


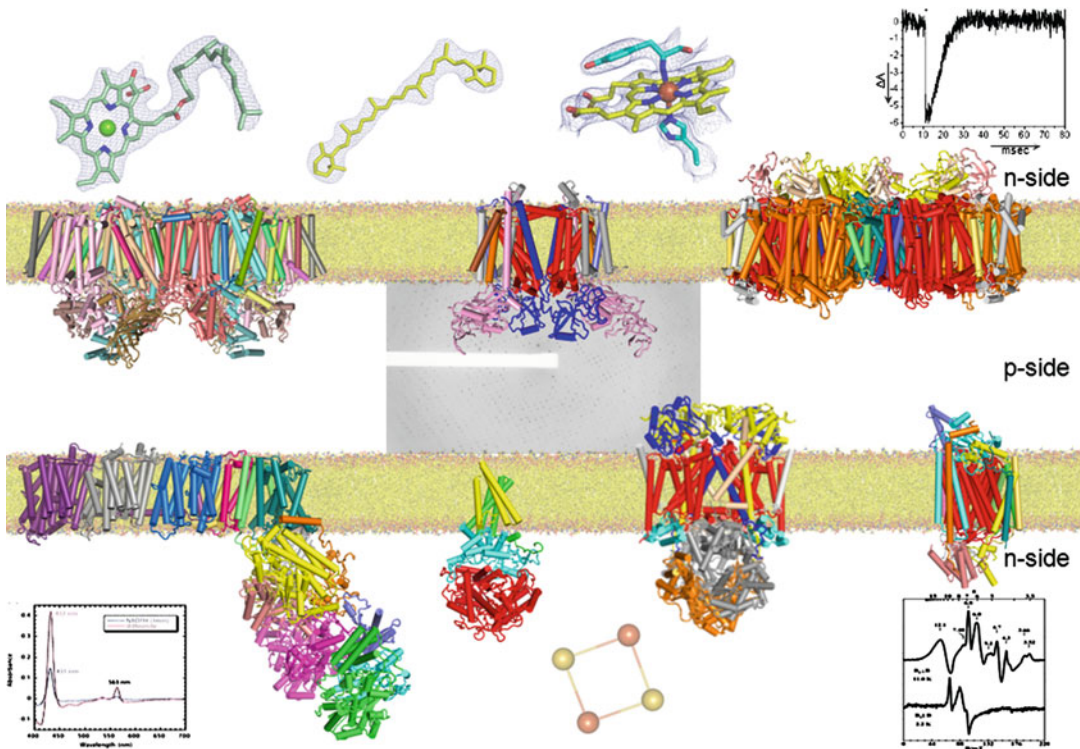
Advances in Photosynthesis and Respiration 41  
Including Bioenergy and Related Processes

William A. Cramer  
Toivo Kallas *Editors*



# Cytochrome Complexes: Evolution, Structures, Energy Transduction, and Signaling

# Cytochrome Complexes: Evolution, Structures, Energy Transduction, and Signaling



**Experimental Information Important for Understanding Properties of Photosynthetic Cytochromes.** Along the top are stick diagrams and electron density of pigments involved in light-harvesting – Chl-*a*,  $\beta$ -carotene, and heme of cytochrome *f* with unusual Tyr–His axial ligation (pdb, protein data base code, 4OGQ). This is followed by a flash kinetic trace of cytochrome oxidation-reduction. Along the bottom is a redox difference spectrum of the cytochrome *b<sub>6</sub>f* complex, the [2Fe-2S] cluster in the Rieske iron-sulfur protein (pdb 4OGQ), and electron spin resonance spectra showing the unique  $g = 12$  signal for the heme  $b_n$ – $c_n$  couple in the cytochrome *b<sub>6</sub>f* complex. In the center is an X-ray diffraction pattern of cytochrome *b<sub>6</sub>f* crystals (pdb 4OGQ). **Protein structures** (left to right); **upper bilayer**: Photosynthetic electron transfer chain – Photosystem II (pdb 2WU2), cytochrome *b<sub>6</sub>f* complex (pdb 4OGQ), Photosystem I (pdb 1JB0); **lower bilayer**: Mitochondrial electron transport chain – NDH complex (pdb 4HEA), succinate dehydrogenase (pdb 1NEN), cytochrome *bc<sub>1</sub>* complex (pdb 3CX5), cytochrome *c* oxidase (pdb 1V54). The lipid bilayer is a homogeneous DOPC bilayer generated with the CHARMM program. *Abbreviations*: p, n-side, electrochemically positive and negative side of the membrane (drawing by S. Saif Hasan)

# **Advances in Photosynthesis and Respiration Including Bioenergy and Related Processes**

---

**VOLUME 41**

---

*Series Editors:*

**GOVINDJEE\***

*(University of Illinois at Urbana-Champaign, IL, U.S.A)*

**THOMAS D. SHARKEY**

*(Michigan State University, East Lansing, MI, U.S.A)*

*\* Founding Series Editor*

*Advisory Editors:*

Roberta CROCE, *University of Amsterdam, The Netherlands*

Basanti BISWAL, *Sambalpur University, Jyoti Vihar, Odisha, India*

Robert E. BLANKENSHIP, *Washington University, St Louis, MO, U.S.A.*

Ralph BOCK, *Max Planck Institute of Molecular Plant Physiology,  
Postdam-Golm, Germany*

Julian J. EATON-RYE, *University of Otago, Dunedin, New Zealand*

Guillaume TCHERKEZ, *Australian National University, Canberra, Australia*

Joy K. WARD, *University of Kansas, U.S.A.*

Johannes MESSINGER, *Umeå University, Umeå, Sweden*

Davide ZANNONI, *University of Bologna, Bologna, Italy*

Xinguang ZHU, *Shanghai Institutes for Biological Sciences,  
Chinese Academy of Sciences, Shanghai, China*

The book series *ADVANCES IN PHOTOSYNTHESIS AND RESPIRATION Including Bioenergy and Related Processes* provides a comprehensive and state-of-the-art account of research in photosynthesis, respiration and related processes. Virtually all life on our planet Earth ultimately depends on photosynthetic energy capture and conversion to energy-rich organic molecules. These are used for food, fuel, and fiber. Photosynthesis is the source of almost all bioenergy on Earth. The fuel and energy uses of photosynthesized products and processes have become an important area of study, and competition between food and fuel has led to resurgence in photosynthesis research. This series of books spans topics from physics to agronomy and medicine; from femtosecond processes through season-long production to evolutionary changes over the course of the history of the Earth; from the photophysics of light absorption, excitation energy transfer in the antenna to the reaction centers, where the highly-efficient primary conversion of light energy to charge separation occurs, through the electrochemistry of intermediate electron transfer, to the physiology of whole organisms and ecosystems; and from X-ray crystallography of proteins to the morphology of organelles and intact organisms. In addition to photosynthesis in natural systems, genetic engineering of photosynthesis and artificial photosynthesis is included in this series. The goal of the series is to offer beginning researchers, advanced undergraduate students, graduate students, and even research specialists, a comprehensive, up-to-date picture of the remarkable advances across the full scope of research on photosynthesis and related energy processes. The purpose of this series is to improve understanding of photosynthesis and respiration at many levels both to improve basic understanding of these important processes and to enhance our ability to use photosynthesis for the improvement of the human condition.

For further volumes:

[www.springer.com/series/5599](http://www.springer.com/series/5599)

# Cytochrome Complexes: Evolution, Structures, Energy Transduction, and Signaling

*Edited by*

**William A. Cramer**

*Department of Biological Sciences  
Hockmeyer Building of Structural Biology  
Purdue University  
West Lafayette, Indiana  
USA*

and

**Toivo Kallas**

*Department of Biology  
Halsey Science Center  
University of Wisconsin-Oshkosh  
Oshkosh, Wisconsin  
USA*

*Editors*

William A. Cramer  
Department of Biological Sciences  
Hockmeyer Building of Structural Biology  
Purdue University  
West Lafayette, Indiana-47917, USA

Toivo Kallas  
Department of Biology  
Halsey Science Center  
University of Wisconsin-Oshkosh  
Oshkosh, Wisconsin-54901, USA

ISSN 1572-0233                      ISSN 2215-0102 (electronic)  
Advances in Photosynthesis and Respiration  
ISBN 978-94-017-7479-6              ISBN 978-94-017-7481-9 (eBook)  
DOI 10.1007/978-94-017-7481-9

Library of Congress Control Number: 2016934058

© Springer Science+Business Media Dordrecht 2016

This work is subject to copyright. All rights are reserved by the Publisher, whether the whole or part of the material is concerned, specifically the rights of translation, reprinting, reuse of illustrations, recitation, broadcasting, reproduction on microfilms or in any other physical way, and transmission or information storage and retrieval, electronic adaptation, computer software, or by similar or dissimilar methodology now known or hereafter developed.

The use of general descriptive names, registered names, trademarks, service marks, etc. in this publication does not imply, even in the absence of a specific statement, that such names are exempt from the relevant protective laws and regulations and therefore free for general use.

The publisher, the authors and the editors are safe to assume that the advice and information in this book are believed to be true and accurate at the date of publication. Neither the publisher nor the authors or the editors give a warranty, express or implied, with respect to the material contained herein or for any errors or omissions that may have been made.

Printed on acid-free paper

This Springer imprint is published by Springer Nature  
The registered company is Springer Science+Business Media B.V. Dordrecht

# From the Series Editors

## **Advances in Photosynthesis and Respiration Including Bioenergy and Related Processes**

### ***Volume 41: Cytochrome Complexes: Evolution, Structures, Energy Transduction, and Signaling***

We are delighted to announce the publication of Volume 41 in this series on *Advances in Photosynthesis and Respiration Including Bioenergy and Related Processes*. Oxygenic photosynthesis begins with conversion of light energy into chemical energy at two photochemical reaction centers in two separate photosystems (PS) I and II; this is followed by oxidation of water to molecular oxygen, reduction of pyridine nucleotide NADP<sup>+</sup> (nicotinamide adenine dinucleotide phosphate) to NADPH, and synthesis of ATP from ADP and inorganic phosphate by ATP synthase, the latter using the proton motive force produced across the thylakoid membrane during electron transport from water to NADP<sup>+</sup>. Four protein complexes are essential for the completion of the entire process that leads to the formation of O<sub>2</sub>, NADPH, and ATP: (1) Photosystem II (PSII); (2) Photosystem I (PSI); (3) Cytochrome (Cyt) *b<sub>6</sub>f* complex; and (4) ATP synthase. Volume 22 in our Series, edited by T. Wydrzynski and K. Satoh and published in 2005, covered in great depth structure and function of PSII (Water-Plastoquinone Oxidoreductase); and volume 24, edited by J.H. Golbeck and published in 2006, did the same for PSI (Plastocyanin-ferredoxin oxidoreductase). Now, in 2016, we are fortunate to be able to present a complete structure-function description of not only Cyt *b<sub>6</sub>f* complex but related complexes from mitochondria as well as from anoxygenic photosynthesis. This book (volume 41), *Cytochrome Complexes: Evo-*

*lution, Structures, Energy Transduction, and Signaling*, was edited by two international authorities in biology, biochemistry, and biophysics: William A. Cramer and Toivo Kallas. In oxygenic photosynthesis, Cyt *b<sub>6</sub>f* provides the link between PSII and PSI; it takes plastoquinol (PQH<sub>2</sub>) made by PSII and reduces plastocyanin, which, in turn, is the source of electrons to reduce ferredoxin (and, thus, NADP<sup>+</sup>) by PSI. In addition, the cytochrome complex functions in the so-called Q cycle that is essential in generating an electrochemical proton gradient sufficient to generate the necessary ATP.

This book starts, appropriately, with a chapter by the late Derek S. Bendall, where he described the historical background of the field as well as the cytochrome notation. The book includes a discussion of the evolution of cytochromes and their functions. Students will benefit by an extensive exposure to both the experiments and the theory underlying electron transfer in proteins, as well as that of the molecular structures of cytochromes and even supercomplexes from both eukaryotes and prokaryotes. Essentially, one has, for the first time, as one would say, “*All we wanted to know about cytochromes, but could not bring ourselves to ask.*” Yes, the book includes authoritative information even on macromolecular assembly, regulation, and signaling via the Cyt *b<sub>6</sub>f* complex.

Because volume 41 covers an extensive subset of the cytochrome complexes that are involved not only in oxygenic photosynthesis

but also in anoxygenic photosynthesis, as well as in respiration, one is confident that this book will be used in educating undergraduate and graduate students and researchers not only in plant and agricultural sciences but animal sciences as well as in microbiology. And since the book covers in depth the structure and function, the molecular biology, and the biochemistry as well as the biophysics of these cytochrome complexes (see Preface as well as Table of Contents of this book for further details), it can be used by students in molecular & cell biology, biochemistry, chemical biology, and biophysics. Further, one can see its significance in areas of agricultural and chemical engineering and in biotechnology, all of which should contribute to the significance of this book.

### Authors of Volume 41

We note with great pride that the current volume is truly an international book; it has authors from 13 countries: Finland (1); France (6); Germany (10); Italy (3); Ireland (3); Israel (2); Japan (8); Lithuania (2); Poland (6); Russia (10); Switzerland (1); UK (8); and USA (25).

We begin by specifically mentioning here two authors, who are also editors of this volume: William A. Cramer of Purdue University, Indiana, USA, and Toivo Kallas of University of Wisconsin Oshkosh, Wisconsin, USA (see their biographies in this volume). Cramer's theme of research is the structure and function of membrane proteins, with a major focus on photosynthetic energy transduction via the cytochrome  $b_6f$  protein complex. We recommend that you visit his websites since they provide information on him as well as on his research: <https://www.bio.purdue.edu/lab/cramer/>; [https://www.bio.purdue.edu/People/faculty\\_dm/directory.php?refID=12](https://www.bio.purdue.edu/People/faculty_dm/directory.php?refID=12) Kallas's theme of research is overall photosynthesis, but in particular, electron transport through the cytochrome  $b_6f$  complex. His work has often focused on cyanobacteria; his web page is at <http://www.uwosh.edu/facstaff/kallas>.

There are 80 authors (including the two editors), who are experts in the field of their research, especially cytochromes. Alphabetically (by last names), they are Jean Alric, Eva-Mari Aro, Danas Baniulis, Adrian C. Barbrook, Carl E. Bauer, the late Derek S Bendall, Gabor Bernat, Edward Berry, Wojciech Bialek, Robert E. Blankenship, Elisa Bombarda, Martin Caffrey, William A. Cramer, Fevzi Daldal, Miguel A. De la Rosa, Irene Díaz-Moreno, Antonio Díaz-Quintana, Timothy J. Donohue, Anne-Lise Ducluzeau, Seda Ekici, Robert Ekiert, Lothar Esser, Giovanni Finazzi, Maria Luisa Genova, Patrice Hamel, Shigeharu Harada, S. Saif Hasan, Florian Hilbers, Christopher J. Howe, Li-shar Huang, Saheed Imam, Daniel Ken Inaoka, Giles N. Johnson, Toivo Kallas, Bahia Khalfaoui-Hassani, Kiyoshi Kita, Hans-Georg Koch, Piotr Kolesinski, David Kramer, Lev I. Krishtalik, Genji Kurisu, Giorgio Lenaz, Joseph A. Lyons, Erica L.W. Majumder, Alizée Malnoë, Benjamin May, Yuval Mazor, I. Miliute, Jun Minagawa, Anthony L. Moore, Frank Müh, Lars Mueller, Nathan Nelson, Robert H. Nimmo, Wolfgang Nitschke, Daniel R. Noguera, Artur Osyczka, Jean-David Rochaix, Matthias Rögner, Marcin Sarewicz, Georg Schmetterer, Dirk Schneider, Tomoo Shiba, Toshiharu Shikanai, Namita Shroff, Melanie A. Spero, Andrzej Szczepaniak, Petru-Iulian Trasnea, G. Matthias Ullmann, Marcel Utz, Andreia F. Verissimo, Di Xia, Shinya Yoshikawa, Luke Young, Chang-An Yu, Sébastien Zappa, Fei Zhou, Francesca Zito, and Athina Zouni.

### Our Books

We list below information on the 40 volumes that have been published thus far (see <http://www.springer.com/series/5599> for the series website). Electronic access to individual chapters depends on subscription (ask your librarian) but Springer provides free downloadable Preface, sample pages and Table of Content for nearly all volumes. The available websites of the books in the Series are listed below.

- **Volume 40 (2014): Non-Photochemical Quenching and Energy Dissipation in Plants, Algae and Cyanobacteria**, edited by Barbara Demmig-Adams, Győző Garab, William W. Adams III, and Govindjee from USA and Hungary. Twenty-eight chapters, 649 pp, Hardcover ISBN 978-94-017-9031-4, eBook ISBN 978-94-017-9032-1 [<http://www.springer.com/life+sciences/plant+sciences/book/978-94-017-9031-4>]
- **Volume 39 (2014): The Structural Basis of Biological Energy Generation**, edited by Martin F. Hohmann-Marriott from Norway. Twenty-four chapters, 483 pp, Hardcover ISBN 978-94-017-8741-3, eBook ISBN 978-94-017-8742-0 [<http://www.springer.com/life+sciences/book/978-94-017-8741-3>]
- **Volume 38 (2014): Microbial BioEnergy: Hydrogen Production**, edited by Davide Zannoni and Roberto De Phillipis, from Italy. Eighteen chapters, 366 pp, Hardcover ISBN 978-94-017-8553-2, eBook ISBN 978-94-017-8554-9 [<http://www.springer.com/life+sciences/plant+sciences/book/978-94-017-8553-2>]
- **Volume 37 (2014): Photosynthesis in Bryophytes and Early Land Plants**, edited by David T. Hanson and Steven K. Rice, from USA. Eighteen chapters, approx. 342 pp, Hardcover ISBN 978-94-007-6987-8, eBook ISBN 978-94-007-6988-5 [<http://www.springer.com/life+sciences/plant+sciences/book/978-94-007-6987-8>]
- **Volume 36 (2013): Plastid Development in Leaves during Growth and Senescence**, edited by Basanti Biswal, Karin Krupinska and Udaya Biswal, from India and Germany. Twenty-eight chapters, 837 pp, Hardcover ISBN 978-94-007-5723-33, eBook ISBN 978-94-007-5724-0 [<http://www.springer.com/life+sciences/plant+sciences/book/978-94-007-5723-3>]
- **Volume 35 (2012): Genomics of Chloroplasts and Mitochondria**, edited by Ralph Bock and Volker Knoop, from Germany. Nineteen chapters, 475 pp, Hardcover ISBN 978-94-007-2919-3 eBook ISBN 978-94-007-2920-9 [<http://www.springer.com/life+sciences/plant+sciences/book/978-94-007-2919-3>]
- **Volume 34 (2012): Photosynthesis – Plastid Biology, Energy Conversion and Carbon Assimilation**, edited by Julian Eaton-Rye, Baishnab C. Tripathy, and Thomas D. Sharkey, from New Zealand, India, and USA. Thirty-three chapters, 854 pp, Hardcover, ISBN 978-94-007-1578-3, eBook ISBN 978-94-007-1579-0 [<http://www.springer.com/life+sciences/plant+sciences/book/978-94-007-1578-3>]
- **Volume 33 (2012): Functional Genomics and Evolution of Photosynthetic Systems**, edited by Robert L. Burnap and Willem F.J. Vermaas, from USA. Fifteen chapters, 428 pp, Hardcover ISBN 978-94-007-1532-5, Softcover ISBN 978-94-007-3832-4, eBook ISBN 978-94-007-1533-2 [<http://www.springer.com/life+sciences/book/978-94-007-1532-5>]
- **Volume 32 (2011): C<sub>4</sub> Photosynthesis and Related CO<sub>2</sub> Concentrating Mechanisms**, edited by Agepati S. Raghavendra and Rowan Sage, from India and Canada. Nineteen chapters, 425 pp, Hardcover ISBN 978-90-481-9406-3, Softcover ISBN 978-94-007-3381-7, eBook ISBN 978-90-481-9407-0 [<http://www.springer.com/life+sciences/plant+sciences/book/978-90-481-9406-3>]
- **Volume 31 (2010): The Chloroplast: Basics and Applications**, edited by Constantin Rebeiz (USA), Christoph Benning (USA), Hans J. Bohnert (USA), Henry Daniell (USA), J. Kenneth Hooper (USA), Hartmut K. Lichtenthaler (Germany), Archie R. Portis (USA), and Baishnab C. Tripathy (India). Twenty-five chapters, 451 pp, Hardcover ISBN 978-90-481-8530-6, Softcover ISBN 978-94-007-3287-2, eBook ISBN 978-90-481-8531-3 [<http://www.springer.com/life+sciences/plant+sciences/book/978-90-481-8530-6>]
- **Volume 30 (2009): Lipids in Photosynthesis: Essential and Regulatory Functions**, edited by Hajime Wada and Norio Murata, both from Japan. Twenty chapters, 506 pp, Hardcover ISBN 978-90-481-2862-4, Softcover ISBN 978-94-007-3073-1 eBook ISBN 978-90-481-2863-1 [<http://www.springer.com/life+sciences/plant+sciences/book/978-90-481-2862-4>]



- **Volume 29 (2009): Photosynthesis in Silico: Understanding Complexity from Molecules**, edited by Agu Laisk, Ladislav Nedbal, and Govindjee, from Estonia, The Czech Republic, and USA. Twenty chapters, 525 pp, Hardcover ISBN 978-1-4020-9236-7, Softcover ISBN 978-94-007-1533-2, eBook ISBN 978-1-4020-9237-4 [<http://www.springer.com/life+sciences/plant+sciences/book/978-1-4020-9236-7>]
- **Volume 28 (2009): The Purple Phototrophic Bacteria**, edited by C. Neil Hunter, Fevzi Daldal, Marion C. Thurnauer and J. Thomas Beatty, from UK, USA and Canada. Forty-eight chapters, 1053 pp, Hardcover ISBN 978-1-4020-8814-8, eBook ISBN 978-1-4020-8815-5 [<http://www.springer.com/life+sciences/plant+sciences/book/978-1-4020-8814-8>]
- **Volume 27 (2008): Sulfur Metabolism in Phototrophic Organisms**, edited by Christiane Dahl, Rüdiger Hell, David Knaff and Thomas Leustek, from Germany and USA. Twenty-four chapters, 551 pp, Hardcover ISBN 978-4020-6862-1, Softcover ISBN 978-90-481-7742-4, eBook ISBN 978-1-4020-6863-8 [<http://www.springer.com/life+sciences/plant+sciences/book/978-1-4020-6862-1>]
- **Volume 26 (2008): Biophysical Techniques Photosynthesis**, Volume II, edited by Thijs Aartsma and Jörg Matysik, both from The Netherlands. Twenty-four chapters, 548 pp, Hardcover, ISBN 978-1-4020-8249-8, Softcover ISBN 978-90-481-7820-9, eBook ISBN 978-1-4020-8250-4 [<http://www.springer.com/life+sciences/plant+sciences/book/978-1-4020-8249-8>]
- **Volume 25 (2006): Chlorophylls and Bacteriochlorophylls: Biochemistry, Biophysics, Functions and Applications**, edited by Bernhard Grimm, Robert J. Porra, Wolfhart Rüdiger, and Hugo Scheer, from Germany and Australia. Thirty-seven chapters, 603 pp, Hardcover, ISBN 978-1-40204515-8, Softcover ISBN 978-90-481-7140-8, eBook ISBN 978-1-4020-4516-5 [<http://www.springer.com/life+sciences/plant+sciences/book/978-1-4020-4515-8>]
- **Volume 24 (2006): Photosystem I: The Light-Driven Plastocyanin: Ferredoxin Oxidoreductase**, edited by John H. Golbeck, from USA. Forty chapters, 716 pp, Hardcover ISBN 978-1-40204255-3, Softcover ISBN 978-90-481-7088-3, eBook ISBN 978-1-4020-4256-0 [<http://www.springer.com/life+sciences/plant+sciences/book/978-1-4020-4255-3>]
- **Volume 23 (2006): The Structure and Function of Plastids**, edited by Robert R. Wise and J. Kenneth Hooper, from USA. Twenty-seven chapters, 575 pp, Softcover, ISBN: 978-1-4020-6570-6; Hardcover ISBN 978-1-4020-4060-3, Softcover ISBN 978-1-4020-6570-5, eBook ISBN 978-1-4020-4061-0 [<http://www.springer.com/life+sciences/plant+sciences/book/978-1-4020-4060-3>]
- **Volume 22 (2005): Photosystem II: The Light-Driven Water: Plastoquinone Oxidoreductase**, edited by Thomas J. Wydrzynski and Kimiyuki Satoh, from Australia and Japan. Thirty-four chapters, 786 pp, Hardcover ISBN 978-1-4020-4249-2, eBook ISBN 978-1-4020-4254-6 [<http://www.springer.com/life+sciences/plant+sciences/book/978-1-4020-4249-2>]
- **Volume 21 (2005): Photoprotection, Photoinhibition, Gene Regulation, and Environment**, edited by Barbara Demmig-Adams, William W. Adams III and Axtar K. Mattoo, from USA. Twenty-one chapters, 380 pp, Hardcover ISBN 978-14020-3564-7, Softcover ISBN 978-1-4020-9281-7, eBook ISBN 978-1-4020-3579-1 [<http://www.springer.com/life+sciences/plant+sciences/book/978-1-4020-3564-7>]
- **Volume 20 (2006): Discoveries in Photosynthesis**, edited by Govindjee, J. Thomas Beatty, Howard Gest and John F. Allen, from USA, Canada and UK. One hundred and eleven chapters, 1304 pp, Hardcover ISBN 978-1-4020-3323-0, eBook ISBN 978-1-4020-3324-7 [<http://www.springer.com/life+sciences/plant+sciences/book/978-1-4020-3323-0>]
- **Volume 19 (2004): Chlorophyll *a* Fluorescence: A Signature of Photosynthesis**, edited by George C. Papageorgiou and Govindjee,

- from Greece and USA. Thirty-one chapters, 820 pp, Hardcover, ISBN 978-1-4020-3217-2, Softcover ISBN 978-90-481-3882-1, eBook ISBN 978-1-4020-3218-9 [<http://www.springer.com/life+sciences/biochemistry+%26+biophysics/book/978-1-4020-3217-2>]
- **Volume 18 (2005): Plant Respiration: From Cell to Ecosystem**, edited by Hans Lambers and Miquel Ribas-Carbo, from Australia and Spain. Thirteen chapters, 250 pp, Hardcover ISBN 978-1-4020-3588-3, Softcover ISBN 978-90-481-6903-0, eBook ISBN 978-1-4020-3589-0 [<http://www.springer.com/life+sciences/plant+sciences/book/978-1-4020-3588-3>]
  - **Volume 17 (2004): Plant Mitochondria: From Genome to Function**, edited by David Day, A. Harvey Millar and James Whelan, from Australia. Fourteen chapters, 325 pp, Hardcover, ISBN: 978-1-4020-2399-6, Softcover ISBN 978-90-481-6651-0, eBook ISBN 978-1-4020-2400-9 [<http://www.springer.com/life+sciences/cell+biology/book/978-1-4020-2399-6>]
  - **Volume 16 (2004): Respiration in Archaea and Bacteria: Diversity of Prokaryotic Respiratory Systems**, edited by Davide Zannoni, from Italy. Thirteen chapters, 310 pp, Hardcover ISBN 978-1-4020-2002-5, Softcover ISBN 978-90-481-6571-1, eBook ISBN 978-1-4020-3163-2 [<http://www.springer.com/life+sciences/plant+sciences/book/978-1-4020-2002-5>]
  - **Volume 15 (2004): Respiration in Archaea and Bacteria: Diversity of Prokaryotic Electron Transport Carriers**, edited by Davide Zannoni, from Italy. Thirteen chapters, 350 pp, Hardcover ISBN 978-1-4020-2001-8, Softcover ISBN 978-90-481-6570-4 (no eBook at this time) [<http://www.springer.com/life+sciences/biochemistry+%26+biophysics/book/978-1-4020-2001-8>]
  - **Volume 14 (2004): Photosynthesis in Algae**, edited by Anthony W. Larkum, Susan Douglas and John A. Raven, from Australia, Canada and UK. Nineteen chapters, 500 pp, Hardcover ISBN 978-0-7923-6333-0, Softcover ISBN 978-94-010-3772-3, eBook ISBN 978-94-007-1038-2 [<http://www.springer.com/life+sciences/plant+sciences/book/978-0-7923-6333-0>]
  - **Volume 13 (2003): Light-Harvesting Antennas in Photosynthesis**, edited by Beverley R. Green and William W. Parson, from Canada and USA. Seventeen chapters, 544 pp, Hardcover ISBN 978-07923-6335-4, Softcover ISBN 978-90-481-5468-5, eBook ISBN 978-94-017-2087-8 [<http://www.springer.com/life+sciences/plant+sciences/book/978-0-7923-6335-4>]
  - **Volume 12 (2003): Photosynthetic Nitrogen Assimilation and Associated Carbon and Respiratory Metabolism**, edited by Christine H. Foyer and Graham Noctor, from UK and France. Sixteen chapters, 304 pp, Hardcover ISBN 978-07923-6336-1, Softcover ISBN 978-90-481-5469-2, eBook ISBN 978-0-306-48138-3 [<http://www.springer.com/life+sciences/plant+sciences/book/978-0-7923-6336-1>]
  - **Volume 11 (2001): Regulation of Photosynthesis**, edited by Eva-Mari Aro and Bertil Andersson, from Finland and Sweden. Thirty-two chapters, 640 pp, Hardcover ISBN 978-0-7923-6332-3, Softcover ISBN 978-94-017-4146-0, eBook ISBN 978-0-306-48148-2 [<http://www.springer.com/life+sciences/plant+sciences/book/978-0-7923-6332-3>]
  - **Volume 10 (2001): Photosynthesis: Photobiochemistry and Photobiophysics**, edited by Bacon Ke, from USA. Thirty-six chapters, 792 pp, Hardcover ISBN 978-0-7923-6334-7, Softcover ISBN 978-0-7923-6791-8, eBook ISBN 978-0-306-48136-9 [<http://www.springer.com/life+sciences/plant+sciences/book/978-0-7923-6334-7>]
  - **Volume 9 (2000): Photosynthesis: Physiology and Metabolism**, edited by Richard C. Leegood, Thomas D. Sharkey and Susanne von Caemmerer, from UK, USA and Australia. Twenty-four chapters, 644 pp, Hardcover ISBN 978-07923-6143-5, Softcover ISBN 978-90-481-5386-2, eBook ISBN 978-0-306-48137-6 [<http://www.springer.com/life+sciences/plant+sciences/book/978-0-7923-6143-5>]
  - **Volume 8 (1999): The Photochemistry of Carotenoids**, edited by Harry A. Frank, Andrew J. Young, George Britton and Richard J. Cogdell, from USA and UK. Twenty chapters, 420 pp, Hardcover ISBN 978-0-7923-5942-5, Softcover ISBN

- 978-90-481-5310-7, eBook ISBN 978-0-306-48209-0 [<http://www.springer.com/life+sciences/plant+sciences/book/978-0-7923-5942-5>]
- **Volume 7 (1998): The Molecular Biology of Chloroplasts and Mitochondria in *Chlamydomonas***, edited by Jean David Rochaix, Michel Goldschmidt-Clermont and Sabeeha Merchant, from Switzerland and USA. Thirty-six chapters, 760 pp, Hardcover ISBN 978-0-7923-5174-0, Softcover ISBN 978-94-017-4187-3, eBook ISBN 978-0-306-48204-5 [<http://www.springer.com/life+sciences/plant+sciences/book/978-0-7923-5174-0>]
  - **Volume 6 (1998): Lipids in Photosynthesis: Structure, Function and Genetics**, edited by Paul-André Siegenthaler and Norio Murata, from Switzerland and Japan. Fifteen chapters, 332 pp. Hardcover ISBN 978-0-7923-5173-3, Softcover ISBN 978-90-481-5068-7, eBook ISBN 978-0-306-48087-4 [<http://www.springer.com/life+sciences/plant+sciences/book/978-0-7923-5173-3>]
  - **Volume 5 (1997): Photosynthesis and the Environment**, edited by Neil R. Baker, from UK. Twenty chapters, 508 pp, Hardcover ISBN 978-07923-4316-5, Softcover ISBN 978-90-481-4768-7, eBook ISBN 978-0-306-48135-2 [<http://www.springer.com/life+sciences/plant+sciences/book/978-0-7923-4316-5>]
  - **Volume 4 (1996): Oxygenic Photosynthesis: The Light Reactions**, edited by Donald R. Ort and Charles F. Yocum, from USA. Thirty-four chapters, 696 pp, Hardcover ISBN 978-0-7923-3683-9, Softcover ISBN 978-0-7923-3684-6, eBook ISBN 978-0-306-48127-7 [<http://www.springer.com/life+sciences/plant+sciences/book/978-0-7923-3683-9>]
  - **Volume 3 (1996): Biophysical Techniques in Photosynthesis**, edited by Jan Amesz and Arnold J. Hoff, from The Netherlands. Twenty-four chapters, 426 pp, Hardcover ISBN 978-0-7923-3642-6, Softcover ISBN 978-90-481-4596-6, eBook ISBN 978-0-306-47960-1 [<http://www.springer.com/life+sciences/plant+sciences/book/978-0-7923-3642-6>]
  - **Volume 2 (1995): Anoxygenic Photosynthetic Bacteria**, edited by Robert E. Blankenship, Michael T. Madigan and Carl E. Bauer, from USA. Sixty-two chapters, 1331 pp, Hardcover ISBN 978-0-7923-3682-8, Softcover ISBN 978-0-7923-3682-2, eBook ISBN 978-0-306-47954-0 [<http://www.springer.com/life+sciences/plant+sciences/book/978-0-7923-3681-5>]
  - **Volume 1 (1994): The Molecular Biology of Cyanobacteria**, edited by Donald R. Bryant, from USA. Twenty-eight chapters, 916 pp, Hardcover, ISBN 978-0-7923-3222-0, Softcover ISBN 978-0-7923-3273-2, eBook ISBN 978-94-011-0227-8 [<http://www.springer.com/life+sciences/plant+sciences/book/978-0-7923-3222-0>]
- Further information on these books and ordering instructions is available at <http://www.springer.com/series/5599>. Contents of volumes 1–28 can also be found at < <http://www.life.uiuc.edu/govindjee/photosynSeries/ttocs.html>>.
- Special 25 % discounts are available to members of the International Society of Photosynthesis Research, ISPR <http://www.photosynthesisresearch.org/>. See <http://www.springer.com/ispr>.

### Future Advances in Photosynthesis and Respiration and Other Related Books

The readers of the current series are encouraged to watch for the publication of the forthcoming books (not necessarily arranged in the order of future appearance):

- *Canopy Photosynthesis: From Basics to Applications* (Editors: Kouki Hikosaka, Ülo Niinemets and Niels P.R. Anten); it is already available; see < <http://www.springer.com/us/book/9789401772907>>
- *Photosynthesis and Climate Change* (working title) (Editor: Joy K. Ward)

- *Cyanobacteria* (Editor: Donald Bryant)
- *Leaf Photosynthesis* (Editors: William W. Adams III and Ichiro Terashima)
- *Photosynthesis in Algae* (Editors: Anthony Larkum and Arthur Grossman)
- *Plant Respiration* (Editor: Guillaume Tcherkez)

In addition to the above contracted books, the following topics are under consideration:

- Algae, Cyanobacteria: Biofuel and Bioenergy
- Artificial Photosynthesis
- ATP Synthase: Structure and Function
- Bacterial Respiration II
- Carotenoids II
- Evolution of Photosynthesis
- Green Bacteria and Heliobacteria
- Interactions between Photosynthesis and other Metabolic Processes
- Limits of Photosynthesis: Where do we go from here?
- Photosynthesis, Biomass and Bioenergy
- Photosynthesis under Abiotic and Biotic Stress

*If you have any interest in editing/coediting any of the above listed books, or being an author, please send an e-mail to Tom Sharkey ([tsharkey@msu.edu](mailto:tsharkey@msu.edu)) and/or to Govindjee ([gov@illinois.edu](mailto:gov@illinois.edu)). Suggestions for additional topics are also welcome.*

Instructions for writing chapters in books in our series are available by sending e-mail requests to one or both of us; they may also be downloaded from Govindjee's website <http://www.life.illinois.edu/govindjee> as the fourth item under "Announcements" on the main page.

## Acknowledgments

We take this opportunity to thank and congratulate William A. Cramer and Toivo Kallas for their outstanding editorial work; they have indeed done a fantastic job, not only in editing but also in organizing this book for all of us, and for their highly professional dealing with the reviewing process. We thank all the 81 authors of this book (see the list given earlier); without their authoritative chapters, there would be no such volume. We give special thanks to S. Koperundevi of SPi Global, India, for directing the typesetting of this book; her expertise has been crucial in bringing this book to completion. We owe Jacco Flipsen, Andre Tournois, and Ineke Ravesloot (of Springer) thanks for their friendly working relation with us that led to the production of this book.

**March 15, 2016**

**Govindjee**

Department of Plant Biology  
Department of Biochemistry and Center  
of Biophysics & Quantitative Biology  
University of Illinois  
at Urbana-Champaign, Urbana  
IL 61801, USA  
[gov@illinois.edu](mailto:gov@illinois.edu)

**Thomas D. Sharkey**

Department of Biochemistry  
and Molecular Biology  
Michigan State University  
East Lansing, MI 48824, USA  
[tsharkey@msu.edu](mailto:tsharkey@msu.edu)



# Series Editors



**Govindjee** is the founding series editor of *Advances in Photosynthesis*, as it was called then, with volume 1 (*The Molecular Biology of Cyanobacteria*, 1994). In addition to being co-series editor (with Tom Sharkey) since volume 31 (*The Chloroplast: Basics and Applications*, 2010), he has coedited (1) Volume 19 (*Chlorophyll a Fluorescence: A Signature of Photosynthesis*, 2004); (2) Volume 20 (*Discoveries in Photosynthesis*, 2006); (3) Volume 29 (*Photosynthesis In Silico: Understanding Complexity from Molecules to Ecosystems*, 2009); and (4) Volume 40 (*Non-Photochemical Quenching and Energy Dissipation in Plants, Algae and Cyanobacteria*, 2014).

Govindjee, who uses one name only, has been Professor Emeritus of Biochemistry, Biophysics, and Plant Biology at the University of Illinois at Urbana-Champaign (UIUC), since 1999. His short evolving biography can be found in each volume of *Advances in Photosynthesis and Respiration*, and other information on him and his activities is available at his website <http://www.life.illinois.edu/govindjee>. An interview for Annual Reviews Inc., by

Don Ort, is available at <https://www.youtube.com/watch?v=cOzuL0vxEi0>. His recent publications are listed at [http://www.life.illinois.edu/govindjee/recent\\_papers.html](http://www.life.illinois.edu/govindjee/recent_papers.html), and earlier publications since 1955 are at <http://www.life.illinois.edu/govindjee/pubschron.html>.

Govindjee was trained in Plant Physiology (1952–1956) by Shri Ranjan (a student of Felix Frost Blackman of UK), in Biology and Biochemistry of Photosynthesis (1956–1958) by Robert Emerson (a student of the Nobel laureate Otto Warburg), and in Biophysics of Photosynthesis (1958–1961) by Eugene Rabinowitch (a postdoc student of the Nobel laureate James Franck). After his Ph.D. in Biophysics in 1960 from the UIUC, he has learned many concepts and techniques from many others including Louis N.M. Duysens (Leiden, The Netherlands); C. Stacy French (Stanford, California, USA); Herbert S. Gutowsky (Urbana, Illinois, USA); Bessel Kok (Baltimore, Maryland, USA); Jean Lavorel (Gif-sur-Yvette, France); Gregorio Weber (Urbana, Illinois); and Horst Witt (Berlin, Germany).

Govindjee's discoveries, with his coworkers and graduate students, include the participation of chlorophyll (Chl) *a* (in what we now call Photosystem (PS) II); proof of the existence of two light reactions in NADP reduction, and in Chl *a* fluorescence; temperature dependence of excitation energy transfer down to 4° K in algae and cyanobacteria; molecular understanding of both the fast and slow Chl *a* fluorescence (both prompt and delayed) changes—that includes participation of membrane potential, pH gradient, “traffic jam” in PSI, and the so-called state changes; first picosecond measurements on the primary photochemistry of PSI and PSII; unique role of bicarbonate in electron transfer and protonation events at the Q<sub>B</sub> binding site; first comprehensive theory of thermoluminescence in plants; and the first use of lifetime of Chl *a* fluorescence measurements in understanding photoprotection in plants.

Govindjee's activities include, besides research on “Light Reactions of Photosynthesis,” honoring others (Robert Blankenship; Bob Buchanan; Andre Jagendorf; Wolfgang Junge; Hartmut Lichtenthaler; George Papageorgiou; William Ogren; Vladimir Shuvalov; and Diter Von Wettstein; see Govindjee's website) in the field, as well as participating in writing and editing obituaries and tributes (Lou Duysens; Colin Wraight; Al Bassham; Rene Marcelle; V.S.R. Rama Das; Prasanna Mohanty; Jalal Aliyev; Al Frenkel; and Andy Benson). In addition, he enjoys lecturing on the

history of photosynthesis research and in teaching photosynthesis by having students act as molecules and demonstrating the path of electrons in photosynthesis by having them enact a drama. He has had many honors, but he cherishes five of them dearly: 2006 Lifetime Achievement Award of the Rebeiz Foundation for Basic Biology; 2007 Communication Award of the International Society of Photosynthesis Research; 2008 Liberal Arts & Sciences Lifetime Achievement Award of UIUC; 2015 Dr. B.M. Johri Memorial Award for Excellence in Plant Biology, from the Society of Plant Research, India; and a 2016 Distinguished Alumnus Award from his High School (Colonelganj Inter College) in Allahabad. In addition, he has enjoyed what others have written on him at his 75th and 80th birthdays (see *Photosynth Res* **93**:1–5 (2007); **94**: 153–178 (2007); **100**: 49–55 (2009); **116**: 107–110; 111–144 (2013); **122**: 113–119); also see <<https://www.linkedin.com/pulse/govindjee-living-legend-i-met-dr-ravi-sharma>>. (To see this site, click on “living-legend”.) A rather useful effort in teaching others is through the article “Photosynthesis Web Resources” <<http://www.life.illinois.edu/govindjee/photoweb/>>. Also see a collection of education books at <http://www.life.illinois.edu/govindjee/g/Books.html>. He is always delighted to respond to questions on both photosynthesis research and education (e-mail: [gov@illinois.edu](mailto:gov@illinois.edu)).



**Thomas D. (Tom) Sharkey** obtained his Bachelor's degree in Biology in 1974 from Lyman Briggs College, a residential science college at Michigan State University, East Lansing, Michigan, USA. After 2 years as a research technician, Tom entered a Ph.D. program in the Department of Energy Plant Research Laboratory at Michigan State University under the mentorship of Klaus Raschke and finished in 1979. Postdoctoral research was carried out with Graham Farquhar at the Australian National University, in Canberra, where he coauthored a landmark review on photosynthesis and stomatal conductance. For 5 years he worked at the Desert Research Institute, Reno, Nevada. After Reno, Tom spent 20 years as Professor of Botany at the University of Wisconsin in Madison. In 2008, Tom became Professor and Chair of the Department of Biochemistry and Molecular Biology at Michigan State University. Tom's research interests center on the exchange of gases between plants and the atmosphere and carbon metabolism of photosynthesis. The biochemistry and biophysics underlying carbon dioxide uptake and isoprene emission from plants form the two major research topics in his laboratory. Among his contributions are measurement of the carbon dioxide concentration inside leaves, an

exhaustive study of short-term feedback effects in carbon metabolism, and a significant contribution to elucidation of the pathway by which leaf starch breaks down at night. In the isoprene research field, Tom is recognized as the leading advocate for thermotolerance of photosynthesis as the explanation for why plants emit isoprene. In addition, his laboratory has cloned many of the genes that underlie isoprene synthesis and he has published many important papers on the biochemical regulation of isoprene synthesis. Tom's work has been cited over 21,000 times according to Google Scholar in 2015. He has been named an Outstanding Faculty member by Michigan State University and in 2015, he was honored, and named as a University Distinguished Professor. Tom has coedited three books, the first on trace gas emissions from plants in 1991 (with Elizabeth Holland and Hal Mooney), volume 9 of this series (with Richard Leegood and Susanne von Caemmerer) on the *Physiology of Carbon Metabolism of Photosynthesis* in 2000, and volume 34 (with Julian Eaton-Rye and Baishnab C. Tripathy) entitled *Photosynthesis: Plastid Biology, Energy Conversion and Carbon Assimilation*. Tom has been co-series editor of this series since volume 31.





# Contents

<b>From the Series Editors</b>	<b>v</b>
<b>Series Editors</b>	<b>xiii</b>
<b>Preface</b>	<b>xxix</b>
<b>Editors</b>	<b>xxxix</b>
<b>Remembrances</b>	<b>xxxv</b>
<b>Contributors</b>	<b>xli</b>

## ***Part I: Diversity and Evolution***

---

<b>1 Keilin, Cytochrome and Its Nomenclature</b>	<b>3–11</b>
<i>Derek S. Bendall (deceased)</i>	
Summary	3
I. The Cytochromes and History	3
References	10
<b>2 When Did Hemes Enter the Scene of Life? On the Natural History of Heme Cofactors and Heme-Containing Enzymes</b>	<b>13–24</b>
<i>Anne-Lise Ducluzeau and Wolfgang Nitschke</i>	
Summary	13
I. Introduction	14
II. Hemes in LUCA; Pros and Cons	15
III. An Alternative Scenario	19
IV. Why All the Fuzz?	21
Acknowledgments	22
References	22
<b>3 The Diversity of Photosynthetic Cytochromes</b>	<b>25–50</b>
<i>Erica L.-W. Majumder and Robert E. Blankenship</i>	
Summary	25
I. Introduction	26
II. Cytochromes in Anoxygenic Photosynthetic Electron Transport Chains	26

III. Cytochromes in Oxygenic Photosynthetic Electron Transport Chains	40
IV. Conclusions	44
Acknowledgments	44
References	44

#### **4 Evolution of Photosynthetic NDH-1: Structure and Physiological Function** **51–70**

*Toshiharu Shikanai and Eva-Mari Aro*

Summary	51
I. Introduction	52
II. Function and Structure of Cyanobacterial NDH-1	53
III. Chloroplast NDH-1 and Cyclic Electron Transport Around PSI	57
IV. Structure of Chloroplast NDH-1	58
V. Evolution of Chloroplast NDH-1 in Land Plants	60
VI. Physiological Reason for Evolutionary Increase in Complexity of Chloroplast NDH-1	63
VII. The Origin of Photosynthetic NDH-1	64
VIII. Concluding Remarks	64
Acknowledgements	65
References	65

### ***Part II: Theoretical Aspects of Electron Transfer***

---

#### **5 Fundamentals of Electron Transfer in Proteins** **73–98**

*Lev I. Krishtalik*

Summary	73
I. Introduction	74
II. The General Theory of Charge Transfer Reactions in Polar Media: An Outline	74
III. Proteins as Specific Structured Polar Media	83
IV. Equilibrium Energies of Electron Transfer	85
V. Reorganization Energy and Activation Energy	90
VI. Long-Range Electron Transfer	93
References	95

#### **6 Theoretical Analysis of Electron Transfer in Proteins: From Simple Proteins to Complex Machineries** **99–127**

*G. Matthias Ullmann, Lars Mueller, and Elisa Bombarda*

Summary	99
I. Introduction	100
II. Theoretical Description of Electron Transfer Reactions	102
III. Electrostatic Methods for Estimating Reaction Free Energies and Reorganization Energies	108

IV. Complex Electron Transfer Proteins	120
V. Conclusions	122
Acknowledgements	125
References	125

## **Part III: Molecular Structures and Functions of Cytochrome Complexes**

---

<b>A. Photosynthetic Reaction Centers and Linked Cytochromes (Chapters 7 and 8)</b>	
<b>7 Higher Plant and Cyanobacterial Photosystem I: Connected Cytochrome Pathways</b>	<b>131–142</b>
<i>Yuval Mazor and Nathan Nelson</i>	
Summary	131
I. Introduction	132
II. Cytochrome <i>bc</i> Complex and Its Central Role in Photosynthetic and Respiratory Electron Transport Chains	132
III. Oceanic Photosynthesis	133
IV. Interactions Between Photosystem I and Small Electron Donors	134
V. Phage Encoded PSI Complex	139
References	140
<b>8 Cytochrome <i>b</i><sub>559</sub> in Photosystem II</b>	<b>143–175</b>
<i>Frank Müh and Athina Zouni</i>	
Summary	144
I. Introduction	144
II. Structure	146
III. Redox Properties	158
IV. Function of Cytochrome <i>b</i> <sub>559</sub>	167
V. Conclusions and Outlook	169
Acknowledgements	170
References	170
<b>B. Structure-Function of Cytochrome <i>bc</i><sub>1</sub> and <i>b</i><sub>6</sub><i>f</i> Complexes (Chapters 9, 10, 11, 12, 13, 14 and 15)</b>	
<b>9 Structure-Function of the Cytochrome <i>b</i><sub>6</sub><i>f</i> Lipoprotein Complex</b>	<b>177–207</b>
<i>William A. Cramer and S. Saif Hasan</i>	
Summary	178
I. Introduction	179
II. Historical Perspective	179
III. Cytochrome <i>b</i> <sub>6</sub> <i>f</i> and <i>bc</i> <sub>1</sub> Complexes; General Aspects	180
IV. Structure-Function of the Cyt <i>b</i> <sub>6</sub> <i>f</i> Complex	180
V. Lipids in the <i>b</i> <sub>6</sub> <i>f</i> Lipoprotein Complex	190

VI. Pathways of Cyclic Electron Transport (CET)	191
VII. Functions of the $b_6f$ Complex in the Linear Electron Transport (LET) Pathway; the Q Cycle	194
VIII. Quinone-Mediated $H^+$ Transfer Pathways; n-Side to Quinone Binding Site: Heme $c_n$ ; p-Side PEWY Exit Pathway with Invaginated $H_2O$ Pocket	197
IX. The Cytochrome $b_6f$ Complex as a Hetero-Oligomeric Membrane Lipoprotein	200
Acknowledgements	200
References	200

## 10 Structure-Function Studies of the Cytochrome $bc_1$ Complex of Anoxygenic Photosynthetic Purple Bacteria **209–235**

*Lothar Esser, Fei Zhou, Chang-An Yu, and Di Xia*

Summary	210
I. Introduction	211
II. The Mechanism of Electron Transfer (ET)-Coupled Proton Translocation Function of Cyt $bc_1$ Complexes	215
III. Comparison of Crystal Structures Between Bacterial and Mitochondrial Cyt $bc_1$ Complexes	216
IV. Structural Studies of Cyt $bc_1$ with Bound Inhibitors	222
V. Experimental Verification of the Bifurcated ET Mechanism	225
VI. The Mechanisms of Proton Uptake at the $Q_N$ Site and Exit at the $Q_P$ Site	227
VII. Future Perspective	229
Acknowledgements	230
References	230

## 11 Rieske Iron-Sulfur Protein Movement and Conformational Changes in Cytochrome $bc$ – $bf$ Complexes **237–251**

*Li-shar Huang and Edward Berry*

Summary	237
I. Introduction	237
II. Requirement for Movement of the ISP Extrinsic Domain to Shuttle Electrons	238
III. Classification and Depiction of Different Positions of the ISP-ED	238
IV. Conformational Changes in the ISP Hinge Region	243
V. Does the ISP-ED Undergo Internal Conformation Changes?	248
Acknowledgements	249
References	249

## 12 Structural Perspective of Ferredoxin NAD(P)H Reductase Reactions with Cytochrome $b_6f$ Complexes **253–264**

*Genji Kurisu*

Summary	253
I. The Perspective	253
References	263

<b>13 Alternative Rieske Iron-Sulfur Subunits and Small Polypeptides of Cyanobacterial Cytochrome <math>b_6f</math> Complexes</b>	<b>265–279</b>
<i>Gábor Bernát, Dirk Schneider, and Matthias Rögner</i>	
Summary	265
I. Introduction	266
II. Multiple Rieske-Proteins and Cytochrome $b_6f$ Heterogeneity	268
III. Small <i>bona fide</i> Cytochrome $b_6f$ Subunits	272
IV. Loosely Bound Subunits	273
Acknowledgements	275
References	275
<b>14 Inter-Monomer Electron Transfer in Cytochrome <math>bc</math> Complexes</b>	<b>281–294</b>
<i>Marcin Sarewicz, Robert Ekiert, and Artur Osyczka</i>	
Summary	281
I. Introduction	282
II. Implications from Structures for Inter-Monomer Electron Transfer	282
III. Theoretical Prediction for the Time Scale of Heme $b_L$ - $b_L$ Electron Transfer	283
IV. Experimental Evidence for Inter-Monomer Electron Transfer	285
V. Mechanistic Consequences of Inter-Monomer Electron Transfer	288
VI. Physiological Significance of Inter-Monomer Electron Transfer	289
VII. Conclusions	290
Acknowledgements	291
References	291
<b>15 Heme <math>c_i</math> or <math>c_n</math> of the Cytochrome <math>b_6f</math> Complex, A Short Retrospective</b>	<b>295–306</b>
<i>Francesca Zito and Jean Alric</i>	
Summary	295
I. Introduction	296
II. Early Evidence: Heme $c_i$ of the Cytochrome $b_6f$ Complex, A Functional Retrospective	297
III. Tridimensional Structure	300
IV. Heme $c_i/Q_i$ Site Directed Mutants	301
V. NQNO, A Not-So-Good Inhibitor of the $Q_i$ Site of the Cytochrome $b_6f$ Complex	303
VI. Concluding Remarks	303
Acknowledgements	304
References	305

## C. Cytochrome Oxidases (Chapters 16, 17, 18 and 19)

### 16 Structure and Function of Bacterial Cytochrome *c* Oxidases

307–329

*Joseph A. Lyons, Florian Hilbers,  
and Martin Caffrey*

Summary	307
I. Introduction	308
II. Respiratory Chain	308
III. Heme Copper Oxidases	309
IV. Pathways Within HCO	315
V. Electron Transfer	319
VI. Oxygen Channel	320
VII. The Catalytic Cycle	321
VIII. Side Reactions in CcO	323
IX. Conclusions	324
Acknowledgements	324
References	324

### 17 The Respiratory Terminal Oxidases (RTOs) of Cyanobacteria

331–355

*Georg Schmetterer*

Summary	331
I. Introduction	332
II. Types of RTOs Occurring in Cyanobacteria and Definitions	332
III. Genes Encoding Putative Subunits of Cyanobacterial RTOs	341
IV. Mitochondrial-Type Cytochrome <i>c</i> Oxidases (Cox)	342
V. Alternate Respiratory Terminal Oxidases (ARTOs)	343
VI. <i>cbb</i> <sub>3</sub> Type Cytochrome <i>c</i> Oxidases	345
VII. Homologs of Cytochrome <i>bd</i> Quinol Oxidases	346
VIII. Plastidic-Type Terminal Oxidases (Ptox)	347
IX. Cellular Location of Cyanobacterial RTOs	348
X. Regulation of Expression of Cyanobacterial RTOs	349
Acknowledgements	351
References	351

### 18 XFEL Studies on Bovine Heart Cytochrome *c* Oxidase

357–373

*Shinya Yoshikawa*

Summary	357
I. Introduction	358
II. Properties of the Resting Oxidized Form of Bovine Heart CcO	359
III. Redox Properties of the Resting Oxidized Bovine Heart CcO	360
IV. Resonance Raman Analysis of the Resting Oxidized CcO	362
V. X-ray Structural Analyses of the Resting Oxidized CcO Using Third Generation Synchrotron Radiation Facilities	362

VI. X-ray Structural Analyses of the Resting Oxidized CcO Obtained at an XFEL Facility	366
VII. Picobiology	368
Acknowledgements	371
References	372

## **19 Structure and Mechanism of Action of the Alternative Quinol Oxidases** **375–394**

*Luke Young, Benjamin May, Tomoo Shiba, Shigeharu Harada, Daniel Ken Inaoka, Kiyoshi Kita, and Anthony L. Moore*

Summary	375
I. General Introduction	376
II. Overall Structure of the Alternative Oxidases	377
III. Mechanism of Di-oxygen Reduction by the Alternative Oxidases	385
IV. Concluding Remarks	391
Acknowledgements	392
References	392

## **Part IV: Superoxide Generation in Cytochrome *bc* Complexes**

---

### **20 Mechanisms of Superoxide Generation and Signaling in Cytochrome *bc* Complexes** **397–417**

*Danas Baniulis, S. Saif Hasan, Inga Miliute, and William A. Cramer*

Summary	397
I. Introduction	398
II. Mechanisms of Superoxide Generation in Cytochrome <i>bc</i> Complexes	400
III. Signaling Function of ROS Produced by Cytochrome <i>bc</i> Complexes	405
References	410

### **21 Electron Transfer Reactions at the Q<sub>o</sub> Site of the Cytochrome *bc*<sub>1</sub> Complex: The Good, the Bad, and the Ugly** **419–434**

*Nicholas Fisher, Michael K. Bowman, and David M. Kramer*

Summary	419
I. Introduction	420
II. Superoxide Production by the <i>bc</i> <sub>1</sub> Complex and the Question of SQ <sub>o</sub> Reactivity	421
III. Structure and Mechanism of the Q <sub>o</sub> Site: Keeping the Chemistry Under Control	422
Acknowledgements	430
References	431



## **Part V: Cytochrome Complexes, Signaling, and Regulation**

---

### **22 The Cytochrome $b_6f$ Complex: A Regulatory Hub Controlling Electron Flow and the Dynamics of Photosynthesis? 437–452**

*Giovanni Finazzi, Jun Minagawa,  
and Giles N. Johnson*

Summary	437
I. Introduction	438
II. $H^+/e^-$ Coupling in the Cytochrome $b_6f$ Complex and Its Role in Photosynthetic Control	440
III. A Redox Kinetic Control of Cytochrome $b_6f$ ?	443
IV. Linear Versus Cyclic Electron Flow	445
V. Role of Cytochrome $b_6f$ in State Transitions	446
VI. Conclusions	449
Acknowledgements	449
References	449

### **23 A Supercomplex of Cytochrome $bf$ and Photosystem I for Cyclic Electron Flow 453–462**

*Jun Minagawa*

Summary	453
I. Introduction	454
II. Cyclic Electron Flow Is Essential	454
III. Cyclic Electron Flow and the Redox Status of the Chloroplast	456
IV. A Supercomplex in Charge of Cyclic Electron Flow in <i>Chlamydomonas</i>	456
V. Perspectives	460
Acknowledgements	461
References	461

### **24 State Transition Kinases and Redox Signal Transduction in Chloroplasts 463–477**

*Jean-David Rochaix*

Summary	463
I. Introduction	464
II. The Role of the Stt7/STN7 Protein Kinase in State Transitions	466
III. Mobility and Location of LHClI	468
IV. How Is the Stt7/STN7 Kinase Activated?	469
V. Involvement of Stt7/STN7 in the Long Term Response	470
VI. Relationship Between Stt7/STN7 and Cyclic Electron Flow	471
VII. Conclusions and Perspectives	473
Acknowledgements	474
References	474

<b>25 Regulating Synthesis of Cytochromes</b>	<b>479–498</b>
<i>Sébastien Zappa and Carl E. Bauer</i>	
Summary	479
I. Introduction	480
II. The Bi- and Tri-furcated Tetrapyrrole Pathway	481
III. Regulating Heme Biosynthesis	482
IV. Regulating Cytochrome Apoprotein Synthesis	487
V. Metal Homeostasis and Cytochrome Regulation	490
VI. Concluding Remarks	493
References	493

## **Part VI: Assembly of Cytochrome Complexes and Super-Complexes**

---

<b>26 Cofactor Assembly of Cytochrome <math>bc_1</math>-<math>b_6f</math> Complexes</b>	<b>501–525</b>
<i>Sara Guenthner Cline, Stéphane Thierry Gabilly, Nitya Subrahmanian, and Patrice Paul Hamel</i>	
Summary	502
I. Introduction	502
II. Prosthetic Groups in $bc_1$ and $b_6f$	503
III. Pathways for the Covalent Attachment of Heme	505
Acknowledgements	517
References	517
<b>27 Biogenesis of Cytochrome c Complexes: From Insertion of Redox Cofactors to Assembly of Different Subunits</b>	<b>527–554</b>
<i>Bahia Khalfaoui-Hassani, Andreia F. Verissimo, Namita P. Shroff, Seda Ekici, Petru-Iulian Trasnea, Marcel Utz, Hans-Georg Koch, and Fevzi Daldal</i>	
Summary	527
I. Introduction	528
II. The $cbb_3$ -Cox	530
Acknowledgements	546
References	546
<b>28 Assembly of Transmembrane <math>b</math>-Type Cytochromes and Cytochrome Complexes</b>	<b>555–584</b>
<i>Hans-Georg Koch and Dirk Schneider</i>	
Summary	555
I. Introduction	556
II. Transmembrane $b$ -Type Cytochromes in Respiratory and Photosynthetic $e^-$ -Transfer Chains	559
III. Targeting and Membrane Insertion of $b$ -Type Apo-Cytochromes	559

IV. Structural Features Determining Heme Binding to Membrane-Bound Apo-Cytochromes	567
V. Assembly of Individual Transmembrane Holo-Cytochromes	569
VI. Naturally Occurring and Designed Transmembrane Four-Helix Bundle <i>b</i> -Type Cytochromes	574
VII. Assembly of Cytochrome <i>b</i> -Containing Membrane Protein Complexes	576
Acknowledgements	578
References	578

## **29 Respiratory Cytochrome Supercomplexes** **585–628**

*Giorgio Lenaz and Maria Luisa Genova*

Summary	585
I. Introduction	586
II. Distribution and Composition of Respiratory Supercomplexes	589
III. Structure of Supercomplexes	592
IV. Functions of Respiratory Supercomplexes	600
V. A Role of Supercomplexes in Cell Physiology	616
References	617

## **Part VII: Branched Pathways and Cryptic Cytochromes**

---

### **30 The Interaction Between Cytochrome *f* and Plastocyanin or Cytochrome *c*<sub>6</sub>** **631–655**

*Derek S. Bendall (deceased) and Christopher J. Howe*

Summary	631
I. Introduction	632
II. Evolution of Plastocyanin and Cytochrome <i>c</i> <sub>6</sub>	633
III. Structure of Cytochrome <i>f</i>	635
IV. Structure of Plastocyanin and Cytochrome <i>c</i> <sub>6</sub>	636
V. Structure of Specific Complexes	637
VI. Dynamics of Interaction	639
VIII. The Reaction In Vivo	646
Acknowledgements	649
References	649

### **31 Cytochrome *c*<sub>6</sub> of Cyanobacteria and Algae: From the Structure to the Interaction** **657–677**

*Irene Díaz-Moreno, Antonio Díaz-Quintana, and Miguel A. De la Rosa*

Summary	657
I. Introduction	658
II. Cytochrome <i>c</i> <sub>6</sub> Structure and Properties	658
III. C <i>c</i> <sub>6</sub> -Involving Photosynthetic Complexes	662

IV. C <sub>6</sub> -Involving Respiratory Complexes	667
V. Conclusions and Perspectives	671
Acknowledgements	671
References	671
<b>32 Electron Partitioning in Anoxic Phototrophic Bacteria</b>	<b>679–700</b>
<i>Melanie A. Spero, Saheed Imam, Daniel R. Noguera, and Timothy J. Donohue</i>	
Summary	680
I. Introduction	680
II. Competition for Electrons of the Quinone Pool	681
III. The Role of Cytoplasmic “Electron Sinks” During Photoheterotrophic Growth	685
IV. Recycling Reducing Power Captured in Pyridine Nucleotides	688
V. Modeling the Metabolism of Photosynthetic Organisms	692
VI. Concluding Remarks and Future Directions	694
Acknowledgements	694
References	695
<b>33 Cytochrome c<sub>6A</sub> of Chloroplasts</b>	<b>701–712</b>
<i>Christopher J. Howe, Robert H. Nimmo, Adrian C. Barbrook, and Derek S. Bendall (deceased)</i>	
Summary	701
I. Introduction	702
II. The Protein	703
III. ‘Omics Studies	706
IV. Distribution Outside the Green Plant Lineage	707
V. Possible Functions	708
VI. Evolution of Cytochrome c <sub>6A</sub>	709
VII. General Conclusions	710
Acknowledgements	711
References	711
<b>34 Cryptic c<sub>6</sub>-Like and c<sub>M</sub> Cytochromes of Cyanobacteria</b>	<b>713–734</b>
<i>Wojciech Bialek, Andrzej Szczepaniak, Piotr Kolesinski, and Toivo Kallas</i>	
Summary	713
I. Introduction	714
II. Discovery of the c <sub>6</sub> -Like and c <sub>M</sub> Cytochromes	714
III. Cytochromes c <sub>6C</sub> and c <sub>6B</sub>	715
IV. Cytochrome c <sub>M</sub>	722
V. Possible Functions of c <sub>6</sub> -Like and c <sub>M</sub> Cytochromes	725
VI. Concluding Remarks	729
Acknowledgements	730
References	730
<b>Index</b>	<b>735–739</b>



# Preface

Why study cytochrome complexes? An answer is provided by the range of subtopics in the book, “evolution, structures, energy, and signaling,” which are described in the book title. Studies on the cytochrome family of proteins encompass a uniquely wide area of basic and applied research. Research in this field utilizes a range of theoretical and computational approaches, as well as a broad cross section of experimental techniques. Understanding obtained on the structure and function of the cytochromes and cytochrome complexes utilizes an extraordinary range of experimental approaches, including computational biology, genetics, macromolecular biochemistry, molecular biology, physics of charge transfer reactions, structure analysis using x-ray and electron diffraction, and ultrafast spectroscopy.

As reflected in the book title, the information and understanding gained in the field has an influence on a wide range of subjects, including evolution, mechanisms of membrane-based respiratory and photosynthetic energy transduction, theory of charge transfer in proteins, structure-function of large hetero-oligomeric membrane proteins, including lipid-protein interactions, and transmembrane signaling.

A special aspect of cytochromes, cytochrome complexes, as well as other proteins involved in bioenergetics and charge transfer is that they allow function to be quantitatively analyzed. Thus, in this group of proteins, it is possible to determine that a protein or protein complex is functional before committing a large amount of time to crystallization and analysis of structure. Dating back to the 1988 Nobel Prize in Chemistry, given to J. Deisenhofer, H. Michel, and R. Huber for determination of the crystal structure of the bacterial photosynthetic reaction center, the majesty of the crystal structures of hetero-

oligomeric membrane proteins obtained in the subsequent 10 years were of energy-transducing proteins. Of these, a substantial fraction involved cytochrome complexes.

*The Logic of the Collection* The book starts with an Introduction by Derek Bendall describing cytochrome notation, which is connected to the history of the field, focusing on research in England in the pre-World War II era. An *ab initio* “start with the beginning” logic then leads to a discussion of the evolution of cytochromes and hemes. Before presentation of the many individual cytochrome systems, the fundamentals of the theory of electron transfer in proteins are presented, followed by an extensive description of the molecular structures of cytochromes and cytochrome complexes from eukaryotic and prokaryotic sources, including those derived from photosynthetic reaction centers. The presentation of atomic structure information has a major role in these discussions, including the relatively new subject of “supercomplexes.” This structure information has a major niche in the broad field of membrane structure-function. Expanding the perspective beyond structure-function applied to charge transfer and energy storage, the problems of protein and macromolecule assembly, regulation, and signaling, including transmembrane signaling, which have conceptual connections to central areas of biochemistry, biophysics, and cell biology, are considered. Regarding subjects related to cutting-edge areas of biology and plant biology, the up-to-date presentation of the topics of *Regulation* and *Signaling* is noted here.

The broad extent of fundamental intellectual and research areas that are represented in this book makes it a useful resource for teaching of academic courses and presentation of seminars on fundamental and

broad aspects of biological energy transduction to advanced undergraduates and graduate students with interests in biology, biochemistry, biological engineering, chemistry, and biophysics.

As a last entry to the Introduction to this book, we note, sadly, the passing of Derek S. Bendall and Bernard L. Trumpower, whose achievements in this field are substantial and of fundamental importance. The Remembrances in this volume that are dedicated to them are of historical importance and note their many contributions to the subjects discussed herein.

**March 15, 2016**

**William A. Cramer**

Department of Biological Sciences  
Hockmeyer Building of Structural Biology  
Purdue University  
West Lafayette, IN 47917, USA  
[waclab@purdue.edu](mailto:waclab@purdue.edu)

**Toivo Kallas**

Department of Biology  
Halsey Science Center  
University of Wisconsin-Oshkosh  
Oshkosh, WI 54901, USA  
[kallas@uwosh.edu](mailto:kallas@uwosh.edu)

# Editors



**William A. Cramer (WAC)** received a B.S. (Physics, 1959) from the Massachusetts Institute of Technology (MIT), Boston, Mass., USA. From MIT, WAC went to the University of Chicago, where he obtained his M.S. in Physics; he initially worked and published in muon physics and birefringence of muscle proteins, and obtained a Ph.D. in Biophysics (1965), studying with R.B. Uretz. Subsequently, he carried out postdoctoral studies on photosynthetic electron transport with Warren L. Butler at the University of California/San Diego. He is currently the Henry Koffler Distinguished Professor in the Department of Biological Sciences at Purdue University, West Lafayette, Indiana. His research is focused on the relationship between structure and function of membrane proteins, including those involved in photosynthetic energy transduction. He is an authority on the cytochrome (cyt)  $b_6f$  complex, a hetero-oligomeric lipoprotein complex in the cytochrome  $bc$  family that functions in the photosynthetic and respiratory electron transport chains. The

$b_6f$  complex generates a major fraction of the transmembrane electrochemical potential and proton gradient; it is also responsible for significant generation of superoxide, and for a unique redox-controlled mechanism of transmembrane signaling that activates a kinase responsible for phosphorylation of the light-harvesting chlorophyll protein. Cramer also studies the membrane-mediated mechanism of cellular import of bacterial cytotoxins.

Some of the conceptual and experimental bases for his chapters in this book have been discussed in the 1991 textbook by him and the late David B. Knaff, entitled *Energy Transduction in Biological Membranes*, published by Springer-Verlag, as well as reviews on the cytochrome complex and the mechanism of cytotoxin import, including those in the Annual Reviews (Biophysics, Biochemistry, Plant Biology, and Genetics). WAC has served as the Chair of the Gordon Research Conferences on Photosynthesis (1990) and Bioenergetics (2001). He has served as the Chair of the Bioenergetics



Subgroup, and as the Program Chair (1996), of the National Meeting (1996) of the American Biophysical Society. He has been a recipient of the Charles F. Kettering Award of the American Society of Plant

Physiology for “Excellence in Photosynthesis” (1996), a Guggenheim Fellow (1992), and is a Fellow of the Alexander von Humboldt Foundation and of the Biophysical Society.



**Toivo Kallas** is a Distinguished Professor of Microbial Genetics and Biotechnology at the University of Wisconsin (UW) – Oshkosh, USA. He holds a B.A. from Carleton College, Minnesota, and a Ph.D. in Microbiology from the University of Oregon where he worked with Richard Castenholz on thermophilic cyanobacteria. He did postdoctoral work with Germaine Cohen-Bazire (Stanier), Institut Pasteur (Paris, France), on aerobic nitrogen fixation by unicellular cyanobacteria and with Richard Malkin, University of California (UC), Berkeley, on the cytochrome *b<sub>6</sub>f* electron transfer complex of photosynthesis. He spent sabbaticals with Francis-André Wollman and Catherine de Vitry, Institut Biologie Physico-Chimique (Paris, France), on regulation and electron transfer kinetics in *Chlamydomonas* and cyanobacteria and Michael Sussman, UW Madison Biotechnology Center, on proteomics of silica cell wall biogenesis in diatoms. His research at UW Oshkosh has focused on electron transfer proteins, energy transduction, gene expression, and metabolic engineering of cyanobacteria. Some 80 undergraduate students, 24 Master's students, and several postdoctoral and visiting scientists have participated in this research funded by grants from the US National Science

Foundation, US Department of Agriculture, UW Oshkosh, and UW WiSys Technology Foundation.

Over the past several years, Kallas, Matthew Nelson (UW Oshkosh), and Eric Singaas (Natural Resources Research Institute, University of Minnesota, Duluth, USA) have worked on metabolic engineering of cyanobacteria and photobioreactor design to convert solar energy and waste CO<sub>2</sub> into high-value isoprene-terpene bioproducts and biofuels. This project has reached several milestones, and the team recently founded Algoma Algal Biotechnology (AABT), a limited liability company (LLC), to develop both biomass conversion and microalgal carbon capture as avenues for sustainable hydrocarbon production. Kallas has published two detailed authoritative reviews on the cytochrome *bf* complex for the *Advances in Photosynthesis and Respiration* series (volumes 1 and 34) and has coedited (with Anne Ruffing, of Sandia National Labs, Albuquerque, New Mexico, USA) a recent special issue on Cyanobacteria, the Green *E. coli* for *Frontiers in Bioengineering and Biotechnology*. He co-organized (with Jack Meeks, UC Davis) the 2007 Cyanobacterial Workshop and has co-organized two Midwest-Southeast Photosynthesis Conferences (in 2001 and

2010). His current work on CO<sub>2</sub> capture, isoprene production, and AABT business development is funded by Small Business Technology Transfer (STTR) Phase I and IB grants from the US National Science

Foundation and a supplement from the UW Center for Technology Commercialization. Further information on Toivo Kallas is available at his website <http://www.uwosh.edu/facstaff/kallas>.

# Remembrances



## Remembering Professor Derek S. Bendall

The distinguished biochemist Derek S. Bendall, whose last written scientific work is presented in this volume, passed away in December 2014 at the age of 84 years. We would like to contribute to a celebration of Derek's life with personal reflections on Derek and his scientific legacy and our experiences working closely with him on a collaborative project.

Derek's research passion was redox reactions of biological systems, a topic that he pursued for nearly 60 years. In particular, he was fascinated by the problem of how solar energy is transduced into chemical energy in green plants, and on the mechanism of photosynthetic oxygen evolution. His research journey began with his scientific training as an undergraduate in Cambridge in the UK, where he was awarded a first class degree in 1953. His evolving interests in photosynthesis led him to studies of plant microsomes and mitochondria for a dissertation project with Robin Hill in the Biochemistry Department. He was awarded a Ph.D. in 1957

from Cambridge University and then spent a year working in Louvain, Belgium, where he studied methods for preparing mammalian mitochondria fractions for characterization. Derek then worked for the Nyasaland Tea Association in both Africa and Cambridge before becoming a demonstrator (1960) and lecturer (1965) in the Biochemistry Department in Cambridge. His early work demonstrated that mitochondria have a cytochrome oxidase, and he analyzed cytochromes in chloroplasts. He studied the cycling of electron transfer around photosystem I, and how this helps to protect against the effects of rapid changes in light level. Under this condition, electrons are transferred from the plastoquinone pool or terminal oxidase rather than photosystem I to reduce backup of photosynthetic electron transfer.

The mechanism of biological electron transfer and, in particular, transient protein-protein interactions mediating such reactions was of special interest to him, and he edited and contributed to an excellent book on the

subject, entitled *Protein Electron Transfer*, which was published in 1996 before Derek's official "retirement." For Jonathan Worrall, this book holds special memories and was a source of continuous background reading during his Ph.D. and early postdoc years. It was with great pleasure therefore that upon attending a meeting in Denmark focused on transient protein-protein interactions, Jonathan was awarded the poster prize and received from Derek a signed copy of his book.

Not content to follow retirement in the traditional sense, Derek joined Chris Howe's laboratory in the Biochemistry Department in Cambridge, where he continued earlier collaborative work that they had started on various projects. He continued studies on protein targeting in cyanobacteria, and in particular on the distribution of photosystem proteins in the membrane, following up earlier studies in which they had found evidence for the localization of some proteins in the cytoplasmic membrane. In addition he continued his interest in weak protein-protein interactions, particularly those of the electron transfer complex formed between cytochrome *f* and plastocyanin.

His interest in cytochromes attracted him to a mysterious cytochrome  $c_6$  homologue, encoded in the genome of several land plants and algae, but possessing a more negative redox potential than its bacterial counterparts. To distinguish this homologue from the bacterial proteins, Derek suggested that it should be named cytochrome  $c_{6A}$ . We worked with Derek to initially characterize the crystal structure of cytochrome  $c_{6A}$  in reduced and oxidized forms. Derek's driving enthusiasm to understand why cytochrome  $c_{6A}$  possessed a redox potential some 250 mV lower than bacterial cytochrome  $c_6$  proteins led to further collaboration with us and to experimental support for a mechanism of redox potential control by the interactions of side chains around the heme. The chapters

presented in this book written with his long-term collaborator, Chris Howe, describe his last work on cytochrome  $c_{6A}$ .

Derek was also involved in translational projects during his retirement. He worked on renewable energy projects using cyanobacteria, studying direct electron transport from cyanobacteria and algal cells onto electrodes to make direct photovoltaic devices. He was also involved in engineering cyanobacteria to explore terminal oxidases in the process of direct electron transfer.

Derek had a long-standing interest in tea, both as a tea-drinker connoisseur and as a subject for scientific investigation. He studied the biochemical processes of tea fermentation, and his work, including preparation and characterization of catechol oxidase, resulted in several reports on the fermentation process. His passion for botany was also expressed in his activities as a keen gardener.

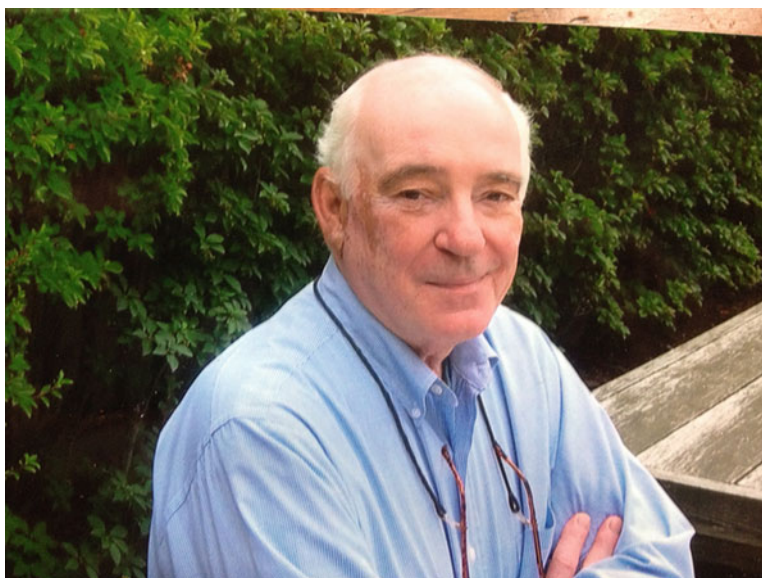
Through our work with Derek on the cytochrome  $c_{6A}$ , we had an opportunity for extensive interactions that involved hypothesis formulation and testing, and these were stimulating interactions. We were struck by Derek's knowledge and scientific imagination, by his gentle character and modest nature. Like many other colleagues, we feel very fortunate to have had the opportunity to work with him and to have benefited from these interactions.

For further information and references to Bendall's key papers, see C.J. Howe, P.R. Rich and M. Ubbink (2015) Derrek Bendall (1930–2015) *Photosynth Res* 124: 249–252.

**March 15, 2016**

**Jonathan Worrall**  
Cambridge University

**Ben Luisi**  
Cambridge University



### Remembering Professor Bernard L. Trumpower

The news that Bernard had passed away on the Christmas day of 2014 spread rapidly among his friends, colleagues, former Ph.D. students, and postdocs. Together with the personal sorrow that inevitably comes with such a message, I immediately felt struck by the gap created within our scientific community. “Bernie,” as we used to call him, when I had the privilege to work as a postdoc in his laboratory, was clearly a leading figure in the field of bioenergetics for many years. Here, I can only try to give an account of his fundamental contributions to our understanding of the structure and function of the mitochondrial cytochrome  $bc_1$  complex.

Bernard L. Trumpower studied Chemistry at the University of Pittsburgh and completed his Ph.D. in Biochemistry at St. Louis University, Missouri, USA, in 1969, where he worked with Robert E. Olson on the biosynthesis of ubiquinone-9. During his postdoctoral studies with Efraim Racker at Cornell University, Ithaca, N.Y. (1969-1972), he became acquainted with the membrane protein complexes of the oxidative phosphorylation system that use ubiquinone as a substrate. This set the stage for his successful career of

more than 40 years studying the structure and function of the cytochrome  $bc_1$  complex that made him a leader in the field of Molecular Bioenergetics.

In 1972, when Bernard was appointed Assistant Professor of Biochemistry at Dartmouth Medical School, the molecular mechanism of this central complex of the respiratory chain was still enigmatic. Early on, he had realized the key role of the Rieske iron-sulfur protein, and the usefulness of specific inhibitors for studying the intricate mechanism of the enzyme. This allowed him to provide decisive experimental proof for the proton-motive Q-cycle, soon after Peter Mitchell published this hypothesis for the redox-driven proton translocation by the cytochrome  $bc_1$  complex in 1975. Shortly after Bernard was promoted to Associate Professor in 1978, he published a series of landmark papers showing the activation of cytochrome  $bc_1$  complex function by reconstitutively active Rieske iron-sulfur protein (Trumpower and Edwards 1979), establishing the use of Electron Paramagnetic Resonance (EPR) spectroscopy with Tomoko Ohnishi to study catalytic intermediates (Ohnishi and Trumpower 1980,

Trumpower et al. 1980), and introducing novel ubiquinone analogues as specific inhibitors of the cytochrome  $bc_1$  complex (Bowyer and Trumpower 1980). When he became a full Professor of Biochemistry at Dartmouth in 1983, he was just performing groundbreaking functional studies together with Gebhard von Jagow using myxothiazol, the first representative of another new class of specific inhibitors. In a classical experiment, later known as the “double-kill,” they were able to demonstrate unambiguously and characterize functionally the two distinct ubiquinone-binding sites of the cytochrome  $bc_1$  complex, thereby confirming a central postulate of the proton-motive Q-cycle hypothesis (von Jagow et al. 1984).

Following Efraim Racker’s pledge “*Don’t waste clean thinking on dirty enzymes.*” Bernard developed simple and efficient protocols to purify cytochrome  $bc_1$  complexes from mitochondria and bacterial membranes still applied today that were among the first to demonstrate the usefulness of the now widely used detergent dodecyl-maltoside to purify membrane protein complexes (Ljungdahl et al. 1987). This paved the way for a series of important studies on the kinetic properties of the bacterial enzyme seminal to understanding central aspects of the proton-motive Q-cycle.

Again leading the field, Bernard recognized soon the enormous potential of molecular biology that became widely applicable in the 1980s. In his quest to understand all aspects of structure and function of the cytochrome  $bc_1$  complex, he spent time with Gerry Fink at Harvard University (Cambridge, Massachusetts) to learn yeast genetics. Using this powerful approach, Bernard’s laboratory subsequently cloned several genes of all so-called supernumerary subunits of the complex from yeast mitochondria and characterized their function by genomic deletion and structure/function studies (see Zara et al. (2009) for a review). Exhaustive site-directed mutagenesis of the Rieske iron-sulfur protein were a straightforward extension of his early work and led to the identification of the functionally critical domains (Graham et al. 1993).

Returning to the roots of his early research, Bernard then used the X-ray structures of the cytochrome  $bc_1$  complex that finally became available in the late 1990s as a guide for fundamental studies to understand the molecular basis of the proton-motive Q-cycle. Intrigued by the fact that the structures showed the cytochrome  $bc_1$  complex to be a constitutive dimer, he indeed defined a functional role for this remarkable structural feature (Covian and Trumpower 2008).

In the years before retirement and becoming Professor Emeritus from the Dartmouth Medical School in 2013, he also dived into an important medical aspect demonstrating the societal impact of his research: The molecular target of the widely used antimalarial Atoquavone is the ubiquinol oxidation site of the cytochrome  $bc_1$  complex. Bernard applied his profound knowledge on structure and function of enzymes, to design quinone derivatives binding to this site that are less susceptible to drug resistance (Hughes et al. 2011).

The groundbreaking research contributions by Bernard L. Trumpower were honored through a number of national and international awards including the Humboldt Prize in 1984 and the Merit Award of the National Institute of Health (NIH) in 1994. He served the scientific community in many ways, as editor of several leading biomedical journals, member of NIH Study Sections, and organizer of a number of major national and international conferences.

Reaching far beyond the dry facts that can be documented in a list of his publications, Bernard had a truly lasting impact as a guide and a role model for his students and young colleagues. Never content with a superficial answer, he taught us to stay focused, to be thorough, persistent, and self-critical. I will never forget that when we finally reached a conclusion in an intense and controversial scientific discussion, his next sentence would usually start with “But...” to express that there is always another side of the problem to explore.

For me, his unconditional quest for perfection best characterizes Bernard not

only as a scientist. It can be experienced nicely by looking at the series of wonderful photographs he made after his retirement (<https://www.dartmouth.edu/~grnhouse/brotut.php>) showcasing the beauty and elegance of orchids.

**March 15, 2016**

**Ulrich Brandt**

Nijmegen Center for Mitochondrial Disorders (NCMD)  
Radboud University Medical Center  
Geert Grooteplein Zuid 10, Route 772  
6525 GA Nijmegen, The Netherlands  
([ulrich.brandt@radboudumc.nl](mailto:ulrich.brandt@radboudumc.nl))

## References

- Bowyer JR, Trumpower BL (1980) Inhibition of the oxidant-induced reduction of cytochrome *b* by a synthetic analogue of ubiquinone. *FEBS Lett* 115:171–174
- Covian R, Trumpower BL (2008) Regulatory interactions in the dimeric cytochrome *bc*<sub>1</sub> complex: the advantages of being a twin. *Biochim Biophys Acta* 1777:1079–1091
- Graham LA, Brandt U, Sargent JS, Trumpower BL (1993) Mutational analysis of assembly and function of the iron-sulfur protein of the cytochrome *bc*<sub>1</sub> complex in *Saccharomyces cerevisiae*. *J Bioenerg Biomembr* 25:245–257
- Hughes LM, Lanteri CA, O’Neil MT, Johnson JD, Gribble GW, Trumpower BL (2011) Design of anti-parasitic and anti-fungal hydroxy-naphthoquinones that are less susceptible to drug resistance. *Mol Biochem Parasitol* 177:12–19
- Ljungdahl PO, Pennoyer JD, Robertson DE, Trumpower BL (1987) Purification of highly active cytochrome *bc*<sub>1</sub> complexes from phylogenetically diverse species by a single chromatographic procedure. *Biochim Biophys Acta* 89:227–241
- Ohnishi T, Trumpower BL (1980) Differential effects of antimycin on ubisemiquinone bound in different environments in isolated succinate:cytochrome *c* reductase complex. *J Biol Chem* 255:3278–3284
- Trumpower BL, Edwards CA (1979) Identification of oxidation factor as a reconstitutively active form of the iron-sulfur protein of the cytochrome *b-c*<sub>1</sub> segment of the respiratory chain. *FEBS Lett* 100:13–16.
- Trumpower BL, Edwards CA, Ohnishi T (1980) Reconstitution of the iron-sulfur protein responsible for the *g* = 1.90 electron paramagnetic resonance signal and associated cytochrome *c* reductase activities to depleted succinate-cytochrome *c* reductase complex. *J Biol Chem* 255:7487–7493.
- von Jagow G, Ljungdahl PO, Graf P, Ohnishi T, Trumpower BL (1984) An inhibitor of mitochondrial respiration which binds to cytochrome *b* and displaces quinone from the iron-sulfur protein of the cytochrome *bc*<sub>1</sub> complex. *J Biol Chem* 259:6318–6326.
- Zara V, Conte L, Trumpower BL (2009) Biogenesis of the yeast cytochrome *bc*<sub>1</sub> complex. *Biochim Biophys Acta* 1793:89–96





# Contributors

**Jean Alric (Chapter 15)**

IBEB/SBVME/LB3M, Bât 161, CEA de Cadarache, Saint Paul Lez Durance cedex, France

[jean.alric@cea.fr](mailto:jean.alric@cea.fr)

**Eva-Mari Aro (Chapter 4)**

Department of Biochemistry, and Molecular Plant Biology, University of Turku, Turku, Finland

[evaaro@utu.fi](mailto:evaaro@utu.fi)

**Danas Baniulis (Chapter 20)**

Institute of Horticulture, Lithuanian Research Centre for Agriculture and Forestry, Kaunas, Lithuania

[d.baniulis@lsdi.lt](mailto:d.baniulis@lsdi.lt)

**Adrian C. Barbrook (Chapter 33)**

Department of Biochemistry, University of Cambridge, Cambridge, UK

[acb18@cam.ac.uk](mailto:acb18@cam.ac.uk)

**Carl E. Bauer (Chapter 25)**

Department of Molecular and Cellular Biochemistry, Indiana University, Bloomington, IN, USA

[bauer@indiana.edu](mailto:bauer@indiana.edu)

**Derek S. Bendall (Chapters 1, 30 & 33; deceased)**

Department of Biochemistry, University of Cambridge, Cambridge, UK

**Gábor Bernát (Chapter 13)**

Laboratory of Photosynthesis, Centre Algatech, Institute of Microbiology, Academy of Sciences of the Czech Republic, Třeboň, Czech Republic

[bernat@alga.cz](mailto:bernat@alga.cz)

**Edward Berry (Chapter 11)**

Biochemistry and Molecular Biology, SUNY Upstate Medical University, Syracuse, NY, USA

[berrye@upstate.edu](mailto:berrye@upstate.edu)

**Wojciech Bialek (Chapter 34)**

Faculty of Biotechnology, University of Wrocław, Wrocław, Poland

[wojciech.bialek@uwr.edu.pl](mailto:wojciech.bialek@uwr.edu.pl)

**Robert E. Blankenship (Chapter 3)**

Department of Chemistry, and Department of Biology, Washington University, St. Louis, MO, USA

[Blankenship@wustl.edu](mailto:Blankenship@wustl.edu)

**Elisa Bombarda (Chapter 6)**

Experimental Physics IV, University of Bayreuth, Universitätsstr., Bayreuth, Germany

[elisa.bombarda@uni-bayreuth.de](mailto:elisa.bombarda@uni-bayreuth.de)

**Michael K. Bowman (Chapter 21)**

Department of Chemistry, The University of Alabama, Tuscaloosa, AL, USA

[mkbowman@ua.edu](mailto:mkbowman@ua.edu)

**Martin Caffrey (Chapter 16)**

School of Medicine and School of Biochemistry and Immunology, Trinity College Dublin, Dublin, Ireland

[martin.caffrey@inmesolabs.net](mailto:martin.caffrey@inmesolabs.net)

**Sara Guenther Cline (Chapter 26)**

Department of Mathematics, Computer and Natural Sciences, Athens State University, Athens, AL, USA

[sara.cline@athens.edu](mailto:sara.cline@athens.edu)

**William A. Cramer (Chapters 9 & 20)**

Department of Biological Sciences, Hockmeyer Building of Structural Biology, Purdue University, West Lafayette, IN, USA

[wacrlab@purdue.edu](mailto:wacrlab@purdue.edu)

**Fevzi Daldal (Chapter 27)**

Department of Biology, University of Pennsylvania, Philadelphia, USA

[fdaldal@sas.upenn.edu](mailto:fdaldal@sas.upenn.edu)

**Miguel A. De la Rosa (Chapter 31)**

Instituto de Bioquímica Vegetal y  
Fotosíntesis, Centro de Investigaciones  
Científicas Isla de la Cartuja, Universidad de  
Sevilla-CSIC, Sevilla, Spain  
[marosa@us.es](mailto:marosa@us.es)

**Irene Díaz-Moreno (Chapter 31)**

Instituto de Bioquímica Vegetal y  
Fotosíntesis, Centro de Investigaciones  
Científicas Isla de la Cartuja, Universidad de  
Sevilla-CSIC, Sevilla, Spain  
[idiazmoreno@us.es](mailto:idiazmoreno@us.es)

**Antonio Díaz-Quintana (Chapter 31)**

Instituto de Bioquímica Vegetal y  
Fotosíntesis, Centro de Investigaciones  
Científicas Isla de la Cartuja, Universidad de  
Sevilla-CSIC, Sevilla, Spain  
[gzaida@us.es](mailto:gzaida@us.es)

**Timothy J. Donohue (Chapter 32)**

Department of Bacteriology, University of  
Wisconsin-Madison, Madison, WI,  
USA  
[tdonohue@bact.wisc.edu](mailto:tdonohue@bact.wisc.edu)

**Anne-Lise Ducluzeau (Chapter 2)**

School of Fisheries and Ocean Sciences,  
University of Alaska-Fairbanks, Fairbanks,  
USA  
[aducluzeau@alaska.edu](mailto:aducluzeau@alaska.edu)

**Seda Ekici (Chapter 27)**

Department of Biology, University of  
Pennsylvania, Philadelphia, PA, USA  
[seda@sas.upenn.edu](mailto:seda@sas.upenn.edu)

**Robert Ekiert (Chapter 14)**

Department of Molecular Biophysics,  
Faculty of Biochemistry, Biophysics and  
Biotechnology, Jagiellonian University,  
Kraków, Poland  
[robert.ekiert@uj.edu.pl](mailto:robert.ekiert@uj.edu.pl)

**Lothar Esser (Chapter 10)**

Laboratory of Cell Biology, Center for  
Cancer Research, National Cancer Institute,  
National Institutes of Health, Bethesda, MD,  
USA  
[lessen@helix.nih.gov](mailto:lessen@helix.nih.gov)

**Giovanni Finazzi (Chapter 22)**

Centre National Recherche Scientifique,  
Unité Mixte Recherche 5168, Laboratoire  
Physiologie Cellulaire et Végétale,  
Grenoble, France  
[giovanni.finazzi@cea.fr](mailto:giovanni.finazzi@cea.fr)

**Nicholas Fisher (Chapter 21)**

MSU-DOE Plant Research Laboratory, and  
Department of Biochemistry and Molecular  
Biology, Michigan State University, East  
Lansing, MI, USA  
[nefisher@msu.edu](mailto:nefisher@msu.edu)

**Stéphane Thierry Gabilly (Chapter 26)**

Department of Plant and Microbial Biology,  
University of California, Berkeley, CA, USA  
[stephane.gabilly@berkeley.edu](mailto:stephane.gabilly@berkeley.edu)

**Maria Luisa Genova (Chapter 29)**

Section of Biochemistry, Department of  
Biomedical and Neuromotor Sciences  
(DIBINEM), University of Bologna,  
Bologna, Italy  
[marialuisa.genova@unibo.it](mailto:marialuisa.genova@unibo.it)

**Patrice Paul Hamel (Chapter 26)**

Department of Molecular Genetics and  
Department of Biological Chemistry and  
Pharmacology, The Ohio State University,  
Columbus, OH, USA  
[hamel.16@osu.edu](mailto:hamel.16@osu.edu)

**Shigeharu Harada (Chapter 19)**

Department of Applied Biology, Graduate  
School of Science and Technology, Kyoto  
Institute of Technology, Kyoto, Japan  
[harada@kit.ac.jp](mailto:harada@kit.ac.jp)

**S. Saif Hasan (Chapters 9 & 20)**

Department of Biological Sciences,  
Hockmeyer Building of Structural Biology,  
Purdue University, West Lafayette,  
IN, USA  
[sshasan@purdue.edu](mailto:sshasan@purdue.edu)

**Florian Hilbers (Chapter 16)**

Department of Molecular Biology and  
Genetics, Aarhus University, Aarhus,  
Denmark  
[hilbers@mbg.au.dk](mailto:hilbers@mbg.au.dk)

**Christopher J. Howe (Chapters 30 & 33)**

Department of Biochemistry, University of  
Cambridge, Cambridge, UK  
[c.j.howe@bioc.cam.ac.uk](mailto:c.j.howe@bioc.cam.ac.uk);  
[ch26@cam.ac.uk](mailto:ch26@cam.ac.uk)

**Li-shar Huang (Chapter 11)**

Biochemistry and Molecular Biology, SUNY  
Upstate Medical University, Syracuse, NY,  
USA  
[BerryL@upstate.edu](mailto:BerryL@upstate.edu)

**Saheed Imam (Chapter 32)**

Program in Cellular and Molecular Biology,  
University of Wisconsin-Madison, Madison,  
WI, USA  
[saheedrimam@gmail.com](mailto:saheedrimam@gmail.com)

**Daniel Ken Inaoka (Chapter 19)**

Department of Biomedical Chemistry,  
Graduate School of Medicine, The  
University of Tokyo, Tokyo, Japan  
[danielkeninaoka@yahoo.co.jp](mailto:danielkeninaoka@yahoo.co.jp)

**Giles N. Johnson (Chapter 22)**

Faculty of Life Sciences, University of  
Manchester, Manchester, UK  
[giles.johnson@manchester.ac.uk](mailto:giles.johnson@manchester.ac.uk)

**Toivo Kallas (Chapter 34)**

Department of Biology, University  
of Wisconsin-Oshkosh, Oshkosh, WI,  
USA  
[kallas@uwosh.edu](mailto:kallas@uwosh.edu)

**Bahia Khalfaoui-Hassani (Chapter 27)**

Department of Biology, University of  
Pennsylvania, Philadelphia, PA, USA  
[kbahia@sas.upenn.edu](mailto:kbahia@sas.upenn.edu)

**Kiyoshi Kita (Chapter 19)**

Department of Biomedical Chemistry,  
Graduate School of Medicine,  
The University of Tokyo,  
Tokyo, Japan  
[kitak@m.u-tokyo.ac.jp](mailto:kitak@m.u-tokyo.ac.jp)

**Hans-Georg Koch (Chapters 27 & 28)**

Institut für Biochemie und  
Molekularbiologie, Albert-Ludwigs-  
Universität Freiburg, Freiburg, Germany  
[hans-georg.koch@biochemie.uni-freiburg.de](mailto:hans-georg.koch@biochemie.uni-freiburg.de)

**Piotr Kolesinski (Chapter 34)**

Faculty of Biotechnology, University of  
Wroclaw, Wroclaw, Poland  
[piotr.kolesinski@uwr.edu.pl](mailto:piotr.kolesinski@uwr.edu.pl)

**David M. Kramer (Chapter 21)**

Department of Biochemistry and Molecular  
Biology, Michigan State University, East  
Lansing, MI, USA  
[kramerd8@msu.edu](mailto:kramerd8@msu.edu)

**Lev I. Krishtalik (Chapter 5)**

A. N. Frumkin Institute of Physical  
Chemistry and Electrochemistry,  
Russian Academy of Sciences, Moscow,  
Russia  
[lkrishtalik@mail.ru](mailto:lkrishtalik@mail.ru)

**Genji Kurisu (Chapter 12)**

Institute for Protein Research, Osaka  
University, Osaka, Japan  
[gkurisu@protein.osaka-u.ac.jp](mailto:gkurisu@protein.osaka-u.ac.jp)

**Giorgio Lenaz (Chapter 29)**

Section of Biochemistry, Department of  
Biomedical and Neuromotor Sciences  
(DIBINEM), University of Bologna,  
Bologna, Italy  
[giorgio.lenaz@unibo.it](mailto:giorgio.lenaz@unibo.it)

**Joseph A. Lyons (Chapter 16)**

Department of Molecular Biology and  
Genetics, Aarhus University, Aarhus,  
Denmark  
[lyons@mbg.au.dk](mailto:lyons@mbg.au.dk)

**Erica L.-W. Majumder (Chapter 3)**

Department of Chemistry, and Department  
of Biology, Washington University,  
St. Louis, MO, USA  
[erica.majumder@gmail.com](mailto:erica.majumder@gmail.com)

**Benjamin May (Chapter 19)**

Biochemistry and Molecular Sciences,  
School of Life Sciences, University of  
Sussex, Brighton, UK  
[ozmay@me.com](mailto:ozmay@me.com)

**Yuval Mazor (Chapter 7)**

Department of Biochemistry, and Molecular  
Biology, Tel Aviv University, Tel Aviv,  
Israel  
[yuval.mazor@gmail.com](mailto:yuval.mazor@gmail.com)

**Inga Miliute (Chapter 20)**

Institute of Horticulture, Lithuanian  
Research Centre for Agriculture and  
Forestry, Kaunas LT, Lithuania  
[i.miliute@lsdi.lt](mailto:i.miliute@lsdi.lt)

**Jun Minagawa (Chapters 22 & 23)**

Division of Environmental Photobiology,  
National Institute for Basic Biology (NIBB),  
Okazaki, Japan  
[minagawa@nibb.ac.jp](mailto:minagawa@nibb.ac.jp)

**Anthony L. Moore (Chapter 19)**

Biochemistry and Molecular Sciences,  
School of Life Sciences, University of  
Sussex, Brighton, UK  
[a.l.moore@sussex.ac.uk](mailto:a.l.moore@sussex.ac.uk)

**Lars Mueller (Chapter 6)**

Structural Biology/Bioinformatics,  
University of Bayreuth, Universitätsstr.,  
Bayreuth, Germany  
[lars.mueller@uni-bayreuth.de](mailto:lars.mueller@uni-bayreuth.de)

**Frank Müh (Chapter 8)**

Institut für Theoretische Physik, Johannes  
Kepler Universität Linz, Linz, Austria  
[Frank.Mueh@jku.at](mailto:Frank.Mueh@jku.at)

**Nathan Nelson (Chapter 7)**

Department of Biochemistry, and  
Molecular Biology, Tel Aviv University, Tel  
Aviv, Israel  
[nelson@post.tau.ac.il](mailto:nelson@post.tau.ac.il)

**Robert H. Nimmo (Chapter 33)**

Department of Biochemistry, University of  
Cambridge, Cambridge, UK  
[rn269@cam.ac.uk](mailto:rn269@cam.ac.uk)

**Wolfgang Nitschke (Chapter 2)**

Laboratoire de Bioénergétique et Ingénierie  
des Protéines UMR 7281 CNRS/AMU  
FR3479, Marseille Cedex 20, France  
[nitschke@imm.cnrs.fr](mailto:nitschke@imm.cnrs.fr)

**Daniel R. Noguera (Chapter 32)**

Department of Civil and Environmental  
Engineering, University of Wisconsin-  
Madison, Madison, WI, USA  
[noguera@engr.wisc.edu](mailto:noguera@engr.wisc.edu);  
[dnoguera@wisc.edu](mailto:dnoguera@wisc.edu)

**Artur Osyczka (Chapter 14)**

Department of Molecular Biophysics,  
Faculty of Biochemistry, Biophysics and  
Biotechnology, Jagiellonian University,  
Kraków, Poland  
[artur.osyczka@uj.edu.pl](mailto:artur.osyczka@uj.edu.pl)

**Jean-David Rochaix (Chapter 24)**

Departments of Molecular Biology and Plant  
Biology, University of Geneva, Geneva,  
Switzerland  
[Jean-David.Rochaix@unige.ch](mailto:Jean-David.Rochaix@unige.ch)

**Matthias Rögner (Chapter 13)**

Lehrstuhl für Biochemie der Pflanzen,  
Ruhr-Universität Bochum, Bochum,  
Germany  
[Matthias.Roegner@ruhr-uni-bochum.de](mailto:Matthias.Roegner@ruhr-uni-bochum.de)

**Marcin Sarewicz (Chapter 14)**

Department of Molecular Biophysics,  
Faculty of Biochemistry, Biophysics and  
Biotechnology, Jagiellonian University,  
Kraków, Poland  
[marcin.sarewicz@uj.edu.pl](mailto:marcin.sarewicz@uj.edu.pl)

**Georg Schmetterer (Chapter 17)**

Institute of Biophysical Chemistry,  
University of Vienna, Vienna,  
Austria  
[georg.schmetterer@univie.ac.at](mailto:georg.schmetterer@univie.ac.at)

**Dirk Schneider (Chapters 13 & 28)**

Institut für Pharmazie und Biochemie,  
Johannes Gutenberg-Universität Mainz,  
Mainz, Germany  
[Dirk.Schneider@uni-mainz.de](mailto:Dirk.Schneider@uni-mainz.de)

**Tomoo Shiba (Chapter 19)**

Department of Applied Biology,  
Graduate School of Science and Technology,  
Kyoto Institute of Technology, Kyoto,  
Japan  
[tshiba@kit.ac.jp](mailto:tshiba@kit.ac.jp)

**Toshiharu Shikanai (Chapter 4)**

Department of Botany, Graduate School of  
Science, Kyoto University, Sakyo-ku, Kyoto,  
Japan  
[shikanai@pmg.bot.kyoto-u.ac.jp](mailto:shikanai@pmg.bot.kyoto-u.ac.jp)

**Namita P. Shroff (Chapter 27)**

Department of Biology, University of Pennsylvania, Philadelphia, PA, USA  
[namita.shroff@gmail.com](mailto:namita.shroff@gmail.com)

**Melanie A. Spero (Chapter 32)**

Department of Bacteriology, University of Wisconsin-Madison, Madison, WI, USA  
[spero@wisc.edu](mailto:spero@wisc.edu); [spero@caltech.edu](mailto:spero@caltech.edu)

**Nitya Subrahmanian (Chapter 26)**

Department of Molecular Genetics and Department of Biological Chemistry and Pharmacology, The Ohio State University, Columbus, OH, USA  
[subrahmanian1@osu.edu](mailto:subrahmanian1@osu.edu)

**Andrzej Szczepaniak (Chapter 34)**

Faculty of Biotechnology, University of Wrocław, Wrocław, Poland  
[andrzej.szczepaniak@ibmb.uni.wroc.pl](mailto:andrzej.szczepaniak@ibmb.uni.wroc.pl)

**Petru-Iulian Trasnea (Chapter 27)**

Institut für Biochemie und Molekularbiologie, Albert-Ludwigs Universität Freiburg, Freiburg, Germany  
[petru-iulian.trasnea@biochemie.uni-freiburg.de](mailto:petru-iulian.trasnea@biochemie.uni-freiburg.de); [trasnea.iulian@yahoo.com](mailto:trasnea.iulian@yahoo.com)

**G. Matthias Ullmann (Chapter 6)**

Structural Biology/Bioinformatics, University of Bayreuth, Universitätsstr., Bayreuth, Germany  
[matthias.ullmann@uni-bayreuth.de](mailto:matthias.ullmann@uni-bayreuth.de)

**Marcel Utz (Chapter 27)**

Institut für Biochemie und Molekularbiologie, Albert-Ludwigs Universität Freiburg, Freiburg, Germany  
[utz.marcel@googlemail.com](mailto:utz.marcel@googlemail.com)

**Andreia F. Verissimo (Chapter 27)**

Department of Biology, University of Pennsylvania, Philadelphia, PA, USA  
[andreia@sas.upenn.edu](mailto:andreia@sas.upenn.edu)

**Di Xia (Chapter 10)**

Laboratory of Cell Biology, Center for Cancer Research, National Cancer Institute, National Institutes of Health, Bethesda, MD, USA  
[xiad@mail.nih.gov](mailto:xiad@mail.nih.gov)

**Shinya Yoshikawa (Chapter 18)**

Picobiology Institute, Graduate School of Life Sciences, University of Hyogo, Ako, Japan  
[yoshi@sci.u-hyogo.ac.jp](mailto:yoshi@sci.u-hyogo.ac.jp)

**Luke Young (Chapter 19)**

Biochemistry and Molecular Sciences, School of Life Sciences, University of Sussex, Brighton, UK  
[ley20@sussex.ac.uk](mailto:ley20@sussex.ac.uk)

**Chang-An Yu (Chapter 10)**

Department of Biochemistry and Molecular Biology, Oklahoma State University, Stillwater, OK, USA  
[changan.yu@okstate.edu](mailto:changan.yu@okstate.edu)

**Sébastien Zappa (Chapter 25)**

Department of Molecular and Cellular Biochemistry, Indiana University, Bloomington, IN, USA  
[szappa@indiana.edu](mailto:szappa@indiana.edu)

**Fei Zhou (Chapter 10)**

Laboratory of Cell Biology, Center for Cancer Research, National Cancer Institute, National Institutes of Health, Bethesda, MD, USA  
[fei.zhou@nih.gov](mailto:fei.zhou@nih.gov)

**Francesca Zito (Chapter 15)**

Institut Biologie Physico-Chimique, UMR7099, CNRS/Université Paris Diderot, Paris, France  
[zito@ibpc.fr](mailto:zito@ibpc.fr)

**Athina Zouni (Chapter 8)**

Institut für Biologie, Humboldt Universität zu Berlin, Berlin, Germany  
[athina.zouni@hu-berlin.de](mailto:athina.zouni@hu-berlin.de)

# Part I

## **Diversity and Evolution**

# Chapter 1

## Keilin, Cytochrome and Its Nomenclature

Derek S. Bendall (deceased)

Department of Biochemistry, University of Cambridge,  
Cambridge, UK

Summary.....	3
I. The Cytochromes and History.....	3
References.....	10

### Summary

D. S. Bendall describes the micro-spectroscopic studies on bacteria, tissue, and plant samples that took place in Cambridge in the years just preceding World War II, which provided the rationale for the modern-day notation for cytochromes and hemes. This history includes the discovery of ‘cytochromes’ by D. Keilin and his original description of a respiratory chain that occurred in the background of the studies on respiration and fermentation by O. Warburg. Bendall notes the subsequent development of the high resolution difference spectrophotometry of turbid samples by B. Chance and W. L. Butler that has been crucial in studies of biological electron transport chains.

### I. The Cytochromes and History

Cell respiration was still a black box in the decade following the end of the First World War. Attempts to throw light on the mechanisms involved mainly made use of the interplay between the concepts of specific enzymes and unspecific surface forces associated with colloids or membranes. The outstanding problem became how to reconcile two opposing notions (Keilin 1966; Kohler 1973). On the one hand, there was activation of hydrogen in metabolic substrates followed by an unspecific reduction of oxygen (Wieland and Thunberg), as could be beautifully and simply demonstrated by the reduction of methylene blue in a ‘Thunberg tube’. On the other hand there was

Warburg’s theory of the ‘*atmungsferment*’ which postulated an iron compound that could be reduced by unspecific surface forces but required a specific activation to be reoxidized by oxygen. An elegant series of experiments by Warburg, in which he studied the reversal by light of the effect of carbon monoxide on respiration and fermentation in yeast, led eventually to an absorption spectrum with maxima at 578, 546 and 436 nm which suggested to him that the *atmungsferment* was related to haemoglobin, which also forms a light-sensitive compound with carbon monoxide (Warburg 1927).

David Keilin’s discovery of cytochrome, which was to resolve this problem, was the serendipitous result of a study of haemoglobin in the horse bot fly, *Gas-*



*terophilus intestinalis*, and depended absolutely on his use of a simple but powerful instrument, the microspectroscope ocular, invented by Sorby in the late 1860s. The singular advantage of this instrument was that by virtue of its low dispersion, which sharpened absorption bands, and the fact that it allowed an intense beam of light to be focused on the sample placed on the microscope stage, absorption spectra of intact tissues or of turbid suspensions could be observed. Conventional spectroscopes and spectrophotometers, already available in the 1920s, were confined to the study of clear solutions, and even today this ability of commercial instruments is the exception rather than the rule. A variety of techniques were tried for overcoming this; opal glass was the key to one, but the most successful was a large end-window photomultiplier to collect the maximum amount of scattered light. This was used by Warren Butler, for example, but the most accessible were the dual-wavelength (double-beam) and split beam spectrophotometers developed by Britton Chance and colleagues at the Johnson Research Foundation in Philadelphia, which led to commercial instruments. The microspectroscope, however, remains a quick and simple way of getting a good idea of what you have in a coloured sample. It is also a curious fact that the way the eye interprets the absorption bands means that a shoulder on an otherwise symmetrical band is immediately obvious in the microspectroscope, but could easily be missed in a cursory examination of the spectrum given by a conventional spectrophotometer—try looking at the  $\alpha$ -band of cytochrome *f* with a microspectroscope.

Keilin was a parasitologist, inspired by his association with Maurice Caullery in Paris. He became interested in the life cycles of parasitic insects and especially the evolutionary adaptations of respiration in dipterous larvae. In 1915 he moved to Cambridge to join George Nuttall who had been elected as the first Quick Professor of Biology. Keilin's work became concentrated on the behaviour of *Gasterophilus*. Larvae of this fly find their home in the stomach of the horse in an

environment low in oxygen and in compensation their tracheal cells become rich in haemoglobin. Eventually they are voided in the faeces, burrow into the soil and pupate, and several weeks later adult flies emerge. The problem to be solved was the fate of the high concentration of haemoglobin in the larvae as the mature fly develops, and without his use of the microspectroscope the solution, and the discovery of cytochrome, would have been long delayed. The spectrum of haemoglobin gradually disappeared during pupation and was replaced in the thoracic wing muscles of the adult by a distinct four-banded spectrum. The obvious conclusion would have been that the pigment responsible for this spectrum was derived from haemoglobin. Keilin, however, was a biologist and before jumping to a conclusion looked at the spectra of intact thoracic muscles from several insects, especially *Galleria mellonella*, the wax moth which parasitises bees' nests. These moths were cultured in the laboratory and showed no haemoglobin at any stage. All his samples showed the same four-banded spectrum, and he also found it in cultures of *Bacillus subtilis* which had been used for culturing the insects, and eventually in yeast and plant tissues (chlorophyll free). Thus *Gasterophilus*, *Galleria* and the microspectroscope pointed the way, in Keilin's hands, to the discovery of cytochrome.

At this point, Keilin's literature searches led to his unearthing of the papers of MacMunn published between 1880 and 1890 in which he reports the occurrence of the characteristic four-banded spectrum in a variety of animal tissues (MacMunn 1886). MacMunn gave the names myohaematin and histoematin to the pigment responsible and concluded that it was a respiratory pigment distinct from haemoglobin and its derivatives. Hoppe-Seyler would not accept MacMunn's conclusion, claiming that the spectrum observed by MacMunn, which he had not looked for himself, was in fact derived from haemoglobin in different ways (ignoring MacMunn's finding of it in invertebrates which lack haemoglobin) (MacMunn 1890). MacMunn's work was gradually forgotten.

Keilin's first paper *On Cytochrome* (Keilin 1925), was outstanding in various ways. To a novice scientist entering the field in the mid 1950s it seemed like the ideal model for a scientific paper. The whole of the Introduction is devoted to a discussion of MacMunn's observations and the way in which they had been misunderstood and eventually ignored. He then gives an account of his own observations, starting with the occurrence of the characteristic spectrum in a wide range of animal tissues and also, most significantly, in some bacteria, yeast and plant tissues. This is followed by a series of simple and elegant experiments from which he was able to argue conclusively about the physiological function of the pigment and its chemical constitution. The pigment was introduced under the name "*Cytochrome*, signifying merely 'cellular pigment', pending the time when its composition shall have been properly determined." The change of name was justified by the much wider distribution of the pigment than had been envisaged by MacMunn. Moreover, Keilin showed that cytochrome was not a single pigment, as MacMunn had thought, but the superposition of three. Thus the names cytochrome *a*, *b* and *c* became established from the beginning, corresponding to the  $\alpha$ -bands at about 605, 560 and 550 respectively. The fourth band in the cytochrome spectrum at around 520 nm was the fused  $\beta$ -bands of the three components (in case anyone should think that this arbitrary name system was in the wrong order, note that in a direct-vision spectroscopy long wavelengths appear towards the left and short wavelengths to the right). The three components were haemochromogen-like (haemochrome-like) substances, giving slightly different haemochromogens when denatured with KOH. Cytochrome *c* was obtained separate from the others in an aqueous extract of yeast. Anson and Mirsky had established that the characteristic haemochromogen spectrum (sharp  $\alpha$ -band, more diffuse  $\beta$ -band) is formed by the following reaction

Reduced haem

+ nitrogen compound  $\rightleftharpoons$  haemochromogen

(Anson and Mirsky 1925a). The three components could be related to haemoglobin only by the common possession of haem groups (Anson and Mirsky 1925b).

The most important observation (Keilin 1925) was that cytochrome could be reversibly oxidized and reduced in vivo depending on the availability of oxygen. MacMunn had demonstrated the existence of oxidized and reduced states because the four-banded spectrum only appeared in the reduced state and disappeared when oxidized, but he had only shown this using chemical reagents. Thus Keilin had demonstrated that cytochrome is involved in cell respiration in virtually all aerobic organisms. By 1929 he was able to state clearly that the role of cytochrome in cell respiration is to connect the reducing systems of Wieland and Thunberg with an oxidase, as in Fig. 1.1, this being the first formulation of the respiratory chain (Keilin 1929). The oxidase was equated with what had previously been described as indophenol oxidase and also with Warburg's *atmungsferment*. The more appropriate name, first suggested by Malcolm Dixon, was of course cytochrome oxidase (Dixon 1929). The arrangement of the individual cytochrome components, especially cytochrome *b*, was not clear at that time.

The term cytochrome could then logically be applied to any intracellular haemochromogen-like substance the function of which is to undergo reversible oxidation and reduction in an electron transfer process. Thus, as new cytochrome components were discovered that did not readily fit into Keilin's *a*, *b*, *c* system for respiration, it became natural to extend this arbitrary lettering system. Cytochromes *e*, *f*, *h* and *o* were soon described.

Cytochrome *e* is now forgotten, but was the name given by Keilin and Hartree (1949) to a component revealed in their particulate cytochrome preparation from heart muscle by application of their new technique

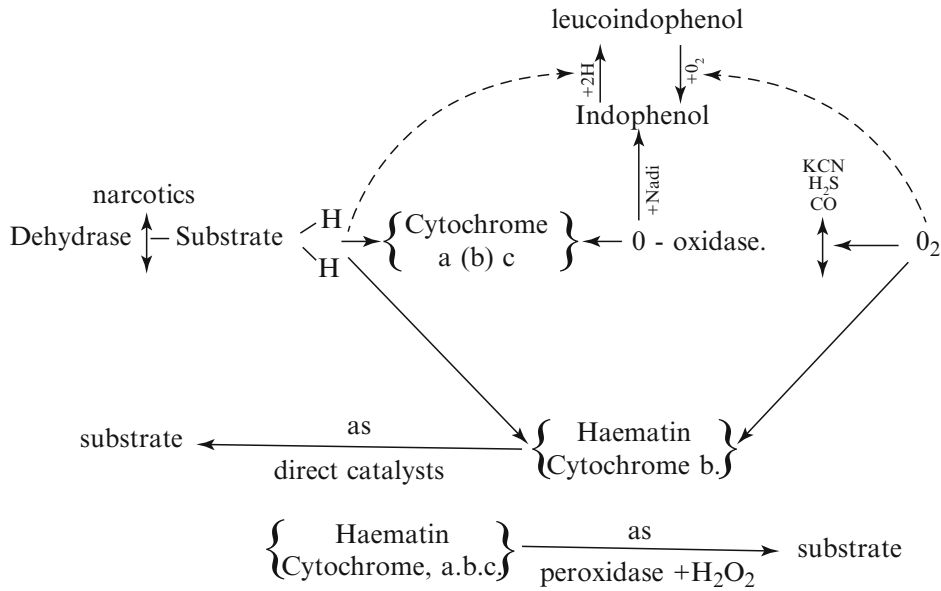


Fig. 1.1. The first formulation of the function of cytochrome in a respiratory chain (From Keilin 1929).

for sharpening and intensifying absorption bands by cooling a suspension in 50 % glycerol down to 77 K with liquid air or liquid nitrogen. They later realised, however, that cytochrome *e* was identical with a component previously discovered by Yakushiji and Okunuki in heart muscle preparations after extraction of all the cytochrome *c* and to which they had given the name cytochrome  $c_1$ . The name cytochrome *e* was therefore abandoned (Keilin and Hartree 1955).

Cytochrome *f* we are all familiar with. Robin Hill worked in the Biochemistry Department in Cambridge, but was closely associated with Keilin, a few yards away in the Molteno Institute of Parasitology. Hill had done original work on the chemistry of haem compounds and had published with Keilin on the nature of the haem of cytochrome *c*. His real passion was the chemistry of plants, and following Keilin's work he was keen to discover whether cytochrome also had a role in photosynthesis. Looking for cytochrome in leaves was not straightforward because of the high concentration of chlorophyll which masked the spectra of cytochrome components. Hill and Kamala Bhagvat had succeeded in isolating a partic-

ulate preparation from plants that possessed succinate and cytochrome oxidase activities (Bhagvat and Hill 1951; Hill and Bhagvat 1939) and, around this time and immediately following the end of the war, the generality of the cytochrome system in plant respiration was being demonstrated in several laboratories, concentrating mostly on chlorophyll-free tissues. Rosenberg and Ducet (1949), however, found cytochrome oxidase activity in impure preparations of chloroplasts while Hill and Scarisbrick were able to extract cytochrome *c* from leaves (Hill and Scarisbrick 1951; Scarisbrick 1947). Hill and Scarisbrick first sought to observe cytochrome in leaves by examining acetone powders, free of chlorophyll, and found that the spectrum was dominated by a strong band centred at 554 nm. They were soon able to extract this component into solution with ethanol-ammonia as solvent. It was clearly different from cytochrome *c* both in its absorption spectrum and redox potential, and was also incapable of being oxidized by cytochrome oxidase. Furthermore, its concentration in leaves was an order of magnitude higher than that of cytochrome *c* and, unlike cytochrome *c*, it was confined to the green tissues of

plants. To emphasise its distinctive association with leaves they named it cytochrome *f* (Latin *frons* as stated by Hill and Scarisbrick, or *folium*), a name which has turned out to be too convenient to lose, even though an attempt was later made to rename it cytochrome *c*<sub>6</sub> once its formal classification as a *c*-type cytochrome became apparent.

Cytochrome *h* is no longer well known, but is closely related to helicorubin which is like an extracellular *b*-type cytochrome occurring in the intestinal tract of snails and some other molluscs and crustaceans. Cytochrome *h* occurs in the digestive gland of snails and was purified by Joan Keilin (1956, 1957) from *Helix pomatia*, hence the name. Although it appears to be a protein similar to helicorubin, the exact relationship is still not clear, and unlike helicorubin the haem group is not released by treatment with acid acetone. Thus cytochrome *h* is more likely to turn out to be a *c*-type cytochrome.

Cytochrome *o* is the name given by Castor and Chance (1959) to a bacterial oxidase which was clearly distinct from *a*-type oxidases and which they had discovered with their new technique for measuring the photochemical action spectrum of CO-inhibited respiration. This turns out to be the oxygen-reacting component of a quinol oxidase occurring in a number of bacterial species (Poole 1983). It has often been assumed to be a *b*-type component despite the strong reservations of Castor and Chance, and the Nomenclature Committee of the IUB even goes so far as to recommend that the name cytochrome *o* should be abandoned in favour of cytochrome *b*', the prime indicating it is not strictly a haemochromogen as the 6th ligand position of the iron is free for combination with CO or O<sub>2</sub>. The situation has been clarified by Wikström and colleagues (Puustinen and Wikström 1991; Wu et al. 1992) who have demonstrated unequivocally that haem *o* differs from protohaem in that one of the vinyl sidechains has become farnesylhydroxyethyl as in haem *a*, but differs from haem *a* in not possessing a formyl sidechain. Nevertheless, the high-spin haem *o* is associated with a second, low-spin

haem and also a copper atom, suggesting that the enzyme belongs to the cytochrome *aa*<sub>3</sub> family of oxidases. The low-spin haem can be either protohaem or haem *o* depending on the source of enzyme, and both function equally well. The enzyme is usually referred to as cytochrome *bo* or *bo*<sub>3</sub>, the subscript indicating homology with the cytochrome *aa*<sub>3</sub> oxidase as suggested by Puustinen and Wikström (1991), although no cytochromes *o*<sub>1</sub> or *o*<sub>2</sub> are currently known. It is one of two ubiquinol oxidases occurring in *Escherichia coli*, and has a relatively low affinity for oxygen.

The arbitrary assignment of letters to different cytochrome components was based on the position of the  $\alpha$ -band of the reduced form, but it soon became apparent that since they were all haem proteins a more satisfactory classification could be based on their respective pyridine haemochromogens. The pyridine haemochromogens would give more consistent spectra, based on the chemical nature of the haem group. Anson and Mirsky had shown that cytochrome preparations contained the same haem as haemoglobin, that is protohaem, and this could be assigned to cytochrome *b*. The pyridine haemochromogen of cytochrome *c*, which could be extracted into solution free of the other components, was clearly different. Hill and Keilin (1930) obtained porphyrin *c* and showed that it was related to haematoporphyrin in which the vinyl sidechains of protoporphyrin are replaced by hydroxyethyl groups, but the nature of its attachment to the protein was not established until Theorell (1938) demonstrated that it was bound through thioether linkages to cysteine residues. The distinctive feature of haem *a*, which shifts its  $\alpha$ -band to the red end of the spectrum, is the possession of a formyl group as sidechain in place of the methyl group at position 8 of the porphyrin ring, and it also contains a long alkyl sidechain at position 2 in place of vinyl (Caughey et al. 1975).

The classification of cytochromes was thus based upon structure as well as function, which is the case for the formal classification of enzymes. Newly discovered cytochromes,

if they did not fit readily into Keilin's respiratory chain, could be named as being type *a*, *b* or *c* according to the position of the  $\alpha$ -band of the pyridine haemochromogen (587, 557 and 550 nm respectively) and given a subscript number. Hence we have, for example, cytochromes *a*<sub>1</sub>, *a*<sub>2</sub> and *a*<sub>3</sub>. Cytochromes *a*<sub>1</sub> and *a*<sub>2</sub> are bacterial components initially so named because their  $\alpha$ -bands lie at the red end of the spectrum, but different from cytochrome *a*. Castor and Chance (1959) showed that they are oxidases from the action spectra for photodissociation of CO complexes. Subsequent analysis of the pyridine haemochromogens, however, has shown that in many cases the assignment to type *a* was a mistake, although cytochrome *a*<sub>3</sub> is correctly assigned.

Cytochromes *a*<sub>1</sub> and *a*<sub>2</sub>, with  $\alpha$ -bands around 590 and 630 nm respectively (Keilin 1934, 1966; Poole 1983), have had somewhat chequered careers. Cytochrome *a*<sub>1</sub> has been purified from *Acetobacter aceti* and shown to be a ubiquinol oxidase that possesses one haem *a* and one haem *b* (Matsushita et al. 1990), and thus should be named cytochrome *ba* or perhaps more appropriately *ba*<sub>3</sub>. On the other hand in *Escherichia coli* *a*<sub>1</sub> and *a*<sub>2</sub> occur together in the second ubiquinol oxidase (the other being cytochrome *bo*<sub>3</sub>) which has a high affinity for oxygen and contains no haem *a* (Castor and Chance 1959). In this case what was previously described spectroscopically as cytochrome *a*<sub>1</sub> actually contains a high-spin *b*-type haem with an  $\alpha$ -band in the reduced form at 595 nm and now referred to as cytochrome *b*<sub>595</sub> (Lorence et al. 1986). The haem of so-called cytochrome *a*<sub>2</sub> was shown by Barrett (1956) to be of a new type which contains a dihydroporphyrin or chlorin in which the porphyrin ring is partially reduced. This is now known as haem *d*, the structure of which was established in detail by Timkovich et al. (1985). This second oxidase contains another *b*-type haem which is low-spin and has its  $\alpha$ -band at 558 nm, but there is no copper to provide a binuclear centre to react with oxygen. Evidence has accumulated that cytochrome *d* and cytochrome *b*<sub>595</sub> together

form a binuclear centre but no crystal structure is yet available. These enzymes are usually referred to as cytochrome *bd* oxidases. The distinguishing feature of haem *d* is that the porphyrin ring is partially saturated with one reduced pyrrole ring, and so is a chlorin as shown by Barrett. In addition to the oxidases, however, a bacterial nitrite reductase also contains a partially reduced haem group, but with a different set of sidechains and a pair of carbonyl groups attached to adjacent pyrrole rings. This has been named haem *d*<sub>1</sub>. The enzymes containing haem *d*<sub>1</sub> carry out the one electron reduction of nitrite to nitric oxide, but they are also capable of reducing oxygen to water, which is a four-electron reaction (Timkovich et al. 1984).

One more type of enzyme that has not conventionally been described as a cytochrome, but in fact conforms to the general definition of a haem protein involved in intracellular electron transfer, is the assimilatory sulphite reductase of sulphate reducing bacteria which carries out the six electron reduction of sulphite to sulphide. The haem prosthetic group has been given the name sirohaem to indicate its involvement in sulphite reduction, and like haem *d*<sub>1</sub> has a pair of saturated pyrrole rings (although with different sidechains) making it an isobacteriochlorin (Murphy and Siegel 1973). It could thus be regarded as a type *d* cytochrome with the name cytochrome *d*<sub>2</sub>.

The use of the wavelength maximum of the  $\alpha$ -band to describe a cytochrome component was first suggested by Scarisbrick (1947) and was normally written on the line hyphenated to the haem type, for example cytochrome *c*-553. This was convenient for a new component which had not been clearly established in terms of either structure or function, but suffered from the disadvantage that it might not represent a unique component. Cytochrome *c*-553 (sometimes *c*-552) was the term being used to describe the so-called soluble cytochrome *f* to distinguish it from the bound cytochrome *f* but when it became clear that the soluble component and the true

membrane-bound cytochrome *f* have distinct functions in the photosynthetic electron transport chain (Wood 1977) the name *c*-553 was relinquished in favour of the more definitive *c*<sub>6</sub>. The wavelength maximum has frequently been written as a subscript, as *b*<sub>558</sub> and *b*<sub>595</sub>, but this notation is best reserved for those cases, as here, in which it describes a well-established component.

The naming and numbering of cytochrome components often seems arbitrary, but has been determined by the history of their discovery, and well known names tend to be perpetuated, even if strictly erroneous. The many different kinds of *b*-type cytochromes illustrate this point. Cytochrome *b*-559 associated with the reaction centre of photosystem II is an example. It is frequently referred to as cytochrome *b*<sub>559</sub>, which is preferable, but even so the true wavelength maximum is at 559.6 nm, so a more accurate name would be cytochrome *b*<sub>560</sub> (Cramer 2004). It would have been possible to avoid the nomenclature problems by defining this component as cytochrome *b*<sub>9</sub>, but the name *b*<sub>559</sub> seems too well established for change to be accepted.

Cytochrome *b*<sub>5</sub> is well known as a distinctive component with widespread occurrence in microsomal membranes and the outer mitochondrial membrane. Cytochrome *b*<sub>6</sub> has proved a useful name for the component of the cytochrome *b*<sub>6</sub>*f* complex to distinguish its properties from those of the mitochondrial cytochrome *b* occurring in complex III, the cytochrome *bc*<sub>1</sub> complex. Previously the name cytochrome *b*<sub>2</sub> had been used to describe the flavocytochrome which is the yeast lactate dehydrogenase. These numbers, however, leave puzzling gaps for *b*<sub>1</sub> and *b*<sub>3</sub>. Cytochrome *b*<sub>1</sub> was used by Keilin (1934) to describe the principal component of *Escherichia coli*, which did not belong to his classical *a*, *b*, *c* group. More recently cytochrome *b*<sub>1</sub> has been shown to be a multisubunit protein identical with bacterioferritin, an iron-storage protein (Smith et al. 1988). On the other hand, little is known about cytochrome *b*<sub>3</sub>. In their initial study of the cytochrome components of leaves Hill

and Scarisbrick (Scarisbrick 1947) found two cytochromes in aqueous extracts which had been allowed to stand overnight to allow all chloroplast fragments to aggregate. These were cytochromes *c* and a new *b*-component which they named *b*<sub>3</sub>, both of which also occurred in non-green tissues. Cytochrome *b*<sub>3</sub> had an  $\alpha$ -band at 559 nm, was autoxidisable and could be reduced by ascorbate. Martin and Morton (1955) suggested that it is derived by autolysis from a component of the microsomal fraction of certain plant tissues on the basis of the similarity in properties of the two, which is plausible but has not been directly demonstrated. Rich and Bendall (1975) showed that the main components of plant microsomes are cytochromes *b*-559.5 and *b*-562 with similar properties, *b*<sub>5</sub> and P450, but that the relative amounts varied widely between different tissues. Nothing is known about the function of cytochrome *b*-559 (nor *b*<sub>3</sub>).

This volume celebrates the fact that cytochromes often occur in relatively large protein complexes containing more than one polypeptide and frequently more than one haem group with possibly additional redox centres. The first example of this was the mitochondrial cytochrome *aa*<sub>3</sub>, first described by Keilin and Hartree (1938). The first clear expression of the concept of protein complexes with catalytic activity in electron transfer was made by Hatefi and other colleagues of David Green in the Institute for Enzyme Research at the University of Wisconsin in 1962 (Hatefi et al. 1962). This was the origin of the idea of the mitochondrial respiratory chain being divided into four discrete complexes which could be individually purified, hence complex I (DPNH—coenzyme Q reductase), complex II (succinic—coenzyme Q reductase), complex III (QH<sub>2</sub>—cytochrome *c* reductase) complex IV (cytochrome *c* oxidase). The emphasis was on the proteins and the enzymic activities, rather than the cytochromes, but complex IV was equivalent to Keilin and Hartree's cytochrome oxidase and complex III was what we now know alternatively as a cytochrome *bc* complex.

The activities of these complexes were linked by two diffusible components, the lipid soluble coenzyme Q (ubiquinone) and the water soluble cytochrome *c*. Since that time the concept of cytochrome complexes has burgeoned, especially with regard to photosynthetic systems, both eukaryotic and prokaryotic, the complex processes occurring in cytochrome *bc* complexes, and the rich field of bacterial oxidases.

This brings us to the last example concerning cytochrome nomenclature. At present bacterial oxidases fall into two broad classes, those containing a haem-copper binuclear centre with a high spin haem, and those that contain haem *d* together with a second high-spin haem ( $b_{595}$ ) instead of the copper. A low spin haem compound, usually of type *a*, *b* or sometimes *o*, is always associated with the binuclear centre as electron donor, and occasionally there is an additional bound cytochrome *c* as well. The high spin haem of haem-copper enzymes may be type *a*, *b* or *o*, and is usually given the subscript 3, following  $a_3$  of the mitochondrial enzyme. There is no known example of a high spin haem *c* in this role, and the name cytochrome  $c_3$  has been appropriated by a low-potential, low spin, multihaem cytochrome in sulphate reducing bacteria (Postgate 1956). Nevertheless, a high-spin cytochrome *c*, originally described as pseudo-hemoglobin and later RHP (Rhodospirillum heme protein) but now designated cytochrome *c'*, was discovered in aqueous extracts of *Rhodospirillum rubrum* by Vernon and Kamen (1954). Its function has long been a puzzle, but it may play a role in redox poisoning to prevent over reduction or over oxidation of the cyclic electron transfer system (Meyer and Cusanovich 2003).

In 1925 Keilin justified use of the new term cytochrome by the fact that it is much more widely distributed than had been envisaged by MacMunn and established the defining feature that it is involved in intracellular electron transfer. The second and crucial point demonstrated by Keilin is that there is more than one cytochrome compo-

nent (hence the respiratory chain) and that they are all haem compounds. But at the same time he thought of cytochrome as a temporary term "pending the time when its composition shall have been properly determined". He could not have imagined (as early as 1925) how the numbers of known cytochrome components would expand in subsequent years, nor how much detailed information about their composition would accumulate. Incomplete as our knowledge and understanding is, we can nevertheless say that they are all proteins with no common structure or evolutionary origin. In other words Keilin's two defining characteristics are the only ones we can apply to all cytochromes. So we end with names, established by custom and usage, of a series of cytochrome components each with its own type of haem, *a*, *b*, *c*, *d* or *o* which may have a subscript number defining its function. Recognizing the importance of habit in the use of names we make an honourable exception to this rather crude formulation for cytochrome *f*, and as we have seen, a strictly consistent nomenclature is difficult to achieve and probably undesirable.

## References

- Anson ML, Mirsky AE (1925a) On haemochromogen and the relation of protein to the properties of the haemoglobin molecule. *J Physiol* 60:50–67
- Anson ML, Mirsky AE (1925b) On haem in nature. *J Physiol* 60:161–174
- Barrett J (1956) The prosthetic group of cytochrome  $a_2$ . *Biochem J* 64:626–639
- Bhagvat K, Hill R (1951) Cytochrome oxidase in higher plants. *New Phytol* 50:112–120
- Castor LN, Chance B (1959) Photochemical determinations of the oxidases of bacteria. *J Biol Chem* 234:1587–1592
- Caughey WS, Smythe GA, O'Keeffe DH, Maskasky JE, Smith ML (1975) Heme A of cytochrome *c* oxidase. *J Biol Chem* 250:7602–7622
- Cramer WA (2004) *Ironies* in photosynthetic electron transport: a personal perspective. *Photosynth Res* 80:293–305
- Dixon M (1929) Oxidation mechanisms in animal tissues. *Biol Rev* 4:352–397

- Hatefi Y, Haavik AG, Fowler LR, Griffiths DE (1962) Studies on the electron transfer system XLII Reconstitution of the electron transfer system. *J Biol Chem* 237:2661–2669
- Hill R, Bhagvat K (1939) Cytochrome oxidase in flowering plants. *Nature* 143:726
- Hill R, Keilin D (1930) The porphyrin of component *c* of cytochrome and its relationship to other porphyrins. *Proc R Soc B* 107:286–292
- Hill R, Scarisbrick R (1951) The haematin compounds of leaves. *New Phytol* 50:98–111
- Keilin D (1925) On cytochrome, a respiratory pigment, common to animals, yeast, and higher plants. *Proc R Soc B* 98:312–339
- Keilin D (1929) Cytochrome and respiratory enzymes. *Proc R Soc B* 104:206–252
- Keilin D (1934) Cytochrome and the supposed direct spectroscopic observation of oxidase. *Nature* 133:290–291
- Keilin J (1956) Helicorubin and cytochrome *h*. *Biochem J* 64:663–676
- Keilin J (1957) Properties of helicorubin and cytochrome *h*. *Nature* 180:427–429
- Keilin D (1966) *The History of Cell Respiration and Cytochrome*. Cambridge University Press, Cambridge
- Keilin D, Hartree EF (1938) Cytochrome *a* and cytochrome oxidase. *Nature* 141:870–871
- Keilin D, Hartree EF (1949) Effect of low temperature on the absorption spectra of haemoproteins; with observations on the absorption spectrum of oxygen. *Nature* 164:254–259
- Keilin D, Hartree EF (1955) Relationship between certain components of the cytochrome system. *Nature* 176:200–206
- Kohler RE (1973) The background to Otto Warburg's conception of the *Atmungsferment*. *J Hist Biol* 6:171–192
- Lorence RM, Koland JG, Gennis RB (1986) Coulometric and spectroscopic analysis of the purified cytochrome *d* complex of *Escherichia coli*: evidence for the identification of “cytochrome *a*<sub>1</sub>” as cytochrome *b*<sub>595</sub>. *Biochemistry* 25:2314–2321
- MacMunn CA (1886) Researches on myohaematin and the histohaematins. *Phil Trans R Soc* 177:267–2980
- MacMunn CA (1890) Ueber das myohämatin. *Hoppe-Seyl Z* 14:328–329
- Martin EM, Morton RK (1955) Cytochrome *b*<sub>3</sub> of microsomes from plant tissues. *Nature* 176:113–114
- Matsushita K, Shinagawa E, Adachi O, Ameyama M (1990) Cytochrome *a*<sub>1</sub> of *Acetobacter acetii* is a cytochrome *ba* functioning as ubiquinol oxidase. *Proc Natl Acad Sci USA* 87:9863–9867
- Meyer TE, Cusanovich MA (2003) Discovery and characterization of electron transfer proteins in the photosynthetic bacteria. *Photosynth Res* 76:111–126
- Murphy MJ, Siegel LM (1973) Siroheme and sirohydrochlorin. The basis for a new type of porphyrin-related prosthetic group common to both assimilatory and dissimilatory sulfite reductases. *J Biol Chem* 248:6911–6919
- Poole RK (1983) Bacterial cytochrome oxidases. A structurally and functionally diverse group of electron-transfer proteins. *Biochim Biophys Acta* 726:205–243
- Postgate JR (1956) Cytochrome *c*<sub>3</sub> and Desulphoviridin; pigments of the anaerobe *Desulphovibrio desulphuricans*. *J Gen Microbiol* 14:545–572
- Puustinen A, Wikström M (1991) The heme groups of cytochrome *o* from *Escherichia coli*. *Proc Natl Acad Sci USA* 88:6122–6126
- Rich PR, Bendall DS (1975) Cytochrome components of plant microsomes. *Eur J Biochem* 55:333–341
- Rosenberg AJ, Ducet GL (1949) Activité cytochromoxydasique chez l'épinard. *CR Acad Sci Paris* 229:391–393
- Scarisbrick R (1947) Haematin compounds in plants. *Ann Rep Prog Chem* 44:226–236
- Smith JMA, Quirk AV, Plank RWH, Diffin FM, Ford GC, Harrison PM (1988) The identity of *Escherichia coli* bacterioferritin and cytochrome *b*<sub>1</sub>. *Biochem J* 255:737–740
- Theorell H (1938) The chemical constitution of the cytochromes *c*. *Biochem Z* 298:242–267
- Timkovich R, Cork MS, Taylor PV (1984) Proposed structure for the noncovalently associated heme prosthetic group of dissimilatory nitrite reductases. *J Biol Chem* 259:1577–1585
- Timkovich R, Cork MS, Gennis RB, Johnson PY (1985) Proposed structure of heme *d*, a prosthetic group of bacterial terminal oxidases. *J Am Chem Soc* 107:6069–6075
- Vernon LP, Kamen MD (1954) Hematin compounds in photosynthetic bacteria. *J Biol Chem* 211:643–662
- Warburg O (1927) Über die Wirkung von Kohlenoxyd und Stickoxyd auf Atmung und Gärung. *Biochem Z* 189:354–380
- Wood PM (1977) The roles of *c*-type cytochromes in algal photosynthesis. Extraction from algae of a cytochrome similar to higher plant cytochrome *f*. *Eur J Biochem* 72:605–612
- Wu W, Chang CK, Varotsis C, Babcock GT, Puustinen A, Wikström M (1992) Structure of the heme *o* prosthetic group from the terminal quinol oxidase of *Escherichia coli*. *J Am Chem Soc* 114:1182–1187



# Chapter 2

## When Did Hemes Enter the Scene of Life? On the Natural History of Heme Cofactors and Heme-Containing Enzymes

Anne-Lise Ducluzeau<sup>a</sup> and Wolfgang Nitschke<sup>b,\*</sup>

<sup>a</sup>*School of Fisheries and Ocean Sciences, University of Alaska-Fairbanks, 245 O'Neill Bldg., Fairbanks, AK 757220, USA*

<sup>b</sup>*Laboratoire de Bioénergétique et Ingénierie des Protéines UMR 7281 CNRS/AMU FR3479, F-13402 Marseille Cedex 20, France*

Summary.....	13
I. Introduction.....	14
II. Hemes in LUCA; Pros and Cons.....	15
A. Does Ubiquity Automatically Translate into Deep Ancestry?.....	15
B. Phylogenies of Heme-Bearing Bioenergetic Enzymes Suggest a Red LUCA.....	15
C. The Dichotomy of Heme Biosynthesis Enzymes.....	16
1. Does the Existence of Two Distinct Pathways Necessarily Argue for an Anemic LUCA?.....	18
III. An Alternative Scenario.....	19
A. A Scenario Potentially Reconciling Molecular Phylogeny of Heme Enzymes and Pathway Dichotomy.....	19
B. Is the Heme-Biosynthesis-Pathway Dichotomy Related to Other Major Pathway Dichotomies?.....	20
IV. Why All the Fuzz?.....	21
Acknowledgments.....	22
References.....	22

### Summary

Heme proteins are almost ubiquitous both in Archaea and in Bacteria. The last universal common ancestor (LUCA) of the two prokaryotic domains was, therefore, assumed until recently to already have made use of heme cofactors, a notion bolstered by molecular phylogenies of several heme-bearing enzymes. The discovery of a second pathway for heme biosynthesis, predominantly present in Archaea, was subsequently interpreted to indicate independent origins of heme biosynthesis in each of the two prokaryotic domains (Lane and Martin (Cell 151:1406–1416, 2012)), implying that the LUCA might have been entirely devoid of hemes and heme proteins. In this contribution, we outline the presently

---

\*Author for correspondence, e-mail: [nitschke@imm.cnrs.fr](mailto:nitschke@imm.cnrs.fr)

available evidence in favour of either scenario and propose a new model reconciling the seemingly contradictory messages sent by molecular phylogeny of heme-bearing enzymes and the biosynthesis pathway dichotomy. A possible relation to other biosynthesis pathway dichotomies is suggested, and the far-reaching repercussions of the ultimate resolution of the controversy on our understanding of free energy conversion in the LUCA and at life's origin are emphasized.

## I. Introduction

From the point of view of thermodynamics, living organisms fundamentally are free energy converting systems transforming environmental redox disequilibria into the extraordinary entropy decrease that characterizes cellular life (Branscomb and Russell 2013). One of the quintessential attributes of life therefore is its ability to perform redox reactions and to channel reducing equivalents from the environmental electron donating to the accepting substrates. Redox compounds therefore can safely be assumed to be crucial elements of life in general and thus must have already played a paramount role at its origin. Obvious candidates for such redox compounds at life's inception are centres made up from environmental transition metals such as iron, nickel, molybdenum, tungsten, manganese, cobalt etc.

Indeed, several redox cofactors found in extant life have been proposed based on molecular phylogeny to be as old as life itself, that is, iron sulphur clusters (Eck and Dayhoff 1966), nickel-iron centres (Vignais et al. 2001) and molybdenum/tungsten compounds (Schoepp-Cothenet et al. 2012). Iron-sulphur clusters and Mo/W-centres are indeed basically ubiquitous in extant life. However, another iron-based redox centre, i.e. heme, likely is almost as widely distributed in living organisms as are iron-sulphur and Mo/W-centres.

The heme cofactors in heme proteins overwhelmingly serve as electron transferring redox centres operating in an impressively wide range of electrochemical potentials. The major part of contributions to this volume indeed deals with electron transferring heme proteins. However, hemes can also play the roles of small-molecule transporters (e.g. Suzuki and Imai 1998) and sensors (Cutruzzolà et al. 2014; Martinkova et al. 2013; Pokkuluri et al. 2008) or even directly participate in catalysis (e.g. P<sub>450</sub>, O<sub>2</sub>-reductase *alias* cytochrome oxidase or *cd*<sub>1</sub>-type nitrite reductase). The listed examples imply that in the context of this contribution, the term “heme” will refer to substituted Fe-tetrapyrroles in general, encompassing not only Fe-protoporphyrin IX (FePPIX), i.e. heme *b* and its derived heme *c*, but also differently substituted Fe-tetrapyrroles such as sirohemes or heme *a*, heme *o*, etc. This extension of scope becomes ineluctable in the evolutionary context since, as we will see, the synthesis pathways of differently substituted protoporphyrins are heavily convoluted and individual pathways can therefore not be dealt with separately.

Until a few years ago, the occurrence of heme proteins and hence necessarily of hemes in the oldest cellular entity which we can define, i.e. the last universal common ancestor (LUCA) of Bacteria and Archaea, was tacitly taken for granted by a large part of the heme protein community. A number of recent articles have challenged this view (Lane and Martin 2012; Sousa et al. 2013, Sousa and Martin 2014), and the previously held opinion on the evolutionary ancestry of all kinds of heme proteins are consequently called into question. Our contribution aims at providing the readers with a better understanding of the pros and cons of both

---

*Abbreviations:* Ahb-pathway – Alternative heme biosynthesis pathway; (B)Chl – (Bacterio)Chlorophyll; FePPIX – Iron-protoporphyrin IX; GOE – Great oxidation event; HGT – Horizontal gene transfer; LUCA – Last universal common ancestor of Archaea and Bacteria; Mo/W – Molybdenum/tungsten; NOR – NO reductase; O<sub>2</sub>R – O<sub>2</sub> reductase

the “heme-bearing” and the “heme-free LUCA” paradigms and of the evolutionary consequences at stake in either scenario.

## II. Hemes in LUCA; Pros and Cons

### *A. Does Ubiquity Automatically Translate into Deep Ancestry?*

In the realm of the prokaryotes, only a small number of taxonomic groups are known thus far, the members of which are devoid of heme and the most conspicuous examples likely are certain methanogenic Archaea, the homoacetogenic Bacteria from the clostridial phylum or strict fermenters such as the Thermotogales (Sousa et al. 2013). Pervasive presence of a specific trait in both Archaea and Bacteria is frequently taken as indicating the presence of this trait already prior to the Archaea/Bacteria divergence (see for example the case made for aerobic respiration in the LUCA by Brochier-Armanet et al. 2009). As we have argued in the past (van Lis et al. 2011; Nitschke and Russell 2013; Ducluzeau et al. 2014a), we consider this line of reasoning as fraught with problems. The existence of horizontal gene transfer (HGT) between the prokaryotic domains is a well-established fact (haloarchaeal genomes provide an extreme example, see Nelson-Sathi et al. 2012) and a novel trait providing a substantial increase in evolutionary fitness is likely to be widely distributed within the prokaryotes via this mechanism. The evolutionary driving force for trait-dissipation is further augmented if the novel trait is specifically adapted to altered ambient conditions following large-scale environmental transitions. Such transitions have almost certainly occurred several times during the roughly four billion years of life’s history on planet Earth and the most conspicuous and best-studied example is the so-called Great-Oxidation-Event (GOE) occurring about 2.3 billion years ago. The GOE has indeed turned the basically O<sub>2</sub>-free primordial planet into an “aerobic”

world. Whether the GOE had resulted in a persistent oxygenation of the biosphere or was followed by a substantial drop in O<sub>2</sub>-levels between 1.9 and about one billion years ago is presently debated (Partin et al. 2013). While the “phylogenomic distribution argument” thus considers that scarce traits have a poor chance of having been present in the LUCA whereas ubiquitous ones are good candidates, we would argue that the undisputable occurrence of profound, one-way, changes of the planet’s geo-environment substantially diminishes the logical basis of this argument. In our view, evolutionary traits favourable during life’s infancy have a non-negligible chance of becoming outcompeted following major changes in the environment by traits evolving as a result of such environmental overturning and subsequently being widely dispersed through HGT.

All this thus means that the mere pervasive presence of heme cofactors in both Archaea and Bacteria likely is insufficient to conclude on a heme-bearing LUCA. A more stringent approach, albeit prone to a number of experimental difficulties (as discussed in Ducluzeau et al. 2014a) consists in the application of molecular phylogeny (Zuckerlandl and Pauling 1965). The obvious difficulty here is that hemes as organic, transition-metal bearing, cofactors are not (directly) encoded by genes and therefore don’t feature (gene- or amino acid-) sequences. However, enzymes using hemes as crucial cofactors as well as the proteins involved in heme biosynthesis do. Which kind of messages can be extracted from the molecular memories of these systems?

### *B. Phylogenies of Heme-Bearing Bioenergetic Enzymes Suggest a Red LUCA*

In the following, we will restrict our discussion to cover only enzymes participating in bioenergetic electron transfer. To the best of our knowledge, heme-dependent enzymes from other types of cellular processes have so far not been studied in great detail with

respect to their deep evolutionary history. Furthermore, the paramount importance for life of free energy converting mechanisms guarantees a good species coverage for individual enzymes and thus improves the reliability of derived phylogenetic trees. Last but not least, the bioenergetic cytochrome systems are what readers of this volume will be most interested in.

Examples for bioenergetic enzymes which involve heme cofactors in a functionally crucial manner are provided by the Rieske/cytb complexes (encompassing the *bc*<sub>1</sub> and *b*<sub>6f</sub> complexes as well as their homologs), the superfamily of O<sub>2</sub>- and NO-reductases and the *cd*<sub>1</sub>-type nitrite reductases. Other enzymes feature heme-containing subunits involved in electron transfer from or to the catalytic centre while their reaction turnover is not or only marginally dependent on the presence or absence of these heme proteins. Representatives of the latter class are for instance Group 1 [Ni-Fe]-hydrogenases (Pandelia et al. 2012), the superfamily of Mo/W-bisPGD-enzymes (Schoepp-Cothenet et al. 2012), succinate dehydrogenases/fumarate reductases (Lemos et al. 2002), certain types of heterodisulphide reductases (Thauer et al. 2008) or several enzymes involved in the bioenergetics of sulphur compounds (Grein et al. 2013). The heme subunits in these enzymes typically serve to link redox reactions in the soluble phase (i.e. the peri- or cytoplasm) to membrane-integral lipophilic hydrogen carriers such as quinones and methanophenazines (Schoepp-Cothenet et al. 2013). The vast majority of these heme-subunits belong to one of three structural groups (Baymann et al. 2003; Schoepp-Cothenet et al. 2013; Grimaldi et al. 2013).

Only a few of the proteins mentioned have been studied by molecular phylogeny so far. Prominent examples are the Rieske/cytb complexes (Schütz et al. 2000; Dibrova et al. 2013; Kao and Hunte 2014), the O<sub>2</sub>R/NOR superfamily (Pereira et al. 2001; Ducluzeau et al. 2009, 2014; Gribaldo et al. 2009; Sousa et al. 2012), the cytochrome subunits of Group 1 [Ni-Fe]-hydrogenases (Pandelia et al. 2012) and *cd*<sub>1</sub>-type nitrite reductases

(van Lis et al. 2011). For the majority of these heme proteins, the reconstructed phylogenetic trees support their presence prior to the Archaea/Bacteria divergence and they have consequently been proposed to be “pre-LUCA” enzymes. For the case of the O<sub>2</sub>R/NOR superfamily, a controversy persists as to which of the subfamilies is the most ancient (Gribaldo et al. 2009 vs. Ducluzeau et al. 2014b) while all studies advocate the presence of ancestral members of the superfamily in the LUCA (as discussed in Ducluzeau et al. 2014a). For the case of the Rieske/cytb complexes, one article (Dibrova et al. 2013) challenges the conclusion on a pre-LUCA presence repeatedly arrived at over the last two decades (Castresana et al. 1995; Schütz et al. 2000; Lebrun et al. 2006; Ducluzeau et al. 2009; ten Brink et al. 2013) as well as most recently (Kao and Hunte 2014).

As we have pointed out in the past (Ducluzeau et al. 2014a), molecular phylogeny is prone to a number of methodological and database problems and the results obtained (i.e. the phylogenetic trees) from this approach represent likelihoods rather than certainties. With this caveat having been clearly stated, we would nevertheless hold that molecular phylogenies of heme-carrying proteins and enzymes are by and large in favour of the presence of heme proteins in the LUCA.

### C. The Dichotomy of Heme Biosynthesis Enzymes

Two distinct pathways have been found enabling prokaryotes to synthesize FePPIX (heme *b*) (Fig. 2.1). The earlier discovered pathway was elucidated mainly in crown-group proteobacteria (and in particular in *E. coli*) and in Firmicutes (Bacilli) (for a recent review, see Bali et al. 2014). More recently, a distinct pathway was discovered in sulphate-reducing  $\delta$ -proteobacteria (Ishida et al. 1998; Bali et al. 2011) and was shown to be abundant among Archaea (Bali et al. 2011). The earlier deciphered pathway is now frequently referred to as the

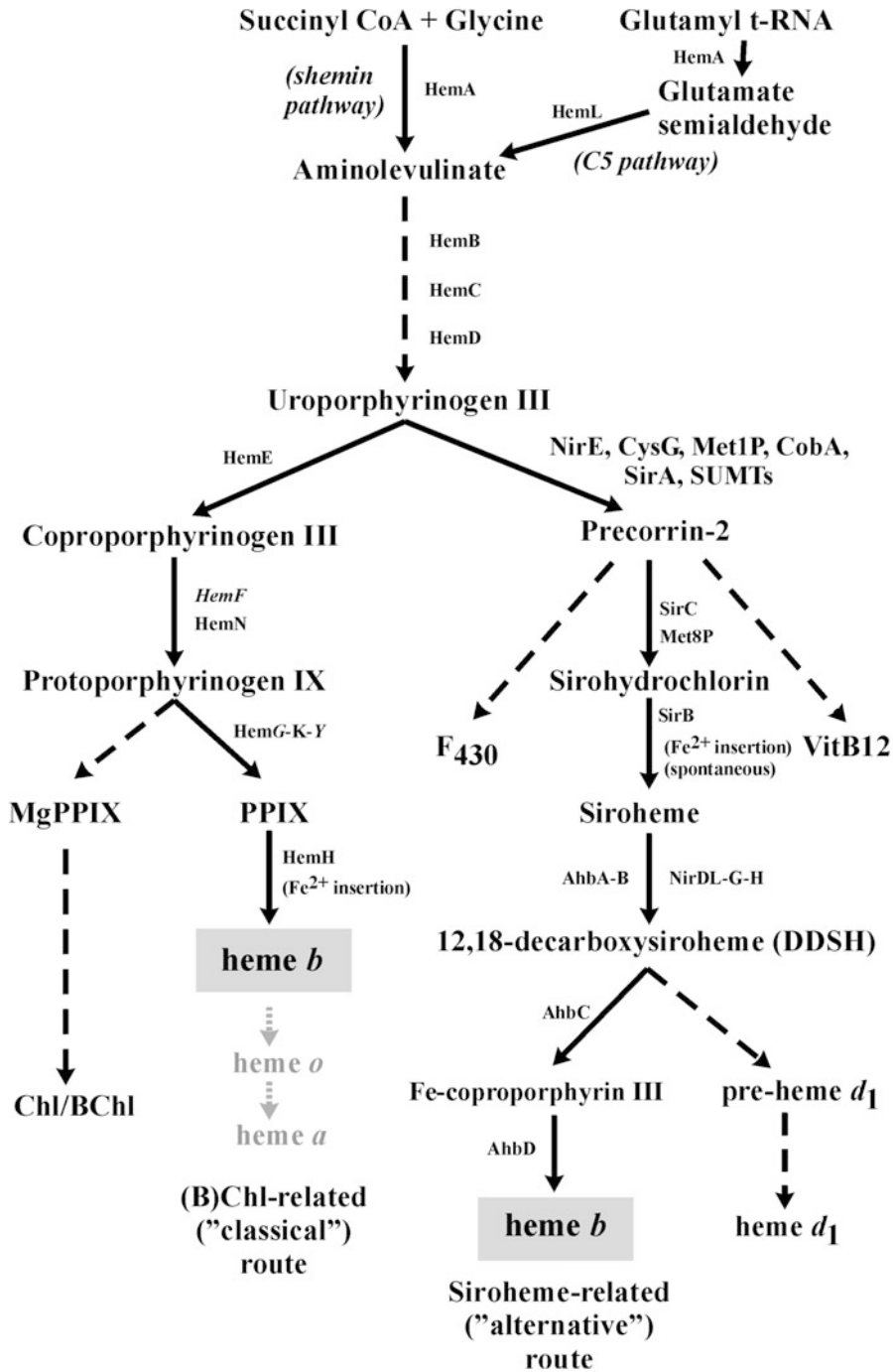


Fig. 2.1. Schematic representation of the two biosynthetic pathways yielding heme *b* and its close relatives together with their relationship to the biosynthesis routes for (B)Chl- and corrin-derived cofactors. Dashed arrows denote shortcuts summarising several consecutive steps. The corresponding enzymes catalysing specific conversions are marked next to the arrows. O<sub>2</sub>-dependent enzymes are highlighted in italics.

“classical” route (Bali et al. 2011, 2014). It is closely connected to the biosynthesis of (bacterio)chlorophylls and branches from the (bacterio)chlorophyll-pathways at the level of protoporphyrinogen IX (Fig. 2.1, left branch). The second route, now generally termed the “alternative heme biosynthesis” (Ahb-) pathway (Fig. 2.1, right branch), sequentially features corrins and sirohemes as intermediates on the way to heme *b* (Bali et al. 2011) rather than porphyrins as in the traditional pathway. Both routes share the common intermediate uroporphyrinogen III and all steps leading up to this compound (see Fig. 2.1).

### 1. Does the Existence of Two Distinct Pathways Necessarily Argue for an Anemic LUCA?

Several recent articles have interpreted the dichotomy of heme biosynthesis pathways as indicating that LUCA had not yet invented hemes and hence must have been devoid of heme-carrying enzymes (Lane and Martin 2012; Sousa et al. 2013; Sousa and Martin 2014). In the line of these authors’ argu-

ments, the fact that Archaea mainly synthesize hemes via the Ahb-pathway while the majority of Bacteria utilize the classical one, means that the two routes must have evolved independently, one in Archaea and the other one in Bacteria (Fig. 2.2a) and that the LUCA therefore must have operated on types of metabolism not calling upon the catalytic or electron transfer properties of hemes. An inventory of genes coding for enzymes involved in one or the other pathway over all available genomes (Sousa et al. 2013) confirmed the predominance of the Ahb-route in Archaea and the classical pathway in Bacteria. Exceptions to this rule detected in this study, some of which have already been pointed out previously (Bali et al. 2011), were taken to be due to HGT events.

The apparent overall correlation between type of prokaryotic domain and type of biosynthesis pathway certainly is intriguing. However, are these observations sufficient to unambiguously draw a conclusion about a heme-free LUCA? A number of general considerations and a few details of the pathways indicate that the story may be more complicated:

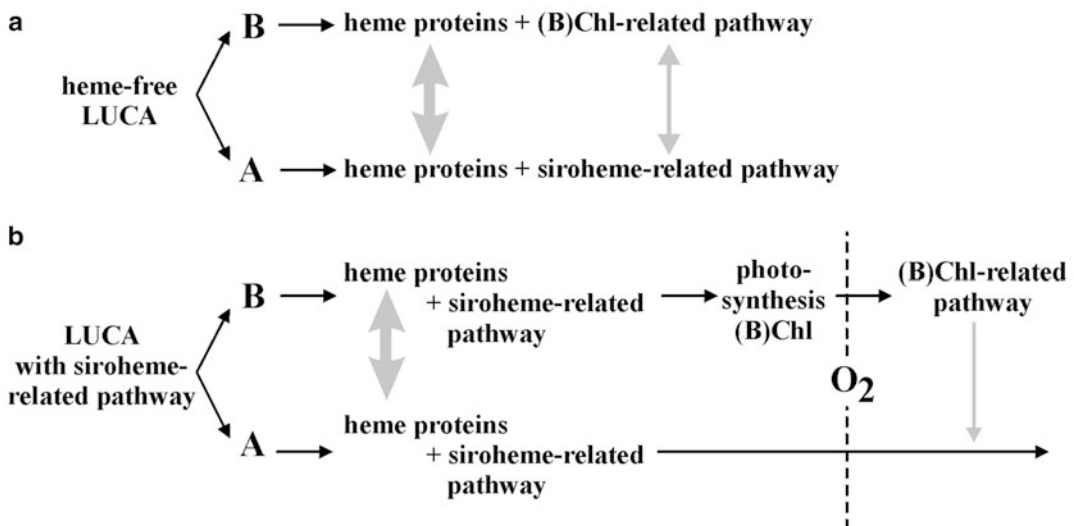


Fig. 2.2. Schematic representation of (a) the evolutionary scenario accounting for pathway dichotomy as proposed by Lane and Martin (2012), Sousa et al. (2013) and (b) our “alternative” model as described in the text. A and B stand for Archaea and Bacteria, respectively. The (B)Chl- and the siroheme-related pathways correspond to the “classical” and the “Ahb”-routes as defined by Bali et al. (2014), respectively.

- The Ahb-pathway appears substantially more widely distributed over both Archaea and Bacteria whereas the traditional pathway, abundant in several bacterial phyla, is only very rarely present in Archaea (see Fig. 7 in Sousa et al. 2013).
- The classical pathway is related to the synthesis of (B)Chl. In the past, the standard interpretation of this relationship was that (B)Chl synthesis evolved from the heme-biosynthetic pathway. This was based on the consideration that hemes are likely to be evolutionarily older than (B)Chls. Photosynthesis indeed appears to have originated “relatively” late within the bacterial domain (Baymann et al. 2001). This scenario appeared inevitable while the classical pathway was still thought to be life’s only way to make hemes, i.e. before the discovery of the Ahb route. The present picture of the topology of reaction schemes shown in Fig. 2.1, however, allows alternative, plausible scenarios. Given the existence of a parallel heme-biosynthesis pathway, the evolutionary sequence of a (B)Chl route growing out of an ancestral Ahb-pathway, and a second route for heme synthesis evolving only later as a derivative of the (B)Chl scheme, is at least as plausible as the original “(B)Chl-from-heme” model. The plausibility of this latter scenario is reinforced by the fact (Fig. 2.1) that the Ahb-pathway is part of the route providing not only heme *b* but also vitamin B<sub>12</sub>, siroheme, and cofactor F<sub>430</sub> (a molecule involved in crucial reaction steps of archaeal methanogenesis, Thauer et al. 2008). The credentials of a “good-for-everything” pathway as the more ancestral appear much stronger to us than those of a system specialized to making only heme *b* (plus *a* and *o*) such as the classical route. An analogous set of arguments has already been considered by Bali et al. (2014).
- Counting from their common precursor, that is, uroporphyrinogen III, the classical pathway goes through three major intermediates before reaching FePPIX (heme *b*) while the Ahb pathway passes through five such reaction intermediates.
- Intriguingly, the classical pathway features several steps which are dependent on the presence of O<sub>2</sub> (the respective enzymes are

denoted by italics in Fig. 2.1). In the absence of O<sub>2</sub>, alternative enzymes catalyse these conversions through chemically differing reaction schemes (for a review, see Bali et al. 2014).

### III. An Alternative Scenario

#### A. A Scenario Potentially Reconciling Molecular Phylogeny of Heme Enzymes and Pathway Dichotomy

In addition to the above detailed “independent and domain-inherent origins”-model, at least one additional distinct scenario is thus in principle possible. In this scenario, one of the two pathways would have been present in the LUCA and consequently been inherited by both Archaea and Bacteria. The other pathway would have been a later innovation featuring some kind of evolutionary advantage over the ancestral pathway. This novel pathway might have appeared either in Bacteria or in Archaea and then have supplanted the ancestral pathway in many species due to its evolutionary edge over the other route. An analogous sequence of events has, for example, been invoked to rationalize the evolutionary history of O<sub>2</sub>- and NO-reductases (Ducluzeau et al. 2014b).

In the light of the above listed pathway idiosyncrasies we will in the following tentatively outline a more detailed version of this alternative scenario of the evolutionary history of heme biosynthesis. In this scenario, the Ahb-pathway is the ancestral route for the biosynthesis of heme *b*, siroheme, Vit B<sub>12</sub>, F<sub>430</sub> and likely further related cofactors (Fig. 2.2b). This pathway was already present in the LUCA and operated under strictly anaerobic conditions which likely characterized the primordial planet. It was subsequently vertically inherited into both Archaea and Bacteria. At some point in evolutionary history, certainly prior to 2.5 billion years ago, i.e. prior to the GOE, certain Bacteria evolved photosynthesis with tetrapyrroles as light-responsive cofactors (in contrast

to archaeal photosynthesis which is based on light-induced conformational changes of opsins and which eventually gave “vision” to life). Optimization of tetrapyrrol-based photosynthesis towards higher absorption efficiency for solar photons in the wavelength window not filtered out by the atmosphere led to the emergence of the (B)Chl branch of Fig. 2.1. Hemes, by contrast, were still synthesized via the Ahb-route. The ultimate advent of non-negligible amounts of O<sub>2</sub> in the biosphere (Fig. 2.2b) induced by oxygenic photosynthesis (although probably only after a significant time lag due to geochemical buffering of the O<sub>2</sub> produced) allowed the emergence of a plethora of biochemical pathways making profitable use of the newly available, highly reactive and strongly oxidizing molecular oxygen (Raymond and Segrè 2006). Among them was an energetically more economical pathway for heme *b* biosynthesis. Since the oxygenic photosynthesizers likely were among the very first to encounter increasing levels of O<sub>2</sub>, it seems plausible that this novel heme biosynthesis pathway evolved within these species and was related to the (B)Chl route due to co-regulation. When O<sub>2</sub> had become pervasive in the biosphere (i.e. after 2.3 billion years ago), this pathway became strongly favourable even for non-O<sub>2</sub>-producers generating an evolutionary driving force for its dissemination towards other aerobic organisms throughout the prokaryotes. The Ahb-route was increasingly overgrown by the more modern “classical” pathway except in organisms that remained confined to the shrinking anaerobic niches and never ventured out into oxygenated environments. Aerobic species having entirely lost the Ahb-route, however, were obliged to develop alternative O<sub>2</sub>-independent enzymes if they were to recolonise O<sub>2</sub>-poor or anaerobic habitats, which rationalizes the presence of O<sub>2</sub>-dependent and O<sub>2</sub>-independent enzymes at certain biosynthesis steps in the (B)Chl-related pathway (Fig. 2.1).

The wording of the preceding paragraph highlights the psychological hurdles entailed

by the current pathway nomenclature. Referring to a “classical” and an “alternative” route subliminally opposes the notion that the “alternative” pathway might have been THE ancestral route while the “classical” one might in fact represent the actual alternative route that had emerged only at a later time. As will be discussed below, the same nomenclature scheme is in use in the field of menaquinone biosynthesis (Hiratsuka et al. 2008). We do think that it is time to adopt less suggestive terms to identify these pathways. For obvious reasons (see Fig. 2.1), we propose the terms “(B)Chl-related pathway” for the “classical” route and “siroheme-related pathway” for the “alternative” one. We have used this scheme to denote pathways in Fig. 2.2.

It seems obvious to us that both the above sketched “heme-free-LUCA” and the “Ahb-in-LUCA” scenarios are generally in line with presently available evidence. To decide between these two alternatives, global phylogenies of enzymes involved in all (i.e. encompassing heme-, (B)Chl-, siroheme-) biosynthesis pathways are required. Such a study would represent an impressive and highly time-consuming task, but we would argue that it will be indispensable for progressing on the question of the evolutionary history of hemes and heme proteins.

### *B. Is the Heme-Biosynthesis-Pathway Dichotomy Related to Other Major Pathway Dichotomies?*

The scenario of an Ahb-pathway in the LUCA which was later outcompeted (likely after the onset of oxygenic photosynthesis some 2.7 billion years ago) by a more recently emerged system was stimulated by the fact that several other intriguingly analogous pathway dichotomies may find an explanation in the same manner. Two prominent ones are those of the menaquinone- and the iron-sulphur cluster biosynthesis systems. Menaquinones (MK), likely the most ancestral of respiratory quinones (Schoepp-Cothenet et al. 2009, 2013) are



synthesized in prokaryotes via two distinct routes, i.e. the (once again) “classical” Men-pathway (predominantly studied in *E. coli* (Bentley and Meganathan 1983) and the “alternative” futasine-pathway (Hiratsuka et al. 2008). The dichotomy of MK-biosynthetic routes has been argued to again indicate the absence of quinones in the LUCA (Lane and Martin 2012; Sousa et al. 2013). Phylogenies of several enzymes involved in both pathways have been reconstructed and appear to show that the futasine pathway is more ancestral than the Men-route (Zhi et al. 2014). However, when it comes to deciding whether the futasine pathway was present in the LUCA, the published data so far are inconclusive. Phylogenetic tree reconstruction based on different algorithms yields divergent results and no clear answer is therefore possible at present.

A further pathway dichotomy has been found for iron-sulphur cluster biosynthesis. The quite distinct “Isc”- and “Suf”- pathways are scattered over the realm of the prokaryotes with some species containing either one or the other, while others use both pathways differentially as a function of growth conditions and predominantly of oxidative stress (Roche et al. 2013). To the best of our knowledge, no detailed and evolutionarily deep molecular phylogenies of the involved enzymes have been reported so far. However, while heme- and quinone-biosynthesis may indeed be argued to have been absent from the LUCA, we would hold that an iron-sulphur-cluster-free LUCA does not figure in any of the presently proposed scenarios. Parallel, independent, origins of the Isc- and Suf-systems in Archaea and Bacteria, as proposed by Lane and Martin (2012) for heme and quinone biosynthesis, therefore seem highly unlikely. Both in the Fe-S and in the MK-biosynthesis pathways, O<sub>2</sub>-dependent/resistant enzymes are asymmetrically distributed and seem to be more frequent in the Men- and the Suf-routes. Since Fe-S centres are highly O<sub>2</sub>-labile, it seems more likely to us that emergence of an “aerobic” system (likely the Suf-pathway) was

driven by the need to harden the Fe-S-cluster transporting biosynthesis enzymes against the deleterious effects of O<sub>2</sub> rather than by favourable O<sub>2</sub>-mediated biosynthetic steps.

The occurrence of all these pathway dichotomies therefore may well indicate the late origins of O<sub>2</sub>-dependent routes supplanting anaerobic ones instead of the independent emergences of two pathways in Archaea and Bacteria, respectively. We have proposed in the past that a very similar scenario perfectly rationalizes the convoluted evolutionary history of O<sub>2</sub>- and NO-reductases (Ducluzeau et al. 2014). The advent of molecular O<sub>2</sub> on planet Earth certainly represented one of the most profound geochemical revolutions of the environment. It seems to make perfect sense to us that the appearance of the novel and powerful reactant O<sub>2</sub> would drive the emergence of pathways that reap benefits from the opportunity of unprecedented reaction schemes. If the mentioned pathway dichotomies should indeed reflect the late emergence of O<sub>2</sub>-related systems, a better understanding of the source organisms, i.e., the species wherein these novel pathways emerged, will substantially further our understanding of life’s ways to weather the biochemical turmoil that must have been associated with the GOE.

#### IV. Why All the Fuzz?

The controversy concerning the detailed evolutionary scenario accounting for the origin of heme cofactors may appear purely academic and of interest only to a very restricted community of molecular phylogeny geeks. However, as we have discussed recently (Ducluzeau et al. 2014a), the resolution to this problem will have substantial consequences for our understanding of energy conversion at the origin of life. Approaches attempting to retrodict bioenergetic mechanisms operating in the LUCA from what we see in extant life to our mind represents a much more “empirical” way to study the origin of life than the conceiving of “*ab-initio*” hypotheses based

solely on chemical and geochemical plausibility arguments (discussed in Schoepp-Cothenet et al. 2013). A scenario remarkably successful in rationalizing the emergence of chemiosmotic free energy conversion, while being perfectly in agreement with thermodynamic requirements, was proposed by Martin and Russell (2003, 2007) as a biochemical incarnation of the seminal hypothesis stipulating alkaline hydrothermal vents as the cradle of life (Russell and Hall 1997). This scenario stipulates Wood-Ljungdahl-type energy conversion (Martin and Russell 2007) and carbon fixation as the ancestral types of metabolism in the LUCA and inorganic versions thereof back to the very origin of life. The Wood-Ljungdahl pathways mainly rely on Fe-S- and Ni-containing cofactors for catalysis but are devoid of quinones and hemes (Lane and Martin 2012). More recently, a variant of this scenario was proposed based on a re-evaluation of the inventory of likely redox substrates present in presumed locales for life's origin (Nitschke and Russell 2013). This scenario still maintains the importance of catalytic steps featuring in the Wood-Ljungdahl pathway (if partially in the reverse direction of catalysis), but adds an oxidative branch resembling anaerobic respiration necessarily implicating quinones and hemes. Whereas the first scenario stipulates only H<sub>2</sub> and CO<sub>2</sub> as providing the environmental redox disequilibrium which drove the emergence of life, the second one envisages a wider cocktail of substrates involving at least H<sub>2</sub> and CH<sub>4</sub> as reductants and CO<sub>2</sub>, nitrate, nitrite and potentially Fe<sup>3+</sup>, Mn<sup>4+</sup> etc. (Russell et al. 2014) as oxidants resulting in a substantially stronger and multifaceted environmental redox disequilibrium tapped by nascent life. Whereas quinones and hemes are conceivable in the LUCA, they are more difficult to envisage at life's very origin. Inorganic metal-complexes able to have played the roles later taken over by quinones and hemes have therefore been proposed (Nitschke et al. 2013). However, if the LUCA had been devoid of hemes and quinones altogether, the types of energy metabolism pro-

posed to have fuelled the LUCA in the more recent scenario (Nitschke and Russell 2013) are precluded and by extension have little chance of having operated at life's origin.

The question whether the LUCA was red or "anemic" therefore by far exceeds the mere evolutionary history of heme proteins and has crucial repercussions for our understanding of life's origin.

## Acknowledgments

We thank Shilpa Bali (Oxford/UK) for stimulating discussions and for providing manuscripts prior to publication. We furthermore are grateful to Mike Russell (Pasadena/USA) and Bill Cramer (Purdue/USA) for critical reading of our manuscript. Innumerable stimulating discussions with Barbara Schoepp-Cothenet and Frauke Baymann (both Marseille/France) are gratefully acknowledged. ALD is supported by the Moore Foundation and by NSF's Division of Polar Programs (grant number 1203262).

## References

- Bali S, Lawrence AD, Lobo SA, Saraiva LM, Golding BT, Palmer DJ, Howard MJ, . . . , Warren MJ (2011) Molecular hijacking of siroheme for the synthesis of heme and d1 heme. *Proc Natl Acad Sci USA* 108:18260–18265
- Bali S, Palmer DJ, Schroeder S, Ferguson SJ, Warren MJ (2014) Recent advances in the biosynthesis of modified tetrapyrroles: the discovery of an alternative pathway for the formation of heme and heme d<sub>1</sub>. *Cell Mol Life Sci* 71:2837–2863
- Baymann F, Brugna M, Mühlenhoff U, Nitschke W (2001) Daddy, where did (PS) I come from? *Biochim Biophys Acta Bioenerg* 1507:291–310
- Baymann F, Lebrun E, Brugna M, Schoepp-Cothenet B, Giudici-Orticoni M-T, Nitschke W (2003) The redox protein construction kit: pre last universal common ancestor evolution of energy-conserving enzymes. *Philos Trans R Soc Lond B Biol Sci* 358:267–274
- Bentley R, Meganathan R (1983) Biosynthesis of vitamin K (menaquinone) in bacteria. *Microbiol Rev* 46:241–280

- Branscomb E, Russell ML (2013) Turnstiles and bifurcators: the disequilibrium converting engines that put metabolism on the road. *Biochim Biophys Acta Bioenerg* 1827:62–78
- Brochier-Armanet C, Talla E, Gribaldo S (2009) The multiple evolutionary histories of dioxygen reductases: implications for the origin and evolution of aerobic respiration. *Mol Biol Evol* 26:285–297
- Castresana J, Lübben M, Saraste M (1995) New archaeobacterial genes coding for redox proteins: implications for the evolution of aerobic metabolism. *J Mol Biol* 250:202–210
- Cutruzzola F, Arcovito A, Giardina G, della Longa S, D'Angelo P, Rinaldo S (2014) Distal-proximal crosstalk in the heme binding pocket of the NO sensor DNR. *Biomaterials* 27:736–773
- Dibrova DV, Cherepanov DA, Galperin MY, Skulachev VP, Mulikidjanian AY (2013) Evolution of cytochrome *bc* complexes: from membrane-anchored dehydrogenases of ancient bacteria to triggers of apoptosis in vertebrates. *Biochim Biophys Acta Bioenerg* 1827:1407–1427
- Ducluzeau A-L, van Lis R, Duval S, Schoepp-Cothenet B, Russell MJ, Nitschke W (2009) Was nitric oxide the first strongly oxidizing terminal electron sink? *Trends Biochem Sci* 34:9–15
- Ducluzeau A-L, Schoepp-Cothenet B, Baymann F, Russell MJ, Nitschke W (2014a) Free energy conversion in the LUCA: Quo vadis? *Biochim Biophys Acta Bioenerg* 1837:982–988
- Ducluzeau A-L, Schoepp-Cothenet B, van Lis R, Baymann F, Russell MJ, Nitschke W (2014b) The evolution of the respiratory O<sub>2</sub>/NO reductases; an out-of-the-phylogenetic-box perspective. *J R Soc Interface* 11:20140196
- Eck RV, Dayhoff MO (1966) Evolution of the structure of ferredoxin based on living relics of primitive amino acid sequences. *Science* 152:363–366
- Grein F, Ramos AR, Venceslau SS, Pereira IAC (2013) Unifying concepts in anaerobic respiration: insights from dissimilatory sulfur metabolism. *Biochim Biophys Acta Bioenerg* 1827:145–160
- Gribaldo S, Talla E, Brochier-Armanet C (2009) Evolution of the haem copper oxidases superfamily: a rooting tale. *Trends Biochem Sci* 34:375–381
- Grimaldi S, Cécaldi P, Schoepp-Cothenet B, Guigliarelli B, Magalon A (2013) The prokaryotic Mo/W-bisPGD enzymes family: a catalytic workhorse in bioenergetics. *Biochim Biophys Acta Bioenerg* 1827:1048–1085
- Hiratsuka T, Furihata K, Ishikawa J, Yamashita H, Itoh N, Seto H, Dairi T (2008) An alternative menaquinone biosynthetic pathway operating in microorganisms. *Science* 321:1670–1673
- Ishida T, Yu L, Akutsu H, Ozawa K, Kawanishi S, Seto A, Inubushi T, Sano S (1998) A primitive pathway of porphyrin biosynthesis and enzymology in *D. vulgaris*. *Proc Natl Acad Sci USA* 95:4853–4858
- Kao W-C, Hunte C (2014) The molecular evolution of the Qo motif. *Genome Biol Evol* 6:1894–1910
- Lane N, Martin WF (2012) The origin of membrane bioenergetics. *Cell* 151:1406–1416
- Lebrun E, Santini JM, Brugna M, Ducluzeau A-L, Ouchane S, Schoepp-Cothenet B, Baymann F, Nitschke W (2006) The Rieske protein: a case study on the pitfalls of multiple sequence alignments and phylogenetic reconstruction. *Mol Biol Evol* 23:1180–1191
- Lemos RC, Fernandes AS, Pereira MM, Gomes CM, Teixeira M (2002) Quinol:fumarate oxidoreductases and succinate:quinone oxidoreductases: phylogenetic relationships, metal centres and membrane attachment. *Biochim Biophys Acta Bioenerg* 1553:158–170
- Martin W, Russell MJ (2003) On the origins of cells: a hypothesis for the evolutionary transitions from abiotic geochemistry to chemoautotrophic prokaryotes, and from prokaryotes to nucleated cells. *Philos Trans R Soc Lond B Biol Sci* 358:59–83
- Martin WF, Russell MJ (2007) On the origin of biochemistry at an alkaline hydrothermal vent. *Philos Trans R Soc Lond B Biol Sci* 362:1887–1925
- Martinkova M, Kitanishi K, Shimizu T (2013) Heme-based globin-coupled oxygen sensors: linking oxygen binding to functional regulation of diguanylate cyclase, histidine kinase and methyl-accepting chemotaxis. *J Biol Chem* 288:27702–27711
- Nelson-Sathi S, Dagan T, Landan G, Janssen A, Steel M, McInerney JO, Deppenmeier U, Martin WF (2012) Acquisition of 1,000 eubacterial genes physiologically transformed a methanogen at the origin of Haloarchaea. *Proc Natl Acad Sci USA* 109:20537–20542
- Nitschke W, Russell MJ (2013) Beating the acetyl-CoA pathway to the origin of life. *Philos Trans R Soc Lond B Biol Sci* 368:20120258
- Nitschke W, McGlynn S, Milner-White J, Russell MJ (2013) On the antiquity of metalloenzymes and their substrates in bioenergetics. *Biochim Biophys Acta Bioenerg* 1827:871–881
- Pandelia ME, Lubitz W, Nitschke W (2012) Evolution and diversification of Group 1 [NiFe] hydrogenases. Is there a phylogenetic marker for O<sub>2</sub> tolerance? *Biochim Biophys Acta Bioenerg* 1817:1565–1575

- Partin CA, Bekker A, Planavsky NJ, Scott CT, Gill BC, Li C, Podkovyrov V, . . . , Lyons TW (2013) Large-scale fluctuations in Precambrian atmosphere and oceanic oxygen levels from the record of U in shales. *Earth Planet Sci Lett* 369–370:284–293
- Pereira MM, Santana M, Teixeira M (2001) A novel scenario for the evolution of haem-copper oxygen reductases. *Biochim Biophys Acta Bioenerg* 1505:185–208
- Pokkuluri PR, Pessanha M, Londer YY, Wood SJ, Duke NEC, Wilton R, Catarino T, . . . , Schiffer M (2008) Structures and solution properties of two novel periplasmic sensor domains with c-type heme from chemotaxis proteins of *Geobacter sulfurreducens*: implications for signal transduction. *J Mol Biol* 377:1498–1517
- Raymond J, Segrè D (2006) The effect of oxygen on biochemical networks and the evolution of complex life. *Science* 311:1764–1767
- Roche B, Aussenl, Ezraty B, Mandin P, Py B, Barras F (2013) Iron/sulfur proteins biogenesis in prokaryotes: formation, regulation and diversity. *Biochim Biophys Acta Bioenerg* 1827:455–469
- Russell MJ, Hall AJ (1997) The emergence of life from iron-monosulphide bubbles at a submarine hydrothermal redox and pH front. *J Geol Soc Lond* 154:377–402
- Russell MJ, Barge LM, Bhartia R, Bocanegra D, Bracher PJ, Branscomb E, Kidd R, . . . , Kanik I (2014) The drive to life on wet and icy worlds. *Astrobiology* 14:308–343
- Schoepp-Cothenet B, Lieutaud C, Baymann F, Verméglio DD, Friedrich T, Kramer DM, Nitschke W (2009) Menaquinone as pool quinone in a purple bacterium. *Proc Natl Acad Sci USA* 106: 8549–8554
- Schoepp-Cothenet B, van Lis R, Philippot P, Magalon A, Russell MJ, Nitschke W (2012) The ineluctable requirement for the trans-iron elements molybdenum and/or tungsten in the origin of life. *Sci Rep* 2:263
- Schoepp-Cothenet B, van Lis R, Atteia A, Baymann F, Capowiez L, Ducluzeau A-L, Duval S, . . . , Nitschke W (2013) On the universal core of bioenergetics. *Biochim Biophys Acta Bioenerg* 1827:79–93
- Schütz M, Brugna M, Lebrun E, Baymann F, Huber R, Stetter K-O, Hauska G, . . . , Nitschke W (2000) Early evolution of cytochrome bc complexes. *J Mol Biol* 300:663–675
- Sousa FL, Alves RJ, Ribeiro MA, Pereira-Leal JB, Teixeira M, Pereira MM (2012) The superfamily of heme-copper oxygen reductases: types and evolutionary considerations. *Biochim Biophys Acta Bioenerg* 1817:629–637
- Sousa FL, Thiergart T, Landan G, Nelson-Sathi S, Pereira IA, Allen JF, Lane N, Martin WF (2013) Early bioenergetic evolution. *Phil Trans R Soc London* 368:1622
- Sousa FL, Martin WF (2014) Biochemical fossils of the ancient transition from geoenergetics to bioenergetics in prokaryotic one carbon compound metabolism. *Biochim Biophys Acta, Bioenerg* 1837:964–981
- Suzuki T, Imai K (1998) Evolution of myoglobin. *Cell Mol Life Sci* 54:979–1004
- ten Brink F, Schoepp-Cothenet B, van Lis R, Nitschke W, Baymann F (2013) Multiple Rieske/cytb complexes in a single organism. *Biochim Biophys Acta Bioenerg* 1827:1392–1406
- Thauer RK, Kaster AK, Sedorf H, Buckel W, Hedderich R (2008) Methanogenic archaea: ecologically relevant differences in energy conservation. *Nat Rev Microbiol* 6:579–591
- van Lis R, Ducluzeau A-L, Nitschke W, Schoepp-Cothenet B (2011) The nitrogen cycle in the Archaean; an intricate interplay of enzymatic and abiotic reactions. In: Moir JWB (ed) *Nitrogen Cycling in Bacteria: Molecular Analysis*. Caister Academic, Norfolk, pp 1–21
- Vignais PM, Billoud B, Meyer J (2001) Classification and phylogeny of hydrogenases. *FEMS Microbiol Rev* 25:455–501
- Zhi X-Y, Yao J-C, Tang S-K, Huang Y, Li H-W, Li W-J (2014) The futasoline pathway played an important role in menaquinone biosynthesis during early prokaryote evolution. *Genome Biol Evol* 6: 149–160
- Zuckermandl E, Pauling L (1965) Molecules as documents of evolutionary history. *J Theor Biol* 8: 357–366

# Chapter 3

## The Diversity of Photosynthetic Cytochromes

Erica L.-W. Majumder and Robert E. Blankenship\*  
*Department of Chemistry, and Department of Biology,  
Washington University, Brookings Dr., Campus Box, 1134,  
St. Louis, MO 63130, USA*

Summary.....	25
I. Introduction.....	26
II. Cytochromes in Anoxygenic Photosynthetic Electron Transport Chains.....	26
A. Cytochromes in Type I and II Reaction Centers.....	27
1. Cytochromes in Type I Reaction Centers.....	28
2. Cytochromes in Type II Reaction Centers.....	32
B. Cytochromes in <i>bc</i> Complexes.....	34
1. Cytochrome <i>bc</i> <sub>1</sub> Complex.....	35
2. Cytochrome <i>bc</i> Complexes.....	36
3. Alternative Complex III.....	38
C. Soluble Cytochromes in Anoxygenic Cyclic Electron Transport.....	39
III. Cytochromes in Oxygenic Photosynthetic Electron Transport Chains.....	40
A. Cytochromes in Photosystems I and II.....	40
1. Photosystem I.....	41
2. Photosystem II.....	41
B. Cytochromes in <i>b<sub>6</sub>f</i> Complexes.....	42
C. Soluble Cytochromes in Oxygenic Cyclic Electron Transport.....	43
IV. Conclusions.....	44
Acknowledgments.....	44
References.....	44

### Summary

This chapter explores the myriad of cytochromes involved in the photosynthetic process that generates the most energy and oxygen on Earth. All photosynthetic organisms rely on cytochromes to move electrons around the cell and drive the photosynthetic mechanism. Although cytochromes have many jobs in many environments, only a few types of cytochromes are involved in these electron transport chains. The hemes vary in axial ligation to meet the needs and reduction potential of each specific role. Some cytochromes

---

\*Author for correspondence, e-mail: [Blankenship@wustl.edu](mailto:Blankenship@wustl.edu)

diverge from the typical alpha helical structure, such as cytochrome *f* with beta sheet secondary structure. Whether in membranes or in the cytoplasm, diverse cytochromes keep photosynthesis pumping in many ecosystems.

## I. Introduction

The photosynthetic process, in both anoxygenic and oxygenic phototrophs, is the major producer of available energy on Earth. Photosynthesis converts sunlight into stable chemical energy through a series of excitation energy transfer, electron transfer and enzymatic steps (Blankenship 2014). Proteins in the cells perform these functions, and the activity is often centered on the metal atom housed in the proteins. A major class of electron transport metalloproteins ubiquitous across the tree of life is cytochrome proteins. Cytochrome proteins contain at least one heme molecule and move electrons via redox reactions. Phototrophic organisms use cytochromes as subunits in membrane protein complexes as well as free soluble proteins to transfer electrons around the cell (Cramer and Whitmarsh 1977).

Phototrophs belong to taxa from the smallest bacteria up through the giant redwood trees. The first photosynthetic organisms were bacteria. Bacterial phyla that contain phototrophic representatives include: Green Sulfur Bacteria, Purple Bacteria, Heliobacteria, Chloroacidobacteria, Cyanobacteria, Filamentous Anoxygenic Phototrophs and Gemmatimonadetes (Blankenship 2014; Zeng et al. 2014). All of these except cyanobacteria carry out anoxygenic (non-oxygen-evolving) photosynthesis. Cyanobacteria developed the

ability to perform oxygenic photosynthesis, and the cyanobacteria were the source of the chloroplast of photosynthetic eukaryotes by endosymbiosis (Margulis 1992). Eukaryotic phototrophs range from algae to plants of all sorts. Cytochromes persisted in the evolutionary jump from anoxygenic to oxygenic photosynthesis because, in order to accommodate the new surroundings, the organisms incorporated different types of cytochromes into the photosynthetic machinery including both *b* and *c* type cytochromes (Moore and Pettigrew 1990) (Fig. 3.1a, b). Table 3.1 summarizes all of the cytochromes discussed in this chapter in the order of appearance.

## II. Cytochromes in Anoxygenic Photosynthetic Electron Transport Chains

The earliest forms of bacterial photosynthesis emerged before the presence of oxygen in the Earth's atmosphere. These pioneering organisms found a way to use solar energy to drive cellular processes without oxygen as an electron source (Blankenship 2010). Anoxygenic phototrophs continue to thrive today in extreme or niche environments such as the under-layers of microbial mats, sulfur springs or deep sea hydrothermal vents (Lau and Pointing 2009) because they utilize a variety of electron sources and electron shuttles (Meyer and Donohue 1995; Ritchie and Runcie 2012). This variety of electron donors and acceptors is seen in Fig. 3.1a. The basic components of a photosynthetic electron transport chain, whether anoxygenic or oxygenic, are a light harvesting antenna, a pigment-protein reaction center, a proton pumping complex, intermembrane electron shuttles and soluble

---

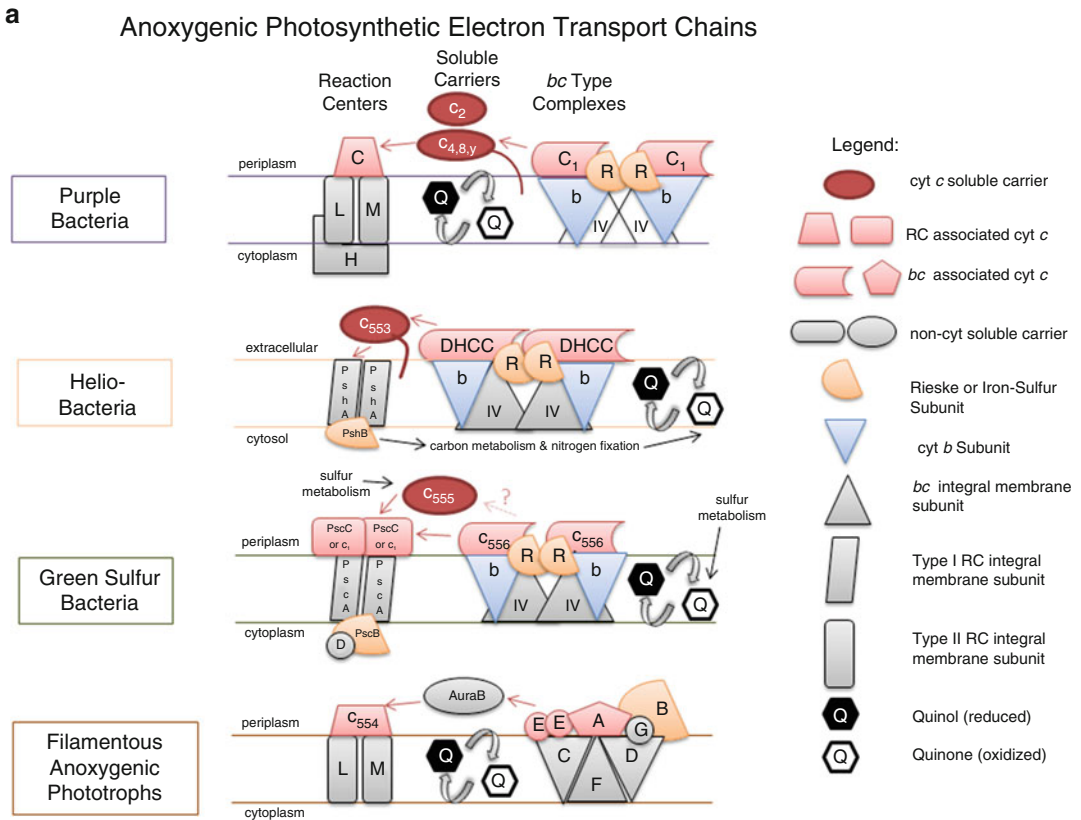
*Abbreviations:* ACIII – Alternative Complex III; CEF – Cyclic Electron Flow; CF<sub>X</sub> – *Chloroflexus aurantiacus*; cyt – Cytochrome; ETC – Electron Transport Chain; FAP – Filamentous Anoxygenic Phototroph; GSB – Green Sulfur Bacteria; LEF – Linear Electron Flow; OEC – Oxygen Evolving Complex; PB – Purple Bacteria; PSI – Photosystem I; PSII – Photosystem II; Q<sub>i</sub> – Quinone Reduction Site; Q<sub>o</sub> – Quinone Oxidation Site; RC – Reaction Center; RFX – *Roseiflexus castenholzii*

electron carriers. As explored throughout this chapter, cytochromes form key subunits of the reaction center and proton pumping complexes. They are also the most common form of soluble electron carrier used. Intermembrane carriers are quinols or other small molecules. Anoxygenic phototrophs rely on a diverse collection of cytochromes to survive in their challenging environments.

**A. Cytochromes in Type I and II Reaction Centers**

The Reaction Center (RC) is the pigment-protein complex to which excitation energy is transferred to drive charge separation, thereby converting solar energy into redox

free energy. The primary charge separation process is carried out by pigments, known as the special pair, and does not involve cytochromes in the primary process. Cytochromes, however, function in RCs to reduce the pigments after the primary electron transfer (Parson 1968). RCs are classified into type I and type II as determined by their final electron acceptors, and the iron sulfur clusters or quinones that they carry, respectively, but are thought to all have a common ancestor (Hohmann-Marriott and Blankenship 2011). The cytochromes associated with type I and type II RCs in anoxygenic phototrophs are found on the periplasmic side of the RC and have the function of special pair re-reduction.



*Fig. 3.1.* Photosynthetic electron transport chains. Schematics of electron transport chains in representative families of (a) anoxygenic and (b) oxygenic photosynthetic organisms. Legend is included in part A. Arrows represent the flow of electrons. Cytochrome and FeS subunits are in color and labeled with their common name, see Table 3.1 for full names.

b

## Oxygenic Photosynthetic Electron Transport Chains

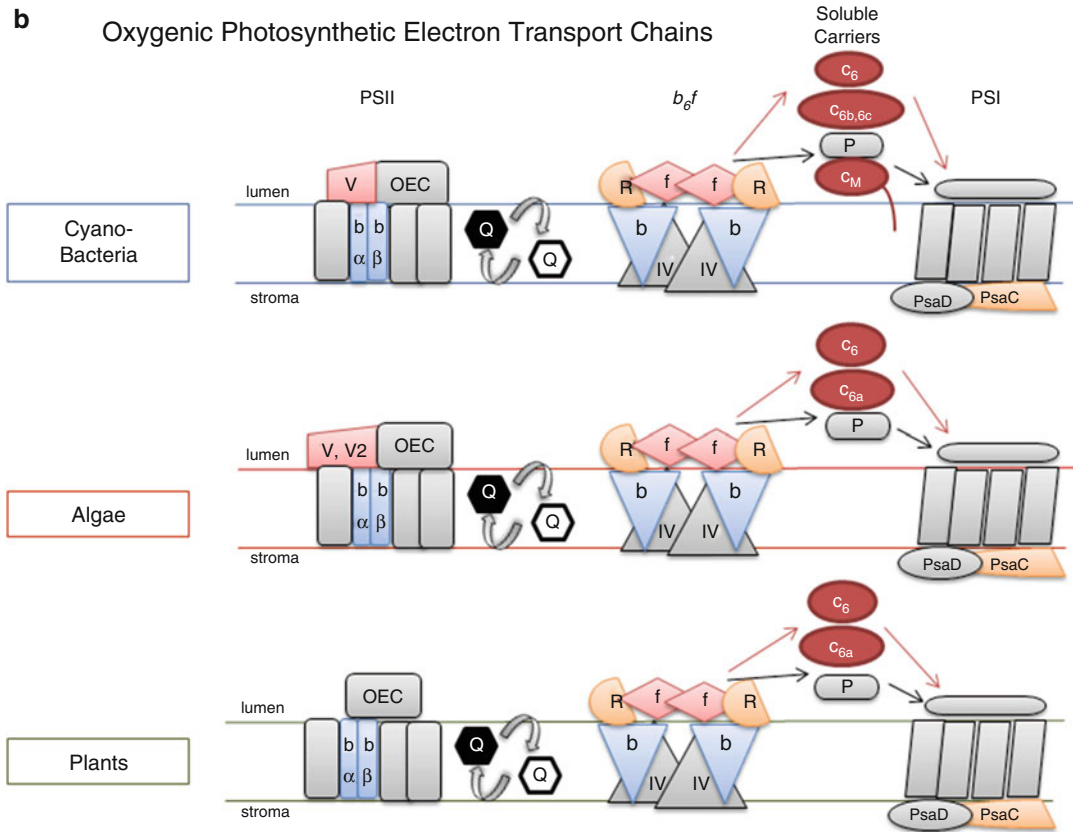


Fig. 3.1. (continued)

### 1. Cytochromes in Type I Reaction Centers

Prokaryotic anoxygenic type I photosynthetic Reaction Centers are found in Green Sulfur Bacteria (GSB), Chloroacidobacteria and Heliobacteria (Azai et al. 2010). Type I RC's exist as homodimers and are more primitive than their oxygenic counterparts, appearing early in the evolution of photosynthesis (Williamson et al. 2011). Light energy striking the special pair pigments, P800 or P840, causes charge separation and subsequent electron transfer through the RC iron-sulfur clusters, designated Fe-S<sub>x</sub>, Fe-S<sub>A</sub>, and Fe-S<sub>B</sub>, to a soluble carrier, typically a member of the ferredoxin family, small iron-sulfur cluster proteins. The *c*-type monoheme cytochrome *c<sub>Z</sub>* of Green Sulfur Bacteria and *c<sub>553</sub>* of Heliobacteria

function in the periplasm to re-reduce the special pair bacteriochlorophylls after charge separation has occurred (Oh-oka et al. 1998; Azai et al. 2010). While performing the same basic function, the differences of these two monoheme *c*-type cytochromes represent the diversity of anoxygenic type I RC associated cytochromes.

For GSB, the RC associated cytochrome is *c<sub>Z</sub>*, also known as PscC or by its absorption peak *c<sub>551</sub>*. Formal identification of *c<sub>Z</sub>* spanned several decades from initial observation in the 1970s by membrane flash kinetics to more sophisticated techniques in the 1990s (Fowler et al. 1971; Prince and Olson 1976; Okkels et al. 1992; Oh-oka et al. 1995). Cyt *c<sub>Z</sub>* is held in place with three N-terminal helices that anchor the cytochrome to the RC complex. This three helix structure on the N-terminus is unique among cytochromes and



Table 3.1. Representative cytochromes in photosynthesis.

Cytochrome	Other names	Major organism Family/ies	Location in cell & attachment	Complex or Shuttle	Function	Special features
<i>c<sub>z</sub></i>	PscC, <i>c<sub>551</sub></i>	GSB	Periplasm, n complex	T1 RC	Re-reduce special pair	Interacts with <i>c<sub>555</sub></i> & <i>c<sub>556</sub></i>
<i>c<sub>553</sub></i>	PetJ	Helio	Periplasm, soluble/complex, anchor	T1 RC	<i>bc</i> to RC	Anchor tail, direct reduces special pair
<i>c<sub>554</sub></i>	tetraheme <i>cyt c</i> , RC <i>cyt c</i>	PB, FAP	Periplasm, in complex	T2 RC	Re-reduce special pair	Surprise in crystal structure, uphill energy transfer
Cyt <i>b</i> anoxy	<i>b<sub>H</sub></i> & <i>b<sub>L</sub></i> , <i>b<sub>p</sub></i> & <i>b<sub>n</sub></i> , <i>b<sub>O</sub></i> & <i>b<sub>i</sub></i>	All	Integral membrane	<i>bc</i>	Q cycle	Helio version is PsbE precursor
<i>c<sub>1</sub></i>		PB & mitochondria	Periplasm, in complex	<i>bc<sub>1</sub></i>	Rieske to soluble acceptor	Interacts with far moving Rieske
DHCC	diheme	Helio	Periplasm, in complex	<i>bc</i>	Rieske to soluble acceptor	Has two hemes
<i>c<sub>556</sub></i>		GSB	Periplasm, in complex	<i>bc</i>	Rieske to soluble acceptor	Can directly interact with <i>cz</i>
ActA	pentaheme	FAP	Periplasm, in complex	ACIII	FeS to soluble acceptor	has five hemes
ActE	monoheme	FAP	Periplasm, in complex	ACIII	FeS to soluble acceptor	Two copies of the subunit
<i>c<sub>2</sub></i>		PB	Periplasm, soluble	shuttle	<i>bc</i> to RC	Rapid kinetics
<i>c<sub>y</sub></i>		PB	Periplasm, soluble, anchor	shuttle	<i>bc</i> to RC	Alternative <i>c<sub>2</sub></i> , anchor tail
<i>c<sub>4</sub></i>		PB	Periplasm, soluble	shuttle	<i>bc</i> to RC	Alternative <i>c<sub>2</sub></i>
<i>c<sub>8</sub></i>		PB	Periplasm, soluble	shuttle	<i>bc</i> to RC	Alternative <i>c<sub>2</sub></i>
<i>c'</i>	CycP	Anoxygenic	Soluble	De-nitrication	Binds NO & CO	Sequence similarities to <i>c<sub>556</sub></i>
<i>c<sub>555</sub></i>	CycA	GSB	Periplasm, soluble	shuttle	<i>bc</i> to RC	Can be reduced by sulfur metabolism
<i>b<sub>559</sub></i>	PSII <i>cyt b</i> , PsbE&F	Oxygenic	Integral membrane	PSII	unknown	$\alpha$ & $\beta$ with heme bridged, 4 potentials

(continued)

Table 3.1. (continued)

Cyto-chrome	Other names	Major organism Family/ies	Location in cell & attachment	Complex or Shuttle	Function	Special features
V	PsbV, cyt <i>c</i> <sub>550</sub>	Cyano, red algae	Lumen, in complex	PSII	Ion gating	Near OEC
V2	PsbV2	Cyano, red algae	Lumen, in complex	PSII	Replace V under stress	Alternative to PsbV, His/Cys axial ligation
Cyt <i>b</i> oxy	<i>b</i> <sub>H</sub> & <i>b</i> <sub>L</sub> , <i>b</i> <sub>p</sub> & <i>b</i> <sub>n</sub> , <i>b</i> <sub>O</sub> & <i>b</i> <sub>i</sub>	Oxygenic	Integral membrane	<i>b</i> <sub>6f</sub>	Q cycle	Has pigments
<i>c</i> <sub>i</sub>	<i>c</i> <sub>n</sub> , <i>c</i> <sub>x</sub>	Oxygenic	Integral membrane	<i>b</i> <sub>6f</sub>	Q cycle	Surprise in crystal structure
Cyt <i>f</i>		Oxygenic	Lumen, in complex	<i>b</i> <sub>6f</sub>	Rieske to soluble acceptor	Beta barrel, unique structure, unknown evolution
<i>c</i> <sub>6</sub>	PetJ, Cyt <i>c</i> <sub>553</sub>	Oxygenic	Lumen, soluble	shuttle	<i>b</i> <sub>c</sub> to RC	Alternative <i>c</i> <sub>6</sub> , di-thio cyt
<i>c</i> <sub>6a</sub>		Green algae & plants	Lumen, soluble	shuttle	<i>b</i> <sub>c</sub> to RC, forms disulfide bridges?	
<i>c</i> <sub>6b</sub>	Pet J1	Cyano	Lumen, soluble	shuttle	<i>b</i> <sub>c</sub> to RC	Alternative <i>c</i> <sub>6</sub>
<i>c</i> <sub>6c</sub>	Pet J2	Cyano	Lumen, soluble	shuttle	<i>b</i> <sub>c</sub> to RC	Alternative <i>c</i> <sub>6</sub>
<i>c</i> <sub>M</sub>		Cyano	Lumen, soluble, anchor	shuttle	<i>b</i> <sub>c</sub> to RC & donation to COX	Alternative <i>c</i> <sub>6</sub>

was assigned its own class, V, of cytochrome protein structures (Azai et al. 2010). Cytochrome  $c_z$  reduced the special pair pigments on the 40  $\mu\text{s}$  timescale (Oh-oka et al. 1998). The anchoring allows for the rapid re-reduction of the special pair by keeping the cytochrome in an ideal place for electron transfer rather than letting the dynamics be diffusion controlled.

Besides the unique structure of the three helix anchor on the N-terminus, the *cyt c<sub>z</sub>* C-terminus domain also contained structural surprises. The soluble C-terminal portion of *cyt c<sub>z</sub>* has been overexpressed, characterized, crystallized, and its structure solved (Hirano et al. 2010). Despite the low amino acid sequence similarity, this domain of *cyt c<sub>z</sub>* surprisingly showed structural similarity to class I cytochromes (Higuchi et al. 2009; Hirano et al. 2010). Class I cytochromes are *c*-type low spin hemes with heme attachment near the N-terminus histidine and a sixth coordinating axial ligand, methionine. The unique structure may contribute to its second proposed role of accepting electrons.

In addition to special pair reduction, *cyt c<sub>z</sub>* has been implicated in direct electron transfer from the *cyt bc<sub>1</sub>* complex. It was shown to enhance the 150  $\mu\text{s}$  time-scale of electron transfer between the RC and the *cyt bc<sub>1</sub>* complex by interacting directly with the periplasmic subunit of the *bc<sub>1</sub>* complex, cytochrome *c<sub>556</sub>* (Oh-oka et al. 1998). In other bacterial cyclic electron transport chains, an additional free soluble electron carrier would shuttle electrons from the *bc<sub>1</sub>* to the RC. However, in GSB, no such additional carrier has been observed. One possibility to fill this functional role was the GSB soluble carrier *cyt c<sub>555</sub>*, also known as *CycA* when involved in sulfur metabolism, but it was unable to shuttle electrons between *c<sub>556</sub>* and the  $c_z$ . This implied that the two peripheral cytochrome subunits of the RC and *bc<sub>1</sub>* complex may directly contact each other to move electrons without an intermediate (Oh-oka et al. 1998; Tsukatani et al. 2008). Although *CycA*, *cyt c<sub>555</sub>*, was not shown to shuttle between RC and *bc<sub>1</sub>*, in the GSB *Chlorobium tepidum*, *cyt c<sub>555</sub>* donated electrons to

*cyt c<sub>z</sub>* on the same timescale as *cyt c<sub>556</sub>* (Azai et al. 2008; Tsukatani et al. 2008). This finding does not detract from the direct electron transfer between RC and *bc<sub>1</sub>* hypothesis. *Cyt c<sub>z</sub>* of the GSB type I RC's is a unique cytochrome structurally and in choice of reaction partners.

Apart from *cyt c<sub>z</sub>*, another type I RC cytochrome has been characterized, *cyt c<sub>553</sub>* (PetJ) in Heliobacteria. Unlike GSB, Heliobacteria are gram-positive, lacking a periplasmic space and restricting mobile cytochromes to the cytoplasmic space. Cytochrome *c<sub>553</sub>* is therefore found in the cytoplasm and thought to be linked to the membrane via the terminal cysteine residue forming covalent bonds with lipid fatty acids (Azai et al. 2010). When the full Heliobacterial RC complex was purified, *cyt c<sub>553</sub>* was integrated as a subunit (Sarrou et al. 2012). The subunit was also expressed and characterized. It displayed with similar function and a redox potential, + 217 mV, to the native RC preparation (Kashey et al. 2014).

Functionally, GSB *cyt c<sub>553</sub>* donates electrons to the RC special pair, P800, with an electron transfer donation rate about  $5 \times 10^3 \text{ s}^{-1}$ , similar to that of *cyt c<sub>z</sub>* (Tsukatani et al. 2008). This rate is ten times larger than in purple bacteria, which have type II RCs and are discussed in the next section (Azai et al. 2010). The tenfold rate enhancement of type I to type II suggests that the hemes and special pairs of the type I RC's are better aligned for efficient electron transfer. Also like GSB, *cyt c<sub>553</sub>* can shuttle electrons directly from the *cyt bc<sub>1</sub>* complex to the RC (Azai et al. 2010; Sattley and Blankenship 2010). Periplasm type I RC cytochromes transfer electrons to re-reduce the RC special pair. *Cyt c<sub>z</sub>* and *c<sub>553</sub>* are doing the same job at about the same rate with different structures and attachments showing how organisms can use a variety of cytochromes conditioned to their habitat. *Cyt c<sub>z</sub>* and *c<sub>553</sub>* of prokaryotic type I RC's demonstrate the similarity and differences amongst this large family of proteins and reflect the diverse environments in which the proteins function.

## 2. Cytochromes in Type II Reaction Centers

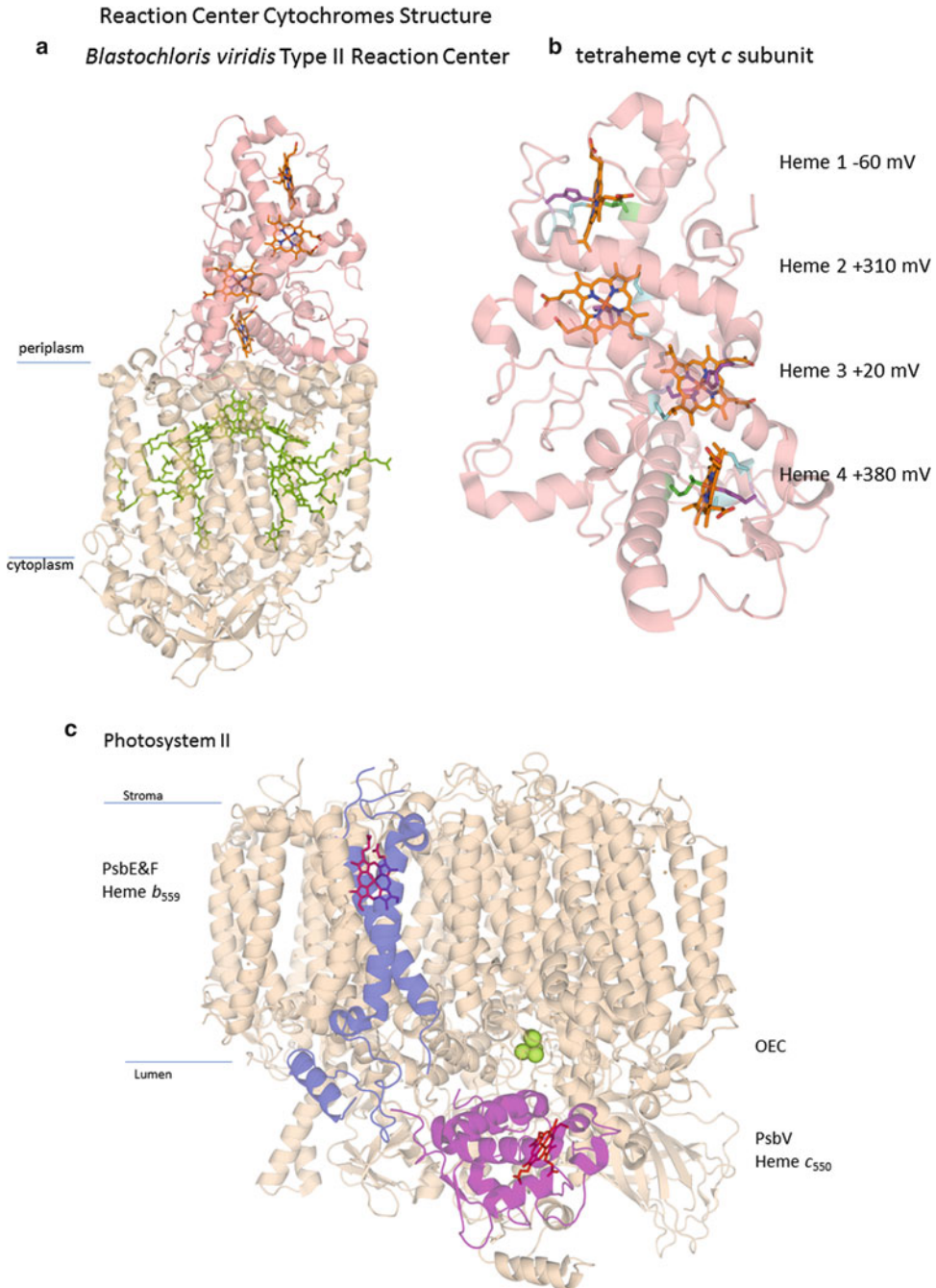
Type II Reaction Center protein complexes have been characterized more extensively than their type I counterparts due to enhanced stability and relative ease of purification. Type II RCs typically have a Light Harvesting (LH) subunit attached to or surrounding the Reaction Center complexes, unlike type I's the only have the charge separation and electron transfer subunits (Westerhuis 1996). Type II RC cytochromes are usually involved in cyclic rather than linear electron transfer in prokaryotes (Blankenship 2014). The special pair, P870 will receive the excitation energy from light and completes charge separation by quickly passing the charge down bacteriochlorophyll and bacteriopheophytin pigments. The electron is passed through two quinones, from  $Q_A$  to  $Q_B$  and then to another quinone that will carry the electron through the membrane. The special pair is re-reduced by a cytochrome so that the process can start again.

Anoxygenic Type II RCs, as exemplified by Purple Bacteria (PB), contain three integral membrane subunits: L, M, H and, in many cases, a fourth periplasmic cytochrome subunit. As in the type I RC's, they utilize a cytochrome to re-reduce the special pair of pigments responsible for charge separation (Allen et al. 1987). Many of the purple bacteria contain a tightly bound tetraheme cytochrome that reduces the RC special pair after photo-induced electron transfer (Jones 2009). However, some purple bacterial RCs do not have a bound cytochrome *c* subunit. Instead, they depend on a soluble cytochrome  $c_2$  that is discussed below or other soluble electron transfer protein (Ortega et al. 1999; Axelrod and Okamura 2005).

The tetraheme cytochrome *c* RC subunit in Purple Bacteria is a periplasmic subunit with four hemes responsible for accepting electrons from a soluble carrier and re-reducing the RC special pair. It belongs to class III of cytochrome proteins, which are defined by their multihemes with low redox potentials (Coutinho and Xavier 1994).

Early biochemical work on PB RC's had focused on *Rhodobacter sphaeroides* or *Rhodobacter capsulatus*, which do not have the tetraheme cytochrome subunit (Allen et al. 1987; Bauer et al. 1988). Thus, it had been thought that the PB RC's lacked an attached cytochrome. Additionally, the RC cyt *c* subunit can remain firmly attached during purification, but it is sometimes lost, which made it difficult to detect or characterize. However, an important advance in the knowledge and understanding of the PB RC, and in particular the cytochrome subunit, was the crystal structure of the RC of *Blastochloris viridis*, (formerly known as *Rhodospseudomonas viridis*) (Fig. 3.2a) (Deisenhofer et al. 1985). This was the first photosynthetic RC crystallized and revealed a surprise, the tetra-heme cytochrome *c*. The discovery and characterization of the tetraheme cytochrome in the *Bl. viridis* structure altered the perception not only of PB RC's, but of all cytochrome donors of reaction center complexes. The discovery spurred questions such as: Why are there four hemes? Does each heme have a distinct redox potential? and How do electrons flow through the hemes?

This tetraheme subunit, known as cyt  $c_{554}$  or RC cyt *c*, accepts electrons from a periplasmic soluble electron donor, and transfers an electron to the special pair of pigments to re-reduce the pair after charge separation has occurred (Hara 1998; Roszak et al. 2012) Cyt  $c_{554}$  is analogous to cyt  $c_z$  in type I RC's, but has four hemes and no transmembrane anchor helix. The crystal structure revealed a bound tetraheme cytochrome *c* subunit with a roughly vertically stacked heme alignment (Fig. 3.2b) that had not previously been observed in any cytochrome protein (Deisenhofer et al. 1985). This arrangement was postulated to direct the flow of electron transfer and was confirmed with the assignment of the redox potentials. The redox potentials are heme 1 at  $-60$  mV, heme 2 at  $+310$  mV, heme 3 at  $+20$  mV, and heme 4 at  $+380$  mV in *Bl. viridis* (Dracheva et al. 1988). The subunit has two low potential and two high potential



*Fig. 3.2.* Crystal Structures of photosynthetic reaction center cytochromes. **(a)** *Blastochloris viridis* RC (PDBID 3T6D). The tetraheme subunit is in red and the integral membrane subunits are in tan. Heme cofactors are orange and special pair pigments are green. **(b)** The tetraheme subunit alone. Chain is in red and hemes are in orange. Heme binding amino acid side chains are shown as cysteine in cyan, histidine in purple and methionine in green. **(c)** *Thermosynechococcus elongatus* Photosystem II (PDBID 3BZ1). PSII integral membrane subunits are tan, cyt  $b_{559}$  subunit is in blue, PsbV is in purple, b-type hemes are pink, c-type hemes are red and OEC is in green.

hemes (Nogi et al. 2005). The function of each heme and order of electron transfer within this subunit corresponds to the redox potential. A Low Potential-High Potential-Low Potential-High Potential-Special Pair electron flow pathway was established (Dracheva et al. 1988).

Another unique feature of cyt  $c_{554}$  is the ability of the subunit to move electrons uphill against the redox potential gradient. Overall in cyclic electron transport, the distal heme of the tetraheme cytochrome has a much lower redox potential ( $-60$  mV) than donor, cyt  $c_2$  ( $+345$  mV), yet donates within  $60$   $\mu$ s to the electron acceptor special pair, as characterized in *Bl. viridis* (Blankenship 2014). Somehow the tetraheme subunit is able to overcome this energy barrier; likely from overall downhill thermodynamics of the electron transfer from cyt  $c_2$  to the RC.

Attached tetraheme cytochromes are not only found in PB, but they are observed in other anoxygenic photosynthetic prokaryotic families such as the Filamentous Anoxygenic Phototrophs (FAPs) (Collins et al. 2010). Many FAPs differ from PBs by growing in warmer environments, being filaments versus rods and having different light harvesting antenna (Tang et al. 2011). Their RCs also lack the H subunit but are still type II RC's (Collins et al. 2009). FAPs are represented by the closely related *Chloroflexus aurantiacus* (CFX) and *Roseiflexus castenholzii* (RFX), but differ in that CFX has a large peripheral light harvesting complex, the chlorosome, and RFX does not (Yamada et al. 2005; Cao et al. 2012). Additionally, the tetraheme cytochrome  $c$  subunit of RFX stays firmly attached to the RC during purification but that of CFX does not (Meyer et al. 1989). Despite the loss during purification, the CFX subunit was characterized, and re-reduction of the RC cyt  $c_{554}$  was observed in vitro (Meyer et al. 1989). Likewise, the intact RFX RC complex has been purified and characterized (Collins et al. 2010). The re-reduction of the RC special pair by the tetraheme cyt  $c$  kinetics in RFX were similar to that of CFX (Xin et al. 2011). The structure of the FAP RC's has not been determined, but a high sequence similarity between the FAP and PB

RCs suggests that structure would be similar (Gardiner et al., unpublished data).

In addition to promoting uphill electron transfer, the presence of an attached cytochrome  $c$  subunit has been shown to increase the photocurrent detected for a Light Harvesting Reaction Center (LHRC) complex versus an LHRC with no cyt  $c$  subunit during in vitro photochemical cell assays (Friebe & Majumder, unpublished data). This increase in photocurrent is attributed to the attached cytochrome  $c$  subunit because then the electron donor binding is not the rate limiting step and the assay is not dependent on diffusion and binding of the carrier cyt  $c$ . The tetraheme cyt  $c$  enhances function of the RC by contributing to the reaction rate and overcoming an energy barrier. The tetraheme cyt  $c$  of PB and FAPs adds to the structural and functional diversity of anoxygenic photosynthetic RC cytochromes.

### B. Cytochromes in *bc* Complexes

After RCs complete charge separation, electrons move through the cyclic or non-cyclic electron transport chain. The electron movement generates a proton-motive force that ultimately drives ATP synthase forming chemical energy such as ATP (Crofts et al. 2013a). In the RC, two electrons and two protons are donated to a quinone, reducing the quinone to quinol. The reduced quinol diffuses through the membrane to the second large complex of the anoxygenic cyclic electron transport chain, the cytochrome *bc* complex (See Chaps. 9 (Cramer & Hassan) and 10 in this edition) (Hunte 2003). This complex oxidizes the quinol, sending the electrons through the *bc* complex via a process known as the Q-cycle and simultaneously translocates protons to the positive side of the membrane periplasmic or P side (Cape et al. 2006). The proton translocation against the electrochemical gradient contributes to the proton motive force. The electrons, after going through the Q-cycle are loaded onto a soluble carrier, typically a cytochrome (Kramer et al. 2009) which is discussed in the next section.

The cytochrome *bc* complexes are named for their major cofactors, *b* and *c*-type hemes. A few key differences distinguish *b* and *c* type hemes: *c* type hemes are covalently linked to the protein via thioether bonds while *b* type hemes have vinyl groups in those positions. In typical cytochrome *bc* complexes the *b* and *c* heme cofactors are localized in different subunits. The *b* subunit is usually involved in quinone redox reactions and the *c* subunit in electron transfer with soluble carriers. The proton pumping ability of cyt *bc*-type complexes makes them well suited to electron transport chains for cellular respiration. Cyt *bc* complexes are consequently found in phototrophic and non-phototrophic taxa of prokaryotes including proteobacteria and the in mitochondria of eukaryotes including humans (Cape et al. 2006). The cyt *bc* complexes of anoxygenic photosynthetic prokaryotes discussed in this section are small and simple compared to their eukaryotic counterparts (Esser et al. 2008). However, despite being present on nearly the whole tree of life, the fundamental catalytic components of this protein complex have relatively few forms compared to the variety of species and electron transport chains in which they exist (Berry et al. 2000). This section explores the canonical cyt *bc*<sub>1</sub> complex, the *bc* complex of Heliobacteria, and the novel functional replacement the Alternative Complex III (ACIII).

### 1. Cytochrome *bc*<sub>1</sub> Complex

The proton pumping complex used in most anoxygenic phototrophic bacteria is the cytochrome *bc*<sub>1</sub> complex, which functions to preserve energy within the cell through the Q cycle (Trumpower 1990; Cape et al. 2006). The establishment of the Q cycle mechanism has been the focus of effort in *bc* complexes in recent years and relied heavily on understanding the cytochrome subunits. Typical cyt *bc*<sub>1</sub> complexes have a cytochrome *b* subunit, a cytochrome *c*<sub>1</sub> subunit and a Rieske iron-sulfur cluster subunit (Fig. 3.3a) (Khalfaoui-Hassani et al. 2012). The cytochrome *b* and Rieske

protein subunits start the reactions in the Q cycle by providing the sites for quinol oxidation.

The cyt *b* subunit of the cytochrome *bc*<sub>1</sub> complex has two *b*-type hemes in a classical *b*-type fold with the heme plane parallel to the helix bundle axis (Berry et al. 2013). They belong to the cyt *b* family of proteins defined by their two *b*-type hemes and presence in *bc* complexes (Berry et al. 2000). The subunit has an elongated structure that spans the membrane with about eight transmembrane helices. It is also predicted to be the precursor of the PSII RC cyt *b*<sub>559</sub> discussed in later sections (Shinopoulos and Brudvig 2012). The two *b* hemes within the subunit are named *b*<sub>L</sub> and *b*<sub>H</sub> for their respective low and high redox potential. They can also be called *b*<sub>p</sub> and *b*<sub>n</sub>, corresponding to *b*<sub>L</sub> and *b*<sub>H</sub>, in reference to their locations near the positive and negative sides of the membrane. The hemes are the major cofactors near to the Q<sub>o</sub> and Q<sub>i</sub> sites, also known as Q<sub>p</sub> and Q<sub>n</sub> in the same fashion as the hemes, where quinol is oxidized and quinone is reduced, respectively, during the Q cycle (Czapla et al. 2013). Heme *b*<sub>L</sub> is found near the Q<sub>o</sub> site to match the redox potential needs of quinol oxidation, and heme *b*<sub>H</sub> is found near the Q<sub>i</sub> site because of the redox potential needed to reduce quinone. The specific chemistry at each of these sites and the mechanism of electron transfer through each heme is part of the Q cycle.

To start the Q cycle, the Q<sub>o</sub> site facilitates bifurcated electron transfer. Here we give only a brief description, but see the chapters in this volume by Sarewicz et al. (Chap. 14) and Fisher et al. (Chap. 21) for more information. Two electrons and two protons are extracted from the quinol sequentially (Crofts et al. 2013b). One electron moves onto the Rieske subunit and the other to heme *b*<sub>L</sub>. The now reduced lower potential heme passes its electrons down the energy gradient to heme *b*<sub>H</sub>. In the Q<sub>i</sub> site a quinone is bound and receives the electron from *b*<sub>H</sub> generating a semiquinone radical (Cooley 2010). Another quinol binds to the Q<sub>o</sub> site and the process repeats generating a reduced quinol in the Q<sub>i</sub> that then diffuses into the membrane.

After a quinol is oxidized at the  $Q_0$  site, the second arm of the bifurcation event loads one electron onto the Rieske Fe-S subunit, which moves almost 20 angstroms to dock with the cytochrome  $c_1$  on the periplasmic face of the  $bc_1$  complex (Esser et al. 2008; Osyczka and Cooley 2013). The cytochrome  $c_1$  subunit has a typical cytochrome  $c$  fold around the monoheme and is anchored to the membrane with a C-terminal helix (Fig. 3.3b). It belongs to class I cytochrome  $c$ 's. Cyt  $c_1$  transfers electrons to a soluble cytochrome  $c_2$  or sometimes interacts with a different soluble cytochromes  $c_8$  or  $c_y$  (Fig. 3.1a). The cyt  $c_1$  subunit has a hydrophobic surface with positive and negative patches complementary

to the soluble acceptor cyt  $c_2$  (Figs. 3.3c and 3.4b). The complementary electrostatic surfaces permits  $c_1$  to bind transiently but tightly with the soluble acceptor. Cyt  $c_2$  or the other soluble carriers, as discussed in the next section, serve to re-reduce the RC, thereby completing the Q-cycle (Sanders et al. 2009). Unlike the cyt  $b$  subunit of  $bc$  complexes, which are conserved across nature, there is more variation in the cyt  $c_1$  subunits.

## 2. Cytochrome $bc$ Complexes

Heliobacteria are strictly anaerobic phototrophs that belong to the Firmicutes family, which are Gram positive bacteria and to the class of Clostridia which are anaerobic

### $bc$ Complex Cytochromes Structures

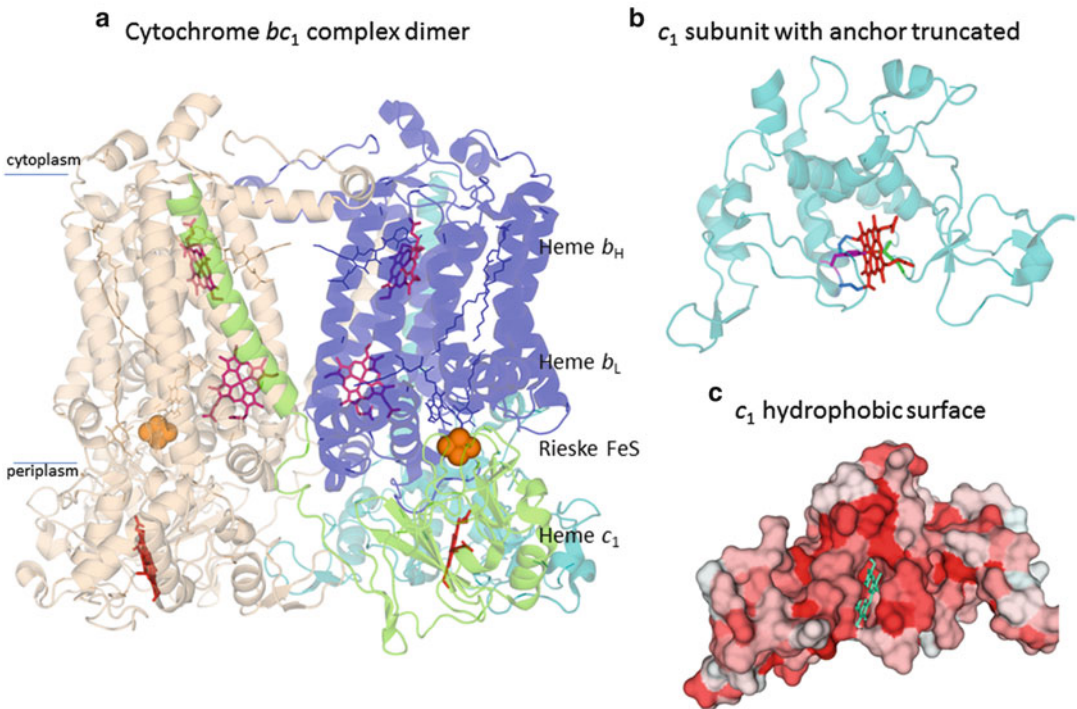


Fig. 3.3. Crystal structures of photosynthetic  $bc$  complex cytochromes. (a) Cytochrome  $bc_1$  complex from *Rhodobacter sphaeroides* (PBDID 2QJK). The complex is shown as the biological dimer with one half color-coded. The cytochrome  $b$  subunit is in blue, the cytochrome  $c_1$  subunit is in teal and the Rieske subunit is in green.  $b$ -type hemes are pink,  $c$ -type hemes are red and FeS is in orange. The chains of the second half of the dimer are in tan. (b) The cytochrome  $c_1$  subunit alone with anchor helix truncated. Chain is in teal and heme is in red. Heme binding amino acid side chains are shown as cysteine in cyan, histidine in purple and methionine in green. (c) Hydrophobic surface of the cytochrome  $c_1$  subunit. The darker the red, the more hydrophobic the area is. Heme is shown in cyan and shown in same orientation as 3B.



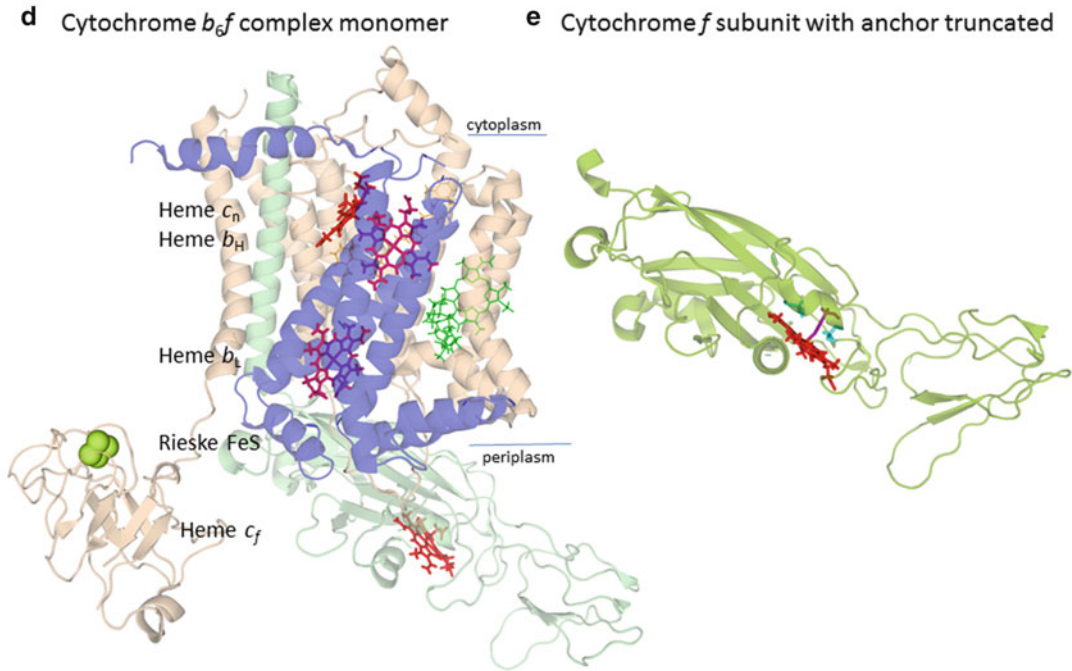


Fig. 3.3. (continued) **(d)** Cytochrome  $b_6f$  complex from *Nostoc sp. PCC7120* (PBDID 4HH4). The complex is shown as half of biological dimer. The cytochrome  $b$  subunit is in *blue*, the cytochrome  $f$  subunit is in *green*.  $b$ -type hemes are *pink*,  $c$ -type hemes are *red* and FeS is in *green*, carotenoid is in *orange* and chlorophyll is in *green*. The other subunits are in *tan*. **(e)** The cytochrome  $f$  subunit alone with anchor helix truncated. Chain is in *green* and heme is in *red*. Heme binding amino acid side chains are shown as cysteine in *cyan*, histidine in *purple* and methionine in *green*.

(Heinrichel and Golbeck 2007). For photosynthetic machinery, they employ Type I Reaction Centers and a *cyt bc* complex that is comparatively simple or smaller than the previously discussed complexes (Redding et al. 2013). From the *cyt bc* complex, the  $b$  subunit in Heliobacteria is the postulated evolutionary precursor for both *cyt b<sub>6f</sub>* and *cyt bc<sub>1</sub>* *cyt b* subunits (Dibrova et al. 2013). The deviation from the conventional pattern is in the periplasmic cytochrome subunit. Instead of a monoheme cytochrome  $c$ , heliobacteria have a diheme cytochrome  $c$ . This protein is predicted to have resulted from a gene duplication event and subsequent fusion (Baymann and Nitschke 2010).

Unlike other DHCCs, in the heliobacterial DHCC, both hemes have equal reduction potentials (Yue et al. 2012). Recent work predicts a structure and mechanism for this complex using homology modeling

in combination with Hydrogen Deuterium Exchange Mass spectrometry (Zhang et al. 2014). In the absence of a crystal structure, the modelled protein has two similar  $c$ -type cytochrome domains with an N-terminal helix anchor. In the predicted mechanism, the electron arrives at DHCC via the iron-sulfur cluster. The N-terminal heme would accept the electron from the iron-sulfur cluster. The electron would then pass to the heme of the C-terminal domain. The C-terminal domain is more flexible and solvent accessible and therefore should donate the electron to the soluble electron carrier. This mechanism involving both hemes in the DHCC subunit would allow the complex to store electrons or be able to turn over even if the soluble carrier has not returned yet (Zhang et al. 2014).

As in Heliobacteria, the complex in Green Sulfur bacteria is also called a *bc* complex because it also an alternative to *cyt c<sub>1</sub>*. GSB

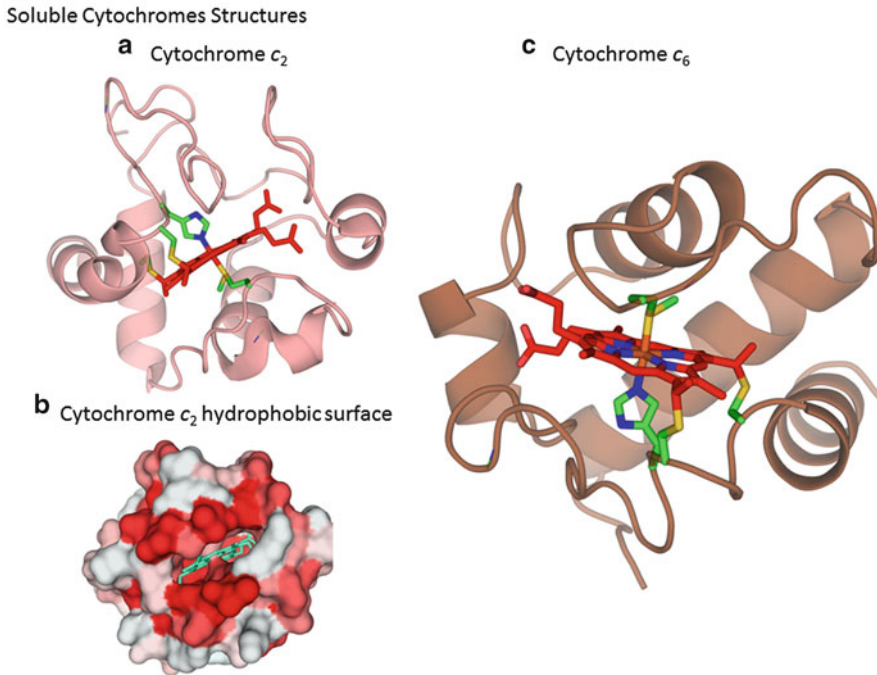


Fig. 3.4. Crystal structures of photosynthetic soluble cytochromes. (a) Cytochrome  $c_2$  from *Blastochloris viridis* (PDBID 1IO3) that interacts with the RC in Fig. 3.2a. Chain is light brown, heme is in red, and the heme binding amino acid side chains are colored by element. (b) Hydrophobic surface of the cytochrome  $c_2$ . The darker the red, the more hydrophobic the area is. Heme is shown in cyan and shown in same orientation as 4A. (c) cyt  $c_6$  from *Chlamydomonas reinhardtii* (PDBID 1CYI) that interacts with the RC in Fig. 3.2c. Chain is brown, heme is in red, and the heme binding amino acid side chains are colored by element.

have a cytochrome  $c_{556}$  that is structurally much like cyt  $c_1$ , but differs in that  $c_{556}$  is predicted to directly donate to the RC cyt  $c_2$  without a soluble intermediate (Oh-oka et al. 1998). There is diversity in the structure and mechanism of anoxygenic photosynthetic cyt  $bc$  complexes.

### 3. Alternative Complex III

Some anoxygenic phototrophs contain novel integral membrane cytochrome complexes that do not fit into either the  $bc_1$  or  $b_6f$  category. They fulfill the same functional role as a major enzyme of the electron transport chain of organism but do not share sequence homology or an evolutionary relationship with the conventional  $bc$  complexes.

An unconventional cytochrome complex that stands in contrast to the cytochrome  $bc$  complex protein family, belonging instead

to the molybdopterin oxidoreductase family, is the Alternative Complex III (ACIII) (Yanyushin et al. 2005; Gao et al. 2009; Majumder et al. 2013). ACIII complexes are found in several families of non-phototrophic bacteria and in photosynthetic prokaryotes, in the Filamentous Anoxygenic Phototrophs (FAPs) family (Refojo et al. 2013). ACIII is predicted to have the function of the  $bc$  complex, but does not resemble the typical complex, having more homology to poly-sulfide reductase (Majumder et al. 2013). It has seven subunits, two of which contain  $c$ -type hemes and does not contain  $b$ -type cytochromes.

The two heme subunits of ACIII that have been characterized in the photosynthetic prokaryote *Chloroflexus aurantiacus* are ActA and ActE. ActA has five hemes, and ActE is a monoheme subunit with two copies present in the full complex. ActA and ActE

are both found in the periplasm. The 5 hemes in ActA have 3 redox potentials of  $-228$  mV (3 hemes),  $-110$  mV (1 heme) and  $+94$  mV (1 heme). ActE has a redox potential of  $+390$  mV (Gao et al. 2010). ActA is predicted to donate electrons to ActE, and ActE is thought to be the final electron acceptor within the complex, much like cyt  $c_1$  in the  $bc$  complexes. ActE has been shown to be necessary for oxido-reductase function (Gao et al. 2013). Furthermore, it is thought to be a dimer (Gao et al. 2010). A homologous protein to ActE has not been identified in the Protein DataBank, and therefore suggests that ActE does not have the typical cytochrome  $c$  fold. The amino acid sequence of ActA, however, aligns with other multiheme proteins such as the *Escherichia coli* hexaheme nitrite reductase, but shows differences that arise from the presence of a N-terminal trans-membrane helix in ActA (Majumder et al. 2013).

Overall, ACIII contains seven hemes to carry out a one-electron process. Other proteins with mutlihemes carry out chemistry that requires more electrons, which poses the question of the mechanism of ACIII (Clarke et al. 2004, 2007). There is no evidence for a Q-cycle-like mechanism in ACIII. A  $Q_o$  site has been identified by inhibitor assays by a HQNO fluorescence assay, but there is no  $Q_i$  site nor  $b$ -type hemes (Refojo et al. 2010). The mechanism of ACIII is expected to be quite different from that of typical cyt  $bc$  complexes. In mechanism and subunit composition, ACIII is a novel member of the photosynthetic cytochromes.

### C. Soluble Cytochromes in Anoxygenic Cyclic Electron Transport

Soluble cytochromes are the mobile components of photosynthetic electron transport chains, shuttling electrons between the large membrane proteins. All known soluble cytochromes in photosynthesis are monoheme  $c$ -type cytochromes, most with the usual  $c$ -type cytochrome protein fold and are located in the periplasm (Azai et al. 2010). Examples of other non-cytochrome soluble

electron carriers are two small blue copper proteins: plastocyanin in oxygenic photosynthetic organisms and auracyanin in the FAPs (King et al. 2013). While some soluble cytochromes are restricted by an anchoring tail that attaches these cytochromes to the membrane surface, other soluble cytochromes are neither attached nor associated with the membrane (Dutton et al. 1975; Kashey et al. 2014). Regardless of membrane attachment, soluble cytochromes proteins are promiscuous binders allowing them to bind two different protein complexes transiently (Myllykallio et al. 1998; Bernroither et al. 2009).

A canonical soluble anoxygenic cytochrome is cyt  $c_2$ , which shuttles electrons from the cyt  $bc_1$  complex to the RC in Purple Bacteria (Dutton et al. 1975; Sponholtz et al. 1976). This protein belongs to the class I  $c$ -type cytochromes having histidine and methionine as axial ligands and the heme attachment near the N-terminus of the protein (Lin et al. 1994). The crystal structures of cyt  $c_2$  from several purple bacterial species have been solved (Fig. 3.4a). The solved cyt  $c_2$  structures all contain an alpha-helical  $c$ -type cytochrome fold. The heme is buried except for one exposed edge surrounded by positively charged lysine residues (Fig. 3.4b) (Axelrod et al. 2009). This feature defines the binding site to the RC and cyt  $bc_1$  which have corresponding regions consisting of complementary negatively charged residues on their surface (Blankenship 2014). This electrostatic interaction allows for tight but transient binding since  $c_2$  must deliver electrons quickly to the two different partners. The flash-induced kinetics for  $c_2$  donation to the RC special pair are multiphasic, representing each step in the electron transfer process: first the diffusion of the reduced  $c_2$  and binding to the RC is seen in the slower kinetic phase and secondly, the fast phase,  $1 \mu\text{s}$ , reflects the rapid oxidation of a bound  $c_2$  (Daldal et al. 2001; Gong et al. 2003).

In Purple Bacteria, cytochromes  $c_y$ ,  $c_8$ ,  $c_4$ , and a HiPIP (High-Potential Iron-Sulfur Protein) have been implicated as alternatives

cyt  $c_2$ , the donor to the RC. Cytochromes  $c_4$  and  $c_8$  are also  $c$ -type soluble cytochromes (Verméglio et al. 2002). The ability of cyt  $c_8$  to donate to the RC in several PB species was established in the 1970s (Tatsuhiko 1970; Samyn and Smet 1996; Hochkoeppler et al. 1997). It has also been observed to function during autotrophic growth (Verméglio et al. 2002). The origin of  $c_8$  may be in the nitrite reduction pathway (Nagashima et al. 2011). Cyt  $c_y$  is unique as one of the few anchored soluble cytochromes, also found in PB (Hochkoeppler et al. 1995). The membrane anchor is a tail that attaches to a membrane lipid moiety. It therefore has a pendulum type motion in shuttling electrons between the large integral membrane complexes. The electron transfer rates in  $c_2$ -less mutants that only use  $c_y$  still showed efficient photosynthetic growth suggesting that  $c_y$  is functional replacement for  $c_2$  (Jenney et al. 1994; Hochkoeppler et al. 1995; Myllykallio et al. 1998). The alternative donors provide PB the flexibility to survive in changing conditions such as light intensity and nutrient concentration.

Another unique class of cytochromes found in phototrophic and aerobic bacteria is cytochrome  $c'$  (Ambler et al. 1981). They are soluble  $c$ -type cytochromes whose function is not well understood. They are designated as  $c$ -type because of the covalent bonds from the heme to cysteines but differ in most other ways. Cytochrome  $c'$  has the heme in a high spin environment, but does not have typical ligands or a  $c$ -type cytochrome fold and is thus pentacoordinate (Weber et al. 1980). This class of alternative cyt  $c$  proteins has their heme binding sites near the C-terminal end of the protein, which similar to  $c_{556}$  from GSB, but has other structure features of cyt  $c_1$  (Ambler et al. 1981). A study of cyt  $c'$  in PB *Rhodobacter sphaeroides* showed that cyt  $c'$  is expressed most during photosynthetic denitrification growth and binds NO and CO (Choi et al. 2005; Russell et al. 2013). Further work will reveal the function of cyt  $c'$ .

The story of soluble cytochromes in other anoxygenic species is not as straightforward. Green Sulfur Bacteria were originally

thought to use a soluble cyt  $c_{555}$ , but it is now known that there are other sources of electrons from sulfur metabolism that enter the photosynthetic cyclic electron transport chain, but they that are not well characterized (Sakurai et al. 1996). As seen in Fig. 3.1a, cyt  $c_{555}$  can take electrons from sulfur metabolism and potentially donate them to  $c_z$  of the RC. As discussed above, Heliobacteria are now believed to have no soluble cytochromes as part of their CET chain and rely solely on membrane-bound cytochromes (Blankenship 2014). The Filamentous Anoxygenic Phototrophs, as mentioned above, rely on the small blue copper protein auracyanin to shuttle electrons between ACIII and the RC (Fig. 3.1a) (Majumder et al. 2013). Whether typical or atypical, many cytochromes are key components in the photosynthetic electron transport chain of anoxygenic bacteria. These cytochromes persisted in their same basic forms during the evolutionary transition to oxygenic photosynthesis.

### III. Cytochromes in Oxygenic Photosynthetic Electron Transport Chains

As the evolution of the Earth progressed, organisms developed the ability to split water and produce oxygen approximately three billion years ago as part of their photosynthetic electron transport (Iverson 2006; Falkowski and Raven 2007). This process developed as part of the great oxygenation event released oxygen into the atmosphere and made possible complex, multicellular life as we know it. This was a phenomenal achievement billions of years in the making. Even in oxygenic eukaryotic organisms, cytochromes perform many of the same functions as in their prokaryotic counterparts (Fig. 3.1b).

#### A. Cytochromes in Photosystems I and II

The oxygenic versions of the Type I and Type II RCs are Photosystem I and Photosystem II. These are very large protein complexes

with around 20–30 subunits and associated light-harvesting proteins (Drop et al. 2014). They function together in linear electron transport with PSII extracting electrons from water and passing them onto PSI (Fig. 3.1b). Cyclic electron transport flow has also been observed around PSI (Iwai et al. 2010; Shinopoulos and Brudvig 2012; Trubitsin et al. 2014). Cytochromes in the Photosystems are found more as integral membrane components with fewer examples of soluble cytochromes being used than their anoxygenic counterparts.

### 1. Photosystem I

Cyanobacteria, algae and plants have a type I Reaction Center Photosystem I, and a type II RC, Photosystem II that will be discussed below. PSI, unlike the anoxygenic type I RCs, contains no cytochromes. PSI is distinct from the other RCs in that it does not have a bound cytochrome subunit (Falkowski and Raven 2007). PSI contains three iron-sulfur clusters and therefore uses non-heme irons on the acceptor side, but do not replace the donor side cytochromes as in other RC's (Blankenship 2014). In some cases, depending on copper and iron content, Photosystem I receives electrons from the cytochrome *b<sub>6</sub>f* complex via the blue copper protein plastocyanin and ultimately reduces ferredoxin to make NADPH (Blankenship 2010). However, most cyanobacteria and some algae contain a cyt *c<sub>6</sub>*, which will be discussed below, that can substitute for plastocyanin, with the expression dependent on copper availability (Hill and Merchant 1992).

### 2. Photosystem II

The Reaction Center with the most subunits and variety of cofactors is Photosystem II (Williamson et al. 2011). PSII is found in cyanobacteria, algae and plants. PSII houses a Mn-containing Oxygen Evolving Complex (OEC) within the protein (Pokhrel and Brudvig 2014). The OEC was a critical development in Earth's evolution providing the oxygen that allowed higher forms of life to

evolve (Blankenship 2010). The OEC, as the electron donor, aides PSII to participate in both cyclic and linear electron flow. The cytochrome subunits of PSII also help the complex function in both of these scenarios (Fig. 3.2c).

Cytochrome *b<sub>559</sub>* in PSII is a heterodimeric monoheme subunit with alpha and beta subunits, each contributing one heme coordinating histidine (Shinopoulos and Brudvig 2012). A single heme being coordinated across two small subunits is a unique structural feature of the cyt *b<sub>559</sub>* compared to other known cytochromes. Cyt *b<sub>559</sub>* is a required subunit for the assembly of PSII (see Müh and Zouni 2015), but it does not appear to function in the electron transport chain and its precise functional role has long been elusive. It has been proposed to have a role in secondary electron transfer pathways such as putative cyclic electron flow around PSII, photoinhibition, or reactive oxygen species protection (Pospíšil 2011; Shinopoulos and Brudvig 2012). Recent work has investigated the enzymatic function of cyt *b<sub>559</sub>* as an oxidoreductase because it was observed that four distinct forms of cyt *b<sub>559</sub>* with different redox potentials appear in vivo under different conditions (Feyziyev et al. 2013; Kaminskaya and Shuvalov 2013; Guerrero et al. 2014). The range of redox potentials for a monoheme cytochrome (see Müh and Zouni 2015 for discussion of functional significance of these potentials) and the bridging of the heme between two proteins make cytochrome *b<sub>559</sub>* a unique cytochrome in photosynthetic electron transport chains.

PSII from some organisms, has two other known cytochromes, PsbV and PsbV2. PsbV and PsbV2 are low redox potential cytochromes, but so far their function is not understood (Fig. 3.2c). These two cytochromes have been found in cyanobacteria and red algae, but not in plants (Kerfeld et al. 2003). The PSII subunit PsbV encodes for a cytochrome *c<sub>550</sub>* and is an extrinsic protein on the luminal side of the cyanobacterial thylakoid membrane. The subunit binds PSII in close proximity

to the Mn cluster of the OEC (Roncel et al. 2012) (see also Chap. 8, Muh and Zouni, this volume). PsbV is one among several cyt's of unknown function in oxygenic phototrophs (Katoh et al. 2001; Roszak et al. 2012). Since PsbV is implicated in PSII's affinity for calcium and chloride ions in the OEC, the presence of the subunit is required for the function and stability of the complex (Kirilovsky et al. 2004). The role of the heme, specifically, in PsbV is still unknown since the heme is not thought to act in the ion affinity function. The heme of PsbV is also not thought to have a redox function in the OEC due to the low redox potential of the heme. Recent data suggest that it protects the Mn atom in the OEC from reductants (Roncel et al. 2012). Additional new mass spectrometry techniques have shown that the disruption of PsbQ affects the stability of PsbV and decreases the overall function of PSII (Liu et al. 2013, 2014).

An alternate protein to PsbV is PsbV2. PsbV2 was found in the genome of thermophilic cyanobacteria immediately following PsbV. The amino acid sequences of PsbV and PsbV2 are highly similar (Kerfeld et al. 2003). PsbV2 has been isolated and purified. Biochemically, it appears to be similar to PsbV and can partially replace PsbV in the event of disruption of PsbV expression. Both proteins have sequence similarity to PetJ or cyt  $c_6$ , formerly referred to as cytochrome  $c_{553}$  (Katoh et al. 2001). The crystal structure of PsbV2 was recently solved revealing a new His/Cys axial heme ligation, but an overall structure like that of cyt  $c_6$  and cyt  $c_{550}$  (Suga et al. 2013). The novel ligation adds a further question to an enzymatic role for the heme of PsbV and PsbV2. The cytochrome subunits of PSII are diverse members of the cytochrome family in their unique heme coordination, ligation and putative functional roles in the RC complex.

### B. Cytochromes in $b_6f$ Complexes

In oxygenic phototrophs, including cyanobacteria, algae and plants, the functional role of the cytochrome  $bc$  complex is filled

by the cytochrome  $b_6f$  complex (Kallas 2012). Unlike anoxygenic photosynthetic organisms, which only have cyclic electron transport, the  $b_6f$  complex is involved in LEF and CEF (Hasan et al. 2013). Their role in CEF mirrors that of the cyt  $bc_1$  complex sending cycles electrons around the RC, PSI. Under conditions of CEF only,  $b_6f$  becomes the sole protein responsible for the proton gradient that drives ATP production. LEF is a feature of oxygenic photosynthetic electron transport chains and involves both photosystems to split water and reduce  $\text{NADP}^+$  with  $b_6f$  in between (Blankenship 2014). Whether in CEF or LEF, cyt  $b_6f$  undergoes a Q cycle that analogous to the mechanism in  $bc_1$ . The mechanism is bifurcated electron transfer mediated by the same classes of cofactors,  $b$  and  $c$  hemes and iron sulfur clusters (Fig. 3.3d). Recent work on the evolution of  $bc$  complexes has pointed to a common ancestor for  $bc_1$  and  $b_6f$  complexes that is closer to the  $bc$  complex from Heliobacteria (Dibrova et al. 2013). After their appearance,  $b_6f$  complexes have remained largely unchanged and are highly similar among species that are separated by hundreds of millions of years of evolution (Cramer et al. 2004).

The cytochrome  $b$  subunit is much like cyt  $b$  of the  $bc_1$  complex with two  $b$  type hemes interacting with the quinone pool. The differences lie in the addition of pigments within the complex, the length of the  $b$  subunit, and the presence of an additional  $c$ -type heme. The anoxygenic and/or prokaryotic cyt  $b$  has a longer amino acid sequence than its oxygenic counterpart (Cramer et al. 2004). The function of the carotenoid and chlorophyll pigments in the  $b_6f$  complex is unknown since the complex is not known to do photochemistry. Reports have suggested a protective mechanism of these pigments against ROS species by capturing the triplet energy of ROS (Stroebel et al. 2003; Cramer et al. 2005). Heme  $c_i$  was a surprise discovery when the crystal structure of the cytochrome  $b_6f$  complex was solved (Fig. 3.3d) (Stroebel et al. 2003). Heme  $c_i$  is located near heme  $b_L$  in the  $Q_i$  site of the complex. It has

at midpoint potential of +100 mV, but no axial ligands and may be accessed by an exogenous ligand (Alric et al. 2005). Mutation to the  $c_i$  resulted in a slowly of b heme reoxidation (de Lacroix de Lavalette et al. 2009). The role of  $c_i$  in the complex is still being investigated (Hasan et al. 2013). The oxygenic cyt *b* subunit of the  $b_6f$  complex, while being similar to its anoxygenic counterpart, is a diverse cytochrome because of the presence of pigments in the subunit.

The most unusual cytochrome protein in photosynthesis is cytochrome *f* (Fig. 3.3e). Cytochrome *f* takes the place of cytochrome  $c_1$  as a *c*-type heme being the last step of electron transfer within the  $b_6f$  complex (Whitmarsh and Cramer 1979; Stroebel et al. 2003). Cyt *f*, however, is primarily a beta-sheet protein that does not resemble the typical alpha helical cytochrome *c* fold. Additionally, the axial coordination of the heme involves an unusual histidine and tyrosine combination (Prince and George 1995). Cyt *f* belongs not to a cytochrome family of proteins but rather to the barrel sandwich hybrid superfamily (Prince and George 1995). Within the crystal structure, it was observed that heme-binding residues are located on alpha helices of only a few residues in length (Fig. 3.3e) (Martinez et al. 1994). Fundamental work by Hill and coworkers in the early 1950's first identified and then isolated cytochrome *f* (Davenport and Hill 1952). By the late 1970s, cytochrome *f* was known, and its role in the cell was being clarified (Whitmarsh and Cramer 1979). Today, even with hundreds of cyt *f* genes sequences and high-resolution crystal structures, the origin and evolution of the cytochrome *f* remains a mystery. It is speculated to be an important link in the transition from anoxygenic to oxygenic photosynthesis (Blankenship 2014).

### C. Soluble Cytochromes in Oxygenic Cyclic Electron Transport

Soluble cytochromes in oxygenic cyclic electron transport are not as widely utilized as is the case in their anoxygenic photosynthetic

counterparts. Oxygenic organisms have several alternative soluble electron carriers. A small blue copper protein, plastocyanin, fills the major role of shuttling electrons between the cyt  $b_6f$  complex and PSI in plant and algal chloroplasts and in many cyanobacteria (Gupta et al. 2002). Likewise, electrons arrive to the special pair in PSII from water splitting in the OEC. Small molecules such as ferredoxin or NADPH also serve as electron carriers in oxygenic electron transport chains (Nelson and Ben-Shem 2004). Soluble cytochromes are still valuable oxygenic photosynthesis. In many cyanobacteria, cyt  $c_6$  is the sole known electron donor to PSI (Kerfeld and Krogmann 1998). Cytochromes can also have new functions during stress conditions providing flexibility for the organisms (Rutherford et al. 2012; Simon and Klotz 2013).

One family of soluble oxygenic photosynthetic cytochromes is cyt  $c_6$  and cyt  $c_{6a}$ . They are luminal electron carriers found in cyanobacteria and eukaryotic algae and plants (Figs. 3.1b and 3.4c). Cyt  $c_6$  has been shown to replace plastocyanin donation to PSI when the medium is copper limited (Hill and Merchant 1992). Cyt  $c_6$  is a class I *c*-type cytochrome of about 10 kDa with standard histidine and methionine axial ligands (Kerfeld and Krogmann 1998). The flash-induced kinetics of cyt  $c_6$  donation to PSI were compared in many organisms and situations (Hill et al. 1991; Hervas et al. 1995). The cyt  $c_6$  of the chlorophyll-*d* containing cyanobacterium *Acaryochoris marina* has also been purified and characterized. It was found to weigh 8.9 kDa, have alpha helical structure and a midpoint potential of +327 mV (Bell et al. 2009). The work by Bell et al. also suggested that cyt  $c_6$  was the electron acceptor from cyt  $b_6f$  rather than plastocyanin. Characterization of the cyt  $c_6$  family has continued with new techniques and new species. Recent work has characterized the rapid electron transfer between cytochrome *f* and cyt  $c_6$ , shedding light on the efficiency of this process (Díaz-Moreno et al. 2014) (see also Bialek et al. 2015).

The cyt  $c_{6a}$  designation emerged amid evidence that higher plants had by evolution eliminated cyt  $c_6$  from their chloroplasts (Gupta et al. 2002). Oxygenic organisms have a very high degree of conservation in their photosynthetic machinery within their families. Cyanobacteria predominantly use cyt  $c_6$  to interact with cyt  $b_{6f}$ . Algae use both cyt  $c_6$  and plastocyanin and plants only express and use plastocyanin (Hippler 1999). The discovery of cyt  $c_{6a}$  in *Arabidopsis* challenged this notion. Compared to the sequence of cyt  $c_6$ , cyt  $c_{6a}$  has an insertion of 12 amino acids with two conserved cysteine residues. It also has a particularly low potential heme that is 200 mV lower than cyt  $c_6$  (Gupta et al. 2002). This indicates that cyt  $c_{6a}$  could not effectively donate electrons to PSI. This low potential was surprising because the axial heme coordination is the same as cyt  $c_6$  (Worrall et al. 2008). The exact functional role of low potential cyt  $c_{6a}$  is not clear (Howe et al. 2006, 2015).

Besides cyt  $c_{6a}$ , there are other known alternatives to cyt  $c_6$ . In cyanobacteria, two other forms of cyt  $c_6$  have been identified as  $c_{6b}$  and  $c_{6c}$ . These cytochromes were identified from the *petJ1* gene and a *petJ1*-like gene, *petJ2*, in *Synechococcus* sp. PCC 7002. The *petJ1* gene encodes a typical cyt  $c_6$ , which is the only known electron carrier between the cyt  $b_{6f}$  complex and PSI in *Synechococcus* 7002 and many other cyanobacteria. *PetJ2* had a much lower midpoint potential +148 mV, compared to +319 of *PetJ1*, and was designated as the cyt  $c_{6c}$  class of cytochromes, which are widely distributed among cyanobacteria (Bialek et al. 2008). Cytochrome cyt  $c_M$  from cyanobacteria is another possible  $c_6$  substitute and is an example of a protein that may be used in both CEF and LEF. Cyt  $c_M$  was shown to donate electrons to cytochrome  $c$  oxidase cyanobacterial respiration during in vitro assays as rapidly as cyt  $c_6$  and faster than plastocyanin (Bernroither et al. 2009). However, there is no available evidence to show that cyt  $c_M$  is expressed at sufficient levels in vivo to support such functions (Mullineaux 2014). The varied soluble

oxygenic cytochromes allow organisms to adapt to stress conditions or different living environments.

#### IV. Conclusions

From large membrane protein complexes to small soluble proteins, cytochromes play crucial roles in electron transport chains, accomplishing the major processes of energy conversion and oxygen production on the planet. Most that have been studied are  $b$  or  $c$ -type cytochromes, but significant variations exist despite overall similarity in functions. Most cytochromes share evolutionary origins, with the notable exception of cytochrome  $f$ , whose origin remains obscure. Photosynthetic organisms take advantage of the diversity of cytochromes to adapt to different environments and metabolic needs.

#### Acknowledgments

We would like to acknowledge the Olin Fellowship for Women for funding ELWM.

#### References

- Allen JP, Feher G, Yeates TO, Komiya H, Rees DC (1987) Structure of the reaction center from *Rhodobacter sphaeroides* R-26: the protein subunits. *Proc Natl Acad Sci USA* 84:6162–6166
- Alric J, Pierre Y, Picot D, Lavergne J, Rappaport F (2005) Spectral and redox characterization of the heme  $c_i$  of the cytochrome  $b_6f$  complex. *Proc Natl Acad Sci USA* 102:15860–15865
- Ambler RP, Bartsch RG, Daniel M, Kamen MD, McLellan L, Meyer TE, Van Beeumen J (1981) Amino acid sequences of bacterial cytochromes  $c'$  and  $c$ -556. *Proc Natl Acad Sci USA* 78:6854–6857
- Axelrod HL, Okamura MY (2005) The structure and function of the cytochrome  $c_2$ : reaction center electron transfer complex from *Rhodobacter sphaeroides*. *Photosynth Res* 85:101–114
- Axelrod H, Miyashita O, Okamura M (2009) Structure and function of the cytochrome  $c_2$ : reaction center complex from *Rhodobacter sphaeroides*. In: Hunter CN, Daldal F, Thurnauer MC, Beatty JT (eds) *Purple Phototrophic Bact.* Springer, Dordrecht, pp 323–336



- Azai C, Tsukatani Y, Miyamoto R, Kondo T, Murakami H, Itoh S, Oh-oka H (2008) Bifurcated electron donations from quinol oxidoreductase and soluble C<sub>ycA</sub> to cytochrome *c<sub>z</sub>* of the photosynthetic reaction center complex in the green sulfur bacterium *Chlorobium tepidum*. In: Allen JF, Gantt E, Golbeck JH, Osmond B (eds) Photosynthesis. Energy from the Sun. Springer, The Netherlands, pp 549–552
- Azai C, Tsukatani Y, Itoh S, Oh-oka H (2010) C-type cytochromes in the photosynthetic electron transfer pathways in green sulfur bacteria and heliobacteria. *Photosynth Res* 104:189–199
- Bauer CE, Young DA, Marrs BL (1988) Analysis of the *Rhodobacter capsulatus* *puf* operon. Location of the oxygen-regulated promoter region and the identification of an additional *puf*-encoded gene. *J Biol Chem* 263:4820–4827
- Baymann F, Nitschke W (2010) Heliobacterial Rieske/cytb complex. *Photosynth Res* 104:177–187
- Bell PD, Xin Y, Blankenship RE (2009) Purification and characterization of cytochrome *c*(6) from *Acaryochloris marina*. *Photosynth Res* 102:43–51
- Bernroither M, Tangl D, Lucini C, Furtmüller PG, Peschek GA, Obinger C (2009) Cyanobacterial cytochrome *c*(M): probing its role as electron donor for Cu(A) of cytochrome *c* oxidase. *Biochim Biophys Acta* 1787:135–143
- Berry EA, Guergova-Kuras M, Huang LS, Crofts AR (2000) Structure and function of cytochrome *bc* complexes. *Annu Rev Biochem* 69:1005–1075
- Berry EA, De Bari H, Huang L-S (2013) Unanswered questions about the structure of cytochrome *bc*1 complexes. *Biochim Biophys Acta Bioenerg*
- Bialek W, Nelson M, Tamiola K, Kallas T, Szczepaniak A (2008) Deeply branching *c*<sub>6</sub>-like cytochromes of cyanobacteria. *Biochemistry* 47:5515–5522
- Bialek W, Szczepaniak A, Kolesinski P, Kallas T (2015) Cryptic *c*<sub>6</sub>-like and *c*<sub>M</sub> cytochromes of cyanobacteria. In: Cramer WA, Kallas T (eds) *Cytochrome Complexes: Evolution, Structures, Energy Transduction, and Signaling*. Springer, Dordrecht
- Blankenship RE (2010) Early evolution of photosynthesis. *Plant Physiol* 154:434–438
- Blankenship RE (2014) *Molecular Mechanisms of Photosynthesis*. Blackwell Science, Malden, MA
- Cao L, Bryant DA, Schepmoes AA, Vogl K, Smith RD, Lipton MS, Callister SJ (2012) Comparison of *Chloroflexus aurantiacus* strain J-10-fl proteomes of cells grown chemoheterotrophically and photoheterotrophically. *Photosynth Res* 110:153–168
- Cape JL, Bowman MK, Kramer DM (2006) Understanding the cytochrome *bc* complexes by what they don't do. The Q-cycle at 30. *Trends Plant Sci* 11:46–55
- Choi PS, Grigoryants VM, Abruña HD, Scholes CP, Shapleigh JP (2005) Regulation and function of cytochrome *c'* in *Rhodobacter sphaeroides* 2.4.3. *J Bacteriol* 187:4077–4085
- Clarke TA, Dennison V, Seward HE, Burlat B, Cole JA, Hemmings AM, Richardson DJ (2004) Purification and spectropotentiometric characterization of *Escherichia coli* NrfB, a decaheme homodimer that transfers electrons to the decaheme periplasmic nitrite reductase complex. *J Biol Chem* 279:41333–41339
- Clarke TA, Cole JA, Richardson DJ, Hemmings AM (2007) The crystal structure of the pentahaem c-type cytochrome NrfB and characterization of its solution-state interaction with the pentahaem nitrite reductase NrfA. *Biochem J* 19–30
- Collins AM, Xin Y, Blankenship RE (2009) Pigment organization in the photosynthetic apparatus of *Roseiflexus castenholzii*. *Biochim Biophys Acta* 1787:1050–1056
- Collins AM, Qian P, Tang Q, Bocian DF, Hunter CN, Blankenship RE (2010) Light-harvesting antenna system from the phototrophic bacterium *Roseiflexus castenholzii*. *Biochemistry* 49:7524–7531
- Cooley JW (2010) A structural model for across membrane coupling between the Q<sub>o</sub> and Q<sub>i</sub> active sites of cytochrome *bc*1. *Biochim Biophys Acta* 1797:1842–1848
- Coutinho IB, Xavier AV (1994) Inorganic microbial sulfur metabolism. *Methods Enzymol* 243:119–140
- Cramer W, Whitmarsh J (1977) Photosynthetic cytochromes. *Annu Rev Plant Physiol* 28:133–172
- Cramer WA, Zhang H, Yan J, Kurisu G, Smith JL (2004) Evolution of photosynthesis: time-independent structure of the cytochrome *b*6f complex. *Biochemistry* 43:5921–5929
- Cramer WA, Yan J, Zhang H, Kurisu G, Smith JL (2005) Structure of the cytochrome *b*6f complex: new prosthetic groups, Q-space, and the “hors d'oeuvres hypothesis” for assembly of the complex. *Photosynth Res* 85:133–143
- Crofts AR, Hong S, Wilson C, Burton R, Victoria D, Harrison C, Schulten K (2013a) The mechanism of ubihydroquinone oxidation at the Q(o)-site of the cytochrome *bc*(1) complex. *Biochim Biophys Acta*. doi:10.1016/j.bbabi.2013.01.009
- Crofts AR, Hong S, Wilson C, Burton R, Victoria D, Harrison C, Schulten K (2013b) The mechanism of ubihydroquinone oxidation at the Q<sub>o</sub>-site of the cytochrome *bc*1 complex. *Biochim Biophys Acta Bioenerg* 1827:1362–1377
- Czapla M, Cieluch E, Borek A, Sarewicz M, Osyczka A (2013) Catalytically-relevant electron transfer between two hemes *bL* in the hybrid cytochrome

- bc1-like complex containing a fusion of *Rhodobacter sphaeroides* and *capsulatus* cytochromes b. *Biochim Biophys Acta*. doi:10.1016/j.bbabi.2013.02.007
- Daldal F, Mandaci S, Winterstein C, Myllykallio H, Duyck K, Zannoni D (2001) Mobile cytochrome c2 and membrane-anchored cytochrome cy are both efficient electron donors to the cbb3- and aa3-type cytochrome c oxidases during respiratory growth of *Rhodobacter sphaeroides*. *J Bacteriol* 183:2013–2024
- Davenport HE, Hill R (1952) The preparation and some properties of cytochrome f. *Proc R Soc B Biol Sci* 139:327–345
- De Lacroix de Lavalette A, Barucq L, Alric J, Rapaport F, Zito F (2009) Is the redox state of the c heme of the cytochrome b6f complex dependent on the occupation and structure of the Qi site and vice versa? *J Biol Chem* 284:20822–20829
- Deisenhofer J, Epp O, Miki K, Huber R, Michel H (1985) Structure of the protein subunits in the photosynthetic reaction centre of *Rhodospseudomonas viridis* at 3 Å resolution. *Nature* 318: 618–624
- Díaz-Moreno I, Hulsker R, Skubak P, Foerster JM, Cavazzini D, Finiguerra MG, Díaz-Quintana A, . . . , Ubbink M (2014) The dynamic complex of cytochrome c6 and cytochrome f studied with paramagnetic NMR spectroscopy. *Biochim Biophys Acta*. doi:10.1016/j.bbabi.2014.03.009
- Dibrova DV, Cherepanov DA, Galperin MY, Skulachev VP, Mulikdjanian AY (2013) Evolution of cytochrome bc complexes: from membrane-anchored dehydrogenases of ancient bacteria to triggers of apoptosis in vertebrates. *Biochim Biophys Acta* 1827:1407–1427
- Dracheva SM, Drachev LA, Konstantinov AA, Semenov AY, Skulachev VP, Arutjunjan AM, Shuvalov VA, Zaberezhnaya SM (1988) Electrogenic steps in the redox reactions catalyzed by photosynthetic reaction-centre complex from *Rhodospseudomonas viridis*. *Eur J Biochem* 171:253–264
- Drop B, Webber-Birungi M, Yadav SKN, Filipowicz-Szymanska A, Fusetti F, Boekema EJ, Croce R (2014) Light-harvesting complex II (LHCII) and its supramolecular organization in *Chlamydomonas reinhardtii*. *Biochim Biophys Acta Bioenerg* 1837:63–72
- Dutton PL, Petty KM, Bonner HS, Morse SD (1975) Cytochrome c2 and reaction center of *Rhodospseudomonas spheroides* Ga. membranes. Extinction coefficients, content, half-reduction potentials, kinetics and electric field alterations. *Biochim Biophys Acta Bioenerg* 387:536–556
- Esser L, Elberry M, Zhou F, Yu CA, Yu L, Xia D (2008) Inhibitor-complexed structures of the cytochrome bc1 from the photosynthetic bacterium *Rhodobacter sphaeroides*. *J Biol Chem* 283:2846–2857
- Falkowski PG, Raven JA (2007) *Aquatic Photosynthesis*. Princeton University Press, Princeton, p 512
- Feyziyev Y, Deák Z, Styring S, Bernát G (2013) Electron transfer from Cyt b(559) and tyrosine-D to the S2 and S3 states of the water oxidizing complex in photosystem II at cryogenic temperatures. *J Bioenerg Biomembr* 45:111–120
- Fowler CF, Nugent NA, Fuller RC (1971) The isolation and characterization of a photochemically active complex from *Chloropseudomonas ethylica*. *Proc Natl Acad Sci USA* 68:2278–2282
- Gao X, Xin Y, Blankenship RE (2009) Enzymatic activity of the alternative complex III as a menaquinol:auracyanin oxidoreductase in the electron transfer chain of *Chloroflexus aurantiacus*. *FEBS Lett* 583:3275–3279
- Gao X, Xin Y, Bell PD, Wen J, Blankenship RE (2010) Structural analysis of alternative complex III in the photosynthetic electron transfer chain of *Chloroflexus aurantiacus*. *Biochemistry* 49:6670–6679
- Gao X, Majumder EW, Kang Y, Yue H, Blankenship RE (2013) Functional analysis and expression of the mono-heme containing cytochrome c subunit of alternative complex III in *Chloroflexus aurantiacus*. *Arch Biochem Biophys* 535:197–204
- Gong X-M, Paddock ML, Okamura MY (2003) Interactions between cytochrome c2 and photosynthetic reaction center from *Rhodobacter sphaeroides*: changes in binding affinity and electron transfer rate due to mutation of interfacial hydrophobic residues are strongly correlated. *Biochemistry* 42:14492–14500
- Guerrero F, Zurita JL, Roncel M, Kirilovsky D, Ortega JM (2014) The role of the high potential form of the cytochrome b559: study of *Thermosynechococcus elongatus* mutants. *Biochim Biophys Acta* 1837:908–919
- Gupta R, He Z, Luan S (2002) Functional relationship of cytochrome c(6) and plastocyanin in *Arabidopsis*. *Nature* 417:567–571
- Hara M (1998) Redox properties of an H-subunit-depleted photosynthetic reaction center from *Rhodospseudomonas viridis*. *Biochim Biophys Acta Bioenerg* 1363:199–208
- Hasan SS, Yamashita E, Baniulis D, Cramer WA (2013) Quinone-dependent proton transfer pathways in the photosynthetic cytochrome b6f complex. *Proc Natl Acad Sci USA* 110:4297–4302

- Heinrich M, Golbeck JH (2007) Heliobacterial photosynthesis. *Photosynth Res* 92:35–53
- Hervas M, Navarro JA, Diaz A, Bottin H, De la Rosa MA (1995) Laser-flash kinetic analysis of the fast electron transfer from Plastocyanin and Cytochrome c6 to photosystem I. Experimental evidence on the evolution of the reaction mechanism. *Biochemistry* 34:11321–11326
- Higuchi M, Hirano Y, Kimura Y, Oh-oka H, Miki K, Wang ZY (2009) Overexpression, characterization, and crystallization of the functional domain of cytochrome c(z) from *Chlorobium tepidum*. *Photosynth Res* 102:77–84
- Hill KL, Merchant S (1992) In vivo competition between plastocyanin and a copper-dependent regulator of the *Chlamydomonas reinhardtii* cytochrome c6 gene. *Plant Physiol* 100:319–326
- Hill K, Li H, Singer J, Merchant S (1991) Isolation and structural characterization of the *Chlamydomonas reinhardtii* gene for cytochrome c6. Analysis of the kinetics and metal specificity of its copper-responsive expression. *J Biol Chem* 266:15060–15067
- Hippler M (1999) Insertion of the N-terminal part of PsaF from *Chlamydomonas reinhardtii* into photosystem I from *Synechococcus elongatus* enables efficient binding of Algal plastocyanin and cytochrome c6. *J Biol Chem* 274:4180–4188
- Hirano Y, Higuchi M, Azai C, Oh-oka H, Miki K, Wang ZY (2010) Crystal structure of the electron carrier domain of the reaction center cytochrome c(z) subunit from green photosynthetic bacterium *Chlorobium tepidum*. *J Mol Biol* 397:1175–1187
- Hochkoeppler A, Jenney FJ, Lang S, Zannoni D, Daldal F (1995) Membrane-associated cytochrome cy of *Rhodobacter capsulatus* is an electron carrier from the cytochrome bc1 complex to the cytochrome c oxidase during respiration. *J Bacteriol* 177:608–613
- Hochkoeppler A, Ciurli S, Kofod P, Venturoli G, Zannoni D (1997) On the role of cytochrome c8 in photosynthetic electron transfer of the purple non-sulfur bacterium *Rhodospirillum rubrum*. *Photosynth Res* 53:13–21
- Hohmann-Marriott MF, Blankenship RE (2011) Evolution of photosynthesis. *Annu Rev Plant Biol* 62:515–548
- Howe CJ, Schlarb-Ridley BG, Wastl J, Purton S, Bendall DS (2006) The novel cytochrome c6 of chloroplasts: a case of evolutionary bricolage? *J Exp Bot* 57:13–22
- Howe CJ, Nimmo RH, Barbrook AC, Bendall DS (2015) Cytochrome c<sub>6a</sub> of chloroplasts. In: Cramer WA, Kallas T (eds) *Cytochrome Complexes: Evolution, Structures, Energy Transduction, and Signaling*. Springer, Dordrecht
- Hunte C (2003) Protonmotive pathways and mechanisms in the cytochrome bc1 complex. *FEBS Lett* 545:39–46
- Iverson TM (2006) Evolution and unique bioenergetic mechanisms in oxygenic photosynthesis. *Curr Opin Chem Biol* 10:91–100
- Iwai M, Takizawa K, Tokutsu R, Okamuro A, Takahashi Y, Minagawa J (2010) Isolation of the elusive supercomplex that drives cyclic electron flow in photosynthesis. *Nature* 464:1210–1213
- Jenney FE, Prince RC, Daldal F (1994) Roles of the soluble cytochrome c2 and membrane-associated cytochrome cy of *Rhodobacter capsulatus* in photosynthetic electron transfer. *Biochemistry* 33:2496–2502
- Jones MR (2009) Structural plasticity of reaction centers from purple bacteria. In: Hunter CN, Daldal F, Thurnauer MC, Beatty JT (eds) *Purple Phototrophic Bact*. Springer, Dordrecht, pp 295–321
- Kallas T (2012) Cytochrome b6/f complex at the heart of energy transduction and redox signaling. In: Eaton-Rye JJ, Tripathy BC, Sharkey TD (eds) *Photosynthesis*. Springer, Dordrecht, pp 501–560
- Kaminskaya OP, Shuvalov VA (2013) Biphasic reduction of cytochrome b559 by plastoquinol in photosystem II membrane fragments: evidence for two types of cytochrome b559/plastoquinone redox equilibria. *Biochim Biophys Acta* 1827:471–483
- Kashey TS, Cowgill JB, McConnell MD, Flores M, Redding KE (2014) Expression and characterization of cytochrome c553 from *Heliobacterium modesticaldum*. *Photosynth Res*. doi:10.1007/s11120-014-9982-y
- Katoh H, Itoh S, Shen JR, Ikeuchi M (2001) Functional analysis of psbV and a novel c-type cytochrome gene psbV2 of the thermophilic cyanobacterium *Thermosynechococcus elongatus* strain BP-1. *Plant Cell Physiol* 42:599–607
- Kerfeld CA, Krogmann DW (1998) Photosynthetic cytochromes c in cyanobacteria, algae, and plants. *Annu Rev Plant Physiol Plant Mol Biol* 49:397–425
- Kerfeld CA, Sawayama M, Bottin H, Tran KT, Sugiura M, Cascio D, Desbois A, . . . , Boussac A (2003) Structural and EPR characterization of the soluble form of cytochrome c-550 and of the psbV2 gene product from the cyanobacterium *Thermosynechococcus elongatus*. *Plant Cell Physiol* 44:697–706
- Khalifaoui-Hassani B, Lanciano P, Lee D-W, Darrouzet E, Daldal F (2012) Recent advances in cytochrome bc(1): inter monomer electronic communication? *FEBS Lett* 586:617–621

- King JD, McIntosh CL, Halsey CM, Lada BM, Niedzwiedzki DM, Cooley JW, Blankenship RE (2013) Metalloproteins diversified: the auracyanins are a family of cupredoxins that stretch the spectral and redox limits of blue copper proteins. *Biochemistry* 52:8267–8275
- Kirilovsky D, Roncel M, Boussac A, Wilson A, Zurita JL, Ducruet JM, Bottin H, . . . , Rutherford AW (2004) Cytochrome c550 in the cyanobacterium *Thermosynechococcus elongatus*: study of redox mutants. *J Biol Chem* 279:52869–52880
- Kramer D, Wolfgang N, Cooley JW (2009) The cytochrome bc 1 and related bc complexes: the rieske/cytochrome b complex as the functional core of a central electron/proton transfer complex. In: Hunter CN, Daldal F, Thurnauer MC, Beatty JT (eds) *Purple Phototrophic Bact.* Springer, Dordrecht, pp 451–473
- Lau MCY, Pointing SB (2009) Vertical partitioning and expression of primary metabolic genes in a thermophilic microbial mat. *Extremophiles* 13:533–540
- Lin X, Williams JC, Allen JP, Mathis P (1994) Relationship between rate and free energy difference for electron transfer from cytochrome c2 to the reaction center in *Rhodobacter sphaeroides*. *Biochemistry* 33:13517–13523
- Liu H, Chen J, Huang RY, Weisz D, Gross ML, Pakrasi HB (2013) Mass spectrometry-based footprinting reveals structural dynamics of loop E of the chlorophyll-binding protein CP43 during photosystem II assembly in the cyanobacterium *Synechocystis* 6803. *J Biol Chem* 288:14212–14220
- Liu H, Zhang H, Weisz DA, Vidavsky I, Gross ML, Pakrasi HB (2014) MS-based cross-linking analysis reveals the location of the PsbQ protein in cyanobacterial photosystem II. *Proc Natl Acad Sci USA* 111:4638–4643
- Majumder ELW, King JD, Blankenship RE (2013) Alternative complex III from phototrophic bacteria and its electron acceptor auracyanin. *Biochim Biophys Acta Bioenerg* 1827:1383–1391
- Margulis L (1992) *Symbiosis in Cell Evolution*, 2nd edn. W.H. Freeman, San Francisco
- Martinez SE, Huang D, Szczepaniak A, Cramer WA, Smith JL (1994) Crystal structure of chloroplast cytochrome f reveals a novel cytochrome fold and unexpected heme ligation. *Structure* 2: 95–105
- Meyer TE, Donohue TJ (1995) Cytochromes, iron-sulfur, and copper proteins mediating electron transfer from the Cyt bc 1 complex to photosynthetic reaction center complexes. In: Blankenship RE, Madigan MT, Bauer CE (eds) *Anoxygenic Photosynthetic Bacteria*. Springer, Dordrecht, pp 725–745
- Meyer TE, Tollin G, Cusanovich MA, Freeman JC, Blankenship RE (1989) In vitro kinetics of reduction of cytochrome c554 isolated from the reaction center of the green phototrophic bacterium, *Chloroflexus aurantiacus*. *Arch Biochem Biophys* 272: 254–261
- Moore GR, Pettigrew GW (1990) *Cytochromes c: Evolutionary, Structural, and Physicochemical Aspects*. Springer, Berlin/New York, p 478
- Müh F, Zouni A (2015) Cytochrome *b*<sub>559</sub> in photosystem II. In: Cramer WA, Kallas T (eds) *Cytochrome Complexes: Evolution, Structures, Energy Transduction, and Signaling*. Springer, Dordrecht
- Mullineaux CW (2014) Co-existence of photosynthetic and respiratory activities in cyanobacterial thylakoid membranes. *Biochim Biophys Acta* 1837: 503–511
- Myllykallio H, Drepper F, Mathis P, Daldal F (1998) Membrane-anchored cytochrome cy mediated microsecond time range electron transfer from the cytochrome bc1 complex to the reaction center in *Rhodobacter capsulatus*. *Biochemistry* 37:5501–5510
- Nagashima S, Shimada K, Verméglio A, Nagashima KVP (2011) The cytochrome c<sub>8</sub> involved in the nitrite reduction pathway acts also as electron donor to the photosynthetic reaction center in *Rubrivivax gelatinosus*. *Biochim Biophys Acta* 1807: 189–196
- Nelson N, Ben-Shem A (2004) The complex architecture of oxygenic photosynthesis. *Nat Rev Mol Cell Biol* 5:971–982
- Nogi T, Hirano Y, Miki K (2005) Structural and functional studies on the tetraheme cytochrome subunit and its electron donor proteins: the possible docking mechanisms during the electron transfer reaction. *Photosynth Res* 85:87–99
- Oh-oka H, Kamei S, Matsubara H, Iwaki M, Itoh S (1995) Two molecules of cytochrome c function as the electron donors to P840 in the reaction center complex isolated from a green sulfur bacterium, *Chlorobium tepidum*. *FEBS Lett* 365: 30–34
- Oh-oka H, Iwaki M, Itoh S (1998) Membrane-bound cytochrome cz couples quinol oxidoreductase to the P840 reaction center complex in isolated membranes of the green sulfur bacterium *Chlorobium tepidum*. *Biochemistry* 37:12293–12300
- Okkels JS, Kjaer B, Hansson O, Svendsen I, Møller BL, Scheller HV (1992) A membrane-bound monoheme cytochrome c551 of a novel type is the immediate electron donor to P840 of the *Chlorobium vibrioforme* photosynthetic reaction center complex. *J Biol Chem* 267:21139–21145

- Ortega JM, Drepper F, Mathis P (1999) Electron transfer between cytochrome c2 and the tetraheme cytochrome c in *Rhodospseudomonas viridis*. *Photosynth Res* 59:147–157
- Osyczka A, Cooley JW (2013) Protein conformational changes involved in the cytochrome bc<sub>1</sub> complex catalytic cycle. *Biochim Biophys Acta Bioenerg* 1827:1340–1345
- Parson WW (1968) The role of P870 in bacterial photosynthesis. *Biochim Biophys Acta* 153:248–259
- Pokhrel R, Brudvig G (2014) Oxygen-evolving complex of photosystem II: correlating structure with spectroscopy. *Phys Chem Chem Phys*. doi:10.1039/c4cp00493k
- Pospišil P (2011) Enzymatic function of cytochrome b559 in photosystem II. *J Photochem Photobiol B* 104:341–347
- Prince RC, George GN (1995) Cytochrome f revealed. *Trends Biochem Sci* 20:217–218
- Prince RC, Olson JM (1976) Some thermodynamic and kinetic properties of the primary photochemical reactants in a complex from a green photosynthetic bacterium. *Biochim Biophys Acta* 423:357–362
- Redding KE, Sarrou I, Rappaport F, Santabarbara S, Lin S, Reifschneider KT (2013) Modulation of the fluorescence yield in heliobacterial cells by induction of charge recombination in the photosynthetic reaction center. *Photosynth Res*. doi:10.1007/s11120-013-9957-4
- Refojo PN, Teixeira M, Pereira MM (2010) The alternative complex III of *Rhodothermus marinus* and its structural and functional association with caa(3) oxygen reductase. *Biochim Biophys Acta–Bioenerg* 1797:1477–1482
- Refojo PN, Ribeiro MA, Calisto F, Teixeira M, Pereira MM (2013) Structural composition of alternative complex III: variations on the same theme. *Biochim Biophys Acta Bioenerg* 1827:1378–1382
- Ritchie RJ, Runcie JW (2012) Photosynthetic electron transport in an anoxygenic photosynthetic bacterium *Afifella* (*Rhodospseudomonas*) *marina* measured using PAM fluorometry. *Photochem Photobiol*. doi:10.1111/j.1751-1097.2012.01241.x
- Roncel M, Kirilovsky D, Guerrero F, Serrano A, Ortega JM (2012) Photosynthetic cytochrome c550. *Biochim Biophys Acta* 1817:1152–1163
- Roszak AW, Moulisová V, Reksodipuro ADP, Gardiner AT, Fujii R, Hashimoto H, Isaacs NW, Cogdell RJ (2012) New insights into the structure of the reaction centre from *Blastochloris viridis*: evolution in the laboratory. *Biochem J* 442:27–37
- Russell HJ, Hardman SJO, Heyes DJ, Hough MA, Greetham GM, Towrie M, Hay S, Scrutton NS (2013) Modulation of ligand-heme reactivity by binding pocket residues demonstrated in cytochrome c' over the femtosecond-second temporal range. *FEBS J* 280:6070–6082
- Rutherford AW, Osyczka A, Rappaport F (2012) Back-reactions, short-circuits, leaks and other energy wasteful reactions in biological electron transfer: redox tuning to survive life in O(2). *FEBS Lett* 586:603–616
- Sakurai H, Kusumoto N, Inoue K (1996) Function of the reaction center of green sulfur bacteria. *Photochem Photobiol* 64:5–13
- Samyn B, Smet L (1996) A high-potential soluble cytochrome C-551 from the purple phototrophic bacterium *chromatium vinosum* is homologous to cytochrome C8 from denitrifying. *Eur J Biochem* 236:689–696
- Sanders C, Turkarslan S, Onder O, Frawley ER, Kranz RG, Koch HG, Daldal F (2009) Biogenesis of c-type Cytochromes and Cytochrome Complexes. In: Hunter CN, Daldal F, Thurnauer MC, Beatty JT (eds) *Purple Phototrophic Bact*. Springer, Dordrecht, pp 407–423
- Sarrou I, Khan Z, Cowgill J, Lin S, Brune D, Romberger S, Golbeck JH, Redding KE (2012) Purification of the photosynthetic reaction center from *Heliobacterium modesticaldum*. *Photosynth Res* 111:291–302
- Sattley WM, Blankenship RE (2010) Insights into heliobacterial photosynthesis and physiology from the genome of *Heliobacterium modesticaldum*. *Photosynth Res* 104:113–122
- Shinopoulos KE, Brudvig GW (2012) Cytochrome b559 and cyclic electron transfer within photosystem II. *Biochim Biophys Acta* 1817:66–75
- Simon J, Klotz MG (2013) Diversity and evolution of bioenergetic systems involved in microbial nitrogen compound transformations. *Biochim Biophys Acta* 1827:114–135
- Sponholtz DL, Brautigan DL, Loach PA, Margoliash E (1976) Preparation of cytochrome c2 from *Rhodospirillum rubrum*. *Anal Biochem* 72:255–260
- Stroebel D, Choquet Y, Popot J-L, Picot D (2003) An atypical haem in the cytochrome b(6)f complex. *Nature* 426:413–418
- Suga M, Lai T-L, Sugiura M, Shen JR, Boussac A (2013) Crystal structure at 1.5 Å resolution of the PsbV2 cytochrome from the cyanobacterium *Thermosynechococcus elongatus*. *FEBS Lett* 587:3267–3272
- Tang KH, Barry K, Chertkov O, Dalin E, Han CS, Hauser LJ, Honchak BM, . . . , Blankenship RE (2011) Complete genome sequence of the filamentous anoxygenic phototrophic bacterium *Chloroflexus aurantiacus*. *BMC Genomics* 12:334

- Tatsuhiko Y (1970) Solubilization, purification and properties of particulate hydrogenase from *Desulfovibrio vulgaris*. *J Biochem* 68:649–657
- Trubitsin BV, Mamedov MD, Semenov AY, Tikhonov AN (2014) Interaction of ascorbate with photosystem I. *Photosynth Res*
- Trumpower BL (1990) Cytochrome bc<sub>1</sub> complexes of microorganisms. *Microbiol Mol Biol Rev* 54:101–129
- Tsukatani Y, Azai C, Kondo T, Itoh S, Oh-Oka H (2008) Parallel electron donation pathways to cytochrome c(z) in the type I homodimeric photosynthetic reaction center complex of *Chlorobium tepidum*. *Biochim Biophys Acta* 1777:1211–1217
- Verméglio A, Li J, Schoepp-Cothenet B, Pratt N, Knaff DB (2002) The role of high-potential iron protein and cytochrome c<sub>8</sub> as alternative electron donors to the reaction center of *Chromatium vinosum*. *Biochemistry* 41:8868–8875
- Weber PC, Bartsch RG, Cusanovich MA, Hamlin RC, Howard A, Jordan SR, Kamen MD, . . . , Salemme FR (1980) Structure of cytochrome c': a dimeric, high-spin haem protein. *Nature* 286:302–304
- Westerhuis WHJ (1996) Consequences for the organization of reaction center-light harvesting antenna 1 (LH1) core complexes of *Rhodobacter sphaeroides* arising from deletion of amino acid residues from the C terminus of the LH1 alpha polypeptide. *J Biol Chem* 271:3285–3292
- Whitmarsh J, Cramer WA (1979) Cytochrome f function in photosynthetic electron transport. *Biophys J* 26:223–234
- Williamson A, Conlan B, Hillier W, Wydrzynski T (2011) The evolution of Photosystem II: insights into the past and future. *Photosynth Res* 107:71–86
- Worrall JAR, Luisi BF, Schlarb-Ridley BG, Bendall DS, Howe CJ (2008) Cytochrome c<sub>6A</sub>: discovery, structure and properties responsible for its low haem redox potential. *Biochem Soc Trans* 36:1175–1179
- Xin Y, Pan J, Collins AM, Lin S, Blankenship RE (2011) Excitation energy transfer and trapping dynamics in the core complex of the filamentous photosynthetic bacterium *Roseiflexus castenholzii*. *Photosynth Res*. doi:10.1007/s11120-011-9669-6
- Yamada M, Zhang H, Hanada S, Nagashima KV, Shimada K, Matsuura K (2005) Structural and spectroscopic properties of a reaction center complex from the chlorosome-lacking filamentous anoxygenic phototrophic bacterium *Roseiflexus castenholzii*. *J Bacteriol* 187:1702–1709
- Yanyushin MF, del Rosario MC, Bruno DC, Blankenship RE (2005) New class of bacterial membrane oxidoreductases. *Biochemistry* 44:10037–10045
- Yue H, Kang Y, Zhang H, Gao X, Blankenship RE (2012) Expression and characterization of the di-heme cytochrome c subunit of the cytochrome bc complex in *Heliobacterium modesticaldum*. *Arch Biochem Biophys* 517:131–137
- Zeng Y, Feng F, Medová H, Dean J, Koblížek M (2014) Functional type 2 photosynthetic reaction centers found in the rare bacterial phylum Gemmatimonadetes. *Proc Natl Acad Sci USA* 111:7795–7800
- Zhang Y, Majumder EL-W, Yue H, Blankenship RE, Gross ML (2014) Structural analysis of di-heme cytochrome C by hydrogen-deuterium exchange mass spectrometry and homology modeling. *Biochemistry* 53:5619–5630

# Chapter 4

## Evolution of Photosynthetic NDH-1: Structure and Physiological Function

Toshiharu Shikanai<sup>a,\*</sup> and Eva-Mari Aro<sup>b</sup>

<sup>a</sup>*Department of Botany, Graduate School of Science, Kyoto University, Kitashirakawa, Sakyo-ku, Kyoto 606-8502, Japan*

<sup>b</sup>*Department of Biochemistry, and Molecular Plant Biology, University of Turku, FIN-20014, Turku, Finland*

Summary.....	51
I. Introduction.....	52
II. Function and Structure of Cyanobacterial NDH-1.....	53
III. Chloroplast NDH-1 and Cyclic Electron Transport Around PSI.....	57
IV. Structure of Chloroplast NDH-1.....	58
V. Evolution of Chloroplast NDH-1 in Land Plants.....	60
VI. Physiological Reason for Evolutionary Increase in Complexity of Chloroplast NDH-1.....	63
VII. The Origin of Photosynthetic NDH-1.....	64
VIII. Concluding Remarks.....	64
Acknowledgements.....	65
References.....	65

### Summary

Chloroplast and cyanobacterial NADH dehydrogenase-like complex (photosynthetic NDH-1) is structurally related to the multi-subunit-type NADH dehydrogenase present in bacteria and mitochondria (respiratory NDH-1). They both have a common ancestor, namely the group 4 membrane-bound hydrogenases, including energy-converting hydrogenase (Ech). During its evolution, respiratory NDH-1 (complex 1) acquired the electron input N module that functions in NADH oxidation. Homologs of the N module have not been identified in photosynthetic NDH-1. The electron donor system for photosynthetic NDH-1 has apparently remained similar to that in the common ancestor and accepts electrons directly from ferredoxin (Fd). Indeed, the discovery of the NdhS protein required for high-affinity binding of Fd to NDH-1 in chloroplasts and cyanobacteria supports the idea that photosynthetic NDH-1 accepts electrons from Fd. Through modification of its subunit composition NDH-1 in cyanobacteria is involved in divergent functions, including the concentration of CO<sub>2</sub>

---

\*Author for correspondence, e-mail: [shikanai@pmg.bot.kyoto-u.ac.jp](mailto:shikanai@pmg.bot.kyoto-u.ac.jp)

by NDH-1MS complexes. Nonetheless, chloroplast NDH-1 originated from cyanobacterial NDH-1L that in the light mediates cyclic electron transport around photosystem I (PSI) and in darkness regulates respiratory electron transport. Consistent with this, chloroplast NDH-1 also mediates PSI cyclic electron transport as well as chlororespiratory reduction of the plastoquinone pool in order to maintain redox homeostasis in chloroplasts. During the evolution of land plants, the number of subunits of chloroplast NDH-1 increased and it became associated with PSI to form a supercomplex in flowering plants, the process which is necessary to stabilize NDH-1. Despite conservation of the core skeleton forming the L-shape, photosynthetic NDH-1 is likely to have undergone evolution distinct from that of respiratory NDH-1. Consequently, photosynthetic NDH-1 has gained different physiological functions and operates, at least partially, by molecular mechanisms different from those of respiratory NDH-1.

## I. Introduction

Multi-subunit-type NADH dehydrogenase (complex I) couples electron transfer from NADH to quinone, with translocation of protons (or cations) across the membrane. The complex consists of a peripheral arm mediating electron transfer and a membrane arm consisting of the proton-transfer machinery, forming an L-shaped skeleton (Baradaran et al. 2013). NADH-dependent quinone reduction is also mediated by a single-subunit-type enzyme (NDH-2), but this reaction is not coupled with proton translocation (Melo et al. 2004). Multi-subunit proton/cation-transferring enzymes are referred to as NDH-1 to distinguish them from NDH-2. A prototype of NDH-1 is a prokaryotic enzyme consisting of a minimum set of 14 subunits (Friedrich and Scheide 2000) in three distinct modules (N, Q, and P). The peripheral arm contains all of the redox cofactors and is subdivided into the electron-input NADH oxidizing (N) module (composed of NuoE, F, and G in *Escherichia coli* NDH-1) and the Q module mediating electron transfer to the quinone-binding site (composed of NuoB, C, D, and I in *E. coli* NDH-1). The membrane arm forms

the proton-translocating P module composed of 6 subunits (NuoA, J, K, L, M, and N in *E. coli* NDH-1). NuoH does not belong to any module and connects the Q and P modules (Efremov and Sazanov 2012).

Complete sequencing of chloroplast genomes has revealed 11 *ndh* genes in tobacco (*Nicotiana tabacum*) and liverwort (*Marchantia polymorpha*) (Ohyama et al. 1986; Shinozaki et al. 1986). This set of genes encodes 4 subunits of the Q module, 6 subunits of the P module, and NdhA, corresponding to NuoH (Matsubayashi et al. 1987). Why do the chloroplast genomes encode subunits of the respiratory complex? Chloroplasts originated via endosymbiotic events from cyanobacteria, in which photosynthetic and respiratory electron transport share a common quinone pool in the thylakoid membrane (Mullineaux 2014). Reflecting this evolutionary scenario, some electron transport routes in the thylakoid membrane resemble respiratory electron transport in mitochondria. Both NDH-1 and NDH-2 reduce the plastoquinone (PQ) pool, which in turn is oxidized by plastid terminal oxidase (PTOX), which is related to alternative oxidase (AOX) in mitochondria (Rumeau et al. 2007). Chlororespiration is electron transport mediated by these components; particularly high chlororespiration activity has been reported in *Chlamydomonas reinhardtii* (Peltier and Schmidt 1991; Peltier and Cournac 2002). However, the green algae,

---

*Abbreviations:* BN – Blue native; Fd – Ferredoxin; Lhc – Light harvesting complex; NPQ – Nonphotochemical quenching; pmf – Proton motive force; PQ – Plastoquinone; PSI/II – Photosystem I/II; PTOX – Plastid terminal oxidase



including *Chlamydomonas*, have lost their chloroplast NDH-1, and their chlororespiration depends on NDH-2 (Desplats et al. 2009). Even though chloroplast NDH-1 is structurally closely related to respiratory NDH-1, the enzymes have experienced differential evolution and are likely to have acquired different functions from the common ancestor. On the basis of its distinct difference from “respiratory NDH-1” in bacteria and mitochondria, here we call the NDH-1 in chloroplasts and cyanobacteria “photosynthetic NDH-1.” In fact, photosynthetic NDH-1 is unlikely to be a true NADH dehydrogenase and the term “NDH” has been proposed to represent the NADH dehydrogenase-like complex in cyanobacteria and chloroplasts (Ifuku et al. 2011; Yamamoto et al. 2011). Here, we summarize our knowledge about the evolution of cyanobacterial NDH-1 from the common ancestor with respiratory NDH-1. This prototype of photosynthetic NDH-1 further experienced evolution in land plant chloroplasts. We do not yet understand the reasons for this evolution, but we summarize the current progress in research toward elucidation of the mysterious features of the photosynthetic NDH complex. To avoid overlap with recent reviews (Suorsa et al. 2009; Battchikova et al. 2011a; Peng et al. 2011b), we specifically focus on the evolution of photosynthetic NDH-1.

## II. Function and Structure of Cyanobacterial NDH-1

To review the research history of photosynthetic NDH-1, it is natural to start with the story of the M55 mutant of *Synechocystis* sp. PCC 6803 (Ogawa 1991). The M55 mutant was isolated on the basis of its requirement for a high CO<sub>2</sub> concentration for growth; the mutation was identified in the *ndhB* gene encoding an NDH-1 subunit. The discovery was followed by extensive physiological research, the results of which supported the idea that NDH-1 mediates cyclic electron transport around photosystem

I (PSI) (Mi et al. 1992). However, the original idea that NDH-1 operates in PSI cyclic electron transport in order to energize the CO<sub>2</sub>-concentrating machinery was soon found to be overly simplified and was actually an erroneous assumption. Most of the cyanobacterial *ndh* genes are present as a single copy per genome; *ndhD* and *ndhF* are the only exceptions (Table 4.1). The *Synechocystis* genome has 6 *ndhD* genes (*ndhD1* to *ndhD6*) and 3 *ndhF* genes (*ndhF1*, *ndhF3*, and *ndhF4*) (Kaneko et al. 1996). Selective knockout of specific *ndhD* genes has elucidated the distinct functions of NDH-1 (Ohkawa et al. 2000). *NdhD1* and *NdhD2* (but not *Ndh5* and *Ndh6*), which are related to chloroplast *NdhD*, and their double knockout results in a low rate of respiration (Bernát et al. 2011) and impaired photo-heterotrophic growth. The NDH-1 complex containing *NdhD1* or *NdhD2* mediates electron transport from the electron donor to the PQ pool in respiratory electron transport in the dark and in PSI cyclic electron transport in the light. These conclusions made from mutant phenotypes have been supported by proteomics analysis of thylakoid membrane complexes separated by blue native (BN) gels (Herranen et al. 2004; Zhang et al. 2004). In the BN gel, two bands represent distinct forms of NDH-1, namely the NDH-1L (~490 KDa) and the NDH-1M (~350 KDa) complexes (Battchikova et al. 2005). NDH-1L and NDH-1M share all other subunits except for *NdhD1/D2* and *NdhF1*, which are specifically present only in NDH-1L (Prommeenate et al. 2004; Battchikova et al. 2005). Nevertheless, the original idea based on the mutant phenotypes (low rate of respiration and impaired photo-heterotrophic growth) may require modification, because succinate dehydrogenase, at least in *Synechocystis* sp. PCC 6803, has been shown to mainly donate electrons to the PQ pool in darkness (Cooley and Vermaas 2001); thus the role of NDH-1 in respiration may be related to light conditions. Moreover, cyanobacterial NDH-1 includes *NdhS* (see the discussion on the electron donor for chloroplast NDH-1) and

Table 4.1. A list of genes encoding NDH-1 subunits.

SC <sup>a</sup>	Subunit	Other name	<i>At</i> <sup>b</sup>	<i>Mp</i> <sup>c</sup>	<i>Syn</i> <sup>d</sup>	<i>E. coli</i>	motif
M	NdhA		<i>ndhA</i>	<i>ndhA</i>	slr0851	NuoH	TM <sup>e</sup>
	NdhB		<i>ndhB</i>	<i>ndhB</i>	slI0223	NuoN	TM, H <sup>+</sup> translocation
	NdhC		<i>ndhC</i>	<i>ndhC</i>	slr1279	NuoA	TM
	NdhD		<i>ndhD</i>	<i>ndhD</i>	slr0331 (D1) slr1291 (D2)	NuoM	TM, H <sup>+</sup> translocation
	NdhD'				slI1733 (D3) slI0027 (D4)		TM
					slr2007 (D5) slr2009 (D6)		TM
					slI0522	NuoK	TM
					slr0844 (F1) slI1732 (F3) slI0026 (F4)	NuoL	TM, H <sup>+</sup> translocation TM
					slI0521	NuoJ	TM
					slr0261	NuoD	TM
A					slI0520	NuoI	TM
					slr1281	NuoC	TM
					slr1280	NuoB	TM
					ssr1386		
					slI1623		
					slI1262		
					ssI1690		
						NuoE	
						NuoF	NADH binding
						NuoG	
N <sup>f</sup>							

B	PnsB1	NDH48/NDF1	At1g15980	HE855895		
	PnsB2	NDH45/NDF2	At1g64770	HE855896		
	PnsB3	NDF4	At3g16250	HE855897		TM
	PnsB4	NDF6	At1g18730	HE855898	sml0013 (NdhP)	TM
	PnsB5	NDH18	At5g43750	HE855899		TM
L	NdhQ				slr1311	PsbP-like
	PnsL1	PPL2	At2g39470			PsbQ-like
	PnsL2	PQL	At1g14150			PsbQ-like
	PnsL3	PQL	At3g01440			PsbQ-like
	PnsL4	FKBP16-2	At4g39710			FKBP— type PPIase
ED	PnsL5	AtCYP20-2	At5g13120	HE855903		PPIase
	NdhS	CRR31	At4g23890	HE855892	ssl0352	SH3-like fold
	NdhT	CRRJ	At4g09350	HE855893		J domainTM
	NdhU	CRRL	At5g21430	HE855894		J-like domainTM
	NdhV		At2g04039	CUFF.9031		DUF2996
1S <sup>g</sup>	CupA				sl0272	
	CupB				sl11734	
	CupS				slr1302	
LK <sup>h</sup>	Lhca5		At1g45474			Lhcl
	Lhca6		At1g19150			Lhcl

The bolditalics indicate chloroplast-encoded genes

<sup>a</sup>Subcomplex

<sup>b</sup>*Arabidopsis thaliana*

<sup>c</sup>*Marchantia polymorpha*

<sup>d</sup>*Synechocystis* sp. PCC 6803

<sup>e</sup>trans-membrane domain

<sup>f</sup>N module

<sup>g</sup>NDH-1S

<sup>h</sup>Linkers

probably accepts electrons from ferredoxin (Fd) rather than from NAD(P)H (Battchikova et al. 2011b). It is highly conceivable that our original concept of photosynthetic NDH-1 was influenced too much by the homology with respiratory NDH-1.

In contrast to the *Synechocystis*  $\Delta ndhD1/\Delta ndhD2$  mutant, the  $\Delta ndhD3/\Delta ndhD4$  mutant is defective in CO<sub>2</sub> uptake, in addition to PSI cyclic electron transfer, and requires increased levels of CO<sub>2</sub> for optimal growth (Ohkawa et al. 2000; Shibata et al. 2001). *ndhD3* is co-transcribed with *ndhF3* and *cupA/chpY* from an operon induced at low CO<sub>2</sub> concentrations (Maeda et al. 2002; Wang et al. 2004; Zhang et al. 2004). On the other hand, *ndhD4* is constitutively expressed with *ndhF4* and *cupB/chpX*. These subunits, which are specific for the CO<sub>2</sub> concentrating machinery, form NDH-1S complexes, which associate with NDH-1M to form active NDH-1MS complexes (Zhang et al. 2004, 2005). NDH-1MS complexes are involved in CO<sub>2</sub> concentration. The M55 mutant is defective in NdhB, which is present in both NDH-1L and NDH-1MS complexes; this results in disruption of both functions. This research history has been extensively reviewed in other articles (Battchikova and Aro 2007; Ogawa and Mi 2007).

Like the *Thermus thermophilus* and *E. coli* NDH-1 complexes, which consist of a minimal set of 14 subunits (Sazanov et al. 2013) and have been characterized as the prototypes of mitochondrial NDH-1, cyanobac-

terial NDH-1 can be regarded as a model for chloroplast NDH-1. As discussed below in greater detail, photosynthetic NDH-1 lacks the N module composed of three subunits in *E. coli* NDH-1, indicating that 11 subunits form a core conserved both in the respiratory and photosynthetic NDH-1 complexes (Table 4.1). In addition to these 11 subunits, the cyanobacterial NDH-1 contains the NdhL, M, N, and O subunits (Ogawa 1992; Prommeenate et al. 2004; Battchikova et al. 2005). These 15 subunits (NdhA to NdhO), at a minimum, form the core of photosynthetic NDH-1. The crystal structure of NDH-1 has been determined only in the prototypical bacterial enzymes (Efremov et al. 2010; Efremov and Sazanov 2011; Baradaran et al. 2013). Nevertheless, single-particle electron microscopy has provided structural information about cyanobacterial NDH-1 (Arteni et al. 2006). In *Thermosynechococcus elongatus* BP-1, NDH-1 forms an L-shaped structure with a relatively short peripheral hydrophilic arm, which probably reflects the lack of the N module (Fig. 4.1). However, a minor population of the complex contains a longer peripheral arm, implying the presence of an unknown electron input module. Another low-abundance type of the complex forms a U-shaped structure, probably corresponding to the NDH-1MS complex (Arteni et al. 2006; Folea et al. 2008). By adding a YFP-tag to the subunits, the positions of NdhL, M, N, and O have been determined by single-particle

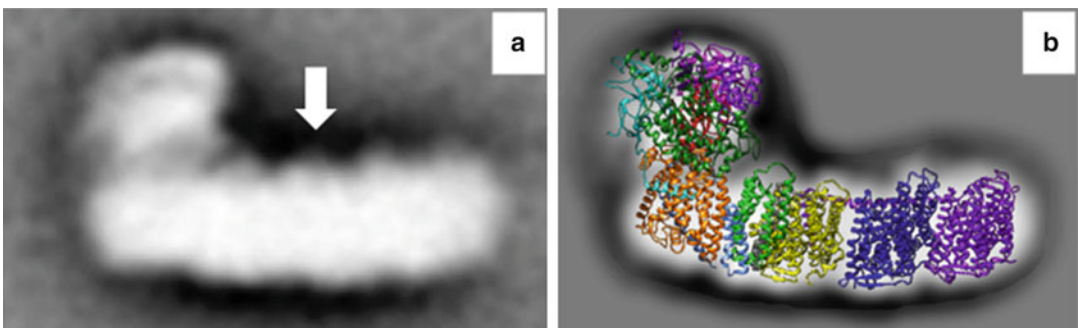


Fig. 4.1. Single-particle images of cyanobacterial NDH-1L (side view). An arrow in (a) indicates the position of NdhL, M, N, and O. (b) Overlap with the crystal structure of respiratory NDH-1, from which the N module is omitted (Single-particle images were kindly provided by E. J. Boekema).

analysis (Birungi et al. 2010). Unexpectedly, the NdhL, M and N subunits were localized to the central part of the membrane arm, which is inconsistent with the *Arabidopsis* model based on genetic and biochemical evidence (Peng et al. 2009, 2012) (see below).

### III. Chloroplast NDH-1 and Cyclic Electron Transport Around PSI

A breakthrough in cyanobacterial study made it possible to seriously reconsider the enigmatic occurrence of NDH-1 in chloroplasts. Meanwhile, a technique for plastid transformation was established (Svab and Maliga 1993), enabling knockouts of the chloroplast *ndh* genes (Burrows et al. 1998; Kofer et al. 1998; Shikanai et al. 1998; Horváth et al. 2000). The initial physiological characterization of the NDH knockout tobacco has been a topic of another review (Shikanai 2007) and is only briefly discussed here. Chloroplast NDH-1 mediates electron transport from the stromal electron pool (see information below on the electron donor) to the PQ pool. However, knockout of the NDH-1 complex has no influence on photosynthetic electron transport under greenhouse conditions (Burrows et al. 1998; Shikanai et al. 1998). This is also true for *Arabidopsis* mutants defective in chloroplast NDH-1 (Hashimoto et al. 2003; Munekage et al. 2004). Chlororespiratory reduction of the PQ pool shares a route with cyclic electron transport around PSI in the light. However, the contribution of chloroplast NDH-1 to the total proton motive force (pmf;  $\Delta\text{pH}$  plus membrane potential) is small, at least in tobacco and *Arabidopsis*. The phenotypes of the NDH-1 mutants have been detected from the post-illumination changes in chlorophyll fluorescence and from  $\text{P700}^+$  levels (Burrows et al. 1998; Shikanai et al. 1998; Hashimoto et al. 2003; Munekage et al. 2004). Importantly, virtually no phenotype has been able to be monitored during steady-state photosynthesis. For example, it has not been possible to monitor the reduction in the extent of non-photochemical quenching

(NPQ) of chlorophyll fluorescence, which in leaves reflects the size of  $\Delta\text{pH}$ . This is also true for attempted measurements of the activity of Fd-dependent PQ reduction in ruptured chloroplasts, which is smaller than the main, antimycin A-sensitive, PGR5-dependent pathway (Okegawa et al. 2008). Although there is evidence that NDH-1-deficient tobacco is sensitive to various environmental stresses (Endo et al. 1999; Horváth et al. 2000), the exact molecular mechanism of the resistance provided by photosynthetic NDH-1 remains obscure.

PSI cyclic electron transport mediates the recycling of electrons from Fd to the PQ pool, contributing to the formation of pmf without accumulation of NADPH (Shikanai 2007). The *Arabidopsis pgr5* (*proton gradient regulation 5*) mutant is defective in the main pathway of PSI cyclic electron transport (Munekage et al. 2002) and this pathway corresponds to the antimycin A-sensitive route of electrons, initially discovered by the group of Arnon (Tagawa et al. 1963; Joët et al. 2001; Munekage et al. 2002; Hertle et al. 2013; Sugimoto et al. 2013). *Arabidopsis* double mutants defective in both the NDH-1- and PGR5-dependent pathways of PSI cyclic electron transport exhibit very severe phenotypes of photosynthesis and plant growth (Munekage et al. 2004), providing genetic evidence that PGR5-dependent and NDH-1-dependent pathways partly redundantly contribute to the formation of pmf. On the basis of the *pgr5* mutant phenotype in *Arabidopsis* (Munekage et al. 2002, 2004) and rice (Nishikawa et al. 2012), the physiological function of PSI cyclic electron transport can be summarized as (Shikanai 2014): (1) Acidification of the thylakoid lumen to induce NPQ (Munekage et al. 2002) and downregulation of the activity of the cytochrome *b<sub>6</sub>f* complex (Suorsa et al. 2012), both of which are required to protect PSI from photodamage (Munekage et al. 2002; Suorsa et al. 2012). This process is especially important for growth under fluctuating light conditions (Suorsa et al. 2012; Kono et al. 2014). (2)

The pmf formed by PSI cyclic electron transport, as well as that formed by linear electron transport, contributes to the ATP supply for CO<sub>2</sub> fixation (Munekage et al. 2002, 2008; Nishikawa et al. 2012). The defect in chloroplast NDH-1 accelerates the *pgr5* phenotype (Munekage et al. 2004), suggesting that NDH-1 also contributes to the formation of pmf in chloroplasts by mediating PSI cyclic electron transport. This was also supported by the direct analysis of the size of pmf in the double mutants (Wang et al. 2015).

Although the contribution of chloroplast NDH-1 to pmf formation is minor during steady-state photosynthesis, it may regulate the redox state of the PQ pool under certain conditions in combination with PTOX (Joët et al. 2002; Trouillard et al. 2012). The variegated phenotype of the PTOX mutant (*immutans*) is alleviated by the absence of chloroplast NDH-1, suggesting that chlororespiration has a regulatory function in maintaining the proper redox state of the PQ pool during early chloroplast development (Okegawa et al. 2010). PGR5-dependent PQ reduction also contributes substantially to redox homeostasis at this stage (Okegawa et al. 2010). Nevertheless, the question remains regarding the physiological function of NDH-dependent PSI cyclic electron transport in mature chloroplasts. This topic is discussed further below, on the basis of the different phenotypes of NDH-1-deficient mutants between flowering plants and *Marchantia*.

#### IV. Structure of Chloroplast NDH-1

Respiratory NDH-1 in *E. coli* is composed of 3 modules, whereas photosynthetic NDH-1 in chloroplasts consists of 5 subcomplexes assigned as subcomplexes A, B, ED, L, and M (Ifuku et al. 2011). Eleven core subunits, which are homologous to those forming the Q and P modules in *E. coli*, are encoded by the chloroplast genome (Table 4.1). NdhH, I, J, and K form the core of subcomplex A, which corresponds to the Q module in *E. coli*,

whereas NdhB, C, D, E, F, and G are core components of subcomplex M (membrane), corresponding to the P module. NdhA corresponds to NuoH in *E. coli* NDH-1, which connects the Q and P modules. In addition to the 4 plastid-encoded subunits, the subcomplex A of chloroplast NDH-1 contains NdhL, M, N, and O, which are encoded in the nuclear genomes in eukaryotes (Rumeau et al. 2005; Shimizu et al. 2008). Although single-particle analysis has detected NdhL, M and N in the center of the stromal surface of subcomplex M in cyanobacteria (Fig. 4.1), genetic evidence suggests that they are components of subcomplex A in chloroplasts (Peng et al. 2011b). This is in accordance with a recent report, which re-localizes the NdhO subunit to the peripheral hydrophilic arm of cyanobacterial NDH-1 (Zhao et al. 2014). In-depth research on the assembly of subcomplex A in the stroma also provide support for this localization in *Arabidopsis* (Peng et al. 2012): (1) In the assembly intermediates of subcomplex A in the stroma, the stability of NdhK depends on NdhM, implying that there is an interaction between the two proteins. (2) NdhO forms the scaffold for further assembly with NdhH and the assembly factor CRR41, implying that NdhO also directly interacts with NdhH. (3) Finally, NdhL and NdhN are probably needed for incorporation of the peripheral arm into the proper position of the membrane arm. Thus, NdhL and NdhN should be located close to the peripheral arm. More study is needed to determine the exact positions of these subunits specific to photosynthetic NDH-1.

Although the exact positions of NdhL, M, N, and O are still unclear, 8 subunits in total form subcomplex A in chloroplast NDH-1 (Table 4.1). NdhL has 2 trans-membrane domains and was first discovered in cyanobacteria (Ogawa 1992); subsequently, its homolog with an additional trans-membrane domain was identified in *Arabidopsis* (Shimizu et al. 2008). NdhL likely interacts with NdhA, which interconnects subcomplexes A and M. NdhL is essential for NDH activity but is not required for stabilizing NDH-1 subunits in

cyanobacteria (Ogawa 1992). In contrast, the *ndhL* defect destabilizes subcomplex A in *Arabidopsis* (Shimizu et al. 2008). In *Arabidopsis*, subcomplex A is assembled in the stroma (Peng et al. 2012) as is the Q module in mitochondria (Mimaki et al. 2012). NdhL may be required for placing subcomplex A in the proper position on subcomplex M to build the L-shape. It is likely that the assembly factor CRR7 is required for this process (Peng et al. 2010) and that NdhN is incorporated into the NDH-1 complex in this step, because NdhN has not been detected—even in the final assembly intermediate—in the stroma (Peng et al. 2012). In the absence of NdhL, subcomplex A may be placed in a wrong position on subcomplex M, thereby rendering the subcomplex A subunits more susceptible to proteolytic attack in chloroplasts than in cyanobacteria. Probably reflecting this assembly step, the individual proteins of the M, L, and B subcomplexes are stable in the absence of subcomplex A and remain associated with PSI (Peng et al. 2008, 2009).

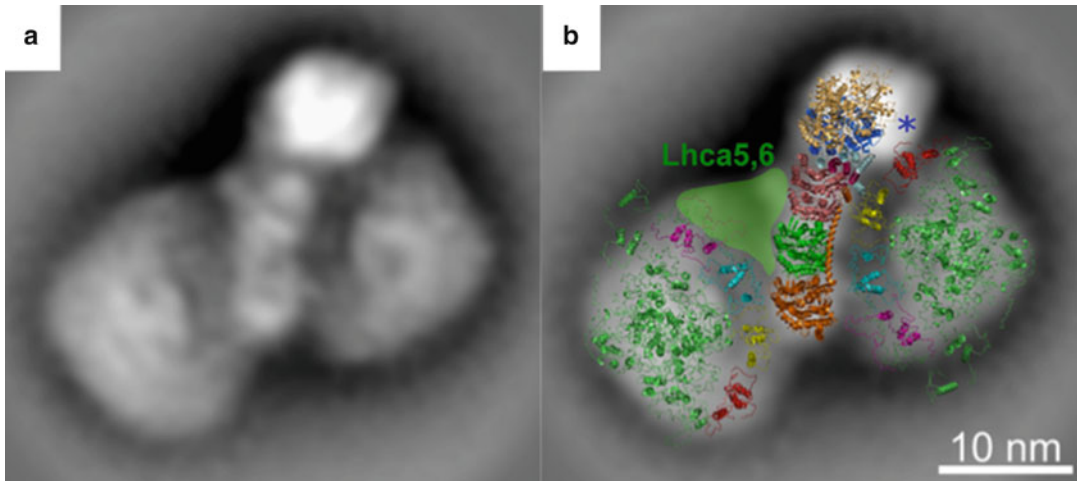
Compared with cyanobacterial NDH-1, a striking structural difference in chloroplast NDH-1 is the presence of additional B and L (lumen) subcomplexes (Table 4.1). Subcomplex B, composed of 5 protein subunits, was first believed to be specific to chloroplast NDH-1, but recently a novel NDH-1 subunit, NdhP was discovered in cyanobacteria; it shows weak similarity to PnsB4/NDF6 in the region including the trans-membrane domain (Nowaczyk et al. 2011; Ishikawa et al. 2008). Chloroplast NDH-1 may have required more accessory subunits that interact with PnsB4.

In *Arabidopsis* mutants defective in subcomplex L, the stability of subcomplex A is drastically affected, suggesting that subcomplex L interacts with NdhL, a sole subcomplex A subunit with trans-membrane domains, thereby stabilizing the entire subcomplex A (Peng et al. 2009). Unexpectedly, 3 subunits of subcomplex L are homologs of the oxygen-evolving complex of PSII. PnsL1 is a PsbP-like protein 2 (PPL2), whereas PnsL2 and PnsL3 are PsbQ-like proteins (PQLs) (Ishihara et al.

2007; Suorsa et al. 2010; Yabuta et al. 2010). On the basis of the amino acid sequence, we categorized PnsL3 into subcomplex L, but its stability is more closely related to that of subcomplex B (Yabuta et al. 2010). Most likely, PnsL3 attaches to the luminal side of subcomplex B, possibly via interaction with PnsB4 or PnsB5, or both (Ifuku et al. 2011).

Subcomplex ED (electron-donor binding) was finally identified in a proteomics study of the NDH-1 complex in *Arabidopsis* and is composed of NdhS, T, and U (Yamamoto et al. 2011). Subcomplex ED most likely interacts with subcomplex A, but the subunit stability is largely independent of the other subcomplexes, distinguishing this subcomplex from others. Recently, NdhV was shown to be required for the stability of subcomplexes A and ED (Fan et al. 2015). NdhV is likely to be a member of subcomplex ED. Subcomplex ED forms the binding site of NDH-1 to the electron donor (Fd); this topic is discussed below in detail.

In *Arabidopsis*, chloroplast NDH-1 forms a supercomplex with PSI (Peng et al. 2008). Lhca5 and Lhca6 are minor LhcI proteins that mediate this interaction (Peng et al. 2009). Chloroplast NDH-1 has been proposed to interact with at least two copies of PSI (Peng et al. 2009), as determined by the mobility in BN gels of the supercomplexes isolated from *lhca5* and *lhca6* single mutants and an *lhca5 lhca6* double mutant. Consistent with this, single-particle electron microscopy has revealed that NDH-1 is sandwiched between two copies of the PSI-LhcI supercomplex, in which the LhcI side faces NDH-1 (Fig. 4.2; Kouřil et al. 2014). The interaction of NDH-1 with one of the two PSI copies is probably weak, because often a partial supercomplex with only one PSI copy is detected. An unassigned protein density has been observed between NDH-1 and another copy of PSI adjacent to Lhca2 and Lhca3; this area has been proposed to represent both Lhca5 and Lhca6 (Kouřil et al. 2014). However, this model cannot explain the phenotype of *lhca5* and *lhca6* single mutants simply; each mutant lacks a



**Fig. 4.2.** Single-particle images of the NDH-1-PSI supercomplex (*top view*). An averaged projection map (**a**) and overlaps with the crystal structures of the PSI complex (*both sides*) and the respiratory NDH-1 (*center*) (**b**). The N module, which is missing in photosynthetic NDH-1, is omitted from the structure of respiratory NDH-1. Each PSI complex interacts with NDH-1 via the surface, composed of 4 Lhca molecules (Lhca1 to 4). The *blue asterisk* indicates an assigned density in the hydrophilic arm. The *green area* was assigned to Lhca5 and 6 in the original manuscript (Kouřil et al. 2014), but further research is needed for this to be conclusive (see text) (Pictures were kindly provided by R. Kouřil).

single copy of PSI, suggesting that Lhca5 and Lhca6 independently interact with PSI (Peng et al. 2009). The unassigned space may be for subcomplex B, which is absent in cyanobacterial NDH-1 except for PnsB4 (Ifuku et al. 2011). Because the sequence of Lhca6 is similar to that of Lhca2, one copy of Lhca2 (possibly in the weakly-associated PSI) may be substituted by Lhca6 to form the supercomplex with NDH-1. However, it is unlikely that both copies of Lhca2 are substituted by Lhca6, because Lhca2 has been detected in the NDH-PSI supercomplex (Peng et al. 2009). Because Lhca5 interacts with Lhca2 and Lhca3 in the PSI supercomplex (Lucinski et al. 2006), it is conceivable that the unassigned space includes Lhca5, as well as the subcomplex B.

## V. Evolution of Chloroplast NDH-1 in Land Plants

Liverwort (*M. polymorpha*) is highlighted as an emerging model plant because of its earliest divergence in the evolution of land

plants (Qiu et al. 2006). Because transformation techniques for both nuclear and plastid genomes have been established, *Marchantia* is an ideal model plant for organelle research (Chiyoda et al. 2007; Ishizaki et al. 2008). We took advantage of this available genome information to survey the nuclear-encoded genes for NDH-1 subunits (Table 4.1). In flowering plants, NDH-1 interacts with PSI to form a supercomplex (Peng et al. 2008, 2009), but the *Marchantia* genome does not encode Lhca6. Consistent with this, the NDH-1-PSI supercomplex has not been detected in BN gels (Ueda et al. 2012). The high levels of sequence identity between Lhca2 and Lhca6 suggest that Lhca6 originated from Lhca2 after gene duplication, but the origin of Lhca5 is unclear. In fact, a gene has been annotated as Lhca5 in *Physcomitrella patens* (Alboresi et al. 2010), and small amounts of NDH-1 subunits have been detected in high-molecular weight positions on BN gels (Armbruster et al. 2013). Functional analysis is necessary to conclude whether *Physcomitrella* has Lhca5. In Arabidopsis, Lhca6 plays a key role in stabilizing the NDH-1 complex (Peng et al. 2009), and



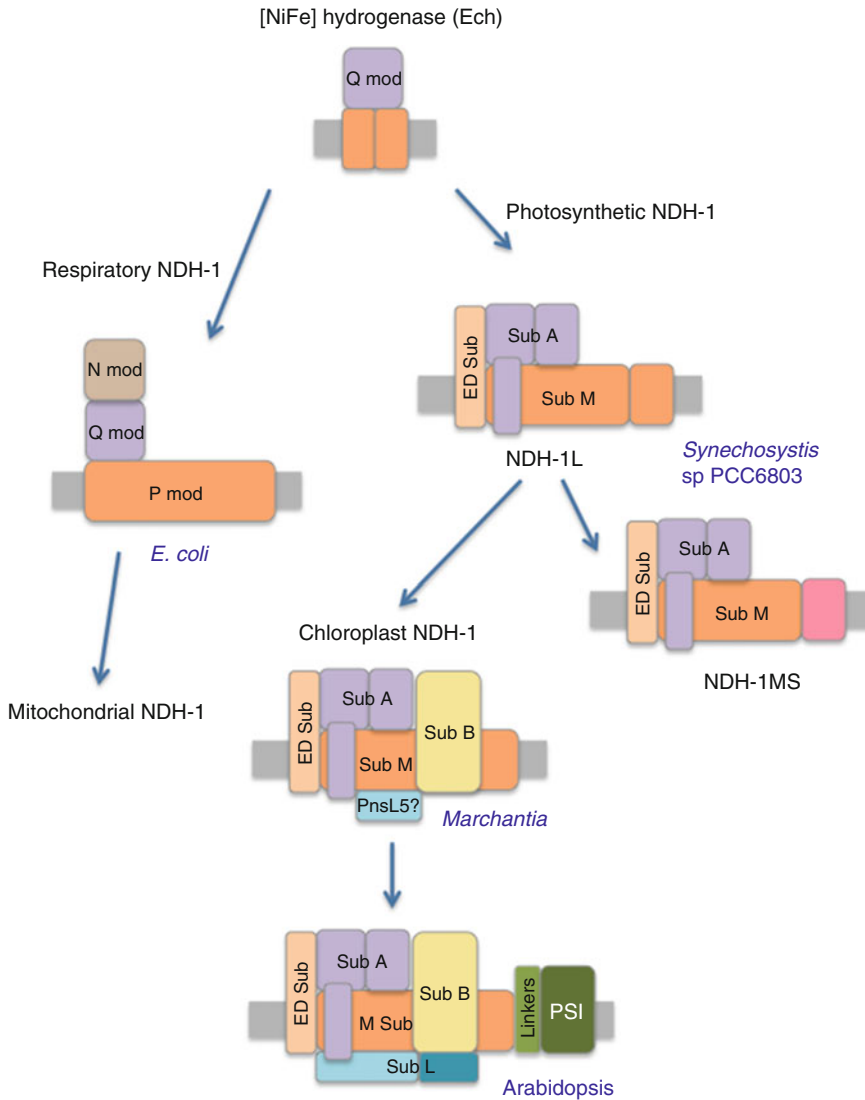


Fig. 4.3. Model for the evolution of NDH-1 complexes. Both respiratory and photosynthetic NDH-1 complexes are considered to have originated from energy-converting hydrogenase (Ech). During the evolution of respiratory NDH-1, the enzyme acquired an N module to accept electrons from NADH. Chloroplast NDH-1 originated from cyanobacterial NDH-1L and increased its number of subunits during the evolution of land plants. In flowering plants, chloroplast NDH-1 associates with PSI.

*Physcomitrella* is unlikely to have completed evolution in regard to flowering plant-type supercomplex formation (Fig. 4.3).

What is the physiological significance of NDH-1-PSI supercomplex formation in flowering plants? In the *Arabidopsis lhca6* mutant, NDH-1 is destabilized in mature leaves and Lhca5 has a similar function, especially at high light intensity

(Peng and Shikanai 2011). Because NDH-1 activity is detected in immature leaves of the *lhca5 lhca6* double mutant, supercomplex formation is not necessary for enzyme activity (Peng et al. 2009). The phenotype of *lhca5 lhca6* is probably explained by the reduced stability of NDH-1 in chloroplasts. The question is: How is the NDH-1 complex stabilized in *Marchantia* and cyanobacteria,

in which NDH-1 does not interact with PSI? High light intensity decreases the stability of NDH-1 in the *lhca5 lhca6* double mutant (Peng et al. 2009). In flowering plants that are adapted to adverse light environments, the protein complexes in the thylakoid membrane may require an additional device for stability. The exact reason for the evolution of the supercomplex is still unclear.

The *Marchantia* genome does not encode the genes for subcomplex L, with the exception of that for PnsL5 (Ueda et al. 2012). This is also true for *Physcomitrella* (Armbruster et al. 2013). PnsL5 is an unusual subunit of chloroplast NDH-1 in *Arabidopsis* and may possess peptidyl-prolyl isomerase (PPIase) activity (Sirpiö et al. 2009). This is not specific to PnsL5. PnsL4 is FKBP (FK506-binding protein) 16–2, which has been annotated as a chloroplast-lumen targeting immunophilin (Peng et al. 2009). NdhT and U form subcomplex ED with NdhS and are J and J-like proteins, respectively (Yamamoto et al. 2011). It is unclear why chloroplast NDH-1 incorporated these proteins, which may be involved in protein folding, as subunits. These subunits may retain the original enzyme activity in the complex and may be necessary for the assembly of NDH-1. In *Marchantia*, the PnsL5 homolog may be conserved as PPIase and may not be a genuine NDH-1 subunit. This is likely, because the stability of PnsL5 in *Arabidopsis* depends on other subunits of the subcomplex L (Peng et al. 2009).

Although it is unclear whether PnsL5 is an NDH-1 subunit in *Marchantia*, the entire subcomplex L was likely acquired during the evolution of land plants. In *Arabidopsis*, the mutant phenotype suggests that subcomplex L stabilizes subcomplex A (Peng et al. 2009). However, NDH-1 lacks subcomplex L in *Marchantia* and cyanobacteria, suggesting that this straightforward hypothesis based simply on the mutant phenotype is unlikely to explain the function of subcomplex L in the wild type. The occurrence of the subcomplex L coincides with supercomplex formation

with PSI (Fig. 4.3), and this may be the reason for the evolution of subcomplex L.

The exact reason for the structural difference in chloroplast NDH-1 between *Marchantia* and flowering plants is unclear, but we can extend our speculation a little further. Both the full subcomplex L and supercomplex formation with PSI may be required for stabilizing NDH-1 in the chloroplasts of flowering plants. To test this hypothesis, a straightforward strategy would be the introduction of *Marchantia*-type or cyanobacterial-type NDH-1 into chloroplasts of flowering plants. However, our technology is still premature for handling such huge multi-subunit complexes in transgenic research. Chloroplasts are the sites of reactive oxygen generation, and the thylakoid lumen is acidified to less than pH 6.0 to induce NPQ and downregulation of the cytochrome *b<sub>6</sub>f* complex. Assembly and stabilization of the protein complexes in the thylakoid membrane may have required additional machineries in the course of land plant evolution. As described above, a defect in *ndhL* has a different impact on the stability of subcomplex A in cyanobacteria and flowering plants (Ogawa 1992; Shimizu et al. 2008). This structural adaptation might have been particularly important because of the concomitant disappearance of some photoprotective pathways in the course of evolution. One example is the disappearance of flavodiiron proteins in angiosperms, suggesting that switching of the systems regulating photosynthetic electron transport occurred during the evolution of land plants (Allahverdiyeva et al. 2013; Zhang et al. 2012). On the other hand, more assembly factors were recruited to photosynthetic NDH-1 in the course of land plant evolution. In *Arabidopsis*, the assembly of subcomplex A requires the non-subunit factors CRR41 and CRR42, the functions of which are not conserved in cyanobacteria (Peng et al. 2012). In *Marchantia* chloroplasts, NdhH is folded properly with the assistance of the Cpn60 complex. In *Arabidopsis*, however, the evolution of an unusual  $\beta$  subunit (Cpn60 $\beta$ 4) was necessary for the folding

of NdhH, although the NdhH sequence is highly conserved between *Marchantia* and *Arabidopsis* (Peng et al. 2011a). We speculate that adaptation to the severe light conditions of terrestrial environments required the more robust assembly, or a stabilizing system, of protein complexes in the thylakoid membrane.

## VI. Physiological Reason for Evolutionary Increase in Complexity of Chloroplast NDH-1

How does the structural difference in chloroplast NDH-1 between flowering plants and *Marchantia* reflect differences in physiological function? As in flowering plants, knockout of *ndhB* does not affect the growth of thalli in *Marchantia* (Ueda et al. 2012). Consistently, photosynthetic electron transport is not drastically affected in the mutants. Similar to the case in flowering plants, chloroplast NDH-1 is unlikely to mediate the main route of electrons that contributes substantially to pmf formation in *Marchantia*. At low light intensity, however, the PQ pool is slightly more reduced by electrons in the *ndhB* mutant, suggesting that chloroplast NDH-1 is required for redox homeostasis in *Marchantia* chloroplasts. A similar phenotype has been observed in rice NDH-1-deficient mutants (Yamori et al. 2011). The contribution of NDH-1 to pmf is not negligible, at least in these plants at low light intensity. Actually, we observed a minor but statistically significant decline in pmf even in the *Arabidopsis* NDH-less mutants (Wang et al. 2015). The difference in mutant phenotypes among plant materials may depend on the activity of other, alternative, electron transport pathways, including the water-water cycle. The physiological function of NDH-1 has been analyzed by focusing on stress tolerance (Endo et al. 1999; Horváth et al. 2000), and it is conceivable that chloroplast NDH-1 is involved in redox homeostasis in chloroplasts under various stress conditions and may even

be involved in the plant immune response (García-Andrade et al. 2013). Fine-tuning of the chloroplast redox state may be necessary for plant fitness. Despite the obscure physiological function of chloroplast NDH-1, its molecular function is clear: Chloroplast NDH-1 couples electron transport from Fd to PQ with proton/cation translocation across the thylakoid membrane. The direct consequence of an NDH-1 defect should be reduced pmf, as in the *Arabidopsis pgr5* mutant. In flowering plants, PGR5-dependent PSI cyclic electron transport is essential for survival under field conditions, through ATP synthesis and also through regulatory processes via lumenal acidification (Suorsa et al. 2012; Shikanai 2014). Indeed, both *Marchantia* and flowering plants possess at least two pathways of PSI cyclic electron transport, which differ substantially in terms of rates of electron transport. A central question is how plants selectively use the two pathways of PSI cyclic electron transport.

C<sub>4</sub> photosynthesis requires additional ATP for recycling phosphoenolpyruvate, and this ATP is believed to be synthesized by PSI cyclic electron transport (Nakamura et al. 2013). Bundle sheath cells of maize contain higher levels of NDH-1 than do mesophyll cells, suggesting that some C<sub>4</sub> plants utilize NDH-1-dependent PSI cyclic electron transport to energize the CO<sub>2</sub>-concentrating machinery (Takabayashi et al. 2005). Chloroplast NDH-1 is likely to have proton-pumping activity; this machinery seems to be superior to that of the PGR5/PGRL1 complex for pmf formation. In C<sub>3</sub> plants, however, ΔpH formation is required not only for ATP synthesis but also for regulation of photosynthesis, NPQ induction (Munekage et al. 2002), and downregulation of the cytochrome *b<sub>6</sub>f* complex (Suorsa et al. 2012). It is likely that, for these purposes, the PGR5-dependent pathway was selected over chloroplast NDH-1. Bundle sheath cells of maize contain only small amounts of PSII, and regulation of photosynthesis in these plants via low lumen pH is probably not necessary. In *Marchantia*, NDH-1—rather than the main machinery

for pmf formation—may have a regulatory function; this is probably true also for C<sub>3</sub> plants.

## VII. The Origin of Photosynthetic NDH-1

Among the protein complexes related to NDH-1, cyanobacterial and chloroplast (photosynthetic) NDH-1 is unique because of the absence of the N module. In *E. coli* NDH-1, the N module consists of NuoE, F, and G and functions in oxidizing NADH (Friedrich and Scheide 2000). Because, in cyanobacteria and higher plants, despite complete genome sequencing of nearly 100 different oxygenic photosynthetic organisms, no orthologs of *E. coli* N module subunits have been identified, a completely different electron input module for photosynthetic NDH-1 has started to emerge. Indeed, for decades the nature of the electron donors for photosynthetic NDH-1 has raised confusion, and conflicting results have been reported from physiological and biochemical studies. In *Arabidopsis*, NDH-1-dependent PQ reduction is strictly dependent on Fd (Munekage et al. 2004) when ruptured chloroplasts are used as an assay system, but NAD(P)H has also been shown to donate electrons to the same complex in spinach (Endo et al. 1997), potato (Corneille et al. 1998), and barley (Bernhard Teicher and Vibe Scheller 1998). A purified NDH complex from pea chloroplasts also showed NADH dehydrogenase activity (Sazanov et al. 1998), although the purified complex apparently lacked many subunits. The dilemma regarding identification of the various functional electron donors for photosynthetic NDH-1 is at least partly due to the fragile nature of the complex. It is also possible that soluble or membrane-bound FNR has contributed to NAD(P)H dehydrogenase activity (Guedeney et al. 1996). More problematically, there has been no consensus among researchers on how to measure photosynthetic NDH-1 activity: The conclusions drawn are fully dependent on

the methods used (Johnson 2005; Leister and Shikanai 2013).

Sequence identity between NDH-1 and [NiFe] hydrogenase was discovered more than two decades ago (Böhm et al. 1990) and led to the idea that the two enzymes share a common ancestor (Friedrich and Weiss 1997; Friedrich and Scheide 2000). Photosynthetic NDH-1 especially shares structural similarity with group 4 membrane-bound [NiFe] hydrogenase (Fig. 4.3; Efremov and Sazanov 2012; Marreiros et al. 2013). In this group of hydrogenases, the Q module directly accepts electrons from Fd to reduce protons (Marreiros et al. 2013). Independent of conflicting physiological and biochemical analyses, this sequence identity suggests that photosynthetic NDH-1 accepts electrons from Fd.

NdhS/CRR31 is a subunit of chloroplast NDH-1 discovered in the NDH-1-PSI supercomplex of *Arabidopsis* (Yamamoto et al. 2011). The Src homology 3 domain-like fold of NdhS is structurally similar to that of PsaE, which forms the Fd-binding site in PSI, as well as to that of PsaC (Sétif et al. 2002; Ben-Shem et al. 2003). In ruptured chloroplasts, NdhS is required for high-affinity binding of Fd to chloroplast NDH-1 in order to reduce PQ; NdhS is also required for NDH-1 activity *in vivo* (Yamamoto et al. 2011). As in the case of other Fd-interacting proteins, binding of Fd to NdhS also depends on electrostatic interaction. Arginine 193 of NdhS is required for the formation of a positively-charged pocket in the domain; this pocket is required for high-affinity Fd binding (Yamamoto and Shikanai 2013). This function of NdhS is conserved in cyanobacterial NDH-1 (Battchikova et al. 2011b), suggesting that NDH-1 accepts electrons from Fd also in cyanobacteria.

## VIII. Concluding Remarks

Since the discovery of 11 *ndh* genes in chloroplast genomes (Matsubayashi et al. 1987), our knowledge of this enigmatic enzyme has progressively improved. However,

several fundamental questions related to its activity and physiological function still remain. Some of these questions are common to all photosynthetic NDH-1 complexes, from cyanobacteria to flowering plants, whereas some are related to changes that have occurred in the course of evolution of the land plants. If photosynthetic NDH-1 accepts electrons directly from Fd, how are electrons transferred from Fd to the iron-sulfur cluster present in NdhI? Are some subunits still missing from our models? Photosynthetic NDH-1 is considered to possess proton-pumping activity, but the experimental evidence is totally missing. It has become clear that regulation of pmf components ( $\Delta\text{pH}$  and membrane potential) is important, because both  $\Delta\text{pH}$  and membrane potential contribute to pmf but only  $\Delta\text{pH}$  triggers the regulation of photosynthesis (by induction of NPQ, at least in chloroplasts, and down-regulation of the cytochrome *b<sub>6</sub>f* complex) (Carraretto et al. 2013). Is it possible that photosynthetic NDH-1 pumps cations rather than protons? Hopefully the answers will be found at the level of the crystal structure. What is the function of cyanobacterial NDH-1 in the light and in darkness? Does the function in light of photosynthetic NDH-1 in cyanobacteria differ from that in chloroplasts of flowering plants? What is the exact reason for the supercomplex formation with PSI in flowering plants and for the appearance of the B and L subcomplexes during the evolution of land plants? Despite the low levels of NDH-1 in chloroplasts, genetic approaches have identified many assembly factors specifically required for chloroplast NDH-1 (Peng et al. 2010, 2011a, b, 2012; Armbruster et al. 2013). Chloroplast NDH-1 can be an excellent model for the assembly of huge protein complexes, the subunits of which are encoded by both nuclear and chloroplast genomes. The exact physiological function of chloroplast NDH-1 is also unclear. We have to bridge the gap between the slow rate of NDH-1-dependent electron transport observed *in vivo* and the drastic phenotypes of *Arabidopsis* double mutants defective in both NDH-1 and PGR5

(Munekage et al. 2004). The central question is the physiological function of chloroplast NDH-1 in the wild type.

## Acknowledgements

Research in authors' laboratories is supported by CREST (JST) and Grant 25251032 (JSPS) (TS) and by the Academy of Finland projects 271832 and 273870 (EMA). The authors acknowledge to Takayuki Kohchi and Shohei Yamaoka for the genome information of *Marchantia*. We are grateful for Leinwei Peng, Hiroshi Yamamoto, Natalia Battchikova and other members who contributed to the work in our groups.

## References

- Alboresi A, Caffarri S, Nogue F, Bassi R, Morosinotto T (2010) *In silico* and biochemical analysis of *Physcomitrella patens* photosynthetic antenna: identification of subunits which evolved upon land adaptation. PLoS ONE 3:e2033
- Allahverdiyeva Y, Mustila H, Ermakova M, Bersanini L, Richaud P, Ajlani G, Battchikova N, ... , Aro E-M (2013) Flavodiiron proteins Flv1 and Flv3 enable cyanobacterial growth and photosynthesis under fluctuating light. Proc Natl Acad Sci USA 110:4111–4116
- Armbruster U, Rühle T, Kreller R, Strotbek C, Zühlke J, Tadini L, Blunder T, ... , Leister D (2013) The photosynthesis affected mutant68-like protein evolved from a PSII assembly factor to mediate assembly of the chloroplast NAD(P)H dehydrogenase complex in Arabidopsis. Plant Cell 25:3926–3943
- Arteni AA, Zhang P, Battchikova N, Ogawa T, Aro E-M, Boekema EJ (2006) Structural characterization of NDH-1 complexes of *Thermosynechococcus elongatus* by single particle electron microscopy. Biochim Biophys Acta 1757:1469–1775
- Baradaran R, Berrisford JM, Minhas GS, Sazanov LA (2013) Crystal structure of the entire respiratory complex I. Nature 494:443–448
- Battchikova N, Aro E-M (2007) Cyanobacterial NDH-1 complexes: multiplicity in function and subunit composition. Physiol Plant 131:22–32
- Battchikova N, Zhang P, Rudd S, Ogawa T, Aro E-M (2005) Identification of NdhL and Ssl 1690

- (NdhO) in NDH-1L and NDH-1M complexes of *Synechocystis* sp. PCC 6803. *J Biol Chem* 280:2587–2595
- Battchikova N, Eisenhut M, Aro E-M (2011a) Cyanobacterial NDH-1 complexes: novel insights and remaining puzzles. *Biochim Biophys Acta* 1807:935–944
- Battchikova N, Wei L, Du L, Bersanini L, Aro E-M, Ma W (2011b) Identification of novel Ssl0352 protein (NdhS), essential for efficient operation of cyclic electron transport around photosystem I, in NADPH:plastoquinone oxidoreductase (NDH-1) complexes of *Synechocystis* sp. PCC 6803. *J Biol Chem* 286:36992–37001
- Ben-Shem A, Frolov F, Nelson N (2003) Crystal structure of plant photosystem I. *Nature* 426:630–635
- Bernhard Teicher H, Vibe Scheller H (1998) The NAD(P)H dehydrogenase in barley thylakoids is photoactivatable and uses NADPH as well as NADH. *Plant Physiol* 117:525–532
- Bernát G, Appel J, Ogawa T, Rögner M (2011) Distinct roles of multiple NDH-1 complexes in the cyanobacterial electron transport network as revealed by kinetic analysis of P700<sup>+</sup> reduction in various Ndh-deficient mutants of *Synechocystis* sp. strain PCC6803. *J Bacteriol* 193(1):292–295
- Birungi M, Folea M, Battchikova N, Xu M, Mi H, Ogawa T, Aro E-M, Boekema EJ (2010) Possibilities of subunit localization with fluorescent protein tags and electron microscopy exemplified by a cyanobacterial NDH-1 study. *Biochim Biophys Acta* 1797:1681–1686
- Böhm R, Sauter M, Böck A (1990) Nucleotide sequence and expression of an operon in *Escherichia coli* coding for formate hydrogenlyase components. *Mol Microbiol* 4:231–243
- Burrows PA, Sazanov LA, Svab Z, Maliga P, Nixon PJ (1998) Identification of a functional respiratory complex in chloroplasts through analysis of tobacco mutants containing disrupted plastid *ndh* genes. *EMBO J* 17:868–876
- Carraretto L, Formentin E, Teardo E, Checchetto V, Tomizioli M, Morosinotto T, Giacometti GM, . . . , Szabó I (2013) A thylakoid-located two-pore K<sup>+</sup> channel controls photosynthetic light utilization in plants. *Science* 342:114–118
- Chiyoda S, Linley PJ, Yamato KT, Fukuzawa H, Yokota A, Kohchi T (2007) Simple and efficient plastid transformation system for the liverwort *Marchantia polymorpha* L. suspension-culture cells. *Transgenic Res* 16:41–49
- Cooley JW, Vermaas WF (2001) Succinate dehydrogenase and other respiratory pathways in thylakoid membranes of *Synechocystis* sp. strain PCC 6803: capacity comparisons and physiological function. *J Bacteriol* 183:4251–4258
- Corneille S, Cournac L, Guedeney G, Havaux M, Peltier G (1998) Reduction of the plastoquinone pool by exogenous NADH and NADPH in higher plant chloroplasts. Characterization of a NAD(P)H-plastoquinone oxidoreductase activity. *Biochim Biophys Acta* 1363:59–69
- Desplats C, Mus F, Cuiñé S, Billon E, Cournac L, Peltier G (2009) Characterization of Nda2, a plastoquinone-reducing type II NAD(P)H dehydrogenase in *Chlamydomonas* chloroplasts. *J Biol Chem* 284:4148–4157
- Efremov RG, Sazanov LA (2011) Structure of the membrane domain of respiratory complex I. *Nature* 476:414–420
- Efremov RG, Sazanov LA (2012) The coupling mechanism of respiratory complex I—a structural and evolutionary perspective. *Biochim Biophys Acta* 1817:1785–9517
- Efremov RG, Baradaran R, Sazanov LA (2010) The architecture of respiratory complex I. *Nature* 465:441–445
- Endo T, Mi H, Shikanai T, Asada K (1997) Donation of electrons to plastoquinone by NAD(P)H dehydrogenase and by ferredoxin-quinone reductase in spinach chloroplasts. *Plant Cell Physiol* 38:1272–1277
- Endo T, Shikanai T, Takabayashi A, Asada K, Sato F (1999) The role of chloroplastic NAD(P)H dehydrogenase in photoprotection. *FEBS Lett* 457:5–8
- Fan X, Zhang J, Li W, Peng L (2015) The NdhV subunit is required to stabilize the chloroplast NADH dehydrogenase-like complex in Arabidopsis. *Plant J* 82:221–231
- Folea IM, Zhang P, Nowaczyk MM, Ogawa T, Aro E-M, Boekema EJ (2008) Single particle analysis of thylakoid proteins from *Thermosynechococcus elongatus* and *Synechocystis* 6803: localization of the CupA subunit of NDH-1. *FEBS Lett* 582:249–254
- Friedrich T, Scheide D (2000) The respiratory complex I of bacteria, archaea and eukarya and its module common with membrane-bound multisubunit hydrogenases. *FEBS Lett* 479:1–5
- Friedrich T, Weiss H (1997) Modular evolution of the respiratory NADH:ubiquinone oxidoreductase and the origin of its modules. *J Theor Biol* 187:529–540
- García-Andrade J, Ramírez V, López A, Vera P (2013) Mediated plastid RNA editing in plant immunity. *PLoS Pathog* 9:e1003713
- Guedeney G, Corneille S, Cuiñé S, Peltier G (1996) Evidence for an association of *ndh* B, *ndh* J gene products and ferredoxin-NADP-reductase as components of a chloroplastic NAD(P)H dehydrogenase complex. *FEBS Lett* 378:277–280

- Hashimoto M, Endo T, Peltier G, Tasaka M, Shikanai T (2003) A nucleus-encoded factor, CRR2, is essential for the expression of chloroplast *ndhB* in Arabidopsis. *Plant J* 36:541–549
- Herranen M, Battchikova N, Zhang P, Graf A, Sirpiö S, Paakkariinen V, Aro E-M (2004) Towards functional proteomics of membrane protein complexes in *Synechocystis* sp. PCC 6803. *Plant Physiol* 134:470–481
- Hertle AP, Blunder T, Wunder T, Pesaresi P, Pribil M, Armbruster U, Leister D (2013) PGRL1 is the elusive ferredoxin-plastoquinone reductase in photosynthetic cyclic electron flow. *Mol Cell* 49:511–523
- Horváth EM, Peter SO, Joët T, Rumeau D, Cournac L, Horváth GV, Kavanagh TA, . . . , Medgyesy P (2000) Targeted inactivation of the plastid *ndhB* gene in tobacco results in an enhanced sensitivity of photosynthesis to moderate stomatal closure. *Plant Physiol* 123:1337–1350
- Ifuku K, Endo T, Shikanai T, Aro E-M (2011) Structure of the chloroplast NADH dehydrogenase-like complex: nomenclature for nuclear-encoded subunits. *Plant Cell Physiol* 52:1560–1568
- Ishihara S, Takabayashi A, Ido K, Endo T, Ifuku K, Sato F (2007) Distinct functions for the two PsbP-like proteins PPL1 and PPL2 in the chloroplast thylakoid lumen of Arabidopsis. *Plant Physiol* 145:668–679
- Ishikawa N, Takabayashi A, Ishida S, Hano Y, Endo T, Sato F (2008) NDF6: a thylakoid protein specific to terrestrial plants is essential for activity of chloroplastic NAD(P)H dehydrogenase in Arabidopsis. *Plant Cell Physiol* 49:1066–1073
- Ishizaki K, Chiyoda S, Yamato KT, Kohchi T (2008) *Agrobacterium*-mediated transformation of the haploid liverwort *Marchantia polymorpha* L., an emerging model for plant biology. *Plant Cell Physiol* 49:1084–1091
- Joët T, Cournac L, Horváth EM, Medgyesy P, Peltier G (2001) Increased sensitivity of photosynthesis to antimycin A induced by inactivation of the chloroplast *ndhB* gene. Evidence for a participation of the NADH-dehydrogenase complex to cyclic electron flow around photosystem I. *Plant Physiol* 125:1919–1929
- Joët T, Genty B, Josse EM, Kuntz M, Cournac L, Peltier G (2002) Involvement of a plastid terminal oxidase in plastoquinone oxidation as evidenced by expression of the *Arabidopsis thaliana* enzyme in tobacco. *J Biol Chem* 277:31623–31630
- Johnson GN (2005) Cyclic electron transport in C<sub>3</sub> plants: fact or artefact? *J Exp Bot* 56:407–416
- Kaneko T, Sato S, Kotani H, Tanaka A, Asamizu E, Nakamura Y, Miyajima N, . . . , Tabata S (1996) Sequence analysis of the genome of the unicellular cyanobacterium *Synechocystis* sp. strain PCC6803. II. Sequence determination of the entire genome and assignment of potential protein-coding regions. *DNA Res* 3:109–136
- Kofer W, Koop H-U, Wanner G, Steinmüller K (1998) Mutagenesis of the genes encoding subunits A, C, H, I, J and K of the plastid NAD(P)H-plastoquinone-oxidoreductase in tobacco by polyethylene glycol-mediated plastome transformation. *Mol Gen Genet* 258:166–173
- Kono M, Noguchi K, Terashima I (2014) Roles of the cyclic electron flow around PSI (CEF-PSI) and O<sub>2</sub>-dependent alternative pathways in regulation of the photosynthetic electron flow in short-term fluctuating light in *Arabidopsis thaliana*. *Plant Cell Physiol* 55:990–1004
- Kouřil R, Strouhal O, Nosek L, Lenobel R, Chamrád I, Boekema EJ, Sebelá M, Ilík P (2014) Structural characterization of a plant photosystem I and NAD(P)H dehydrogenase supercomplex. *Plant J* 77:568–576
- Leister D, Shikanai T (2013) Complexities and protein complexes in the antimycin A-sensitive pathway of cyclic electron flow in plants. *Front Plant Sci* 4:161
- Lucinski R, Schmid VH, Jansson S, Klimmek F (2006) Lhca5 interaction with plant photosystem I. *FEBS Lett* 580:6485–6488
- Maeda S, Badger MR, Price GD (2002) Novel gene products associated with NdhD3/D4-containing NDH-1 complexes are involved in photosynthetic CO<sub>2</sub> hydration in the cyanobacterium, *Synechococcus* sp. PCC7942. *Mol Microbiol* 43:425–435
- Marreiros BC, Batista AP, Duarte AM, Pereira MM (2013) A missing link between complex I and group 4 membrane-bound [NiFe] hydrogenases. *Biochim Biophys Acta* 1827:198–209
- Matsubayashi T, Wakasugi T, Shinozaki K, Yamaguchi-Shinozaki K, Zaita N, Hidaka T, Meng BY, . . . , Sugiura M (1987) Six chloroplast genes (*ndhA-F*) homologous to human mitochondrial genes encoding components of the respiratory chain NADH dehydrogenase are actively expressed: determination of the splice sites in *ndhA* and *ndhB* pre-mRNAs. *Mol Gen Genet* 210:385–393
- Melo AM, Bandejas TM, Teixeira M (2004) New insights into type II NAD(P)H:quinone oxidoreductases. *Microbiol Mol Biol Rev* 68:603–616
- Mi H, Endo T, Schreiber U, Ogawa T, Asada K (1992) Electron donation from cyclic and respiratory flows to the photosynthetic intersystem chain is mediated by pyridine-nucleotide dehydrogenase in the cyanobacterium *Synechocystis* PCC6803. *Plant Cell Physiol* 33:1233–1237
- Mimaki M, Wang X, McKenzie M, Thorburn DR, Ryan MT (2012) Understanding mitochondrial complex I assembly in health and disease. *Biochim Biophys Acta* 1817:851–862

- Mullineaux CW (2014) Co-existence of photosynthetic and respiratory activities in cyanobacterial thylakoid membranes. *Biochim Biophys Acta* 1837:503–511
- Munekage Y, Hojo M, Meurer J, Endo T, Tasaka M, Shikanai T (2002) *PGR5* is involved in cyclic electron flow around photosystem I and is essential for photoprotection in *Arabidopsis*. *Cell* 110:361–371
- Munekage Y, Hashimoto M, Miyake C, Tomizawa K, Endo T, Tasaka M, Shikanai T (2004) Cyclic electron flow around photosystem I is essential for photosynthesis. *Nature* 429:579–582
- Munekage YN, Genty B, Peltier G (2008) Effect of *PGR5* impairment on photosynthesis and growth in *Arabidopsis thaliana*. *Plant Cell Physiol* 49:1688–1698
- Nakamura N, Iwano M, Havaux M, Yokota A, Munekage YN (2013) Promotion of cyclic electron transport around photosystem I during the evolution of NADP-malic enzyme-type C<sub>4</sub> photosynthesis in the genus *Flaveria*. *New Phytol* 199:832–842
- Nishikawa Y, Yamamoto H, Okegawa Y, Wada S, Sato N, Taira Y, Sugimoto K, . . . , Shikanai T (2012) *PGR5*-dependent cyclic electron transport around PSI contributes to the redox homeostasis in chloroplasts rather than CO<sub>2</sub> fixation and biomass production in rice. *Plant Cell Physiol* 53:2117–2126
- Nowaczyk MM, Wulfhorst H, Ryan CM, Souda P, Zhang H, Cramer WA, Whitelegge JP (2011) NdhP and NdhQ: two novel small subunits of the cyanobacterial NDH-1 complex. *Biochemistry* 50:1121–1124
- Ogawa T (1991) A gene homologous to the subunit-2 gene of NADH dehydrogenase is essential to inorganic carbon transport of *Synechocystis* PCC6803. *Proc Natl Acad Sci USA* 88:4275–4279
- Ogawa T (1992) Identification and characterization of the *ictA*/*ndhL* gene product essential to inorganic carbon transport of *Synechocystis* PCC6803. *Plant Physiol* 99:1604–1608
- Ogawa T, Mi H (2007) Cyanobacterial NADPH dehydrogenase complexes. *Photosynth Res* 93:69–77
- Ohkawa H, Pakrasi HB, Ogawa T (2000) Two types of functionally distinct NAD(P)H dehydrogenases in *Synechocystis* sp strain PCC6803. *J Biol Chem* 275:31630–31634
- Ohyama K, Fukuzawa H, Kohchi T, Shirai H, Sano T, Sano S, Umezono K, . . . , Ozeki H (1986) Chloroplast gene organization deduced from complete sequence of liverwort *Marchantia polymorpha* chloroplast DNA. *Nature* 322:572–574
- Okegawa Y, Kagawa Y, Kobayashi Y, Shikanai T (2008) Characterization of factors affecting the activity of photosystem I cyclic electron transport in chloroplasts. *Plant Cell Physiol* 49:825–834
- Okegawa Y, Kobayashi Y, Shikanai T (2010) Physiological links among alternative electron transport pathways reducing and oxidizing plastoquinone in *Arabidopsis*. *Plant J* 63:458–468
- Peltier G, Cournac L (2002) Chlororespiration. *Annu Rev Plant Biol* 53:523–550
- Peltier G, Schmidt GW (1991) Chlororespiration: an adaptation to nitrogen deficiency in *Chlamydomonas reinhardtii*. *Proc Natl Acad Sci USA* 88:4791–4795
- Peng L, Shikanai T (2011) Supercomplex formation with photosystem I is required for the stabilization of the chloroplast NADH dehydrogenase-like complex in *Arabidopsis*. *Plant Physiol* 155:1629–1639
- Peng L, Shimizu H, Shikanai T (2008) The chloroplast NAD(P)H dehydrogenase complex interacts with photosystem I in *Arabidopsis*. *J Biol Chem* 283:34873–34879
- Peng L, Fukao Y, Fujiwara M, Takami T, Shikanai T (2009) Efficient operation of NAD(P)H dehydrogenase requires the supercomplex formation with photosystem I via minor LHCI in *Arabidopsis*. *Plant Cell* 21:3623–3640
- Peng L, Cai W, Shikanai T (2010) Chloroplast stromal proteins, CRR6 and CRR7, are required for assembly of the NAD(P)H dehydrogenase subcomplex A in *Arabidopsis*. *Plant J* 63:203–211
- Peng L, Fukao Y, Myouga F, Motohashi R, Shinozaki K, Shikanai T (2011a) A chaperonin subunit with unique structures is essential for folding of a specific substrate. *PLoS Biol* 9, e1001040
- Peng L, Yamamoto T, Shikanai T (2011b) Structure and biogenesis of the chloroplast NAD(P)H dehydrogenase complex. *Biochim Biophys Acta* 1807:945–953
- Peng L, Fukao Y, Fujiwara M, Shikanai T (2012) Multistep assembly of chloroplast NADH dehydrogenase-like subcomplex A requires several nucleus-encoded proteins, including CRR41 and CRR42, in *Arabidopsis*. *Plant Cell* 24:202–214
- Prommeenate P, Lennon AM, Markert C, Hippler M, Nixon PJ (2004) Subunit composition of NDH-1 complexes of *Synechocystis* sp PCC 6803—identification of two new *ndh* gene products with nuclear-encoded homologues in the chloroplast Ndh complex. *J Biol Chem* 279:28165–28173
- Qiu Y-L, Li LB, Wang B, Chen ZD, Knoop V, Groth-Malonek M, Dombrowska O, . . . , Davis CC (2006) The deepest divergences in land plants inferred from phylogenomic evidence. *Proc Natl Acad Sci USA* 103:15511–15516
- Rumeau D, Bécuwe-Linka N, Beyly A, Louwagie M, Garin J, Peltier G (2005) New subunits NDH-M, -N, and -O, encoded by nuclear genes, are essential for plastid Ndh complex functioning in higher plants. *Plant Cell* 17:219–232



- Rumeau D, Peltier G, Cournac L (2007) Chlororespiration and cyclic electron flow around PSI during photosynthesis and plant stress response. *Plant Cell Environ* 30:1041–1051
- Sazanov LA, Burrows PA, Nixon PJ (1998) The plastid *ndh* genes code for an NADH-specific dehydrogenase: isolation of a complex I analogue from pea thylakoid membranes. *Proc Natl Acad Sci USA* 95:1319–1324
- Sazanov LA, Baradaran R, Efremov RG, Berrisford JM, Minhas G (2013) A long road towards the structure of respiratory complex I, a giant molecular proton pump. *Biochem Soc Trans* 41:1265–1271
- Sétif P, Fischer N, Lagoutte B, Bottin H, Rochaix J-D (2002) The ferredoxin docking site of photosystem I. *Biochim Biophys Acta* 1555:204–209
- Shibata M, Ohkawa H, Kaneko T, Fukuzawa H, Tabata S, Kaplan A, Ogawa T (2001) Distinct constitutive and low-CO<sub>2</sub>-induced CO<sub>2</sub> uptake systems in cyanobacteria: genes involved and their phylogenetic relationship with homologous genes in other organisms. *Proc Natl Acad Sci USA* 98:11789–11794
- Shikanai T (2007) Cyclic electron transport around photosystem I: genetic approaches. *Annu Rev Plant Biol* 58:199–217
- Shikanai T (2014) Central role of cyclic electron transport around photosystem I in the regulation of photosynthesis. *Curr Opin Biotechnol* 26: 25–30
- Shikanai T, Endo T, Hashimoto T, Yamada Y, Asada K, Yokota A (1998) Directed disruption of the tobacco *ndhB* gene impairs cyclic electron flow around photosystem I. *Proc Natl Acad Sci USA* 95:9705–9709
- Shimizu H, Peng L, Myouga F, Motohashi R, Shinozaki K, Shikanai T (2008) CRR23/NdhL is a subunit of the chloroplast NAD(P)H dehydrogenase complex in *Arabidopsis*. *Plant Cell Physiol* 49:835–842
- Shinozaki K, Ohme M, Tanaka M, Wakasugi T, Hayashida N, Matsubayashi T, Zaita N, . . . , Sugiura M (1986) The complete nucleotide sequence of tobacco chloroplast genome: its gene organization and expression. *EMBO J* 5:2043–2049
- Sirpiö S, Holmström M, Batchikova N, Aro E-M (2009) AtCYP20-2 is an auxiliary protein of the chloroplast NAD(P)H dehydrogenase complex. *FEBS Lett* 583:2355–2358
- Sugimoto K, Okegawa Y, Tohri A, Long TA, Sarah FS, Hisabori T, Shikanai T (2013) A single amino acid alteration in PGR5 confers resistance to antimycin A in cyclic electron transport around PSI. *Plant Cell Physiol* 54:1525–1534
- Suorsa M, Sirpiö S, Aro E-M (2009) Towards characterization of the chloroplast NAD(P)H dehydrogenase complex. *Mol Plant* 2:1127–1140
- Suorsa M, Sirpiö S, Paakkari V, Kumari N, Holmström M, Aro E-M (2010) Two proteins homologous to PsbQ are novel subunits of the chloroplast NAD(P)H dehydrogenase. *Plant Cell Physiol* 51:877–883
- Suorsa M, Järvi S, Grieco M, Nurmi M, Pietrzykowska M, Rantala M, Kangasjärvi S, . . . , Aro E-M (2012) PROTON GRADIENT REGULATION5 is essential for proper acclimation of *Arabidopsis* photosystem I to naturally and artificially fluctuating light conditions. *Plant Cell* 24:2934–2948
- Svab Z, Maliga P (1993) High-frequency plastid transformation in tobacco by selection for a chimeric *aadA* gene. *Proc Natl Acad Sci USA* 90:913–917
- Tagawa K, Tsujimoto HY, Arnon DI (1963) Role of chloroplast ferredoxin in the energy conversion process of photosynthesis. *Proc Natl Acad Sci USA* 49:567–572
- Takabayashi A, Kishine M, Asada K, Endo T, Sato F (2005) Differential use of two cyclic electron flows around photosystem I for driving CO<sub>2</sub>-concentration mechanism in C<sub>4</sub> photosynthesis. *Proc Natl Acad Sci USA* 102:16898–16903
- Trouillard M, Shahbazi M, Moyet L, Rappaport F, Joliot P, Kuntz M, Finazzi G (2012) Kinetic properties and physiological role of the plastoquinone terminal oxidase (PTOX) in a vascular plant. *Biochim Biophys Acta* 1817:2140–2148
- Ueda M, Kuniyoshi T, Yamamoto Y, Sugimoto K, Ishizaki K, Kohchi T, Nishimura Y, Shikanai T (2012) Composition and physiological function of the chloroplast NADH dehydrogenase-like complex in *Marchantia polymorpha*. *Plant J* 72: 683–693
- Wang HL, Postier BL, Burnap RL (2004) Alterations in global patterns of gene expression in *Synechocystis* sp. PCC 6803 in response to inorganic carbon limitation and the inactivation of *ndhR*, a LysR family regulator. *J Biol Chem* 279:5739–5751
- Wang C, Yamamoto H, Shikanai T (2015) Role of cyclic electron transport around photosystem I in regulating proton motive force. *Biochim Biophys Acta* 1847:931–938
- Yabuta S, Ifuku K, Takabayashi A, Ishihara S, Ido K, Ishikawa N, Endo T, Sato F (2010) Three PsbQ-like proteins are required for the function of the chloroplast NAD(P)H dehydrogenase complex in *Arabidopsis*. *Plant Cell Physiol* 51:866–876
- Yamamoto H, Shikanai T (2013) *In planta* mutagenesis of Src homology 3 domain-like fold

- of NdhS, a ferredoxin-binding subunit of the chloroplast NADH dehydrogenase-like complex in *Arabidopsis*: a conserved Arg-193 plays a critical role in ferredoxin binding. *J Biol Chem* 288: 36328–37363
- Yamamoto H, Peng L, Fukao Y, Shikanai T (2011) An Src homology 3 domain-like fold protein forms a ferredoxin-binding site for the chloroplast NADH dehydrogenase-like complex in *Arabidopsis*. *Plant Cell* 23:1480–1493
- Yamori W, Sakata N, Suzuki Y, Shikanai T, Makino A (2011) Cyclic electron flow around photosystem I via chloroplast NAD(P)H dehydrogenase (NDH) complex performs a significant physiological role during photosynthesis and plant growth at low temperature in rice. *Plant J* 68:966–976
- Zhang P, Battchikova N, Jansen T, Appel J, Ogawa T, Aro E-M (2004) Expression and functional roles of the two distinct NDH-1 complexes and the carbon acquisition complex NdhD3/NdhF3/CupA/Sll1735 in *Synechocystis* sp PCC 6803. *Plant Cell* 16:3326–3340
- Zhang P, Battchikova N, Paakkari V, Katoh H, Iwai M, Ikeuchi M, Pakrasi HB, ... , Aro E-M (2005) Isolation, subunit composition and interaction of the NDH-1 complexes from *Thermosynechococcus elongatus* BP-1. *Biochem J* 390: 513–520
- Zhang P, Eisenhut M, Brandt AM, Carmel D, Silén H, Vass I, Allahverdiyeva Y, ... , Aro E-M (2012) Operon *flv4-flv2* provides cyanobacterial photosystem II with flexibility of electron transfer. *Plant Cell* 24:1952–1971
- Zhao J, Gao F, Zhang J, Ogawa T, Ma W (2014) NdhO, a Subunit of NADPH dehydrogenase, destabilizes medium size complex of the enzyme in *Synechocystis* sp. strain PCC 6803. *J Biol Chem* 289:26669–26676

# Part II

## **Theoretical Aspects of Electron Transfer**

# Chapter 5

## Fundamentals of Electron Transfer in Proteins

Lev I. Krishtalik\*

*A. N. Frumkin Institute of Physical Chemistry and  
Electrochemistry, Russian Academy of Sciences, Leninskii pr.  
31, 119991 Moscow, Russia*

Summary.....	73
I. Introduction.....	74
II. The General Theory of Charge Transfer Reactions in Polar Media: An Outline.....	74
A. Electron Transfer and Charge: Medium Interaction, Activation and Reorganization Energies.....	74
B. Underbarrier Transfer (Quantum—Mechanical Tunneling): Adiabatic and Non-adiabatic Transitions.....	80
III. Proteins as Specific Structured Polar Media.....	83
IV. Equilibrium Energies of Electron Transfer.....	85
A. The Pre-existent Field.....	85
B. The Medium Polarization Energy.....	87
V. Reorganization Energy and Activation Energy.....	90
VI. Long-Range Electron Transfer.....	93
References.....	95

### Summary

An outline of the Marcus–Levich–Dogonadze theory of charge transfer reactions in polar media is given with an emphasis on the physical sense of its concepts rather than on mathematical details. The reorganization energy has been considered as well as the dependence of the activation energy on this parameter and on the reaction energy. The quantum—mechanical treatment of the pre-exponential factor is described, and the regularities of the non-adiabatic and adiabatic electron transfer are qualitatively explained. Regarding intraprotein electron transfer, the electrostatic interaction of a moving charge with its surroundings, primarily with protein and water, is the major factor determining the thermodynamics and kinetics involved. A specific feature of protein structure is the presence of a high concentration of strongly polar groups, mainly of peptide groups. Tight packing of these dipoles inside certain structures substantially restricts their ability to change orientation in an external electric field. This has two consequences: (i) a low static dielectric permittivity (i.e., dielectric constant) of proteins and (ii) the presence of a substantial permanent intraprotein electric field pre-existent before charging of the active site, e.g., redox center. Therefore, the internal environment of proteins can be defined as a pre-organized highly-polar, low-dielectric medium. These specific protein

---

\*Author for correspondence, e-mail: [av164159@akado.ru](mailto:av164159@akado.ru)

features are important for acceleration of electron transfer reactions. The semi-continuum electrostatics approach, viz. description of a protein as a set of point atomic charges in a continuum dielectric is presented. The specificity of quantitative calculations in the framework of this approach of all the parameters determining the activation energy has been considered. It is shown that the intraprotein pre-existing field should be calculated employing the protein's optical permittivity, while for the dielectric response energy one should use the static quantity (in both cases, the static dielectric constant of water). The reorganization energy of a protein does not depend on the pre-existing field. The reorganization energies calculated by microscopic simulations and by semi-continuum electrostatics (including quantum—chemical data) are in reasonable agreement with each other and with experiment. The mechanism of long-range electron transfer is discussed.

## I. Introduction

A great many biochemical processes are essentially electron transfer reactions, i.e., the processes involving transfer of charged particles. The purpose of this chapter is to provide a brief summary of the general theory of charge transfer in condensed polar media, and to discuss the consequences of this theory applied to biochemical processes, namely, charge transfer reactions in the specific polar medium of a protein. Accordingly, the chapter consists of two main parts. The first aims at presenting the physical sense of the theory with an emphasis on the qualitative understanding of its main concepts rather than on the rigorous deduction of its equations, (including the most important formulae). The second part considers the charge transfer reactions in proteins. Its main goal is to show how the general architectural principles of protein structure are reflected in their behavior as media of charge transfer.

---

*Abbreviations:* bpy – Bipyridine; D – Debye the unit of dipole moment; DMF – Dimethylformamide; ESP – Electrostatic potential; HOMO – Highest occupied molecular orbital; im – Imidazole; LUMO – Lowest unoccupied molecular orbital; MD – Molecular dynamics; MM – Molecular mechanics; py – Pyridine; SHE – Standard hydrogen electrode; QM – Quantum mechanics; WT – Wild type

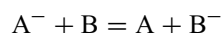
There exists a vast literature on the topic that is impossible to cover completely. Therefore, in many cases, I will cite reviews, the original papers in which some specific problem was first considered, and/or some more recent publications where the reader can find a more detailed bibliography.

## II. The General Theory of Charge Transfer Reactions in Polar Media: An Outline

The foundations of the theory in the framework of the semi-classical approach have been laid by Marcus (1956) (Nobel Prize, 1992), and the rigorous quantum—mechanical theory was first developed by Levich and Dogonadze (1959). The theory has been reviewed many times, and for a more detailed description the reader is referred to representative manuscripts and books (Dogonadze and Kuznetsov 1975, 1983; Ulstrup 1979; Marcus and Sutin 1985; Krishtalik 1986a; Kuznetsov et al. 1988; Marcus 1996; Kuznetsov 1995, 1999; Kuznetsov and Ulstrup 1999).

### A. Electron Transfer and Charge: Medium Interaction, Activation and Reorganization Energies

Let us consider electron transfer from A to B



Any charge in a polar medium causes orientation of its dipoles. The orientation of many dipoles results in medium polarization. In subsequent figures, this polarization is described by the coordinate  $q$ . The energy of the charge-polarization interaction is an important constituent of the system's free energy,  $G$ . The optimum dipole orientation corresponds to the equilibrium state having a minimal energy. Any deviation from this initial optimum polarization  $q_o$  caused by thermal fluctuations of dipole orientations results in an increase in energy. As the dielectric polarization responds linearly to the electric field in the absence of dielectric saturation, the energy depends quadratically on polarization, i.e., the energy as a function of  $q$ , is a parabola (the polarization  $q$  serves as

the reaction coordinate in the framework of the continuum electrostatic description.

In the left panel of Fig. 5.1, curve 1 represents the dependence of the system free energy on the medium polarization for the initial state (electron residing on A). The corresponding equilibrium polarization is  $q_o^i$ . When charge is transferred from one reactant to another (from A to B), a new final equilibrium polarization ( $q_o^f$ ) and a corresponding new equilibrium energy appears, which is described by another energy curve (curve 2, Fig. 5.1, left panel). The energy difference at the minima of these two curves is equal to the reaction free energy,  $\Delta G_0$ .

It should be mentioned that the quadratic dependence of energy on the reaction coordinate was also obtained by molecular

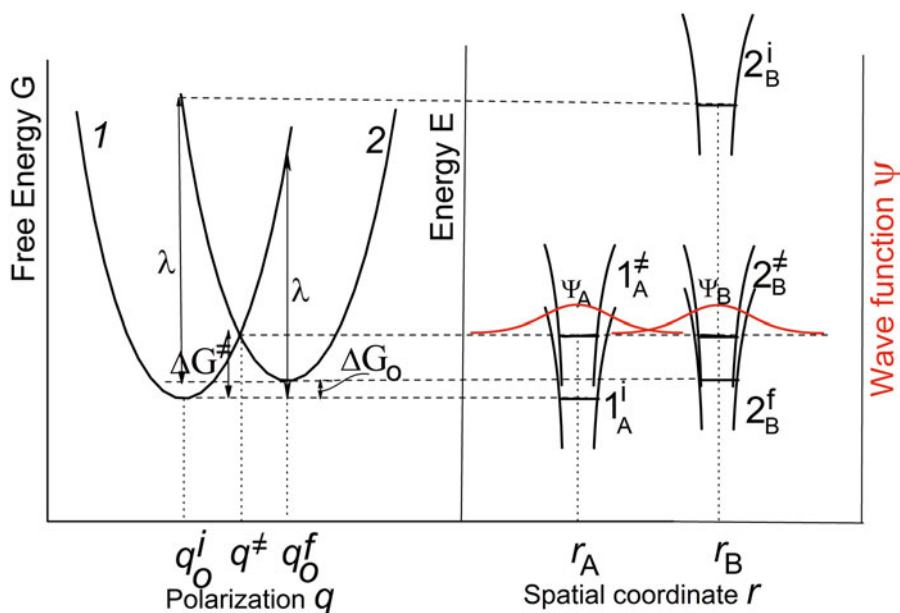


Fig. 5.1. Energy diagrams for the electron transfer process. *Left panel:* System free energy ( $G$ ) dependence on the medium polarization  $q$ . Curve 1 corresponds to the initial state (electron residing on A), curve 2 to the final one (electron on B). The polarizations  $q_o^i$  and  $q_o^f$  are the equilibrium values for initial and final states, polarization  $q^{\neq}$  relates to the intersection point of curves 1 and 2, i.e., to transition state.  $\Delta G_0$  is the equilibrium reaction free energy, and  $\Delta G^{\neq}$  the activation energy. *Right panel:* The intra-atom electron potential energy dependence on its spatial coordinate  $r$  (black curves). Curves  $1_A$  correspond to the electron residing on A, curves  $2_B$ —on B. Superscript  $i$  means that the polarization coordinate equals to  $q_o^i$ , superscript  $f$  relates to polarization  $q_o^f$ , superscript  $\neq$  — to  $q^{\neq}$ . Horizontal bars inside the electronic wells show the electron energy levels, occupied for A, and empty for B. The states with equal energies in the left and right panels are connected by thin horizontal dashed lines. The wave functions of electron on A or B ( $\psi_A$  and  $\psi_B$ ) are represented as red curves.

dynamics simulations for some concrete systems (e.g., Yadav et al. 1991; Simonson 2002; see also Sect. V). Hence, the microscopic simulations support the continuum dielectric description.

The potential energy curves for electron as a function of the spatial coordinate  $r$  are represented (Fig. 5.1, right panel). The potential wells for the electron in the atom or an atomic group are approximately hyperbolic. Curve  $1_A^i$  relates to the initial state (electron residing on A); curve  $2_B^f$ —to the final state (electron on B). The electron energy levels shown here (horizontal bars in the potential wells described by curves  $1_A^i$  and  $2_B^f$ ) relate to an equilibrium, i.e., they are at the same energy as the minima of the curves 1 and 2 at the left panel (the equivalent states in the left and right panels are connected by dashed horizontal lines).

Let us consider now the process of the electron transfer from A to B. At the dipole coordinates corresponding to the equilibrium initial state ( $q_o^i$ ), the electron energy level is shown at the curve  $1_A^i$  (right panel) when the electron is on A, and at curve  $2_B^i$  when it is on B. The energy of the system with the electron on B at dipole coordinates  $q_o^i$  is described by curve 2, left panel. Due to the great difference in masses, the rate of the electron movement is many orders of magnitude faster than that of the heavy particles (dipoles) movement. Therefore, the electron transfer should proceed at practically constant coordinates of heavy particles (nuclei), and the latter can be considered as practically immobile in the course of this process. This very important statement is called the Franck-Condon principle. We see that, at the constant coordinate  $q_o^i$ , the electron levels in the initial and final states are quite different, and hence the electron cannot jump from one reactant to the other without an input of energy from an external source. In this system, there are no other energy sources except thermal motion of the molecules, but molecular motion is too slow in comparison to electron movement. Therefore, the electron cannot borrow energy from this source. Thus, electron transfer at the equilibrium

polarization  $q_o^i$  is impossible as it contradicts the law of energy conservation.

The situation changes when, as a result of relatively slow thermal fluctuation of dipole orientation, the system comes to the intersection point of the potential curves of the initial and final states (Fig. 5.1, left panel,  $q^\ddagger$ ). At this coordinate, the energy levels of the electron at A and B become equal (curves  $1_A^\ddagger$  and  $2_B^\ddagger$ , right panel) and electron transfer becomes possible. Thereby, this electron transition should be preceded by a thermal activation bringing the system to the top of the barrier. This barrier is called the Franck-Condon barrier. The probability of the electron transition from A to B at the top of the barrier will be considered in the next Sect. (II.B).

The height of the barrier (activation energy  $\Delta G^\ddagger$ ) is determined by the equilibrium energy gap between two states,  $\Delta G_o$ , and the shape of the energy curves. In the case of dielectric polarization of the medium, only the positions of the charge in the initial and final states are different, but not its interaction with the medium; therefore, the two parabolic curves 1 and 2 have the same curvature. Their shape can be characterized by the quantity called the reorganization energy,  $\lambda$ . As shown in Fig. 5.1,  $\lambda$  is the energy necessary to bring the system from the initial to final equilibrium polarization (coordinates,  $q_o^i$  and  $q_o^f$ ) under the condition that electron remains in the initial configuration, i.e., resides on A; this means that the system reaches the final polarization  $q_o^f$  remaining on curve 1. As shown in Fig. 5.1, the same quantity,  $\lambda$ , corresponds to charge transfer in the opposite direction, from  $q_o^f$  to  $q_o^i$ . The activation energy,  $\Delta G^\ddagger$  is the difference between the initial equilibrium energy and the energy at the intersection point of the two parabolae. The corresponding formula (the Marcus equation; Marcus 1956) is

$$\Delta G^\ddagger = \frac{(\lambda_s + \Delta G_o)^2}{4\lambda_s} \quad (5.1)$$

The subscript “s” here means that  $\lambda$  relates to reorganization of the medium (solvent).

In principle, reorganization of coordinates of other heavy particles is possible, e.g., change of the covalent bonds lengths inside a complex ion (inner—sphere reorganization,  $\lambda_i$ , as opposed to the outer—sphere reorganization,  $\lambda_s$ ). In that case, Eq. 5.1 should involve the sum of all reorganization energies (at the strongly asymmetric potential curves of the inner coordinates,  $\lambda_i$ 's for the two reaction directions are non-equivalent; in this case, Eq. 5.1 takes a more complex form; however, when these two  $\lambda_i$ 's are not too different (e.g., by more than a factor of two), and markedly smaller than  $\lambda_s$ , one can use their arithmetic mean.

Figure 5.1 presents a one-dimensional scheme of the potential energy curves. The polarization coordinate  $q$  involves coordinates (degrees of freedom) of a great many dipoles, and hence the real picture is a multi-dimensional energy surface. Averaging statistically over all degrees of freedom gives the free energies that enter Eq. 5.1.

As defined above, the reorganization energy,  $\lambda_s$ , is the energy necessary to change the polarization from  $q_o^i$  to  $q_o^f$  with the electron remaining at its initial position. This polarization is due to the orientation of dipoles, i.e., of heavy particles moving slowly relative to electron movement. This kind of polarization is called ‘inertial polarization’ as opposed to the inertia-less electronic polarization of the medium (the electrons of the medium follow instantaneously the movement of the electron being transferred, and hence electronic polarization does not present any obstacle for electron transfer).

To clarify the physical sense of the reorganization energy, we will calculate the value of  $\lambda_s$  following the Marcus scheme. At the first step, we will find the equilibrium energy of a slow charge transfer from A to B in some medium with the static dielectric constant (dielectric permittivity),  $\epsilon_s$ . This static constant reflects the total dielectric response of inertial and inertia-less polarization. The second step is a very fast charge transfer backwards from B to A. This transfer is so fast that only electronic polarization (described

by the optical dielectric constant  $\epsilon_o$ ) has time to adapt itself to the new charge position. Therefore, the inertial polarization remains the same as after the first step. Therefore, as the result of this two-step process, we have the system with the initial charge distribution and with the inertial polarization corresponding to the final charge position. The total energy of this process is nothing else than the reorganization energy. Let us perform these calculations using the simple model of spherical conducting spheres with radii  $a_A$  and  $a_B$ .

The electron transfer from A to B ( $A + B \rightarrow A^+ + B^-$ ) can be described as the charging of A by the positive charge  $+e$  and, simultaneously, charging of B by  $-e$  ( $e$  is the unit electron charge). At some moment in the course of the charging process, a charge  $+q$  resides on A ( $0 \leq q \leq e$ ) and  $-q$  resides on B; then, we add  $+dq$  to A and  $-dq$  to B. The additional charge  $+dq$  is distributed on the surface of A, and is subject to the potential

$$\varphi_A^s = +q/\epsilon_s a_A - q/\epsilon_s R \quad (5.2)$$

The first term is due to the charge of A itself, and the second is the potential set up by the charge of B ( $R$  is the distance between centers of A and B). A similar expression describes the potential at B.

$$\varphi_B^s = -q/\epsilon_s a_B + q/\epsilon_s R \quad (5.3)$$

The work of bringing  $+dq$  to A is  $+\varphi_A dq$ , and the corresponding quantity for  $-dq$  is  $-\varphi_B dq$ , and the total work of the first step of the charging process is obtained by integration over  $q$  from 0 to  $e$

$$\begin{aligned} W_1 = W_s &= \int_0^e \left( \frac{1}{a_A} + \frac{1}{a_B} - \frac{2}{R} \right) \frac{1}{\epsilon_s} q dq \\ &= \frac{e^2}{\epsilon_s} \left( \frac{1}{2a_A} + \frac{1}{2a_B} - \frac{1}{R} \right) \end{aligned} \quad (5.4)$$

The designation  $W_s$  stresses that the process considered is charging in a “static” medium characterized by dielectric constant  $\epsilon_s$ .



Now we shall calculate the charging energy for the second step, i.e., the charging of A by  $-e$ , and charging of B by  $+e$  leaving both reactants uncharged. The situation differs from the first step because the potentials on A and B are not zero before the new charging process, as in the first step, but have some constant values corresponding to the final state after the first charging:

$$\varphi_A^{\text{sf}} = +e/\varepsilon_s a_A - e/\varepsilon_s R \quad (5.5)$$

$$\varphi_B^{\text{sf}} = -e/\varepsilon_s a_B + e/\varepsilon_s R \quad (5.6)$$

The contribution of this field to the charging energy is:

$$\begin{aligned} W_{\text{sf}} &= \int_0^e (\varphi_B^{\text{sf}} dq - \varphi_A^{\text{sf}} dq) \\ &= -\frac{e^2}{\varepsilon_s} \left( \frac{1}{a_A} + \frac{1}{a_B} - \frac{2}{R} \right) \end{aligned} \quad (5.7)$$

Note that  $W_{\text{sf}} = -2 W_s$ . Now we calculate the contribution to the charging energy due to polarization of the “optical” medium (with  $\varepsilon_o$ ) by the charge added. The calculation is quite analogous to the calculation of  $W_s$  (in Eqs. 5.2, 5.3 and 5.4; one should exchange lower indices A and B, and substitute  $\varepsilon_o$  for  $\varepsilon_s$ ):

$$\begin{aligned} W_o &= \int_0^e \left( \frac{1}{a_A} + \frac{1}{a_B} - \frac{2}{R} \right) \frac{1}{\varepsilon_o} q dq \\ &= \frac{e^2}{\varepsilon_o} \left( \frac{1}{2a_A} + \frac{1}{2a_B} - \frac{1}{R} \right) \end{aligned} \quad (5.8)$$

The total work of the second step is

$$W_{\text{II}} = W_{\text{sf}} + W_o \quad (5.9)$$

Correspondingly, the reorganization energy is

$$\begin{aligned} \lambda_s &= W_{\text{I}} + W_{\text{II}} \\ &= e^2 \left( \frac{1}{\varepsilon_o} - \frac{1}{\varepsilon_s} \right) \left( \frac{1}{2a_A} + \frac{1}{2a_B} - \frac{1}{R} \right) \end{aligned} \quad (5.10)$$

For the sake of simplicity, Eq. 5.10 was derived for the initially uncharged reactants. It can be shown that it is valid for any initial charges of reactants because the contribution due to these initial fields cancels out.

Equation 5.10 defines the medium reorganization energy as function of properties both of the reaction complex and of the medium. So, it cannot be ascribed to some reaction in any medium or to some medium for any reaction, but only to a definite reaction in a definite medium. The reaction complex is described by the geometric factor (second parentheses), and the medium properties are represented by the difference of reciprocals of the optical and static dielectric constants. The last quantity is called the coupling constant (it determines coupling of charge movement with the inertial polarization) or the Pekar parameter (it was first introduced by Pekar in the polaron theory; Pekar 1954).

The optical permittivity  $\varepsilon_o$  corresponds to the medium polarization that follows inertialess the electron transfer. First, it is a purely electronic polarization, and it can be calculated as  $\varepsilon_o = n^2$ , where  $n$  is the refraction index for visible light. However, in some media, other vibrational modes can be present that are fast enough to follow the movement of the electron to be transferred. This effect is expressed especially in water due, for instance, to the high-frequency vibrations of O-H bonds. This results in a frequency dependence of the permittivity up to the frequency of the “quantum limit”  $kT/h$  (on the “quantum limit”, see Sect. II.B). This effectively causes an increase in  $\varepsilon_o$  and a corresponding decrease in reorganization and activation energies. However, the influence of this effect on the reaction rate is smaller than one can expect on the basis of the decrease in activation energy: the shift of atoms at frequencies higher than  $kT/h$  proceeds via tunneling, and the rate decreases by factor  $\exp(-\sigma)$  where  $\sigma$  is the medium tunneling factor. On the whole, the effect of the medium quantum vibrations is difficult to estimate quantitatively (Kuznetsov 1955, 1999).

Inspection of Eq. 5.10 shows that it can be rewritten as

$$\lambda_s = W_o - W_s \quad (5.11)$$

Equation 5.10 was derived for a simple model of two spherical reactants in a homogeneous medium. It can be shown that Eq. 5.9 has a quite general character and is valid for any geometry of reactants, their internal charge density distribution, and an inhomogeneous medium. Its application demands a proper calculation of charging energies, i.e., for a solution of the corresponding electrostatic problem; in the case of complex geometries, e.g., redox centers inside a protein globule, this solution can be achieved by numerical methods.

Let us turn again to Eq. 5.1. The reaction activation energy  $\Delta G^\ddagger$  depends on the reaction free energy,  $\Delta G_o$ . With increasing driving force (i.e.,  $\Delta G_o$  more negative), the activation energy decreases. However, this decrease takes place only until  $\Delta G_o$  becomes equal to  $-\lambda$ . At this point, the activation energy becomes zero (activationless process; see scheme in Fig. 5.2, intersection of curves 1 and 2), and the reaction rate achieves its maximal possible value. At more negative values of  $\Delta G$ , in the so-called “inverted region,” the activation energy increases with the increasing driving force (intersection of curves 1 and 3, Fig. 5.1. Curve 3 corresponds to an equilibrium energy  $\Delta G_1 < \Delta G_o$ , and the activation energy  $\Delta G_1^\ddagger > 0$ ). Due to the quadratic form of Eq. 5.1, the dependence of the activation energy  $\Delta G^\ddagger$  on  $\Delta G_o$  has a symmetric parabolic form with a minimum ( $\Delta G^\ddagger = 0$ ) at  $\Delta G_o = -\lambda$  (the corresponding dependence for the rate constant has a maximum). However, the experimental dependencies are asymmetric—the decrease in the rate constant at high driving forces is markedly slower than its increase at lower absolute values of  $\Delta G_o$ . The explanation of such behavior lies in the involvement in the process of the vibrationally excited states of the products. Eq. 5.1 relates to both initial reactants and final products being in their

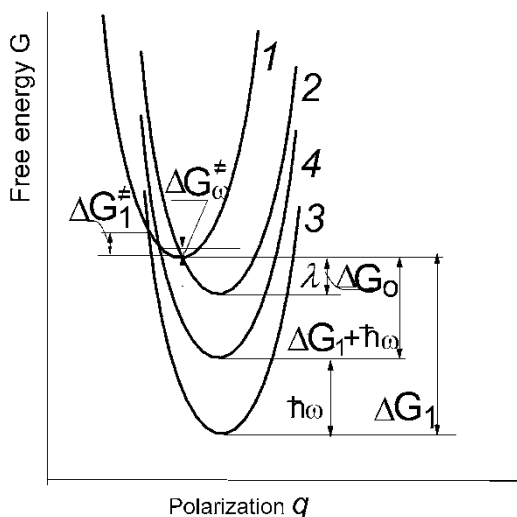


Fig. 5.2. Free energy diagrams for activationless and inverted regions. System free energy dependence on the medium polarization  $q$ . Curve 1—initial state, curves 2–4—different final states. Intersection of curves 1 and 2 at the minimum of curve 1 ( $\lambda = -\Delta G_o$ ) results in activation energy equal to zero (activationless process). At more negative free energy ( $-\Delta G_1 > \lambda$ , curve 3) activation energy ( $\Delta G_1^\ddagger$ ) increases. When in the final state, a vibrationally-excited level of the product is involved (curve 4), its energy becomes higher by the value of the vibrational quantum  $\hbar\omega$  (the reaction free energy ( $\Delta G_1 + \hbar\omega$ ) becomes less negative). Correspondingly, the activation energy  $\Delta G_o^\ddagger < \Delta G_1^\ddagger$ . The situation described by curves 3 and 4 is called the “inverted region”.

ground states. This is the most favorable pathway before the reaction rate maximum. However, at very negative  $\Delta G$ 's, formation of a vibrationally-excited product decreases the absolute value of  $\Delta G$  by the energy of the vibration quantum,  $\hbar\omega$  ( $\Delta G_1 + \hbar\omega$ ) decreasing the activation energy  $\Delta G_o^\ddagger$  (intersection of curves 1 and 4 in Fig. 5.2). For some products, more than one vibrational state, and even an electronically excited state, may be involved.

Equation 5.1 describes the activation free energy inside a reaction complex having some optimal configuration of reactants. Often, some work ( $W_i$ ) associated with approach of reactants must be expended to achieve this optimum configuration (inter-reactant distances, and orientation). In this case,

$$\Delta G^\ddagger = W_i + \frac{(\lambda_s + \Delta G)^2}{4\lambda_s} \quad (5.12)$$

Here  $\Delta G$  is the free energy of the elementary act of reaction inside the reaction complex; it differs from the reaction free energy for the separated reactants  $\Delta G_o$  by the difference of the energies of approach for initial reactants and final products

$$\Delta G = \Delta G_o + W_f - W_i \quad (5.13)$$

The quantity  $\Delta G_o$  in Eqs. 5.1 and 5.13 refers to the process inside the reaction complex, According to its physical sense, it is independent of the presence of the reactants outside the complex, and of their concentration in the bulk solution. This concentration-independent quantity is called the configurational free energy  $\Delta G_c$  which depends on the configuration of the reactants but not on their concentration. It differs from the total free energy of reaction by the difference of the free energies of mixing of initial and final reactants with the solvent:

$$\Delta G_c = \Delta G_o + RT \sum_1^n \ln X_{oi} - RT \sum_1^m \ln X_{of} \quad (5.14)$$

Here  $\Delta G_o$  is the standard free energy of the reaction in solution, and  $X_{oi}$  and  $X_{of}$  are the molar fractions of  $n$  initial and  $m$  final reactants in solution in their standard states. The origin of the last two terms in this equation is purely entropic: a decrease in the fraction of some substance increases the number of transpositions of its molecules with other molecular species (normalized to one mole of this substance), and hence increases the probability of the state, i.e., increases the molar entropy.

Equation 5.12 allows one to calculate  $\Delta G_c$ , which should enter Eqs. 5.1 and 5.13 as  $\Delta G_o$ , when the standard free energy is known. If the standard states of all reactants are the same (e.g., 1 M), and the number of molecules does not change upon the reaction

( $n = m$ ), the last two terms in Eq. 5.11 cancel out, and  $\Delta G_c = \Delta G_o$ . That means that the free energy expenditure necessary to take the dissolved reactants from the bulk and gather them into the reaction complex (the demixing process that is accompanied by a decrease in entropy) is exactly compensated for by the free energy of mixing of the products with solution. In other, also frequently occurring cases, the correction according to Eq. 5.12 is large, and thereby substantially influences the reaction equilibrium and rate (Krishtalik 1986b).

### B. Underbarrier Transfer (Quantum—Mechanical Tunneling): Adiabatic and Non-adiabatic Transitions

The electron transfer from the initial to the final position is described as an underbarrier transition (quantum—mechanical tunneling). For any particle, there are two possible pathways of transition—classical ‘overbarrier’ and quantum—mechanical ‘underbarrier’. In the case that the distance between two neighboring energy levels (for harmonic oscillator  $\hbar\omega$ ) is smaller than the average energy of thermal fluctuations,  $kT$ , the predominant pathway is the classical overbarrier transition. In the opposite case ( $\hbar\omega > kT$ ) the particle transfer proceeds through a quantum—mechanical underbarrier pathway. Let us qualitatively describe how this underbarrier transition proceeds.

For the particle behaving quantum—mechanically, its state is described by the wave function  $\psi$ , and this function is not confined in the space inside the well, but protrudes outside it; in the “outer space” it decays approximately exponentially with distance. The probability of finding the particle at some position is determined by its wave function, so it is not zero outside the well. With two wells not too far from each other, the wave functions corresponding to an electron in wells A and B ( $\psi_A$  and  $\psi_B$ , red curves in Fig. 5.1) overlap. In the region of this overlap, the electron belongs simultaneously to both atoms—it has a common wave function and the same energy.

Therefore, it can transfer from one atom to the other; the probability of this transition is larger, the greater the overlap of the wave functions (more precisely, the stronger is the interaction between the initial and final states, see below). It decays exponentially with increasing distance.

Not only electrons, but any particle can in principle, behave quantum-mechanically. In special cases, the proton also undergoes an underbarrier transition, and the process is accompanied by a substantial kinetic isotope effect (Krishtalik 2000).

In the preceding considerations, we have used potential curves (more strictly, free energy surfaces) corresponding to the initial and final states separately. These energy curves, unaffected by the interaction of the reactants are called “diabatic curves”. However, the interaction of reactants can influence the form of potential curves and the position of the corresponding energy levels. This interaction is substantial when the electron has time to rearrange its wave function, i.e., zero time for a transition from one potential well to the other (from the initial  $i$  to the final  $f$ ). Let us designate this time,  $\tau_{if}$ . According to the Franck-Condon principle, this transition can take place only near the top of the barrier along the  $q$  coordinate. On the other hand, the coordinate  $q$  changes continuously because of thermal fluctuations, and the slow classical subsystem remains near the barrier top only for some restricted time  $\tau_c$ .

When  $\tau_c \ll \tau_{if}$ , the interaction between initial and final states does not have sufficient time to develop, the system remains in the diabatic state, and the barrier height is determined by intersection of the diabatic curves. In the course of its thermal fluctuations, the classical subsystem will pass the crossing point many times before the particle jumps to its final position. Therefore, at the top of the classical barrier, the transfer probability is much less than unity and is close, within an order of magnitude, to the ratio  $\tau_c/\tau_{if}$ . Such reactions are called “non-adiabatic.”

In contrast, when  $\tau_c \gg \tau_{if}$ , the electron can exchange many times between the re-

actants before the system leaves the region of the barrier top. Therefore, they can interact effectively and form a unified state (this is possible near the barrier top where the energies of the two reactants are similar). More exactly, from two initially existing states ( $i$  and  $f$ ) two new states appear, one which is lower than the intersection point of the diabatic curves by the interaction energy (coupling matrix element)  $V_{if}$ , and the other lying higher by the same energy difference. These curves (free energy surfaces) are called “adiabatic” (Fig. 5.3, left panel). The intersection region of diabatic curves are shown Fig. 5.3 by the dashed segments of curves 1 and 2, and the adiabatic curves are presented as solid lines. Two adiabatic curves correspond to two different electronic states and, instead of one energy level in each potential well (dashed curves in the right panel of Fig. 5.3), two levels appear (solid lines, Fig. 5.3, right). In the course of a slow movement of the classical subsystem, at any moment the electron has enough time to adjust adiabatically to the new coordinates, and hence when the system goes over the  $q$ -barrier, the electron can transit readily to the final state. Such a transition called adiabatic, and it has a probability of 1.

As is explained below the rate constant  $k$  can be written as

$$k = \frac{\omega_{\text{eff}}}{2\pi} P \exp\left(-\frac{\Delta G^\ddagger}{kT}\right) \quad (5.15)$$

In addition to the purely electrostatic treatment, the medium can be described also as a set of harmonic oscillators, or one oscillator with an effective circular frequency  $\omega_{\text{eff}}$ . In Eq. 5.15,  $\omega_{\text{eff}}/2\pi$  is the number of the classical subsystem’s oscillations, and  $\exp(-\Delta G^\ddagger/kT)$  determines the fraction of these oscillations having an energy sufficient to reach the barrier top.  $P$  is the probability of the electron transition to the final state when the system has reached the barrier top, where the electron levels in the initial and final states become equal. For a non-adiabatic process, the quantum mechanical Levich—Dogonadze theory gives

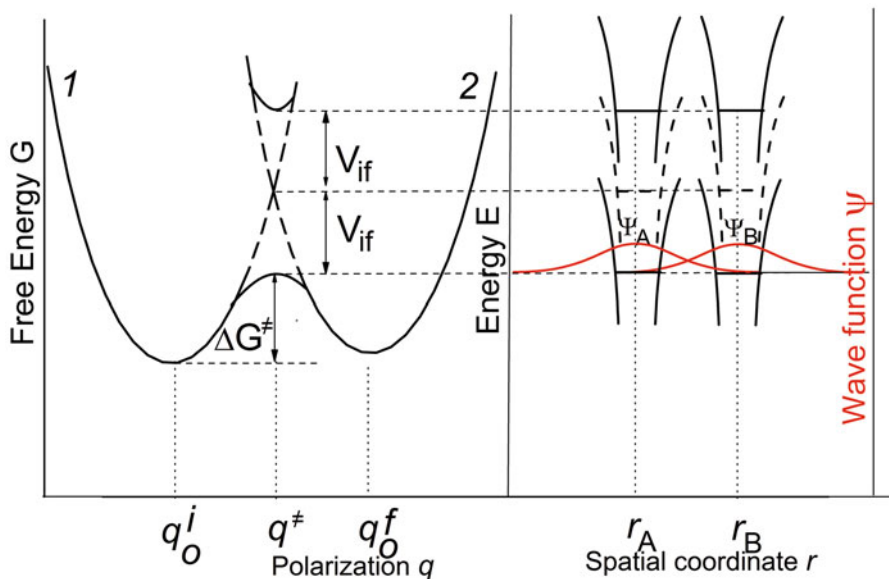


Fig. 5.3. Energy diagrams for the adiabatic electron transfer process. Plotted similarly to Fig. 5.1, the designations are also similar. On the *left panel*, two continuous *solid lines* relates to two adiabatic curves with the upper and lower energies at the transition polarization  $q^\ddagger$ .  $V_{if}$  is the interaction energy. The *dashed* segments represent the diabatic curves for the initial and final states. On the *right panel*, the *dashed* potential wells correspond to the diabatic state, i.e., the situation where the interaction of initial and final states is absent (the point of intersection of diabatic curves on the *left panel*). The *solid* potential wells relate to two electronic (adiabatic) states at the transition point  $q^\ddagger$ ; their energy levels are separated by  $2V_{if}$ .

the following expression for the rate constant:

$$k = 2\pi \frac{V_{if}^2}{h} \left( \frac{\pi}{kT\lambda_s} \right)^{1/2} \exp\left(-\frac{\Delta G^\ddagger}{kT}\right) \quad (5.16)$$

Let us explain qualitatively some features of this formula. As to its strict description, we refer the reader to the references cited at the beginning of Sect. II, especially to Kuznetsov (1995, 1999).

We have seen that the system behavior depends substantially on the ratio  $\tau_c/\tau_{if}$ . The value of  $\tau_c$  depends on two factors. The first is the width of the transition region that should be crossed by the slow subsystem; it increases with increasing  $V_{if}$ , and decreases with the increasing curvature of the potential curves in the vicinity of their intersection that depends on  $\lambda_s$ . The second factor is the velocity of crossing the transition region which is proportional to the frequency of the classical oscillator (medium oscillator)  $\omega_{eff}$ .

As a result,  $\tau_c$  is inversely proportional to  $\omega_{eff}$ . Therefore, the frequencies in the numerator and denominator cancel out, and the rate constant is independent of  $\omega_{eff}$ . The physical basis is that an increasing  $\omega_{eff}$  implies a higher frequency of barrier crossings, but simultaneously a larger velocity of this crossing, and hence a compensating decrease in transition probability at each crossing event.

On the other hand, the crossing time  $\tau_{if}$  is inversely proportional to  $V_{if}$  (it equals  $h/V_{if}$  by approximately an order of magnitude). The stronger the interaction, the faster the transformation of the electronic cloud. This explains why  $k$  is proportional to  $V_{if}^2$ .

For the non-adiabatic reaction, the small value of  $V_{if}$  corresponds usually to a weak overlap of the wave functions  $\psi_A$  and  $\psi_B$  (see Fig. 5.1, right panel). In this case, the activation energy  $\Delta G^\ddagger$  is determined by the intersection of two diabatic curves. The activation energy is expressed through the reorganization energy  $\lambda_s$  and the free

energy of the elementary act,  $\Delta G_o$ , by the usual quadratic expression of the Marcusian type.

For adiabatic reactions, the activation barrier is lower than the crossing point of two diabatic curves by the value of the interaction energy  $V_{if}$  (see Fig. 5.3, left panel; in this figure, the large  $V_{if}$  corresponds to the strong overlapping of the wave functions). At the same time, the probability  $P$  for these reactions equals one. Hence, the medium vibration frequency enters the rate equation explicitly (Eq. 5.13).

### III. Proteins as Specific Structured Polar Media

The properties of proteins as polar media are determined by the distinctive features of their structure (for review, see Krishtalik 2012). The main principle underlying protein ‘architectonics’ is the formation of a linear sequence of amino acid residues linked together by strong peptide bonds and rather tightly packed into secondary and tertiary structures. The main elements of this structure, peptide groups, are characterized by a large dipole moment. For example, the dipole moments of many free amides are close to 4D; there is evidence that the formation of certain secondary structures, such as  $\alpha$ -helices, leads to mutual polarization of peptide bonds and enhancement of their dipole moment up to  $\sim 6D$ . Tight packing of peptide sequences and polar-side chains inside certain structures substantially restricts the ability of protein dipoles to change orientation (to reorient) under the action of an external electric field. Of course, the dipoles retain some mobility but their orientation is constrained to narrow limits. This has two important consequences:

First, the dielectric response of a protein to the external electric field is very weak (the extent of their reorientation is small), and hence its static dielectric permittivity is low. For certain dry proteins, the dielectric permittivity was found to be  $\sim 3.5$ – $4.0$  (Pethig

1979); similar values were obtained with different variants of microscopic simulations for regions inside protein molecules (e.g., Gilson and Honig 1986; Simonson 1998). At the same time, liquid low-molecular weight amides with practically the same or a lower concentration of polar amide groups are characterized by high dielectric permittivity (e.g., 37 for dimethylformamide). Second, an important difference between proteins and low-molecular weight polar solvents lies in the existence of a permanent intraprotein electric field. The electric potential created by dipoles at any point of a low-molecular weight liquid at an arbitrary time can differ from zero. However, random fluctuations of dipole orientation make the time averaged potential equal to zero. The averaged dipole orientation ceases to be random only after an ion is introduced into the liquid; then, the potential created by the dipoles assumes a definite value. Unlike dipole orientation in liquids, that in proteins is determined by their structure. Certainly, dipole orientation in proteins undergoes fluctuations but the permissible variations are very limited. This accounts for the existence of a permanent time-averaged electric field at any point in the protein molecule. The field is present prior to the introduction of a new free charge; therefore, it may be called a ‘pre-existent field’. Dipoles in proteins are intrinsically ordered, whereas in liquids their ordering develops only after the introduction of a charge. The pre-existent field is organized in such a way to facilitate charge transfer (see below, Sects. IV.A and V). For this reason, proteins can be described as ‘pre-organized polar media’ (Krishtalik 1974).

The proteins as pre-organized media possess one more feature different from that of liquid dielectrics. In liquid solvents, the main contribution to the solvation energy is brought about by the interaction of the ion with the nearest molecules; the more distant dipoles are less oriented because the field of the ion at larger distance is weaker. In proteins, the orientation of dipoles is determined by the entire protein structure, and therefore one can observe in some cases that

the dominant effect is the interaction not only with the nearest ion's neighbors but with the larger number of more distant dipoles.

It follows from the foregoing that proteins are highly-polar, low-dielectric media, i.e., they exhibit a combination of properties that can never be found in low-molecular weight liquids showing practically unlimited dipole mobility. Therefore, there is no sense, in the case of proteins, to consider a high polarity and a low dielectric permittivity to be antithetical properties.

In real biological systems, proteins practically never function as the sole dielectric phase; they are usually in contact with other dielectrics, e.g., water or lipids. The long-range action of Coulomb forces accounts for the substantial interaction of charges inside the protein with a non-protein phase that must be necessarily taken into consideration in the quantitative description of charge transfer processes. The introduction of a certain effective dielectric permittivity, sometimes proposed to describe an averaged description of the response of the two phases, is a rough approximation having no clear physical sense.

The aqueous environment influences both the energy of interaction between the charge and dipoles created by polarization and the strength of the pre-existent field. The latter is due to the shielding of the charge field in a protein by polarization of its aqueous environment, characterized by high dielectric permittivity. This effect was first reported, in quantitative terms in the classic work by Tanford and Kirkwood (1957) for the field of charged groups in the model of a homogeneous dielectric sphere. For dipole fields, the effect of aqueous surroundings was first considered in the microscopic model by Warshel and Levitt (1976). For the field of free charges and dipoles in the protein of a real geometry, the first accurate computations in the framework of a semi-continuum model, were performed by Warwicker and Watson (1982). At present, a few programs, e.g., DelPhi (Nicholls and Honig 1991) and MEAD (Bashford and Karplus 1990) are available for the electrostatic calculation

of arbitrarily shaped macromolecules in an electrolyte solution. The point in question is the numerical solution of the Poisson–Boltzmann equation (solution of the Poisson equation taking account of the Boltzmann distribution of the surrounding electrolyte ions in the Debye–Hückel approximation).

Structural constraints on the mobility of dipoles affect not only the permissible degree of their orientation, but also their rotation rate. A wide range of different-scale movements are known to occur in proteins, with different activation barriers and, therefore, with different characteristic times (see, e.g., Brooks et al. 1988). Dipole rotation associated with different types of protein movements correspond to different dielectric response rates reflected in the broad spectrum of dielectric relaxation times (from hundreds of femtoseconds to a few seconds). This situation can be phenomenologically described as a set of effective dielectric permittivities, each corresponding to a certain time interval (Krishtalik 1996).

To summarize, the consequences of common principles of the protein architecture are low dielectric permittivity, the presence of a permanent intraprotein electric field, and a wide range of dielectric relaxation times. How these specific features of proteins as dielectric media manifest themselves in the rate of electron transfer will be discussed in the following sections.

An exhaustive theoretical analysis of the charge transfer reactions in proteins demands a quantum-mechanical treatment of all parts of the system—reactants, protein and its surroundings. However, it is an extremely difficult task even for modern powerful computers, and therefore more tractable multi-scale models were developed (Karplus, Levitt, Warshel, Nobel Prize in Chemistry, 2013). In these models, the reactants are treated quantum-mechanically (QM), and the protein and its surroundings by various classical mechanics methods—molecular mechanics (MM), molecular dynamics (MD) (reviewed by Shurki and Warshel 2003).

For the processes involving bond breaking—bond formation, and hence

the mutual movement of reacting groups, MM/QM or MD/QM are the computational methods of choice. However, for reactions of the pure electronic transfer, another approach can be used; the redox centers are treated quantum-chemically (QC) or (more often) by a combination of QC with the experimental data, and the protein and surroundings—by classical electrostatics. For the protein, the semi-continuum model is used: a set of point charges (full and partial) imbedded in a continuum dielectric (the latter can be inhomogeneous one). A comparison of these two approaches has been discussed in a review by Simonson (2008), and the conclusion was that for redox reactions both these methods give reasonably similar results. In practical applications, both microscopic and semi-continuum electrostatics models have to resort to various approximations and simplifications. For these approaches, the approximations used are different, and therefore it is instructive to compare their results for the same concrete system. Some examples of such a comparison will be given below (Sect. V).

In the following, we will employ the semi-continuum protein description. First, in our opinion, it gives a more transparent general physical picture. Second, the calculations in this model consume, by orders of magnitude, less computer time than any microscopic simulation. We will analyze the problems in the framework of the Marcus–Levich–Dogonadze formalism, described above in Sect. II (also, see Chap. 6 by G. Matthias Ullmann et al. 2015).

#### IV. Equilibrium Energies of Electron Transfer

The free energy of the elementary act of charge transfer is the sum of the energy determined by the inherent properties of reactants (e.g., ionization potential) and the energy of interaction between the charge and its environment. The latter energy, in turn, comprises two components. One is the en-

ergy of polarization,  $\Delta G_{\text{pol}}$ , of the dielectric medium by the charge. The polarization energy generated by the dielectric response of the medium is manifested in both low-molecular weight liquids and proteins, where it differs only quantitatively in agreement with the difference of their static dielectric permittivities.

The usual polarization of the medium by the charge is supplemented in protein media by a qualitatively new effect absent in liquid dielectrics; namely, the pre-existing field effect mentioned in Sect. III. A charge introduced into a protein (or transferred from one of its sites to another) interacts not only with the polarization it induces but also with the pre-existing intraprotein electric field, giving a contribution,  $\Delta G_{\text{p.f.}}$ .

##### A. The Pre-existent Field

The effect of the pre-existent field of protein dipoles, and not only of superficial charged groups, described in the early 1970s (Johanin and Kellersohn 1972; Krishtalik 1974; Warshel and Levitt 1976) was later extensively investigated. However, the analysis of electrostatic effects in proteins was for a long time inconsistent due to the ambiguity of the notion of dielectric permittivity used in these calculations (see, e.g., Schutz and Warshel 2001). In many calculations, the same static permittivity  $\epsilon_s$  was used for evaluation of both the pre-existing field and the polarization energy. Warshel and coworkers (King et al. 1991) noticed a contradiction inherent in such an approach. Indeed, it suggests that permanent dipoles not only create an intraprotein field but also screen it; in other words, the permanent dipole field is shielded by the dipoles themselves which is physically unreasonable. This contradiction can be resolved by the following considerations (Krishtalik et al. 1997).

In the framework of the semi-continuum approximation, we consider a protein as some set of charges imbedded in a continuum dielectric medium. Hence, we substitute the true electron density



distribution over all atoms of the protein by certain effective partial atomic charges obtained in quantum chemical calculations of small molecules or their fragments, which describe the field outside these molecules. The field of each fragment distorts the electron density distribution of all other fragments by inducing respective dipole moments. In the framework of the semi-continuum approximation, mutual electronic polarization of protein molecule fragments is averaged and described by a certain mean electronic (optical) dielectric permittivity  $\epsilon_0$ . The optical permittivity is used to calculate the pre-existent field, because the coordinates of all the atoms are specified and their shift under the action of the pre-existing field should not be taken into consideration. The appearance in the protein of a new free charge (e.g., attachment of electrons or protons to a group) causes both displacement of the medium (protein) heavy atoms (and/or dipole rotation, an analog of atomic and orientational polarization of ordinary dielectrics) and polarization of all electron shells. Therefore, all types of polarizability are responding, and the effect of the interaction of the new charge with the polarization it induces is determined by the total, i.e., static, dielectric permittivity,  $\epsilon_s$ . This suggests an algorithm for the  $\Delta G$  calculation in which  $\Delta G_{p.f.}$  and  $\Delta G_{pol}$  are calculated using the protein dielectric constants,  $\epsilon_0$  and  $\epsilon_s$ , respectively.

The optical dielectric permittivity of liquid amides is close to 2. However, at the practically identical polarizability of an amide molecule and each link of the polypeptide chain, the protein density is approximately 30 % higher. According to the Clausius-Mosotti equation (Atkins 1978), that elevates  $\epsilon_0$  to 2.5. Extrapolation of refraction indices of  $\alpha$ -chymotrypsin aqueous solutions yields a similar value (Mertz and Krishtalik 1999).

Let us consider a typical case when a certain group, e.g., a center for oxidation-reduction, has some definite charge (including zero) under conditions in which the protein structure is determined. The additional

charging of this group would cause a change in protein dipole orientation. Therefore, the potential created by its charge at other points must be calculated with the use of static permittivity,  $\epsilon_s$ . This potential is added to that created by all the remaining protein's charges (full and partial) giving the pre-existent field and computed based on the optical permittivity,  $\epsilon_0$ .

The choice of atomic partial charges is important. These values are inaccessible to any direct experiment, and hence are determined as effective values that describe the extramolecular field corresponding to the electronic density distribution obtained from quantum chemical calculations (so called electrostatic potentials ESP). Various systems of parameterized partial charges have been proposed. We deem it necessary to choose, in the first place, values of partial charges that correspond to the experimentally measurable characteristic of a given molecule that is directly related to its charge density distribution, i.e., the dipole moment. Quantum chemical calculations can provide the electric field of a molecule in a vacuum with the  $\epsilon$  inside the molecule set to be equal to one. Because we describe proteins as continuous media with  $\epsilon_0$  when calculating the pre-existent field, the same optical permittivity is automatically attributed to the inner region of each molecular fragment. Such 'filling' of a fragment with a medium having  $\epsilon_0 > 1$  weakens its field. In order to retain the correct field value outside the fragment, the 'vacuum' partial charges should be multiplied by a coefficient close to  $(\epsilon_0 + 2)/3$  (the field of a dipole placed in a sphere with  $\epsilon_0$  is  $3/(\epsilon_0 + 2)$  times weaker than the field of the same dipole in a vacuum). This coefficient relates only to the partial charges of dipoles or other electro-neutral groups. Free charges must not be corrected (the field outside the charged sphere being independent of dielectric permittivity inside the sphere).

It should be noted that most of the modern systems (such as CHARMM, AMBER etc.) that employ partial charges increase them over the values that correspond

to the experimental dipole moments of small molecules, thereby achieving better agreement of MD simulations. In particular, the PARSE set of charges (Sitkoff et al. 1994) generates intraprotein fields close to results obtained with charges that are corrected as described above, for the effect of filling of the fragment “body” by  $\epsilon_0$  (Ptushenko et al. 2008).

In real biological systems, a protein is surrounded by different media, water, and lipids for intra-membrane proteins. Therefore, calculations must be performed for a heterogeneous system. Unlike atomic coordinates in proteins, the coordinates of the surrounding water molecules are not fixed, and its dielectric response includes all types of polarizability; this means that the pre-existing field must be calculated using  $\epsilon_0$  for the protein and at the same time the static permittivity (dielectric constants)  $\epsilon_{sw}$  for water and  $\epsilon_{si}$  for lipids.

As shown above, the energy of polarization of the dielectric medium,  $\Delta G_{pol}$ , is computed using the static permittivity of both the protein and the surrounding water. Since the  $\epsilon_s$  of protein is much smaller than that of water, the absolute value of the energy,  $\Delta G_{pol}$ , in the protein-water system is significantly lower than in the purely aqueous environment. This makes charge transfer from water into a low-dielectric medium energetically disadvantageous, as is well known from the Born formula (discussed below). An ion can exist in the protein environment only when the loss of the solvation energy is compensated by the action of the intraprotein pre-existing field. Such more or less full compensation has been observed many times (e.g., Gunner et al 2000; reviewed in Krishtalik 2012). A drawback of most of these studies is that the pre-existing field was calculated with the use of protein static permittivity; the use of optical permittivity enhances the field and makes compensation for the low solvation energy a more reliably established fact. This compensation is especially substantial in the case of multi-charged ions; here, the difference between the more accurate computations using  $\epsilon_0$  and

the traditional approach where only one permittivity is employed, namely the static one, becomes very large. For example, the corresponding error in calculation of the redox potentials of multi-charged  $Fe_4S_4$  clusters (in the Photosystem I and in ferredoxins) reaches 0.8–1.0 V (Ptushenko et al. 2008).

Concluding this section, let us mention that besides the well-known structural specificity of enzymatic catalysis, which is due to the structure of active sites, an additional structural factor exists. This is the spatial configuration of the intraprotein field that is needed to ensure a favorable energy of charge transfer. As was described in Sect. III, this field depends not only on the amino acid composition of the active site, but also on a large number of dipoles of peptide groups and surrounding side chains.

### B. The Medium Polarization Energy

The notion of the ion solvation energy as due to the interaction of the ion’s charge with the dielectric’s polarization induced by it dates back to the famous paper by Born (1920). Born described the solvation energy of a spherical ion of radius ‘a’ as a difference of its charging energies by charge  $e$  in vacuum and sample dielectric,  $\epsilon_s$ .

$$\Delta G = \frac{e^2}{2a} \left( 1 - \frac{1}{\epsilon_s} \right) \quad (5.17)$$

Notice the similarity of this formula with the Marcus equation for the reorganization energy (Eq. 5.10)—both are based on continuum electrostatics.

It is well known that the Born equation, although it provides a clear physical picture, does not provide quantitative results. This is due to the discreteness of solvents. Most common inorganic ions are small compared to solvent molecules and water clusters. Their electric field at small distances, less than the size of solvent molecules, changes rapidly, and inside the solvent molecule it cannot be described as a field in a continuum medium.

The foregoing suggests that for ions larger than solvent molecules the Born equation

may be sufficiently accurate. However, the “chemical solvation energy”, i.e., the energy only due to interaction with the solvent, cannot be determined experimentally by any thermodynamically correct experiment; only the so-called “real solvation energy” that includes, in addition to the chemical energy, the energy of ion transfer across the solvent-dependent surface potential difference at the liquid/air boundary is experimentally accessible. The surface potential components cancel out when we determine the sum of solvation energies for cation and anion or difference of solvation energies for two ions of the same sign. Such a determination was performed for the cationic and anionic forms of cobaltocene  $\text{CoCp}_2$  (bis-cyclopentadienylcobalt  $\text{Co}(\text{C}_5\text{H}_5)_2$ ) that have an effective radius  $3.7 \text{ \AA}$  as well as for two anionic forms of bis-*o*-dicarbollylnickel  $\text{NiCb}_2$  ( $\text{Ni}(\text{C}_2\text{B}_9\text{H}_{11})_2$ ), which has an effective radius of  $4.17 \text{ \AA}$  (Krishtalik et al. 1991; this and subsequent studies summarized in Krishtalik 2008). The data presented in Fig. 5.4 show that for  $\text{CoCp}_2$  the Born equation is fulfilled practically quantitatively in a wide interval of static dielectric constants from 65 to 7, the latter a permittivity close to those of proteins, especially at their active sites. Similar data were obtained for  $\text{NiCb}_2$  (but in a narrower range of permittivities, 65–21).

In proteins, the size of redox centers (e.g., hemes, flavins) is much larger than the size of the peptide group or the polar ends of side chains. Therefore, the results described above may serve as some substantiation of the continuum electrostatics approximation in these systems. The shape of redox centers is far from spherical, and hence the Born equation in its simple form cannot be applied. However, the existing programs for numerical solution of the Poisson equation allow calculations of the dielectric response energy for a reactant of any shape.

For computation of redox potentials one employs two methods—the first based on quantum—chemical calculations, and

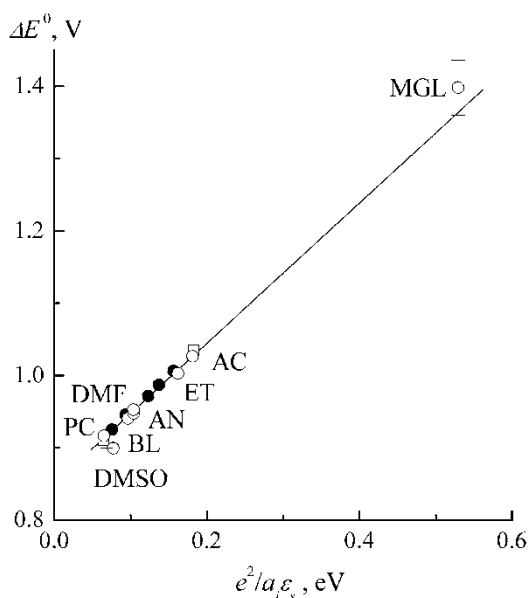


Fig. 5.4. Dependence of the redox potential difference of the  $\text{CoCp}_2^+/\text{CoCp}_2$  and  $\text{CoCp}_2/\text{CoCp}_2^-$  couples on the sum of charging energies of cation and anion, calculated according to Born equation. Designations: *circles* are the results obtained with a mercury electrode; *squares* are the results obtained with a platinum electrode. These charging energies are calculated assuming the same electronic density distribution for each of the components in all solvents. However, DMSO is more polarizable than the other solvents studied (electronic dielectric permittivity 2.2 compared to 1.8), and therefore interacts stronger with solute; as a result, in this solvent the covalent bond in  $\text{CoCp}_2^-$  is more polar, making the charging energy somewhat lower. The cross presents the point for DMSO with the charging energy recalculated on the basis of quantum-chemical data (An. Kuznetsov et al. 2009); open points correspond to propylene-carbonate (PC), butyrolactone (BL), dimethylsulfoxide (DMSO), dimethylformamide (DMF), acetonitrile (AN), ethanol (ET), acetone (AC), monoglyme (dimethoxyethane) (MGL); *black circles* correspond to mixtures of PC and AC.

the second—on the experimental data and quantum—chemical results.

In the first method, one computes the ionization energy of the corresponding group in a gas phase, and then calculates the difference of the electrostatic transfer energies from gas to protein for the reduced and oxidized forms (including both the dielectric response energies and the energies in the pre-existing intraprotein electric field). These transfer energies are the chemical ones.

The electron formed in the gas phase should be used for reduction of the other oxidized species, for instance  $H^+$  with the final formation of  $\frac{1}{2}H_2$ . Their transfer energies (with an account for half of the  $H_2$  dissociation energy) give the potential of the standard hydrogen electrode (SHE). The difference of the corresponding energies of the redox couple under study and the potential of the hydrogen electrode gives the redox potential relative to the standard hydrogen electrode— an experimentally measurable quantity.

In these calculations, very frequently one employs the so-called absolute SHE potential defined by Reiss and Heller (1985). This potential is actually nothing else than the potential suggested for the first time by Kanevskii (1952). This ‘absolute’ potential can be strictly computed thermodynamically from experimental data, as the sum of the metal work function and the potential difference at the metal-solution interface at a given electrode potential, specifically the SHE potential. However, the calculations described above employ the chemical solvation energies, and hence should use the hydrogen electrode potential based on the ‘chemical’ hydration energy (An. Kuznetsov et al. 2008). Unlike this potential, Kanevskii’s potential is determined by the ‘real’ hydration energy, including the water surface potential,  $\chi$

$$\Delta G_{\text{real}} = \Delta G_{\text{chem}} + \chi q \quad (5.18)$$

The ‘chemical’ hydration energy enters the so-called Trasatti potential  $E_T$  (1974), differing from the Kanevskii potential  $E_K$  by the water surface potential,  $\chi$ .

$$E_K = E_T + \chi \quad (5.19)$$

The Trasatti potential should be employed in calculations of redox potentials.

Determination of the water-gas potential jump implies the use of extra-thermodynamic assumptions. Different assumptions were applied by Trasatti (1974) and Krishtalik (2008), but they give similar

values close to 0.14 V. In conjunction with the known experimental value of  $E_K = 4.44$  V, it yields  $E_T = 4.30 \pm 0.02$  V.

Calculations of this type were performed for the Rieske iron-sulfur protein that functions in respiratory and photosynthetic electron transport, using  $E_T$  and the optical dielectric permittivity for the calculation of the intraprotein field. Their agreement with the experimental data is reasonably close. It is interesting that the distortion of the  $Fe_2S_2$  cluster due to the steric restrictions imposed by the protein matrix affects the redox potential substantially (An. Kuznetsov et al. 2010).

The second type of computation uses quantum-chemical data for the charge distribution in the reactants that are necessary for electrostatic calculations, and experimental data for the redox potential in some, usually aprotic, solvents. One calculates the electrostatic transfer energies from the solvent into the protein for both reduced and oxidized forms, and adds this component to the experimental redox potential. However, there is a pitfall similar to that in the first method—the unknown liquid junction potential between solution in the nonaqueous solvent and the aqueous solution of the reference electrode, e.g., SHE. This potential is caused by a nonequivalent distribution of cations and anions of the background electrolyte between water and the organic solvent due to the difference of their transfer energies. This quantity is inaccessible to direct measurement and hence, for its evaluation, one needs to resort to some extra-thermodynamic assumptions. The correction is minimal if one has measured the redox potential relative to a proper internal standard in the same solvent, e.g., the  $FeCp_2^+/FeCp_2$  couple; for this couple, there are good estimates of its redox potential in aprotic solvents relative to an aqueous reference electrode. This approach combined with quantum—chemical data, data on the distribution of static dielectric permittivity, and the employment of the optical permittivity for the intraprotein field evaluation, resulted in a reasonable agreement with the experiment for ten

cofactors of the Photosystem I and two soluble ferredoxins (Ptushenko et al. 2008).

## V. Reorganization Energy and Activation Energy

Let us start by considering the simple case of charge transfer in a homogeneous medium. According to the Marcus equation (5.10), the medium reorganization energy is determined by its optical and static dielectric permittivities,  $\epsilon_0$  and  $\epsilon_s$ , as it is expressed via the so-called polaron coupling constant (Pekar constant)  $C = 1/\epsilon_0 - 1/\epsilon_s$ , (as discussed in Sect. II.A). For the usual polar solvents, ‘C’ depends weakly on static permittivity. For example, for water,  $\epsilon_0 = 1.8$ ,  $\epsilon_s = 78$  at 25 °C, and  $C = 0.54$ ; for DMF,  $\epsilon_0 = 2.04$ ,  $\epsilon_s = 36.7$ ,  $C = 0.46$ . However, the low static dielectric permittivity of proteins has a dramatic effect on their reorganization energy. At typical values of the optical and static permittivity of proteins (roughly 2.5 and 4) the C value is as low as 0.15. Hence, the protein reorganization energy can be expected to be several times lower than for water and other polar solvents. The low reorganization energy of charge transfer in proteins (together with the pre-existing field favoring the electron transfer; see below) is one of the main physical causes of low activation energy and, therefore, of high catalytic activity of enzymes.

As was discussed in Sect. III, a specific property of proteins is the presence of a pre-existing electric field. This field is due to the full and partial charges of the amino acid residues, but is not dependent on the charge that is transferred to the reacting group. Therefore, it is the same during the charging and discharging processes used for determination of the reorganization energy as described in Sect. II.A. In the charging process, this field contributes the energy

$$\sum_i \varphi_i q,$$

where  $\varphi_i$  designates the field set up by the protein atom  $i$  on the reactant (but not the po-

tential created by the reacting group), and  $q$  is the charge transferred to the reactant (usually distributed over the reactant’s atoms). This energy is a part of the total reaction energy,  $\Delta G$ , and hence has an important role in charge transfer in proteins.

In the second step of the reorganization energy computation, viz. discharge in an optical medium, the potential of the pre-existing field is the same, and the charge transferred is  $-q$ . Hence, the corresponding energy is

$$-\sum_i \varphi_i q$$

The sum of these two expressions is zero, and hence the pre-existing field does not affect the reorganization energy. The latter is the same as in the structureless medium with the same spatial distribution of dielectric permittivities. Therefore, the reorganization energy calculation in the framework of the semi-continuum approximation is insensitive to the choice of a parameter such as the partial charge of protein atoms.

In real systems, one deals with an inhomogeneous medium, i.e., proteins (that can have some spatial distribution of permittivities), reactants, and the surrounding aqueous electrolyte solution. In a general case, one can employ a numerical solution of the Poisson–Boltzmann equation to find the dielectric response energies in optical and static media,  $W_o$  and  $W_s$  (Eq. 5.9) using a program that accounts for the presence of several dielectric regions. A more detailed description of the algorithm is given in Krishtalik (2011, 2012).

The reorganization energy semi-continuum calculation is independent on the partial charges of the protein atoms while the molecular-dynamics calculations employ this parameter explicitly. It is interesting to compare the results of these quite different methods. Below, some examples related to cytochromes and similar systems are given (Krishtalik 2011).

The experimental evaluation of the reorganization energy of horse heart cytochrome  $c$ , in electrochemical reaction on the electrode, modified by a covalently tethered long-chain

aliphatic alcohol gives a value of 0.58 eV (Terrettaz et al. 1996). These experimental data are related to electron transfer into metal for a distance determined by the thickness of the adsorbed layer, while the calculations were performed for the electron transfer to an infinite distance. The corresponding extrapolation results in a value of 0.64 eV (Krishtalik 2011).

The calculated reorganization energy of the medium turned out to be 0.45–0.48 eV, about half of it due to the reorganization of surrounding water. To obtain the full reorganization energy, one should add other terms. First, there is the inner-sphere reorganization energy of a liganded heme equaling about 0.04 eV. There is one more component of the medium reorganization energy associated with a marked displacement upon the heme charging of water molecule 156, as well as of Asn-152, Tyr-57, and Thr-78 adjoining the heme (this is the standard numbering of residues for the horse cytochrome *c*). This shift cannot be described in the usual dielectric approximation that suggests a linear response, which is feasible in practice only for small displacements of atoms. Our quantum chemical calculations yielded 0.28 eV for this ‘non-linear dielectric reorganization’ of the environment. The total reorganization energy is 0.77–0.80 eV.

Microscopic simulations of cytochrome *c* yielded a reorganization energy of 0.4–0.65 eV (Muegge et al. 1997) and 0.77 eV (Simonson 2002; the latter study employed a much longer molecular dynamic simulation), in reasonable agreement with the results of experimental measurements and semi-continuum calculations.

Gray and coworkers have studied the electron transfer between the heme of cytochrome *c* and a ruthenium complex covalently tethered to Nε2 of His33 of the protein. For a series of Ru-ammonia-pyridine modified Zn-cytochromes *c*, the reorganization energy was estimated to be  $1.20 \pm 0.05$  eV (Gray and Winkler 1996, 2003; Meade et al. 1989).

The calculation for the Ru(NH<sub>3</sub>)<sub>5</sub> derivative gives  $\lambda_s = 1.12$ – $1.18$  eV, for the

more typical members of the series studied, viz. the Ru(NH<sub>3</sub>)<sub>4</sub>-pyridine derivative, the medium reorganization energy equals to 0.95–1.01 eV. It is somewhat smaller than the experimental value due to the aforementioned contributions of the inner-sphere reorganization and, especially, the shift of some residues in the vicinity of the heme (the data for the Zn-substituted cytochrome are unknown, but one can expect an effect of the same order of magnitude).

Blumberger and coworkers (Tipmanee et al. 2010) have studied the reorganization energy for three amine-ruthenated cytochromes using a quantum mechanical–molecular mechanical approach. For Ru(NH<sub>3</sub>)<sub>5</sub>—substituted cytochrome *c*, a total reorganization energy was found to be 1.34 eV, which is close to the experimental data and to our estimates. An important finding is the good agreement with experiment obtained using only the ‘polarizable force field’ model (Tipmanee et al. 2010). Without accounting for the molecular electronic polarizability, the calculated reorganization energies are substantially overestimated by 40 %. This is in line with the idea of the dielectric continuum theory where optical (electronic) dielectric permittivity plays an important role (Sect. II.A, this Sect. V, above).

For the Ru(bpy)<sub>2</sub>(im) derivative (bpy = bipyridine, im = imidazole), a value  $\lambda = 1.26$  eV was calculated (Tipmanee et al. 2010). In our calculations,  $\lambda_s$  for this system equals to 0.70–0.74 eV. The approximate experimental estimate for the total  $\lambda$  is 0.75 eV (Mines et al. 1996).

The reorganization energy for the electron transfer between heme *a* and heme *a*<sub>3</sub> in cytochrome *c* oxidase was roughly estimated from the kinetic data by Jasaitis et al. (2005) as lying between 0.05 and 0.20 eV (the last figure seems to be more probable). A semi-continuum calculation gives the value of 0.2 eV; the same result was obtained by molecular dynamics simulations (Kailaa et al. 2010).

Concluding, one can state that in the computation of reorganization energies, the microscopic modeling and semi-continuum

electrostatics (plus quantum chemistry) approach are generally in good correspondence, and similarly agree with experiment.

The activation energy is determined by two quantities—the reaction free energy and the reorganization energy. Therefore, one should consider the protein's influence on both of these quantities together (Krishtalik 1974, 1985, 2012). The contribution of the aqueous surroundings to the reorganization energy depends on its accessibility to the active site of the protein. In the examples given above, the heme of cytochrome *c* lies close to the protein surface, and hence the effect of water reorganization is substantial. It plays an even greater role for amine-ruthenated cytochromes because the ruthenium complex is surrounded by water. However, for interheme electron transfer in cytochrome *c* oxidase, it is only of minor importance, as the reactants are situated deep in the membrane protein. In any case, the presence of aqueous surroundings somewhat increases the reorganization energy.

For the reaction free energy, the effect of the aqueous phase depends on the direction of charge transfer. When the charge is transferred from the interior of the protein towards its surface, the charge interaction with the high-dielectric phase makes  $\Delta G$  more negative, and therefore decreases the activation energy. The opposite direction of charge transfer makes  $\Delta G$  more positive. Therefore, for several enzymes with two-step processes, the step that would be less favorable in a homogeneous medium proceeds with the charge transfer from inside to outside, compensating in this way for energy consumption.

In globular proteins, the active site is usually situated close to the globule surface to ensure effective interaction with the reaction partners. An increase in the globule radius results in better screening of the opposite side of the active site from interaction with water. This screening results in both the reorganization energy and the activation energy of the slow step of the charge transfer decreasing with increasing globule radius; for

small values of the radius, this decrease is initially relatively rapid. This suggests the existence of a range of optimal radii within which the activation energy is almost minimal, while the consumption of protein for the globule formation is also not too high. The initially fast decrease in the activation energy with increasing protein radius accounts for the experimentally observed fact that the size of enzyme globules is, as a rule, substantially greater than the size of the active site proper—an additional volume of protein insures better screening of the charge in the active site from the interaction with water.

As discussed in Sect. III, the main principle of protein structure results in two consequences: a low static dielectric permittivity (dielectric constant) and the presence of a permanent intraprotein electric field. On the one hand, the low static permittivity of proteins results in a small reorganization energy. On the other, the low dielectric permittivity accounts for the disadvantage of the presence of charged groups in a protein that may, in principle, cause an increase in the reaction activation energy compared with its value in an aqueous medium. A consistent comparison of these two media implies taking account of the energy of charge transfer,  $\Delta G_{tr}$ , from one medium to the other. The effective activation energy is expressed as

$$\Delta G_{eff}^{\neq} = \Delta G^{\neq} + \Delta G_{tr} \quad (5.20)$$

The activation energy for certain typical reactions (charge separation, neutralization, transport of charges from an initially charged reactant to an uncharged one, etc.) has been analyzed (Krishtalik 1985, 2012). The activation energy of the elementary act proper in a medium with low dielectric permittivity  $\Delta G^{\neq}$  can be in some cases lower than in water, and greater in the other cases. However, the effective activation energy in the low-dielectric medium is invariably higher than in the high-dielectric one. In other words, the additional energy expenditure necessary to transfer a charge into a low-dielectric permittivity medium (or generate a charge in such a

medium) always outweighs the gain due to a decrease in reorganization energy.

This inference holds for a structureless dielectric for which the polarization interaction between the charge and its environment (Born solvation energy) is the sole contribution to the electrostatic energy of the system. However, proteins are highly structured systems possessing a permanent electric field, and the energy of the reactant charge in this field is an essential constituent of the system's electrostatic energy; usually, it compensates for the loss of the Born solvation energy given a proper potential in the region of the reactant localization. The existence of a strong intraprotein electric field confers on proteins one of their evolutionary preferences over many other possible biopolymers (Krishtalik 1985).

In conclusion, it should be stressed that only the joint action of two factors, the low reorganization energy and the intraprotein electric field, ensures a substantial reduction in the activation energy, i.e., the high catalytic activity of enzymes. Both effects directly follow from the general principles and architecture of protein structural organization.

It is relevant to add some additional comments.

The compensation effect of the intraprotein field may be either slightly smaller or greater than the loss of the Born solvation energy; it is important that the total  $\Delta G$  value must be reduced to a mechanistically feasible level. Excessive stabilization of the charge is sometimes unfavorable because it may hamper realization of a subsequent electron transfer, or release of a free ion.

Often, one sees the statement that the intraprotein field stabilizes the transition state. This is literally correct as far as heavy particle transfer reactions are concerned when the transition state has a definite charge. However, the notion of transition state charge makes no sense for the non-adiabatic electron transfer that is widespread in biochemical reactions. In these processes, the charge is wholly concentrated at one of the reactants, either in the initial or final states of the reaction. In such a situation, one may speak

of electrostatic stabilization of the reaction product relative to the initial reactants, which lowers the activation barrier. In other words, a decrease in the transition state energy is an indirect result of a decreased  $\Delta G$  of the reaction rather than the consequence of a direct action of the field on the transition state charge. Let us notice that the transition state includes not only the reactive groups proper, but also the surrounding medium in a non-equilibrium configuration. The behavior of this medium is governed by its reorganization energy, which does not depend on the intraprotein electric field; its low value is due to the protein's weak dielectric response as described in this section.

## VI. Long-Range Electron Transfer

In the great majority of biological systems, two redox centers are not in the direct contact that assures the adiabatic electron transfer, but are situated at a longer distance resulting in non-adiabatic transfer. So, there is a "tunneling barrier" formed by the protein matrix. In the last two—three decades, this problem has been the subject of intensive studies, both experimental and theoretical.

For non-adiabatic electron transfer its probability decreases strongly with increasing distance. A useful empirical formula describing the distance dependence has been proposed by the Dutton's group (Moser et al. 1992; review, Moser et al. 2010). It has the form

$$\log_{10}k = 13 - 0.8(1.2 - \rho)(R - 3.6) - 3.1 \frac{(\Delta G + \lambda)^2}{\lambda} \quad (5.21)$$

In this formula, the constant '13' is the logarithm of  $kT/h$ , i.e., the pre-exponential in Eyring's absolute rate theory. The quantity  $\rho$  is the packing factor (calculated for some pathway connecting the donor and acceptor); it accounts for the difference in the tunneling probabilities through the protein atoms and through the empty space (the former term substantially higher); the generic value



of  $\rho \approx 0.76$ .  $R$  (in Å) is the edge-to-edge distance between the redox partners (for the molecules with conjugated bonds, like heme, the molecular orbitals encompass the entire molecule, and decay exponentially outside the molecule); 3.6 is the approximate sum of the donor-acceptor van der Waals radii, so  $(R-3.6)$  presents the distance at which the electron transfer becomes non-adiabatic. The last term has a usual Marcusian form but the empirical coefficient equals to 3.1 instead of the value of 4.2 in the Marcus formula (energies expressed in eV) and is supposed to account for a decrease in activation energy due to the involvement of quantum modes as described in Sect. II.A above. In the derivation of this formula, several approximations are made. For example,  $\lambda$  has been assigned the same value for all reactions and reactions at all distances, which seems to be an oversimplification. Notice, however, that the described  $R$ -dependence was observed for the activationless processes where the last term of Eq. 5.17 equals zero. In spite of all approximations, this formula works well in many cases (Moser et al. 2010).

Often one considers the exponential dependence on the distance as due to the

electron tunneling through a rectangular barrier according to the Gamow equation (Gamow 1928), and estimates the proper barrier height. However, these estimates give values too low compared to the barrier height expected from physical considerations. The most probable mechanism of the long-range electron transfer in proteins as well as the transfer through synthetic spacers is the so called “super-exchange” via some “pathway” (Beratan and Onuchic 1989; for review see Gray and Winkler 2010). Let us describe qualitatively the latter mechanism using a simple scheme presented in Fig. 5.5.

As shown above (Fig. 5.1), when the classical subsystem reaches the top of the barrier, the electronic levels in initial and final states become equal; in (Fig. 5.5) these are the levels of donor D and acceptor A. However, direct electron transfer from D to A is impractical because the donor-acceptor distance is too large, and hence the overlapping of their wave functions is negligible. At the same time, the wave function of D overlaps markedly with the wave function of the molecular orbital (LUMO) of the intermediate protein group P1 (Fig. 5.5); the same takes place for A and P4. The simple elec-

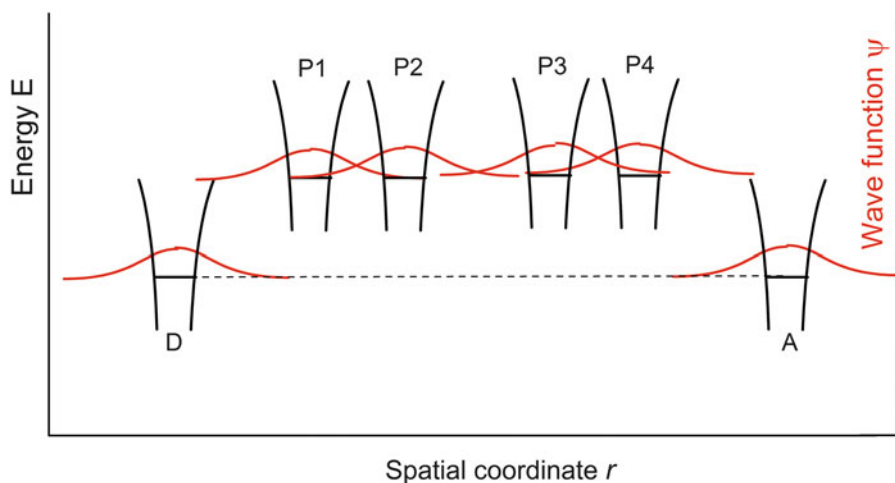


Fig. 5.5. Scheme of the super-exchange electron transfer through intervening protein. Plotted similarly to the right panel of Fig. 5.1. The black curves represent the electron potential energy  $E$  versus its spatial coordinate  $r$ , the horizontal bars inside the potential wells mark the electron energy levels. Designations of potential wells: D—donor, A—acceptor, P1–P4—groups of the protein that form the pathway. Horizontal dashed line shows that the energies of electronic levels in D and A are equal. Red curves represent the corresponding wave functions.

tron transfer from D to P1 is impossible because they have different energies. However, the substantial overlapping of wave functions from P1 to P4 makes possible the overlap between D and A via the chain P1–P4. This chain is called “the pathway”. One should not understand this term as some trajectory of a real electron movement (the electron cannot jump from D to P1 or from P4 to A). It rather means “the combination of protein orbitals which dominates the coupling between donor and acceptor” (Beratan and Onuchic 1989). A similar picture holds true for the hole transfer from A to D; in this case, the HOMO's of the intervening protein are employed.

In Fig. 5.5, the distances between P1 and P2 as well as between P3 and P4, are drawn shorter than the P2–P3 distance. The former correspond to covalent bonds, the latter to the space between unboundatoms. As seen from the shape of the wave functions, the electronic coupling through the covalent bond is substantially stronger than through-space. The extent of these couplings can be estimated on the basis of quantum—chemical analysis. The various calculations give somewhat different results. For through-bond coupling, the decrease in  $\log_{10}k$  is 0.45–0.6 per covalent  $\sigma$ -bond. The through-space coupling is strongly distance– dependent, with the rate constant,  $k$ , changing by  $\Delta\log_{10}k = -1.5 R_{\text{space}}$  where  $R_{\text{space}}$  is the length of this interval (Jones et al. 2002). The distance between donor and acceptor  $R$  is approximately proportional to the number of bonds connecting them ( $n$ ). For the synthetic compounds with D and A linked by some regular covalent chain;  $R$  and  $n$  are strictly proportional. Therefore, both the density model (Eq. 5.18) and the pathway model usually yield qualitatively similar results. A detailed comparison of these two models was done by Jones et al. (2002). For 33 of 38 donor–acceptor pairs in 28 proteins a linear correlation of coupling parameters was found. The slope of the best—fit linear function = 0.7, which is due primarily to the difference in the through–space parameters used in these models. The correlation observed is understandable

because both approaches have a similar physical basis, viz. the difference between the transfer probabilities, through-bond and through-space.

For five systems, a substantial deviation from the common fit/linear function was observed. It was caused by a non-coincidence of the optimal pathway with the shortest Donor–Acceptor distance or by a large difference in the estimation of the role of through–space coupling.

In some model systems, a strong discrepancy between the pathway approach and distance dependence was observed. For example, Niki et al. (2003) studied the electron transfer to cytochrome *c* from a metal coated with a covalently tethered layer of long-chain carboxylic acid. Several lysines, surrounding the heme edge are attracted to caboxylates. Using the WT and various mutants, it was shown that only one of the mutations (eliminating Lys 13) results in a drastic, approximately six orders of magnitude, decrease in the reaction rate, and it is precisely that residue which is connected to the heme by the shortest chain of covalent bonds. The distance to the electrode for the WT and different mutants is similar, but the pathways from the different Lys's to the heme are quite different.

Another example is the electrochemical reduction of hemin through the physically adsorbed (and hence more flexible) carboxylic acid monolayer (Khanova and Krishtalik 2005). An alteration in the orientation of hydrocarbon chains of the carboxylic acid upon a change in pH of the solution results in a twofold decrease in the layer thickness. However, the reaction rate remains practically unaltered because the number of covalent bonds between the electrode and hemin does not change.

## References

- Atkins PW (1978) Physical Chemistry. Oxford University Press, Oxford
- Bashford D, Karplus M (1990) The pKa's of ionizable groups in proteins: atomic detail from a continuum electrostatic model. *Biochemistry* 29:10219–10225

- Beratan DN, Onuchic JN (1989) Electron tunneling pathways in proteins: influences on the transfer rate. *Photosynth Res* 22:173–186
- Born M (1920) Volumen und Hydratationwärme der Ionen. *Z Phys* 1:45–48
- Brooks CL, Karplus M, Pettitt BM (1988) *Proteins. A Theoretical Perspective of Dynamics, Structure, and Thermodynamics*. Wiley, New York
- Dogonadze RR, Kuznetsov AM (1975) Theory of Charge Transfer Kinetics at Solid-Polar Liquid Interfaces, *Progress in Surface Science*. Pergamon, Oxford, vol 6, pp 1–42
- Dogonadze RR, Kuznetsov AM (1983) Quantum electrochemical kinetics. In: Conway BE, Bockris JO'M, Yeager E, Khan SUM, White RE (eds) *Comprehensive Treatise of Electrochemistry*. Plenum, New York, pp 1–40
- Gamow GA (1928) Zur Quantentheorie des Atomkernes. *Z Phys* 51:204–212
- Gilson MK, Honig BH (1986) The dielectric constant of a folded protein. *Biopolymers* 25:2097–2119
- Gray HB, Winkler JR (1996) Electron transfer in proteins. *Annu Rev Biochem* 65:537–561
- Gray HB, Winkler JR (2003) Electron tunneling through proteins. *Q Rev Biophys* 36:341–372
- Gray HB, Winkler JR (2010) Electron flow through metalloproteins. *Biochim Biophys Acta* 1797:1563–1572
- Gunner M, Saleh M, Cross E, ud-Doula A, Wise M (2000) Backbone dipoles generate positive potentials in all proteins: origins and implications of the effect. *Biophys J* 78:1126–1144
- Jasaitis A, Rappaport F, Pilet E, Liebl U, Vos MH (2005) Activationless electron transfer through the hydrophobic core of cytochrome c oxidase. *Proc Natl Acad Sci USA* 102:10882–10886
- Johannin G, Kellersohn N (1972) An estimate of intraproteic electrostatic fields values originated by the peptide groups in  $\alpha$ -chymotrypsin. *Biochem Biophys Res Commun* 49:321–327
- Jones ML, Kurnikov IV, Beratan DN (2002) The nature of tunneling: pathway and average packing density models for protein-mediated electron transfer. *J Phys Chem A* 106:2002–2006
- Kailaa VRI, Johansson MP, Sundholm D, Wikström M (2010) Interheme electron tunneling in cytochrome c oxidase. *Proc Natl Acad Sci USA* 107:21470–21475
- Kanevskii EA (1952) On the theory of electrode potential. III. Calculation of free energies of electrode processes and thermodynamic electrode potentials. *Zh Fiz Khim* 26:633–641
- Khanova LA, Krishtalik LI (2005) Long – range electron transfer: what is rate-determining – the geometric distance or the pathway? *Electrochim Acta* 50:1085–1099
- King G, Lee FS, Warshel A (1991) Microscopic simulations of macroscopic dielectric constants of solvated proteins. *J Chem Phys* 95:4366–4377
- Krishtalik LI (1974) The specific features of enzyme as a polar medium and their role in the mechanism of enzymatic process. *Molekulyarnaya Biologiya (Mosc)* 8:91–99
- Krishtalik LI (1985) Effective activation energy of enzymatic and nonenzymatic reactions. Evolution imposed requirements to enzyme structure. *J Theor Biol* 112:251–264
- Krishtalik LI (1986a) *Charge Transfer Reactions in Electrochemical and Chemical Processes*. Plenum, New York
- Krishtalik LI (1986b) Energetics of multielectron reactions. *Photosynthetic oxygen evolution*. *Biochim Biophys Acta* 849:162–171
- Krishtalik LI (1996) Intramembrane electron transfer: processes in photosynthetic reaction center. *Biochim Biophys Acta* 1273:139–149
- Krishtalik LI (2000) The mechanism of the proton transfer: an outline. *Biochim Biophys Acta* 1458:6–27
- Krishtalik LI (2008) Solvation energy of metallocenes pilot ions: beyond the Born approximation. *Electrochim Acta* 53:3722–3733, Corrigendum, *ibid* (2009) 54:4741
- Krishtalik LI (2011) The medium reorganization energy for the charge transfer reactions in proteins. *Biochim Biophys Acta – Bioenerg* 1807:1444–1456
- Krishtalik LI (2012) Proteins as specific polar media for charge transfer processes. *Physics – Uspekhi* 55:1192–1213
- Krishtalik LI, Alpatova NM, Ovsyannikova EV (1991) Electrostatic ion – solvent interaction. *Electrochim Acta* 36:435–445
- Krishtalik LI, Kuznetsov AM, Mertz EL (1997) Electrostatics of proteins: description in terms of two dielectric constants simultaneously. *Proteins Struct Funct Genet* 28:174–182
- Kuznetsov AM (1995) *Charge Transfer in Physics, Chemistry and Biology*. Gordon and Breach Publisher, Amsterdam
- Kuznetsov AM (1999) *Stochastic and Dynamic Views of Chemical Reaction Kinetics in Solutions*. Press Polytechniques et Universitaires Romandes, Lausanne
- Kuznetsov AM, Ulstrup J (1999) *Electron Transfer in Chemistry and Biology. An Introduction to the Theory*. Wiley, New York
- Kuznetsov AM, Ulstrup J, Vorotyntsev MA (1988) Solvent effects in charge transfer processes. In: Dogonadze RR, Kálmán E, Kornyshev AA, Ulstrup J (eds) *The Chemical Physics of Solvation, Part C*. Elsevier, Amsterdam, p 163

- Kuznetsov AM, Maslii AN, Krishtalik LI (2008) Quantum chemical model of solvation for calculation of electrode potentials of redox processes involving ferrocene, cobaltocene, and their ions. *Russ J Electrochem* 44:34–42
- Kuznetsov AM, Maslii AN, Krishtalik LI (2009) Solvation of ferrocene, cobaltocene, and their ions by the data of quantum-chemical calculations. *Russ J Electrochem* 45:87–92
- Kuznetsov AM, Zueva EM, Masliy AN, Krishtalik LI (2010) Redox potential of the Rieske iron–sulfur protein. Quantum-chemical and electrostatic study. *Biochim Biophys Acta – Bioenerg* 1797:347–359
- Levich VG, Dogonadze RR (1959) Theory of radiationless electronic transitions between ions in solutions. *Proc Acad Sci USSR Phys Chem Sect* 124:9–13
- Marcus RA (1956) On the theory of oxidation-reduction reactions involving electron transfer. I. *J Chem Phys* 24:966–978
- Marcus RA (1996) Electron transfer reactions in chemistry. Theory and experiment. In: Bendall DS (ed) *Protein Electron Transfer*. BIOS Scientific Publishers Ltd, Oxford, pp 249–272
- Marcus RA, Sutin N (1985) Electron transfers in chemistry and biology. *Biochim Biophys Acta* 811:265–322
- Matthias Ullmann G, Mueller L, Bombarda E (2015) Theoretical analysis of electron transfer in proteins, from simple proteins to complex machineries. In: Cramer WA, Kallas T (eds) *Cytochrome Complexes: Evolution, Structures, Energy Transduction, and Signaling*. Springer, Cham
- Meade TJ, Gray HB, Winkler JR (1989) Driving-force effects on the rate of long-range electron transfer in ruthenium-modified cytochrome *c*. *J Am Chem Soc* 111:4353–4356
- Mertz EL, Krishtalik LI (1999) Free energy of charge transfer and intraprotein electric field: method of calculation depends on the charge state of protein at a given structure. *Bioelectrochem Bioenerg* 48:397–405
- Mines GA, Bjerrum MJ, Hill MG, Casimiro DR, Chang I-J, Winkler JR, Gray HB (1996) Rates of heme oxidation and reduction in Ru(His33)cytochrome *c* at very high driving forces. *J Am Chem Soc* 118:1961–1965
- Moser CC, Keske JM, Warncke K, Farid RS, Dutton PL (1992) Nature of biological electron-transfer. *Nature* 355:796–802
- Moser CC, Anderson JLR, Dutton PL (2010) Guidelines for tunneling in enzymes. *Biochim Biophys Acta* 1797:1573–1586
- Muegge I, Qi PX, Wand AJ, Chu ZT, Warshel A (1997) The reorganization energy of cytochrome *c* revisited. *J Phys Chem B* 101:825–836
- Nicholls A, Honig BJ (1991) A rapid finite-difference algorithm, utilizing successive over-relaxation to solve the Poisson-Boltzmann equation. *Comput Chem* 12:435–445
- Niki K, Hardy WR, Hill MG, Li H, Sprinkle JR, Margoliash E, Fujita K, ..., Gray HB (2003) Coupling to Lysine-13 promotes electron tunneling through carboxylate-terminated alkanethiol self-assembled monolayers to cytochrome *c*. *J Phys Chem B* 107:9947–9949
- Pekar SI (1954) Untersuchungen über die Electronentheorie der Kristalle. Akademie Verlag, Berlin
- Pethig R (1979) Dielectric and Electronic Properties of Biological Materials. Wiley, Chichester
- Pushenko VV, Cherepanov DA, Krishtalik LI, Semenov AY (2008) Semi-continuum electrostatic calculations of redox potentials in Photosystem I. *Photosynth Res* 97:55–74
- Reiss H, Heller A (1985) The absolute potential of the standard hydrogen electrode—a new estimate. *J Phys Chem* 89:4207–4213
- Schutz CN, Warshel A (2001) What are the dielectric “constants” of proteins and how to validate electrostatic models? *Proteins Struct Funct Genet* 44:400–417
- Shurki A, Warshel A (2003) Structure / function correlations of proteins using MM, QM/MM, and related approaches: methods, concepts, pitfalls, and current progress. *Adv Protein Chem* 66:249–313
- Simonson T (1998) Dielectric constant of cytochrome *c* from simulations in a water droplet including all electrostatic interactions. *J Am Chem Soc* 120:4875–4876
- Simonson T (2002) Gaussian fluctuations and linear response in an electron transfer protein. *Proc Natl Acad Sci USA* 99:6544–6549
- Simonson T (2008) Dielectric relaxation in proteins: the computational perspective. *Photosynth Res* 97:21–32
- Sitkoff D, Sharp KA, Honig B (1994) Accurate calculation of hydration free energies using macroscopic solvent models. *J Phys Chem* 98:1978–1988
- Tanford C, Kirkwood JG (1957) Theory of protein titration curves I. General equations for impenetrable spheres. *J Am Chem Soc* 79:5333–5339
- Terrettaz S, Cheng J, Miller CJ, Guiles RD (1996) Kinetic parameters for cytochrome *c* via insulated electrode voltammetry. *J Am Chem Soc* 118:7857–7858

- Tipmanee V, Oberhofer H, Park M, Kim KS, Blumberg J (2010) Prediction of reorganization free energies for biological electron transfer. A comparative study of Ru-modified cytochromes and a 4-helix bundle protein. *J Am Chem Soc* 132:17032–17040
- Trasatti S (1974) The concept of absolute electrode potential. An attempt at a calculation. *J Electroanal Chem* 52:313–329
- Ulstrup J (1979) Charge Transfer Processes in Condensed Media, Lecture Notes in Chemistry. Springer, Berlin
- Warshel A, Levitt M (1976) Theoretical studies of enzymic reactions: dielectric, electrostatic and steric stabilization of the carbonium ion in the reaction of lysozyme. *J Mol Biol* 103:227–249
- Warwicker J, Watson H (1982) Calculation of the electrostatic potential in the active site cleft due to a helix dipoles. *J Mol Biol* 157:671–679
- Yadav A, Jackson RM, Holbrook JJ, Warshel A (1991) Role of solvent reorganization energies in the catalytic activity of enzymes. *J Am Chem Soc* 113:4800–4805

# Chapter 6

## Theoretical Analysis of Electron Transfer in Proteins: From Simple Proteins to Complex Machineries

G. Matthias Ullmann<sup>a,\*</sup>, Lars Mueller<sup>a</sup>, and Elisa Bombarda<sup>b</sup>

<sup>a</sup>*Structural Biology/Bioinformatics, University of Bayreuth,  
Universitätsstr. 30, NW I, 95447 Bayreuth, Germany*

<sup>b</sup>*Experimental Physics IV, University of Bayreuth, Universitätsstr.  
30, 95447 Bayreuth, Germany*

Summary.....	99
I. Introduction.....	100
II. Theoretical Description of Electron Transfer Reactions.....	102
A. Marcus Theory of Electron Transfer.....	102
B. Electronic Coupling.....	104
C. Reorganization Energy.....	105
D. Reaction Free Energy.....	106
E. Moser-Dutton Ruler.....	106
F. Tuning of Electron Transfer Rates in Proteins.....	107
III. Electrostatic Methods for Estimating Reaction Free Energies and Reorganization Energies... 108	108
A. The Poisson-Boltzmann Equation.....	108
B. Calculating the Outer Sphere Reorganization Energies.....	110
C. Calculating Redox Potentials of Proteins.....	111
D. Interacting Redox Active Groups.....	112
E. Looking at the Coupling of Reduction Reactions to Protonation Reaction.....	116
F. Influence of Membrane Potential and Transmembrane Gradients.....	117
IV. Complex Electron Transfer Proteins.....	120
A. Simulating Complex Electron Transfer Networks.....	120
B. Analyzing Calculated Electron Transfer Networks.....	121
C. Electron Transfer from the C-Subunit of the Photosynthetic Reaction Center to the Special Pair.....	121
V. Conclusions.....	122
Acknowledgements.....	125
References.....	125

### Summary

Electron transfer plays a central role in many biological processes such as, for instance, photosynthesis or oxidative phosphorylation, but also in other bioenergetic processes such as denitrification or sulfate and sulfite reduction. Moreover, electron transfer is a key step in

---

\*Author for correspondence, e-mail: [ullmann@uni-bayreuth.de](mailto:ullmann@uni-bayreuth.de)

many enzymatic reactions. The framework of Marcus theory provides the theoretical basis to describe the kinetics of these reactions. The parameters to calculate rate constants can be estimated using protein crystal structures. Namely, the electronic coupling is related to the edge-to-edge distance between the redox-active sites. The reaction free energy and the reorganization energy can be obtained, for instance, from continuum electrostatic calculations. However, to perform complicated tasks, proteins often combine many redox cofactors and couple the redox reactions to protonation reactions or conformational changes. Moreover, electron transfer proteins are often embedded in membranes, and thus membrane potential and concentration gradients influence the reactions. One approach to describe such complex systems is the so-called microstate model, in which each state of a system is represented by a vector in which each component defines the status of each site (for instance oxidized or reduced, protonated or deprotonated). On the basis of this microstate description, it is possible to calculate the thermodynamics and kinetics of a complex protein system. In this article, we will review the principle features of the microstate model and explain how the parameters of the microstate model can be calculated using continuum electrostatics. The microstate model provides the theoretical framework to go from molecular structures to the mechanism of complex protein machines.

## I. Introduction

Electron transfer reactions are central in many biological processes such as photosynthesis and oxidative phosphorylation, to name just the most prominent biochemical pathways. Additionally, electron transfer also plays a central role in biochemical pathways such as the nitrogen cycle and the sulfur cycle that are of geochemical relevance. In recent years, the biochemical electron transfer processes also raised an increased interest because of its use in microbial fuel cells (Logan 2008; Zhou et al. 2013). Electron transfer reactions are even possible candidates to be processes at the origin of life in hydrothermal vents where electron transfer reactions are driven by pH gradients (Martin et al. 2008). These reactions are in some respect just the reverse of the chemi-osmotic theory of Mitchell (1961) and may thus help to explain the origin of the non-equilibrium state that is characteristic for living organisms.

Considering the central role of redox reactions in biochemical systems, it is not surprising that the redox potential is tightly controlled in the cell (Banerjee 2008). In fact, there are several redox buffering systems in the cell that are interconnected through

various complex enzymatic systems. One of the most prominent biological redox buffers is glutathione, a tri-peptide which forms dimers through its thiol group upon oxidation (Deponte 2013). Glutathione functions as an antioxidant in plants, animals, fungi, and some bacteria and archaea and prevents harmful reactions which can be caused by reactive oxygen species such as free radicals and peroxides. Oxidized glutathione is reduced by nicotinamide adenine dinucleotide phosphate (NADP) through a reaction that is catalyzed by glutathione reductase. Glutathione reductase links the redox buffer glutathione to the anabolic redox pool of NADPH, which is mainly generated in the pentose phosphate pathway and, in the case of plants and cyanobacteria, in the light phase of photosynthesis. The major catabolic redox coenzyme is nicotinamide adenine dinucleotide (NAD) which lacks one phosphate group in comparison to NADP and thus has different binding properties, enabling enzymes to differentiate between NAD and NADP. The redox pools of NAD/NADH and NADP/NADPH are connected through the enzyme nicotine amide nucleotide transhydrogenase, a multi-domain membrane protein (Pedersen et al. 2008). Quinones, especially ubiquinone,

plastoquinone, menaquinone and related molecules play a central role in many bioenergetic reactions. Quinones take up electrons from various metabolic reactions and can channel their redox-energy into the Q-cycle that is catalyzed by *bc*-type cytochromes (Mitchell 1976; Crofts 2004). These membrane-linked redox buffers are in contact with the redox buffers in the aqueous medium in the cell through several enzymes. A description of the mechanism of *bc*-type cytochromes are discussed in articles by Xia et al. Trumpower and Hasan et al. in this volume. Although this short discussion of the different redox reactions in the cell shows only the tip of the iceberg, it underlines the prevalence and importance of complex biological redox reactions for biochemical processes. Many more different redox reactions play a central role in the metabolism and we are only at the beginning of understanding what is happening in the cells and how complex enzymes direct and use the electron flow in the cell.

There are two groups of proteins that can undergo redox changes: (i) the electron transport proteins that simply take up electrons from a protein complex and transport them further to other complexes (e.g. monomeric cytochromes, ferredoxins, flavodoxins, thioredoxins, and cupredoxins); (ii) the large group of oxido-reductase enzymes which catalyze redox reactions often with the help of metal ions or other prosthetic groups. The first group played an important role in the theoretical analysis of electron transport in proteins since they are relatively simple and therefore allow a detailed study of the electron transfer reactions. Much of our understanding of electron transfer reactions in proteins originates from studies of such small proteins such as cytochrome *c* or azurin in connection with non-natural electron transfer partners (Gray and Winkler 1996). Complex oxido-reductase enzymes are instead a challenge, since they often involve many redox-active sites and couple the redox reactions for instance to protonation

reactions or conformational changes. The theoretical understanding of these complex reactions is still in its infancy, however much of the theoretical framework developed from simple electron transfer reactions can be employed.

Although electron transfer proteins often contain cofactors, there are also a few proteinogenic amino acids that are redox-active. In particular, pairs of cysteine residues, which can form disulfide bridges, are common redox-regulated motives, for instance in thioredoxins and also in many other redox sensitive proteins (Woycechowsky and Raines 2000). Furthermore, also tyrosine and tryptophan residues are known to undergo redox state changes in proteins (Warren et al. 2012). Another amino acid that can undergo redox changes in proteins is glycine, which can form radicals (Stubbe and van der Donk 1998). These glycine radicals in conjunction with a cysteine residue can catalyze complex chemical reactions in so-called glycine radical enzymes (Stubbe and van der Donk 1998). In the resting form of the enzyme, a radical is localized at a glycine residue. Upon substrate binding, the glycy radical abstracts a hydrogen atom from an adjacent cysteine residue, which then performs the actual catalytic reaction. Another redox-active amino acid that is sometimes found in proteins is seleno-cysteine in which the thiol group is replaced by a selenol group. The  $pK_a$  value of the selenol is 5.2, much lower than that of a thiol (8.3), and its redox properties are also considerably shifted (Wessjohann et al. 2007). Besides these redox-active aminoacids, there are also protein-derived cofactors that are post-translationally formed by chemical modifications of amino acids (Davidson 2007). Examples of such groups are trihydroxyphenyl-alanine quinone, lysine tyrosylquinone, cysteine tryptophylquinone or tryptophan tryptophylquinone. Other cofactors are generated by cross-linking aminoacids such as, for instance, tyrosine and histidine in the active site of cytochrome *c* oxidase.



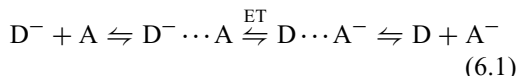
However, the large majority of electron transfer proteins bind redox cofactors as prosthetic groups. Such cofactors can be organic cofactors such as flavins or quinones; pure metal clusters such as copper centers, iron sulfur centers, non-heme iron centers, nickel-iron or molybdenum-iron centers, or manganese centers; or they can be of mixed organic/inorganic origin such as hemes or molybdopterin-centers (da Silva and Williams 2001). A special role is played by chlorophyll molecules, which are tetrapyrrole cofactors, similar to hemes, with a non-redox-active magnesium ion in the center of the ring. Pheophytins have an identical organic scaffold but lack any central ion. These later two cofactors are normally involved in light harvesting and participate in electron transfer only in photosynthetic reaction centers.

Many of the redox enzymes that perform complex reactions contain more than one redox center. Famous examples are the photosynthetic reaction center, which couples photoexcitation to charge separation, and the cytochrome  $bc_1$  and cytochrome  $b_6f$  complexes, which generate a trans-membrane proton electrochemical gradient through bifurcation reactions, and cytochrome  $c$  oxidase, which couples the exergonic reduction of oxygen to an endergonic proton transfer across the membrane. Some examples are shown in Fig. 6.1. A crucial point for the understanding of the mechanism of these enzymes is the coupling of the electron transfer reactions to proton transfer reactions, to conformational changes and to other electron transfer reactions. A theoretical analysis of electron transfer reactions can help to reveal the mechanism of complex enzymes. In order to properly model complex electron transfer reactions that are coupled to conformational changes, to proton transfer reactions, or to other chemical reactions, different theoretical methods need to be combined. In this article, we will review the most important methods and explain the theoretical framework for analyzing complex reactions.

## II. Theoretical Description of Electron Transfer Reactions

### A. Marcus Theory of Electron Transfer

Even if biological redox reactions can involve association and dissociation reactions and can thus be bimolecular (Eq. 6.1), the actual electron transfer reaction is monomolecular:



This system consists of two redox active sites, the donor (D) and the acceptor (A). In the reactant state ( $D^- \cdots A$ ), the electron is localized at the donor and in the product state ( $D \cdots A^-$ ), the electron is localized at the acceptor. The actual electron transfer step can be described by transition state theory, i.e. to obtain the following rate constants for the forward ( $k_{for}$ ) and for the backward ( $k_{back}$ ) reaction. One can write:

$$k_{for} = \frac{\zeta}{\beta h} \exp\left(-\beta G^\ddagger\right) \quad (6.2)$$

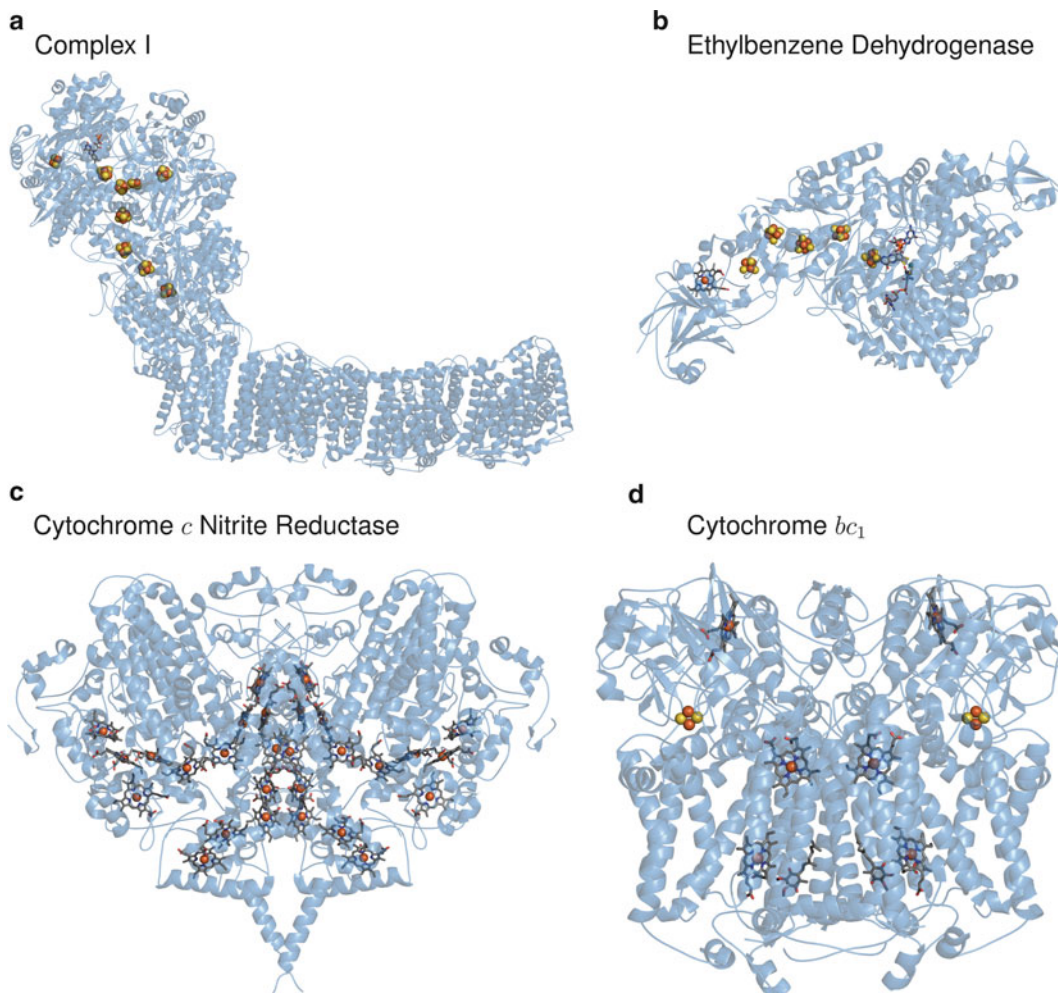
$$k_{back} = \frac{\zeta}{\beta h} \exp\left(-\beta(G^\ddagger + \Delta G^\circ)\right) \quad (6.3)$$

where  $G^\ddagger$  is the free activation energy,  $\Delta G^\circ$  is the reaction free energy,  $\zeta$  is the transmission coefficient which accounts for the probability of being reactive once the transition state is reached,  $\beta$  is  $1/k_B T$  ( $k_B$  is the Boltzmann constant,  $T$  the absolute temperature), and  $h$  the Planck constant (see Fig. 6.2).

For long range electron transfer reactions, the donor and the acceptor are only weakly electronically coupled. Thus, the reaction is non-adiabatic and its rate can be obtained from Fermi's golden rule (Marcus and Sutin 1985).

$$k_{ET} = \frac{2\pi}{h} H_{DA}^2 (FC) \quad (6.4)$$

where  $H_{DA}^2$  is the electronic coupling between the reactant state and the product state (sometimes called donor state and acceptor state, respectively) and  $(FC)$  is the



*Fig. 6.1.* Multicenter redox proteins. **(a)** Complex I catalyzes the transfer of electrons from NADH to ubiquinone. The electron transfer via several iron sulfur centers drives a proton transfer across the membrane in a not understood way. **(b)** Ethylbenzene Dehydrogenase is a molybdopterin enzyme. The electron transfer to the active site occurs via one heme and several iron-sulfur centers. **(c)** Cytochrome *c* Nitrite Reductase catalyzes the six-electron reduction of nitrite to ammonia. The electrons are provided by several heme centers in the protein. This enzyme couples the reduction of ammonia to the quinone/quinol pool in the membrane. **(d)** Cytochrome *bc*<sub>1</sub> uses the driving force of the electron transfer from ubiquinol to cytochrome *c* to generate a proton gradient. This proton pumping is achieved by a complex redox loop reaction called the Q-cycle.

Franck-Condon weighted density of states, i.e. the Franck-Condon factor. Equation 6.4 separates the electronic factors (represented by the electronic coupling) from the nuclear factors (represented by the Franck-Condon factor which accounts for the structural adaptation of the donor site, the acceptor site, and their surroundings) (Marcus and Sutin 1985). A classical form of the

Franck-Condon factor is given by the following expression:

$$(FC) = \frac{1}{\sqrt{4\pi\beta^{-1}\lambda}} \exp\left(-\beta \frac{(\Delta G^\circ + \lambda)^2}{4\lambda}\right) \quad (6.5)$$

where  $\lambda$  is the reorganization energy and  $\Delta G^\circ$  is the reaction free energy. The reor-

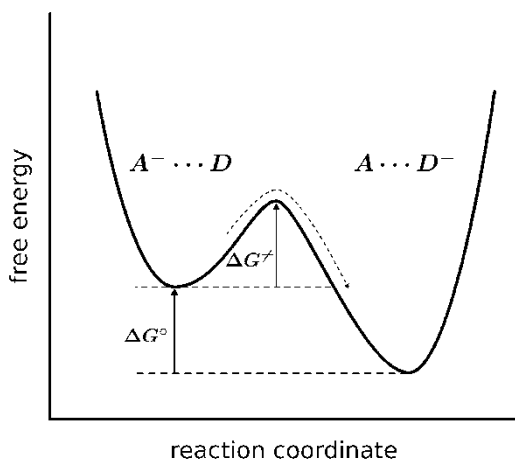


Fig. 6.2. The transition from the reactant state (or donor state) to the product state (or acceptor state) occurs over a barrier  $\Delta G^\ddagger$ . The free energy difference between the two states is  $\Delta G^\circ$ . Thus, the back reaction has a barrier that is the sum of the two energies  $\Delta G^\ddagger + \Delta G^\circ$ .

ganization energy accounts for the structural reorganization of the reactant state to the product state upon the reaction. Comparing Eq. 6.2 with Eqs. 6.4 and 6.5, one can recognize that the term  $\frac{(\Delta G^\circ + \lambda)^2}{4\lambda}$  corresponds to the activation free energy. Instead, the electronic coupling together with the preexponential factor of Eq. 6.5 are related to the transmission coefficient  $\zeta$  in Eq. 6.2.

In summary, electron transfer reactions are influenced by three energetic parameters: the electronic coupling of the donor and the acceptor, the reaction free energy, and the reorganization energy. Each of these parameters can be estimated from molecular structures using various theoretical models as discussed below.

### B. Electronic Coupling

The electronic coupling quantifies how easily an electron can move from the donor to the acceptor. The closer the donor site and the acceptor site the more rapid the transfer. If the distance between the redox centers in a protein becomes larger than 20 Å, the electron transfer rate between them is so slow

that it is basically inconsequential. The actual electron transfer is a tunneling event, in which the electronic states of the protein are used as a bridge. Several theoretical methods have been developed to calculate the tunneling efficiency.

In the simplest model, an electron with the mass  $m$  tunnels between two narrow wells that are separated by a uniform energy barrier of the height  $V$ . The electronic coupling in such a system decreases exponentially with the distance  $R$  between the wells (Gamow 1928; Gray and Winkler 2005).

$$\begin{aligned} H_{DA}^2 &= H_{DA}^{\circ 2} \exp\left(-\frac{2\sqrt{2mV}}{\hbar}(R-R_0)\right) \\ &= H_{DA}^{\circ 2} \exp\left(-b(R-R_0)\right) \end{aligned} \quad (6.6)$$

This model describes reasonably well the distance and the barrier height dependence of electron transfer between two cofactors embedded in a protein matrix. This picture captures the view that the electronic coupling between redox cofactors in a protein medium is mainly dependent on the distance between the cofactors. The intervening medium represents a barrier to the electron. The protein medium lowers the barrier compared to the vacuum and provides an electronic bridge. To estimate electronic coupling between cofactors in a protein, different models have been developed ranging from methods based on quantum chemical calculations (Stuchebrukhov 2003), to electron transfer pathways (Gray and Winkler 1996), or a simple, experimentally parametrized distance dependence (Moser et al. 1992; Page et al. 1999) just to name some of the models [also see Krishtalik in this volume]. In the later model, the specific nature of the intervening protein medium such as secondary or tertiary structure is not taken into consideration. Surprisingly, the different methods gave similar results leading to an exponential decay of the electronic coupling as a function of the distance between the donor site and the acceptor site. This finding indicates that the

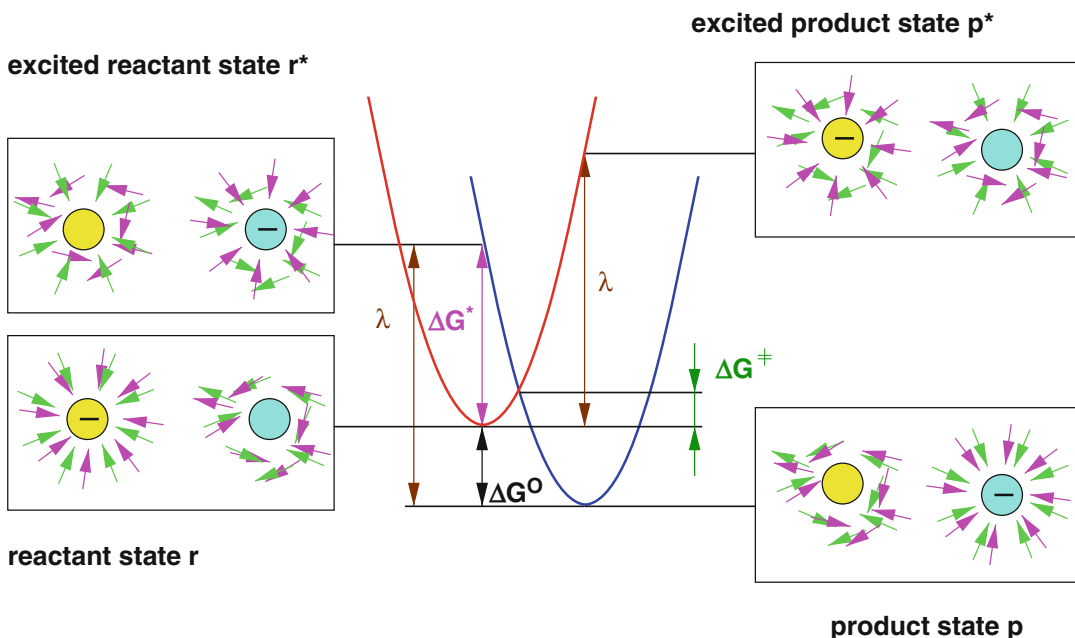


Fig. 6.3. The Marcus model of electron transfer. The reactant and the product states are described as *red* and *blue* harmonic potentials, respectively. The energy difference between the two states, i.e. the reaction free energy, is given by  $\Delta G^\circ$ . The energy  $\Delta G^*$  represents the vertical excitation energy leading to the Franck-Condon state. The reorganization energy  $\lambda$  is the energy required to adopt the nuclear configuration of the product state without leaving the potential energy curve of the reactant state. The same reorganization energy can be defined for the backward reaction. As can be seen,  $\lambda = \Delta G^\circ + \Delta G^*$ . The activation free energy  $\Delta G^\ddagger$  can be obtained from the reorganization energy and the reaction free energy. The idea of Marcus was to separate the fast relaxing electronic polarization (represented by *magenta arrows*) from the slowly relaxing solvent polarization (represented by *green arrows*). In the equilibrium states, both polarizations adapt fully to the given charge distribution, while in the vertically excited Franck-Condon state only the electronic polarization is adapted to the charge distribution.

electronic coupling is not much influenced by the specific nature of the protein medium.

### C. Reorganization Energy

The reorganization energy  $\lambda$  accounts for the structural reorganization of the reactant and the product state including the surrounding medium. Figure 6.3 shows the meaning of the reorganization energy. Assuming a harmonic potential, the reorganization energy is the energy required to adapt the geometry of the product state in the reactant state and vice versa. The potential energy of the two states can then be expressed as

$$V_r(\vec{x}) = G_r + \frac{1}{2}k(\vec{x} - \vec{x}_r)^2 \quad (6.7)$$

$$V_p(\vec{x}) = G_p + \frac{1}{2}k(\vec{x} - \vec{x}_p)^2 \quad (6.8)$$

where  $\vec{x}$  represents the collective coordinates of the system, i.e. the position of all atoms, the index  $p$  indicates the product state, the index  $r$  the reactant state, and  $k$  is a force constant. The reorganization energy is given by

$$\lambda = \frac{1}{2}k(\vec{x}_p - \vec{x}_r)^2 \quad (6.9)$$

Since the electron transfer reaction is accompanied with large changes in the electrostatic potential because of the transferred charge, the effects on the medium surrounding the redox-active sites can be rather long range (on the order of 20 Å). Therefore, it is appropriate to separate the reorganization energy into an inner sphere reorganization

energy  $\lambda_i$  and an outer sphere reorganization energy  $\lambda_o$ .

$$\lambda = \lambda_i + \lambda_o \quad (6.10)$$

The inner sphere reorganization energy is mainly connected to changes in the redox active site itself and can be calculated by an expression that is similar to Eq. 6.9. The outer reorganization energy is connected to changes in the surrounding medium such as the solvent or the protein environment. Marcus suggested that the outer sphere reorganization energy can be calculated on the basis of a continuum electrostatic model (Marcus 1956). Namely, the idea is to separate the fast electronic response ( $10^{-15} \dots 10^{-16}$  s) from the slow molecular (orientational) response ( $10^{-11} \dots 10^{-14}$  s) as explained in Fig. 6.3. This part can be described by an electrostatic model as will be discussed below (section “III.B. Calculating the Outer Sphere Reorganization Energies”).

#### D. Reaction Free Energy

The reaction free energy  $\Delta G^\circ$  is often approximated by the difference between the donor and acceptor redox groups. Even if this approximation is often justified, it is not always correct, since the interaction between the redox active groups influences the reaction free energy (Ullmann and Bombarda 2013). The situation becomes even more complex when the redox reaction is coupled to proton binding or the protein contains many redox active cofactors. Instead, it is always correct to consider the reaction free energy as the energy difference between the product state and the reactant state:

$$\Delta G = G_p - G_r \quad (6.11)$$

The microstate model (Becker et al. 2007; Bombarda and Ullmann 2011; Ullmann and Bombarda 2013), which will be explained in section “III.D. Interacting Redox Active Groups,” takes this energy difference correctly into account.

#### E. Moser-Dutton Ruler

A practical although not exclusive way of calculating electron transfer rate constants is the Moser-Dutton ruler (Moser et al. 1992; Page et al. 1999), which represents an empirical formula for electron transfer rates that relies on the theoretical basis of Marcus theory. The parameters were obtained by fitting known electron transfer rates to a linear equation of the form

$$\lg k_{et}^{ex} = A - B(R - R_o) - C \frac{(\Delta G^\circ + \lambda)^2}{\lambda} \quad (6.12)$$

$A$  was found to be 13.0;  $B$  has an average value of  $0.6 \text{ \AA}^{-1}$  (a more complex expression can be used if the packing density is considered (Page et al. 1999));  $C$  has a value of  $3.1 (\text{eV})^{-1}$ .  $R_o$  is the van der Waals contact distance, which was assumed to be  $3.6 \text{ \AA}$ . For endergonic reaction, Eq. 6.12 was extended to account for the uphill step (Eq. 6.13) with  $D = 0.06 \text{ eV}$ .

$$\lg k_{et}^{ex} = A - B(R - R_o) - C \frac{(-\Delta G^\circ + \lambda)^2}{\lambda} - \frac{\Delta G^\circ}{D} \quad (6.13)$$

The justification of Eq. 6.13 has been discussed in the literature and an alternative formulation based on the Marcus equation was proposed (Crofts and Rose 2007).

There are several other methods to estimate electron transfer rates. One of the more popular methods is the pathway model that was developed by Gray, Beratan, Onuchic, and coworkers (Gray and Winkler 1996). This model estimates the electronic coupling as a product of through-bond/through-space/through-hydrogen-bond couplings. Other methods rely on quantum chemical methods (Stuchebrukhov 2003). However, a major advantage of the Moser-Dutton ruler is its simplicity and its clear connection to molecular structures. The parameter  $R$  is the edge-to-edge distance between the cofactors involved in the electron transfer process. This distance can be estimated from

crystal structures of the relevant proteins. The other two parameters, namely the reorganization energy  $\lambda$  and the reaction free energy  $\Delta G^\circ$ , can be also estimated from the structure either by molecular mechanics calculations (Beveridge and DiCapua 1989; Muegge et al. 1997) or by continuum electrostatic calculations (Sharp 1998; Ullmann and Knapp 1999).

#### F. Tuning of Electron Transfer Rates in Proteins

The protein can tune electron transfer rate constants by adapting the three energetic parameters of the Marcus equation: the electronic coupling, the reorganization energy and the reaction free energy. As discussed above, the electronic coupling between the redox cofactors can only be efficiently varied by changing the distance between them. Changing protein residues in the electron pathways between the donor moiety and the acceptor moiety has

only minor effects presumably because the packing between the donor and the acceptor does not change very much and thus the electron always finds pathways that are equally well-suited to transfer the electron (Ullmann and Kostić 1995). Thus, in a given protein fold, the electron coupling cannot be much changed unless larger conformational changes occur. An example of such a conformational change affecting electron transfer reactions is the movement of the Rieske-head domain in cytochrome  $bc_1$  shown in Fig. 6.4 (Zhang et al. 1998).

As discussed above, another parameter of the Marcus equation is the reorganization energy. The inner sphere reorganization energy is mainly connected to the nature of the redox active group (Olsson et al. 1998; Ryde and Olsson 2001). The protein can influence this parameter only to some extent, for instance through strain exerted on the redox center. The outer sphere reorganization energy is connected to the solvent and protein reorganization. Thus, this parameter cannot also be

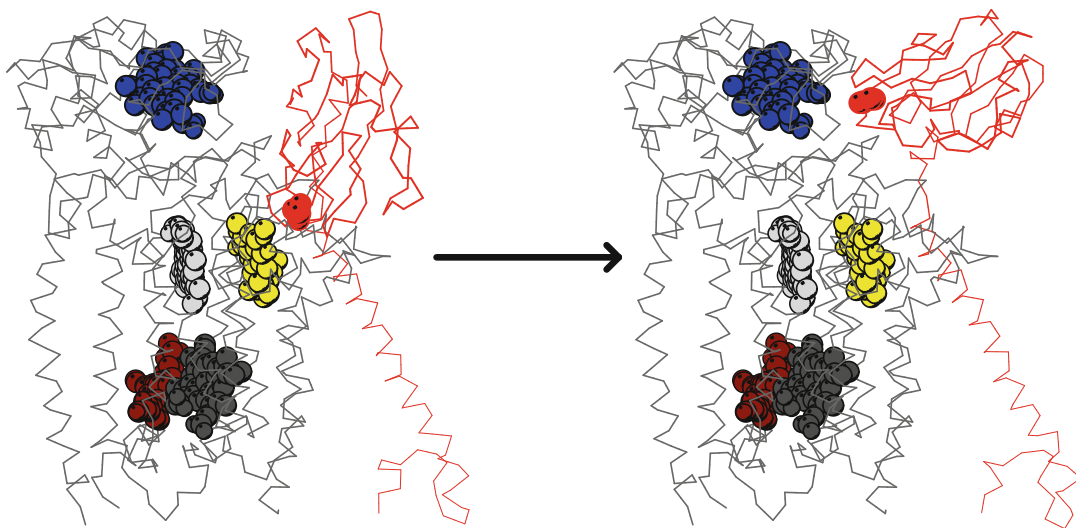


Fig. 6.4. Movement of the Rieske-Domain in cytochrome  $bc_1$ . The Rieske iron sulfur center (red balls) receives an electron from an ubiquinol (yellow) and transports this electron to cytochrome  $c_1$ . The second electron of the ubiquinol is transferred to the heme  $b_p$  (light grey) and from there further to the heme  $b_n$  (dark grey) and a quinone (brown). The subscript  $p$  or  $n$  indicate whether the heme is closer to the electrochemically positive or negative side of the membrane, respectively. The conformational change of the Rieske domain (shown in red) facilitates the electron transfer from the Rieske iron sulfur center to cytochrome  $c_1$  by changing the electronic coupling between the redox centers. The movement of the Rieske domain is a key element of the Q-cycle through which the cytochrome  $bc_1$  complex can generate a proton gradient.

much influenced in a given protein scaffold, since the protein has a low polarizability. Nevertheless, the outer sphere reorganization energy is influenced by the solvent exposure of the redox active group and the polarity of the protein medium.

The parameter that is most easily influenced by the protein environment is the reaction free energy. Biological systems have several ways to tune the redox properties of a particular site. The nature of the redox active site is the most crucial. Depending on whether an iron-sulfur cluster or a heme is chosen as a redox site, the redox potential will be different. Also the nature of the ligands of the metal center influences the redox properties. Thus, for instance it is known from model compounds of heme proteins, that the change from a histidine-histidine ligated heme to a histidine-methionine ligated heme decreases the redox potential from  $-70$  to  $-220$  mV (Wilson 1983). The protein environment is probably most important for the fine tuning of redox properties of a redox-active site (Zheng and Gunner 2009). The protein environment can tune the redox potential by (i) placement of charges or dipoles in the vicinity of the redox active site (for instance hydrogen bonds or salt bridges), (ii) changing the solvent accessibility of the redox active site, and (iii) coupling of the reduction to the protonation of a nearby site (redox-Bohr effect).

### III. Electrostatic Methods for Estimating Reaction Free Energies and Reorganization Energies

The protein can electrostatically tune the redox potential of a redox active group. This tuning can be understood theoretically by using a continuum electrostatic model of the protein.

#### A. The Poisson-Boltzmann Equation

Electrostatic interactions are the most important interactions in biomolecules. Most of the effects in biochemical systems are

dominated by electrostatics. It is therefore not too surprising that an electrostatic model can describe very well many features of biomolecular systems. This model relies on the Poisson-Boltzmann equation.

The basic idea of the Poisson-Boltzmann model is to describe the protein as a region with a low dielectric permittivity which is embedded in a region of high dielectric permittivity (aqueous solvent). The charge distribution of the protein is described by a fixed charge distribution in the low dielectric region, which is given by the molecular structure of the protein. Charges and dipoles are modeled by (fractional) point charges that are placed at the center of the atoms. The dissolved ions are represented by a Boltzmann-distributed charge density. The boundary of the low dielectric region is defined by the solvent accessible surface of the protein (Connolly 1983). Mathematically, the whole system is described by the Poisson-Boltzmann equation (Eq. 6.14) (Warwicker and Watson 1982; Honig and Nicholls 1995),

$$\nabla [\varepsilon(\mathbf{r})\nabla\phi(\mathbf{r})] = -\rho_f(\mathbf{r}) - \sum_{i=1}^K c_i^{\text{bulk}} Z_i e_0 \times \exp\left(\frac{-Z_i e_0 \phi(\mathbf{r})}{RT}\right) \quad (6.14)$$

where  $\nabla$  is the differential operator,  $\varepsilon(\mathbf{r})$  is the spatially varying dielectric permittivity,  $\rho_f(\mathbf{r})$  is the spatially fixed charge density which is usually defined by point charges at the positions of the nuclei of the solute molecule;  $c_i^{\text{bulk}}$  is the bulk concentration of the ionic species  $i$  with the charge  $Z_i$  ( $e_0$  is the elementary charge). The sum runs over all  $K$  ionic species in the solvent and describes a Boltzmann distribution of the ions in the electrostatic potential  $\phi(\mathbf{r})$  of the protein. The electrostatic potential  $\phi(\mathbf{r})$  can be obtained by solving Eq. 6.14.

Generally, non-linear partial differential equations like the one in Eq. 6.14 are difficult to solve even numerically. However by approximating the exponential term as a

series, Eq. 6.14 can be linearized. With the common definitions of the ionic strength

$$I = \frac{1}{2} \sum_{i=1}^K c_i^{\text{bulk}} Z_i^2 \quad \text{and the modified inverse}$$

Debye length  $\bar{\kappa} = \sqrt{\frac{2N_A e_0^2 I}{k_B T}}$  the linearized Poisson-Boltzmann equation assumes the form that is found in biophysics text books (Eq. 6.15).

$$\nabla [\varepsilon(\mathbf{r}) \nabla \phi(\mathbf{r})] = -\rho_{\text{prot}}(\mathbf{r}) + \bar{\kappa}^2(\mathbf{r}) \phi(\mathbf{r}) \quad (6.15)$$

In Eq. 6.15, the term  $\varepsilon(\mathbf{r})$  reflects the spatially varying permittivity (or dielectric constant). The first term on the right hand side describes the spatially fixed charge distribution in the protein and the second term describes the charge distribution due to the mobile ions which adopt a Boltzmann distribution in the field of the protein.

The Poisson-Boltzmann equation in its linearized form can be solved analytically only for particular geometries. However, there are several methods that can solve the Poisson-Boltzmann equation numerically for arbitrary geometries. The solution of the Poisson-Boltzmann equation can be expressed as a potential that is composed of two contributions:

$$\phi(\mathbf{r}) = \sum_{i=1}^M \frac{q_i}{4\pi \varepsilon_p |\mathbf{r} - \mathbf{r}'_i|} + \phi_{\text{rf}}(\mathbf{r}) \quad (6.16)$$

First, the Coulomb potential at the position  $\mathbf{r}$  caused by  $M$  point charges  $q_i$  at positions  $\mathbf{r}'_i$  in a medium with a permittivity  $\varepsilon_p$ , and second, the reaction field potential arising from the  $M$  point charges  $q_i$  and the dielectric boundary between the protein and the solvent, as well as from the distribution of ions in the solution. The reaction field potential originates from the polarization of the solvent by the solute. Usually, the reaction field potential stabilizes charged states. At the molecular level, a smaller part of this polarization originates from the deformation of the electron density of the solvent due to the presence of the solute, while the larger part originates from the orientational polarization of the solvent molecules.

The total electrostatic energy of a system in aqueous solution consists of two parts: the interaction between the components of the system and the interaction of the system with the solvent. The first contribution is obtained by charging the charge set  $\rho_2$  in the presence of the electrostatic potential caused by charge  $\rho_1$ . Assuming that the charge set  $\rho_2$  consists of a single charge  $q_f$ , the interaction energy becomes

$$G_{\text{inter}} = \int_0^{q_f} \phi(\rho_1, \mathbf{r}_q) dq = \phi(\rho_1, \mathbf{r}_q) q_f \quad (6.17)$$

Since the potential  $\phi(\rho_1, \mathbf{r}_q)$  at the position  $\mathbf{r}_q$  of the charge  $q_f$  is totally independent of the charge  $q_f$  itself, the integration in Eq. 6.17 reduces to a simple multiplication. Equation 6.17 can be generalized to the interaction between two disjunct sets of charges  $\{q\}$  and  $\{p\}$ , which is given by

$$G_{\text{inter}} = \sum_{i=1}^{N_q} q_i \phi(\{p\}, \mathbf{r}_{q_i}) = \sum_{i=1}^{N_p} p_i \phi(\{q\}, \mathbf{r}_{p_i}) \quad (6.18)$$

where  $N_q$  and  $N_p$  are the number of charges in the charge sets  $\{q\}$  and  $\{p\}$ , respectively,  $\phi(\{p\}, \mathbf{r}_{q_i})$  is the potential caused by the charge set  $\{p\}$  at the position of the charge  $q_i$  and  $\phi(\{q\}, \mathbf{r}_{p_i})$  is the potential caused by the charge set  $\{q\}$  at the position of the charge  $p_i$ . As can be seen from Eq. 6.18, this interaction energy is symmetric.

The second contribution is the reaction field energy, which is also sometimes called “self-energy”. This energy originates from the interaction energy of the charge set  $\{q\}$  with its own reaction field potential  $\phi_{\text{rf}}$ . To obtain this energy, one imagines the charging of a particle in a dielectric medium, and asks what is the energy of this charging process. Analogous to Eq. 6.17, we can write

$$G_{\text{rf}} = \int_0^{q_f} \phi_{\text{rf}}(q, \mathbf{r}_q) dq \quad (6.19)$$

In contrast to the situation in Eq. 6.17, the reaction field potential  $\phi_{\text{rf}}$  depends on the



charge of the particle. For simplicity, one assumes a linear response, i.e.  $\phi_{rf}(q_f, \mathbf{r}_q) = Cq_f$ . From Eq. 6.19, we obtain

$$G_{rf} = \int_0^{q_f} Cq \, dq = \frac{1}{2} Cq_f^2 = \frac{1}{2} \phi_{rf}(q_f, \mathbf{r}_q) q_f \quad (6.20)$$

Equation 6.20 can be generalized to obtain the reaction field energy of a charge set  $\{q\}$

$$G_{rf} = \frac{1}{2} \sum_{i=1}^{N_q} q_i \phi_{rf}(\{q\}, \mathbf{r}_{q_i}) \quad (6.21)$$

As shown above, the factor  $\frac{1}{2}$  in this equation is a consequence of the linear response approach.

The reaction field energy can be used to calculate the electrostatic contribution of the solvation energy, which is the energy to transfer from vacuum into a solvent with a given dielectric constant  $\epsilon_s$ . This approach was used by Max Born to calculate the solvation energy of a ion with the radius  $r$  and the charge  $Z$  (Born 1920)

$$\Delta G_{solv} = -\frac{1}{4\pi\epsilon_o} \frac{(Ze_o)^2}{2r} \left(1 - \frac{1}{\epsilon_s}\right) \quad (6.22)$$

This equation is part of an expression for the outer reorganization energy derived by Marcus (1956), which will be discussed in the next section.

Although the continuum electrostatic approach is relatively simple, it is surprising how well it works to understand the energetics of biochemical systems (Ullmann et al. 2008). It can be used to analyze electron and proton transfer reactions as will be explained in the following.

### B. Calculating the Outer Sphere Reorganization Energies

By separating the fast and the slow polarization, Marcus derived a simple expression for the outer sphere reorganization energy for the transfer of the charge  $\Delta e$  between two spherical ions with the radii  $a_1$  and  $a_2$

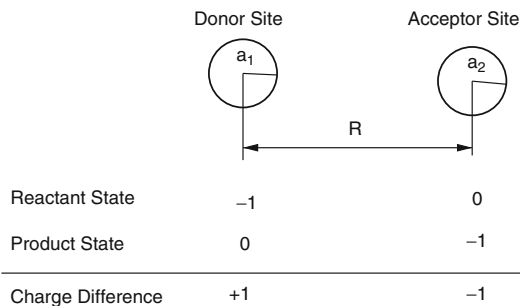


Fig. 6.5. Model of the charge transfer between two spheres at a separation  $R$  with the radii  $a_1$  and  $a_2$ , respectively. The charge difference between the product state and the reactant state can be used to calculate the outer sphere reorganization energy and leads to Eq. 6.23.

at a distance  $R$  (Marcus 1956), leading to Eq. 6.23

$$\lambda_o = \frac{\Delta e^2}{4\pi\epsilon_o} \left( \frac{1}{2} \left( \frac{1}{a_1} + \frac{1}{a_2} \right) - \frac{1}{R} \right) \left( \frac{1}{\epsilon_{op}} - \frac{1}{\epsilon_s} \right) \quad (6.23)$$

where  $\epsilon_{op}$  is the optical dielectric constant and  $\epsilon_s$  is the dielectric constant of the solvent (Fig. 6.5). The optical dielectric constant takes into account only the electronic polarization and thus has a value of about 2.

Equation 6.23 can be interpreted as having two contributions: (i) the difference between the solvation energy of ions in a low dielectric medium with a purely electronic polarization ( $\epsilon_{op}$ ) and a solvent with a higher dielectric constant  $\epsilon_s$  and (ii) interaction energy of the charge difference between the reactant and the product state. Since the charge difference is considered, the charge at the donor site and the acceptor site is  $+1$  and  $-1$ , respectively. The interaction between these charges gives rise to the  $1/R$  term. The solvation energy difference is related to the Born formula (Eq. 6.22). Thus, the influence of the reaction field originating from the donor site is neglected at the acceptor site and vice versa. This approximation is valid if  $R$  is large. The outer sphere reorganization energy is always a positive number, since the optical dielectric constant, which

accounts only for the purely electronic polarization, is much smaller than the solvent dielectric constant and the separation between the charges is much larger than the radius of the spheres.

The idea that underlies Eq. 6.23 can be generalized such that it can be used to calculate the reorganization energy of a protein (Sharp 1998). For proteins, the numerical solution of the Poisson-Boltzmann equation must be used instead of the Born formula. The outer sphere reorganization energy in this frame work is given by

$$\lambda_o = \frac{1}{2} \sum_i \left( \phi_{r^*-r}(\{\Delta q\}, \mathbf{r}_i) - \phi_{p-r}(\{\Delta q\}, \mathbf{r}_i) \right) \Delta q_i \quad (6.24)$$

where the charge set  $\{\Delta q\}$  is the difference between charges assigned to the product state and the reactant state, respectively

$$\Delta q_i = q_i^p - q_i^r \quad (6.25)$$

In Eq. 6.24, the term  $\phi_{r^*-r}(\{\Delta q\}, \mathbf{r}_i)$  reflects the potential considering the fast electronic relaxation and is the numerical solution of Eq. 6.26

$$\nabla \varepsilon_{op} \nabla \phi_{r^*-r}(\{\Delta q\}) = -\rho(\{\Delta q\}) \quad (6.26)$$

The term  $\phi_{p-r}(\{\Delta q\}, \mathbf{r}_i)$  represents the potential considering slow orientational relaxation which is given by the numerical solution of Eq. 6.27

$$\nabla \varepsilon(\mathbf{r}) \nabla \phi_{p-r}(\{\Delta q\}) = -\rho(\{\Delta q\}) + \bar{\kappa}^2 \phi_{p-r}(\{\Delta q\}) \quad (6.27)$$

With this approach, the reorganization energy of a charge transfer reaction can be easily calculated on the basis of molecular structures using the numerical solution of the Poisson-Boltzmann equation. Interestingly, in this approach the outer sphere reorganization energy depends only on the charge difference between the reactant state and the donor state and to a minor extent on the shape of the low dielectric region defined by the protein. Thus, in the frame

work of this continuum electrostatic model, the surrounding protein residues do not have much influence on the outer sphere reorganization energy except by defining the dielectric boundaries. Consequently, one would expect that the reorganization energy cannot be much altered by mutations.

### C. Calculating Redox Potentials of Proteins

The redox potential of a group characterizes the energetics of an electron transfer reaction, since it is proportional to the energy change upon electron release or uptake. The calculation of absolute redox potentials requires very high-level quantum chemical calculations and is often not very accurate. However, changes in the redox potentials arising from the protein are mainly caused by electrostatic interactions. Thus, it is possible to determine the changes of the redox potential of a group  $A$  due to the protein environment compared to a model compound of the group for which the redox potential  $E_{\text{model},A}^o$  is known. There are two contributions to the redox potential shift, one originates from the changes of the reaction field when the model compound is moved from the aqueous solution into the protein ( $\Delta \Delta G_{\text{Born},A}^{\text{redox}}$ ). The other originates from the interaction of the redox active group with the charges and dipoles of the protein ( $\Delta \Delta G_{\text{back},A}^{\text{redox}}$ ). The redox potential in the protein  $E_{\text{intr},A}^o$  is thus expressed by

$$E_{\text{intr},A}^o = E_{\text{model},A}^o - \frac{1}{F} (\Delta \Delta G_{\text{Born},A}^{\text{redox}} + \Delta \Delta G_{\text{back},A}^{\text{redox}}) \quad (6.28)$$

where

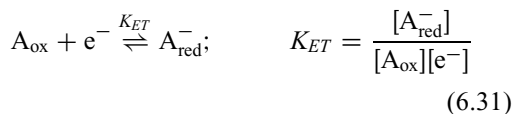
$$\begin{aligned} \Delta \Delta G_{\text{Born},A}^{\text{redox}} &= \frac{1}{2} \sum_{i=1}^{N_{Q,A}} Q_{i,A}^{\text{red}} [\phi_p(\mathbf{r}_i; Q_A^{\text{red}}) - \phi_m(\mathbf{r}_i; Q_A^{\text{red}})] \\ &\quad - \frac{1}{2} \sum_{i=1}^{N_{Q,A}} Q_{i,A}^{\text{ox}} [\phi_p(\mathbf{r}_i; Q_A^{\text{ox}}) - \phi_m(\mathbf{r}_i; Q_A^{\text{ox}})] \end{aligned} \quad (6.29)$$

$$\begin{aligned}
\Delta\Delta G_{\text{back},A}^{\text{redox}} &= \sum_{i=1}^{N_p} q_i [\phi_p(\mathbf{r}_i; Q_A^{\text{red}}) - \phi_p(\mathbf{r}_i; Q_A^{\text{ox}})] \\
&\quad - \sum_{i=1}^{N_m} q_i [\phi_m(\mathbf{r}_i; Q_A^{\text{red}}) - \phi_m(\mathbf{r}_i; Q_A^{\text{ox}})]
\end{aligned} \tag{6.30}$$

The summations in Eq. 6.29 run over the  $N_{Q,A}$  atoms of group  $A$  that have different charges  $Q_{i,A}^{\text{ox}}$  and  $Q_{i,A}^{\text{red}}$  in the oxidized (ox) and in the reduced (red) state, respectively. The first summation in Eq. 6.30 runs over the  $N_p$  charges of the protein that belong to atoms in non-titratable groups. The second summation in Eq. 6.30 runs over the  $N_m$  charges of atoms of the model compound that do not have different charges in the different redox states. The terms  $\phi_m(\mathbf{r}_i, Q_A^{\text{ox}})$ ,  $\phi_m(\mathbf{r}_i, Q_A^{\text{red}})$ ,  $\phi_p(\mathbf{r}_i, Q_A^{\text{ox}})$ , and  $\phi_p(\mathbf{r}_i, Q_A^{\text{red}})$  denote the values of the electrostatic potential at the position  $\mathbf{r}$  of the atom  $i$ . The electrostatic potential can be obtained by solving the Poisson-Boltzmann equation numerically using the shape of either the protein (subscript  $p$ ) or the model compound (subscript  $m$ ) as dielectric boundary and assigning the charges of the redox-active group  $A$  in either the oxidized ( $Q_A^{\text{ox}}$ ) or the reduced ( $Q_A^{\text{red}}$ ) form to the respective atoms.

The background energy  $\Delta\Delta G_{\text{back},A}^{\text{redox}}$  reflects the interaction of the redox-active group with charges of the protein. Thus, it is this term that is mainly influenced by mutations of residues or by variations of the protonation state of nearby residues. The Born term  $\Delta\Delta G_{\text{Born},A}^{\text{redox}}$  is sensitive to changes in the protein shape and thus it may change in case the border between protein and solvent is modified by mutations or by conformational changes in the vicinity of the active site.

The equilibrium between the redox couple  $A_{\text{ox}}/A_{\text{red}}^-$  is defined by



where  $K_{ET}$  is the equilibrium constant. One can define the solution redox potential  $E$  and the redox potential  $E^0$  of the redox couple  $A_{\text{ox}}/A_{\text{red}}^-$  as  $E = -RT/F \ln \gamma [e^-]$  and  $E^0 = RT/F \ln K_{ET}$ , respectively. With the factor  $RT/F$ , where  $F$  is the Faraday constant, one obtains  $E$  and  $E^0$  in the units volts;  $\gamma$  is the activity coefficient. The relation between  $E^0$  and the standard reaction free energy  $G_{\text{redox}}^0$  is given by  $G_{\text{redox}}^0 = FE^0$ . With these definitions and Eq. 6.31, one obtains the Nernst equation for a single electron reduction:

$$E = E^0 + \frac{RT}{F} \ln \frac{[A_{\text{ox}}]}{[A_{\text{red}}^-]} \tag{6.32}$$

The probability  $\langle x \rangle$  that a redox-active group is in its oxidized state is defined as  $\langle x \rangle = [A_{\text{ox}}]/([A_{\text{red}}^-] + [A_{\text{ox}}])$ . The relation between the probability  $\langle x \rangle$ , the solution redox potential  $E$ , and the redox potential  $E^0$  is given by

$$\langle x \rangle = \frac{\exp\left(\frac{F}{RT}(E - E^0)\right)}{1 + \exp\left(\frac{F}{RT}(E - E^0)\right)} \tag{6.33}$$

Consequently, the free energy  $G_{\text{redox}}$  required to oxidize a one-electron redox-active group at a given redox potential of the solution  $E$  is given by Eq. 6.34.

$$G_{\text{redox}} = -F(E - E^0) = -RT \ln \frac{\langle x \rangle}{1 - \langle x \rangle} \tag{6.34}$$

#### D. Interacting Redox Active Groups

In many redox proteins, there is more than one redox active group and these redox active groups interact. Because of these interactions, the titration curves of the individual redox active sites can become irregular. These irregular titration curves originate from the population of several microstates. The simplest case is a system with two interacting sites.

Such a system has four possible microstates: fully reduced, reduced at one group, reduced at the other group, and fully oxidized (Fig. 6.6). These states can be respectively described by their redox

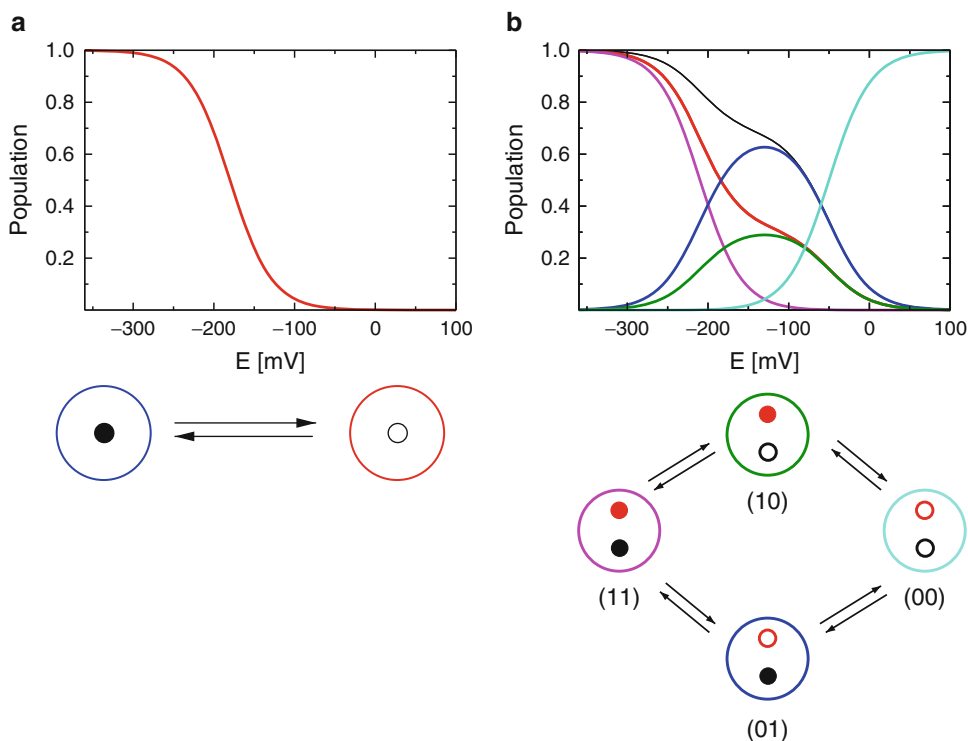


Fig. 6.6. Titration behavior of molecules with one and two redox-active groups. (a) Titration curve of a single redox-active group. The titration curve has a sigmoidal shape. (b) Titration curve of a molecule with two titratable groups. The contributions of the populations of the different microstates lead to non-sigmoidal titration curves. The microstates and their populations, the titration curves and the sites are color coded in the reaction scheme and in the diagram. For instance, the titration curve of the *red* site is the sum of the probability of the microstate population curve of the state (11) in *magenta* and the microstate population curve of state (10) in *green*.

state vectors: 11, 10, 01, and 00, where 1 marks that the group is reduced and 0 that it is oxidized. In order to obtain the titration curve of group one, the probabilities of all microstates in which this group is reduced need to be added. For instance the titration curve of group one is given by  $\langle x_1 \rangle = \langle 10 \rangle + \langle 11 \rangle$ . The titration curves of such groups can considerably deviate from standard sigmoidal titration curves and can show highly irregular features because of electrostatic interactions between the groups. The assignment of an  $E^\circ$  value to one particular group is in such cases difficult if not impossible. To eliminate the difficulties, the problem can be reformulated. Instead of considering a protein as a system of groups with a certain probability of being reduced, the problem can be formulated in terms of

well-defined microstates of the protein which have a certain probability of occurrence as will now be outlined.

Let us consider a system that possesses  $K$  redox-active sites. Such a system can adopt  $M = 2^K$  states assuming that each sites can exist in two forms. The interaction between them can be modeled electrostatically. Each state of the system can be written as a  $K$ -dimensional vector  $\vec{x} = (x_1, \dots, x_K)$ , where  $x_i$  is 1 or 0 if site  $i$  is reduced or oxidized, respectively. Each state of the system has a well-defined energy which depends on the redox energetics of the individual sites ( $E_i^{\text{intr}}$ ) and the interaction between sites ( $W_{ij}$ ). The energy of a state  $\vec{x}_v$  is given by (Bashford and Karplus 1990; Ullmann and Knapp 1999; Ullmann 2000; Gunner et al. 2006; Nielsen and McCammon 2003):

$$G(\vec{x}_v) = \sum_{i=1}^K (x_{v,i} - x_i^\circ) F(E - E_i^{\text{intr}}) + \frac{1}{2} \sum_{i=1}^K \sum_{j=1}^K (x_{v,i} - x_i^\circ)(x_{v,j} - x_j^\circ) W_{ij} \quad (6.35)$$

where  $R$  is the gas constant,  $T$  the absolute temperature, and  $F$  the Faraday constant;  $x_{v,i}$  denotes the redox form of the site  $i$  in state  $\vec{x}_v$ ,  $x_i^\circ$  is the reference form of site  $i$ ;  $E_i^{\text{intr}}$  is the redox potential that site  $i$  would have if all other sites are in their reference state (this value is also called the intrinsic redox potential; see section “III.C. Calculating Redox Potentials of Proteins”);  $E$  is the reduction potential of the solution;  $W_{ij}$  represents the interaction energy between site  $i$  and  $j$ . It can be calculated from Eq. 6.36.

$$W_{ij} = \sum_{A=1}^{N_{Q,A}} [Q_{i,A}^{\text{red}} - Q_{i,A}^{\text{ox}}] [\phi_p(\mathbf{r}_A, Q_j^{\text{red}}) - \phi_p(\mathbf{r}_A, Q_j^{\text{ox}})] \quad (6.36)$$

Equation 6.35 can be used to calculate either microscopic redox potentials or also microscopic reaction free energies by subtracting the appropriate microstate energies from each other. For example, if we consider a system with two sites as depicted in Fig. 6.6, we can calculate a microscopic redox potential from the energy difference between the states (1,0) and (1,1). This microscopic redox potential will differ from the microscopic redox potential between the states (0,0) and (0,1) because of electrostatic interactions between the two groups. The reaction free energy is given by the energy difference between the states (0,1) and (1,0). This reaction free energy can be used in Marcus theory to calculate electron transfer rates.

The equilibrium properties of a physical system are completely determined by the energies of its states. To keep the notation concise, states will be numbered by Greek indices in the subscript, i.e., for state energies we write  $G_\nu$  instead of  $G(\vec{x}_\nu)$ . For site indices, the roman letters  $i$  and  $j$  will be used.

The equilibrium probability of a single state  $\vec{x}_\nu$  is given by

$$p_\nu^{\text{eq}} = \frac{e^{-\beta G_\nu}}{Z} \quad (6.37)$$

with  $\beta = 1/RT$  and  $Z$  being the partition function of the system.

$$Z = \sum_{\nu=1}^M e^{-\beta G_\nu} \quad (6.38)$$

The sum runs over all  $M$  possible states. Properties of single sites can be obtained from Eq. 6.37 by summing up the individual contributions of all states. For example, the probability of site  $i$  being reduced is given by

$$\langle x_i \rangle = \sum_{\nu} x_{\nu,i} p_\nu^{\text{eq}} \quad (6.39)$$

where  $x_{\nu,i}$  denotes the redox form of site  $i$  in the charge state  $\vec{x}_\nu$ . For small systems, this sum can be evaluated explicitly. For larger systems, Monte-Carlo techniques can be used to determine these probabilities (Beroza et al. 1991; Ullmann and Ullmann 2012).

In general, the titration curves in such a system do not have to be sigmoidal and can even be non-monotonic (Onufriev et al. 2001). However as a consequence of statistical thermodynamics, it can be proven that the macroscopic titration curve of a system can be always decomposed into standard titration curves (Nernst functions) as long as there is no positive cooperativity (Ullmann 2003; Ullmann and Bombarda 2013).

In principle,  $2^{K-1}$  different microscopic redox potentials can be assigned to each redox-active group in a protein, where  $K$  is the number of redox active groups in the molecule. Since however, most of the interactions are relatively weak, most of these microscopic redox potentials will be very similar. But in case of strong interactions, a larger variation of the redox potential can be observed. As an example, Fig. 6.7 shows the calculated redox potentials of the hemes

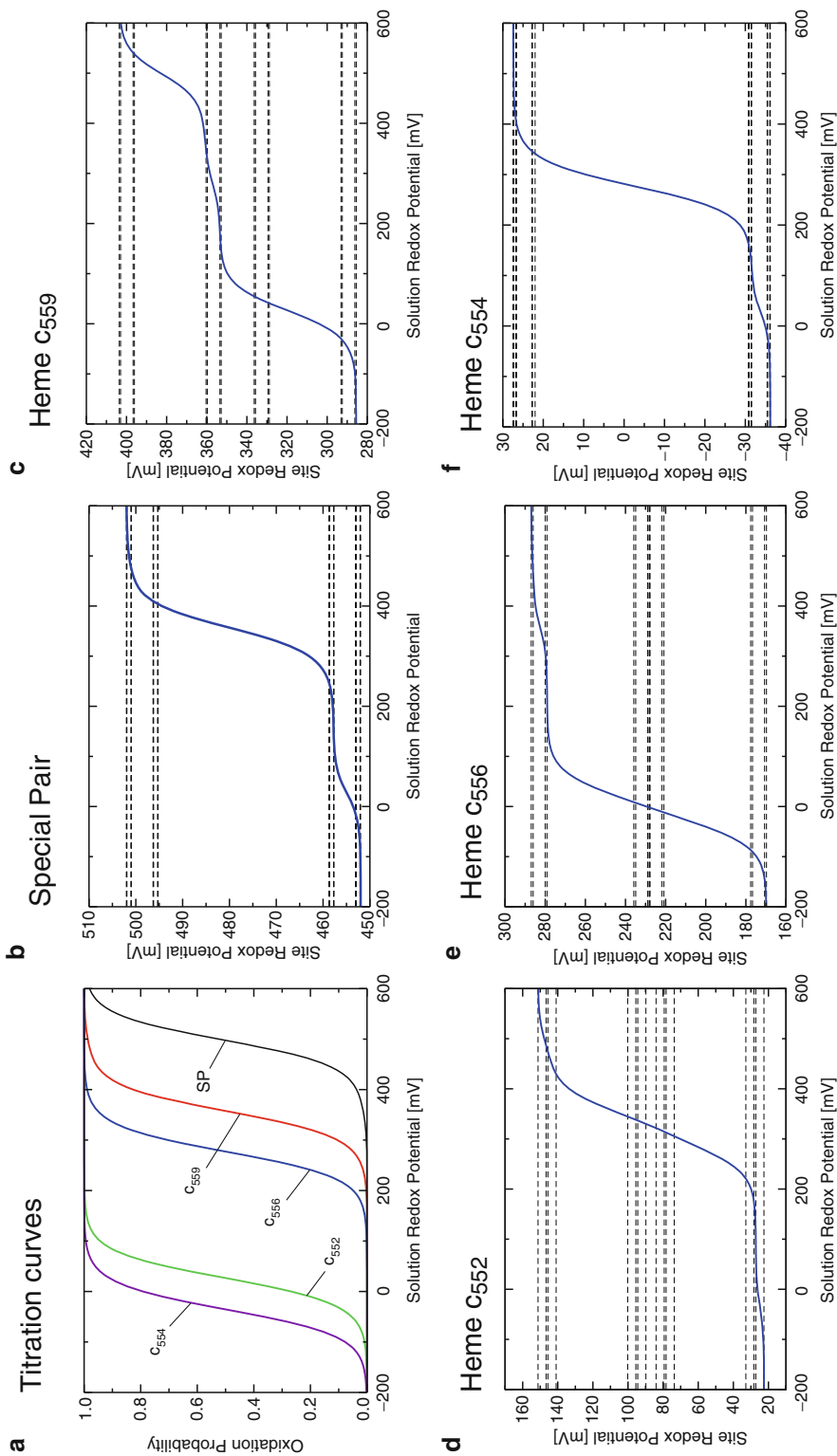


Fig. 6.7. Calculated redox titration behavior of special pair (SP) and the hemes of the RC from *B. viridis*. (a) Probability of the oxidized form of the redox-active sites; (b) to (f) solution redox-potential dependence of the site redox potential of the special pair (b), heme  $c_{559}$  (c), heme  $c_{552}$  (d), heme  $c_{556}$  (e), heme  $c_{554}$  (f). The *dashed lines* show the different microscopic redox potentials, the *blue lines* show the average redox-potential which depends on the solution redox potential.

and the special pair of bacteriochlorophylls in the photosynthetic reaction center from *B. viridis*. This protein possesses four heme groups that facilitate the rereduction of the special pair after photooxidation (Fig. 6.10). As can be seen from the graphs in Fig. 6.7, the microscopic redox potentials may vary quite substantially and cannot necessarily be read as midpoint potentials directly from the titration curves which are depicted in Fig. 6.7a. An effective redox potential or midpoint potential can be defined from the redox potential-dependent reduction probability

$$E_i^{\circ} = E - \frac{RT}{F} \left( \ln \frac{\langle x_i \rangle}{1 - \langle x_i \rangle} \right) \quad (6.40)$$

This effective midpoint potential can depend on the solution redox potential because of the interaction between the redox active sites. It represents an equilibrium redox potential (Ullmann and Bombarda 2013). The value of this effective midpoint potential varies between the most extreme microscopic redox potentials (see Fig. 6.7). However, it must be underlined that this effective midpoint potential is not necessarily the functionally relevant redox potential at which an enzyme is working as will be shown later (section “IV. Complex Electron Transfer Proteins”).

#### E. Looking at the Coupling of Reduction Reactions to Protonation Reaction

Redox reactions are often coupled to protonation reactions. Such a coupling can be very strong, meaning that as soon as an electron binds a proton also binds stoichiometrically. In other cases, the coupling is relatively weak, meaning that the coupling is substoichiometric. Biologically, this coupling of protonation and reduction can help on the one hand to tune the redox potential of a redox active group; on the other hand, it is essential for the electron transfer driven proton transfer that plays a central role in biological energy transduction (Nicholls and Ferguson 2013).

Since protonation and redox reactions can be considered in general as binding reactions, they are basically all described by the same underlying theory. Figure 6.8 summarizes and compares the similarity among the description of protonation reactions by the Henderson-Hasselbalch equation, redox equilibria by the Nernst equation, and a general thermodynamic description of binding equilibria. Because of this resemblance, protonation equilibria can be described by the same theoretical tools as redox equilibria. Since there are usually several protonatable groups in a protein, one has to consider the interaction between the protonatable groups and the mutual interaction between the protonatable groups and the redox active groups. The state vector defined above needs to be extended to a  $2^{N+K}$  dimensional vector where  $N$  is the number of protonatable groups and  $K$  is number of redox active groups. Equation 6.35 needs to be extended to include the effect of the pH.

$$G(\vec{x}_v) = \sum_{i=1}^N (x_{v,i} - x_i^{\circ}) RT \ln 10 (\text{pH} - \text{p}K_{a,i}^{\text{intr}}) + \sum_{i=1}^K (x_{v,i} - x_i^{\circ}) F (E - E_i^{\text{intr}}) + \frac{1}{2} \sum_{i=1}^{N+K} \sum_{j=1}^{N+K} (x_{v,i} - x_i^{\circ}) (x_{v,j} - x_j^{\circ}) W_{ij} \quad (6.41)$$

In this equation,  $\text{p}K_{a,i}^{\text{intr}}$  is the intrinsic  $\text{p}K_a$  value, i.e., the  $\text{p}K_a$  value that the site would have if all other titratable groups are in their respective reference state. By analogy to the intrinsic redox potential, the intrinsic  $\text{p}K_a$  value is calculated using an appropriate model compound and takes into account the protonation energy shift due to the change in the solvation energy ( $\Delta\Delta G_i^{\text{Borm}}$ ) and the change due to the interaction with non-titrating background charges ( $\Delta\Delta G_i^{\text{back}}$ ).

$$\text{p}K_{a,i}^{\text{intr}} = \text{p}K_a^{\text{model}} - \frac{1}{RT \ln 10} (\Delta\Delta G_i^{\text{Borm}} + \Delta\Delta G_i^{\text{back}}) \quad (6.42)$$

Protonation	Reduction	General Binding
$\text{HA} \xrightleftharpoons{K_a} \text{A}^- + \text{H}^+$	$\text{A}_{\text{ox}} + \text{e}^- \xrightleftharpoons{K_{\text{ET}}} \text{A}_{\text{red}}^-$	$\text{R} + \text{L} \xrightleftharpoons{K} \text{RL}$
Henderson-Hasselbalch Equation	Nernst Equation	Binding Equilibrium
$\text{p}K_a = \text{pH} - \lg \frac{[\text{A}^-]}{[\text{HA}]}$	$E^\circ = E + \frac{1}{\beta F} \ln \frac{[\text{A}_{\text{red}}^-]}{[\text{A}_{\text{ox}}]}$	$G^\circ = \mu_L + \frac{1}{\beta} \ln \left( \frac{[\text{R}]}{[\text{RL}]} \right)$
pH Value	Solution Redox Potential	Chemical Potential
$\text{pH} = -\lg \left( \gamma [\text{H}^+] \right)$	$E = -\ln \left( \gamma [\text{e}^-] \right)$	$\mu_L = \mu_L^\circ + \ln \left( \gamma [\text{L}] \right)$
Protonation Energy at a given pH value	Reduction Energy at a given solution redox potential	Binding Energy at a given chemical potential
$G^{\text{prot}} = -\beta^{-1} \ln 10 (\text{p}K_a - \text{pH})$	$G^{\text{red}} = -F(E^\circ - E)$	$G^{\text{bind}} = -(G^\circ - \mu_L)$
Protonation Probability	Reduction Probability	Binding Probability
$\langle x \rangle = \frac{e^{-\ln 10 (\text{pH} - \text{p}K_a)}}{1 + e^{-\ln 10 (\text{pH} - \text{p}K_a)}}$	$\langle x \rangle = \frac{e^{-\beta F (E - E^\circ)}}{1 + e^{-\beta F (E - E^\circ)}}$	$\langle x \rangle = \frac{e^{-\beta (G^\circ - \mu_L)}}{1 + e^{-\beta (G^\circ - \mu_L)}}$

Fig. 6.8. Comparison of the theoretical formulations of protonation equilibria, redox equilibria and general binding equilibria. The direct comparison shows the equivalence of the formulations and the relationship between the corresponding terms. Moreover, it allows to see the relation protonation reactions and reduction reactions to a more general binding formalism. The meaning of the symbols is explained in the text.

These energy shifts as well as the interaction energy  $W_{ij}$  between two groups can be calculated on the basis of the Poisson-Boltzmann equation as described above (Bashford and Karplus 1990; Ullmann and Knapp 1999).

The formalism described here is applicable only to sites that have two states, i.e., either protonated and deprotonated or oxidized and reduced. For some redox active sites such as quinones or flavins, the situation is more complicated, because they have multiple redox and protonation states for just one site. Furthermore, changes in the conformation of the amino acids side chain (rotamers) as well as larger conformational changes may

need to be considered. For all such cases, the formalism needs to be extended (Ullmann and Ullmann 2012). The equations become slightly more complicated; nevertheless, the basic philosophy stays the same and the microstate model can be applied.

#### F. Influence of Membrane Potential and Transmembrane Gradients

Many electron transfer proteins are embedded in membranes and generate an electrochemical gradient consisting of a proton gradient and a membrane potential across these membranes. This electrochemical



transmembrane gradient is used by ATP-synthase membrane protein complex to transduce the electrochemical energy into chemical energy in the form of ATP. Thus, the effect of transmembrane gradients and membrane potentials also need to be considered to describe energy transduction processes properly.

The influence of a membrane potential on the energetics of a membrane protein can be incorporated in the Poisson-Boltzmann theory (Roux 1997). The linearized Poisson-Boltzmann equation (see section “III.A. The Poisson-Boltzmann Equation”) of a membrane system with a membrane potential  $\Psi$  present is given by

$$\nabla [\varepsilon(\mathbf{r})\nabla\phi(\mathbf{r})] = -\rho_f(\mathbf{r}) + \varepsilon(\mathbf{r})\bar{\kappa}(\mathbf{r})^2 [\phi(\mathbf{r}) - \Psi\Theta(\mathbf{r})] \quad (6.43)$$

where  $\Theta(\mathbf{r})$  is a simple step function which is equal to zero at the extracellular side and equal to one at the cytoplasmic side (Heaviside step function). The potential  $\phi(\mathbf{r})$  which is obtained as the numerical solution of Eq. 6.43 can be expressed as (You and Bashford 1995; Roux 1997)

$$\phi(\mathbf{r}) = \sum_{i=1}^M \frac{q_i}{\varepsilon_p |\mathbf{r} - \mathbf{r}'_i|} + \phi_{\text{rf}}(\mathbf{r}) + \Psi\chi_{\text{mp}}(\mathbf{r}) \quad (6.44)$$

As in Eq. 6.16, the first term describes the Coulomb electrostatic potential at the position  $\mathbf{r}$  caused by  $M$  point charges  $q_i$  at positions  $\mathbf{r}'_i$  in a medium with a dielectric permittivity  $\varepsilon_p$ . The second term describes the reaction field potential  $\phi_{\text{rf}}(\mathbf{r})$  originating from the dielectric boundary between the protein and the solvent as well as from the distribution of ions in the solution, and the third term describes the potential originating from the transmembrane potential. In Eq. 6.44,  $\chi_{\text{mp}}(\mathbf{r})$  is a dimensionless function, which depends on the dielectric properties of the system and the ion distribution in the medium but not on the charge distribution within the protein. The function  $\chi_{\text{mp}}(\mathbf{r})$  has

the property that  $0 \leq \chi_{\text{mp}}(\mathbf{r}) \leq 1$  (Roux 1997). This function  $\chi_{\text{mp}}(\mathbf{r})$  describes how the membrane potential is modulated inside the membrane protein and can deviate from a simple linear function (Roux 1997).

The ions, protons and electrons that are transferred across the membrane are also influenced by the membrane potential. By analogy to the chemical potential  $\mu_c$  of a substance  $c$ , one can define the electrochemical potential  $\bar{\mu}_c$  for the ionic species  $c$  with charge  $z_c$  and activity  $\gamma[c]$  in a system with a membrane potential  $\Psi$ :

$$\bar{\mu}_c = \mu_c + z_c F \Theta(\mathbf{r}) \Psi \quad (6.45)$$

with

$$\mu_c = \bar{\mu}_c = \mu_c^\circ + RT \ln \gamma[c] \quad (6.46)$$

The energy for moving an ion across a membrane has thus two contributions: one arising from the work against the concentration difference between the two sides of the membrane and a second arising from work against the membrane potential  $\Psi$  (Cramer and Knaff 1991; Nicholls and Ferguson 2013). The work required to transfer an ion from one side of the membrane to the other is given by the difference between the electrochemical potential at the two sides of the membrane.

In order to account for the membrane potential in the energy calculation of a microstate, it is necessary to include the effect of the membrane potential on the binding energetics. Moreover, also the ligand concentrations on the two sides of the membrane may be different. Thus, a generalized version of Eq. 6.41 which uses binding free energies and electrochemical potentials instead of redox potentials,  $\text{p}K_a$  values and pH values defines the state energy for a transmembrane protein with  $N$  sites connected to the extracellular region (EC), and  $K$  sites connected to the cytoplasmic region (CP) (Calimet and Ullmann 2004; Bombarda et al. 2006) is

$$\begin{aligned}
G_n(\overline{\mu}_{c,i}^{\text{EC}}, \overline{\mu}_{h,j}^{\text{CP}}) &= \sum_{i=1}^N (x_i^n - x_i^\circ) (\overline{G}_{\text{intr},i}^\circ - \overline{\mu}_i^{\text{EC}}) \\
&+ \sum_{j=1}^K (x_j^n - x_j^\circ) (\overline{G}_{\text{intr},j}^\circ - \overline{\mu}_j^{\text{CP}}) \\
&+ \frac{1}{2} \sum_{i=1}^{N+K} \sum_{j=1}^{N+K} W_{ij} (x_i^n - x_i^\circ) (x_j^n - x_j^\circ)
\end{aligned} \tag{6.47}$$

where  $\overline{\mu}_i^{\text{EC}}$  and  $\overline{\mu}_j^{\text{CP}}$  are the electrochemical potentials of the ligand (for instance electrons or protons) binding to site  $i$  at the extracellular and site  $j$  at the cytoplasmic side, respectively. As before, the intrinsic binding energy ( $\overline{G}_{\text{intr},i}^\circ$ ) is the binding energy that the site  $i$  would have in the presence of a membrane potential if all the other titratable sites are in their reference state. The intrinsic binding energy  $\overline{G}_{\text{intr},i}^\circ$  has several contributions (For sites  $j$ , an analogous expression has to be used):

$$\overline{G}_{\text{intr},i}^\circ = G_{\text{model},i}^\circ + \Delta\Delta G_i^{\text{solv}} + \Delta\Delta G_i^{\text{back}} + \Delta\Delta G_i^\Psi \tag{6.48}$$

i.e., in addition to the terms in Eq. 6.28, Eq. 6.48 includes the interaction with the membrane potential  $\Delta\Delta G_i^\Psi$ , which can be obtained from

$$\begin{aligned}
\Delta\Delta G_i^\Psi &= F\Psi \Gamma_i \\
&= F\Psi \sum_{k=1}^{M_i} \chi_{\text{mp}}(\mathbf{r}_k) (Q_{k,i}^b - Q_{k,i}^u)
\end{aligned} \tag{6.49}$$

where the quantity  $\Gamma_i$  describes the relative effect of the membrane potential on the energy;  $\chi_{\text{mp}}(\mathbf{r})$  is the dimensionless function defined in Eq. 6.44;  $M_i$  is the number of charges of residue  $i$  that change during the reaction;  $Q_{k,i}^b$  and  $Q_{k,i}^u$  are the charges of atom  $k$  of residue  $i$  in the bound and unbound form, respectively.

It is important to realize that due to the membrane potential, there is an important

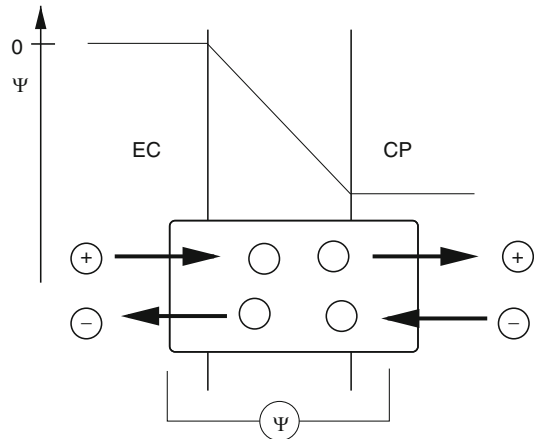


Fig. 6.9. Schematic representation of the ion, proton or electron flow in a membrane. In this scheme the membrane potential  $\Psi = \psi_{\text{CP}} - \psi_{\text{EC}} < 0$ , with  $\psi_{\text{CP}}$  and  $\psi_{\text{EC}}$  being the potential in the cytoplasm (CP) and in the extracellular space (EC), respectively. In case of protons, one could make the assumption that the hydrogen bond network connects the titratable sites to either the EC region or to the CP region (i.e. protons cannot flow through the protein). Proton displacement along one hydrogen bond network is favored in the direction of decreasing potential, electrons would flow in the opposite direction. Under the condition that the protons cannot pass the membrane, the membrane potential will increase the protonation probability of a titratable site receiving a proton from the EC region and it will decrease the protonation probability of a titratable site receiving a proton from the CP region. The opposite is true for electrons.

difference between the sites connected to the cytoplasm and the sites connected to the extracellular region (Bombarda et al. 2006). For example, a negative membrane potential as in Fig. 6.9 favors the protonation of sites connected to the extracellular side, since proton uptake is energetically downhill with regard to the membrane potential (Fig. 6.9). In contrast, protonation of sites connected to the cytoplasm is hindered in the presence of a negative membrane potential, since proton uptake is uphill with regard to the membrane potential (Bombarda et al. 2006). The opposite behavior will be found for electrons, i.e. the reduction from the extracellular side will be disfavored in the presence of a negative membrane potential, but favored from the cytoplasmic side.

## IV. Complex Electron Transfer Proteins

### A. Simulating Complex Electron Transfer Networks

To explore possible mechanisms of large protein complexes such as for instance the photosynthetic reaction center or also cytochrome *bc* complexes, it is often required to examine many different possibilities. Sometimes, even many mechanisms may be possible simultaneously and a single answer may not exist. Such complex reaction schemes can be investigated using the microstate model introduced in section “III.D. Interacting Redox Active Groups”. The kinetics of such reactions can be simulated by a master equation approach. The rate constants which are required for such simulations can be calculated using the methods introduced above. Thus, combined with a master equation approach, continuum electrostatics offers a possibility to access the non-equilibrium behavior of biomolecular systems. In the microstate formalism, charge transfer events are described as transitions between well-defined microstates of a system. The time dependence of the population of each microstate can be simulated using a master equation

$$\frac{d}{dt}p_v(t) = \sum_{\mu=1}^M k_{v\mu}p_{\mu}(t) - \sum_{\mu=1}^M k_{\mu v}p_v(t) \quad (6.50)$$

where  $p_v(t)$  denotes the probability that the system is in charge state  $v$  at time  $t$ ,  $k_{v\mu}$  denotes the probability per unit time that the system will change its state from  $\mu$  to  $v$ . In Eq. 6.50, first sum includes all the reactions that form state  $v$ , the second sum includes all the reactions that annihilate state  $v$ . The summations run over all possible states  $\mu$ . Simulating charge transfer by Eq. 6.50 assumes that these processes can be described as a Markovian stochastic process. This assumption implies that the probability of a given charge transfer depends only on

the current state of the system and not on the pathway in which the system has reached this state. The system given by Eq. 6.50 is a system of coupled linear differential equations with constant coefficients, which can be written in the form

$$\frac{d\mathbf{p}(t)}{dt} = \mathbf{A}\mathbf{p}(t) \quad (6.51)$$

The diagonal element  $A_{vv}$  of the matrix  $\mathbf{A}$  is the negative of the sum over all the rate constants  $k_{\mu v}$  annihilating the state  $v$ . The off-diagonal element  $A_{v\mu}$  is the rate constant  $k_{v\mu}$  for the conversion of state  $\mu$  to state  $v$  (Becker et al. 2007). The analytical solution for such equations can be written as (Ferreira and Bashford 2006; Becker et al. 2007)

$$p_v(t) = \sum_{\mu}^M c_{\mu}v_{\mu,v}e^{-\alpha_{\mu}t} \quad (6.52)$$

where  $\alpha_{\mu}$  is the  $\mu$ th eigenvalue of the matrix  $\mathbf{A}$ , and  $v_{\mu,v}$  is the  $v$ th element of the  $\mu$ th eigenvector of matrix  $\mathbf{A}$ ;  $c_{\mu}$  are integration constants determined from the initial probabilities  $\mathbf{p}$  at  $t = 0$  (i.e. all the terms  $e^{\alpha_{\mu}t} = 1$ ).

$$\mathbf{c} = \mathbf{V}^{-1}\mathbf{p}(0) \quad (6.53)$$

where  $\mathbf{V}^{-1}$  is the inverse of the matrix containing the eigen vectors of  $\mathbf{A}$ .

Equation 6.52 describes the time dependence of the probability distribution of microstates of the system. For these microstates, energies  $G_v$  and transition probabilities  $k_{v\mu}$  can be assigned unambiguously. The time-dependent probability of finding a single site in a particular form can be obtained by summing up individual contributions from the time-dependent probabilities  $p_v(t)$ .

$$\langle x_i \rangle(t) = \sum_v^M x_{v,i}p_v(t) \quad (6.54)$$

If the reactions are electron transfer reactions, their rate constants can be estimated using, for example, the rate laws developed

by Moser and Dutton (Moser et al. 1992; Page et al. 1999) described in section “II.E. Moser-Dutton Ruler”.

### B. Analyzing Calculated Electron Transfer Networks

For the analysis of a complex charge transfer system, it is of particular interest to follow the flow of charges through the system, i.e., the charge flux. The flux from state  $\nu$  to state  $\mu$  is determined by the population of state  $\nu$  times the probability per unit time that state  $\nu$  will change into state  $\mu$ , i.e., by  $k_{\mu\nu}P_\nu(t)$ . The net flux between states  $\mu$  and  $\nu$  is thus given by

$$J_{\nu\mu}(t) = k_{\nu\mu}P_\mu(t) - k_{\mu\nu}P_\nu(t) \quad (6.55)$$

$J_{\nu\mu}$  (Eq. 6.55) is positive if there is a net flux from state  $\mu$  to state  $\nu$ . This flux analysis allows deduction of the reaction mechanism from even very complex reaction schemes (Becker et al. 2007).

In cases where the number of possible microstates is too large, the differential equation can not be solved analytically. Thus, approximations and simulations need to be applied. One attractive simulation is a dynamic Monte Carlo simulation scheme (Gillespie 2001; Till et al. 2008), which allows the simulation of very complex reaction mechanisms such as proton transfer through a protein matrix. Again, the reaction parameter can be obtained using simple approximations such as continuum electrostatics. Each simulation describes one particular reaction path through the possible states of the system. A reaction mechanism can then be inferred from the analysis of many such trajectories. Up to now, this method was only applied to relatively simple systems (Till et al. 2008). However, future application to enzymes which involve chemical transformation, proton and electron transfer, as well as conformational changes, seems possible and is a promising future road for analyzing enzyme functions.

### C. Electron Transfer from the C-Subunit of the Photosynthetic Reaction Center to the Special Pair

The microstate model described above has been used to simulate the kinetics of electron transfer between the tetraheme-subunit and the special pair of the photosynthetic reaction center of *Blastochloris viridis* (Becker et al. 2007; Bombarda and Ullmann 2011). The comparison with the experimental data (Ortega and Mathis 1993) shows that continuum electrostatic calculations can be used in combination with the empirical rate law of Eq. 6.12 to reproduce measurements on the re-reduction kinetics of the photo-oxidized special pair (SP) in the bacterial photosynthetic reaction center.

Re-reduction of the SP in *B. viridis* is facilitated by the cytochrome C-subunit

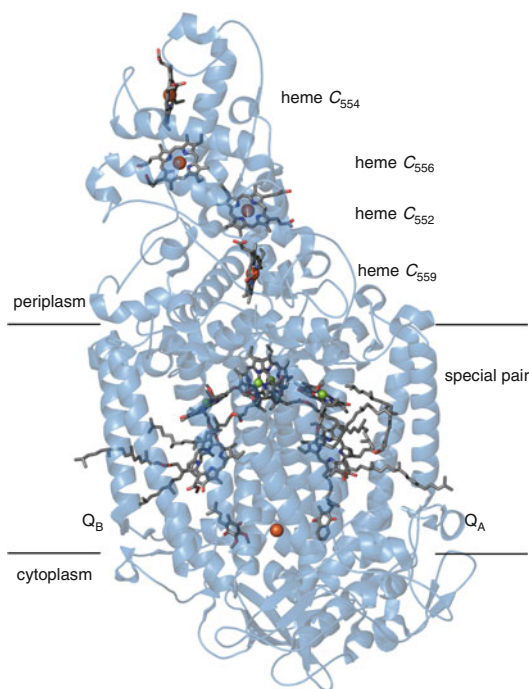


Fig. 6.10. Photosynthetic reaction center from *B. viridis*. In addition to the special pair, the accessory chlorophylls, the pheophytins and the quinones, this reaction center possesses four heme groups that re-reduce the special pair after photooxidation. The re-reduction kinetics of this protein has been well investigated experimentally.

(Fig. 6.10). The C-subunit, contains four heme cofactors forming a transfer chain. The heme groups are commonly labeled according to their absorbance maxima (subscripts) as heme  $c_{559}$ , heme  $c_{552}$ , heme  $c_{556}$  and heme  $c_{554}$ . To simulate electron transfer within the C-subunit and between the C-subunit and the SP, a model was constructed consisting of the five redox-active groups. Redox potentials of these groups and interaction energies for pairs of these groups were calculated using the model with pure electrostatic interaction. In addition, the available structural information was used to calculate reorganization energies for all different pairs of redox-active groups (Becker et al. 2007; Bombarda and Ullmann 2011).

In the experimental studies, Ortega et al. (1993) exposed the reaction center of *B. viridis* to different redox-potentials. The system was prepared experimentally in charge configurations with 4, 3 and 2 electrons distributed over the system consisting of the four hemes and the SP. The re-reduction kinetics of the SP was measured after photo-induced oxidation. These experimental setups can be mimicked by simulations. To illustrate the kinetics seen in such simulations, the result obtained for a system starting from 3 electrons distributed over the four heme groups is shown in Fig. 6.11. In Fig. 6.11a, the time-dependent probability distribution of the accessible microstates is shown. The corresponding oxidation probabilities for the hemes and the SP are shown in Fig. 6.11b. It can be seen that only a limited number of microstates contribute significantly to the probability distribution in the pico- to microsecond time domain. However, this feature does not imply that only this limited number of microstates is important for the kinetics of the system. The detailed information available from the simulation data allows to track the electron fluxes between microstates and thus electron movements between individual sites in a reaction scheme (Fig. 6.12).

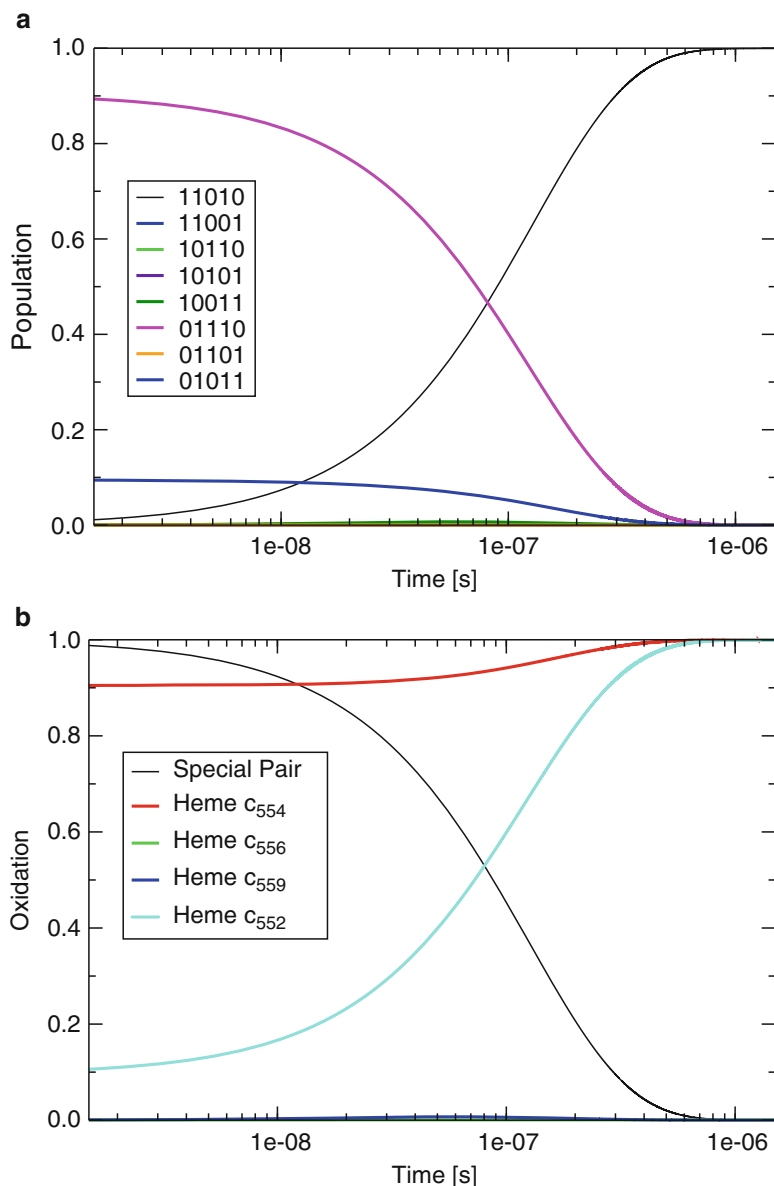
The redox microstates can be denoted as vectors of 1 (reduced sites) and 0 (oxidized

sites). The first element denotes the redox state of the special pair, the next four elements denote redox states of the hemes in the order of their distance to the SP, starting from the nearest. The kinetics depicted in Fig. 6.11 suggests a rather simple picture for the time dependence of the population of accessible microstates. Starting from a population of the two microstates (0,1,1,1,0) (90%) and (0,1,0,1,1) (10%) after photooxidation, the system relaxes towards an equilibrium distribution which is mainly given by one microstate (1,1,0,1,0). However, the underlying transfer dynamics of the system as depicted in Fig. 6.12 is considerably more complex. The highly populated initial state (0,1,1,1,0) can rapidly decay into the final state via just one intermediate, (1,0,1,1,0). In contrast, the initial state (0,1,0,1,1) has to relax towards the final state via a succession of several intermediates. These intermediate states are only transiently populated. Each flux into one of the intermediates is accompanied by an equally high flux out of these intermediates. For example, the transition from the initial state to the intermediate (1,0,0,1,1) is rapidly followed by a transition to a second intermediate state (1,0,1,0,1). This intermediate state in turn either decays into state (1,0,1,1,0) via an electron transfer from heme  $c_{554}$  to heme  $c_{556}$ , or alternatively to state (1,1,0,0,1) via electron transfer from heme  $c_{552}$  to heme  $c_{559}$ .

The procedure outlined here can also be applied to proton transfer reactions. Thus, the strategy to combine continuum electrostatics with the master equation represents an important method to understand the mechanism of complex charge transfer systems.

## V. Conclusions

In this article, we reviewed how our understanding of the electron transfer in proteins on the basis of Marcus theory can help to analyze the mechanism of complex protein machines that can couple redox reactions to proton transfer reactions. Even the effect of membrane potentials and transmembrane



*Fig. 6.11.* Simulation of the re-reduction kinetics of the special pair of the photosynthetic reaction center in a system with three electrons. **(a)** The time-dependent probability distribution of microstates after photo-oxidation of the SP. The state vector is given in the order (SP, heme  $c_{559}$ , heme  $c_{552}$ , heme  $c_{556}$ , heme  $c_{554}$ ). In the state vector, 1 denotes a reduced site and 0 an oxidized site. States that are not shown are not significantly populated. **(b)** Oxidation probabilities of the four hemes and the SP. Initially, three electrons are distributed over the four hemes.

concentration gradients can be included in the calculations. The theoretical basis of the analysis of complex protein machines is the microstate model. In this model, the protein is divided into several functional groups, which can be, for instance, redox-

active centers (like hemes or iron sulfur clusters), protonatable residues (like histidine or glutamate), or enzymatic active sites. The part of the protein that does not belong to a functional group is considered a background that interacts with the functional groups.

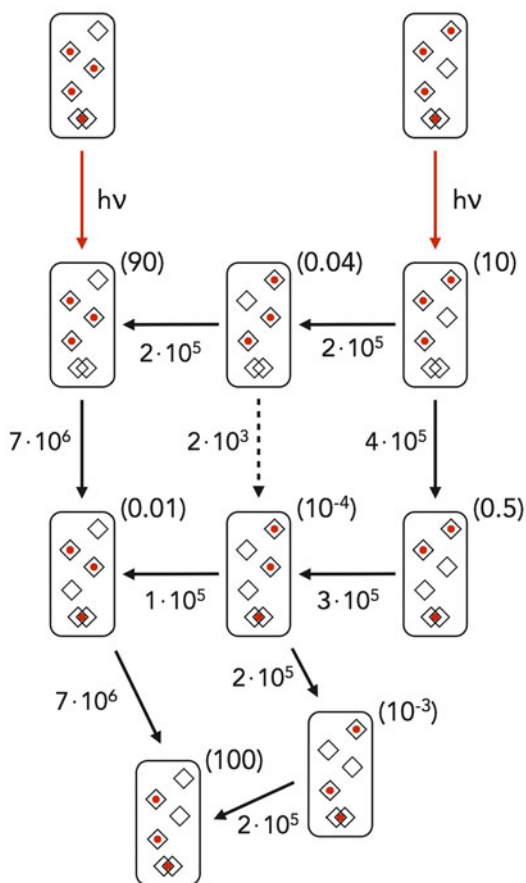


Fig. 6.12. Reaction scheme for the rereduction kinetics of the special pair of the photosynthetic reaction center in a system with three electrons. The reaction scheme is deduced from the flux analysis. Each *rectangle* represents a microstate of the photosynthetic reaction center, the *rhombi* inside the *rectangle* represent the hemes (the order top to bottom: heme  $c_{554}$ , heme  $c_{556}$ , heme  $c_{552}$ , heme  $c_{559}$ ), the overlapping *rhombi* represent the special pair. The reduced state of the cofactors is indicated by a *red sphere*. After photooxidation of the special pair (*red arrows*), several electron transfer reactions lead to the new equilibrium. The microstates representing the starting and the final configurations of the system in the simulation are depicted in the top and the bottom row, respectively. The values in parentheses denote the maximal probability observed during the simulation. Only fluxes (in  $s^{-1}$ ) contributing significantly are indicated by *arrows* and their maximum value is given.

The state of the protein is characterized by defining the state of each functional group (for instance redox state or protonation state). In this picture, a protein with  $N$  sites has many states (precisely  $\prod_{i=1}^N s_i$ , where  $s_i$  is the number of states of site  $i$ ). The energy of a particular state is defined by the sum of the energies of each particular site and the interactions between the sites. In this energy sum, the interaction with membrane potentials or other external fields can also be included.

Thermodynamic properties can be calculated by averaging over all possible states of the systems using statistical thermodynamics. If the system has so many states that explicit averaging is not possible, Metropolis Monte Carlo can be applied. To simulate the kinetic behavior of the protein, a master equation including all transitions between the states can be used. A flux analysis can help to extract mechanistic information from the simulation.

The microstate model is fairly general and does not rely on any particular way by which the state energies or the transition rate constants are calculated. In this article, we showed that the use of continuum electrostatic theory on the basis of the Poisson-Boltzmann equation is particularly useful, since, even for very large systems, the calculations are still tractable and lead to biophysically and biochemically meaningful results. The energies and rate constants of the microstate model could also be calculated with more accurate methods. However, it is important to realize that proteins that contain many cofactors cannot be regarded as a sum of these cofactors. Instead such proteins can exist in many states. Which states are functionally important, for instance, in catalytic cycles can be revealed by the analysis described in this article. We are convinced that the methods described here will allow analysis of many complex enzymatic reactions.

## Acknowledgements

This work was supported by the DFG RTG 1640 (Photophysics of Synthetic and Biological Multichromophoric Systems) and by the DFG Grant BO 3578/1.

## References

- Banerjee R (2008) Redox biochemistry. Wiley, Hoboken
- Bashford D, Karplus M (1990)  $pK_a$ s of ionizable groups in proteins: atomic detail from a continuum electrostatic model. *Biochemistry* 29:10219–10225
- Becker T, Ullmann RT, Ullmann GM (2007) Simulation of the electron transfer between the tetraheme-subunit and the special pair of the photosynthetic reaction center using a microstate description. *J Phys Chem B* 111:2957–2968
- Beroza P, Fredkin DR, Okamura MY, Feher G (1991) Protonation of interacting residues in a protein by a Monte Carlo method: application to lysozyme and the photosynthetic reaction center. *Proc Natl Acad Sci USA* 88:5804–5808
- Beveridge DL, DiCapua FM (1989) Free energy via molecular simulation: applications to chemical and biomolecular systems. *Ann Rev Biophys Biochem* 18:431–492
- Bombarda E, Ullmann GM (2011) Continuum electrostatic investigations of charge transfer processes in biological molecules using a microstate description. *Faraday Discuss* 148:173–193
- Bombarda E, Becker T, Ullmann GM (2006) The influence of the membrane potential on the protonation of bacteriorhodopsin: insights from electrostatic calculations into the regulation of proton pumping. *J Am Chem Soc* 128:12129–12139
- Born M (1920) Volumen und Hydratationswärme der Ionen. *Z Physik* 1:45–48
- Calimet N, Ullmann GM (2004) The influence of a transmembrane pH gradient on protonation probabilities of bacteriorhodopsin: the structural basis of the back-pressure effect. *J Mol Biol* 339:571–589
- Connolly M (1983) Solvent-accessible surfaces of proteins and nucleic acids. *Science* 221:709–713
- Cramer WA, Knaff DB (1991) Energy transduction in biological membranes. Springer, New York
- Crofts AR, Rose S (2007) Marcus treatment of endergonic reactions: a commentary. *Biochim Biophys Acta* 1767:1228–1232
- Crofts AR (2004) The cytochrome bc1 complex: function in the context of structure. *Ann Rev Physiol* 66:689–733
- da Silva JF, Williams R (2001) The biological chemistry of the elements – the inorganic chemistry of life. Oxford University Press, New York
- Davidson VL (2007) Protein-derived cofactors. Expanding the scope of post-translational modifications. *Biochemistry* 46:5283–5292
- Deponce M (2013) Glutathione catalysis and the reaction mechanisms of glutathione-dependent enzymes. *Biochim Biophys Acta* 1830:3217–3266
- Ferreira A, Bashford D (2006) Model for proton transport coupled to protein conformational change: application to proton pumping in the bacteriorhodopsin photocycle. *J Am Chem Soc* 128:16778–16790
- Gamow G (1928) Zur Quantentheorie des Atomkernes. *Z Physik* 51:204–212
- Gillespie DT (2001) Approximate accelerated stochastic simulation of chemically reacting systems. *J Chem Phys* 115:1716–1733
- Gray HB, Winkler JR (1996) Electron transfer in proteins. *Annu Rev Biochem* 65:537–561
- Gray HB, Winkler JR (2005) Long-range electron transfer. *Proc Natl Acad Sci USA* 102:3534–3539
- Gunner MR, Mao J, Song Y, Kim J (2006) Factors influencing the energetics of electron and proton transfers in proteins. What can be learned from calculations. *Biochim Biophys Acta* 1757:942–968
- Honig B, Nicholls A (1995) Classical electrostatics in biology and chemistry. *Science* 268:1144–1149



- Logan BE (2008) Microbial fuel cells. Wiley, Hoboken
- Marcus RA, Sutin N (1985) Electron transfer in chemistry and biology. *Biochim Biophys Acta* 811:265–322
- Marcus RA (1956) On the theory of oxidation-reduction reactions involving electron transfer. *J Chem Phys* 24:966–978
- Martin W, Baross J, Kelley D, Russell MJ (2008) Hydrothermal vents and the origin of life. *Nat Rev Microbiol* 6:805–814
- Mitchell P (1961) Coupling of phosphorylation to electron and hydrogen transfer by a chemi-osmotic type of mechanism. *Nature* 191:144–148
- Mitchell P (1976) Possible molecular mechanisms of the protonmotive function of cytochrome systems. *J Theor Biol* 62:327–367
- Moser CC, Keske JM, Warneke K, Farid RS, Dutton PL (1992) Nature of biological electron transfer. *Nature* 355:796–802
- Muegge I, Qi PX, Wand AJ, Chu ZT, Warshel A (1997) The reorganization energy of cytochrome *c* revisited. *J Phys Chem B* 101:825–836
- Nicholls DG, Ferguson S (2013) Bioenergetics, 4th edn. Elsevier, Amsterdam
- Nielsen JE, McCammon JA (2003) Calculating pKa values in enzyme active sites. *Protein Sci* 12:1894–1901
- Olsson MHM, Ryde U, Roos BO (1998) Quantum chemical calculation of the reorganization energy of blue copper proteins. *Prot Sci* 81:6554–6558
- Onufriev A, Case DA, Ullmann GM (2001) A novel view on the pH titration of biomolecules. *Biochemistry* 40:3413–3419
- Ortega JM, Mathis P (1993) Electron transfer from the tetraheme cytochrome to the special pair in isolated reaction centers of *Rhodospseudomonas viridis*. *Biochemistry* 32:1141–1151
- Page CC, Moser CC, Chen X, Dutton PL (1999) Natural engineering principles of electron tunneling in biological oxidation-reduction. *Nature* 402:47–52
- Pedersen A, Karlsson GB, Rydström J (2008) Proton-translocating transhydrogenase: an update of unsolved and controversial issues. *J Bioenerg Biomemb* 40:463–473
- Roux B (1997) The influence of the membrane potential on the free energy of an intrinsic protein. *Biophys J* 73:2981–2989
- Ryde U, Olsson MHM (2001) Structure, strain and reorganization energy of blue copper models in the protein. *Int J Quant Chem* 81:335–347
- Sharp KE (1998) Calculation of electron transfer reorganization energies using the finite difference poisson-Boltzmann model. *Biophys J* 73:1241–1250
- Stubbe J, van der Donk WA (1998) Protein radicals in enzyme catalysis. *Chem Rev* 98:705–776
- Stuchebrukhov A (2003) Long-distance electron tunneling in proteins. *Theor Chem Acc* 110:314–344
- Till MS, Becker T, Essigke T, Ullmann GM (2008) Simulating the proton transfer in Gramicidin A by a sequential dynamical Monte Carlo method. *J Phys Chem B* 112:13401–13410
- Ullmann GM, Bombarda E (2013) pK(a) values and redox potentials of proteins. What do they mean? *Biol Chem* 394:611–619
- Ullmann GM, Knapp EW (1999) Electrostatic computations of protonation and redox equilibria in proteins. *Eur Biophys J* 28:533–551
- Ullmann GM, Kostić NM (1995) Electron-tunneling paths in various electrostatic complexes between cytochrome *c* and plastocyanin. Anisotropy of the copper-ligand interactions and dependence of the iron-copper electronic coupling on the metalloprotein orientation. *J Am Chem Soc* 117:4766–4774
- Ullmann RT, Ullmann GM (2012) GMCT: a Monte Carlo simulation package for macromolecular receptors. *J Comput Chem* 33:887–900
- Ullmann GM, Kloppmann E, Essigke T, Krammer EM, Klingens AR, Becker T, Bombarda E (2008) Investigating the mechanisms of photosynthetic proteins using continuum electrostatics. *Photosynth Res* 97:33–53
- Ullmann GM (2000) The coupling of protonation and reduction in proteins with multiple redox centers: theory, computational method, and application to cytochrome *c*<sub>3</sub>. *J Phys Chem B* 104:6293–6301
- Ullmann GM (2003) Relations between protonation constants and titration curves in polyprotic acids: a critical view. *J Phys Chem B* 107:6293–6301
- Warren JJ, Winkler JR, Gray HB (2012) Redox properties of tyrosine and related molecules. *FEBS Lett* 586:596–602
- Warwicker J, Watson HC (1982) Calculation of the electrostatic potential in the active site cleft due to the  $\alpha$ -helix dipoles. *J Mol Biol* 186:671–679
- Wessjohann LA, Schneider A, Abbas M, Brandt W (2007) Selenium in chemistry and biochemistry in comparison to sulfur. *Biol Chem* 388:997–1006
- Wilson GS (1983) Electrochemical studies of porphyrin redox reactions as cytochrome models. *Bioelectrochem Bioenerg* 1:172–179
- Woycechowsky K, Raines R (2000) Native disulfide bond formation in proteins. *Curr Opin Chem Biol* 4:533–539

- You T, Bashford D (1995) Conformation and hydrogen ion titration of proteins: a continuum electrostatic model with conformational flexibility. *Biophys J* 69:1721–1733
- Zhang Z, Huang L, Shulmeister VM, Chi YI, Kim KK, Hung LW, Crofts AR, Berry EA, Kim SH (1998) Electron transfer by domain movement in cytochrome bc<sub>1</sub>. *Nature* 392:677–684
- Zheng Z, Gunner MR (2009) Analysis of the electrochemistry of hemes with E(m)s spanning 800 mV. *Proteins* 75:719–734
- Zhou M, Wang H, Hassett DJ, Gu T (2013) Recent advances in microbial fuel cells (MFCs) and microbial electrolysis cells (MECs) for wastewater treatment, bioenergy and bioproducts. *J Chem Tech Biotech* 88:508–518

# Part III

## **Molecular Structures and Functions of Cytochrome Complexes**

- A. Photosynthetic Reaction Centers and Linked Cytochromes (Chapters 7 and 8)
- B. Structure-Function of the Cytochrome  $bc_1$   $b_6f$  Complexes (Chapters 9, 10, 11, 12, 13, 14 and 15)
- C. Cytochrome Oxidases (Chapters 16, 17, 18 and 19)

# Chapter 7

## Higher Plant and Cyanobacterial Photosystem I: Connected Cytochrome Pathways

Yuval Mazor and Nathan Nelson\*

*Department of Biochemistry, and Molecular Biology,  
Tel Aviv University, Ramat Aviv, Tel Aviv 6997801, Israel*

Summary.....	131
I. Introduction.....	132
II. Cytochrome <i>bc</i> Complex and Its Central Role in Photosynthetic and Respiratory Electron Transport Chains.....	132
III. Oceanic Photosynthesis.....	133
IV. Interactions Between Photosystem I and Small Electron Donors.....	134
V. Phage Encoded PSI Complex.....	139
References.....	140

### Summary

Oxygenic photosynthesis is the principal converter of sunlight into chemical energy on earth. The conversion of solar energy is catalyzed by four multi-subunit membrane protein complexes: photosystem I (PSI), photosystem II (PSII), the cytochrome *b6-f* complex (*cytb<sub>6</sub>f*) and ATP-synthase ( $F_0F_1$ ). These protein complexes are connected by soluble electron carriers that are vital not only for the proper function of ATP and NADPH production but also to render the system highly efficient in different organisms and various environments, some of which are quite harsh. While the main fabric of the membrane complexes is highly conserved, their surfaces and interaction with the soluble factors provide the specificity and fine regulation of the operating system. One of the prime examples for this phenomenon is the cyanobacterial photosynthetic electron transport chain that is situated alongside with respiratory complexes, yet it stays unique by virtue of the interacting soluble components. Cyanobacteria contain many different cytochromes that potentially can donate electrons to both PSI and cytochrome oxidase, yet the two systems can operate separately in a synchronous mode. The crystal structure determination of photosynthetic and respiratory protein complexes shed light on the various partial reactions and explains how they can function alongside each other.

---

\*Author for correspondence, e-mail: [nelson@post.tau.ac.il](mailto:nelson@post.tau.ac.il)

## I. Introduction

Over 3 billion years ago our planet was under anaerobic conditions and most of the elements were present in their reduced-valence states (Barber 2008; Nelson 2011). Thus, the atmosphere was rich in nitrogen in the form of ammonia (NH<sub>3</sub>) or N<sub>2</sub>, carbon as CO or CO<sub>2</sub>, and oxygen as H<sub>2</sub>O (Bendall et al. 2008), and the Earth's surface was covered by water that contained not only minerals but also organic molecules. Porphyrins may have been one of the earliest complex organic molecules present on earth. Porphyrins can be synthesized abiotically in a primordial soup Urey-Miller type experiments (Szutka 1966), and can bind a wide variety of metal ions over a range of oxidation states. The biosynthetic pathways leading to chlorophylls and cytochromes are still connected, stemming from a common precursor, 5-aminolevulinic acid (ALA) (Smith and Witty 2002).

In spite of their common evolutionary origin, presently hemes and chlorophylls serve very different functions. Chlorophylls, by far the most abundant porphyrins in nature, serve mainly as light harvesting pigments, while heme-containing cytochromes participate in electron transfer reactions. Of course, within all photosynthetic reaction centers, special chlorophylls participate in very fast charge separation and electron transfer reactions as well.

The hallmark of oxygenic photosynthesis is the coupling of two unique reaction centers within the same membrane system. In spite of the fact that oxygenic photosynthesis evolved early in the evolution of the biosphere, approximately 3 billion years ago, today we can still point to cyanobacteria as the evolutionary ancestors of all known oxygenic photosynthetic membrane systems. The link between the two photosystems is

mainly provided by the cytochrome *b<sub>6</sub>f* and the small soluble Cyt *c<sub>6</sub>* or Pc proteins.

## II. Cytochrome *bc* Complex and Its Central Role in Photosynthetic and Respiratory Electron Transport Chains

The cytochrome *bc* complex that operates at mild redox potentials has homologs in most photosynthetic and respiratory electron transport chains. Initial biochemical studies have determined the composition of the mitochondrial *bc<sub>1</sub>* complex that contains two heme *b*, one heme *c* and a non-heme iron cluster. Preparation of isolated complex contained all those factors and was shown to function in a quinone-cytochrome *c* oxydoreduction reaction (Hurt and Hauska 1981). The use of detergents for solubilizing membranes was introduced and the isolation of functional cytochrome *bc<sub>1</sub>* complex was aided by the strong spectroscopic background of scientists in the area of bioenergetics (Rieske et al. 1964; Chance et al. 1967; Fan and Cramer 1970). The study of cytochrome *b<sub>6</sub>f* complex of oxygenic photosynthesis was hampered by the fact that the same detergents used in mitochondria were useless for photosynthetic membranes and the spectroscopic studies were hampered by the high absorbance of the numerous pigments, especially chlorophylls, present in photosynthetic membranes. Eventually cytochrome *b<sub>6</sub>f* complex was isolated and was shown to be spectroscopically highly similar to its mitochondrial counterpart (Fan and Cramer 1970; Nelson and Neumann 1972). Albeit the two are quite similar, the main difference was the electron acceptor of the complex that is cytochrome *c* in mitochondria and plastocyanin in chloroplasts (Hauska et al. 1971). Those two soluble factors totally differentiated between the two systems. In any case, in plants the two systems are distinguished by the two separate compartments that are separated by 1.5 billion years of evolution

---

*Abbreviations:* ALA – 5-aminolevulinic acid; Cyt *c<sub>6</sub>* – Cytochrome C6; Fd – Ferredoxin; NDH1 – NADH:ubiquinone oxidoreductase I; Pc – Plastocyanin; PSI – Photosystem I; PSII – Photosystem II; PTOX – Plastoquinol terminal

(Hauska et al. 1971). Cyanobacteria went against this dogma by having the two reactions in similar compartments and using soluble cytochromes for both photosynthesis and respiration. Thus the fine tuning of respiratory and photosynthetic electron transport activity required a richer gallery of soluble c-type cytochromes.

The existence of respiratory complexes in the thylakoid membranes of both cyanobacteria and plants has been known for quite some time. Cyanobacteria in particular contain what appears to be a complete respiratory chain in their thylakoid membrane (Pesceck et al. 2004). The electron flow rate through this chain is much lower (1–5 %) than the rate of the photosynthetic electron transport. However, under particular physiological conditions, prolonged dark growth or in various stress conditions, this rate can increase substantially (Molitor et al. 1986; Pesceck et al. 2004). Plants and algae contain NDH1, the complex I equivalent of photosynthesis. The function of respiratory electron chains in the thylakoid membranes of cyanobacteria is usually associated with various forms of cyclic electron flow, mostly revolving around the NDH1 complex (Battchikova et al. 2010).

### III. Oceanic Photosynthesis

Earth's oceans contribute 50 % of the global photosynthetic activity to our biosphere. The majority of this contribution is carried out by microorganisms, either cyanobacteria or algae. Here we will focus on oceanic cyanobacteria. The global oceanic population of cyanobacteria is mostly made up of two very similar genera, the *Prochlorococcus* and *Synechococcus*. *Synechococcus* dominate in nutrient rich waters close to coastal areas while *Prochlorococcus* dominates the vast, oligotrophic regions that encompass most of the ocean (Partensky et al. 1999; Scanlan et al. 2009). These bacteria can reach significant densities (up to  $10^5$  cells/ml in certain depths) in spite of the inhospitable nature of their environment

and can inhabit waters up to 200 m deep. The end result of these two facts is that an incredibly large population of these cyanobacteria exists globally ( $\sim 10^{27}$  cells) and this population makes a significant contribution to the Earth's oxygen and carbon cycle (Partensky et al. 1999). While *Prochlorococcus* and *Synechococcus* are quite similar, very significant differences exist between them. The most noticeable among them is the size, *Prochlorococcus* is the smallest known photosynthetic cell, the small size ( $\sim 0.6 \mu\text{m}$ ) is accompanied by the smallest genome ( $\sim 1.7$  Mbp) of any oxygenic photosynthesizer (Dufresne et al. 2003; Rocap et al. 2003; Partensky and Garczarek 2010). In addition, *Prochlorococcus* synthesizes unusual a- and b-type chlorophylls (Chisholm et al. 1992) and, in contrast, to most other cyanobacteria does not contain phycobilisomes but relies on membrane bound IsiA type antennas for both of its photosystems (Bibby et al. 2003). The antenna genes for *Prochlorococcus* evolved to accommodate the different light regimes (in both intensity and spectrum), and the full complexity of their interaction with the photosynthetic machinery is still not sufficiently explored (Garczarek et al. 2000). It is clear that *Prochlorococcus* contains interesting adaptations to its environment, thus enabling its success. Some of these adaptations can be found in its photosynthetic genes and they provide unique versions of the otherwise highly conserved photosynthetic complexes.

An important element within the environment of oceanic cyanobacteria are cyanophages. The phage population in the ocean outnumbers their hosts ten to one (Suttle 2007). This, together with the highly diverse nature of their genomes points to this population as a huge source for genetic innovation, which can flow into their host population. A particularly relevant example is the presence of photosynthetic genes in the genomes of a large fraction of the oceanic phages. The initial discovery was made in 2003 after the full sequence of one such virus revealed the presence of both D1 and D2 (the reaction

center polypeptides of photosystem II) in its genome (Mann et al. 2003). Since then, many experiments were done on phage-host interactions and on the phylogenetic relationships between viruses and between their photosynthetic genes. Several important facts rose from these studies. First, it was found that the viral D1 and D2 genes are expressed and translated by the cyanobacterium host (Lindell et al. 2005). Secondly, it became clear that certain phage families can infect both *Prochlorococcus* and *Synechococcus*, while other families have a narrow host range (Sullivan et al. 2003). Third, the viral D1 and D2 proteins are distinct from the host proteins (Zeidner et al. 2005). However, presently, there is no known instance where a phage mutation/variant is associated with a unique function (or dysfunction). In fact, due to the highly conserved nature of both D1 and D2, it is still not certain that the viral proteins can fully replace the host D1 and D2. Fourth, from sequence analysis it seems that the viral genes can recombine with host genes and thus increase the genetic variability of the D1 and D2 pool (Zeidner et al. 2005).

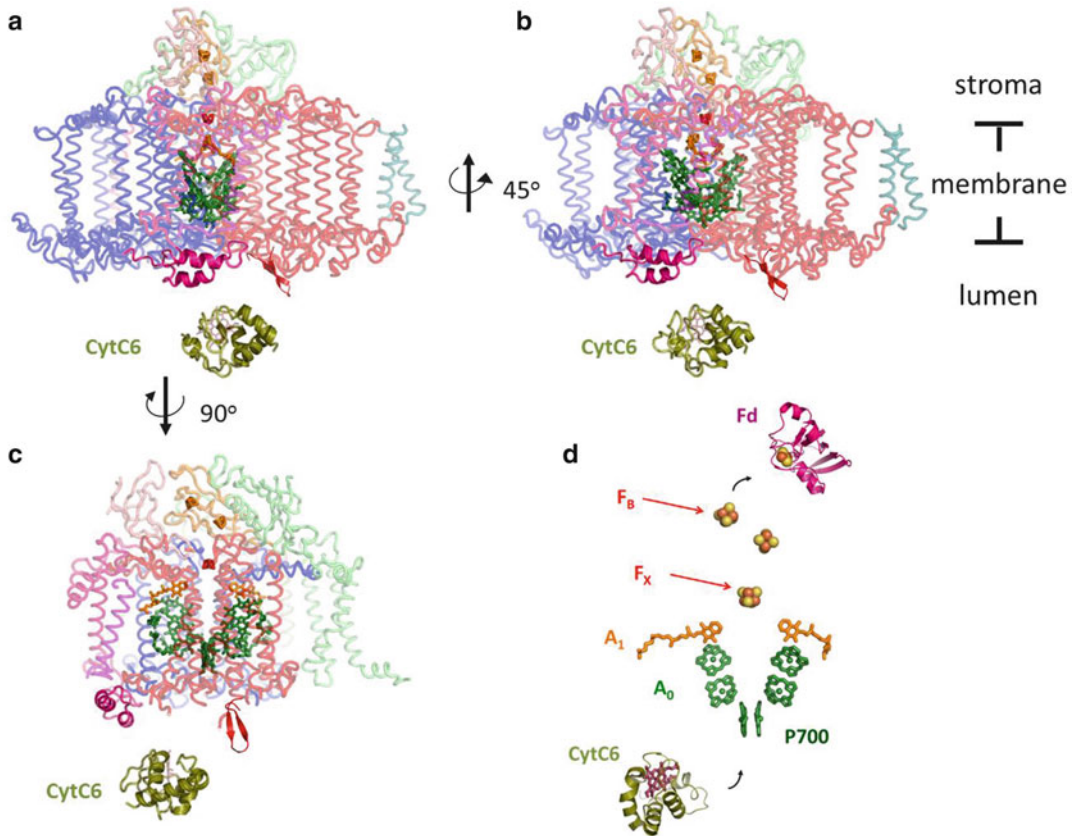
In the past decade genomic studies conducted in the ocean added large amounts of sequence information to the database (Rusch et al. 2007; Dinsdale et al. 2008). The improved sampling of the ocean's genetic landscape resulted in a much richer picture of the gene content of phages and expanded their putative interaction with the host photosynthetic and respiratory electron transport chains well beyond the initial observation. The current list of phage-encoded photosynthesis-related genes includes D1 and D2, plastoquinol terminal oxidase (PTOX), Ferredoxin (Fd), Plastocyanin, some NDHI, and FoF1 subunits, and an entire PSI operon which will be presented in depth in the following sections of this chapter (Sullivan et al. 2006; Sharon et al. 2009, 2011; Mazor et al. 2014). Initially, the rationale employed to explain the role of viral photosystem II subunits was focused on the short half-life of D1, making it the most vulnerable point of the photosynthetic electron transport chain

during phage infection (since phage proteins are transcribed and translated preferentially during infection). This line of thinking is definitely valid for Photosystem II. However, most of the other virally encoded photosynthetic chain members are not particularly short-lived in known photosynthetic model organisms. An additional explanation for the function of the photosynthetic phage-encoded proteins is that they induce an alternative cyclic flow of electrons in the photosynthetic electron transport chain. This is mainly based on the occurrence of the NDHI subunits and on the unusual composition and sequence of the virally encoded PSI operon (Sharon et al. 2009; Alperovitch-Lavy et al. 2011).

#### IV. Interactions Between Photosystem I and Small Electron Donors

Compared with the active sites of “simple”, single subunit enzymes, the large complexes, which participate in electron transfer reactions, contain extremely complicated active “sites”, usually spanning the entire membrane. In the case of Photosystem I, the active “site” can be thought of as a molecular wire selectively linking two poles across the membrane (Fig. 7.1). Charge separation originates at P700 or, according to more recent findings at the electron acceptor A0 (Muller et al. 2003), and then travels across several cofactors to finally reach  $F_B$ , the reducing terminus of PSI (Fig. 7.1). The oxidized P700<sup>+</sup> is reduced back by plastocyanin (Pc) or cytochrome c6 (Cyt c6).

A large body of work has accumulated on the interaction between Pc/Cyt c6 and PSI leading to the identification of the N-terminus of PsaF and a hydrophobic patch juxtaposition to P700 as the most important elements of this interaction (Farah et al. 1995; Sun et al. 1999; Sommer et al. 2002). One of the main differences between cyanobacteria and eukaryotes is their interaction with the small protein electron donor. In the eukaryotic system, a fast phase

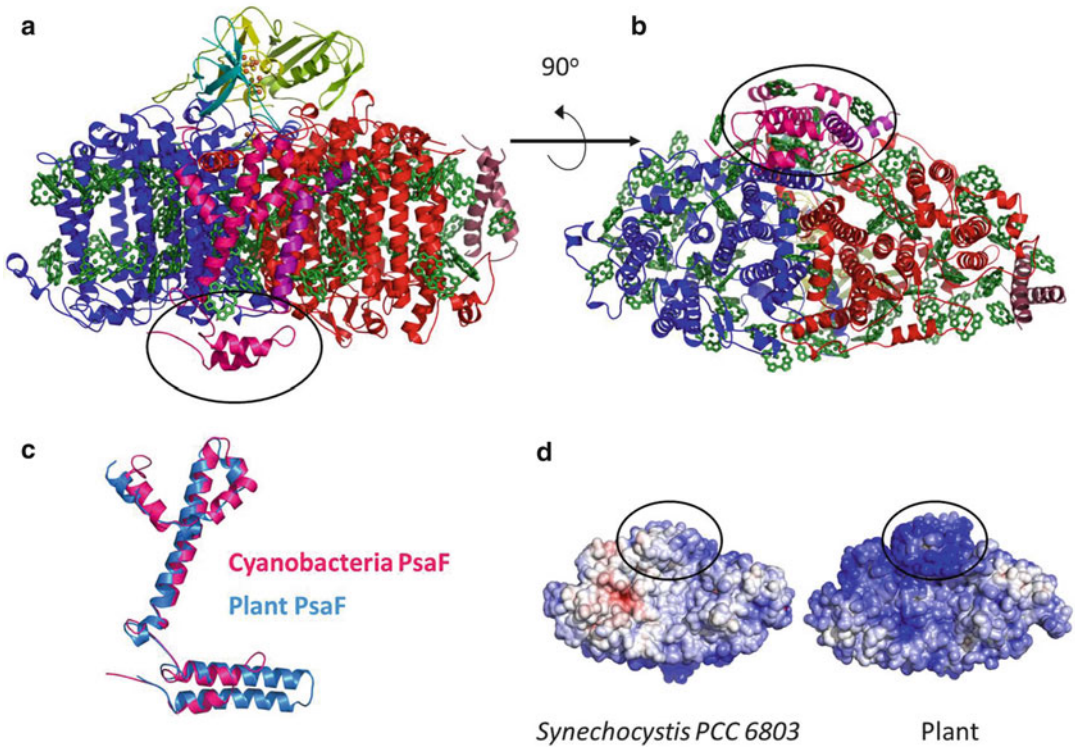


*Fig. 7.1.* Electron transport in PSI. Ribbon representation of photosystem I subunits. Only the central ligands, involved in electron transport are shown. PsaA is colored in red, PsaB in blue and PsaF in pink. The N-terminus of PsaF and the luminal loop of PsaA are shown as cartoons at the bottom of every complex to illustrate their potential in controlling the Cyt *c*<sub>6</sub> binding site. Cyt *c*<sub>6</sub> (colored in olive) was manually placed close to its binding site and its orientation does not reflect any experimental data. (a) and (b) side views of PSI from the membrane plane. (c) a 90° rotation compared to A. with a portion of PsaA removed to reveal the components of the ETC. (d) representation of the ETC in the same orientation as c, showing the flow of electrons from Cyt *c*<sub>6</sub> to Fd (PDB codes for PSI and Cyt *c*<sub>6</sub> are 1JB0 and 4EIC respectively).

( $t_{1/2}$ , several  $\mu$ s) in PSI reduction kinetics has been taken as the manifestation of a stable PSI-Pc complex (Bottin and Mathis 1985; Delosme 1991). In cyanobacteria, this PSI-Pc complex is not as common and several modes of interaction were observed, in line with the highly diverse nature of this group (Baymann et al. 2001; Hervas et al. 2005). However, there is evidence for a stable complex between PSI and Cyt *c*<sub>6</sub> in some cyanobacteria and a fast phase should not be taken as a strictly “eukaryotic” property (Baymann et al. 2001).

The key to the differences between cyanobacteria and eukaryotes can be found in two places. First, the N-terminus of PsaF has changed considerably in both structure and physical properties (Fig. 7.2) and secondly the small donors are very similar in eukaryotes while being very diverse in cyanobacteria (Table 7.1) (Jordan et al. 2001; Ben-Shem et al. 2003). The electrostatic differences between the cyanobacterial PSI and the eukaryotic one are shown in Fig. 7.2, in which the luminal face of PSI is colored according to electrostatic





**Fig. 7.2.** PsaF determines the shape and charge of the Pc/Cyt  $c_6$  binding surface in PSI. **(a)** PSI from *Synechocystis* is shown, in view parallel to the plane of the membrane, with chlorophylls represented as rings only, colored in *green*. **(b)** The luminal face of PSI with the N-terminus of PsaF encircled with a *black ellipse*. **(c)** The PsaF subunits of cyanobacteria (*pink*) and plant (*blue*), superimposed, showing the two helix extension in the eukaryotic PsaF subunit. **(d)** Electrostatic properties of the luminal surface of PSI showing the positive N-terminal domain in the eukaryotic complex. Electrostatic surfaces were calculated using the APBS plugin for Pymol (Baker et al. 2001), and colored *blue* for positive and *red* for negative. The LHC belt was omitted from the eukaryotic complex for ease of comparison (its occlusion did not affect the charge around the PsaF subunit). PDB id for cyanobacteria and plant PSI are 4KT0 and 3LW5.

potential. It is clear that a patch of positive charge, shielding a segment that is negatively charged, has been added in eukaryotes. This is accompanied by the extension of the two-helix domain of PsaF shown in Fig. 7.2. Cross linking experiments showed the Pc and Cyt  $c_6$  bind this positive patch directly in *Chlamydomonas* and higher plants (Wynn and Malkin 1988; Hippler et al. 1996) and that positively charged residues are important for binding (Hippler et al. 1998). In contrast to the clear findings in *Chlamydomonas*, PsaF mutants in *Synechocystis* show no obvious phenotype *in vivo* or *in vitro*

(Chitnis et al. 1991; Farah et al. 1995; Hippler et al. 1996; Mazor et al. 2014). The N-terminus of cyanobacterial PsaF still carries some positive charges and this together with highly acidic donors can lead to stable complex between PSI and its donor. This suggests that the evolution of reaction mechanisms in cyanobacteria mostly took place on the donor side of the two partners (Hervas et al. 2005).

The mechanism of interaction between PSI and Pc/CytC6 was explored in detail using mutants of each of the small donors. The results revealed two sites, one involved

Table 7.1. Calculated PI of Cyt  $c_6$ /Pc. PI values were calculated using the Compute pI/MW tool on ExpASY ([http://web.expasy.org/compute\\_pi/](http://web.expasy.org/compute_pi/)). Only completely sequenced organisms were used in the table, allowing us to reach a conclusion on the absence of Pc or Cyt  $c_6$ . Sequences were retrieved from multiple blast searches using various query sequences and aligned using MUSCLE to assign cytochrome type (Edgar 2004). Cyt  $c_{6A}$  sequences are highlighted in yellow, Cyt  $c_{6B-C}$  in purple and Cyt  $c_M$  in red.

Occurrence of small electron donors within photosynthetic organisms.

	CytC6			CytC <sub>M</sub>	Pc
<b>cyanobacteria</b>					
Synechocystis sp. PCC 6803	6.7			6.2	6.3
Prochlorococcus marinus str. MIT9202				5.8	
Prochlorococcus marinus str. CCMP1986				6.9	4.7
Prochlorococcus marinus str. MIT9215				5.4	4.7
Prochlorococcus marinus str. MIT9301		9.5		5.4	4.7
Prochlorococcus marinus str. MIT9211		7.8		6.1	5.0
Prochlorococcus marinus str. MIT9312		9.5		6.4	4.9
Prochlorococcus marinus str. NATL1A		8.3		5.3	4.9
Prochlorococcus marinus str. CCMP1375		9.2		4.9	5.0
Prochlorococcus marinus str. NATL2A		8.8		5.3	4.9
Prochlorococcus marinus str. MIT9303	5.0	8.8		6.0	4.5
Prochlorococcus marinus str. MIT9313	5.0	9.2		5.8	4.5
Synechococcus sp. BL107	4.5	6.0		4.9	4.7
Synechococcus sp. CB0101	5.4	6.1		8.6	no PC
Synechococcus sp. CC9311	4.9	5.7	5.9	8.6	4.9
Synechococcus sp. CC9605	4.8	6.1		4.9	5.4
Synechococcus sp. JA-3-3Ab	8.6			6.2	9.3
Synechococcus sp. RCC307	5.1	5.3		6.5	no PC
Synechococcus sp. RS9916	4.5	9.2	4.7	6.2	5.0
Synechococcus sp. WH5701	5.4	9.6		9.2	4.8
Synechococcus sp. WH7803	4.4	5.5	4.8	9.2	4.9
Synechococcus sp. WH8016	5.2	6.5	5.6	6.8	4.9
Synechococcus sp. WH8102	4.7	7.8		5.4	4.9
Synechococcus elongatus PCC 7942	6.0	9.1	9.8	7.8	5.5
Synechococcus sp. PCC 7335	4.9	9.6		no cM	6.7
Synechococcus sp. PCC 6312	6.5			7.9	5.7
Synechococcus sp. PCC 7002	6.5	9.3		7.8	no PC
Thermosynechococcus sp. BP-1	7.7			7.8	no PC
Anabaena variabilis ATCC 29413	6.1	9.4	9.3	7.8	9.1
Cyanothece sp. ATCC 51142	6.5	9.2		6.0	5.5
Cyanothece sp. PCC 7425	8.6	7.8		5.8	no PC
Gloeobacter violaceus PCC 7421	5.6	9.6		6.6	9.4
<b>red algae</b>					
Calliarthron tuberculosum	4.6				no PC
Chondrus crispus	4.9				no PC
Cyanidioschyzonmerolae	5.5				no PC
Nannochloropsis gaditana	4.7	9.9			no PC
Porphyra purpurea	4.8				no PC
<b>green algae</b>					
Chlamydomonas reinhardtii	8.7	7.7			6.3
Chlorella variabilis	5.7				4.2
Volvox carteri	9.1				5.6
Micromonas pusilla CCMP1545	9.1				5.5
<b>green plants</b>					
Theobroma Cacao	8.5				4.8
Vitis vinifera	8.2				5.3
Lotus japonicus	9.1				5.0
Medicago truncatula	8.2				5.0
ArabidopsisThaliana	5.1				5.7
Cicer arietinum	9.1				5.0
Cucumis sativus	8.5				4.9

in electrostatic interaction and one involved in hydrophobic interactions located on analogous patches on both proteins (De la Cerda et al. 1997, 1999). These results match the sites identified on PSI, creating a complementary fit (Hervas et al. 2003).

The calculated PI of a large number of small PSI electron donors from cyanobacteria, red and green algae and higher plants, with the purpose of illustrating the most common and divergent points in the architecture of the small electron donors, has been compiled (Table 7.1).

The most diverse group in this table is clearly cyanobacteria with many species containing multiple Cyt c<sub>6</sub> species, alongside with examples of complete loss of either Pc or Cyt c<sub>6</sub>.

Land plants contain a single Cyt c<sub>6</sub> like protein called Cyt c<sub>6A</sub>. The function of this cytochrome is still under debate. Initial claims to its involvement in photosynthetic electron transport proved to be wrong (Molina-Heredia et al. 2003; Weigel et al. 2003). Its relatively low Em (0.14 V) suggests that it cannot accept electrons from the b<sub>6</sub>f complex and its electron donation to PSI was shown to be negligible (Molina-Heredia et al. 2003). Cyt c<sub>6A</sub> contains a small insertion loop with an S-S bond and it was suggested that this S-S bond may play a role in oxidative stress resistance (Marcaida et al. 2006). Currently, the function of this cytochrome in plant and green algae is still not clear. During the evolution of land plants, the functional Cyt c<sub>6</sub> of green algae was therefore lost. The reasons for this loss are not entirely clear. Red algae, a diverse and successful group, appear to have gone the opposite way, losing Pc from their genomes (Table 7.1). It therefore seems unlikely that environmental stresses contributed to these loss events and we think that they simply represent random events fixed by evolution.

Pc and Cyt c<sub>6</sub> are interchangeable but cyanobacteria cannot survive without at least one of them (Duran et al. 2004). The relative levels of Pc and Cyt c<sub>6</sub> are affected by the iron and copper concentrations in some species. As can be seen in Table 7.1, Pc and

Cyt c<sub>6</sub> have a similar charge in *Synechocystis* PCC 6803. In the case of *Synechocystis* these values were determined experimentally and the values in the table are in reasonable agreement with experimentally determined values (~5.5 for Cyt c<sub>6</sub>, Cyt c<sub>M</sub> and Pc). The similar charge of Pc and Cyt c<sub>6</sub> is reflects their similar function. However, as more and more genomes are sequenced the full richness of the Cyt c<sub>6</sub> pool in photosynthetic organisms begins to be appreciated and opens possible routes to new functions.

Two new groups of c<sub>6</sub> type cytochromes were found, Cyt c<sub>6B</sub> and Cyt c<sub>6C</sub> (Bialek et al. 2008). These two groups are colored separately in Table 7.1 and we have somewhat expanded the analysis to include additional sequences (Bialek et al. 2008). The differences between Cyt c<sub>6</sub> and c<sub>6B-C</sub> were shown to be highly significant. The PI of the Cyt c<sub>6B</sub> from *Synechococcus* sp. PCC 7002 is basic at around 9 and its Em (~0.15 V) is significantly lower than that of Cyt c<sub>6</sub> (which is around 0.35 V) (Bialek et al. 2008). The heme pockets of Cyt c<sub>6A-C</sub> are related and this is the reason for their low and similar Em values (Worrall et al. 2007; Zatwarnicki et al. 2013). As with Cyt c<sub>6A</sub>, it is not likely that Cyt c<sub>6B</sub> or Cyt c<sub>6C</sub> can receive electrons from the b<sub>6</sub>f complex and their involvement in photosynthetic electron transport remains to be determined.

Most of the Cyt c<sub>6B</sub> and Cyt c<sub>6C</sub> sequences are found in marine *Synechococcus* and *Prochlorococcus* (Table 7.1). In the case of *Prochlorococcus*, they are the only cytochromes present (with the exception of the MIT9313 and MIT9303 strains which are very similar to *Synechococcus*). If, indeed, they do not donate electrons to PSI then *Prochlorococcus* as a family seem to utilize only Pc in its photosynthetic electron transport chain, in line with the minimalist nature of these organisms, as exemplified in their minimalist genome.

Another cytochrome with a cryptic function is Cyt c<sub>M</sub>. This cytochrome was discovered well before the completion of the *Synechocystis* genome sequence (Malakhov et al. 1994). However, its function is still

unknown. Cyt  $c_M$  is present in virtually all cyanobacterial species and thus it probably carries some unique function (Bernroither et al. 2009). The  $E_m$  of Cyt  $c_M$  as measured for the *Synechocystis* protein is  $\sim 0.15$  V and so, like Cyt  $c_{6A-C}$ , it is not a good candidate for an electron acceptor from the  $b_6f$  complex (Cho et al. 2000; Molina-Heredia et al. 2002). The expression of Cyt  $c_M$  is induced under stress conditions and in vitro it can donate electrons to the terminal oxidase as efficiently as Cyt  $c_6/Pc$  (Malakhov et al. 1999; Bernroither et al. 2009).

To summarize, there is a large group of cytochrome  $c_6$ -like proteins. These proteins are probably imported into the luminal and periplasmic space of cyanobacteria. Their  $E_m$  prevents them from receiving electrons from the  $b_6f$  complex and their interaction with the PSI complex is less efficient than that of Cyt  $c_6/Pc$ . These cytochromes may transfer electrons from the PQ pool to any one of the terminal oxidases in cyanobacteria in times of stress, and may donate electrons to PSI under rare conditions. The nature of the electron donor to this cytochrome pool is still a mystery. This putative activity, which bypasses the  $b_6f$  complex, is probably transient in nature, stems from the PQ pool, and should be tightly controlled. As we discussed in the following section, some of this control may be found in the PSI complex.

## V. Phage Encoded PSI Complex

The GOS expedition and other initiatives dramatically increased the amount of sequence information available in the form of environmental samples. Searching these databases for PSI related sequences revealed a phage-encoded PSI operon (Sharon et al. 2009). The phage operon codes for PsaA, PsaB, PsaC, PsaD, PsaE, PsaJF and PsaK. The operon is unique in both its subunit composition and the sequence of some individual subunits. The presence of 7 subunits out of the known 11 or 12 PSI subunits in cyanobacteria is unusual. However the present subunits can form a fully functional, “minimal” complex,

which probably functions as a monomer in its host membrane (Mazor et al. 2012, 2014). Two noticeable alterations in the sequence of the phage PSI operon provide clues to its function.

The first is the fused PsaJF subunit, in which the PsaJ subunit is fused with a PsaF subunit, which lacks the entire N-terminal domain. As mentioned previously, the function of the cyanobacterial PsaF is not entirely clear as it was shown to be dispensable for  $Pc/Cyt\ c_6$  binding in vitro and in vivo. We proposed that deleting the N-terminus of PsaF will result in a promiscuous PSI complex, a complex that can accept electrons from a wide spectrum of donors. A phage mimetic complex constructed in *Synechocystis* proved to have faster reaction kinetics with a mammalian respiratory cytochrome (which is a very basic protein) when compared to the wild type PSI complex (Mazor et al. 2014).

In addition to the PsaJF subunit, which is only found in phages, the PsaA subunit is missing one of the most highly conserved loops in PSI (624–633 in the *Synechococcus elongatus* structure (Jordan et al. 2001)). This PSI deletion is present in all *Prochlorococcus* PsaA sequences (Mazor et al. 2012). The function of this loop has not been examined experimentally but its proximity to P700 and its high conservation from cyanobacteria to plants suggest that it plays a role in  $Pc/Cyt\ c_6$  binding.

The prevalence of Cyt  $c_6$ -like proteins in *Prochlorococcus* may be related to this alteration in PSI and indicates that the *Prochlorococcus* PSI is inherently promiscuous, also for example, accepting electrons from the Cyt  $c_{6B}$  proteins.

To summarize, cyclic electron flow around PSI affects both the bioenergetic efficiency of photosynthetic membranes and its production of toxic radicals. The existence of respiratory activities in the photosynthetic membranes is now a proven fact, but our knowledge of all of the relevant components and their interaction with the photosynthetic electron transport chain is still lacking. The new groups of cytochrome  $c_6$ -like proteins are

probably an important part of this story and future studies will surely reveal the pathways through which this pool receives and donates electrons *in vivo*. We suggest that some of the pathway insulation between photosynthesis and respiration is accomplished inherently by the PSI complex through the N-terminus of PsaF and through a lumen-extended loop in PsaA. Future genomics efforts will provide additional clues to the function of photosynthetic electron flow in the environment and these efforts must be accompanied by equally thorough experimental validation.

## References

- Alperovitch-Lavy A, Sharon I, Rohwer F, Aro EM, Glaser F, Milo R, Nelson N, Béjà O (2011) Reconstructing a puzzle: existence of cyanophages containing both photosystem-I and photosystem-II gene suites inferred from oceanic metagenomic datasets. *Environ Microbiol* 13:24–32
- Baker NA, Sept D, Joseph S, Holst MJ, McCammon JA (2001) Electrostatics of nanosystems: application to microtubules and the ribosome. *Proc Natl Acad Sci U S A* 98:10037–10041
- Barber J (2008) Photosynthetic generation of oxygen. *Philos Trans R Soc Lond Ser B Biol Sci* 363:2665–2674
- Battchikova N, Eisenhut M, Aro EM (2010) Cyanobacterial NDH-1 complexes: novel insights and remaining puzzles. *Biochim Biophys Acta* 1807:935–944
- Baymann F, Rappaport F, Joliot P, Kallas T (2001) Rapid electron transfer to photosystem I and unusual spectral features of cytochrome c6 in *Synechococcus* sp. PCC 7002 *in vivo*. *Biochemistry* 40:10570–10577
- Bendall DS, Howe CJ, Nisbet EG, Nisbet RE (2008) Photosynthetic and atmospheric evolution. Introduction. *Philos Trans R Soc Lond B Biol Sci* 363:2625–2628
- Ben-Shem A, Frolow F, Nelson N (2003) Crystal structure of plant photosystem I. *Nature* 426:630–635
- Bernroither M, Tangl D, Lucini C, Furtmüller PG, Peschek GA, Obinger C (2009) Cyanobacterial cytochrome c M: probing its role as electron donor for Cu A of cytochrome c oxidase. *Biochim Biophys Acta (BBA)-Bioenerg* 1787:135–143
- Bialek W, Nelson M, Tamiola K, Kallas T, Szczepaniak A (2008) Deeply branching c6-like cytochromes of cyanobacteria. *Biochemistry* 47:5515–5522
- Bibby TS, Mary I, Nield J, Partensky F, Barber J (2003) Low-light-adapted *Prochlorococcus* species possess specific antennae for each photosystem. *Nature* 424:1051–1054
- Bottin H, Mathis P (1985) Interaction of plastocyanin with the photosystem I reaction center: a kinetic study by flash absorption spectroscopy. *Biochemistry* 24:6453–6460
- Chance B, Lee CP, Mela L (1967) Control and conservation of energy in the cytochrome chain. *Fed Proc* 26:1341–1354
- Chisholm SW, Frankel SL, Goerick R, Olson RJ, Palenik B, Waterbury JB, West-Johnsrud L, Zettler ER (1992) *Prochlorococcus marinus* nov. gen. nov. sp.: a marine prokaryote containing divinylchlorophyll a and b. *Arch Microbiol* 157:297–300
- Chitnis PR, Purvis D, Nelson N (1991) Molecular cloning and targeted mutagenesis of the gene *psaF* encoding subunit III of photosystem I from the cyanobacterium *Synechocystis* sp. PCC 6803. *J Biol Chem* 266:20146–20151
- Cho YS, Pakrasi HB, Whitmarsh J (2000) Cytochrome cM from *synechocystis* 6803. Detection in cells, expression in *Escherichia coli*, purification and physical characterization. *Eur J Biochem* 267:1068–1074
- De la Cerda B, Navarro JA, Hervás M, De la Rosa MA (1997) Changes in the reaction mechanism of electron transfer from plastocyanin to photosystem I in the cyanobacterium *Synechocystis* sp. PCC 6803 as induced by site-directed mutagenesis of the copper protein. *Biochemistry* 36:10125–10130
- De la Cerda B, Diaz-Quintana A, Navarro JA, Hervás M, De la Rosa MA (1999) Site-directed mutagenesis of cytochrome c6 from *Synechocystis* sp. PCC 6803. The heme protein possesses a negatively charged area that may be isofunctional with the acidic patch of plastocyanin. *J Biol Chem* 274:13292–13297
- Delosme R (1991) Electron transfer from cytochrome f to photosystem I in green algae. *Photosynth Res* 29:45–54
- Dinsdale EA, Edwards RA, Hall D, Angly F, Breitbart M, Brulc JM, Furlan M, . . . , Rohwer F (2008) Functional metagenomic profiling of nine biomes. *Nature* 452:629–632
- Dufresne A, Salanoubat M, Partensky F, Artiguenave F, Axmann IM, Barbe V, Duprat S, . . . , Hess WR (2003) Genome sequence of the cyanobacterium *Prochlorococcus marinus* SS120, a nearly minimal oxyphototrophic genome. *Proc Natl Acad Sci U S A* 100:10020–10025
- Duran RV, Hervás M, De La Rosa MA, Navarro JA (2004) The efficient functioning of photosynthesis and respiration in *Synechocystis* sp. PCC 6803 strictly requires the presence of either cytochrome c6 or plastocyanin. *J Biol Chem* 279:7229–7233

- Edgar RC (2004) MUSCLE: multiple sequence alignment with high accuracy and high throughput. *Nucleic Acids Res* 32:1792–1797
- Fan HN, Cramer WA (1970) The redox potential of cytochromes b-559 and b-563 in spinach chloroplasts. *Biochim Biophys Acta* 216:200–207
- Farah J, Rappaport F, Choquet Y, Joliot P, Rochaix JD (1995) Isolation of a psaF-deficient mutant of *Chlamydomonas reinhardtii*: efficient interaction of plastocyanin with the photosystem I reaction center is mediated by the PsaF subunit. *EMBO J* 14:4976–4984
- Garczarek L, Hess WR, Holtzendorff J, van der Staay GW, Partensky F (2000) Multiplication of antenna genes as a major adaptation to low light in a marine prokaryote. *Proc Natl Acad Sci U S A* 97:4098–4101
- Hauska GA, McCarty RE, Berzborn RJ, Racker E (1971) Partial resolution of the enzymes catalyzing photophosphorylation. VII. The function of plastocyanin and its interaction with a specific antibody. *J Biol Chem* 246:3524–3531
- Hervas M, Navarro JA, De La Rosa MA (2003) Electron transfer between membrane complexes and soluble proteins in photosynthesis. *Acc Chem Res* 36:798–805
- Hervas M, Diaz-Quintana A, Kerfeld CA, Krogmann DW, De la Rosa MA, Navarro JA (2005) Cyanobacterial Photosystem I lacks specificity in its interaction with cytochrome c(6) electron donors. *Photosynth Res* 83:329–333
- Hippler M, Reichert J, Sutter M, Zak E, Altschmied L, Schröder U, Herrmann RG, Haehnel W (1996) The plastocyanin binding domain of photosystem I. *EMBO J* 15:6374–6384
- Hippler M, Drepper F, Haehnel W, Rochaix JD (1998) The N-terminal domain of PsaF: precise recognition site for binding and fast electron transfer from cytochrome c6 and plastocyanin to photosystem I of *Chlamydomonas reinhardtii*. *Proc Natl Acad Sci U S A* 95:7339–7344
- Hurt E, Hauska G (1981) A cytochrome f/b6 complex of five polypeptides with plastoquinol-plastocyanin-oxidoreductase activity from spinach chloroplasts. *Eur J Biochem* 117:591–595
- Jordan P, Fromme P, Witt HT, Klukas O, Saenger W, Krauss N (2001) Three-dimensional structure of cyanobacterial photosystem I at 2.5 Å resolution. *Nature* 411:909–917
- Lindell D, Jaffe JD, Johnson ZI, Church GM, Chisholm SW (2005) Photosynthesis genes in marine viruses yield proteins during host infection. *Nature* 438:86–89
- Malakhov MP, Wada H, Los DA, Semenenko VE, Murata N (1994) A new type of cytochrome c from *Synechocystis* PCC6803. *J Plant Physiol* 144:259–264
- Malakhov MP, Malakhova OA, Murata N (1999) Balanced regulation of expression of the gene for cytochrome cM and that of genes for plastocyanin and cytochrome c6 in *Synechocystis*. *FEBS Lett* 444:281–284
- Mann NH, Cook A, Millard A, Bailey S, Clokie M (2003) Marine ecosystems: bacterial photosynthesis genes in a virus. *Nature* 424:741
- Marcaida MJ, Schlarb-Ridley BG, Worrall JA, Wastl J, Evans TJ, Bendall DS, Luisi BF, Howe CJ (2006) Structure of cytochrome c6A, a novel dithiocytochrome of *Arabidopsis thaliana*, and its reactivity with plastocyanin: implications for function. *J Mol Biol* 360:968–977
- Mazor Y, Greenberg I, Toporik H, Beja O, Nelson N (2012) The evolution of photosystem I in light of phage-encoded reaction centres. *Philos Trans R Soc Lond B Biol Sci* 367:3400–3405
- Mazor Y, Nataf D, Toporik H, Nelson N (2014) Crystal structures of virus-like photosystem I complexes from the mesophilic cyanobacterium *Synechocystis* PCC 6803. *Elife* 3:e01496
- Molina-Heredia FP, Balme A, Hervás M, Navarro JA, De la Rosa MA (2002) A comparative structural and functional analysis of cytochrome cM cytochrome c6 and plastocyanin from the cyanobacterium *Synechocystis* sp. PCC 6803. *FEBS Lett* 517:50–54
- Molina-Heredia FP, Wastl J, Navarro JA, Bendall DS, Hervás M, Howe CJ, De La Rosa MA (2003) Photosynthesis: a new function for an old cytochrome? *Nature* 424:33–34
- Molitor VR, Erber W, Peschek GA (1986) Increased levels of cytochrome oxidase and sodium-proton antiporter in the plasma membrane of *Anacystis nidulans* after growth in sodium-enriched media. *FEBS Lett* 204:251–256
- Muller MG, Niklas J, Lubitz W, Holzwarth AR (2003) Ultrafast transient absorption studies on Photosystem I reaction centers from *Chlamydomonas reinhardtii*. I. A new interpretation of the energy trapping and early electron transfer steps in Photosystem I. *Biophys J* 85:3899–3922
- Nelson N (2011) Photosystems and global effects of oxygenic photosynthesis. *Biochim Biophys Acta* 1807:856–863
- Nelson N, Neumann J (1972) Isolation of a cytochrome b 6 -f particle from chloroplasts. *J Biol Chem* 247:1817–1824

- Partensky F, Garczarek L (2010) Prochlorococcus: advantages and limits of minimalism. *Ann Rev Mar Sci* 2:305–331
- Partensky F, Hess WR, Vaulot D (1999) Prochlorococcus, a marine photosynthetic prokaryote of global significance. *Microbiol Mol Biol Rev* 63:106–127
- Peschek GA, Obinger C, Paumann M (2004) The respiratory chain of blue-green algae (cyanobacteria). *Physiol Plant* 120:358–369
- Rieske JS, Zaugg WS, Hansen RE (1964) Studies on the electron transfer system. Lix. Distribution of iron and of the component giving an electron paramagnetic resonance signal at  $G = 1.90$  in subfractions of complex 3. *J Biol Chem* 239:3023–3030
- Rocap G, Larimer FW, Lamerdin J, Malfatti S, Chain P, Ahlgren NA, Arellano A, . . . , Chisholm SW (2003) Genome divergence in two Prochlorococcus ecotypes reflects oceanic niche differentiation. *Nature* 424:1042–1047
- Rusch DB, Halpern AL, Sutton G, Heidelberg KB, Williamson S, Yoosay S, Wu D, . . . , Venter JC (2007) The Sorcerer II Global Ocean Sampling expedition: northwest Atlantic through eastern tropical Pacific. *PLoS Biol* 5:e77
- Scanlan DJ, Ostrowski M, Mazard S, Dufresne A, Garczarek L, Hess WR, Post AF, . . . , Partensky F (2009) Ecological genomics of marine picocyanobacteria. *Microbiol Mol Biol Rev* 73:249–299
- Sharon I, Alperovitch A, Rohwer F, Haynes M, Glaser F, Atamna-Ismael N, Pinter RY, . . . , Beja O (2009) Photosystem I gene cassettes are present in marine virus genomes. *Nature* 461:258–262
- Sharon I, Battchikova N, Aro EM, Gligione C, Meinnel T, Glaser F, Pinter RY, . . . , Bèjà O (2011) Comparative metagenomics of microbial traits within oceanic viral communities. *ISME J* 5:1178–1190
- Smith A, Witty M (2002) Heme, Chlorophyll, and Bilins: Methods and Protocols. Humana Press, Totowa
- Sommer F, Drepper F, Hippler M (2002) The luminal helix I of PsaB is essential for recognition of plastocyanin or cytochrome c6 and fast electron transfer to photosystem I in *Chlamydomonas reinhardtii*. *J Biol Chem* 277:6573–6581
- Sullivan MB, Waterbury JB, Chisholm SW (2003) Cyanophages infecting the oceanic cyanobacterium Prochlorococcus. *Nature* 424:1047–1051
- Sullivan MB, Lindell D, Lee JA, Thompson LR, Bielawski JP, Chisholm SW (2006) Prevalence and evolution of core photosystem II genes in marine cyanobacterial viruses and their hosts. *PLoS Biol* 4, e234
- Sun J, Xu W, Hervás M, Navarro JA, Rosa MA, Chitnis PR (1999) Oxidizing side of the cyanobacterial photosystem I. Evidence for interaction between the electron donor proteins and a luminal surface helix of the PsaB subunit. *J Biol Chem* 274:19048–19054
- Suttle CA (2007) Marine viruses – major players in the global ecosystem. *Nat Rev Microbiol* 5:801–812
- Szutka A (1966) Formation of pyrrolic compounds by ultra-violet irradiation of delta-aminolevulinic acid. *Nature* 212:401–402
- Weigel M, Varotto C, Pesaresi P, Finazzi G, Rappaport F, Salamini F, Leister D (2003) Plastocyanin is indispensable for photosynthetic electron flow in *Arabidopsis thaliana*. *J Biol Chem* 278:31286–31289
- Worrall JA, Schlarb-Ridley BG, Reda T, Marcaida MJ, Moorlen RJ, Wastl J, Hirst J, . . . , Howe CJ (2007) Modulation of heme redox potential in the cytochrome c6 family. *J Am Chem Soc* 129:9468–9475
- Wynn RM, Malkin R (1988) Interaction of plastocyanin with photosystem I: a chemical cross-linking study of the polypeptide that binds plastocyanin. *Biochemistry* 27:5863–5869
- Zatwarnicki P, Barciszewski J, Krzywda S, Jaskolski M, Kolesinski P, Szczepaniak A (2013) Cytochrome c(6B) of *Synechococcus* sp. WH 8102 – crystal structure and basic properties of novel c(6)-like family representative. *Biochem Biophys Res Commun* 443:1131–1135
- Zeidner G, Bielawski JP, Shmoish M, Scanlan DJ, Sabehi G, Bèjà O (2005) Potential photosynthesis gene recombination between Prochlorococcus and *Synechococcus* via viral intermediates. *Environ Microbiol* 7:1505–1513

# Chapter 8

## Cytochrome $b_{559}$ in Photosystem II

Frank Müh<sup>a</sup> and Athina Zouni<sup>b,\*</sup>

<sup>a</sup>*Institut für Theoretische Physik, Johannes Kepler Universität  
Linz, Altenberger Strasse 69, A-4040 Linz, Austria*

<sup>b</sup>*Institut für Biologie, Humboldt Universität zu Berlin,  
Leonor-Michaelis-Haus, Philippstrasse 13, D-10099 Berlin,  
Germany*

Summary.....	144
I. Introduction.....	144
II. Structure.....	146
A. Genes and Polypeptides.....	146
B. Insights from X-Ray Crystallography.....	150
C. Subunit Interactions and Structural Relationships.....	151
1. A PQH <sub>2</sub> /Herbicide Binding Site Between PsbD and PsbF?.....	154
2. A Role of PsbD-PsbF Interaction in PSIIcc Assembly or Repair?.....	156
D. A Closer Look at the Heme Site.....	156
III. Redox Properties.....	158
A. Different Redox Potential Forms.....	158
B. Factors Influencing the Redox Potential.....	163
1. pH Dependence.....	163
2. Polarity and Position Relative to $\alpha$ -Helices.....	164
3. Axial Ligation and Interaction with Aromatic Amino Acid Residues.....	166
4. Nonplanarity of the Heme.....	166
5. Binding of Quinone-Like Molecules.....	167
6. Presence of Lipids, Detergent, and PsbY.....	167
IV. Function of Cytochrome $b_{559}$ .....	167
A. Side-Path Electron Transfer and Photoprotective Role.....	167
B. "Save-the-Carotene" Model.....	168
C. Plastoquinol Oxidase and Oxygen Reductase.....	168
D. Superoxide Reductase and Oxidase.....	169
E. Role in PSIIcc Assembly.....	169
V. Conclusions and Outlook.....	169
Acknowledgments.....	170
References.....	170

---

Dedicated to the memory of Gernot Renger

\*Author for correspondence, e-mail: [athina.zouni@hu-berlin.de](mailto:athina.zouni@hu-berlin.de)



## Summary

The photosystem II core complex (PSIIcc) is a complicated membrane protein occurring in oxygenic photosynthetic organisms that catalyzes a key reaction, the light-induced oxidation of water. It consists of 17 membrane-spanning  $\alpha$ -helical and three membrane-extrinsic protein subunits and binds nearly 100 cofactors. Among them is a heme protein composed of one heme *b* group ligated by two low molecular weight subunits with one transmembrane helix each, referred to as cytochrome (cyt) *b*<sub>559</sub>. Despite extensive research, the role of cyt *b*<sub>559</sub> in PSIIcc is still not known. In the present chapter, the structure of cyt *b*<sub>559</sub> is reviewed based on recent crystallographic work together with its unusually complex redox behavior, and some ideas are discussed concerning a possible function of this unique heme protein.

## I. Introduction

Cytochrome (cyt) *b*<sub>559</sub><sup>1</sup> is a heme protein that is an essential component of the photosystem II core complex (PSIIcc). PSIIcc is one of the two light-absorbing and light-driven molecular machines situated in the thylakoid membrane that provide the energy for redox processes in oxygenic photosynthesis (Renger 2008). The activity of PSIIcc ultimately results in the net transfer of electrons and protons from water to plastoquinone (Fig. 8.1). More precisely,

there are three coupled processes: The photon-triggered one-electron transfer in the reaction center (RC), the four-electron water splitting chemistry catalyzed by the water-oxidizing complex (WOC) located at the lumenal side of the RC (the donor side) and the two-electron quinone reduction chemistry at the stromal (or cytoplasmic) side of the RC (the acceptor side). According to our present knowledge, cyt *b*<sub>559</sub> is not involved in these primary processes. Nonetheless, cyt *b*<sub>559</sub> is essential, as PSIIcc cannot assemble without it. Although there is no lack of hypotheses and discussions, the actual purpose of cyt *b*<sub>559</sub> in the assembled PSIIcc is still unclear. In addition, cyt *b*<sub>559</sub> exhibits a redox behavior of bewildering complexity, existing in at least three different redox potential forms. This together with the inability to assign to cyt *b*<sub>559</sub> a clear-cut functional role contributes to the enigmatic character of this heme protein.

The aim of the present chapter is to give an up-to-date overview of the structural and redox potential properties of cyt *b*<sub>559</sub> and a discussion of ideas concerning its function. Earlier reviews on cyt *b*<sub>559</sub> have been given (Cramer and Whitmarsh 1977; Faller et al. 2005; Shinopoulos and Brudvig 2012; Stewart and Brudvig 1998; Whitmarsh and Pakrasi 1996). We also mention the review by Pospisil, focusing on enzymatic properties of cyt *b*<sub>559</sub> (Pospisil 2011), and reviews discussing low molecular weight subunits of PSIIcc (Müh et al. 2008; Shi et al. 2012; Shi

---

*Abbreviations:* Car –  $\beta$ -carotene; Chl – Chlorophyll; Cyt – Cytochrome; DCMU – 3-(3,4-dichlorophenyl)-1,1-dimethylurea; DQH<sub>2</sub> – Duroquinol; EPR – Electron paramagnetic resonance; HP – High potential; IP – Intermediate potential; LMW – Low molecular weight subunit; LP – Low potential; PQ – Plastoquinone; PQH<sub>2</sub> – Plastoquinol; PSII – Photosystem II; PSIIcc – Photosystem II core complex; RC – Reaction center; ROS – Reactive oxygen species; RR – Resonance Raman; TMH – Trans-membrane helix; VLP – Very low potential; WOC – Water-oxidizing complex

<sup>1</sup>The subscript number refers to the first observation of cyt *b*<sub>559</sub> due to a difference spectrum peak at 559 nm (Boardman and Anderson 1967). Curiously, the absorption maximum was later found to be rather close to 560 nm (Tae et al. 1993), and it was proposed to use the notation “cyt *b*<sub>560</sub>” (Cramer 2004). Nonetheless, the common nomenclature “cyt *b*<sub>559</sub>” appears to be irreversibly established, so that we use it here.

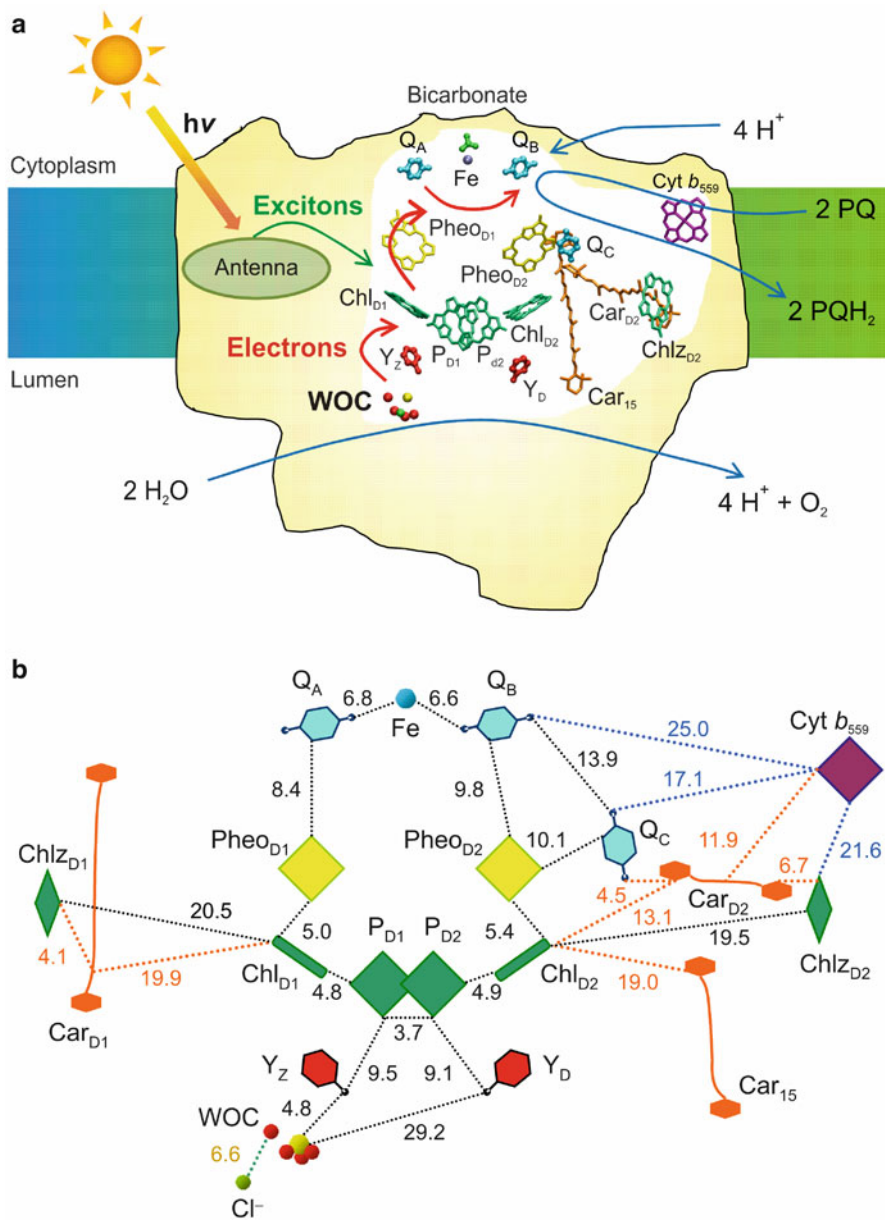


Fig. 8.1. (a) Arrangement of cofactors in and around PSII-RC of *T. elongatus* (made with VMD (Humphrey et al. 1996) based on PDB 3BZ1 (Guskov et al. 2009)) and relative to the perimeter of PSIIcc situated in the thylakoid membrane. Excitation by sunlight (yellow/orange arrow) or exciton transfer from outer antenna creates excitons in the core antenna system that are transferred to the RC (green arrow). Exciton-induced electron transfer in the RC (red arrows) ultimately leads to the reduction of quinones at the acceptor side (top) and oxidation of the WOC at the donor side (bottom). The reduced Q<sub>B</sub> takes up protons from the cytoplasm (or stroma) forming PQH<sub>2</sub> and is exchanged with PQ in the thylakoid membrane (plastoquinone pool), while the oxidized WOC catalyzes the splitting of water into O<sub>2</sub> and protons released into the lumen (blue arrows). (b) Schematic representation of the cofactor arrangement in (a) along with edge-to-edge distances given in Å.

and Schröder 2004; Thornton et al. 2005) as well as a review about plastoquinone (PQ) reduction in PSIIcc that also contains a chapter about *cyt b<sub>559</sub>* (Müh et al. 2012).

## II. Structure

### A. Genes and Polypeptides

PSIIcc is composed of at least 20 different polypeptide chains, a significant part of which (17) are membrane-spanning  $\alpha$ -helical proteins. Besides the four large subunits PsbA, B, C, D comprising the RC and the core antenna of PSIIcc, there is a number of so-called low molecular weight (LMW) subunits consisting of only one trans-membrane helix (TMH) with the exception of PsbZ possessing two such helices (Müh et al. 2008; Shi et al. 2012; Shi and Schröder 2004; Thornton et al. 2005). For reasons that will become apparent below, the most interesting LMWs in the context of the present review are PsbE, F, J, X, and Y. Outstanding among these are the two polypeptides that constitute *cyt b<sub>559</sub>* itself, PsbE and PsbF, also known as the  $\alpha$ - and  $\beta$ -subunit, respectively, of *cyt b<sub>559</sub>*. These are the subunits ligating the heme group. The crystallographic work discussed below shows that PsbJ, X and Y are located close to *cyt b<sub>559</sub>* in PSIIcc.

In cyanobacteria and plants, the two genes *psbE* and *psbF* coding for the two *cyt b<sub>559</sub>* subunits are adjacent and part of an operon that also includes the genes for two other LMWs, *psbL* and *psbJ* (Whitmarsh and Pakrasi 1996). The situation is different in the green alga *Chlamydomonas reinhardtii* (Mor et al. 1995). Deletion of either the entire *psbEFLJ* operon or the individual *psbE* or *psbF* genes results in a significant destabilization of PSIIcc. Studies on the mesophilic cyanobacterium *Synechocystis* PCC 6803 (henceforth referred to as *S. 6803*) showed that in these mutants the large subunit PsbD (also known as the D2 protein) is not integrated into the thylakoid membrane in a stable form, while significant amounts of the other large subunits are

accumulated (Whitmarsh and Pakrasi 1996). Work on tobacco demonstrated that PsbE and PsbF each require the other for a stable insertion into the membrane, and without these subunits, PsbA (the D1 protein) is also not stable (Swiatek et al. 2003). These data clearly show that PSIIcc cannot be assembled without *cyt b<sub>559</sub>*, and that the heme protein has at least a structure-stabilizing role.

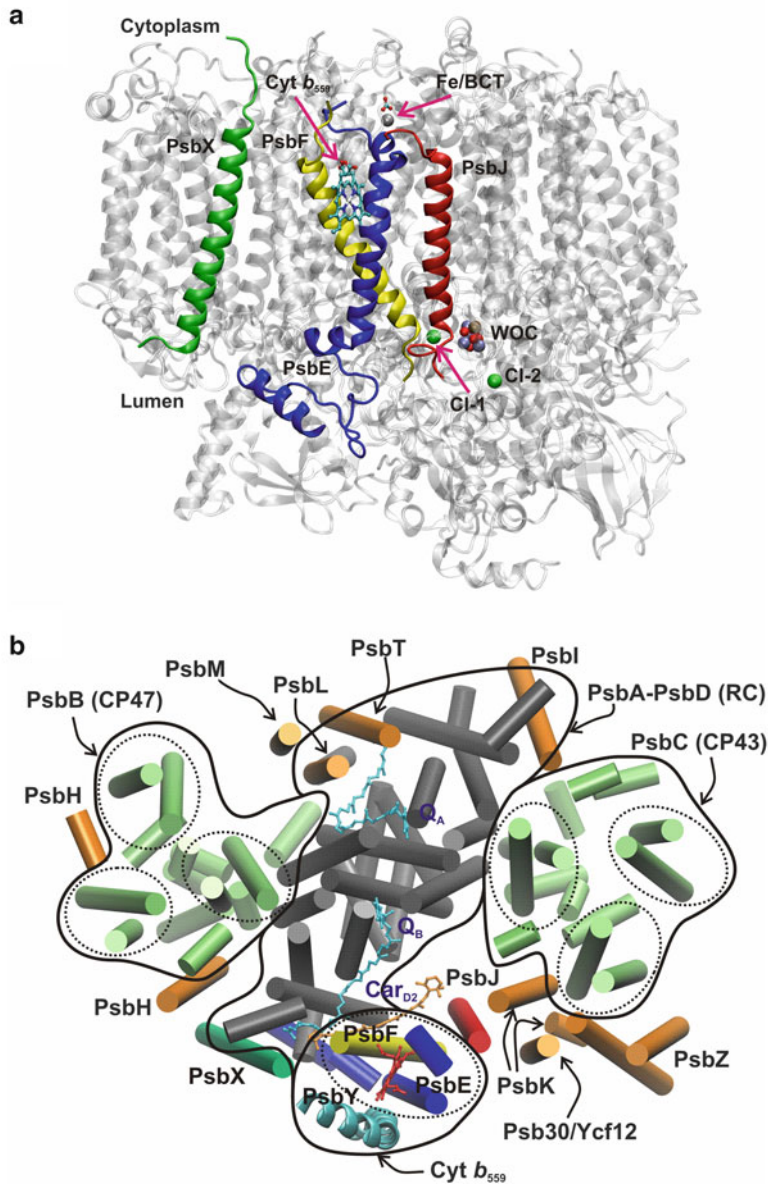
*Cyt b<sub>559</sub>* was first isolated and purified by Garewal and Wasserman (Garewal and Wasserman 1974a, b) and later sequenced (Herrmann et al. 1984; Widger et al. 1985). Amino acid sequences from different organisms are compiled in Fig. 8.2. Analyses of the sequences of PsbE and PsbF indicated the presence of one membrane-spanning  $\alpha$ -helix in each of these polypeptides (Herrmann et al. 1984; Pakrasi et al. 1988), which was later confirmed by X-ray crystallography (see Fig. 8.2). The only potential heme ligands in this region are histidine residues, namely His E23 in the  $\alpha$ -protein and His F24 in the  $\beta$ -protein (highlighted in orange in Fig. 8.2). Indeed, it was shown by combining optical, resonance Raman (RR), and electron paramagnetic resonance (EPR) spectroscopy, that the fifth and sixth ligands to the heme iron of *cyt b<sub>559</sub>* are histidine nitrogens (Babcock et al. 1985) indicating that the whole heme protein consists of at least two  $\alpha$ -helical subunits. The importance of a proper heme ligation was demonstrated by site-directed mutagenesis: The replacement of either E23 or F24 by Leu resulted in complete loss of PSII activity in *S. 6803* (Pakrasi et al. 1991). However, there still remained the different possibilities that *cyt b<sub>559</sub>* is a homodimer ( $\alpha_2$  or  $\beta_2$ ) or an  $\alpha\beta$ -heterodimer. Chemical crosslinking experiments remained inconclusive in this respect (Moskalenko et al. 1992). Finally, X-ray crystallography unveiled *cyt b<sub>559</sub>* to be an  $\alpha\beta$ -heterodimer, at last confirming the model proposed by Herrmann et al. (1984). Another problem that bothered researchers was the orientation of the two TMHs of *cyt b<sub>559</sub>* in the membrane which, because of the positions of the axially ligating histidines, is intimately related to the question of whether the heme group

PsbE	
<i>T. elongatus</i> BP1	MAGTTGERPFSDIITS <b>VR</b> <u>RYWV</u> <b>HSIT</b> IPALFIAGWLFVS TGLAYDVFGTTPRPDSYYAQEQRSIPLVTRDFEAKQVETVFLEQLK
<i>S. PCC 6803</i>	MSGTTGERPFSDIVTS <b>IR</b> <u>YWV</u> <b>HSIT</b> IPMLFIAGWLFVS TGLAYDAFGTTPRPDEYFTQTRQELPILQERYDINQEIQEFNQ
<i>A. thaliana</i>	SFADIITS <b>IR</b> <u>YWV</u> <b>HSIT</b> IPSLFIAGWLFVS TGLAYDVFGSPRPNEYFTESRQGIPLITGRFDPLEQLDEFSSRSF
PsbF	
<i>T. elongatus</i> BP1	MTSNTPNQEPVSYPI <b>FT</b> <b>VR</b> <u>WVAV</u> <b>HTLAVPT</b> IFFLGAIAAM QFIQR
<i>S. PCC 6803</i>	MATQNPNQPVTYPI <b>FT</b> <b>VR</b> <u>WLAV</u> <b>HTLAVPSV</b> FFVGAIAAM QFIQR
<i>A. thaliana</i>	MTIDRTYPI <b>FT</b> <b>VR</b> <u>WLAV</u> <b>HGLXVPT</b> VSFLGSISAM QFIQR
PsbJ	
<i>T. elongatus</i> BP1	MMSEGGRIPLWIVATVAGMGVIVIVGLFFYGA YAGLGSSL
<i>S. PCC 6803</i>	MFAEGRIPLWVGVVAGIGAVLGLFFYGA YAGLGSSM
<i>A. thaliana</i>	MADTTGRIPLWVIGTVAGILVIGLIGIFFYGS YSGLGSSL
PsbX	
<i>T. elongatus</i> BP1	MTITPSLKG <u>FFIGLLSGAVVGLTFAVLI</u> AIS QIDKVQRSL
<i>S. PCC 6803</i>	MTPSLAN <u>FLWSLVLGAAIVLIPATVGLIF</u> I SQDKITRS
<i>A. thaliana</i>	AGSGISPSLKN <u>FLLSIASGGLVLTVIIGVVV</u> GVSNFDPVKRT
PsbY	
<i>T. elongatus</i> BP1	M DWRVLVLLPVL <sup>A</sup> LAGWAVRNI LPYAVKQVQKLLQKAKAA
<i>S. PCC 6803</i>	M DWRVIVVVPL <sup>L</sup> IAATWAAINI GAAAIRQLQDVLGREA
<i>A. thaliana</i> A1	IQQIAQLAAANASS <u>DNRGLALLP</u> IVPAIAWVLYNI LQPAINQVNMKRE
A2	AAEAAAASS <u>DSRGQLLLIVVTPALLWVLYNI</u> LQPALNQINKMRSGD

Fig. 8.2. Amino acid sequence alignment of low molecular weight subunits of PSIIcc related to cyt  $b_{559}$  for the thermophilic cyanobacterium *Thermosynechococcus elongatus* BP1, the mesophilic cyanobacterium *Synechocystis* PCC 6803, and the representative higher plant *Arabidopsis thaliana* (mouse-ear cress). PsbE and PsbF are the  $\alpha$ - and  $\beta$ -subunit, respectively, of cyt  $b_{559}$ , ligating the heme group with the histidine residues highlighted in orange. Other residues forming the heme binding pocket are highlighted in yellow (see also Fig. 8.8). PsbJ and PsbX together with PsbE/F define the openings of the two putative plastoquinone diffusion pathways in PSIIcc (see Fig. 8.4). PsbY is in close contact with cyt  $b_{559}$  (see Figs. 8.3b and 8.5). The transmembrane regions of the peptides, as identified from the crystal structures, are *underlined*. In the case of *A. thaliana*, PsbX and PsbY are nuclear-encoded; corresponding signal sequences (Kim et al. 1996; Mant and Robinson 1998) are omitted. A1 and A2 refer to the two variants of the mature protein in *A. thaliana* contained in the precursor protein pPsbY (Thompson et al. 1999).

is located closer to the cytoplasm (stroma) or to the lumen. Various methods were applied including protease digestion (Tae et al. 1988; Tae and Cramer 1994) as well as immuno-gold labeling and electron microscopy (Vallon et al. 1989) to provide evidence that the N-termini point into the cytoplasmic phase as confirmed later by the crystal structures. Determining the number of cyt  $b_{559}$   $\alpha\beta$ -heterodimers per PSIIcc has been another problem as discussed in greater detail by Whitmarsh and Pakrasi (1996). At least for cyanobacterial PSIIcc, this problem is solved, as the crystal structures clearly show that there is only one cyt  $b_{559}$  per RC. A crystal structure of plant PSIIcc is not yet available. However, structural information about supercomplexes at 12 Å resolution from electron microscopy (Caffarri et al. 2009) suggests that there is a high degree of homology between cyanobacterial and plant PSIIcc and that there is no space for a second cyt  $b_{559}$  in the latter.

The LMW subunit PsbJ is not only of interest here, because its gene is contained in the same operon as those of PsbE and PsbF, but also because it is structurally located close to cyt  $b_{559}$  (Fig. 8.3). Deletion of the *psbJ* gene affects the photoautotrophic growth and the PSII oxygen evolution to an extent that depends on the type of organism (Shi et al. 2012; Shi and Schröder 2004). The polypeptide possesses one TMH (Fig. 8.2), and its N-terminus points into the cytoplasm. Together with PsbE/F, it forms the entrance “gate” of one of the putative PQ diffusion channels in PSIIcc (Fig. 8.4). Thus, one can expect an influence of PsbJ on the PQ/PQH<sub>2</sub> exchange with the quinone pool in the membrane (cf. Fig. 8.1). Indeed, deletion of PsbJ in *S. 6803* results in a longer lifetime of reduced Q<sub>A</sub> and diminished oxygen evolution rates, although it is not essential for PSII activity (Lind et al. 1993; Ohad et al. 2004; Regel et al. 2001). In higher plants, PsbJ is indispensable (Hager et al. 2002). The latter



*Fig. 8.3.* Position of cyt  $b_{559}$  in one monomer of PSIIc. **(a)** Ribbon representation of the protein backbone with PsbE in blue, PsbF in yellow, PsbJ in red and the remaining subunits in light grey; view along the membrane plane. Also shown is the heme group of cyt  $b_{559}$ , the non-heme iron with bound bicarbonate (Fe/BCT) as well as the WOC and the chloride ions close to the WOC as spheres. PsbX is shown in green and PsbY is omitted for clarity. **(b)** View from the cytoplasmic side showing  $\alpha$ -helices as columns except for PsbY, which is shown in ribbon representation (cyan). The colors of PsbE, F, J and X are the same as in **(a)**, the PsbA/D dimer (RC) is shown in grey, the two core antenna subunits PsbB (CP47) and PsbC (CP43) in orange. For clarity, the two-TMH bundles contained in PsbB, PsbC, and cyt  $b_{559}$  are enclosed by dotted ellipses. Also shown are the two plastoquinones  $Q_A$  and  $Q_B$  in cyan, the carotenoid Car $_{D2}$  in orange as well as the heme group of cyt  $b_{559}$  in red (see also Fig. 8.1). Note that  $Q_B$  marks the position of quinone diffusion channel II (see Fig. 8.4), while channel I runs between cyt  $b_{559}$  and PsbJ.  $Q_C$  is not present in the 2.1 Å resolution structure (Koua et al. 2013), from which this figure is derived. Figure made with VMD (Humphrey et al. 1996).

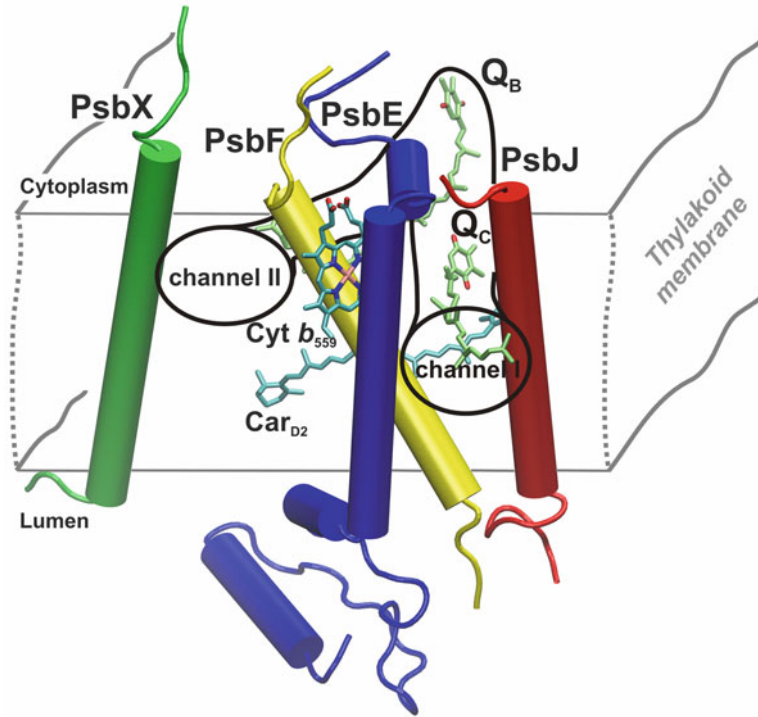


Fig. 8.4. Arrangement of *cyt b<sub>559</sub>* (i.e., subunits PsbE, blue, and PsbF, yellow, binding the heme group) as well as subunits PsbJ (red) and PsbX (green) relative to the thylakoid membrane and the putative PQ/PQH<sub>2</sub> diffusion channels I and II in PSIIcc.  $\alpha$ -Helices are represented as columns. The isoprenoid tail of the PQ occupying the Q<sub>B</sub> site lies along channel II (in the background), while Q<sub>C</sub> is located in channel I. Also shown is the  $\beta$ -carotene cofactor Car<sub>D2</sub>. With the exception of PsbX, all N-termini of the protein subunits are located in the cytoplasm. Figure made with VMD (Humphrey et al. 1996) based on PDB 3BZ1 (Guskov et al. 2009).

fact might be related to the observation that PsbP, an extrinsic subunit pertaining to plant PSIIcc (Bricker et al. 2012), is lacking in  $\Delta psbJ$  mutants (Hager et al. 2002; Suorsa et al. 2004).

The situation is more complicated in the thermophilic cyanobacterium *Thermosynechococcus elongatus*, as the effects of deleting PsbJ seem to depend on the type of D1 protein present. Cyanobacteria possess several genes encoding a number of PsbA-isoforms that are expressed differentially under various growth conditions (Mulo et al. 2009, 2012). There are three *psbA* genes in *T. elongatus* (Nakamura et al. 2002) that encode the three isoforms PsbA1, PsbA2, and PsbA3 (Nowaczyk et al. 2010). Under normal culture conditions, such as those used to obtain PSIIcc preparations that yield crystals (Kern et al. 2005; Zouni 2008),

PsbA1 prevails (Loll et al. 2008). PsbA3 is incorporated to about 70 % into PSIIcc under high light conditions, which is accompanied by some changes in functional properties (Kato et al. 2012; Sander et al. 2010; Sugiura et al. 2010b, 2014). The variant PsbA2 is induced under microaerobic conditions (Sicora et al. 2009), affects electron transfer reactions involving the redox-active tyrosine Y<sub>Z</sub> at the donor side of PSIIcc (Sugiura et al. 2012), and a new hemoprotein is expressed in *T. elongatus* mutants containing only PsbA2 (Boussac et al. 2013). Interesting differences were observed when performing the *psbJ* deletion in *T. elongatus* strains expressing either only PsbA1 or PsbA3 (Sugiura et al. 2010a): While PsbA3-PSIIcc seems to be unaffected by the lack of PsbJ, PsbA1-PSIIcc shows a reduced stability and modified EPR spectra of *cyt b<sub>559</sub>*. In

addition, many other subunits besides PsbJ are lacking in isolated PSIIcc of the PsbA1-variant. In a recent independent study, the core complex isolated from a PsbJ-deletion mutant of *T. elongatus* was found to consist mainly of a monomeric form of PSIIcc exhibiting an exchange of PsbA1 with PsbA3 despite the use of standard growth light conditions, lacking only PsbJ, and containing two additional subunits Psb27 and Psb28, which are involved in the biogenesis and repair of PSII (Nowaczyk et al. 2012).

The second putative quinone diffusion channel is located at the other side of cyt *b*<sub>559</sub> and its mouth is flanked by the TMH of PsbX (Fig. 8.4). In line with this location is the finding that a knock-out of PsbX from *T. elongatus* results in a somewhat less efficient turnover of quinones at the Q<sub>B</sub> site (Kato and Ikeuchi 2001), which might be related to an influence on the diffusion of quinones to or from this site through channel II. Knock-out mutants of higher plants have not been constructed so far, but there is an *Arabidopsis thaliana* antisense plant containing less than 10 % of PsbX. These plants show a reduced level of functionally assembled PSIIcc and a severely reduced phosphorylation level of the core subunits PsbA (D1), PsbC (CP43) and PsbD (D2), which is interpreted in terms of a more oxidized quinone pool in the membrane (García-Cerdán et al. 2009). These findings suggest a structure-stabilizing role of PsbX and again an influence on the quinone turnover.

Based on studies of PsbY-deletion mutants, it was concluded that this subunit is not essential for normal function of PSII in *S. 6803* (Meetam et al. 1999). Knock-out mutants of *A. thaliana* have been obtained and were reported to show phenotypic changes at cyt *b*<sub>559</sub> (Shi et al. 2012) in accordance with the idea that PsbY is attached to the PsbE/F heterodimer as in cyanobacterial PSIIcc (Fig. 8.3b).

### B. Insights from X-Ray Crystallography

The location of cyt *b*<sub>559</sub> could be determined already in the first three-dimensional crystal

structure of the dimeric PSII core complex (dPSIIcc) from *T. elongatus* at 3.8 Å resolution by virtue of the electron density of its heme iron (Zouni et al. 2001). It was also possible to identify helices, and the two TMHs close to the heme group were assigned to the α- and β-subunit of cyt *b*<sub>559</sub>. The two subunits could be distinguished, because the C-terminus of PsbE extends significantly into the lumen as known from the amino acid sequence (Fig. 8.2). The electron density was consistent with an orientation of the π-plane of the heme group perpendicular to the membrane plane in agreement with EPR data (Bergström and Vänngård 1982; Crowder et al. 1982) and models based on the assignment of the axially ligating histidines (Babcock et al. 1985). What was new, however, was the observation, that the two TMHs of PsbE and PsbF are tilted with respect to the membrane normal and with respect to each other, giving the impression that they form a pair of tongs holding the heme group (see Figs. 8.3a and 8.4). Also apparent from this structure was the substantial distance between cyt *b*<sub>559</sub> and the RC cofactors of PSIIcc (see also Fig. 8.1b).

Some assignments of α-helices to LMWs were made in this structure and the following refinements (Biesiadka et al. 2004; Ferreira et al. 2004; Kamiya and Shen 2003; Loll et al. 2005), but remained difficult until at a resolution of 2.9 Å (Guskov et al. 2009) a definite assignment was provided as shown in Fig. 8.3 for the subunits of interest here. The location of PsbY close to cyt *b*<sub>559</sub> was in agreement with an independent crystallographic study of a PsbY-deletion mutant (Kawakami et al. 2007). A peculiar feature of the 2.9 Å resolution structure of PSIIcc was that, besides the usual primary (Q<sub>A</sub>) and secondary (Q<sub>B</sub>) quinones, a third PQ named Q<sub>C</sub> was discovered ((Guskov et al. 2009), for pictures of the electron density, see (Guskov et al. 2010; Müh et al. 2012)). It is located in one of the two putative quinone diffusion channels that were identified on the basis of a theoretical analysis of the crystal structure (Guskov et al. 2009). It is of particular interest that these channels are located

on both sides of the PsbE/PsbF-heterodimer (Fig. 8.4), suggesting that the transport of PQ and/or PQH<sub>2</sub> between the Q<sub>B</sub> site (the active site of PQ reduction) and the thylakoid membrane (PQ pool) is somehow related to cyt  $b_{559}$ . Also, the close proximity of PsbJ and PsbX to the channel mouths (Fig. 8.4) suggests an influence of these LMWs on quinone turnover, which is indeed observed as discussed above. It is not known, how the quinone transport itself takes place. An attractive hypothesis is that one channel is used by PQ, the oxidized form, to approach the Q<sub>B</sub> site, whereas after light-induced reduction, PQH<sub>2</sub> uses channel II to reach the PQ pool, but there are other possibilities (Müh et al. 2012).

In contrast to PsbE, F, and J, the N-termini of PsbX and Y point into the lumen. In the case of PsbY, the electron density was still poor at 2.9 Å resolution. The assignment of this LMW and its orientation was made on the basis of characteristic bends in the helix due to proline residues (for amino acid sequence, see Fig. 8.2) in agreement with an earlier proposal (Kashino et al. 2007) and the above-mentioned crystal structure of a deletion mutant (Kawakami et al. 2007). Nonetheless, PsbY could only be modeled as a poly-Ala chain without structural details. It was clearly a major breakthrough in the structural biology of photosynthesis that the crystal structure of dPSIIcc from *T. vulcanus* could be improved to a resolution of 1.9 Å (Umena et al. 2011). Unfortunately, PsbY is missing in this structure. Subsequently, a crystal structure of dPSIIcc from *T. vulcanus*, in which the calcium ion of the WOC was replaced with strontium, was obtained at 2.1 Å resolution (Koua et al. 2013). This structure features PsbY in one monomer and allows a first detailed look at this subunit.

### C. Subunit Interactions and Structural Relationships

Cyt  $b_{559}$  is located on the periphery of PSIIcc. This is not only apparent from the cofactor arrangement (Fig. 8.1), but also immediately evident from the  $\alpha$ -helix

array shown for one PSIIcc monomer in Fig. 8.3b (Note that not only TMHs are shown). When PSIIcc forms dimers (or rods of dimers as in the thylakoid membrane of cyanobacteria (Mörschel and Schatz 1987) or supercomplexes as in plant thylakoids (Caffarri et al. 2009)), cyt  $b_{559}$  is still at the outside. This location is meaningful, as cyt  $b_{559}$  marks the openings of the quinone diffusion channels, which have to be free to allow for quinone turnover. The central part of PSIIcc is dominated by the two large RC subunits PsbA and PsbD, each with five TMHs (grey) that are flanked by the two large antenna subunits PsbB and PsbC (green). The six TMHs of each of the latter are grouped in antiparallel two-helix bundles that are enclosed by dotted ellipses in Fig. 8.3b. The inner core of these four subunits is decorated at the outside with the various LMWs (orange). According to the present structural information, cyt  $b_{559}$  is actually a three-helix bundle composed of the heme-coordinating subunits PsbE (blue) and PsbF (yellow) forming a parallel two-helix bundle (enclosed by a dotted ellipse in Fig. 8.3b) as well as the additional subunit PsbY (cyan ribbon) which is oriented antiparallel to PsbE. Notably, cyt  $b_{559}$  makes contact with the inner core of PSIIcc only via PsbD, i.e., there is mainly an interaction between the TMH of PsbF and TMH-a, the first TMH along the amino acid sequence of the D2 protein. The putative quinone diffusion channel II as indicated by the isoprenoid tail of Q<sub>B</sub> in Fig. 8.3b is located between these two TMHs. The channel opens to the lipid phase of the thylakoid membrane between the TMHs of PsbE and PsbX, while channel I opens between the TMHs of PsbE and PsbJ (Fig. 8.4). The region between PsbJ and PsbC is effectively filled up by the LMWs PsbK, Psb30 (also known as Ycf12) and, more peripheral, PsbZ, which thus block quinone diffusion in this direction (Fig. 8.3b). Thus, on the basis of the crystal structure, it seems that the possible quinone transport pathways are designed to make PQ or PQH<sub>2</sub> pass close by cyt  $b_{559}$  and that some of the LMWs are crucial in this

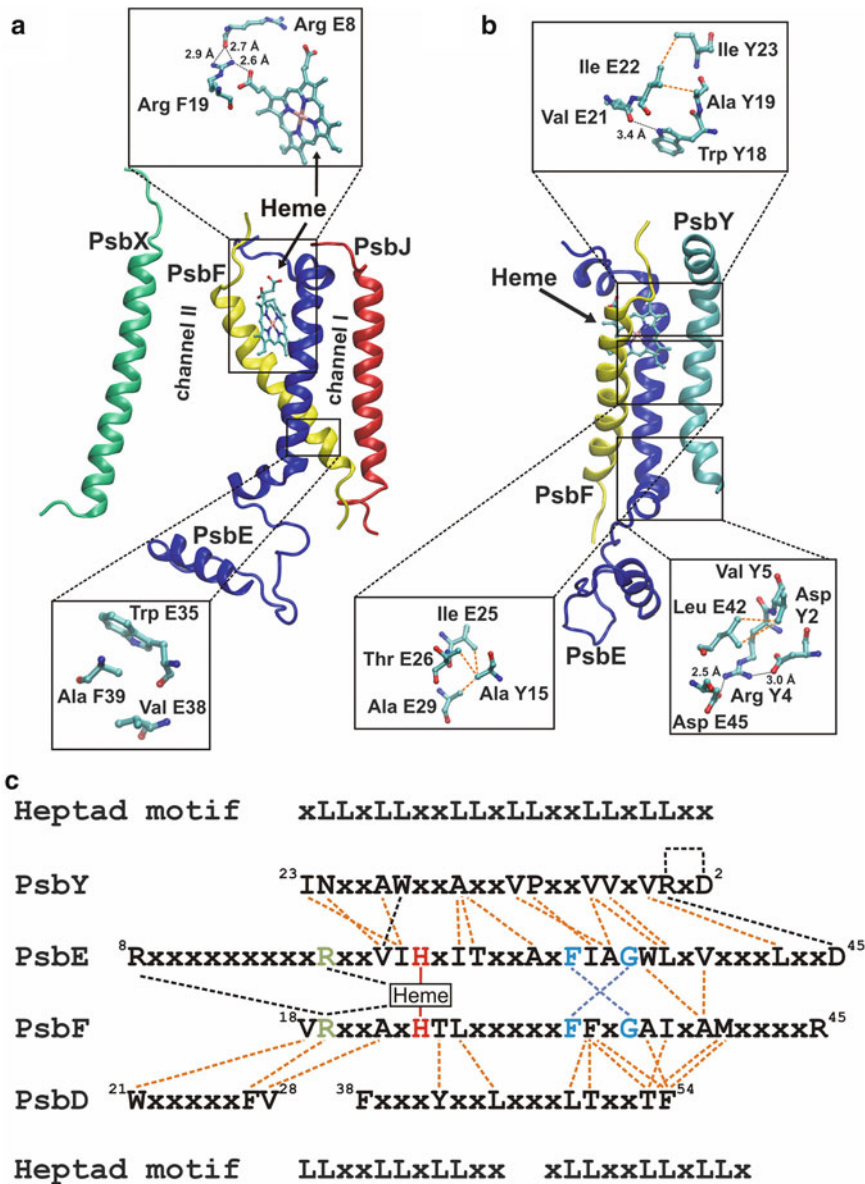


respect. The protein-free region between these LMWs and the large subunits is filled with lipids (not shown). In particular, there is a “bilayer island” composed of eight lipid molecules that is enclosed by protein, thus forming a kind of internal piece of membrane within PSIIcc (Guskov et al. 2009; Kern and Guskov 2011). Perpendicular to the channels and within the membrane plane lies the  $\beta$ -carotene cofactor Car<sub>D2</sub> (Figs. 8.3b and 8.4), which sticks out from all carotenoids bound to PSIIcc because of its unusual orientation and relative vicinity to the RC cofactors (Fig. 8.1). This carotenoid is believed to be involved in slow electron transfer processes involving cyt *b*<sub>559</sub> and the RC (Brose et al. 2013; Faller et al. 2005; Frank and Brudvig 2004; Renger and Schlodder 2011; Shinopoulos and Brudvig 2012). Recent studies on site-directed mutations provide further evidence for this involvement (Shinopoulos et al. 2014).

The two TMHs of PsbE and PsbF cross at an angle of  $-40^\circ$ . The minus sign implies that, when looking on the PsbE/PsbF heterodimer from the PsbE side as in Fig. 8.5a, the TMH of PsbE is rotated clockwise with respect to that of PsbF. This follows the usual sign convention for rotation angles (Chothia et al. 1977). The particular arrangement of the two helices is also referred to as a right-handed crossing. Note that it implies a form of chirality: A counter-clockwise rotation of PsbE with respect to PsbF would have created the mirror image, a left-handed crossing motif. An angle of about  $-40^\circ$  is frequently found in crossing motifs of parallel TMHs (Walters and DeGrado 2006). Helix-helix interactions are found to be promoted by typical amino acid sequences such as the prototypical GxxxG-motif of glycophorin A, an erythrocyte protein of unknown function (Langosch and Arkin 2009; Moore et al. 2008). The glycine residues may be replaced by other residues with small side chains such as Ala or Ser, which is why the motif, in the case of right-handed crossing, is also referred to as GAS<sub>Right</sub> motif (Moore et al. 2008). The GAS<sub>Right</sub> motif may be

supplemented by aromatic residues such as Trp or may be extended to an FxxGxxxG motif (Langosch and Arkin 2009). Indeed, the motifs found in cyt *b*<sub>559</sub> are exactly like that: The sequence <sup>31</sup>FxxGWxxV<sup>38</sup> in PsbE interacts with the homologous sequence <sup>32</sup>FxxGxxxA<sup>39</sup> in PsbF (see the central part of Fig. 8.5c). The two glycine residues Gly E34 and Gly F35 define the region of closest approach of the two TMHs. The side chains of the two phenylalanine residues Phe E31 and Phe F32 are symmetry-related to each other and are attached to the Gly residues of the respective other subunit (blue in Fig. 8.5c), presumably by a C<sub>α</sub>-H... $\pi$  interaction (not shown, but see (Brandl et al. 2001) for prototypical examples of such interactions). Further downstream the amino acid sequence in the interaction motif, the side chains of Trp E35 and Val E38 form a pair of tongs holding the side chain of Ala F39 by van-der-Waals interactions (see lower inset to Fig. 8.5a). These interactions very likely already determine the crossing angle of  $-40^\circ$ . Notwithstanding, binding of the heme group will further stabilize the structure. This view is supported by recent EPR studies of a spin-labeled  $\beta_2$ -homodimer referred to as cyt *b*<sub>559</sub>, showing that heme binding is not needed for dimerization, but tightens the heme binding site (Akdogan et al. 2012). In the native  $\alpha\beta$ -heterodimer, this stabilization of the structure is accomplished not only by the ligation of the central iron of the heme by the two histidine side chains E23 and F24 as well as the formation of salt bridges between the propionate substituents of the heme and the two arginine residues E18 and F19 (see below), but also by the additional formation of a hydrogen bond between one of these arginines (F19) and the backbone carbonyl of Arg E8 in the cytoplasmic extension of PsbE (see the upper inset to Fig. 8.5a). The latter bond establishes a further direct interaction between the two subunits.

When the crossing angle of two interacting TMHs is close to  $0^\circ$ , the interaction motif has to cover the full length of the trans-membrane domain. Typical for



*Fig. 8.5.* Interactions between protein subunits of *cyt b<sub>559</sub>*.  $\alpha$ -Helices are represented as ribbons. View along the membrane plane with cytoplasm at the *top* (a) Relative arrangement of PsbE (blue), PsbF (yellow), PsbJ (red), and PsbX (green) (b) Relative arrangement of PsbE (blue), PsbF (yellow), and PsbY (cyan). Insets show enlarged views of specific amino acid interactions (c) Alignment of amino acid sequences in the interaction region of protein subunits PsbD, PsbE, PsbF, and PsbY. The sequence of the latter is shown in reverse order, because the TMH of PsbY is oriented antiparallel to those of the other subunits. The two histidine residues ligating the central iron ion of the heme are colored in red and the two arginine residues forming salt bridges with propionate substituents of the heme in green. Residues colored in blue belong to the central interaction region at the crossing point of PsbE and PsbF (GAS<sub>Right</sub> motif). Dashed lines indicate  $C_{\alpha}$ -H $\cdots$  $\pi$  interactions (blue), van-der-Waals interactions (orange), and hydrogen bonds (including salt-bridges, black). For comparison, prototypical heptad repeat motifs characteristic for membrane-spanning leucine zippers are shown in the *top* and in the *bottom*. Figures made with VMD (Humphrey et al. 1996) based on PDB 4IL6 (Koua et al. 2013).

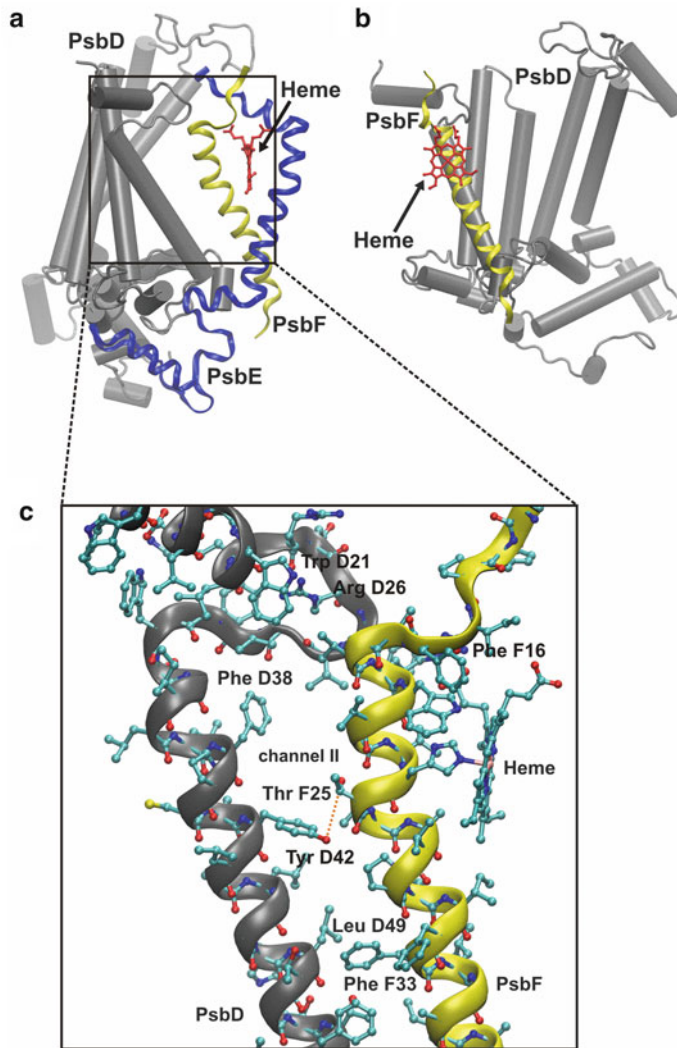
interactions of this kind are heptad repeat motifs of the form LLxxLLxLLxxLLx, where Leu residues are located at positions suitable for interaction with their counterpart in the second helix, while the “x” residues point into a different direction (Gurezka et al. 1999). Such motifs are referred to as membrane-spanning leucine zippers. However, there is no strict requirement for the residues at the “L” positions to be leucines (Gurezka and Langosch 2001) and not even to be apolar (Choma et al. 2000; Zhou et al. 2000). A leucine zipper has been identified in the center of the PSIIcc dimer, where the two PsbM subunits interact (Guskov et al. 2009). Here, the interaction motif is  ${}^6\text{LxxLIxxxLxxLVxxVxxIIxxV}^{27}$ . Similar heptad motifs are found in the interaction region of PsbE and PsbY, although the helices run antiparallel. This is the reason, why the sequence of PsbY is shown in reverse order in Fig. 8.5c. The reverse zipper sequence  ${}^{19}\text{AxxxAxxVPxxVV}^7$  in PsbY contacts the sequence  ${}^{22}\text{IxxITxxAxxIAxxL}^{36}$  in PsbE. The occurrence of the more polar threonine in the latter sequence might be surprising, but in fact, it behaves like an apolar residue by contributing a methyl group to van-der-Waals interactions (see the lower left inset to Fig. 8.5b). These transmembrane helix-helix contacts between PsbE and PsbY are supplemented by further interactions at both ends of the helices that also involve hydrogen bonds and salt bridges (see the upper and lower right inset to Fig. 8.5c).

Cyt  $b_{559}$  makes contact with the inner core of PSIIcc only at TMH-a of PsbD (Fig. 8.6). The interaction between this TMH and that of PsbF is special: When looking along a certain direction in the membrane plane, one notices that the crossing angle is  $0^\circ$ , i.e., the TMHs run parallel as the N-termini of both subunits lie in the cytoplasm (Fig. 8.6b). However, when looking from a perpendicular direction in the membrane plane (Fig. 8.6a), one readily sees that the TMHs make an angle, i.e., they are further apart towards the cytoplasm than towards the lumen. Most

likely, the reason for this arrangement is to clear a space for quinone diffusion. In fact, the region between these two TMHs is a bottleneck of channel II. The interactions between the protein subunits are described accordingly. There is contact between heptad motifs only in the lower part of the helices towards the luminal side (Fig. 8.5c). In the middle of the helices, there is a special interaction between Tyr D42 and Thr F25 without hydrogen bonding (Fig. 8.6c). This point marks the lower boundary of channel II. Additional interactions in the cytoplasmic loops of PsbD and PsbF contribute to maintain the angle between the helices and thus to keep the channel open. This region is particularly interesting for two reasons, as we shall discuss in the remainder of this subsection: (i) the possible existence of a PQH<sub>2</sub>/herbicide binding site and (ii) a possibly crucial role in PSIIcc assembly/repair.

### 1. A PQH<sub>2</sub>/Herbicide Binding Site Between PsbD and PsbF?

Several studies point to the possibility that there are more quinone binding sites in PSIIcc than just the two of Q<sub>A</sub> and Q<sub>B</sub>. A third PQ labeled Q<sub>C</sub> (see Fig. 8.4) was identified in the crystal structure at 2.9 Å resolution (Guskov et al. 2009), but not in any other structure. Kruk and Strzalka investigated electron transfer between cyt  $b_{559}$  and exogenous quinones and found that the low-potential form of cyt  $b_{559}$  (see Sect. III) interacts with the quinones in a way that suggests the presence of two additional distinct binding sites termed “Q<sub>C</sub>” and Q (Kruk and Strzalka 2001). Since DCMU, a herbicide known to occupy the Q<sub>B</sub> pocket ((Müh and Zouni 2013) and references therein), has no influence on these electron transfer reactions, it was concluded that Q<sub>B</sub> is not involved. Furthermore, the new binding sites showed a preference for polar quinones. In contrast, the crystallographically detected Q<sub>C</sub> resides in a fairly apolar environment and is located relatively far away from cyt  $b_{559}$ . Therefore, we think – in agreement with recent sugges-



*Fig. 8.6.* Interaction of cyt  $b_{559}$  with the N-terminal part of the RC subunit PsbD (D2 protein) (a) Location of TMHs of PsbE (blue ribbon) and PsbF (yellow ribbon) relative to those of PsbD (gray columns). The helix of PsbD closest to PsbF is TMH-a. The heme group of cyt  $b_{559}$  is shown in red. View along the  $\pi$ -plane of the heme lying vertical and along the plane of the thylakoid membrane lying horizontal. The black rectangle indicates the region shown enlarged in (c) (b) View rotated by  $90^\circ$  relative to (a) demonstrating that the TMH of PsbF (yellow ribbon) and TMH-a of the PsbD (gray column) have the same orientation in this direction. The heme group of cyt  $b_{559}$  is shown in red. PsbE is omitted for clarity. (c) Region of closest interaction between PsbD and PsbF in the thylakoid membrane. The only polar groups of the two subunits facing each other inside the membrane are Tyr D42 and Thr F25 approaching hydrogen bonding distance, but without forming such a bond (The indicated distance is that between the hydroxyl oxygen of Tyr and carbon  $C_\beta$  of Thr). Note that channel II (see Fig. 8.4) runs above these two residues and is relatively narrow in this region (see also Fig. 8.8d in (Müh et al. 2012)). Figures made with VMD (Humphrey et al. 1996) based on PDB 4IL6 (Koua et al. 2013).

tions (Cardona et al. 2012; Kaminskaya and Shuvalov 2013) – that the “ $Q_C$ ” site proposed by Kruk and Strzalka (2001) is different from the  $Q_C$  site identified by Guskov et al. (2009).

The herbicides DCMU and dinoseb were found to influence the redox potential of the high-potential form of cyt  $b_{559}$ , suggesting that they bind close to cyt  $b_{559}$  (Kaminskaya

et al. 2007). Since both reagents also bind to the  $Q_B$  pocket, it was suggested that the new site close to *cyt b<sub>559</sub>* may also accommodate the structurally similar PQ or PQH<sub>2</sub>. More recently, the photoreduction of *cyt b<sub>559</sub>* in PSII membrane fragments was investigated and shown to be due to PQH<sub>2</sub> from the quinone pool (Kaminskaya and Shuvalov 2013). *Cyt b<sub>559</sub>* can also be reduced by the analogous duroquinol (DQH<sub>2</sub>), and dinoseb competes with DQH<sub>2</sub>, whereas DCMU does not. These data suggest the existence of a binding site close to *cyt b<sub>559</sub>* specific for quinone-like molecules and accessible from the membrane phase, but different from the crystallographic  $Q_C$  site. It was proposed to call this site  $Q_D$  (Kaminskaya and Shuvalov 2013).

As discussed elsewhere (Müh et al. 2012), the idea exists that channel II is specific for PQH<sub>2</sub>. It is then reasonable – as a first guess – to search for the  $Q_D$  site along this channel. In this respect, the region around the bottleneck between TMH-a of PsbD and the TMH of PsbF is an interesting candidate, because it likely constitutes a barrier to quinol diffusion and features a number of specific side chains pointing into the channel that may interact with PQH<sub>2</sub>. For example, the hydroxyl group of Thr F25 is one of only a few possibilities to form a hydrogen bond (Fig. 8.6c). Also, of the few aromatic side chains pointing into the channel, which might bind quinols by  $\pi$ -stacking (Waters 2002), some are located in this area such as Phe D38 or Tyr D42. The region is located close to the heme group suitable for electron transfer and is near the membrane surface, which is more polar than the membrane interior and thus suitable for quinols or more polar quinones (Nowicka and Kruk 2010). Finally, some titratable groups such as Arg D26 (Fig. 8.6c) or Asp X35 (not shown) are nearby in the cytoplasmic region. These groups are potential proton acceptors that might be important to support one-electron oxidation of a quinol (Buser et al. 1992; Kaminskaya and Shuvalov 2013). As dinoseb competes with quinols for the binding place,

a crystal structure of PSIIcc subjected to this herbicide would be of interest to identify the  $Q_D$  site.

## 2. A Role of PsbD-PsbF Interaction in PSIIcc Assembly or Repair?

According to current models of PSIIcc assembly (see (Nixon et al. 2010) for a review), the subunits PsbD, PsbE, and PsbF, on one hand, as well as PsbI and a precursor of PsbA (pD1, containing an extended C-terminus that has to be removed to allow assembly of the WOC) on the other hand, form pre-complexes in the thylakoid membrane: the D2-*cyt b<sub>559</sub>* and pD1-PsbI complex, respectively, which subsequently combine to a larger RC complex. Given the subunit interactions in the fully assembled PSIIcc (Fig. 8.3b), the existence of a D2-*cyt b<sub>559</sub>* complex is reasonable. Then, it is obvious that the peculiar interaction between TMH-a of PsbD and the TMH of PsbF is already present in this sub-complex, and that the involved amino acid residues are important for its assembly. Based on the structure of PSIIcc, one may further assume that the PsbD-PsbF interaction is kept up during the PSII repair cycle, in which the damaged D1 protein is replaced (Nixon et al. 2010). Provided the  $Q_D$  site discussed above is indeed located in this region, it is likely also present in the D2-*cyt b<sub>559</sub>* complex and during D1-exchange. This would enable electron transfer reactions between quinones/quinols and *cyt b<sub>559</sub>* under these conditions with possible functional implications. We would like to stress that the search for a functional role of *cyt b<sub>559</sub>* should not be restricted to the fully assembled PSIIcc, but a role may well be found in subcomplexes related to PSIIcc assembly and repair.

### D. A Closer Look at the Heme Site

The heme group of *cyt b<sub>559</sub>* is well shielded from the environment by the protein, as is apparent from the space-filling representation in Fig. 8.7. The major part of this enclo-

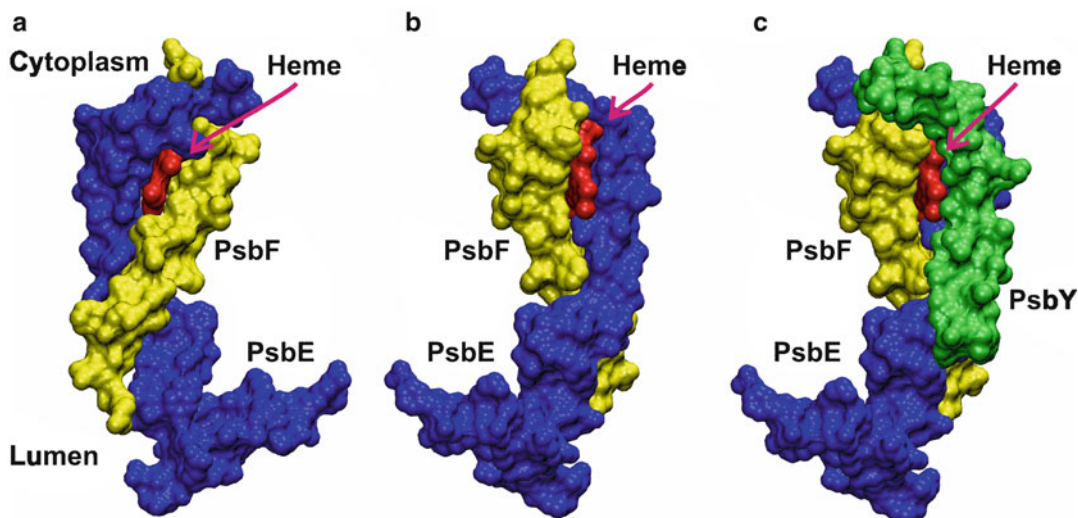


Fig. 8.7. Space filling representation of *cyt*  $b_{559}$  with the heme group in red, PsbE in blue, PsbF in yellow, and PsbY in green. (a) and (b) show views from different directions in the absence of PsbY. The view in (c) is the same as in (b), but with PsbY present. Figures made with VMD (Humphrey et al. 1996) based on PDB 4IL6 (Koua et al. 2013).

sure is already provided by PsbE and PsbF, including an effective shielding against the cytoplasmic phase. However, the shielding by just two TMHs is unavoidably incomplete, as can be seen by the red spots that show the heme in Figs. 8.7a, b, indicating contact of the heme with the membrane phase along the  $\pi$ -plane of the heme group. Notably, a significant fraction of the contact surface at the outside of PSIIcc is covered by PsbY (Fig. 8.7c). Thus, we propose that the role of PsbY is to protect *cyt*  $b_{559}$  against unwanted side reactions due to contact with redox active molecules in the thylakoid membrane, e.g., quinones or dioxygen.

A closer look at the heme itself reveals that it is distorted in an unusual way (Fig. 8.8a). The two pyrrole rings pointing towards the lumen are practically within the  $\pi$ -plane of the tetrapyrrole, whereas those facing the cytoplasm are significantly bent out of this plane giving the heme a propeller-like appearance. Clearly, the reason for this non-planarity is the interaction of the two propionate substituents with arginine residues in the two protein subunits (Arg E18 and F19). In this way, it appears that the heme conformation is coupled to the crossing angle of the

two TMHs of PsbE and PsbF. It is unclear, however, to what extent this angle is variable and whether a conformational distortion of the heme is of functional importance as has been discussed for other heme proteins (Shel-nutt et al. 1998).

The  $\pi$ -systems of the two axially ligating histidines (E23 and F24) are almost in plane, i.e., make an angle of  $\sim 30^\circ$  (Fig. 8.8a), which is not generally the case for *b*-type cytochromes (for a recent counter-example, see the structure of *cyt*  $b_{561}$  from *A. thaliana*, where the angle is close to  $90^\circ$  (Lu et al. 2014)). A possible meaning of this angle is discussed in Sect. III below. Another special feature is the  $\pi$ -stacking of the axially ligating histidines with other aromatic residues as shown for the PsbF-side in Fig. 8.8b. Note that there are various forms of  $\pi$ -stacking (Waters 2002), implying that the  $\pi$ -systems of the stacking side chains need not be in plane, but may also be oriented perpendicular to each other as seen for Trp F20 and Phe F16. These interactions link the orientation of the histidine  $\pi$ -systems with respect to that of the heme to the protein conformation, but the functional significance of such a link is not clear.

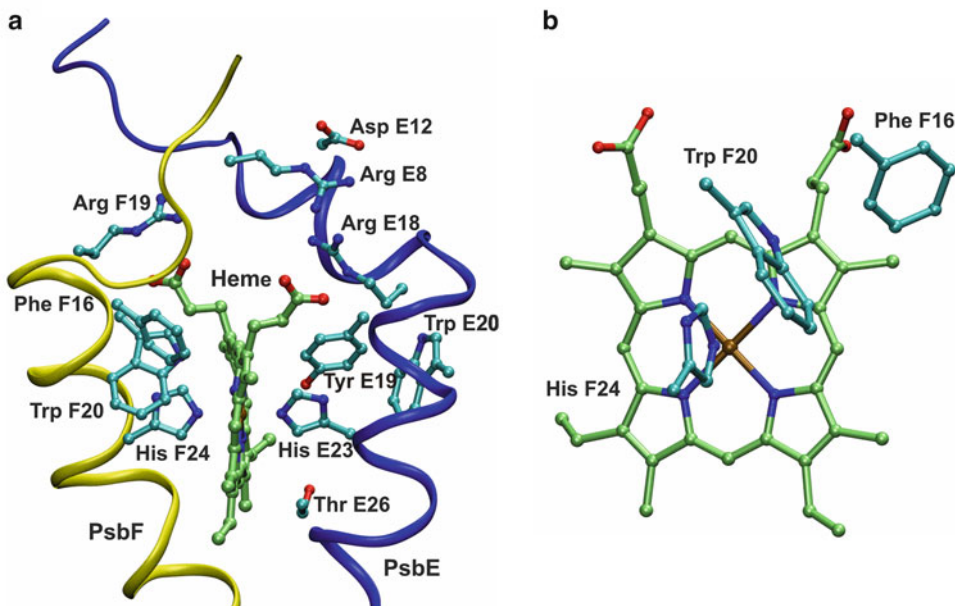


Fig. 8.8. A closer look at the heme site of *cyt b*<sub>559</sub>. (a) View along the  $\pi$ -plane of the heme (carbon atoms green) with selected amino acid side chains (carbon atoms cyan) and the peptide backbone (ribbons) of PsbE (blue) and PsbF (yellow) (b) View on top of the  $\pi$ -plane of the heme with selected amino acid side chains from PsbF (same colors as in a). Figures made with VMD (Humphrey et al. 1996) based on PDB 4IL6 (Koua et al. 2013).

### III. Redox Properties

#### A. Different Redox Potential Forms

The redox midpoint potential of *b*-type cytochromes is normally found in the range of  $-150 \text{ mV} < E_m < +150 \text{ mV}$  (Bérczi and Moller 2000; Cramer and Whitmarsh 1977; Gámiz-Hernández et al. 2010). Indeed, the redox potential of the so-called low-potential (LP) form of cytochrome *b*<sub>559</sub> is in this range (Iwasaki et al. 1995; Kaminskaya et al. 1999; McNamara and Gounaris 1995; Ortega et al. 1988; Roncel et al. 2001; Shuvalov et al. 1994; Thompson et al. 1989). However, in PSII-enriched membrane preparations and untreated chloroplasts of higher plants, the prevailing form is the high-potential (HP) form with  $350 \text{ mV} < E_m < 450 \text{ mV}$  (Horton and Croze 1977; Iwasaki et al. 1995; Kaminskaya et al. 1999, 2007; McNamara and Gounaris 1995; Ortega et al. 1988; Roncel et al. 2001; Thompson et al. 1989). Some authors distinguish in

addition an intermediate potential (IP) form with  $E_m \sim +200 \text{ mV}$  (Ahmad et al. 1993; Horton and Croze 1977; Kaminskaya et al. 2005, 2007; Ortega et al. 1988; Roncel et al. 2001; Shuvalov et al. 1994; Thompson et al. 1989) and a very low potential (VLP) form with  $E_m \sim -200 \text{ mV}$  (Kaminskaya et al. 1999; Shuvalov 1994). An overview is given in Table 8.1. It is evident that a variety of conditions exists, under which the different forms are observed.

In samples that are close to physiological conditions, i.e. untreated chloroplasts or membrane fragments, one usually observes a mixture of HP, IP, and LP form, indicating that all these forms are related to the native behavior of *cyt b*<sub>559</sub>. Although the HP form is prevailing in intact membranes, it has been found to be very labile in the dark toward conversion to a form with a lower potential (Cramer and Whitmarsh 1977). There is a clear tendency to reduce the amount of the HP form, when the isolation procedure is pushed forward, i.e., to

Table 8.1. Redox potential forms of cyt *b*<sub>559</sub>.

Organism	Sample type	Preparation conditions	pH	Form	<i>E</i> <sub>m</sub> (mV)	Reference	
Pea	RC	2 mM βDM <sup>a</sup>	8.0	HP 28 %	430	Ahmad et al. (1993)	
				IP 62 %	180		
				LP 10 %	25		
	PSII membranes Chloroplasts	Kuwabara and Murata (1982) Untreated	5.0–10.0 7.5	IP → LP	203 → 110	Roncel et al. (2001)	
				HP 58 %	383	Horton and Croze (1977)	
				LP 31 %	77		
				IP 58 %	240		
	Spinach	RC	NH <sub>2</sub> OH-treated(dark) NH <sub>2</sub> OH-treated (light) 0.1 % (w/v) βDM <sup>a</sup>	7.2	LP 42 %	93	Shuvalov et al. (1994)
					LP 95 %	90	
					HP 4 %	380	
IP 48 %					150		
LP 48 %					-45		
HP 4 %					400		
IP 48 %					150		
LP 24 %					40		
VLP 24 %					-220		
LP 100 %					115 → 50		
PSIIcc	Nanba and Satoh (1987) 0.025 % (w/v) βDM <sup>a</sup>	4.0–9.0 6.5–9.3	LP 86 %	118	Shibamoto et al. (2008)		
			VLP 14 %	-147	Kaminskaya et al. (1999)		
			HP	360	Ortega et al. (1988); Roncel et al. (2001); Thompson et al. (1989)		
			IP → LP	203 → 110			
PSII membranes	Kuwabara and Murata (1982) Berthold et al. (1981); Beck et al. (1985) Untreated	5.0–10.0 6	HP 44 %	375			
			IP 31 %	228			
			LP 25 %	57			

(continued)



Table 8.1. (continued)

Organism	Sample type	Preparation conditions	pH	Form	$E_m$ (mV)	Reference		
Spinach	PSII membranes	NaCl-washed		HP 18 % IP 42 % LP 40 %	375 171 3	McNamara and Gounaris (1995)		
		Chapman et al. (1988)		HP 90 % LP 10 %	353 81			
		Untreated oxidative	6.0	HP 49 % LP 51 %	390 125			
		Untreated reductive		LP 100 %	96			
		In the presence of 0.05 % $\beta$ DM a		LP 100 %	109			
		Treated with 0.5 % Triton X-100		HP 75 %	398			
		Treated with NaCl in the dark		LP 25 %	149			
		Treated with NaCl in dim light		IP 100 %	179			
		Treated with $MgCl_2$		IP 100 %	167			
		Treated with $CaCl_2$		IP 100 %	169			
		Radmer et al. (1986)						Iwasaki et al. (1995)
		Untreated		6.5	HP 66 % IP 19 % LP 14 %		437 259 26	
		$NH_2OH$ -treated			HP 54 % IP 24 % LP 22 %		435 237 45	
		$NH_2OH$ -treated and exposed to heat-filtered white light at 22 °C			HP 24–54 % IP 17–41 % IP 24–54 % LP 19–56 %		435 342–360 175–237 28–61	

Sugar beet	RC	0.1 % (w/v) $\beta$ DM <sup>a</sup>	6.5–9.3	LP 100 %	60	Kaminskaya et al. (1999)
		Liposomes	9.3–9.7	LP 100 %	40–60	
		Berthold et al. (1981); Völker et al. (1985)	6.8–9.5	LP 100 %	25–100	
	PSII membranes	Berthold et al. (1981); Völker et al. (1985)	6.0–9.2	HP 64 → 34 % IP 21 → 47 %	351–387 196–242	
	PSII membranes	Berthold et al. (1981); Völker et al. (1985)	6.5	LP 15 → 19 % HP 70–75 % IP 10–15 %	11–101 386–404 169–228	Kaminskaya et al. (2007)
		Without additive		LP 10–20 %	0–109	
		With 640 $\mu$ M DCMU <sup>b</sup>		HP 75 %	355	
				IP 15 %	225	
				LP 10 %	100	
		With 110 $\mu$ M dinoseb <sup>c</sup>		HP 81 %	318	
				IP 8 %	217	
				LP 11 %	101	
		With 30 $\mu$ M TPB <sup>d</sup>		HP 54 %	265	
				IP 24 %	171	
				LP 22 %	–7	
		With 20 $\mu$ M CCCP <sup>e</sup>		HP 66 %	316	
				IP 11 %	107	
				LP 23 %	–12	
<i>Phormidium</i> laminosum	PSII membrane	Stewart and Bendall (1980)	7.5	HP (variable amounts)	330–350	Stewart and Bendall (1980)
<i>Synechocystis</i> 6803	PSII membranes	Ortega et al. (1994)	7.5	LP (small amounts) IP 100 %	0–100 170	Ortega et al. (1994)

(continued)

Table 8.1. (continued)

Organism	Sample type	Preparation conditions	pH	Form	$E_m$ (mV)	Reference	
<i>T. elongatus</i>	PSIIcc	0.02 % (w/v) $\beta$ DM <sup>a</sup> (Kern et al. 2005)	6.5	IP 100 %	244	Kaminskaya et al. (2005)	
		0.03 % (w/v) $\beta$ DM <sup>a</sup>				Roncel et al. (2003)	
	Untreated	His-tagged (Sugiura and Inoue 1999)		6.5–8.5	HP 50 %	390	
					IP 50 %	275	
				9.5	HP 30 %	380	
		Tris-washed <sup>f</sup>		6.5	IP 70 %	260	
		After mild heating		6.5	HP 30 %	380	
			6.5	IP 70 %	277		
			6.5	HP 15 %	390		
<i>T. elongatus</i>	PSIIcc	0.03 % (w/v) bDM <sup>a</sup>	6.5	IP 85 %	250		
		His-tagged (Sugiura and Inoue 1999)		HP 85 %	394	Guerrero et al. (2014)	
				IP 15 %	240		

Note that some authors call LP what we here refer to as IP for consistency

<sup>a</sup>n-dodecyl- $\beta$ -D-maltoside, a detergent used to solubilize the thylakoid membrane

<sup>b</sup>3-(3,4-dichlorophenyl)-1,1-dimethylurea, a herbicide

<sup>c</sup>2,4-dinitro-6-sec-butylphenol, a herbicide

<sup>d</sup>tetraphenylboron

<sup>e</sup>carbonylcyamide-*m*-chlorophenylhydrazone

<sup>f</sup>tris(hydroxymethyl)aminomethane

isolated core complexes or RC preparations. This is an indication that interaction with the detergent used to solubilize the membrane is one factor destabilizing the HP form. In particular, the VLP form is only observed in these preparations and preferably at high pH (Shuvalov et al. 1994). It is of note that crystallizable cyanobacterial PSIIcc (isolated from *T. elongatus*) only exhibits the IP form with  $E_m = 244$  mV at pH = 6.5 (Kaminskaya et al. 2005), although preparations from other strains have been reported to also show the HP form (Guerrero et al. 2014; Roncel et al. 2003). These results have to be taken into account, when trying to link the redox properties of cyt  $b_{559}$  to the crystal structure.

Various treatments aiming at a manipulation of the donor side of PSIIcc have been reported to change the composition of redox potential forms of cyt  $b_{559}$  in the samples. These treatments include washing with NaCl to remove some of the extrinsic protein subunits of PSIIcc at the luminal side or incubation with  $\text{NH}_2\text{OH}$  to reduce and eventually destroy the WOC. Since all these experiments have been performed on plant material, and plant PSIIcc differs from cyanobacterial PSIIcc with respect to the extrinsic protein subunits (Bricker et al. 2012; Bricker and Burnap 2005), it is presently difficult to draw any conclusions from the crystal structures concerning these treatments. In the case of cyanobacterial PSIIcc, washing with the buffer Tris at pH 9.0 was reported to also destabilize the HP form (Roncel et al. 2003). This treatment is expected to remove manganese from the WOC and thus to modify the donor side of PSIIcc (Yamashita 1986). It is not clear, how this could affect the redox potential of cyt  $b_{559}$ . However, due to its luminal extension (Fig. 8.3a), PsbE may be sensitive to manipulations of the donor side.

### B. Factors Influencing the Redox Potential

Long-standing questions concerning the redox behavior of cyt  $b_{559}$  are: Why is the redox potential of the HP form so high? And how is the HP form converted to the other

forms? There are still no clear-cut answers to these questions, but a number of factors that may influence the redox potential of cyt  $b_{559}$  have been discussed in the literature. In the following, we shall go through a list of these factors, but also add some points that have not been mentioned in earlier reviews.

#### 1. pH Dependence

The redox potential of the HP form appears to be pH-independent (Ahmad et al. 1993; Ortega et al. 1988; Roncel et al. 2001, 2003), although Kaminskaya et al. (1999) observed a linear drift from 387 to 351 mV between pH 6.0 and 9.2. The behavior of the IP and LP forms is more complicated. In cyanobacterial PSIIcc, Roncel et al. (2003) observed what they call LP to be pH-independent (We call it IP, because  $E_m \sim 275$  mV; see Table 8.1). With plant material, Kaminskaya et al. (1999) demonstrated the pH-dependence of the IP and LP forms to vary in a complicated manner with sample types and conditions. A somewhat simpler picture emerges from the experiments by Ortega et al. (1988) and Roncel et al. (2001) on plant PSII-membranes: The data suggest that the IP and LP form are connected, i.e., that they are just the low-pH and high-pH variant, respectively, of the same form. The results of Roncel et al. (2001) are reproduced in the upper part of Fig. 8.9. The dashed curve is a fit to the Nernst-Clark equation:

$$E_m = E_0 - \frac{RT}{F} \ln \left( \frac{K_{a,\text{ox}} + a_{\text{H}}}{K_{a,\text{red}} + a_{\text{H}}} \right) \quad (8.1)$$

describing the pH-dependence of the midpoint potential  $E_m$  of a redox-active group that is electrostatically coupled to a titratable group, i.e., a group that can release a proton. Here,  $E_0$  is the midpoint potential of the redox-active group at low pH,  $R$  is the gas constant,  $T$  the temperature,  $a_{\text{H}}$  is the proton activity in the medium ( $a_{\text{H}} = 10^{-\text{pH}}$ ), and  $K_{a,\text{ox}}$  and  $K_{a,\text{red}}$  are the equilibrium constants for the deprotonation of the titratable group, when the redox-active group is oxidized and reduced, respectively, related to the

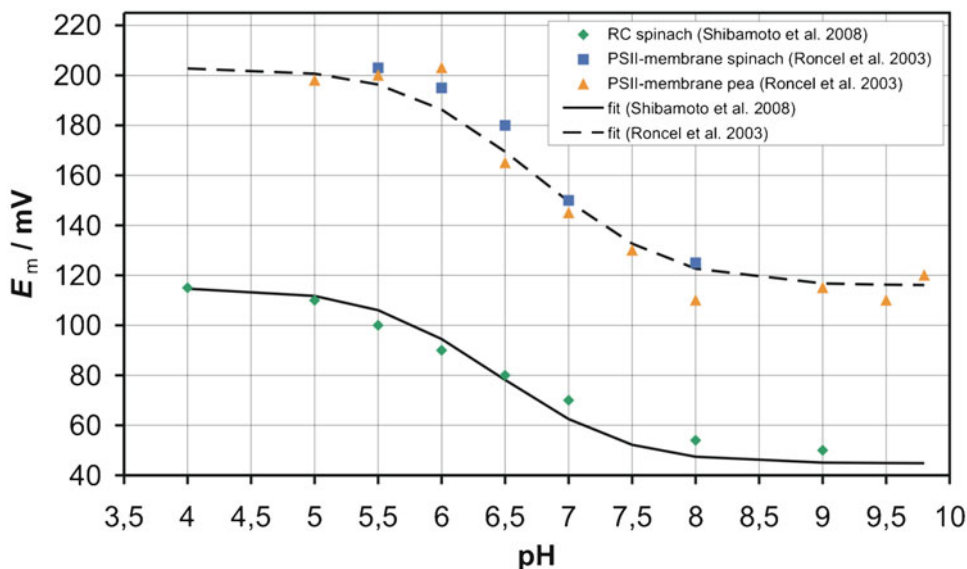


Fig. 8.9. pH-dependence of the redox midpoint potential  $E_m$  (versus normal hydrogen electrode) of cyt  $b_{559}$  in spinach PSII-enriched membranes according to Roncel et al. (2003) and in spinach PSII-RC complexes according to Shibamoto et al. (2008). The curves are fits to the Nernst-Clark equation.

corresponding  $pK_a$  values  $pK_{a,ox}$  and  $pK_{a,red}$ . Based on such a fit, the data can be interpreted in terms of a single titratable group interacting with cyt  $b_{559}$  with  $pK_{a,ox} = 6.0$  and  $pK_{a,red} = 7.5$ . However, the fit can be improved by considering at least two titratable groups interacting with cyt  $b_{559}$  (Roncel et al. 2001). Based on a chemical modification of histidine residues with the agent diethylpyrocarbonate, a model was proposed, according to which the deprotonation of one of the axial histidyl ligands to the heme is responsible for the pH-dependent transformation from the IP to the LP form, while the HP form originates from a reorientation of the protonated histidine side chain and the formation of a hydrogen bond accompanied by structural changes (Roncel et al. 2001). This model is interesting, but problematic in view of the crystal structure (see below, Sect. III.B.3), and the question remains unanswered, why this pH-dependence is not observed in cyanobacterial cyt  $b_{559}$  (Roncel et al. 2003).

In 2008, the pH-dependence was re-investigated by thin-layer cell spectroelectrochemistry using plant PSII-RCs. The obtained data are shown in the lower part

of Fig. 8.9 (Shibamoto et al. 2008) and are consistent with those of Roncel et al. (2001) concerning the pH-dependence, if one allows for slight changes of  $pK_{a,ox}$  and  $pK_{a,red}$  due to the isolation of the RC. It is striking, however, that both the low- and the high-pH form have a significantly lower redox potential in the RC compared to native membrane samples. This result suggests that there is at least one other factor that influences the redox potential independent of the titratable groups.

## 2. Polarity and Position Relative to $\alpha$ -Helices

There is a substantial electrostatic field in proteins due to polar groups (carrying partial charges), titratable residues (in their charged protonation state) and the fields induced by this permanent charge distribution in the polarizable medium (reaction fields). These fields on the whole determine the redox potential of a protein-bound heme group and not just those of the titratable groups causing the pH-dependence discussed above. This influence is due to the fact that

the heme group itself changes its charge and charge distribution when going from the reduced to the oxidized state. The two charge distributions interact differently with the permanent charge distribution of the surrounding protein and induce different reaction fields in the polarizable medium. In particular, the redox potential of a heme group is increased in an apolar medium compared to a polar medium due to the loss of the electrostatic solvation energy. The latter can be estimated based on the Born formula for ion solvation

$$\Delta G_{\text{Born}} = \frac{(Ze)^2}{8\pi\epsilon_0 r} \left( \frac{1}{\epsilon_m} - \frac{1}{\epsilon_w} \right) \quad (8.2)$$

where  $e$  is the elementary charge,  $Z$  the charge number of the ion (or charge difference between redox states, i.e.,  $Z = 1$  for the one-electron oxidation of the heme group),  $r$  is the ion radius (or effective radius assumed for a heme group),  $\epsilon_0$  is the vacuum permittivity, and  $\epsilon_m$  and  $\epsilon_w$  are the static dielectric constants of the membrane and the aqueous phase, respectively. This formula describes the free energy change for shifting an ion from water into the membrane interior. Using  $r = 6.5 \text{ \AA}$ ,  $\epsilon_m = 4$  and  $\epsilon_w = 80$ , one can estimate the contribution of the low dielectric constant of the membrane phase to the redox potential increase to be  $\sim 260 \text{ mV}$ . Similar values were obtained based on a simple geometric model of two TMHs binding a heme group in a lipid bilayer that also takes into account the polarizability of the protein part and the positioning of the heme close to the dielectric boundary between lipid and aqueous phase (Krishtalik et al. 1993). However, medium polarizability is unlikely to fully explain the potential difference between the HP form and the IP or LP forms of cyt  $b_{559}$ , as this would require substantial structural changes that lead to a shift of the heme group from an apolar medium to an essentially aqueous phase. The latter may occur, when cyt  $b_{559}$  disintegrates and the heme is at least partially released. It is thus possible that changes in medium po-

larizability contribute to the observation of lower potentials in damaged or aged samples depending on the degree of heme release and its effect on the absorption spectrum. Certain types of treatments such as trypsinization or heating may also cause a heme release, and one has to be careful with the interpretation of the observed low-potential forms. On the other hand, a distinct structural change from an intact HP form to intact IP or LP forms is unlikely to cause such drastic changes in the polarizability of the heme environment, so that the contribution of polarizability to a transition between these forms can be expected to be smaller than  $260 \text{ mV}$ . A precise determination of this contribution is impossible without detailed structural information about the different forms of cyt  $b_{559}$ .

An important aspect in protein electrostatics is that not only the side chains of polar amino acid residues create electrostatic fields, but also the protein backbone due to the dipole moment of the peptide bond. The form of the fields created by the backbone depends on the secondary structure. In particular,  $\alpha$ -helices create a strong dipole field because of the practically parallel alignment of their peptide bonds. The electrostatic potential due to the backbone of an  $\alpha$ -helix is similar to that of two partial charges of opposite sign (i.e., about  $\pm 0.5 e$ ) positioned at the ends of the helix (Sheridan et al. 1982). Hence, a molecule experiences a different field depending on whether it is located close to the N-terminus, the center or the C-terminus of the helix (Krishtalik et al. 1993). In cyt  $b_{559}$ , the heme group is bound close to the N-termini of the TMHs belonging to PsbE and PsbF. Krishtalik et al. (1993) estimated an increase of the redox potential by about  $200 \text{ mV}$  due to this position based on their structural model, but also discussed carefully the limits of the model. Indeed, the value of  $200 \text{ mV}$  is uncertain for the following reasons: (i) The heme group is positioned somewhat farther away from the N-termini of the helices in the crystal structure than in the model, which may decrease the potential up-shift due to the helix dipoles. (ii) The TMHs

are tilted with respect to each other, which on the basis of model calculations by Krishtalik et al. (1993) may increase the redox potential by up to 100 mV for a tilt angle of  $30^\circ$ . Based on the tilt angle of actually  $40^\circ$  (see above), the upshift may be even larger. (iii) The TMH of P<sub>sb</sub>Y is close by and contributes the field of a helix dipole in antiparallel orientation. This may in fact decrease the redox potential by a yet unknown amount. In addition, as stated above, one has to take into account the electrostatic field of the protein as a whole, so that it is anyway unclear, whether the dipoles of TMHs play a dominating role in determining the redox potential of cyt *b*<sub>559</sub>. More detailed calculations based on the recent crystal structures will be necessary to resolve this issue.

### 3. Axial Ligation and Interaction with Aromatic Amino Acid Residues

There is now doubt that the axial ligands of the central iron ion influence the redox potential of the heme group. According to earlier spectroscopic work (Babcock et al. 1985) and the crystal structures, cyt *b*<sub>559</sub> has a typical bis-histidine ligation. The question is, whether this ligation is changed in a transition from one to another redox potential form of cyt *b*<sub>559</sub>. The enzymatic activity discussed for cyt *b*<sub>559</sub> (Pospisil 2011) indeed may involve the displacement of one axial ligand to pave the way for a substrate such as superoxide to ligate to the iron. However, nothing of the sort appears to be responsible for the transition between redox potential forms, i.e., the iron remains ligated by two histidines. Rather, it has been proposed that the orientation of the two histidine ligands with respect to each other is different in the HP and LP forms (Babcock et al. 1985). On the basis of the crystal structure, though, such a reorientation is difficult to envision due to the strong interaction of the histidine imidazole rings with the protein environment. In particular, there are hydrogen bonds between the second imidazole nitrogen (i.e., not coordinating the iron) of each ligand

with a peptide backbone carbonyl group not uncommon for histidine-ligated cytochromes and predicted by Fourier transform infrared spectroscopy (Berthomieu et al. 1992). Furthermore, as mentioned above, there are  $\pi$ -stacking interactions with adjacent aromatic residues (Fig. 8.8). Therefore, any rotational motion of the imidazole rings is coupled to the surrounding protein and likely hindered. A possibility that remains is that the protein is rotated together with the imidazole rings. This would imply a change of the crossing angle of the two TMHs of P<sub>sb</sub>E and P<sub>sb</sub>F or a bending of the helices. A conformational change including whole TMHs could be a means to communicate changes at the donor side to the heme site.

An interesting detail is that Trp F20 points with the NH-group of its indole ring towards the heme macrocycle (Fig. 8.8). This arrangement suggests a kind of N–H... $\pi$  interaction that could contribute to heme binding. The influence of this type of interaction on the redox potential is presently unknown.

### 4. Nonplanarity of the Heme

It is known for some time that a nonplanar distortion of the heme tetrapyrrole macrocycle alters the redox properties (Barkigia et al. 1988; Shelnuitt et al. 1998). In a systematic study on site-directed mutants of the heme nitric oxide/oxygen binding (H-NOX) protein from *Thermoanaerobacter tengcongensis*, interactions of the heme with non-polar side chains were modified and hence the distortion of the heme manipulated and confirmed by X-ray crystallography (Olea et al. 2008, 2010). The measured redox potential shows a clear correlation with heme distortion: The flatter the tetrapyrrole macrocycle, the smaller the redox potential. The explanation is that heme distortion leads to less electron density at the heme iron due to a perturbation of the metal site away from an octahedral geometry. By analogy, we can conclude that the nonplanar distortion of the heme in cyt *b*<sub>559</sub> contributes to an increase of the redox potential. The question remains

open, whether the different redox potential forms have a different degree of nonplanarity of the heme.

### 5. Binding of Quinone-Like Molecules

The existence of a possible binding site for quinone-like molecules (i.e., PQ, PQH<sub>2</sub>, herbicides) close to cyt  $b_{559}$  (see Sect. II.C.1) implies that binding of these molecules could lead to structural perturbations of the heme site affecting the redox properties. Indeed, Kaminskaya et al. (2007) reported evidence for a strong influence of herbicides on the redox potentials of the various forms, but a weaker influence on the amount of each form (Table 8.1). A straightforward interpretation is that binding of such a molecule close to cyt  $b_{559}$  would not cause a switch between redox potential forms, but merely modulate the potential of the pre-existing form, i.e., mainly that of the HP form. Depending on the specificity of the binding site for PQ or PQH<sub>2</sub>, it is possible that the redox potential of the HP form is thus modulated by the redox state of the quinone pool in the thylakoid membrane. The physiological significance of such a modulation remains obscure.

### 6. Presence of Lipids, Detergent, and PsbY

Cyt  $b_{559}$  interacts with surrounding lipids and PsbY. Clearly, upon perturbation of the thylakoid membrane during the preparation of membrane fragments, core complexes or RCs, the lipids might be extracted or replaced with detergent molecules, and PsbY might be lost. Quantifying the consequences of these changes for the redox potential is difficult, but the data available (e.g., Table 8.1) suggest that overall the disruption of the membrane leads to a destabilization of the HP form. It would be desirable to analyse the lipid/detergent and protein subunit content in the various samples in greater detail in the future in order to establish a possible connection between redox potential shifts and these components.

## IV. Function of Cytochrome $b_{559}$

In the literature, one frequently encounters sentences like the following: “Despite extensive research, the role of cyt  $b_{559}$  is still unclear.” This statement remains true even though we have nowadays high-resolution crystal structures of PSIIcc at our disposal. Notwithstanding, numerous hypotheses concerning the function of cyt  $b_{559}$  have been proposed. In the following, we discuss those that are important in view of the recent literature.

### A. Side-Path Electron Transfer and Photoprotective Role

The photon-triggered electron transfer in the RC ultimately leads to the oxidation of a special chlorophyll (Chl)  $a$  pigment and thus the formation of a strong oxidant that is able to take electrons from water by virtue of the WOC and the redox-active tyrosine Y<sub>Z</sub> (Fig. 8.10). This strong oxidant is traditionally referred to as “P680<sup>+</sup>”, but is very likely P<sub>D1</sub><sup>•+</sup> (Renger and Schlodder 2011). If the native electron transfer from the WOC is impaired, P<sub>D1</sub><sup>•+</sup> could be accumulated and may cause damage by oxidizing other components of PSIIcc. This is referred to as donor side photoinhibition (Vass 2012). It has been proposed that cyt  $b_{559}$  acts as an electron donor to P<sub>D1</sub><sup>•+</sup> and thus provides protection against donor side photoinhibition (Barber and De Las Rivas 1993; Thompson and Brudvig 1988). Meanwhile, there is plenty of evidence for a side-path electron transfer (Faller et al. 2005), in which P<sub>D1</sub><sup>•+</sup> gets electrons from cyt  $b_{559}$  via the intermediate Car<sub>D2</sub>, probably sharing electrons with Chl<sub>ZD2</sub> (blue arrows in Fig. 8.10). However, other pigments might be involved as well. Recent progress in characterizing secondary electron transfer has been reviewed (Shinopoulos and Brudvig 2012). We note that the crystallographically detected PQ in the Q<sub>C</sub> site (Guskov et al. 2009) is located close to Car<sub>D2</sub> (see Figs. 8.1 and 8.4), and one may speculate that it acts as mediator in



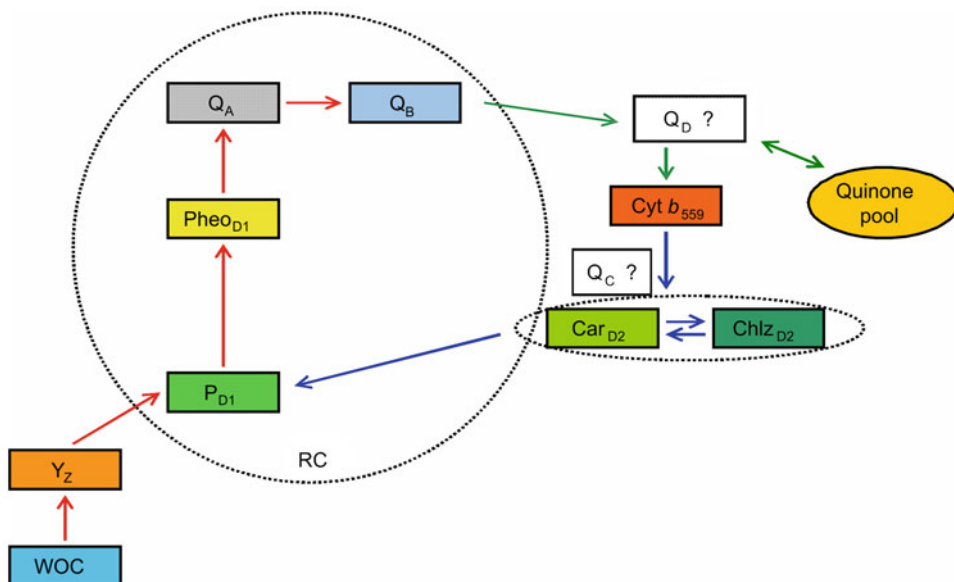


Fig. 8.10. Scheme of PSIIcc-cofactors involved in primary (red arrows), secondary (blue arrows), and putative (green arrows) electron transfer processes. For the real spatial arrangement of cofactors, see Fig. 8.1a. Q<sub>C</sub> is the crystallographically detected PQ (Guskov et al. 2009), while Q<sub>D</sub> indicates a hypothetical PQH<sub>2</sub> binding site close to cyt *b*<sub>559</sub> (Kaminskaya and Shuvalov 2013).

side-path electron transfer. Furthermore, cyt *b*<sub>559</sub> needs electrons to fulfill its protective role. A likely source of electrons is either the RC itself via the Q<sub>B</sub> site or the quinone pool (green arrows in Fig. 8.10). In both cases, a hypothetical quinone binding site close to cyt *b*<sub>559</sub> such as the proposed Q<sub>D</sub> site (see above) could be important for efficient electron delivery. However, there is a problem with this photoprotective role of cyt *b*<sub>559</sub>: The electron donation to P<sub>D1</sub><sup>•+</sup> from the side path is extremely inefficient and slow. In particular, it is not able to compete with P<sub>D1</sub><sup>•+</sup>Q<sub>A</sub><sup>•-</sup> charge recombination. Therefore, it has been argued that such a protection mechanism is actually invalid (Faller et al. 2005).

### B. “Save-the-Carotene” Model

Another source of photodamage is the formation of Chl triplet states either through inter-system crossing from Chl singlet states or through radical pair recombination (Vass 2012). The Chl triplets can act as sensitizer to produce the harmful singlet oxygen.

Carotenoids serve a photoprotective role by quenching the Chl triplets or the singlet oxygen (Pogson et al. 2005). It has been proposed that the purpose of Car<sub>D2</sub> is actually to quench singlet oxygen generated in the RC from Chl triplets (Faller et al. 2005). The peculiar positioning of Car<sub>D2</sub> relative to the RC is a compromise between being close enough to serve as effective quencher and being not too close to avoid oxidation by P<sub>D1</sub><sup>•+</sup>. Nonetheless, Car<sub>D2</sub> is oxidized by P<sub>D1</sub><sup>•+</sup> at a low quantum yield. The role of the side path electron transfer from cyt *b*<sub>559</sub> would then be to repair the Car<sub>D2</sub> quencher by reduction, i.e., to save the carotene (Cardona et al. 2012; Faller et al. 2005).

### C. Plastoquinol Oxidase and Oxygen Reductase

There is a second type of photoinhibition referred to as acceptor side photoinhibition (Vass 2012). It occurs, when the quinone pool is reduced and can no longer deliver PQ to the Q<sub>B</sub> site. This leads to the stabi-

lization of  $Q_A^{\bullet-}$  with the major consequence of enhanced triplet formation by radical pair recombination. It was proposed that PQH<sub>2</sub> oxidation by cyt  $b_{559}$  serves as a protective mechanism against acceptor side photoinhibition (Barber and De Las Rivas 1993). Indeed, there is evidence that PQH<sub>2</sub> can reduce cyt  $b_{559}$  as discussed above in the context of the putative Q<sub>D</sub> site. In addition, it has been proposed that the dark oxidation of PQH<sub>2</sub> by cyt  $b_{559}$  results in the formation of superoxide,  $O_2^{\bullet-}$  (Bondarava et al. 2003; Kruk and Strzalka 1999), where electron transfer from the heme to O<sub>2</sub> requires the LP form of cyt  $b_{559}$ . Independent evidence for an oxygen reductase activity of the LP form exists as reviewed by Pospisil (2011). Since  $O_2^{\bullet-}$  is a harmful reactive oxygen species (ROS), the question arises, how detoxification can be accomplished.

#### D. Superoxide Reductase and Oxidase

Based on the observation that the photooxidation of the HP form of cyt  $b_{559}$  is prevented by exogenous  $O_2^{\bullet-}$  scavengers (Tiwari and Pospisil 2009), it was proposed that cyt  $b_{559}$  acts as a superoxide reductase, whereby a protonated form of superoxide, the hydroperoxyl radical HO<sub>2</sub><sup>•</sup>, binds to the heme iron. The result of this reaction would be the formation of H<sub>2</sub>O<sub>2</sub> and a transformation of cyt  $b_{559}$  to the IP form (Pospisil 2011). The H<sub>2</sub>O<sub>2</sub> might be eliminated by catalase. The oxidized IP form of cyt  $b_{559}$  in turn was proposed to act as superoxide oxidase, transforming  $O_2^{\bullet-}$  into O<sub>2</sub> while being switched back into the HP form. Thus, a possible role of cyt  $b_{559}$  is to remove ROS.

#### E. Role in PSIIcc Assembly

There is biochemical evidence that cyt  $b_{559}$  is required for the assembly of PSIIcc in the thylakoid membrane (Komenda et al. 2004, 2008; Morais et al. 1998; Müller and Eichacker 1999; Nixon et al. 2010; Tae and Cramer 1992). It has been proposed that cyt

$b_{559}$  functions as a nucleus for the assembly of PSIIcc that is under redox control (Morais et al. 1998). In this context, the ability of cyt  $b_{559}$  to bind redox-active molecules such as PQ/PQH<sub>2</sub>, probably in conjunction with the D2 protein as discussed above, could be of importance. We would like to stress that during assembly of PSIIcc (Nixon et al. 2010), many subcomplexes occur that cannot oxidize water, but are able to perform light-induced charge separation in the RC, eventually with a non-functional acceptor side. This photochemistry is prone to the formation of harmful side products such as ROS. It is quite possible that cyt  $b_{559}$  puts into effect its protective role in these subcomplexes rather than in the fully assembled PSIIcc. The question remains, whether the corresponding electron transfer processes are more efficient under these conditions.

## V. Conclusions and Outlook

It is fair to say that we are still far away from understanding the function of cyt  $b_{559}$ . As usual, the crystal structures do not give immediately answers to all questions, but rather form a basis, whereupon future work can be build. When surveying the literature, we got the impression that research on cyt  $b_{559}$  is not as systematic as it should be. Many labs use different organisms and different types of preparations under various buffer conditions (see Table 8.1), and it is hard to draw a unified picture based upon this material. We also note that our description may have gaps, and we apologize for any omission. From the viewpoint of structural biology and related theoretical biophysics, it is clear that more work must be done to better characterize cyt  $b_{559}$  in crystallizable samples such as dimeric PSIIcc from *T. elongatus* in order to understand what the available crystal structures represent. Eventually, it may be possible to crystallize PSIIcc in another state or with another form of cyt  $b_{559}$ . This kind of research will likely shed more light on the “enigma”.

## Acknowledgments

This work was supported by the Deutsche Forschungsgemeinschaft through SFB 1078 (project A5) and Cluster of Excellence “Uni-Cat” coordinated by the Technische Universität Berlin (project E3/D3).

## References

- Ahmad I, Giorgi LB, Barber J, Porter G, Klug DR (1993) Redox potentials of cytochrome *b*-559 in the D1/D2/cytochrome *b*-559 reaction centre of Photosystem II. *Biochim Biophys Acta* 1143:239–242
- Akdogan Y, Anbazhagan V, Hinderberger D, Schneider D (2012) Heme binding constricts the conformational dynamics of the cytochrome *b*<sub>559</sub> heme binding cavity. *Biochemistry* 51:7149–7156
- Babcock GT, Widger WR, Cramer WA, Oertling WA, Metz JG (1985) Axial ligands of chloroplast cytochrome *b*-559: identification and requirement for a heme-cross-linked polypeptide structure. *Biochemistry* 24:3638–3645
- Barber J, De Las Rivas J (1993) A functional model for the role of cytochrome *b*<sub>559</sub> in the protection against donor and acceptor side photoinhibition. *Proc Natl Acad Sci USA* 90:10942–10946
- Barkigia KM, Chantranupong L, Smith KM, Fajer J (1988) Structural and theoretical models of photosynthetic chromophores. Implications for redox, light absorption properties and vectorial electron flow. *J Am Chem Soc* 110:7566–7567
- Beck WF, de Paula JC, Brudvig GW (1985) Active and resting states of the O<sub>2</sub>-evolving complex of Photosystem II. *Biochemistry* 24:3035–3043
- Bérczi A, Moller IM (2000) Redox enzymes in the plant plasma membrane and their possible roles. *Plant Cell Environ* 23:1287–1302
- Bergström J, Vänngård T (1982) EPR signals and orientation of cytochromes in the spinach chloroplast thylakoid membrane. *Biochim Biophys Acta* 682:452–456
- Berthold DA, Babcock GT, Yocum CF (1981) A highly resolved, oxygen-evolving Photosystem II preparation from spinach thylakoid membranes – EPR and electron-transport properties. *FEBS Lett* 134:231–234
- Berthomieu C, Boussac A, Mäntele W, Breton J, Navedryk E (1992) Molecular changes following oxidoreduction of cytochrome *b*<sub>559</sub> characterized by Fourier-transform infrared difference spectroscopy and electron paramagnetic resonance – photooxidation in Photosystem II and electrochemistry of isolated cytochrome *b*<sub>559</sub> and iron protoporphyrin IX-bisimidazole model compounds. *Biochemistry* 31:11460–11471
- Biesiadka J, Loll B, Kern J, Irrgang KD, Zouni A (2004) Crystal structure of cyanobacterial Photosystem II at 3.2 Å resolution: a closer look at the Mn-cluster. *Phys Chem Chem Phys* 6:4733–4736
- Boardman NK, Anderson JM (1967) Fractionation of photochemical systems of photosynthesis. 2. Cytochrome and carotenoid contents of particles isolated from spinach chloroplasts. *Biochim Biophys Acta* 143:187–203
- Bondarava N, de Pascalis L, Al-Babili S, Goussias C, Golecki JR, Beyer P, Bock R, Krieger-Liszskay A (2003) Evidence that cytochrome *b*<sub>559</sub> mediates the oxidation of reduced plastoquinone in the dark. *J Biol Chem* 278:13554–13560
- Boussac A, Koyama K, Sugiura M (2013) The TII0287 protein is a hemoprotein associated with the PsbA2-Photosystem II complex in *Thermosynechococcus elongatus*. *Biochim Biophys Acta* 1827:1174–1182
- Brandl M, Weiss MS, Jabs A, Sühnel J, Hilgenfeld R (2001) C – H ⋯ π-interactions in proteins. *J Mol Biol* 307:357–377
- Bricker TM, Burnap RL (2005) The extrinsic proteins of Photosystem II. In: Wydrzynski T, Satoh K (eds) *Photosystem II: The Light-Driven Water: Plastoquinone Oxidoreductase*. Springer, Dordrecht, pp 95–120
- Bricker TM, Roose JL, Fagerlund RD, Frankel LK, Eaton-Rye JJ (2012) The extrinsic proteins of Photosystem II. *Biochim Biophys Acta* 1817:121–142
- Brose K, Zouni A, Müh F, Mroginski MA, Maultzsch J (2013) Simulations of the polarisation-dependent Raman intensity of β-carotene in Photosystem II crystals. *Chem Phys* 418:65–73
- Buser CA, Diner BA, Brudvig GW (1992) Photooxidation of cytochrome *b*<sub>559</sub> in oxygen-evolving Photosystem II. *Biochemistry* 31:11449–11459
- Caffarri S, Kouril R, Kereiche S, Boekema EJ, Croce R (2009) Functional architecture of higher plant Photosystem II supercomplexes. *EMBO J* 28:3052–3063
- Cardona T, Sedoud A, Cox N, Rutherford AW (2012) Charge separation in Photosystem II: a comparative and evolutionary overview. *Biochim Biophys Acta* 1817:26–43
- Chapman DJ, Gounaris K, Barber J (1988) Electron-transport properties of the isolated D1-D2-cytochrome *b*-559 Photosystem II reaction centre. *Biochim Biophys Acta* 933:423–431
- Choma C, Gratkowski H, Lear JD, DeGrado WF (2000) Asparagine-mediated self-association of a model transmembrane helix. *Nat Struct Biol* 7:161–166

- Chothia C, Levitt M, Richardson D (1977) Structure of proteins – packing of  $\alpha$ -helices and pleated sheets. *Proc Natl Acad Sci USA* 74:4130–4134
- Cramer WA (2004) Ironies in photosynthetic electron transport: a personal perspective. *Photosynth Res* 80:293–305
- Cramer WA, Whitmarsh J (1977) Photosynthetic cytochromes. *Annu Rev Plant Physiol* 28:133–172
- Crowder MS, Prince RC, Bearden A (1982) Orientation of membrane-bound cytochromes in chloroplasts, detected by low-temperature EPR spectroscopy. *FEBS Lett* 144:204–208
- Faller P, Fufezan C, Rutherford AW (2005) Side-path electron donors: cytochrome *b*<sub>559</sub>, chlorophyll Z and  $\beta$ -carotene. In: Wydrzynski T, Satoh K (eds) *Photosystem II: The Light-Driven Water: Plastoquinone Oxidoreductase*. Springer, Dordrecht, pp 347–365
- Ferreira KN, Iverson TM, Maghlaoui K, Barber J, Iwata S (2004) Architecture of the photosynthetic oxygen-evolving center. *Science* 303:1831–1838
- Frank HA, Brudvig GW (2004) Redox functions of carotenoids in photosynthesis. *Biochemistry* 43:8607–8615
- Gámiz-Hernández AP, Kieseritzky G, Galstyan AS, Demir-Kavuk O, Knapp EW (2010) Understanding properties of cofactors in proteins: redox potentials of synthetic cytochromes *b*. *ChemPhysChem* 11:1196–1206
- García-Cerdán JG, Sveshnikov D, Dewez D, Jansson S, Funk C, Schröder WP (2009) Antisense inhibition of the PsbX protein affects PSII integrity in the higher plant *Arabidopsis thaliana*. *Plant Cell Physiol* 50:191–202
- Garewal HS, Wasserman AR (1974a) Triton X-100-4 M urea as an extraction medium for membrane proteins. I. Purification of chloroplast cytochrome *b*<sub>559</sub>. *Biochemistry* 13:4063–4071
- Garewal HS, Wasserman AR (1974b) Triton X-100-4 M urea as an extraction medium for membrane proteins. II. Molecular properties of pure cytochrome *b*<sub>559</sub>: a lipoprotein containing small polypeptide chains and a limited lipid composition. *Biochemistry* 13:4072–4079
- Guerrero F, Zurita JL, Roncel M, Kirilovsky D, Ortega JM (2014) The role of the high potential form of the cytochrome *b*<sub>559</sub>: study of *Thermosynechococcus elongatus* mutants. *Biochim Biophys Acta* 1837:908–919
- Gurezka R, Langosch D (2001) In vitro selection of membrane-spanning leucine zipper protein-protein interaction motifs using POSSYCCAT. *J Biol Chem* 276:45580–45587
- Gurezka R, Laage R, Brosig B, Langosch D (1999) A heptad motif of leucine residues found in membrane proteins can drive self-assembly of artificial transmembrane segments. *J Biol Chem* 274:9265–9270
- Guskov A, Kern J, Gabdulkhakov A, Broser M, Zouni A, Saenger W (2009) Cyanobacterial Photosystem II at 2.9 Å resolution: role of quinones, lipids, channels and chloride. *Nat Struct Mol Biol* 16:334–342
- Guskov A, Gabdulkhakov A, Broser M, Glöckner C, Hellmich J, Kern J, Frank J, . . . , Zouni A (2010) Recent progress in the crystallographic studies of photosystem II. *ChemPhysChem* 11:1160–1171
- Hager M, Hermann M, Biehler K, Krieger-Liszkay A, Bock R (2002) Lack of the small plastid-encoded PsbJ polypeptide results in a defective water-splitting apparatus of Photosystem II, reduced Photosystem I levels, and hypersensitivity to light. *J Biol Chem* 277:14031–14039
- Herrmann RG, Alt J, Schiller B, Widger WR, Cramer WA (1984) Nucleotide-sequence of the gene for apocytochrome *b*-559 on the spinach plastid chromosome – implications for the structure of the membrane protein. *FEBS Lett* 176:239–244
- Horton P, Croze E (1977) The relationship between activity of chloroplast Photosystem II and the midpoint oxidation-reduction potential of cytochrome *b*-559. *Biochim Biophys Acta* 462:86–101
- Humphrey W, Dalke A, Schulten K (1996) VMD: visual molecular dynamics. *J Mol Graph* 14:33–38
- Iwasaki I, Tamura N, Okayama S (1995) Effects of light stress on redox potential forms of cyt *b*-559 in Photosystem II membranes depleted of water-oxidizing complex. *Plant Cell Physiol* 36:583–589
- Kaminskaya OP, Shuvalov VA (2013) Biphasic reduction of cytochrome *b*<sub>559</sub> by plastoquinol in Photosystem II membrane fragments evidence for two types of cytochrome *b*<sub>559</sub>/plastoquinone redox equilibria. *Biochim Biophys Acta* 1827:471–483
- Kaminskaya O, Kurreck J, Irrgang KD, Renger G, Shuvalov VA (1999) Redox and spectral properties of cytochrome *b*<sub>559</sub> in different preparations of Photosystem II. *Biochemistry* 38:16223–16235
- Kaminskaya O, Kern J, Shuvalov VA, Renger G (2005) Extinction coefficients of cytochromes *b*<sub>559</sub> and *c*<sub>550</sub> of *Thermosynechococcus elongatus* and cyt *b*<sub>559</sub>/PS II stoichiometry of higher plants. *Biochim Biophys Acta* 1708:333–341
- Kaminskaya O, Shuvalov VA, Renger G (2007) Evidence for a novel quinone-binding site in the Photosystem II (PS II) complex that regulates the redox potential of cytochrome *b*<sub>559</sub>. *Biochemistry* 46:1091–1105

- Kamiya N, Shen JR (2003) Crystal structure of oxygen-evolving Photosystem II from *Thermosynechococcus vulcanus* at 3.7 Å resolution. *Proc Natl Acad Sci USA* 100:98–103
- Kashino Y, Takahashi T, Inoue-Kashino N, Ban A, Ikeda Y, Satoh K, Sugiura M (2007) Ycf12 is a core subunit in the Photosystem II complex. *Biochim Biophys Acta* 1767:1269–1275
- Kato Y, Shibamoto T, Yamamoto S, Watanabe T, Ishida N, Sugiura M, Rappaport F, Boussac A (2012) Influence of the PsbA1/PsbA3, Ca<sup>2+</sup>/Sr<sup>2+</sup> and Cl<sup>-</sup>/Br<sup>-</sup> exchanges on the redox potential of the primary quinone Q<sub>A</sub> in Photosystem II from *Thermosynechococcus elongatus* as revealed by spectroelectrochemistry. *Biochim Biophys Acta* 1817:1998–2004
- Katoh H, Ikeuchi M (2001) Targeted disruption of *psbX* and biochemical characterization of Photosystem II complex in the thermophilic cyanobacterium *Synechococcus elongatus*. *Plant Cell Physiol* 42:179–188
- Kawakami K, Iwai M, Ikeuchi M, Kamiya N, Shen JR (2007) Location of PsbY in oxygen-evolving Photosystem II revealed by mutagenesis and X-ray crystallography. *FEBS Lett* 581:4983–4987
- Kern J, Guskov A (2011) Lipids in Photosystem II: multifunctional cofactors. *J Photochem Photobiol B* 104:19–34
- Kern J, Loll B, Lüneberg C, DiFiore D, Biesiadka J, Irrgang KD, Zouni A (2005) Purification, characterisation and crystallisation of Photosystem II from *Thermosynechococcus elongatus* cultivated in a new type of photobioreactor. *Biochim Biophys Acta* 1706:147–157
- Kim SJ, Robinson D, Robinson C (1996) An *Arabidopsis thaliana* cDNA encoding PS II-X, a 4.1 kDa component of Photosystem II: a bipartite presequence mediates SecA/delta pH-independent targeting into thylakoids. *FEBS Lett* 390:175–178
- Komenda J, Reisinger V, Müller BC, Dobáková M, Granvogl B, Eichacker LA (2004) Accumulation of the D2 protein is a key regulatory step for assembly of the Photosystem II reaction center complex in *Synechocystis* PCC 6803. *J Biol Chem* 279:48620–48629
- Komenda J, Nickelsen J, Tichy M, Prasil O, Eichacker LA, Nixon PJ (2008) The cyanobacterial homologue of HCF136/YCF48 is a component of an early Photosystem II assembly complex and is important for both the efficient assembly and repair of Photosystem II in *Synechocystis* sp. PCC 6803. *J Biol Chem* 283:22390–22399
- Koua FH, Umena Y, Kawakami K, Shen JR (2013) Structure of Sr-substituted Photosystem II at 2.1 Å resolution and its implications in the mechanism of water oxidation. *Proc Natl Acad Sci USA* 110:3889–3894
- Krishtalik LI, Tae GS, Cherepanov DA, Cramer WA (1993) The redox properties of cytochromes *b* imposed by the membrane electrostatic environment. *Biophys J* 65:184–195
- Kruk J, Strzalka K (1999) Dark reoxidation of the plastoquinone-pool is mediated by the low-potential form of cytochrome *b*-559 in spinach thylakoids. *Photosynth Res* 62:273–279
- Kruk J, Strzalka K (2001) Redox changes of cytochrome *b*<sub>559</sub> in the presence of plastoquinones. *J Biol Chem* 276:86–91
- Kuwabara T, Murata N (1982) Inactivation of photosynthetic oxygen evolution and concomitant release of three polypeptides in the Photosystem II particles of spinach-chloroplasts. *Plant Cell Physiol* 23:533–539
- Langosch D, Arkin IT (2009) Interaction and conformational dynamics of membrane-spanning protein helices. *Protein Sci* 18:1343–1358
- Lind LK, Shukla VK, Nyhus KJ, Pakrasi HB (1993) Genetic and immunological analyses of the cyanobacterium *Synechocystis* sp. PCC 6803 show that the protein encoded by the *psbJ* gene regulates the number of Photosystem II centers in thylakoid membranes. *J Biol Chem* 268:1575–1579
- Loll B, Kern J, Saenger W, Zouni A, Biesiadka J (2005) Towards complete cofactor arrangement in the 3.0 Å resolution structure of Photosystem II. *Nature* 438:1040–1044
- Loll B, Broser M, Kos PB, Kern J, Biesiadka J, Vass I, Saenger W, Zouni A (2008) Modeling of variant copies of subunit D1 in the structure of Photosystem II from *Thermosynechococcus elongatus*. *Biol Chem* 389:609–617
- Lu PL, Ma D, Yan CY, Gong XQ, Du MJ, Shi YG (2014) Structure and mechanism of a eukaryotic transmembrane ascorbate-dependent oxidoreductase. *Proc Natl Acad Sci USA* 111:1813–1818
- Mant A, Robinson C (1998) An *Arabidopsis* cDNA encodes an apparent polyprotein of two non-identical thylakoid membrane proteins that are associated with Photosystem II and homologous to algal *ycf32* open reading frames. *FEBS Lett* 423:183–188
- McNamara VP, Gounaris K (1995) Granal Photosystem II complexes contain only the high redox potential form of cytochrome *b*-559 which is stabilized by the ligation of calcium. *Biochim Biophys Acta* 1231:289–296
- Meetam M, Keren N, Ohad I, Pakrasi HB (1999) The PsbY protein is not essential for oxygenic photosynthesis in the cyanobacterium *Synechocystis* sp. PCC 6803. *Plant Physiol* 121:1267–1272

- Moore DT, Berger BW, DeGrado WF (2008) Protein-protein interactions in the membrane: sequence, structural, and biological motifs. *Structure* 16:991–1001
- Mor TS, Ohad I, Hirschberg J, Pakrasi HB (1995) An unusual organization of the genes encoding cytochrome *b*<sub>559</sub> in *Chlamydomonas reinhardtii*: *psbE* and *psbF* genes are separately transcribed from different regions of the plastid chromosome. *Mol Gen Genet* 246:600–604
- Morais F, Barber J, Nixon PJ (1998) The chloroplast-encoded a subunit of cytochrome *b*-559 is required for assembly of the Photosystem two complex in both the light and the dark in *Chlamydomonas reinhardtii*. *J Biol Chem* 273:29315–29320
- Mörschel E, Schatz GH (1987) Correlation of Photosystem II complexes with exoplasmic freeze-fracture particles of thylakoids of the cyanobacterium *Synechococcus* sp. *Planta* 172:145–154
- Moskalenko AA, Barbato R, Giacometti GM (1992) Investigation of the neighbour relationships between Photosystem II polypeptides in the two types of isolated reaction centres (D1/D2/cyt<sub>b</sub><sub>559</sub> and CP47/D1/D2/cyt *b*<sub>559</sub> complexes). *FEBS Lett* 314:271–274
- Müh F, Zouni A (2013) The nonheme iron in Photosystem II. *Photosynth Res* 116:295–314
- Müh F, Renger T, Zouni A (2008) Crystal structure of cyanobacterial Photosystem II at 3.0 Å resolution: a closer look at the antenna system and the small membrane-intrinsic subunits. *Plant Physiol Biochem* 46:238–264
- Müh F, Glöckner C, Hellmich J, Zouni A (2012) Light-induced quinone reduction in Photosystem II. *Biochim Biophys Acta* 1817:44–65
- Müller B, Eichacker LA (1999) Assembly of the D1 precursor in monomeric Photosystem II reaction center precomplexes precedes chlorophyll *a*-triggered accumulation of reaction center II in barley etioplasts. *Plant Cell* 11:2365–2377
- Mulo P, Sicora C, Aro EM (2009) Cyanobacterial *psbA* gene family: optimization of oxygenic photosynthesis. *Cell Mol Life Sci* 66:3697–3710
- Mulo P, Sakurai I, Aro EM (2012) Strategies for *psbA* gene expression in cyanobacteria, green algae and higher plants: from transcription to PSII repair. *Biochim Biophys Acta* 1817:247–257
- Nakamura Y, Kaneko T, Sato S, Ikeuchi M, Katoh H, Sasamoto S, Watanabe A, . . . , Tabata S (2002) Complete genome structure of the thermophilic cyanobacterium *Thermosynechococcus elongatus* BP-1. *DNA Res* 9:123–130, Suppl. 135–148
- Nanba O, Satoh K (1987) Isolation of a Photosystem II reaction center consisting of D-1 and D-2 polypeptides and cytochrome *b*-559. *Proc Natl Acad Sci USA* 84:109–112
- Nixon PJ, Michoux F, Yu JF, Boehm M, Komenda J (2010) Recent advances in understanding the assembly and repair of Photosystem II. *Ann Bot* 106:1–16
- Nowaczyk MM, Sander J, Grasse N, Cormann KU, Rexroth D, Bernat G, Rögner M (2010) Dynamics of the cyanobacterial photosynthetic network: communication and modification of membrane protein complexes. *Eur J Cell Biol* 89:974–982
- Nowaczyk MM, Krause K, Mieseler M, Sczibilanski A, Ikeuchi M, Rögner M (2012) Deletion of *psbJ* leads to accumulation of Psb27-Psb28 Photosystem II complexes in *Thermosynechococcus elongatus*. *Biochim Biophys Acta* 1817:1339–1345
- Nowicka B, Kruk J (2010) Occurrence, biosynthesis and function of isoprenoid quinones. *Biochim Biophys Acta* 1797:1587–1605
- Ohad I, Dal Bosco C, Herrmann RG, Meurer J (2004) Photosystem II proteins PsbL and PsbJ regulate electron flow to the plastoquinone pool. *Biochemistry* 43:2297–2308
- Olea C, Boon EM, Pellicena P, Kuriyan J, Marletta MA (2008) Probing the function of heme distortion in the H-NOX family. *ACS Chem Biol* 3:703–710
- Olea C, Kuriyan J, Marletta MA (2010) Modulating heme redox potential through protein-induced porphyrin distortion. *J Am Chem Soc* 132:12794–12795
- Ortega JM, Hervás M, Losada M (1988) Redox and acid-base characterization of cytochrome *b*-559 in Photosystem II particles. *Eur J Biochem* 171:449–455
- Ortega JM, Hervas M, Delarosa MA, Losada M (1994) Redox properties of cytochrome *b*559 in photosynthetic membranes from the cyanobacterium *Synechocystis* sp. PCC 6803. *J Plant Physiol* 144:454–461
- Pakrasi HB, Williams JG, Arntzen CJ (1988) Targeted mutagenesis of the *psbE* and *psbF* genes blocks photosynthetic electron transport: evidence for a functional role of cytochrome *b*<sub>559</sub> in Photosystem II. *EMBO J* 7:325–332
- Pakrasi HB, Deciechi P, Whitmarsh J (1991) Site directed mutagenesis of the heme axial ligands of cytochrome *b*559 affects the stability of the Photosystem II complex. *EMBO J* 10:1619–1627
- Pogson BJ, Rissler HM, Frank HA (2005) The role of carotenoids in energy quenching. In: Wydrzynski T, Satoh K (eds) *Photosystem II: The Light-Driven Water: Plastoquinone Oxidoreductase*. Springer, Dordrecht, pp 515–537
- Pospisil P (2011) Enzymatic function of cytochrome *b*<sub>559</sub> in Photosystem II. *J Photochem Photobiol B* 104:341–347

- Radmer R, Cammarata K, Tamura N, Ollinger O, Cheniae G (1986) Depletion of Photosystem II-extrinsic proteins. 1. Effects on O<sub>2</sub>-flash and N<sub>2</sub>-flash yields and steady-state O<sub>2</sub> evolution. *Biochim Biophys Acta* 850:21–32
- Regel RE, Ivleva NB, Zer H, Meurer J, Shestakov SV, Herrmann RG, Pakrasi HB, Ohad I (2001) Deregulation of electron flow within Photosystem II in the absence of the PsbJ protein. *J Biol Chem* 276:41473–41478
- Renger G (ed) (2008) Primary Processes of Photosynthesis – Principles and Apparatus, vol 1, 2, Comprehensive Series in Photochemistry and Photobiology, vol 8, 9. RSC Publishing, Cambridge
- Renger T, Schlodder E (2011) Optical properties, excitation energy and primary charge transfer in Photosystem II: theory meets experiment. *J Photochem Photobiol B* 104:126–141
- Roncel M, Ortega JM, Losada M (2001) Factors determining the special redox properties of photosynthetic cytochrome *b559*. *Eur J Biochem* 268:4961–4968
- Roncel M, Boussac A, Zurita JL, Bottin H, Sugiura M, Kirilovsky D, Ortega JM (2003) Redox properties of the Photosystem II cytochromes *b559* and *c550* in the cyanobacterium *Thermosynechococcus elongatus*. *J Biol Inorg Chem* 8:206–216
- Sander J, Nowaczyk M, Buchta J, Dau H, Vass I, Deak Z, Dorogi M, . . . , Rögner M (2010) Functional characterization and quantification of the alternative PsbA copies in *Thermosynechococcus elongatus* and their role in photoprotection. *J Biol Chem* 285:29851–29856
- Shelnutt JA, Song XZ, Ma JG, Jia SL, Jentzen W, Medforth CJ (1998) Nonplanar porphyrins and their significance in proteins. *Chem Soc Rev* 27:31–41
- Sheridan RP, Levy RM, Salemme FR (1982)  $\alpha$ -helix dipole model and electrostatic stabilization of 4- $\alpha$ -helical proteins. *Proc Natl Acad Sci USA* 79:4545–4549
- Shi LX, Schröder WP (2004) The low molecular mass subunits of the photosynthetic supracomplex, Photosystem II. *Biochim Biophys Acta* 1608:75–96
- Shi LX, Hall M, Funk C, Schröder WP (2012) Photosystem II, a growing complex: updates on newly discovered components and low molecular mass proteins. *Biochim Biophys Acta* 1817:13–25
- Shibamoto T, Kato Y, Watanabe T (2008) Spectroelectrochemistry of cytochrome *b559* in the D1-D2-Cyt *b559* complex from spinach. *FEBS Lett* 582:1490–1494
- Shinopoulos KE, Brudvig GW (2012) Cytochrome *b559* and cyclic electron transfer within Photosystem II. *Biochim Biophys Acta* 1817:66–75
- Shinopoulos KE, Yu J, Nixon PJ, Brudvig GW (2014) Using site-directed mutagenesis to probe the role of the D2 carotenoid in the secondary electron-transfer pathway of Photosystem II. *Photosynth Res* 120:141–152
- Shuvalov VA (1994) Composition and function of cytochrome *b559* in reaction centers of Photosystem II of green plants. *J Bioenerg Biomembr* 26:619–626
- Shuvalov VA, Schreiber U, Heber U (1994) Spectral and thermodynamic properties of the two hemes of the D1D2cytochrome *b-559* complex of spinach. *FEBS Lett* 337:226–230
- Sicora CI, Ho FM, Salminen T, Styring S, Aro EM (2009) Transcription of a “silent” cyanobacterial *psbA* gene is induced by microaerobic conditions. *Biochim Biophys Acta* 1787:105–112
- Stewart AC, Bendall DS (1980) Photosynthetic electron transport in a cell-free preparation from the thermophilic blue-green alga *Phormidium laminosum*. *Biochem J* 188:351–361
- Stewart DH, Brudvig GW (1998) Cytochrome *b559* of Photosystem II. *Biochim Biophys Acta* 1367:63–87
- Sugiura M, Inoue Y (1999) Highly purified thermostable oxygen-evolving Photosystem II core complex from the thermophilic cyanobacterium *Synechococcus elongatus* having His-tagged CP43. *Plant Cell Physiol* 40:1219–1231
- Sugiura M, Iwai E, Hayashi H, Boussac A (2010a) Differences in the interactions between the subunits of Photosystem II dependent on D1 protein variants in the thermophilic cyanobacterium *Thermosynechococcus elongatus*. *J Biol Chem* 285:30008–30018
- Sugiura M, Kato Y, Takahashi R, Suzuki H, Watanabe T, Noguchi T, Rappaport F, Boussac A (2010b) Energetics in Photosystem II from *Thermosynechococcus elongatus* with a D1 protein encoded by either the *psbA1* or *psbA3* gene. *Biochim Biophys Acta* 1797:1491–1499
- Sugiura M, Ogami S, Kusumi M, Un S, Rappaport F, Boussac A (2012) Environment of Tyr<sub>Z</sub> in Photosystem II from *Thermosynechococcus elongatus* in which PsbA2 is the D1 protein. *J Biol Chem* 287:13336–13347
- Sugiura M, Azami C, Koyama K, Rutherford AW, Rappaport F, Boussac A (2014) Modification of the pheophytin redox potential in *Thermosynechococcus elongatus* Photosystem II with PsbA3 as D1. *Biochim Biophys Acta* 1837:139–148
- Suorsa M, Regel RE, Paakkarinen V, Battchikova N, Herrmann RG, Aro EM (2004) Protein assembly of Photosystem II and accumulation of subcomplexes in the absence of low molecular mass subunits PsbL and PsbJ. *Eur J Biochem* 271:96–107

- Swiatek M, Regel RE, Meurer J, Wanner G, Pakrasi HB, Ohad I, Herrmann RG (2003) Effects of selective inactivation of individual genes for low-molecular-mass subunits on the assembly of Photosystem II, as revealed by chloroplast transformation: the *psbEFLJ* operon in *Nicotiana tabacum*. *Mol Genet Genomics* 268:699–710
- Tae GS, Cramer WA (1992) Truncation of the COOH-terminal domain of the *psbE* gene product in *Synechocystis* sp. PCC 6803: requirements for Photosystem II assembly and function. *Biochemistry* 31:4066–4074
- Tae GS, Cramer WA (1994) Topography of the heme prosthetic group of cytochrome *b*-559 in the Photosystem II reaction center. *Biochemistry* 33:10060–10068
- Tae GS, Black MT, Cramer WA, Vallon O, Bogorad L (1988) Thylakoid membrane protein topography: transmembrane orientation of the chloroplast cytochrome *b*-559 *psbE* gene product. *Biochemistry* 27:9075–9080
- Tae GS, Everly RM, Cramer WA, Madgwick SA, Rich PR (1993) On the question of the identity of cytochrome *b*<sub>560</sub> in thylakoid stromal membranes. *Photosynth Res* 36:141–146
- Thompson LK, Brudvig GW (1988) Cytochrome *b*-559 may function to protect Photosystem II from photoinhibition. *Biochemistry* 27:6653–6658
- Thompson LK, Miller AF, Buser CA, de Paula JC, Brudvig GW (1989) Characterization of the multiple forms of cytochrome *b*<sub>559</sub> in Photosystem II. *Biochemistry* 28:8048–8056
- Thompson SJ, Robinson C, Mant A (1999) Dual signal peptides mediate the signal recognition particle/sec-independent insertion of a thylakoid membrane polyprotein, PsbY. *J Biol Chem* 274:4059–4066
- Thornton LE, Roose JL, Pakrasi HB, Ikeuchi M (2005) The low molecular weight proteins of Photosystem II. In: Wydrzynski T, Satoh K (eds) *Photosystem II: The Light-Driven Water: Plastoquinone Oxidoreductase*. Springer, Dordrecht, pp 121–137
- Tiwari A, Pospisil P (2009) Superoxide oxidase and reductase activity of cytochrome *b*<sub>559</sub> in Photosystem II. *Biochim Biophys Acta* 1787:985–994
- Umena Y, Kawakami K, Shen JR, Kamiya N (2011) Crystal structure of oxygen-evolving Photosystem II at a resolution of 1.9 Å. *Nature* 473:55–60
- Vallon O, Tae GS, Cramer WA, Simpson D, Hoyer-Hansen G, Bogorad L (1989) Visualization of antibody binding to the photosynthetic membrane: the transmembrane orientation of cytochrome *b*-559. *Biochim Biophys Acta* 975:132–141
- Vass I (2012) Molecular mechanisms of photodamage in the Photosystem II complex. *Biochim Biophys Acta* 1817:209–217
- Völker M, Ono T, Inoue Y, Renger G (1985) Effect of trypsin on PSII particles. Correlation between hill-activity, Mn-abundance and peptide pattern. *Biochim Biophys Acta* 806:25–34
- Walters RFS, DeGrado WF (2006) Helix-packing motifs in membrane proteins. *Proc Natl Acad Sci USA* 103:13658–13663
- Waters ML (2002) Aromatic interactions in model systems. *Curr Opin Chem Biol* 6:736–741
- Whitmarsh J, Pakrasi HB (1996) Form and function of cytochrome *b*-559. In: Ort DR, Yocum CF (eds) *Oxygenic Photosynthesis: The Light Reactions*. Kluwer, Dordrecht, pp 249–264
- Widger WR, Cramer WA, Hermodson M, Herrmann RG (1985) Evidence for a hetero-oligomeric structure of the chloroplast cytochrome *b*-559. *FEBS Lett* 191:186–190
- Yamashita T (1986) Modification of oxygen evolving center by tris-washing. *Photosynth Res* 10:473–481
- Zhou FX, Cocco MJ, Russ WP, Brunger AT, Engelman DM (2000) Interhelical hydrogen bonding drives strong interactions in membrane proteins. *Nat Struct Biol* 7:154–160
- Zouni A (2008) From cell growth to the 3.0 Å resolution crystal structure of cyanobacterial Photosystem II. In: Renger G (ed) *Primary Processes of Photosynthesis, Principles and Apparatus*, vol 2. RSC Publishing, Cambridge, MA, pp 193–236
- Zouni A, Witt HT, Kern J, Fromme P, Krauss N, Saenger W, Orth P (2001) Crystal structure of Photosystem II from *Synechococcus elongatus* at 3.8 Å resolution. *Nature* 409:739–743



# Chapter 9

## Structure-Function of the Cytochrome $b_6f$ Lipoprotein Complex

William A. Cramer\* and S. Saif Hasan

*Department of Biological Sciences, Hockmeyer Building of  
Structural Biology, Purdue University, West Lafayette, IN 47907,  
USA*

Summary.....	178
I. Introduction.....	179
II. Historical Perspective.....	179
III. Cytochrome $b_6f$ and $bc_1$ Complexes; General Aspects.....	180
IV. Structure-Function of the Cyt $b_6f$ Complex.....	180
A. Problems in Crystallization.....	180
B. General Structure Features of the Cyt $b_6c$ Complex.....	182
C. Unique Chlorophyll $a$ and $\beta$ -Carotene.....	183
D. Trans-Membrane Hemes, $b_n$ and $b_p$ .....	183
1. Hemes, $b_n$ and $b_p$ , Oxidation-Reduction Potentials.....	185
2. Reducibility of $b$ Hemes; Heterogeneity of Internal Dielectric Constants.....	186
E. The High Potential [2Fe-2S] Rieske Iron-Sulfur Protein (ISP).....	186
1. ISP Electron Transfer; a p-Side Conformation/Mobility Problem.....	186
F. Differences Between $b_6f$ and $bc_1$ Complexes.....	187
1. Comparison of Cytochromes $f$ and $c_1$ .....	187
G. The Four Small Peripheral Subunits, Pet G, L, M, and N; a Late Addition in Evolution?.....	187
H. Peripheral Subunits Not Seen in the $b_6f$ Crystal Structure.....	188
I. Distribution of Aromatic Residues in the Trans-Membrane Domain.....	189
J. Inhibitors; Differences Between the $bc$ Complexes.....	189
V. Lipids in the $b_6f$ Lipoprotein Complex.....	190
A. Lipid Content; Anionic Lipid, an Assembly Factor.....	190
VI. Pathways of Cyclic Electron Transport (CET).....	191
A. Cyclic Electron Transport (CET) and the n-Side of the $b_6f$ Complex.....	191
B. The Proton Shortfall; Cyclic Electron Transport.....	192
C. Protein and Redox Components in the CET Pathway.....	193
D. Other Candidates for the Ferredoxin-Plastoquinone Reductase (FQR).....	193
1. A Role for NADPH Dehydrogenase (Ndh).....	194
2. PTOX.....	194
3. PGRL Components.....	194
VII. Functions of the $b_6f$ Complex in the Linear Electron Transport (LET) Pathway; the Q Cycle... 194	
A. Complexity of the $b_6f$ Complex; Some Inconsistencies.....	195
B. Alternative Q Cycle Model.....	195

---

\*Author for correspondence, e-mail: [waclab@purdue.edu](mailto:waclab@purdue.edu)

VIII. Quinone-Mediated H <sup>+</sup> Transfer Pathways; n-Side to Quinone Binding Site: Heme c <sub>n</sub> ; p-Side PEWY Exit Pathway with Invaginated H <sub>2</sub> O Pocket.....	197
A. n-Side Entry Pathway to Heme c <sub>n</sub> Quinone Binding Site.....	197
B. p-Side PEWY-Dependent Exit Pathway.....	198
C. Intrusion of Water in the p-Side Exit Pathway.....	199
IX. The Cytochrome b <sub>6</sub> f Complex as a Hetero-Oligomeric Membrane Lipoprotein.....	200
Acknowledgments.....	200
References.....	200

## Summary

The cytochrome *b<sub>6</sub>f* complex (*f*, derived from “leaf” in Latin, “folium,” or French, “feuille”, see D. S. Bendall, this volume) is responsible for the proton-coupled electron transfer reactions that link the two light-trapping photosystem reaction centers in the electron transport chain of oxygenic photosynthesis, and contains the rate-limiting step of the entire electron transport chain. The understanding of the functions of the intra-membrane cytochrome *b<sub>6</sub>f* complex in its role as the central electron transport complex in the photosynthetic electron transport chain has greatly increased in recent years because of the solving of the atomic structure of the complex, as well as its extrinsic electron transfer domains solved separately, by X-ray crystallographic analysis. The electron transfer and proton translocation functions of the cytochrome *b<sub>6</sub>f* complex are discussed in a context that focuses on function in the context of structure. The structure considerations are based on the recently determined high resolution (2.50 Å) crystal structure (PDB, protein data base, accession 4OGQ). The complex consists of a 280 kDa hetero-oligomeric intra-membrane lipo-protein complex containing, per monomer, 13 trans-membrane  $\alpha$ -helices and seven prosthetic groups, the latter consisting of five hemes, one chlorophyll *a* molecule and one  $\beta$ -carotene. In addition, each monomer contains 23 lipid binding sites, the function of which crosses into a completely new area of structure-function, both for the *b<sub>6</sub>f* complex and for the entire broader field of membrane proteins. Considering energy-transducing membrane protein complexes, the *b<sub>6</sub>f* complex, along with other hetero-oligomeric electron transfer membrane proteins provides a unique perspective in the broad field of membrane protein structure-function that encompasses transport and channel proteins, and extends beyond photosynthesis and bioenergetics to biomedicine. The additional perspective arises from the fact that the function of the cytochrome complexes, along with those of other redox proteins, can be assayed quantitatively through various high resolution spectroscopies.

A major theme in the present article is the comparison of structure and function of the *b<sub>6</sub>f* and the cytochrome *bc<sub>1</sub>* complex, which is located in the mitochondrial respiratory chain and in purple photosynthetic bacteria. One purpose of the comparison is to illustrate that although the two complexes are phylogenetically related, and there are many similarities in structure-function, there are many differences. An analysis and comparison of structures and functions implies that all charge mechanisms determined for *bc<sub>1</sub>* should not apply without exception or modification to the *b<sub>6</sub>f* complex.

---

*Abbreviations:* AFM – Atomic force microscopy; *b<sub>p</sub>*, *b<sub>n</sub>* – *b*-type hemes on electrochemically positive, negative sides of membrane; *C. reinhardtii* – *Chlamydomonas reinhardtii*; CET – Cyclic electron transport; chl – Chlorophyll-*a*; Cyt – Cytochrome; EM – Electron microscopy; E<sub>m7</sub> – Mid-point oxidation-reduction

---

potential at pH 7; EPR – Electron paramagnetic resonance; ETC – Electron transport chain; Fd – Ferredoxin; FNR – Ferredoxin-NADP<sup>+</sup> reductase; ISP – Rieske iron-sulfur protein; *k* – Boltzmann’s constant; LET – Linear electron transport; LHCII – Light-harvesting chlorophyll protein-

## I. Introduction

The cytochrome *b*<sub>6</sub>*f* complex of oxygenic photosynthesis is discussed from three perspectives: (i) mechanisms of electron/proton transfer that underlie its energy-transducing function, derived from biochemical, genetic, and crystallographic structure analysis; (ii) comparison of the structure and mechanisms in the cyt *b*<sub>6</sub>*f* complex with those operating in the *bc*<sub>1</sub> complex of mitochondria and purple anoxygenic photosynthetic bacteria; and (iii) in a brief overview, structure properties of the *bc* complexes in the context of other hetero-oligomeric membrane protein structures that function differently. The present chapter inevitably includes some key aspects of recent previous reviews from ourselves and others (Crofts and Berry 1998; Berry et al. 2000, 2013; Crofts 2004a; Osyczka et al. 2005; Baniulis et al. 2008; Cramer et al. 2008, 2010, 2011; Crofts et al. 2008; Mulkidjanian 2010; Nitschke et al. 2010; Bernat and Roegner 2011; Berry and Huang 2011; Hasan and Cramer 2012, 2014; Kallas 2012; Dibrova et al. 2013; Hasan et al. 2013c; Osyczka 2013; ten Brink et al. 2013; Kao and Hunte 2014; Tikhonov 2014). In a number of instances, however, an updated perspective is presented based on recent structure data, which are utilized to discuss some controversial questions of function.

Crystal structures for cytochrome *bc* complexes (*b*<sub>6</sub>*f* and *bc*<sub>1</sub>) have been obtained for: (i) Cyt *b*<sub>6</sub>*f* complex from the green alga, *C. reinhardtii* (Stroebel et al. 2003) and cyanobacteria (Kurusu et al. 2003; Yan et al.

2006; Yamashita et al. 2007; Baniulis et al. 2009; Hasan et al. 2013b; Hasan and Cramer 2014); (ii) for the Cyt *bc*<sub>1</sub> complex (a) from several mitochondrial sources, reviewed recently by (Berry et al. 2013; Kao and Hunte 2014), with the best resolution, 1.9 Å, obtained for the yeast complex (Solmaz and Hunte 2008) and (b) from anoxygenic photosynthetic bacteria (Esser et al. 2004, 2008, 2015). We also refer the readers to Chap. 1 in this volume by D. S. Bendall for the origin of heme protein notation, and Chaps. 10 and 11 by A. Esser et al. and L. Huang and E. Berry, respectively, for discussions of the structure of the bacterial Cyt *bc*<sub>1</sub> complex.

## II. Historical Perspective

The historical development of concepts governing the mechanisms of membrane energization and function of the cytochrome *bc* complex in proton translocation is based initially on studies of the cytochrome *bc*<sub>1</sub> complex in mitochondria and purple photosynthetic bacteria (Chance and Williams 1956; Dutton and Jackson 1972; Wikström and Berden 1972; Mitchell 1976, 1979; Zhu et al. 1982; Trumpower and Gennis 1994; Berry et al. 2000, 2013; Hunte 2001; Crofts 2004a, b; Lanciano et al. 2013). A consequence is that it has often been assumed that models and concepts developed for the *bc*<sub>1</sub> complex apply in all detail to the *b*<sub>6</sub>*f* complex, and that concepts of structure-function developed for the *bc*<sub>1</sub> complex can be completely applied to the *b*<sub>6</sub>*f* complex. We suggest that this practice in the literature can be confusing, particularly in the teaching of the subject. Regarding notation, the ubiquitous use of ‘i’ and ‘o,’ to describe the two sides of the cytochrome complex and the membrane, and the sidedness of the two *b* hemes that span the membrane can cause confusion in the teaching of the subject. Thus, with respect to the direction of vectorial proton translocation, the inside (“i”), the matrix domain, of the mitochondrion, and the cytoplasmic domain of gram-negative including photosynthetic bacteria, corresponds to the

---

II; M. lamosus – *Mastigocladus lamosus*; Ndh – NADH dehydrogenase; p n-side – Electrochemically positive, negative sides of membranes; PC – Plastocyanin; PDB – Protein data bank; PET – Photosynthetic electron transfer; PEWY – Proline-glutamate-tryptophan-tyrosine; PGRL1 PGRL5 – Proton gradient regulator 1 and 5; PQ-9 – Plastoquinone-9; PSI II – Photosystem I, II; PTOX – Plastoquinol terminal oxidase; Q<sub>p</sub>, Q<sub>n</sub> – Quinone binding site on p-, n-side of membrane; ROS – Reactive oxygen species; subIV – Subunit IV; TDS – Tridecyl-stigmatellin; TMH – Trans-membrane helix;  $\Delta\tilde{\mu}_{\text{H}}^+$  – Trans-membrane difference of proton electrochemical potential

outside (“o”) of the chloroplast thylakoid membrane. The definition of ‘i’ and ‘o’ as the sides corresponding to proton ‘input’ and ‘output’ arose from definitions of Peter Mitchell, who conceived the central role of the trans-membrane proton electrochemical potential gradient,  $\Delta\sim\mu_{\text{H}}^+$ , in membrane energy transduction (Mitchell 1966, 1979). However, the more obvious meaning of ‘i’ and ‘o’ to the uninitiated not accustomed to the colloquial language of the field, is “inside” and “outside.” It is suggested that a more conceptually useful notation is “n” and “p”, referring to the thermodynamically defined electrochemically negative and positive sides of the membrane. This notation is used below to describe the orientation of the redox and protein components that function in the linear and cyclic electron transport pathways of oxygenic photosynthesis (Fig. 9.1a, b).

### III. Cytochrome $b_6f$ and $bc_1$ Complexes; General Aspects

The position of the cytochrome  $bc_1$  and  $b_6f$  (together  $bc$ ) complexes in the phylogenetic tree and their evolution is discussed elsewhere (Widger et al. 1984; Schutz et al. 2000; Nitschke et al. 2010; Hasan and Cramer 2012; Dibrova et al. 2013). The crystal structures of the mitochondrial and bacterial  $bc_1$  complexes contain 11 and 3 polypeptide subunits, respectively, compared to eight in the Cyt  $b_6f$  complex from cyanobacteria (Kurusu et al. 2003; Hasan and Cramer 2014) and the green alga, *C. reinhardtii* (Stroebel et al. 2003). This subunit count refers to the tightly bound subunits that remain in the complex after the purification and crystallization procedures, and do not include weakly bound peripheral subunits that may be important for function but are lost during the process of purification and crystallization. The molecular weights, pI values, and coding origin, nuclear or organelle (Schwenkert et al. 2007), for the eight subunits of the  $b_6f$  complex are summarized (Table 9.1). Core

subunits containing key redox prosthetic groups with a high degree of conservation between  $b_6f$  and  $bc_1$  complexes are: (i) cytochrome  $b$  in the  $bc_1$  complex, which is equivalent in many structure-function aspects to cyt  $b$  and subunit IV in the  $b_6f$  complex (Widger et al. 1984); and (ii) the high potential ( $E_{\text{m}7} = +300$  mV) iron-sulfur [2Fe-2S] protein, often called the “Rieske” iron-sulfur protein because of the origin of its discovery (Rieske et al. 1964a, b). The protein subunit containing the covalently bound  $c$ -type cytochrome, cyt  $f$  and  $c_1$ , respectively, is not conserved between  $b_6f$  and  $bc_1$  complexes.

## IV. Structure-Function of the Cyt $b_6f$ Complex

### A. Problems in Crystallization

Earlier studies on purification of the  $b_6f$  complex (Nelson and Neumann 1972; Hurt and Hauska 1981) provided a foundation for its eventual crystallization and determination of a high resolution crystal structure (Kurusu et al. 2003, 2004; Stroebel et al. 2003; Yan et al. 2006; Yamashita et al. 2007; Baniulis et al. 2009; Hasan et al. 2013b), presently 2.50 Å (Hasan and Cramer 2014). High resolution structures of a C-terminal soluble domain of the 250 residue extrinsic C-terminal domain of cytochrome  $f$  (Martinez et al. 1992, 1994, 1996), and of the N-terminal soluble domain of the Rieske protein (Carrell et al. 1997), were obtained prior to their determination in the intact cytochrome complex. In retrospect, two reasons for the delay in crystallization of the intact cyanobacterial  $b_6f$  complex were: (i) a lack of appreciation for the critical role of internal lipid in the native structure of the cytochrome complex (Zhang et al. 2003; Hasan et al. 2011, 2013a; Hasan and Cramer 2014). The problem was ultimately solved through the addition of synthetic lipid at a stoichiometry of ten lipid molecules/cyt  $f$  to the purified complex (Kurusu et al. 2003;

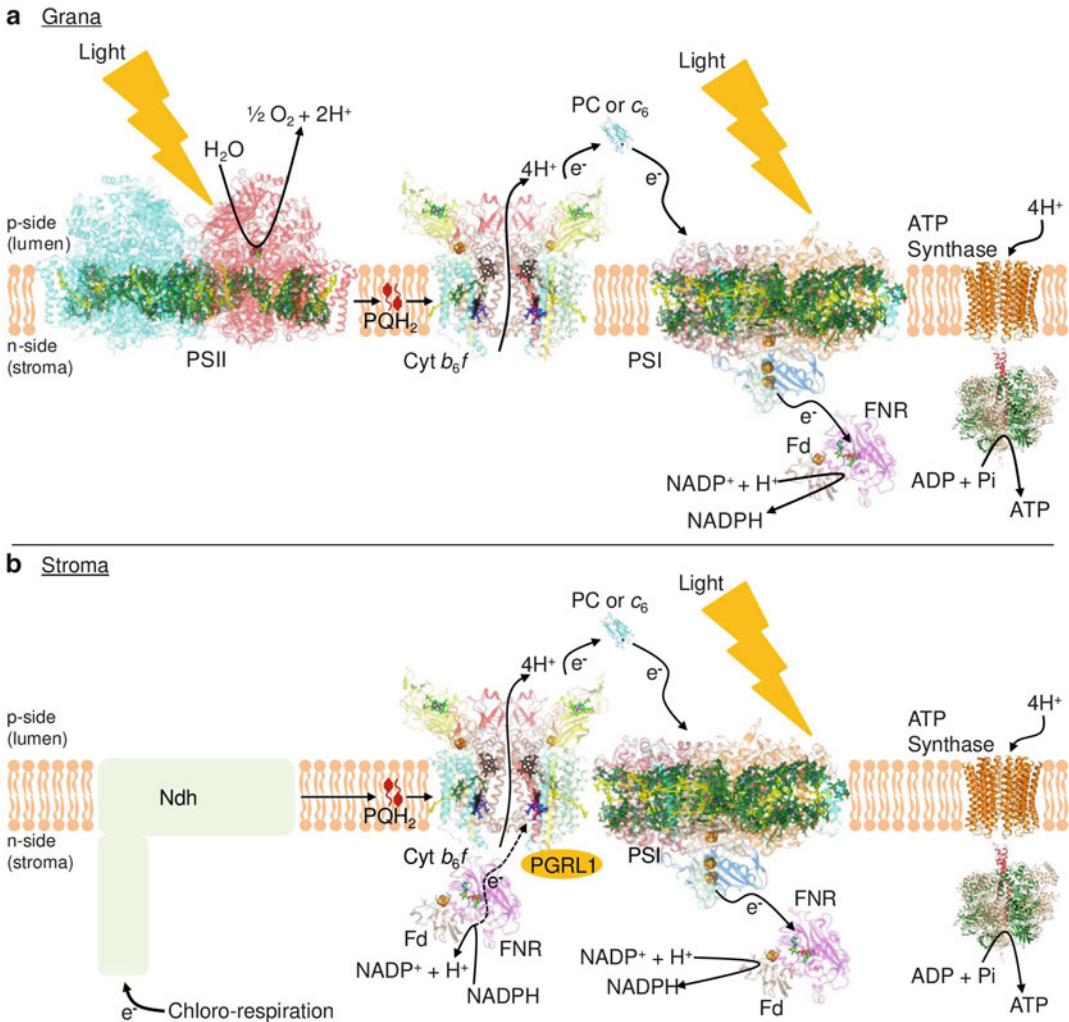


Fig. 9.1. Non-cyclic (“linear”) (a) and cyclic (b) electron transport pathways for oxygenic photosynthetic electron transfer and proton translocation in a format emphasizing the membrane protein structures of the three major hetero-oligomeric membrane protein complexes which, along with plasto-hydroquinol/quinone (PQH<sub>2</sub>/PQ), define the electron transport pathways: (a) photosystem II reaction center complex, PSII (Umena et al. 2011), 20 subunits, MW ≈ 350 kDa; PDB 3WU2; (b) cyt  $b_6f$  complex, 8 subunits, dimer MW = 250 kDa (PDB 4OQG, 2.5 Å crystal structure; (c) PS I reaction center (RC) complex (Jordan et al. 2001), trimer MW ≈ 1 MDa (PDB 1JB0), is connected to the ferredoxin-dependent “cyclic pathway” (Johnson 2011; Joliot and Johnson 2011), which channels electrons back to the PQ pool via “ferredoxin – PQ reductase” whose identity is debated (see below). Electrons are transferred from cyt  $f$  to the P700 special pair via plastocyanin (PC,  $Cu^+/Cu^{2+}$  redox prosthetic group) or a c-type cytochrome ( $Fe^{2+}/Fe^{3+}$ ). Light absorption by PSI RC results in  $10^{-12}$  s (psec) electron transfer from an RC excited state to a ferredoxin-FNR complex (Kurusu et al. 2001) that reduces  $NADP^+$ .

Zhang et al. 2003). (ii) Monomerization of the detergent-extracted complex, resulting in inactive and un-crystallizable material, was partly attributed to the action of a native, as yet unidentified (Baniulis et al. 2009),

protease present in the unicellular cyanobacteria *Synechocystis*, *Synechococcus*, and thermophilic *T. elongatus* (Zhang and Cramer 2005) that were initially used as sources of the complex (Zhang and Cramer

Table 9.1. Fundamental parameters of subunits of cytochrome *b<sub>6</sub>f* complex.

Subunit	MW (kDa)	pI
Cyt <i>f</i> <sup>a</sup>	30.9	4.7
Cyt <i>b</i> <sup>a</sup>	24.7	8.5
ISP <sup>a</sup>	19.3	5.3
SubIV <sup>a</sup>	17.5	7.8
Pet G <sup>a</sup>	3.9	8.1
Pet L <sup>a</sup>	3.2	9.9
Pet M <sup>a</sup>	3.5	4.3
Pet N <sup>a</sup>	3.3	9.5
FNR <sup>b</sup>	35.4	6.3
PetO <sup>c</sup>	15.1	9.6
PetP <sup>d</sup>	7.4	8.2

<sup>a</sup>From cyanobacterium *Nostoc* sp. PCC 7120

<sup>b</sup>PetH; Resolved on SDS-PAGE of spinach prep; MW in *A. Thaliana*

<sup>c</sup>PetO, *C. reinhardtii*

<sup>d</sup>PetP, *A. platensis*

2005). The proteolysis itself may not have caused the monomerization, but rather facilitated the weakening of inter-monomer hydrophobic interactions. Monomerization associated with the delipidation and loss of the single chlorophyll and the small PetL subunit, has been observed in the complex derived from the alga *C. reinhardtii* (Breyton et al. 1997). The problem of proteolysis and monomerization of the complex was found to be less severe in filamentous cyanobacteria (Yamashita et al. 2007; Baniulis et al. 2009), although the quality of the crystals initially prepared remained relatively poor. This was ultimately realized, as mentioned above, to be a consequence of delipidation of the complex in the purification protocol dedicated to purity of the protein moiety of the complex (Zhang et al. 2003). Properties of the extensive lipid population inside the complex are discussed below (Sect. V). Electron transfer activity, which is an indicator of the quality of the preparation, and consequently its ability to crystallize, is greatly reduced in monomeric *b<sub>6</sub>f* complex. Dimeric crystallizable *b<sub>6</sub>f* complex was ultimately isolated from fila-

mentous cyanobacteria (Kurusu et al. 2003; Baniulis et al. 2009), in which the problem of monomerization upon extraction was significantly smaller. A dimeric complex has recently been obtained from the thermophilic cyanobacterium *T. elongatus* (Rexroth et al. 2014).

### B. General Structure Features of the Cyt *b<sub>6</sub>c* Complex

The crystallized complex is a symmetric (C<sub>2</sub> symmetry) dimer that consists of eight trans-membrane polypeptide subunits in plants, green algae, and cyanobacteria (Kurusu et al. 2003). The analogous Cyt *bc*<sub>1</sub> complex consists of 11 subunits in the yeast, PDB 3CX5 (Hunte et al. 2000) and bovine, PDB 1QCK, 1BE3 (Iwata et al. 1998) complex, and three in the complex from the photosynthetic bacterium, *Rps. sphaeroides* (Esser et al. 2008). In all cases, the dimeric structure of the complex is required for a physiologically significant electron transfer activity, 250–400 electrons transferred (cyt f-sec)<sup>-1</sup> (Pierre et al. 1995; Zhang et al. 2001; Rexroth et al. 2014). This is presumably because of (i) the defined inter-monomer quinol entry pathway and (ii) increased stability of the dimer (Fig. 9.2a) in a hydrophobic membrane environment. Proximity of the two monomers is also necessary for inter-monomer cross-over in rapid trans-membrane electron transfer (Swierczek et al. 2010; Khalfauoui-Hassani et al. 2012).

A ribbon diagram of the dimeric *b<sub>6</sub>f* complex (PDB 2ZT9, 4H44, 4OGQ) derived from crystal analysis of the filamentous cyanobacterium *Nostoc* sp. PCC 7120 (Baniulis et al. 2009; Hasan et al. 2013b; Hasan and Cramer 2014), is shown in two views differing by a 180° rotation in order to display more clearly the arrangement of the 8 subunits that span the membrane with 13 TMH per monomer containing 7 prosthetic groups, including 5 with redox function consisting of 4 hemes and the [2Fe-2S] cluster, 1 chlorophyll a (Huang et al. 1994) and one β-carotene (Zhang et al. 1999) (Fig. 9.2a, b; Table 9.1).

### C. Unique Chlorophyll $a$ and $\beta$ -Carotene

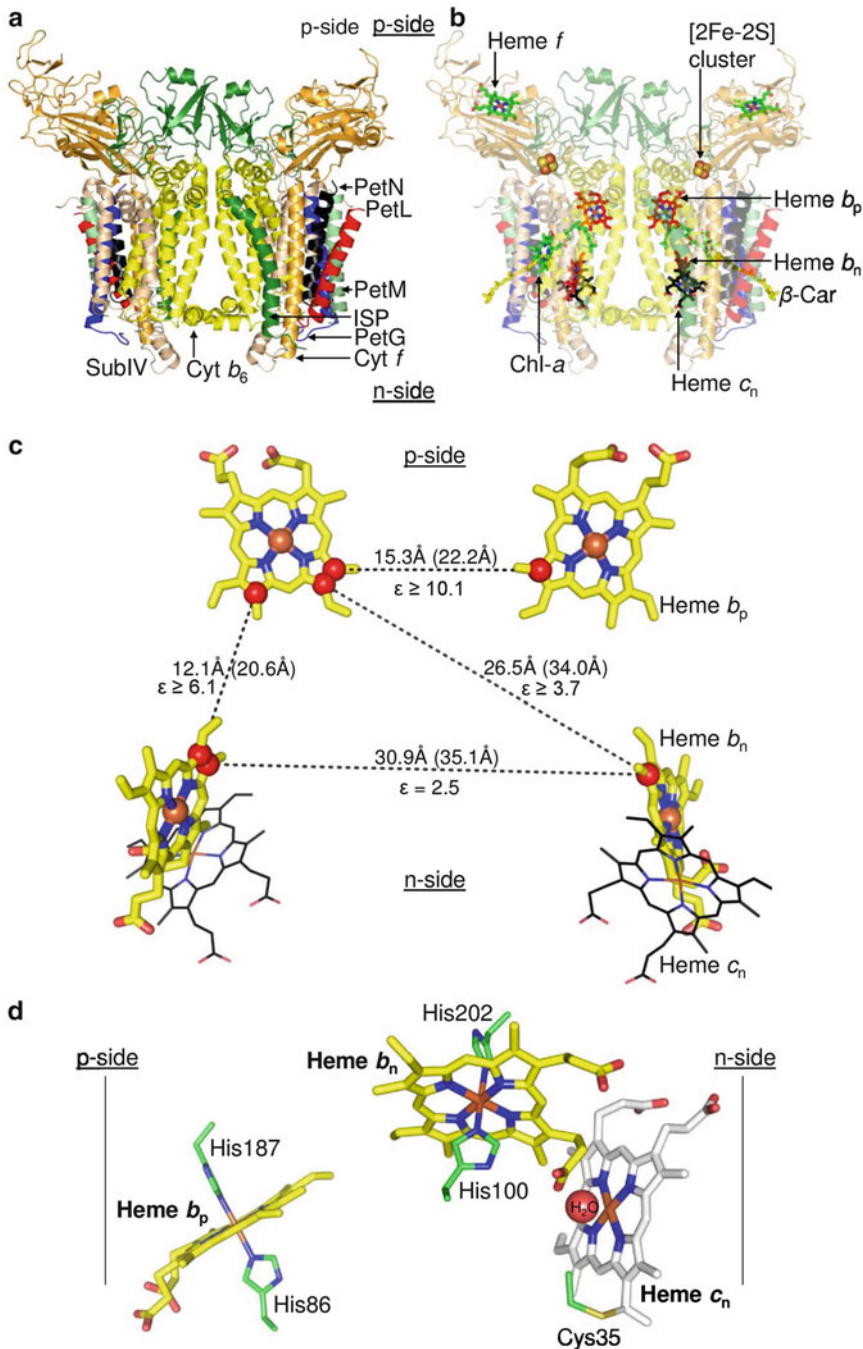
The presence of the single copy of the lipidic chlorophyll  $a$  (Huang et al. 1994; Pierre et al. 1997; Dashdorj et al. 2005) and  $\beta$ -carotene (Zhang et al. 1999) in each monomer of the complex, first determined in the absence of structure data, initially seems enigmatic. As shown in the first structures, the  $\beta$ -carotene is separated by 14 Å from the chlorophyll (Kurusu et al. 2003; Stroebel et al. 2003). Therefore, on the basis of the physics alone the  $\beta$ -carotene cannot quench a chlorophyll excited triplet state (Kim et al. 2005a). A mechanism of long-range transfer through an internal  $O_2$  chain has been considered (Kim et al. 2005b). Recent inferences about the functions of the two pigments are: (i) the relevant group on the chlorophyll is not the tetra-pyrrole ring, but the elongate flexible phytyl chain that gates the passage of plastoquinone(ol) through the portal connecting its p-side binding site with the inter-monomer cavity and bulk membrane (Hasan et al. 2014a). (ii) Regarding the  $\beta$ -carotene, it protrudes by approximately 11 Å from the complex between the TMH of Pet G and that of Pet M (Fig. 9.2b), and thus is in a position analogous to that of cardiolipin in the cytochrome  $bc_1$  complex, which seems to function in the mitochondrial respiratory chain as a glue between the major electron transport complexes (Wenz et al. 2009). It is therefore suggested that the  $\beta$ -carotene functions as a ‘latch’ that connects the  $b_6f$  complex to the PSI reaction center, forming a super-complex (Iwai et al. 2010), analogous to that described for the mitochondrial respiratory chain (Althoff et al. 2011).

### D. Trans-Membrane Hemes, $b_n$ and $b_p$

Of the eight subunits in the monomer, all but two, the heme binding cyt  $b$  subunit and subunit IV (subIV), are monotopic (1 membrane span). For later discussion, it is noted that the two polytopic subunits, the 24 kDa cyt  $b_6$  subunit with 4 TMH (labeled A-D), and the 18 kDa suIV with 3 TMH (E-G),

respectively, share major sequence (Widger et al. 1984) and structure identity with the 42 kDa cyt  $b$  major subunit of the  $bc_1$  complex that has eight TMH, i.e., one more TMH, the ‘H’ helix, than the  $b_6f$  complex. The evolutionary origin of the latter difference between the  $b_6f$  and  $bc_1$  complexes is a subject of discussion (Mulkiđjanian 2010; Nitschke et al. 2010; Hasan and Cramer 2012). The cyt  $b$  subunit also contains a short surface helix, formed by the N-terminal 28–29 amino acids, which is associated with the n-side membrane surface. The four TMH of the cyt  $b_6$  subunit are connected by loops at the p- and n-side membrane interfaces. SubIV (~17 kDa) has three TMH (E–G) that form a p-side saddle around the four helix bundle of cyt  $b_6$ . Helix E of SuIV is located in proximity to the A- and B-helices of cyt  $b_6$  while the F and G-TMH span the four helix bundle, close, respectively, to the C, D and B-TMH (Fig. 9.3). The C-terminus of the E-TMH is separated from the N-terminus of the F-TMH by a distance of ~40 Å, which is bridged by the p-side ef-loop. This seven TMH assembly forms the conserved core of the  $b_6f$  complex, which is bounded in each monomer by the four subunit hydrophobic picket fence.

The arrangement of the two pairs of trans-membrane  $b$ -hemes,  $b_p$  and  $b_n$ , with inter-heme edge-edge and center-center (Fe-Fe) distances (in parentheses) is shown (Fig. 9.2c), along with the heterogeneity of the inter-heme dielectric constants (Hasan et al. 2014b), and the complex of heme  $b_n$  with a skeleton of the covalently bound  $c$ -type heme  $c_n$  (Stroebel et al. 2003; Alric et al. 2005; Zatsman et al. 2006; Baymann et al. 2007; Twigg et al. 2009). The heme  $b_n$ - $c_n$  complex, a unique feature of the  $b_6f$  compared to the  $bc_1$  complexes, in which the close proximity of the two hemes results in sharing of the 3d electronic shells is displayed in a  $g = 12$  EPR signal (Zatsman et al. 2006; Baymann et al. 2007), is shown in more detail (Fig. 9.2d). This proximity is considered relevant to the possibility of a two electron transfer mechanism at the  $Q_n$  site.



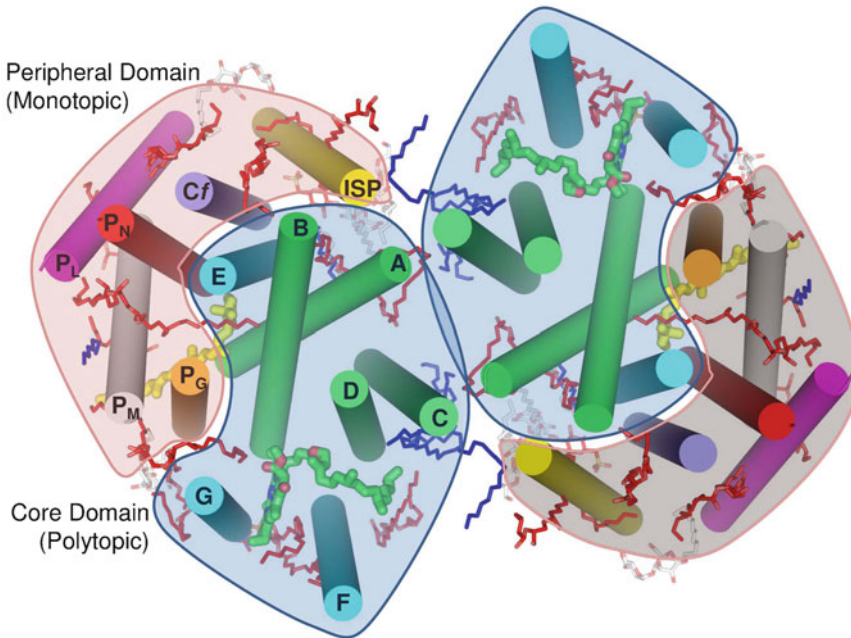
*Fig. 9.2.* The dimeric cytochrome  $b_6f$  complex. **(a)** Polypeptide subunits from the cyanobacterium *Nostoc* sp. PCC 7120 (PDB ID 4OGQ) are shown in ribbon format- cyt  $b_6$  (yellow), subIV (light brown), cyt  $f$  (orange), ISP (dark green), PetL (red), PetM (light green), PetG (blue), PetN (black). **(b)** Prosthetic groups of  $b_6f$  complex. Trans-membrane hemes  $b_p$ ,  $b_n$  (red/blue), and  $c_n$  (black/blue) are shown as sticks. On the p-side, heme  $f$  (green/blue) is shown as sticks, the [2Fe-2S] cluster as spheres (brown/yellow), and the Chl- $a$  (green/blue) and  $\beta$ -car (yellow) as sticks. **(c)** Heme-heme distances within the trans-membrane domain of the complex (PDB ID 4OGQ). Distances shown as black dashes. Heme edge-edge, and center-center (Fe-Fe) distances are shown, respectively, outside and inside parentheses (selected atoms shown as spheres).



### 1. Hemes, $b_n$ and $b_p$ , Oxidation-Reduction Potentials

Determination of the oxidation-reduction potentials of these hemes in the  $bc_1$  complex are consistent in showing a separation of 100–150 mV between the midpoint redox potentials of the two hemes, which are thus often labeled  $b_h$  and  $b_l$  (high and low

potential hemes). For the two hemes in the  $b_6f$  complex, there is disagreement as to whether the mid-point potentials of the two hemes are (Kramer and Crofts 1994) or are not (Girvin 1985; Furbacher et al. 1989; Rich et al. 1991) separable in a redox titration of thylakoid membranes. A simulation shows that a mid-point potential difference of 50 mV or less of a one electron titration could not be resolved



*Fig. 9.3.* Domain structure of  $b_6f$  complex (PDB ID 4OGQ). Central hydrophobic core consisting of polytopic subunits cyt  $b_6$  and subunit IV is organized as a symmetric dimer, each monomer further divided into a core polytopic domain (light blue) and peripheral domain (pink). Polytopic domain consists of cyt  $b_6$  (TMH “A–D”; green) and subunit IV (“E–F”; cyan). The peripheral domain consists of single helix subunits- cyt  $f$  (“C $_f$ ”; blue), ISP (yellow), PetG (“P $_G$ ”; light orange), PetL (“P $_L$ ”; magenta), PetM (“P $_M$ ”; gray) and PetN (“P $_N$ ”; red). Lipids, red sticks; detergent UMQ, red/white; acyl chains, blue sticks. Chl- $a$  and  $\beta$ -car, green/blue/red and yellow. The cyt  $b_6$ /subunit IV core is conserved in  $bc$  complexes from mitochondria, chloroplasts, and photosynthetic bacteria (Widger et al. 1984). p and n sides of the complex possess negative and positive surface potentials (Cramer et al. 2006), respectively, which presumably have a role, as yet undefined, in the organization of peripherally bound subunits, which are not retained in the crystals (Sect. IV.H). Left and right-side panels show view from electrochemically positive and negative sides of membrane.

*Fig. 9.2.* (continued) The dielectric constant,  $\epsilon_{ij}$ , between each pair of hemes,  $\epsilon_{n_1,p_1}$ ,  $\epsilon_{n_1,p_2}$ ,  $\epsilon_{n_2,p_1}$ , etc. (Hasan et al. 2014b) is shown. (d) Trans-membrane heme ligation in the cytochrome  $b_6f$  complex. The central Fe atom of heme  $b_p$  and  $b_n$  is axially ligated, respectively, by residues His86/His187 and His100/His202 which bridge the B and D TMH of the cyt  $b$  subunit, Heme  $c_n$  is covalently attached to the protein via Cys35. Heme  $c_n$  is unique as it lacks an amino acid axial ligand, and the central Fe-atom is penta-coordinated. The sole ligand of heme  $c_n$ , is provided by  $H_2O$  or  $OH^-$  on the heme  $b_n$  side. Fe of heme  $c_n$  separated by 4.0 Å from a propionate oxygen of heme  $b_n$ , which results in electronic coupling, a high spin  $g = 12$  EPR signal (Zatsman et al. 2006; Baymann et al. 2007), and an oxidase-like reaction with nitric oxide (Twigg et al. 2009). Electrochemically positive, negative sides of membrane labeled p, n.

experimentally. For isolated complex, the midpoint potentials of the 2 *b* hemes have been found to be separated by 90–95 mV (Alric et al. 2005; Nelson et al. 2005).

## 2. Reducibility of *b* Hemes; Heterogeneity of Internal Dielectric Constants

Excitonically split circular dichroism (CD) spectra of the  $bc_1$  (Palmer and Degli Esposti 1994) and  $b_6f$  complex (Schoepp et al. 2000; Hasan et al. 2014b) arise from interactions of the reduced hemes. Determination for isolated complex of the time course of heme reduction and the onset of the split CD spectra shows that the heme pair that is preferentially reduced is the intra-monomer pair,  $b_p$  and  $b_n$ . This result contrasts with that which is expected. If heme  $b_n$ , whatever its exact redox potential, has a more positive potential in isolated  $b_6f$  complex than heme  $b_p$ , the two hemes  $b_n$  should be preferentially reduced under equilibrium conditions. The straight-forward explanation is that the protein medium between hemes  $b_p$  and  $b_n$  is more polarizable, i.e., has a higher dielectric constant, than the medium between the two hemes  $b_n$  (Hasan et al. 2014b), implying that the dielectric constant in the complex is heterogeneous and anisotropic (Fig. 9.2c).

## E. The High Potential [2Fe-2S] Rieske Iron-Sulfur Protein (ISP)

Because the degree of sequence conservation between the Rieske proteins in chloroplasts and mitochondria is greater than between the cytochrome  $c_1$  and  $f$  subunits of the complex, for which sequence identity is negligible except for the heme binding motif (Martinez et al. 1996), it has been proposed that a better nomenclature for these  $bc$  complexes would be the “*b* – FeS complex” (Nitschke et al. 2010). To avoid confusion, however, in referencing, the notation “ $b_6f$ ” will be retained in the present discussion. As discussed below, whatever title is given to these complexes, although there is a significant commonality in evolutionary origin

and many similarities in structure/function, it is important to realize that there are major differences in both structure and function between the respiratory and photosynthetic  $bc_1$  complexes on the one hand, and the photosynthetic  $b_6f$  complex on the other. It is noted that the electron transport pathway in the anoxygenic photosynthetic bacteria is discussed as a purely cyclic (CET) pathway (Petty and Dutton 1976; Bowyer and Crofts 1981; Cramer and Crofts 1981; Gennis et al. 1993; Berry et al. 2000), in which there is no energy-coupled diversion of electrons from the cyclic loop. In contrast to these bacteria, and to mitochondria that function through a linear chain, the electron transport pathway associated with oxygenic photosynthesis contains both linear (LET) and cyclic (CET) electron transport chains.

## 1. ISP Electron Transfer; a *p*-Side Conformation/Mobility Problem

A structure-function enigma is that the distance of closest approach of the cytochrome  $f$  heme to the 2Fe-2S cluster in the  $b_6f$  complex is 28 Å, which is much too large to support physiologically meaningful msec electron transfer rates (Moser et al. 1992; Gray and Winkler 1996). Then, how does the Rieske FeS protein transfer electrons to cytochrome  $f$ ? A major gap in understanding the *p*-side electron transfer reactions for the  $b_6f$  complex results from the absence of structure data that would allow kinetically competent electron transfer from the [2Fe-2S] cluster to the heme of cytochrome  $f$ . Given the documented conformation change determined from crystal structure data for the avian mitochondrial  $bc_1$  complex (Zhang et al. 1998; Huang and Berry 2015), electron transfer from the [2Fe-2S] cluster to the *cyt f* heme must involve a rotational-translational conformational change in the ISP (Hasan et al. 2013a). It has not yet been possible, however, to obtain similar structure-based data for the  $b_6f$  complex. An inhibitory effect on cytochrome  $f$  reduction of increased ambient viscosity, achieved in the presence of added glycerol (Heimann et al. 2000),

implies a requirement for motion of the extrinsic domain of the ISP. Extensive site-directed mutagenesis implies that the “hinge” segment of the ISP that connects the [2Fe-2S] cluster-bearing domain in one monomer of the  $b_6f$  complex with its TMH in the second monomer is more flexible than in the similar domain of the mitochondrial  $bc_1$  complex (Yan and Cramer 2003; de Vitry et al. 2004). This flexibility may not apply in situ to all degrees of freedom (Soriano et al. 2002).

Crystallographic evidence for a significant conformation change of the ISP extrinsic domain has been inferred from the disorder of the ISP extrinsic domain observed in crystals of the  $b_6f$  complex formed in the presence of anionic lipid, compared to a largely ordered ISP structure observed in the  $b_6f$  complex supplemented with neutral lipids. A conformation change associated with the disorder is attributed to electrostatic interactions arising from the presence of anionic lipids (Hasan et al. 2013a), which are known to have a central role in the structure of the mitochondrial cyt  $bc_1$  complex (Arnarez et al. 2013) and the respiratory chain (Pfeiffer et al. 2003). Crystal structure evidence for movement of the [2Fe-2S] cluster in the  $b_6f$  complex, comparable to that documented in the mitochondrial  $bc_1$  complex (Zhang et al. 1998), which would provide structure-based documentation for the predicted domain movement of the extrinsic domain of the ISP, and document the mechanism of electron transfer from the ISP to the heme of cytochrome  $f$ , is presently missing.

## F. Differences Between $b_6f$ and $bc_1$ Complexes

### 1. Comparison of Cytochromes $f$ and $c_1$

In contrast to the conserved nature of the cytochrome  $b$  subunit, for the cytochrome  $c_1$  and  $f$  subunits, except for their single TMH that binds the subunit to the complex and the membrane, the structures are different in the  $b_6f$  and  $bc_1$  complexes (Fig. 9.5), the only conserved sequence segment is the Cys-X-Y-Cys-His motif, responsible for

covalent binding of the  $c$ -type heme. The p-side heme binding domain has a completely different secondary structure,  $\alpha$  and  $\beta$ , respectively in  $b_6f$  and  $bc_1$  (Martinez et al. 1992, 1994, 1996). The cyt  $c_1$  and cyt  $f$  subunits of the  $bc_1$  complex, each bound to the complex through one TMH (Fig. 9.4a, b), differ markedly in the structures of the p-side domain that bind the  $c$ -type heme. The secondary structure of the protein housing the  $c_1$  and  $f$  hemes on the p-side of the complex is predominantly  $\beta$  and  $\alpha$ , respectively (Fig. 9.4c, d). All three of the p-side electron transfer proteins that are part of the  $b_6f$  complex, or interact with it, the Rieske [2Fe-2S] protein, cyt  $f$ , and plastocyanin, that mediate electron transfer between the quinol hydrogen donor and the P700 PSI reaction center are predominantly in the  $\beta$ -conformation. Cyt  $f$  and cyt  $c_1$  each have a relatively high potential, +370 mV and +260 mV, respectively, sufficient to provide an oxidant for the ISP, and each contains a covalently bound heme, and is bound to the complex through a single TMH orthogonal to the membrane plane. Otherwise, the structures are completely different, cyt  $f$  and  $c_1$ , respectively, having  $\beta$  sheet and  $\alpha$ -helical secondary structure. Along with the dissimilarity in structure, the evolutionary origin of cyt  $f$  is unclear (Martinez et al. 1994).

## G. The Four Small Peripheral Subunits, *Pet G, L, M, and N*; a Late Addition in Evolution?

A unique lattice of four short (3.3–4.1 kDa), single TMH “hydrophobic sticks,” denoted as *PetG*, *PetL*, *PetM*, and *PetN* (Table 9.1), provides a hydrophobic lattice, or “picket fence,” around each monomer, a structure which is unique among all known integral membrane protein structures. Of these four subunits, *PetM* (Schwenkert et al. 2007), along with the Rieske ISP, are the only subunits among the 13 in the complex that are nuclear-encoded. Specific functions of these four subunits are not defined, although *PetL* interacts sterically with the TMH of the

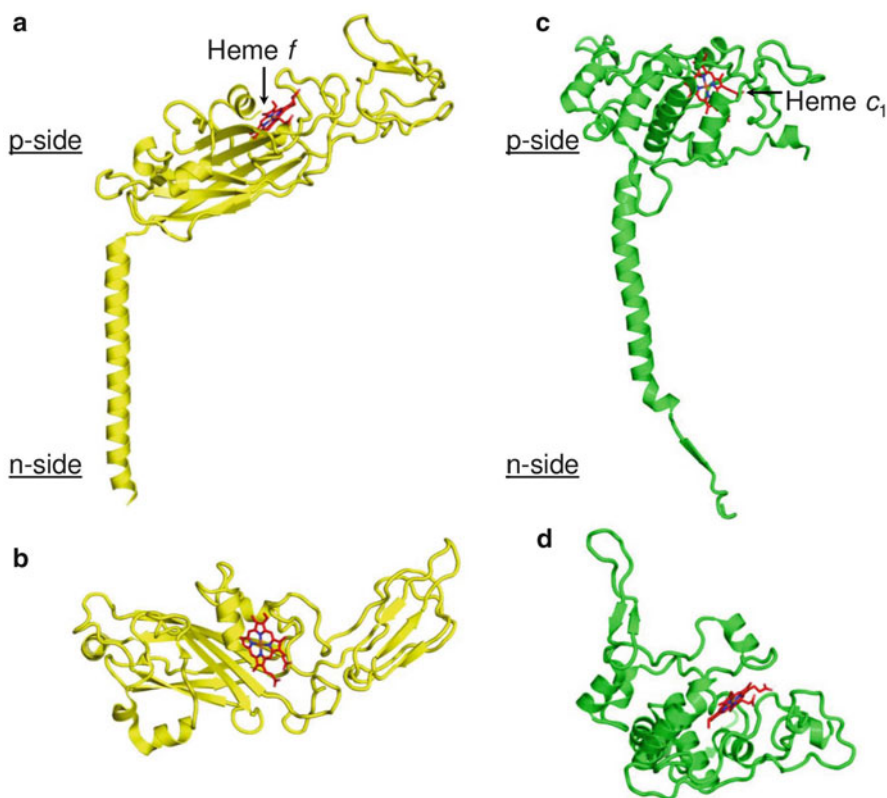


Fig. 9.4. Terminal electron acceptors of cytochrome *bc* complexes, *cyt f* of the *b<sub>6</sub>f* complex (Martinez et al. 1992, 1994, 1996) and *cyt c<sub>1</sub>*. (a, b) *Cyt f* subunit of *b<sub>6</sub>f* complex attached to the complex and membrane through one TMH. The *cyt f* subunit binds a high potential *c*-type heme (“heme *f*”, shown as red/blue sticks) in the p-side predominantly  $\beta$ -sheet extrinsic domain (panel b). (c, d) The *cyt c<sub>1</sub>* subunit of the *bc<sub>1</sub>* complex is also bound to the complex through one TMH (c). In contrast to *cyt f*, the p-side extrinsic domain of *cyt c<sub>1</sub>*, in which the *c*-type heme is covalently bound (red/blue sticks), is predominantly  $\alpha$ -helical (panel d). b, d panels rotated 90° around horizontal axis relative to presentation in a, b, respectively.

Rieske ISP and may provide a constraint on the membrane-spanning orientation of the latter. The position of much of the lipid in the complex between the Pet picket fence and the conserved *cyt b*-sulV core of the complex suggests a “boundary lipid” function and that the “picket fence” may have been added to the core of the complex relatively late in the evolution of the complex.

#### H. Peripheral Subunits Not Seen in the *b<sub>6</sub>f* Crystal Structure

These subunits are PetP (Rexroth et al. 2001), PetO (Hamel et al. 2000), PetH (FNR) (Zhang et al. 2001) and Stt7

(Rochaix 2014). The FNR unit is seen in SDS-PAGE of purified *b<sub>6</sub>f* complex isolated from spinach, usually at an estimated stoichiometry <1 per monomer (Zhang et al. 2001), and in the “super-complex” obtained from *C. reinhardtii* that includes *b<sub>6</sub>f* and the photosystem I reaction center (Iwai et al. 2010). The inability to crystallize the complex from spinach *b<sub>6</sub>f* complex is attributed at least partly to incomplete presence of the petH subunit in the *b<sub>6</sub>f* complex (Zhang et al. 2001), which would result from its concentration in the stromal compartment of the thylakoid membrane (Joliot et al. 2004).

### I. Distribution of Aromatic Residues in the Trans-Membrane Domain

Aromatic residues, Phe, Tyr, and Trp, differ in physical properties due to the absence (Phe) or presence (Tyr and Trp) of polar atoms within the aromatic side chain. The relatively polar Tyr and Trp residues are located preferentially proximal to the lipid-water interface of membrane proteins (Yau et al. 1998; Granseth et al. 2005), where they can interact with the polar head-groups of lipids (Killian and von Heijne 2000). In addition, binding of the phospholipids requires a niche that consists of aromatic residues as well as basic amino acids to neutralize the anionic lipid head-group phosphate (Palsdottir and Hunte 2004b). In this regard, protein complexes associated with the thylakoid membrane, including the  $b_6f$  complex, interact with the unique phosphate-free, neutral galactolipids (Gounaris et al. 1986). The absence of an anionic phosphate group eliminates the need for a basic residue for intra-membrane lipid binding. The recent advances in crystallographic studies of lipid-protein interactions of the  $b_6f$  complex in a synthetic neutral lipid environment has revealed a heterogeneous, bi-planar distribution of aromatic residues within the hydrophobic trans-membrane domain of the  $b_6f$  dimer (Fig. 9.5).

Despite the difference in lipid composition in thylakoid membranes, i.e., the dominant presence of galactolipids, the distribution of Tyr and Trp near the lipid-water interface, first noted in the crystal structure of the photosynthetic reaction center, is conserved in the cytochrome  $b_6f$  complex (Fig. 9.5), where Tyr-Trp residues lie within an interaction distance of the lipid carbonyl groups and polar head groups. The more hydrophobic Phe residues are embedded closer to the membrane center, distal from the lipid-water interface.

### J. Inhibitors; Differences Between the bc Complexes

Commonly used quinone-analogue Inhibitors that bind with sub- $\mu$ molar to  $\mu$ molar affinity to the p- and n-side quinone-binding niche, are: (a) for the  $bc_1$  complex, stigmatellin and antimycin A, respectively, in the p- and n-side quinone binding niches. Antimycin is known to reside with a high degree of preference at the n-side quinone binding site (Huang et al. 2005), and binds tightly enough that it induces trans-membrane conformational changes that are detected by g-value shifts of the EPR signal of the p-side Rieske 2Fe-2S complex (Cooley et al. 2009; Sarewicz et al. 2009; Cooley 2010). (b) In the  $b_6f$  complex, a major problem in studies on electron transport pathways is that there is no well defined high affinity n-side quinone analog inhibitor: (i) association of antimycin A with the  $Q_n$  site is equivocal, as discussed below in the context of cyclic electric transport (Sect. VI.B). (ii) NQNO, whose presence results in an increased amplitude of light-induced heme b (assumed to be heme bn) reduction (Joliot and Joliot 1988; Furbacher et al. 1989) is also a marginally effective (5–10  $\mu$ M) n-side inhibitor of linear electron transport (Jones and Whitmarsh 1988; Rich et al. 1991; Baniulis et al. 2013), which may result from a second binding site of the inhibitor at the  $Q_p$  site. (iii) the preferential side of action of stigmatellin inhibition, n vs. p, is reversed, relative to  $bc_1$ , as stigmatellin is known to be ineffective in p-side inhibition (Hope and Valente 1996), and is found bound at the n-side quinone binding niche in a crystal structure (Hasan et al. 2014a). (iv) Tridecyl-stigmatellin, with a less branched structure, is seen in crystal structures to bind at both  $Q_p$  (Kurisu et al. 2003; Stroebel et al. 2003) and  $Q_n$  sites (Yamashita et al. 2007). (v) The compound MOA-stilbene (Rich et al. 1992) has been proposed to be an n-side inhibitor although

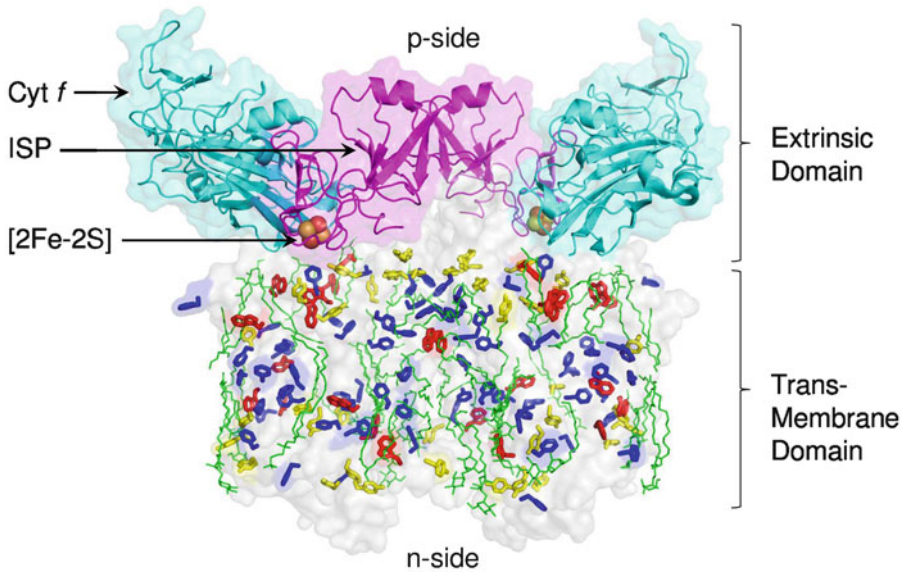


Fig. 9.5. Distribution of aromatic residues in the hydrophobic trans-membrane domain of the *cyt b<sub>6</sub>f* dimeric complex (PDB 4OGQ). Phenylalanine (Phe, *blue sticks*) is distributed predominantly within the core of the trans-membrane domain, while tyrosine (Tyr, *yellow sticks*) and tryptophan (Trp, *red sticks*) are mainly restricted to the periphery, proximal to the lipid-water interface. Many lipids and detergent molecules are crystallographically ordered and are shown as *green sticks*. On the p-side, *cyt f* (*cyan*) and ISP (*pink*) extrinsic domains are shown as ribbons, and the [2Fe-2S] cluster associated with the ISP extrinsic domain as *brown/yellow spheres*. It has been shown recently that the primary determinant of dimer stability is inter-monomer interactions between tryptophan residues and not the inter-monomer connection between the ISP extrinsic domain and its trans-membrane  $\alpha$ -helix (Agarwal et al. 2015).

is relatively unstudied; (vi) DBMIB is unquestionably a Qp –site inhibitor (Bohme et al. 1971; Rich et al. 1991), although it may utilize two p-side binding sites (Roberts and Kramer 2001; Roberts et al. 2004; Yan et al. 2006).

## V. Lipids in the *b<sub>6</sub>f* Lipoprotein Complex

“Boundary lipids” define a domain structure. Because the conserved *cyt b<sub>6</sub>-SU IV* core of the complex is separated by a lipid layer from the “picket fence” (Fig. 9.3), it is implied, as noted above, that the “picket fence,” was added to the core structure at a later stage in the evolution of the *b<sub>6</sub>f* complex, perhaps to facilitate interaction with the reaction center complexes. As noted above, the  $\beta$ -carotene, which protrudes from the surface of the picket fence, may act as a “latch”

to facilitate super-complex formation with the PSI reaction center complex (Iwai et al. 2010).

### A. Lipid Content; Anionic Lipid, an Assembly Factor

The high lipid content, at least 23 lipid binding sites per monomer (Hasan and Cramer 2014) (Fig. 9.6), defines *b<sub>6</sub>f* as a lipoprotein complex with an intimate role of lipids in its structure, function, and assembly. Translocon-based models (e.g., Egea and Stroud 2010), of membrane protein assembly have not yet considered the additional problems associated with hetero-oligomeric membrane lipoproteins and lipid specificity, known in the case of the mitochondrial *bc<sub>1</sub>* complex and super-complex (Althoff et al. 2011) to include a requirement for the di-anionic lipid, cardiolipin, as an assembly factor (Pfeiffer

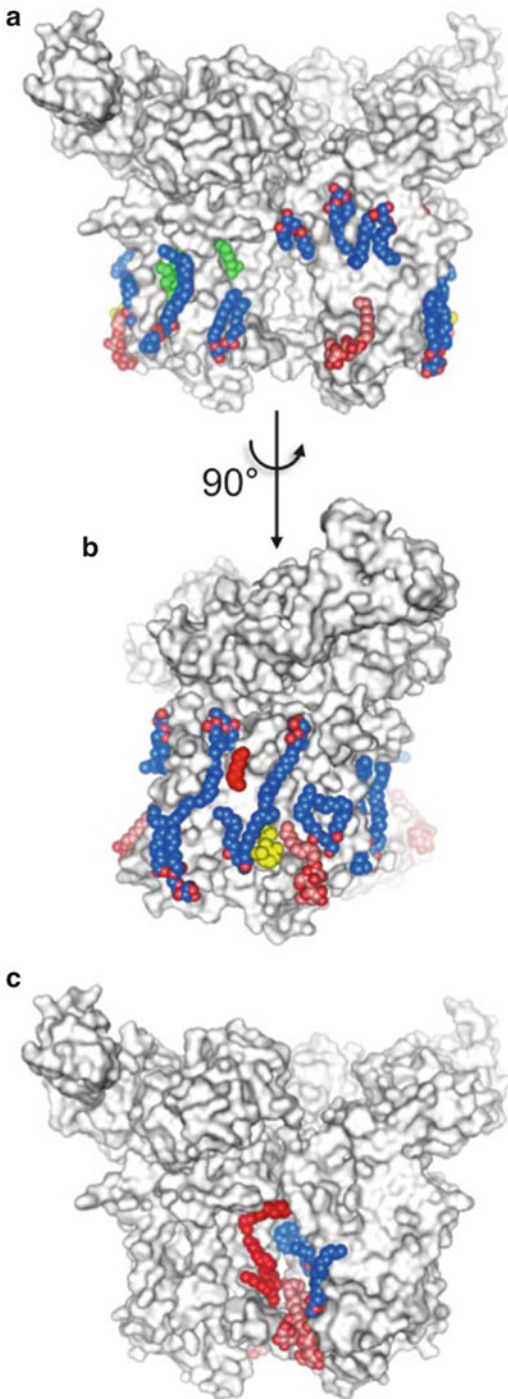


Fig. 9.6. Lipids in the cytochrome  $b_6f$  complex (PDB 4OGQ). (a, b) Peripheral lipidic sites associated with the  $b_6f$  complex shown in two orthogonal views. Lipids shown as blue/red spheres, alkyl chains as red spheres, and detergent molecules as pink/red spheres. Pigments Chl- $a$  and  $\beta$ -car (carotene) are shown as

et al. 2003). The anionic lipids in the  $b_6f$  complex are sulfolipid (sulfoquinovosyl-diacylglycerol) and phosphatidyl-glycerol (Hasan et al. 2011; Arnarez et al. 2013; Hasan and Cramer 2014), which may act “as assembly factors.”

## VI. Pathways of Cyclic Electron Transport (CET)

### A. Cyclic Electron Transport (CET) and the $n$ -Side of the $b_6f$ Complex

[cf., Chaps. 22 and 23 by Finazzi et al. and Minagawa in this volume]. Some details of the cyclic electron transport (CET) pathway from reduced ferredoxin to quinol in the main chain (Fig. 9.1b) are controversial. Independently of these complications, there is an energetic necessity for an additional contribution to the  $\Delta\tilde{\mu}_H^+$  needed for ATP synthesis generated in a CET pathway. As much as two-thirds of the proton gradient used for trans-membrane free energy storage in oxygenic photosynthesis is generated by the  $b_6f$  complex. Considering the 4 electrons needed to form the 2 NADPH molecules required for fixation of one  $\text{CO}_2$  by the Calvin-Benson mechanism, as many as 3  $\text{H}^+$  can be translocated across the membrane for every electron transferred through the chain, i.e.,  $\text{H}^+/\text{e} = 1$  for water splitting and as many as 2 for the  $b_6f$  complex. Thus, per 4 electrons transferred, 12  $\text{H}^+$  can be translocated to the electrochemically positive (p) side of the membrane and thus made available for discharge through the  $\text{F}_o$   $c$ -ring of the ATP synthase, which would ideally be sufficient if the  $c$ -ring contained  $\leq 12$  subunits, as has been proposed (Jiang et al. 2001). Based, however, on data obtained subsequently by

←  
 Fig. 9.6. (continued) green, yellow spheres. (c) Lipidic sites within the inter-monomer cavity. Protein subunits are marked but not colored. Lipids within the inter-monomer cavity are implicated in modulation of dielectric properties that affect electron storage and transfer (Hasan et al. 2014b).

atomic force microscopy (AFM), 12  $H^+$  are insufficient to drive sufficient ATP synthesis in oxygenic photosynthesis, resulting in a mechanistic problem. In more detail, the AFM visualization of the ATPase c-subunit stoichiometry defines 14  $H^+$  conducting c-ring subunits, implying an  $H^+/ATP$  ratio of 4.7 (14/3) in the ATP synthase associated with spinach chloroplasts (Seelert et al. 2000, 2003). Thus, there is a problem of an insufficiency of protons (12–14 = –2). Furthermore, an  $H^+/ATP$  ratio of 5 is implied for the cyanobacterium, *Spirulina platensis*, in which 15 c-subunits were seen (Pogoryelov et al. 2005). The deficiency (12–15 = –3) between the maximum number of protons generated by the linear electron transport chain and those needed for ATP synthesis in one rotation of the c-ring would be even greater.

The requirement for the free energy derived from the proton electro-chemical potential gradient,  $\Delta\tilde{\mu}_{H^+}$ , is a substantially more formidable requirement than exists in bovine mitochondria, where the c-ring contains only 8 subunits (Watt et al. 2010), through which only 8  $H^+$  need be translocated for the synthesis of three ATP per complete revolution of the c-ring. The variability of the size of the F1 ATPase ring is a fascinating problem in the evolution of the structure of the energy transducing molecular apparatus.

### B. The Proton Shortfall; Cyclic Electron Transport

The ATP/2e ratio measured in thylakoid membranes is 1.25 and 1.6 under conditions of LET and CET using methyl viologen and ferredoxin, respectively, as the electron acceptor to define non-cyclic (LET) and PSI cyclic (CET) electron transport (Hosler and Yocum 1987). The recently determined value of the  $H^+/ATP$  stoichiometry in plant chloroplasts is 4.7 (Petersen et al. 2012). Assuming that each complete rotation of the proton translocating c-ring results in the synthesis of 3 ATP (Ferguson 2010; Watt et al. 2010), the maximum efficiency

(ATP/2e) of ATP synthesis would be 1.3 (6  $H^+/2e$  divided by 4.7  $H^+/ATP$ ) or 1.2 (6  $H^+/2e/5 H^+/ATP$ ) via LET coupled to water oxidation and a Q cycle operating at full efficiency, i.e.,  $H^+/e=2$ , in the  $b_6f$  complex (Mitchell 1975a), yielding an  $H^+/2e$  ratio = 6 for the LET chain. *n. b.*, an experimental nuance is that the experimental determination of the pH change associated with a full  $H^+/e$  ratio = 2 in the Q cycle mechanism requires addition of an ionophore to collapse the  $\Delta\tilde{\mu}_{H^+}$  (Fowler and Kok 1976; Graan and Ort 1983; Willms et al. 1987; Berry and Rumberg 1999). The value of 1.25 measured for the ATP/2e stoichiometry in LET mode is appreciably smaller than the value of 1.5 needed to account for the ATP/NADPH stoichiometry. Thus, in addition to the LET pathway including the Q cycle driven through the  $b_6f$  complex (Fig. 9.1a), an additional pathway coupled to proton pumping is required to generate a  $\Delta\tilde{\mu}_{H^+}$  sufficient for synthesis of ATP with the known efficiency. A solution to this problem is utilization of the pathway of photosystem I-ferredoxin-dependent cyclic electron transport, i.e., CET (Joliot and Joliot 2005, 2006; Breyton et al. 2006; Fisher and Kramer 2014), (Fig. 9.1b). Thus, LET alone cannot generate a  $\Delta\tilde{\mu}_{H^+}$  sufficient to account for the measured maximum efficiency of ATP synthesis. CET can be viewed as a modulator of the rate of ATP synthesis, which is an increasing function of the ambient light intensity (Kramer et al. 2004).

By what detailed mechanism, and with what efficiency, the cyclic pathway is coordinated to the main chain or non-cyclic pathway is not well established. It has been estimated that in newly illuminated previously dark-adapted leaves of *Arabidopsis*, cyclic electron flow can operate in dark-adapted leaves at a rate, approximately  $130 s^{-1}$  (Joliot et al. 2004) which is comparable to the rate-limiting step of LET, and that as much as 50 % of the light-dependent ATP synthesis can be derived from the cyclic pathway (Joliot and Joliot 2006). However, there is not a consensus on the pathway and redox



proteins involved in the connection of the physiological low potential electron donor, ferredoxin, to the main chain. Based on inhibition of ferredoxin-mediated cyclic phosphorylation by antimycin A (Tagawa et al. 1963; Arnon et al. 1967), a classical inhibitor of the mitochondrial  $bc_1$  complex that blocks the oxidation of heme  $b_n$  (Chance and Williams 1956; von Jagow and Link 1986), it was proposed that the electron connection of ferredoxin with the main electron transport chain occurred via the cytochrome  $b_6f$  complex (Slovacek et al. 1979; Slovacek and Hind 1980). This result was, however, not confirmed (Moss and Bendall 1984; Bendall and Manasse 1995). The interpretation of the latter result was that cyt  $b_6$  is not involved in the pathway of CET and led to different proposals for the identity of the ferredoxin-plastoquinone reductase (see below). To explain the two different results for the effect of antimycin A on heme  $b_6$  reduction, it can be noted that 12 different isomers of “antimycin” are found in its Internet listing at the NCBI PubChem, and that different antimycin isomers with different specificity may have been used in the two studies on the effect of antimycin on the amplitude of the flash-induced reduction of heme  $b_n$ . It has also been noted that the binding of antimycin A at the n- side of the  $b_6f$  complex must differ from that in the  $bc_1$  complex, and is likely to be of lower affinity, as a consequence of partial occupancy of the  $Q_n$  binding site (Yamashita et al. 2007; Cramer et al. 2011) by the unique heme  $c_n$  (Stroebel et al. 2003; Alric et al. 2005; Zatsman et al. 2006; Baymann et al. 2007; Twigg et al. 2009) of the antimycin binding site in the  $bc_1$  complex.

### C. Protein and Redox Components in the CET Pathway

Information on the identity of additional components involved in CET-dependent electron transport is contained in the isolated PSI reaction center “super-complex” (Iwai et al. 2010) which, in addition to PSI, contains the  $b_6f$  complex, FNR, and the

integral membrane protein PGRL1 that is implicated in CET (Shikanai 2007; Hertle et al. 2013). Participation of FNR with  $b_6f$  complex in the cyclic pathway in plant/algal thylakoid membranes was suggested by the association of FNR with isolated spinach  $b_6f$  complex (Zhang et al. 2001). However, neither the Trol nor the Tic62 proteins that are known to be involved in the bonding of FNR to the thylakoid membrane (Mulo 2011) have been detected in the  $b_6f$  complex (Zhang et al. 2001). The less than stoichiometric binding of FNR to the  $b_6f$  complex (Zhang et al. 2001) would be consistent with the proposal that when FNR functions in CET, it binds only to the fraction of the  $b_6f$  population that resides in the non-appressed membrane fraction in the laterally inhomogeneous membrane (Anderson 2002), where CET is concentrated (Joliot and Joliot 2005) (Fig. 9.1b). An isolated complex containing both FNR and the  $b_6f$  complex implies a connection between the two, suggesting that the n-side of the cytochrome complex provides entry for electrons donated by ferredoxin to the main chain (G. Kurisu, this volume, Chap. 12), and that a ferredoxin-plastoquinone reductase provides the connection necessary for CET between the low potential redox components of the PSI reaction center and the high potential redox centers of the LET chain. A ubiquitous role of FNR in a cyclic pathway, however, is unlikely as it is not found in the cyanobacterial  $b_6f$  complex (Kurisu et al. 2003; Zhang et al. 2003; Yamashita et al. 2007; Baniulis et al. 2009, 2011; Hasan et al. 2013b; Hasan and Cramer 2014; Rexroth et al. 2014), nor in  $b_6f$  complex isolated from *C. reinhardtii* (Pierre et al. 1995; Stroebel et al. 2003), although it is possible that it is loosely bound and lost in purification or crystallization (cf., Sect. IV.H).

### D. Other Candidates for the Ferredoxin-Plastoquinone Reductase (FQR)

Alternative proposals for the identity of this reductase, which are necessary for cyanobac-

teria that do not have a bound FNR, are shown (Fig. 9.1).

### 1. A Role for NADPH Dehydrogenase (Ndh)

Ndh, or Ndh-1 in cyanobacteria (Battchikova et al. 2011) in the cyclic pathway was suggested by: (i) studies on chloroplast mutants in the model plant, *Arabidopsis thaliana* (Livingston et al. 2010); (ii) reduction of the plastoquinone pool in tobacco leaves by a chloroplast Ndh complex whose rate was not documented to be kinetically competent (Sazanov et al. 1998), and (iii) an isolated 550 kDa Ndh complex suggested to function as a respiratory complex dispensable for plant growth under optimum conditions (Burrows et al. 1998). The characterization of this complex from cyanobacteria, particularly by electron microscopy, has been facilitated by a fluorescence tagging approach (Birungi et al. 2010). Although the latter study is a significant advance, it has not yet been possible to characterize a physiologically significant redox activity of the Ndh complex coupled to reaction with a known component in the LET.

### 2. PTOX

An NADH dehydrogenase may also function in a “chlororespiration” system terminated by a plastoquinol terminal oxidase (PTOX) that functions when the quinone pool is over-reduced. The biochemical identity of the PTOX is unknown (McDonald et al. 2011), and the only known redox component in the ETC that has properties resembling an oxidase is the novel heme  $c_n$  in the  $b_6f$  complex, discussed below, which has been shown through EPR spectral analysis to bind nitric oxide (Twigg et al. 2009).

### 3. PGRL Components

A 35.7 kDa ( $pI = 5.2$ ) protein, “PGRL1,” present at unknown stoichiometry in the PSI super-complex *C. reinhardtii* (Iwai et al. 2010), and at a stoichiometry comparable to,

although smaller (0.5:1), that of the Rieske [2Fe-2S] protein in *Arabidopsis thaliana*, has been inferred to be the ferredoxin-quinone reductase (Hertle et al. 2013). The absence of the protein results in a partial decrease of the chlorophyll fluorescence yield that results from reduction of the quinone pool. The redox function is believed to be derived from the six cysteine residues in the protein, perhaps in conjunction with iron that is present in the preparation. PQRL1 is also inferred to be able to bind to the  $b_6f$  complex (Hertle et al. 2013), although it has not been detected in mass spectroscopic analysis of isolated  $b_6f$  complex (Whitelegge et al. 2002). It may be appropriate to include PGRL1 to the list of proteins listed above in Sect. IV.H that are weakly bound to the  $b_6f$  complex. In addition, It is noted: (a) the fluorescence yield effects ascribed to PGRL1 are perhaps not quantitative indicators of an obligatory function in the ETC, as they involve changes of a factor of 2–3 on a time scale of 10 s, approximately a factor of 1000 times slower than the rate-limiting step of electron transport in this region of the ETC; (b) the rate of P700 reduction, a standard kinetically competent assay for cyclic electron transport, in the presence and absence of the peptide has not been reported. (c) Details of the chemical nature and quantitative properties of the hexaCys-Fe redox moiety in PQRL1, proposed to serve as the redox group responsible for FQR activity, are not presently available.

## VII. Functions of the $b_6f$ Complex in the Linear Electron Transport (LET) Pathway; the Q Cycle

Plastoquinone (PQ) is reduced by the PSII reaction center to PQH<sub>2</sub> concomitant with H<sup>+</sup> uptake, and is the second source, besides H<sub>2</sub>O, of H<sup>+</sup> translocated to the p-side of the membrane to form the  $\Delta pH$  component of the  $\Delta \tilde{\mu}_H^+$ . PQH<sub>2</sub> enters an intramembrane pool of 5–10 PQ/PQH<sub>2</sub> per  $b_6f$  (Stiehl and Witt 1969; Graan and Ort 1984). Oxidation of PQH<sub>2</sub> from this pool by the  $b_6f$

complex provides the second site in the LET, and a second mechanism, for generation of the  $\Delta\sim\mu_H^+$ . This second mechanism, centered on the functions of the  $b_6f$  complex, is the “Q cycle” (Fig. 9.7a).

The historical development and evolution of the Q cycle model from its original formulation based on studies of the mitochondrial respiratory chain by Mitchell (1975a, b), and many experimental and conceptual problems associated with it, has been discussed recently in a perspective involving both  $bc_1$  and  $b_6f$  complexes (Mulikidjanian 2010). The major points in the latter critique that apply to data obtained for the function of the  $b_6f$  complex are: (a) the initial suggestion of Mitchell that the quinone bound at the n-side of the complex could be reduced enzymatically (Mitchell 1975a, b); (b) historically, elucidation of the Q-cycle mechanism operating in  $bc_1$  complexes was facilitated by utilization of the photosynthetic  $\alpha$ -proteobacteria, *Rhodobacter sphaeroides* and *Rhodobacter capsulatus* (Crofts and Wraight 1983); (c) the relatively short electron transfer distance, 10–13 Å between the two  $b_p$  hemes, summarized for known structures of cytochrome  $bc$  complexes (Cramer et al. 2011) should allow electron transfer between the two monomers of the complex (Soriano et al. 1999; Sarewicz et al. 2010; Swierczek et al. 2010; Khalfaoui-Hassani et al. 2012). (d) An enigma associated with the Q cycle mechanism of trans-membrane electron transfer across the two hemes  $b_p$  and  $b_n$  is that it has not been possible to obtain an additive photo- (i.e., flash) induced reduction in situ of the two hemes from either the  $bc_1$  (Klishin et al. 2002) or  $b_6f$  (Furbacher et al. 1989) complexes. (e) There are additional experimental problems associated with the analysis of the redox events involving the trans-membrane hemes in the  $b_6f$  complex: the wavelength maxima ( $\lambda_m$ ) of the absorbance difference (reduced minus oxidized) spectra of hemes  $b_p$  and  $b_n$  are spectrophotometrically indistinguishable ( $\Delta\lambda_m \leq 1$  nm) at the measuring light bandwidths usually employed. The consequence

is that it is not possible to experimentally determine which heme,  $b_n$  or  $b_p$ , undergoes photo-reduction. (f) As discussed above (Sect. IV.J), there is no n-side chemical inhibitor of cyt  $b$  redox reactions in the  $b_6f$  complex that acts with the efficacy of antimycin A on heme  $b_n$  in the  $bc_1$  complex.

#### A. Complexity of the $b_6f$ Complex; Some Inconsistencies

With seven redox centers, four hemes ( $f$ ,  $b_p$ ,  $b_n$ , and  $c_n$ ), plastoquinone/ol at two binding sites, and the [2Fe-2S] ISP, present in each monomer of the  $b_6f$  complex that are involved in redox and proton transfer reaction associated with a Q cycle, the associated redox and proton transfer reactions are inevitably complex. The number of disparities (e.g., Girvin and Cramer 1984; Rich 1988; Furbacher et al. 1989; Joliot and Joliot 1994) or variations (Ponamarev and Cramer 1998; Heimann et al. 2000) observed in the anticipated charge transfer parameters of the proposed Q cycle is significant. Many have been discussed previously (Mulikidjanian 2010). Some of the inconsistencies with the predictions of the Q cycle (Girvin and Cramer 1984) involve the slow electrochromic band shift associated with trans- or intra- membrane charge transfer (Joliot and Delosme 1974; Rich 1988).

#### B. Alternative Q Cycle Model

Here, a modified alternative Q cycle model is suggested in the context of some of the perceived inconsistencies in the canonical Q cycle model described above. To accomplish this goal, the participation of the cyclic pathway described above (Sect. VI) is included in the model to supply the second electron to the n-side plastoquinone. This avoids the necessity for turnover of two quinols on the p-side of the complex: thus, (i) plastoquinol, formed in the PSII reaction center by electrons donated from water and protons obtained from the n- (stromal) side of the membrane (Fig. 9.1a), enters the  $b_6f$  complex through the inter-

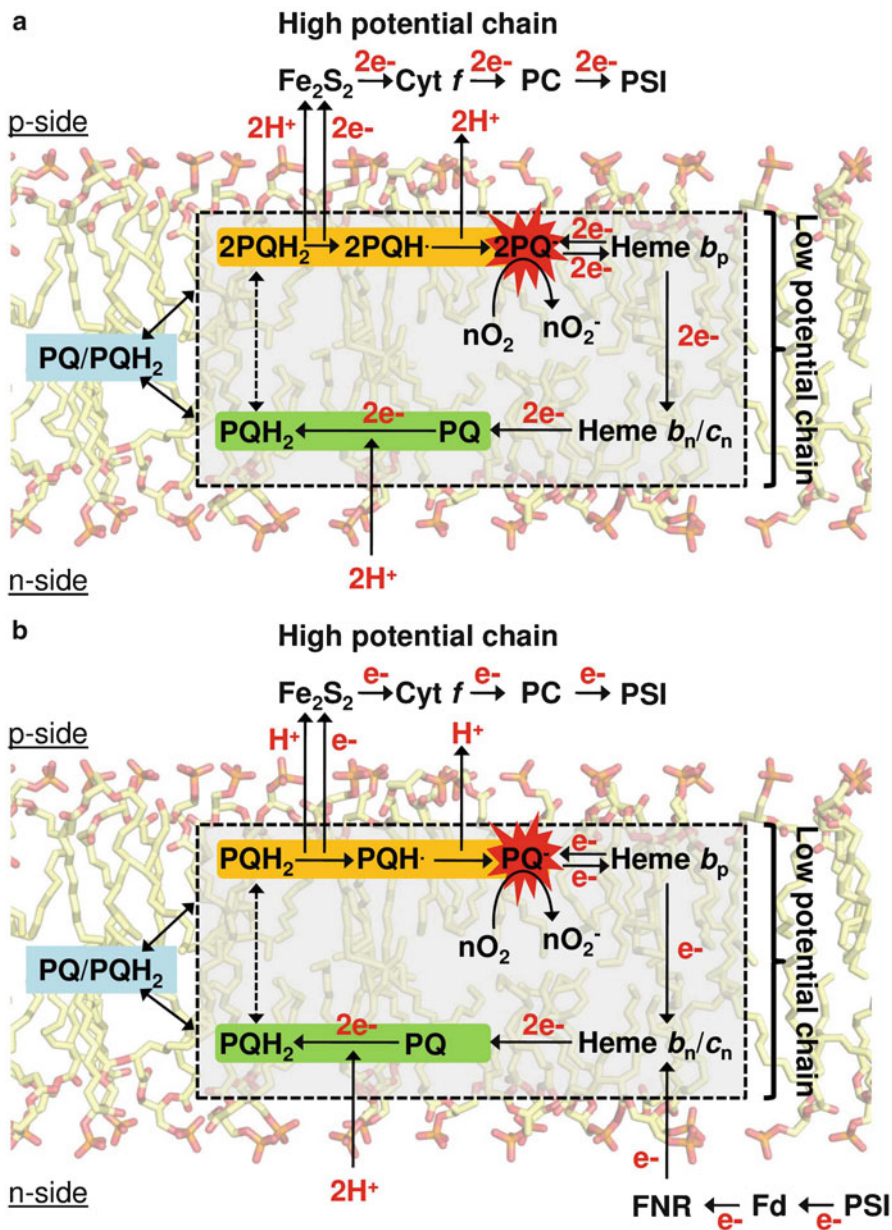


Fig. 9.7. Electron-proton transfer pathways in the cytochrome *b<sub>6</sub>f* complex (Hasan et al. 2013b). Trans-membrane core represented as light gray dashed box, and lipid bilayer as sticks in the background. p-side plastoquinol deprotonation/oxidation (Q<sub>p</sub>) site, n-side plastoquinone reduction/protonation site (Q<sub>n</sub>) shown, respectively, as yellow and green boxes. Intra-membrane plastoquinone (PQ/PQH<sub>2</sub>) pool highlighted as blue box. (a) p-side one electron oxidative/deprotonation reactions: PQH<sub>2</sub> bound within Q<sub>p</sub>-site proximal to 2Fe-2S cluster transfers H<sup>+</sup> to His129 of the ISP and oxidation to neutral semi-plastoquinone (PQH<sup>•</sup>). Anionic semi-plastoquinone (PQ<sup>•-</sup>) (in red) generated either by deprotonation of the neutral semi-plastoquinone (PQH<sup>•</sup>) via the conserved PEWY (Widger et al. 1984) domain (Fig. 9.8). Anionic semi-quinone reduction of molecular oxygen to superoxide (O<sub>2</sub><sup>-</sup>) (Baniulis et al. 2013). The prefix “n” in front of molecular oxygen (O<sub>2</sub>) and superoxide (O<sub>2</sub><sup>-</sup>) in the reaction scheme is a “scale factor” that describes the stoichiometry of superoxide generation within the cytochrome complex, which is 0.02 relative to the LET rate through the cytochrome complex, and approximately 20-fold larger than in the *bc<sub>1</sub>* complex (Baniulis et al. 2013). The prefix “2” associated with the trans-membrane electron transfer, denotes the stoichiometry of the p-side quinol oxidation reactions required for the n-side quinone reaction. (b) An alternative mechanism utilizes the cyclic pathway, in which one of the two electrons required for n-side reduction of plastoquinone is provided by the CET pathway from the PSI complex to the *b<sub>6</sub>f* complex via ferredoxin and, at least in the plant system, FNR, and other possible cofactors.

monomer cavity of the dimeric complex (Fig. 9.2a, b) and quinone entry-exit portal (Hasan et al. 2014a), donates electrons and protons to the p-side [2Fe-2S] cluster of the  $b_6f$  complex (Hasan et al. 2014a). (ii) In the canonical Q-cycle mechanism (Mitchell 1975a; Joliot and Joliot 1985, 1988; Kramer and Crofts 1994; Cape et al. 2006) PQH<sub>2</sub> oxidation by the  $b_6f$  complex occurs through a split pathway involving high (2Fe-2S → cyt f → PC or cyt c → P700) and low (heme  $b_p$  → heme  $b_n$  → PQ<sub>n</sub>) potential ET chains (Fig. 9.7a). This results in a theoretically maximum H<sup>+</sup>/e ratio = 2 contributed by the  $b_6f$  complex and, as discussed above (Sects. VI.A and VI.B), a total H<sup>+</sup>/e ratio of 3 when the contribution from water splitting is included. Pathways of H<sup>+</sup> transfer on the p- and n-sides of the complex are described in Fig. 9.7a.

The Q cycle pathway described in Fig. 9.7b is, in two respects, an alternative to the conventional model shown in Fig. 9.7a, and is based on fundamental differences between the properties of the  $b_6f$  and  $bc_1$  complex. The  $bc_1$  complex differs by having: (a) no cyclic pathway in the mitochondrial respiratory chain operating from the high potential end of the LET; (b) no low potential reductant in the photosynthetic bacteria such as ferredoxin or heme  $c_n$ . The  $b_6f$  complex is distinguished by a unique tight coupling and sharing of electrons between hemes  $b_n$  and  $c_n$  on the n-side of the membrane, which results in the  $g = 12$  EPR signal (Zatsman et al. 2006). Thus, for the n-side of the complex, it is proposed: (i) the heme couple  $b_n$ - $c_n$  reduces quinone via a two electron mechanism that avoids the problem of quinol production via one electron transfer of a reactive semiquinone intermediate; (ii) one of the electrons that reduces PQ<sub>n</sub> in the plant/algal Q cycle system can be donated by ferredoxin. This mechanism would explain why no more than one  $b$  heme in the  $b_6f$  complex can be rapidly reduced by multiple closely spaced short duration light flashes (Furbacher et al. 1989).

The mechanism for the canonical Q cycle described in Fig. 9.7a involves oxidation of

one p-side plastoquinol molecule which provides one electron to the high potential chain, for transfer to the PSI reaction center complex. Oxidation of two p-side plastoquinol molecules is required to completely reduce one n-side plastoquinone to plastoquinol. The individual deprotonation and oxidation steps during the p-side redox reactions of plastoquinol, respectively, involve the transfer of only one proton and electron. Two electrons can be stored in the n-side heme  $b_n/c_n$  couple, to perform two closely spaced plastoquinone (PQ) reduction-protonation reactions, which would preclude/decrease semi-plastoquinone formation on the n-side. A mechanism alternative to that in the  $bc_1$  complex, shown in Fig. 9.7b, is provided by utilization of the PSI cyclic pathway, in which one of the two electrons required for n-side reduction of plastoquinone would be provided by the CET pathway, from the reducing side of the PSI reaction center via ferredoxin to the  $b_6f$  complex. Under such conditions, the requirement of p-side plastoquinol molecules is decreased from two to one for the complete n-side reduction of plastoquinone (PQ) to plastoquinol (PQH<sub>2</sub>). This would remove the requirement in the conventional Q cycle model for a mechanism to coordinate the delivery of two quinol molecules in a msec time interval to the Q<sub>p</sub> site.

### VIII. Quinone-Mediated H<sup>+</sup> Transfer Pathways; n-Side to Quinone Binding Site: Heme $c_n$ ; p-Side PEWY Exit Pathway with Invaginated H<sub>2</sub>O Pocket

#### A. n-Side Entry Pathway to Heme $c_n$ Quinone Binding Site

This domain consists of heme  $b_n$ , the unique heme  $c_n$ , whose close proximity to heme  $b_n$  (4 Å between the  $c_n$  heme Fe and propionate oxygen of heme  $b_n$ ) is reflected in a unique  $g = 12$  EPR signal (Zatsman et al. 2006; Baymann et al. 2007), and the quinone binding defined by these

prosthetic groups. The  $H^+$  uptake pathway from the electrochemically negative (n) aqueous phase to the n-side quinone binding site of the complex has been defined in the 2.70-Å crystal structure (PDB 4H44; (Hasan et al. 2013b)), and in structures with bound quinone analog inhibitors, inferred from crystal structures with the quinone analogue inhibitors tridecyl-stigmatellin and 2-nonyl-4-hydroxyquinoline N-oxide, with a resolution of 3.07 Å and 3.25 Å, respectively (Yamashita et al. 2007). The simplest n-side proton transfer pathway, which does not contain any as yet resolved proton transferring water molecules, extends from the n-side bulk aqueous phase via Asp20 to Arg207 (Arg 214 in *Synechococcus* PCC 7002) in the cyt *b* subunit to quinone bound axially to the heme  $c_n$ . This is a unique structure aspect of the  $b_{6f}$  compared to the  $bc_1$  complex (Fig. 9.8a), and provides a function for the previously enigmatic heme  $c_n$ , whose presence in the  $b_{6f}$  complex is a unique property relative to  $b_{6f}$ . Additional possible n-side  $H_2O$ -containing  $H^+$  – transfer pathways to the heme  $c_n$  quinone binding site have been proposed (Hasan et al. 2013b).

### B. p-Side PEWY-Dependent Exit Pathway

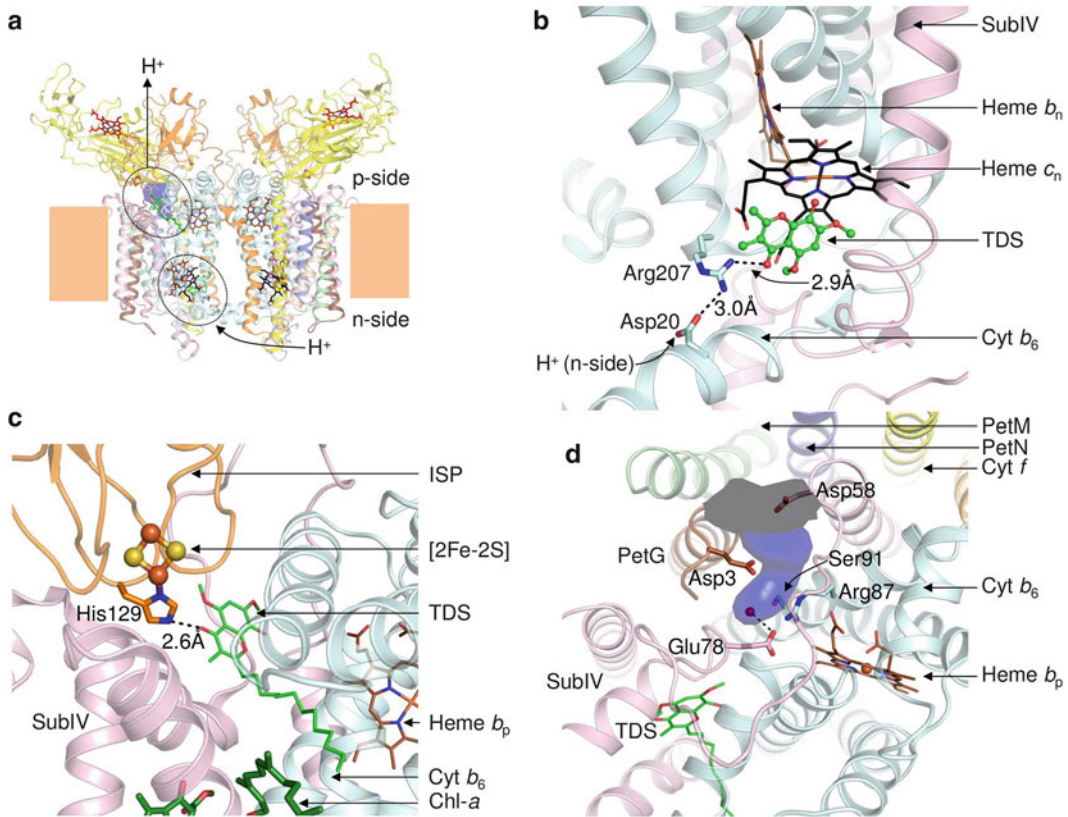
The p-side  $H^+$  transfer pathway in the  $b_{6f}$  complex (Fig. 9.8b) is structurally and conceptually similar to that previously described for the  $bc_1$  complex in mitochondria (Solmaz and Hunte 2008; Berry et al. 2013; Kao and Hunte 2014) and purple photosynthetic bacteria (Esser et al. 2004, 2008). Information on details of the p-side  $H^+$  transfer pathway were obtained from crystal structures of the  $b_{6f}$  complex obtained in the absence and presence of quinone-analog inhibitors from: (a) filamentous cyanobacteria, *M. laminosus* (Kurisu et al. 2003; Yamashita et al. 2007; Baniulis et al. 2009; Hasan et al. 2013b); PDB 1VF5, 2E74, 2E75, 2E76 and *Nostoc* PCC 7120 (PDB 2ZT9, 4H44, 4H0L, 4H13,

and 4OGQ for the highest resolution attained, 2.50 Å); (b) the green alga, *C. reinhardtii* ((Stroebe et al. 2003), PDB 1Q90). The exit pathway for the first proton donated by plastoquinol ( $PQH_2 \rightarrow PQH^- + H^+$ ), based on the structure obtained with the p-side quinone analogue, tri-decyl-stigmatellin (TDS), PDB 2E76 (Yamashita et al. 2007), involves His129 of the Rieske ISP in the p-side binding site (Qp) of  $PQH_2$ . His129 is located within an H-bond distance from O4 of the chromone ring of TDS (Yamashita et al. 2007), and can provide a route for transfer of the first proton donated by plastoquinol ( $PQH_2$ ) to the p-side bulk aqueous phase. The structures of the cyanobacterial complex obtained subsequently at higher resolution, up to 2.5 Å (PDB 4OGQ), imply that, as inferred for the  $bc_1$  complex (Solmaz and Hunte 2008), a different route to the p-side aqueous phase is taken by the second proton. The p-side EF loop of the  $bc_1$  complex and subunit IV ( $b_{6f}$ ) has a conserved sequence motif, PEWY, as noted in the initial description of the membrane topology of the cytochrome *b* subunit in energy transducing membranes (Widger et al. 1984). Crystal structures of the mitochondrial (Solmaz and Hunte 2008; Kao and Hunte 2014), and chromatophore (Esser et al. 2004, 2008)  $bc_1$  complex with quinone analog inhibitors imply that Glu272 in the PEWY sequence undergoes rotation from a quinol-liganding position distal to heme  $b_p$  to a heme  $b_p$ -proximal position. The Glu-78 residue of the PEWY sequence in  $b_{6f}$  is implicated in a similar function, participating in the exit of the second  $H^+$  from the Qp-site (Zito et al. 1998, 1999). A difference in the function of the Glu residue at this position is that in its *trans*-position distal to the quinone, it forms a salt bridge with Arg87 (Hasan et al. 2013b), and is thus inferred to lengthen the lifetime of the protonated plastoquinone (Hasan et al. 2013b), perhaps providing an explanation for the elevated level of super-oxide production relative to the mitochondrial  $bc_1$  complex (Baniulis et al. 2013).

### C. Intrusion of Water in the p-Side Exit Pathway

The side chain carboxylate of the conserved Glu78 in the  $b_6f$  complex faces a water channel (Fig. 9.8) lined by polar residues that is connected to the p-side bulk aqueous phase. Despite some similarities between the  $b_6f$  and the  $bc_1$  complex in the transfer mechanism of the second proton to the aqueous

phase, there is a major difference in the organization of the p-side water network. In the yeast  $bc_1$  complex, an extended water channel from a heme  $b_p$  propionate oxygen extends via hydrogen bonds in a network of water molecules to the p-side aqueous phase (Hunte et al. 2000). In the  $b_6f$  complex, a short channel from Glu78 to a water-filled invagination in the complex is provided by a conserved polar residue, Glu3, from the



**Fig. 9.8.** Proton transfer pathways in the cytochrome  $b_6f$  complex. **(a)** Proton entry into the complex occurs on the electrochemically negative (n) side, and proton exit takes place from the electrochemically positive (p) side of the complex. The plane of the lipid bilayer is shown as *orange blocks*. **(b)** Proton entry has been suggested to involve the residues Asp20 and Arg207 of cyt  $b_6$ , which form a pathway for proton translocation from the n-side aqueous phase to the quinone reduction/protonation site, marked by the quinol analog TDS (*green/red ball and sticks*) (PDB ID 4H44). For simplicity, the TDS tail has been omitted. Proton exit on the p-side of the complex involves two distinct pathways. **(c)** The first proton released from the reduced quinol (QH<sub>2</sub>) involves the ISP surface residue His129 (PDB ID 4H13). The position of the quinol is marked by the bound TDS (*green/red sticks*). **(d)** The second proton is extracted from the semiquinone by Glu78 of subunit IV (PDB ID 4H44). The position of the semiquinone is marked by the quinone analogue inhibitor, TDS, which has been superposed from PDB ID 4H13. The Glu78 side chain connects via a water molecule (water-316, PDB ID 4H44) to a hydrophilic cavity (*blue surface*), which provides a pathway for proton exit to the p-side bulk aqueous phase. The cavity is lined by Asp3 (PetG), Arg87 (cyt  $b_6$ ), Ser91 (cyt  $b_6$ ), and Asp58 (subIV).

peripheral PetG subunit in the  $b_6f$  complex, for which there is no analogue in the  $bc_1$  complex. pKa calculations indicate that Glu3 ( $pK \approx 4.6$ ), which borders the  $H_2O$  channel and is a conserved residue, is consistent with its participation in proton transfer during the p-side proton exit process (Hasan et al. 2013b). It is noted that pronounced water-filled invagination is a common feature of integral membrane transport proteins such as the *lac* permease (Smirnova et al. 2011).

## IX. The Cytochrome $b_6f$ Complex as a Hetero-Oligomeric Membrane Lipoprotein

In addition to its function in photosynthetic and membrane energy transduction, the structure studies on the cytochrome  $bc$  complexes provide information on fundamental properties of multi-subunit relatively complicated hetero-oligomeric membrane proteins (Althoff et al. 2011). Studies on protein-lipid interactions of the  $bc_1$  (Palsdottir and Hunte 2004a; Wenz et al. 2009) and  $b_6f$  complexes I (Hasan et al. 2011, 2014b; Hasan and Cramer 2014) are of general interest in the membrane protein field. The  $b_6f$  complex has at least 23 lipid binding sites per monomer (see Sect. V, Fig. 9.6). In addition to conventional absorbance spectroscopy, the use of other spectrophotometric approaches provided by the hemes to analyze the state of the complex (e.g., Hasan et al. 2014b) confers a unique handle for analysis of conformational changes of the complicated integral membrane lipoprotein complex.

## Acknowledgments

The studies of the authors described in this article have been supported by the National Institutes of Health (GMS-038323), the Henry Koffler Professorship (WAC), and a Fellowship from Purdue University (SSH). For recent discussions that have contributed

to this article, we thank S. D. Zakharov, S. Singh, R. Agarwal, D. Baniulis, H. Zhang, and E. Yamashita.

## References

- Agarwal R, Hasan SS, Jones LM, Stofleth JT, Ryan CM, Whitelegge JP, Kehoe DM, Cramer WA (2015) Role of domain swapping in the hetero-oligomeric cytochrome  $b_6f$  Lipoprotein Complex. *Biochemistry* 54:151–163
- Alric J, Pierre Y, Picot D, Lavergne J, Rappaport F (2005) Spectral and redox characterization of the heme  $c_1$  of the cytochrome  $b_6f$  complex. *Proc Natl Acad Sci U S A* 102:15860–15865
- Althoff T, Mills D, Popot JL, Kühlbrandt W (2011) Arrangement of electron transport chain components in bovine mitochondrial supercomplex I1III2IV1. *EMBO J* 30:4652–4664
- Anderson JM (2002) Changing concepts about the distribution of Photosystems I and II between grana-appressed and stroma-exposed thylakoid membranes. *Photosynth Res* 73:157–164
- Arnarez C, Mazat JP, Elezgaray J, Marrink SJ, Periole X (2013) Evidence for cardiolipin binding sites on the membrane-exposed surface of the cytochrome  $bc_1$ . *J Am Chem Soc* 135:3112–3120
- Arnon DI, Tsujimoto HY, McSwain BD (1967) Ferredoxin and photosynthetic phosphorylation. *Nature* 214:562–566
- Baniulis D, Yamashita E, Zhang H, Hasan SS, Cramer WA (2008) Structure-function of the cytochrome  $b_6f$  complex. *Photochem Photobiol Sci* 84:1349–1358
- Baniulis D, Yamashita E, Whitelegge JP, Zatsman AI, Hendrich MP, Hasan SS, Ryan CM, Cramer WA (2009) Structure-function, stability, and chemical modification of the cyanobacterial cytochrome  $b_6f$  complex from *nostoc* sp. PCC 7120. *J Biol Chem* 284:9861–9869
- Baniulis D, Zhang H, Yamashita E, Zakharova T, Hasan SS, Cramer WA (2011) Purification and crystallization of the cyanobacterial cytochrome  $b_6f$  complex. In: Carpentier R (ed) *Methods in Molecular Biology, Photosynthesis Research Protocols*. Humana Press, Totowa, pp 65–77
- Baniulis D, Hasan SS, Stofleth JT, Cramer WA (2013) Mechanism of enhanced superoxide production in the cytochrome  $b_6f$  complex of oxygenic photosynthesis. *Biochemistry* 52:8975–8983
- Batchikova N, Eisenhut M, Aro EM (2011) Cyanobacterial NDH-1 complexes: novel insights and remaining puzzles. *Biochim Biophys Acta* 1807:935–944



- Baymann F, Giusti F, Picot D, Nitschke W (2007) The *ci/bH* moiety in the *b<sub>6</sub>f* complex studied by EPR: a pair of strongly interacting hemes. *Proc Natl Acad Sci U S A* 104:519–524
- Bendall DS, Manasse RS (1995) Cyclic phosphorylation and electron transport. *Biochim Biophys Acta* 1229:23–38
- Bernat G, Roegner M (2011) Center of the cyanobacterial electron transfer network: the cytochrome *b<sub>6</sub>f* complex. In: Peschek GA (eds) *Bioenergetic Processes of Cyanobacteria*. Springer, Dordrecht, pp 573–606
- Berry EA, Huang LS (2011) Conformationally linked interaction in the cytochrome *bc<sub>1</sub>* complex between inhibitors of the Q(o) site and the Rieske iron-sulfur protein. *Biochim Biophys Acta* 1807:1349–1363
- Berry S, Rumberg B (1999) Proton to electron stoichiometry in electron transport of spinach thylakoids. *Biochim Biophys Acta* 1410:248–261
- Berry EA, Guergova-Kuras M, Huang L-S, Crofts AR (2000) Structure and function of cytochrome *bc* complexes. *Annu Rev Biochem* 69:1005–1075
- Berry EA, De Bari H, Huang LS (2013) Unanswered questions about the structure of cytochrome *bc<sub>1</sub>* complexes. *Biochim Biophys Acta* 1827:1258–1277
- Birungi M, Folea M, Battchikova N, Xu M, Mi H, Ogawa T, Aro E-M, Boekema EJ (2010) Possibilities of subunit localization with fluorescent protein tags and electron microscopy exemplified by a cyanobacterial NDH-1 study. *Biochim Biophys Acta* 1797:1681–1686
- Bohme H, Reimer S, Trebst A (1971) Role of plastoquinone in photosynthesis – effect of dibromothymoquinone, an antagonist of plastoquinone, on non cyclic and cyclic electron flow systems in isolated chloroplasts. *Z Naturforsch Part B-Chem Biochem Biophys Biol Verw Geb B* 26:341
- Bowyer JR, Crofts AR (1981) On the mechanism of photosynthetic electron transfer in *Rhodospseudomonas capsulata* and *Rhodospseudomonas sphaeroides*. *Biochim Biophys Acta* 636:218–233
- Breyton C, Tribet C, Olive J, Dubacq J-P, J-L P (1997) Dimer to monomer conversion of the cytochrome *b<sub>6</sub>f* complex. *J Biol Chem* 272:21892–21900
- Breyton C, Nandha B, Johnson GN, Joliot P, Finazzi G (2006) Redox modulation of cyclic electron flow around photosystem I in C3 plants. *Biochemistry* 45:13465–13475
- Burrows PA, Sazanov LA, Svab Z, Maliga P, Nixon PJ (1998) Identification of a functional respiratory in chloroplasts through analysis of tobacco mutants containing disrupted plastid *ndh* genes. *EMBO J* 17:868–876
- Cape JL, Bowman MK, Kramer DM (2006) Understanding the cytochrome *bc* complexes by what they don't do. The Q-cycle at 30. *Trends Plant Sci* 11:46–55
- Carrell CJ, Zhang H, Cramer WA, Smith JL (1997) Biological identity and diversity in photosynthesis and respiration: structure of the lumen-side domain of the chloroplast Rieske protein. *Structure* 5:1613–1625
- Chance B, Williams GB (1956) The respiratory chain and oxidative phosphorylation. *Adv Enzymol* 17:65–135
- Cooley JW (2010) A structural model for across membrane coupling between the Q<sub>o</sub> and Q<sub>i</sub> active sites of cytochrome *bc<sub>1</sub>*. *Biochim Biophys Acta* 1797:1842–1848
- Cooley JW, Lee DW, Daldal F (2009) Across membrane communication between the Q<sub>o</sub> and Q<sub>i</sub> active sites of cytochrome *bc<sub>1</sub>*. *Biochemistry* 48:1888–1899
- Cramer WA, Crofts AR (1981) Electron and proton transfer. In: Govindjee (ed) *Photosynthesis: Energy Conversion by Plants and Bacteria*. Academic, New York, pp 387–467
- Cramer WA, Zhang H, Yan J, Kurisu G, Smith JL (2006) Trans-membrane traffic in the cytochrome *b<sub>6</sub>f* complex. *Annu Rev Biochem* 75:769–790
- Cramer WA, Zhang H, Yan J, Kurisu G, Yamashita E, Dashdorj N, Kim H, Savikhin S (2008) Structure-function of the cytochrome *b<sub>6</sub>f* complex: a design that has worked for three billion years. In: Renger G (ed) *Comprehensive Series in Photochemistry and Photobiology*. Royal Society of Chemistry, Cambridge, pp 417–446
- Cramer WA, Yamashita E, Baniulis D, Hasan SS (2010) The cytochrome *b<sub>6</sub>f* complex of oxygenic photosynthesis. In: Messerschmidt A (ed) *Handbook of Metalloproteins*. Wiley, Chichester
- Cramer WA, Hasan SS, Yamashita E (2011) The Q cycle of cytochrome *bc* complexes: a structure perspective. *Biochim Biophys Acta* 1807:788–802
- Crofts AR (2004a) The cytochrome *bc<sub>1</sub>* complex: function in the context of structure. *Annu Rev Physiol* 66:689–733
- Crofts AR (2004b) The Q-cycle – a personal perspective. *Photosynth Res* 80:223–243
- Crofts AR, Berry EA (1998) Structure and function of the cytochrome *bc<sub>1</sub>* complex of mitochondria and photosynthetic bacteria. *Curr Opin Struct Biol* 8:501–509
- Crofts AR, Wraight CA (1983) The electrochemical domain of photosynthesis. *Biochim Biophys Acta* 726:149–185
- Crofts AR, Holland JT, Victoria D, Kolling DR, Dikanov SA, Gilbreth R, Sangmoon L, Kuras MG

- (2008) The Q-cycle reviewed: how well does a monomeric mechanism of the  $bc_1$  complex account for the function of a dimeric complex? *Biochim Biophys Acta* 1777:1001–1019
- Dashdorj N, Zhang H, Kim H, Yan J, Cramer WA, Savikhin S (2005) The single chlorophyll  $a$  molecule in the cytochrome  $b_6f$  complex: unusual optical properties protect the complex against singlet oxygen. *Biophys J* 88:4178–4187
- de Vitry C, Ouyang Y, Finazzi G, Wollman FA, Kallas T (2004) The chloroplast Rieske iron-sulfur protein. At the crossroad of electron transport and signal transduction. *J Biol Chem* 279:44621–44627
- Dibrova DV, Cherepanov DA, Galperin MY, Skulachev VP, Mulikidjanian AY (2013) Evolution of cytochrome  $bc$  complexes: from membrane-anchored dehydrogenases of ancient bacteria to triggers of apoptosis in vertebrates. *Biochim Biophys Acta* 1827:1407–1427
- Dutton PL, Jackson JB (1972) Thermodynamic and kinetic characterization of electron transfer components in situ in *Rhodospseudomonas spheroides* and *Rhodospirillum rubrum*. *Eur J Biochem* 30:495–510
- Egea PF, Stroud RM (2010) Lateral opening of a translocon upon entry of protein suggests the mechanism of insertion into membranes. *Proc Natl Acad Sci U S A* 107:17182–17187
- Esser L, Quinn B, Li YF, Zhang M, Elberry M, Yu L, Yu C-A, Xia D (2004) Crystallographic studies of quinol oxidation site inhibitors: a modified classification of inhibitors for the cytochrome  $bc_1$  complex. *J Mol Biol* 341:281–302
- Esser L, Elberry M, Zhou F, Yu CA, Yu L, Xia D (2008) Inhibitor-complexed structures of the cytochrome  $bc_1$  from the photosynthetic bacterium *Rhodobacter sphaeroides*. *J Biol Chem* 283:2846–2857
- Esser L, Zhou F, Yu C-A, Xia D (2015) Cytochrome complexes: evolution, structures, energy transduction, and signaling. In: Cramer WA, Kallas T (eds) *Cytochrome Complexes: Evolution, Structures, Energy Transduction, and Signaling*. Springer, Dordrecht
- Ferguson S (2010) ATP synthase: from sequence to ring size to the P/O ratio. *Proc Natl Acad Sci U S A* 107:16755–16756
- Fisher N, Kramer DM (2014) Non-photochemical reduction of thylakoid redox carriers in vitro: relevance to cyclic electron flow around photosystem I. *Biochim Biophys Acta/Bioenergetics* 1837:1944–1954
- Fowler CF, Kok B (1976) Determination of  $H^+/e^-$  ratios in chloroplasts with flashing light. *Biochim Biophys Acta* 423:510–523
- Furbacher PN, Girvin ME, Cramer WA (1989) On the question of interheme electron transfer in the chloroplast cytochrome  $b_6$  in situ. *Biochemistry* 28:8990–8998
- Gennis RB, Barquera B, Hacker B, Van Doren SR, Arnaud S, Crofts AR, Davidson E, Daldal F (1993) The  $bc_1$  complexes of *Rhodobacter sphaeroides* and *Rhodobacter capsulatus*. *J Bioenerg Biomembr* 25:195–209
- Girvin ME (1985) Electron and proton transfer in the quinone-cytochrome  $bf$  region of chloroplasts, PhD thesis, Purdue University, West Lafayette
- Girvin ME, Cramer WA (1984) A redox study of the electron transport pathway responsible for generation of the slow electrochromic phase in chloroplasts. *Biochim Biophys Acta* 767:29–38
- Gounaris K, Barber J, Harwood JL (1986) The thylakoid membranes of higher plant chloroplasts. *Biochem J* 237:313–326
- Graan T, Ort DR (1983) Initial events in the regulation of electron transfer in chloroplasts. *J Biol Chem* 258:2831–2836
- Graan T, Ort DR (1984) Quantitation of the rapid electron donors to P700, the functional plastoquinone pool, and the ratio of the photosystems in spinach chloroplasts. *J Biol Chem* 259:14003–14010
- Granseth E, von Heijne G, Elofsson A (2005) A study of the membrane-water interface region of membrane proteins. *J Mol Biol* 346:377–385
- Gray HB, Winkler JR (1996) Electron transfer in proteins. *Annu Rev Biochem* 65:537–562
- Hamel P, Olive J, Pierre Y, Wollman FA, deVitry C (2000) A new subunit of cytochrome  $b_6f$  complex undergoes reversible phosphorylation upon state transition. *J Biol Chem* 275:17072–17079
- Hasan SS, Cramer WA (2012) Lipid functions in cytochrome  $bc$  complexes: an odd evolutionary transition in a membrane protein. *Philos Trans R Soc Lond B* 367:3406–3411
- Hasan SS, Cramer WA (2014) Internal lipid architecture of the hetero-oligomeric cytochrome  $b_6f$  complex. *Structure* 22:1008–1015
- Hasan SS, Yamashita E, Ryan CM, Whitelegge JP, Cramer WA (2011) Conservation of lipid functions in cytochrome  $bc$  complexes. *J Mol Biol* 414:145–162
- Hasan SS, Stofleth JT, Yamashita E, Cramer WA (2013a) Lipid-induced conformational changes within the cytochrome  $b_6f$  complex of oxygenic photosynthesis. *Biochemistry* 52:2649–2654
- Hasan SS, Yamashita E, Baniulis D, Cramer WA (2013b) Quinone-dependent proton transfer pathways in the photosynthetic cytochrome  $b_6f$  complex. *Proc Natl Acad Sci U S A* 110:4297–4302

- Hasan SS, Yamashita E, Cramer WA (2013c) Trans-membrane signaling and assembly of the cytochrome *b<sub>6</sub>*-lipidic charge transfer complex. *Biochim Biophys Acta* 1827:1295–1308
- Hasan SS, Proctor EA, Yamashita E, Dokholyan NV, Cramer WA (2014a) Traffic within the cytochrome *b<sub>6</sub>f* lipoprotein complex: gating of the quinone portal. *Biophys J* 107:1620–1628
- Hasan SS, Zakharov SD, Chauvet A, Stadnytskyi V, Savikhin S, Cramer WA (2014b) A map of dielectric heterogeneity in a membrane protein: the hetero-oligomeric cytochrome *b<sub>6</sub>f* complex. *J Phys Chem B* 118:6614–6625
- Heimann S, Ponamarev MV, Cramer WA (2000) Movement of the Rieske iron-sulfur protein in the p-slide bulk aqueous phase: effect of luminal viscosity on redox reactions of the cytochrome *b<sub>6</sub>(f)* complex. *Biochemistry* 39:2692–2699
- Hertle AP, Blunder T, Wunder T, Pesaresi P, Pribil M, Armbruster U, Leister D (2013) PGRL1 is the elusive ferredoxin-plastoquinone reductase in photosynthetic cyclic electron flow. *Mol Cell* 49: 511–523
- Hope AB, Valente P (1996) Inhibitor binding to isolated chloroplast cytochrome *b<sub>6</sub>f* complex. *Photosynth Res* 49:37–48
- Hosler JP, Yocum CF (1987) Regulation of cyclic photophosphorylation during ferredoxin-mediated electron transport: effect of DCMU and the NADPH/NADP ratio. *Plant Physiol* 83:965–969
- Huang L-S, Berry EA (2015) Rieske iron-sulfur protein movement and conformational changes in cytochrome *bc – bf* complexes. In: Cramer WA, Kallas T (eds) *Cytochrome Complexes: Evolution, Structures, Energy Transduction, and Signaling*. Springer, Dordrecht
- Huang D, Everly RM, Cheng RH, Heymann JB, Schägger H, Sled V, Ohnishi T, Cramer WA (1994) Characterization of the chloroplast cytochrome *b<sub>6</sub>f* complex as a structural and functional dimer. *Biochemistry* 33:4401–4409
- Huang LS, Cobessi D, Tung EY, Berry EA (2005) Binding of the respiratory chain inhibitor antimycin to the mitochondrial *bc<sub>1</sub>* complex: a new crystal structure reveals an altered intramolecular hydrogen-bonding pattern. *J Mol Biol* 351:573–597
- Hunte C (2001) Insights from the structure of the yeast cytochrome *bc<sub>1</sub>* complex: crystallization of membrane proteins with antibody fragments. *FEBS Lett* 504:126–132
- Hunte C, Koepke J, Lange C, Rossmannith T, Michel H (2000) Structure at 2.3 Å resolution of the cytochrome *bc<sub>1</sub>* complex from the yeast *Saccharomyces cerevisiae* with an antibody Fv fragment. *Struct Fold Des* 8:669–684
- Hurt EC, Hauska G (1981) A cytochrome *f/b<sub>6</sub>* complex of five polypeptides with plastoquinol-plastocyanin-oxidoreductase activity from spinach chloroplasts. *Eur J Biochem* 117:591–599
- Iwai M, Takizawa K, Tokutsu R, Okamoto A, Takahashi Y, Minagawa J (2010) Isolation of the supercomplex that drives cyclic electron flow in photosynthesis. *Nature* 464:1210–1213
- Iwata S, Lee JW, Okada K, Lee JK, Iwata M, Rasmussen B, Link TA, Jap BK (1998) Complete structure of the 11-subunit bovine mitochondrial cytochrome *bc<sub>1</sub>* complex. *Science* 281: 64–71
- Jiang W, Hermolin J, Fillingame RH (2001) The preferred stoichiometry of c subunits in the rotary motor sector of *Escherichia coli* ATP synthase is 10. *Proc Natl Acad Sci U S A* 98:4966–4971
- Johnson GN (2011) Physiology of PSI cyclic electron transport in higher plants. *Biochim Biophys Acta* 1807:384–389
- Joliot P, Delosme R (1974) Flash-induced 519 nm absorption change in green algae. *Biochim Biophys Acta* 357:267–284
- Joliot P, Johnson GN (2011) Regulation of cyclic and linear electron flow in higher plants. *Proc Natl Acad Sci U S A* 108:13317–13322
- Joliot P, Joliot A (1985) Mechanism of proton-pumping in the cytochrome *b/f* complex. *Photosynth Res* 9:113–124
- Joliot P, Joliot A (1988) The low-potential electron-transfer chain in the cytochrome *bf* complex. *Biochim Biophys Acta* 933:319–333
- Joliot P, Joliot A (1994) Mechanism of electron transfer in the cytochrome *bf* complex of algae: evidence for a semiquinone cycle. *Proc Natl Acad Sci U S A* 91:1034–1038
- Joliot P, Joliot A (2005) Quantification of cyclic and linear flows in plants. *Proc Natl Acad Sci U S A* 102:4913–4918
- Joliot P, Joliot A (2006) Cyclic electron flow in C3 plants. *Biochim Biophys Acta* 1757:362–368
- Joliot P, Beal D, Joliot A (2004) Cyclic electron flow under saturating excitation of dark-adapted *Arabis* leaves. *Biochim Biophys Acta* 1656: 166–176
- Jones RW, Whitmarsh J (1988) Inhibition of electron transfer and electrogenic reaction in the cytochrome *b/f* complex by 2-n-nonyl-4-hydroxyquinoline N-oxide (NQNO) and 2,5-dibromo-3-methyl-6-isopropyl-p-benzoquinone (DBMIB). *Biochim Biophys Acta* 933:258–268
- Jordan P, Fromme P, Witt HT, Klukas O, Saenger W, Krauss N (2001) Three-dimensional structure of cyanobacterial photosystem I at 2.5 Å resolution. *Nature* 411:909–917

- Kallas T (2012) Cytochrome b(6)f complex at the heart of energy transduction and redox signaling. In: Eaton-Rye JJ et al (eds) Photosynthesis: plastid biology, energy conversion and carbon assimilation. Advances in photosynthesis and respiration, vol 34. Springer, Dordrecht, pp 501–560
- Kao WC, Hunte C (2014) The molecular evolution of the Qo motif. *Genome Biol Evol* 6:1894–1910
- Khalifaoui-Hassani B, Lanciano P, Lee DW, Darrouzet E, Daldal F (2012) Recent advances in cytochrome bc(1): inter monomer electronic communication? *FEBS Lett* 586:617–621
- Killian JA, von Heijne G (2000) How proteins adapt to a membrane-water interface. *Trends Biochem Sci* 25:429–434
- Kim H, Dashdorj N, Zhang H, Yan J, Cramer WA, Savikhin S (2005a) An anomalous distance dependence of intra-protein chlorophyll-carotenoid triplet energy transfer. *Biophys J* 89:28–30
- Kim H, Zhang H, Dashdorj N, Yan J, Cramer WA, Savikhin S (2005b) Evidence for long range triplet state energy transfer from chlorophyll *a* to beta-carotene in the cytochrome b6f complex of oxygenic photosynthesis. In: van der Est AB, Bruce D (eds) Thirteenth International Photosynthesis Congress. ACG, Montreal
- Klishin SS, Junge W, Mulikidjanian AY (2002) Flash-induced turnover of the cytochrome bc1 complex in chromatophores of *Rhodobacter capsulatus*: binding of Zn<sup>2+</sup> decelerates likewise the oxidation of cytochrome b, the reduction of cytochrome c1 and the voltage generation. *Biochim Biophys Acta* 1553:177–182
- Kramer DM, Crofts AR (1994) Re-examination of the properties and function of the *b* cytochromes of the thylakoid cytochrome *bf* complex. *Biochim Biophys Acta* 1184:193–201
- Kramer DM, Avenson TJ, Edwards GE (2004) Dynamic flexibility in the light reactions of photosynthesis governed by both electron and proton transfer reactions. *Trends Plant Sci* 9:349–357
- Kurusu G, Kusunoki M, Katoh E, Yamazaki T, Teshima K, Onda Y, Kimata-Aruga Y, Hase T (2001) Structure of the electron transfer complex between ferredoxin and ferredoxin-NADP<sup>+</sup> reductase. *Nat Struct Biol* 8:117–121
- Kurusu G, Zhang H, Smith JL, Cramer WA (2003) Structure of the cytochrome *b<sub>6</sub>f* complex of oxygenic photosynthesis: tuning the cavity. *Science* 302:1009–1014
- Kurusu G, Zhang H, Smith JL, Cramer WA (2004) Structure and function of the cytochrome b6f complex of oxygenic photosynthesis. *Protein, Nucleic Acid Enzyme* 49:1265–1273
- Lanciano P, Khalifaoui-Hassani B, Selamoglu N, Ghelli A, Rugolo M, Daldal F (2013) Molecular mechanisms of superoxide production by complex III: a bacterial versus human mitochondrial comparative case study. *Biochim Biophys Acta* 1827:1332–1337
- Livingston AK, Cruz JA, Kohzuma K, Dhingra A, Kramer DM (2010) An Arabidopsis mutant with high cyclic electron flow around photosystem I (hcef) involving the NADPH dehydrogenase complex. *Plant Cell* 22:221–233
- Martinez SE, Smith JL, Huang D, Szczepaniak A, Cramer WA (1992) Crystallographic studies of the lumen-side domain of turnip cytochrome *f*. In: Murata N (ed) Research in Photosynthesis. Kluwer, Dordrecht, pp 495–498
- Martinez SE, Huang D, Szczepaniak A, Cramer WA, Smith JL (1994) Crystal structure of the chloroplast cytochrome *f* reveals a novel cytochrome fold and unexpected heme ligation. *Structure* 2:95–105
- Martinez S, Huang D, Ponamarev M, Cramer WA, Smith JL (1996) The heme redox center of chloroplast cytochrome *f* is linked to a buried five-water chain. *Protein Sci* 5:1081–1092
- McDonald AE, Ivanov AG, Bode R, Maxwell DP, Rodermel SR, Huner NP (2011) Flexibility in photosynthetic electron transport: the physiological role of plastoquinol terminal oxidase (PTOX). *Biochim Biophys Acta* 1807:954–967
- Mitchell P (1966) Chemiosmotic coupling in oxidative and photosynthetic phosphorylation. *Biol Rev* 41:445–502
- Mitchell P (1975a) Protonmotive redox mechanism of the cytochrome b-c1 complex in the respiratory chain: protonmotive ubiquinone cycle. *FEBS Lett* 56:1–6
- Mitchell P (1975b) The protonmotive Q cycle: a general formulation. *FEBS Lett* 59:137–139
- Mitchell P (1976) Possible molecular mechanisms of the protonmotive function of cytochrome systems. *J Theor Biol* 62:327–367
- Mitchell P (1979) Keilin's respiratory chain concept and its chemiosmotic consequences. *Science* 206:1148–1159
- Moser CC, Keske JM, Warncke K, Farid RS, Dutton PL (1992) Nature of biological electron transfer. *Nature* 355:796–802
- Moss DA, Bendall DS (1984) Cyclic electron transport in chloroplasts. The Q-cycle and the site of action of antimycin. *Biochim Biophys Acta* 767:389–395
- Mulikidjanian AY (2010) Activated Q cycle as a common mechanism for cytochrome *bc<sub>1</sub>* and *b<sub>6</sub>f* complexes. *Biochim Biophys Acta* 1797:1858–1868
- Mulo P (2011) Chloroplast-targeted ferredoxin-NADP(+) oxidoreductase (FNR): structure, function and location. *Biochim Biophys Acta* 1807:927–934

- Nelson N, Neumann J (1972) Isolation of a cytochrome *b<sub>6</sub>f* particle from chloroplasts. *J Biol Chem* 247:1817–1824
- Nelson ME, Finazzi G, Wang QJ, Middleton-Zarka KA, Whitmarsh J, Kallas T (2005) Cytochrome *b<sub>6</sub>* arginine 214 of *Synechococcus sp.* PCC 7002, a key residue for quinone-reductase site function and turnover of the cytochrome *bf* complex. *J Biol Chem* 280:10395–10402
- Nitschke W, van Lis R, Schoepp-Cothenet B, Baymann F (2010) The “green” phylogenetic clade of Rieske/cyt *b* complexes. *Photosynth Res* 104:347–355
- Osyczka A (2013) Mitochondrial complex III and related bc-complexes. *Biochim Biophys Acta* 1827:1257
- Osyczka A, Moser CC, Dutton PL (2005) Fixing the Q cycle. *Trends Biochem Sci* 30:176–182
- Palmer G, Degli Esposti M (1994) Application of excitation coupling theory to the structure of mitochondrial cytochrome *b*. *Biochemistry* 33:176–185
- Palsdottir H, Hunte C (2004) Lipids in membrane protein structures. *Biochim Biophys Acta* 1666:2–18
- Petersen J, Forster K, Turina P, Graber P (2012) Comparison of the H<sup>+</sup>/ATP ratios of the H<sup>+</sup> –ATP synthases from yeast and from chloroplast. *Proc Natl Acad Sci U S A* 109:11150–11155
- Petty KM, Dutton PL (1976) Ubiquinone-cytochrome *b* electron and proton transfer: a functional pK on cytochrome *b<sub>50</sub>* in *Rhodopseudomonas sphaeroides* membranes. *Arch Biochem Biophys* 172:346–353
- Pfeiffer K, Gohil V, Stuart RA, Hunte C, Brandt U, Greenberg ML, Schagger H (2003) Cardiolipin stabilizes respiratory chain supercomplexes. *J Biol Chem* 278:52873–52880
- Pierre Y, Breyton C, Kramer D, Popot JL (1995) Purification and characterization of the cytochrome *b<sub>6</sub>f* complex from *Chlamydomonas reinhardtii*. *J Biol Chem* 270:29342–29349
- Pierre Y, Breyton C, Lemoine Y, Robert B, Vernotte C, Popot J-L (1997) On the presence and role of a molecule of chlorophyll a in the cytochrome *b<sub>6</sub>f* complex. *J Biol Chem* 272:21901–21908
- Pogoryelov D, Yu J, Meier T, Vonck J, Dimroth P, Muller DJ (2005) The c15 ring of the *Spirulina platensis* F-ATP synthase: F1/F0 symmetry mismatch is not obligatory. *EMBO Rep* 6:1040–1044
- Ponamarev MV, Cramer WA (1998) Perturbation of the internal water chain in cytochrome *f* of oxygenic photosynthesis: loss of the concerted reduction of cytochromes *f* and *b<sub>6</sub>*. *Biochemistry* 37:17199–17208
- Rexroth S, Rexroth D, Veit S, Plohnke N, Cormann KU, Novaczyk MM, Roegner M (2014) Functional characterization of the small regulatory subunit PetP from the cytochrome *b<sub>6</sub>f* complex in *Thermosynechococcus elongatus*. *Plant Cell* 26:3425–3448
- Rich PR (1988) A critical examination of the supposed variable proton stoichiometry of the chloroplast cytochrome *bf* complex. *Biochim Biophys Acta* 932:33–42
- Rich PR, Madgwick SA, Moss DA (1991) The interactions of duroquinol, DBMIB, and NQNO with the chloroplast cytochrome *bf* complex. *Biochim Biophys Acta* 1058:312–328
- Rich PR, Madgwick SA, Brown S, Von Jagow G, Brandt U (1992) MOA-stilbene, a new tool for investigation of the chloroplast *bf* complex. *Photosynth Res* 34:465–477
- Rieske JS, Hansen RE, Zaugg WS (1964a) Studies on the electron transfer system. 58. Properties of a new oxidation-reduction component of the respiratory chain as studied by electron paramagnetic resonance spectroscopy. *J Biol Chem* 239:3117–3022
- Rieske JS, Zaugg WS, Hansen RE (1964b) Studies on the electron transfer system. Lix. Distribution of iron and of the component giving an electron paramagnetic resonance signal at G = 1.90 in subfractions of complex 3. *J Biol Chem* 239:3023–3030
- Roberts AG, Kramer DM (2001) Inhibitor double occupancy in the Q<sub>o</sub> pocket of the chloroplast cytochrome *b<sub>6</sub>f* complex. *Biochemistry* 40:13407–13412
- Roberts AG, Bowman MK, Kramer DM (2004) The inhibitor DBMIB provides insight into the functional architecture of the Q<sub>o</sub> site in the cytochrome *b<sub>6</sub>f* complex. *Biochemistry* 43:7707–7716
- Rochaix JD (2014) Regulation and dynamics of the light-harvesting system. *Annu Rev Plant Biol* 65:287–309
- Sarewicz M, Dutka M, Froncisz W, Osyczka A (2009) Magnetic interactions sense changes in distance between heme b(L) and the iron-sulfur cluster in cytochrome bc(1). *Biochemistry* 48:5708–5720
- Sarewicz M, Borek A, Cieluch E, Swierczek M, Osyczka A (2010) Discrimination between two possible reaction sequences that create potential risk of generation of deleterious radicals by cytochrome bc(1). Implications for the mechanism of superoxide production. *Biochim Biophys Acta* 1797:1820–1827
- Sazanov LA, Burrows PA, Nixon PJ (1998) The chloroplast Ndh complex mediates the dark reduction of the plastoquinone pool in response to heat stress in tobacco leaves. *FEBS Lett* 429:115–118

- Schoepp B, Chabaud E, Breyton C, Vermeglio A, Popot JL (2000) On the spatial organization of hemes and chlorophyll in cytochrome b(6)f. A linear and circular dichroism study. *J Biol Chem* 275:5275–5283
- Schutz M, Brugna M, Lebrun E, Baymann F, Huber R, Stetter KO, Hauska G, Nitschke W (2000) Early evolution of cytochrome bc complexes. *J Mol Biol* 300:663–675
- Schwenkert S, Legen J, Takami T, Shikanai T, Herrmann RG, Meurer J (2007) Role of the low-molecular-weight subunits PetL, PetG, and PetN in assembly, stability, and dimerization of the cytochrome b6f complex in tobacco. *Plant Physiol* 144:1924–1935
- Seelert H, Poetsch A, Dencher NA, Engel A, Stahlberg H, Muller DJ (2000) Structural biology. Proton-powered turbine of a plant motor. *Nature* 405:418–419
- Seelert H, Dencher NA, Muller DJ (2003) Fourteen promoters compose the oligomer III of the proton rotor in spinach chloroplast ATP synthase. *J Mol Biol* 333:337–344
- Shikanai T (2007) Cyclic electron transport around photosystem I: genetic approaches. *Annu Rev Plant Biol* 58:199–217
- Slovacek R, Hind G (1980) Energetic factors affecting carbon dioxide fixation in isolated chloroplasts. *Plant Physiol* 65:526–532
- Slovacek RE, Crowther D, Hind G (1979) Cytochrome function in the cyclic electron transport pathway of chloroplasts. *Biochim Biophys Acta* 547:138–148
- Smirnova I, Kasho V, Kaback HR (2011) Lactose permease and the alternating access mechanism. *Biochemistry* 50:9684–9693
- Solmaz SR, Hunte C (2008) Structure of complex III with bound cytochrome *c* in reduced state and definition of a minimal core interface for electron transfer. *J Biol Chem* 283:17542–17549
- Soriano GM, Ponamarev MV, Carrell CJ, Xia D, Smith JL, Cramer WA (1999) Comparison of the cytochrome *bc*<sub>1</sub> complex with the anticipated structure of the cytochrome *b*<sub>6</sub>f complex: Le plus ca change le plus c'est la meme chose. *J Bioenerg Biomembr* 31:201–213
- Soriano GM, Guo LW, De Vitry C, Kallas T, Cramer WA (2002) Electron transfer from the Rieske iron-sulfur protein (ISP) to cytochrome *f* in vitro. Is a guided trajectory of the ISP necessary for competent docking? *J Biol Chem* 277:41865–41871
- Stiehl HH, Witt HT (1969) Quantitative treatment of the function of plastoquinone in photosynthesis. *Z Naturforsch* 24b:1588–1598
- Stroebel D, Choquet Y, Popot J-L, Picot D (2003) An atypical heme in the cytochrome *b*<sub>6</sub>f complex. *Nature* 426:413–418
- Swierczek M, Cieluch E, Sarewicz M, Borek A, Moser CC, Dutton PL, Osyczka A (2010) An electronic bus bar lies in the core of cytochrome *bc*<sub>1</sub>. *Science* 329:451–454
- Tagawa K, Tsujimoto HY, Arnon DL (1963) Role of chloroplast ferredoxin in the energy conversion process of photosynthesis. *Biochemistry* 49:567–572
- ten Brink F, Schoepp-Cothenet B, van Lis R, Nitschke W, Baymann F (2013) Multiple Rieske/cytb complexes in a single organism. *Biochim Biophys Acta* 1827:1392–1406
- Tikhonov AN (2014) The cytochrome b6f complex at the crossroad of photosynthetic electron transport pathways. *Plant Physiol Biochem* 81:163–183
- Trumpower BL, Gennis RB (1994) Energy transduction by cytochrome complexes in mitochondrial and bacterial respiration: the enzymology of coupling electron transfer reactions to transmembrane proton translocation. *Annu Rev Biochem* 63:675–716
- Twigg AI, Baniulis D, Cramer WA, Hendrich MP (2009) EPR detection of an O<sub>2</sub> surrogate bound to heme *c*<sub>n</sub> of the cytochrome *b*<sub>6</sub>f complex. *J Am Chem Soc* 131:12536–12537
- Umena Y, Kawakami K, Shen JR, Kamiya N (2011) Crystal structure of oxygen-evolving photosystem II at a resolution of 1.9 Å. *Nature* 473:55–60
- von Jagow G, Link TA (1986) Use of specific inhibitors on the mitochondrial bc<sub>1</sub> complex. *Methods Enzymol* 126:253–271
- Watt IN, Montgomery MG, Runswick MJ, Leslie AG, Walker JE (2010) Bioenergetic cost of making an adenosine triphosphate molecule in animal mitochondria. *Proc Natl Acad Sci U S A* 107:16823–16827
- Wenz T, Hielscher R, Hellwig P, Schagger H, Richers S, Hunte C (2009) Role of phospholipids in respiratory cytochrome *bc*<sub>1</sub> complex catalysis and supercomplex formation. *Biochim Biophys Acta* 1787:609–616
- Whitelegge JP, Zhang H, Taylor R, Cramer WA (2002) Full subunit coverage liquid chromatography electrospray-ionization mass spectrometry (LCMS<sup>+</sup>) of an oligomeric membrane protein complex: the cytochrome *b*<sub>6</sub>f complex from spinach and the cyanobacterium, *M. laminosus*. *Mol Cell Proteomics* 1:816–827
- Widger WR, Cramer WA, Herrmann RG, Trebst A (1984) Sequence homology and structural similarity between the *b* cytochrome of mitochondrial complex III and the chloroplast *b*<sub>6</sub>f complex: position of the cytochrome *b* hemes in the membrane. *Proc Natl Acad Sci U S A* 81:674–678

- Wikström MKF, Berden JA (1972) Oxido-reduction of cytochrome *b* in the presence of antimycin. *Biochim Biophys Acta* 283:403–420
- Willms I, Malkin R, Chain RK (1987) Oxidation-reduction reactions of cytochrome *b<sub>6</sub>-f* complex. *Arch Biochem Biophys* 258:248–258
- Yamashita E, Zhang H, Cramer WA (2007) Structure of the cytochrome *b<sub>6</sub>f* complex: quinone analogue inhibitors as ligands of heme *c<sub>n</sub>*. *J Mol Biol* 370:39–52
- Yan J, Cramer WA (2003) Functional insensitivity of the cytochrome *b<sub>6</sub>f* complex to structure changes in the hinge region of the Rieske iron-sulfur protein. *J Biol Chem* 278:20925–20933
- Yan J, Kurisu G, Cramer WA (2006) Intraprotein transfer of the quinone analogue inhibitor 2,5-dibromo-3-methyl-6-isopropyl-p-benzoquinone in the cytochrome *b<sub>6</sub>f* complex. *Proc Natl Acad Sci U S A* 103:69–74
- Yau WM, Wimley WC, Gawrisch K, White SH (1998) The preference of tryptophan for membrane interfaces. *Biochemistry* 37:14713–14718
- Zatsman AI, Zhang H, Gunderson WA, Cramer WA, Hendrich MP (2006) Heme-heme interactions in the cytochrome *b<sub>6</sub>f* complex: EPR spectroscopy and correlation with structure. *J Am Chem Soc* 128:14246–14247
- Zhang H, Cramer WA (2005) Problems in obtaining diffraction-quality crystals of hetero-oligomeric integral membrane proteins. *J Struct Funct Genom* 6:219–223
- Zhang Z, Huang L, Shulmeister VM, Chi YI, Kim KK, Hung LW, Crofts AR, Kim SH (1998) Electron transfer by domain movement in cytochrome *bc<sub>1</sub>*. *Nature* 392:677–684
- Zhang H, Huang D, Cramer WA (1999) Stoichiometrically bound beta-carotene in the cytochrome *b<sub>6</sub>f* complex of oxygenic photosynthesis protects against oxygen damage. *J Biol Chem* 274:1581–1587
- Zhang H, Whitelegge JP, Cramer WA (2001) Ferredoxin:NADP<sup>+</sup> oxidoreductase is a subunit of the chloroplast cytochrome *b<sub>6</sub>f* complex. *J Biol Chem* 276:38159–38165
- Zhang H, Kurisu G, Smith JL, Cramer WA (2003) A defined protein-detergent-lipid complex for crystallization of integral membrane proteins: the cytochrome *b<sub>6</sub>f* complex of oxygenic photosynthesis. *Proc Natl Acad Sci U S A* 100:5160–5163
- Zhu QS, Berden JA, Devries S, Slater EC (1982) On the role of ubiquinone in the respiratory-chain. *Biochim Biophys Acta* 680:69–79
- Zito F, Finazzi G, Joliot P, Wollman FA (1998) Glu78, from the conserved PEWY sequence of subunit IV, has a key function in cytochrome *b<sub>6</sub>f* turnover. *Biochemistry* 37:10395–10403
- Zito F, Finazzi G, Delosme R, Nitschke W, Picot D, Wollman FA (1999) The Qo site of cytochrome *b(6)f* complexes controls the activation of the LHCII kinase. *EMBO J* 18:2961–2969

# Chapter 10

## Structure-Function Studies of the Cytochrome $bc_1$ Complex of Anoxygenic Photosynthetic Purple Bacteria

Lothar Esser<sup>a</sup>, Fei Zhou<sup>a</sup>, Chang-An Yu<sup>b</sup>, and Di Xia<sup>a,\*</sup>

<sup>a</sup>Laboratory of Cell Biology, Center for Cancer Research,  
National Cancer Institute, National Institutes of Health, Bethesda,  
MD 20892, USA

<sup>b</sup>Department of Biochemistry and Molecular Biology, Oklahoma  
State University, Stillwater, OK 74078, USA

Summary.....	210
I. Introduction.....	211
A. Anoxygenic Photosynthetic Purple Bacteria's Ability to Convert Light into Chemical Energy.....	211
B. Enzymatic Functions of Bacterial Cyt $bc_1$ .....	213
1. Electron-Transfer-Coupled Proton Translocation.....	213
2. Superoxide Generation.....	213
C. Composition of Cyt $bc_1$ Complexes from Photosynthetic Bacteria and Mitochondria.....	213
II. The Mechanism of Electron Transfer (ET)-Coupled Proton Translocation Function of Cyt $bc_1$ Complexes.....	215
A. The Q-cycle Mechanism.....	215
B. Proposed Mechanisms of the Bifurcated ET at the Quinol Oxidation Site and Proton Translocation.....	215
III. Comparison of Crystal Structures Between Bacterial and Mitochondrial Cyt $bc_1$ Complexes.....	216
A. Structural Studies of Cyt $bc_1$ Complexes.....	216
B. Structural Differences between Mitochondrial and Bacterial $bc_1$ .....	218
1. Structural Differences Observed in the Cyt $b$ Subunit.....	218
2. Structural Differences Observed in Cyt $c_1$ .....	220
3. Structural Differences Observed in the Iron-Sulfur-Protein Subunit.....	222
IV. Structural Studies of Cyt $bc_1$ with Bound Inhibitors.....	222
A. Crystal Structures of Cyt $bc_1$ in Complex with Inhibitors.....	223
B. Inhibitor Binding-Induced Conformation Switch in ISP-ED.....	223
C. Structural Basis of the Mechanism of Electron Bifurcation at the $Q_p$ Site: The Surface-Affinity-Modulated ISP-ED Conformation Switch Mechanism.....	223

---

\*Author for correspondence, e-mail: [xiad@mail.nih.gov](mailto:xiad@mail.nih.gov)



V.	Experimental Verification of the Bifurcated ET Mechanism.....	225
	A. Mutagenesis in Cyt <i>bc</i> <sub>1</sub> Supports the Functional Importance of ISP-ED Movement.....	226
	B. Mutagenesis in <i>bc</i> <sub>1</sub> Supports the Presence of a Control Mechanism for the ISP-ED Conformation Switch.....	226
	C. The Balance of Inter- and Intra-Monomer ET of the Cyt <i>bc</i> <sub>1</sub> Complex.....	227
VI.	The Mechanisms of Proton Uptake at the Q <sub>N</sub> Site and Exit at the Q <sub>P</sub> Site.....	227
	A. Conformational Changes at the Q <sub>N</sub> and Q <sub>P</sub> Site for Possible Proton Uptake and Exit.....	227
	B. Mutational Studies Help to Define Proton Movement Pathways.....	228
VII.	Future Perspective.....	229
	A. The Mechanism of Superoxide Generation by Cyt <i>bc</i> <sub>1</sub> .....	229
	B. Interactions of Cyt <i>bc</i> <sub>1</sub> with Other Protein or Non-protein Factors.....	230
	C. Structure-Based Drug Design to Overcome Widespread Resistance.....	230
	Acknowledgments.....	230
	References.....	230

## Summary

Photosynthetic non-oxygenic purple bacteria possess various energy-conserving machineries that allow them to grow either photosynthetically, anaerobically or aerobically. The photosynthetic and respiratory branches of the power system in purple bacteria are connected via the cytochrome *bc*<sub>1</sub> complex (cyt *bc*<sub>1</sub>), which catalyzes electron transfer from quinol to cyt *c* and couples this reaction to proton translocation across the photosynthetic membrane, generating a trans-membrane proton gradient essential for various cellular activities including ATP synthesis. Crystal structures of wild-type and mutant cyt *bc*<sub>1</sub> complexes have been determined for the closely related photosynthetic bacteria *R. sphaeroides* and *R. capsulatus* in the presence of various inhibitors or substrates. These structures are remarkably similar to their mitochondrial counterparts but do feature insertions or deletions that are characteristic of the bacterial enzyme complexes. Thus, it is expected that bacterial cyt *bc*<sub>1</sub> complexes function in a manner similar to mitochondrial enzymes, justifying their use as model systems. The roles of insertions in bacterial cyt *bc*<sub>1</sub> function are discussed in relation to the subunit compositions of bacterial complexes and to mutagenesis studies. The mechanism of cyt *bc*<sub>1</sub> function is also discussed in the context of the architecture of quinol oxidation and quinone reduction sites, as revealed by inhibitor binding studies of both mitochondrial and bacterial *bc*<sub>1</sub> complexes.

---

*Abbreviations:* *Btbc*<sub>1</sub> – *Bos taurus* mitochondrial *bc*<sub>1</sub>; cyt *bc*<sub>1</sub> – Ubiquinol-cytochrome *c* oxidoreductase cytochrome *bc*<sub>1</sub> or *bc*<sub>1</sub>; cyt – Cytochrome; famoxadone – (*S*)-5-Methyl-5-(4-phenoxy-phenyl)-3-(phenyl-amino)-1,3-oxazolidine-2,4-dione; fenamidone – (*RS*)-5-Methyl-2-(methylsulfanyl)-5-phenyl-3-(phenyl-amino)-3,5-dihydro-4*H*-imidazol-4-one; *Ggbc*<sub>1</sub> – *Gallus gallus* mitochondrial *bc*<sub>1</sub>; IMS – Inter-membrane space; ISP – Iron-sulfur protein; ISP-ED – Extrinsic domain of ISP; JG144 – 3-anilino-5-(2,4-difluoro-phenyl)-5-methyl-oxazol-idine-2,4-dione; LHC – Light-harvesting complex; *Mtbc*<sub>1</sub> –

---

Mitochondrial *bc*<sub>1</sub>; NCS – Non-crystallographic symmetry; *Pdbc*<sub>1</sub> – *bc*<sub>1</sub> from *Paracoccus denitrificans*; pmf – Proton motive force; Q – Ubiquinone; QH<sub>2</sub> – Ubiquinol; Q<sub>N</sub> – Ubiquinone reduction; Q<sub>P</sub> – Ubiquinol oxidation; RC – Bacterial reaction center; *Rcbc*<sub>1</sub> – *bc*<sub>1</sub> from *Rhodobacter capsulatus*; rms deviation – Root-mean square deviation; *Rsb*<sub>1</sub> – *bc*<sub>1</sub> from the photosynthetic bacterium *Rhodobacter sphaeroides*; SAMICS – Surface affinity-modulated ISP-ED conformation switch mechanism; *Scbc*<sub>1</sub> – *Saccharomyces cerevisiae* mitochondrial *bc*<sub>1</sub>; TM – Trans-membrane

## I. Introduction

As part of the cellular respiratory chain and photosynthetic apparatus, cytochrome  $bc_1$  complexes (cyt  $bc_1$  or  $bc_1$ ) translocate protons endergonically across the membrane and propel the proton movement by energetic electron transfer (ET) from ubiquinol ( $QH_2$ ) to cyt  $c$  (cyt  $c_2$ ). The activity of  $bc_1$  thus contributes to the trans-membrane potential or proton motive force (pmf) that is vital to various cellular activities (Trumpower and Gennis 1994). As in all areas of research, much of our understanding of the mechanism that underlies the function of cyt  $bc_1$  came from studies of many laboratories using various technical approaches. This paper, however, will focus on  $bc_1$  function from a structural perspective, based on detailed 3-dimensional structures determined by X-ray crystallography. Over the past two decades, structures of  $bc_1$  from different kingdoms of life have been determined to near atomic resolution, providing an opportunity to examine differences in structures and relate these differences to different aspects of the reaction mechanism as well as to functional variations of the evolutionarily related enzymes. Based on our recent work on the crystal structures of cyt  $bc_1$  from the anoxygenic, photosynthetic purple bacterium *Rhodobacter sphaeroides* (*Rsb $c_1$* ) (Esser et al. 2006, 2008a), we will provide a structural interpretation of  $bc_1$  function and discuss functional implications of the features unique to bacterial  $bc_1$  in comparison to their mitochondrial counterparts.

### A. Anoxygenic Photosynthetic Purple Bacteria's Ability to Convert Light into Chemical Energy

Photosynthesis is arguably the most important reaction on planet earth, as it converts sunlight into chemical energy. Photosynthetic purple bacteria are believed to be one of the most primitive life forms on earth (Woese 1987). In contrast to oxygen-evolving bacteria such as cyanobacteria,

anoxygenic photosynthetic bacteria, as the name indicates, are incapable of producing molecular dioxygen by oxidizing water and are distinct by having only one reaction center (RC) that resembles photosystem II of green plants.

In anoxygenic, facultative photosynthetic bacteria such as *Rhodobacter sphaeroides*, the presence of light and oxygen induces the development of the machineries for both photosynthetic and respiratory growth (Fig. 10.1). In fact, these bacteria can grow aerobically, anaerobically, or photosynthetically. Depending on growth conditions, respiratory and/or photosynthetic apparatus are selectively produced. Under continuous exposure to light, respiration is slowed or inhibited due to the well-known inhibitory build-up of membrane potential or possibly, by competition between the photosynthetic reaction center (RC) and the cyt  $c$  oxidase for reduced cyt  $c_2$  (Oh and Kaplan 2001). Cyt  $bc_1$  lies at the center of the two processes: phototropic and chemotropic electron transfer (ET). The bacterial photosynthetic apparatus consists of membrane-bound light harvesting complexes (LHCs), photosynthetic reaction centers (RCs), cyt  $bc_1$  complexes and the soluble electron carrier cyt  $c_2$ . In the presence of oxygen, the machinery for cellular respiration is produced, including NADH and succinate dehydrogenases, cyt  $bc_1$  complex, and various terminal oxidases. Most of the respiratory complexes contribute to the buildup of the pmf (Fig. 10.1).

Under light conditions and in the absence of molecular oxygen, all photosynthetic bacteria rely on a functioning cyt  $bc_1$  complex for growth, making it essential for photosynthetic growth. To ensure an efficient collection of light energy, the purple bacteria usually contain two types of LHC: LH1 and LH2. After light absorption by the LHCs, the excitation energy is transferred to the RC, where a charge separation occurs between donor and acceptor molecules. The photo-oxidized primary electron donor, a dimer of bacteriochlorophyll (Bchl) molecules, is reduced by the high potential electron carrier

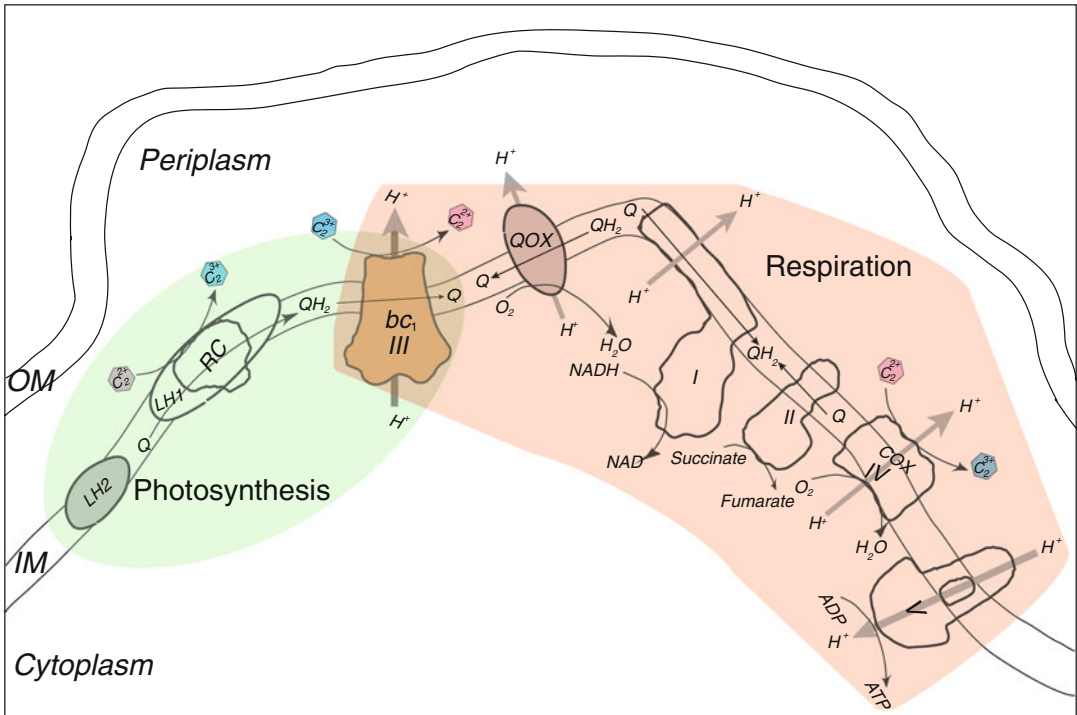


Fig. 10.1. Photosynthetic and respiratory apparatus in *R. sphaeroides*. The two branches of the energy-conserving membrane (chromatophore) are shown. The photosynthetic branch, shaded in green, consists of light harvesting complexes (LH1 and LH2), a reaction center (RC), and the *cyt bc<sub>1</sub>* complex (Complex III or III), where light energy is transduced by RC to reduce quinone (Q) into quinol (QH<sub>2</sub>). The *cyt bc<sub>1</sub>* complex in turn passes electrons from QH<sub>2</sub> to *cyt c<sub>2</sub>* and couples the electron transfer reaction to protons pumping across the membrane. The respiratory branch, shaded in red, is composed of various dehydrogenases including NADH-quinol oxidoreductase (Complex I or I), succinate-quinol oxidoreductase (Complex II or II), and the *cyt bc<sub>1</sub>* complex, a number of oxidases such as *cyt c* oxidase (Complex IV, IV or COX) and quinol oxidases (QOX), and ATP synthase (Complex V or V). The *cyt bc<sub>1</sub>* complex is part of both branches.

*cyt c<sub>2</sub>*, which is in turn reduced by the *cyt bc<sub>1</sub>* complex (Fig. 10.1). To complete the cyclic electron transfer, the *bc<sub>1</sub>* complex oxidizes the QH<sub>2</sub> and then reduces mobile *cyt c<sub>2</sub>* (Vermeglio and Joliet 1999).

When switched from photosynthetic growth to aerobic growth, expressions of the photosynthetic apparatus, as shown by RNA synthesis, are down regulated, while those for aerobic growth are up regulated. Interestingly, many respiratory complexes such as NADH-quinol oxidoreductase, *cyt bc<sub>1</sub>* complex, as well as a number of *cyt c* oxidases are also down regulated (Arai et al. 2008), suggesting a complex regulatory mechanism. Nevertheless, under aerobic conditions, electrons flow downhill

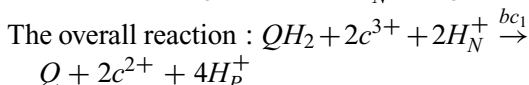
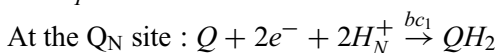
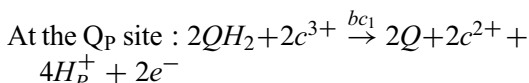
energetically through various respiratory complexes, ending in molecular oxygen. This ET path is coupled to proton pumping across the membrane, contributing to the pmf.

Under anaerobic or photosynthetic growth conditions, bacteria are sensitive to both *bc<sub>1</sub>* inhibitors and mutations that render them non-functional. This is in sharp contrast to growth under aerobic conditions where respiration is supported by alternate oxidases in the absence of *bc<sub>1</sub>*. The key difference to the alternate oxidase pathway is that *cyt bc<sub>1</sub>* couples the oxidation of ubiquinol more efficiently to proton translocation. As it turns out, it is this growth-mode switch feature that renders photosynthetic bacteria useful tools in the study of respiratory components.

## B. Enzymatic Functions of Bacterial Cyt $bc_1$

### 1. Electron-Transfer-Coupled Proton Translocation

All cyt  $bc_1$  complexes catalyze the same antimycin-sensitive ET reaction from the lipophilic substrate  $QH_2$  to cyt  $c$  (cyt  $c_2$  in *R. sphaeroides*), coupled with proton translocation across the membrane (Trumpower and Gennis 1994). This reaction contributes to the maintenance of a potential gradient across the cytoplasmic (mitochondrial in eukaryotes) membrane. As a result of this reaction, four protons are deposited on the positive side of the membrane and two molecules of cyt  $c_2$  are reduced for every  $QH_2$  molecule oxidized. This net stoichiometry of the ET reaction, not necessarily reflecting the underlying mechanism, is presented in the following equations, where  $QH_2$  and  $Q$  represent lipid-soluble reduced and oxidized ubiquinone, respectively,  $c^{3+}$  and  $c^{2+}$  represent oxidized and reduced cyt  $c$ , and  $H^+_N$  and  $H^+_P$  represent protons on the negative and positive side of membrane.



### 2. Superoxide Generation

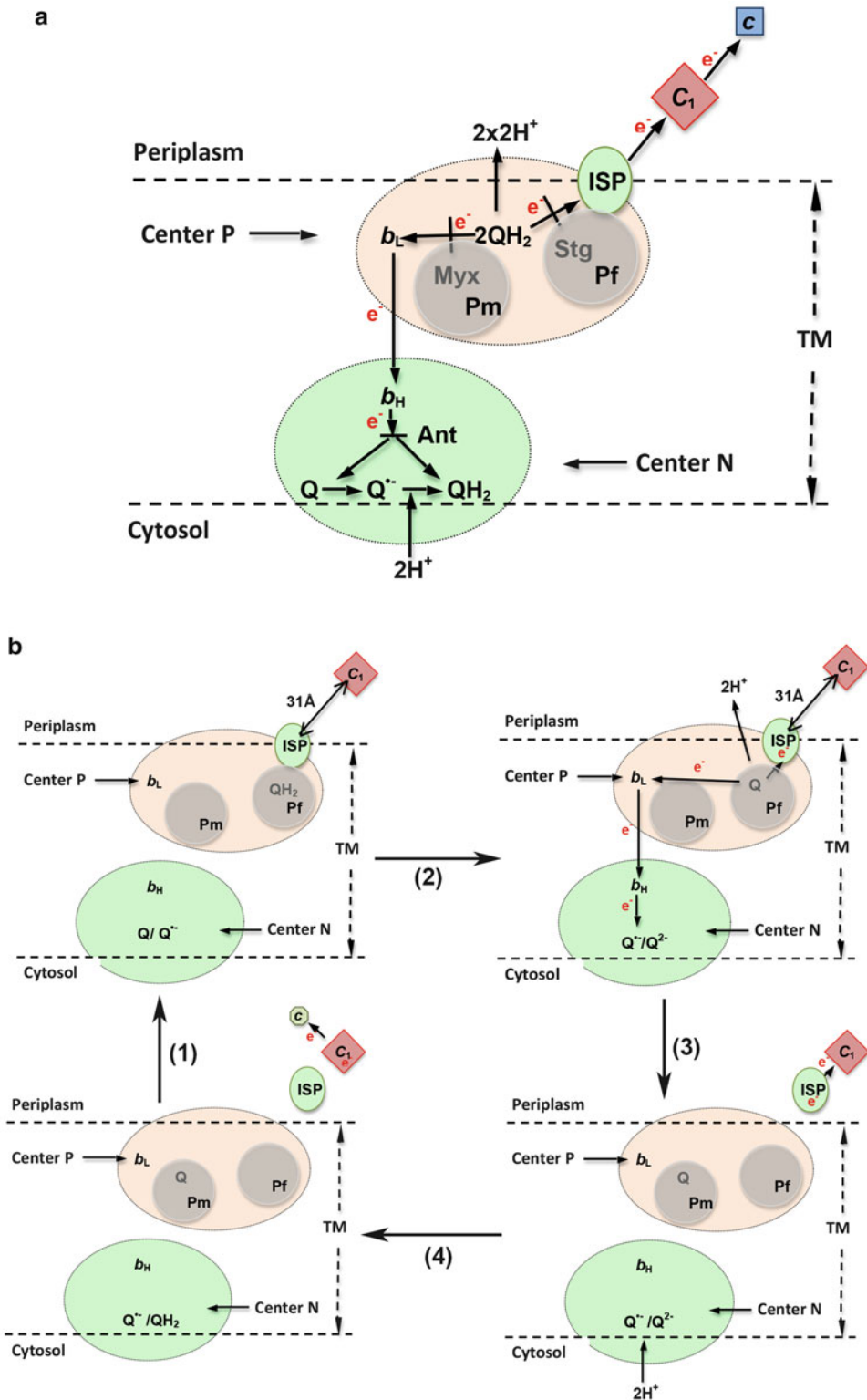
Under normal respiration conditions, the ET from  $QH_2$  to cyt  $c$  catalyzed by the  $bc_1$  complex is accompanied by the production of a small amount of superoxide anions presumably through electron leakage to molecular oxygen, which increases dramatically when the ET within the  $bc_1$  complex is blocked by specific  $bc_1$  inhibitors such as antimycin A or when the ET chain becomes over reduced (Boveris and Chance 1973; Korshunov et al. 1997; Rottenberg et al.

2009). The proposed sites for superoxide anion generation under normal ET conditions are at the  $Q_P$  site and the low-potential cyt  $b$  heme ( $b_L$  heme). Mutations in the cyt  $b$  subunit result in not only impaired ET activity but also increased amounts of superoxide anions. The role played by the small amount of superoxide anions generated under physiological conditions is not clear but they are thought to be part of cellular signaling mechanisms (Muller et al. 2004; Staniek et al. 2002; Yee et al. 2014).

### C. Composition of Cyt $bc_1$ Complexes from Photosynthetic Bacteria and Mitochondria

The cyt  $bc_1$  complexes are multi-subunit, integral membrane protein complexes. Three subunits are essential for the ET-coupled proton translocation function: cyt  $b$ , cyt  $c_1$ , and Rieske iron-sulfur protein (ISP) and they are universally present in all  $bc_1$  complexes. Any additional polypeptide components of a given  $bc_1$  complex are called supernumerary subunits (Trumpower 1990; Yang and Trumpower 1988). Not participating in the catalytic function, these supernumerary subunits are believed to be involved in complex assembly and stability. Mitochondrial  $bc_1$  complexes ( $Mtbc_1$ ) have seven or eight supernumerary subunits, as in yeast or bovine  $bc_1$  (Gao et al. 2002; Hunte et al. 2000), while bacterial  $bc_1$  complexes do not have as many. For example, *R. sphaeroides*  $bc_1$  ( $Rsb_1$ ) has only one additional subunit, but the closely related *R. capsulatus* ( $Rc_1$ ) has none (Berry et al. 2004; Xia et al. 2008).

The cyt  $b$  subunit of  $Mtbc_1$  is the only subunit encoded by the mitochondrial genome. It features two non-covalently bound heme moieties: a low potential ( $b_L$ ,  $E_m = -103$  mV for bovine  $bc_1$  at pH 7.2) and a high potential ( $b_H$ ,  $E_m = +125$  mV at pH 7.2) heme (Dutton et al. 1970). The cyt  $c_1$  subunit is associated with cyt  $b$  by a C-terminal



*Fig. 10.2.* The Q-cycle mechanism and bifurcated ET at the  $Q_P$  site. (a) The modified Q-cycle defines two active sites within the photosynthetic membrane. The center P ( $Q_P$ ) is near the periplasm and center N ( $Q_N$ )

trans-membrane (TM) helix. Its N-terminal domain, which contains a covalently bound type-*c* heme, resides in the inter-membrane space (IMS) for mitochondrial  $bc_1$  or in the periplasm for bacterial  $bc_1$ . Finally, the ISP is bound to the membrane protein via a single N-terminal TM helix. Its functional domain, carrying the 2Fe-2S cluster, is exposed to the aqueous phase and is a neighbor of cyt  $c_1$ .

## II. The Mechanism of Electron Transfer (ET)-Coupled Proton Translocation Function of Cyt $bc_1$ Complexes

### A. The Q-cycle Mechanism

The modified Q-cycle mechanism is based on Mitchell's original work (Mitchell 1972, 1976) and has found general acceptance on the basis of overwhelming biochemical, biophysical and structural evidence (Fig. 10.2a) (Crofts et al. 1983; Garland et al. 1975; Trumpower 1976). According to this mechanism, cyt  $bc_1$ , embedded in the lipid membrane bilayer, contains two distinct binding sites for both quinol ( $Q_P$  or quinol oxidation) and quinone ( $Q_N$  or quinone reduction) near the electrochemically positive and negative ('p' and 'n', respectively) sides of the membrane, respectively. Each site is characterized by the presence of a *b*-type heme ( $b_L$  or

$b_H$ ) necessary for the obligatory electronic coupling of the oxidation of quinol on the one side to the reduction of quinone on the other. In one complete cycle, two molecules of quinol are oxidized in succession and their four protons are released into the positive side. Simultaneously, one quinone molecule is reduced, requiring the uptake of two protons from the negative side. This means that in one half-cycle, a single electron enters the 2Fe-2S cluster of the ISP and is delivered to the final electron acceptor within  $bc_1$ , cyt  $c_1$ . At this point, a net imbalance of charge exists, as only one electron from quinol was removed to the p-side aqueous phase, but both of its protons enter the p-side (protons exit  $bc_1$  on the positive side of the membrane). The remaining electron takes a transverse path to the n-side of the membrane through the cyt *b* hemes. It transiently reduces the proximal heme  $b_L$ , followed by the remote  $b_H$  and ends up on a quinone (Q) or quinone radical ( $Q^\bullet$ ). Protons coming from the n-side aqueous phase of the membrane compensate the sequential arrival of negative charges at the  $Q_N$  site (Fig. 10.2a).

### B. Proposed Mechanisms of the Bifurcated ET at the Quinol Oxidation Site and Proton Translocation

While the overall outline of the process is well accepted of the  $bc_1$  complex (See article by Hason et al. in this volume for

---

Fig. 10.2. (continued) is near the cytosol. In a complete Q cycle, two  $QH_2$  molecules are consumed at the  $Q_P$  site and one  $QH_2$  is generated at the  $Q_N$  site. The ET reaction at the  $Q_N$  site can be blocked by antimycin (Ant). At the  $Q_P$  site, the two electrons from a substrate  $QH_2$  diverge, the first going to the high potential chain (ISP,  $c_1$  and *c*) and the second going to the low potential chain ( $b_L$ ,  $b_H$  and  $Q/Q^\bullet$ ). Reactions at the  $Q_P$  site can be inhibited by stigmatellin (stg) or myxothiazol (myx). From crystallographic studies, stigmatellin fixes the conformation of ISP ( $P_f$  site), whereas myxothiazol mobilizes the ISP ( $P_m$  site). (b) The surface-affinity-modulated ISP conformation switch mechanism (SAMICS). The key feature of the mechanism is that when a substrate  $QH_2$  enters the  $Q_P$  pocket, it binds to the  $P_f$  site first and fixes the conformation of ISP, creating a 31-Å gap between the ISP and cyt  $c_1$ . This gap prevents ET between ISP and cyt  $c_1$ . ET follows with the first electron entering the ISP, which is a one-electron carrier and remains fixed in place. The second electron moves to the  $b_L$  heme. Once the second electron arrives at the  $Q_N$  site, the product Q at the  $Q_P$  pocket is able to move to the  $P_m$  site, which liberates the ISP, allowing it to deliver the first electron to cyt  $c_1$ , and subsequently to cyt *c*. The reduced  $Q^{2*}$  at the completion of the Q-cycle picks up two  $H^+$  from the cytosol to form a  $QH_2$ .

discussion of Q cycle in  $b_6f$  complex), exactly how the separation or bifurcation of electrical charges at the  $Q_P$  site as well as how coupled proton flow is accomplished remain the subject of much debate and research. For the electron bifurcation, a number of models with varying degrees of acceptance and refinement have been proposed: (1) catalytic switch model (Brandt and von Jagow 1991), (2) double-occupancy  $Q_P$  site model (Ding et al. 1992), (3) proton-gated charge-transfer mechanism (Brandt 1996), (4) logic-gated fit mechanism (Rich 2004), (5) sequential model (Cape et al. 2007; Crofts and Wang 1989), (6) concerted model (Crofts et al. 1983; Zhu et al. 2007), (7) R-complex model (Berry and Huang 2003) and (8) surface-affinity modulated ISP conformation switch (SAMICS) (Fig. 10.2b) (Esser et al. 2006, 2008b; Xia et al. 2007, 2013).

Proton transport from the n-side of the membrane (matrix or cytosol) to the positively charged periplasm (IMS in mitochondria) is achieved within  $bc_1$  with a stoichiometry of two protons per electron transferred. The two protons translocated are mechanistically non-identical. One is called ‘scalar’ and the other is ‘vectorial’ (Guerrieri and Nelson 1975; Leung and Hinkle 1975), reflecting the exit of protons on the positive side and uptake from the negative side, respectively. The proton exit must be coupled with ET, as  $cyt\ bc_1$  activity is pH dependent with a maximum activity at pH 8.0 under steady state conditions for  $Mtbc_1$  (Hsueh et al. 2010; Lin et al. 2006; Link et al. 1992; Prince and Dutton 1976; Ugulava and Crofts 1998). Two protonatable histidine residues bound to the 2Fe-2S cluster with pK 6.6 and 9.2, respectively, have been identified as responsible for the pH dependency (Brandt and Okun 1997). Not surprisingly, various proposals exist on how such coupling might take place. Similarly, a number of mechanisms for proton uptake from the negative side of the membrane have been proposed (Gao et al. 2003; Lange et al. 2001).

### III. Comparison of Crystal Structures Between Bacterial and Mitochondrial $Cyt\ bc_1$ Complexes

#### A. Structural Studies of $Cyt\ bc_1$ Complexes

Prior to the availability of high-resolution crystal structures, mitochondrial  $cyt\ bc_1$  complexes were studied by 2-D electron microscopy, which revealed the dimeric nature of the complexes (Akiba et al. 1996; Leonard et al. 1981). Crystal structures of mitochondrial  $cyt\ bc_1$  complexes from bovine, chicken, and yeast revealed the subunit arrangement, the locations of the prosthetic groups, namely the hemes  $b_L$ ,  $b_H$ , and  $c_1$ , the 2Fe-2S cluster and bound substrate ubiquinone. They also clearly delineated the locations for ubiquinol oxidation ( $Q_P$ ) and ubiquinone reduction ( $Q_N$ ) (Hunte et al. 2000; Iwata et al. 1998; Kim et al. 1998; Xia et al. 1997; Zhang et al. 1998b) (Fig. 10.3). These studies were followed by structure determinations of the related  $cyt\ b_6f$  complexes from the cyanobacteria *Mastigocladus laminosus* (Baniulis et al. 2009; Hasan et al. 2013; Kurisu et al. 2003; Yamashita et al. 2007) and from alga *Chlamydomonas reinhardtii* (Stroebel et al. 2003), revealing structural features unique to the  $b_6f$  complexes, most notably the presence of heme  $c_n$  at the  $Q_N$  site (Nogueira et al. 2013). More recently, the structures of  $cyt\ bc_1$  from photosynthetic purple bacteria *R. capsulatus* ( $Rcbc_1$ ) (Berry et al. 2004) and *R. sphaeroides* ( $Rsb_1$ ) (Esser et al. 2006, 2008a) as well as the soil bacterium *Paracoccus denitrificans* ( $Pdbc_1$ ) (Kleinschroth et al. 2011) were reported (Table 10.1).

The bacterial forms of  $bc_1$  from  $\alpha$ -proteobacteria  $Rcbc_1$  and  $Rsb_1$  have a long history of being model systems for the study of functional aspects of the enzyme, as they are more amenable to genetic manipulations than their mitochondrial counterparts. Because they are part of

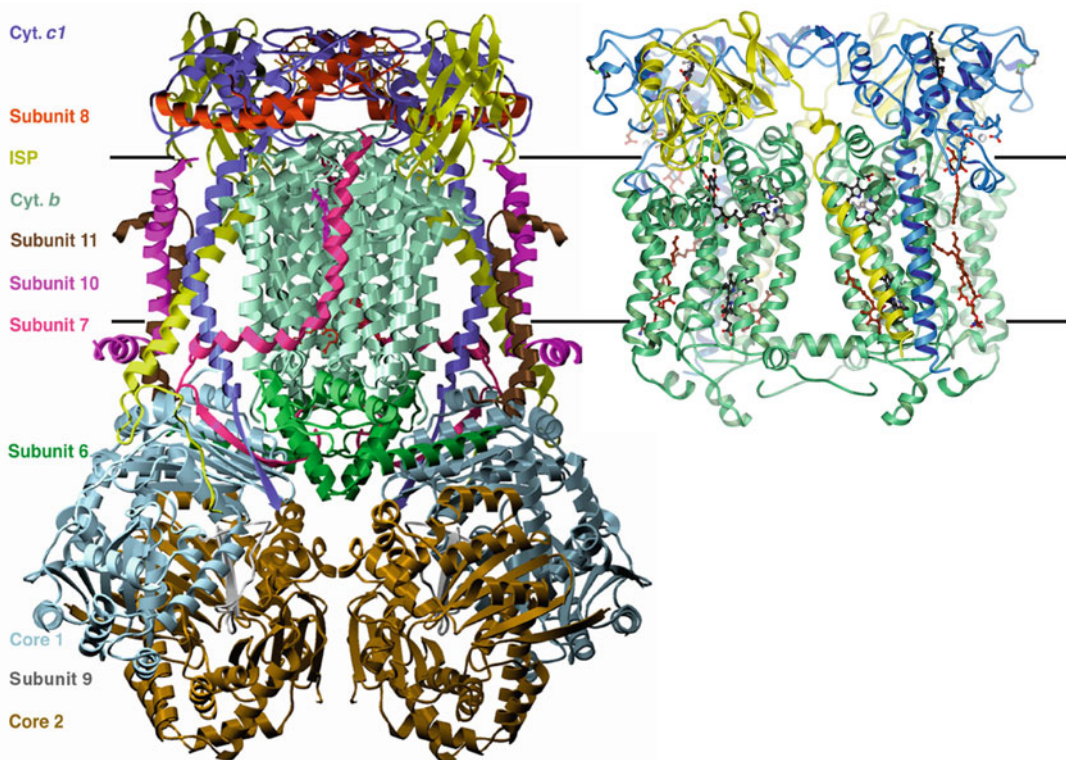


Fig. 10.3. Structures of cyt  $bc_1$  from bovine mitochondria and photosynthetic bacterium *R. sphaeroides*. Dimeric mitochondrial  $bc_1$  is shown on the left with labels for each individual subunit and bacterial  $bc_1$  is shown on the right.

the photosynthetic apparatus (Fig. 10.1), the bacterial cyt  $bc_1$  complexes can be studied less invasively in their native lipid environment (Mulikidjanian 2007). Even more effective using the bacterial  $bc_1$  are the functional studies analyzing spontaneous revertants in response to point mutations introduced to impair or influence the function of  $bc_1$  or the action of a  $bc_1$  ( $Q_P$  or  $Q_N$  site) inhibitor. Furthermore, the relatively close genetic relationship of *Rhodobacterales* to *Rickettsiales* (Andersson et al. 1998), which are the precursors of mitochondria, allows one to extend mechanistic conclusions obtained from bacterial  $bc_1$  to its mitochondrial analogues (Crofts and Wang 1989). Solved crystal structures of native, and if possible, mutant forms would help to ascertain that biochemically obtained results from mutational studies are based on the expected local changes and are not due to

unintended changes to the overall structure. This can be achieved much more easily in bacterial  $bc_1$  than in their mitochondrial counterparts. Since the mitochondrion and with it the  $bc_1$  enzyme arose from bacteria that underwent endosymbiotic incorporation into eukaryotic cells, a comparative analysis between evolutionarily derived and modified forms of  $bc_1$  should shed significant light on the function of supernumerary subunits as well as the process of evolution in general.

Because of the advantages of bacterial cyt  $bc_1$  complexes with respect to their structural simplicity, low cost and ease of use in genetic manipulations, high-resolution structures of bacterial enzymes were sought for many years in laboratories worldwide. A decade ago in 2004, the crystal structure of the  $bc_1$  complex from *R. capsulatus* ( $Rcbc_1$ ) (Berry et al. 2004) was reported at 3.8 Å resolution (Table 10.1). This was the first  $bc_1$  structure



Table 10.1. Available crystal structures of cyt  $bc_1$  from prokaryotic organisms.

Pdb ID	Species	Mutation	Q <sub>P</sub> occupant	Q <sub>N</sub> occupant	Res. (Å)	References
1ZRT	<i>R. capsulatus</i>	wt	Stigmatellin	None	3.8	Berry et al. (2004)
2FYN	<i>R. sphaeroides</i>	<sup>b</sup> S287R/ <sup>ISP</sup> V135S	Stigmatellin	None	3.2	Esser et al. (2006)
2QJP	<i>R. sphaeroides</i>	wt	Stigmatellin	Antimycin A	2.6	Esser et al. (2008a)
2QJK	<i>R. sphaeroides</i>	<sup>b</sup> S287R/ <sup>ISP</sup> V135S	Stigmatellin	Antimycin A	3.1	Esser et al. (2008a)
2QJY	<i>R. sphaeroides</i>	<sup>b</sup> S287R/ <sup>ISP</sup> V135S	Stigmatellin	Ubiquinone	2.4	Esser et al. (2008a)
2YIU	<i>P. denitrificans</i>	wt	Stigmatellin	None	2.7	Kleinschroth et al. (2011)

from a prokaryotic organism and confirmed the overall similarity to mitochondrial  $bc_1$ ; however, it lacked sufficient detail to reveal reliably the unique structural features of the bacterial form. Higher resolution structures of *R. sphaeroides* (*Rsb<sub>c1</sub>*) could initially only be obtained when the stabilizing double mutations, S287R (cyt *b*)/V135S (ISP), were introduced. Crystallization succeeded in the presence of stigmatellin, which has been known to immobilize the extrinsic domain of the ISP subunit (Esser et al. 2006; Xia et al. 2008) (Fig. 10.3, Table 10.1). Crystal structures of wild-type and mutant *Rsb<sub>c1</sub>* in complex with inhibitors and substrates were subsequently determined up to 2.4 Å resolution (Esser et al. 2008a) (Table 10.1). The purified *Rsb<sub>c1</sub>* was crystallized in a number of different crystal forms and required the presence of histidine for stability of the dimer and monodispersity of the protein sample in detergent solutions (Xia et al. 2008).

### B. Structural Differences between Mitochondrial and Bacterial $bc_1$

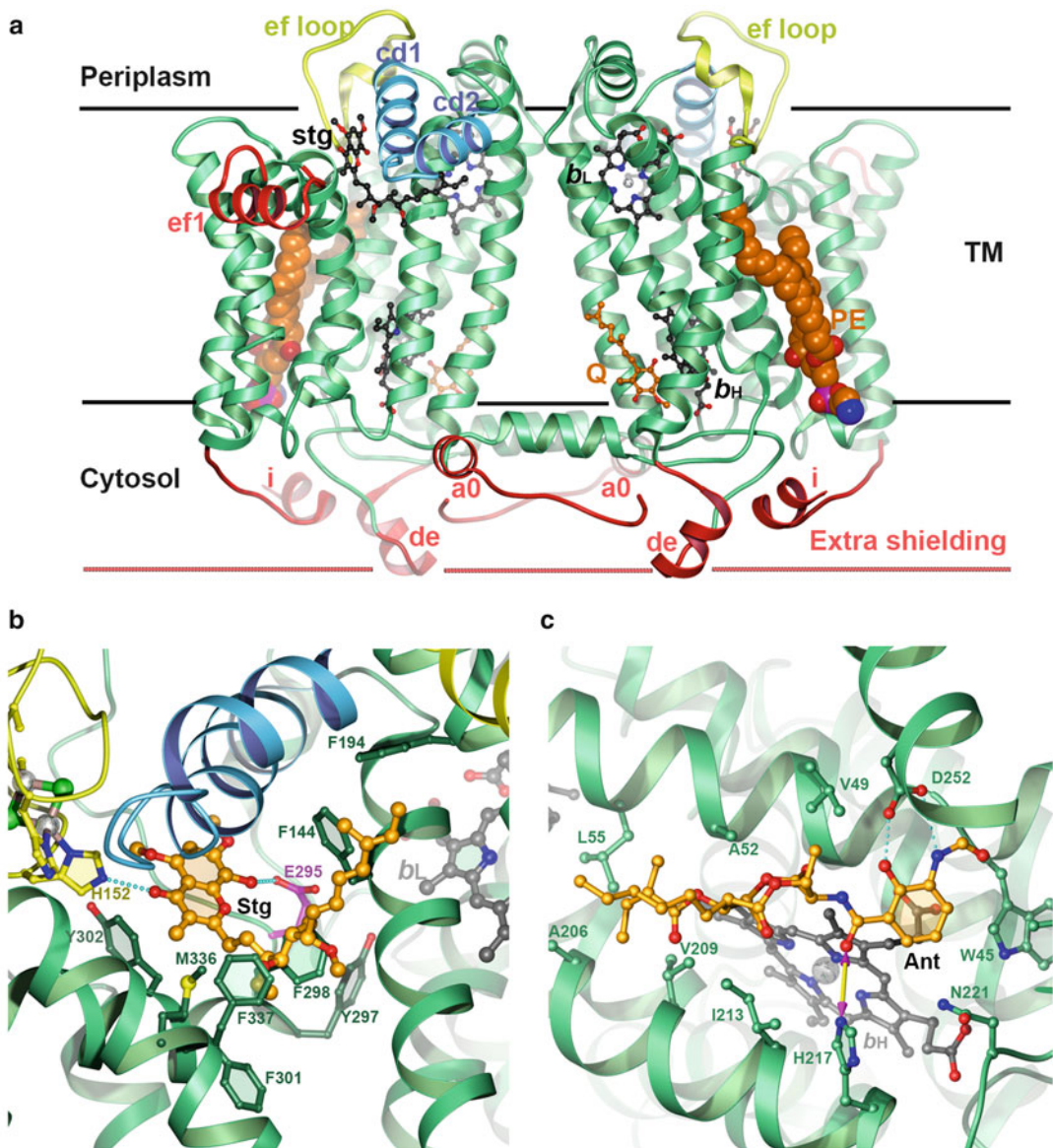
Although all  $bc_1$  complexes catalyze the same reaction, conservation of protein sequences is usually limited to the active sites across different organisms, making it difficult to correlate the sequence differences with functional variations. The availability of a large number of  $bc_1$  structures from different species allows one to perform structure-based sequence alignments. These alignments coupled to the large number of available sequences (for example, >10,000 for cyt *b*) from all kingdoms of life reveal

a wealth of information encompassing commonalities, strict conservation, and the correct identification of insertions and corresponding deletions that are organism-specific environmental or functional adaptations.

To compare bacterial with mitochondrial cyt  $bc_1$ , it is necessary to find a consensus on available bacterial structures. While the two high-resolution structures of *Rsb<sub>c1</sub>* and *Pdbc<sub>1</sub>*, determined at 2.4 and 2.7 Å Bragg spacing, respectively, agree well with each other, the same cannot be said concerning the structure of *Rcbc<sub>1</sub>*. In the latter case, unfortunately due to diffraction limitations, the structural features that are unique to this and many other prokaryotic enzymes could only be modeled as polyalanine segments (PDB: 1ZRT). A structure of *Rcbc<sub>1</sub>* at higher resolution has not since been reported. In the following sections, we will use *Rsb<sub>c1</sub>* and *Pdbc<sub>1</sub>* as representatives of bacterial  $bc_1$  for comparison with mitochondrial complexes.

#### 1. Structural Differences Observed in the Cyt *b* Subunit

At first glance, a major difference between bacterial and mitochondrial  $bc_1$  complexes is the lack of supernumerary subunits on the cytoplasmic side of the membrane in bacterial  $bc_1$  (Fig. 10.3). A proposed function for these additional subunits is to shield the portion of the enzyme complex, which is embedded in the membrane bilayer against proton and or water leakage. Supporting this hypothesis is the fact that the sequence of *Rs* cyt *b* is 66 residues ( $\geq 15\%$ ) longer than the bovine sequence (Fig. 10.4a). Furthermore,



**Fig. 10.4.** Structures of bacterial *cyt b* and its inhibitor complexes. **(a)** Ribbon diagram of the dimeric *cyt b* of *RsbC1* is given. The insertions unique to the bacterial *cyt b* are highlighted in red and labeled, most of which are on the cytosolic side of the membrane, creating an extra layer of shielding. The cd1 and cd2 helices are shown in blue. The yellow elements belong to the ef loop. The heme moieties and bound Q<sub>P</sub>-site stigmatellin are shown in stick models with carbon in black, oxygen red and nitrogen blue. The substrate ubiquinone bound to the Q<sub>N</sub>-site is also shown as the stick model with carbon in gold. The bound lipid molecule is rendered as ball model with carbon also in gold color. **(b)** Close-up view of the quinol oxidation site with bound stigmatellin in the *cyt b* subunit of *RsbC1*. Structural elements from the *cyt b* subunit are colored green except for cd1 and cd2 helices, which are in blue. Structural elements from ISP are colored yellow. Residues contributing to the Q<sub>P</sub> environment are labeled and shown as the ball-and-stick models. **(c)** Close-up view of the antimycin A-binding site in the *cyt b* subunit of *RsbC1*.

the insertions and extensions are concentrated on the negative side of the membrane, suggesting that their function(s) were eventually taken over by the two large core subunits in *Mtbc*<sub>1</sub>. In fact, bacterial *cyt b* has significant extensions at both its N-terminus (see helix a0) and at its C-terminus (helix i). In the crystal structures of all bacterial forms, the first ordered residue (as judged by electron density) for *cyt b* starts at position 3 and ends at residue 430. This suggests that the 15 remaining C-terminal residues are highly flexible and can in fact be deleted without affecting the function of the enzyme in *R. sphaeroides* (Liu et al. 2004). The extra helices a0, de and i enable *cyt b* to interact with lipid molecules molded as PE, as shown in Fig. 10.4a, apparently creating additional shielding for enhanced membrane impermeability.

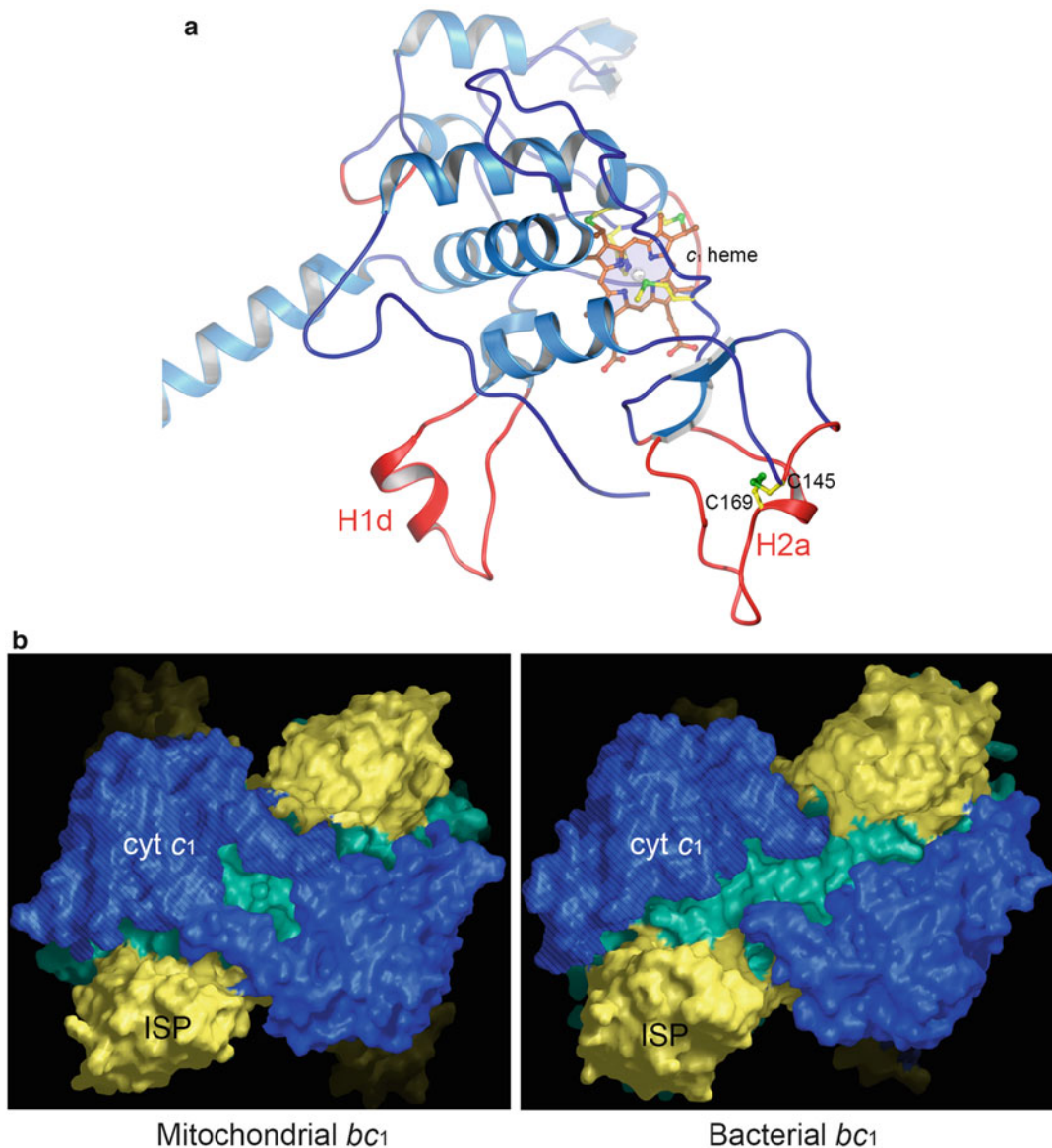
Located near the positive side of the membrane, the insertion of 18 residues (310–327) provides an additional structural element in *R. sphaeroides* and *R. capsulatus* denoted as the efl helix (Fig. 10.4a). As seen in the high-resolution crystal structures of *Rsb*c<sub>1</sub> the N-terminal side of the efl helix interacts with lipid-like molecules (as deduced from the residual density that is not shown in Fig. 10.4a), which so far defied attempts to model them as lipids or possibly detergent molecules. However, it has been shown that deletion of residues 309–326 (efl helix) or as little as the point mutation S322A significantly impairs the function of *bc*<sub>1</sub> (Esser et al. 2006). Since mitochondrial *cyt b* does not have the efl helix, its direct involvement in catalysis or structural integrity can be ruled out. This protruding element may be needed to interact with membrane lipids, providing help to orient the complex in the membrane environment, as seen in Fig. 10.4a.

## 2. Structural Differences Observed in Cyt c<sub>1</sub>

Among the three bacterial species with known 3-D coordinates, the sequence identities range from 59 % to 63 %. Comparing mitochondrial *cyt c*<sub>1</sub> sequences,

one finds approximately the same degree of conservation (58 %). However, the sequence identity drops to 33–40 % between bacteria and mitochondria. Most notably, the bacterial *cyt c*<sub>1</sub> sequence suffers a loss of two major structural elements and a gain of two smaller insertions (Fig. 10.5a). In the following sections, *R. sphaeroides* sequence numbers are used, since the *cyt c*<sub>1</sub> structure of *Rsb*c<sub>1</sub> shows the highest degree of completeness and therefore lends itself most conveniently as the reference. First, the C<sup>36</sup>XXC<sup>39</sup>H<sup>40</sup> signature motif for *c*-type heme groups is perfectly conserved including the remote M185, which forms together with H40 the two axial ligands to the heme iron. R107 is also conserved; it forms a salt bridge with one of the propionate groups of the heme and is located on the surface of *cyt c*<sub>1</sub> that interacts transiently with the moving extrinsic domain of ISP (ISP-ED). A superposition of coordinates (C $\alpha$  positions) reveals a very high degree of preservation of structural elements, and in particular the position of the important heme redox group as well as the C-terminal TM helix. Two insertions have occurred in mitochondrial *cyt c*<sub>1</sub> after position 76 and 94 (bovine sequence), both of which contribute to a closing-up of *cyt c*<sub>1</sub> including the establishment of a direct bridge between the two *cyt c*<sub>1</sub> units of the homo-dimeric *bc*<sub>1</sub> complex (Fig. 10.5b).

A prominent loop is inserted into the sequences of *R. sphaeroides* and *R. capsulatus* containing a stabilizing disulfide bridge C<sup>145</sup>-C<sup>169</sup>. Remarkably, the disulfide bridge is absent in *P. denitrificans* (Fig. 10.5a), which features instead a highly charged foreshortened loop. In fact, *P. denitrificans* *cyt c*<sub>1</sub> resembles mitochondrial *cyt c*<sub>1</sub> more closely with respect to the “missing” disulfide-linked loops. Mitochondrial *cyt c*<sub>1</sub>, however, recruits subunits 7 and 8 to gain stability. Subunit 8 is a disulfide-linked helical hairpin guarding the perimeter of *cyt c*<sub>1</sub>, which suggests a compensatory function for the loss of secondary structure in *cyt c*<sub>1</sub>. Another highlighted feature of bacterial *cyt c*<sub>1</sub> is the largely helical insertion between



**Fig. 10.5.** Structural comparison of  $cyt\ c_1$  between  $Rsb c_1$  and  $Btbc_1$ . **(a)** Ribbon diagram of  $cyt\ c_1$  of  $Rsb c_1$  is shown with insertions highlighted in red and labeled. The C145 and C169 residues that form a disulfide bond are shown as stick models. The heme  $c_1$  is also labeled. **(b)** Comparison of mitochondrial and bacterial  $cyt\ c_1$  in the context of dimeric  $bc_1$  showing the presence and absence of bridging, respectively, in the two symmetrically related structures of  $cyt\ c_1$  (mitochondrial and bacterial).

residues 107 and 125 (Fig. 10.5a). This element, designated h1d helix, has been deleted from mitochondrial forms of  $cyt\ c_1$  without any discernable compensation. The high degree of flexibility of this loop rendered it “invisible” in the structures of

*R. capsulatus* and *P. denitrificans*  $cyt\ c_1$  but could be modeled with high temperature factors in  $Rsb c_1$ . Here the lateral displacement of the helix away from the globular  $cyt\ c_1$  core revealed a cavity that appears to provide space for a lipid head group of

a phosphatidylethanolamine (PE). However, the high degree of disorder in this region prevented it from being included in the final model. While the exact nature of the function of this loop awaits further investigation, it may be another demonstration that the three core subunits of bacterial *bc*<sub>1</sub> not only fulfill their redox catalytic functions but also deal with proper partitioning of the complex into lipids, a task that appears to be shared to a large degree with supernumerary subunits in mitochondria.

A strontium ion ( $\text{Sr}^{2+}$ ) from the crystallization additive has been shown to bind to the side chains of D8, E14 and E129 and the backbone carbonyl oxygen atom of V9 in *R. sphaeroides* *cyt c*<sub>1</sub>. As the crystallization conditions of *Rbc*<sub>1</sub> and *Pdbc*<sub>1</sub> did not contain equivalent metal ions, their respective, but otherwise perfectly conserved, residues remain free. While the  $\text{Sr}^{2+}$  ion is most likely not a physiological substrate, it was shown that the presence of  $\text{Ca}^{2+}$  ions can prevent the binding of subunit IV of *Rsb*<sub>1</sub>, possibly through blocking the acidic cluster of residues meant to bind a basic portion of *Rsb*<sub>1</sub>'s only supernumerary unit. The purpose of this site in *Rbc*<sub>1</sub> and *Pdbc*<sub>1</sub>, which are not known to require an additional subunit, remains unclear. In mitochondrial *bc*<sub>1</sub> this site is structurally but not electronically maintained, as the amino acids D8 and E14 have been replaced by neutral, polar or even basic ones. Only vestiges of the formerly acidic site remain. Residue E129 was replaced by D125 (bovine) or D189 (yeast), forming hydrogen bonds to the indole group of W12 (or W76), which replaced F11 in bacterial sequences.

### 3. Structural Differences Observed in the Iron-Sulfur-Protein Subunit

The ISP is anchored to the membrane via its N-terminal TM helix. The TM helix is connected to the extrinsic domain of ISP (ISP-ED) by a flexible linker, which enables ISP-ED to relay the electron from the QP site to *cyt c*<sub>1</sub>. The ISP is well conserved among species but structure-based sequence

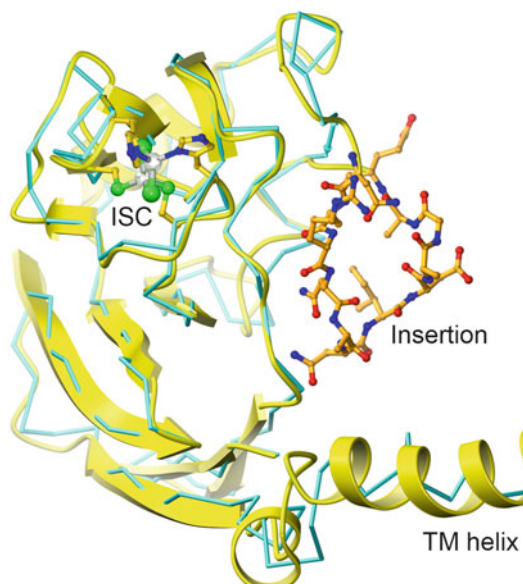


Fig. 10.6. Structure of bacterial ISP and comparison to its mitochondrial counterpart. The model of bacterial ISP is shown in a yellow ribbon diagram. Superimposed is a  $\alpha$ -trace of the bovine ISP in cyan. Unique to the bacterial ISP is the globular-shaped insertion, which is illustrated as a ball-and-stick model.

alignments highlight one  $\sim 12$ -residue long globular insertion in the bacterial ISP featuring three  $\beta$ -turns and an inverse  $\gamma$ -turn (Fig. 10.6). Despite the remoteness of this element from the iron-sulfur cluster (20–25 Å), an interruption in its hydrogen bonding network by more than one point mutation results in a failure to integrate this subunit into *bc*<sub>1</sub> (Xiao et al. 2004).

## IV. Structural Studies of *Cyt bc*<sub>1</sub> with Bound Inhibitors

To gain a survival advantage, many bacterial and fungal species developed the ability to produce quinol or quinone binding site inhibitors, some of which are close chemical analogues of the substrates as well (Esser et al. 2014). Inhibitors targeting *bc*<sub>1</sub> have helped unravel the mechanism of electron flow including the elucidation of the phenomenon of oxidant-induced *cyt b* reduction in the presence of antimycin (Slater 1973;

Wikstrom and Berden 1972). Because complex III is not only present in a large number of diverse organisms but also structurally well conserved, cyt  $bc_1$  complexes have been selected as the targets of modern pesticides and specific antibiotics in agriculture and medicine (Bueno et al. 2012; Esser et al. 2014).

#### A. Crystal Structures of Cyt $bc_1$ in Complex with Inhibitors

In contrast to the many published mitochondrial  $bc_1$  structures from beef, chicken and yeast with a good cross-section of bound  $Q_P$ - (Berry and Huang 2011; Gao et al. 2002; Xia et al. 1997) and  $Q_N$ -site (Gao et al. 2003; Kim et al. 1998) inhibitors, crystal structures of bacterial complexes are still rare. At the  $Q_P$  site, the only inhibitor bound to bacterial  $bc_1$  in all published structures is stigmatellin (Fig. 10.4b) (Berry et al. 2004; Esser et al. 2008a; Kleinschroth et al. 2011). This is not surprising, since crystallization depends on conformational stability or overall rigidity of the protein and stigmatellin effectively arrests the motion of ISP-ED. Serendipitously, many mitochondrial  $bc_1$  crystals have insulated the IMS domains of cyt  $c_1$  and ISP from crystal contacts by providing interactions exclusively from several supernumerary subunits. As far as  $Q_N$  site inhibitors are concerned, so far, only one crystal structure of wild-type *Rsb* $c_1$  with the stigmatellin at  $Q_P$  and antimycin at  $Q_N$  has been published (Fig. 10.4c) (Esser et al. 2008a) (Table 10.1). Despite the small number of inhibitor-complexed structures for bacterial  $bc_1$ , conclusions obtained from those studies using mitochondrial  $bc_1$  are applicable to the bacterial enzymes.

#### B. Inhibitor Binding-Induced Conformation Switch in ISP-ED

The binding of inhibitors has a profound effect on the spectra of *b*-type hemes and on the redox potential of ISP (Link et al. 1993; von Jagow and Link 1986). Inhibitor binding was also recognized to be

a function of the redox state of the enzyme (Brandt and von Jagow 1991). However, these phenomena were difficult to explain in the absence of structural information. In 1998, less than a year after the first  $bc_1$  structure was published, Kim et al. reported crystallographic observations demonstrating the conformational switch of ISP-ED in response to binding of different types of  $bc_1$  inhibitors to the  $Q_P$  site (Kim et al. 1998). One type of inhibitors, including stigmatellin, UHDBT, and famoxadone, led to fixation of ISP-ED conformation at the  $Q_P$  site of cyt *b* (*b*-site) and another type, including myxothiazol, azoxystrobin, and MOA stilbene, mobilized ISP-ED (Table 10.2). These two types of inhibitors were named  $P_f$ - and  $P_m$ -type inhibitors, respectively, according to their ability to fix or mobilize ISP-ED (Esser et al. 2004). High-resolution crystallographic data also showed that these two types of inhibitors bind to two different sites, the  $P_f$ - or  $P_m$ -sites, within the  $Q_P$  pocket (Fig. 10.2a), driving movement of the highly conserved cd1 helix in a bi-directional fashion (Esser et al. 2006) (Fig. 10.2a). Since the cd1 helix forms part of the ISP-ED binding surface, this bi-directional movement was hypothesized to modulate the binding affinity of ISP-ED, leading to a conformation switch (Esser et al. 2006; Xia et al. 2013).

#### C. Structural Basis of the Mechanism of Electron Bifurcation at the $Q_P$ Site: The Surface-Affinity-Modulated ISP-ED Conformation Switch Mechanism

Elucidating the mechanism that enforces bifurcation of the electrons in an energy conserving process of  $bc_1$  was not expected to be trivial, as evidenced by many proposed mechanisms (see Sect. II.B). In the first publication on the crystal structures of bovine  $bc_1$  (Xia et al. 1997), the ISP-ED was found to be disordered in both native and inhibitor-bound (antimycin A or myxothiazol) structures, demonstrating its mobility. However, the 2Fe-2S cluster of ISP-ED left an unmistakable signal in the anomalous

Table 10.2. Conformation switch of the ISP-ED in the presence of different types of inhibitors.

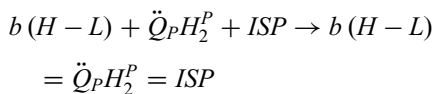
Ligand at Q <sub>P</sub> site	Space group	Inhibitor type	Normalized ISC anomalous peak	ISC-cyt <i>c</i> <sub>1</sub> distance (Å)	Estimated ET rate (s <sup>-1</sup> )	References
None	<i>I</i> 4 <sub>1</sub> 22	–	0.45	27.7	2.1 × 10 <sup>-5</sup>	Kim et al. (1998)
Azoxystrobin	<i>I</i> 4 <sub>1</sub> 22	Pm	0.36	27.7	2.1 × 10 <sup>-5</sup>	Esser et al. (2006)
MOAS	<i>I</i> 4 <sub>1</sub> 22	Pm	0.23	27.7	2.1 × 10 <sup>-5</sup>	Esser et al. (2006)
Famoxadone	<i>I</i> 4 <sub>1</sub> 22	Pf	1.02	27.7	2.1 × 10 <sup>-5</sup>	Esser et al. (2006)
Stigmatellin	<i>I</i> 4 <sub>1</sub> 22	Pf	1.20	27.7	2.1 × 10 <sup>-5</sup>	Esser et al. (2006)
UHDBT	<i>I</i> 4 <sub>1</sub> 22	Pf	0.96	27.7	2.1 × 10 <sup>-5</sup>	Esser et al. (2006)
None	<i>P</i> 6 <sub>5</sub>	–	–	23.6	0.007	Iwata et al. (1998)
None	<i>P</i> 6 <sub>5</sub> 22	–	–	7.8	2.9 × 10 <sup>7</sup>	Iwata et al. (1998)

difference Fourier map, placing it very far (~31 Å) away from the cyt *c*<sub>1</sub> heme iron. This distance is incompatible with the observed turnover rate of *bc*<sub>1</sub> reaction, as it would prohibit efficient ET between ISP and cyt *c*<sub>1</sub>. Subsequent crystal structures showed that ISP-ED can be in different locations in different crystal forms (Table 10.2), leading to the proposal that ET between ISP and cyt *c*<sub>1</sub> can be accomplished by domain movement (Iwata et al. 1998; Zhang et al. 1998b). The discovery of the motion of ISP-ED through crystal structure analyses of mitochondrial *bc*<sub>1</sub> solved only part of the problem of electron bifurcation in that it enabled an understanding of the mechanism that relays electrons from the quinol oxidation site to the remote cyt *c*<sub>1</sub> electron acceptor. The mobility of ISP-ED also complicated the system by allowing the head domain of ISP to become a second substrate, binding adjacent to ubiquinol in the enzyme-substrate complex. Furthermore, despite much effort, the reaction product bound in an enzyme-product complex at the Q<sub>P</sub> site has not been identified by crystallographic methods; the best approximations are complexes with inhibitors that closely resemble quinone.

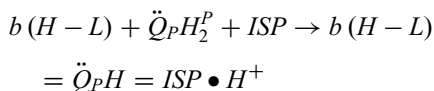
The essence of the operation of *bc*<sub>1</sub> is separation of the electrons from substrate quinol, which is initiated after the binding of the substrate and the docking of the mobile ISP-ED at the Q<sub>P</sub> site of cyt *b*, bringing the high-potential 2Fe-S2 cluster into close prox-

imity to the substrate. Since direct structural details on several critical waypoints along the reaction coordinate are not yet available, researchers remain cautious not to overinterpret observations including thermodynamic data that would (at times strongly) suggest a certain sequence of events. Nevertheless, the experimental observations of ISP-ED conformation switch in the presence of two different types of inhibitors suggested a mechanism for the bifurcated ET at the Q<sub>P</sub> site. As shown in Fig. 10.2b, ISP-ED must be in a fixed conformation when substrate QH<sub>2</sub> enters the Q<sub>P</sub> pocket, occupying first the P<sub>T</sub>-site. It remains fixed in place during the first electron transfer to the one-electron carrier ISP. At the same time, the two protons transfer to their respective receptors, the glutamate of the PEWY motif and a histidine ligand to 2Fe-2S. Because of the 31 Å separation between the 2Fe-2S and heme *c*<sub>1</sub>, ET between these two redox partners will not occur for as long as the reduced ISP-ED remains fixed at this position. The resulting highly unstable Q• radical, is however electronically coupled with hemes *b*<sub>L</sub> and *b*<sub>H</sub>, allowing the second electron to reduce the Q<sub>N</sub> site occupant. Once the 2nd electron reaches the Q<sub>N</sub> site, the now fully oxidized quinone substrate Q moves to the P<sub>m</sub>-site, releasing ISP-ED from the *b*-site to deliver the first electron to cyt *c*<sub>1</sub>. This surface-affinity modulated ISP-ED conformation switch mechanism or SAMICS can be summarized with the following formulae in six steps:

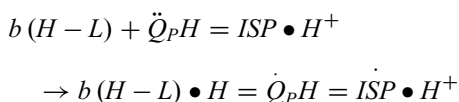
Step 1: cyt  $b$ ,  $QH_2$  and ISP form a complex



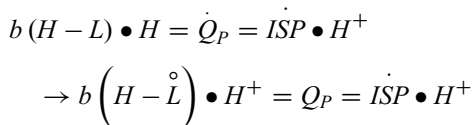
Step 2:  $QH_2$  transfers a proton to ISP



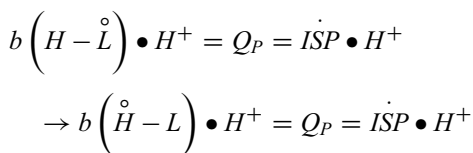
Step 3: QH transfers the first electron to ISP and another proton to cyt  $b$



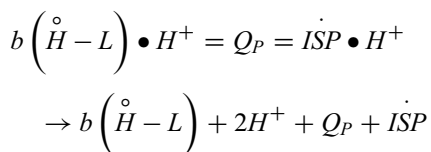
Step 4: Q radical transfers the remaining electron to  $b_L$  heme of cyt  $b$



Step 5:  $b_L$  heme delivers the electron to  $b_H$  heme



Step 6: ISP and Q dissociate from cyt  $b$



This hypothesis is consistent with a large body of biochemical, biophysical and genetic evidence: (1) it provides a functional explanation for the extraordinary sequence conservation of the  $cd1$  helix. (2) A logical consequence of this hypothesis is that the reduction of  $b$  hemes precedes that of cyt  $c_1$ , as shown by the pre-steady state kinetic analysis

(Bowyer and Crofts 1981; Gupta et al. 1998; Hansen et al. 2000; Zhu et al. 2007). (3) The strict inhibition of  $bc_1$  by antimycin A, which binds exclusively to the remote  $Q_N$  site (Gao et al. 2003), can be readily explained by SAMICS, whereas an unregulated, mobile ISP-ED would be incompatible with the observed antimycin inhibition.

## V. Experimental Verification of the Bifurcated ET Mechanism

As mentioned above, cyt  $bc_1$  is required for bacteria under photosynthetic growth conditions (Fig. 10.1). During the photosynthetic energy conversion process, electrons are shuttled back and forth between RCs and cyt  $bc_1$  by cyt  $c_2$  and quinol/quinone. Importantly, there is no exogenous electron donor or final acceptor in this cyclic ET pathway and light energy is converted to the pmf for ATP synthesis. However, the quinol oxidation activity catalyzed by  $bc_1$  can be bypassed when photosynthetic bacteria are grown under aerobic conditions, which is an important feature that allows an impaired or defective  $bc_1$  to be experimentally examined (Gennis et al. 1993; Thony-Meyer 1997).

In *R. sphaeroides*, the  $fbc$ FBC operon encoding the three core subunits of the cyt  $bc_1$  complex is only 3.3 kb (Yun et al. 1990). A separate gene  $fbcQ$  encoding the subunit IV is approximately 278 kb away from the  $fbc$ FBC operon. Thus, the *R. sphaeroides* strain BC17 that has the  $fbc$ FBC and  $fbcQ$  operons removed from the chromosome cannot grow photosynthetically. It must grow aerobically. A  $bc_1$  expression system that affords easy manipulation was created by inserting  $fbc$ FBC and  $fbcQ$  genes into the low copy number expression vector pRKD418 (Mather et al. 1995) and transforming it into BC17 (Yun et al. 1990). This system was further modified by inserting a hexahistidine tag into the C-terminus of cyt  $c_1$  (Tian et al. 1998), permitting affinity purification of the  $bc_1$  complexes from *R. sphaeroides* cells. A similar system that was developed for cyt  $bc_1$



in *R. capsulatus* has also been widely used (Gennis et al. 1993).

#### A. Mutagenesis in Cyt *bc*<sub>1</sub> Supports the Functional Importance of ISP-ED Movement

Mutations were introduced into cyt *b* and ISP of *Rsb*<sub>c1</sub>, *Rbc*<sub>c1</sub> and also into *Scb*<sub>c1</sub> to determine whether the mobility of ISP-ED is a critical and vital aspect of the *bc*<sub>1</sub> function. The matter of a mobile ISP-ED arose immediately from the first structure determination of *Mtbc*<sub>1</sub> (Kim et al. 1998; Xia et al. 1997), which placed the 2Fe-2S cluster at a distance too far from its oxidation partner cyt *c*<sub>1</sub> for rapid electron transfer. With a globular head domain connected to a single TM through a flexible “neck” region, the ISP has all the structural features required to swivel between cyt *b* to cyt *c*<sub>1</sub> carrying one electron at a time. Mutations that modify the neck region of ISP to make it more rigid, more flexible, or mutations that alter the length (deletion or insertion mutants) clearly inhibit or even abolish the enzymatic activity of *bc*<sub>1</sub> (Darrouzet et al. 2000a, b; Obungu et al. 2000; Tian et al. 1998, 1999). To leave no doubt about the mobility of the ISP-ED, the Yu lab (Ma et al. 2008; Xiao et al. 2000) produced a double cysteine mutant of *Rsb*<sub>c1</sub>. The mutation sites, one in cyt *b* and one in the ISP-ED, are spatially close so that a disulfide bridge could be formed under oxidizing conditions or broken under reduction or alkylation. Thus, manipulation of the disulfide bridge provided an effective and reversible on-off switch for the mobile ISP head domain (Xiao et al. 2000).

#### B. Mutagenesis in *bc*<sub>1</sub> Supports the Presence of a Control Mechanism for the ISP-ED Conformation Switch

On the basis of structural analysis of mitochondrial *bc*<sub>1</sub> in the presence of P<sub>f</sub>- or P<sub>m</sub>-type inhibitors, the SAMICS mechanism was proposed (Esser et al. 2006; Xia et al. 2013). A requirement of this mechanism is that the ISP-ED remains fixed at the Q<sub>p</sub> site

or the *b*-position until the transfers of the second electron and protons from ubiquinol are completed, which effortlessly explains the high fidelity of the bifurcation of the electron pathway. This hypothesis also predicts that mutations in residues of the cyt *b* subunit lining the surface of the ISP-ED binding site would significantly alter the dynamics of ISP-ED movement, thus affecting *bc*<sub>1</sub> activity. The ISP-ED binding surface at the *b*-site consists of residues from the cd1 helix and EF loop with a total of 13 residues, five on the cd1 helix and eight on the EF loop, that have their side chains exposed to the binding surface (Fig. 10.7). The mutations introduced into these residues produced effects that agreed well with the prediction of altered ET kinetics between the ISP and cyt *c*<sub>1</sub> but these mutations rarely influence the substrate binding. For instance, mutations W142R/T/K/S (W141 in *Btbc*<sub>1</sub>) were introduced to *Scb*<sub>c1</sub> (Bruehl et al. 1995) and T160Y/S (T144 in *Btbc*<sub>1</sub>) to *Rsb*<sub>c1</sub> (Mather et al. 1995), both on the cd1 helix, resulting in a dramatic reduction in *bc*<sub>1</sub> activity and altered cyt *c*<sub>1</sub> reduction kinetics; yet substrate binding was not affected. Similar observations were made to residues on the EF loop as in K329A of *R. sphaeroides* (K287 *Btbc*<sub>1</sub>) (Esser et al. 2006), L286 and I292 (I268 *Btbc*<sub>1</sub>) of *R. sphaeroides* (Rajagukguk et al. 2007), K329 of *R. sphaeroides* (Crofts et al. 1995), Y279 of yeast (Wenz et al. 2007), and Y302 in *R. capsulatus* (Lee et al. 2011).

A number of these mutants were purified and ET rates between ISP and cyt *c*<sub>1</sub> were measured by rapid photooxidation of a laser-excitable ruthenium cluster (Millett and Durham 2009). For example, residue I292 on the EF loop was mutated to I292L/M/V/E/R and the ET rate between ISP and *c*<sub>1</sub> dropped precipitously for all mutants, when compared to the wild-type *bc*<sub>1</sub>. In particular, the I292A and I292M mutants behaved like *bc*<sub>1</sub> inhibited by the P<sub>f</sub> inhibitor famoxadone (Rajagukguk et al. 2007).

The current hypothesis also predicts that limiting the movement of the cd1 helix leads to a modification in the activity of the complex depending on the size of substitution, as

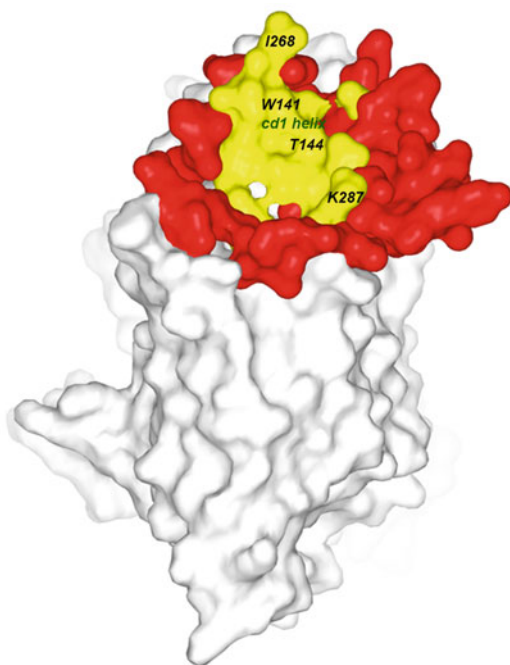


Fig. 10.7. The binding surface in the cyt  $b$  subunit for the ISP-ED. A van der Waals surface plot for the cyt  $b$  subunit is given in gray and the ISP-0 binding surface is a shallow depression shown in red. Residues that are in direct contact with ISP-ED when it is fixed at the  $b$ -position in the presence of  $P_f$  inhibitors like stigmatellin are shown in yellow. Those residues that have been mutated are labeled.

seen in S155 of *R. sphaeroides* (Tian et al. 1997) and in G158 of *R. capsulatus* (Ding et al. 1995).

### C. The Balance of Inter- and Intra-Monomer ET of the Cyt $bc_1$ Complex

According to the SAMICS mechanism, before the ISP-ED is released to reduce cyt  $c_1$ , the second ET must take place. This demands a clear ET passage to the  $Q_N$  site. To avoid charge congestion, nature has apparently evolved a backup mechanism by making the coupled system larger. In the first dimeric cyt  $bc_1$  structure, the distance between the two  $b_L$  hemes was determined to be as short as  $\sim 14$  Å (Xia et al. 1997), which remains unchanged in the dimeric *Rsb* $c_1$  and

permits inter-monomer ET. Indeed, the ET rate between the two  $b_L$  hemes was estimated to be 0.025–0.25 ms (Osyczka et al. 2004). Communications between the monomers of the dimeric  $bc_1$  was also demonstrated experimentally in *P. denitrificans* by deactivating the  $Q_P$  site of one monomer, which was fully active but was unable to stimulate the second site in response to antimycin binding at the  $Q_N$  site (Castellani et al. 2010). In a more elegant investigation of inter-monomer ET, a fully functional dimeric  $bc_1$  with a covalently linked cyt  $b$  dimer was engineered (denoted B-B dimer vs. BB dimer for the wild type) (Swierczek et al. 2010). Using site-directed mutagenesis, each of the four redox sites within the cyt  $b$  dimer could be deactivated alone or in groups. The quinol oxidation site can be deactivated by a point mutation that prevents quinone binding through a G158W change. The fused, but otherwise unaltered cyt  $b$  dimer, assembled into a cyt  $bc_1$  complex, performs catalysis at the same turnover rate (B-B dimer:  $60.0$  s $^{-1}$ ) as the wild-type  $bc_1$  dimer (denoted BB dimer:  $56.4$  s $^{-1}$ ). Inactivating one entire branch by a double mutation reduces the performance to 60–70 %. Simultaneous deactivations of the  $Q_P$  site of one monomer and the  $Q_N$  site on the opposite side (denoted with  ${}_W$ B-B $^N$ ) indeed decreases the enzyme's activity to about 50 % of the wild type (Swierczek et al. 2010).

## VI. The Mechanisms of Proton Uptake at the $Q_N$ Site and Exit at the $Q_P$ Site

### A. Conformational Changes at the $Q_N$ and $Q_P$ Site for Possible Proton Uptake and Exit

In a complete catalytic cycle, a ubiquinone molecule at the  $Q_N$  site receives two electrons from the  $b_H$  heme and two protons from the negative side of the membrane; this process is specifically inhibited by antimycin A and NQNO. In a number of published crystal structures, the substrate ubiquinone,

with either two or six isoprenoid repeats, was modeled into the electron density in the  $Q_N$  site of the  $bc_1$  complexes (Esser et al. 2008a; Gao et al. 2003; Hunte et al. 2000; Lange et al. 2001). Structures of bovine mitochondrial  $bc_1$  in the presence of antimycin A<sub>1</sub> or NQNO were also reported (Fig. 10.4c). Interestingly, ubiquinone and antimycin A were found to occupy overlapping but different portions of the  $Q_N$  pocket. Mechanistically, proton uptake at the  $Q_N$  site was considered in the context of a lipid environment; two potential proton uptake pathways were proposed based on analysis of bound water molecules (Lange et al. 2001). By comparing bovine and yeast  $bc_1$  structures with ubiquinone at the  $Q_N$  site, a mechanism based on conformational changes in residues H201, K227 and D228 and a ubiquinone protonation pathway via two water molecules was also proposed (Gao et al. 2003).

Proton exit at the  $Q_P$  site has been proposed to be coupled to the bifurcated ET events. The complexity of the reaction is compounded by the number of participants involving the cyt *b* subunit, the substrate  $QH_2$ , and the ISP-ED. Without dismissing differences of various mechanisms, it is generally agreed that the two protons of  $QH_2$  are extracted and exported sequentially (Crofts et al. 2006). Lacking the crystal structures showing the binding of substrate  $QH_2$  at the  $Q_P$  site, most recent discussions in the literature on the proton exit pathway were based on modeling of substrate binding using existing inhibitors such as stigmatellin (Fig. 10.4b), which is sandwiched between H161 of ISP and E271 of cyt *b* (bovine sequence). Thus, these two residues are primary candidates for moving protons out of the complex to the inter-membrane space or periplasm. Indeed, both residues were seen to undergo conformational changes upon  $bc_1$  binding to different inhibitors (Esser et al. 2004; Gao et al. 2002). However, other structural elements, such as cd1 and cd2 helices, and residues mostly in the cyt *b* subunit, such as Y131 and Y287, undergo large conformational changes as well and the roles of these residues in

proton pumping are not known (Esser et al. 2004; Gao et al. 2002).

### B. Mutational Studies Help to Define Proton Movement Pathways

Although the concept of ET-coupled proton translocation has been widely accepted, details describing the paths the protons take and how their movements are coupled to ET remain elusive. Because the bacterial cyt  $bc_1$  complexes from *R. rubrum* and *R. capsulatus* consist of only three subunits and are able to carry out full proton transfer activity (Guner et al. 1991; Robertson et al. 1993), the proton translocation must be accomplished by the three essential subunits. The accessible surface of bacterial  $bc_1$  complex is not completely closed off to the cytosolic side especially at the  $Q_N$  site so as to provide possible proton uptake pathways (Esser et al. 2008a). Because the proton movement at the  $Q_P$  site is proposed to couple to the electron bifurcation (Brandt 1996; Brandt and von Jagow 1991; Crofts et al. 2006; Link 1997; Rich 2004) and the cyt  $bc_1$ 's surface facing the periplasm is completely sealed, proton exit to the periplasm must be accompanied by some sort of conformational change of the protein. One particular residue, E271 of bovine cyt *b*, is nearly universally conserved and was believed to be involved in proton pumping as a general base at the  $Q_P$  site. Indeed, in *R. sphaeroides* cyt *b*, the corresponding residue E295 was mutated to E295Q/G/D, which severely reduced  $bc_1$  activity (Crofts et al. 1999). Kinetic analysis of these mutants suggested that the interactions between hydroxyl groups of quinol and side chains of E295 of cyt *b* and H152 of ISP are essential for proton pumping out of the enzyme. Some studies have supported the role of the iron-sulfur cluster (ISC) in proton exiting. Protons can enter and leave the  $bc_1$  complex when the ISC is chemically or genetically destroyed (Gurung et al. 2005; Miki et al. 1991). Similarly, when the ISP head domain was removed by thermolysin digestion, a decrease in proton pumping activity and an increase in

proton leakage were observed (Gurung et al. 2005). Based on these results, the protons are thought to exit via the histidine ligand of the ISC and glutamate of the -PEWY- motif.

## VII. Future Perspective

Although a full review of what has been accomplished in the structural study of cyt  $bc_1$  from photosynthetic bacteria is beyond the scope of this manuscript, it would be incomplete without at least providing a brief outlook on future research efforts from a structural perspective. It has been more than one and half decades since the first crystal structure of cyt  $bc_1$  complex debuted, and now over 50 entries of structures of  $bc_1$  and related  $b_6f$  complexes are available in the Protein Data Bank for detailed scrutiny by researchers. Reliable structural information is now available for  $bc_1$  from mitochondrial origins to bacterial species. Furthermore, structures of native and mutant  $bc_1$  with a variety of inhibitors and substrates bound are beginning to shed light on details of the reaction mechanism. Despite the progress that has been made, the following areas deserve special attention from structural biologists.

### A. The Mechanism of Superoxide Generation by Cyt $bc_1$

Reactive oxygen species (ROS) are well known contributors to oxidative stress (Andreyev et al. 2005; Barja 2004; Van Remmen and Richardson 2001), causing damage to DNA/RNA, proteins, carbohydrates, and lipids. Damage caused by ROS has been linked to a number of diseases, including cancer, inflammation and aging (Moro et al. 2005; Sadek et al. 2003; Shigenaga et al. 1994). As a progenitor of ROS, superoxide is generated by electron leakage from the oxidative phosphorylation pathway (Boveris et al. 1972) with a significant contribution from the cyt  $bc_1$  complexes (McLennan and Degli Esposti 2000; Nohl and Jordan 1986; Turrens et al. 1985). More significantly, ROS generated by cyt  $bc_1$  has more impact on the

cytosolic concentration of ROS than those generated by other respiratory complexes (Muller et al. 2004). Mechanistically, identifying the source of electron leakage has been a centerpiece of ROS research on the  $bc_1$  complex. It is known that under normal catalytic conditions, very small amounts of ROS are generated by  $bc_1$ . But the amount increases dramatically when  $bc_1$  is inhibited by antimycin A at the  $Q_N$  site or when the membrane is fully energized (Andreyev et al. 2005; Quinlan et al. 2011; Zhang et al. 1998a).

It has been reported that the production of superoxide by  $bc_1$  is reciprocally related to its ET activity. Bovine cyt  $bc_1$  has 10 times higher ET activity than  $Rsb_{c_1}$  but produces superoxide only at one-tenth of that generated by the  $Rsb_{c_1}$  (Yin et al. 2009). The  $\Delta IV$ -subunit mutant of  $Rsb_{c_1}$ , in which the only supernumerary subunit is deleted, has lower ET activity but shows four times higher superoxide generation activity than that of the wild type (Tso et al. 2006; Yin et al. 2009). Mutations introduced to conserved residues often lead to changes in superoxide activity. For example, mutations introduced to Y302 of *R. capsulatus* cyt  $b$ , the equivalent of Y278 in human and Y279 in bovine cyt  $b$ , all have decreased ET activity and an increased rate of superoxide generation (Lee et al. 2011). Similarly, the M183L mutant in cyt  $c_1$  of *Rcb\_{c\_1} was unable to grow photosynthetically due to cyt  $c_1$  inactivation (Gray et al. 1992), but a higher superoxide generation activity was observed (Borek et al. 2008).*

Two possible sites for electron leakage have been considered: one is the ubisemiquinone radical ( $Q^{\cdot}$ ) at the  $Q_P$  site (Muller et al. 2002; Nohl and Jordan 1986; Turrens et al. 1985) and the other site involves the reversed electron flow to heme  $b_L$  (Drose and Brandt 2008). The lack of detection of the  $Q^{\cdot}$  radical under normal conditions at the  $Q_P$  site obscures the  $Q^{\cdot}$ -mediated mechanism. The reduced  $b_L$ -mediated mechanism has gained support from the observation that superoxide production is maximal when the quinol pool is partially oxidized. This view is difficult

to reconcile with the observation that the *Rsb<sub>c1</sub>* mutant lacking heme *b<sub>L</sub>* produces as much superoxide as the wild type (Yang et al. 2008).

Thus, the mechanism of superoxide generation in atomic detail remains obscure. Although a direct demonstration of trapped superoxide in the cyt *bc<sub>1</sub>* structure seems distant, indirect evidence may be within reach. Analogues of superoxide could be included in crystallization experiments to reveal potential binding sites for both wild-type and mutant *bc<sub>1</sub>* complexes. The readers are encouraged to read contributions by Baniulus et al., Osychka et al., and Kramer et al. in this volume on related topic.

### *B. Interactions of Cyt *bc<sub>1</sub>* with Other Protein or Non-protein Factors*

As part of the cellular respiratory chain, the activity of the cyt *bc<sub>1</sub>* complex is regulated by redox potential and by the concentration of substrates. It has been known for some time that many factors regulate *bc<sub>1</sub>* activity, though the physiological significance of these effects was not fully appreciated. Molecules as small as ions and as large as entire proteins were found to interact with cyt *bc<sub>1</sub>*, and seem to be able to regulate its activity at least in vitro. Ions or small molecules that are reported to interfere with *bc<sub>1</sub>* activity are Zn<sup>2+</sup> (Skulachev et al. 1967), ATP (Lorusso et al. 1990), and dioxygen (Zhou et al. 2012). Recently, cyt *bc<sub>1</sub>* has been reported to form a supercomplex with other respiratory chain components (Schagger and Pfeiffer 2000) as well as to interact with matrix proteins such as malate dehydrogenase (Wang et al. 2010). Detailed interactions at sub-molecular resolution and their physiological roles in regulating *bc<sub>1</sub>* activities remain to be elucidated.

### *C. Structure-Based Drug Design to Overcome Widespread Resistance*

The cyt *bc<sub>1</sub>* complex is a time-tested and highly effective target of numerous antibiotics and fungicides. Nearly all cyt *bc<sub>1</sub>* in-

hibitors act on either the Q<sub>P</sub> or Q<sub>N</sub> site. The emergence of drug resistance, however, has had devastating economic and social consequences. The primary cause of resistance to *bc<sub>1</sub>* inhibitors is target site mutations, creating a need for novel agents that act on alternative sites within the cyt *bc<sub>1</sub>* (Esser et al. 2014). The accumulation of crystallographic data of *bc<sub>1</sub>* complexes with and without inhibitors bound offers rich information on the inhibitor binding modes, conformational changes upon inhibitor binding of side chains in the active site and large-scale domain movements of the iron-sulfur protein subunit, providing the structural basis for rational drug design. The challenge before us is to make use of the existing knowledge and devise novel strategies that would allow the discovery of better agents for disease control in a more efficient manner.

## Acknowledgments

The authors wish to thank George Leiman for editorial assistance. This research was supported by the Intramural Research Program of the NIH, National Cancer Institute, Center for Cancer Research.

## References

- Akiba T, Toyoshima C, Matsunaga T, Kawamoto M, Kubota T, Fukuyama K, Namba K, Matsubara H (1996) Three-dimensional structure of bovine cytochrome *bc<sub>1</sub>* complex by electron cryomicroscopy and helical image reconstruction. *Nat Struct Biol* 3:553–561
- Andersson SG, Zomorodipour A, Andersson JO, Sicheritz-Ponten T, Alsmark UC, Podowski RM, Naslund AK, . . . , Kurland CG (1998) The genome sequence of *Rickettsia prowazekii* and the origin of mitochondria. *Nature* 396:133–140
- Andreyev AY, Kushnareva YE, Starkov AA (2005) Mitochondrial metabolism of reactive oxygen species. *Biochem Biokhimiia* 70:200–214
- Arai H, Roh JH, Kaplan S (2008) Transcriptome dynamics during the transition from anaerobic photosynthesis to aerobic respiration in *Rhodospirillum rubrum* 2.4.1. *J Bacteriol* 190:286–299

- Baniulis D, Yamashita E, Whitelegge JP, Zatsman AI, Hendrich MP, Hasan SS, Ryan CM, Cramer WA (2009) Structure-function, stability, and chemical modification of the cyanobacterial cytochrome *bc*<sub>1</sub> complex from *Nostoc* sp. PCC 7120. *J Biol Chem* 284:9861–9869
- Barja G (2004) Free radicals and aging. *Trends Neurosci* 27:595–600
- Berry EA, Huang LS (2003) Observations concerning the quinol oxidation site of the cytochrome *bc*<sub>1</sub> complex. *FEBS Lett* 555:13–20
- Berry EA, Huang LS (2011) Conformationally linked interaction in the cytochrome *bc*<sub>1</sub> complex between inhibitors of the Q(o) site and the Rieske iron-sulfur protein. *Biochim Biophys Acta* 1807:1349–1363
- Berry EA, Huang L, Saechao LK, Pon NG, Valkova-Valchanova M, Daldal F (2004) X-ray structure of *Rhodobacter capsulatus* cytochrome *bc*<sub>1</sub>: comparison with its mitochondrial and chloroplast counterparts. *Photosynth Res* 81:251–275
- Borek A, Sarewicz M, Osyczka A (2008) Movement of the iron-sulfur head domain of cytochrome *bc*<sub>1</sub> transiently opens the catalytic Q(o) site for reaction with oxygen. *Biochemistry* 47:12365–12370
- Boveris A, Chance B (1973) The mitochondrial generation of hydrogen peroxide. General properties and effect of hyperbaric oxygen. *Biochem J* 134:707–716
- Boveris A, Oshino N, Chance B (1972) The cellular production of hydrogen peroxide. *Biochem J* 128:617–630
- Bowyer JR, Crofts AR (1981) On the mechanism of photosynthetic electron transfer in *Rhodospseudomonas capsulata* and *Rhodospseudomonas sphaeroides*. *Biochim Biophys Acta* 636:218–233
- Brandt U (1996) Bifurcated ubihydroquinone oxidation in the cytochrome *bc*<sub>1</sub> complex by proton-gated charge transfer. *FEBS Lett* 387:1–6
- Brandt U, Okun JG (1997) Role of deprotonation events in ubihydroquinone: cytochrome *c* oxidoreductase from bovine heart and yeast mitochondria. *Biochemistry* 36:11234–11240
- Brandt U, von Jagow G (1991) Analysis of inhibitor binding to the mitochondrial cytochrome *c* reductase by fluorescence quench titration: evidence for a ‘catalytic switch’ at the Q<sub>o</sub> center. *Eur J Biochem* 195:163–170
- Bruel C, di Rago J, Slonimski PP, Lemesle-Meunier D (1995) Role of the evolutionarily conserved cytochrome *b* tryptophan 142 in the ubiquinol oxidation catalyzed by the *bc*<sub>1</sub> complex in the yeast *Saccharomyces cerevisiae*. *J Biol Chem* 270:22321–22328
- Bueno JM, Herreros E, Angulo-Barturen I, Ferrer S, Fiandor JM, Gamo FJ, Gargallo-Viola D, Derimanov G (2012) Exploration of 4(1H)-pyridones as a novel family of potent antimalarial inhibitors of the plasmoidal cytochrome *bc*<sub>1</sub>. *Future Med Chem* 4:2311–2323
- Cape JL, Bowman MK, Kramer DM (2007) A semiquinone intermediate generated at the Q<sub>o</sub> site of the cytochrome *bc*<sub>1</sub> complex: importance for the Q-cycle and superoxide production. *Proc Natl Acad Sci U S A* 104:7887–7892
- Castellani M, Covian R, Kleinschroth T, Anderka O, Ludwig B, Trumpower BL (2010) Direct demonstration of half-of-the-sites reactivity in the dimeric cytochrome *bc*<sub>1</sub> complex: enzyme with one inactive monomer is fully active but unable to activate the second ubiquinol oxidation site in response to ligand binding at the ubiquinone reduction site. *J Biol Chem* 285:502–510
- Crofts AR, Wang ZG (1989) How rapid are the internal reactions of the ubiquinol-cytochrome-C<sub>2</sub> oxidoreductase. *Photosynth Res* 22:69–87
- Crofts AR, Meinhardt SW, Jones KR, Snozzi M (1983) The role of the quinone pool in the cyclic electron-transfer chain of *Rhodospseudomonas sphaeroides*: a modified Q-cycle mechanism. *Biochim Biophys Acta* 723:202–218
- Crofts AR, Barquera B, Bechmann G, Guergova M, Salcedo-Hernandez R, Hacker B, Hong S, Gennis RB (1995) Structure and function in the *bc*<sub>1</sub>-complex of *Rb. sphaeroides*. In: Pathis P (ed) *Photosynthesis: from light to biosphere*, vol 2. Kluwer, Dordrecht, pp 493–500
- Crofts AR, Hong S, Ugulav N, Barquera B, Gennis R, Guergova-Kuras M, Berry EA (1999) Pathways for proton release during ubihydroquinone oxidation by the *bc*<sub>1</sub> complex. *Proc Natl Acad Sci U S A* 96:10021–10026
- Crofts AR, Lhee S, Crofts SB, Cheng J, Rose S (2006) Proton pumping in the *bc*<sub>1</sub> complex: a new gating mechanism that prevents short circuits. *Biochim Biophys Acta* 1757:1019–1034
- Darrouzet E, Valkova-Valchanova M, Daldal F (2000a) Probing the role of the Fe-S subunit hinge region during Q(o) site catalysis in *Rhodobacter capsulatus bc*<sub>1</sub> complex. *Biochemistry* 39:15475–15483
- Darrouzet E, Valkova-Valchanova M, Moser CC, Dutton PL, Daldal F (2000b) Uncovering the [2Fe2S] domain movement in cytochrome *bc*<sub>1</sub> and its implications for energy conversion. *Proc Natl Acad Sci U S A* 97:4567–4572
- Ding H, Robertson DE, Daldal F, Dutton PL (1992) Cytochrome *bc*<sub>1</sub> complex [2Fe-2S] cluster and its interaction with ubiquinone and ubihydroquinone at the Q<sub>o</sub> site: a double-occupancy Q<sub>o</sub> site model. *Biochemistry* 31:3144–3158

- Ding H, Moser CC, Robertson DE, Tokito MK, Daldal F, Dutton PL (1995) Ubiquinone pair in the Qo site central to the primary energy conversion reactions of cytochrome bc1 complex. *Biochemistry* 34:15979–15996
- Drose S, Brandt U (2008) The mechanism of mitochondrial superoxide production by the cytochrome bc1 complex. *J Biol Chem* 283:21649–21654
- Dutton PL, Wilson DF, Lee CP (1970) Oxidation-reduction potentials of cytochromes in mitochondria. *Biochemistry* 9:5077–5082
- Esser L, Quinn B, Li Y, Zhang M, Elberry M, Yu L, Yu CA, Xia D (2004) Crystallographic studies of quinol oxidation site inhibitors: a modified classification of inhibitors for the cytochrome bc1 complex. *J Mol Biol* 341:281–302
- Esser L, Gong X, Yang S, Yu L, Yu CA, Xia D (2006) Surface-modulated motion switch: capture and release of iron-sulfur protein in the cytochrome bc1 complex. *Proc Natl Acad Sci U S A* 103:13045–13050
- Esser L, Elberry M, Zhou F, Yu CA, Yu L, Xia D (2008a) Inhibitor complexed structures of the cytochrome bc1 from the photosynthetic bacterium *Rhodobacter sphaeroides* at 2.40 Å resolution. *J Biol Chem* 283:2846–2857
- Esser L, Yu L, Yu C, Xia D (2008b) Insights into the mechanisms of quinol oxidation in cytochrome bc1 in light of the structure of bacterial complex. *Biophys Rev Lett* 2:229–257
- Esser L, Yu CA, Xia D (2014) Structural basis of resistance to anti-cytochrome bc1 complex inhibitors: implication for drug improvement. *Curr Pharm Des* 20:704–724
- Gao X, Wen X, Yu C, Esser L, Tsao S, Quinn B, Zhang L, . . . , Xia D (2002) The crystal structure of mitochondrial cytochrome bc1 in complex with famoxadone: the role of aromatic-aromatic interaction in inhibition. *Biochemistry* 41:11692–11702
- Gao X, Wen X, Esser L, Yu L, Yu CA, Xia D (2003) Structural basis for the quinone reduction in bc1 complex: a comparative analysis of crystal structures of mitochondrial cytochrome bc1 with bound substrate and inhibitors. *Biochemistry* 42:9067–9080
- Garland PB, Clegg RA, Doxer D, Downie JA, Haddock BA (1975) Proton-translocating nitrate reductase of *Escherichia coli*. In: Quagliariello E, Papa S, Falmieri F, Slater EC, Siliprandi N (eds) *Electron Transfer Chains and Oxidative Phosphorylation*. North-Holland Publishing Co., Amsterdam, pp 351–358
- Gennis RB, Barquera B, Hacker B, Van Doren SR, Arnaud S, Crofts AR, Davidson E, . . . , Daldal F (1993) The bc1 complexes of *Rhodobacter sphaeroides* and *Rhodobacter capsulatus*. *J Bioenerg Biomembr* 25:195–209
- Gopta OA, Feniouk BA, Junge W, Mulikdjanian AY (1998) The cytochrome bc1 complex of *Rhodobacter capsulatus*: ubiquinol oxidation in a dimeric Q-cycle? *FEBS Lett* 431:291–296
- Gray KA, Davidson E, Daldal F (1992) Mutagenesis of methionine-183 drastically affects the physicochemical properties of cytochrome c1 of the bc1 complex of *Rhodobacter capsulatus*. *Biochemistry* 31:11864–11873
- Guerrieri F, Nelson BD (1975) Studies on the characteristics of a proton pump in phospholipid vesicles inlaid with purified complex III from beef heart mitochondria. *FEBS Lett* 54:339–342
- Guner S, Robertson DE, Yu L, Qiu ZH, Yu CA, Knaff DB (1991) The *Rhodospirillum rubrum* cytochrome bc1 complex: redox properties, inhibitor sensitivity and proton pumping. *Biochim Biophys Acta* 1058:269–279
- Gurung B, Yu L, Xia D, Yu CA (2005) The iron-sulfur cluster of the Rieske iron-sulfur protein functions as a proton-exiting gate in the cytochrome bc1(1) complex. *J Biol Chem* 280:24895–24902
- Hansen KC, Schultz BE, Wang G, Chan SI (2000) Reaction of *Escherichia coli* cytochrome bo3 and mitochondrial cytochrome bc1 with a photoreleasable decylubiquinol. *Biochim Biophys Acta* 1456:121–137
- Hasan SS, Yamashita E, Baniulis D, Cramer WA (2013) Quinone-dependent proton transfer pathways in the photosynthetic cytochrome b6f complex. *Proc Natl Acad Sci U S A* 110:4297–4302
- Hsueh KL, Westler WM, Markley JL (2010) NMR investigations of the Rieske protein from *Thermus thermophilus* support a coupled proton and electron transfer mechanism. *J Am Chem Soc* 132:7908–7918
- Hunte C, Koepke J, Lange C, Rossmann T, Michel H (2000) Structure at 2.3 Å resolution of the cytochrome bc1(1) complex from the yeast *Saccharomyces cerevisiae* co-crystallized with an antibody Fv fragment. *Structure* 15:669–684
- Iwata S, Lee JW, Okada K, Lee JK, Iwata M, Rasmussen B, Link TA, . . . , Jap BK (1998) Complete structure of the 11-subunit bovine mitochondrial cytochrome bc1 complex [see comments]. *Science* 281:64–71
- Kim H, Xia D, Yu CA, Xia JZ, Kachurin AM, Zhang L, Yu L, Deisenhofer J (1998) Inhibitor binding changes domain mobility in the iron-sulfur protein of the mitochondrial bc1 complex from bovine heart. *Proc Natl Acad Sci U S A* 95:8026–8033

- Kleinschroth T, Castellani M, Trinh CH, Morgner N, Brutschy B, Ludwig B, Hunte C (2011) X-ray structure of the dimeric cytochrome *bc*(1) complex from the soil bacterium *Paracoccus denitrificans* at 2.7-Å resolution. *Biochim Biophys Acta* 1807:1606–1615
- Korshunov SS, Skulachev VP, Starkov AA (1997) High protonic potential actuates a mechanism of production of reactive oxygen species in mitochondria. *FEBS Lett* 416:15–18
- Kurisu G, Zhang H, Smith JL, Cramer WA (2003) Structure of the cytochrome *b6f* complex of oxygenic photosynthesis: tuning the cavity. *Science* 302:1009–1014
- Lange C, Nett JH, Trumpower BL, Hunte C (2001) Specific roles of protein-phospholipid interactions in the yeast cytochrome *bc*1 complex structure. *EMBO J* 20:6591–6600
- Lee DW, Selamoglu N, Lanciano P, Cooley JW, Forquer I, Kramer DM, Daldal F (2011) Loss of a conserved tyrosine residue of cytochrome *b* induces reactive oxygen species production by cytochrome *BC*1. *J Biol Chem* 286:18139–18148
- Leonard K, Wingfield P, Arad T, Weiss H (1981) Three-dimensional structure of ubiquinol: cytochrome *c* reductase from *Neurospora* mitochondria determined by electron microscopy of membrane crystals. *J Mol Biol* 149:259–274
- Leung KH, Hinkle PC (1975) Reconstitution of ion transport and respiratory control in vesicles formed from reduced coenzyme Q-cytochrome *c* reductase and phospholipids. *J Biol Chem* 250:8467–8471
- Lin IJ, Chen Y, Fee JA, Song J, Westler WM, Markley JL (2006) Rieske protein from *Thermus thermophilus*: 15N NMR titration study demonstrates the role of iron-ligated histidines in the pH dependence of the reduction potential. *J Am Chem Soc* 128:10672–10673
- Link TA (1997) The role of the ‘Rieske’ iron sulfur protein in the hydroquinone oxidation (Q<sub>p</sub>) site of the cytochrome *bc*1 complex – the ‘proton-gated affinity change’ mechanism. *FEBS Lett* 412:257–264
- Link TA, Pierik AJ, Assmann C, von Jagow G (1992) Determination of the redox properties of the Rieske [2Fe-2S] cluster of bovine heart *bc*1 complex by direct electrochemistry of a water-soluble fragment. *Eur J Biochem* 208:685–691
- Link TA, Haase U, Brandt U, von Jagow G (1993) What information do inhibitors provide about the structure of the hydroquinone oxidation site of ubiquinol: cytochrome *c* oxidoreductase? *J Bioenerg Biomembr* 25:221–232
- Liu X, Yu CA, Yu L (2004) The role of extra fragment at the C-terminal of cytochrome *b* (Residues 421–445) in the cytochrome *bc*1 complex from *Rhodobacter sphaeroides*. *J Biol Chem* 279:47363–47371
- Lorusso M, Cocco T, Minuto M, Papa S (1990) Effect of ATP on the activity of bovine heart mitochondrial *b-c*1 complex. *FEBS Lett* 267:103–106
- Ma H-W, Yang S, Yu L, Yu C-A (2008) Formation of engineered intersubunit disulfide bond in cytochrome *bc*1 complex disrupts electron transfer activity in the complex. *Biochim Biophys Acta (BBA) – Bioenerg* 1777:317–326
- Mather MW, Yu L, Yu CA (1995) The involvement of threonine 160 of cytochrome *b* of *Rhodobacter sphaeroides* cytochrome *bc*1 complex in quinone binding and interaction with subunit IV. *J Biol Chem* 270:28668–28675
- McLennan HR, Degli Esposti M (2000) The contribution of mitochondrial respiratory complexes to the production of reactive oxygen species. *J Bioenerg Biomembr* 32:153–162
- Miki T, Yu L, Yu CA (1991) Hematoporphyrin-promoted photoinactivation of mitochondrial ubiquinol-cytochrome *c* reductase: selective destruction of the histidine ligands of the iron-sulfur cluster and protective effect of ubiquinone. *Biochemistry* 30:230–238
- Millett F, Durham B (2009) Chapter 5 use of ruthenium photooxidation techniques to study electron transfer in the cytochrome *bc*1 complex. *Methods Enzymol* 456:95–109
- Mitchell P (1972) Chemiosmotic coupling in energy transduction: a logical development of biochemical knowledge. *J Bioenerg* 3:5–24
- Mitchell P (1976) Possible molecular mechanisms of the protonmotive function of cytochrome systems. *J Theor Biol* 62:327–367
- Moro MA, Almeida A, Bolanos JP, Lizasoain I (2005) Mitochondrial respiratory chain and free radical generation in stroke. *Free Radic Biol Med* 39:1291–1304
- Mulki-djanian AY (2007) Proton translocation by the cytochrome *bc*1 complexes of phototrophic bacteria: introducing the activated Q-cycle. *Photochem Photobiol Sci* 6:19–34
- Muller F, Crofts AR, Kramer DM (2002) Multiple Q-cycle bypass reactions at the Q<sub>o</sub> site of the cytochrome *bc*1 complex. *Biochemistry* 41:7866–7874
- Muller FL, Liu Y, Van Remmen H (2004) Complex III releases superoxide to both sides of the inner mitochondrial membrane. *J Biol Chem* 279:49064–49073
- Nogueira C, Barros J, Sa MJ, Azevedo L, Taipa R, Torracca A, Meschini MC, . . . , Santorelli FM (2013)



- Novel TTC19 mutation in a family with severe psychiatric manifestations and complex III deficiency. *Neurogenetics* 14:153–160
- Nohl H, Jordan W (1986) The mitochondrial site of superoxide formation. *Biochem Biophys Res Commun* 138:533–539
- Obungu VH, Amyot S, Wang Y, Beattie DS (1998) Amino acids involved in the putative movement of the iron-sulfur protein of the BC1 complex during catalysis. *FASEB J* 12:A1394
- Obungu VH, Wang YD, Amyot SM, Gocke CB, Beattie DS (2000) Mutations in the tether region of the iron-sulfur protein affect the activity and assembly of the cytochrome BC1 complex of yeast mitochondria. *Biochim Biophys Acta* 1457:36–44
- Oh JI, Kaplan S (2001) Generalized approach to the regulation and integration of gene expression. *Mol Microbiol* 39:1116–1123
- Osyczka A, Moser CC, Daldal F, Dutton PL (2004) Reversible redox energy coupling in electron transfer chains. *Nature* 427:607–612
- Prince RC, Dutton PL (1976) Further studies on the Rieske iron-sulfur center in mitochondrial and photosynthetic systems: a pK on the oxidized form. *FEBS Lett* 65:117–119
- Quinlan CL, Gerencser AA, Treberg JR, Brand MD (2011) The mechanism of superoxide production by the antimycin-inhibited mitochondrial Q-cycle. *J Biol Chem* 286:31361–31372
- Rajagukguk S, Yang S, Yu CA, Yu L, Durham B, Millett F (2007) Effect of mutations in the cytochrome b<sub>ef</sub> loop on the electron-transfer reactions of the Rieske iron-sulfur protein in the cytochrome bc<sub>1</sub> complex. *Biochemistry* 46:1791–1798
- Rich PR (2004) The quinone chemistry of bc complexes. *Biochim Biophys Acta* 1658:165–171
- Robertson DE, Ding H, Chelminski PR, Slaughter C, Hsu J, Moomaw C, Tokito M, . . . , Dutton PL (1993) Hydroubiquinone-cytochrome c<sub>2</sub> oxidoreductase from *Rhodobacter capsulatus*: definition of a minimal, functional isolated preparation. *Biochemistry* 9:1310–1317
- Rottenberg H, Covian R, Trumpower BL (2009) Membrane potential greatly enhances superoxide generation by the cytochrome bc<sub>1</sub> complex reconstituted into phospholipid vesicles. *J Biol Chem* 284:19203–19210
- Sadek HA, Nulton-Persson AC, Szweda PA, Szweda LI (2003) Cardiac ischemia/reperfusion, aging, and redox-dependent alterations in mitochondrial function. *Arch Biochem Biophys* 420:201–208
- Schagger H, Pfeiffer K (2000) Supercomplexes in the respiratory chains of yeast and mammalian mitochondria. *EMBO J* 19:1777–1783
- Shigenaga MK, Hagen TM, Ames BN (1994) Oxidative damage and mitochondrial decay in aging. *Proc Natl Acad Sci U S A* 91:10771–10778
- Skulachev VP, Chistyakov VV, Jasaitis AA, Smirnova EG (1967) Inhibition of the respiratory chain by zinc ions. *Biochem Biophys Res Commun* 26:1–6
- Slater EC (1973) The mechanism of action of the respiratory inhibitor, antimycin. *Biochim Biophys Acta* 301:129–154
- Staniek K, Gille L, Kozlov AV, Nohl H (2002) Mitochondrial superoxide radical formation is controlled by electron bifurcation to the high and low potential pathways. *Free Radic Res* 36:381–387
- Stroebel D, Choquet Y, Popot JL, Picot D (2003) An atypical haem in the cytochrome b<sub>6</sub>f complex. *Nature* 426:413–418
- Swierczek M, Cieluch E, Sarewicz M, Borek A, Moser CC, Dutton PL, Osyczka A (2010) An electronic bus bar lies in the core of cytochrome bc<sub>1</sub>. *Science* 329:451–454
- Thony-Meyer L (1997) Biogenesis of respiratory cytochromes in bacteria. *Microbiol Mol Biol Rev* 61:337–376
- Tian H, Yu L, Mather MW, Yu CA (1997) The involvement of serine 175 and alanine 185 of cytochrome b of *Rhodobacter sphaeroides* cytochrome bc<sub>1</sub> complex in interaction with iron-sulfur protein. *J Biol Chem* 272:23722–23728
- Tian H, Yu L, Mather MW, Yu CA (1998) Flexibility of the neck region of the rieske iron-sulfur protein is functionally important in the cytochrome bc<sub>1</sub> complex. *J Biol Chem* 273:27953–27959
- Tian H, White S, Yu L, Yu CA (1999) Evidence for the head domain movement of the rieske iron-sulfur protein in electron transfer reaction of the cytochrome bc<sub>1</sub> complex. *J Biol Chem* 274:7146–7152
- Trumpower BL (1976) Evidence for a protonmotive Q cycle mechanism of electron transfer through the cytochrome b-c<sub>1</sub> complex. *Biochem Biophys Res Commun* 70:73–80
- Trumpower BL (1990) Cytochrome bc<sub>1</sub> complexes of microorganisms. *Microbiol Rev* 54:101–129
- Trumpower BL, Gennis RB (1994) Energy transduction by cytochrome complexes in mitochondrial and bacterial respiration: the enzymology of coupling electron transfer reactions to transmembrane proton translocation. *Annu Rev Biochem* 63:675–716
- Tso SC, Yin Y, Yu CA, Yu L (2006) Identification of amino acid residues essential for reconstitutive activity of subunit IV of the cytochrome bc<sub>1</sub> complex from *Rhodobacter sphaeroides*. *Biochim Biophys Acta* 1757:1561–1567

- Turrens JF, Alexandre A, Lehninger AL (1985) Ubisemiquinone is the electron donor for superoxide formation by complex III of heart mitochondria. *Arch Biochem Biophys* 237:408–414
- Ugulava NB, Crofts AR (1998) CD-monitored redox titration of the Rieske Fe-S protein of *Rhodobacter sphaeroides*: pH dependence of the midpoint potential in isolated bc1 complex and in membranes. *FEBS Lett* 440:409–413
- Van Remmen H, Richardson A (2001) Oxidative damage to mitochondria and aging. *Exp Gerontol* 36:957–968
- Vermeglio A, Joliot P (1999) The photosynthetic apparatus of *Rhodobacter sphaeroides*. *Trends Microbiol* 7:435–440
- von Jagow G, Link TA (1986) Use of specific inhibitors on the mitochondrial bc1 complex. *Methods Enzymol* 126:253–271
- Wang Q, Yu L, Yu CA (2010) Cross-talk between mitochondrial malate dehydrogenase and the cytochrome bc1 complex. *J Biol Chem* 285:10408–10414
- Wenz T, Covian R, Hellwig P, Macmillan F, Meunier B, Trumpower BL, Hunte C (2007) Mutational analysis of cytochrome b at the ubiquinol oxidation site of yeast complex III. *J Biol Chem* 282:3977–3988
- Wikstrom MK, Berden JA (1972) Oxidoreduction of cytochrome-B in presence of antimycin. *Biochim Biophys Acta* 283:403–420
- Woese CR (1987) Bacterial evolution. *Microbiol Rev* 51:221–271
- Xia D, Yu CA, Kim H, Xia JZ, Kachurin AM, Zhang L, Yu L, Deisenhofer J (1997) Crystal structure of the cytochrome bc1 complex from bovine heart mitochondria. *Science* 277:60–66
- Xia D, Esser L, Yu L, Yu CA (2007) Structural basis for the mechanism of electron bifurcation at the quinol oxidation site of the cytochrome bc1 complex. *Photosynth Res* 92:17–34
- Xia D, Esser L, Elberry M, Zhou F, Yu L, Yu CA (2008) The road to the crystal structure of the cytochrome bc1 complex from the anoxygenic, photosynthetic bacterium *Rhodobacter sphaeroides*. *J Bioenerg Biomembr* 40:485–492
- Xia D, Esser L, Tang WK, Zhou F, Zhou Y, Yu L, Yu CA (2013) Structural analysis of cytochrome bc1 complexes: implications to the mechanism of function. *Biochim Biophys Acta* 1827:1278–1294
- Xiao K, Yu L, Yu CA (2000) Confirmation of the involvement of protein domain movement during the catalytic cycle of the cytochrome bc1 complex by the formation of an intersubunit disulfide bond between cytochrome b and the iron-sulfur protein. *J Biol Chem* 275:38597–38604
- Xiao KH, Liu XY, Yu CA, Yu L (2004) The extra fragment of the iron-sulfur protein (residues 96–107) of *Rhodobacter sphaeroides* cytochrome bc(1) complex is required for protein stability. *Biochemistry* 43:1488–1495
- Yamashita E, Zhang H, Cramer WA (2007) Structure of the cytochrome *b6f* complex: quinone analogue inhibitors as ligands of heme cn. *J Mol Biol* 370:39–52
- Yang X, Trumpower BL (1988) Protonmotive Q cycle pathway of electron transfer and energy transduction in the three-subunit ubiquinol-cytochrome c oxidoreductase complex of *Paracoccus denitrificans*. *J Biol Chem* 263:11962–11970
- Yang S, Ma HW, Yu L, Yu CA (2008) On the mechanism of quinol oxidation at the QP site in the cytochrome bc1 complex: studied using mutants lacking cytochrome bL or bH. *J Biol Chem* 283:28767–28776
- Yee C, Yang W, Hekimi S (2014) The intrinsic apoptosis pathway mediates the pro-longevity response to mitochondrial ROS in *C. elegans*. *Cell* 157:897–909
- Yin Y, Tso SC, Yu CA, Yu L (2009) Effect of subunit IV on superoxide generation by *Rhodobacter sphaeroides* cytochrome bc(1) complex. *Biochim Biophys Acta* 1787:913–919
- Yun C, Beci R, Crofts AR, Kaplan S, Gennis RB (1990) Cloning and DNA sequencing of the *fb* operon encoding the cytochrome bc1 complex from *Rhodobacter sphaeroides*. *Eur J Biochem* 194:399–411
- Zhang L, Yu L, Yu CA (1998a) Generation of superoxide anion by succinate-cytochrome c reductase from bovine heart mitochondria [in process citation]. *J Biol Chem* 273:33972–33976
- Zhang Z, Huang L, Shulmeister VM, Chi YI, Kim KK, Hung LW, Crofts AR, . . . , Kim SH (1998b) Electron transfer by domain movement in cytochrome bc1. *Nature* 392:677–684
- Zhou F, Yin Y, Su T, Yu L, Yu CA (2012) Oxygen dependent electron transfer in the cytochrome bc(1) complex. *Biochim Biophys Acta* 1817:2103–2109
- Zhu J, Egawa T, Yeh S, Yu L, Yu CA (2007) Simultaneous reduction of iron-sulfur protein and cytochrome bL during ubiquinol oxidation in cytochrome bc1 complex. *Proc Natl Acad Sci U S A* 104:4864–4869

# Chapter 11

## Rieske Iron-Sulfur Protein Movement and Conformational Changes in Cytochrome *bc*–*bf* Complexes

Li-shar Huang and Edward Berry\*

*Biochemistry and Molecular Biology, SUNY Upstate Medical University, 750 E. Adams Street, Syracuse, NY 13210, USA*

Summary.....	237
I. Introduction.....	237
II. Requirement for Movement of the ISP Extrinsic Domain to Shuttle Electrons.....	238
III. Classification and Depiction of Different Positions of the ISP-ED.....	238
IV. Conformational Changes in the ISP Hinge Region.....	243
V. Does the ISP-ED Undergo Internal Conformation Changes?.....	248
Acknowledgements.....	249
References.....	249

### Summary

A detailed description is provided of the different positions observed for the Rieske iron-sulfur protein in different crystal structures of the *bc*<sub>1</sub> complex, and the conformational changes taking place in the “neck” or “linker” region to make those positions possible. Significant movement in the neck is limited to residues 69–71. The effect of neck mutations is interpreted in terms of their effect on the tension exerted by the neck on the extrinsic domain, rather than flexibility of the neck.

### I. Introduction

The cytochrome *bc*<sub>1</sub> complex has proved to be a particularly productive target for crystallization, perhaps because of the large extrin-

sic domains on both sides of the membrane with the mitochondrial complex. Today there are ~40 structures of cyt *bc*<sub>1</sub>, from 6 different organisms, in 11 different crystal forms, in the Protein Databank (PDB). There are

---

*Abbreviations:* Cyt – Cytochrome; ED – Extrinsic domain; HHDBT UHDBT – 5-n-heptyl or 5-n-undecyl –6-hydroxy-4,7-dioxobenzothiazole “*bc* complex” is used as a generic term referring to the superfamily of enzymes including a cyt *b* homolog Rieske ISP, and c-type cytochrome including *bc*<sub>1</sub> *b*<sub>6f</sub>, *b*<sub>6c1</sub>, and *b*-*cc* complexes; ISP – Iron sulfur protein; *Pc.d.*

---

– *Paracoccus denitrificans*; PDB – Protein Databank ([www.pdb.org](http://www.pdb.org)); Q<sub>N</sub> – Quinol reduction site; Q<sub>P</sub> – Quinol oxidation site of *bc*–*bf* complexes; *Rb.c.* – *Rhodobacter capsulatus*; *Rb.s.* – *Rhodobacter sphaeroides*; *T. thermophilus* – *Thermus thermophilus*; – Structures in the PDB are referred to by their 4-letter accession code

---

\*Author for correspondence, e-mail: [berrye@upstate.edu](mailto:berrye@upstate.edu)

12 structures of the *b<sub>6</sub>f* complex from three different organisms, in two different crystal forms. Many of the crystal forms contain more than one monomer in the asymmetric unit, giving us multiple crystallographically independent structures from a single crystal.

Comparing these structures allows us to identify conformational changes. Some of these just reflect plasticity of the protein, as it is influenced by different crystal contacts in the different crystal forms. Other changes represent significant changes that may be related to the function of the enzyme. Describing these changes, and deducing their significance, if any, for the mechanism, is important for getting the most understanding from the structures.

The most significant changes observed in the *bc<sub>1</sub>* complex structures have involved different positions of the Rieske iron-sulfur protein. At the least these involve different positions of a tethered, soluble, electron carrier as it diffuses between electron donor and acceptor. However, as described below, it is likely that it involves a carefully orchestrated movement that is important for ensuring the strict bifurcation of electron transfer at the Q<sub>p</sub> site, and thus the efficiency of energy conservation by the *bc<sub>1</sub>* complex. Herein we focus mainly on the detailed description of the conformational changes without overly emphasizing the possible interpretations, which have been covered in a number of reviews. In particular we provide a detailed description of conformational changes occurring in the “neck” of the iron-sulfur protein.

## II. Requirement for Movement of the ISP Extrinsic Domain to Shuttle Electrons

The Rieske iron-sulfur protein (ISP) consists of a hydrophilic globular domain of approximately 120 residues which includes the Fe<sub>2</sub>S<sub>2</sub> cluster (the ISP extrinsic domain or ED), anchored to the membrane by a single transmembrane helix (TMH). There is a short, flexible linker between the ISP-ED and the transmembrane helix, referred to as the

linker, neck, tether, or hinge; and the ED is mobile as indicated by different orientations in different crystal structures. As pointed out by Iwata et al. (1996), this arrangement suggests that the ISP may have arisen as a soluble periplasmic electron carrier that became anchored to the membrane and recruited into the complex to improve efficiency of electron transfer. Another advantage in the case of a bacterial complex could be in preventing loss through a leaky outer membrane.

The first evidence for mobility of the ED came from the poor order (high B-factor, unclear electron density) of this protein in crystal structures (Xia et al. 1997) and the observation of different positions in different structures (Iwata et al. 1998; Zhang et al. 1998). There seemed to be a mechanistic requirement for movement, since none of the positions for the cluster seen in crystals were close enough to both the presumed site of the electron donor at the Q<sub>p</sub> site in cytochrome *b* and the electron acceptor, heme *c<sub>1</sub>*, to allow electron transfer between them at a kinetically competent rate. Various mutations, both spontaneous and site-directed, have also provided evidence for the importance of mobility (Tian et al. 1999; Darrouzet et al. 2000a; Obungu et al. 2000; Xiao et al. 2000; Ghosh et al. 2001; Darrouzet and Daldal 2002; Rajagukguk et al. 2007; Ma et al. 2008).

## III. Classification and Depiction of Different Positions of the ISP-ED

Different positions of the ISP-ED seen in the various mitochondrial *bc<sub>1</sub>* structures, in different crystal forms and with different inhibitors bound, have been reviewed (Berry and Huang 2011). The fixed, or *b* position, which is seen for example in all structures with stigmatellin bound, has the Rieske protein tightly docked in the binding crater on cytochrome *b*, with maximal buried surface area between cyt *b* and the ISP-ED and an H-bond from stigmatellin to cluster-ligand His161 of the ISP. This position is also seen in structures with H- or U- HDBT, atovaquone, or ascochlorin, which form

similar bonds to cluster-ligand histidine. And it is also seen, at lower occupancy, in the tetragonal crystals of bovine  $bc_1$  with no inhibitor. We assume that electron transfer from ubiquinone to the ISP occurs in this position, with ubiquinol in the place of the inhibitor.

In the presence of MOA<sup>1</sup> inhibitors, the tetragonal crystals (1sqb, 1sqq, 1sqj) disengage the cluster-bearing end of the ISP-ED from the binding crater by about 4 Å. Since this state promoted by MOA inhibitors is known as the released state, we have called this the released position. But the ISP-ED is present here at low occupancy as judged by the cluster's Fe anomalous signal, and in fact the truly released ISP-ED are the majority that we don't see in these crystals because they occupy a large number of different positions in very low occupancy. This ensemble of invisible positions is assumed to include some that are competent for electron transfer to cyt  $c_1$ . Nonetheless, the position close to cyt  $b$ , that is modeled in the structures of these crystals in the presence of MOA inhibitors, is in fact "released" from its tight binding to cyt  $b$  as indicated by a decreased number of H-bonds and decreased buried surface area between the ISP-ED and cyt  $b$ , compared to the fixed position (Esser et al. 2006), concomitant with its 4 Å retraction of the cluster tip from the binding crater.

This released position is still too far (26 Å) from cyt  $c_1$  for kinetically competent delivery of the electron. Other structures show the cluster within electron transfer (<14 Å) distance of heme  $c_1$ , in what has been called the  $c_1$  or "distal" position(s). These are found in the chicken crystals, either with MOA inhibitors or with no inhibitor (Zhang et al. 1998), and in the P6<sub>5</sub>22 bovine crystals (Iwata et al. 1998).

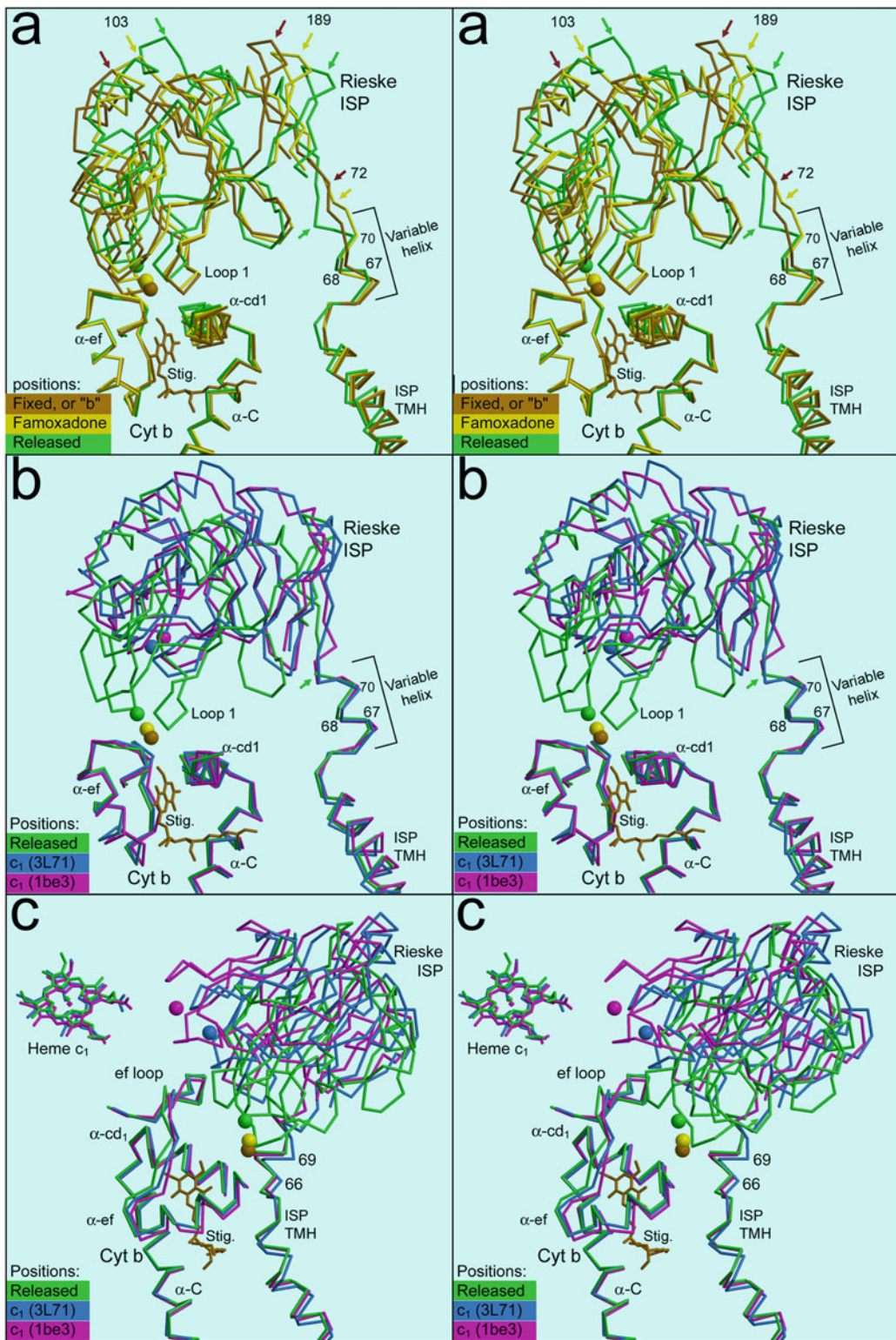
Factors governing the different positions seen in crystals, and the relation between these positions and the mobility required by the reaction, are not clear. Mechanisms invoking gated motion (or position) of the ISP to enforce the bifurcated reaction at the Q<sub>P</sub> site have been proposed (Link 1997; Brandt 1998; Esser et al. 2006), and it may be that

different inhibitors mimic different intermediates in the reaction cycle resulting in different positions of the ED.

We assume that electron transfer from ubiquinol occurs when the ISP is in the "fixed", or "b" position, H-bonded to ubiquinol at the Q<sub>P</sub> site by cluster-ligand His161, much as it is H-bonded to stigmatellin, nHDBT, or atovaquone in various crystal structures. The second electron may be transferred to cyt  $b_L$  either subsequently (Link 1997; Junemann et al. 1998) or concertedly (Snyder et al. 2000), leaving the reduced ISP H-bonded to the oxidized ubiquinone in a product complex similar to that giving rise to the  $gx = 1.8$  epr signal observed when membranes containing endogenous ubiquinone are treated with ascorbate to reduce the ISP (Ding et al. 1992). This complex would dissociate with some rate/frequency. Alternatively, the semiquinone may dissociate after the first electron is transferred to the cluster, and move to a more proximal location from which the second electron is transferred to cyt  $b$  (Crofts et al. 1999; Victoria et al. 2013). In either case the reduced, protonated ISP is released, allowing it to transfer the electron to cyt  $c_1$  and release one proton on the P side of the membrane.

While the static X-ray structures do not describe the actual path of movement, the positions that have been seen in various crystals can be assumed to be accessible and can be used to map out a possible path for the ISP-ED between its position docked at the Q<sub>P</sub> site on cyt  $b$  and that with the cluster in proximity of heme  $c_1$  where the electron is delivered. In this we are also guided by a "steered" molecular dynamics simulation of the movement reported by Izrailev et al. (1999).

Figure 11.1a illustrates in stereo the first part of the path of the ISP-ED from the fixed or  $b$  position to the  $c_1$  position. This is the movement from the fixed position (brown trace) seen for example in the presence of stigmatellin, to the "released" position (green) seen in the tetragonal beef crystals in the presence of MOA inhibitors. This is a



see-saw or rotational motion, with the cluster end of the molecule moving away from its docking position in *cyt b* by about 4 Å while the opposite end, to which the linker is attached, moves toward the membrane. This allows the helix in the linker to grow, and take up the slack, as discussed in the next section. The Fe<sub>2</sub> atom of the cluster is modeled as a sphere of the same color as the respective trace, showing how far the cluster moves.

Also shown in Fig. 11.1a is an intermediate position seen with the famoxadone-like inhibitors, JG144 in this case (yellow trace). This class of inhibitors does not form an H-bond with the ISP but for reasons that are not well understood results in fixing the ISP near *cyt b*. The cluster-ligand His161 (which H-bonds the inhibitor in structures with stigmatellin) H-bonds Y279 of *cyt b*. Before it was ever observed in an actual x-ray structure, this H-bond was seen at one point along the simulated trajectory of steered molecular dynamics (Izrailev et al. 1999). This more distal H-bonding partner pushes His166 of the ISP, and cluster-bearing loop 2 to which it is attached, farther from *cyt b*. Loop 1 maintains essentially the same interactions with *cyt b*. This results in pivoting the ED about a point in loop 1 by about 10°, in turn resulting in movement of the opposite end (around residue 103 or 106) of the ISP by about 6 Å between the *cyt b* position and the famoxadone position, while Fe<sub>2</sub> of the cluster moves away from *cyt b* by a little over 1.5 Å.

Figure 11.1b and c illustrate the motion from the released position of the tetragonal crystals (green) to the “*cyt c<sub>I</sub>*” position of the chicken crystals (blue) and the extreme *cyt c<sub>I</sub>*

position of the hexagonal beef crystal 1be3 (magenta). Figure 11.1b is a side view with the cluster on our left and the linker on the right, in the same orientation as Fig. 11.1a. However, the motion is different from the seesaw motion in that figure, as here the rotation is about an axis that passes near the attachment point of the linker (approximately in the plane of the paper). It thus does not involve any significant change in length of the tether, as can be seen in Fig. 11.1b, while the cluster (large sphere) rotates upwards and away from the viewer. The hinge for this motion is mainly in residues 72 and 73, with flexion but very little translation of these residues. Figure 11.1c shows the same structures, but looking roughly down the rotation axis, with the cluster toward the viewer and the linker attachment in the rear. Notice how Fe<sub>2</sub> of the cluster swings upward and to the (viewer’s) left to face the heme of *cyt c<sub>I</sub>* (The Fe<sub>2</sub> atom for the fixed and famoxadone positions are included in Fig. 11.1b and c for completeness).

Unlike mitochondrial cytochrome *c* and other “large” Class I cytochromes, which have a loop covering the heme propionates, cytochrome *c<sub>I</sub>* has the propionates exposed (Zhang et al. 1998). They are approached by the cluster-bearing tip of the ISP in the *c<sub>I</sub>* positions, and in the structure 1be3 there is a hydrogen bond between the cluster-ligand His166 and the “D” heme propionate. The heme is also exposed (as in other class I cytochromes), at the surface of the heme binding cleft, where the C pyrrole ring protrudes. This is where it interacts with its acceptor, cytochrome *c* (Broger et al. 1980; Stonehuerner et al. 1985; Hunte et al.

←  
 Fig. 11.1. Trajectory of the ISP-ED from the Q<sub>p</sub> site to *cyt c<sub>I</sub>*. Illustrated by stereo views of crystal structures with the ISP-ED in different positions. (a) In moving from the fixed position to the released position, the ED rotates clockwise lifting the Fe<sub>2</sub>S<sub>2</sub> cluster (round ball at position of Fe<sub>2</sub>) out of the Q<sub>p</sub> site, while the variable helix in the linker takes up the slack by adding another turn. Arrows along the upper edge indicate the same residue in different positions. (b) Viewed from the same orientation as in (a), the ISP rotates about an axis roughly horizontal in the plane of the picture, turning the cluster to face *cyt c<sub>I</sub>* without affecting the variable helix. (c) shows the same motion as (b) viewed along the rotation axis to illustrate the path of the cluster. The structures used are 1sqx (stigmatellin), 2fyu (famoxadone), 1sqb (beef azoxystrobin), 3 L71 (chicken azoxystrobin), 1be3 (beef P6<sub>5</sub>22) for fixed, famoxadone, released, *c<sub>I</sub>*, and extreme *c<sub>I</sub>* positions. Stigmatellin from 1sqx is included in all three views to indicate the Q<sub>p</sub> site.

2002). Thus rather than interacting with its donor and acceptor using the same surface, as the ISP does, and requiring movement to disengage from the donor before interacting with the acceptor, cyt  $c_1$  can interact with both simultaneously to mediate electron transfer from the ISP to cyt  $c$ .

The ef-loop, which has been considered a barrier obstructing movement between the  $b$  and  $c_1$  positions (Darrouzet and Daldal 2002) or a support stabilizing the  $c_1$  position (Berry et al. 2013), has also been rendered in Fig. 11.1c. The effect of “mobility” mutants in the ef loop will be discussed below in relation to mutations in the neck region.

The ED is often referred to as the “head” of the Rieske ISP, with the linker as the “neck”. To extend this analogy we can describe these two steps of the motion in cartoon form as first (Fig. 11.1a) lifting the head to raise the snout out of the binding crater where it receives the electron from the Q<sub>P</sub> site, and then (Fig. 11.1c) turning the head (twisting the neck) to face heme  $c_1$ , where the electron will be deposited.

It can be assumed that the Rieske ISP of the b<sub>6</sub>f complex also undergoes movement to deliver electrons from the QP site to cytochrome  $f$ , as again the distance is too great to be traversed by direct electron transfer (Kurusu et al. 2003). Also, the rate of electron transfer from the QP site to cyt  $f$  is sensitive to viscosity (Yan and Cramer 2003). Despite large differences in the linker region of the ISP as compared with the bc<sub>1</sub> complex (discussed in the next section), similar positions of the ISP have been observed.

The three b<sub>6</sub>f structures with the stigmatellin analog TDS (1Q90, 2E76, 4H13) have the ED tightly docked in its binding crater with cluster ligand His129 H-bonded to the inhibitor, as in the fixed or “ $b$ ” position of the bc<sub>1</sub> complex. The Fe<sub>2</sub>S<sub>2</sub> cluster and cluster-bearing loops in these structures superimpose well with mitochondrial bc<sub>1</sub> structures in the presence of stigmatellin, when the structures are superimposed based on cytochrome  $b$ .

Structures without inhibitor (1vf5, 2e74, 2e75, 2d2c, 2zt9, 4h0L, 4 h44, 4ogq)

have the cluster a little farther from cyt  $b$ , as in the released position of the tetragonal beef crystals. Specifically, the Fe<sub>2</sub> atom of the cluster in the structures with an empty Q<sub>P</sub> site is 3.5–4.0 Å from its position in 4H13 (with TDS). There are no structures as yet illustrating the position in which the b<sub>6</sub>f ISP transfers an electron to cytochrome  $f$ . However a recent structure (4i7z) of the cyanobacterial complex treated with anionic phospholipids has a disordered ISP-ED, which is interpreted as meaning that it is fully released from cytochrome  $b$  and distributed over a large number of distal positions with low occupancy in any one position (Hasan et al. 2013).

The electron acceptor from the b<sub>6</sub>f ISP, cytochrome  $f$ , bears little similarity to cytochrome  $c_1$  other than presence of a c-type heme and a C-terminal membrane anchor. Superposition of cytochromes bc<sub>1</sub> and b<sub>6</sub>f by the transmembrane helices of cyt  $b$ /SU<sub>IV</sub> places the heme iron of cyt  $f$  18 Å from that of cyt  $c_1$ , but both c-type hemes are about the same distance from the Fe<sub>2</sub>S<sub>2</sub> cluster docked in the  $b$  position. While the heme of cyt  $c_1$  faces the ISP edge-on with its propionates, that of cyt  $f$  is flat-on with its axial ligand His26 (His25 in *Chlamydomonas*) directed toward the ISP.

Rather than being inserted into a binding cleft perpendicular to the protein surface, the heme of cyt  $f$  is lying nearly flat on the surface opposite the ISP, partly covered by the N-terminal helix and the other axial ligand Tyr1. The axial ligand, His26, is buried under the heme as seen from this side but is near the surface on the side facing the ISP. It has been estimated that a rotation of the ISPED by 25°, with 14 Å movement of the cluster, would bring the cluster into a favorable position for electron transfer to the heme of cyt  $f$  via Leu27 and His 26 (Kurusu et al. 2003).

Plastocyanin is believed to interact with the hydrophobic patch around Tyr1 (Ubbink et al. 1998; Diaz-Moreno et al. 2005). Thus it is likely that cyt  $f$ , like cyt  $c_1$ , has separate binding sites for its electron donor and acceptor allowing it to interact with both simultaneously, the heme acting as an electron wire between the ISP and plastocyanin.



#### IV. Conformational Changes in the ISP Hinge Region

There is no indication of conformational flexibility in the transmembrane helix anchor of the ISP. Assuming for now (but see next section) that the extrinsic domain moves as a rigid body, the mobility of that body thus results from conformational changes in the short linker region, connecting it to the transmembrane helix. As described in the previous section, in *bc<sub>1</sub>* complexes this region not only provides a flexible hinge but also takes up slack by adding a turn to the variable helix as the ED rotates. A possible function for this helix in “spring-loading” the ED to facilitate leaving the *b* position has been discussed (Berry et al. 2000, 2013; Crofts et al. 2002).

Having accurate atomic models for the *bc<sub>1</sub>* complex with the ISP in a wide range of positions allows us to pinpoint the region of flexibility in the neck and describe the conformational changes taking place there. Here we use the sequence numbering of the mature vertebrate ISP. By convention the yeast protein uses the numbering of the apoprotein, which adds 20 to the number of each residue relative to the vertebrate sequences. Proteobacterial (*Rhodobacter* and *Paracoccus*) proteins have shorter N-termini even than the mature mitochondrial proteins, and the residue numbers in the conserved neck region are smaller by 25 (Rb.) or 20 (Pc) than the corresponding vertebrate residues. Table 11.1 provides the vertical alignment of sequences for which structures are available.

The transmembrane helix ends at about residue 61 in the vertebrate numbering. The stretch between 61 and 66, although appearing unstructured when the subunit is depicted by itself, is packed into a dense structure with cytochrome *b* from both dimers, called the “clamp” or “vise” region, and does not vary significantly in the different structures. Figure 11.2a shows these contacts in a stereo ribbon diagram. The vise consists of the conserved di-glycine at 167,168 in *cyt b* of the monomer with which the extrinsic domain interacts, and

Table 11.1. Vertical sequence alignment of residues in and around the ISP neck.

SS <sup>a</sup>	Beef	Chick	Yeast	Rb.s	Rb.c	Pc.d
HH	S56	T56	E76	W32	W32	W36
HH	Q57	Q57	T77	P33	P33	T37
HH	F58	F58	F78	L34	L34	L38
HH	V59	I59	I79	I35	I35	V39
HH	S60	S60	S80	N36	N36	N40
HH	S61	S61	S81	Q37	Q37	Q41
--	M62	L62	M82	M38	M38	M42
--	S63	S63	T83	N39	N39	N43
--	A64	A64	A84	P40-S <sup>b</sup>	A40	P44
--	S65	S65	T85	S41	S41	S45
GH	A66	A66	A86L <sup>c</sup>	A42-SΔ <sup>d</sup>	A42	A46
GH	D67	D67	D87	D43  Δ	D43	D47
GH	V68	V68	V88	V44-SΔ	V44P <sup>e</sup>	V48
-H	L69	L69	L89	Q45	K45P	Q49
-T	A70	A70	A90	A46-S	A46P	A50
-T	M71	L71	M91	L47	M47P	L51
-T	S72	S72	A92	A48	A48P	A52
--	K73	K73	K93	S49	S49P	S53
EE	I74	I74	V94	I50	I50	I54
EE	E75	E75	E95	F51	F51	Q55

<sup>a</sup>SS: Secondary structure assignment by DSSP algorithm (Kabsch and Sander 1983). The first column gives the assignment (H  $\alpha$ -helix, G  $3_{10}$  helix, T turn, E sheet, - random coil) for structure 1PPI, in the “*b*” position, while the second is for structure 3L70 in the “*c<sub>1</sub>*” position

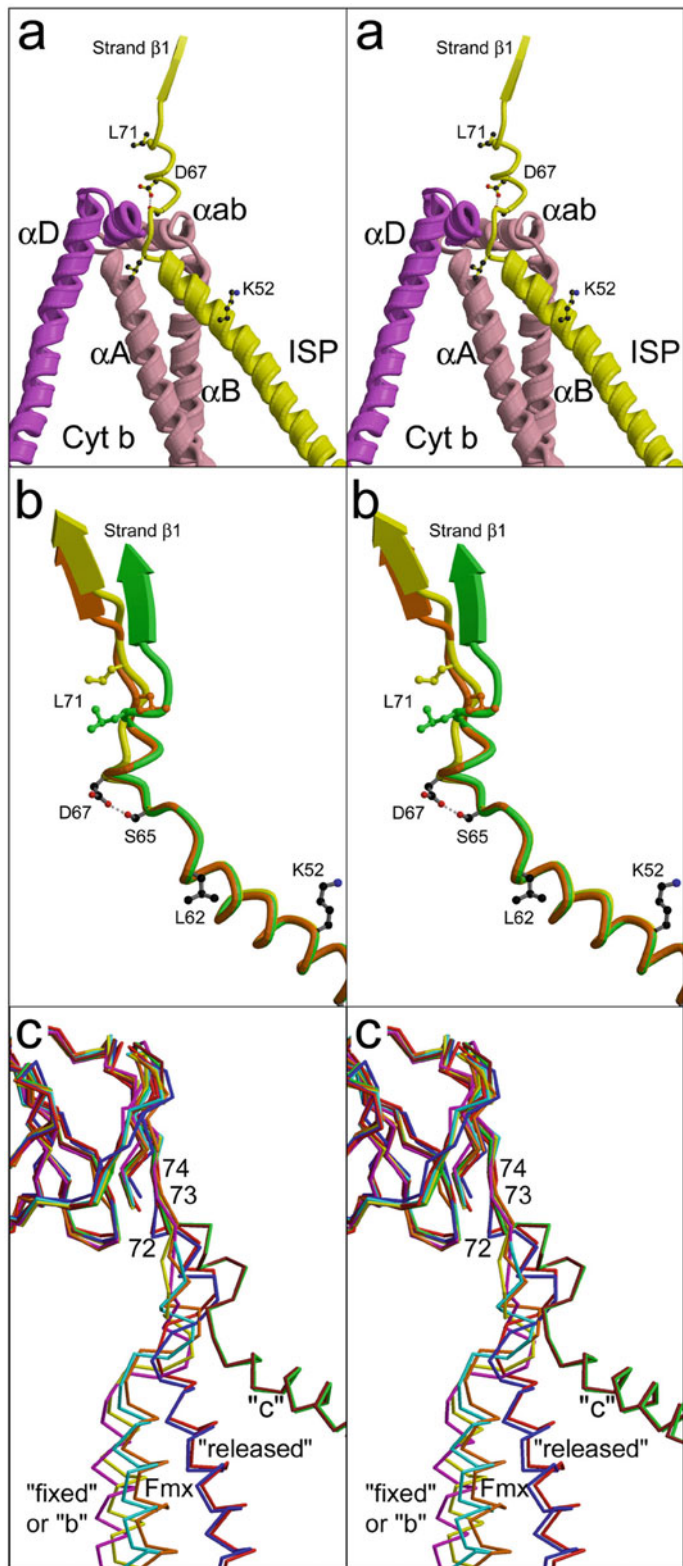
<sup>b</sup>S: Cys mutants of Tian et al. (1999)

<sup>c</sup>L: A86L mutation of Obungu et al. (2000)

<sup>d</sup>Δ: residues deleted in ΔADV mutant of Tian et al. (1998)

<sup>e</sup>P: residues mutated to Pro or Gly in the 6-Pro, 6-Gly mutants of Daldal and coworkers (Darrouzet et al. 2000a)

residues 73–75 (at the turn before the start of helix  $\alpha$ B) of the other monomer. Van-der-Waals contacts and H-bonds hold this stretch immobile during the movement of the ED. Given this entrapment in the *cyt b* dimer interface, it may seem surprising that the ISP can be removed by fairly gentle treatment, and reconstituted into ISP-depleted complex to restore activity, but this has been demonstrated by a number of groups (Trumpower and Edwards 1979; Trumpower et al. 1980; Hovmoller et al. 1981; Engel et al. 1983; Shimomura et al. 1984; Gonzalez-Halphen et al. 1991; Valkova-Valchanova et al. 1998).



In Fig. 11.2a there appears to be a gap through which the neck could pop out of the vise. Alternatively, the ISP-depleted complex may reversibly dissociate into monomers (Musatov and Robinson 1994) that can bind the ISP on reassembly. That reconstitution does in fact involve specific reinsertion of the transmembrane helix is supported by the fact that a transmembrane fragment inhibits (Gonzalez-Halphen et al. 1991), and by the failure of the soluble fragment to reconstitute activity (Valkova-Valchanova et al. 1998).

An H-bond between the side chains of conserved pair Ser(Thr)65 and Asp67 holds residues 65, 66, and 67 in a non-helical loop which also does not vary between structures. It may also hold residues 66 and 67 in a conformation to seed formation of a helix, as these two residues are shown by secondary structure analysis to be part of the helix in either the condensed or stretched conformation of the neck.

Figure 11.2b shows a superposition of the ISP backbones from chicken crystals in the presence of azoxystrobin, famoxadone, and stigmatellin, with the superposition based on the transmembrane helices of *cyt b*. Comparing the three structures, the first residue that shows significant movement is 69. The motion consists of stretching the neck by partially unwinding a variable helix involving residues 66–71. In the presence of azoxystrobin, when the cluster is away from the  $Q_P$  site in the *c* position, the neck is shortest, with  $\alpha$ -helical H-bonds reaching as far as residue 71. In the presence of stigmatellin, when the cluster-bearing tip of the ISP is deep in the binding crater and binding to stigmatellin in the  $Q_P$  site, the neck is maximally extended. In this position only one  $3_{10}$  H-bond remains (between residues 65 and 68),

as noted for the yeast structure with stigmatellin (Hunte et al. 2000). Residues 69–71 have been pulled out of the helix by stretching.

Essentially all the flexibility of the neck is exhibited by residues 69–72, with everything from residue 73 on moving as a rigid body with the extrinsic domain. This can be shown by superimposing the ISP from different structures based on the extrinsic domain as in Fig. 11.2c. Residue 74 is the beginning of the first strand of beta sheet 1, and 72–73 form H-bonds with Trp91 and Arg92 of the globular domain, both in the structure of the soluble fragment Irie (Iwata et al. 1996) and in the  $bc_1$  complex. Stretching of the helix occurs between the “fixed” and “released” positions, while the much larger movement of the ED between the released and  $c_I$  positions is accommodated by rotation about bonds in the range 72–73. This implies that the full energy of formation of the helix contributes to moving the cluster from its bound “*b*” position to the position in the released state of the tetragonal crystals (a distance of only 4 Å).

The stretching and “melting” of the helix is quantitatively documented in Table 11.2, which classifies the available mitochondrial  $bc_1$  structures into (i) fixed, (ii) famoxadone, (iii) released, or (iv)  $c_I$  positions. The length of the neck, measured as distance from  $C^\alpha$  of residue 65 to  $C^\alpha$  of residue 74, is provided in the first numerical column. The range is from 17 Å in the released or  $c_I$  position to 22–24 Å in the *b* position. Among the structures with the *b*-position, the length varies from 21.5 to 24.5, probably due to different crystal contacts. Of these the longest necks are in the chicken crystals, which have no significant crystal contacts on the ISPED.

←  
 Fig. 11.2. Details of the linker segment of the  $bc_1$  Rieske ISP. (a) Ribbon diagram showing how the ISP is clamped between the two monomers of *cyt b*. One side of the clamp consists of the conserved di-glycine turn at 167, 168 (between helix  $cd_2$  and D) in *cyt b* of the monomer with which the extrinsic domain interacts, and residues 73–75 (at the turn before the start of helix  $\alpha B$ ) of the other *cyt b* monomer. (b) linker region of the ISP of chicken  $bc_1$  in three different positions superimposed based on *cyt b*. Yellow, position (3h1h). Brown, famoxadone (3 L74). Green,  $c_I$  position (3 L71). Side chains of K52, L62, S65, and D67 are shown for 3 L71, and L71 is shown for each. (c) Superposition of ISP based on the ED. Residues from 73 on move as a rigid body with the ED.

Table 11.2. ISP “Neck” length and H-bond distances in structures with different ISP ED positions.

	C <sup>α</sup> –C <sup>α</sup>	N->O								
PDBID	65–74	68–65*	69–65	69–66*	70–66	70–67*	71–67	71–68*	72–68	72–69*
Position: stigmatellin										
3h1i	24.48	3.82								
3h1j	24.24	3.34	4.41							
1 pp9	21.41	3.00	3.42	3.38	3.59	3.47	–	–	–	–
1ppj	21.78	2.91	3.49	3.59	3.93	3.95	–	–	–	–
2a06	21.73	3.03	3.63	3.51	–	–	–	–	–	–
1sqx	22.75	3.47	3.92	4.01	–	–	–	–	–	–
3cx5	22.12	3.18	3.97	4.17	–	–	–	–	–	–
1 kb9	22.18	2.95	3.78	3.88	–	–	–	–	–	–
Position: PHDBT										
1p84	22.29	3.04	3.75	3.91	–	–	–	–	–	–
Position: ascochlorin										
3h1L	24.40	4.05	–	–	–	–	–	–	–	–
Famoxadone, fenamidone, JG144										
3 174	21.05	2.91	3.00	3.30	3.13	3.34	–	–	–	–
3 175	21.15	2.83	3.00	3.35	3.13	3.38	–	–	–	–
2fyu	21.02	2.73	3.26	3.67	3.85	4.48	–	–	–	–
Released position: MOA inhibitor in tetragonal crystals										
1sqb	16.91	2.75	3.18	3.64	3.29	4.18	4.08	3.13	3.74	3.58
1sqq	16.13	2.85	2.96	3.47	3.22	4.46	4.52	3.30	4.06	3.61
1sqq	17.97	2.64	2.87	3.78	3.55	4.38	4.02	3.00	4.34	2.95
c <sub>1</sub> position: empty site or MOA (or int position: 1bgy)										
1be3	13.72	3.26	2.68	3.63	3.18	3.54	3.89	3.65	3.37	2.50
1bgy	15.09	2.96	2.85	3.55	2.62	3.44	4.00	2.81	3.42	3.31
3h1h	16.79	2.84	2.98	3.19	2.96	3.60	3.91	2.98	3.30	2.90
3h1k	16.79	3.18	2.94	3.44	3.11	2.72	3.23	3.72	3.31	3.22
3 170	16.84	2.72	2.96	3.39	2.87	3.36	3.66	2.87	3.32	2.82
3 171	16.86	2.72	2.99	3.47	2.96	3.52	3.81	2.94	3.38	2.72
3 172	17.01	2.98	2.83	3.13	2.99	3.12	3.51	3.59	3.55	2.95
3 173	16.79	2.65	2.87	3.53	2.99	3.29	3.86	3.04	3.50	2.78
3tgu	17.12	3.06	2.85	3.29	2.95	3.25	3.67	3.19	3.65	2.77

The first column lists the structures used, arranged by the position of the ED. The second column gives the overall neck length, measured from a point in the transmembrane helix to a point in the ED. Then for each residue from 65 to 69, the length of two putative hydrogen bonds, one (3<sub>10</sub>, marked\*) from the amide N of the residue 3 ahead to the carbonyl of that residue, and one ( $\alpha$ -helix) from the N of the residue 4 ahead is given. A typical  $\alpha$  – helical H-bond is  $\sim 2.7$  Å. Values over 3.5 Å are not compatible with a strong H-bond, and values over 4.5 Å are not shown. For the yeast structures, the residues aligning with these vertebrate residues were used

The shortest are the beef orthorhombic crystals. In these crystals there are contacts (described in Bowman et al. 2004) which are likely to be pushing the back end of the ISPED down, shortening the neck. Notably

the cluster positions, and the residues around the clusters, superimpose very closely in all these *b*-position structures (Fig. 1 of Berry et al. 2013). It seems that in the *b*-position the ISPED is anchored by interactions of

the cluster binding domain with the binding crater and pivots about that contact, while the other end is not much constrained by the stretched-out linker, accounting for the variability in its length in this position.

Table 11.2 also lists the lengths of potential helical H-bonding pairs in the variable helix. As mentioned above only the single  $3_{10}$  bond between 65 and 68 remains in the *b* position, and that is really stretched out of existence in the longest necks (3.82 in 3h1i, 4.05 in 3h1L). As the ED moves to the released or  $c_I$  position, H-bonds to the carbonyl O's of residues 66–69 begin to form. Distances are listed for each of these from the residue three ahead in the sequence ( $3_{10}$  helical bond) as well as the residue four ahead ( $\alpha$ -helical). In many cases the two are nearly equal, indicating the helix is still more stretched than a canonical  $\alpha$ -helix.

The neck region has been subjected to extensive site-directed mutagenesis to probe its role in the function and assembly of the complex. While these mutations were originally conceived and discussed mainly with respect to their effect on flexibility of the linker, it has been argued (Berry et al. 2013) that they can better be rationalized in terms of the tension exerted by the tether on the extrinsic domain, pulling it away from its binding crater on the surface of cytochrome *b*. As discussed above, docking of the ISP in the *b* position results in dissolution of all but one turn of the  $\alpha$ -helix that is present in the linker in the  $c_I$  position or “released” state. This partial melting of the helix requires energy, which must detract from the energy of binding the ISP at the *b* position.

The three movable residues in the helix, 69–71, are usually Leu, Ala, or Lys69; Ala70; and Met or Leu71. These four amino acids are among the five with the highest helical propensity (O’Neil and DeGrado 1990), providing a relatively strong force for helix formation and the resulting dissociation of the ISP from its *b* position. Substitution of these helical residues with low-helical-propensity Gly or Pro (Darrouzet et al. 2000a) or Ile (Obungu et al. 2000), or insertion of additional Ala residues (Darrouzet et al. 2000b;

Obungu et al. 2000), results in a partially or completely inactive complex.

Replacement of these residues individually with Ala (which has a high helical propensity) had no effect (Darrouzet et al. 2000a), ruling out the need for a specific side chain. Insertion of extra residues in the neck led to loss of function. The 6-Pro or 6-Gly substitutions regained function by spontaneous loss of three of the residues to give a shorter than normal chain. This would not be expected if the defect is due to loss of flexibility in the 6-Pro mutant, but is consistent with the deletion overcoming excessive length due to failure of the Pro or Gly residues to form a helix.

Investigation of the 6-Pro substitution by EPR spectroscopy and flash kinetics indicated that the  $[\text{Fe}_2\text{S}_2]$  cluster is present in the  $\text{Q}_P$  site and unable to transfer electrons to cyt  $c_I$  (Darrouzet et al. 2000a). EPR spectra supported that position for the 6-gly (Darrouzet et al. 2000a) and alanine insertion (Darrouzet et al. 2000b) mutants as well. This is consistent with stabilization of the ISP at its docking site on cyt *b* as a result of the reduced tension due to low helix-forming propensity or the increased length of the neck.

On the other hand the “box 1” mutations (in the cluster-bearing loop 1 of the ISP) around the first His cluster ligand (Liebl et al. 1997) (140 and 142 in the vertebrate sequence, 134 and 136 in Rhodobacter) or mutations in the ef loop of cyt *b* (Darrouzet and Daldal 2002, 2003), produce results consistent with destabilizing the *b* position relative to the  $c_I$  position, such as weak or no interaction with quinone at the  $\text{Q}_P$  site and rapid re-reduction of cyt  $c_I$  in the presence of myxothiazol. While either class of mutation is deleterious, they apparently counterbalance each other, so that 2nd site revertant to the box 1 mutations L136G or H arise in the neck region, while the +1Ala neck mutation reverted via a mutation in the ef loop (Darrouzet and Daldal 2002). Such complementary balancing interactions, together with complementary effects on the apparent midpoint potential of the ISP cluster- from

about 320 mv in wild type to 370, 410, and 460 mv in the +Ala, +2Ala, and 6Pro neck mutants (Darrouzet et al. 2002), or 255–270 mv in T288 ef-loop mutants (Darrouzet and Daldal 2002, 2003) – can be rationalized in terms of relative stabilization of the *b* vs *c<sub>1</sub>* positions (Berry et al. 2013). While the ef loop and box 1 residues affect the equilibrium because they are involved in different interfaces in the two states, the neck residues are proposed to affect the equilibrium by adjusting the tension of the tether.

Deletion of up to five residues in the neck was tolerated but with considerably decreased activity and with increased tendency to lose the ISP during purification (Darrouzet et al. 2000a). Deletion of the conserved Asp making the H-bond with Ser had a similar effect (Obungu et al. 2000). Even with no helix, it seems unlikely that a neck shortened by five residues would be compatible with the *b* position, unless the neck binds higher up in the cyt *b* clamp by a few residues. Such non-specific binding might result in easy dissociation, as might loss of the turn enforced by the Asp-Ser H-bond.

One series of neck mutations which originally seemed to demonstrate the need for movement may need to be re-evaluated in light of current knowledge of the structures. Tian et al. (1999) substituted pairs of cysteine residues in the *Rb.s.* ISP in the region 40–46 (corresponding to 64–70 in the bovine sequence, see Table 11.1). The mutant with cysteines at 40 and 42 was inactive under oxidizing condition, and that with 42 and 44 had reduced activity. Those with 44 and 46, or 42 and 46, were unaffected. Now it is clear that 40 and 42 are in the immobile region within the cytochrome *b* clamp, so the effect was more likely due to interference with binding than to decreased flexibility. The two mutants involving 46 would cross-link the variable helix and prevent it from extending, but given the results with deletion mutants this would not be expected to abolish activity. Notably all three showed loss of ISP from the *bc<sub>1</sub>* complex upon purification (Tian et al. 1999).

Given the requirement of the neck residues in the *bc<sub>1</sub>* complex for high helical propensity and defined length, it is surprising that the linker in the *b<sub>6f</sub>* ISP consists mainly of glycines and is insensitive to substitution with proline or changes in length. The mutations which change the length of the linker do affect sensitivity to inhibitors in a way consistent with the idea that a long linker favors binding to inhibitors in the Q<sub>P</sub> site, but clearly there is no need for tension from the tether to facilitate dissociation of the product complex during turnover. It could be that compensating mutations in the interface between cyt *b<sub>6</sub>*/SU<sub>IV</sub> and the ISP destabilize the *b* position. In this regard the “box 1” region of the ISP is exactly the same in the *b<sub>6f</sub>* and *bc<sub>1</sub>* complexes, but in fact the ef loop shows the same mutation as the L286F mutation found in a revertant of the +1Ala mutation in *Rb.c.*: In the *b<sub>6f</sub>* complex the corresponding residue is F69 in subunit IV. This could be a contributing factor.

## V. Does the ISP-ED Undergo Internal Conformation Changes?

In describing the original high-resolution structure of bovine Rieske fragment, Iwata et al. (1996) emphasized the “high stability . . . maintained both through a strong salt bridge/hydrogen-bonding network as well as through the presence of a disulfide bridge”. In most mitochondrial *bc<sub>1</sub>* structures in which the ISP is sufficiently ordered to discriminate, it appears that the structure is the same as in the bovine soluble fragment, regardless of the position of the ISP-ED or the presence of inhibitors. This suggests that the ED moves as a rigid body during electron transfer.

There were some early indications to the contrary, however (Iwata et al. 1998, 1999). In structure 1BGY the cluster binding fold was found rotated by 6° relative to the base fold, resulting in 2 Å displacement of the cluster. In this structure the peptide bond linking conserved proline P175 with the previous residue was modeled in a *cis* config-

uration, where the soluble fragment and the other  $bc_1$  structures have *trans*.

No other structures of mitochondrial ISP show significant deviation from the structure of the high-resolution ISP fragment (1rie), and the diffraction data were never released for structure 1BGY so it is impossible to evaluate the evidence. It is tempting to discount it as an artifact of refining a moving target: the cluster-bearing tip is most ordered when contacting cyt *b* in the fixed position, while the end to which the linker is attached is most ordered in the released and  $c_1$  positions, when the linker is short and helical. Thus given a mixture of positions, the observed density might shift between them as you go from one end of the ED to the other. The ISP of 1BGY was not in the fixed or released position but in a unique “int” position, but the same principle could apply if there is some heterogeneity in its position.

Interestingly, the high resolution structure (1RFS, 1.83 Å) of the  $b_6f$  Rieske protein (Carrell et al. 1997) has the residue corresponding to P175 terminating a *cis* peptide as in the 1BGY Rieske. The soluble Rieske fragment from a cyanobacterium, *Thermosynechococcus elongatus* (3AZC, 2.0 Å), also has a *cis* peptide here (Veit et al. 2012), while that from *T. thermophilus* (1NYK, 1.3 Å) has a *trans* peptide in this place (Hunsicker-Wang et al. 2003). Structures of the entire  $b_6f$  complex are evenly divided as to whether this should be a *cis* peptide in the  $b_6f$  protein. However, given the lower resolution of these structures and the relatively high B factors of the ISP-ED in the complex due to its mobility, this should probably not be taken as evidence of *cis* – *trans* conformational switching in the protein.

There is some evidence for proline isomerization, if not large scale conformational change, in the *T. thermophilus* ISP. Markley and coworkers (Hsueh et al. 2013) used NMR to look at possible changes in conformation with oxidation and reduction of the soluble *T. thermophilus* Rieske fragment, and found evidence suggesting that the residues P152 and P170, corresponding to vertebrate P159 and

P175, might go from *trans* in the oxidized state to *cis* in the reduced state. However no evidence was seen by NMR for a large-scale conformational change of the protein.

## Acknowledgements

The authors were supported by a start-up grant from the State University of New York to EAB during the time this manuscript was prepared.

## References

- Berry EA, Huang LS (2011) Conformationally linked interaction in the cytochrome bc(1) complex between inhibitors of the Q(o) site and the Rieske iron-sulfur protein. *Biochim Biophys Acta* 1807:1349–1363
- Berry EA, Guergova-Kuras M, Huang LS, Crofts AR (2000) Structure and function of cytochrome bc complexes. *Annu Rev Biochem* 69:1005–1075
- Berry EA, De Bari H, Huang LS (2013) Unanswered questions about the structure of cytochrome bc<sub>1</sub> complexes. *Biochim Biophys Acta* 1827:1258–1277
- Bowman MK, Berry EA, Roberts AG, Kramer DM (2004) Orientation of the g-tensor axes of the Rieske subunit in the cytochrome bc<sub>1</sub> complex. *Biochemistry* 43:430–436
- Brandt U (1998) The chemistry and mechanics of ubihydroquinone oxidation at center P (Qo) of the cytochrome bc<sub>1</sub> complex. *Biochim Biophys Acta* 1365:261–268
- Broger C, Nalecz MJ, Azzi A (1980) Interaction of cytochrome c with cytochrome bc<sub>1</sub> complex of the mitochondrial respiratory chain. *Biochim Biophys Acta* 592:519–527
- Carrell CJ, Zhang H, Cramer WA, Smith JL (1997) Biological identity and diversity in photosynthesis and respiration: structure of the lumen-side domain of the chloroplast Rieske protein. *Structure* 5:1613–1625
- Crofts AR, Barquera B, Gennis RB, Kuras R, Guergova-Kuras M, Berry EA (1999) Mechanism of ubiquinol oxidation by the bc(1) complex: different domains of the quinol binding pocket and their role in the mechanism and binding of inhibitors. *Biochemistry* 38:15807–15826
- Crofts AR, Shinkarev VP, Dikanov SA, Samoilova RI, Kolling D (2002) Interactions of quinone with

- the iron-sulfur protein of the bc(1) complex: is the mechanism spring-loaded? *Biochim Biophys Acta* 1555:48–53
- Darrouzet E, Daldal F (2002) Movement of the iron-sulfur subunit beyond the ef loop of cytochrome b is required for multiple turnovers of the bc<sub>1</sub> complex but not for single turnover Qo site catalysis. *J Biol Chem* 277:3471–3476
- Darrouzet E, Daldal F (2003) Protein-protein interactions between cytochrome b and the Fe-S protein subunits during QH<sub>2</sub> oxidation and large-scale domain movement in the bc<sub>1</sub> complex. *Biochemistry* 42:1499–1507
- Darrouzet E, Valkova-Valchanova M, Daldal F (2000a) Probing the role of the Fe-S subunit hinge region during Q(o) site catalysis in *Rhodobacter capsulatus* bc(1) complex. *Biochemistry* 39:15475–15483
- Darrouzet E, Valkova-Valchanova M, Moser CC, Dutton PL, Daldal F (2000b) Uncovering the [2Fe2S] domain movement in cytochrome bc<sub>1</sub> and its implications for energy conversion. *Proc Natl Acad Sci U S A* 97:4567–4572
- Darrouzet E, Valkova-Valchanova M, Daldal F (2002) The [2Fe-2S] cluster E(m) as an indicator of the iron-sulfur subunit position in the ubihydroquinone oxidation site of the cytochrome bc<sub>1</sub> complex. *J Biol Chem* 277:3464–3470
- Diaz-Moreno I, Diaz-Quintana A, De la Rosa MA, Ubbink M (2005) Structure of the complex between plastocyanin and cytochrome f from the cyanobacterium *Nostoc* sp. PCC 7119 as determined by paramagnetic NMR. The balance between electrostatic and hydrophobic interactions within the transient complex determines the relative orientation of the two proteins. *J Biol Chem* 280:18908–18915
- Ding H, Robertson DE, Daldal F, Dutton PL (1992) Cytochrome bc<sub>1</sub> complex [2Fe-2S] cluster and its interaction with ubiquinone and ubihydroquinone at the Qo site: a double-occupancy Qo site model. *Biochemistry* 31:3144–3158
- Engel WD, Michalski C, von Jagow G (1983) Reconstitution of the ubiquinol: cytochrome c reductase from a bc<sub>1</sub> subcomplex and the 'Rieske' iron-sulfur protein isolated by a new method. *Eur J Biochem* 132:395–407
- Esser L, Gong X, Yang S, Yu L, Yu CA, Xia D (2006) Surface-modulated motion switch: capture and release of iron-sulfur protein in the cytochrome bc<sub>1</sub> complex. *Proc Natl Acad Sci U S A* 103:13045–13050
- Ghosh M, Wang Y, Ebert CE, Vadlamuri S, Beattie DS (2001) Substituting leucine for alanine-86 in the tether region of the iron-sulfur protein of the cytochrome bc<sub>1</sub> complex affects the mobility of the [2Fe2S] domain. *Biochemistry* 40:327–335
- Gonzalez-Halphen D, Vazquez-Acevedo M, Garcia-Ponce B (1991) On the interaction of mitochondrial complex III with the Rieske iron-sulfur protein (subunit V). *J Biol Chem* 266:3870–3876
- Hasan SS, Stofleth JT, Yamashita E, Cramer WA (2013) Lipid-induced conformational changes within the cytochrome b<sub>6</sub>f complex of oxygenic photosynthesis. *Biochemistry* 52:2649–2654
- Hovmoller S, Leonard K, Weiss H (1981) Membrane crystals of a subunit complex of mitochondrial cytochrome reductase containing the cytochromes b and c<sub>1</sub>. *FEBS Lett* 123:118–122
- Hsueh KL, Tonelli M, Cai K, Westler WM, Markley JL (2013) Electron transfer mechanism of the Rieske protein from *Thermus thermophilus* from solution nuclear magnetic resonance investigations. *Biochemistry* 52:2862–2873
- Hunsicker-Wang LM, Heine A, Chen Y, Luna EP, Todaro T, Zhang YM, Williams PA, . . . , Fee JA (2003) High-resolution structure of the soluble, respiratory-type Rieske protein from *Thermus thermophilus*: analysis and comparison. *Biochemistry* 42:7303–7317
- Hunte C, Koepke J, Lange C, Rossmannith T, Michel H (2000) Structure at 2.3 Å resolution of the cytochrome bc(1) complex from the yeast *Saccharomyces cerevisiae* co-crystallized with an antibody Fv fragment. *Struct Fold Des* 8:669–684
- Hunte C, Solmaz S, Lange C (2002) Electron transfer between yeast cytochrome bc(1) complex and cytochrome c: a structural analysis. *Biochim Biophys Acta* 1555:21–28
- Iwata S, Saynovits M, Link TA, Michel H (1996) Structure of a water soluble fragment of the 'Rieske' iron-sulfur protein of the bovine heart mitochondrial cytochrome bc<sub>1</sub> complex determined by MAD phasing at 1.5 Å resolution. *Structure* 4:567–579
- Iwata S, Lee JW, Okada K, Lee JK, Iwata M, Rasmussen B, Link TA, . . . , Jap BK (1998) Complete structure of the 11-subunit bovine mitochondrial cytochrome bc<sub>1</sub> complex. *Science* 281:64–71
- Iwata M, Bjorkman J, Iwata S (1999) Conformational change of the Rieske [2Fe-2S] protein in cytochrome bc<sub>1</sub> complex. *J Bioenerg Biomembr* 31:169–175
- Izrailev S, Crofts AR, Berry EA, Schulten K (1999) Steered molecular dynamics simulation of the Rieske subunit motion in the cytochrome bc(1) complex. *Biophys J* 77:1753–1768
- Junemann S, Heathcote P, Rich PR (1998) On the mechanism of quinol oxidation in the bc<sub>1</sub> complex. *J Biol Chem* 273:21603–21607
- Kabsch W, Sander C (1983) Dictionary of protein secondary structure: pattern recognition of hydrogen-bonded and geometrical features. *Biopolymers* 22:2577–2637



- Kurusu G, Zhang H, Smith JL, Cramer WA (2003) Structure of the cytochrome b6f complex of oxygenic photosynthesis: tuning the cavity. *Science* 302:1009–1014
- Liebl U, Sled V, Brasseur G, Ohnishi T, Daldal F (1997) Conserved nonliganding residues of the *Rhodobacter capsulatus* Rieske iron-sulfur protein of the bc<sub>1</sub> complex are essential for protein structure, properties of the [2Fe-2S] cluster, and communication with the quinone pool. *Biochemistry* 36:11675–11684
- Link TA (1997) The role of the ‘Rieske’ iron sulfur protein in the hydroquinone oxidation (Q(P)) site of the cytochrome bc<sub>1</sub> complex. The ‘proton-gated affinity change’ mechanism. *FEBS Lett* 412:257–264
- Ma HW, Yang S, Yu L, Yu CA (2008) Formation of engineered intersubunit disulfide bond in cytochrome bc<sub>1</sub> complex disrupts electron transfer activity in the complex. *Biochim Biophys Acta* 1777:317–326
- Musatov A, Robinson NC (1994) Detergent-solubilized monomeric and dimeric cytochrome bc<sub>1</sub> isolated from bovine heart. *Biochemistry* 33:13005–13012
- O’Neil KT, DeGrado WF (1990) A thermodynamic scale for the helix-forming tendencies of the commonly occurring amino acids. *Science* 250:646–651
- Obungu VH, Wang Y, Amyot SM, Gocke CB, Beattie DS (2000) Mutations in the tether region of the iron-sulfur protein affect the activity and assembly of the cytochrome bc(1) complex of yeast mitochondria. *Biochim Biophys Acta* 1457:36–44
- Rajagukguk S, Yang S, Yu CA, Yu L, Durham B, Millett F (2007) Effect of mutations in the cytochrome b ef loop on the electron-transfer reactions of the Rieske iron-sulfur protein in the cytochrome bc<sub>1</sub> complex. *Biochemistry* 46:1791–1798
- Shimomura Y, Nishikimi M, Ozawa T (1984) Isolation and reconstitution of the iron-sulfur protein in ubiquinol-cytochrome c oxidoreductase complex. Phospholipids are essential for the integration of the iron-sulfur protein in the complex. *J Biol Chem* 259:14059–14063
- Snyder CH, Gutierrez-Cirlos EB, Trumppower BL (2000) Evidence for a concerted mechanism of ubiquinol oxidation by the cytochrome bc<sub>1</sub> complex. *J Biol Chem* 275:13535–13541
- Stonehuerner J, O’Brien P, Geren L, Millett F, Steidl J, Yu L, Yu CA (1985) Identification of the binding site on cytochrome c1 for cytochrome c. *J Biol Chem* 260:5392–5398
- Tian H, Yu L, Mather MW, Yu CA (1998) Flexibility of the neck region of the Rieske iron-sulfur protein is functionally important in the cytochrome bc<sub>1</sub> complex. *J Biol Chem* 273:27953–27959
- Tian H, White S, Yu L, Yu CA (1999) Evidence for the head domain movement of the Rieske iron-sulfur protein in electron transfer reaction of the cytochrome bc<sub>1</sub> complex. *J Biol Chem* 274:7146–7152
- Trumppower BL, Edwards CA (1979) Purification of a reconstitutively active iron-sulfur protein (oxidation factor) from succinate. Cytochrome c reductase complex of bovine heart mitochondria. *J Biol Chem* 254:8697–8706
- Trumppower BL, Edwards CA, Ohnishi T (1980) Reconstitution of the iron-sulfur protein responsible for the g = 1.90 electron paramagnetic resonance signal and associated cytochrome c reductase activities to depleted succinate-cytochrome c reductase complex. *J Biol Chem* 255:7487–7493
- Ubbink M, Ejdeback M, Karlsson BG, Bendall DS (1998) The structure of the complex of plastocyanin and cytochrome f, determined by paramagnetic NMR and restrained rigid-body molecular dynamics. *Structure* 6:323–335
- Valkova-Valchanova MB, Saribas AS, Gibney BR, Dutton PL, Daldal F (1998) Isolation and characterization of a two-subunit cytochrome b-c1 subcomplex from *Rhodobacter capsulatus* and reconstitution of its ubihydroquinone oxidation (Qo) site with purified Fe-S protein subunit. *Biochemistry* 37:16242–16251
- Veit S, Takeda K, Tsunoyama Y, Rexroth D, Rogner M, Miki K (2012) Structure of a thermophilic cyanobacterial b6f-type Rieske protein. *Acta Crystallogr D Biol Crystallogr* 68:1400–1408
- Victoria D, Burton R, Crofts AR (2013) Role of the -PEWY-glutamate in catalysis at the Q(o)-site of the Cyt bc(1) complex. *Biochim Biophys Acta* 1827:365–386
- Xia D, Yu CA, Kim H, Xia JZ, Kachurin AM, Zhang L, Yu L, Deisenhofer J (1997) Crystal structure of the cytochrome bc<sub>1</sub> complex from bovine heart mitochondria. *Science* 277:60–66
- Xiao K, Yu L, Yu CA (2000) Confirmation of the involvement of protein domain movement during the catalytic cycle of the cytochrome bc<sub>1</sub> complex by the formation of an intersubunit disulfide bond between cytochrome b and the iron-sulfur protein. *J Biol Chem* 275:38597–38604
- Yan J, Cramer WA (2003) Functional insensitivity of the cytochrome b6f complex to structure changes in the hinge region of the Rieske iron-sulfur protein. *J Biol Chem* 278:20925–20933
- Zhang Z, Huang L, Shulmeister VM, Chi YI, Kim KK, Hung LW, Crofts AR, . . . , Kim SH (1998) Electron transfer by domain movement in cytochrome bc<sub>1</sub>. *Nature* 392:677–684

## Structural Perspective of Ferredoxin NAD(P)H Reductase Reactions with Cytochrome *b<sub>6</sub>f* Complexes

Genji Kurisu\*

*Institute for Protein Research, Osaka University, Osaka, Japan*

Summary.....	253
I. The Perspective.....	253
References.....	263

### Summary

The reaction of FNR with the Cytochrome *b<sub>6</sub>f* complex (Cyt *bf*) implies a role in cyclic electron transport. FNR is not a membrane protein but is also involved as a component of a cyclic electron transport ‘super-complex.’ It has been reported that FNR in higher plant chloroplasts is localized peripherally on the stromal side of thylakoid membranes through association with an intrinsic protein. Although several high-resolution X-ray structures of plant-type FNR are available, the exact binding mode of FNR to Cyt *bf* is still elusive. However, as high-resolution structures of Cyt *bf* and membrane bound FNR (L-FNR1) have become available, and possible patterns of the interaction can be structurally discussed through them.

### I. The Perspective

In green plants, algae, cyanobacteria, and photosynthetic bacteria, light energy is trapped by the antenna proteins and converted to a stable chemical form. The principal function of the light-dependent reactions of photosynthesis is to generate

the NADPH and ATP required for carbon reduction. This is accomplished through a series of reactions that constitute the electron transport chain which can be classified in two groups: (i) oxygenic photosynthesis in green plants, algae and cyanobacteria, and (ii) anoxygenic photosynthesis in purple and green sulfur bacteria.

*Abbreviations:* CEF – Cyclic electron transport; Cyt – Cytochrome; FAD – Flavin adenine dinucleotide; Fd – Ferredoxin; FNR – Ferredoxin NAD(P)<sup>+</sup> reductase; LET – Linear electron transport; LHC – Light harvesting chlorophyll protein; NADH – Nicotinamide adenine dinucleotide; NADPH – Nicotinamide adenine

dinucleotide phosphate; PAGE – Polyacryl amide gel electrophoresis; PBS – Phycobilisome; PC – Plastocyanin; PDB – Protein Data Bank; PS – Photosystem; Tic – Translocon at the inner envelope of chloroplast; Trx – Thioredoxin

\*Author for correspondence, e-mail: [gkurisu@protein.osaka-u.ac.jp](mailto:gkurisu@protein.osaka-u.ac.jp)

In oxygenic photosynthesis, there are two photosystems (photosystem II and I in series) that are linked by the cytochrome *b<sub>6</sub>f* complex (Cyt *b<sub>6</sub>f*). A sequential arrangement of three macromolecular membrane protein complexes extracts low-energy electrons from water and reduces Ferredoxin (Fd) that is finally used to produce a strong reductant, NADPH, via Fd NAD(P)H reductase ([EC 1.1.1.14], FNR). This flow of electrons is known as linear electron transport (LET). In the thylakoid membrane, however, photosystem II (PSII) and photosystem I (PSI) are not always physically linked, but are unevenly distributed between grana and stroma thylakoids. To produce extra ATP per NADPH molecule, PSI and Cyt *b<sub>6</sub>f* can transport electrons independently of PSII, a pathway known as a cyclic electron transport (CET). The FNR reaction with Cyt *b<sub>6</sub>f* implies a role in CET, and it has been suggested that FNR could be involved in modulating the two photosynthetic energy flows. FNR is not a membrane protein but is also involved as a component of CET super complex, which generates a proton gradient that results in ATP synthesis, with minimal water splitting and reduction of NADP<sup>+</sup>. The functional implication of FNR in photosynthetic electron partitioning has

led to interest in the mechanism and location of FNR binding to the thylakoid membrane (Fig. 12.1).

FNR is an ubiquitous Fd-dependent enzyme containing a flavin adenine dinucleotide (FAD) as a prosthetic group, which generally catalyzes the reversible redox reaction between the electron carrier protein, Fd, and NAD(P)<sup>+</sup>/NAD(P)H. Based on phylogenetic and structural information, FNRs are classified into two families; glutathione reductase (GR)-type and plant-type (Aliverti et al. 2008). The former is further divided into three groups; Adrenodoxin reductase (AdR)-like, Oxygenase-coupled NADH-ferredoxin reductase (ONFRs)-like and Thioredoxin reductase (TrxR)-like FNR. The latter is also divided into two groups; bacterial FNR that is involved in nitrogen fixation and response to oxidative stress, and plastidic FNR (Fig. 12.2). The group of plant-type plastidic FNR contains FNRs from green plants, algae and cyanobacteria. High-resolution crystal structures of several plant-type FNRs have shown that the FAD binding and NADPH binding domains are arranged sequentially in the primary structure (Karplus et al. 1991; Bruns and Karplus 1995; Deng et al. 1999; Dorowski et al. 2001; Kurisu et al. 2001) (Fig. 12.3).

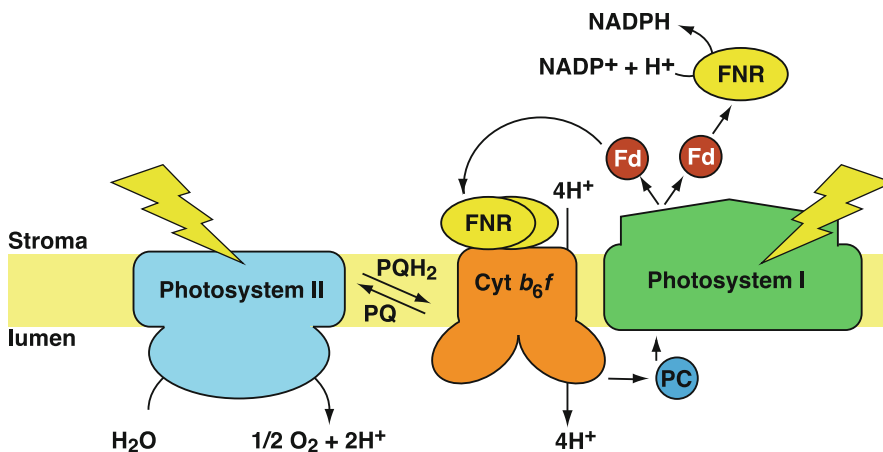
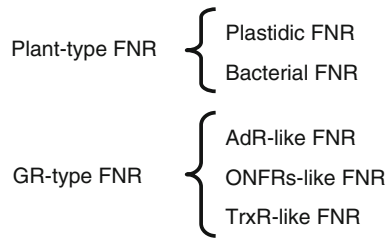
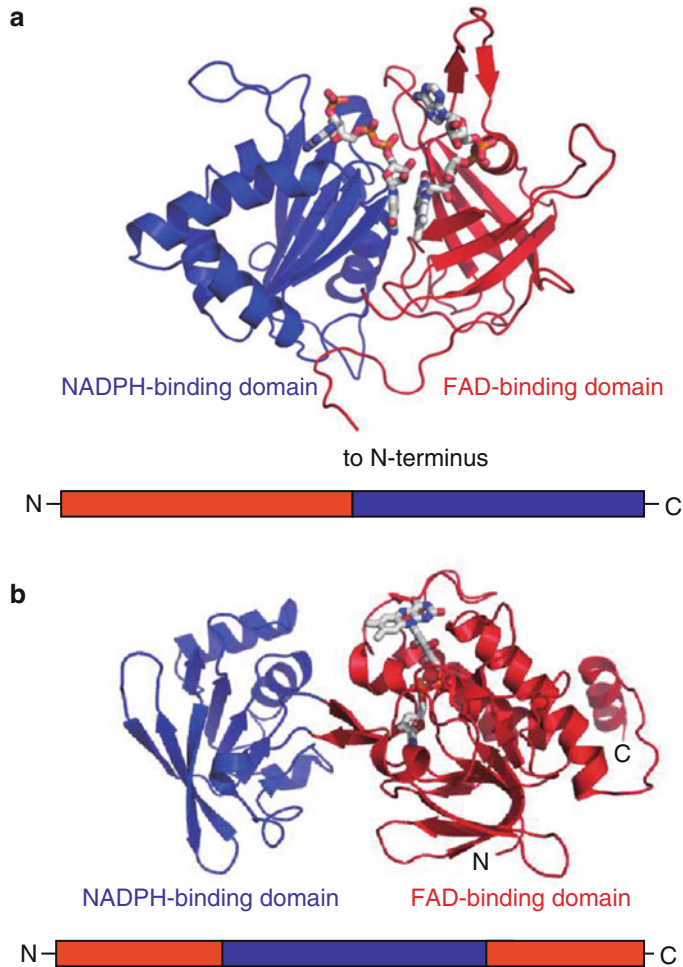


Fig. 12.1. Photosystem II, Photosystem I, and the cytochrome *b<sub>6</sub>f* complex (Cyt *b<sub>6</sub>f*) in the thylakoid membrane are responsible for oxygenic photosynthetic electron transport. The small electron transfer proteins, Ferredoxin (Fd) and Plastocyanin (PC), mediate electron transfer on the membrane. FNR functions in the two electron transfer pathways; linear and cyclic electron transport.



*Fig. 12.2.* Classification of FNRs. FNRs from higher plants and cyanobacteria are classified as Plastidic FNR. Those from purple and green sulfur bacteria are classified as Bacterial FNR and TrxR-like FNR, respectively.



*Fig. 12.3.* Three-dimensional structure and domain organization of plant-type and GR-type FNRs. FAD and NADPH molecules are shown in ball-and-stick models. (a) Y308S mutant of pea FNR complexed with NADPH (PDB ID 1QFZ, chain A). (b) FNR from the green sulfur bacterium *Chlorobaculum tepidum* (PDB ID 3AB1, chain A.).

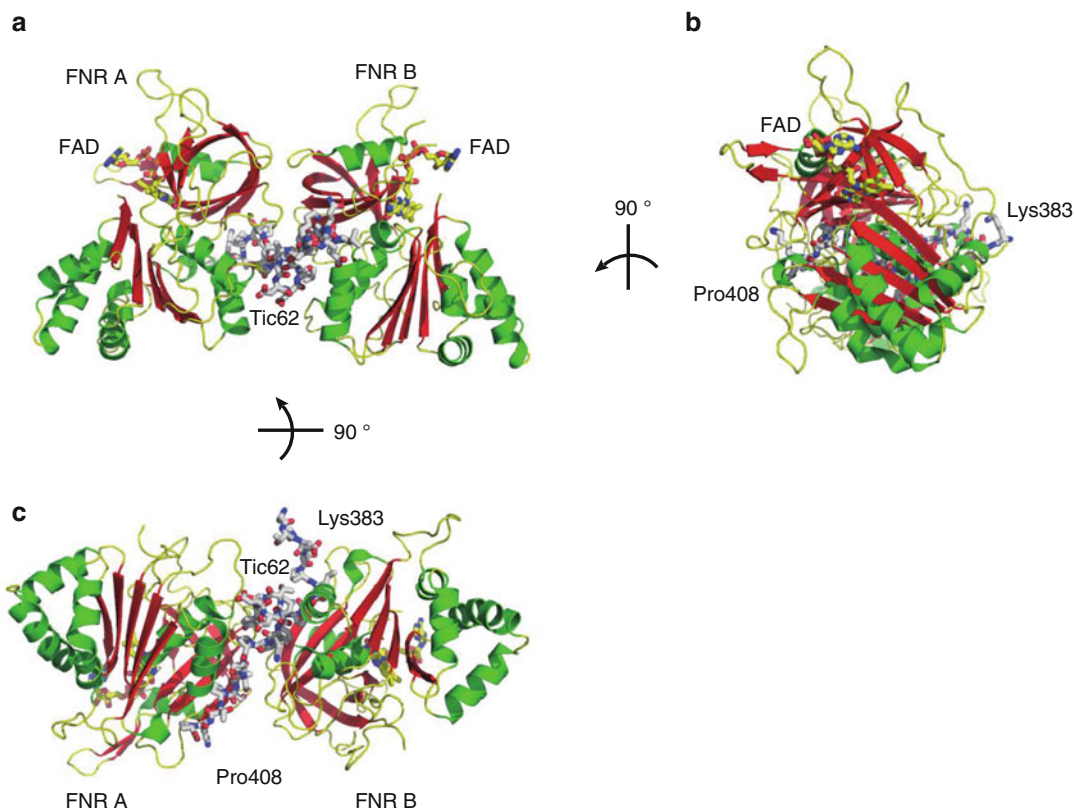
FNRs from purple bacteria belong to plant-type bacterial FNR (Nogués et al. 2005; Bortolotti et al. 2009, 2014), while that from green sulfur bacterium is classified as GR-type TrxR-like FNR (Seo and Sakurai 2002; Muraki et al. 2010) (Fig. 12.3).

FNR from green plants is localized mainly in chloroplasts. FNR in the leaf (L-FNR), which is bound to the thylakoid and also present as a soluble protein in the chloroplast stroma, catalyzes the photosynthetic reduction of NADP<sup>+</sup> to NADPH via reduced Fd (Hanke et al. 2005; Lintala et al. 2007). It has been reported that FNR in higher plant chloroplasts is localized peripherally on the stromal side of thylakoid membranes through association with the intrinsic proteins; PSI (Andersen et al. 1992), Cyt *bf* (Zhang et al. 2001; Okutani et al. 2005), NAD(P)H dehydrogenase complex (Quiles et al. 2000), TROL (Juric et al. 2009) and Tic62 (Benz et al. 2009). Among them, only Tic62 has been structurally characterized as an FNR binding-protein (Alte et al. 2010), and this protein was recently identified in the model plant organism, *Arabidopsis thaliana*. The others protein directly participate in photosynthesis, but Tic62 has no direct photosynthetic role. It seems rather to stabilise FNR. An FNR binding region containing a Ser/Pro-rich motif has been identified in both TROL and Tic62. In the X-ray structure of the complex between FNR and Tic62 polypeptide, FNR dimerizes around this Ser/Pro-rich motif of the peptide (Fig. 12.4). This interaction increases the surface area available for FNR:FNR binding from 380 Å<sup>2</sup> to 2070 Å<sup>2</sup>. The strength of this binding interaction is reported to be pH-dependent (Alte et al. 2010).

In the detergent-soluble Cyt *bf* from spinach (*Spinacia oleracea*) leaves, L-FNR was tightly bound after exposure to hydrophobic extraction at high ionic strength, hydrophobic chromatography, and sucrose gradient separation. L-FNR bound to Cyt *bf* was enzymatically active (Zhang et al. 2001), implying a functional role of the Cyt *bf* complex in the CET pathway.

FNRs from green plants are encoded by a small multiple gene family as shown by the recent whole-genome analysis of model plants (Duvick et al. 2008). The presence of multiple isoenzymes at the protein level has been reported in several plant species. Maize (*Zea mays*) leaves contain three separate FNR isoproteins (L-FNR1, L-FNR2, L-FNR3). Although their capacity for electron transfer is similar, these three FNRs have distinct membrane association patterns. L-FNR1 is restricted to the thylakoid, L-FNR3 is only recovered from chloroplasts as a soluble protein, while L-FNR2 is found in both membrane-bound and unbound states. In order to determine whether the interaction between L-FNR and Cyt *bf* is isoenzyme specific, a Cyt *bf* partially purified from maize leaves was analyzed by SDS-PAGE (Okutani et al. 2005). Proteins of L-FNR1 and L-FNR2 in roughly equal quantities were co-purified with Cyt *bf*, and their identity was confirmed by western blotting.

Unlike C3 plants such as spinach or *Arabidopsis* in which FNR has been studied extensively, maize is a C4 plant and therefore contains two differentiated photosynthetic cell types. Mesophyll cells perform predominantly LET, while bundle sheath cells have very low PS II activity, and so utilize mainly CET. Using maize as a model therefore provides an opportunity to discover what determines the different membrane association behavior of FNR proteins, and how Fds contribute to two different photosynthetic electron transport pathways, LET and CET. In maize (*Zea mays*), two ferredoxin isoproteins, Fd I and Fd II, are expressed specifically in mesophyll and bundle-sheath cells, respectively (Kimata and Hase 1989). The two cell type-specific Fds differentially modulate electron flow around photosystem I (Fig. 12.5). Two cDNAs encoding Fd I and Fd II were introduced separately into the cyanobacterium *Plectonema boryanum* with a disrupted endogenous Fd. The resulting transformants expressing maize Fd I and Fd II in place of the endogenous cyanobacterial Fd showed significant differences in the two



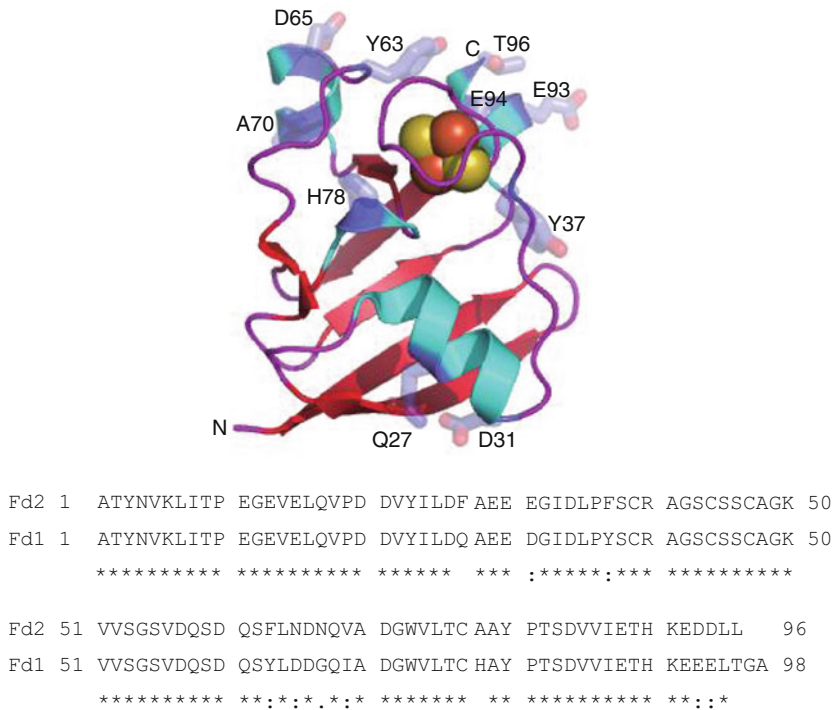
*Fig. 12.4.* Complex structure of the pea FNR and the C-terminal peptide of Tic62. Ribbon drawings of the complex viewed from (a) the front, (b) the side, and (c) the bottom (PDB ID 3MHP) of the complex. Peptide of Tic62 peptide drawn in ball-and-stick models with *white carbon atoms* is sandwiched by two FNR molecules. FAD molecules are also drawn in ball-and-stick with *yellow carbon atoms*.

pathways, thus causing marked changes in the balance of cellular levels of ATP and NADPH (Kimata-Arigo et al. 2000).

As mentioned above, maize contains three chloroplast L-FNR proteins with totally different membrane association. It has been confirmed that these three proteins have a variable distribution between cells conducting predominantly CET (bundle sheath) and LET (mesophyll), which is similar but not so simple as the case of Fd I and Fd II. Membrane-bound forms were detected in both the bundle sheath and mesophyll cells, with the ratio of L-FNR1 to L-FNR2 higher in the bundle sheath than the mesophyll cells. By comparison, soluble proteins were only detected in the mesophyll cells, where L-FNR2 is abundant and L-FNR3 is poor (Twachtmann et al. 2012).

The higher portion of membrane bound L-FNRs distributed together with Cyt *bf* in the bundle sheath therefore correlates with a higher demand for CET, while the greater abundance of soluble FNR occurs in cell types with a greater demand for LET in mesophyll cell.

Although there are several high-resolution X-ray structures of plant-type FNR are available, the exact binding mode of L-FNR to Cyt *bf* is still elusive (Karplus et al. 1991; Bruns and Karplus 1995; Deng et al. 1999; Dorowski et al. 2001; Kurisu et al. 2001). A large hydrophobic cavity in the NADP<sup>+</sup> binding domain of the crystal structure of spinach L-FNR was suggested as a possible binding region to the membrane, when the first structure of plastidic FNR was solved (Karplus et al. 1991; Bruns and Karplus



*Fig. 12.5.* Crystal structure of maize Fd I (PDB ID 3B2F) and amino acid sequence alignment of Fd I and Fd II from maize. Side chains of non-conserved residues are shown in transparent stick models that are mainly distributed on the surface surrounding the [2Fe-2S] cluster on the top of the molecule.

1995). Then, the crystal structure analysis of L-FNR from pea, paprika and maize was obtained (Deng et al. 1999; Dorowski et al. 2001; Kurisu et al. 2001). Later, the crystal structures of maize L-FNR isozymes, L-FNR1-3, became available (Twachtmann et al. 2012). The three structures of L-FNR1-3 resemble each other with the major differences between them being the orientation of the N-terminal 20 residues and the interface of back-to-back dimer formation (Fig. 12.6). All three maize FNRs were crystallized as a dimer in the crystallographic asymmetric unit. The dimeric arrangement of L-FNR1 and L-FNR2 is very similar to that of pea L-FNR complexed with the C-terminal peptide of Tic62, but that of soluble L-FNR3 is obviously different from the others. It should be noted that two molecules of maize L-FNR1 proteins interacted with two N-terminal regions extended from crystallographic neighboring molecules (2:2 stoichiometry). This

type of interaction at the crystallographic dimer interface of L-FNR can be found also in the structure of pea L-FNR mutants (PDB ID:1QFY), and would be widely distributed in the case of membrane bound FNRs.

In the LET participated by soluble FNRs, the resulting NADPH fuels carbon fixation by the Calvin cycle and drives other reductive metabolism in the stroma or outside the chloroplast. In higher plant roots, genetically distinct root-type FNR (R-FNR) enzymes catalyze the NADPH-dependent reduction of Fd to provide reducing power to the many Fd-dependent enzymes involved in assimilation of nitrogen and sulfur, etc. Contrary to L-FNRs, R-FNR exists as a soluble form and it does not interact with the thylakoid membrane (Aliverti et al. 2001). Although the crystal structure of R-FNR from maize exhibited some unique structural features distinct from L-FNRs, the entire structure including the characteristic of molecular sur-

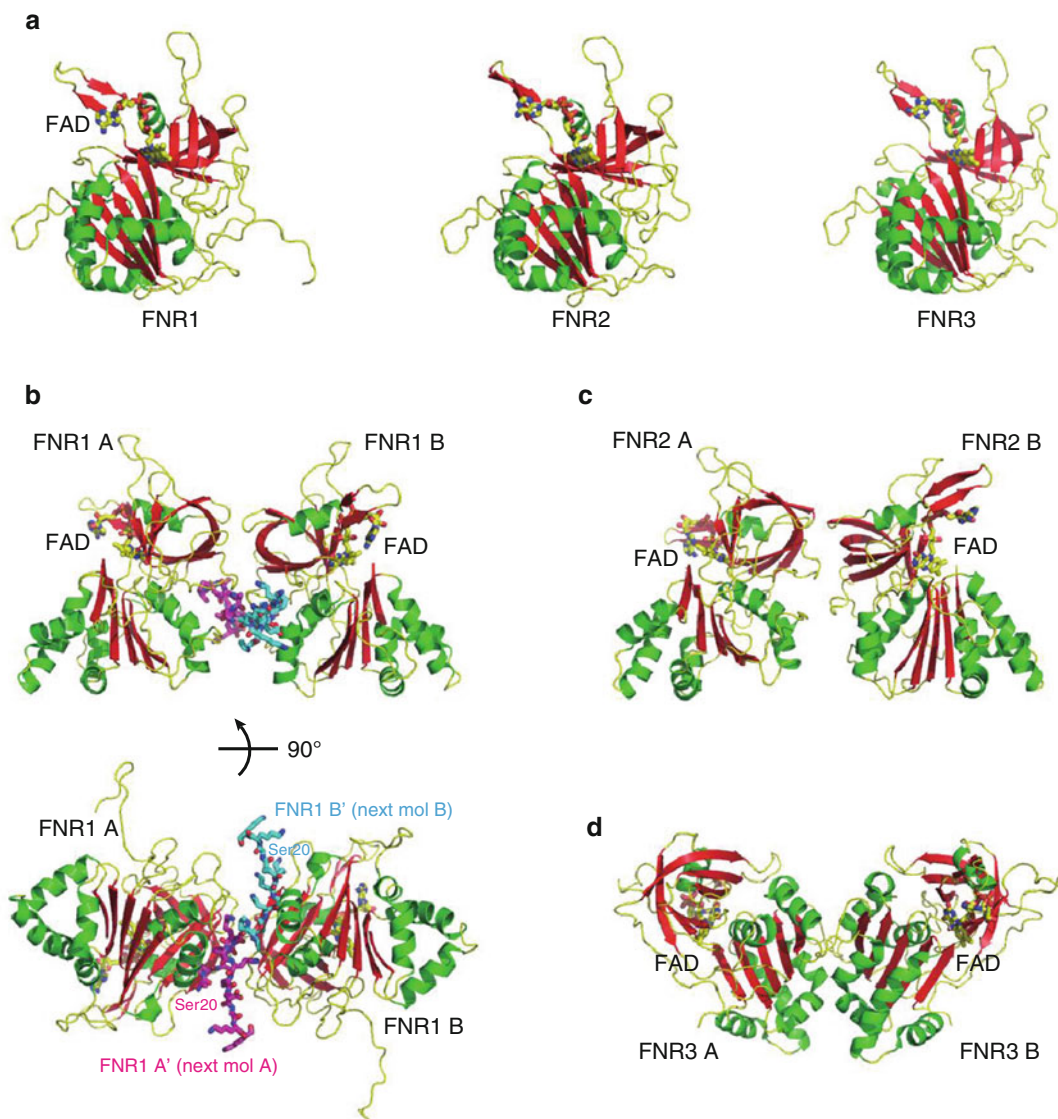


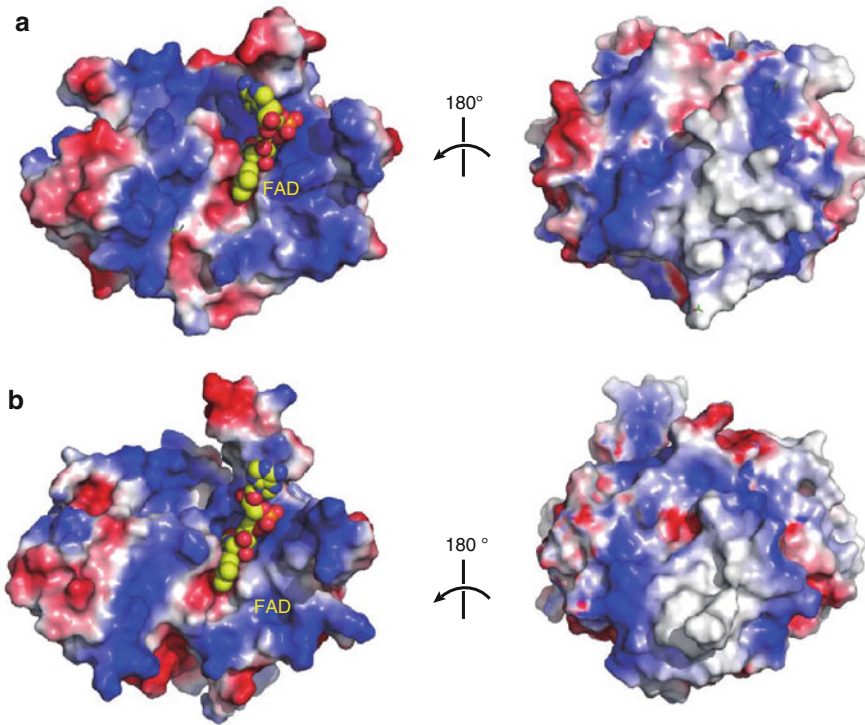
Fig. 12.6. Crystal structures of maize L-FNR1 (PDB ID 1GAW), L-FNR2 (PDB ID 3VO1) and L-FNR3 (PDB ID 3VO2). (a) monomeric forms, and (b) the crystallographic dimer of L-FNR1, (c) L-FNR2 and (d) L-FNR3. Interactions between the dimeric L-FNR1 and the N-terminal regions that extend from crystallographic neighboring molecules are highlighted in *cyan* and *magenta* stick models in (b).

face is quite similar to that of soluble L-FNR3 (Fig. 12.7). Soluble FNRs have shown an independent dimerization feature distinct from those of membrane-bound FNRs.

The Cyt *bf* is a dimeric trans-membrane complex consisting of eight polypeptide subunits per monomer; cytochrome *f*, cytochrome *b*<sub>6</sub>, the Rieske iron-sulfur protein

(ISP), and subunit IV as well as four small hydrophobic subunits, PetG, PetL, PetM, and PetN (latest structure, 2.5 Å, PDB ID 4OGQ). To date, X-ray crystal structures of the Cyt *bf* complex have been obtained from the cyanobacteria *Mastigocladus laminosus* (Hasan et al. 2013a; Yamashita et al. 2007; Kurisu et al. 2003), *Nostoc*





*Fig. 12.7.* Comparison of the molecular surfaces of soluble FNRs. Electrostatic potentials mapped on the molecular surface of (a) L-FNR3 (PDB ID 3VO2) and (b) R-FNR (PDB ID 3LVB), both of which exist in a soluble form.

PCC7120 (Hasan and Cramer 2014; Hasan et al. 2013b; Baniulis et al. 2009), and the green alga *Chlamydomonas reinhardtii* (Stroebel et al. 2003). Although there are several differences between these X-ray structures, the arrangement of eight subunits and composition of prosthetic groups are fundamentally the same. In the recently solved X-ray structure of Cyt *bf* from *Nostoc* PCC7120 at the highest resolution of 2.5 Å, it is proposed that the niche formed between the F and G trans-membrane helices (subunit IV) may represent the binding site for the LHClI kinase for state transition, based on the structural comparison between the mitochondrial Cytochrome *bc*<sub>1</sub> complex (Cyt *bc*<sub>1</sub>) and Cyt *bf* and the non-physiological binding of augmented synthetic lipid (Hasan et al. 2013c). Compared to the case of LHClI kinase, biochemical evidence is not available to determine the binding site for FNR to Cyt *bf* complex. However, a possible pattern of

the interaction can be structurally predicted referring to the high-resolution structures of Cyt *bf* and membrane-bound FNR (L-FNR1).

Cyt *bf* has dimensions of  $90 \times 55$  Å on the lumen side and of  $120 \times 75$  Å on the stromal side. The lumen side of the membrane has two large extrinsic domains, cytochrome *f* and the ISP. The hydrophobic trans-membrane region has formed the functionally indispensable quinone/quinol-exchanging cavities between two monomers. In contrast, the stromal side has no globular domains but has only short loops and several chain termini, which have not been functionally annotated yet. If the back-to-back arrangement of FNR tethering discussed above is common to the case of interaction with Cyt *bf* complex, the structure of Cyt *bf* must have interacting terminal polypeptides on the stromal side of the membrane. There are four candidates

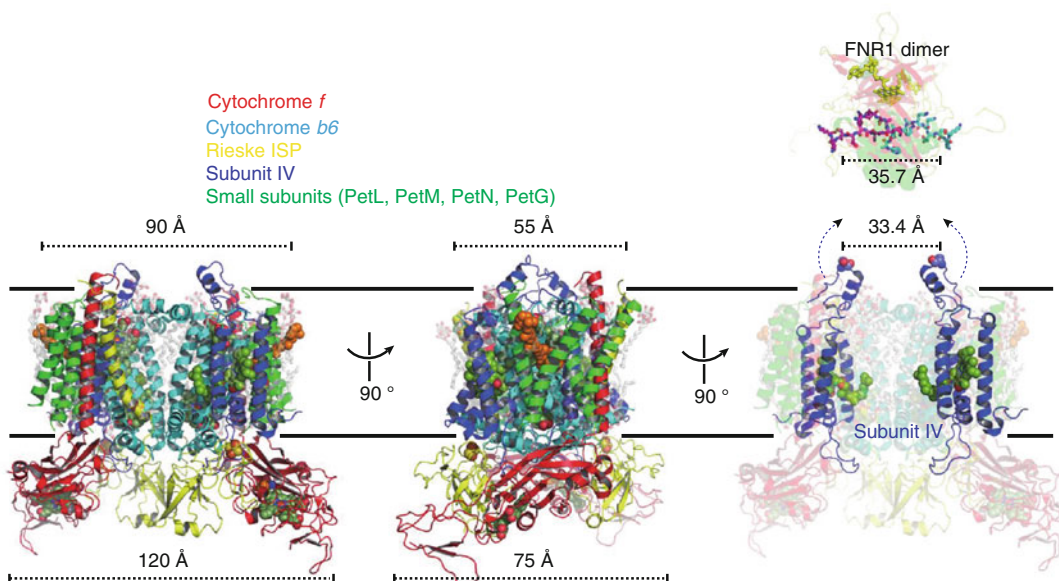


Fig. 12.8. Crystal structure of cyanobacterial Cyt *bf* (PDB ID 4OGQ) and the membrane-bound FNR (L-FNR1, PDB ID 1GAW) viewed normal to the plane of the membrane. Cyt *bf* is colored in each subunit: Cytochrome *f* in red, Cytochrome *b*<sub>6</sub> in cyan, the Rieske-ISP protein in yellow, subunit IV in blue, and four small subunits in green. Molecules of detergents and lipids are shown in transparent stick models. Hemes, iron-sulfur clusters, chlorophylls and carotenoids are drawn in CPK models. In the right panels, two pairs of subunit IV molecules in the Cyt *bf* and the neighboring N-terminal peptide proposed to interact with FNRs are highlighted. Dimensions of Cyt *bf* and the particular distances written in the text are also shown.

from major functional subunits of Cyt *bf*; the N-terminus of cyt *f*, the C-terminus of the ISP, the N-terminus of cyt *b*<sub>6</sub> and the N-terminus of subunit IV (Fig. 12.8). The C-terminal end of cyt *b*<sub>6</sub> can be excluded because it is structurally occluded by subunit IV and PetG.

Based on the L-FNR1 crystal structure, the length of the N-terminal polypeptides interacting with crystallographic adjacent FNR molecule is 35.7 Å (Fig. 12.8, C $\alpha$  carbon of Ser 20, Maize numbering). Possible counterparts of Cyt *bf* must have the flexible terminal regions with corresponding distances. The two ends of the secondary structure (Fig. 12.8, C $\alpha$  carbons of Ser 10, *Nostoc* PCC7120 numbering) of subunit IV are 33.4 Å apart, while those of cyt *f*, the ISP and cyt *b*<sub>6</sub>, are separated by 77, 66 and 58 Å, respectively. Furthermore, the N-terminal region of subunit IV protrudes from the trans-membrane region. It looks favorable for the interaction of globular L-FNR1.

According to this structural information, it is proposed that L-FNR/Cyt *bf* interacts through the N-terminal regions of subunit IV. Supporting structure evidence can be obtained from the comparison between two structures of Cyt *bf* from *Nostoc* and *Chlamydomonas*. Structural plasticity indicated between two structures around Pro12 of subunit IV has suggested the possible rearrangement of polypeptide when interacting with membrane-bound L-FNRs. Based on these structural observation, the N-terminal region of subunit IV may have the highest probability for a binding site of L-FNR.

Involvement of subunit IV in the L-FNR/Cyt *bf* interaction implies that Cyt *bf* activity might be tuned by complex formation. The rate-limiting step of the oxygenic photosynthetic electron transport chain is located in the proton-coupled electron transfer through the Cyt *bf* complex. There is a consensus that the coupling of the redox-

coupled trans-membrane proton transfer to the p-side aqueous phase limits the rate of electron transfer. In the presence of low intensity illumination and/or small  $\Delta\mu_{\text{H}}^+$ , the 26 Å distance measured between the [2Fe-2S] cluster and the heme of cytochrome *f* in the Cyt *bf* crystal structure would seem to impose a major barrier to electron transfer (Heimann et al. 2000; Yan and Cramer 2003). A second possibility for a kinetic limitation is oxidation of the bulky lipophilic quinol. Intra-molecular quinone/quinol exchange cavity has a portal to the  $Q_p$  site of Cyt *bf*. The bent trans-membrane helix (F-helix) of Subunit IV forms a wall of the exchange portal. Based on the mutagenesis of this F-helix, it is proposed that a rate limitation of electron transport in Cyt *bf* may arise from steric constraints in the portal to  $Q_p$  site (Hasan and Cramer 2012). Since the N-terminal region of subunit IV is structurally close to the stromal end of F-helix (for example, an  $C\alpha$  distance between Lys20 and Lys119 is 10.95 Å), it may also be relevant for possible tuning of the activity in the membrane through the L-FNR/Cyt *bf* interaction.

In the case of cyanobacterial FNR, early reports suggested the unique membrane localization pattern of FNR is totally different from that of plastidic FNR. The molecular mass of a typical cyanobacterial FNR is similar to that of higher plants (ca. 35 kDa) (Serre et al. 1996; Hermoso et al. 2002). However, the FNR encoded by a cyanobacterial gene (*petH*) was reported to have an estimated molecular mass of 45 kDa. The larger than anticipated molecular mass of this protein arises from the presence of a small domain attached to the N-terminus of NAD(P)H binding domain, which displays significant sequence similarity with the phycobilisome (PBS) binding protein CpcD. It has been proposed that the full-length cyanobacterial FNR is located in close proximity to the thylakoid membrane through the binding to PBS (van Thor et al. 1999, 2000; Arteni et al. 2009). Three forms of FNR can be purified from the thermophilic cyanobacterium

*Thermosynechococcus elongatus* BP-1: (i) a 34 kDa form lacking the CpcD-like domain (probably due to proteolytic cleavage at the hinge region); (ii) a 45 kDa form with an intact CpcD-like domain; and (iii) a 78 kDa form in complex with phycocyanin, which is a major pigment-protein complex of PBS (Nakajima et al. 2002). Although the three-dimensional arrangement of the CpcD-like domain relative to the other domains is still unclear, it is noted that cyanobacteria have a unique system utilizing PBS to tether the FNR close proximity to the membrane probably suitable for CET.

Although the apparatus of anoxygenic photosynthesis is very diverse, coupling of electron and proton transfer mediated by the Cyt *bf* or *bc*<sub>1</sub> complex is indispensable for the photosynthetic electron transfer pathways except for the green thermophilic photosynthetic bacterium *Chloroflexus aurantiacus* that has an alternative complex III (Gao et al. 2010; Tang et al. 2011). In contrast to the case of Cyt *bf* or *bc*<sub>1</sub>, purple and green sulfur bacteria may or may not have FNRs for the light-dependent reactions. The green sulfur bacterium *Chlorobaculum tepidum* (formerly *Chlorobium tepidum*) possesses an iron-sulfur type reaction center which is evolutionarily related to photosystem I in chloroplasts and is able to reduce Fd photosynthetically. It was anticipated that *C. tepidum* might possess a homologue of the plant-type FNR because the electron transfer reactions involving Fd are quite similar to those that occur in the chloroplast. Instead, *C. tepidum* has a GR-type FNR distinct from previously characterized plant-type FNRs distinct in its oligomerization state and amino acid sequence (Seo and Sakurai 2002; Muraki et al. 2010). Since anoxygenic phototynthetic bacteria like *C. tepidum* are living under much simpler photosynthetic conditions, i. e., shallow lakes and marshes near volcano producing H<sub>2</sub>S gas, it seems that there is no need and no chance for *C. tepidum* FNR to interact with the Cyt *bc* complex by environmental adaptation.

## References

- Aliverti A, Faber R, Finnerty CM, Ferioli C, Pandini V, Negri A, Karplus PA, ... , Zanetti G (2001) Biochemical and crystallographic characterization of ferredoxin-NADP(+) reductase from nonphotosynthetic tissues. *Biochemistry* 40:14501–14508
- Aliverti A, Pandini V, Pennati A, de Rosa M, Zanetti G (2008) Structural and functional diversity of ferredoxin-NADP(+) reductases. *Arch Biochem Biophys* 474:283–291
- Alte F, Stengel A, Benz JP, Petersen E, Soll J, Groll M, Bölter B (2010) Ferredoxin:NADPH oxidoreductase is recruited to thylakoids by binding to a polyproline type II helix in a pH-dependent manner. *Proc Natl Acad Sci* 107:19260–19265
- Andersen B, Scheller HV, Moller BL (1992) The PSI-E subunit of photosystem I binds ferredoxin:NADP+ oxidoreductase. *FEBS Lett* 311:169–173
- Arteni AA, Ajlani G, Boekema EJ (2009) Structural organisation of phycobilisomes from *Synechocystis* sp. strain PCC6803 and their interaction with the membrane. *Biochim Biophys Acta* 1787:272–279
- Baniulis D, Yamashita E, Whitelegge JP, Zatsman AI, Hendrich MP, Hasan SS, Ryan CM, ... , Cramer WA (2009) Structure-function, stability, and chemical modification of the cyanobacterial cytochrome b6f complex from *Nostoc* sp. PCC 7120. *J Biol Chem* 284:9861–9869
- Benz JP, Stengel A, Lintala M, Lee YH, Weber A, Philippar K, Gügel IL, ... , Bölter B (2009) Arabidopsis Tic62 and ferredoxin-NADP(H) oxidoreductase form light-regulated complexes that are integrated into the chloroplast redox poise. *Plant Cell* 21:3965–3983
- Bortolotti A, Pérez-Dorado I, Goñi G, Medina M, Hermoso JA, Carrillo N, Cortez N (2009) Coenzyme binding and hydride transfer in *Rhodobacter capsulatus* ferredoxin/ flavodoxin NADP (H) oxidoreductase. *Biochim Biophys Acta* 1794:199–210
- Bortolotti A, Sánchez-Azqueta A, Maya CM, Velázquez-Campoy A, Hermoso JA, Medina M, Cortez N (2014) The C-terminal extension of bacterial flavodoxin-reductases: involvement in the hydride transfer mechanism from the coenzyme. *Biochim Biophys Acta* 1837:33–43
- Bruns CM, Karplus PA (1995) Refined crystal structure of spinach ferredoxin reductase at 1.7 Å resolution: oxidized, reduced and 2'-phospho-5'-AMP bound states. *J Mol Biol* 247:125–145
- Deng Z, Aliverti A, Zanetti G, Arakaki AK, Ottado J, Orellano EG, Calcaterra NB, ... , Karplus PA (1999) A productive NADP+ binding mode of ferredoxin-NADP+ reductase revealed by protein engineering and crystallographic studies. *Nat Struct Biol* 6:847–853
- Dorowski A, Hofmann A, Steegborn C, Boicu M, Huber R (2001) Crystal structure of paprika ferredoxin-NADP+ reductase. Implications for the electron transfer pathway. *J Biol Chem* 276:9253–9263
- Duvick J, Fu A, Muppurala U, Sabharwal M, Wilkerson MD, Lawrence CJ, Lushbough C, ... , Brendel V (2008) PlantGDB: a resource for comparative plant genomics. *Nucleic Acids Res* 36:D959–D965
- Gao X, Xin Y, Bell PD, Wen J, Blankenship RE (2010) Structural analysis of alternative complex III in the photosynthetic electron transfer chain of *Chloroflexus aurantiacus*. *Biochemistry* 49:6670–6679
- Hanke GT, Okutani S, Satomi Y, Takao T, Suzuki A, Hase T (2005) Multiple iso-proteins of FNR in Arabidopsis: evidence for different contributions to chloroplast function and nitrogen assimilation. *Plant Cell Environ* 28:1146–1157
- Hasan SS, Cramer WA (2012) On rate limitations of electron transfer in the photosynthetic cytochrome b6f complex. *Phys Chem Chem Phys* 14:13853–13860
- Hasan SS, Cramer WA (2014) Internal lipid architecture of the hetero-oligomeric cytochrome b6f complex. *Structure* 22:1008–1015
- Hasan SS, Stoffeth JT, Yamashita E, Cramer WA (2013a) Lipid-induced conformational changes within the cytochrome b6f complex of oxygenic photosynthesis. *Biochemistry* 52:2649–2654
- Hasan SS, Yamashita E, Baniulis D, Cramer WA (2013b) Quinone-dependent proton transfer pathways in the photosynthetic cytochrome b6f complex. *Proc Natl Acad Sci U S A* 110:4297–4302
- Hasan SS, Yamashita E, Cramer WA (2013c) Transmembrane signaling and assembly of the cytochrome b6f-lipidic charge transfer complex. *Biochim Biophys Acta* 1827:1295–1308
- Heimann S, Ponamarev MV, Cramer WA (2000) Movement of the Rieske iron-sulfur protein in the p-side bulk aqueous phase: effect of luminal viscosity on redox reactions of the cytochrome b6f complex. *Biochemistry* 39:2692–2699
- Hermoso JA, Mayoral T, Faro M, Gomez-Moreno C, Sanz-Aparicio J, Medina M (2002) Mechanism of coenzyme recognition and binding revealed by crystal structure analysis of ferredoxin-NADP+ reductase complexed with NADP+. *J Mol Biol* 319:1133–1142

- Jurić S, Hazler-Pilepić K, Tomašić A, Lepeduš H, Jeličić B, Puthiyaveetil S, Bionda T, . . . , Fulgosi H (2009) Tethering of ferredoxin:NADP+ oxidoreductase to thylakoid membranes is mediated by novel chloroplast protein TROL. *Plant J* 60: 783–794
- Karplus PA, Daniels MJ, Herriott JR (1991) Atomic structure of ferredoxin-NADP+ reductase: prototype for a structurally novel flavoenzyme family. *Science* 251:60–66
- Kimata Y, Hase T (1989) Localization of ferredoxin isoproteins in mesophyll and bundle sheath cell in maize leaf. *Plant Physiol* 89:1193–1197
- Kimata-Arigo Y, Matsumura T, Kada S, Fujimoto H, Fujita Y, Endo T, Mano J, . . . , Hase T (2000) Differential electron flow around photosystem I by two C4-photosynthetic-cell-specific ferredoxins. *EMBO J* 19:5041–5050
- Kurisu G, Kusunoki M, Katoh E, Yamazaki T, Teshima K, Onda Y, Kimata-Arigo Y, Hase T (2001) Structure of the electron transfer complex between ferredoxin and ferredoxin-NADP+ reductase. *Nat Struct Biol* 8:117–121
- Kurisu G, Zhang H, Smith JL, Cramer WA (2003) Structure of the cytochrome b6f complex of oxygenic photosynthesis: tuning the cavity. *Science* 302:1009–1014
- Lintala M, Allahverdiyeva Y, Kidron H, Piippo M, Battchikova N, Suorsa M, Rintamäki E, . . . , Mulo P (2007) Structural and functional characterization of ferredoxin-NADP-oxidoreductase using knockout mutants of *Arabidopsis*. *Plant J* 49:1041–1052
- Muraki N, Seo D, Shiba T, Sakurai T, Kurisu G (2010) Asymmetric dimeric structure of ferredoxin-NAD(P)+ oxidoreductase from the green sulfur bacterium *Chlorobaculum tepidum*: implications for binding ferredoxin and NADP+. *J Mol Biol* 401:403–414
- Nakajima M, Sakamoto T, Wada K (2002) The complete purification and characterization of three forms of ferredoxin-NADP+ oxidoreductase from a thermophilic cyanobacterium *Synechococcus elongatus*. *Plant Cell Physiol* 43:484–493
- Nogués I, Pérez-Dorado I, Frago S, Bittel C, Mayhew SG, Gómez-Moreno C, Hermoso JA, . . . , Carrillo N (2005) The ferredoxin-NADP(H) reductase from *Rhodobacter capsulatus*: molecular structure and catalytic mechanism. *Biochemistry* 44:11730–11740
- Okutani S, Hanke GT, Satomi Y, Takao T, Kurisu G, Suzuki A, Hase T (2005) Three maize leaf ferredoxin:NADPH oxidoreductases vary in subchloroplast location, expression, and interaction with ferredoxin. *Plant Physiol* 139:1451–1459
- Quiles MJ, Garcia A, Guello J (2000) Separation by blue-native PAGE and identification of the whole NAD(P)H dehydrogenase complex from barley stroma thylakoids. *Plant Physiol Biochem* 38: 225–232
- Seo D, Sakurai H (2002) Purification and characterization of ferredoxin-NAD(P)(+) reductase from the green sulfur bacterium *Chlorobium tepidum*. *Biochim Biophys Acta* 1597:123–132
- Serre L, Vellieux FM, Medina M, Gomez-Moreno C, Fontecilla-Camps JC, Frey M (1996) X-ray structure of the ferredoxin:NADP+ reductase from the cyanobacterium *Anabaena PCC 7119* at 1.8 Å resolution, and crystallographic studies of NADP+ binding at 2.25 Å resolution. *J Mol Biol* 263:20–39
- Stroebel D, Choquet Y, Popot JL, Picot D (2003) An atypical haem in the cytochrome b6f complex. *Nature* 426:413–418
- Tang KH, Barry K, Chertkov O, Dalin E, Han CS, Hauser LJ, Honchak BM, . . . , Blankenship RE (2011) Complete genome sequence of the filamentous anoxygenic phototrophic bacterium *Chloroflexus aurantiacus*. *BMC Genomics* 12:334
- Twachtmann M, Altmann B, Muraki N, Voss I, Okutani S, Kurisu G, Hase T, Hanke GT (2012) N-terminal structure of maize ferredoxin:NADP+ reductase determines recruitment into different thylakoid membrane complexes. *Plant Cell* 24:2979–2991
- van Thor JJ, Gruters OW, Matthijs HC, Hellingwerf KJ (1999) Localization and function of ferredoxin:NADP+ reductase bound to the phycobilisomes of *Synechocystis*. *EMBO J* 18: 4128–4136
- van Thor JJ, Jeanjean R, Havaux M, Sjollem KA, Joset F, Hellingwerf KJ, Matthijs HC (2000) Salt shock-inducible photosystem I cyclic electron transfer in *Synechocystis PCC6803* relies on binding of ferredoxin:NADP+ reductase to the thylakoid membranes via its CpcD phycobilisome-linker homologous N-terminal domain. *Biochim Biophys Acta* 1457:129–144
- Yamashita E, Zhang H, Cramer WA (2007) Structure of the cytochrome b6f complex: quinone analogue inhibitors as ligands of heme cn. *J Mol Biol* 370: 39–52
- Yan J, Cramer WA (2003) Functional insensitivity of the cytochrome b6f complex to structure changes in the hinge region of the Rieske iron-sulfur protein. *J Biol Chem* 278:20925–20933
- Zhang H, Whitelegge JP, Cramer WA (2001) Ferredoxin:NADP+ oxidoreductase is a subunit of the chloroplast cytochrome b6f complex. *J Biol Chem* 276:38159–38165

# Chapter 13

## Alternative Rieske Iron-Sulfur Subunits and Small Polypeptides of Cyanobacterial Cytochrome *b<sub>6</sub>f* Complexes

Gábor Bernát<sup>a,\*</sup>, Dirk Schneider<sup>b</sup>, and Matthias Rögner<sup>c</sup>

<sup>a</sup>Laboratory of Photosynthesis, Centre Algatech, Institute of Microbiology, Academy of Sciences of the Czech Republic, Opatovický mlyn, Třeboň CZ-379 81, Czech Republic

<sup>b</sup>Institut für Pharmazie und Biochemie, Johannes Gutenberg-Universität Mainz, D-55128 Mainz, Germany

<sup>c</sup>Lehrstuhl für Biochemie der Pflanzen, Ruhr-Universität Bochum, D-44780 Bochum, Germany

Summary.....	265
I. Introduction.....	266
II. Multiple Rieske-Proteins and Cytochrome <i>b<sub>6</sub>f</i> Heterogeneity.....	268
III. Small <i>bona fide</i> Cytochrome <i>b<sub>6</sub>f</i> Subunits.....	272
IV. Loosely Bound Subunits.....	273
Acknowledgements.....	275
References.....	275

### Summary

The cytochrome (cyt) *b<sub>6</sub>f* complex is a central component of both, photosynthetic and respiratory electron- and proton transport processes in cyanobacteria. Among its eight *bona fide* subunits, the Rieske [2Fe-2S] protein is encoded by multiple genes in most cyanobacterial genomes. However, the significance of the resulting protein heterogeneity is essentially not yet understood. The following chapter provides an overview on the Rieske [2Fe-2S] protein diversity in cyanobacteria, and related aspects. In addition, potential roles of small cyt *b<sub>6</sub>f* complex subunits are discussed.

---

\*Author for correspondence, e-mail: [bernat@alga.cz](mailto:bernat@alga.cz)

## I. Introduction

About 50 years ago, John S. Rieseke and his co-workers discovered a new type of iron-sulfur protein, which later became known as ‘Rieseke’ proteins (Rieseke et al. 1964). The catalytic center of these proteins is formed by a unique [2Fe-2S] cluster. In contrast to the bis-cysteine ligation found in ferredoxin-type [2Fe-2S] clusters, one of the two Fe ions is coordinated by two histidine residues in Rieseke-type [2Fe-2S] clusters (Fig. 13.1) (Liu et al. 2014). Two inorganic sulfide ions bridge the two Fe ions, forming together a flat, rhombic cluster. Rieseke proteins are essential subunits of different types of bacterial non-heme oxygenases (Ferraro et al. 2005), and of all *cyt bc* complexes, *i.e.*, *cyt bc*<sub>1</sub> (complex III), *cyt b*<sub>6f</sub> and related complexes. Hence, Rieseke proteins have a central role in biological energy transduction in most living organisms (Dibrova et al. 2013).

3D structures of various dimeric *cyt bc*-type complexes are available at high resolution, including structures of the *cyt b*<sub>6f</sub> complexes of the green alga *Chlamydomonas reinhardtii* and three cyanobacteria *Mastigocladus laminosus*, *Nostoc* sp. PCC

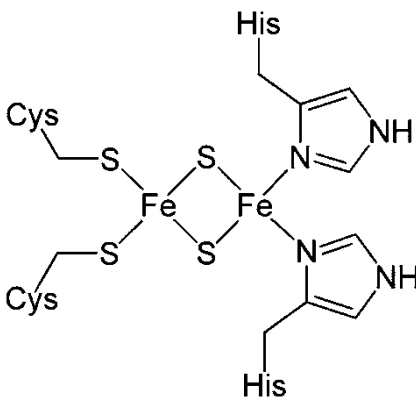


Fig. 13.1. Catalytic center of Rieske-type [2Fe-2S] proteins.

**Abbreviations:** *cyt* – Cytochrome; *Fd* – Ferredoxin; *FNR* – Ferredoxin:NADP<sup>+</sup> oxidoreductase; *HL* – High light; *LHCII* – Light harvesting system of PSII; *PQH*<sub>2</sub> – Plastoquinol; *PS* – Photosystem

7120, and *Fremyella diplosiphon* SF33 (Fig. 13.2) (Stroebel et al. 2003; Kurisu et al. 2003; Yamashita et al. 2007; Baniulis et al. 2009; Hasan and Cramer 2014; Agarwal et al. 2015). A *cyt b*<sub>6f</sub> monomer consists of the four large (17.5–32 kDa) subunits: *cyt f* (*PetA*), *cyt b*<sub>6</sub> (*PetB*), the Rieske [2Fe-2S] protein (*PetC*) and subunit IV (*SU IV*, *PetD*), as well as of four small (3.3–4.1 kDa) subunits (*PetG*, *–L*, *–M* and *–N*) at unit stoichiometry (for a more detailed description see the Chap. 9 by Cramer and Hasan in this volume). The typical Rieske [2Fe-2S] protein consists of 180–183 amino acids and has a molecular mass of ~19 kDa (Schneider and Schmidt 2005). The protein consists of a single N-terminal transmembrane helix and a large soluble domain of ~140 residues, located in the thylakoid lumen (Fig. 13.2). The two domains are connected by a flexible hinge region (Fig. 13.3). Within a *cyt b*<sub>6f</sub> homodimer, the membrane-spanning  $\alpha$ -helical anchor is swapped and the soluble domain of one Rieske monomer is anchored to the membrane by a transmembrane helix, which is part of the adjacent monomer. According to recent data, the domain-swapped structure is necessary for function (see below) but not essential for maintaining the dimeric structure of the complex (Agarwal et al. 2015). The soluble Rieske protein domain mainly consists of  $\beta$ -sheets and can be further divided into a large and a small subdomain (Carrell et al. 1997) with the Rieske [2Fe-2S] center being localized in the small subdomain (Fig. 13.3). Its ordinary form (see below) has a midpoint potential of 300–320 mV (Nitschke et al. 1992; Zhang et al. 1996; Schneider et al. 2002).

As discussed in greater detail in the Chap. 9 by Cramer and Hasan, a central feature of the *cyt b*<sub>6f</sub> complex is the bifurcation of electron transport at the *Q*<sub>o</sub> (or *Q*<sub>p</sub>) plastoquinol (*PQH*<sub>2</sub>) binding site, which is located close to the luminal surface of the thylakoid membrane. One of the two electrons carried by *PQH*<sub>2</sub> is transferred to the energetically favored, so-called high-potential chain, which gives rise to a downhill electron transport

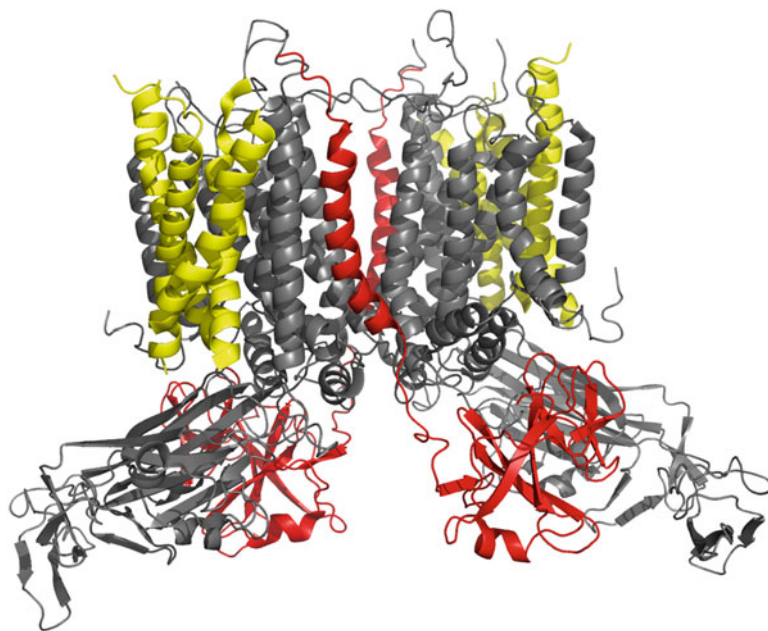


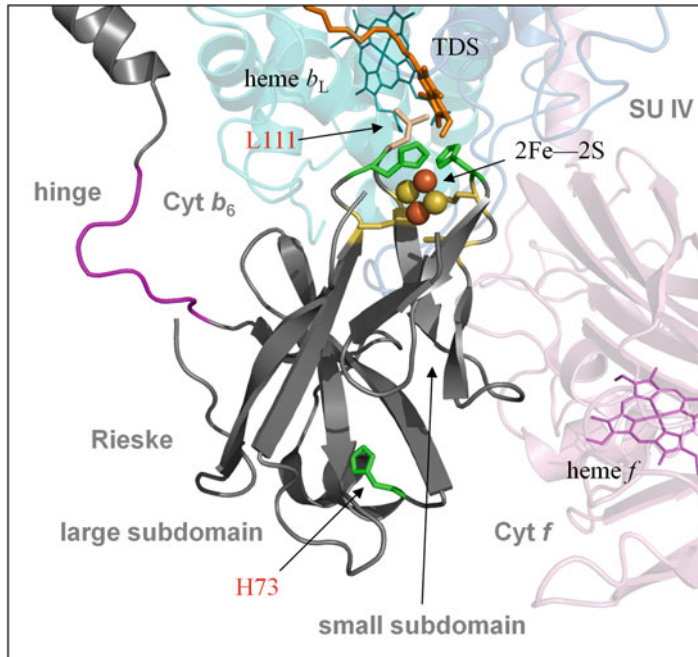
Fig. 13.2. Side view of a dimeric *cyt b<sub>6f</sub>* complex (PDB, 1vf5; Kurisu et al. 2003). Most  $\alpha$ -helices of the complex are membrane integrated, whereas the  $\beta$ -sheet-dominated parts are the water-soluble domains, which extend into the thylakoid lumen. The two Rieske subunits of the complex are colored in red, the small subunits are marked in yellow, and all other subunits are shown in gray. While each small subunit has only a single membrane spanning transmembrane helix, the Rieske [2Fe–2S] polypeptide consists of two domains: a membrane-anchored transmembrane helix and a large water-soluble domain, which are connected by a flexible hinge region. These two domains are swapped between the two monomers in the *cyt b<sub>6f</sub>* homodimer. For further details see Fig. 13.3 and the text.

towards plastocyanin/*cyt c<sub>6</sub>* and photosystem I (PS I) via the Rieske [2Fe–2S] cluster and *cyt f*. The Rieske [2Fe–2S] center is 8–10 Å (edge-to-edge) away from the bound quinol with a leucine and a histidine residue in between (Fig. 13.3). After reduction of the Rieske [2Fe–2S] cluster, the electron is subsequently transferred to *cyt f* via movement (“tethered diffusion”) of the soluble domain of the Rieske [2Fe–2S] protein towards *cyt f* (Heimann et al. 2000; see also the Chap. 11 by Huang and Berry in this volume). Beyond participating in electron transport, the Rieske [2Fe–2S] center is also involved in PQH<sub>2</sub> deprotonation. As proposed by Crofts (Crofts et al. 2000; Crofts 2004), one of the two electrons and protons of the quinol, respectively, is transferred in a concerted action to the [2Fe–2S] center, which results in protonation of one of its histidine ligands. This proton can thereafter be released into

the thylakoid lumen via an internal water bridge located within *cyt f* (Martinez et al. 1996; Ponamarev and Cramer 1998; Cramer et al. 2006). The second electron is “recycled” through the so-called low-potential chain, which consists of a *b*-type heme (*cyt b<sub>L</sub>*) and a *b*-type/*c*-type heme couple (*cyt b<sub>H</sub>*/*cyt c<sub>i</sub>*) transferring electrons across the membrane to the Q<sub>i</sub> (or Q<sub>n</sub>) quinone-binding site, where PQ molecules are reduced back to PQH<sub>2</sub> in the so-called Q-cycle (Mitchell 1975; see also the Chaps. 9, 10 and 21 by Cramer and Hasan, Esser et al. and Fisher et al.). The second proton may predominantly be released via Glu78, which is part of a conserved Pro-Glu-Trp-Tyr (PEWY) sequence in the *ef* loop of SU IV (Zito et al. 1998; Finazzi 2002; Cramer et al. 2006).

The four small *cyt b<sub>6f</sub>* subunits, PetG, –L, –M and –N, are located at the periphery of the complex and form a so-called “picket





*Fig. 13.3.* The soluble domain of the Rieske [2Fe—2S] protein and its molecular environment (PDB, 1vf5 and 2e76; Kurisu et al. 2003 and Yamashita et al. 2007, respectively). The  $Q_o$  plastoquinol binding site is shown with the bound quinone analog tridecyl-stigmatellin (TDS, orange). While subunits cyt  $b_6$ , SU IV, and cyt  $f$  are marked by transparent cyan, sky blue, and pink, respectively, the Rieske [2Fe—2S] subunit is colored in grey. For clarity, residues 142–144 and the last 16 residues of the Rieske C-terminus are omitted. The following color codes have been used: Rieske [2Fe—2S] center (yellow/orange spheres), hemes  $b_L$  and  $f$  (cyan and pink lines, respectively), four cysteine and two histidine residues around the [2Fe—2S] cluster (yellow and green sticks/cartoons, respectively), His73, part of a potential metal binding site (green sticks/cartoon, red identifier), the leucine residue (Leu111) located between the [2Fe—2S] center and the bound quinol (wheat sticks/cartoon, red identifier), hinge region between water soluble domain and transmembrane helix of the Rieske [2Fe—2S] protein (magenta). Transmembrane helix (upper left) and the water soluble domain of the Rieske protein (center) belong to opposing monomers. For details see text.

fence” structure (Fig. 13.2) (Stroebel et al. 2003; Kurisu et al. 2003; Yamashita et al. 2007; Baniulis et al. 2009; Hasan and Cramer 2014). Besides their important role in assembly and/or stability of the cyt  $b_6f$  complex, there are also experimental findings suggesting regulatory functions of these polypeptides. Beyond the eight *bona fide* cyt  $b_6f$  subunits, there is evidence for further protein components interacting transiently and/or loosely with the cyt  $b_6f$  complex. Though data strongly indicate involvement in electron transport and/or signal transduction processes of some of these partners, the nature of most of these interactions are still poorly understood.

## II. Multiple Rieske-Proteins and Cytochrome $b_6f$ Heterogeneity

In higher plants and green algae, as well as in some cyanobacteria, such as *Thermosynechococcus elongatus* and *Gloeobacter violaceus*, the Rieske protein of the cyt  $b_6f$  complex is encoded by a single *petC* gene. In chloroplasts as well as in cyanobacteria, this canonical *petC* gene is organized in an operon together with the *petA* gene coding for cyt  $f$  (Kallas et al. 1988). However, the vast majority of cyanobacterial genomes display a family of different *petC* genes. In most of these cyanobacteria, including the well-

<b>PetC1</b>	1	MTQISGSPDVPDLGRRQFMNLLTFGTITGVAAGALYPAVK	40
<b>PetC2</b>	1	-MDNTQAIAPPSSYSRRQLLNFLAGTTVAVTASAGAYAMGK	39
<b>PetC3</b>	1	-----MVKRRKLI <b>SYTAFST</b> IAVITG <b>CF</b> -----	24
<b>PetC1</b>	41	YLIPP- <u>SSGSGGGV</u> TAKDALGNDVKVTEFLASH <b>SH</b> NAGDRV	79
<b>PetC2</b>	40	FFVPPAEKGGAGGGI <b>I</b> AKDVLGNPIPASQILA-EAPGTRA	78
<b>PetC3</b>	25	--- <b>GNSSNGQGQ</b> -----TVNVGTMADLKAKG--E	49
<b>Box I</b>			
<b>PetC1</b>	80	LAQGLK <b>GDPT</b> YIIVVQGD <b>DTI</b> ANYGINAV <b>CTHLGC</b> VVPWNA	119
<b>PetC2</b>	79	LVAGLAG <b>GDPT</b> YLIVKEDGSLDSIGIVDS <b>CTHLGC</b> TFPWNG	118
<b>PetC3</b>	50	LKGNTPK <b>GF</b> -VTVVPNGNSGQISAVNPT <b>CTHNGC</b> QVNWKK	88
<b>Box II</b>			
<b>PetC1</b>	120	SENKFM <b>CPCHGS</b> QYNAEGKVVR <b>GPAPLS</b> LALAHATVTD <b>DD</b>	159
<b>PetC2</b>	119	NDQEF <b>QCPCHGS</b> RYHPDGSVARG <b>GPAPLPL</b> LKIVQVAVVD-D	157
<b>PetC3</b>	89	ANGKFV <b>CPCHGA</b> EFAATGKVLK <b>GPAIRD</b> LPTYATQVSGNN	128
<b>PetC1</b>	160	KLVLSTWTETDFRTDEDPWWA	181
<b>PetC2</b>	158	QIFISPWTDLDPRTGEKPWWV	179
<b>PetC3</b>	129	ILVKA-----	133

Fig. 13.4. Sequence alignment of the three PetC proteins of *Synechocystis* sp. PCC 6803. Identical residues, as well as conservative substitutions, are marked by the colored background. Iron-sulfur binding sites (Box I and II) are highlighted in yellow, while amino acids forming putative transmembrane helices are shown in bold. Potential metal binding PetC1-His73 and lipid binding PetC3-Cys23 residues are highlighted by red color. The position of the hinge region is underlined.

characterized cyanobacteria *Synechocystis* sp. PCC 6803, *Nostoc punctiforme* and *Synechococcus* sp. PCC 7002, three Rieske isoforms are encoded (PetC1–3), from which PetC1 is organized with *petA* in an operon and shows the highest similarity to the chloroplast PetC (Schneider et al. 2002). In *Synechocystis* sp. PCC 6803 PetC1, PetC2 and PetC3 are encoded by the open reading frames *sll1316*, *slr1185* and *sll1182* localized in the chromosome at positions 1166186–1166728 (543 bp), 3527045–3527581 (537 bp) and 1848301–1848702 (402 bp), respectively. Nucleotide sequences show 53 %, 49 % and 42 % identities between *petC1* vs. *petC2*, *petC1* vs. *petC3* and *petC2* vs. *petC3*, corresponding to 44 %, 33 % and 24 % identity on the amino acid sequence level. This indicates a much closer relationship between PetC1

and PetC2 than between any of them and PetC3. In some other cyanobacteria, such as *Nostoc* PCC 7120, even an additional fourth Rieske protein (PetC4) is encoded (for a review see (Schneider and Schmidt 2005); for a sequence alignment of PetC1–PetC3 see Fig. 13.4).

Homologous genes encoding different protein isoforms and the resulting heterogeneity in protein complex compositions are well described. One of the most prominent examples in biological energy transduction is the *psbA* gene family, which encodes different (up to five) copies of the D1 protein of PS II in cyanobacteria, expressed differently according to the light conditions (see e.g., Mulo et al. 2009; Nowaczyk et al. 2010). In general, heterogeneity within protein complexes allows organisms to acclimate to changing environmental

conditions. Under normal conditions, typically one gene product is predominantly active, whereas the other (typically silent) gene(s) are expressed only under certain physiological (often stress) conditions. In case of the cyanobacterium *Synechococcus* sp. PCC 7002, the deletion of the canonical *petC* gene (i.e., *petC1*) (Yan and Cramer 2003) was not tolerated, suggesting that only *petC1* encodes a functional Rieske protein. In contrast, *petC1* could be deleted successfully in *Synechocystis* sp. PCC 6803. In this organism, all three *petC* genes (*petC1–3*) were deleted individually; also, two *petC* double deletion strains could be generated, resulting in the generation of five  $\Delta petC$  mutant strains in total. Importantly, only the  $\Delta petC1/\Delta petC2$  double deletion strain turned out to be lethal (Schneider et al. 2004a), suggesting that either PetC1 or PetC2 have to be present and they can, at least partially, substitute each other. This is in good agreement with their high sequence similarity (see above and Fig. 13.4) and their predicted similar midpoint potentials (Schneider et al. 2002, 2004b).

The above mentioned *Synechococcus* data, as well as an in depth *in vivo* analysis of the various *Synechocystis* PCC 6803  $\Delta petC$  mutant strains further supported the assumption that PetC1, which is phylogenetically closest to the group of chloroplast Rieske proteins (Schneider et al. 2002), is the major Rieske iron-sulfur protein in cyanobacteria.

Very recently, the structure of the water-soluble extrinsic domain of the canonical Rieske [2Fe–2S] protein of *T. elongatus* was determined at high (2 Å) resolution (Veit et al. 2012, PDB: 3azc). Three internal water molecules (wat202, wat204, and wat208) have been identified in the structure as well as an unidentified metal ion in close proximity to wat202, which is hydrogen bonded to Tyr69, Asp77, and Val91. Interestingly, His73 (Figs. 13.3 and 13.4), which is located in a loop together with Tyr69 and Asp77, has already been proposed to be part of a potential inhibitory  $Cu^{2+}$  binding site (Rao et al. 2000). Thus, the metal binding site identified in the crystal structure might have a regula-

tory function in the Rieske protein. Notably, a membrane facing hydrophobic pocket has also been identified, suggesting either the binding of a lipophilic ligand (e.g., plastoquinone, lipid, chlorophyll or carotenoid molecule), or of hydrophobic residues from another protein to this hydrophobic cavity. Especially plastocyanin, which binds to cyt *b<sub>6</sub>f* (as it does to PSI) via both hydrophilic and hydrophobic domains (Crowley et al. 2001; Haddadian and Gross 2006), would be a good candidate as binding partner (see also the Chaps. 30 and 31 by Bendall and Howe, and Diaz-Moreno et al. in this volume). This is also in agreement with experimental data, which suggest an electron transfer through the cyt *b<sub>6</sub>f* complex without involvement of cyt *f* (Fernández-Velasco et al. 2001). Remarkably, both the proposed metal-binding motif and the hydrophobic pocket are absent in the PetC2 Rieske variant, indicating differences in the function and/or regulation of PetC1 and PetC2, respectively.

Although cyt *f* re-reduction kinetics indicated very similar catalytic activities of PetC1- and PetC2-type [2Fe–2S] centers under near-single turnover conditions (Ranade and Kallas, unpublished), the  $\delta petC1$  mutant shows a remarkably low electron transport rate through the cyt *b<sub>6</sub>f* complex. However, it could be shown that this is caused by the low cyt *f* content in the  $\delta petC1$  strain, due to co-expression with *petC1* in the *petCA* operon (Schneider et al. 2002). Eventually, this results in low amounts of functional PetC2–cyt *b<sub>6</sub>f* complexes (Schultze et al. 2009; Tsunoyama et al. 2009), causing concomitant accumulation of PQH<sub>2</sub> and a severely reduced capability ( $\leq 30\%$ ) to perform state transitions (Tsunoyama et al. 2009; Krause, Bernát and Rögner, unpublished; Ranade and Kallas, unpublished). These are accompanied by a significantly increased sensitivity towards high light stress, a decreased PS II/PS I ratio, and an enhanced cyt *bd* oxidase activity (Schneider et al. 2004a; Tsunoyama et al. 2009).

Besides this, there is also a low amount of PetC2 even in wild type *Synechocystis* PCC 6803 cells under stress conditions

with significantly increased transcript levels, which suggests a regulatory role of this polypeptide. This is indirectly confirmed by an atypically high growth rate of the  $\Delta petC2$  strains under high light (HL) conditions (Tsunoyama et al. 2009). Generally, stress conditions, including HL treatment (Tsunoyama et al. 2009), low oxygen tension (Summerfield et al. 2008),  $H_2O_2$ - (more than 200-fold increase!) or  $Zn^{2+}$ -treatment (Houot et al. 2007), and cold- or heat stress in the presence of novobiocin (Prakash et al. 2009), induce high PetC2 transcript levels in wild type *Synechocystis*. While novobiocin may induce changes in DNA supercoiling (Prakash et al. 2009), all other observations link the *petC2* expression to the PQ redox level. Notably,  $Zn^{2+}$  (like  $Cu^{2+}$ , see above) has been shown to inhibit electron transport via the high potential chain (Rao et al. 2000; Roberts et al. 2002). Possibly, binding of these metal ions affects the interaction of the Rieske [2Fe-2S] protein with the  $Q_o$  site of the complex, preventing PQH<sub>2</sub> binding and oxidation (Rao et al. 2000; Roberts et al. 2002). Replacing PetC1 by PetC2, which lacks the inhibitory metal binding site (see above), might therefore maintain photosynthetic electron transport through the cyt *b<sub>6</sub>f* complex even under metal stress conditions. However, the benefit of a metal-sensitive variant among two otherwise similar proteins is quite unclear and has to be explored in more detail. Nevertheless, the ability of the  $\Delta petC1$  mutant to perform state transitions – albeit to a lower extent (see above) – indicates that both PetC1- and PetC2-containing cyt *b<sub>6</sub>f* complexes play a role in redox-regulated light energy distribution between the two photosystems in cyanobacteria (Mao et al. 2002).

For PetC3, an involvement in electron transport processes was indicated by combined ferredoxin (Fd)-chromatography/mass spectrometry analysis showing Fd-PetC3 interaction (Hanke et al. 2011) and by significant (fourfold) upregulation of *petC3* expression in a  $\Delta lepB1$  *Synechocystis* strain with a low functional cyt *b<sub>6</sub>f* population

(Zhang et al. 2013). Besides, PetC3 was reported to induce an upregulation of the cyclic electron flow and to be involved in long-term light adaptation processes (Tsunoyama et al. 2009). However, the distinct features of PetC3 prevent a direct substitution of PetC1 or PetC2 in a cyt *b<sub>6</sub>f*-complex. Notably, the N-terminus of PetC3 lacks more than ten residues in comparison to PetC1 and PetC2, the sequence of its putative transmembrane helix is poorly conserved and the connected hinge region is absent (Fig. 13.4; Schneider et al. 2002). Furthermore, the midpoint redox potential of 135 mV (vs. 300–320 mV for PetC1/PetC2) excludes the oxidation of PQH<sub>2</sub>, i.e., a role in the linear electron transport chain (Schneider et al. 2002, 2004b). In contrast to PetC1 and PetC2, which apparently are exclusively located in the thylakoid membrane, PetC3 is exclusively located in the cytoplasmic membrane, with all other major cyt *b<sub>6</sub>f* subunits being absent (Aldridge et al. 2008; Schultze et al. 2009). Consequently, the cyanobacterial cytoplasmic membrane most probably does not contain a functional cyt *b<sub>6</sub>f* complex, which, in turn, excludes a linear or cyclic photosynthetic electron transport and allows only a truncated electron transport chain via the PQ-pool (Schultze et al. 2009; for a review see Bernát and Rögner 2011). In conclusion, PetC3 is probably not a component of a classical cyt *b<sub>6</sub>f* complex. Rather, as predicted by its N-terminal sequence, it might be a lipoprotein with a potential lipid binding site at Cys23 (Fig. 13.4). Based on sequence alignments [e.g., with KILIM\_005\_00710 of *Kineosphaera limosa* or SMUL\_3119 of *Sulfospirillum multivorans* (accession numbers: K6X6L5 and W6EI55, respectively, at UniProt (<http://www.uniprot.org>))], PetC3 is predicted to be a subunit of an arsenite oxidase. Typically, arsenite oxidases are membrane-bound periplasmic enzymes, where the Rieske-type [2Fe–2S] center has a midpoint potential of +60 to +100 mV (Lebrun et al. 2003). The midpoint redox potential of PetC3 (135 mV, see above)

is close to this range, which supports the prediction that the PetC3 Rieske-type protein is a component of an arsenite oxidase. As arsenite was proposed as a potential electron donor to the PQ-pool (Nagy et al. 2014), PetC3 might be involved in this alternative electron transport pathway.

The PetC4 protein in *Nostoc* PCC 7120 has a high sequence similarity to PetC1 and PetC2 and apparently plays a role in nitrogen fixation and/or heterocyst formation and is proposed to be a redox sensor (Arnold et al. 2005).

### III. Small *bona fide* Cytochrome *b<sub>6</sub>f* Subunits

The four small *bona fide* cyt *b<sub>6</sub>f* subunits PetG, –L, –M and –N are located at the periphery of the dimeric cyt *b<sub>6</sub>f* complex and form a so-called “picket fence” structure (Fig. 13.2). While PetM and PetL are positioned peripherally, PetG and PetN are located more deeply inside the complex (Stroebel et al. 2003; Yamashita et al. 2007; Baniulis et al. 2009). This localization is also reflected in the phenotypes of the deletion mutants: While deletion of *petG* or *petN* genes, encoding the partly buried subunits, was impossible and/or showed dramatic effects (*i.e.*, lethal/bleached phenotypes, which are unable to grow photosynthetically) in *Synechocystis* sp. PCC 6803 (Schneider et al. 2007), *C. reinhardtii* ( $\delta$ *petG*, Berthold et al. 1995), and tobacco (Hager et al. 1999; Schwenkert et al. 2007) deletions of *petL* resulted only in moderate phenotypes. Irrespective of pro- or eukaryotic sources, PetL-depleted cyt *b<sub>6</sub>f* complexes were functional, although complex accumulation and stability as well as electron transport rates were affected (Takahashi et al. 1996; Zito et al. 2002; Schneider et al. 2007; Schöttler et al. 2007; Schwenkert et al. 2007). In contrast, deletion of *petM* resulted in different phenotypes in cyanobacteria and higher plants. While PetM is non-essential in the cyanobacterium *Synechocystis* sp. PCC 6803 and the  $\Delta$ *petM* deletion strain

accumulated wild type levels of cyt *b<sub>6</sub>f* complex (Schneider et al. 2001), *petM* RNAi tobacco plants were unable to assemble functional cyt *b<sub>6</sub>f* complexes. This may result from functional differences in the corresponding PetM subunits (Hojka et al. 2014) and/or the different chemical nature of the essential carotenoid prosthetic group (9-*cis*  $\beta$ -carotene in *C. reinhardtii* and higher plants and echinenone in cyanobacteria (Wenk et al. 2005)), which is bound between the PetG and PetM helices.

As with other small proteins (see e.g., Hobbs et al. 2011), the physiological role of the four low molecular weight cyt *b<sub>6</sub>f* complex subunits is only little understood. Besides their important role in assembly and/or stability of the cyt *b<sub>6</sub>f* complex (as discussed above), other – still to be elucidated – functions of these small polypeptides may be predictable or can be suggested based on available experimental data. One example is the proposed regulatory role of PetM in *Synechocystis* sp. PCC 6803, based on a significantly altered stoichiometry of photosynthetic protein complexes in the *petM* knockout strain, while the activity of the cyt *b<sub>6</sub>f* complex was unchanged (Schneider et al. 2001). Furthermore, large-scale protein interaction analyses revealed at least six *Synechocystis* proteins interacting with PetG (Sato et al. 2005). Three of them (gene products of the open reading frames *slI0040*, *slr0594*, and *slr1866*) are classified as unknown/hypothetical proteins, while three others are members of known protein families, among them a RND (Resistance-Nodulation-Division) multidrug efflux transporter (Slr0454, AcrB) and a penicillin-binding protein (SlI0002, PonA). As the functions of these polypeptides are not directly related to known cyt *b<sub>6</sub>f* functions, further data are required for the elucidation of these interactions. Also the function of the sixth interacting partner (SlI0798, RppB, NrsS, Hik30) is still under debate. It is suggested to be a two-component sensor histidine kinase, functioning possibly as a nickel sensor (López-Maury et al. 2002) or as a redox-responsive regulator

of photosynthesis and photopigment related gene expression (Li and Sherman 2000). Based on the finding that low CO<sub>2</sub> reduces expression of *sll0798* – similar to other two-component regulators – a multiple regulatory role was proposed (Wang et al. 2003), potentially involving an up-regulation of the cyclic electron flow, as observed under these conditions (Eisenhut et al. 2007). As the *cyt b<sub>6</sub>f* complex is considered the branching point for cyclic vs. linear electron flow (see e.g., Cramer and Zhang 2006; Cramer et al. 2006, 2010), a control directly at the complex would be straight forward. Present results indicate that PetG and Sll0798 might be involved in such a regulatory mechanism in cyanobacteria. Notably, interaction of Sll0798 with Fd was also reported (Hanke et al. 2011), which again suggests an involvement of this protein in the regulation of electron transport processes.

#### IV. Loosely Bound Subunits

Besides the eight *bona fide* *cyt b<sub>6</sub>f* complex subunits identified in the X-ray structures, there is evidence for further protein components, interacting transiently and/or loosely with the *cyt b<sub>6</sub>f* complex. As discussed above, protein interaction analysis revealed proteins interacting with the small subunit PetG in *Synechocystis* PCC 6803 (Sato et al. 2005). While the physiological role of these interactions is still enigmatic, only one of the three categorized proteins is directly related to electron transport and/or signal transduction processes (see above), *i.e.*, the basic functions of the *cyt b<sub>6</sub>f* complex.

Although it cannot be considered as a small subunit, it should also be noted that the *cyt b<sub>6</sub>f* complex and the ferredoxin: NADP<sup>+</sup> oxidoreductase (FNR; MW = 32–36 kDa) can be co-isolated from higher plants (Clark et al. 1984; Zhang et al. 2001; Iwai et al. 2010; Szymańska et al. 2011; see also the Chap. 23 by Minagawa on *cyt b<sub>6</sub>f* supercomplexes). A central role of

this interaction in cyclic electron transport processes was suggested, which is discussed in detail elsewhere (Cramer et al. 2006, 2010, 2011; Cramer and Zhang 2006; see also the Chaps. 9 and 12 by Cramer and Hasan, and Kurisu).

Besides mediating electron flow, the *cyt b<sub>6</sub>f* complex also has a central role in regulation of state transitions, the short-term regulation of light energy distribution between the two photosystems (Vener et al. 1995; for reviews see Wollman 2001; Allen 2003; Finazzi and Forti 2004; Lemeille and Rochaix 2010; Rochaix 2011; Minagawa 2011; and Chaps. 22 and 24 by Finazzi et al. and Rochaix in this volume). In eukaryotic photoautotrophs, occupation of the *cyt b<sub>6</sub>f* Q<sub>o</sub> site by PQH<sub>2</sub> leads to activation of the Stt7/STN7 kinase, which is a prerequisite for phosphorylation of the light harvesting system of PSII (LHCII) and the subsequent LHCII displacement from PSII to PSI (*i.e.*, state 1 to state 2 transition) (Depège et al. 2003; Bellafiore et al. 2005; Lemeille et al. 2009). Activation of Stt7/STN7 includes transient association with the *cyt b<sub>6</sub>f* complex. Notably, both *cyt b<sub>6</sub>f* and Stt7 have dimeric structures (see Lemeille and Rochaix 2010); however, due to steric reasons it is very unlikely that the dimeric Stt7 can match the C2 symmetry of the *cyt b<sub>6</sub>f* complex. This *cyt b<sub>6</sub>f* complex-associated Stt7/STN7 kinase is inactivated under high light by the ferredoxin-thioredoxin system, most probably in order to prevent potential damage under these conditions (Martinsuo et al. 2003; Puthiyaveetil 2011). Further details are discussed in the Chap. 24 by Rochaix. In *C. reinhardtii*, state 1 to state 2 transitions are also combined with phosphorylation of a 15.2 kDa transmembrane protein (PetO), which is peripherally associated with the *cyt b<sub>6</sub>f* complex (Hamel et al. 2000). PetO was shown to be a component of the *cyt b<sub>6</sub>f*–PSI–FNR–LHCII supercomplex, which is engaged in cyclic electron flow (Iwai et al. 2010). This protein was suggested as *Chlamydomonas*-analog of the PGR5 regulator, which was found attached to the analogous supercomplex in higher plants

(DalCorso et al. 2008; Iwai et al. 2010). Thus, phosphorylation of PetO might be part of the signaling pathway in *Chlamydomonas* (Hamel et al. 2000). Interestingly, while neither PetO nor PGR5 is encoded in cyanobacterial genomes, the hypothetical cyanobacterial protein Ssr2016, which may have a role in cyclic electron flow (Yeremenko et al. 2005), shows a remarkably high similarity to the amino acid sequence of the PGR5 N-terminus. In contrast to the dogma that state 1 to state 2 transitions are generally combined with an increased cyclic vs. linear electron flow (Finazzi et al. 1999, 2002; Wollman 2001), recent results suggest an independent regulation of cyclic electron flow and state transitions (Takahashi et al. 2013; see also Rochaix 2011). Notably, while the molecular regulatory mechanism of state transitions in cyanobacteria is essentially unknown, the triggering mechanism may be similar to that in chloroplasts (Mullineaux and Emlyn-Jones 2005).

Highly purified cyt *b<sub>6</sub>f* complexes from *Synechocystis* sp. PCC 6803 and *T. elongatus* contain an additional associated polypeptide with a molecular mass of ~7 kDa. This potential 9th subunit of the (cyanobacterial) cyt *b<sub>6</sub>f* complex was named PetP (Volkmer et al. 2007; Gendrullis et al. 2008). It is encoded by the open reading frame *ssr2998* in *Synechocystis* PCC 6803 and *tsr0524* in *T. elongatus*, respectively, and is highly conserved in all cyanobacterial genomes (Volkmer et al. 2007). In accordance with its amino acid sequence, predicting a cytoplasmically localized soluble polypeptide, proteomic analyses suggest that PetP is a membrane associated (*i.e.*, not membrane integral) protein (Wang et al. 2009). Combined cross-linking and mass spectrometry analyses, showing direct interaction between the N-termini of SU IV and PetP in *T. elongatus*, further support this view (Rexroth et al. 2014). Although this subunit has not been identified in any of the solved structures of cyanobacterial cyt *b<sub>6</sub>f* complexes (Kurusu et al. 2003; Yamashita et al. 2007; Baniulis et al. 2009; Hasan and Cramer 2014), selected reaction monitoring (SRM) shows a 1:1:1 stoichiometry between

Rieske protein, SU IV and PetP (Rexroth et al. 2014), which therefore appears to be only loosely/temporarily associated with the complex. Functional analysis of *petP* deletion strains showed twofold slower growth rates than wild type cells, especially under HL conditions (Volkmer et al. 2007; Gendrullis et al. 2008; Rexroth et al. 2014). Also, flash-induced absorption change measurements indicated slower re-reduction kinetics relative to wild type of both cyt *f*<sup>+</sup> and P<sub>700</sub><sup>+</sup> by a factor of 1.7–3.1 in the mutants (Volkmer et al. 2007; Gendrullis et al. 2008; Rexroth et al. 2014), whereas the PQ-pool was highly reduced. Interestingly, the electron transport rates through the high-potential/linear electron transport chain was much more affected than the cyclic electron transport around the cyt *b<sub>6</sub>f* complex (Rexroth et al. 2014) and through the low-potential chain within the complex which was basically unaffected (Nowaczyk et al. 2010). These kinetic alterations are accompanied by a strongly decreased stability of the complex isolated from PetP-depleted *T. elongatus* (Rexroth et al. 2014). Thus, although PetP is not an essential cyt *b<sub>6</sub>f* subunit, these observations suggest a combined structural and regulatory role for PetP, which seems to be indispensable for maintaining the maximal photosynthetic activity under changing environmental conditions. In good accordance with this, time-lagged profiles of the transcriptional response of *ssr2998* indicate a close correlation with some genes encoding different PSII and phycobilisome subunits under fluctuating light (Schmitt et al. 2004). Also, screening for interaction partners of heterologously overexpressed PetP revealed, besides essential phycobilisome and cyt *b<sub>6</sub>f* subunits, three PSI subunits, NdhF3, and Fd as potential interaction partners of PetP (Rexroth et al. 2014). Putting these together with the kinetic data above suggests a potential role of PetP in electron transport processes and, like PetO in *C. reinhardtii* (see above), formation of a cyt *b<sub>6</sub>f*–PSI super-complex in cyanobacteria.

It should also be mentioned that depletion of the integral membrane protein Ycf34, a

prototype of a new class of [4Fe-4S] proteins, shows – depending on light conditions – a similar phenotype as several cyt  $b_6f$  mutants (see above), *i.e.*, impaired electron transport through the complex (Wallner et al. 2012). This suggests a – direct or indirect – interaction between Ycf34 and the cyt  $b_6f$  complex.

## Acknowledgements

We thank Sandra K. Gridley and Toivo Kallas for careful reading of the manuscript. Financial support by SFB 480 (project C1, MR) is acknowledged. GB was supported by project Algaman (CZ.1.07/2.3.00/20.0203) of the Ministry of Education, Youth and Sports (MŠMT), Czech Republic.

## References

- Agarwal R, Hasan SS, Jones LM, Stofleth JT, Ryan CM, Whitelegge JP, Kehoe DM, Cramer WA (2015) Role of domain swapping in the hetero-oligomeric cytochrome  $b_6f$  lipoprotein complex. *Biochemistry* 54:3151–3163
- Aldridge A, Spence E, Kirkilionis MA, Frigerio L, Robinson C (2008) Tat-dependent targeting of Rieske iron-sulfur proteins to both the plasma and thylakoid membranes in the cyanobacterium *Synechocystis* PCC 6803. *Mol Microbiol* 70:140–150
- Allen JF (2003) State transitions – a question of balance. *Science* 299:1530–1532
- Arnold M, Hauska G, Maldener I (2005) A special isoform of the Rieske–FeS protein is involved in heterocyst function of the cyanobacterium *Anabaena* sp PCC 7120. In: van der Est A, Bruce D (eds) *Photosynthesis: Fundamental Aspects to Global Perspectives*. Allen Press, Lawrence, pp 443–446
- Baniulis D, Yamashita E, Whitelegge JP, Zatsman AI, Hendrich MP, Hasan SS, Ryan CM, Cramer WA (2009) Structure-function, stability, and chemical modification of the cyanobacterial cytochrome  $b_6f$  complex from *Nostoc* sp PCC 7120. *J Biol Chem* 284:9861–9869
- Bellafore S, Barneche F, Peltier G, Rochaix JD (2005) State transitions and light adaptation require chloroplast thylakoid protein kinase STN7. *Nature* 433:892–895
- Bernát G, Rögner M (2011) Center of the cyanobacterial electron transport network: the cytochrome  $b_6f$  complex. In: Peschek GA, Obinger C, Renger G (eds) *The Bioenergetic Processes in Cyanobacteria – From Evolutionary Singularity to Ecological Diversity*. Springer, Dordrecht/New York, pp 573–606
- Berthold DA, Schmidt CL, Malkin R (1995) The deletion of *petG* in *Chlamydomonas-Reinhardtii* disrupts the cytochrome  $bf$  complex. *J Biol Chem* 270:29293–29298
- Carrell CJ, Zhang HM, Cramer WA, Smith JL (1997) Biological identity and diversity in photosynthesis and respiration: structure of the lumen-side domain of the chloroplast Rieske protein. *Structure* 5: 1613–1625
- Clark RD, Hawkesford MJ, Coughlan SJ, Hind G (1984) Association of ferredoxin-NADP<sup>+</sup> oxidoreductase with the chloroplast cytochrome  $bf$  complex. *FEBS Lett* 174:137–142
- Cramer WA, Zhang HM (2006) Consequences of the structure of the cytochrome  $b_6f$  complex for its charge transfer pathways. *Biochim Biophys Acta* 1757:339–345
- Cramer WA, Zhang HM, Yan JS, Kurisu G, Smith JL (2006) Transmembrane traffic in the cytochrome  $b_6f$  complex. *Annu Rev Biochem* 75:769–790
- Cramer WA, Yamashita E, Baniulis D, Hasan SS (2010) The cytochrome  $b_6f$  complex of oxygenic photosynthesis. In: Messerschmidt A (ed) *The Handbook of Metalloproteins*. Wiley, Chichester, pp 16–28
- Cramer WA, Hasan SS, Yamashita E (2011) The Q cycle of cytochrome  $bf$  complexes: a structure perspective. *Biochim Biophys Acta* 1807:788–802
- Crofts AR (2004) Proton-coupled electron transfer at the Q<sub>o</sub>-site of the  $bc_1$  complex controls the rate of ubiquinone oxidation. *Biochim Biophys Acta* 1655:77–92
- Crofts AR, Guergova-Kuras M, Kuras R, Ugulava N, Li JY, Hong SJ (2000) Proton-coupled electron transfer at the Q<sub>o</sub> site: what type of mechanism can account for the high activation barrier? *Biochim Biophys Acta* 1459:456–466
- Crowley PB, Otting G, Schlarb-Ridley BG, Canters GW, Ubbink M (2001) Hydrophobic interactions in cyanobacterial plastocyanin-cytochrome  $f$  complex. *J Am Chem Soc* 123:10444–10453
- DalCorso G, Pesaresi P, Masiero S, Aseeva E, Schünnemann D, Finazzi G, Joliot P, . . . , Leister D (2008) A complex containing PGRL1 and PGRL5 is involved in the switch between linear and cyclic electron flow in Arabidopsis. *Cell* 132:273–285



- Depège N, Bellaïf S, Rochaix JD (2003) Role of chloroplast protein kinase Stt7 in LHCII phosphorylation and state transition in *Chlamydomonas*. *Science* 299:1572–1575
- Dibrova DV, Cherepanov DA, Galperin MY, Skulachev VP, Mulikidjanian AY (2013) Evolution of cytochrome *bc* complexes: from membrane-anchored dehydrogenases of ancient bacteria to triggers of apoptosis in vertebrates. *Biochim Biophys Acta* 1827:1407–1427
- Eisenhut M, Aguirre von Wobeser E, Jonas L, Schubert H, Ibelings BW, Bauwe H, HC Matthijs, Hagemann M (2007) Long-term response toward inorganic carbon limitation in wild type and glycolate turnover mutants of the cyanobacterium *Synechocystis* sp. strain PCC 6803. *Plant Physiol* 144:1946–1959
- Fernández-Velasco JG, Jamshidi A, Gong XS, Zhou J, Ueng RY (2001) Photosynthetic electron transfer through the cytochrome *b<sub>6</sub>f* complex can bypass cytochrome *f*. *J Biol Chem* 276:30589–30607
- Ferraro DJ, Gakhar L, Ramaswamy S (2005) Rieske business: structure-function of Rieske non-heme oxygenases. *Biochem Biophys Res Commun* 338:175–190
- Finazzi G (2002) Redox-coupled proton pumping activity in cytochrome *b<sub>6</sub>f*, as evidenced by the pH dependence of electron transfer in whole cells of *Chlamydomonas reinhardtii*. *Biochemistry* 41:7475–7482
- Finazzi G, Forti G (2004) Metabolic flexibility of the green alga *Chlamydomonas reinhardtii* as revealed by the link between state transitions and cyclic electron flow. *Photosynth Res* 82:327–338
- Finazzi G, Furia A, Barbagallo RP, Forti G (1999) State transitions, cyclic and linear electron transport and photophosphorylation in *Chlamydomonas reinhardtii*. *Biochim Biophys Acta* 1413:117–129
- Finazzi G, Rappaport F, Furia A, Fleischmann M, Rochaix JD, Zito F, Forti G (2002) Involvement of state transitions in the switch between linear and cyclic electron flow in *Chlamydomonas reinhardtii*. *EMBO Rep* 3:280–285
- Gendrullis M, Dyczmons N, Gomolla D, Gathmann S, Bernát G, Schneider D, Rögner M (2008) PetP, a new cytochrome *b<sub>6</sub>f* subunit, and cytochrome *bd* oxidase – two potential regulatory players of cyanobacterial electron transport? In: Allen JF, Gantt JH, Golbeck JH, Osmond B (eds) *Photosynthesis Energy from the Sun*. Springer, Dordrecht, pp 585–589
- Haddadian EJ, Gross EL (2006) A Brownian dynamics study of the effects of cytochrome *f* structure and deletion of its small domain in interaction with cytochrome *c<sub>6</sub>* and plastocyanin in *Chlamydomonas reinhardtii*. *Biophys J* 90:566–577
- Hager M, Biehler K, Illerhaus J, Ruf S, Bock R (1999) Targeted inactivation of the smallest plastid genome-encoded open reading frame reveals a novel and essential subunit of the cytochrome *b<sub>6</sub>f* complex. *EMBO J* 18:5834–5842
- Hamel P, Olive J, Pierre Y, Wollman FA, de Vitry C (2000) A new subunit of cytochrome *b<sub>6</sub>f* complex undergoes reversible phosphorylation upon state transition. *J Biol Chem* 275:17072–17079
- Hanke GT, Satomi Y, Shinmura K, Takao T, Hase T (2011) A screen for potential ferredoxin electron transfer partners uncover new, redox dependent interactions. *Biochim Biophys Acta* 1814:366–374
- Hasan SS, Cramer WA (2014) Internal lipid architecture of the hetero-oligomeric cytochrome *b<sub>6</sub>f* complex. *Structure* 22:1008–1015
- Heimann S, Ponamarev MV, Cramer WA (2000) Movement of the Rieske iron–sulfur protein in the *p*-side bulk aqueous phase: effect of luminal viscosity on redox reactions of the cytochrome *b<sub>6</sub>f* complex. *Biochemistry* 39:2692–2699
- Hobbs EC, Fontaine F, Yin X, Storz G (2011) An expanding universe of small proteins. *Curr Opin Microbiol* 14:167–173
- Hojka M, Thiele W, Tóth SZ, Lein W, Bock R, Schöttler MA (2014) Inducible repression on nuclear-encoded subunits of the cytochrome *b<sub>6</sub>f* complex in tobacco reveals an extraordinarily long lifetime of the complex. *Plant Physiol* 165:1632–1646
- Houot L, Floutier M, Marteyn B, Michaut M, Picciocchi A, Legrain P, Aude JC, Cassier-Chauvat F (2007) Cadmium triggers an integrated reprogramming of the metabolism of *Synechocystis* sp. PCC 6803, under the control of the Slr 1738 regulator. *BMC Genomics* 8:350
- Iwai M, Takizawa K, Tokutsu R, Okamuro A, Takahashi A, Minagawa J (2010) Isolation of the super-complex that drives cyclic electron flow in photosynthesis. *Nature* 464:1210–1213
- Kallas T, Spiller S, Malkin R (1988) Characterization of 2 operons encoding the cytochrome-*b<sub>6</sub>f* complex of the cyanobacterium *Nostoc* PCC 7906 – highly conserved sequences but different gene organization than in chloroplasts. *J Biol Chem* 263:14334–14342
- Kurisu G, Zhang HM, Smith JL, Cramer WA (2003) Structure of the cytochrome *b<sub>6</sub>f* complex of oxygenic photosynthesis: tuning the cavity. *Science* 302:1009–1014
- Lebrun E, Brugna M, Baymann F, Müller D, Lièvreumont D, Lett MC, Nitschke W (2003) Arsenite oxidase, an ancient bioenergetic enzyme. *Mol Biol Evol* 20:686–693

- Lemeille S, Rochaix JD (2010) State transition at the crossroad of thylakoid signaling pathways. *Photosynth Res* 106:33–46
- Lemeille S, Willig A, Depège-Fargeix N, Delessert C, Bassi R, Rochaix JD (2009) Analysis of the chloroplast protein kinase Stt7 during state transitions. *PLoS Biol* 7:e1000045
- Li H, Sherman LA (2000) A redox-responsive regulator of photosynthesis gene expression in the cyanobacterium *Synechocystis* sp. strain PCC 6803. *J Bacteriol* 182:4268–4277
- Liu J, Chakraborty S, Hosseinzadeh P, Yu Y, Tian S, Petrik I, Bhagi A, Lu Y (2014) Metalloproteins containing cytochrome, iron-sulfur, or copper redox centers. *Chem Rev* 114:4366–4469
- López-Maury L, García-Domínguez M, Florencio FJ, Reyes JC (2002) A two-component signal transduction system involved in nickel sensing in the cyanobacterium *Synechocystis* sp. PCC 6803. *Mol Microbiol* 43:247–256
- Mao HB, Li GF, Ruan X, Wu QY, Gong YD, Zhang XF, Zhao NM (2002) The redox state of plastoquinone pool regulates state transitions via cytochrome *b<sub>6</sub>f* complex in *Synechocystis* sp. PCC 6803. *FEBS Lett* 519:82–86
- Martínez SE, Huang D, Ponomarev M, Cramer WA, Smith JL (1996) The heme redox center of chloroplast cytochrome *f* is linked to a buried five-water chain. *Protein Sci* 5:1081–1092
- Martinsuo P, Pursiheimo S, Aro EM, Rintamäki E (2003) Dithiol oxidant and disulfide reductant dynamically regulate the phosphorylation of light-harvesting complex II proteins in thylakoid membranes. *Plant Physiol* 133:37–46
- Minagawa J (2011) State transitions – the molecular remodeling of photosynthetic supercomplexes that controls energy flow in chloroplast. *Biochim Biophys Acta* 1807:897–905
- Mitchell P (1975) Protonmotive redox mechanism of cytochrome-*bc<sub>1</sub>* complex in respiratory chain – protonmotive ubiquinone cycle. *FEBS Lett* 56:1–6
- Mullineaux CW, Emlyn-Jones D (2005) State transitions: an example of acclimation to low-light stress. *J Exp Bot* 56:389–393
- Mulo P, Sicora C, Aro EM (2009) Cyanobacterial *psbA* family: optimization of oxygenic photosynthesis. *Cell Mol Life Sci* 66:3697–3710
- Nagy CI, Vass I, Rákhely G, Vass IZ, Tóth A, Duzs Á, Peca L, . . . , Kós PB (2014) Coregulated genes link sulfide: quinone oxidoreductase and arsenic metabolism in *Synechocystis* sp. strain PCC 6803. *J Bacteriol* 196:3430–3440
- Nitschke W, Joliot P, Liebl U, Rutherford WA, Hauska G, Müller A, Riedel A (1992) The pH dependence of the redox midpoint potential of the 2Fe2S cluster from cytochrome *b<sub>6</sub>f* complex (the ‘Rieske centre’). *Biochim Biophys Acta* 1102:266–268
- Nowaczyk MM, Sander J, Grasse N, Cormann KU, Rexroth D, Bernát G, Rögner M (2010) Dynamics of the cyanobacterial photosynthetic network: communication and modification of membrane protein complexes. *Eur J Cell Biol* 89:974–982
- Ponomarev MV, Cramer WA (1998) Perturbation of the internal water chain in cytochrome *f* of oxygenic photosynthesis: loss of the concerted reduction of cytochromes *f* and *b<sub>6</sub>*. *Biochemistry* 37:17199–17208
- Prakash JSS, Sinetova M, Zorina A, Kupriyanova E, Suzuki I, Murata N, Los DA (2009) DNA supercoiling regulates the stress-inducible expression of genes in the cyanobacterium *Synechocystis*. *Mol Biosyst* 5:1904–1912
- Puthiyaveetil S (2011) A mechanism for regulation of chloroplast LHC II kinase by plastoquinol and thioredoxin. *FEBS Lett* 585:1717–1721
- Rao BKS, Tyrshkin AM, Roberts AG, Bowman MK, Kramer DM (2000) Inhibitory copper binding site on the spinach cytochrome *b<sub>6</sub>f* complex: implications for Q<sub>o</sub> site catalysis. *Biochemistry* 39:3285–3296
- Rexroth S, Rexroth D, Veit S, Plohnke N, Cormann KU, Nowaczyk MM, Rögner M (2014) Functional characterization of the small regulatory subunit PetP from the cytochrome *b<sub>6</sub>f* complex in *Thermosynechococcus elongatus*. *Plant Cell* 26:3435–3448
- Rieske JS, MacLennan DH, Coleman R (1964) Isolation and properties of an iron-protein from the (reduced coenzyme Q)-cytochrome C reductase complex of the respiratory chain. *Biochem Biophys Res Commun* 15:338–344
- Roberts AG, Bowman MK, Kramer DM (2002) Certain metal ion are inhibitors of cytochrome *b<sub>6</sub>f* complex ‘Rieske’ iron–sulfur protein domain movements. *Biochemistry* 41:4070–4079
- Rochaix JD (2011) Reprint of: regulation of photosynthetic electron transport. *Biochim Biophys Acta* 1807:878–886
- Sato S, Shimoda Y, Muraki A, Kohara M, Nakamura Y, Tabata A (2005) A large-scale protein-protein analysis in *Synechocystis* sp. PCC 6803. *DNA Res* 14:207–216
- Schmitt WA Jr, Raab RM, Stephanopoulos G (2004) Elucidation of gene interaction networks through time-lagged correlation analysis of transcriptional data. *Genome Res* 14:1654–1663
- Schneider D, Schmidt CL (2005) Multiple Rieske proteins in prokaryotes: where and why? *Biochim Biophys Acta* 1710:1–12

- Schneider D, Berry S, Rich P, Seidler A, Rögner M (2001) A regulatory role of the PetM subunit in a cyanobacterial cytochrome *b<sub>6</sub>f* complex. *J Biol Chem* 276:16780–16785
- Schneider D, Skrzypczak S, Anemüller S, Schmidt CL, Seidler A, Rögner M (2002) Heterogeneous Rieske proteins in the cytochrome *b<sub>6</sub>f* complex of *Synechocystis* PCC 6803? *J Biol Chem* 277:10949–10954
- Schneider D, Berry S, Volkmer T, Seidler A, Rögner M (2004a) PetC1 is the major Rieske iron-sulfur protein in the cytochrome *b<sub>6</sub>f* complex of *Synechocystis* sp PCC 6803. *J Biol Chem* 279:39383–39388
- Schneider D, Volkmer T, Berry S, Seidler A, Rögner M (2004b) Characterisation of the PETC gene family in the cyanobacterium *Synechocystis* PCC 6803. *Cell Mol Biol Lett* 9:51–55
- Schneider D, Volkmer T, Rögner M (2007) PetG and PetN, but not PetL, are essential subunits of the cytochrome *b<sub>6</sub>f* complex from *Synechocystis* PCC 6803. *Res Microbiol* 158:45–50
- Schöttler MA, Flügel C, Thiele W, Bock R (2007) Knock-out of the plastid-encoded PetL subunit results in reduced stability and accelerated leaf age-dependent loss of the cytochrome *b<sub>6</sub>f* complex. *J Biol Chem* 282:976–985
- Schultze M, Forberich B, Rexroth S, Dyczmons NG, Rögner M, Appel J (2009) Localization of cytochrome *b<sub>6</sub>f* complexes implies an incomplete respiratory chain in cytoplasmic membranes of the cyanobacterium *Synechocystis* sp PCC 6803. *Biochim Biophys Acta* 1787:1479–1485
- Schwenkert S, Legen J, Takami T, Shikanai T, Herrmann RG, Meurer J (2007) Role of the low-molecular-weight subunits PetL, PetG, and PetN in assembly, stability, and dimerization of the cytochrome *b<sub>6</sub>f* complex in tobacco. *Plant Physiol* 144:1924–1935
- Stroebel D, Choquet Y, Popot JL, Picot D (2003) An atypical haem in the cytochrome *b<sub>6</sub>f* complex. *Nature* 426:413–418
- Summerfield TC, Toepel J, Sherman LA (2008) Low-oxygen induction of normally cryptic *psbA* genes in cyanobacteria. *Biochemistry* 40:411–417
- Szymańska R, Dłużewska J, Ślesak I, Kruk J (2011) Ferredoxin:NADP<sup>+</sup> oxidoreductase bound to cytochrome *b<sub>6</sub>f* complex is active in plastoquinone reduction: implications for cyclic electron transport. *Phys Plant* 141:289–298
- Takahashi Y, Rahire M, Breyton C, Popot JL, Joliot P, Rochaix JD (1996) The chloroplast *ycf7* (*petL*) open reading frame of *Chlamydomonas reinhardtii* encodes a small functionally important subunit of the cytochrome *b<sub>6</sub>f* complex. *EMBO J* 15:3498–3506
- Takahashi H, Clowez S, Wollman FA, Vallon O, Rapaport F (2013) Cyclic electron flow is redox-controlled but independent of state transition. *Nat Commun* 4:1954
- Tsunoyama Y, Bernát G, Dyczmons NG, Schneider D, Rögner M (2009) Multiple Rieske proteins enable short- and long-term light adaptation of *Synechocystis* sp PCC 6803. *J Biol Chem* 284:27875–27883
- Veit S, Takeda K, Tsunoyama Y, Rexroth D, Rögner M, Miki K (2012) Structure of a thermophilic cyanobacterial *b<sub>6</sub>f*-type Rieske protein. *Acta Crystallogr D* 68:1400–1408
- Vener AV, van Kan PJM, Gal A, Andersson B, Ohad I (1995) Activation deactivation cycle of redox-controlled thylakoid protein-phosphorylation – role of plastoquinol bound to the reduced cytochrome *b<sub>6</sub>f* complex. *J Biol Chem* 270:25225–25232
- Volkmer T, Schneider D, Bernát G, Kirchhoff H, Wenk SO, Rögner M (2007) Ssr2998 of *Synechocystis* sp PCC 6803 is involved in regulation of cyanobacterial electron transport and associated with the cytochrome *b<sub>6</sub>f* complex. *J Biol Chem* 282:3730–3737
- Wallner T, Hagiwara Y, Bernát G, Sobotka R, Reijerse EJ, Frankenberg-Dinkel N, Wilde A (2012) Inactivation of the conserved open reading frame *ycf34* of *Synechocystis* sp. PCC 6803 interferes with the photosynthetic electron transport chain. *Biochim Biophys Acta* 1817:2016–2026
- Wang HL, Postier BL, Burnap RL (2003) Alterations in global patterns of gene expression in *Synechocystis* sp. PCC 6803 in response to inorganic carbon limitation and the inactivation of *ndhR*, a LysR family regulator. *J Biol Chem* 279:5739–5751
- Wang Y, Xu Y, Chitnis PR (2009) Identification and bioinformatic analysis of the membrane proteins of *Synechocystis* sp. PCC 6803. *Proteome Sci* 7:11
- Wenk SO, Schneider D, Boronowsky U, Jäger C, Klughammer C, de Weerd FL, van Roon H, . . . , Rögner M (2005) Functional implications of pigments bound to a cyanobacterial cytochrome *b<sub>6</sub>f* complex. *FEBS J* 272:582–592
- Wollman FA (2001) State transitions reveal the dynamics and flexibility of the photosynthetic apparatus. *EMBO J* 20:3623–3630
- Yamashita E, Zhang H, Cramer WA (2007) Structure of the cytochrome *b<sub>6</sub>f* complex: quinone analogue inhibitors as ligands of heme *c<sub>n</sub>*. *J Mol Biol* 370:39–52
- Yan JS, Cramer WA (2003) Functional insensitivity of the cytochrome *b<sub>6</sub>f* complex to structure changes in the hinge region of the Rieske iron-sulfur protein. *J Biol Chem* 278:20925–20933
- Yeremenko N, Jeanjean R, Prommeenate P, Krasikov V, Nixon PJ, Vermaas WFJ, Havaux M, Matthijs

- HCP (2005) Open reading frame *ssr2016* is required for antimycin A-sensitive photosystem I-driven cyclic electron flow in the cyanobacterium *Synechocystis* sp PCC 6803. *Plant Cell Physiol* 46:1433–1436
- Zhang H, Carrell CJ, Huang D, Sled V, Ohnishi T, Smith JL, Cramer WA (1996) Characterization and crystallization of the lumen side domain of the chloroplast Rieske iron-sulfur protein. *J Biol Chem* 271:31360–31366
- Zhang HM, Whitelegge JP, Cramer WA (2001) Ferredoxin: NADP<sup>+</sup> oxidoreductase is a subunit of the chloroplast cytochrome  $b_6f$  complex. *J Biol Chem* 276:38159–38165
- Zhang L, Selão TT, Pisareva T, Qian J, Sze SK, Carlberg I, Norling B (2013) Deletion of *Synechocystis* sp. PCC 6803 leader peptidase LepB1 affects photosynthetic complexes and respiration. *Mol Cell Proteomics* 12:1193–1203
- Zito F, Finazzi G, Joliot P, Wollman FA (1998) Glu78, from the conserved PEWY sequence of subunit IV, has a key function in cytochrome  $b_6f$  turnover. *Biochemistry* 37:10395–10403
- Zito F, Vinh J, Popot JL, Finazzi G (2002) Chimeric fusions of subunit IV and PetL in the  $b_6f$  complex of *Chlamydomonas reinhardtii* – structural implications and consequences on state transitions. *J Biol Chem* 277:12446–12455

# Chapter 14

## Inter-Monomer Electron Transfer in Cytochrome *bc* Complexes

Marcin Sarewicz, Robert Ekiert, and Artur Osyczka\*  
*Department of Molecular Biophysics, Faculty of Biochemistry,  
Biophysics and Biotechnology, Jagiellonian University,  
30-387 Kraków, Poland*

Summary.....	281
I. Introduction.....	282
II. Implications from Structures for Inter-Monomer Electron Transfer.....	282
III. Theoretical Prediction for the Time Scale of Heme $b_L$ - $b_L$ Electron Transfer.....	283
IV. Experimental Evidence for Inter-Monomer Electron Transfer.....	285
V. Mechanistic Consequences of Inter-Monomer Electron Transfer.....	288
VI. Physiological Significance of Inter-Monomer Electron Transfer.....	289
VII. Conclusions.....	290
Acknowledgments.....	291
References.....	291

### Summary

Crystal structures of cytochrome  $bc_1/b_6f$  revealed that these complexes assemble as homodimers. An intriguing feature of redox cofactor spatial arrangement in the dimers is the relatively short distance between two low potential hemes  $b_L$  located in separated monomers. Theoretical calculations suggested that with this distance a two-heme bridge can support inter-monomer electron transfer on the catalytic time scale. While this electron exchange was incorporated in several models describing the molecular mechanism of catalysis, its experimental verification has been hampered by a high degree of structural symmetry and the fact that such a reaction  $bc$  can be considered as virtual self-exchange. Recently, the construction of cytochrome  $bc_1$  derivatives with broken symmetry between the monomers provided experimental evidence that the heme  $b_L$ - $b_L$  electron transfer does take place on the catalytically-relevant time scale. In this chapter we summarize these recent developments and discuss the mechanistic consequences and possible physiological meaning of this inter-monomer connection.

---

\*Author for correspondence, e-mail: [Arthur.osyczka@uj.edu.pl](mailto:Arthur.osyczka@uj.edu.pl)

## I. Introduction

All known cytochrome  $bc_1/b_6f$  complexes are homodimers characterized by high structural symmetry between the monomers. The symmetry concerns both the architecture of cofactor chains and the amino-acid composition/structure of the proteins (Berry et al. 2004; Xia et al. 2013). Intriguingly, the architecture of cofactor chains, as described by crystal structures of  $bc_1/b_6f$  complexes (Xia et al. 1997; Zhang et al. 1998; Hunte et al. 2000; Kurisu et al. 2003; Stroebel et al. 2003; Hasan et al. 2013), indicated that the two monomers are separated in such a way that they do not exchange electrons, except for one point where closely-positioned hemes  $b_L$  (each coming from different monomer) make catalytically-relevant electron transfer between monomers possible. Accordingly, several groups have suggested that this electronic connection may be an inherent part of enzymatic turnover, either as a straightforward electron transfer route that competes with intra-monomer electron transfer (Osyczka et al. 2004, 2005; Shinkarev and Wraight 2007), or as an element of more elaborate pathways involving conformational changes or substrate exchanges that gate various processes (Gupta et al. 1998; Covian et al. 2004; Covian and Trumpower 2006, 2008; Cooley et al. 2009; Castellani et al. 2010).

However, from the structural point of view, as each monomer is equipped with all elements necessary to perform the catalytic

Q-cycle described in detail in other chapters in this volume (see also Sarewicz and Osyczka 2015 for a recent review), both the existence of the inter-monomer electron transfer and its possible role became a matter of intense debate (Shinkarev and Wraight 2007; Crofts et al. 2008, 2013; Mulkidjanian 2010; Cramer et al. 2011; Khalfaoui-Hassani et al. 2012; Bazil et al. 2013; Hasan et al. 2014). In searching for the ways of verifying whether the inter-monomer electron transfer exists, the experiments based on studying the effects of mutated residues lying between the two hemes  $b_L$  at the monomer:monomer interface (Gong et al. 2005), or the effects of sub-stoichiometric concentrations of inhibitors were initially described (Covian and Trumpower 2005). However, the results of those experiments are opened to interpretation (Shinkarev and Wraight 2007; Crofts et al. 2008).

Recently, a direct evidence of inter-monomer electron transfer was provided by the experiments in which the structural symmetry of the dimer was broken to expose the inter-monomer connection for kinetic testing *in vitro* and functional testing *in vivo* (Świerczek et al. 2010; Lanciano et al. 2011, 2013a; Czaplą et al. 2012a, 2013; Ekiert et al. 2014). In this chapter, we focus on those recent advances and present them along with background of structural and theoretical rationales to describe the current state of knowledge on inter-monomer electron transfer in cytochrome  $bc$  complexes and its possible physiological meaning.

---

*Abbreviations:* A – Electron acceptor; B-B – Cytochrome  $bc_1$ -like complex containing fusion protein of two *R. capsulatus* cytochromes  $b$  (cytochrome  $bb$ ) in place of two separate cytochrome  $b$  subunits; B<sub>S</sub>-B – Cytochrome  $bc_1$ -like complex containing a hybrid-fusion protein of *R. sphaeroides* and *R. capsulatus* cytochromes  $b$  (cytochrome  $b_{SB}$ ) in place of two separate cytochrome  $b$  subunits; D – Electron donor; Fe-S – Rieske protein, subunit of cytochrome  $bc_1$  complex containing [2Fe-2S] cluster; Q<sub>i</sub> – Quinone reduction site of cytochrome  $bc_1$  also known as Q<sub>n</sub>; Q<sub>o</sub> – Quinol oxidation site of cytochrome  $bc_1$  also known as Q<sub>p</sub>; *R.* – *Rhodobacter*; ROS – Reactive Oxygen Species; UQ – Ubiquinone; UQH<sub>2</sub> – Ubihydroquinone

## II. Implications from Structures for Inter-Monomer Electron Transfer

As the structural details of cytochrome  $bc$  complexes are described in other chapters of this book, we highlight just those elements that are essential to the topic of this section.

Cytochrome  $bc_1$  complex assembles as a homodimer, where each monomer consists of three catalytically active subunits: cytochrome  $b$ , cytochrome  $c_1$  and the Fe-S protein. The accessory subunits that are

present in some structures, especially in mitochondrial complex III, do not play a role in redox reactions catalyzed by the enzyme. The core cytochrome  $b$  subunit in each monomer contains two catalytic quinone-binding sites,  $Q_i$  and  $Q_o$ , localized near the two opposite sides of the membrane: inside (matrix) and outside (inter-membrane). These two sites are electronically connected by heme  $b_L$  and heme  $b_H$  that form the low potential  $b$ -chain. The cofactors of other core subunits, heme  $c_1$  of cytochrome  $c_1$  and Rieske [2Fe-2S] cluster of the Fe-S protein, form the high potential  $c$ -chain connecting the  $Q_o$  site with soluble electron carriers (such as cytochrome  $c$ ) (Berry et al. 2000; Xia et al. 2013).

Despite the differences in the genetic and protein amino-acid sequences, the general spatial arrangement of cofactors and catalytic sites in mitochondrial complex III, cytochrome  $b_{6f}$  and bacterial cytochrome  $bc_1$  is highly conserved. When crystal structures of  $bc_1$  homologues from various organisms are superimposed, the catalytic core of the enzymes reveals no significant differences, especially within the central hydrophobic protein core of cytochrome  $b$  and within the arrangement of all four hemes  $b$  in the dimer (Fig. 14.1a). The arrangement of cofactors in cytochrome  $b_{6f}$  exhibits some differences in the peripheral parts of the chains: the location of heme  $f$  is shifted in comparison to heme  $c_1$ , and additionally, an atypical heme  $c_i$  is present near heme  $b_H$  and the  $Q_i$  binding site of cytochrome  $b_{6f}$  (Kurisu et al. 2003; Stroebel et al. 2003) [also see Hasan et al., this volume]. However, the other cofactors of cytochrome  $b_{6f}$  overlay with those from cytochrome  $bc_1$  counterparts. Interestingly, the edge-to-edge distance between the two hemes  $b_L$  in the dimer varies between 13.2 and 15.2 Å, depending on the structure. Such distances fall within the limits of the electron transfer rate required for the fast catalytic turnover of enzymes (Page et al. 1999). Conversely, other cofactors of the opposite monomers are positioned farther apart, preventing any catalytically-relevant electron exchange.

The cofactor arrangement suggests the existence of a highly symmetric H-shaped electron transfer system built of two upper and two lower branches connected by a bridge formed by the two hemes  $b_L$  (Fig. 14.1b). In this system, the heme  $b_L$ - $b_L$  bridge constitutes a structural element supporting the inter-monomer electron transfer.

### III. Theoretical Prediction for the Time Scale of Heme $b_L$ - $b_L$ Electron Transfer

Direct measurements of the rate of possible electron transfer between hemes  $b_L$  in cytochrome  $bc_1$  are generally difficult because of several reasons, including the high symmetry of the dimer and the fact that such reaction can be considered as virtual self-exchange. The magnitude of the rate of electron transfer between two hemes  $b_L$  can, however, be estimated by theoretical calculations.

The general view of electron transfer theory is discussed in detail in Sect. II of this book. Here, we introduce those aspects that directly relate to calculations of heme  $b_L$ - $b_L$  electron transfer. The nature of electron transfer process is quantum mechanical and relies on quantum mechanical tunneling phenomenon, which means that electron can cross an insulating barrier between donor (D) and acceptor (A) even when the thermal energy is much lower than the energy gap between those of the electron donor and acceptor (Marcus and Sutin 1985; Moser et al. 1992; Barbara et al. 1996). The characteristic rate constant of such electron tunneling between D and A molecules follows Fermi's golden rule and depends on a product of two terms: the electronic ( $V^2$ ) and the nuclear ( $FC$ ):

$$k_{ET} = \frac{2\pi}{\hbar} V^2 FC \quad (14.1)$$

where,  $k_{ET}$  is the rate of electron tunneling,  $V^2$  is the electronic coupling between D and

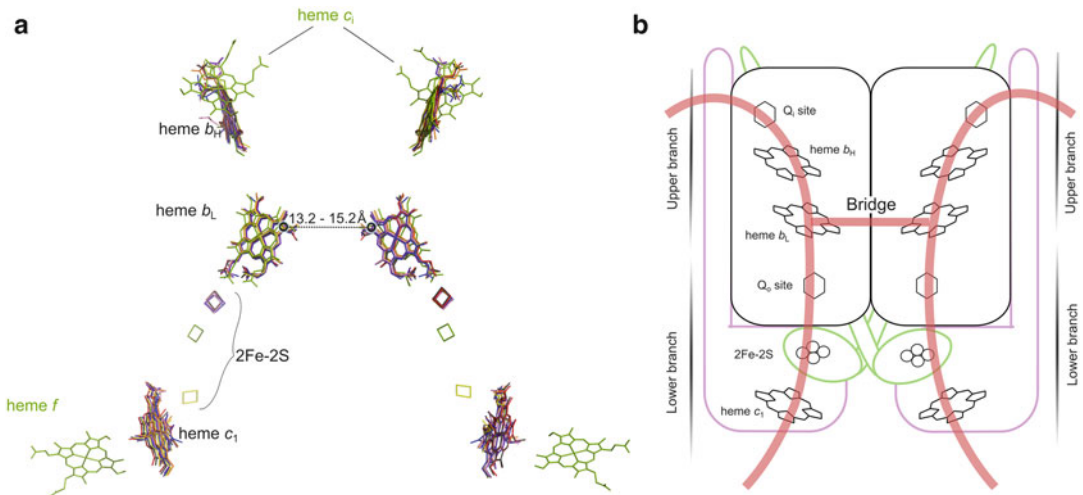


Fig. 14.1. Arrangement of cofactors in dimeric cytochrome  $bc_1/b_6f$  complexes. (a) Cofactors from the superimposed crystal structures of cytochrome  $bc_1$  of bacteria (*Rhodobacter capsulatus*, 1ZRT (Berry et al. 2004), *Rhodobacter sphaeroides*, 2QJP (Esser et al. 2008), *Paracoccus denitrificans*, 2YIU (Kleinschroth et al. 2011)), yeast (*Saccharomyces cerevisiae*, 1KYO (Lange and Hunte 2002), 3CXH (Solmaz and Hunte 2008)), chicken (*Gallus gallus*, 3H1H (Zhang et al. 1998)), bovine (*Bos taurus*, 2A06 (Huang et al. 2005)) and cytochrome  $b_6f$  of the cyanobacterium (*Mastigocladus laminosus*, 1VF5 (Kurisu et al. 2003)). Numbers above the dashed line show the range of the edge-to-edge distances between hemes  $b_L$  in those structures. (b) Cofactors embedded in cytochrome  $bc_1$  subunits of a dimer form an H-shaped electron transfer system (thick lines) consisting of two upper branches, two lower branches and the heme  $b_L$ - $b_L$  bridge.

A electronic states,  $FC$  is density of states weighted Frank – Condon factor and  $\hbar$  is the reduced Planck constant.

The first electronic term  $V^2$  is temperature independent and falls exponentially with increasing the distance between D and A:

$$V^2 = V_0^2 \exp(-\beta R) \quad (14.2)$$

where:  $V_0^2$  is the maximum coupling in the case when D and A are in van der Waals contact,  $R$  is the edge-to-edge distance between D and A and  $\beta$  is the scaling factor, which determines how fast the coupling decays with the distance  $R$ . The scaling factor  $\beta$  depends on the nature of the medium between A and D and is in the range between  $\sim 2.8 \text{ \AA}^{-1}$  for vacuum to  $\sim 0.7 \text{ \AA}^{-1}$  for covalently bonded system. Extensive studies of electron transfer in proteins showed that  $\beta = 1.4 \text{ \AA}^{-1}$  is a good approximation and may vary slightly with packing density (Page et al. 1999). This equation is similar to those describing the decrease of the frequency of spin-spin

exchange interaction (detected by electron paramagnetic resonance) with increased distance between two paramagnetic species (Likhtenshtein 1996). If so, then  $\beta$  should also be somewhat sensitive to the possible hydrogen bonds formed between D and A molecules, as they facilitate propagation of electronic density over larger distances along the bonds (Fournel et al. 1998; Calvo 2007).

The second term,  $FC$ , is associated with changes in the nuclear coordinates of D and A and surrounding solvent molecules caused by electron transfer. It depends on the reorganization energy,  $\lambda$ , and on the free energy change of the reaction,  $\Delta G$ , which is the difference between energy of products and reactants. The rate of electron transfer is expected to be the largest when  $\Delta G$  is equal to the reorganization energy, i.e.  $\Delta G = -\lambda$ . In case of electron transfer between hemes  $b_L$ , the reaction can be considered as self-exchange, assuming that the properties of hemes  $b_L$  do not depend significantly on conformational changes in the other parts of



the protein; therefore, in this case,  $\Delta G = 0$  (Marcus and Sutin 1985).

Calculation of reorganization energy is generally difficult due to the enormous complexity of the system. However, in proteins, studies on electron transfer between cofactors separated by different distances and of different redox potentials allowed estimation of the general value of  $\lambda$  of about 0.7 eV. These studies also provided the general phenomenological equation useful for calculating the electron transfer rate between most of the protein cofactors (Page et al. 1999; Moser et al. 2006, 2010):

$$\log(k_{ET}) = 13 - (1.2 - 0.8\rho)(R - 3.6) - 3.1 \frac{(\Delta G + \lambda)^2}{\lambda} \quad (14.3)$$

In this formula parameter  $\rho$  defines the packing density factor of protein between cofactors (Page et al. 1999). The value  $\rho = 1$  corresponds to the fully packed matrix ( $\beta = 0.9 \text{ \AA}^{-1}$ ), while  $\rho = 0$  corresponds to vacuum ( $\beta = 2.8 \text{ \AA}^{-1}$ ). For most proteins the packing density factor is about 0.76 (Page et al. 1999).

Taking the typical values of  $\rho$  and  $\lambda$  determined for proteins, the equation (14.3) can be simplified and  $k_{ET}$  is given by the following formula that has only a single parameter (distance  $R$ ) that influences the electron transfer rate between cofactors (Moser et al. 2006):

$$\log(k_{ET}) = 12.8 - 0.6R \quad (14.4)$$

Despite the fact that this equation is only a crude approximation of  $k_{ET}$  for electron transfer between cofactors, it can be used to obtain an order of magnitude for the rate of electron transfer between hemes  $b_L$  in cytochrome  $bc$  complexes. The rate of this process calculated for edge-to-edge distances between hemes from various cytochrome  $bc_1$  structures (Fig. 14.2, dotted lines) exceeds the range of catalytic turnover rate. This means that the heme  $b_L$ - $b_L$  electron transfer, when connecting the catalytic  $Q_o$  and  $Q_i$  sites, should not limit the overall turnover rate of the enzyme.

#### IV. Experimental Evidence for Inter-Monomer Electron Transfer

Mechanistic studies on cytochrome  $bc_1$  catalysis are often performed with photosynthetic bacteria *Rhodobacter capsulatus* or *Rhodobacter sphaeroides*. These simple organisms allow straightforward genetic manipulations while the light-induced catalytic cycle makes detailed analyses of the electron transfer reactions possible (Gray and Daldal 1995; Berry et al. 2009). Experimentally, the most unambiguous way to expose the inter-monomer electron transfer for functional testing would seem through the cross-inactivation of complementary parts of electron transfer chains of the dimer to enforce the inter-monomer connection as the only possible link between the  $Q_o$  and  $Q_i$  catalytic sites. This, however, required specific modifications to the genetic system used for mutagenesis which, due to the fact that the genes of cytochrome  $bc_1$  naturally do not differentiate between the monomers, only enabled introducing mutations symmetrically in both monomers. Breaking the symmetry of the dimeric  $bc_1$  complex has been accomplished recently in experiments that used two approaches. One approach was based on an idea of fusing two cytochrome  $b$  subunits of the dimer (Świerczek et al. 2010; Czapla et al. 2012b, 2013), the other – on using two different plasmids (Castellani et al. 2010; Lanciano et al. 2011, 2013a; Khalfaoui-Hassani et al. 2013).

Construction of the fusion protein involved replacing the cytochrome  $b$  gene in *R. capsulatus* with its duplicated version, in which two parts of the same gene were connected by a linker (Fig. 14.3a). Such protein folded into an enzymatically-active complex (named B-B) consisting of the cytochrome  $bb$  core containing all four quinone catalytic sites, to which cytochrome  $c_1$  and Fe-S subunits assembled in a way that overall topography resembled the dimeric  $bc_1$  complex (Świerczek et al. 2010; Czapla et al. 2012b). A variant of the fusion protein system was also developed using cytochrome  $b$  genes from different, but closely related

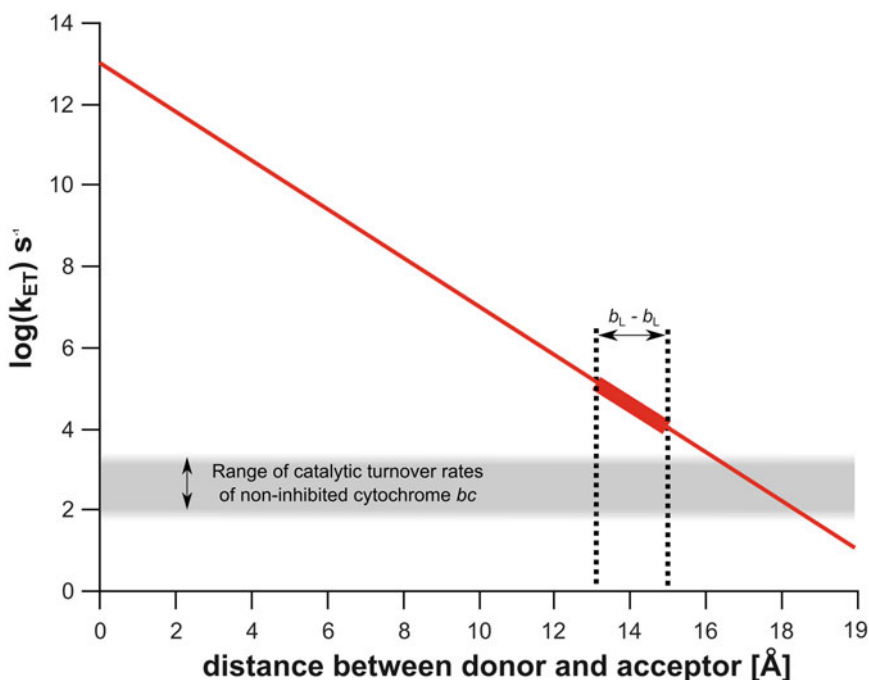


Fig. 14.2. The distance dependence of the rate for heme  $b_L$ - $b_L$  electron transfer. The distance dependence of the rate (red line) was calculated using simplified equation (14.4). The range of edge-to-edge distances between hemes  $b_L$  (dotted vertical lines) defines the range of expected rates for heme  $b_L$ - $b_L$  electron transfer (thick red line). The range of distances corresponds to that shown in Fig. 14.1a. Gray area represents the span of cytochrome  $bc_1$  catalytic turnover rates implicated from flash-induced electron transfer measurements and steady-state enzymatic turnover assays.

species: *R. sphaeroides* and *R. capsulatus* (Fig. 14.3b). Such hybrid fusion protein (cytochrome  $b_Sb$ ) was also assembled into functional  $bc_1$ -like complex (named  $B_S$ - $B$ ) (Czapla et al. 2013). With these systems, it was possible to create cross-inactivated forms in which mutations knocking out the individual cofactors were placed asymmetrically in different halves of the fusion protein. These mutations inactivated the upper branch of one monomer (H212N mutation, preventing heme  $b_H$  assembly, thus disrupting the electronic connection with the  $Q_i$  site (Osyczka et al. 2004)) and the lower branch of the other monomer (G158W, rendering the  $Q_o$  site inactive (Ding et al. 1995)) and leaving the path involving the inter-monomer electron transfer as the only connection between the active  $Q_i$  and  $Q_o$  catalytic sites.

Flash-induced kinetic measurements in membranes with cross-inactivated  $B$ - $B$  or

$B_S$ - $B$  revealed that the electron transfer between the monomers takes place in the millisecond time scale, matching the enzymatic turnover time and thus suggesting its catalytic relevance (Świerczek et al. 2010; Czapla et al. 2013). The measurements of the enzymatic activities of the purified cross-inactivated  $B$ - $B$  mutant confirmed that inter-monomer electron transfer can support multiple turnovers (Czapla et al. 2012a). In addition, using cells expressing cross-inactivated  $B_S$ - $B$  complexes, it was possible to demonstrate that the inter-monomer electronic connection can support the  $bc_1$ -dependent photoheterotrophic growth. Such growth was not supported when the same branches were knocked out in  $B_S$ - $B$  (both upper or both lower branches) (Ekiert et al. 2014).

The “two-plasmid” system involved the use of two plasmids coding for the

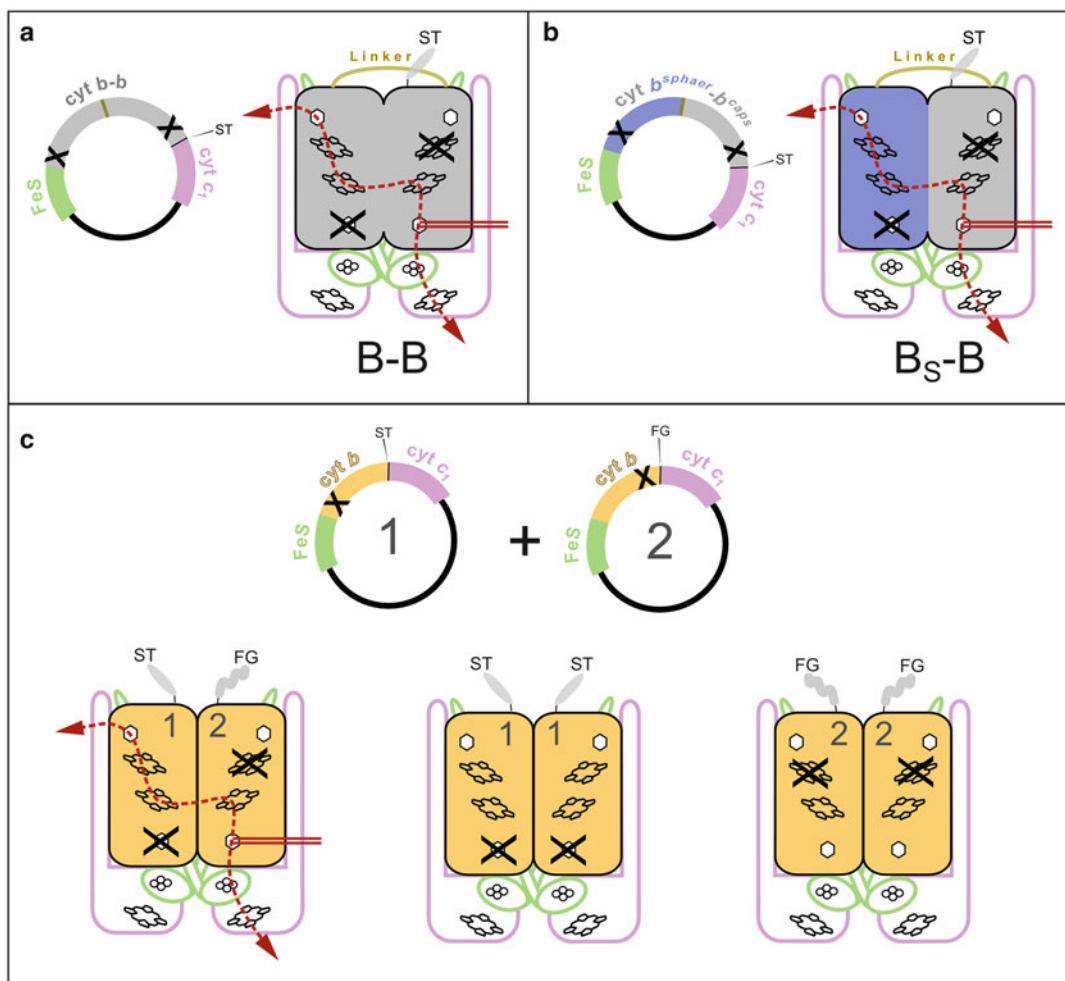


Fig. 14.3. Experimental systems used to expose the inter-monomer electron transfer in the *Rhodobacter capsulatus* cytochrome  $bc_1$ . For each system, mutations disabling individual branches of the H-shaped electron transfer system (black crosses) are shown at the levels of plasmid and protein complex. Cross-inactivation disrupts the functional link between  $Q_0$  and  $Q_i$  sites within each monomer, leaving the path involving inter-monomer electron transfer via the heme  $b_L$ - $b_L$  bridge as the only pathway to connect the catalytic sites in a dimer (dotted arrow lines). *ST* Strep-tag, *FG* FLAG-tag. (a) Fusion protein system – two cytochrome  $b$  subunits in the dimer are replaced by a fusion consisting of two cytochromes  $b$  identical in primary amino-acid sequence. (b) Hybrid fusion protein system – two cytochrome  $b$  subunits in the dimer are replaced by a hybrid fusion of cytochromes  $b$  of *R. sphaeroides* and *R. capsulatus*. (c) Two-plasmid system – mixture of homo- and heterodimers identifiable by different composition of polypeptide tags.

cytochrome  $b$  protein tagged with different polypeptide labels (Fig. 14.3c). Mutations inactivating opposite branches of the electron flow used in this system affected the  $Q_0$  site (Y147A; (Saribas et al. 1995)) or inactivated the  $Q_i$  site or heme  $b_H$  (H217L or H212N, respectively (Gray et al. 1994; Oszycza et al. 2004)). Mutated cytochromes

$b$  were randomly distributed into dimeric  $bc_1$  complexes assembled in *R. capsulatus* cells. Flash-induced kinetic measurements in membranes showed the millisecond electronic connection between the monomers of  $bc_1$  complex (Lanciano et al. 2011, 2013a). Two rounds of protein purification, using the tags distinctive for each of the

mutated plasmids, resulted in obtaining the cross-inactivated complexes, which were enzymatically active. Moreover, it was observed that these complexes were able to support the photoheterotrophic growth of the cells (Lanciano et al. 2013a).

The results of these independent sets of experiments using both approaches not only provided consistent evidence for the existence of inter-monomer electron transfer in the catalytic time scale, but also indicated that inter-monomer electron transfer can support function of cytochrome *bc*<sub>1</sub> *in vivo*.

## V. Mechanistic Consequences of Inter-Monomer Electron Transfer

Electron transfer between the two hemes *b*<sub>L</sub> has several important mechanistic consequences. It converts the independent cofactor chains in the dimer into an H-shaped electron transfer as indeed implicated from the structure (Fig. 14.1). This system connects electronically all four quinone catalytic sites. It consists of two uprights connected by a bridge. Each upright is formed by one upper and one lower branch that together encompass the *c*- and *b*-chains of one monomer. The bridge allows for connection of the lower branch of one monomer with the upper branch of the other monomer. It also links two upper branches together and two lower branches together. All these additional links increase, in principle, a number of possible electron transfer paths connecting the catalytic sites of the dimer, if compared to a simple connection of upper and lower branch within the upright of one monomer.

The catalytic Q-cycle requires functional connection of the Q<sub>o</sub> site with the Q<sub>i</sub> site (Mitchell 1975; Crofts et al. 1983; Brandt and Trumpower 1994), which, given all possible links of the H-shaped electron transfer system, can involve intra- and/or inter-monomer electron transfers. Intra-monomer electron transfer (within one

upright) connects the Q<sub>o</sub> and Q<sub>i</sub> sites of the same monomer, while the path involving inter-monomer electron transfer connects the Q<sub>o</sub> and Q<sub>i</sub> sites across the dimer. From the experimental point of view it appears that both ways of connecting the sites support enzymatic function. This means that the H-shaped electron transfer system, in its basic engineering principle, allows any connection between the catalytic sites of the opposite sides of the membrane to be enzymatically competent (Świerczek et al. 2010). On thermodynamic grounds, the net electron flow in this system can be understood as a result of consecutive changes in transition probabilities between the fully reversible partial reactions in the chain (Osyczka et al. 2004; Shinkarev and Wraight 2007; Cieluch et al. 2010), with the main rationale that electron “blindly” uses any path that is available at a given point in time.

However, an obligatory coupling of two turnovers of the Q<sub>o</sub> site with one turnover of the Q<sub>i</sub> site, inherent to the Q-cycle, opens the possibility for other, more elaborated, mechanistic schemes for the operation of the H-shaped electron transfer system. Indeed, specific sequences of electron transfer within the dimer, involving the inter-monomer electron transfer, are proposed in various models that assume allosteric interactions within/between monomers. In these schemes, conformational constraints at certain steps act to impose the specific direction of electron flow. One mechanistic element often evoked is an allosteric control over the position of the Fe-S head domain by the occupants of the Q<sub>i</sub> site, which in various models is differently ascribed (Covian and Trumpower 2006, 2008; Cooley et al. 2009; Mulkidjanian 2010).

An intriguing consequence of inter-monomer electron connection is a possibility of electron transfer between the Q<sub>i</sub> sites through reactions involving just the two upper branches and the bridge. Such tunneling equilibration between all four hemes *b* in a dimer, occurring on a time scale of Q<sub>o</sub> site catalysis and in a manner

independent of the  $Q_o$  site, can in principle, lead to dismutation of two semiquinones that are present simultaneously at two  $Q_i$  sites of two monomers. In effect, this removes the strict coupling between two turnovers of one  $Q_o$  site and one  $Q_i$  site described in traditional scheme of the Q-cycle (Osyczka et al. 2004).

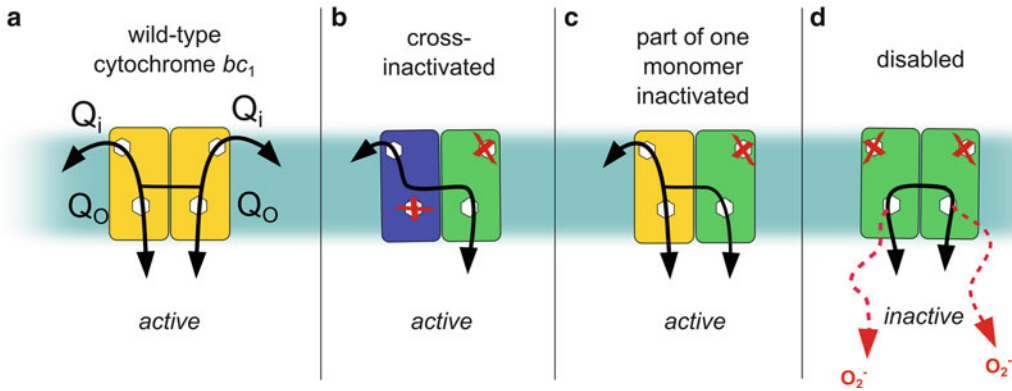
## VI. Physiological Significance of Inter-Monomer Electron Transfer

The physiological meaning of the H-shaped electron transfer system remains an open issue. Considering currently available information on the thermodynamics of the reactions in cytochrome  $bc_1$  it can be anticipated that electron transfer between hemes  $b_L$  and  $b_H$  of each monomer is favored over the heme  $b_L$ - $b_L$  electron transfer (inter-monomer electron transfer) as long as there are no factors that influence the electron transfer route (Shinkarev and Wraight 2007). One such factor is membrane potential, inherently present and dynamically changing in bioenergetically active organelles in living cells. An increase in membrane potential impedes the electron transfer from heme  $b_L$  to heme  $b_H$  (Shinkarev et al. 2001; Rottenberg et al. 2009), but at the same time it may increase the fraction of electrons that travel through the heme  $b_L$ - $b_L$  bridge. Therefore, the membrane potential can be considered as one of the prominent factors that effectively modulate the inter- vs intra-monomer electron transfer.

Inter-monomer electron transfer, creating the conditions that do not preclude the dismutation of two semiquinones that occupy two  $Q_i$  sites of the dimer, gives the enzyme a possibility to reduce one ubiquinone (UQ) molecule to ubihydroquinone (UQH<sub>2</sub>) in one of the  $Q_i$  sites using two electrons, each delivered from a different  $Q_o$  site. This option of completing enzymatic turnovers may provide physiological advantage for the cells, as it enhances the efficiency of the Q-cycle under a shortage of UQH<sub>2</sub> in the quinone pool.

Another possible physiological advantage of the H-shaped electron transfer system is related with its flexibility to use more than one electronic path that functionally connects the  $Q_o$  site with the  $Q_i$  site. This built-in redundancy allows physiological function of the enzyme even after operational damage of one part (Fig. 14.4). Such damage can be associated with the occurrence of certain mutations, especially within the cytochrome  $b$  subunit. In eukaryotic cells, this is particularly relevant to the process of accumulation of mitochondrial damage inherent to aging and/or a progress of development of several mitochondria-related diseases (DiMauro 2004; Kujoth et al. 2007; Tuppen et al. 2010). Given that mtDNA-located gene coding for cytochrome  $b$  subunit does not differentiate between monomers, the presence of mutations in just a part of the copies of the gene (mtDNA is present in several copies in mitochondria) is likely to result in expression of both symmetrically and asymmetrically mutated dimers of cytochrome  $bc_1$ , as indeed observed in bacterial two-plasmid systems (Castellani et al. 2010; Lanciano et al. 2011, 2013a). It is thus possible that upon accumulation of mtDNA mutations, the amount of the asymmetrically damaged complexes increases. Such partially-damaged enzymes are likely to retain their physiological function as long as any of the connections between the operational  $Q_o$  and  $Q_i$  sites in the dimer is preserved (Sarewicz and Osyczka 2015).

Yet another possible physiological advantage of the H-shaped electron transfer system is related to the reactive oxygen species (ROS) generation by cytochrome  $bc_1$ . Current discussions on ROS generation by this enzyme consider the prolonged state of reduced heme  $b_L$  as condition increasing the probability of superoxide generation by the  $Q_o$  site (Kramer et al. 2004; Cape et al. 2006; Dröse and Brandt 2012; Bleier and Dröse 2013; Lanciano et al. 2013b). Such conditions arise when a semiquinone at the  $Q_o$  site (Cape et al. 2007; Zhang et al. 2007; Sarewicz et al. 2013) is given the opportunity to interact with oxygen. In one scenario, this occurs when reduced heme



*Fig. 14.4.* Possible advantage of H-shaped electron transfer in cytochrome  $bc_1$  in the context of mutational damage. (a) In wild-type cytochrome  $bc_1$ , four active branches and a bridge connect catalytic  $Q_o$  and  $Q_i$  sites. (b) Mutational inactivation of complementary branches on each of the monomers does not abolish enzymatic activity of a dimer, as long as the cross-communication between the opposite  $Q_o$  and  $Q_i$  sites is maintained through the bridge. (c) Inactivation of a part of one monomer does not inactivate a dimer. (d) Assembly of similarly damaged monomers (for example with both upper branches disabled) leads to the formation of an inactive enzyme, which additionally may become the source of superoxide radical.

$b_L$  reduces ubiquinone to semiquinone as a part of reverse electron transfer (Dröse and Brandt 2008; Sarewicz et al. 2010). In this case, the highest probability of reaction of semiquinone with oxygen is when the [2Fe-2S] cluster is remote from the site and unable to interact with occupant of the  $Q_o$  site at the time of semiquinone formation (Borek et al. 2008; Sarewicz et al. 2013). The other scenario assumes that when semiquinone formed as a result of one-electron reduction of [2Fe-2S] cluster by  $UQH_2$  cannot immediately reduce heme  $b_L$  (as this heme is already reduced and unable to take electrons from it), it reacts with oxygen instead (Muller et al. 2002; Forquer et al. 2006; Quinlan et al. 2011).

Typically, heme  $b_L$  becomes reduced for prolonged time when the electron outflow from the  $Q_i$  site is blocked or suppressed by inhibition or mutation and an active  $Q_o$  site is exposed to an excess of substrate  $UQH_2$ . If such damage or inhibition occurs asymmetrically in a dimer (is present only in one monomer), the connection between monomers may help removing electrons from hemes in the b-chain, decreasing the chance of superoxide formation by the enzyme. Considering that

cytochrome  $bc_1$  evolved in anoxygenic environment, it is not clear whether possible protective role of geometric proximity of two hemes  $b_L$  against ROS was a coincidental effect or an evolutionarily-driven design. Nevertheless, one cannot exclude possibility that some tuning of energy levels might have occurred throughout evolution (Rutherford et al. 2012), for example to minimize the probability of direct reaction of reduced heme  $b_L$  with oxygen.

## VII. Conclusions

The inter-monomer electron connection emerges as an integral part of the electron transfer system of cytochrome  $bc$  complexes. This intriguing feature of the dimer, implicated from the crystal structures and electron transfer calculations, is now supported by experimental evidence at both *in vitro* and *in vivo* levels. *In vitro*, the kinetic measurements established that inter-monomer electron transfer connects functionally the quinone binding sites on the opposite sides of the membrane and occurs on a time scale of milliseconds or faster and thus does not limit the enzymatic turnover.

*In vivo*, it was shown that specifically-mutated enzymes that rely on the inter-monomer electron transfer to connect the catalytic sites are competent in supporting the cytochrome  $bc_1$ -dependent growth of the cells. The existence of inter-monomer electron connection converts the independent redox chains of cytochrome  $bc_1$  dimer into the H-shaped electron transfer system that enables any connection between the catalytic quinone binding sites on the opposite sides of the membrane to be enzymatically competent. Details of electronic distribution in this system in living cells and the physiological meaning of inter-monomer electron transfer, especially in the context of the radical-generating activity of cytochrome  $bc$  complexes, still remain to be elucidated.

## Acknowledgments

AO acknowledges The Wellcome Trust for International Senior Research Fellowship. RE is a recipient of Homing Plus grant from Foundation for Polish Science and a Fellowship from the Jagiellonian University within the SET project, co-financed by the European Union.

## References

- Barbara PF, Meyer TJ, Ratner MA (1996) Contemporary issues in electron transfer research. *J Phys Chem* 100:13148–13168
- Bazil JN, Vinnakota KC, Wu F, Beard DA (2013) Analysis of the kinetics and bistability of ubiquinol:cytochrome  $c$  oxidoreductase. *Biophys J* 105:343–355
- Berry EA, Guergova-Kuras M, Huang L, Crofts AR (2000) Structure and function of cytochrome  $bc$  complexes. *Annu Rev Biochem* 69:1005–1075
- Berry EA, Huang L-S, Saechao LK, Pon NG, Valkova-Valchanova M, Daldal F (2004) X-ray structure of *Rhodobacter capsulatus* cytochrome  $bc_1$ : comparison with its mitochondrial and chloroplast counterparts. *Photosynth Res* 81:251–275
- Berry EA, Lee D-W, Huang L-S, Daldal F (2009) Structural and mutational studies of the cytochrome  $bc_1$  complex. In: Daldal F, Thurnauer MC, Beatty JT, Hunter CN (eds) *Purple Phototrophic Bacteria*. Springer, Dordrecht, pp 425–450
- Bleier L, Dröse S (2013) Superoxide generation by complex III: from mechanistic rationales to functional consequences. *Biochim Biophys Acta* 1827:1320–1331
- Borek A, Sarewicz M, Osyczka A (2008) Movement of the iron-sulfur head domain of cytochrome  $bc_1$  transiently opens the catalytic  $Q_o$  site for reaction with oxygen. *Biochemistry* 47:12365–12370
- Brandt U, Trumpower B (1994) The protonmotive Q cycle in mitochondria and bacteria. *Crit Rev Biochem Mol Biol* 29:165–197
- Calvo R (2007) EPR measurements of weak exchange interactions coupling unpaired spins in model compounds. *Appl Magn Reson* 31:271–299
- Cape JL, Bowman MK, Kramer DM (2006) Understanding the cytochrome  $bc$  complexes by what they don't do. The Q cycle at 30. *Trends Plant Sci* 11:46–54
- Cape JL, Bowman MK, Kramer DM (2007) A semiquinone intermediate generated at the  $Q_o$  site of the cytochrome  $bc_1$  complex: importance for the Q-cycle and superoxide production. *Proc Natl Acad Sci U S A* 104:7887–7892
- Castellani M, Covian R, Kleinschroth T, Anderka O, Ludwig B, Trumpower BL (2010) Direct demonstration of half-of-the-sites reactivity in the dimeric cytochrome  $bc_1$  complex: enzyme with one inactive monomer is fully active but unable to activate the second ubiquinol oxidation site in response to ligand binding at the ubiquinone reduction site. *J Biol Chem* 285:502–510
- Cieluch E, Pietryga K, Sarewicz M, Osyczka A (2010) Visualizing changes in electron distribution in coupled chains of cytochrome  $bc_1$  by modifying barrier for electron transfer between the FeS cluster and heme  $c_1$ . *Biochim Biophys Acta* 1797:296–303
- Cooley JW, Lee D-W, Daldal F (2009) Across membrane communication between the  $Q_o$  and  $Q_i$  active sites of cytochrome  $bc_1$ . *Biochemistry* 48:1888–1899
- Covian R, Trumpower BL (2005) Rapid electron transfer between monomers when the cytochrome  $bc_1$  complex dimer is reduced through center N. *J Biol Chem* 280:22732–22740
- Covian R, Trumpower BL (2006) Regulatory interactions between ubiquinol oxidation and ubiquinone reduction sites in the dimeric cytochrome  $bc_1$  complex. *J Biol Chem* 281:30925–30932
- Covian R, Trumpower BL (2008) Regulatory interactions in the dimeric cytochrome  $bc_1$  complex: the advantages of being a twin. *Biochim Biophys Acta* 1777:1079–1091

- Covian R, Gutierrez-Cirlos EB, Trumpower BL (2004) Anti-cooperative oxidation of ubiquinol by the yeast cytochrome *bc*<sub>1</sub> complex. *J Biol Chem* 279:15040–15049
- Cramer WA, Hasan SS, Yamashita E (2011) The Q cycle of cytochrome *bc* complexes: a structure perspective. *Biochim Biophys Acta* 1807:788–802
- Crofts AR, Meinhardt SW, Jones KR, Snozzi M (1983) The role of the quinone pool in the cyclic electron-transfer chain of *Rhodospseudomonas sphaeroides*: a modified Q-cycle mechanism. *Biochim Biophys Acta* 723:202–218
- Crofts AR, Holland JT, Victoria D, Kolling DRJ, Dikanov SA, Gilbreth R, Lhee S, . . . , Kuras MG (2008) The Q-cycle reviewed: how well does a monomeric mechanism of the *bc*<sub>1</sub> complex account for the function of a dimeric complex? *Biochim Biophys Acta* 1777:1001–1019
- Crofts AR, Hong S, Wilson C, Burton R, Victoria D, Harrison C, Schulten K (2013) The mechanism of ubihydroquinone oxidation at the Q<sub>o</sub>-site of the cytochrome *bc*<sub>1</sub> complex. *Biochim Biophys Acta* 1827:1362–1377
- Czapla M, Borek A, Sarewicz M, Osyczka A (2012a) Enzymatic activities of isolated cytochrome *bc*<sub>1</sub>-like complexes containing fused cytochrome *b* subunits with asymmetrically inactivated segments of electron transfer chains. *Biochemistry* 51:829–835
- Czapla M, Borek A, Sarewicz M, Osyczka A (2012b) Fusing two cytochromes *b* of *Rhodobacter capsulatus* cytochrome *bc*<sub>1</sub> using various linkers defines a set of protein templates for asymmetric mutagenesis. *Protein Eng Des Sel* 25:15–25
- Czapla M, Cieluch E, Borek A, Sarewicz M, Osyczka A (2013) Catalytically-relevant electron transfer between two hemes *b*<sub>L</sub> in the hybrid cytochrome *bc*<sub>1</sub>-like complex containing a fusion of *Rhodobacter sphaeroides* and *capsulatus* cytochromes *b*. *Biochim Biophys Acta* 1827:751–760
- DiMauro S (2004) Mitochondrial diseases. *Biochim Biophys Acta* 1658:80–88
- Ding H, Moser CC, Robertson DE, Tokito MK, Daldal F, Dutton PL (1995) Ubiquinone pair in the Q<sub>o</sub> site central to the primary energy conversion reactions of cytochrome *bc*<sub>1</sub> complex. *Biochemistry* 34:15979–15996
- Dröse S, Brandt U (2008) The mechanism of mitochondrial superoxide production by the cytochrome *bc*<sub>1</sub> complex. *J Biol Chem* 283:21649–21654
- Dröse S, Brandt U (2012) Molecular mechanisms of superoxide production by the mitochondrial respiratory chain. In: Kadenbach B (ed) *Mitochondrial Oxidative Phosphorylation: Nuclear-Encoded Genes, Enzyme Regulation, and Pathophysiology*. Springer, New York, pp 145–169
- Ekiert R, Czapla M, Sarewicz M, Osyczka A (2014) Hybrid fusions show that inter-monomer electron transfer robustly supports cytochrome *bc*<sub>1</sub> function in vivo. *Biochem Biophys Res Commun* 451:270–275
- Esser L, Elberry M, Zhou F, Yu C-A, Yu L, Xia D (2008) Inhibitor-complexed structures of the cytochrome *bc*<sub>1</sub> from the photosynthetic bacterium *Rhodobacter sphaeroides*. *J Biol Chem* 283:2846–2857
- Forquer I, Covian R, Bowman MK, Trumpower BL, Kramer DM (2006) Similar transition states mediate the Q-cycle and superoxide production by the cytochrome *bc*<sub>1</sub> complex. *J Biol Chem* 281:38459–38465
- Fournel A, Gambarelli S, Guigliarelli B, More C, Asso M, Chouteau G, Hille R, Bertrand P (1998) Magnetic interactions between a [4Fe–4S]<sup>1+</sup> cluster and a flavin mononucleotide radical in the enzyme trimethylamine dehydrogenase: a high-field electron paramagnetic resonance study. *J Chem Phys* 109:10905–10913
- Gong X, Yu L, Xia D, Yu C-A (2005) Evidence for electron equilibrium between the two hemes *b*<sub>L</sub> in the dimeric cytochrome *bc*<sub>1</sub> complex. *J Biol Chem* 280:9251–9257
- Gopta OA, Feniouk BA, Junge W, Mulikidjanian AY (1998) The cytochrome *bc*<sub>1</sub> complex of *Rhodobacter capsulatus*: ubiquinol oxidation in dimeric Q-cycle? *FEBS Lett* 431:291–296
- Gray KA, Daldal F (1995) Mutational studies of the cytochrome *bc*<sub>1</sub> complexes. In: Blankenship RE, Madigan MT, Bauer CE (eds) *Anoxygenic Photosynthetic Bacteria*. Kluwer, Dordrecht, pp 747–774
- Gray KA, Dutton PL, Daldal F (1994) Requirement of histidine 217 for ubiquinone reductase activity (Q<sub>i</sub> site) in the cytochrome *bc*<sub>1</sub> complex. *Biochemistry* 33:723–733
- Hasan SS, Yamashita E, Baniulis D, Cramer WA (2013) Quinone-dependent proton transfer pathways in the photosynthetic cytochrome *b*<sub>6f</sub> complex. *Proc Natl Acad Sci U S A* 110:4297–4302
- Hasan SS, Zakharov SD, Chauvet A, Stadnytskyi V, Savikhin S, Cramer WA (2014) A map of dielectric heterogeneity in a membrane protein: the heterooligomeric cytochrome *b*<sub>6f</sub> complex. *J Phys Chem B* 118:6614–6625
- Huang LS, Cobessi D, Tung EY, Berry EA (2005) Binding of the respiratory chain inhibitor antimycin to the mitochondrial *bc*<sub>1</sub> complex: a new crystal structure reveals an altered intramolecular hydrogen-bonding pattern. *J Mol Biol* 351:573–597



- Hunte C, Koepke J, Lange C, Rossmann T, Michel H (2000) Structure at 2.3 Å resolution of the cytochrome  $bc_1$  complex from the yeast *Saccharomyces cerevisiae* co-crystallized with an antibody Fv fragment. *Structure* 8:669–684
- Khalfaoui-Hassani B, Lanciano P, Lee D-W, Darrouzet E, Daldal F (2012) Recent advances in cytochrome  $bc_1$ : inter monomer electronic communication? *FEBS Lett* 586:617–621
- Khalfaoui-Hassani B, Lanciano P, Daldal F (2013) A robust genetic system for producing heterodimeric native and mutant cytochrome  $bc_1$ . *Biochemistry* 52:7184–7195
- Kleinschroth T, Castellani M, Trinh CH, Morgner N, Brutschy B, Ludwig B, Hunte C (2011) X-ray structure of the dimeric cytochrome  $bc_1$  complex from the soil bacterium *Paracoccus denitrificans* at 2.7-Å resolution. *Biochim Biophys Acta* 1807:1606–1615
- Kramer DM, Roberts AG, Muller F, Cape J, Bowman MK (2004) Q-cycle bypass reactions at the  $Q_o$  site of the cytochrome  $bc_1$  (and related) complexes. *Methods Enzymol* 382:21–45
- Kujoth GC, Bradshaw PC, Haroon S, Prolla TA (2007) The role of mitochondrial DNA mutations in mammalian aging. *PLoS Genet* 3:161–173
- Kurisu G, Zhang H, Smith JL, Cramer WA (2003) Structure of the cytochrome  $b_6f$  complex of oxygenic photosynthesis: tuning the cavity. *Science* 302:1009–1014
- Lanciano P, Lee D-W, Yang H, Darrouzet E, Daldal F (2011) Intermonomer electron transfer between the low-potential  $b$  hemes of cytochrome  $bc_1$ . *Biochemistry* 50:1651–1663
- Lanciano P, Khalfaoui-Hassani B, Selamoglu N, Daldal F (2013a) Intermonomer electron transfer between the  $b$  hemes of heterodimeric cytochrome  $bc_1$ . *Biochemistry* 52:7196–7206
- Lanciano P, Khalfaoui-Hassani B, Selamoglu N, Ghelli A, Rugolo M, Daldal F (2013b) Molecular mechanisms of superoxide production by complex III: a bacterial versus human mitochondrial comparative case study. *Biochim Biophys Acta* 1827:1332–1339
- Lange C, Hunte C (2002) Crystal structure of the yeast cytochrome  $bc_1$  complex with its bound substrate cytochrome  $c$ . *Proc Natl Acad Sci U S A* 99:2800–2805
- Likhtenshtein GI (1996) Role of orbital overlap and local dynamics in long-distance electron transfer in photosynthetic reaction centres and model systems. *J Photochem Photobiol Chem* 96:79–92
- Marcus RA, Sutin N (1985) Electron transfers in chemistry and biology. *Biochim Biophys Acta* 811:265–322
- Mitchell P (1975) The protonmotive Q cycle: a general formulation. *FEBS Lett* 59:137–139
- Moser CC, Keske JM, Warncke K, Farid RS, Dutton PL (1992) Nature of biological electron transfer. *Nature* 355:796–802
- Moser CC, Farid TA, Chobot SE, Dutton PL (2006) Electron tunneling chains of mitochondria. *Biochim Biophys Acta* 1757:1096–1109
- Moser CC, Anderson JLR, Dutton PL (2010) Guidelines for tunneling in enzymes. *Biochim Biophys Acta* 1797:1573–1586
- Mulkidjanian AY (2010) Activated Q-cycle as a common mechanism for cytochrome  $bc_1$  and cytochrome  $b_6f$  complexes. *Biochim Biophys Acta* 1797:1858–1868
- Muller F, Crofts AR, Kramer DM (2002) Multiple Q-cycle bypass reactions at the  $Q_o$  site of the cytochrome  $bc_1$  complex. *Biochemistry* 41:7866–7874
- Osyczka A, Moser CC, Daldal F, Dutton PL (2004) Reversible redox energy coupling in electron transfer chains. *Nature* 427:607–612
- Osyczka A, Moser CC, Dutton PL (2005) Fixing the Q cycle. *Trends Biochem Sci* 30:176–182
- Page CC, Moser CC, Chen X, Dutton PL (1999) Natural engineering principles of electron tunnelling in biological oxidation-reduction. *Nature* 402:47–52
- Quinlan CL, Gerencser AA, Treberg JR, Brand MD (2011) The mechanism of superoxide production by the antimycin-inhibited mitochondrial Q-cycle. *J Biol Chem* 286:31361–31372
- Rottenberg H, Covian R, Trumpower BL (2009) Membrane potential greatly enhances superoxide generation by the cytochrome  $bc_1$  complex reconstituted into phospholipid vesicles. *J Biol Chem* 284:19203–19210
- Rutherford AW, Osyczka A, Rappaport F (2012) Back-reactions, short-circuits, leaks and other energy wasteful reactions in biological electron transfer: redox tuning to survive life in  $O_2$ . *FEBS Lett* 586:603–616
- Sarewicz M, Osyczka A (2015) Electronic connection between the quinone and cytochrome  $c$  redox pools and its role in regulation of mitochondrial electron transport and redox signalling. *Physiol Rev* 95:219–243
- Sarewicz M, Borek A, Cieluch E, Świerczek M, Osyczka A (2010) Discrimination between two possible reaction sequences that create potential risk of generation of deleterious radicals by cytochrome  $bc_1$ . Implications for the mechanism of superoxide production. *Biochim Biophys Acta* 1797:1820–1827

- Sarewicz M, Dutka M, Pintscher S, Osyczka A (2013) Triplet state of the semiquinone-Rieske cluster as an intermediate of electronic bifurcation catalyzed by cytochrome *bc*<sub>1</sub>. *Biochemistry* 52: 6388–6395
- Saribas AS, Ding H, Dutton PL, Daldal F (1995) Tyrosine 147 of cytochrome *b* is required for efficient electron transfer at the ubihydroquinone oxidase site (Q<sub>o</sub>) of the cytochrome *bc*<sub>1</sub> complex. *Biochemistry* 34:16004–16012
- Shinkarev VP, Wraight CA (2007) Intermonomer electron transfer in the *bc*<sub>1</sub> complex dimer is controlled by the energized state and by impaired electron transfer between low and high potential hemes. *FEBS Lett* 581:1535–1541
- Shinkarev VP, Crofts AR, Wraight CA (2001) The electric field generated by photosynthetic reaction center induces rapid reversed electron transfer in the *bc*<sub>1</sub> complex. *Biochemistry* 40: 12584–12590
- Solmaz SR, Hunte C (2008) Structure of complex III with bound cytochrome *c* in reduced state and definition of a minimal core interface for electron transfer. *J Biol Chem* 283: 17542–17549
- Stroebel D, Choquet Y, Popot J-L, Picot D (2003) An atypical haem in the cytochrome *b*<sub>6f</sub> complex. *Nature* 426:413–418
- Świerczek M, Cieluch E, Sarewicz M, Borek A, Moser CC, Dutton PL, Osyczka A (2010) An electronic bus bar lies in the core of cytochrome *bc*<sub>1</sub>. *Science* 329:451–454
- Tuppen HAL, Blakely EL, Turnbull DM, Taylor RW (2010) Mitochondrial DNA mutations and human disease. *Biochim Biophys Acta* 1797:113–128
- Xia D, Yu CA, Kim H, Xia JZ, Kachurin AM, Zhang L, Yu L, Deisenhofer J (1997) Crystal structure of the cytochrome *bc*<sub>1</sub> complex from bovine heart mitochondria. *Science* 277:60–66
- Xia D, Esser L, Tang W-K, Zhou F, Zhou Y, Yu L, Yu C-A (2013) Structural analysis of cytochrome *bc*<sub>1</sub> complexes: implications to the mechanism of function. *Biochim Biophys Acta* 1827:1278–1294
- Zhang Z, Huang L, Shulmeister VM, Chi YI, Kim KK, Hung LW, Crofts AR, . . . , Kim SH (1998) Electron transfer by domain movement in cytochrome *bc*<sub>1</sub>. *Nature* 392:677–684
- Zhang H, Osyczka A, Dutton PL, Moser CC (2007) Exposing the complex III Q<sub>o</sub> semiquinone radical. *Biochim Biophys Acta* 1767:883–887

# Chapter 15

## Heme $c_i$ or $c_n$ of the Cytochrome $b_6f$ Complex, A Short Retrospective

Francesca Zito<sup>a,\*</sup> and Jean Alric<sup>b</sup>

<sup>a</sup>*Institut Biologie Physico-Chimique, UMR7099, CNRS/Université Paris Diderot, 13, rue Pierre et Marie Curie, F-75005 Paris, France*

<sup>b</sup>*IBEB/SBVME/LB3M Bât 161 CEA de Cadarache, Saint Paul Lez Durance Cedex 13108, France*

Summary.....	295
I. Introduction.....	296
II. Early Evidence: Heme $c_i$ of the Cytochrome $b_6f$ Complex, A Functional Retrospective.....	297
III. Tridimensional Structure.....	300
IV. Heme $c_i/Q_i$ Site Directed Mutants.....	301
V. NQNO, A Not-So-Good Inhibitor of the $Q_i$ Site of the Cytochrome $b_6f$ Complex.....	303
VI. Concluding Remarks.....	303
Acknowledgments.....	304
References.....	305

### Summary

The unexpected existence of heme  $c_i$  (or  $c_n$ ) of cytochrome  $b_6f$  complex was revealed to the scientific community in Spring 2003 at the Gordon Bioenergetics conference, taking place at Kimball Union Academy, NH, USA. The three-dimensional structures of the complex were published back-to-back by two independent groups in Fall 2003 (Kurusu et al. *Science* 302:1009–1014, 2003; Stroebel et al. *Nature* 426:413–418, 2003). Further information about the physico-chemical properties of this unusual heme was gathered in the following years. Here we shall re-examine early evidence for the presence of this unusual cytochrome, originally called G (Lavergne. *Biochim Biophys Acta* 725:25–33, 1983; Joliot and Joliot. *Biochim Biophys Acta* 933:319–333, 1988), which show the role that heme  $c_i$  plays in electron transfer in the cytochrome  $b_6f$  complex.

---

\*Author for correspondence, e-mail: [zito@ibpc.fr](mailto:zito@ibpc.fr); [jean.alric@cea.fr](mailto:jean.alric@cea.fr)

## I. Introduction

The cytochrome  $b_6f$  complex (plastoquinol-plastocyanin oxidoreductase) is the inter-system electron carrier *par excellence*. It provides photosystem II (PSII), oxidizing water, with plastoquinones as electron acceptors, and photosystem I (PSI), reducing ferredoxin, FNR and  $\text{NADP}^+$ , with reduced plastocyanins (or  $c_6$  cytochromes) as electron donors. The molecular and functional features of the cytochrome  $b_6f$  complex are described in other chapters of this volume (see the Chap. 9 by Cramer and Hasan) and others in this series (Kallas 2012). Here the focus will be on a peculiar cofactor, present in the plastoquinone-binding pocket of the complex, the  $Q_i$  (or  $Q_n$ ) site, on the stromal side of the thylakoid membrane, or the cytoplasmic side in cyanobacteria. Table 15.1 recapitulates the various terminologies used to discriminate between the quinol-oxidation “o” or “p” and quinone-reduction “i” or “n” sites of cytochrome  $bc$ - $bf$  complexes. The “o” and “i” terminology originates from mitochondrial cytochrome  $bc_1$  complexes whereas “n” and “p” refer to the electronegative and positive sides of the membrane.

Plastoquinols (the reduced and protonated form of plastoquinones) produced by PSII are oxidized and deprotonated at the cytochrome  $b_6f$   $Q_o$  site. Whereas protons are released into the thylakoid lumen, therefore participating to the building of a pH gradient ( $\Delta\text{pH}$ ), only half of the electrons are directed towards the “high-potential chain” (consisting of the Rieske iron-sulfur protein and cytochrome  $f$ ) and then further trans-

Table 15.1. The various names given to the quinone binding sites of cytochrome  $bc$ - $bf$  complexes.

Quinol oxidation site	Quinone reduction site
“o” outside (used in this review)	“i” inside (used in this review)
Intermembrane space (top)	Mitochondrial matrix (bottom)
“p” positively charged	“n” negatively charged
Thylakoid lumen (bottom)	Chloroplast stroma (top)
Periplasm	Cytoplasm
Left (Mitchell 1976)	Right (Mitchell 1976)

ferred along the chain through plastocyanin (or cytochrome  $c_6$ ) to PSI. The other half of the electrons are recycled to the “low-potential chain”, namely through hemes  $b_L$ ,  $b_H$  and  $c_i$  (Stroebel et al. 2003) or  $x$  (Kurisu et al. 2003), or  $c_n$  (Cramer and Zhang 2006), for the reduction and protonation of a quinone at the  $Q_i$  site. The plastoquinol formed at  $Q_i$  can be reoxidized at the  $Q_o$  site, therefore completing a cycle called the Q-cycle (Mitchell 1975). The bifurcation of electron flow at the  $Q_o$  site and the Q-cycle means that the cytochrome  $b_6f$  complex, like the cytochrome  $bc_1$  complex, translocates two protons through the membrane per one electron passing through Cyt  $f$  or Cyt  $c_1$ , resulting in a major contribution to  $\Delta\text{pH}$ .

The oxidoreductase activity and the overall structure of the cytochrome  $b_6f$  complex are not so different from that of the cytochrome  $bc_1$  complex, although a  $c'$ -type heme is found in the  $Q_i$  site of the cytochrome  $b_6f$  complex. Similar to cytochrome  $b_6f$  complex, which transfers electrons with photosystems II and I, the cytochrome  $bc_1$  complex is involved in photosynthetic electron flow in association with either type II or type I reaction centers in purple bacteria and in green-sulfur bacteria, respectively (see the Chaps. 3 and 10 by Majumder and Blankenship, and Esser et al., in this volume). Here we review some of the physico-chemical properties of heme  $c_i$ , discuss its role in redox chemistry of quinones, and its postulated specific roles

Abbreviation:  $b_H$  – High-potential heme  $b$ ;  $b_L$  – Low-potential heme  $b$ ; Cyt  $b_6f$  – Cytochrome  $b_6f$  complex; ECS – Electrochromic shift;  $E_m$  – Midpoint redox potential; FNR – Ferredoxin- $\text{NADP}^+$  reductase; LHC2 – Light Harvesting Complex 2;  $\text{NADP}^+$  – Nicotinamide adenine dinucleotide phosphate; NQNO – *2-n-nonyl-4-hydroxyquinoline N-oxide*; PSI – Photosystem I; PSII – Photosystem II; TMBZ – 3,3',5,5'-tetramethylbenzidine

for cytochrome  $b_6f$  complex function in comparison with the cytochrome  $bc_1$  complex.

## II. Early Evidence: Heme $c_i$ of the Cytochrome $b_6f$ Complex, A Functional Retrospective

Early evidence for the presence of an unusual  $c'$ -type heme associated to the cytochrome  $b_6f$  complex came from a spectroscopic study by Lavergne (1983), and a subsequent one from Joliot and Joliot (1988), using intact cells of the green microalga *Chlorella*. These

thorough studies have provided most of the functional information about heme  $c_i$ . This discovery arose by the combined advances of two unique tools: firstly, the development of highly sensitive flash-spectrophotometers, and secondly the isolation of low-chlorophyll mutants of green microalgae. As shown in Figs. 15.1 and 15.2, heme  $c_i$  shows rather weak absorbance changes ( $\Delta\epsilon_{425\text{ nm}} \approx 60\text{--}70\text{ mM}^{-1}\text{ cm}^{-1}$ ), compared to hemes  $b$  ( $\Delta\epsilon_{433\text{ nm}} \approx 150\text{ mM}^{-1}\text{ cm}^{-1}$ ) or  $f$  ( $\Delta\epsilon_{422\text{ nm}} \approx 150\text{ mM}^{-1}\text{ cm}^{-1}$ ), and it is only observable in the blue region of the spectrum where chlorophyll absorbance is preponderant.

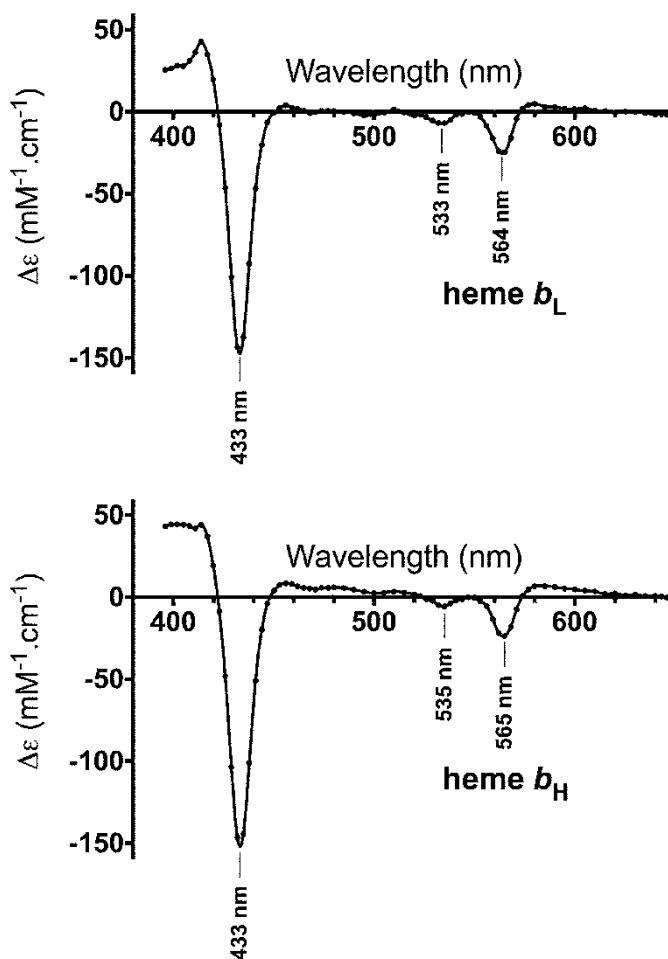


Fig. 15.1. Oxidized-minus-reduced difference spectra of the  $b$  hemes of the purified cytochrome  $b_6f$  complex from *Chlamydomonas reinhardtii* (Redrawn from Alric et al. (2005)).

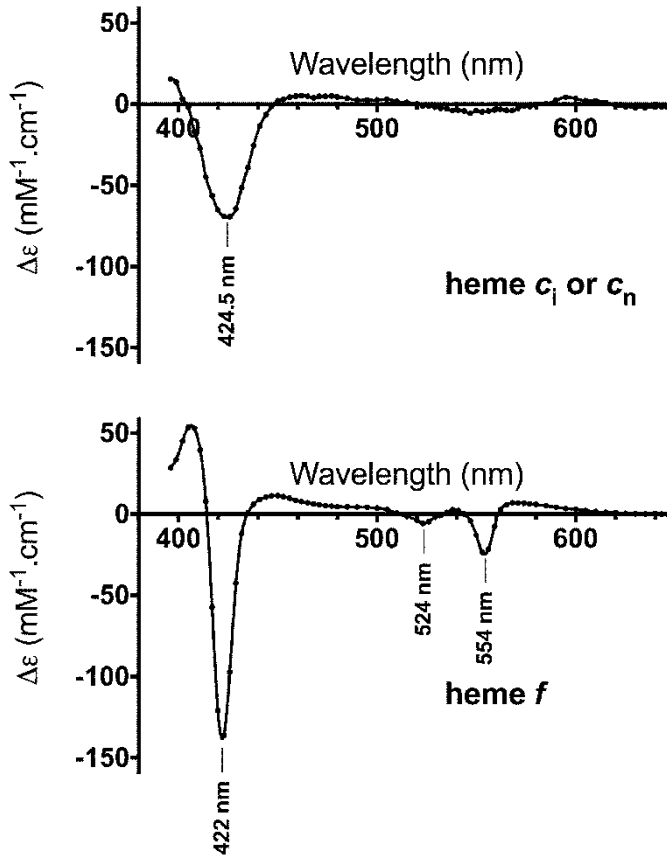


Fig. 15.2. Oxidized-minus-reduced difference spectra of heme  $c_i$  (or  $c_n$  or  $x$ ) and Cyt  $f$  of the purified cytochrome  $b_6f$  complex from *Chlamydomonas reinhardtii* (Redrawn from Alric et al. (2005)).

Light-induced absorbance changes measured *in vivo* are dominated by the large contribution of the electrochromic shift (ECS) of pigments induced by the membrane potential ( $\Delta\Psi$ ) formed during illumination. First reported by Duysens (1954), this signal was later (Witt 1971) ascribed to an absorbance shift (Stark effect) of chlorophylls a and b (bands around 630–700 nm), carotenoids (peak around 515–520 nm), chlorophyll b (trough around 480 nm), or a mixed contribution of chlorophylls and carotenoids (<450 nm) showing sharp bands. Those spectral contributions in the region below 450 nm hinder the absorbance changes in the  $\gamma$ -band of cytochromes specific to oxidation-reduction of hemes  $f$  (~420 nm) or  $b_6$  (~430 nm) from the cytochrome  $b_6f$  complex. Furthermore, absorbance flattening

(Duysens 1956) in the highly absorbing blue region of the spectrum drastically reduces the contribution of the cytochrome's  $\gamma$ -bands (420–430 nm) relative to their  $\alpha$ -bands (550–560 nm).

*Chlorella sorokiniana* has a small cell size compared to other eukaryotic algal species (Shihira and Krauss 1965). It was therefore quickly adopted by the *in vivo* spectroscopists, who appreciated the lower scattering and lower absorption flattening of these intact cells (Lavergne et al. 1984). At this time, mutants were produced and studied that were devoid of the major photosynthetic complexes PSI, PSII, cytochrome  $b_6f$  complex, LHC2 complexes (Lacambra et al. 1984; Lavergne et al. 1984), or chloroplast ATPase (Rappaport et al. 1999). In addition, almost all possible combinations of double

mutants were obtained, providing the experimentalist with a complete set of tools for the *in vivo* analysis of photosynthetic electron flow in the whole visible spectrum range.

Provided with a *Chlorella* strain lacking LHC2 and PSI, and with a Joliot-type spectrophotometer, a highly sensitive flash spectrophotometer designed and built by D. Béal (Joliot et al. 1980), J. Lavergne measured the absorption changes from  $\sim 390$  to  $\sim 580$  nm induced by 1 s of preillumination (Lavergne 1983). He

observed that a spectral component, peaking around 425 nm and differing from the ECS contribution, appeared concomitantly with heme  $b$  oxidation and to the decay of the membrane potential. A pure spectral signature of this new component, that was named carrier G, of the photosynthetic chain was obtained 2 s after preillumination in the presence of the strong membrane uncoupler dicyclohexyl-18-crown-6 see Fig. 15.3 top panel (Lavergne 1983). The electron transfer from G to heme  $b_H$  was completed in less than 100  $\mu$ s. This, with the requirement of a

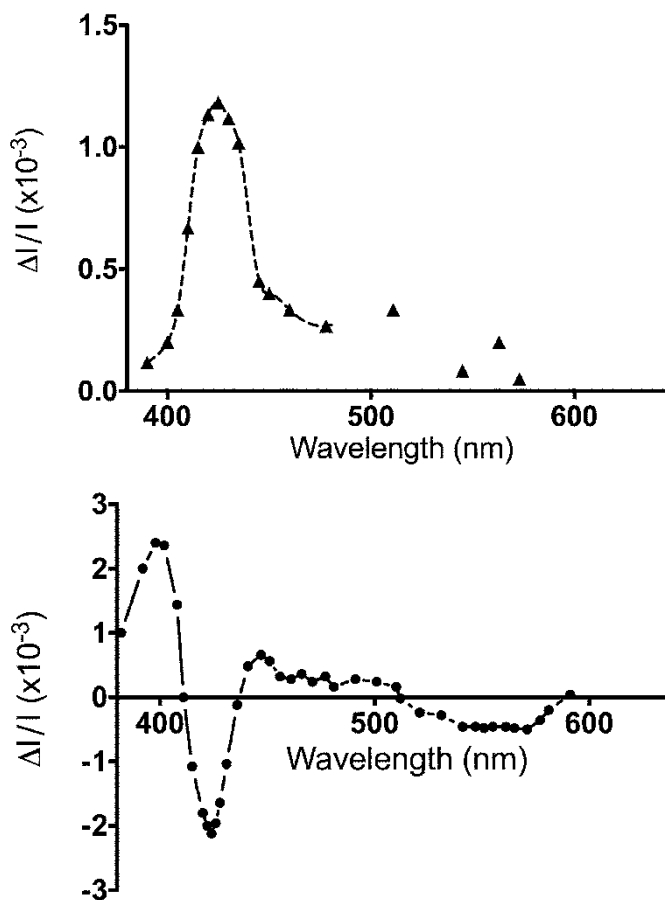


Fig. 15.3. Reduced-minus-oxidized (top) and oxidized-minus-reduced (bottom) difference spectra of heme  $c_i$  (or  $c_n$  or  $x$ ) measured *in vivo* in intact cells of low-chlorophyll mutants of *Chlorella sorokiniana* (Redrawn from Lavergne (1983) and Joliot and Joliot (1988)). In the bottom panel, absorbance changes are distorted at shorter wavelengths ( $<410$  nm) due to the difference between  $b_L$  and  $b_H$  contributions in this range, but the 500–600 nm range is better resolved than in the top panel, matching those of Fig. 15.2. *In vivo*, the amplitude of absorbance changes due to cytochromes is flattened in the  $\gamma$ -band compared to the  $\alpha$ -band (observed here comparing Fig. 15.3, bottom panel to Fig. 15.2, top panel), for absorbance flattening, see (Duysens 1956).

transmembrane location of G, had suggested that it is embedded in (or tightly bound to) cytochrome  $b_6f$  (Lavergne 1983). A few years later, Joliot and Joliot (1988) observed G under similar uncoupled and preilluminated conditions: the same signal appeared in the difference spectrum between untreated and CO-treated samples (Joliot and Joliot 1988), see Fig. 15.3 bottom. The spectral features of G were similar to those of high spin  $c'$  cytochromes that were found in some photosynthetic bacteria.

Functional and biochemical evidence such as the apparent absence of G in spinach thylakoids, and no clear spectral contribution of G in the oxidized-minus-reduced spectra of purified cytochrome  $b_6f$ , suggested that G was not ubiquitous in photosynthesis or that it could be a soluble protein loosely bound to cytochrome  $b_6f$  complex, lost during purification. Despite repeated attempts to further characterize this cytochrome, researchers mistook what was probably its most obvious manifestation: a blue-green smeary band in denaturing electrophoresis gels, appearing after TMBZ staining. Whereas the non-covalently bound  $b$ -type hemes of mitochondrial and bacterial cytochrome  $b$  are lost after denaturation of the complex (Berry et al. 1991), the cytochrome  $b_6$ -subunit of Cyt  $b_6f$  complexes can be stained by TMBZ after electrophoresis (Kuras et al. 1997). One of the  $b$  hemes seemed resilient to solubilization, but no matter how harsh the denaturing treatment was; the hazy blue-colored band appearing in TMBZ-stained gels would not fade away. At that time, the presence of a  $c$ -type heme covalently-bound to the  $b_6$  subunit was so unthinkable that an unusual binding of one of the two  $b$  hemes to the cytochrome  $b_6f$  complex was postulated. For a recent update on the detection of heme  $c_i$  attached to cytochrome  $b_6$  in denaturing gels, see (de Vitry et al. 2004). Other signs of the invisible heme  $c_i$  came from the difficulty of constructing  $Q_i$ -site mutants in *C. reinhardtii* on the basis of the homology with the Cyt  $bc_1$  complex (de Lacroix de Lavalette et al. 2008), and from

mass spectrometry data (Whitelegge et al. 2002).

Despite these apparent inconsistencies, the pre-structure era did collect some solid information on this new cytochrome: (i) the new spectral component 'G' that was identified corresponded to a  $c'$ -type cytochrome (Lavergne 1983; Joliot and Joliot 1988), (ii) this cyt  $c'$  should be tightly bound to or embedded in the cytochrome  $b_6f$  complex, very close to heme  $b_H$  and located on the stromal side of the membrane (Lavergne 1983), (iii) the redox potential of this new cofactor was 30 mV higher than that of  $b_H$ , and the equilibrium constant between  $b_H$  and  $c_i$  was dependent upon the membrane potential (Lavergne 1983), and (iv) the redox potential of this cofactor could be modulated by the presence/absence of axial ligands of the heme iron, such as CO (Joliot and Joliot 1988).

### III. Tridimensional Structure

The two structures of the cytochrome  $b_6f$  complex, published back to back in 2003 (Kurusu et al. 2003; Stroebel et al. 2003) confirmed the high structural homology between cytochrome  $bc_1$  and  $b_6f$  complexes: the inter-cofactor distances are similar and the  $b$  hemes are oriented in the same way. Some differences in the  $b_6f$  complex relative to the cytochrome  $bc_1$  complex were expected: a chlorophyll  $a$  molecule and a  $\beta$ -carotene, retained during purification of the  $b_6f$  complex (Huang et al. 1994; Pierre et al. 1995, 1997), were found in the structure. The big surprise from the crystal structure was a large flat electron density with two lateral extensions, in the  $Q_i$  site, at the stromal side of the complex. The general structure of the  $Q_i$  site is similar in  $b_6f$  and  $bc_1$  complexes, with the exception of the active site showing a larger quinone-binding pocket formed by separate Cyt  $b_6$  and subunit IV components rather than a single Cyt  $b$  protein, and an additional prosthetic group in  $b_6f$  complexes. The latter was likely to correspond to a heme according to the following observations: (i)





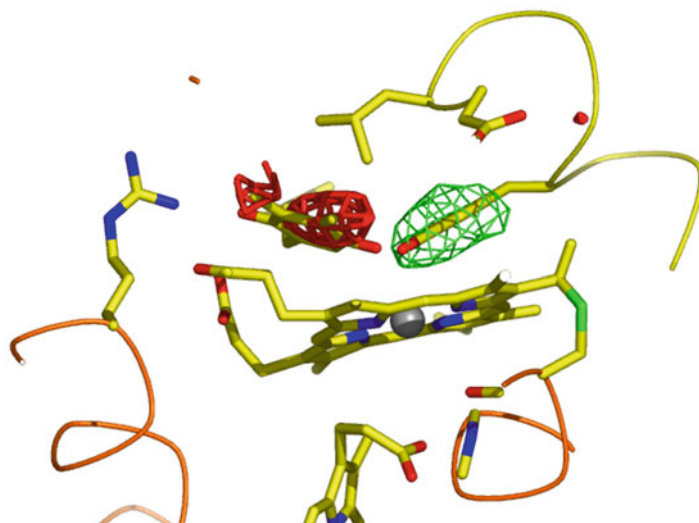


Fig. 15.5. Difference Fourier map between F40Y mutant and wild type of heme  $c_1$  environment. Difference density is contoured at 4 Å positive signal in *green*, negative signal in *red*. The positive electron density around Tyr40, shows a higher occupancy of Tyr for this site than the native Phe, the negative signal suggest the absence of the quinone.

nal redesign of the cavity, to understand the redox chemistry of quinone reduction. The Phe40 from subunit IV was the obvious first mutagenesis target to modulate the interaction between  $c_1$  and the quinone or quinol molecules. When Phe40 was replaced by a Tyr (F40Y mutant) (de Lacroix de Lavalette et al. 2009), Tyr40 served as an axial ligand to the heme, which induced a downshift of the  $c_1$  heme midpoint-potential.

Figure 15.5 shows a stick model of the  $Q_i$  site of the F40Y mutant (Daniel Picot personal communication), where the stick model of the polar head of the quinone is added from the native structure. Here the quinone tail, too disordered in the crystal, could not be modelled (Stroebel et al. 2003). The 3D-contours show the positive (green) and negative (red) differences in electron density maps obtained from mutant and wild type crystals ( $F_{40Y}-F_{wt}$ ). The negative signal shows that the mutation to Tyr has released the quinone. An unexpectedly strong positive electron density also appeared in the difference map, around Tyr40, showing a higher occupancy of Tyr for this site than the native Phe, which had a weaker electron density.

This can be explained because Tyr is tightly coordinated with the  $c_1$  heme group whereas the native Phe at position 40 is somehow more flexible and more readily allows the binding of a quinone to the  $Q_i$  site.

Following a single flash reduction of the  $b$  hemes in the F40Y mutant, their reoxidation was 50 times slower than in the wild type (de Lacroix de Lavalette et al. 2009), showing that Tyr ‘locks’ the cavity and impedes access by quinone. However, under continuous illumination, when the reducing pressure increases on the Cyt  $b_6 f$  complex low-potential chain, the turnover of the mutant  $b_6 f$  complex was largely sufficient to sustain photosynthesis (de Lacroix de Lavalette et al. 2009), suggesting that the Tyr 40 cavity lock can be forced open. Tyr 40 was apparently displaced by carbon monoxide, which ligated to the  $c_1$  heme iron. The kinetics of CO rebinding after photodissociation was only two times slower in the mutant than in the wild type (de Lacroix de Lavalette et al. 2009). All of these data support the idea that the steric hindrance related to the Tyr- $c_1$  heme coordination is relieved under steady-state illumination conditions; in other

words, heme  $c_i$  reduction may control ligand binding and substrate accessibility. Data from heme oxygenase and nitrite reductase (Adachi et al. 1993; Liu et al. 1999; Das et al. 2001) show similar redox-induced changes in heme ligation that control the accessibility of the substrate to the catalytic site. In the wild type cytochrome  $b_6f$  complex, the Phe40 aromatic ring has to move away from the heme iron to accommodate the quinone (D. Picot, personal communication). This movement requires energy that can be partly provided by the  $\Delta G$  of heme  $c_i$  reduction.

### V. NQNO, A Not-So-Good Inhibitor of the $Q_i$ Site of the Cytochrome $b_6f$ Complex

Perhaps a similar redox-control of the  $Q_i$ -site occupancy accounts for the inhibitory effect of NQNO (Jones and Whitmarsh 1988). Rich et al. (1991) noted that “*NQNO concentrations which are sufficient to cause a maximal effect on the quinone reduction site completely inhibit steady state electronic turnover of the bc complexes but have no effect on steady state electronic turnover (Jones and Whitmarsh 1988) or proton translocating stoichiometry (Hope and Rich 1989) of the bf complex. Furthermore, at these inhibitor concentrations oxidant-induced reduction of both haems b is possible in the bc complexes, but oxidant-induced reduction of more than one haem b has never been achieved with the bf complex (Rich 1988; Furbacher et al. 1989). These findings have led to views that the cytochrome bf complex may have a basic reaction cycle which can be different to that of the bc complexes*”.

These early observations may be rationalized by the structural differences in the quinone-binding pocket and from the redox titrations of heme  $c_i$ . Redox titrations show that the  $E_m$  of heme  $c_i$  is  $\sim 240$  mV more electronegative in the presence of NQNO. This shows that NQNO stabilizes the oxidized form of heme  $c_i$ , or destabilizes the reduced form of heme  $c_i$ . In other words,

NQNO binds to the oxidized form of  $c_i$ , or reciprocally NQNO is released upon reduction of  $c_i$ . Because the shift in potential is rather large ( $\sim 240$  mV), the changes in terms of equilibrium constant of the reactions (and therefore association/dissociation constant of the substrate/inhibitor) are rather important (*i.e.*  $10^{240/60} = 10^4$ -fold change). For a structure of the complex with NQNO, see (Yamashita et al. 2007).

In Fig. 15.6, we propose a series of reactions that would depict the residual turnover of the cytochrome  $b_6f$  complex in an NQNO-poisoned sample. These involve electron transfer reactions and binding or release of quinone analogs. Let us first describe the B, C, D, and E states as expected from the redox titrations from (Alric et al. 2005). The  $-60$  mV per pH unit dependence of the redox potential of  $c_i$ , in the inhibited or non-inhibited state show that heme  $c_i$  is protonated while reduced (deprotonated while oxidized). In the presence of NQNO, at pH 7,  $c_i$  and  $b_L$  are nearly equipotential (Alric et al. 2005) (see B and C states,  $K \sim 1$ ), whereas in the absence of inhibitor the reduction of  $c_i$  ( $E_m \sim +100$  mV) is largely favored at the expense of the reduction of  $b_L$  ( $E_m \sim -140$  mV) (see D and E states,  $K_{eq} \sim 10^4$ ). This translates into a dissociation constant  $10^4$ -fold stronger (greatly favoring dissociation) for the reduced form of the heme (see states C and E) than for its oxidized form (see states B and D) and accounts for the leakiness of NQNO. Under steady-state illumination, when the reducing pressure from PSII on the cytochrome  $b_6f$  low-potential chain is strong (heme  $c_i$  reduction), NQNO is released from its site thereby exemplifying the structural difference between cyt  $bc_1$  and cyt  $b_6f$  foreseen by Rich et al. (1991).

### VI. Concluding Remarks

Twenty years elapsed between the discovery of an unusual  $c'$ -type cytochrome signal associated with cytochrome  $b_6f$  turnover (Lavergne 1983) and the proper identification

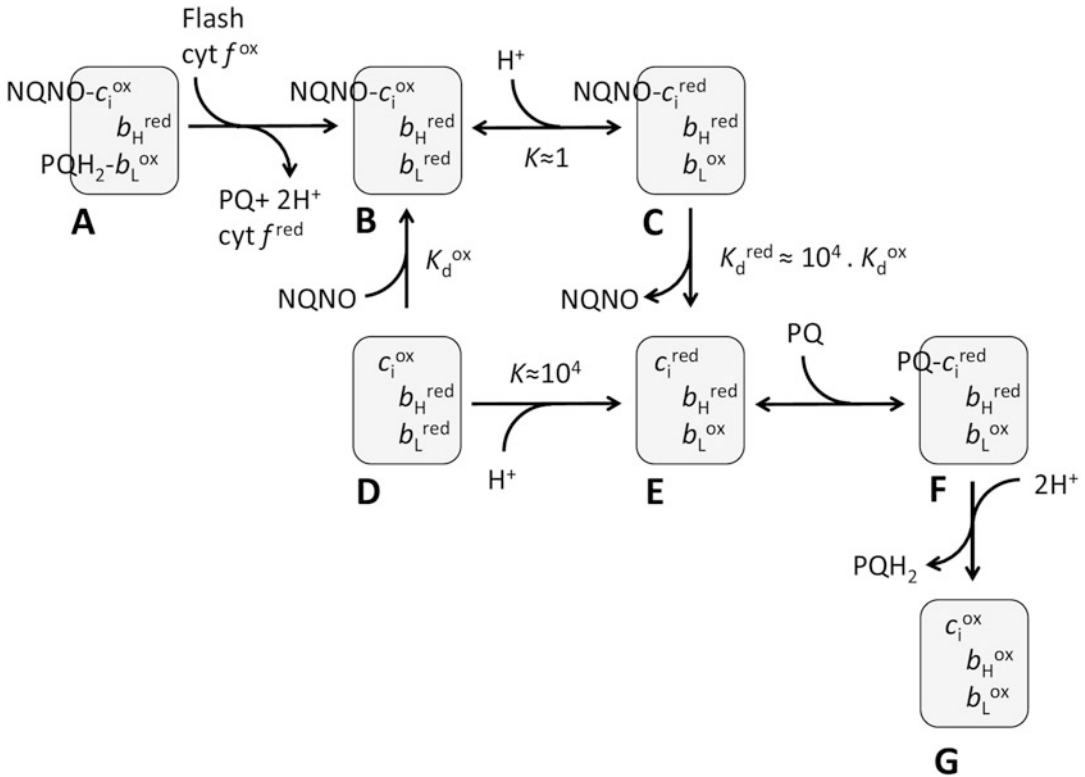


Fig. 15.6. Model for cytochrome  $b_6f$  turnover observed in the presence of NQNO. Upon oxidant-induced single-turnover of the enzyme (Cyt  $f$  oxidized by PSI following a single flash), state B is partly stable and the complex in its inhibited state. Upon continuous illumination, when the reducing pressure builds up on the cytochrome  $b_6f$  low-potential chain, steadily forming  $c_i^{\text{red}}, b_H^{\text{red}}$  and  $b_L^{\text{red}}$ , NQNO is released from the  $Q_i$  site, and oxidation of  $c_i$ - $b_H$  (E-G reactions) is favored. The equilibrium constant,  $K$ , refers to the redox equilibrium between  $c_i$  and  $b_L$  and the dissociation constant,  $K_d$ , refers to the dissociation of NQNO from  $c_i$ .

of this cofactor as an intrinsic component of the complex (Kurisu et al. 2003; Stroebel et al. 2003). This rather long delay was partly due to the very nature of this peculiar heme  $c'$ . More probably, the delay was due to the unexpected existence of such a cofactor in such an improbable place. The specific role heme  $c_i$  plays in the cytochrome  $b_6f$  complex does not appear clearly from comparison with its counterpart, the ancestral cytochrome  $bc_1$  complex. Perhaps the only satisfactory idea is that the closely coupled, two-electron reduction of the plastoquinone (PQ) to plastoquinol ( $\text{PQH}_2$ ) in the  $Q_i$  site by the heme  $c_i$ - $b_H$  “double barreled shotgun” would reduce the half-life of the semi-

quinone and would make the cytochrome  $b_6f$  complex more fit for the oxic environment of oxygenic photosynthesis (Baymann et al. 2007).

## Acknowledgments

We acknowledge Daniel Picot for stimulating discussion and help in drawing Fig. 15.5. Work in FZ laboratory was supported by Unité Mixte de Recherche 7099, CNRS, and Université Paris Diderot and by the “Initiative d’Excellence” program (Grant “DYNAMO,” ANR-11-LABX-0011-01).

## References

- Adachi S, Nagano S, Ishimori K, Watanabe Y, Morishima I, Egawa T, Kitagawa T, Makino R (1993) Roles of proximal ligand in heme proteins: replacement of proximal histidine of human myoglobin with cysteine and tyrosine by site-directed mutagenesis as models for P-450, chloroperoxidase, and catalase. *Biochemistry* 32:241–252
- Alric J, Pierre Y, Picot D, Lavergne J, Rappaport F (2005) Spectral and redox characterization of the heme  $c_i$  of the cytochrome  $b_6f$  complex. *Proc Natl Acad Sci U S A* 102:15860–15865
- Baymann F, Giusti F, Picot D, Nitschke W (2007) The  $c_i/b_H$  moiety in the  $b_6f$  complex studied by EPR: a pair of strongly interacting hemes. *Proc Natl Acad Sci U S A* 104:519–524
- Berry EA, Huang LS, DeRose VJ (1991) Ubiquinol-cytochrome  $c$  oxidoreductase of higher plants. Isolation and characterization of the  $bc_1$  complex from potato tuber mitochondria. *J Biol Chem* 266:9064–9077
- Cramer WA, Zhang H (2006) Consequences of the structure of the cytochrome  $b_6f$  complex for its charge transfer pathways. *Biochim Biophys Acta* 1757:339–345
- Das TK, Wilson EK, Cutruzzola F, Brunori M, Rousseau DL (2001) Binding of NO and CO to the  $d_1$  heme of  $cd_1$  nitrite reductase from *Pseudomonas aeruginosa*. *Biochemistry* 40:10774–10781
- de Lacroix de Lavalette A, Barbagallo RP, Zito F (2008) Why is it so difficult to construct  $Q_i$  site mutants in *Chlamydomonas reinhardtii*? *Comptes Rendus Biol* 331:510–517
- de Lacroix de Lavalette A, Barucq L, Alric J, Rappaport F, Zito F (2009) Is the redox state of the  $c_i$  heme of the cytochrome  $b_6f$  complex dependent on the occupation and structure of the  $Q_i$  site and vice versa? *J Biol Chem* 284:20822–20829
- de Vitry C, Desbois A, Redeker V, Zito F, Wollman FA (2004) Biochemical and spectroscopic characterization of the covalent binding of heme to cytochrome  $b_6$ . *Biochemistry* 43:3956–3968
- Duysens LNM (1954) Reversible changes in the absorption spectrum of *Chlorella* upon irradiation. *Science* 120:353–354
- Duysens LN (1956) The flattening of the absorption spectrum of suspensions, as compared to that of solutions. *Biochim Biophys Acta* 19:1–12
- Furbacher PN, Girvin ME, Cramer WA (1989) On the question of interheme electron transfer in the chloroplast cytochrome  $b_6$  in situ. *Biochemistry* 28:8990–8998
- Hope AB, Rich PR (1989) Proton uptake by the chloroplast cytochrome  $bf$  complex. *Biochim Biophys Acta* 975:96–103
- Huang D, Everly RM, Cheng RH, Heymann JB, Schagger H, Sled V, Ohnishi T, . . . , Cramer WA (1994) Characterization of the chloroplast cytochrome  $b_6f$  complex as a structural and functional dimer. *Biochemistry* 33:4401–4409
- Joliot P, Joliot A (1988) The low-potential electron-transfer chain in the cytochrome  $bf$  complex. *Biochim Biophys Acta* 933:319–333
- Joliot P, Béal D, Frilley B (1980) A new spectrophotometric method for the study of photosynthetic reactions. *J Chim Phys* 77:209–216
- Jones RW, Whitmarsh J (1988) Inhibition of electron-transfer and the electrogenic reaction in the cytochrome  $bf$  complex by 2-normal-nonyl-4-hydroxyquinoline N-oxide (NQNO) and 2,5-dibromo-3-methyl-6-isopropyl-P-benzoquinone (DBMIB). *Biochim Biophys Acta* 933:258–268
- Kallas T (2012) Cytochrome  $b_6f$  complex at the heart of energy transduction and redox signaling. In: Eaton-Rye JJ, Tripathy BC, Sharkey TD (eds) *Photosynthesis*. Springer, Dordrecht, pp 501–560
- Kuras R, de Vitry C, Choquet Y, Girard-Bascou J, Culler D, Buschlen S, Merchant S, Wollman FA (1997) Molecular genetic identification of a pathway for heme binding to cytochrome  $b_6$ . *J Biol Chem* 272:32427–32435
- Kurusu G, Zhang H, Smith JL, Cramer WA (2003) Structure of the cytochrome  $b_6f$  complex of oxygenic photosynthesis: tuning the cavity. *Science* 302:1009–1014
- Lacambra M, Larsen U, Olive J, Bennoun P, Wollman FA (1984) Mutants of *Chlorella sorokiniana*: a new material for photosynthesis studies. I. Characterization of the thylakoid membranes of wild type and mutant strains. *Photobiochem Photobiophys* 8:191–205
- Lavergne J (1983) Membrane potential-dependent reduction of cytochrome  $b_6$  in an algal mutant lacking photosystem-I centers. *Biochim Biophys Acta* 725:25–33
- Lavergne J, Delosme R, Larsen U, Bennoun P (1984) Mutants of *Chlorella sorokiniana*: a new material for photosynthesis studies. II. Improved spectroscopic analysis of electron transfer in mutant strains. *Photobiochem Photobiophys* 8:207–219
- Liu Y, Moenne-Loccoz P, Hildebrand DP, Wilks A, Loehr TM, Mauk AG, Ortiz de Montellano PR (1999) Replacement of the proximal histidine iron ligand by a cysteine or tyrosine converts heme oxygenase to an oxidase. *Biochemistry* 38:3733–3743
- Mitchell P (1975) The protonmotive Q-cycle: a general formulation. *FEBS Lett* 59:137–139
- Mitchell P (1976) Possible molecular mechanisms of the protonmotive function of cytochrome systems. *J Theor Biol* 62:327–367

- Pierre Y, Breyton C, Kramer D, Popot JL (1995) Purification and characterization of the cytochrome *b<sub>6</sub>f* complex from *Chlamydomonas reinhardtii*. *J Biol Chem* 270:29342–29349
- Pierre Y, Breyton C, Lemoine Y, Robert B, Verrotte C, Popot JL (1997) On the presence and role of a molecule of chlorophyll a in the cytochrome *b<sub>6</sub>f* complex. *J Biol Chem* 272: 21901–21908
- Rappaport F, Finazzi G, Pierre Y, Bennoun P (1999) A new electrochemical gradient generator in thylakoid membranes of green algae. *Biochemistry* 38:2040–2047
- Rich PR (1988) A critical-examination of the supposed variable proton stoichiometry of the chloroplast cytochrome-*bf* complex. *Biochim Biophys Acta* 932:33–42
- Rich PR, Madgwick SA, Moss DA (1991) The interactions of duroquinol, dbmib and NQNO with the chloroplast cytochrome-*bf* complex. *Biochim Biophys Acta* 1058:312–328
- Shihira I, Krauss RW (1965) *Chlorella*: Physiology and Taxonomy of Forty-one Isolates. University of Maryland, College Park
- Stroebel D, Choquet Y, Popot JL, Picot D (2003) An atypical haem in the cytochrome *b<sub>6</sub>f* complex. *Nature* 426:413–418
- Whitelegge JP, Zhang H, Aguilera R, Taylor RM, Cramer WA (2002) Full subunit coverage liquid chromatography electrospray ionization mass spectrometry (LCMS+) of an oligomeric membrane protein: cytochrome *b<sub>6</sub>f* complex from spinach and the cyanobacterium *Mastigocladus laminosus*. *Mol Cell Proteomics* 1:816–827
- Witt HT (1971) Coupling of quanta, electrons, fields, ions and phosphorylation in the functional membrane of photosynthesis. Results by pulse spectroscopic methods. *Q Rev Biophys* 4:365–477
- Yamashita E, Zhang H, Cramer WA (2007) Structure of the cytochrome *b<sub>6</sub>f* complex: quinone analogue inhibitors as ligands of heme *c<sub>n</sub>*. *J Mol Biol* 370:39–52

# Chapter 16

## Structure and Function of Bacterial Cytochrome *c* Oxidases

Joseph A. Lyons<sup>a</sup>, Florian Hilbers<sup>a</sup>, and Martin Caffrey<sup>b,\*</sup>

<sup>a</sup>*Department of Molecular Biology and Genetics, Aarhus  
University, Aarhus, Denmark*

<sup>b</sup>*School of Medicine and School of Biochemistry and  
Immunology, Trinity College Dublin, Dublin 2, Ireland*

Summary.....	307
I. Introduction.....	308
II. Respiratory Chain.....	308
III. Heme Copper Oxidases.....	309
A. Overall Structure.....	310
1. Subunit I.....	314
2. Subunit II.....	314
3. Subunit III.....	315
4. Subunit IV.....	315
IV. Pathways Within HCO.....	315
A. Type A.....	316
1. D-Pathway.....	316
2. K-Pathway.....	317
B. Type B and C.....	318
1. An Alternative K-Pathway.....	318
C. Proton and Water Exit Pathways.....	318
V. Electron Transfer.....	319
VI. Oxygen Channel.....	320
VII. The Catalytic Cycle.....	321
VIII. Side Reactions in CcO.....	323
IX. Conclusions.....	324
Acknowledgments.....	324
References.....	324

### Summary

Cytochrome *c* oxidase or complex IV is the terminal enzyme of the aerobic respiratory chain performing the essential process of reducing molecular oxygen to water. The energy resulting from this reaction is exploited to drive proton pumping across the membrane, which in turn contributes to the generation of a proton motive force and the downstream synthesis

---

\*Author for correspondence, e-mail: [martin.caffrey@tcd.ie](mailto:martin.caffrey@tcd.ie)

of ATP. This chapter highlights current progress in the field of bacterial cytochrome *c* oxidase research from the perspective of the structural and functional characterisation of this family of essential enzymes.

## I. Introduction

Energy is a fundamental requirement for all living organisms. Plants, algae and cyanobacteria derive their metabolic energy from photosynthesis while animals derive it from cellular respiration (Stryer et al. 2002). During photosynthesis, solar energy is harnessed by chlorophyll to produce carbohydrates from CO<sub>2</sub> and water, yielding oxygen as a by-product. In cellular respiration different food molecules such as glucose and fatty acids are metabolised into CO<sub>2</sub> and water, releasing energy. This energy is used to synthesise adenosine 5'-triphosphate (ATP), the cell's chemical energy currency. ATP can later be used to drive a myriad of cellular functions ranging from biosynthesis to the active transport of ions and molecules across the membrane. A key protein in the bacterial respiratory chain, cytochrome *c* oxidase, forms the focus of this chapter and is described in detail from a structure and function perspective.

## II. Respiratory Chain

The electron transport chain (Fig. 16.1), also referred to as the respiratory chain, catalyses the final steps of cellular respiration and is located in the plasma membrane of ar-

chaea and bacteria or the mitochondrial inner membrane in higher organisms. The respiratory chain comprises a series of integral membrane protein complexes and two mobile electron carriers required to couple electron transfer, from Complex I to Complex IV (see below), with transmembrane proton pumping and the reduction of oxygen (Fig. 16.1). Structures are available for both the soluble and membrane components of the respiratory chains to various resolutions (Fig. 16.1). The overall function of the respiratory chain is to generate the trans-membrane electrochemical gradient (proton motive force) that is used to drive thermodynamically unfavourable reactions such as the synthesis of ATP by the F<sub>0</sub>F<sub>1</sub>-ATP synthase, in a process known as oxidative phosphorylation. The membrane protein components of the bacterial electron transport chain are as follows (Fig. 16.1):

1. NADH:ubiquinone reductase (Complex I), the first and largest enzyme in the respiratory chain, functions by oxidizing NADH to NAD<sup>+</sup> and reducing ubiquinone to ubiquinol. The process is coupled to the pumping of four protons. In addition, two protons are used to reduce ubiquinone and one proton is released in the oxidation of NADH. Among the electron/proton transfer complexes, Complex I is capable of generating the largest amount of reactive oxygen species (ROS) (Hatefi et al. 1961; Hatefi 1985; Turrens 1997; Brandt 2006, 2011).
2. Succinate dehydrogenase (Complex II) is the second most reducing complex of the respiratory chain. It participates in both the citric acid cycle and the electron transport chain coupling the two processes (see Maklashina and Cecchini 2010). The enzyme reduces ubiquinone to ubiquinol using electrons derived from the oxidation of succinate to fumarate. Unlike Complex I, electron transfer in Complex II is not coupled to proton pumping.

---

*Abbreviations:* ATP – Adenosine tri-phosphate; CcO – Cytochrome *c* oxidase; EPR – Electron paramagnetic resonance; FTIR – Fourier transform infra-red spectroscopy; HCO – Heme copper oxidase; HiPIP – High potential iron-sulfur protein; MD – Molecular dynamics; NAD<sup>+</sup> – Nicotinamide adenine dinucleotide (oxidised form); NADH – Nicotinamide adenine dinucleotide (reduced form); NMR – Nuclear magnetic resonance; N-side – Electrochemically negative side of the membrane; PDB – Protein Data Bank; P-side – Electrochemically positive side of the membrane; ROS – Reactive oxygen species; SU – Subunit



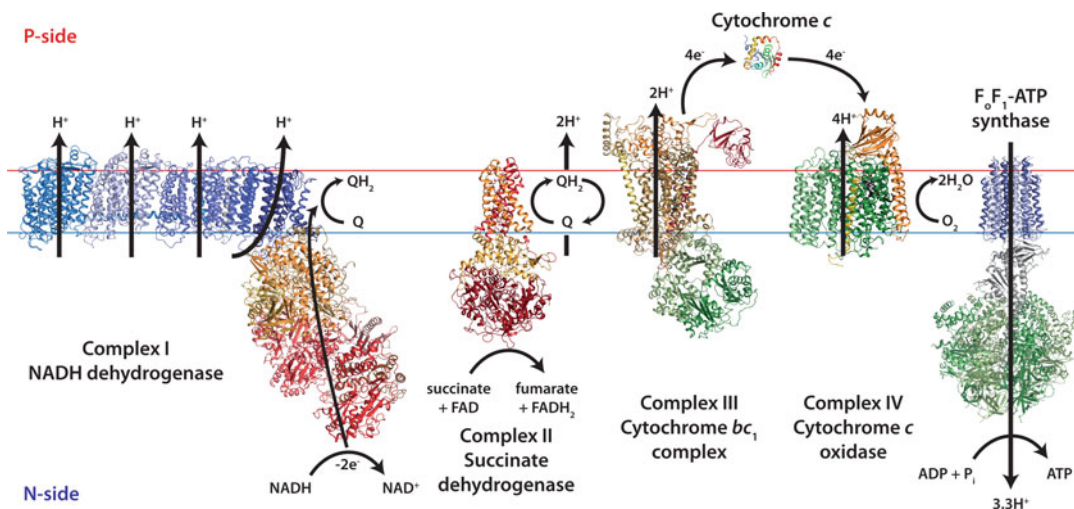


Fig. 16.1. Overview of the electron transport chain. The chain comprises Complex I (*Thermus thermophilus*, PDB entry: 4HEA), Complex II (*Escherichia coli*, PDB entry: 1NEK), Complex III (*Saccharomyces cerevisiae*, PDB entry: 1EZV), cytochrome *c* (*T. thermophilus*, PDB entry: 1C52), Complex IV (*Paracoccus denitrificans*, PDB entry: 1QLE) and ATP synthase (*S. cerevisiae*, PDB entry: 2XOK).

3. The cytochrome *bc*<sub>1</sub> complex (Complex III) is the penultimate enzyme in the respiratory chain. It couples the one-electron reduction of cytochrome *c* to the step-wise oxidation of ubiquinol with the concomitant transfer of protons across the membrane via the Q cycle (Crofts 2004). Cytochrome *c* is a small heme containing protein that acts as a soluble electron carrier between Complex III and IV of the respiratory chain (Fig. 16.1). Like Complex I, Complex III also produce ROS (Hatefi et al. 1961; Hatefi 1985; Turrens 1997).
4. Cytochrome *c* oxidase (CcO, Complex IV) is a member of the Heme Copper Oxidase (HCO) superfamily. It is the terminal enzyme in the respiratory chain of mitochondria and aerobic prokaryotes (Ferguson-Miller and Babcock 1996). CcO uses electrons donated by cytochrome *c* to catalytically reduce molecular oxygen to water (Fig. 16.1). This electron transfer is coupled to the translocation of protons across the membrane.

### III. Heme Copper Oxidases

As the terminal enzyme of the electron transport chain, HCOs have a rich diversity in electron donors, subunit composition, and

heme group types (Ferguson-Miller and Babcock 1996; Pereira et al. 2001, 2008; Sousa et al. 2012). Members of the HCO superfamily are defined by the presence in the most conserved subunit, subunit I (SU I), of a low-spin heme and a hetero-binuclear centre composed of a high spin heme and a copper ion, Cu<sub>B</sub>. In bacteria, the heme group can be of type A, B or O (which differ in porphyrin ring substituents) or derivatives thereof. By contrast, the mitochondrial HCOs contain only A-type hemes (Calhoun et al. 1994; Lubben and Morand 1994).

HCO superfamily members are further classified as Type A, B and C based on amino acid sequence signatures and the degree of conservation of the D- and K-proton pathways (Sect. IV), (Pereira et al. 2001, 2008; Sousa et al. 2012) (Fig. 16.2 and Table 16.1). Type A HCOs include mitochondrial CcOs and their closely related counterparts from bacteria such as *P. denitrificans* and *Rhodobacter sphaeroides*, as well as the *bo*<sub>3</sub>-type ubiquinol oxidase from *Escherichia coli*. This Type A group can be further divided into two subclasses, according to the amino acid composition at the hydrophobic end of the D-pathway. Type A1 contains a highly conserved glutamate in the sequence motif –XGHPEV– on helix

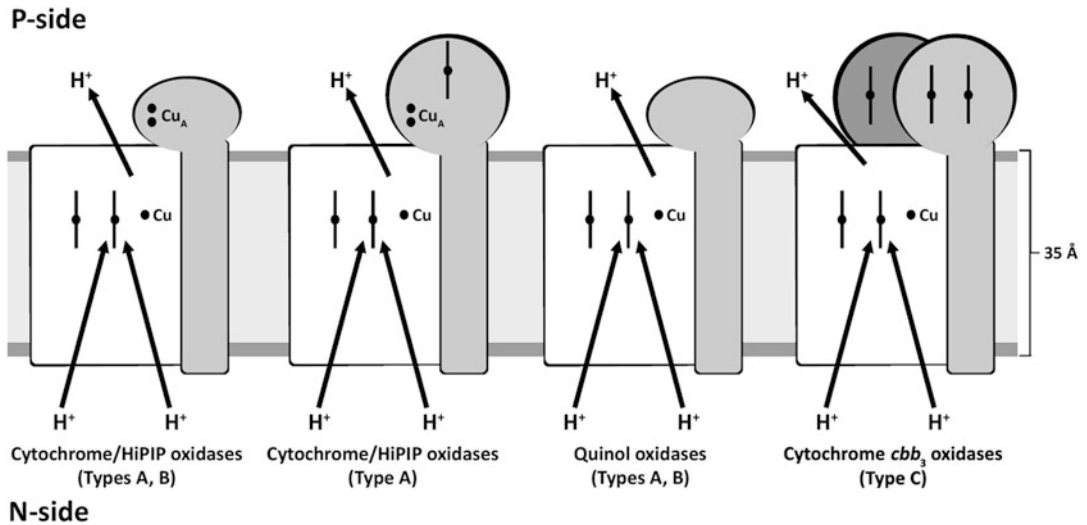


Fig. 16.2. Schematic representation of the architecture and overall mode of action of the various types of heme-copper oxidases. HCOs have been simplified to the catalytic subunits I (white) and II (grey). The structural and functional similarities of SU I are indicated and form the basis for HCO classification. Hemes are illustrated as a black line with a black dot in the centre for the metal. Proton movements are represented by arrows. For HCOs containing Cu<sub>A</sub> and/or heme *c* within their auxilliary subunits, electron donation is via reduced cytochrome *c* or in some cases high potential iron-sulfur proteins (HiPIP). The *cbb*<sub>3</sub>-type CcOs have an additional third subunit involved in electron transport (dark grey) (Redrawn from (Pereira et al. 2001)).

VI. In Type A2, the gating glutamate has been proposed to be replaced spatially by a consecutive tyrosine and serine in a –YSHPXV– motif (Pereira et al. 1999). Both A1 and A2 HCOs have a covalent link between one of the Cu<sub>B</sub> complexing histidines and a tyrosine on the same helix.

HCOs of the Type B variety are found in bacteria and archaea. *T. thermophilus ba*<sub>3</sub>-oxidase is a Type B HCO. It has low sequence homology with the Type A mitochondrial CcO. The B-type HCOs do not contain the canonical K- or D-pathways. Instead they have a proton-pathway similar to the K-pathway of A-type HCOs. B-type HCOs have a His-Tyr cross-link, as observed with Type A HCOs.

Finally, the Type C HCOs are highly divergent from both the Type A and B oxidases with respect to amino acid and subunit composition. This group consists solely of *cbb*<sub>3</sub>-type CcOs. They have an extra subunit that is involved in electron transport, while SU I contains the canonical His-Tyr cross-link and a single proton pathway analogous

to the Type A K-pathway. Unlike Type A and Type B HCOs, where the His-Tyr cross-link is between amino acids on the same helix, in Type C HCOs these residues are on different helices. This chapter will be limited to a discussion on the structure and function of the bacterial CcOs.

### A. Overall Structure

Crystal structures for members of all three major HCO families are available (Type A (A1 and A2), Type B and Type C) (Fig. 16.3). The first bacterial cytochrome *c* oxidase structure was of the four subunit *aa*<sub>3</sub>-type CcO from *P. denitrificans* (Iwata et al. 1995). The structures of the three canonical subunits (Subunits I-III) of the bacterial enzyme were remarkably similar to their mammalian counterpart (Tsukihara et al. 1996). Subsequent to the publication of the first structure of *aa*<sub>3</sub>-type CcO, improvements were made to the quality of the crystallographic data and the models derived through the crystallisation of both

Table 16.1. Structural and biophysical characteristics of the HCO types and sub-types.

HCO family and subfamily	A			C
	A1	A2	B	
Examples	<i>P. denitrificans</i> aa3 <i>R. sphaeroides</i> aa3	<i>T. thermophilus</i> caa3 <i>R. marinus</i> caa3	<i>T. thermophilus</i> ba3 <i>R. marinus</i> ba3	<i>P. stutzeri</i> cbb3
Minimal functional unit				
Subunit I	Low spin heme ( <i>a</i> , <i>b</i> , and <i>a</i> derivatives) High spin heme ( <i>α</i> , <i>o</i> and <i>a</i> derivatives)		Low spin heme ( <i>b</i> ) High spin heme ( <i>a</i> )	Low spin heme ( <i>b</i> ) High spin heme ( <i>b</i> )
Subunit II	Cu <sub>B</sub> Cu <sub>A</sub> or Cu <sub>A</sub> and low spin heme <i>c</i> No prosthetic groups (quinol oxidase)		Cu <sub>B</sub>	Cu <sub>B</sub> FixO/CcoO <sup>a</sup>
Subunit III	No prosthetic groups			Low spin heme <i>c</i> FixP/CcoP <sup>a</sup> Two low spin hemes <i>c</i>
Proton channels:				
D-pathway	Yes	Yes	N/A	N/A
Residue(s) at end of D-pathway	E	YS	N/A	N/A
K-pathway	Yes	Yes	Alternative K-pathway	Alternative K-pathway
Pumping stoichiometry in reconstituted enzymes	0.75–1 H <sup>+</sup> /e <sup>-</sup> Verkhovskiy et al. (1999), Pawate et al. (2002), Richter et al. (2005), Capitanio et al. (2006)	0.8–1 H <sup>+</sup> /e <sup>-</sup> Honnami and Oshima (1984), Pereira et al. (1999)	0.5–0.75 H <sup>+</sup> /e <sup>-</sup> Kammt et al. (1998b)	0.2–0.4 H <sup>+</sup> /e <sup>-</sup> Toledo-Cuevas et al. (1998)

(continued)

Table 16.1. (continued)

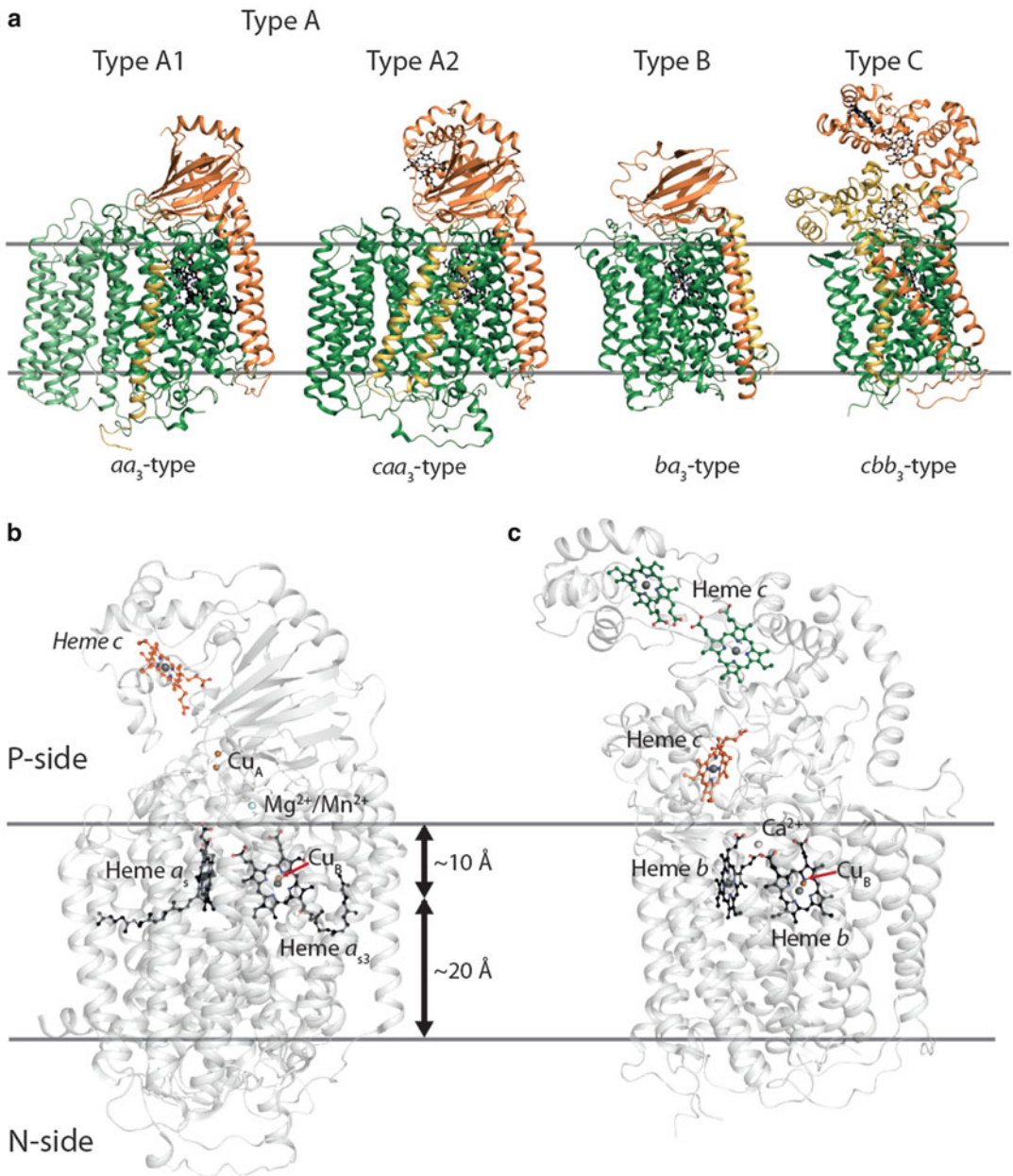
HCO family and subfamily	A		
	A1	A2	B
Readily observable intermediate states	P( $\text{Fe}^{\text{IV}} = \text{O}$ ) <sup>b</sup> F( $\text{Fe}^{\text{IV}} = \text{O}$ ) <sup>b</sup>		Not determined
Tyr-His cross-link	Yes	Yes	Yes <sup>c</sup>

Modified from (Pereira et al. 2001)

<sup>a</sup>The FixO/CcoO and FixP/CcoP subunits found in *cbh3*-type CcoO refer to the mono- and di-heme *c* containing subunits and are not related to SU II and III of the Type A and B HCOs

<sup>b</sup>The P and F intermediates differ with regard to the protonation state of the ligand on C<sub>UB</sub>

<sup>c</sup>In Type C HCOs the Tyr-His cross-link is atypical; it bridges two helices



**Fig. 16.3.** Overview of CcO structures and prosthetic group arrangements. **(a)** Representative models of Type A1 (*aa*<sub>3</sub>-type CcO; PDB entry 1QLE), Type A2 (*caa*<sub>3</sub>-type CcO; PDB entry 2YEV), Type B (*ba*<sub>3</sub>-type CcO; PDB entry 1EHK) and Type C (*cbb*<sub>3</sub>-type CcO; PDB entry 3MK7). Protein is displayed as ribbons with SUs I-IV colored green, orange, light green and yellow for the Type A oxidases, SUs I-IIa colored green, orange, and yellow for Type B and CcoN-P colored green, yellow, and orange for Type C HCOs. **(b)** Architecture of Type A and B HCOs using *caa*<sub>3</sub>-type CcO (*caa*<sub>3</sub>-type CcO; PDB entry 2YEV) as an example. For *aa*<sub>3</sub>-type and *ba*<sub>3</sub>-type CcOs, electron transfer within the enzyme begins from Cu<sub>A</sub>. **(c)** Architecture of Type C HCOs (*cbb*<sub>3</sub>-type CcO; PDB entry 3MK7). In this figure, hemes are displayed as ball and stick with metal ions as spheres. Ligating residues are omitted for clarity. In **b** and **c**, the position of the metal centres relative to the sides of the membrane is indicated by double headed arrows.

the fully-assembled enzyme (SU I-IV) and a complex comprising the catalytically active subunits (SU I & II) of the *P. denitrificans* (Ostermeier et al. 1997; Koepke et al. 2009) and *R. sphaeroides* enzymes (Svensson-Ek et al. 2002; Qin et al. 2006, 2008, 2009). Investigations into the overall structural similarities and subfamily-defining differences of HCOs were made possible upon the elucidation of the *ba*<sub>3</sub>-type CcO (Type B) structure from *T. thermophilus* (Soulimane et al. 2000; Luna et al. 2008; Tiefenbrunn et al. 2011) and more recently the *cbb*<sub>3</sub>-type CcO (Type C) from *P. stutzeri* (Buschmann et al. 2010) and the *caa*<sub>3</sub>-type CcO from *T. thermophilus* (Lyons et al. 2012) (Fig. 16.3), both of which can function as nitric oxide (NO) reductases. Structural descriptions of bacterial CcO from the various HCO types and subtypes follow.

### 1. Subunit I

The HCO defining subunit, SU I, is similar for the three family types and consists of twelve transmembrane (TM) helices that house the aforementioned low spin (6-coordinate) and high spin (5-coordinate) hemes and the copper ion, Cu<sub>B</sub>, as well as the proton pathways required for activity (Fig. 16.2). The heme types vary between Types A, B and C HCOs and are designated heme *x* (low-spin) and heme *x*<sub>3</sub> (high spin), respectively, where *x* denotes the heme type. All three redox centres are buried in the hydrophobic core of the protein and are located at a depth of approximately 1/3 of the low dielectric membrane thickness from the *P*-side of the membrane (Fig. 16.3b) (Iwata et al. 1995; Verkhovsky et al. 1999). The iron of the low spin heme is axially coordinated by two conserved histidines, one on each face of the heme. The high spin heme is axially coordinated by histidine (customarily called the proximal position), while the sixth coordination or distal site remains open for substrate binding. Cu<sub>B</sub> is ligated by three histidine side-chains and is located about 5 Å from the distal side of the heme iron. Furthermore, one of the Cu<sub>B</sub>

coordinating histidines is covalently linked to a neighbouring tyrosine side chain. Together, the high spin heme and Cu<sub>B</sub> constitute the enzyme's active site. Both hemes are positioned with their propionates pointing towards the *P*-side of the membrane.

In addition to the redox centres described above, SU I houses a functionally relevant non-redox active metal centre in Type A and C HCOs. In Type A HCOs, this metal is typically a Mg<sup>2+</sup> or Mn<sup>2+</sup> ion and is found at the interface between SU I and SU II just above the high spin heme propionates. The metal is coordinated by three residues from SU I and SU II as well as three water molecules and resides within a larger water cluster. In Type C HCOs, however, the metal is a Ca<sup>2+</sup> ion, which interacts directly with both the low and high spin hemes, and a glutamate and a serine side chain on SU I (also called CcoN in *cbb*<sub>3</sub>-type CcO) and SU II, respectively. While the divalent cation is not essential for proton pumping in HCOs (Mills et al. 2000), it is most likely part of an exit pathway for water molecules produced during turnover (Florens et al. 2001). A calcium binding site is also present at the periplasmic side in transmembrane helix I of subunit I of the bacterial CcOs. This calcium ion has no known function.

### 2. Subunit II

In Type A HCOs, SU II comprises two N-terminal transmembrane helices and a globular cupredoxin domain that resides in the periplasm in bacteria. The cupredoxin domain, formed from a ten-stranded β-barrel, houses the mixed valence dinuclear copper site, Cu<sub>A</sub>. The copper ions are ~2.5 Å apart and act as the primary electron acceptor of CcO from reduced cytochrome *c*. They are bridged by two cysteines and individually ligated by a histidine – methionine pair and a glutamate peptide carbonyl – histidine pair, respectively. In addition to the cupredoxin domain, Type A HCOs can also contain a C-terminally fused cytochrome *c* domain as in the structure of the *caa*<sub>3</sub>-type CcO from *T. thermophilus* (Lyons et al. 2012).

SU II of Type B HCOs have a similar overall architecture to the Type A HCOs in that they contain a membrane anchored cupredoxin domain. However, the membrane spanning domain comprises a lone helix. Spatially, the missing helix is compensated by an additional subunit consisting of a single TM and is designated SU IIa (Soulimane et al. 2000).

Type C HCOs do not use a dinuclear copper site to receive electrons from reduced cytochrome *c*. Instead, redox centers housed in two auxiliary subunits, designated subunit O and P (CcoO and CcoP), are used. CcoO comprises a single TM helix and a soluble cytochrome *c* domain carrying one heme *c*. In *cbb3*-type CcO from *Pseudomonas stutzeri*, the linkage between the TM helix and the cytochrome *c* domain interacts with the high (active site) and low spin hemes in SU I (CcoN), as well as CcoP. CcoP consists of a pair of N-terminal TM helices connected by a 40 Å long helix to an extramembranal globular domain (Buschmann et al. 2010). The globular unit comprises two cytochrome *c* domains each housing a heme *c*. The third canonical helix in the two cytochromes is domain-swapped.

### 3. Subunit III

In Type A HCOs, SU III comprises seven TM helices that form a V-shaped cleft between two helical bundles and has been modelled with one or more integral phospholipids. The *P. denitrificans* enzyme contains a single phosphatidylcholine molecule while the *R. sphaeroides* enzyme contains two phosphatidylethanolamines (Iwata et al. 1995; Svensson-Ek et al. 2002). The *T. thermophilus caa3*-type CcO has a three-chained thermophilic glycolynergophospholipid in this region (Lyons et al. 2012). The rationale behind this V-shaped packing of helices is not obvious. However, it is possible that the bound lipid facilitates oxygen uptake into SU I to the binuclear centre. It has been shown recently that oxidase enzyme depleted of SU III undergoes suicide inactivation, where increasing amounts of inactive enzyme

appear during catalytic turnover (Haltia et al. 1989; Bratton et al. 1999; Hosler 2004), with a subsequent loss of Cu<sub>B</sub>. Furthermore, the presence of SU III appears to influence the pH dependence of steady state oxygen reduction and is important for maintaining efficient proton flow to the active site via the D-pathway (Gilderson et al. 2003; Mills et al. 2003; Hosler 2004; Mills and Hosler 2005).

### 4. Subunit IV

SU IV, identified in the crystal structures of Type A1 HCOs as a single transmembrane helix, is loosely associated along one side of SU I and III (Fig. 16.3) and has no obvious effect on the enzymatic properties of the enzyme (Iwata et al. 1995). It bears no significant sequence homology with any other known peptide or protein. Hence, its function remains a mystery. Iwata et al. speculated on its role in stabilisation of the enzyme (Iwata et al. 1995). In the case of *caa3*-type CcO from *T. thermophilus* SU IV consists of two TM helices located across the concave membrane exposed surface of SU I/III (Fig. 16.3) (Lyons et al. 2012). To date, no evidence for a SU IV has been found in Type B HCOs, while in the structure of *cbb3*-type CcO electron density for an additional helix was detected. However, its sequence could not be assigned to CcoQ (Buschmann et al. 2010).

## IV. Pathways Within HCO

Internal pathways through HCOs are paramount for protons and oxygen to reach the binuclear centre and for the release of product water and pumped protons across the membrane. These pathways will be described in the following sections for Type A, B and C HCOs.

Crystal structures of the various cytochrome *c* oxidases in conjunction with site-directed mutagenesis studies have identified conserved proton pathways within the assorted HCOs. Type A HCOs have two proton pathways designated as the D- and K-pathways while the Type B and C HCOs

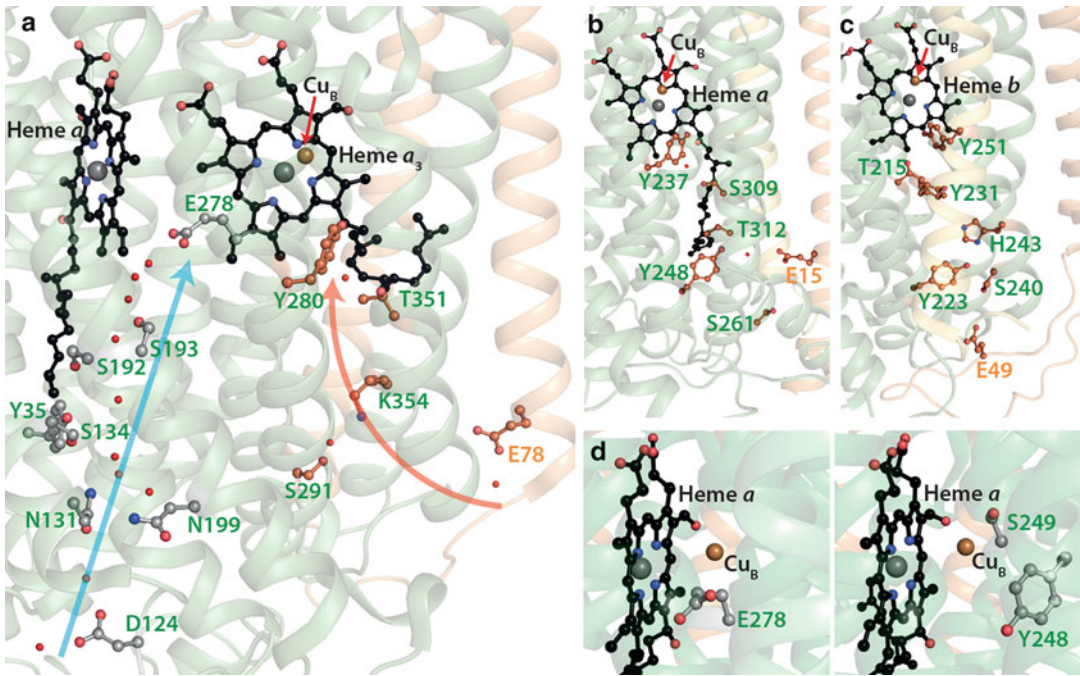


Fig. 16.4. HCO proton pathways. (a) Key residues of the D- and K-pathways for Type A HCO (*aa*<sub>3</sub>-type CcO; PDB entry: 1QLE). The D- and K-pathways are identified by blue and red arrows, respectively. (b–c) The alternative K-pathway for Type B (*ba*<sub>3</sub>-type CcO; PDB entry 1EHK) and Type C (*cbb*<sub>3</sub>-type CcO; PDB entry 3MK7) HCOs. (d) Difference between Type A1 (left, *aa*<sub>3</sub>-type CcO; PDB entry: 1QLE) and A2 (right, *caa*<sub>3</sub>-type CcO; PDB entry 2YEV) HCOs in the composition of the hydrophobic end of the D-pathway. The linings for the K- and D-pathways are gray and orange, respectively. Hemes are displayed as ball and stick with metal ions as spheres. Waters are shown as red non-bonded spheres. Prosthetic group ligands have been excluded for clarity.

contain a single proton pathway analogous to the Type A K-pathway (Fig. 16.4).

## A. Type A

### 1. D-Pathway

In Type A HCOs, the longer D-pathway is named for the conserved and functionally critical aspartate at the pathway entrance (Fig. 16.4a). The importance of the aspartate has been highlighted by an Asp132Asn mutation in *R. sphaeroides* that precludes proton translocation and significantly impairs enzymatic turnover (Thomas et al. 1993; Fetter et al. 1995; Garcia-Horsman et al. 1995). In the *P. denitrificans* enzyme, the pathway starts at Asp 124 on the *N*-side of the membrane and is connected through hydrogen bonding via a lone bridging water molecule to Asn 131. A continuous chain

of water molecules, hydrogen bonded to a number of flanking residues, links Asn 131 to the gating glutamate, Glu 278, (Fig. 16.4a and d). The gating glutamate is located approximately 10 Å from the binuclear centre and is essential for both the proton pumping and oxygen reduction events. The protons can traverse the pathway from the cytoplasm to the active site via the Grotthuss mechanism where protons transfer between hydrogen bonded molecules in the water chain (de Grotthuss 1806). While the water chain is well conserved within the known bacterial Type A1 HCOs structures, the number and arrangement of water molecules vary between the different structures. The most complete chain has been reported for the *aa*<sub>3</sub>-type CcO from *P. denitrificans* where eight waters span the distance between Asp 124 to the gating glutamate Glu 278 (Koepke et al. 2009). Recently, it has been shown that



the structure of the water pathway may be modulated by changes in the redox state of the oxidase that has led to a proposed water gating mechanism (Kim et al. 2007, 2009) with elements of alternating access between the D- and K- pathways (Qin et al. 2009).

In the *T. thermophilus* *caa*<sub>3</sub>-type CcO, a member of the Type A2 HCOs, the D-pathway, is similar to that of the Type A1 HCOs (Lyons et al. 2012). It is formed by a chain of ordered internal waters complete with orienting polar side chains that extend from Asp 103 at the cytoplasmic (N-) side of the membrane to the active site via the hallmark YS “gate” that differentiates the A1 and A2 HCO sub-types (Fig. 16.4d). This gate is functionally equivalent to the aforementioned gating glutamate (Glu 278 *P. denitrificans*) as determined by single-, double- and triple-mutant studies performed on the *P. denitrificans* *aa*<sub>3</sub>-type CcO, which mimics the Type A2 pump configuration in both *T. thermophilus* and *Rhodothermus marinus* (Backgren et al. 2000).

The D-pathway is responsible for transmitting six protons, four of which are pumped to the *P*-side of the membrane; the remaining two are donated to the active site for use in oxygen reduction chemistry. In *P. denitrificans* *aa*<sub>3</sub>-type CcO, Glu 278 has been identified as the gate or branch point responsible for routing protons to the active site or to the pump loading site which leads to the *P*-side of the membrane (Fig. 16.4). This glutamate points towards the *N*-side of the membrane (“down” conformation) from which it can accept protons as indicated by the crystal structures and molecular dynamics simulations (Iwata et al. 1995). For either proton pumping or proton loading of the binuclear centre to occur, the side chain of Glu 278 has been proposed to undergo a rotamer change during turnover to a position pointing towards the *P*-side (“up” conformation) (Riistama et al. 1996; Kaila et al. 2008). Here, it contacts both the active site and pump loading site through individual water networks. In contrast, the protonation state of the YS “gate” side chains in Type A2 HCOs are not modulated by the redox state of

the enzyme as shown by  $pK_a$  calculations on both homology and crystal derived models (Pereira et al. 1999; Lyons et al. 2012). This would indicate that its role is to stabilize particular water wires that are continuous with the active site or the proposed proton exit pathway, supporting a role for a water-gated mechanism.

## 2. K-Pathway

The shorter K-proton pathway (Fig. 16.4) is named after a conserved, centrally located lysine residue, Lys 354 (*P. denitrificans* numbering). It leads to the binuclear centre via the highly conserved residues Lys 354, Thr 351, and the His 276 cross-linked Tyr 280 in the *P. denitrificans* enzyme (Fig. 16.4a). In the known crystal structures, the pathway contains two structurally resolved water molecules. However, a continuous pathway is not evident without the transient movement of key side chains and/or rearrangement of structural waters. The K-pathway is responsible for supplying two protons to the catalytic site as part of the initial reduction of the binuclear centre. In fact, unless proton uptake occurs via the K-pathway, reduction of the binuclear centre is not possible (Adelroth et al. 1998). While the K-pathway is not involved in the oxidative phase of the catalytic cycle (Sect. VI) (Tuukkanen et al. 2006), movement of the protonated lysine side chain towards the binuclear centre has been reported to act as a “dielectric well” stabilizing/neutralizing an otherwise uncompensated electron transfer to the active site (Junemann et al. 1997; Brändén et al. 2001; Rich and Marechal 2013).

The entry point to the K-pathway has been determined by site-directed mutagenesis to be Glu 101 on SU II in *R. sphaeroides* *aa*<sub>3</sub>-type CcO (Branden et al. 2002; Tomson et al. 2003). The entry point to the *P. denitrificans* enzyme is unclear as similar mutagenesis work on the homologous Glu 78 did not affect proton pumping or the rate of heme *a*<sub>3</sub> reduction even though a long range electrostatic interaction between the binuclear active site and Glu 78 has been identified based on

titration curves calculated by Monte Carlo sampling (Kannt et al. 1998a). A recent high resolution structure of the *P. denitrificans* enzyme has identified a chain of ordered water molecules close to Glu 78 that may form the entry for protons in the K-pathway without the need for direct involvement of the glutamate side chain (Koepke et al. 2009).

## B. Type B and C

### 1. An Alternative K-Pathway

Interestingly, proton pathways within the Type B and C HCOs are markedly different from that of the Type A HCOs. Crystal structure analysis of the Type B HCO, (*ba*<sub>3</sub>-type CcO from *T. thermophilus*) identified three putative pathways – a novel Q-pathway and homologs of the Type A D- and K-pathways (Soulimane et al. 2000). The lack of sequence conservation within the putative D- and Q-pathways suggested they were not functional. However, the alternative K-pathway, consisting of a number of polar residues that are conserved across the B-family, could form a proton pathway. These residues reside within SU I (Thr 312, Ser 309, Tyr 248, Ser 261 and Tyr 237) with the exception of the pathway entrance (Glu15) which is on SU II (Fig. 16.4b). Subsequent mutagenesis of these residues showed that this alternative K-pathway is critical for enzyme function (Chang et al. 2009).

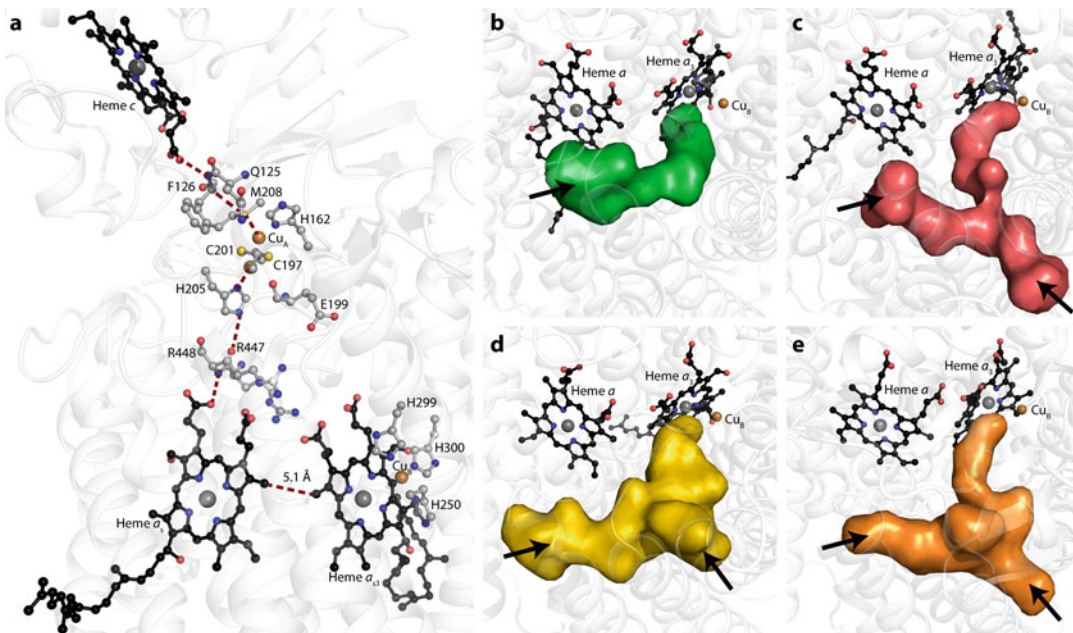
For the Type C *cbb*<sub>3</sub>-type CcO, the putative proton pathway is composed of residues in the CcoN subunit and Glu 49 of the CcoP subunit at the pathway entrance (*P. stutzeri* numbering). The pathway propagates through a number of polar residues (Tyr 223, Ser 240, His 243, Tyr 317, and Thr 215) to Tyr 251 (Fig. 16.4c), which is cross-linked to one of the histidine ligands of Cu<sub>B</sub> and is located ~4 Å from the active site (Rauhamaki et al. 2006; Buschmann et al. 2010). Recently, it has been shown that alanine and glutamine mutants of Glu 25 in the *R. sphaeroides cbb*<sub>3</sub>-type CcO, homologous to Glu 49 of the *P. stutzeri* enzyme, have severely impaired proton uptake from

solution during oxidation of the fully reduced enzyme by O<sub>2</sub>, consistent with this residue playing a critical role in the proton pathway (Lee et al. 2011). Interestingly, the enzyme's ability to reduce NO (a process requiring protons from the periplasmic side of the membrane) remains largely unaffected.

### C. Proton and Water Exit Pathways

Given the sequence diversity across the various HCO types, it is logical to assume that if the pump loading site is common to all, the number of possible candidates for this site is limited. They consist of the six histidines that ligate the heme iron and Cu<sub>B</sub>, the four propionate groups of the two hemes, as well as the internal water cluster over the hemes (Fig. 16.5a) (Chang et al. 2009). Various models have been proposed that have focused on one or more of the Cu<sub>B</sub> ligating histidines, but no convincing evidence has emerged identifying these residues as the proton loading site (Wikstrom 2000; Makhov et al. 2006; Sharpe and Ferguson-Miller 2008; Popovic et al. 2010). The active site heme D-propionate has also been implicated as the pump loading site or as a transient site through which protons transfer to the proton loading site. In Type A and B HCOs, the area above the D-propionate contains two highly conserved arginines which form a salt bridge with the propionate (Ostermeier et al. 1997; Kannt et al. 1998a). However, these arginines are not conserved in Type C HCOs, with this site interacting with a Ca<sup>2+</sup>. Furthermore, site directed mutagenesis of the arginines in the *aa*<sub>3</sub>-type CcO from *R. sphaeroides* also indicate that the D-propionate is unlikely to be the proton loading site. However, its role as a transient site has not been excluded (Lee et al. 2009).

The active site A-propionate is a possible location for the pump loading site based on evidence from computational studies on the *P. denitrificans* enzyme and structural analysis of the HCO family (Wikstrom and Verkhovskiy 2007; Chang et al. 2009; Kaila et al. 2011). The computational analysis identified a transient and reversible



**Fig. 16.5.** Electron transfer pathway and oxygen channels. **(a)** Electron transfer pathway for *caa*<sub>3</sub>-type CcO between heme *c*, Cu<sub>A</sub>, heme *a* and the active site. Figure redrawn based on electron transfer pathways calculated for *P. denitrificans* *aa*<sub>3</sub>-type CcO (Farver et al. 2006) and *caa*<sub>3</sub>-type CcO (Lyons et al. 2012). The ion to ion distances are 17.2 Å, 19.5 Å and 13.6 Å for heme *c* iron to Cu<sub>A</sub>, Cu<sub>A</sub> to heme *a* iron, and heme *a* iron to heme *a*<sub>3</sub> iron, respectively. **(b–e)** Calculated oxygen channels for *aa*<sub>3</sub>-type CcO from *R. sphaeroides* (PDB entry 1 M56), *caa*<sub>3</sub>-type CcO from *T. thermophilus* (PDB entry 2YEV), *ba*<sub>3</sub>-type CcO from *T. thermophilus* (PDB entry 1EHK) and *cbb*<sub>3</sub>-type CcO from *P. stutzeri* (PDB entry 3MK7). Entry points into the channels from the membrane hydrocarbon region are indicated by black arrows. Protein is represented as transparent white cartoon. Hemes and relevant residues are as ball and stick with ions as spheres. Channels were calculated using *Hollow* (Ho and Gruswitz 2008).

conformation change of the A-propionate of heme *a*<sub>3</sub> that could facilitate proton pumping upon heme *a* reduction. This conformational change results in a breaking of the hydrogen bond shared between the propionate and a nearby aspartic acid (Asp 399 of SU I in *aa*<sub>3</sub>-type CcO of *P. denitrificans*). This effectively increases the p*K*<sub>a</sub> of the A-propionate, allowing it to be protonated, thus linking the p*K*<sub>a</sub> of the A-propionate with the redox state of heme *a* (Kaila et al. 2011). The same study also showed that Arg 438 and the D-propionate dissociate. However, this did not correlate to a change in its p*K*<sub>a</sub> implying that the A-propionate is likely the pump site (Kaila et al. 2011).

In the various HCOs, a hydrophilic cavity above the hemes, separating SU I and SU II, has been postulated as the beginning

of the water exit pathway. This portal in Type A and C HCOs is centred on a conserved Mg<sup>2+</sup>/Mn<sup>2+</sup> and Ca<sup>2+</sup> ion, respectively, while in Type B HCOs the cavity is filled with water molecules. These sites are continuous with the periplasmic space via discrete channels (Iwata et al. 1995; Ostermeier et al. 1997; Soulimane et al. 2000; Svensson-Ek et al. 2002; Koepke et al. 2009; Buschmann et al. 2010; Lyons et al. 2012).

## V. Electron Transfer

The elucidation of crystal structures for cytochrome *c* oxidase has provided the distance separating the redox centres, the ligands and surrounding protein, and their relative orientation (Fig. 16.3b and c). This

has allowed for a more detailed exploration of hypotheses into the electron transfer pathways within the protein as outlined below.

Cytochrome *c* oxidase is reduced by four consecutive one-electron transfer events from cytochrome *c*, with the rate limiting step being the formation and disassociation of the cytochrome *c*/cytochrome *c* oxidase complex. In general, electron transfer through cytochrome *c* oxidase proceeds as follows: upon complex formation electrons are rapidly transferred from reduced cytochrome *c* to the Cu<sub>A</sub> centre (in Type A and B HCOs). From the homobinuclear Cu<sub>A</sub> centre, intra-molecular electron transport has been calculated for the *T. thermophilus* enzyme which proceeds via a hydrogen bond to the His 205 side chain of SU II to the amide carbonyl between Arg 447 and Arg 448 in SU I (Fig. 16.5a). Another hydrogen bond connects the peptide nitrogen of Arg 448 to the heme *a* A-propionate (Farver et al. 2006). It has been demonstrated that the inter-heme electron transfer is concomitant with vectorial proton transfer (Belevich et al. 2006). Analogous electron transfer calculations have been made for the bovine heart enzyme that reveal a similar electron transfer path. For an in-depth analysis of electron tunneling see (Moser et al. 2008; Gray and Winkler 2010).

While the cytochrome *c*/cytochrome *c* oxidase complex structure remains elusive to crystallographic methods, efforts have been made to explore the interactions between these two redox partners using mutagenesis, nuclear magnetic resonance (NMR) (Reincke et al. 2001) and molecular dynamics approaches (Roberts and Pique 1999; Flock and Helms 2002; Bertini et al. 2005; Lyubenova et al. 2007; van Dijk et al. 2007). From in vitro interaction studies of the cytochrome *c* oxidase Cu<sub>A</sub> domain and its partner, the soluble cytochrome *c*<sub>552</sub> from *P. denitrificans*, a multi-step mechanism was proposed (Maneg et al. 2003, 2004). First, oppositely charged surface potentials are responsible for the long-range orientation and initial interaction of the two redox partners. Secondly, hy-

drophobic patches on both surfaces govern a fine tuning of the docking. Finally, reduction of Cu<sub>A</sub> proceeds through electron transfer from cytochrome *c* via the conserved Trp 121 side chain of the Cu<sub>A</sub> domain in the *P. denitrificans* enzyme (Drosou et al. 2002). A different scenario has been proposed for the *T. thermophilus* cytochrome *c*<sub>552</sub> and the *ba*<sub>3</sub>-type CcO Cu<sub>A</sub> electron transfer complex where docking is dictated primarily by hydrophobic interactions (Muresanu et al. 2006).

The fused cytochrome *c*/cupredoxin domain in *caa*<sub>3</sub>-type CcO offers a unique view of this complex (Lyons et al. 2012). The cytochrome *c* domain is oriented such that its heme *c* propionates interact directly with the cupredoxin domain, with the most prominent interaction between the heme *c* D-propionate and the *cis*-amide of an aromatic residue conserved across SU II of Type A and B CcOs, i.e., Phe 126 and Trp 121 in *T. thermophilus caa*<sub>3</sub>-type CcO and *P. denitrificans aa*<sub>3</sub>-type CcO, respectively. This *cis*-amide was first identified in *R. sphaeroides aa*<sub>3</sub>-type CcO (Qin et al. 2006). Based on this observation a pathway model was proposed with through-bond and through-space tunneling events.

In the case of *cbb*<sub>3</sub>-type CcO, the primary electron acceptor from cytochrome *c* is the outer most heme *c* of CcoP, whose C and D pyrroles are exposed. This accepted electron is subsequently transferred via the inner heme *c* of CcoP to the heme *c* of CcoO. From CcoO, the electron is shuttled to the CcoN heme *b*. The edge-to-edge distance between heme *c* of CcoO and heme *b* of CcoN is shorter than that between Cu<sub>A</sub> and heme *a* or *b* in *aa*<sub>3</sub>-type CcO in cupredoxin domain containing HCOs. The electron is transferred between heme *b* and *b*<sub>3</sub>, which are in Van der Waal's interaction with each other, and from heme *b*<sub>3</sub> it can equilibrate with Cu<sub>B</sub>.

## VI. Oxygen Channel

Non-polar molecules freely diffuse through the hydrocarbon rich environment of the biological membrane. Structural and computa-

tional analyses of Type A, B and C HCOs have identified possible channels that can be exploited by molecular oxygen to access the active site (Fig. 16.5b–e) (Iwata et al. 1995; Hofacker and Schulten 1998; Svensson-Ek et al. 2002; Luna et al. 2008; Lyons et al. 2012). Early suggestions and calculations for an oxygen pathway in cytochrome *c* oxidase identified a hydrophobic residue lined channel starting at the V-shaped cleft in SU III with the oxygen molecule entering SU I between helices IV and V (Hofacker and Schulten 1998).

For the *aa*<sub>3</sub>-type CcO of *R. sphaeroides* (Svensson-Ek et al. 2002) and the *ba*<sub>3</sub>-type CcO of *T. thermophilus* (Luna et al. 2008; Tiefenbrunn et al. 2011), hydrophobic cavities have been determined from xenon positions upon X-ray analysis of crystals prepressurised with the gas. Xenon is used as an oxygen analog. With a higher atomic number it is easier to identify in electron density maps than oxygen. In these studies, the end of the pathways, proximal to the active site, in both the *R. sphaeroides* and *T. thermophilus* enzymes are in close agreement with previous molecular dynamics calculations (Hofacker and Schulten 1998). A mutation of the highly conserved Val 287 to isoleucine in the *E. coli bo*<sub>3</sub> oxidase resulted in an increase in the  $K_M$  for dioxygen with no effect on  $V_{max}$  when compared to the wild type enzyme (Ristama et al. 1996). This valine, homologous to Val 279 in *P. denitrificans aa*<sub>3</sub>-type CcO, is located one residue away from the gating glutamate position on helix VI in Type A1 HCOs. Given its proximity to the active site, the result of the mutagenesis was interpreted as a partial blocking of oxygen entry to the active site. This observation further supports the location of the calculated and experimentally determined oxygen channels reported to date (Hofacker and Schulten 1998; Luna et al. 2008; Tiefenbrunn et al. 2011; Lyons et al. 2012).

Comparison of the oxygen channels in the Type A and B cytochrome *c* oxidases from *T. thermophilus* highlight a conserved bifurcated pathway with two channels leading to the apolar region of the membrane with

entrances between helices II and III and between helices IV and V (Fig. 16.5c–d) (Luna et al. 2008; Lyons et al. 2012). Interestingly, the oxygen channel in the *ba*<sub>3</sub>-type CcO is larger than that of its type A counterpart. The latter has a constriction where the two branches meet. This difference in channel architecture may be related to the fact that *ba*<sub>3</sub>-type CcO needs to sequester oxygen under low oxygen conditions. Molecular dynamic simulations performed with the *aa*<sub>3</sub>-type CcO of *R. sphaeroides* identified a bifurcated pathway similar to that observed for *caa*<sub>3</sub>-type CcO, with the calculations indicating a role for gating via constriction and dilation within the oxygen channel, which has been postulated to regulate oxygen supply to the active site (Buhrow et al. 2012). A similar bifurcated channel has been described for *ccb*<sub>3</sub>-type CcO (Fig. 16.5e) (Buschmann et al. 2010).

## VII. The Catalytic Cycle

The catalytic cycle of cytochrome *c* oxidase is illustrated in Fig. 16.6. It can be divided into an oxidative (**R** → **O**) and a reductive (**O** → **R**) phase. The cycle involves several intermediate states of the active site, identified by one-letter code. The reaction cycle presented here describes the reduction of oxygen by A-type HCOs. As only limited information for the other two HCO types is available, they will not be described further.

The oxidative phase of the redox cycle begins with the binding of molecular oxygen to the fully reduced binuclear centre (**R** state) forming the **A** state (Fig. 16.6). In this step, molecular oxygen binds to heme *a*<sub>3</sub>. The **A** state spontaneously transforms to the **P<sub>M</sub>** state upon the transfer of four electrons to molecular oxygen. This causes immediate cleavage of the dioxygen bond which, in turn, prevents the formation of reactive oxygen species. Two of these electrons derive from heme *a*<sub>3</sub> and one from Cu<sub>B</sub>. The last electron along with a proton comes from the cross-linked tyrosine, yielding the **P<sub>M</sub>** intermediate with a ferryl iron, Fe[IV] = O, a cupric copper/hydroxyl species and a neutral

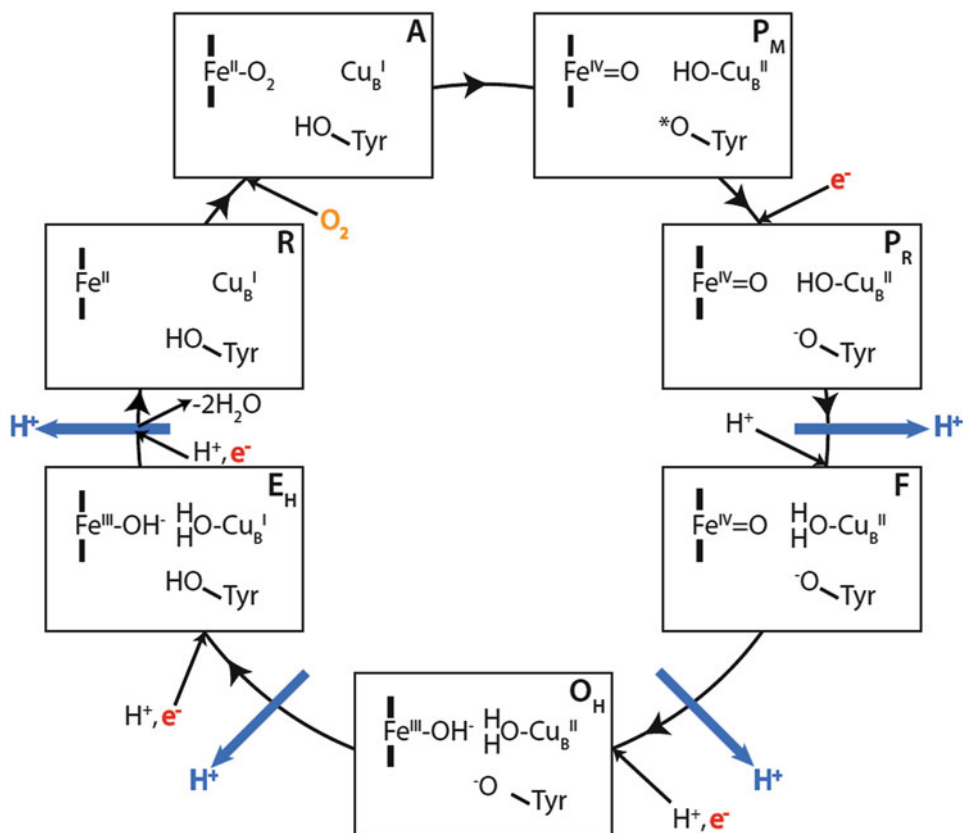


Fig. 16.6. The catalytic cycle of cytochrome *c* oxidase. The catalytic cycle for type A HCOs is drawn clockwise with the name of each intermediate state noted in the upper right corner of each rectangle. For simplicity, only the active site is shown which consists of heme  $a_3$ ,  $\text{Cu}_B$  and the tyrosine of the cross-linked histidine-tyrosine pair. The oxidation states of Fe,  $\text{Cu}_B$ , and the cross-linked tyrosine in the binuclear center are indicated, along with protonation states of the cross-linked tyrosine and metal ligands. Proton pumping events are identified by blue arrows, while electrons and protons consumed during turnover are shown in red and black, respectively. Binding of  $\text{O}_2$  to the binuclear center takes place in the R to A transition (Modified from (Sharma et al. 2013)).

tyrosine radical. The  $\text{P}_M$  state transforms to the  $\text{P}_R$  state accompanied by the addition of an electron to the active site with the tyrosine radical converting to a tyrosylate in the  $\text{P}_R$  state. The latter evolves into the F state through the addition of a proton to the active site with the only observable difference between these states being the ligand on  $\text{Cu}_B$  ( $\text{OH}^-$  vs  $\text{H}_2\text{O}$ ). Experimentally, this has been seen by EPR and UV-VIS spectroscopy measurements on the transformation of the F state into the  $\text{P}_R$  state by the addition of ammonia at high pH, which subsequently ligates to  $\text{Cu}_B$  (as described in detail in von der Hocht et al. (2011)). The first proton pumping event in the catalytic cycle takes

place during the  $\text{P}_R$  to F state transition. The oxidised ferric/cupric  $\text{O}_H$  state is formed by another transfer of an electron and a proton to the binuclear centre with the pumping of the second proton. Transition from the  $\text{O}_H$  to the  $\text{E}_H$  state proceeds with the pumping of the third proton and the uptake of an electron and proton to the active site, resulting in a cuprous  $\text{Cu}_B$  and reprotonation of the tyrosine. The reaction cycle is completed when the R state is regenerated from the  $\text{E}_H$  state during which an electron and a proton are donated to the binuclear centre with the two product waters released and the fourth and final proton pumped (Michel 1999; Kaila et al. 2009, 2011).

Wikström and coworkers observed at least two of these natural intermediates (**P** and **F** states) in mitochondria for the first time when the reaction catalyzed by the  $F_0F_1$ -ATP synthase was reversed (thereby hydrolyzing ATP and pumping protons back across the membrane (Wikstrom 1981)). This generates a positive redox-potential, resulting in the partial reversal of the cytochrome *c* oxidase reaction. Initially, it was believed that the structure of the active site in the **P**-intermediate resembled a peroxy state (hence **P** intermediate) and that of the **F** intermediate a ferryl (or oxoferryl) state. However, Resonance Raman spectroscopy was used to show that both states have an oxoferryl structure (Ogura and Kitagawa 2004). After Wikström's description of intermediates in the reaction cycle, it was found that at least some of these intermediates can easily be generated artificially and exploited to investigate detailed aspects of the reaction cycle. These states are only defined as intermediates with distinct absorption maxima in difference spectra. For example, the **P** and **F** intermediates have distinctive positive signals at 607 and 580 nm, respectively (Wikstrom 1981). The **P** intermediate can be generated artificially by adding 5 molar equivalents of hydrogen peroxide at high pH or by purging with CO. One recently discovered method to generate an artificial **P** intermediate involves adding ammonia at high pH after artificially generating the **F** intermediate by treating the oxidase with 500 molar equivalents of hydrogen peroxide (for a summary see (von der Hocht et al. 2011)). These intermediates were then further studied by a variety of different techniques. Resonance Raman spectroscopy and FTIR were used to probe the exact structure of the active center in different (artificial) intermediate states of the reaction cycle (Hrabakova et al. 2006; Voicescu et al. 2009; Kozuch et al. 2013; Marechal et al. 2013).

To fully reduce dioxygen to water in a single step, four electrons are needed. However, as noted, the metal ions in the active center are only able to provide three electrons. Investigations on artificial intermedi-

ates helped identify possible sources of the fourth electron. The mystery was solved to some degree by applying EPR spectroscopy using a high concentration of hydrogen peroxide (500 molar equivalents) to generate the artificial **F**-state of the cytochrome *c* oxidase (for recent studies see (de Vries 2008; Sharpe et al. 2009; von der Hocht et al. 2011; Yu et al. 2012)). The source of the electron turned out to be a tyrosine or tryptophan radical close to the active site. However, the exact identity of the amino acid providing this electron is still under debate.

The groups of Adelroth and Brzezinski implemented stopped flow methods to monitor the various catalytic intermediates in the reaction cycle (Thornstrom et al. 1988). These groups used a combination of trapped components that deliver electrons upon excitation, together with flash photolysis of CO from CcO, to specifically target and observe different intermediates in the reaction cycle of CcO. Stopped flow measurements have been exploited to calculate rate constants for the generation of the different natural intermediates.

It has recently been shown, by the group of Konstantinov, that a fine tuning of the catalytic activity of cytochrome *c* oxidase happens via a specifically bound  $Ca^{2+}$  ion. This group also showed that a high affinity zinc binding site exists within the CcO and that zinc in this site inhibits the enzyme (Vygodina et al. 2008, 2013).

### VIII. Side Reactions in CcO

Apart from their oxygen reductase activity, all HCOs show a variety of side reactions. C type HCOs, for example, exhibit nitric oxide (NO) reductase activity (Forte et al. 2001). This is not surprising, since NO reductases are closely related to HCOs. Similarly, members of the Type A and B HCO family from *T. thermophilus* have NO reductase activity (Giuffre et al. 1999).

Apart from its established oxidoreductase activity, Type A and C HCOs have been

reported to possess a background catalase-like activity (Orii and Okunuki 1963; Xie et al. 2014). This activity is attributed to the heme component of the enzymes as observed with several other heme-containing proteins such as methemoglobin (Dalziel and O'Brien 1954; Orii and Okunuki 1963; Paco et al. 2009; Bolshakov et al. 2010; Hilbers et al. 2013). Interestingly, *aa3*-type CcO in *P. denitrificans* containing a recombinantly overexpressed SUI (all other subunits were chromosomally encoded) has been shown to exhibit increased catalase activity in comparison to the wild type enzyme. This activity was later linked to co-factor insertion during the biogenesis of recombinant CcO, where SU I was overexpressed on a low copy number plasmid. The catalase activity was shown to be diminished when the protein was co-expressed with a plasmid containing genes which encode chaperones previously reported to be required for correct insertion of Cu and heme *a*, thus increasing the chaperone levels in the cell (Kulajta et al. 2006; Bundschuh et al. 2008; Greiner et al. 2008).

## IX. Conclusions

Although HCOs exhibit a wide diversity in subunit and heme type composition, the fundamental mode of action remains, for the most part, conserved across its various types. Questions relating to the pathways through which the pumped protons exit and the identity of the pump loading site still remain. Given that the majority of information has been obtained from extensive studies of the Type A, and to a lesser extent Type B HCOs, a similar focus on Type C HCOs is in order. Recent structures of the Type A2 and C HCOs, coupled with the available models of the Type A1 and B variants have allowed identification of conserved pathways and channels and provide a framework for further structure-function studies of this important enzyme.

## Acknowledgments

J.A. Lyons is funded through an individual postdoctoral fellowship from the Danish Research Council for Natural Sciences. F. Hilbers is funded through the Danish Research Institute of Translational Neuroscience. M. Caffrey is supported through Science Foundation Ireland (12/IA/1255), COST Action CM1306 and the National Institutes of Health (P50GM073210, U54GM094599).

## References

- Adelroth P, Gennis RB, Brzezinski P (1998) Role of the pathway through K(I-362) in proton transfer in cytochrome *c* oxidase from *R. sphaeroides*. *Biochemistry* 37:2470–2476
- Backgren C, Hummer G, Wikstrom M, Puustinen A (2000) Proton translocation by cytochrome *c* oxidase can take place without the conserved glutamic acid in subunit I. *Biochemistry* 39:7863–7867
- Belevich I, Verkhovsky MI, Wikstrom M (2006) Proton-coupled electron transfer drives the proton pump of cytochrome *c* oxidase. *Nature* 440: 829–832
- Bertini I, Cavallaro G, Rosato A (2005) A structural model for the adduct between cytochrome *c* and cytochrome *c* oxidase. *J Biol Inorg Chem* 10:613–624
- Bolshakov IA, Vygodina TV, Gennis R, Karyakin AA, Konstantinov AA (2010) Catalase activity of cytochrome *c* oxidase assayed with hydrogen peroxide-sensitive electrode microsensor. *Biochemistry (Moscow)* 75:1352–1360
- Brändén M, Sigurdson H, Namslauer A, Gennis RB, Ådelroth P, Brzezinski P (2001) On the role of the K-proton transfer pathway in cytochrome *c* oxidase. *Proc Natl Acad Sci U S A* 98:5013–5018
- Branden M, Tomson F, Gennis RB, Brzezinski P (2002) The entry point of the K-proton-transfer pathway in cytochrome *c* oxidase. *Biochemistry* 41:10794–10798
- Brandt U (2006) Energy converting NADH:quinone oxidoreductase (complex I). *Annu Rev Biochem* 75:69–92
- Brandt U (2011) A two-state stabilization-change mechanism for proton-pumping complex I. *Biochim Biophys Acta* 1807:1364–1369



- Bratton MR, Pressler MA, Hosler JP (1999) Suicide inactivation of cytochrome *c* oxidase: catalytic turnover in the absence of subunit III alters the active site. *Biochemistry* 38:16236–16245
- Buhrow L, Ferguson-Miller S, Kuhn LA (2012) From static structure to living protein: computational analysis of cytochrome *c* oxidase main-chain flexibility. *Biophys J* 102:2158–2166
- Bundschuh FA, Hoffmeier K, Ludwig B (2008) Two variants of the assembly factor SurfI target specific terminal oxidases in *Paracoccus denitrificans*. *Biochim Biophys Acta* 1777:1336–1343
- Buschmann S, Warkentin E, Xie H, Langer JD, Ermler U, Michel H (2010) The structure of *cbb*<sub>3</sub> cytochrome oxidase provides insights into proton pumping. *Science* 329:327–330
- Calhoun MW, Thomas JW, Gennis RB (1994) The cytochrome oxidase superfamily of redox-driven proton pumps. *Trends Biochem Sci* 19:325–330
- Capitanio G, Martino PL, Capitanio N, De Nitto E, Papa S (2006) pH dependence of proton translocation in the oxidative and reductive phases of the catalytic cycle of cytochrome *c* oxidase. The role of H<sub>2</sub>O produced at the oxygen-reduction site. *Biochemistry* 45:1930–1937
- Chang HY, Hemp J, Chen Y, Fee JA, Gennis RB (2009) The cytochrome *ba*<sub>3</sub> oxygen reductase from *Thermus thermophilus* uses a single input channel for proton delivery to the active site and for proton pumping. *Proc Natl Acad Sci U S A* 106:16169–16173
- Crofts AR (2004) The cytochrome *bc*<sub>1</sub> complex: function in the context of structure. *Annu Rev Physiol* 66:689–733
- Dalziel K, O'Brien JR (1954) Spectrophotometric studies of the reaction of methaemoglobin with hydrogen peroxide. 1. The formation of methaemoglobin-hydrogen peroxide. *Biochem J* 56:648–659
- de Grotthuss CJT (1806) Sur la décomposition de l'eau et des corps qu'elle tient en dissolution à l'aide de l'électricité galvanique. *Ann Chim (Paris)* 58:54–73
- de Vries S (2008) The role of the conserved tryptophan272 of the *Paracoccus denitrificans* cytochrome *c* oxidase in proton pumping. *Biochim Biophys Acta* 1777:925–928
- Drosou V, Malatesta F, Ludwig B (2002) Mutations in the docking site for cytochrome *c* on the *Paracoccus* heme *aa*<sub>3</sub> oxidase. Electron entry and kinetic phases of the reaction. *Eur J Biochem* 269:2980–2988
- Farver O, Grell E, Ludwig B, Michel H, Pecht I (2006) Rates and equilibrium of Cu<sub>A</sub> to heme *a* electron transfer in *Paracoccus denitrificans* cytochrome *c* oxidase. *Biophys J* 90:2131–2137
- Ferguson-Miller S, Babcock GT (1996) Heme/copper terminal oxidases. *Chem Rev* 96:2889–2908
- Fetter JR, Qian J, Shapleigh J, Thomas JW, Garcia-Horsman A, Schmidt E, Hosler J, . . . , Ferguson-Miller S (1995) Possible proton relay pathways in cytochrome *c* oxidase. *Proc Natl Acad Sci U S A* 92:1604–1608
- Flock D, Helms V (2002) Protein—protein docking of electron transfer complexes: cytochrome *c* oxidase and cytochrome *c*. *Proteins* 47:75–85
- Florens L, Schmidt B, McCracken J, Ferguson-Miller S (2001) Fast deuterium access to the buried magnesium/manganese site in cytochrome *c* oxidase. *Biochemistry* 40:7491–7497
- Forte E, Urbani A, Saraste M, Sarti P, Brunori M, Giuffrè A (2001) The cytochrome *cbb*<sub>3</sub> from *Pseudomonas stutzeri* displays nitric oxide reductase activity. *Eur J Biochem* 268:6486–6491
- Garcia-Horsman JA, Puustinen A, Gennis RB, Wikstrom M (1995) Proton transfer in cytochrome *bo*<sub>3</sub> ubiquinol oxidase of *Escherichia coli*: second-site mutations in subunit I that restore proton pumping in the mutant Asp135 → Asn. *Biochemistry* 34:4428–4433
- Gilderson G, Salomonsson L, Aagaard A, Gray J, Brzezinski P, Hosler J (2003) Subunit III of cytochrome *c* oxidase of *Rhodobacter sphaeroides* is required to maintain rapid proton uptake through the D pathway at physiologic pH. *Biochemistry* 42:7400–7409
- Giuffrè A, Stubauer G, Sarti P, Brunori M, Zumft WG, Buse G, Soulimane T (1999) The heme-copper oxidases of *Thermus thermophilus* catalyze the reduction of nitric oxide: evolutionary implications. *Proc Natl Acad Sci U S A* 96:14718–14723
- Gray HB, Winkler JR (2010) Electron flow through metalloproteins. *Biochim Biophys Acta* 1797:1563–1572
- Greiner P, Hannappel A, Werner C, Ludwig B (2008) Biogenesis of cytochrome *c* oxidase—*in vitro* approaches to study cofactor insertion into a bacterial subunit I. *Biochim Biophys Acta* 1777:904–911
- Haltia T, Finel M, Harms N, Nakari T, Raitio M, Wikstrom M, Saraste M (1989) Deletion of the gene for subunit III leads to defective assembly of bacterial cytochrome oxidase. *EMBO J* 8:3571–3579
- Hatefi Y (1985) The mitochondrial electron transport and oxidative phosphorylation system. *Annu Rev Biochem* 54:1015–1069
- Hatefi Y, Haavik AG, Griffiths DE (1961) Reconstitution of the electron transport system. I. Preparation and properties of the interacting enzyme complexes. *Biochem Biophys Res Commun* 4:441–446

- Hilbers F, von der Hocht I, Ludwig B, Michel H (2013) True wild type and recombinant wild type cytochrome *c* oxidase from *Paracoccus denitrificans* show a 20fold difference in their catalase activity. *Biochim Biophys Acta* 1827:319–327
- Ho BK, Gruswitz F (2008) HOLLOW: generating accurate representations of channel and interior surfaces in molecular structures. *BMC Struct Biol* 8:49
- Hofacker I, Schulten K (1998) Oxygen and proton pathways in cytochrome *c* oxidase. *Proteins* 30:100–107
- Honnami K, Oshima T (1984) Purification and characterization of cytochrome *c* oxidase from *Thermus thermophilus* HB8. *Biochemistry* 23:454–460
- Hosler JP (2004) The influence of subunit III of cytochrome *c* oxidase on the D pathway, the proton exit pathway and mechanism-based inactivation in subunit I. *Biochim Biophys Acta* 1655:332–339
- Hrabakova J, Ataka K, Heberle J, Hildebrandt P, Murgida DH (2006) Long distance electron transfer in cytochrome *c* oxidase immobilised on electrodes. A surface enhanced resonance Raman spectroscopic study. *Phys Chem Chem Phys* 8:759–766
- Iwata S, Ostermeier C, Ludwig B, Michel H (1995) Structure at 2.8 Å resolution of cytochrome *c* oxidase from *Paracoccus denitrificans*. *Nature* 376:660–669
- Junemann S, Meunier B, Gennis RB, Rich PR (1997) Effects of mutation of the conserved lysine-362 in cytochrome *c* oxidase from *Rhodobacter sphaeroides*. *Biochemistry* 36:14456–14464
- Kaila VR, Verkhovsky MI, Hummer G, Wikstrom M (2008) Glutamic acid 242 is a valve in the proton pump of cytochrome *c* oxidase. *Proc Natl Acad Sci U S A* 105:6255–6259
- Kaila VR, Johansson MP, Sundholm D, Laakkonen L, Wikstrom M (2009) The chemistry of the CuB site in cytochrome *c* oxidase and the importance of its unique His-Tyr bond. *Biochim Biophys Acta* 1787:221–233
- Kaila VR, Sharma V, Wikstrom M (2011) The identity of the transient proton loading site of the proton-pumping mechanism of cytochrome *c* oxidase. *Biochim Biophys Acta* 1807:80–84
- Kannt A, Lancaster CR, Michel H (1998a) The coupling of electron transfer and proton translocation: electrostatic calculations on *Paracoccus denitrificans* cytochrome *c* oxidase. *Biophys J* 74:708–721
- Kannt A, Soulimane T, Buse G, Becker A, Bamberg E, Michel H (1998b) Electrical current generation and proton pumping catalyzed by the *ba*<sub>3</sub>-type cytochrome *c* oxidase from *Thermus thermophilus*. *FEBS Lett* 434:17–22
- Kim YC, Wikstrom M, Hummer G (2007) Kinetic models of redox-coupled proton pumping. *Proc Natl Acad Sci U S A* 104:2169–2174
- Kim YC, Wikstrom M, Hummer G (2009) Kinetic gating of the proton pump in cytochrome *c* oxidase. *Proc Natl Acad Sci U S A* 106:13707–13712
- Koepke J, Olkhova E, Angerer H, Muller H, Peng G, Michel H (2009) High resolution crystal structure of *Paracoccus denitrificans* cytochrome *c* oxidase: new insights into the active site and the proton transfer pathways. *Biochim Biophys Acta* 1787:635–645
- Kozuch J, von der Hocht I, Hilbers F, Michel H, Weidinger IM (2013) Resonance Raman characterization of the ammonia-generated oxo intermediate of cytochrome *c* oxidase from *Paracoccus denitrificans*. *Biochemistry* 52:6197–6202
- Kulajta C, Thumfart JO, Haid S, Daldal F, Koch HG (2006) Multi-step assembly pathway of the *ccb*<sub>3</sub>-type cytochrome *c* oxidase complex. *J Mol Biol* 355:989–1004
- Lee HJ, Ojemyr L, Vakkasoglu A, Brzezinski P, Gennis RB (2009) Properties of Arg481 mutants of the *aa*<sub>3</sub>-type cytochrome *c* oxidase from *Rhodobacter sphaeroides* suggest that neither R481 nor the nearby D-propionate of heme *a*<sub>3</sub> is likely to be the proton loading site of the proton pump. *Biochemistry* 48:7123–7131
- Lee HJ, Gennis RB, Aderoth P (2011) Entrance of the proton pathway in *ccb*<sub>3</sub>-type heme-copper oxidases. *Proc Natl Acad Sci U S A* 108:17661–17666
- Lubben M, Morand K (1994) Novel prenylated hemes as cofactors of cytochrome oxidases. Archaea have modified hemes A and O. *J Biol Chem* 269:21473–21479
- Luna VM, Chen Y, Fee JA, Stout CD (2008) Crystallographic studies of Xe and Kr binding within the large internal cavity of cytochrome *ba*<sub>3</sub> from *Thermus thermophilus*: structural analysis and role of oxygen transport channels in the heme-Cu oxidases. *Biochemistry* 47:4657–4665
- Lyons JA, Aragao D, Slattery O, Pislakov AV, Soulimane T, Caffrey M (2012) Structural insights into electron transfer in *caa*<sub>3</sub>-type cytochrome oxidase. *Nature* 487:514–518
- Lyubenova S, Siddiqui MK, Vries MJ, Ludwig B, Prisner TF (2007) Protein-protein interactions studied by EPR relaxation measurements: cytochrome *c* and cytochrome *c* oxidase. *J Phys Chem B* 111:3839–3846
- Makhov DV, Popovic DM, Stuchebrukhov AA (2006) Improved density functional theory/electrostatic calculation of the His291 protonation state in cytochrome *c* oxidase: self-consistent charges for solvation energy calculation. *J Phys Chem B* 110:12162–12166

- Maklashina E, Cecchini G (2010) The quinone-binding and catalytic site of complex II. *Biochim Biophys Acta* 1797:1877–1882
- Maneg O, Ludwig B, Malatesta F (2003) Different interaction modes of two cytochrome-*c* oxidase soluble Cu<sub>A</sub> fragments with their substrates. *J Biol Chem* 278:46734–46740
- Maneg O, Malatesta F, Ludwig B, Drosou V (2004) Interaction of cytochrome *c* with cytochrome oxidase: two different docking scenarios. *Biochim Biophys Acta* 1655:274–281
- Marechal A, Iwaki M, Rich PR (2013) Structural changes in cytochrome *c* oxidase induced by binding of sodium and calcium ions: an ATR-FTIR study. *J Am Chem Soc* 135:5802–5807
- Michel H (1999) Cytochrome *c* oxidase: catalytic cycle and mechanisms of proton pumping—a discussion. *Biochemistry* 38:15129–15140
- Mills DA, Hosler JP (2005) Slow proton transfer through the pathways for pumped protons in cytochrome *c* oxidase induces suicide inactivation of the enzyme. *Biochemistry* 44:4656–4666
- Mills DA, Florens L, Hiser C, Qian J, Ferguson-Miller S (2000) Where is ‘outside’ in cytochrome *c* oxidase and how and when do protons get there? *Biochim Biophys Acta* 1458:180–187
- Mills DA, Tan Z, Ferguson-Miller S, Hosler J (2003) A role for subunit III in proton uptake into the D pathway and a possible proton exit pathway in *Rhodobacter sphaeroides* cytochrome *c* oxidase. *Biochemistry* 42:7410–7417
- Moser CC, Chobot SE, Page CC, Dutton PL (2008) Distance metrics for heme protein electron tunneling. *Biochim Biophys Acta* 1777:1032–1037
- Muresanu L, Pristovsek P, Lohr F, Maneg O, Mukrasch MD, Ruterjans H, Ludwig B, Lucke C (2006) The electron transfer complex between cytochrome *c*<sub>552</sub> and the Cu<sub>A</sub> domain of the *Thermus thermophilus* *ba*<sub>3</sub> oxidase. A combined NMR and computational approach. *J Biol Chem* 281:14503–14513
- Ogura T, Kitagawa T (2004) Resonance Raman characterization of the P intermediate in the reaction of bovine cytochrome *c* oxidase. *Biochim Biophys Acta* 1655:290–297
- Orii Y, Okunuki K (1963) Studies on cytochrome *a*. X. Effect of hydrogen peroxide on absorption spectra of cytochrome *a*. *J Biochem* 54:207–213
- Ostermeier C, Harrenga A, Ermler U, Michel H (1997) Structure at 2.7 Å resolution of the *Paracoccus denitrificans* two-subunit cytochrome *c* oxidase complexed with an antibody FV fragment. *Proc Natl Acad Sci U S A* 94:10547–10553
- Paco L, Galarneau A, Drone J, Fajula F, Bailly C, Pulvin S, Thomas D (2009) Catalase-like activity of bovine met-hemoglobin: interaction with the pseudo-catalytic peroxidation of anthracene traces in aqueous medium. *Biotechnol J* 4:1460–1470
- Pawate AS, Morgan J, Namslauer A, Mills D, Brzezinski P, Ferguson-Miller S, Gennis RB (2002) A mutation in subunit I of cytochrome oxidase from *Rhodobacter sphaeroides* results in an increase in steady-state activity but completely eliminates proton pumping. *Biochemistry* 41:13417–13423
- Pereira MM, Santana M, Soares CM, Mendes J, Carita JN, Fernandes AS, Saraste M, . . . , Teixeira M (1999) The *caa*<sub>3</sub> terminal oxidase of the thermohalophilic bacterium *Rhodothermus marinus*: a HiPIP: oxygen oxidoreductase lacking the key glutamate of the D-channel. *Biochim Biophys Acta* 1413:1–13
- Pereira MM, Santana M, Teixeira M (2001) A novel scenario for the evolution of haem-copper oxygen reductases. *Biochim Biophys Acta* 1505:185–208
- Pereira MM, Sousa FL, Verissimo AF, Teixeira M (2008) Looking for the minimum common denominator in haem-copper oxygen reductases: towards a unified catalytic mechanism. *Biochim Biophys Acta* 1777:929–934
- Popovic DM, Leontyev IV, Beech DG, Stuchebrukhov AA (2010) Similarity of cytochrome *c* oxidases in different organisms. *Proteins* 78:2691–2698
- Qin L, Hiser C, Mulichak A, Garavito RM, Ferguson-Miller S (2006) Identification of conserved lipid/detergent-binding sites in a high-resolution structure of the membrane protein cytochrome *c* oxidase. *Proc Natl Acad Sci U S A* 103:16117–16122
- Qin L, Mills DA, Buhrow L, Hiser C, Ferguson-Miller S (2008) A conserved steroid binding site in cytochrome *c* oxidase. *Biochemistry* 47:9931–9933
- Qin L, Liu J, Mills DA, Proshlyakov DA, Hiser C, Ferguson-Miller S (2009) Redox-dependent conformational changes in cytochrome *c* oxidase suggest a gating mechanism for proton uptake. *Biochemistry* 48:5121–5130
- Rauhamaa V, Baumann M, Soliymani R, Puustinen A, Wikstrom M (2006) Identification of a histidine-tyrosine cross-link in the active site of the *cb*<sub>b</sub><sub>3</sub>-type cytochrome *c* oxidase from *Rhodobacter sphaeroides*. *Proc Natl Acad Sci U S A* 103:16135–16140
- Reincke B, Perez C, Pristovsek P, Lucke C, Ludwig C, Lohr F, Rogov VV, . . . , Ruterjans H (2001) Solution structure and dynamics of the functional domain of *Paracoccus denitrificans* cytochrome *c*(552) in both redox states. *Biochemistry* 40:12312–12320

- Rich PR, Marechal A (2013) Functions of the hydrophilic channels in protonmotive cytochrome *c* oxidase. *J R Soc Interface* 10:20130183
- Richter OM, Durr KL, Kannt A, Ludwig B, Scandurra FM, Giuffre A, Sarti P, Hellwig P (2005) Probing the access of protons to the K pathway in the *Paracoccus denitrificans* cytochrome *c* oxidase. *FEBS J* 272:404–412
- Riistama S, Puustinen A, García-Horsman A, Iwata S, Michel H, Wikström M (1996) Channelling of dioxygen into the respiratory enzyme. *Biochim Biophys Acta* 1275:1–4
- Roberts VA, Pique ME (1999) Definition of the interaction domain for cytochrome *c* on cytochrome *c* oxidase. *J Biol Chem* 274:38051–38060
- Sharma V, Karlin KD, Wikstrom M (2013) Computational study of the activated O(H) state in the catalytic mechanism of cytochrome *c* oxidase. *Proc Natl Acad Sci U S A* 110:16844–16849
- Sharpe MA, Ferguson-Miller S (2008) A chemically explicit model for the mechanism of proton pumping in heme-copper oxidases. *J Bioenerg Biomembr* 40:541–549
- Sharpe MA, Krzyaniak MD, Xu S, McCracken J, Ferguson-Miller S (2009) EPR evidence of cyanide binding to the Mn(Mg) center of cytochrome *c* oxidase: support for Cu(A)-Mg involvement in proton pumping. *Biochemistry* 48:328–335
- Soulimane T, Buse G, Bourenkov GP, Bartunik HD, Huber R, Than ME (2000) Structure and mechanism of the aberrant *ba*<sub>3</sub>-cytochrome *c* oxidase from *Thermus thermophilus*. *EMBO J* 19:1766–1776
- Sousa FL, Alves RJ, Ribeiro MA, Pereira-Leal JB, Teixeira M, Pereira MM (2012) The superfamily of heme-copper oxygen reductases: types and evolutionary considerations. *Biochim Biophys Acta* 1817:629–637
- Stryer L, Berg JM, Tymoczko JL (2002) *Biochemistry*. W.H. Freeman & Co. Ltd, New York
- Svensson-Ek M, Abramson J, Larsson G, Tornroth S, Brzezinski P, Iwata S (2002) The X-ray crystal structures of wild-type and EQ(I-286) mutant cytochrome *c* oxidases from *Rhodobacter sphaeroides*. *J Mol Biol* 321:329–339
- Thomas JW, Puustinen A, Alben JO, Gennis RB, Wikstrom M (1993) Substitution of asparagine for aspartate-135 in subunit I of the cytochrome *bo* ubiquinol oxidase of *Escherichia coli* eliminates proton-pumping activity. *Biochemistry* 32:10923–10928
- Thornstrom PE, Brzezinski P, Fredriksson PO, Malmstrom BG (1988) Cytochrome *c* oxidase as an electron-transport-driven proton pump: pH dependence of the reduction levels of the redox centers during turnover. *Biochemistry* 27:5441–5447
- Tiefenbrunn T, Liu W, Chen Y, Katritch V, Stout CD, Fee JA, Cherezov V (2011) High resolution structure of the *ba*<sub>3</sub> cytochrome *c* oxidase from *Thermus thermophilus* in a lipidic environment. *PLoS One* 6:e22348
- Toledo-Cuevas M, Barquera B, Gennis RB, Wikstrom M, Garcia-Horsman JA (1998) The *cbb*<sub>3</sub>-type cytochrome *c* oxidase from *Rhodobacter sphaeroides*, a proton-pumping heme-copper oxidase. *Biochim Biophys Acta* 1365:421–434
- Tomson FL, Morgan JE, Gu G, Barquera B, Vygodina TV, Gennis RB (2003) Substitutions for glutamate 101 in subunit II of cytochrome *c* oxidase from *Rhodobacter sphaeroides* result in blocking the proton-conducting K-channel. *Biochemistry* 42:1711–1717
- Tsukihara T, Aoyama H, Yamashita E, Tomizaki T, Yamaguchi H, Shinzawa-Itoh K, Nakashima R, . . . , Yoshikawa S (1996) The whole structure of the 13-subunit oxidized cytochrome *c* oxidase at 2.8 Å. *Science* 272:1136–1144
- Turrens JF (1997) Superoxide production by the mitochondrial respiratory chain. *Biosci Rep* 17:3–8
- Tuukkanen A, Verkhovsky MI, Laakkonen L, Wikstrom M (2006) The K-pathway revisited: a computational study on cytochrome *c* oxidase. *Biochim Biophys Acta* 1757:1117–1121
- van Dijk AD, Ciofi-Baffoni S, Banci L, Bertini I, Boelens R, Bonvin AM (2007) Modeling protein-protein complexes involved in the cytochrome *c* oxidase copper-delivery pathway. *J Proteome Res* 6:1530–1539
- Verkhovsky MI, Jasaitis A, Verkhovskaya ML, Morgan JE, Wikstrom M (1999) Proton translocation by cytochrome *c* oxidase. *Nature* 400:480–483
- Voicescu M, El Khoury Y, Martel D, Heinrich M, Hellwig P (2009) Spectroscopic analysis of tyrosine derivatives: on the role of the tyrosine-histidine covalent linkage in cytochrome *c* oxidase. *J Phys Chem B* 113:13429–13436
- von der Hocht I, van Wonderen JH, Hilbers F, Angerer H, MacMillan F, Michel H (2011) Interconversions of P and F intermediates of cytochrome *c* oxidase from *Paracoccus denitrificans*. *Proc Natl Acad Sci U S A* 108:3964–3969
- Vygodina TV, Zakirzianova W, Konstantinov AA (2008) Inhibition of membrane-bound cytochrome *c* oxidase by zinc ions: high-affinity Zn<sup>2+</sup> –binding site at the P-side of the membrane. *FEBS Lett* 582:4158–4162
- Vygodina T, Kirichenko A, Konstantinov AA (2013) Direct regulation of cytochrome *c* oxidase by calcium ions. *PLoS One* 8:e74436

- Wikstrom M (1981) Energy-dependent reversal of the cytochrome oxidase reaction. *Proc Natl Acad Sci U S A* 78:4051–4054
- Wikstrom M (2000) Mechanism of proton translocation by cytochrome *c* oxidase: a new four-stroke histidine cycle. *Biochim Biophys Acta* 1458:188–198
- Wikstrom M, Verkhovsky MI (2007) Mechanism and energetics of proton translocation by the respiratory heme-copper oxidases. *Biochim Biophys Acta* 1767:1200–1214
- Xie H, Buschmann S, Langer JD, Ludwig B, Michel H (2014) Biochemical and biophysical characterization of the two isoforms of *cbb<sub>3</sub>*-type cytochrome *c* oxidase from *Pseudomonas stutzeri*. *J Bacteriol* 196:472–482
- Yu MA, Egawa T, Shinzawa-Itoh K, Yoshikawa S, Guallar V, Yeh SR, Rousseau DL, Gerfen GJ (2012) Two tyrosyl radicals stabilize high oxidation states in cytochrome *c* oxidase for efficient energy conservation and proton translocation. *J Am Chem Soc* 134:4753–4761

# Chapter 17

## The Respiratory Terminal Oxidases (RTOs) of Cyanobacteria

Georg Schmetterer\*

*Institute of Biophysical Chemistry, University of Vienna, UZA2,  
Althanstrasse 14, A-1090 Vienna, Austria*

Summary.....	331
I. Introduction.....	332
II. Types of RTOs Occurring in Cyanobacteria and Definitions.....	332
III. Genes Encoding Putative Subunits of Cyanobacterial RTOs.....	341
IV. Mitochondrial-Type Cytochrome <i>c</i> Oxidases (Cox).....	342
V. Alternate Respiratory Terminal Oxidases (ARTOs).....	343
VI. <i>cbb<sub>3</sub></i> Type Cytochrome <i>c</i> Oxidases.....	345
VII. Homologs of Cytochrome <i>bd</i> Quinol Oxidases.....	346
VIII. Plastidic-Type Terminal Oxidases (Ptox).....	347
IX. Cellular Location of Cyanobacterial RTOs.....	348
X. Regulation of Expression of Cyanobacterial RTOs.....	349
Acknowledgments.....	351
References.....	351

### Summary

Cyanobacteria are unique in performing oxygenic photosynthesis and aerobic respiration in the same compartment. Therefore the bioenergetic situation of cyanobacteria can be considered to be the most complex among all organisms known. While the components of oxygenic photosynthesis are largely known, the components of cyanobacterial respiration still present a number of mysteries for two reasons: (1) Many cyanobacteria contain several respiratory electron transport chains (up to ten) and (2) there are at least eight types of respiratory terminal oxidases (RTOs) that catalyse the reduction of O<sub>2</sub> to water in cyanobacteria. Starting from a list of all RTOs in all currently sequenced cyanobacterial genomes, this review defines the eight different types of known cyanobacterial RTOs: namely, mitochondrial-type cytochrome *c* oxidase, four types of alternate respiratory terminal oxidases (ARTOs), cytochrome *c* oxidase of the *cbb<sub>3</sub>* type, cytochrome *bd*-type quinol oxidases (cyanide sensitive or cyanide insensitive), and plastidic type terminal oxidase (Ptox). The goal of this chapter is to review current understanding of the function of these RTOs, especially in cyanobacteria that contain more than one RTO. The author starts from the hypothesis that in strains with more than one RTO, each must have a specific function, otherwise the genes encoding “superfluous” RTOs would quickly be lost by spontaneous mutation,

---

\*Author for correspondence, e-mail: [georg.schmetterer@univie.ac.at](mailto:georg.schmetterer@univie.ac.at)

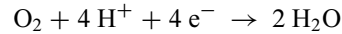
because most RTOs consist of several polypeptide subunits that must be synthesized during every cell division cycle. Two conclusions can be drawn from the available data: (1) Every known cyanobacterium contains at least one RTO, and (2) no one type of RTO is present in all cyanobacteria. Furthermore, the available data probably allow the conclusion that all cyanobacteria contain at least one RTO that catalyzes the transfer of electrons from a soluble cytochrome *c* to O<sub>2</sub> (cytochrome *c* oxidase reaction).

## I. Introduction

There are three primary bioenergetic processes in nature: photosynthesis, respiration, and fermentation. Photosynthesis and respiration are membrane bound processes with light and chemical bond energy as primary energy sources, respectively, while fermentation operates with soluble components using chemical bond energy. Cyanobacteria are defined as prokaryotes (eubacteria) able to perform oxygenic photosynthesis. Therefore, the bioenergetic reactions of cyanobacteria are central to the properties of these organisms. All known cyanobacteria also perform aerobic respiration in the dark and many, perhaps all, also perform these reactions in the light. (Tchernov et al. 2003). Relatively little is known about fermentation in cyanobacteria, which is probably only performed under anaerobic dark conditions. Among cyanobacteria three known modes of growth are photo-litho-autotrophy, photo-organo-heterotrophy, and chemo-organo-heterotrophy.

All cyanobacteria are capable of photo-litho-autotrophy, some are able to grow also photo-organo-heterotrophically, and of these a few are known to possess the capability for chemo-organo-heterotrophy. For the latter strains, respiration is essential,

no cyanobacterium known is able to grow chemo-organo-heterotrophically under anaerobic conditions using fermentation processes for its energy metabolism. For respiration, the only known terminal electron acceptor in cyanobacteria is dioxygen. The reduction of dioxygen to water is the chemical reaction common to all cyanobacterial “Respiratory Terminal Oxidases” (RTOs):



There exist several earlier reviews on the RTOs of cyanobacteria (e.g. Bernroither et al. 2011; Hart et al. 2005; Schmetterer and Pils 2004; Schmetterer 1994). All RTOs are membrane-bound enzymes. The source of the electrons necessary for this reaction can be different for different RTOs. The RTO reaction, independent of which RTO catalyses it, is apparently of great importance for cyanobacteria. One example for this is the observation that in the absence of all RTOs – in *Synechocystis* sp. PCC 6803 – the photochemical reduction of external substrate (specifically ferricyanide) is enhanced 24 times (Bradley et al. 2013). This could be of potential commercial interest by using cyanobacteria that lack RTOs for photo-voltaic systems (Bombelli et al. 2011).

---

*Abbreviations:* Aox – Mitochondrial alternative oxidase; ARTO – Alternate respiratory terminal oxidase; Cbb3 – *cbb3* type cytochrome *c* oxidase; CM – Cytoplasmic membrane; Cox – Mitochondrial-type cytochrome *c* oxidase; Cyd – Homolog of cytochrome *bd*-type quinol oxidase; ICM – Intracytoplasmic membranes (thylakoids); Ptox – Plastidic type terminal oxidase; RTO – Respiratory terminal oxidase; SU – Subunit

## II. Types of RTOs Occurring in Cyanobacteria and Definitions

Table 17.1 lists all genes that encode putative subunits (SU) of RTOs in cyanobacteria in the Joint Genomics Institute, Integrated Microbial Genomes (IMG) database (<https://img.jgi.doe.gov/cgi-bin/mer/main.cgi>). In

Table 17.1. Genes encoding respiratory terminal oxidases of cyanobacteria (December 2013).

---

*Gloeobacter violaceus* PCC 7421

1 cox (gvip300, gvip299, gvip298)

1 cyd (gvip165, gvip164)

1 ptox (gll0601)

1 ARTO2a (incomplete, only gvip077 [CTQLCG], gvip078, no SU3)

*Gloeobacter kilaueensis* JS1

1 cox (GKIL\_3886, GKIL\_3887, GKIL\_3888)

1 ARTO3 (GKIL\_3027 [DSQFSG], GKIL\_3026, GKIL\_3025)

2 ARTO2a, both only SU2 and SU1, no SU3, (GKIL\_2666 [CTQLCG], GKIL\_2665 [WVHHMF]),  
(GKIL\_3016 [CTQLCG], GKIL\_3017 [WVHHMF])

*Prochlorococcus marinus* AS9601

1 cox (A9601\_05011, A9601\_05001, A9601\_04991)

1 ptox (A9601\_03651) (protein lacks 1/3 of normal sequence at the C-terminus, functional?)

*Prochlorococcus* sp. CC9311

1 cox (sync\_2127, sync\_2126, sync\_2125)

1 ARTO3 (sync\_1927 [DAMFSG], sync\_1928, sync\_1929)

*Prochlorococcus* sp. CC9605

1 cox (Syncc9605\_0608, Syncc9605\_0607, Syncc9605\_0606)

1 ARTO1 (Syncc9605\_0981 [DAMFSG] Syncc9605\_0980 [WVHHMF], Syncc9605\_0979)

*Prochlorococcus* sp. CC9902

1 cox (Syncc9902\_1754, Syncc9902\_1755, Syncc9902\_1756)

1 ptox (Syncc9902\_0439)

*Prochlorococcus marinus marinus* CCMP 1375

1 cox (Pro0442, Pro0441, Pro0440)

*Prochlorococcus marinus pastoris* CCMP 1986

1 cox (PMM0446, PMM0445, PMM0444)

1 ptox (PMM0336)

*Prochlorococcus marinus* MIT 9211

1 cox (P9211\_04431, P9211\_04421, P9211\_04411)

*Prochlorococcus marinus* MIT 9215

1 cox (P9215\_05251, P9215\_05241, P9215\_05231)

1 ARTO1 P9215\_16631 [DAMFSG], P9215\_16641 [WVHHMF], P9215\_16651

1 ptox (P9215\_03641)

*Prochlorococcus marinus* MIT 9301

1 cox (P9301\_04701, P9301\_04691, P9301\_04681)

1 ptox (P9301\_03641)

*Prochlorococcus marinus* MIT 9303

1 cox (P9303\_06421, P9303\_06411, P9303\_06401)

*Prochlorococcus marinus* MIT 9312

1 cox (PMT9312\_0445, PMT9312\_0444, PMT9312\_0443)

1 ptox (PMT9312\_0341)

*Prochlorococcus marinus* MIT 9313

1 cox (PMT1341, PMT1342, PMT1343)

*Prochlorococcus marinus* MIT 9515

---

(continued)



Table 17.1. (continued)

---

1 cox (P9515\_05081, P9515\_05071, P9515\_05061)  
1 ARTO1 (P9515\_12631 [DAMFSG], P9515\_12641 [WVHHMF], P9515\_12651)  
*Prochlorococcus marinus* NATL1A  
1 cox (NATL1\_05001, NATL1\_04991, NATL1\_04981)  
1 ptox (NATL1\_11341) (protein lacks 28% of normal sequence, functional?)  
*Prochlorococcus marinus* NATL2A  
1 cox (PMN2A\_1777, PMN2A\_1776, PMN2A\_1775)  
1 ptox (PMN2A\_0429)  
*Prochlorococcus* sp. WH 7803  
1 cox (SynWH7803\_1871, SynWH7803\_1872, SynWH7803\_1873)  
1 ARTO1 (SynWH7803\_0715 [DAMFSG], SynWH7803\_0714 [WVHHMF], SynWH7803\_0713)  
*Prochlorococcus* sp. WH8102  
1 cox (SYNW1861, SYNW1862, SYNW1863)  
1 ARTO3 (SYNW1528 [DAMFSG], SYNW1529, SYNW1530)  
1 ptox (SYNW0887)  
*Synechococcus elongatus* PCC 6301  
1 cox (syc1508\_c, syc1507\_c, syc1506\_c)  
1 cyd (syc2325\_d, syc2326\_d)  
1 cbb3 (syc1309\_d, syc1310\_d)  
*Synechococcus* sp. PCC 6312  
1 ARTO2 (Syn6312\_1832, Syn6312\_1831 [WVHHMF], Syn6312\_1830)  
1 cyd (Syn6312\_1302, Syn6312\_1301)  
*Synechococcus* sp. PCC 7002  
1 cox (SYNPCC7002\_A1162, SYNPCC7002\_A1163, SYNPCC7002\_A1164)  
1 ARTO1 (SYNPCC7002\_A0727 [DSQFSG], SYNPCC7002\_A0726 [WVHHMF], SYNPCC7002\_A0725)  
*Synechococcus* sp. PCC 7336  
1 ARTO2 (Syn7336\_0128, Syn7336\_0127 [WVHHMF], Syn7336\_0126)  
1 cyd (Syn7336\_2230, Syn7336\_2231)  
*Synechococcus* sp. PCC 7502  
1 cox (Syn7502\_01300, Syn7502\_01301, Syn7502\_01302)  
1 cyd (Syn7502\_03463, Syn7502\_03462)  
*Synechococcus elongatus* PCC 7942  
1 cox (Synpcc7942\_2602, Synpcc7942\_2603, Synpcc7942\_2604)  
1 cyd (Synpcc7942\_1767, Synpcc7942\_1766)  
1 cbb3 (Synpcc7942\_0202, Synpcc7942\_0201)  
*Synechococcus* sp. RCC 307  
1 cox (SynRCC307\_0672, SynRCC307\_0671, SynRCC307\_0670)  
1 ARTO3 (SynRCC307\_1937 [DAHFSG], SynRCC307\_1936 + SynRCC307\_1935: sequence complete, but split into 2 ORFs, functional?, SynRCC307\_1934)  
*Synechococcus* sp. WH 8016  
1 cox (Syn8016\_2863, Syn8016\_2864, Syn8016\_2865)  
1 ARTO3 (Syn8016\_0007 [DAMFSG], Syn8016\_0006, Syn8016\_0005)  
*Synechococcus* sp. JA-2-3B'a(2-13)  
1 cox (CYB\_2697, CYB\_2698, CYB\_2700; genes are immediately adjacent)  
1 cyd (CYB\_1208, CYB\_1209)

---

(continued)

Table 17.1. (continued)

---

*Synechococcus* sp. JA-3-3Ab

1 ARTO2 (CYA\_1514, CYA\_1513 [WVHHMF], CYA\_1512)  
1 cyd (CYA\_1764, CYA\_1766; genes are immediately adjacent)

*Synechococcus* sp. KORDI-49

1 cox (KS49-00006190, KS49-00006180, KS49-00006170)  
1 ARTO3 (KS49-00010360 [DAMFSG], KS49-00010350, KS49-00010340)

*Synechococcus* sp. KORDI-100

1 cox (KS100-00007580, KS100-00007570, KS100-00007560)  
1 ARTO3 (KS100-00020350 [DAMFSG], KS100-00020360, KS100-00020370)

*Synechocystis* sp. PCC 6803

1 cox (SYNPCCP\_0713, SYNPCCP\_0714, SYNPCCP\_0715)  
1 ARTO1 (SYNPCCP\_1544 [DSQFSG], SYNPCCP\_1395 [WVHHMF], SYNPCCP\_1396; gene for SU2 far away from putatively associated genes encoding SU1 and SU3!)  
1 cyd (SYNPCCP\_0610, SYNPCCP\_0611)

*Cyanobium gracile* PCC 6307

1 cox (Cyagr\_3213, Cyagr\_3212, Cyagr\_3211)  
1 ARTO1 (Cyagr\_2789 [DSQFSG], Cyagr\_2788 [WVHHMF], Cyagr\_2787)

*Microcystis aeruginosa* NIES-843

1 cox (MAE\_22930, MAE\_22940, MAE\_22950)

*Gloeocapsa* sp. PCC 7428

1 cox (Glo7428\_4450, Glo7428\_4451, Glo7428\_4452)  
1 ARTO1 (Glo7428\_4787 [DSMFSG], Glo7428\_4786 [WVHHMF], Glo7428\_4785)

*Cyanothece* sp. ATCC 51472

1 cox (Cy51472\_2994, Cy51472\_2993, Cy51472\_2992)  
2 ARTO1 (Cy51472\_4951 [DSQFSG], Cy51472\_4950 [WVHHMY], Cy51472\_4949), (Cy51472\_0426 [DSQFSG], Cy51472\_0427 [WVHHMY], Cy51472\_0428)  
1 cyd (Cy51472\_4388, Cy51472\_4387)

*Cyanothece* sp. PCC 7424

1 cox (PCC7424\_4071, PCC7424\_4072, PCC7424\_4073)  
1 ARTO1 (PCC7424\_3139 [DSQFSG], PCC7424\_3140 [WVHHMF], PCC7424\_3141)  
1 cyd (PCC7424\_0151, PCC7424\_0150)

*Cyanothece* sp. PCC 7425

2 cox (Cyan7425\_3958, Cyan7425\_3957, Cyan7425\_3956), (Cyan7425\_1211, Cyan7425\_1212, Cyan7425\_1213)

*Cyanothece* sp. PCC 7822

1 cox (Cyan7822\_4713, Cyan7822\_4712, Cyan7822\_4711)  
1 ARTO1 (Cyan7822\_4378 [DSQFSG], Cyan7822\_4379 [WVHHMF], Cyan7822\_4380)  
1 ARTO3 (Cyan7822\_5867 [DSQFSG], Cyan7822\_5868, Cyan7822\_5869)  
1 cyd (Cyan7822\_1642, Cyan7822\_1641)

*Cyanothece* sp. PCC 8801

1 cox (PCC8801\_0567, PCC8801\_0568, PCC8801\_0569)

*Cyanothece* sp. PCC 8802

1 cox (Cyan8802\_0584, Cyan8802\_0585, Cyan8802\_0586)

*Cyanothece* sp. ATCC 51142

1 cox (cce\_1977, cce\_1976, cce\_1975)

---

(continued)

Table 17.1. (continued)

---

2 ARTO1 (cce\_4109 [DSQFSG], cce\_4110 [WVHHMF], cce\_4111), (cce\_4815 [DSQFSG], cce\_4814 [WVHHMF], cce\_4813)  
1 cyd (cce\_3415, cce\_3414)  
*Cyanothece* sp. ATCC 51472  
1 cox (Cy51472\_2994, Cy51472\_2993, Cy51472\_2992)  
2 ARTO1 (Cy51472\_0426 [DSQFSG], Cy51472\_0427 [WVHHMF], Cy51472\_0428), (Cy51472\_4951 [DSQFSG], Cy51472\_4950 [WVHHMF], Cy51472\_4949)  
1 cyd (Cy51472\_4388, Cy51472\_4387)  
*Halotheca* sp. PCC 7418  
1 cox (PCC7418\_3827, PCC7418\_3826, PCC7418\_3825)  
*Dactylococcopsis salina* PCC 8305  
1 cox (Dacsa\_0127, Dacsa\_0126, Dacsa\_0125)  
1 cyd (Dacsa\_3582, Dacsa\_3581)  
*Thermosynechococcus elongatus* BP-1  
1 ARTO2 (tll2011, tll2010 [WVHHMF], tll2009)  
1 cyd (tll1602, tll1601)  
*Acaryochloris marina* MBIC11017  
1 cox (AM1\_4621, AM1\_4620, AM1\_4619)  
3 ptox (AM1\_A0138), (AM1\_0483), (AM1\_1551)  
*Cyanobacterium aponinum* PCC 10605  
1 cox (Cyan10605\_1220, Cyan10605\_1221, Cyan10605\_1222)  
1 cyd (Cyan10605\_1133, Cyan10605\_1134)  
*Cyanobacterium stanieri* PCC 7202  
1 cox (Cyast\_0400, Cyast\_0401, Cyast\_0402)  
1 cyd (Cyast\_1965, Cyast\_1964)  
*Pleurocapsa* sp. PCC 7327  
1 cox (Ple7327\_1598, Ple7327\_1599, Ple7327\_1600)  
1 ARTO1 (Ple7327\_1318 [DSQYSG], Ple7327\_1317 [WVHHMF], Ple7327\_1316)  
1 incomplete ARTO (no SU2, SU1: Ple7327\_3511 [WVHHMF] incomplete, large part of N-terminaql part is missing, SU3: Ple7327\_3510 consists of 2 ORFs, probably non-functional)  
1 cyd (Ple7327\_3726, Ple7327\_3727)  
*Stanieria cyanosphaera* PCC 7437  
1 cox (Sta7437\_0429, Sta7437\_0428, Sta7437\_0427)  
1 cyd (Sta7437\_2309, Sta7437\_2308)  
*Oscillatoria acuminata* PCC 6304  
1 cox (Oscil6304\_4839, Oscil6304\_4840, Oscil6304\_4841)  
1 cyd (Oscil6304\_4617, Oscil6304\_4616)  
*Oscillatoria nigro-viridis* PCC 7112  
1 cox (Osc7112\_2626, Osc7112\_2627, Osc7112\_2628)  
1 ARTO1 (Osc7112\_1280 [DSQFSG], Osc7112\_1279 [WVHHMF], Osc7112\_1278)  
1 cyd (Osc7112\_1947, Osc7112\_1946)  
2 ptox (Osc7112\_0370), (Osc7112\_4313)  
*Planktothrix* NIVA CYA 15  
1 cox (NIVACYA15\_00041000, NIVACYA15\_00040990, NIVACYA15\_00040980)  
1 ARTO1 (NIVACYA15\_00005730 [DSQYSG], NIVACYA15\_00005740 [WVHHMF], NIVACYA15\_00005750)

---

(continued)

Table 17.1. (continued)

---

*Planktothrix agardhii* NIVA-CYA 34

- 1 cox (DRAFT34\_00040540, DRAFT34\_00040530, DRAFT34\_00040520)
- 1 ARTO1 (DRAFT34\_00025670 [DSQYSG], DRAFT34\_00025660 [WVHHMF], DRAFT34\_00025650)

*Planktothrix agardhii* NIVA-CYA 126/8

- 1 cox (Pagardhii\_20090528\_2646, Pagardhii\_20090528\_2645, Pagardhii\_20090528\_2644)
- 1 ARTO1 (Pagardhii\_20090528\_3646 [DSQYSG], Pagardhii\_20090528\_3647 [WVHHMF], Pagardhii\_20090528\_3648)

*Planktothrix rubescens* NIVA-CYA 98

- 1 cox (Draft98\_00012580 + Draft98\_00012610, Draft98\_00012570, Draft98\_00012560) (functional?, the *coxB* gene contains a putative intron and is therefore annotated as being split into 2 ORFs)
- 1 ARTO1 (Draft98\_00045960 [DSQYSG], Draft98\_00045950 [WVHHMF], Draft98\_00045940)
- 1 cyd (Draft98\_00045930, Draft98\_00045920)

*Planktothrix* NIVA-CYA405

- 1 cox (CYA405DRAFT\_0002.00012730, CYA405DRAFT\_0002.00012720, CYA405DRAFT\_0002.00012710)
- 1 ARTO1 (CYA405DRAFT\_0003.00002480 [DSQYSG], CYA405DRAFT\_0003.00002490 [WVHHMF], YA405DRAFT\_0003.00002500)

*Planktothrix* NIVA-CYA406

- 1 cox (CYA406DRAFT\_0001.00035910 + CYA406DRAFT\_0001.00035930, CYA406DRAFT\_0001.00035940, CYA406DRAFT\_0001.00035950) (functional?, the *coxB* gene contains a putative intron and is therefore annotated as being split into 2 ORFs)
- 1 ARTO1 (CYA406DRAFT\_0001.00002530 [DSQYSG], CYA406DRAFT\_0001.00002540 [WVHHMF], CYA406DRAFT\_0001.00002550)
- 1 cyd (CYA406DRAFT\_0001.00002560, CYA406DRAFT\_0001.00002570)

*Geitlerinema* sp. PCC 7407

- 1 cox (GEI7407\_0253, GEI7407\_0252, GEI7407\_0251)
- 1 cyd (GEI7407\_1752, GEI7407\_1751)
- 1 ptox (GEI7407\_0144)

*Chroococciopsis* sp. PCC 6712

- 1 cox (Chr6712\_0562, Chr6712\_0561, Chr6712\_0560)
- 1 ARTO1 (Chr6712\_1947 [DSQYSG], Chr6712\_1946 [WVHHMF], Chr6712\_1945)
- 1 cyd (Chr6712\_1774, Chr6712\_1773)

*Chroococciopsis thermalis* PCC 7203

- 1 cox (Chro\_4049, Chro\_4050, Chro\_4051)
- 1 ARTO1 (Chro\_0830 [DSMFSG], Chro\_0829 [WVHHMF], Chro\_0828)
- 1 cyd (Chro\_2619, Chro\_2620)

*Crinallium epipsammum* PCC 9333

- 1 cox (Cri9333\_4097, Cri9333\_4098, Cri9333\_4099)
- 1 ptox (Cri9333\_3623), (gene Cri9333\_2513 is a truncated ptox and probably not functional?)

*Calothrix* sp. PCC 6303

- 1 cox (Cal6303\_4202, Cal6303\_4201, Cal6303\_4200)
- 1 ARTO1 (Cal6303\_0060 [DSQFSG], Cal6303\_0061 [WVHHMY], Cal6303\_0062)
- 1 ARTO2 (Cal6303\_2019, Cal6303\_2877 + Cal6303\_2020 [WVHHMF], Cal6303\_2878) (2 far apart loci containing an almost complete set of ARTO2 genes, the sequence for SU1 is split, probably not functional?)
- 1 cyd (Cal6303\_2052, Cal6303\_2051)

*Calothrix* sp. PCC 7507

- 1 cox (Cal7507\_2608, Cal7507\_2609, Cal7507\_2610)
- 

(continued)

Table 17.1. (continued)

---

1 ARTO1 (Cal7507\_4381 [DSQYSG], Cal7507\_4380 [WVHHLY], Cal7507\_4379)  
1 ARTO2a (Cal7507\_0173 [CTELCG], Cal7507\_0172 [WVHHMF], Cal7507\_0171) (1 additional gene for SU3 - Cal7507\_2184 - contains a frameshift in the middle of its sequence and is therefore not functional?)  
1 cyd (Cal7507\_3535, Cal7507\_3534)  
*Fremyella diplosiphon* UTEX 481  
1 cox (SU2: fdiDRAFT73520, SU1: fdiDRAFT73520, separately SU3: fdiDRAFT37390)  
3 ARTO1: (fdiDRAFT79940 [DSQFSGV], fdiDRAFT79920 [WVHHMF], fdiDRAFT79910. 1 small ORF between SU2 and S1 on the opposite DNA strand, function?), (fdiDRAFT45260 [DALFSGV], fdiDRAFT45250 [WVHHMF], fdiDRAFT45240), (SU2: fdiDRAFT08180 [DSQYSG], SU1 and SU3: fdiDRAFT07660 [WVHHLY], fdiDRAFT0750)  
1 ARTO2 (fdiDRAFT83790, fdiDRAFT83780 [WVHHMF], fdiDRAFT83770)  
1 ARTO2a (fdiDRAFT37920 [CTELCG], fdiDRAFT37910 [WVHHMF], 37900)  
2 cyd (fdiDRAFT40960, fdiDRAFT40970), (fdiDRAFT65210, fdiDRAFT65220)  
*Leptolyngbya* sp. PCC 7376  
1 cox (Lepto7376\_1818, Lepto7376\_1819, Lepto7376\_1820)  
1 ptox (Lepto7376\_3160)  
*Microcoleus* sp. PCC 7113  
1 cox (Mic7113\_3734, Mic7113\_3735, Mic7113\_3736)  
1 ARTO1 (Mic7113\_4334 [DSMFSG], Mic7113\_4335 [WVHHMF], Mic7113\_4336 )  
1 ARTO2 (Mic7113\_0967, Mic7113\_0966 [WVHHMF], Mic7113\_0965)  
1 ARTO (incomplete, only genes for SU1 and SU3, functional?) (Mic7113\_3050 [WVHHMF], Mic7113\_3051)  
*Rivularia* sp. PCC 7116  
1 cox (Riv7116\_0273, Riv7116\_0274, Riv7116\_0275)  
2 ARTO1 (Riv7116\_3245 [DSQYSG], Riv7116\_3244 [WVHHMF], Riv7116\_3243), (Riv7116\_3237 [DSQYSG], Riv7116\_3236 [WVHHMF], Riv7116\_3235) (the 2 ARTO1 loci are only ca. 6000bp apart!)  
1 ARTO2a (Riv7116\_6530 [CTELCG], Riv7116\_6529 [WVHHMF], Riv7116\_6528)  
1 cyd (Riv7116\_5466, Riv7116\_5465)  
*Pseudanabaena* sp. PCC 7367  
1 cox (Pse7367\_0191, Pse7367\_0190, Pse7367\_0189)  
1 ptox (Pse7367\_3413)  
*Spirulina major* PCC 6313  
1 ARTO2 (Spi6313\_4172, Spi6313\_4171 [WVHHMF], Spi6313\_4170)  
1 cyd (Spi6313\_1329, Spi6313\_1328)  
*Spirulina subsalsa* PCC 9445  
1 ARTO2 (Spi9445\_0790, Spi9445\_0789 [WVHHMF], Spi9445\_0788)  
1 cyd (Spi9445\_3064, Spi9445\_3063)  
(1 incomplete gene for cyd SU1, encodes potentially only 32 amino acids, probably pseudogene)  
*Arthrospira platensis* NIES-39  
1 cox (NIES39\_O03100, NIES39\_O03090, NIES39\_O03080)  
1 cyd (NIES39\_A01920, NIES39\_A01910)  
*Trichodesmium erythraeum* IMS101  
1 ARTO1 (Tery\_0278 [DSQYSG], Tery\_0277 [WVHHMY], Tery\_0276)  
1 ARTO2 (Tery\_1779, Tery\_1778 [WVHHMF], Tery\_1777)  
*Anabaena* sp. PCC 7108  
1 cox (Ana7108\_3268, Ana7108\_3269, Ana7108\_3270)

---

(continued)

Table 17.1. (continued)

---

2 ARTO1 (Ana7108\_2154 [DSQYSG], Ana7108\_2153 [WVHHMF], Ana7108\_2152), (Ana7108\_0877 [DSQFSG], Ana7108\_0878 [WVHHMF], Ana7108\_0879)

1 ARTO2 (Ana7108\_0810, Ana7108\_0809 [WVHHMF], Ana7108\_0808)

1 cyd (Ana7108\_2333, Ana7108\_2334)

*Anabaena cylindrica* PCC 7122

1 cox (Anacy\_4800, Anacy\_4801, Anacy\_4802)

1 ARTO1 (Anacy\_5413 [DSQYSG], Anacy\_5412 [WVHHMY], Anacy\_5411)

1 ARTO2 (Anacy\_0079, Anacy\_0080 [WVHHMF], Anacy\_0081)

1 cyd (Anacy\_0048, Anacy\_0049)

1 ptox (Anacy\_4546)

*Anabaena variabilis* ATCC 29413

1 cox (Ava\_0528, Ava\_0529, Ava\_0530) (gene for SU2 contains in the middle unusual “insert” of 31 amino acids, function?)

3 ARTO1 (Ava\_B0179 [DSQFSG], Ava\_B0178 [WVHHMF], Ava\_B0177) (located on plasmid A), (Ava\_4298 [DSQYSG], Ava\_4299 [WVHHLY], Ava\_4300), (Ava\_3577 [DSLFSG], Ava\_3576 [WVHHMF], Ava\_3575)

1 ARTO2 (Ava\_0446, Ava\_0447 [WVHHMF], Ava\_0448)

4 cyd (Ava\_1674, Ava\_1675), (Ava\_4048, Ava\_4047) (Ava\_B0175, Ava\_B0174) (located on plasmid A) (Ava\_B0172, Ava\_B0173) (located on plasmid A directly adjacent to the other cyd locus, but encoded on the complementary strand, functional?)

1 ptox (Ava\_1055)

*Anabaena* sp. 90

1 ARTO 1 (ANA\_C20658 [DSQYSG], ANA\_C20657 [WVHHMY], ANA\_C20656) (on plasmid)

2 ARTO2 (ANA\_C13186, ANA\_C13185 [WVHHMF], ANA\_C13184), (ANA\_C10492, ANA\_C10491 [WVHHMF], ANA\_C10490)

*Nostoc azollae* 0708

1 cox (Aazo\_3573, Aazo\_3574, Aazo\_3575)

3 ARTO1 (Aazo\_3660 [DSQYSG], Aazo\_3659 [WVHHMY], Aazo\_3658), (Aazo\_3102 [DALFKG], Aazo\_3101 [WVHHMF], Aazo\_3100), (Aazo\_5318 [DALFSG], Aazo\_5317 [WVHHMF], Aazo\_5316) (located on plasmid pAzo01)

1 ARTO2 (Aazo\_2641, Aazo\_2640 [WVHHMF], Aazo\_2639) (3 putative pseudogenes with high sequence similarity to cox genes, containing only parts of the normal cox sequences: Aazo\_1738 SU2, Aazo\_1737 SU1, Aazo\_3578 SU3)

*Nostoc* sp. PCC 7107

1 cox (Nos7107\_1624, Nos7107\_1625, Nos7107\_1626)

1 ARTO1 (Nos7107\_0351 [DSQYSG], Nos7107\_0352 [WVHHMY], Nos7107\_0353)

1 ARTO2 (Nos7107\_0751, Nos7107\_0750 [WVHHMF], Nos7107\_0749)

1 cyd (Nos7107\_5139, Nos7107\_5138)

*Nostoc* sp. PCC 7120

1 cox (alr0950, alr0951, alr0952)

1 ARTO1 (alr2731 [DSQYSG], alr2732 [WVHHLY], alr2734) (locus is functional, although there is a small ORF - on the other strand - between genes for SU1 and SU3)

1 ARTO2 (alr2514, alr2515 [WVHHMF], alr2516)

1 cyd (all4024, all4023)

1 ptox (all2096)

*Nostoc punctiforme* PCC 73102

1 cox (Npun\_F5532, Npun\_F5533, Npun\_F5534)

---

(continued)

Table 17.1. (continued)

---

2	ARTO1 (Npun_R3537 [DSQYSG], Npun_R3536 [WVHHMY], Npun_R3535) (Npun_R1789 [DSQFSG], Npun_R1788 [WVHHMF], Npun_R1787)
1	ARTO2 (Npun_F0336, Npun_F0337 [WVHHMF], Npun_F0338)
<i>Nostoc</i> sp. PCC 7524	
1	cox (Nos7524_3669, Nos7524_3670, Nos7524_3671)
1	ARTO1 (Nos7524_3778 [DSQYSG], Nos7524_3779 [WVHHMY], Nos7524_3780)
1	ARTO2 (Nos7524_4668, Nos7524_4667 [WVHHMF], Nos7524_4666)
1	cyd (Nos7524_3691, Nos7524_3690)
1	ptox (Nos7524_1144)
<i>Nodularia spumigena</i> CCY9414	
1	cox (NSP_4060, NSP_4050, NSP_4040)
1	ARTO1 (NSP_960 [DSQYSG], NSP_970 [WVHHMY], NSP_980)
1	ARTO2a (NSP_41420 [CTELCG], NSP_41410 [WVHHMF], NSP_41400)
<i>Cyanobacterium</i> sp. UCYN-A	
1	cox (UCYN_12300, UCYN_12290, UCYN_12280)

---

The genes listed were identified by using the BLAST-P program (with a preset E-value of 1e-0) on all finished cyanobacterial genomic sequences in the JGI-IMG database <https://img.jgi.doe.gov/cgi-bin/mer/main.cgi> as of March 2014. The database contains four finished sequences for *Synechocystis* sp. PCC 6803 that were performed to study the development of spontaneous mutations in laboratory-grown cultures. They differ by only a few base pairs and only one of these genomes (that of *Synechocystis* sp. PCC 6803, PCC-P) was considered for this chapter. Partially sequenced genomes were not included, although many potential RTO sequences are present in the incomplete genomic sequences of this database. The BLAST-P program was performed with the following “master gene” query sequences (names as used in the “Cyanobase” database (<http://genome.microbedb.jp/cyanobase>): *coxA* (*Synechocystis* sp. PCC6803 slr 1137), *coxB* (*Synechocystis* sp. PCC6803 slr 1136) *coxC* (*Synechocystis* sp. PCC6803 slr 1138), ARTO-A (*Synechocystis* sp. PCC6803 slr 2082), ARTO-B (*Synechocystis* sp. PCC6803 slr 0813) ARTO-C (*Synechocystis* sp. PCC6803 slr 2038), *cydA* (*Synechocystis* sp. PCC6803 slr 1379), *cydB* (*Synechocystis* sp. PCC6803 slr 1380), *ccoN* (*Synechococcus* sp. PCC 6301 syc1309\_d), *ccoO* (*Synechococcus* sp. PCC 6301 syc1310\_d), *ptox* (*Anabaena* sp. PCC 7120 all2096). Genes thought to encode polypeptides belonging to one protein complex are listed jointly in parenthesis in the following orders: for Cox: *coxBAC*, for ARTO: *ARTO-BAC*, for Cyd: *cydAB* and for *cbb<sub>3</sub>* oxidase *ccoNO*. These are the order in which the genes occur in most genomes. Definitions of the different types of ARTO genes are described in the text. The actual sequence present in the “marker region” of SU1 and SU2 of the ARTOs are given in brackets. The absence of such a bracket after an ARTO subunit implies that the actual “marker sequence” for this ARTO subunit is that of Cox: WAHMHMF for SU1 and CAELCG for SU2. The list includes one organism (*Cyanobacterium* sp. UCYN-A) that does not formally satisfy the definition of a “cyanobacterium,” see text for details. The numbers in front of the RTOs gives the numbers of RTOs for this particular RTO in the strain. For most genes in this list there is no experimental evidence beyond the sequence similarity found and the reader is therefore cautioned when interpreting these data

order to to present a complete picture for each strain, only finished genomes were considered for Table 17.1, although the many partially sequenced strains in this database contain a large number of additional genes encoding putative subunits of RTOs. The author is not a specialist in cyanobacterial nomenclature and the names of the strains are listed as they currently appear in the IMG database. In some cases, the names of strains are controversial, such as for strains PCC 7120 (*Anabaena* or *Nostoc*) and WH8102 (*Synechococcus* or *Prochlorococcus*). The

names of genes are also listed exactly as they appear in the IMG database to allow unequivocal identification.

The RTOs present in cyanobacteria belong to three protein families:

- (A) homologs of heme-copper oxidases
- (B) homologs of cytochrome *bd* quinol oxidases
- (C) homologs of alternative oxidases as found in chloroplasts (Ptox) and mitochondria (Aox)

The homologs of heme-copper oxidases can be further divided into three subgroups

- (A1) mitochondrial-type cytochrome *c* oxidases
- (A2) alternate respiratory terminal oxidases (ARTOs)
- (A3) homologs of cytochrome *cbb<sub>3</sub>* cytochrome *c* oxidases

The homologs of cytochrome *bd* quinol oxidases are either

- (B1) cyanide sensitive or
- (B2) cyanide insensitive

In all mitochondria, there exists a cytochrome *c* oxidase (Cox) that oxidizes reduced soluble cytochrome *c* from the Fe<sup>2+</sup> form to Fe<sup>3+</sup> and transfers the electrons to O<sub>2</sub> with H<sub>2</sub>O as the final product. This chemical reaction is strongly exergonic and part of the liberated energy can be used to generate a proton gradient across the membrane to be used for ATP synthesis and transport processes. Mitochondrial Cox consists of 13 subunits (see e.g. Tsukihara et al. 1996) while related enzymes found in many, but not all (see e.g. Saraste et al. 1991) bacteria have only the three largest subunits found in the mitochondrial complex (see e.g. Iwata et al. 2002). For the purpose of this chapter these three subunits are called CoxA (SU1), CoxB (SU2), and CoxC (SU3), although largely for historical reasons the genes encoding these subunits do not have the same names in all cyanobacteria.

In many cyanobacteria there exist genes encoding homologs of *coxB*, *coxA*, and *coxC* that do not encode cytochrome *c* oxidases. These were first discovered in *Synechocystis* sp. PCC 6803 (Howitt and Vermaas 1998). In this chapter the difference between Cox and ARTO is defined by short characteristic marker sequences present in SU1 and/or SU2. Mitochondrial-type cytochrome *c* oxidases contain the amino acid sequence WAHHMF in SU1 that is involved in binding the heme *a<sub>3</sub>*/ Cu<sub>B</sub> catalytic center. Saraste et al. (1996) first discovered that this sequence can vary. In *Bacillus subtilis* it is WVHHMF. Similarly, there is a marker sequence in SU2, CAELCG, that binds the Cu<sub>A</sub> ion (Yoshikawa et al. 2012),

which is involved in the primary electron transfer from soluble cytochrome *c* to the cytochrome *c* oxidase complex. This sequence has also been characterized in the SU2 of cyanobacterial cytochrome *c* oxidase (Paumann et al. 2004b). All cyanobacterial homologs that have the sequence WAHHMF in their SU1 and CAELCG in their SU2, and only such protein complexes, are considered mitochondrial-type cytochrome *c* oxidases in this chapter. All other homologs of mitochondrial cytochrome *c* oxidase that have a different sequence in at least SU1 or SU2 (or both) will be called Alternate Respiratory Terminal Oxidases (ARTOs, a name introduced by Pils et al. 1997).

### III. Genes Encoding Putative Subunits of Cyanobacterial RTOs

Several interesting general conclusions can be inferred from Table 17.1. First, each cyanobacterium contains at least one RTO, meaning that all known wild type cyanobacteria should be capable of aerobic respiration. It is also evident from Table 17.1 that no single type of RTO is present in every cyanobacterium. The number of different RTO genes in one strain varies widely, from one (in several strains) to ten (in *Anabaena variabilis* ATCC 29413). The latter is currently the organism with the largest known number of putative RTO genes among all living organisms. Even among closely related strains, the types and number of RTOs present can vary widely. For example, strains of *Nostoc* (also known as *Anabaena*) sp. PCC 7120 and *Anabaena variabilis* ATCC 29413 show high sequence similarity for many corresponding genes, but strain PCC 7120 contains only five RTOs. Similarly, the several different, but closely related *Prochlorococcus marinus* strains do not all have the same set of RTOs. To evaluate the function of the several RTOs present in many cyanobacteria, mutants that lack all but one RTO are extremely helpful. Unfortunately, such a set of mutants is currently only available for a single cyanobacterial strain,



*Synechocystis* sp. PCC 6803 (Howitt and Vermaas 1998).

Although there is no experimental evidence for this in cyanobacteria, ARTO type 2 and ARTO type 2a (see below, Sect. V) may actually catalyze the same cytochrome *c* – dioxygen oxidoreductase reaction as mitochondrial-type cytochrome *c* oxidase. This is suggested by the presence of the two cysteine residues that form a key part of the Cu<sub>A</sub> site of SU2, which is essential for the electron transfer reaction from soluble cytochrome *c* to the oxidase complex. The well characterized cytochrome *c* oxidase of *Paracoccus denitrificans* indeed contains the marker sequence CSELCG – rather than CAELCG – in its SU2 (Larsson et al. 1995). All strains listed in Table 17.1 contain at least one of the following three putative cytochrome *c* oxidase complexes: Cox, ARTO type 2, or ARTO type 2a. Thus it can probably be inferred from Table 17.1 that every cyanobacterium contains at least one enzyme that catalyzes the cytochrome *c* oxidase reaction. At least one gene for a soluble cytochrome *c* is present in the genomes of all cyanobacteria analyzed so far. This suggests that the cytochrome *c* oxidase reaction is of central importance for cyanobacteria, probably for generating ATP during dark periods.

The cyanobacterium UCYN-A does not contain a functional Photosystem II (Zehr et al. 2001) and is therefore unable to perform oxygenic photosynthesis. This quite common organism is therefore not a cyanobacterium according to the classical definition (prokaryote capable of oxygenic photosynthesis), but otherwise is very similar to typical cyanobacteria such that its inclusion in the list is warranted. UCYN-A is able to fix dinitrogen (Moisander et al. 2010) and lives as a symbiont of a marine eukaryotic alga (Thompson et al. 2012).

Not listed in Table 17.1, but possibly of biological importance is the occurrence of genes encoding cyanobacterial RTOs in cyanophages. Ignacio-Espinoza and Sullivan (2012) found *ptox* genes in the genomes of 10 cyanophages.

#### IV. Mitochondrial-Type Cytochrome *c* Oxidases (Cox)

Undoubtedly these enzymes are the most important RTOs in cyanobacteria, and no other RTO occurs more often in cyanobacterial genomes. Cyanobacterial Cox always contain three subunits whose genes are arranged in the order *coxBAC*, as in other prokaryotes. No known cyanobacterium contains a gene encoding a polypeptide with sequence similarity to any of the other ten subunits of mitochondrial cytochrome *c* oxidase. It can hardly be a coincidence that these ten subunits are all nucleus-encoded in eukaryotes, while the three largest, SU1, SU2, and SU3, are encoded in the genomes of the mitochondria. There is experimental evidence that Cox is of central importance for dark metabolism in cyanobacteria. For three strains that are capable of chemo-organo-heterotrophic growth, it has been demonstrated that Cox is essential for this growth mode. Cox deletion mutants of *Synechocystis* sp. PCC 6803 (Pils et al. 1997), *Anabaena variabilis* ATCC 29143 (Schmetterer et al. 2001), and *Nostoc* sp. PCC 7120 (Stebegg et al. 2012) have lost the capacity for chemo-organo-heterotrophic growth. Similar experiments on strains that do not encode a Cox in the wild type genome but have ARTO type 2 or ARTO type 2a instead have not yet been performed. The Cox SU2 of *Anabaena variabilis* ATCC 29143 has an “insertion” of 31 amino acids that is not present in any other known Cox SU2. Its origin and significance are unknown. In *Fremyella diplosiphon* UTEX 481, the three genes *coxB*, *coxA*, and *coxC* are localized in two widely separated loci, *coxBA* and *coxC*.

Since cyanobacteria are the only organisms in which oxygenic photosynthesis and aerobic respiration occur in the same compartment, there is interaction between these two electron transport processes. Pils et al. (1997) constructed several mutants of *Synechocystis* sp. PCC 6803 that demonstrate this interaction in vivo. This cyanobacterium contains three small soluble redox proteins

that are possible electron donors to Cox: cytochrome  $c_6$ , cytochrome  $c_M$ , and plastocyanin (for reviews see Ho et al. 2011 and the Chaps. 30, 31 and 34 by Bendall and Howe, Diaz-Moreno et al., and Bialek et al., in this volume). Both cytochrome  $c_6$  and plastocyanin can act as electron donors to Photosystem I (see e.g. Hervás et al. 2005). *Synechocystis* 6803 strain PDJ lacks cytochrome  $c_6$ , strain PDM lacks cytochrome  $c_M$ , and strain PDJM lacks both cytochromes; it is not possible to construct a homozygous double mutant lacking cytochrome  $c_6$  and plastocyanin. All three PD mutant strains are capable of chemo-organo-heterotrophic growth. Since a functional Cox is necessary for this growth mode, the double mutant PDJM must have another electron carrier that allows delivery of electrons to Cox. This is most likely plastocyanin. Similar experiments were performed by Durán et al. (2004). Paumann et al. (2004a) have demonstrated in vitro that electron transfer from plastocyanin to the  $Cu_A$  binding region of cytochrome  $c$  oxidase SU2 of *Synechocystis* sp. PCC 6803 is possible.

One strain in Table 17.1 (*Cyanothece* sp. PCC 7425, also known as *Aphanocapsa*) contains two complete sets of *coxBAC* genes. There are currently no data showing what the specific function of the two gene sets might be, but it is interesting to note that this strain is a unicellular obligate photo-litho-autotroph that is able to fix dinitrogen under microaerobic conditions (Rippka et al. 1979). In this strain the Cox proteins may have an additional function besides the bioenergetic one; for example, in protecting nitrogenase from dioxygen by consuming  $O_2$  via the RTO reaction. On the other hand, Schmetterer et al. (2001) found, in the heterocyst forming strain *Anabaena variabilis* ATCC 29413, that deletion of the *cox* genes leads to a mutant that is still capable of growth on dinitrogen. Two related strains (*Planktothrix rubescens* NIVA-CYA 98, *Planktothrix rubescens* NIVA-CYA406) have a *cox* locus that may contain an intron. Although interesting, there are currently no experimental data that corroborate the functionality of these

introns and *cox* genes. However, the presence and function of introns in cyanobacterial genomes has been verified in tRNA genes (Paquin et al. 1997).

Nomura et al. (2006a) constructed a Cox mutant of *Synechococcus* sp. PCC 7002 and discovered a remarkable phenotype (Nomura et al. 2006b). This mutant strain is very sensitive to high light; but, curiously, a double mutant that lacks both the Cox and the ARTO type 1 (see Table 17.1) is much less sensitive to high light. It is currently not possible to explain this unusual phenotype.

## V. Alternate Respiratory Terminal Oxidases (ARTOs)

For the purpose of this chapter, four types of ARTO are defined based on marker sequences in SU1 and SU2:

- (i) ARTO type 1: has no WAHHMF in SU1, and has no CAELCG in SU2
- (ii) ARTO type 2: has no WAHHMF in SU1, but has CAELCG in SU2
- (iii) ARTO type 2a: has no WAHHMF in SU1, but has CxxxCx in SU2
- (iv) ARTO type 3: has WAHHMF in SU1, but has no CAELCG in SU2

Subunits are defined as belonging to the same protein complex if they are encoded in the genome in the order SU2 → SU1 → SU3, which is by far the most common arrangement. If there is more than one heme-copper RTO in an organism, it would be interesting to know whether a polypeptide encoded by one RTO gene locus can form a functional protein complex with polypeptide(s) encoded by another locus. There is currently no information to answer this question. A few strains listed in Table 17.1 have unusual ARTO gene loci. *Gloeobacter violaceus* PCC 7421 has one locus and *Gloeobacter kilaueensis* JS1 has two loci with two genes each encoding SU2 and SU1 of an ARTO type 2a complex. However, these genomes contain no recognizable gene for a SU3 of this protein complex. Especially in these strains, it would

be interesting to test whether the SU3 of the mitochondrial-type Cox (present in both strains) can substitute to form a functional ARTO type 2a complex. No such experiments have thus far been performed, largely because these interesting organisms are apparently not yet amenable to genetic manipulation. *Synechococcus* sp. RCC 307 has an interrupted SU3 gene that could either be non-functional or “repaired” in a secondary reaction, possibly at the post-transcriptional stage.

Unusual locations for ARTO type 1 genes are observed in *Synechocystis* sp. PCC 6803 and *Fremyella diplosiphon* UTEX 481. The latter strain additionally has two “normal” gene loci for ARTO type 1 enzymes. In both strains, ARTO genes are located in two loci that contain SU1 and SU3 genes, with the SU2 gene in a separate distant locus. In both strains, the ARTO SU2 has high sequence similarity to all other ARTO-type SU2, significantly higher than the sequence similarity to Cox-type SU2. *Synechocystis* sp. PCC 6803 is one of the few strains for which a function of its ARTO has been determined (see below). Thus its genome clearly encodes a functional enzyme. However, it is not known, what polypeptides make up this ARTO enzyme. Similarly, *Microcoleus* sp. PCC 7113 contains a locus with genes for only SU1 and SU3, with no evidence for a gene encoding an ARTO SU2. *Pleurocapsa* sp. PCC 7327 contains an incomplete locus for an ARTO that does not seem to encode a functional polypeptide. Similarly, *Nostoc azollae* 0708 contains three incomplete genes with sequence similarity to ARTO genes that are probably pseudo-genes. *Calothrix* sp. PCC 6303 contains an unusual set of ARTO type 2 genes, with two segments for SU1 that are more than 900,000 bp apart. While these genes may be non-functional, cross-formation of protein complexes from polypeptides encoded by different loci may be possible and thus the synthesis of a biologically functioning enzyme cannot be excluded. For example, the *dnaE* gene of *Synechocystis* sp. PCC 6803 is trans-spliced by an intein dependent mechanism (Wu et al.

1998). *Nostoc* sp. PCC 7120 contains a very unusual ARTO locus, with a small gene located between the coding sequences for SU1 and SU3. Even so, this is one of the few ARTOs for which a function has been established (see below).

The details of the reaction catalyzed by cyanobacterial ARTOs are still unclear. The electron acceptor seems to be dioxygen. A mutant strain of *Synechocystis* sp. PCC 6803 that lacks all RTOs except the ARTO consumes O<sub>2</sub> in a KCN-dependent manner (Pils et al. 1997). This reaction is, however, very slow, compared to the O<sub>2</sub> consumption rate of the other two RTOs (Cox and Cyd) in this strain. Recently, Kranzler et al. (2013) provided evidence that the ARTO type 1 can have another electron acceptor besides O<sub>2</sub>, namely inorganic Fe<sup>3+</sup>, with Fe<sup>2+</sup> as the reaction product. Because many cyanobacterial strains (Table 17.1) contain neither an ARTO type 1 nor any ARTO, the role of an ARTO in iron metabolism cannot be a general one for all cyanobacteria. Even so, this is the first evidence for a cyanobacterial RTO that uses an electron acceptor other than O<sub>2</sub>.

A completely different function for ARTOs has been found in the heterocyst-forming strain *Nostoc (Anabaena)* sp. PCC 7120. Heterocysts are differentiated cells in filamentous cyanobacteria that are specialized for N<sub>2</sub> fixation (for reviews see e.g. Flores and Herrero 2010; Ehira 2013). The nitrogenase enzyme that catalyzes the reduction of N<sub>2</sub> to NH<sub>3</sub>, is one of the most O<sub>2</sub> sensitive proteins known. Valladares et al. (2003) constructed three mutants of *Nostoc (Anabaena)* PCC 7120 lacking either the ARTO type 1 or the ARTO type 2 loci, or both. These were designated *cox3* and *cox2*, respectively, but are now classified as ARTOs. Both enzymes were shown to be expressed only in heterocysts. Only the double mutant was unable to grow on dinitrogen. This was interpreted as these enzymes having the function of removing O<sub>2</sub> from the heterocyst and thus contributing critically to an anaerobic environment for nitrogenase function. Interestingly, the two single mutants lacking only one of the

two ARTOs were able to support growth on N<sub>2</sub>, showing that these ARTOs can, in this respect, fulfill the same function, despite belonging to different ARTO groups.

The molecule donating electrons to ARTO type 1 and type 3 is often assumed to be plastoquinol (e.g. Bernroitner et al. 2011). To my knowledge this has not yet been demonstrated experimentally. Table 17.2 compares all marker sequences for SU2 of ARTO type 1, ARTO type 2a, and ARTO type 3 sequences that appear in Table 17.1. These amino acid sequences are compared with the corresponding sequences present in SU2 of the so-called cytochrome *bo* quinol oxidases present in *Escherichia coli* and their relatives (see e.g. Gennis and Stewart 1996). These cytochrome *bo* enzymes are well characterized and consist of three polypeptides that have significant sequence similarity to the three subunits of prokaryotic (and therefore also cyanobacterial) mitochondrial-type cytochrome *c* oxidase and ARTO. Table 17.2 shows that the “marker sequences” of SU2 cyanobacterial ARTO type 1 and type 3 are very similar to each other, and less similar to the corresponding sequences in cytochrome *bo*. From Table 17.2, the possibility that ARTO type 1 and type 3 are quinol oxidases cannot be inferred but also not excluded, and further studies are necessary to clarify this important point. A search for ARTOs type 1 in other organisms showed that this enzyme seems to occur strictly in cyanobacteria.

## VI. *cbb*<sub>3</sub> Type Cytochrome *c* Oxidases

Two closely related strains (*Synechococcus* sp. PCC 6301 and *Synechococcus* sp. PCC 7942) contain two genes with high sequence similarity to the two largest subunits of the *cbb*<sub>3</sub> type cytochrome *c* oxidase, *ccoN* and *ccoO*. The CcoN protein is clearly related to subunit 1 of mitochondrial-type cytochrome *c* oxidase. The CcoO protein is a

Table 17.2. Marker sequences for subunits of ARTOs in cyanobacteria.

(a) Subunit 2:	
ARTO type 2a:	CTQLCG 3
	CTELCG 3
ARTO type 1 and ARTO type 2	DAMFSG 10
	DSQFSG 18
	DAHFGS 1
	DSMFSG 2
	DSQYSG 21
	DSLFGS 1
	DALFKG 1
	DALFGS 2
<i>Escherichia</i>	SASYSG 30
<i>Salmonella</i>	SASYSG 29
<i>Shigella</i>	SASYSG 7
Mitochondrial cytochrome <i>c</i> oxidase subunit 2:	
	CAELCG
(b) Subunit 1	
ARTO type 1, ARTO type 2, ARTO type 2a:	
	WVHHMF 59
	WVHHMY 11
	WVHHLY 3
<i>Escherichia</i>	WLHHFF 33
<i>Salmonella</i>	WLHHFF 22
<i>Shigella</i>	WLHHFF 0
Mitochondrial cytochrome <i>c</i> oxidase subunit 1:	
	WAHHMF

The table is derived from the data presented in Table 17.1 and shows, the number of times a certain amino acid marker sequence is present in SU2 and SU1, respectively, in the ARTOs of cyanobacterial strains listed in Table 17.1. For comparison, the occurrence of marker sequences for the cytochrome *bo* oxidases of totally sequenced *Escherichia*, *Salmonella*, *Shigella* strains and also mitochondrial Cox are shown. The mitochondrial marker sequences are also present in every cyanobacterial Cox SU2 and SU1 sequence

*c*-type cytochrome and probably acts as the acceptor subunit for electron transfer from soluble cytochrome *c*. A Cu<sub>A</sub> center like that in SU2 of mitochondrial cytochrome *c* oxidase is not present in *cbb*<sub>3</sub> oxidases. *Cbb*<sub>3</sub> type cytochrome *c* oxidases are quite common among bacteria (see e.g. the review by Pitcher and Watmough 2004) and are especially well characterized in purple

bacteria (Oh and Kaplan 2004). The X-ray structure of the *cbb<sub>3</sub>* oxidase from *Rhodobacter spaeroides* shows that the enzyme consists of four subunits encoded by the *ccoNOPQ* genes (Oh and Kaplan 1999). In the related strain, *Rhodobacter capsulatus*, there are five subunits, CcoNOPQH (Ekici et al. 2012). *Synechococcus* strains PCC 6301 and 7942, mentioned above, do not contain any recognizable homologs beyond *ccoN* and *ccoO*. This led Ducluzeau et al. (2008) to suggest that the two genes encoding putative membrane proteins of “unknown function,” immediately downstream of *ccoN* and *ccoO* in these strains, may actually be subunits of a cyanobacterial *cbb<sub>3</sub>* oxidase. While this cannot be ruled out, it is striking that both of these genes for putative membrane proteins have homologs in many other cyanobacteria that clearly do not contain *cbb<sub>3</sub>* type cytochrome *c* oxidases.

We were recently able to show that the *cbb<sub>3</sub>* type oxidase of *Synechococcus* sp. PCC 7942 is an active cytochrome *c* oxidase and is present in this strain in the ICM (thylakoids) and not in the cytoplasmic membrane (CM) (Burgstaller 2012; Schmetterer et al. 2010). Homozygous knock-out mutations in the *cbb<sub>3</sub>* oxidase and, independently, in the mitochondrial-type cytochrome *c* oxidase genes were constructed and the resulting strains tested for in vitro cytochrome *c* oxidase activity in purified membranes (CM or ICM). The Cbb3 mutant exhibited cytochrome *c* oxidation only in the CM, and the Cox mutant only in the ICM, which implies that the *cbb<sub>3</sub>* oxidase is an active cytochrome *c* oxidase and is located only in the ICM of this strain. This is all the more remarkable, since *cbb<sub>3</sub>* oxidases tend to be expressed only under microaerobic conditions in many bacteria (Pitcher and Watmough 2004). This was certainly not the case in the above mentioned studies, since the *Synechococcus* strains were grown under conditions of oxygenic photosynthesis. Indeed both of these *Synechococcus* strains, which carry *ccoN* and *ccoO* genes, are obligate photo-litho-autotrophs.

## VII. Homologs of Cytochrome *bd* Quinol Oxidases

A review by Borisov et al. (2011) lists the categories of enzymes that are collectively called “homologs of cytochrome *bd* quinol oxidase” (here abbreviated Cyd). Such Cyd enzymes are widely distributed among prokaryotes and are always quinol-dioxygen oxidoreductases. Cyd oxidases are not known to occur in any eukaryote. These enzymes contains two subunits, encoded by the *cydAB* genes that are found in this order in genomes. The sequences of CydA proteins can be either “long Q loop” (as e.g. in *E. coli*) or “short Q loop” (as e.g. in *Bacillus stearothermophilus*), the Q loop being the part of the protein where quinol binds. The significance of the additional amino acids in the “long Q loop” enzymes is unknown. All cyanobacteria that contain a Cyd have “short Q-loop” enzymes. It has been shown in *Synechocystis* sp. PCC 6803 that the Cyd enzyme indeed uses plastoquinol as the electron donor (Berry et al. 2002). However, Mogi and Miyoshi (2009) determined that the Cyd from *Synechocystis* sp. PCC 6803 *cydAB* genes expressed in *E. coli* preferred ubiquinol over plastoquinol.

The “*bd*-type” oxidase nomenclature originates from *Escherichia coli*, where the enzyme was found to contain two hemes, a heme *b* and a heme *d*. Many Cyd enzymes, however, contain either no heme *d* or only a small proportion of these proteins present in one cell contain heme *d*. These enzymes are insensitive to KCN. Unfortunately, these KCN-insensitive Cyd enzymes can currently not be recognized from their amino acid sequences. The analysis of the heme content of Cyd enzymes turned out to be tricky because heme *d* is very unstable (Sotiriou and Chang 1988). Indeed, Timkovich et al. (1985) found that extraction of heme *d* from cells or isolated membranes of *E. coli* is not possible because of its severe instability. The chemical structure of heme *d* could be determined only from the isolated enzyme complex. There is a report that heme *d* is present in several cyanobacteria (Fromwald et al. 1996). These

data may be unreliable, however, because the hemes were extracted from isolated membranes in an acidic medium. Recently, it was determined that a mutant form of the *Nostoc* (*Anabaena*) sp. PCC 7120 Cyd enzyme is quite resistant to KCN at 0.67 mM (A. Valladares, unpublished; Mikulic 2013). In this strain, this mutant Cyd enzyme is the only RTO that is rather resistant to KCN. This is remarkable because earlier experiments showed that all RTOs of *Synechocystis* sp. PCC 6803 – and thus also the Cyd oxidase – are sensitive to KCN (Pils et al. 1997). This sensitivity was also found in a *Synechocystis* mutant, in which the Cox and ARTO had been inactivated, and the Cyd was the only remaining RTO (Howitt and Vermaas 1998). In contrast, Mogi and Miyoshi (2009) expressed the *cydAB* genes of *Synechocystis* sp. PCC 6803 in *E. coli* (lacking its wild type RTOs) and found that the expressed *Synechocystis* enzyme behaved like a cyanide-insensitive cyd. The discrepancy may have to do with the content of hemes in the Cyd oxidases in *Synechocystis* relative to *Escherichia coli*. In *E. coli* the heme *d* content of the *Synechocystis* Cyd was found to be much lower than in the *E. coli* wild type Cyd (Mogi and Miyoshi 2009).

Two inhibitors of *Synechocystis* sp. PCC 6803 Cyd are known: 2-heptyl-4-hydroxyquinoline-N-oxide (HQNO) and pentachlorophenol (PCP) (see e.g. Pils et al. 1997). These are specific inhibitors that act only on the Cyd, but not on either the Cox or ARTO enzymes. Note, however, that HQNO and the related NQNO are also partially effective as inhibitors of the quinone-binding  $Q_i$  (or  $Q_n$ ) site of cytochrome *b<sub>6</sub>f* complexes (see the Chap. 15 by Zito and Alric in this volume).

In *E. coli*, the Cyd oxidase can support growth by respiration (Gennis and Stewart 1996). In contrast, in three cyanobacteria (*Anabaena variabilis* ATCC 29413, *Nostoc* (*Anabaena*) sp. PCC 7120, and *Synechocystis* sp. PCC6803), Cox is the enzyme essential for chemo-organo-heterotrophic growth (see Sect. IV). All three strains contain a Cyd (see Table 17.1), but apparently – with respect

to chemo-organo-heterotrophic growth – the Cyd cannot substitute for Cox. The function of the Cyd in cyanobacteria seems therefore not to be a bioenergetic one. Berry et al. (2002) found that the Cyd in *Synechocystis* sp. PCC 6803 seems to function mainly in preventing overreduction of the quinone pool, which could otherwise lead to oxygen radical formation and damage to Photosystem 2 and other proteins. This protective function of the Cyd enzyme in *Synechocystis* sp. PCC 6803 implies that the Cyd must be located in the same membrane as the photosystems, namely the ICM. However, as suggested by Schmetterer (1994), this implies that under normal conditions of photosynthesis, electron flow from the quinone pool to the Cyd must be blocked, because otherwise electrons would be “lost” for transfer to Photosystem 1. The mechanism for this is still not known, but the discovery that expression of the Cyd in *Synechocystis* sp. PCC 6803 is strongly dependent on growth conditions, and especially active under high light (Berry et al. 2002; Gendrullis et al. 2008), implies that the Cyd is an important factor in regulating overall electron transport. The higher activity of Cyd under high light conditions does not result from a higher mRNA level (Gendrullis et al. 2008). Another function for Cyd in *Nostoc* sp. PCC 7120 was discovered recently by Mikulic (2013). A mutant of this heterocyst-forming strain that lacks Cyd was not able to grow diazotrophically. The reason for this is unknown, but it may be the same as that for the ARTOs (see above); i.e. removal of O<sub>2</sub> from the cytoplasm of heterocysts to protect the nitrogenase enzyme from oxidative damage.

## VIII. Plastidic-Type Terminal Oxidases (Ptox)

Ptox and the related Aox (alternative terminal oxidases) are members of the di-iron carboxylate group of proteins. They are quinol-dioxygen oxidoreductases and contain no heme. They were originally found in plant mitochondria (Aox, alternative

oxidase) and chloroplasts (plastidic oxidase, Ptox). Both Aox (Ito et al. 1997) and Ptox from chloroplasts (Josse et al. 2003) are cyanide resistant and function as scavengers for dioxygen to prevent overreduction of the quinone pool and formation of reactive oxygen species (McDonald et al. 2011). Ptox in cyanobacteria was discovered by genome sequencing (McDonald et al. 2003; McDonald and Vanlerberghe 2004; Atteia et al. 2004). McDonald et al. (2003) showed that the gene encoding Ptox is expressed. Recently, two homozygous mutants lacking the *ptox* gene were constructed in *Nostoc (Anabaena)* sp. PCC 7120 (Mikulic 2013). One was in a PCC 7120 wild type background strain and the other in a Cox minus mutant (Stebegg et al. 2012). In both cases, the loss of the *ptox* gene made dark respiration less resistant to KCN. This means that either the Ptox is not solely responsible for KCN resistance or the removal of the Ptox protein induces the biosynthesis of an RTO that is insensitive to KCN, or both. Bailey et al. (2008) studied electron flow from the quinone pool to RTOs in *Synechococcus (Prochlorococcus)* sp. WH 8102 and found spectroscopic evidence that the Ptox protein is used by this strain to prevent overreduction of the quinone pool under iron-limiting conditions. In their experiments, the oxidase was only slightly influenced by KCN, azide or salicylhydroxamic acid, but strongly inhibited by propyl gallate.

Genes with significant sequence similarity to cyanobacterial *ptox* genes were also found in several cyanophages (Sullivan et al. 2010; Ignacio-Espinoza and Sullivan 2012), but the biological significance of this is unclear.

## IX. Cellular Location of Cyanobacterial RTOs

Except for *Gloeobacter* (Rippka et al. 1974), which has only a cytoplasmic membrane (CM), all cyanobacteria have at least two bioenergetically active membranes, the CM and the intracytoplasmic membranes or thylakoids (ICM). The ICM contains

all photosystems and other chlorophyll containing proteins. Some filamentous cyanobacteria are able to differentiate some cells into specialized cells for specific functions: heterocysts for N<sub>2</sub> fixation, akinetes (spores) for surviving nutritionally adverse conditions (e.g. low phosphate, low water) and/or hormogonia with motility for infecting other organisms to form symbioses (for reviews see e.g. Flores and Herrero 2010; Meeks et al. (2002)). In cyanobacteria without cell differentiation, each RTO is – as far as is currently known – located in one membrane only (either CM or ICM). This has important implications for their function, because in the ICM the electron transport chains for respiration and photosynthesis are linked and share common components. Therefore these RTOs must be considered as part of a larger electron transport system that can transfer electrons to O<sub>2</sub> as the terminal acceptor. For the Cyd and Ptox enzymes, this is apparently their major function in cyanobacteria and they may be exclusively found in the ICM. For the heme-copper oxidases the situation is more complex. In *Synechocystis* sp. PCC 6803 it is well established that the Cox and Cyd enzymes are localized in the ICM and the ARTO type 1 in the CM (Schmetterer and Pils 2004). Especially striking are the results of Pisareva et al. (2011) who found in a proteomic study of *Synechocystis* sp. PCC 6803 the two largest ARTO subunits (SU1 and SU2) only in the CM and not in the ICM. Similarly Berry et al. (2002) found no evidence for ARTO in the ICM of *Synechocystis* sp. PCC 6803. The Cyd in this strain was detected only in the ICM (Berry et al. 2002). Ardelean and Peschek (2011) summarize evidence for Cox in the ICM of *Synechocystis* sp. PCC 6803. In contrast, in *Synechococcus* sp. PCC 7942, Schmetterer et al. (2010) found Cox located exclusively in the CM. In this cyanobacterium, the cytochrome *c* oxidase activity of the ICM is due to the *ccb*<sub>3</sub> oxidase (see Sect. VI above). The main conclusion from these studies is that it is not possible to predict the cellular location of an RTO in any cyanobacterium, especially since it

is not yet possible to predict from the amino acid sequence, to which membrane the leader sequence directs the protein. In *Arthrospira* (*Spirulina*) *platensis*, a filamentous strain that does not undergo cell differentiation, purified CM did not show cytochrome *c* oxidase activity (Xu et al. 1994). This implies that in this strain, the single Cox (see Table 17.1) is localized exclusively in the ICM, as in *Synechocystis* sp. PCC 6803.

In heterocysts, there exist three different types of bioenergetically active membranes: CM and two forms of ICM, the photosynthetic thylakoids and the so-called honeycomb membranes that derive from the ICM and are localized close to the heterocyst junctions with adjacent vegetative cells. In heterocysts of *Anabaena cylindrica* strain 629, RTOs were found to be localized in the honeycomb membranes by oxidation of diaminobenzidine, a reaction typical for heme-containing oxidoreductases (Murry et al. 1981). Similar results were obtained (Valladares et al. 2007) when heterocysts of a mutant of *Nostoc* (*Anabaena*) sp. PCC 7120 lacking both ARTO type 2 and ARTO type 1 were subjected to electron microscopy: in the mutant the honeycomb membranes were almost absent. This suggests that these two ARTO proteins are actively involved in the cell differentiation process from vegetative cell to heterocyst that occurs after removal of combined nitrogen from the medium.

## X. Regulation of Expression of Cyanobacterial RTOs

It is clear, even from the comparatively few data on expression of cyanobacterial RTOs, that the expression of these enzymes is highly regulated by multiple external factors. Cyanobacteria are the only prokaryotes that contain an internal circadian clock (for reviews see e.g. Golden et al. 1997; Terauchi and Kondo 2008; Johnson et al. 2011). Liu et al. (1995) first noted that the

number of genes regulated by the circadian clock is very high in *Synechococcus* sp. PCC 7942, especially compared to the number of circadian clock-controlled genes in eukaryotes. Since then, systematic investigations of certain cyanobacterial strains have revealed that some but not all RTOs are subject to regulation by the circadian clock. Specifically, in *Synechococcus* sp. PCC 7942 (Ito et al. 2009), the *coxBAC* genes encoding the Cox enzyme and the *ccoN* and *ccoO* genes encoding the two large subunits of the *cbb<sub>3</sub>* cytochrome *c* oxidase are subject to circadian clock regulation. In contrast, the *cydAB* genes encoding the Cyd quinol oxidase are not regulated by this system. As pointed out above (Sect. VI), only the CcoN and CcoO polypeptides (encoded by adjacent genes) are recognized as probable subunits of cyanobacterial *cbb<sub>3</sub>*, although no other *cbb<sub>3</sub>* cytochrome *c* oxidases with only two subunits are known. The study by Ito et al. (2009) revealed that the two genes downstream of *ccoN* and *ccoO* are regulated by the circadian clock in coordination with *ccoN* and *ccoO*. Nothing is known about these two downstream genes, and they are currently annotated as “hypothetical” (both in the *Synechococcus* sp. PCC 6301 and *Synechococcus* sp. PCC 7942 genomes), but one might speculate that these genes may encode functional subunits of the cyanobacterial *cbb<sub>3</sub>* not present in any *cbb<sub>3</sub>* protein complex from other bacteria. In *Synechocystis* sp. PCC 6803, the expression of the three RTOs is controlled differently by the circadian clock. Whereas the Cox shows a clear rhythmic behavior, the Cyd and the ARTO type 1 do not (Kucho et al. 2005). Experiments that use light/dark growth cycles do not necessarily reflect only circadian gene regulation, but may also reflect the influences of light intensity or quality. This was shown by Lea-Smith et al. (2013) who demonstrated that a *Synechocystis* sp. PCC 6803 mutant lacking both Cox and Cyd is especially sensitive to photooxidative damage in cycles of 12 h high light/12 h darkness. In *Nostoc* (*Anabaena*)



sp. PCC 7120 the Cox and ARTO type 2 are circadian-controlled, whereas the ARTO type 1, Cyd, and Ptox are not (Kushige et al. 2013). In this study, it was also reported that the respiratory activity during cycles of 12 h light/12 h dark was highest from before darkness to about the middle of the dark period. Light regulation has also been found for the Cyd in *Synechocystis* sp. PCC 6803 (Berry et al. 2002), but in this case and also in *Thermosynechococcus elongatus*, a higher Cyd activity in high light did not result from higher *cydAB* mRNA levels in the cells (Gendrullis et al. 2008).

While it is likely that many cyanobacterial RTO-encoding genes are in operons, because many occur adjacent to each other, few cyanobacterial RTO-encoding gene loci have been systematically studied at the mRNA level. Schmetterer et al. (2001) found in the heterocyst-forming strain *Anabaena variabilis* that the Cox locus (*coxBAC* genes) produces three transcripts of different lengths, containing only the *coxB* gene, *coxA* plus *coxC* genes, and all three genes, respectively. Surprisingly the first of these was by far the most abundant, which may have to do with the stability of the primary transcript(s). Although respiration is dramatically higher in heterocysts than in vegetative cells (see e.g. Wolk et al. 1994), the transcripts of the *coxBAC* locus are not very different in filaments containing heterocysts (grown on N<sub>2</sub>) versus filaments without heterocysts (grown on combined nitrogen sources) (Schmetterer et al. 2001). The largest influence on mRNA abundance was found in cells grown with fructose (a heterotrophic growth substrate) relative to cells grown without fructose. Of the two transcriptional start sites identified for this *coxBAC* operon, only one (*tsp2*) was induced by fructose. In the related strain *Nostoc (Anabaena)* sp. PCC 7120, both the *coxBAC* genes and the three homologous genes encoding the ARTO type 2 were found to be within operons encompassing all three genes (Jones and Haselkorn 2002).

The *cydA* gene is expressed at a higher level under microaerobic conditions in *Nostoc (Anabaena)* sp. PCC 7120 (Nicolaisen et al. 2010). This is interesting, because in *E. coli*, the well studied Cyd (cytochrome *bd* quinol oxidase) is also activated under low O<sub>2</sub> conditions and has a higher affinity for O<sub>2</sub> than the other RTO, cytochrome *bo* quinol oxidase (Borisov et al. 2011).

Adaption to changing concentrations of NaCl is very important for cyanobacteria in natural environments (for a review see Hagemann 2011). It has long been known that respiration in cyanobacteria is enhanced in the presence of high NaCl (Fry et al. 1986; Nitschmann and Packer 1992). These studies were performed with *Synechococcus* sp. PCC 6311, for which no genome sequence data are currently available, so the discovery of in vitro cytochrome *c* oxidase activity in this strain in response to high salt (Nitschmann and Packer 1992) cannot be specifically attributed to any Cox, *cbb3*, or ARTO type 2 or 2a enzyme complex. Curiously, an extensive analysis of genes in *Synechocystis* sp. PCC 6803 induced by different stresses, including high NaCl (500 mM), did not identify any gene encoding an RTO subunit (Los et al. 2008), although enhanced, in vitro cytochrome *c* oxidase activity had been detected in high NaCl (550 mM) in this strain (Jeanjean et al. 1993).

Two examples exist of regulation of RTO expression by inorganic ions. Ni deprivation causes upregulation of Cox and Ptox in *Synechococcus (Prochlorococcus)* WH 8102 and of Cox and ARTO type 1 in *Synechococcus* sp. PCC 7002, when these strains are grown with NH<sub>4</sub><sup>+</sup> as the nitrogen source (Dupont et al. 2012). The FurA transcriptional regulator of *Anabaena (Nostoc)* sp. PCC 7120 (González et al. 2012), that was discovered as a regulator of Fe uptake (hence the name), is now known to be a much more general transcriptional regulator. The *coxBAC* operon contains a characteristic DNA sequence, that binds FurA, in front of both the *coxB* and *coxA* genes. For *coxB*, the binding was experimentally verified by

vitro by electrophoretic mobility shift assay (EMSA) experiments (González et al. 2014). Hakkila et al. (2013) discovered that in a *Synechocystis* sp. PCC 6803 mutant that lacks the sigma factors sigC, sigD, and sigE, the RTO genes *coxB*, *coxA*, *coxC*, *cydA* and *cydB* are all downregulated.

Cyanobacteria that are capable of cell differentiation must have complex gene regulation. With respect to RTOs there are few data concerning expression in heterocysts, akinetes, or hormogonia. As mentioned above (Sect. V), transcripts for the genes encoding the ARTO type 1 and ARTO type 2 proteins in *Anabaena* (*Nostoc*) sp. PCC 7120 (see Table 17.1) could only be found in heterocysts (Valladares et al. 2003).

Campbell et al. (2007) performed a unique study with *Nostoc punctiforme* PCC 73102. This filamentous strain is among the most complex cyanobacteria, because it can form all four types of cells that occur in cyanobacteria: vegetative cells, heterocysts, akinetes, and hormogonia. In heterocysts, the ARTO type 2 genes and one of the the ARTO type 1 loci (genes Npun\_R3537, Npun\_R3536, Npun\_R3535) are up-regulated compared to their expression in vegetative cells grown in  $\text{NH}_4^+$ . This is similar to the situation in *Anabaena* (*Nostoc*) sp. PCC 7120 (see above), except that *Nostoc punctiforme* PCC 73102 contains a second ARTO type 1 (see Table 17.1), whose expression is not affected by the cell differentiation process from vegetative cell to heterocyst. The two ARTO 1 enzymes may therefore have different functions despite their high sequence similarity. The differentiation from vegetative cells to akinetes is not accompanied by a change in expression of any of the RTO genes in *Nostoc punctiforme* PCC 73102. In hormogonia, the ARTO type 2 genes and one of the ARTO type 1 gene sets (genes Npun\_R3537, and Npun\_R3535) are upregulated relative to vegetative cells grown in  $\text{NH}_4^+$ , while the *coxC* gene is down regulated.

Clearly, much remains to be learned about the expression and function of RTOs in cyanobacteria.

## Acknowledgments

The author is very grateful to Prof. Annette Rompel, Head of Institute, for hosting him in her Institute of Biophysical Chemistry after his retirement from the Institute of Physical Chemistry at the University of Vienna. Important discussions with Prof. Enrique Flores, CSIC-Universidad de Sevilla, Sevilla, Spain, are gratefully acknowledged.

## References

- Ardelean II, Peschek GA (2011) The site of respiratory electron transport in cyanobacteria and its implication for the photoinhibition of respiration. In: Peschek GA, Obinger C, Renger G (eds) Bioenergetic Processes of Cyanobacteria. Springer, Dordrecht, pp 131–136
- Attea A, van Lis R, van Hellemond JJ, Tielens AGM, Martin W, Henze K (2004) Identification of prokaryotic homologues indicates an endosymbiotic origin for the alternative oxidases of mitochondria (AOX) and chloroplasts (PTOX). *Gene* 330:143–148
- Bailey S, Melis A, Mackey KRM, Cardol P, Finazzi G, van Dijken G, Berg GM, . . . , Grossman A (2008) Alternative photosynthetic electron flow to oxygen in marine *Synechococcus*. *Biochim Biophys Acta* 1777:269–276
- Bernroither M, Zamocky M, Pailer M, Peschek GA, Obinger C (2011) Cyanobacterial respiratory electron transport: heme-copper oxidases and their electron donors. In: Peschek GA, Obinger C, Renger G (eds) Bioenergetic Processes of Cyanobacteria. Springer, Dordrecht, pp 657–682
- Berry S, Schneider D, Vermaas WFJ, Rögner M (2002) Electron transport routes in whole cells of *Synechocystis* sp. strain PCC 6803: the role of the cytochrome *bd*-type oxidase. *Biochemistry* 41:3422–3429
- Bombelli P, Bradley RW, Scott AM, Philips AJ, McCormick AJ, Cruz SM, Anderson A, . . . , Fisher AC (2011) Quantitative analysis of the factors limiting solar power transduction by *Synechocystis* sp. PCC 6803 in biological photovoltaic devices. *Energy Environ Sci* 4:4690–4698
- Borisov VB, Gennis RB, Hemp J, Verkhovsky MI (2011) The cytochrome *bd* respiratory oxygen reductases. *Biochim Biophys Acta* 1807: 1398–1413
- Bradley RW, Bombelli P, Lea-Smith DJ, Howe CJ (2013) Terminal oxidase mutants of the cyanobac-

- terium *Synechocystis* sp. PCC 6803 show increased electrogenic activity in biological photo-voltaic systems. *Phys Chem Chem Phys* 15:13611–13618
- Burgstaller HM (2012) Respiratorische terminale Oxidasen im Cyanobakterium *Synechococcus* sp. Stamm PCC 7942. Diploma thesis, University of Vienna, Austria
- Campbell EL, Summers ML, Christman H, Martin ME, Meeks JC (2007) Global gene expression patterns of *Nostoc punctiforme* in steady-state dinitrogen-grown heterocyst-containing cultures and at single time points during the differentiation of akinetes and hormogonia. *J Bacteriol* 189:5247–5256
- Ducluzeau AL, Ouchane S, Nitschke W (2008) The *cbb<sub>3</sub>* oxidases are an ancient innovation of the domain bacteria. *Mol Biol Evol* 25:1158–1166
- Dupont CL, Johnson DA, Phillippy K, Paulsen IT, Brahmsha B, Palenik B (2012) Response to Ni deprivation in *Synechococcus* sp. strain WH8102. *Appl Environ Microbiol* 78:7822–7832
- Durán RV, Hervás M, De la Rosa M, Navarro JA (2004) The efficient functioning of photosynthesis and respiration in *Synechocystis* sp. PCC 6803 strictly requires the presence of either cytochrome *c<sub>6</sub>* or plastocyanin. *J Biol Chem* 279:7229–7233
- Ehira S (2013) Transcriptional regulation of heterocyst differentiation in *Anabaena* sp. strain PCC 7120. *Russ J Plant Physiol* 60:443–452
- Ekici S, Pawlik G, Lohmeyer E, Koch HG, Daldal F (2012) Biogenesis of *cbb<sub>3</sub>*-type cytochrome *c* oxidase in *Rhodobacter capsulatus*. *Biochim Biophys Acta* 1817:898–910
- Flores E, Herrero A (2010) Compartmentalized function through cell differentiation in filamentous cyanobacteria. *Nat Rev Microbiol* 8:39–50
- Fromwald S, Zoder R, Wastyn M, Lübben M, Peschek GA (1996) Extended heme promiscuity in the cyanobacterial cytochrome *c* oxidase: characterization of native complexes containing hemes A, O, and D, respectively. *Arch Biochem Biophys* 367:122–128
- Fry IV, Hufleijt M, Erber WA, Peschek GA, Packer L (1986) The role of respiration during adaption of the freshwater cyanobacterium *Synechococcus* 6311 to salinity. *Arch Biochem Biophys* 244:686–691
- Gendrullis M, Dyczmons N, Gomolla D, Gathmann S, Bernát G, Schneider D, Rögner M (2008) PetP, a new cytochrome *b<sub>6f</sub>* subunit, and cytochrome *bd* oxidase – two potential regulatory players of cyanobacterial electron transport. In: Allen JF, Gantt E, Golbeck JH, Osmond B (eds) *Photosynthesis, Energy from the Sun*. Springer, Dordrecht, pp 585–589
- Gennis RB, Stewart V (1996) Respiration. In: Neidhardt FC et al (eds) *Escherichia coli and Salmonella*. ASM Press, Washington, DC, pp 217–261
- Golden SS, Ishiura M, Johnson CH, Kondo T (1997) Cyanobacterial circadian rhythms. *Annu Rev Plant Physiol Plant Mol Biol* 48:327–354
- González A, Bes MT, Valladares A, Peleato ML, Fillat MF (2012) FurA is the master regulator of iron homeostasis and modulates the expression of tetrapyrrole biosynthesis in *Anabaena* sp. PCC 7120. *Environ Microbiol* 14:3175–3187
- González A, Espinosa Angarica V, Sancho J, Fillat MF (2014) The FurA regulon in *Anabaena* sp. PCC 7120: *in silico* prediction and experimental validation of novel target genes. *Nucl Acids Res* 42. doi:10.1093/nar/gku123
- Hagemann M (2011) Molecular biology of cyanobacterial salt acclimation. *FEMS Microbiol Rev* 35:87–123
- Hakkila K, Antal T, Gunnelius L, Kurkela J, Matthijs HCP, Tyystjärvi E, Tyystjärvi T (2013) Group 2 sigma factor mutant Δ*sigCDE* of the cyanobacterium *Synechocystis* sp. PCC 6803 reveals functionality of both carotenoids and flavodiiron proteins in photoprotection of photosystem II. *Plant Cell Physiol* 54:1780–1790
- Hart SE, Schlarb-Ridley BG, Bendall DS, Howe CJ (2005) Terminal oxidases of cyanobacteria. *Biochem Soc Trans* 33:832–835
- Hervás M, Diaz-Quintana A, Kerfeld CA, Krogman DW, De la Rosa NA, Navarro JA (2005) Cyanobacterial photosystem I lacks specificity in its interaction with cytochrome *c(6)* electron donors. *Photosynth Res* 83:329–333
- Ho KK, Kerfeld C, Krogman DW (2011) The water soluble cytochromes of cyanobacteria. In: Peschek GA, Obinger C, Renger G (eds) *Bioenergetic Processes of Cyanobacteria*. Springer, Dordrecht, pp 515–540
- Howitt CA, Vermaas WFJ (1998) Quinol and cytochrome oxidases in the cyanobacterium *Synechocystis* sp. PCC 6803. *Biochemistry* 37:17944–17951
- Ignacio-Espinoza JC, Sullivan MB (2012) Phylogenomics of T4 cyanophages: lateral gene transfer in the ‘core’ and origins of host genes. *Environ Microbiol* 14:2113–2126
- Ito Y, Saisho D, Nakazono M, Tsutsumi N, Hirai A (1997) Transcript levels of tandem-arranged alternative oxidase genes in rice are increased by low temperature. *Gene* 203:121–129
- Ito H, Mutsuda M, Murayama Y, Tomita J, Hosokawa N, Terauchi K, Sugita C, ..., Iwasaki H (2009) Cyanobacterial daily life with Kai-based circadian and diurnal genome-wide transcriptional control in

- Synechococcus elongatus*. Proc Natl Acad Sci USA 106:14168–14173
- Iwata S, Ostermeier C, Ludwig B, Michel H (2002) Structure at 2.8 Å resolution of cytochrome *c* oxidase from *Paracoccus denitrificans*. Nature 376:660–669
- Jeanjean R, Matthijs HCP, Onana B, Havaux M, Jost F (1993) Exposure of the cyanobacterium *Synechocystis* PCC6803 to salt stress induces concerted changes in respiration and photosynthesis. Plant Cell Physiol 34:1073–1079
- Johnson CH, Stewart PL, Egli M (2011) The cyanobacterial circadian system: from biophysics to bioevolution. Annu Rev Biophys 40:143–167
- Jones KM, Haselkorn R (2002) Newly identified cytochrome *c* oxidase operon in the nitrogen-fixing cyanobacterium *Anabaena* sp. strain PCC 7120 specifically induced in heterocysts. J Bacteriol 184:2491–2499
- Josse EM, Alcaraz JP, Labouré AM, Kuntz M (2003) *In vitro* characterization of a plastid terminal oxidase (PTOX). Eur J Biochem 270:3787–3794
- Kranzler C, Lis H, Finkel OM, Schmetterer G, Shaked Y, Keren N (2013) Coordinated transporter activity shapes high-affinity iron acquisition in cyanobacteria. ISME J 8:409–417
- Kucho KI, Okamoto K, Tsuchiya Y, Nomura S, Nango M, Kanehisa M, Ishiura M (2005) Global analysis of circadian expression in the cyanobacterium *Synechocystis* sp. strain PCC 6803. J Bacteriol 187:2190–2199
- Kushige H, Kugenuma H, Matsuoka M, Ehira S, Ohmori M, Iwasaki H (2013) Genome-wide and heterocyst-specific circadian gene expression in the filamentous cyanobacterium *Anabaena* sp. strain PCC 7120. J Bacteriol 195:1276–1284
- Larsson S, Källebring B, Wittung P, Malmström BG (1995) The CuA center of cytochrome-*c* oxidase: electronic structure and spectra of models compared to the properties of CuA domains. Proc Natl Acad Sci U S A 92:7167–7171
- Lea-Smith D, Ross N, Zori M, Bendall DS, Dennis JS, Scott SA, Smith AG, Howe CJ (2013) Thylakoid terminal oxidases are essential for the cyanobacterium *Synechocystis* sp. PCC 6803 to survive rapidly changing light intensities. Plant Physiol 162:484–495
- Liu Y, Tsinoremas NF, Johnson CH, Lebedeva NV, Golden SS, Ishiura M, Kondo T (1995) Circadian orchestration of gene expression in cyanobacteria. Genes Dev 9:1469–1478
- Los DA, Suzuki I, Zinchenko VV, Murata N (2008) Stress responses in *Synechocystis*: regulated genes and regulatory systems. In: Herrero A, Flores E (eds) The Cyanobacteria, Molecular Biology, Genomics and Evolution. Caister Academic Press, Norfolk, pp 117–157
- McDonald AE, Vanlerberghe GC (2004) Alternative oxidase and plastoquinol terminal oxidase in marine prokaryotes of the Sargasso Sea. Gene 349:15–24
- McDonald AE, Amirsadeghi S, Vanlerberghe GC (2003) Prokaryotic orthologues of mitochondrial alternative oxidase and plastid terminal oxidase. Plant Mol Biol 53:865–876
- McDonald AE, Ivanov AG, Bode R, Maxwell DP, Rodermel SR, Hüner NPA (2011) Flexibility in photosynthetic electron transport: the physiological role of plastoquinol terminal oxidase (PTOX). Biochim Biophys Acta 1807:954–967
- Meeks JC, Campbell EL, Summers ML, Wong FC (2002) Cellular differentiation in the cyanobacterium *Nostoc punctiforme*. Arch Microbiol 178:395–40
- Mikulic M (2013) Knock-out mutants of respiratory terminal oxidases in the cyanobacterium *Anabaena* sp. strain PCC 7120. Diploma thesis, University of Vienna, Austria
- Mogi T, Miyoshi H (2009) Properties of cytochrome *bd* plastoquinol oxidase from the cyanobacterium *Synechocystis* sp. PCC 6803. J Biochem 145:395–401
- Moisander PH, Beinart RA, Hewson I, White A, Johnson KS, Carlson CA, Montoya JP, Zehr JP (2010) Unicellular cyanobacterial distributions broaden the oceanic N<sub>2</sub> fixation domain. Science 327:1512–1514
- Murry MA, Olafsen AG, Benemann JR (1981) Oxidation of diaminobenzidine in the heterocysts of *Anabaena cylindrica*. Curr Microbiol 6:201–206
- Nicolaisen K, Hahn A, Valdebenito M, Moslavac S, Samborski A, Maldener I, Wilken C, . . . , Schleiff E (2010) The interplay between siderophore secretion and coupled iron and copper transport in the heterocyst-forming cyanobacterium *Anabaena* sp. PCC 7120. Biochim Biophys Acta 1798:2131–2140
- Nitschmann WH, Packer L (1992) NMR studies on Na<sup>+</sup> transport in *Synechococcus* PCC 6311. Arch Biochem Biophys 294:347–352
- Nomura CT, Persson S, Shen G, Inoue-Sakamoto K, Bryant DA (2006a) Characterization of two cytochrome oxidase operons in the marine cyanobacterium *Synechococcus* sp. PCC 7002: inactivation of *ctaDI* affects the PSI:PSII ratio. Photosynth Res 87:215–228
- Nomura CT, Sakamoto T, Bryant DA (2006b) Roles for heme-copper oxidases in extreme high-light and oxidative stress response in the cyanobacterium *Synechococcus* sp. PCC7002. Arch Microbiol 185:471–479

- Oh J-I, Kaplan S (1999) The *cbb<sub>3</sub>* terminal oxidase of *Rhodobacter sphaeroides* 2.4.1: structural and functional implications for the regulation of spectral complex formation. *Biochemistry* 38: 2688–2696
- Oh J-I, Kaplan S (2004) Oxidases as sensors in pigment synthesis. In: Zannoni D (ed) *Respiration in Archaea and Bacteria: Diversity of Prokaryotic Electron Carriers*, vol 15. Springer, Dordrecht, pp 287–309
- Paquin B, Kathe SD, Nierzwicki-Bauer SA, Shub DA (1997) Origin and evolution of group I introns in cyanobacterial tRNA genes. *J Bacteriol* 179:6798–6806
- Paumann M, Bernroither M, Lubura B, Peer M, Jakopitsch C, Furtmüller PG, Peschek GA, Obinger C (2004a) Kinetics of electron transfer between plastocyanin and the soluble Cu<sub>A</sub> domain of cyanobacterial cytochrome *c* oxidase. *FEMS Microbiol Lett* 239:301–307
- Paumann M, Lubura B, Regelsberger G, Feichtinger M, Kollensberger G, Jakopitsch C, Furtmüller PG, . . . , Obinger C (2004b) Soluble Cu<sub>A</sub> domain of cyanobacterial cytochrome *c* oxidase. *J Biol Chem* 279:10293–10303
- Pils D, Gregor W, Schmetterer G (1997) Evidence for in vivo activity of three distinct respiratory terminal oxidases in the cyanobacterium *Synechocystis* sp. strain PCC 6803. *FEMS Microbiol Lett* 152: 83–88
- Pisareva T, Kwon J, Oh J, Kim S, Ge C, Wieslander A, Choi JS, Norling B (2011) Model for membrane organization and protein sorting in the cyanobacterium *Synechocystis* sp. PCC 6803 inferred from proteomics and multivariate sequence analyses. *J Proteome Res* 10:3617–3633
- Pitcher RS, Watmough NJ (2004) The bacterial cytochrome *cbh<sub>3</sub>* oxidases. *Biochim Biophys Acta* 1655:388–399
- Rippka R, Waterbury J, Cohen-Bazire G (1974) A cyanobacterium which lacks thylakoids. *Arch Microbiol* 100:419–436
- Rippka R, Deruelles J, Waterbury JB, Herdman M, Stanier RY (1979) Generic assignments, strain histories and properties of pure cultures of cyanobacteria. *J Gen Microbiol* 111:1–61
- Saraste M, Metso T, Nakari T, Jalli T, Lauraeus M, Van der Oost J (1991) The *Bacillus subtilis* cytochrome-*c* oxidase, variations on a conserved protein theme. *Eur J Biochem* 195:517–525
- Saraste M, Castresana J, Higgins D, Lübben M, Wilmanns M (1996) Evolution of cytochrome oxidase. In: Baltscheffsky H (ed) *Origin and evolution of biological energy conversion*. VCH Publishers, New York, pp 255–289
- Schmetterer G (1994) Cyanobacterial respiration. In: Bryant DA (ed) *The Molecular Biology of Cyanobacteria*. Springer, Dordrecht, pp 409–435
- Schmetterer G, Pils D (2004) Cyanobacterial respiration. In: Zannoni D (ed) *Respiration in Archaea and Bacteria, Diversity of Prokaryotic Respiratory Systems*, vol 16. Springer, Dordrecht, pp 261–278
- Schmetterer G, Valladares A, Pils D, Steinbach S, Pacher M, Muro-Pastor AM, Flores E, Herrero A (2001) The *coxBAC* operon encodes a cytochrome *c* oxidase required for heterotrophic growth in the cyanobacterium *Anabaena variabilis* strain ATCC 29413. *J Bacteriol* 183:6429–6434
- Schmetterer G, Burgstaller H, Mikulic M, Stebegg R (2010) The respiratory terminal oxidases of cyanobacteria. In: Kerfeld C, Schluchter W (eds) *Book of Abstracts, 10th Cyanobacterial Molecular Biology Workshop*. UCLA Conference Center, Lake Arrowhead, p P16
- Sotiriou C, Chang CK (1988) Synthesis of the heme *d* prosthetic group of bacterial terminal oxidase. *J Am Chem Soc* 110:2264–2270
- Stebegg R, Wurzinger B, Mikulic M, Schmetterer G (2012) Chemoheterotrophic growth of the cyanobacterium *Anabaena* sp. strain PCC 7120 dependent on a functional cytochrome *c* oxidase. *J Bacteriol* 194:4601–4607
- Sullivan MB, Katherine H, Huang KH, Ignacio-Espinoza JC, Berlin AM, Kelly L, Weigle PR, . . . , Chisholm SW (2010) Genomic analysis of oceanic cyanobacterial myoviruses compared with T4-like myoviruses from diverse hosts and environments. *Environ Microbiol* 12:3035–3058
- Tchernov D, Silverman J, Luz B, Reinhold L, Kaplan A (2003) Massive light-dependent cycling of inorganic carbon between oxygenic photosynthetic microorganisms and their surroundings. *Photosynth Res* 77:95–103
- Terauchi K, Kondo T (2008) The cyanobacterial circadian clock and the KaiC phosphorylation cycle. In: Herrero A, Flores E (eds) *The Cyanobacteria, Molecular Biology, Genomics and Evolution*. Caister Academic Press, Norfolk, pp 199–216
- Thompson AW, Foster RA, Krupke A, Carter BJ, Musat N, Vault D, Kuypers MMM, Zehr JP (2012) Unicellular cyanobacterium symbiotic with a single-celled eukaryotic alga. *Science* 227:1546–1550
- Timkovich R, Cork MS, Gemis RB, Johnson PY (1985) Proposed structure of heme *d*, a prosthetic group of bacteria. *J Am Chem Soc* 107:6069–6075
- Tsukihara T, Aoyama H, Yamashita E, Tomizaki T, Yamaguchi H, Shinzawa-Itoh K, Nakashima R, . . . , Yoshikawa S (1996) The whole structure of the

- 13-subunit oxidized cytochrome *c* oxidase at 2.8 Å. *Science* 272:1136–1144
- Valladares A, Herrero A, Pils D, Schmetterer G, Flores E (2003) Cytochrome *c* oxidase genes required for nitrogenase activity and diazotrophic growth in *Anabaena* sp. PCC 7120. *Mol Microbiol* 47:1238–1249
- Valladares A, Maldener I, Muro-Pastor AM, Flores E, Herrero A (2007) Heterocyst development and diazotrophic metabolism in terminal respiratory oxidase mutants of the cyanobacterium *Anabaena* sp. strain PCC 7120. *J Bacteriol* 189:4425–4430
- Wolk CP, Ernst A, Elhai J (1994) Heterocyst metabolism and development. In: Bryant DA (ed) *The Molecular Biology of Cyanobacteria*. Kluwer, Dordrecht, pp 770–823
- Wu H, Hu Z, Liu XQ (1998) Protein trans-splicing by a split intein encoded in a split DnaE gene of *Synechocystis* sp. PCC6803. *Proc Natl Acad Sci U S A* 95:9226–9231
- Xu CH, Nejidat A, Belkin S, Boussiba S (1994) Isolation and characterization of the plasma membrane by two-phase partitioning from the alkaliphilic cyanobacterium *Spirulina platensis*. *Plant Cell Physiol* 35:737–741
- Yoshikawa S, Muramoto K, Shinzawa-Itoh K, Mochizuki M (2012) Structural studies on bovine heart cytochrome *c* oxidase. *Biochim Biophys Acta* 1817:579–589
- Zehr JP, Waterbury JB, Turner PJ, Montoya JP, Omoregie E, Steward GF, Hansen A, Karl DM (2001) Unicellular cyanobacteria fix N<sub>2</sub> in the subtropical North Pacific Ocean. *Nature* 412:635–638

# Chapter 18

## XFEL Studies on Bovine Heart Cytochrome *c* Oxidase

Shinya Yoshikawa\*

*Picobiology Institute, Graduate School of Life Sciences,  
University of Hyogo, 3-2-1 Kouto, Kamigori, Ako,  
Hyogo 678-1297, Japan*

Summary.....	357
I. Introduction.....	358
II. Properties of the Resting Oxidized Form of Bovine Heart CcO.....	359
III. Redox Properties of the Resting Oxidized Bovine Heart CcO.....	360
IV. Resonance Raman Analysis of the Resting Oxidized CcO.....	362
V. X-ray Structural Analyses of the Resting Oxidized CcO Using Third Generation Synchrotron Radiation Facilities.....	362
VI. X-ray Structural Analyses of the Resting Oxidized CcO Obtained at an XFEL Facility.....	366
VII. Picobiology.....	368
Acknowledgments.....	371
References.....	372

### Summary

Cytochrome *c* oxidase (CcO) has four redox-active metal sites, Fe<sub>a</sub>, Fe<sub>a3</sub>, Cu<sub>A</sub> and Cu<sub>B</sub>. Each site reversibly receives one electron equivalent. The four electron equivalents required to reduce the bound O<sub>2</sub> are sequentially transferred from cytochrome *c* and each is coupled to the pumping of one proton equivalent. The purified enzyme fraction as prepared (the resting oxidized form) is not involved in catalytic turnover since one electron reduction of the resting oxidized form is not coupled to proton pumping. Redox and resonance Raman data suggest that a peroxide molecule bridges Fe<sub>a3</sub> and Cu<sub>B</sub> in the O<sub>2</sub> reduction site. X-ray structural analyses show that the O-O bond length is 1.7 Å, which is significantly longer than that of the typical peroxide bridge between two metals (1.5 Å), suggesting an activated state of the bound peroxide. On the other hand, investigation of a bacterial CcO produced the proposal that the bound peroxide is not the intrinsic ligand; instead the peroxide is formed from hydroxyl radicals created by the strong X-ray radiation. Establishment of the ligand structure in the O<sub>2</sub> reduction site is a prerequisite for elucidation of the proton-pumping mechanism.

The damage-free X-ray structure of CcO determined using the recently developed femtosecond pulse of an X-ray free-electron laser (XFEL) system shows the existence of a typical peroxide ligand with an O-O distance of 1.55 Å. Thus, the negatively-charged peroxide in the O<sub>2</sub> reduction site blocks the proton-pump upon initial two electron reduction by suppressing the electron transfer from Fe<sub>a</sub> to Fe<sub>a3</sub> (with Fe<sub>a</sub> oxidation driving the proton pump.).

---

\*Author for correspondence, e-mail: [yoshi@sci.u-hyogo.ac.jp](mailto:yoshi@sci.u-hyogo.ac.jp)

This successful determination of a high resolution X-ray structure using femtosecond XFEL pulse validates the system for analysis of changes in X-ray structures over a physiologically-relevant time scale. This chapter includes a discussion for the new field, “Picobiology”, which is made possible by XFEL.

## I. Introduction

Cytochrome *c* oxidase (CcO) is the terminal oxidase of cellular respiration, which reduces  $O_2$  to  $H_2O$  coupled with proton pumping (Yoshikawa et al. 2011). Bovine heart CcO contains 13 different subunits which hold hemes *a* ( $Fe_a$ ) and  $a_3$  ( $Fe_{a_3}$ ),  $Cu_A$  and

$Cu_B$ , each of which reversibly receives one electron equivalent (Tsukihara et al. 1996). Heme  $a_3$ , the  $O_2$  binding site, and  $Cu_B$  form the  $O_2$  reduction site (Yoshikawa et al. 2011). The electron equivalents used to reduce the bound  $O_2$  are sequentially transferred to the  $O_2$  reduction site from cytochrome *c* at the positive side phase (P-phase) of the mitochondrial inner membrane via  $Cu_A$  and heme *a*. The protons in the synthesis of water molecules are transferred from the negative side phase (N-phase) via the two proton conducting pathways (K and D pathways) (Yoshikawa et al. 2011). Each electron transfer from cytochrome *c* is coupled to proton pumping in A type CcOs (Pereira et al. 2008). It is well established that protons are pumped through a proton-conducting pathway (H-pathway) which connects the N-phase to the P-phase in most of animal CcOs (Yoshikawa et al. 2011). On the other hand, either the D or the K pathway has been proposed to function as the proton pumping pathway for eukaryotic (except for most animals) and prokaryotic CcOs (Konstantinov et al. 1997). The structure of the  $O_2$  reduction site which is composed of a high-spin  $Fe_{a_3}^{2+}$  and a  $Cu_B^{1+}$  coordinated with three histidine imidazole groups in a trigonal planar conformation in the reduced state, is completely conserved in all CcOs thus far (Chang et al. 2009). The conservation strongly suggests that there is a common mechanism for  $O_2$  reduction. The completely conserved low spin heme suggests that the heme plays crucial roles in the proton pumping function (Artzbatanov et al. 1978).

It has been established that the  $O_2$  reduction site receives  $O_2$  only when the two metals are in the reduced state (R form) (Dodson et al. 1996) to form the oxygenated form (A form) closely similar to the oxygenated forms of myoglobins (Tsubaki et al. 1980; van Wart and Zimmer 1985)

---

*Abbreviations:* A form – The  $O_2$ -bound form of CcO closely similar to oxymyoglobin, which appears in the catalytic turnover of CcO; A type CcO – Group of CcOs containing three proton conducting pathways D, K, and H; B type CcO – A group of CcOs containing only one proton conducting pathways corresponding to the K pathway of A type CcO; CcO – Cytochrome *c* oxidase;  $Cu_A$  – One of the copper sites of cytochrome *c* oxidase which is the initial electron acceptor from cytochrome *c*;  $Cu_B$  – One of the copper sites of cytochrome *c* oxidase which forms the  $O_2$  reduction site with  $Fe_{a_3}$ ; D-pathway – One of the proton conducting pathways connecting N-phase and the  $O_2$  reduction site for transfer of protons for making water molecules;  $Fe_a$  – The low spin iron ion of one of the two heme As designated as heme *a*, contained in cytochrome *c* oxidase;  $Fe_{a_3}$  – The high spin iron ion of one of the two heme. As designated as heme  $a_3$ , contained in cytochrome *c* oxidase; fs – Femtosecond ( $10^{-15}$  s); H-pathway – The proton conducting pathway connecting the N-phase with the P-phase for proton transfer and pumping; K-pathway – One of the proton conducting pathways connecting the N-phase and the  $O_2$  reduction site for transfer of protons to make water molecules; N-phase – Aqueous phase located in the inside of mitochondrial inner (or bacterial plasma) membrane; O form – The fully oxidized form which appears under turnover conditions; P-phase – Aqueous phase located in the outside of mitochondrial inner (or bacterial plasma) membrane; R form – One of the intermediate species of the catalytic turnover of CcO in which both metals in the  $O_2$  reduction site are in the reduced state and free from any external ligand; SACLA – The nick name of the XFEL facility constructed in Sayo Japan; XFEL – X-ray free electron laser



and of picket-fence heme model compounds (Burke et al. 1978). The transiently bound  $O_2$  at  $Fe_{a3}$  is spontaneously (without any electron donation from the low spin heme (heme *a*)) reduced to two oxides ( $O^{2-}$ ) upon receipt of four electron equivalents from  $Fe_{a3}$ ,  $Cu_B$  and possibly the nearby OH group of Y244 to provide the P form. Then, four electron equivalents are transferred to the  $O_2$  reduction site from cytochrome *c* via  $Cu_A$  and heme *a* to regenerate the R form giving three intermediate species, F, O, E (Yoshikawa et al. 2011). In the O form, all of the redox-active metal sites are in the oxidized form with  $OH^-$  ligands bound to  $Fe_{a3}^{3+}$  and  $Cu_B^{2+}$  (Ogura et al. 1993).

The method for isolation of bovine heart CcO has been well established and yields single crystals which diffract X-rays to 1.3 Å or better resolution. Because the isolation is performed under aerobic conditions, the isolated sample as prepared is in the fully oxidized state. However, although quite stable, the sample as prepared has significantly lower reactivity than that of the fully oxidized state which exists under turnover conditions (the O form described above) in terms of the functions of electron receiving, cyanide binding, and proton pumping (Yoshikawa et al. 2011). Thus, the CcO sample as prepared is known as the “resting oxidized form.” Reductive titration analyses under strict anaerobic conditions indicate that six electrons are required for complete reduction of the resting oxidized form (Mochizuki et al. 1999). Furthermore, a resonance Raman analysis indicates the presence of peroxide bound to the  $O_2$  reduction site (Sakaguchi et al. 2010). These results strongly suggest that peroxide bound to the  $O_2$  reduction site in the resting oxidized CcO blocks the proton pump. The physiological significance of this form has not been well established. However, a detailed structural analysis of resting oxidized CcO would provide various insights into the proton pump mechanism and the coupling between the proton pump and  $O_2$  reduction. Thus, the X-ray structure of the resting oxidized form was examined at SPring-8, a third-generation synchrotron radiation facil-

ity. Significant X-ray damage was detected at the  $O_2$  reduction site, resulting in decreased electron density between the two metals in the  $O_2$  reduction site, with increased X-ray exposure time, which is required to obtain high resolution X-ray diffraction (Aoyama et al. 2009). The X-ray structure without X-ray irradiation, determined by extrapolating the time dependence of the decrease in the electron density, indicates that the O-O bond distance is significantly longer than that of a typical O-O bridge between the two metal atoms (Aoyama et al. 2009). Although the structure may indicate the existence of an activated peroxide molecule bound to the  $O_2$  reduction site, the possibility that the extrapolation was unsuccessful cannot be excluded.

Thus, a damage-free X-ray structural analysis using a recently developed X-ray free electron laser facility (XFEL) was performed for resting oxidized CcO. This investigation concluded that the O-O bond distance is 1.55 Å, a value consistent with the resonance Raman results (Hirata et al. 2014). Thus, binding of peroxide (in the ground state) blocks the proton pump. Careful structural comparison of the resting oxidized form with the O-form (when it is available) would provide various insights in the proton-pump mechanism.

It is noteworthy that the damage-free structural analyses using XFEL pulses of 20 fs validates the feasibility of time resolved X-ray structural analysis, which is a prerequisite for elucidation of the protein function as the chemical reaction (i.e. description of the reaction mechanism in terms of the action of individual atoms).

## II. Properties of the Resting Oxidized Form of Bovine Heart CcO

Evaluation of a method of purifying a protein from its cell is most appropriately and sensitively evaluated by the resolution of the X-ray diffraction obtained from single crystals of the sample isolated by the purification method. In this sense,

the purification method, developed by Okunuki, Yonetani and Yoshikawa groups (Yonetani 1961; Tsukihara et al. 1995; Mochizuki et al. 1999), is the best one since it produces crystals with the highest X-ray diffraction resolution of bovine CcO. Resolution of up to 1.3 Å has been obtained for crystals purified by this method. The CcO sample as prepared is in the fully oxidized state since the purification of the protein with extremely high sensitivity to O<sub>2</sub> is performed under aerobic conditions. However, the sample as prepared by the best method has a much slower cyanide binding compared with that of the fully oxidized form under turnover conditions. This suggests that the O<sub>2</sub>-reduction site of the sample as prepared is not in the same state as the fully oxidized state involved in the catalytic turnover (Mochizuki et al. 1999). Furthermore, some heterogeneity in the cyanide-binding rate has been reported, depending on the purification procedure. Some preparations react with cyanide at a rate of 1–2 M<sup>-1</sup>s<sup>-1</sup> (Naqui et al. 1984; Baker et al. 1987; Mitchell et al. 1992), which is measurable by a standard absorbance spectrophotometer. Other preparations have much slower cyanide binding rates. These preparations are designated as “fast” and “slow” preparations (or forms) (Mitchell et al. 1992). These preparations are also characterized by the Soret band position, at 424 and 418 nm, respectively (Moody 1996). Furthermore, in the dithionite reduction process, the slow form has a much slower reduction rate of heme *a*<sub>3</sub> (time scale of minutes) compared with that of heme *a* (Wrigglesworth et al. 1988). This property also suggests that the slow form is not involved in catalytic turnover. The slow form can be transformed to the fast form by O<sub>2</sub>-pulsing (i.e. complete reduction of the sample followed by exposure of excess O<sub>2</sub>) (Antonini et al. 1977). It is well known that most bovine CcO preparations have variable heterogeneity with respect to the ratio of fast/slow forms (Moody 1996), although purification methods for pure fast and slow forms have been reported (Baker et al. 1987;

Brandt et al. 1989; Cooper and Salerno 1992). Prokaryotic CcOs also demonstrate the slow and fast forms (Cheesman et al. 2004). These results strongly suggest that the slow and fast forms are not due to denatured enzyme preparations, although the physiological functions of the two forms have not been established. The preparation of CcO purified with the method of Okunuki, Yonetani and Yoshikawa groups (Yonetani 1961; Tsukihara et al. 1995; Mochizuki et al. 1999) has the cyanide reactivity, Soret band position and the dithionite reduction rate of the “fast” form. Most of the structural and functional studies on bovine heart CcO have been performed using the “fast” preparation. Thus, in this article, the resting oxidized form is designated as the resting oxidized “fast” form.

### III. Redox Properties of the Resting Oxidized Bovine Heart CcO

Various special precautions are required to obtain an accurate redox titration of CcO, since CcO has the strongest O<sub>2</sub> affinity of the O<sub>2</sub>-reactive proteins in the cell. Repeated evacuation/pure nitrogen-gas equilibration cycles are necessary to completely remove O<sub>2</sub> from the purified sample, which is stabilized by detergents attached to the transmembrane surface. Thus, the stability of the purified sample is crucial. Further, complete removal of contaminating proteins which contain redox-active metals or functional groups is also necessary. In the case of bovine heart CcO, some CcO preparations have been reported to contain contaminant iron proteins which contribute a 30 % higher iron content than that due to heme A. The contaminant proteins are removed only with repeated crystallization (Mochizuki et al. 1999). Thus, a CcO preparation purified by crystallization must be used for redox titration analyses of CcO. A detailed examination of the purity of various bacterial CcO preparations has not been reported thus far.

The most reliable redox titration of bovine heart CcO thus far indicates that six electron equivalents supplied by dithionite are required for complete reduction of the resting oxidized CcO purified by recrystallization (Mochizuki et al. 1999). The slope of the titration curve (generated from the absorbance spectral changes vs the electron equivalents added) during addition of the initial two electron equivalents is significantly less steep than the slope generated by addition of the subsequent four electron equivalents. The oxidative titration of the dithionite-reduced CcO with  $O_2$  indicates that four oxidation equivalents supplied by  $O_2$  are sufficient for re-oxidation of the dithionite-reduced CcO. However, the absorbance spectrum of the  $O_2$ -re-oxidized sample is slightly but significantly different from that of the resting oxidized form existing before the initiation of the dithionite titration. The  $O_2$ -re-oxidized sample after aeration for 30 min requires six electron equivalents from dithionite for complete reduction (Mochizuki et al. 1999). These results strongly suggest that peroxide ( $O_2^{2-}$ ) is bound to the  $O_2$ -reduction site. The shallow titration curve observed during the initial two electron reduction suggests that the electron equivalents are mostly used to reduce the bound  $O_2^{2-}$  to water. The  $O_2$ -re-oxidized sample is likely to correspond to the oxidized form under turnover conditions. The  $O_2$ -re-oxidized sample obtained under strict anaerobic conditions without addition of any external reducing system undergoes slow reduction of both hemes (Mochizuki et al. 1999). These results suggest the presence of slow electron donors in the protein moiety at the  $O_2$  reduction site. Such slow electron donors could reduce  $O_2$  to peroxide when the  $O_2$ -re-oxidized sample is exposed to excess  $O_2$ . Certain amino acid residues such as tryptophan, tyrosine and lysine could serve as two-electron donors and provide stable non-radical products which are not reducible with dithionite (Mochizuki et al. 1999).

It is well known that  $H_2O_2$  reacts with resting oxidized CcO to generate the P

or F form in a manner which depends on the amount of  $H_2O_2$  added (Wrigglesworth 1984; Weng and Baker 1991). Although the mechanism is still unknown, the generation of these forms is well established by absorbance and resonance Raman analyses (Proshlyakov et al. 1994, 1996). Thus, it has been claimed that the peroxide-bound form is unlikely to be stable enough to allow the resting oxidized CcO to be stored in the crystalline state for several months at 4 °C without any significant absorbance spectral change (Kim et al. 2004; Kaila et al. 2010; Wikström 2012). However, as described above, the resting oxidized CcO is formed from the fully oxidized form corresponding to the oxidized form under turnover conditions ( $Fe_{a3}^{3+}-OH^-$ ,  $Cu_B^{2+}-OH^-$ ) by slow spontaneous electron transfer from the protein moiety in the presence of  $O_2$  (Mochizuki et al. 1999). On the other hand,  $H_2O_2$  reacts with the resting oxidized CcO which has a peroxide molecule bound to the  $O_2$  reduction site. Thus, the high reactivity of resting oxidized CcO with  $H_2O_2$  does not provide evidence for the absence of peroxide in the  $O_2$  reduction site of the resting oxidized CcO. It is possible that  $H_2O_2$  functions as a two electron acceptor from the bound peroxide in the resting oxidized CcO to provide the fully oxidized state as follows; one equivalent of  $H_2O_2$  added oxidizes the bound peroxide in [ $Fe_{a3}^{3+}-O-O-Cu_B^{2+}$ ] to provide transiently [ $Fe_{a3}^{3+}$ ,  $Cu_B^{2+}$ ],  $O_2$  and  $2H_2O$ . The  $O_2$  molecule produced in this step is unlikely to interact with the  $O_2$  reduction site. Then the second  $H_2O_2$  is trapped at the  $O_2$  reduction site and generated the P-form, which is characterized by  $Fe_{a3}^{4+} = O^{2-}$ ,  $Cu_B^{2+}-OH^-$  and a Y244 OH radical (Y244 is cross-linked covalently to one of the three histidine imidazole groups coordinated to  $Cu_B$  (Yoshikawa et al. 1998)). An excess amount of  $H_2O_2$  would provide another electron donor to the P-form to generate the F-form. The coupling of the single electron injection with the pumping of one proton equivalent has been well established for all of the intermediate species which appear after the A form (the  $O_2$ -bound form), namely, the

P, F, O and E forms (Verkhovsky et al. 1999; Bloch et al. 2004; Siletsky and Konstantinov 2012). Although single electron reduction of the resting oxidized CcO initiates rapid electron transfer from  $\text{Cu}_A$  to heme  $a$ , no further electron transfer to the  $\text{O}_2$  reduction site from heme  $a$  is detectable (Verkhovsky et al. 2001; Bloch et al. 2004). It appears that the negative charges of the bound peroxide on the  $\text{O}_2$  reduction site prevent the redox-potential of heme  $a_3$  from increasing in heme  $a_3$ . The increased redox potential of heme  $a_3$  is responsible for the electron extraction from heme  $a$ . It is well known that oxidation of heme  $a$  drives the proton pump (Yoshikawa et al. 2011). These results suggest that the structure of the  $\text{O}_2$  reduction site is crucial for proton pump. In other words, the  $\text{O}_2$  reduction site is also involved in proton-pumping. Further, the second single electron reduction flash to the single-electron reduced resting oxidized CcO induces a slower electrogenic phase (135  $\mu\text{s}$ ). However, the intensity is too weak to drive the pumping of a single proton (Verkhovsky et al. 2001).

#### IV. Resonance Raman Analysis of the Resting Oxidized CcO

The peroxide binding is confirmed by resonance Raman analysis excited at 647.1 nm from a  $\text{Kr}^+$  laser. This laser excites the charge transfer band (detectable as a shoulder near 650 nm) characteristic of the resting oxidized CcO to provide a clear band at  $755\text{ cm}^{-1}$ . Cyanide eliminates both the resonance Raman and the absorption bands. A linear relationship between the O-O stretching frequency and the corresponding O-O bond length suggest that the  $755\text{ cm}^{-1}$  band corresponds to the frequency due to the O-O stretch of the bond length of 1.50 Å (Sakaguchi et al. 2010). The bond length is consistent with the O-O bond length detectable in the X-ray structures of various peroxide-bridged inorganic compounds deposited in the Cambridge Database. The absence of the Fe-O stretch mode in the

resonance Raman spectrum of the resting oxidized CcO also supports this assignment (Collman et al. 2003).

#### V. X-ray Structural Analyses of the Resting Oxidized CcO Using Third Generation Synchrotron Radiation Facilities

Although the above redox and resonance Raman characteristics strongly provide strong evidence that peroxide is bound to the  $\text{O}_2$  reduction site of the resting oxidized CcO, X-ray structure at high resolution is indispensable for elucidation of the mechanism of blockage of the proton pump. Thus, an X-ray structural analysis of the resting oxidized CcO has been conducted at SPring-8. As expected, significant X-ray radiation effects were detected in the absorbance spectra of the frozen single crystals as shown in Fig. 18.1 (Aoyama et al. 2009). The visible spectral changes induced by 30 s irradiation of a single crystal of the resting oxidized CcO at 100 K show a significant increase in the  $\alpha$ -band region at 604 and 582 nm (Fig. 18.1). The third peak is detectable between the two peaks near the  $\alpha$ -band peak before X-ray irradiation. The time course of the absorbance changes shows that the maximal changes for both peaks are attained after 20 s of irradiation. No further spectral change is detectable with longer exposure, although the spectrum of CcO in the crystal is clearly different from that of the fully reduced CcO (see Fig. 18.1b). The appearance of the residual peak at 595 nm near the  $\alpha$ -band peak of the oxidized CcO and the residual charge transfer band near 650 nm strongly suggest that reduction of the CcO in the crystals is incomplete. In fact, warming the crystals induces the fully reduced CcO spectrum (Aoyama et al. 2009). The sharp bands at 582 and 604 nm suggest that two different low spin ferrous hemes are induced. The 604 nm band is reasonably assignable to heme  $a$ . Essentially identical absorbance spectral changes are detectable in the bacte-

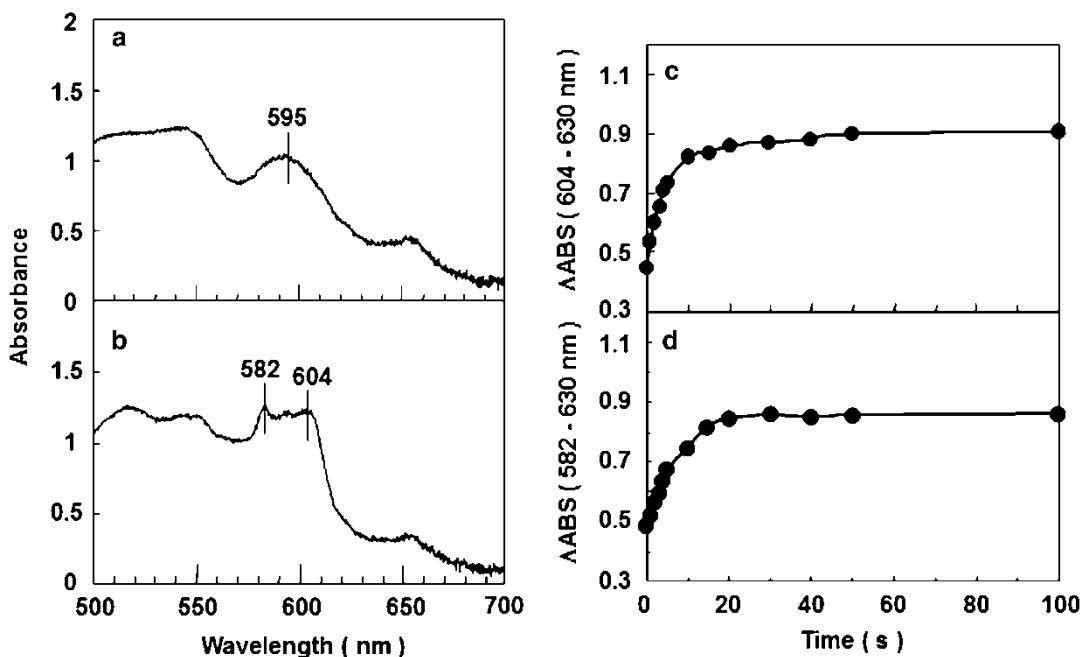


Fig. 18.1. Effects of X-ray irradiation on the visible spectra of the single crystals of the resting oxidized bovine heart cytochrome *c* oxidase. The measuring light beam focused to about 50  $\mu\text{m}$  in diameter was injected perpendicular to the most-extended plane of (010). Visible spectra are shown for the sample before X-ray irradiation (a) and after a 30 s exposure (b). Time course of the increases in the absorbance difference are shown between 604 and 630 nm (c) and between 582 and 630 nm (d) (Reprinted with permission from “Aoyama et al. 2009”).

rial (*R. sherooides*) CcO, which has electron density closely similar to that of bovine heart CcO (Qin et al. 2006).

One of the simplest interpretations of the irradiated spectrum (Fig. 18.1b) is as follows: heme *a* is fully reduced while heme *a*<sub>3</sub> is partially reduced to give a low spin ferrous heme *a*<sub>3</sub> with the 582 nm band and the residual resting oxidized heme *a*<sub>3</sub> exhibiting absorbance bands at 595 and 650 nm. The partial reduction of heme *a*<sub>3</sub> could be induced by uneven crystal packing of CcO in the dimer state. One of the monomers in the dimer is subject to significantly stronger constraints from the adjacent CcO molecules in the crystal, compared with the other monomer. On the other hand, the electron density between the two metals in the O<sub>2</sub> reduction site is weakened by the longer exposure of the crystals to X-ray irradiation. The electron density decrease, which is accompanied by an increase in the O-O bond distance, proceeds af-

ter the maximal absorbance spectral changes are attained following the 20 s irradiation period. Careful refinement of X-ray structural data obtained at various exposure times indicates that electron density assignable to a water molecule hydrogen-bonded to the OH group of Y244 increases as the electron density of the peroxide molecule decreases. The X-ray-irradiation-induced appearance of the water molecule also suggests that the bridging peroxide is reduced by the hydrated electrons which are generated by X-ray irradiation (Aoyama et al. 2009).

In order to obtain an X-ray structure with minimal radiation effects, an X-ray structure was extrapolated to 0 s using X-ray data from a 1 s exposure to a 400 s exposure. The resulting structure with 2.1 Å resolution indicates that the O-O bond distance is 1.7 Å, as given in Fig. 18.2 (Aoyama et al. 2009). It is noteworthy that the Fe<sub>a3</sub>-O distance is significantly longer than that of the typical

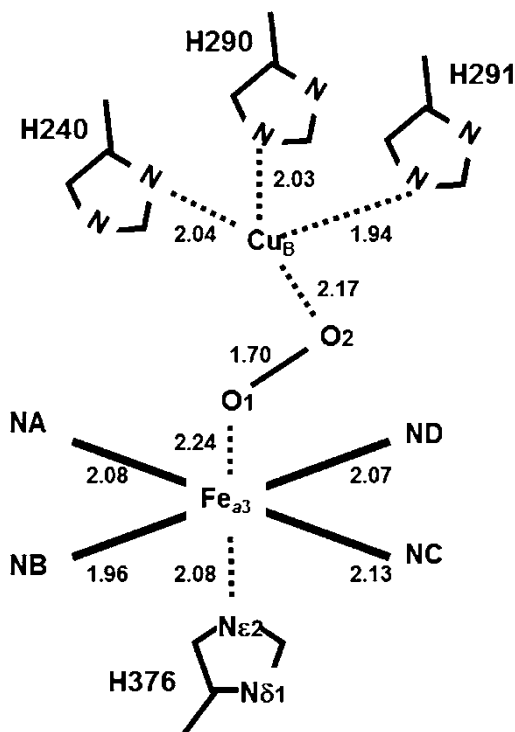


Fig. 18.2. Coordination geometries of the  $O_2$  reduction site of the resting oxidized bovine heart CcO at 2.1 Å resolution, extrapolated to 0 s X-ray exposure. The interatomic distances are given in Å. Other distances and angles are  $Fe_{a3}-Cu_B$ , 4.87 Å;  $N_{\epsilon 2}$  (H376)- $Fe_{a3}-O_1$ , 168.5°;  $Fe_{a3}-O_1-O_2$ , 144.1° and  $O_1-O_2-Cu_B$ , 90.5°. These geometries are fully consistent with those of the X-ray structure determined from the 103.5 s exposures at 1.95 Å resolution (Reprinted with permission from “Aoyama et al. 2009”).

low spin coordination, which is consistent to the proposal that heme  $a_3$  is in the high spin state in the resting oxidized form (Day et al. 1993; Cheesman et al. 2004). On the other hand, the O-O bond distance of the bound peroxide is significantly longer than that of typical bridging peroxides reported thus far. Also, the distance is inconsistent with the resonance Raman results.

One of the possible interpretations of these results is that the extrapolation to 0 s of exposure was unsuccessful and that the X-ray data is contaminated by X-ray-damaged structures. The other interpretation is that the peroxide in the  $O_2$  reduction site is in an activated state which is stable only in the protein. The O-O bond length of 1.5 Å, indicated by the resonance Raman results is based on an empirical relationship between the bond length and the position of the O-

O stretch mode from various inorganic compounds (Sakaguchi et al. 2010). Thus, the resonance Raman result is not conclusive evidence against a bond length of 1.7 Å. On the other hand, the activated state of the peroxide in the  $O_2$  reduction site is inconsistent with the high stability of the resting oxidized CcO, especially in the crystalline state.

The X-ray structure of the fully oxidized state under turnover conditions (the O form) has not been determined. However, the X-ray structures of the fully oxidized azide and cyanide bound forms indicate that significant structural differences between these fully oxidized CcOs are detectable only in the  $O_2$  reduction site. Thus, the structural differences between the O form and the resting oxidized form are likely to be small. An accurate determination of the resting oxidized CcO and comparison of this form with the structure

of the O-form would provide various crucial insights which will contribute to elucidation of the proton-pump mechanism. Thus, an experimental evaluation of the two interpretations described above is highly desirable.

The O<sub>2</sub> reduction site of *R. sphaeroides* CcO has an electron density similar to that of bovine heart CcO (Qin et al. 2006). However, it has been proposed that two equivalents of OH<sup>-</sup> or H<sub>2</sub>O are present instead of one equivalent of peroxide. On the other hand, Michel and coworkers have proposed that the O<sub>2</sub> reduction site in the oxidized *P. denitrificans* CcO has a peroxide bridging between the two metals, i.e. the same assignment as bovine CcO (Koepke et al. 2009). However, it was proposed that the peroxide-bound species is involved in catalytic turnover. A B-type CcO, cytochrome *ba*<sub>3</sub> from *T. thermophiles*, a thermophilic bacteria, provides a clear electron density peak in the O<sub>2</sub> reduction site (1.8 Å resolution) which indicates an O-O distance of 1.50 Å. A peroxide molecule was assigned as the bridging ligand to the fully reduced O<sub>2</sub> reduction site (Tiefenbrunn et al. 2011). It has been proposed that the bridging peroxide is a product generated from two equivalents of hydroxyl radical (•OH) created by the synchrotron radiation beam. The H<sub>2</sub>O<sub>2</sub> ligand is bound to the fully reduced O<sub>2</sub> reduction site (Fe<sub>a3</sub><sup>2+</sup>, Cu<sub>B</sub><sup>1+</sup>) which is formed by reduction of the oxidized CcO by hydrated electrons produced by the strong X-ray beam. This interpretation is consistent with the absorption spectral change induced by the X-ray irradiation which produces a hemochrome-type spectrum characterized by a sharp band in the α-band region (Tiefenbrunn et al. 2011). However, a decrease in electron density induced by long exposure to the X-ray beam, as in the case of bovine CcO, has not been reported for the *ba*<sub>3</sub> type CcO. A plausible interpretation for these results is that *ba*<sub>3</sub> CcO has a weaker sensitivity to X-ray irradiation, compared with that of bovine CcO, and as a result, no further significant radiation effect on the bridging peroxide is detectable. On the other hand, bovine heart CcO is more significantly affected by the

X-ray beam and, therefore, there is a decrease in the electron density due to the bound peroxide coupled with increase in O-O bond length.

However, this interpretation is inconsistent with the observation that the electron density peak between the two metals in the O<sub>2</sub> reduction site after 1 s exposure indicates a clear O-O bond with an intensity consistent with two oxygen atoms linked by a covalent bond, while the 1 s exposure induces less than 10 % of the maximal absorption spectral change (Aoyama et al. 2009). Because the X-ray-irradiation effect is detectable most sensitively by the absorbance spectral change, the 1 s exposure is unlikely to cause significant damage into the conformation of CcO. The hemochrome-type absorbance spectrum showing its maximum intensity at 20 s X-ray exposure more likely arises from a radiation-damaged product originating from Fe<sup>3+</sup>-O-O-Cu<sup>2+</sup> moiety. In the product, the O-O bond has been broken and the heme iron is reduced. This enables binding of a strong ligand of unknown origin which gives rise to the hemochrome spectrum. Furthermore, the stability of the hemochrome spectrum induced by the X-ray irradiation is inconsistent with the proposed structure of Fe<sup>2+</sup>-O-O-Cu<sup>1+</sup>, since the metal site has two electron equivalents which are able to readily reduce the peroxide completely to the oxide (O<sup>2-</sup>) level. Although a theoretical (DFT) calculation indicating the possibility of this structure has been reported (Du and Noodleman 2013), experimental confirmation such as a damage-free X-ray structural analysis is needed for *ba*<sub>3</sub> CcO. Furthermore, the redox titration results (which indicate a requirement of six electron equivalents for complete reduction of the resting oxidized bovine CcO which has not been exposed to any strong X-ray beam) are also inconsistent with the above interpretation. Careful redox titration experiments similar to the bovine heart CcO titrations are desirable for these bacterial CcOs since significant diversity in the function of the O<sub>2</sub> reduction site between bacterial CcOs and bovine CcO cannot be excluded at this stage.

## VI. X-ray Structural Analyses of the Resting Oxidized CcO Obtained at an XFEL Facility

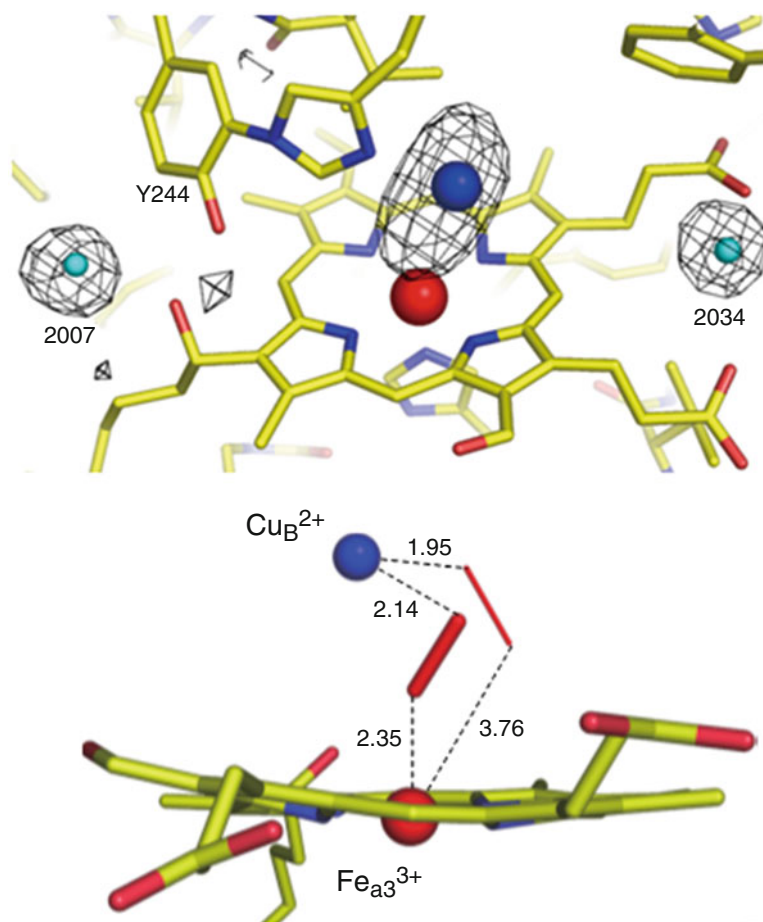
In order to eliminate the radiation damage effect, a newly constructed X-ray free electron laser facility (XFEL, SACLA) has been employed in the X-ray structural analysis of the resting oxidized CcO (Hirata et al. 2014). The facility generates extremely strong and short (20 fs) X-ray pulses which lead to complete and instantaneous destruction of protein molecules in the crystalline array would be destroyed completely by the X-ray pulse. However, before inducing such serious damages the strong X-ray pulse produces X-ray diffraction with sufficient intensity to enable X-ray structural analyses. In the X-ray diffraction experiments using SACLA, the X-ray pulse is sufficiently strong to destroy completely the protein structure and the crystalline array so that partially damaged protein molecules in the crystals which diffract X-rays are not produced during the X-ray diffraction experiments. Thus, only X-ray diffraction from the damage-free protein molecules in the regular array can be collected by this system. However, the pulse beam is too strong and too short to enable the acquisition of oscillation photographs. The position of a single shot of the pulse on a single crystal must be sufficiently separated from any position of the previous shots in order to avoid the X-ray damage effects induced by the previous shots. The extent of propagation of the X-ray irradiation damage was determined for the resting oxidized CcO crystals by evaluating the change in the integrity of the X-ray diffraction pattern at various positions within the crystal, depending on the proximity to the point of an individual XFEL shot. The integrity of the diffraction pattern was determined by an appropriately weakened X-ray beam. In the case of the resting oxidized CcO, a distance 50  $\mu\text{m}$  from neighboring beam foot prints has been found to be sufficient for X-ray diffraction experiments which avoid the influence of X-ray damage propagation from

previous shots (Hirata et al. 2014). However, this distance is likely to be applicable for most protein crystals, since CcO, which has one of the highest redox potentials among the proteins in the cell, is likely to be very sensitive to X-ray radiation damage, which leads to production of hydrated electrons. The newly developed method for X-ray structural determination which does not require oscillation photographs has been reported (Hirata et al. 2014).

The damage-free structure of the resting oxidized form at 1.9  $\text{\AA}$  resolution has been published and is shown in Fig. 18.3. As described above, an electron density peak assignable to a water molecule hydrogen-bonded to Y244 OH group increases with decreasing electron density of the bound peroxide by X-ray irradiation. The X-ray structure of the cyanide-bound oxidized CcO shows a weak electron density peak (37 % of the peak intensity due to a fixed water molecule with a low B-factor), indicating the presence of a partially occupied water molecule-hydrogen bonded to Y244 before X-ray irradiation, since cyanide replaces the bound peroxide in the resting oxidized form completely. As shown in the upper panel of Fig. 18.3, a region of weak electron density (38 % of the peak intensity due to a fixed water molecule with low B-factor) hydrogen-bonded to Y244 is detectable. This region of intensity confirms the absence of any significant radiation damage to the bound peroxide.

The damage free structure (Fig. 18.3, the lower panel) includes contribution from a pair of conformations with 95 % and 5 % occupancies. Both conformers indicate an O-O bond distance of 1.55  $\text{\AA}$ , which indicates that the bound peroxide is not in the activated state as previously proposed. The Fe-O distance is significantly longer than the Cu-O distance. The structure is consistent with the resonance Raman results which indicate an O-O bond length of 1.50  $\text{\AA}$ , although the minor conformer is not detectable in the resonance Raman spectrum. The resonance Raman band position suggests that the species is  $\text{O}_2^{2-}$  rather than  $^-\text{OOH}$  (Nakamoto 1997).





*Fig. 18.3.* X-ray structure of the O<sub>2</sub> reduction site of the resting oxidized bovine heart CcO, determined at an XFEL facility (SACLA). *Upper panel:*  $F_0-F_c$  difference map at 1.90 Å resolution for the XFEL data of CcO. Electron density cages at the  $3\sigma$  level ( $\sigma/0.041 \text{ e}/\text{\AA}^3$ ) are depicted with the structural model including Fe<sub>a<sub>3</sub></sub> (red), Cu<sub>B</sub> (blue), and oxygen atoms (light blue) of two water molecules, 2007 and 2034, which were not included in the structural refinements. The peak heights of both water molecules are  $9.0\sigma$ , while the peak height near Tyr244 is  $3.4\sigma$ . *Lower panel:* a stick model of the O<sub>2</sub> reduction site with a major component (95 %) and a minor component (5 %) of peroxide anions both with an O-O distance of 1.55 Å. The colors for designating atom species are the same as indicated for the upper panel. The numerical values indicated between the metal atoms and the oxygen atoms of the peroxide anions are their distances in Å (Reprinted with permission from “Hirata et al. 2014”).

Thus, in spite of the long Fe<sup>3+</sup>-O distance as a coordination bond, O<sub>2</sub><sup>2-</sup> is bridged between the two metals. This is consistent with the long-standing proposal that Fe<sub>a<sub>3</sub></sub><sup>3+</sup> in the resting oxidized state is in the high spin state (Day et al. 1993; Cheesman et al. 2004).

The negative charges on the bound peroxide in the resting oxidized state are likely to suppress the electron transfer from heme *a* to heme *a*<sub>3</sub> to block the proton pump. (In bovine heart CcO, oxidation of heme *a* to heme

*a*<sub>3</sub> drives proton active transport through the hydrogen bond network of the H pathway, which connects the N-phase and the P-phase (Yoshikawa et al. 2011).) Resonance Raman analyses of the O<sub>2</sub> reduction process by CcO have shown that the O state has OH<sup>-</sup> bound to the Fe<sub>a<sub>3</sub></sub><sup>3+</sup> site (Ogura et al. 1993). The structural difference of the O<sub>2</sub> reduction site between the resting oxidized CcO and the O form confirms the above proposal for the mechanism of blockage of the proton pump

by the bound  $O_2^{2-}$ . It is desirable to obtain a high resolution and damage free X-ray structure of the O form for comparison with the resting oxidized form. Such a comparison is expected to reveal various insights into the mechanism of the proton pump.

It is noteworthy that the successful determination of the damage-free X-ray structure of the resting oxidized CcO by the femtosecond level pulse (20 fs) from the XFEL facility indicates that X-ray structure of any protein can, in principle, be determined at high resolution with a time resolution of 20 fs, a much shorter time resolution than that of any physiological process driven by proteins in the cell. This finding is likely to induce a revolution in the Life Sciences as described in the following chapter.

## VII. Picobiology

Any life phenomenon is comprised of chemical reactions driven by proteins. Thus, elucidation of the mechanism of the protein function as the chemical reaction (namely as the behaviors of the atoms comprised in the functional site of the protein) is indispensable for complete understanding of *in vivo* phenomena. For elucidation of the mechanism of a protein function, the three dimensional location and the chemical reactivity of each atom in the functional site of the protein must be determined accurately by crystallographic (mainly X-ray crystallographic) and vibrational (mainly infrared) spectroscopic analyses, respectively. The chemical reactivity of an individual atom is determined by the characteristic of the chemical bonds to that atom. Vibrational spectroscopy is the best method for examination of the chemical reactivity of any atom. The location and the chemical reactivity of each atom in the functional site undergo significant changes concomitant with the progression of the physiological (or chemical) reaction process driven by the protein. Thus, time-resolved techniques are required for both crystallography and vibrational spectroscopy.

X-ray structures provide atomic coordinates of all the atoms of the protein at a resolution of 0.1 Å at the highest. However, the chemical reactivity of an individual atom is sensitively influenced by chemical bond length differences in the picometer range (in the vicinity of 0.01 Å or  $10^{-12}$  m or shorter). Furthermore, crystallographically-determined electron density of proteins generally does not provide information regarding the chemical reactivity of atoms. The chemical bond length can be determined accurately by infrared spectroscopy at a resolution better than 1 picometer. However, infrared spectroscopy does not provide information regarding the three-dimensional arrangement of atoms. In other words, infrared spectroscopy determines bond length of a chemical bond regardless of the location of the bond in the protein. Thus, both vibrational and crystallographic techniques are indispensable. Therefore, we suggest the term, “picobiology”, as a descriptive term referring to a scientific field which has the objective of understanding the mechanism of protein function in terms of the behavior of atoms (i.e. as a set of chemical reactions) based on structural analyses at the picometer level by using a combination of vibrational and crystallographic techniques.

It should be noted that the functional site of a protein is in most cases buried inside the protein moiety. As a result, the functional site may have a specialized microenvironment for a given chemical reaction which is definitely different from the environment outside of the protein. The chemical reactivity of any atom is sensitively influenced by its environment. For example, the proton affinity of an O atom of a terminal carboxyl group of acetate is highly sensitive to the polarity of the medium. In fact, the pKa value the terminal carboxyl group increases from 5 to 10 upon exchange of the medium from water to methanol (Isaacs 1995). In the functional site, various amino acid residues and cofactor molecules are arranged in three dimensional space to provide various unique microenvironments which cannot be artifi-

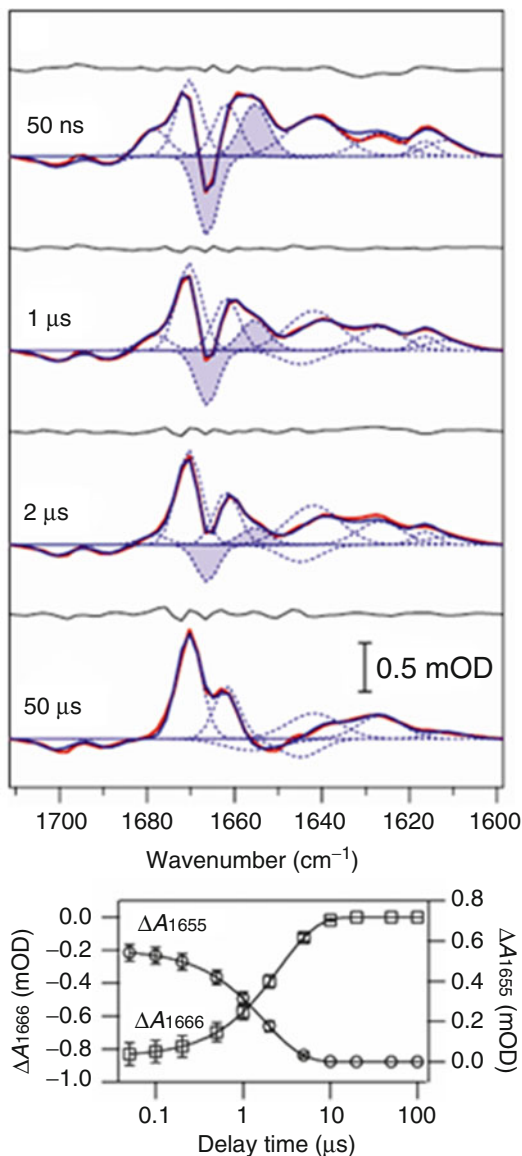
cially duplicated accurately in a non-protein model system. Thus, it is impossible to accurately predict the chemical reactivity of atoms (or functional groups) of a functional site based on an analysis conducted outside of the protein. Therefore, direct measurement of the chemical reactivity of the atoms in the functional site by infrared spectroscopy as well as a determination of the three dimensional location of atoms in the active site of the protein is absolutely necessary in order to elucidate the reaction mechanism. However, infrared spectroscopy is not appropriate for samples in aqueous solution, because water molecules have strong infrared absorption. While most proteins function in aqueous solution, the integral membrane proteins which are embedded in the biological membrane have hydrophilic surfaces at their ends which extend into both aqueous phases. In fact, it is essentially impossible to transfer membrane proteins into organic solvent without denaturation. Thus, even the integral membrane proteins cannot function without aqueous phases.

As described above, X-ray structural information intrinsically does not provide direct information regarding the chemical reactivity of atoms within a protein. Thus, in the past, the mechanisms that produce protein functions have been estimated by X-ray structures determined at various intermediate states experimentally stabilized in its crystals and by assuming that the chemical reactivity of atoms in the functional site is identical or similar to that determined in homogeneous system in the outside of the protein. However, this assumption is not practical as described above. In other words, without the direct infrared information on the chemical reactivity of the atoms, it is essentially impossible to discover the process (or the chemical reaction) which can be driven only by the protein microenvironment.

A time-resolved infrared system applicable for investigation of aqueous protein systems has been recently constructed. This system is equipped with a strong infrared light source created by a femtosecond pulse laser system and a highly sensitive

infrared multichannel detector, and provides time resolution at the picosecond level and sensitivity sufficient for detection of a single C=O stretch band of an  $\alpha$ -helix in the amide I and II region with accuracy of  $\pm 10\%$  at the peak position in H<sub>2</sub>O (Kubo et al. 2013).

This system has been used to examine the process of CO release after flash photolysis of CO-bound CcO which is analogous to the reverse reaction of O<sub>2</sub> binding to Fe<sub>a3</sub><sup>2+</sup>. Figure 18.4 shows the infrared spectral change after CO release in the amide I and II region between 1750 and 1600 cm<sup>-1</sup> and in the time range from 50 ns to 50  $\mu$ s. There is a prominent spectral change that generates peak/trough positions at 1655 and 1666 cm<sup>-1</sup>, respectively. The band positions and intensities suggest that a single main chain C=O group in a bulge conformation (or not involved in  $\alpha$ -helix) becomes incorporated into the  $\alpha$ -helix within the dead time (50 ns, the duration between photolysis and the time when measurement of the spectrum is initiated). The infrared spectral changes in the C-O triple bond stretch region indicate stoichiometric migration of CO from Fe<sub>a3</sub><sup>2+</sup> to Cu<sub>B</sub><sup>1+</sup> within the dead time, followed by release of the CO bound at Cu<sub>B</sub> at  $t_{1/2}$  at about 2  $\mu$ s without rebinding of CO to Fe<sub>a3</sub> (Kubo et al. 2013). Concomitant with the CO release, the 1655/1666 cm<sup>-1</sup> band disappears as shown in Fig. 18.4, indicating formation of a bulge conformation. In order to identify the position of the main chain C=O group, examination of the site-directed isotope shift effect is necessary. However, a cell-free synthesis system for site-directed isotope labeling has not been constructed for bovine heart CcO. On the other hand, X-ray structural results reported thus far indicate that a bulge/ $\alpha$ -helix conformational transition coupled with a  $\alpha$ -helix/bulge conformational transition upon CO binding to the fully reduced CcO is detectable only in the segment of helix X including S382 and V380 (Kubo et al. 2013). Thus, the spectral changes in the 1655/1666 cm<sup>-1</sup> bands are reasonably assignable to the movement (or conformational change) of the S382/V380 segment.



*Fig. 18.4.* Time-resolved infrared difference spectra of CcO in H<sub>2</sub>O buffer. *Upper panel:* Difference of infrared spectrum as a function of time after flash photolysis relative to the spectrum obtained before photolysis (i.e. spectrum after photolysis minus the spectrum of CO-bond CcO). *Red:* measured spectra, *Blue:* Fitted spectra, with each Gaussian component shown by a dotted curve. The fitting residual is also shown for each spectrum. *Lower panel:* Changes in intensities of the peak (1655 cm<sup>-1</sup>) and trough (1666 cm<sup>-1</sup>) of the *shadowed band pair* showing the most prominent spectral changes. *Error bars* represent the standard deviation of five independent experiments performed on different days using different batches of CcO preparation (Reprinted with permission from “Kubo et al. 2013”).

The conformational change plays a crucial role in proton pump. As mentioned above, in bovine heart CcO, protons are pumped through the H-pathway (a proton conducting

pathway) which is composed of a hydrogen-bond network and a water channel operating in tandem (Yoshikawa et al. 2011). Protons for pumping are transferred as hydronium ion

from the N-phase through the water channel to the bottom end of the hydrogen bond network. The protons arriving at the hydrogen-bond network are actively transported to the P-phase by electrostatic repulsion between the protons and the positive charge of heme *a* which is attached to the hydrogen bond network via hydrogen bonds connected to the peripheral groups of heme *a*. The positive charge of heme *a* is created upon electron transfer from  $\text{Fe}_a$  to the  $\text{O}_2$  reduction site. In the fully reduced and ligand-free state, S382, located near the water channel, is included in helix X, while the main chain C=O of V380 is included in the bulge conformation. The bulge has no significant influence on the conformation of the water channel of the H-pathway. The X-ray structural analyses indicate that upon CO binding to  $\text{Fe}_{a3}^{2+}$ , S382 migrates to form a bulge conformation accompanied by incorporation of V380 into helix X (Muramoto et al. 2010). Similar conformational changes are likely to occur also upon  $\text{O}_2$  binding to  $\text{Fe}_{a3}^{2+}$ . This bulge blocks water molecule (or hydronium ion) access through the water channel to the bottom end of the hydrogen-bond network in the H-pathway. Furthermore, the blockage prevents backward leakages of protons from the hydrogen-bond network. Thus, protons for pumping must be drawn into the hydrogen-bond network before  $\text{O}_2$  is bound to  $\text{Fe}_{a3}$ . The intermediate conformation formed within the dead time as shown in Fig. 18.4 is likely to be a conformation which promotes proton collection from the N-phase. Formation of the intermediate conformation is coupled with CO binding to  $\text{Cu}_B$ . This suggests the existence of a relay system between  $\text{Cu}_B$  and S382. The coupling suggests that  $\text{O}_2$  is transiently bound to  $\text{Cu}_B$  before binding to  $\text{Fe}_{a3}$ . This CO binding to  $\text{Cu}_B$  promotes proton collection for pumping before the initiation of  $\text{O}_2$  reduction, which is critical for effective proton pump. Determination of the X-ray structure of the intermediate species induced by the ligand binding to  $\text{Cu}_B$ , as detected by

the time-resolved infrared analysis, is necessary to determine the significance of the infrared data with respect to the intermediate species.

The above time-resolved infrared results show that, using this system, the infrared absorption spectral changes due to a single C=O stretch can be accurately observed even in the frequency region which includes intense absorption by  $\text{H}_2\text{O}$  molecules. This system is applicable for any aqueous protein solution. Thus, one of the two most significant problems encountered in picobiology investigations has now been solved.

The second of the two most significant problems, time-resolved X-ray structural analysis, has been solved recently (Hirata et al. 2014). As described in the preceding chapter, a damage free X-ray structure of the resting oxidized CcO has been determined at 1.9 Å resolution using a femtosecond X-ray pulse generated at an XFEL facility. The results indicate that, in principle, an X-ray structure of any protein can be determined at a time resolution of 20 fs at high resolution. Although a number of issues relating specific analyses of various class of proteins must be solved before practical use of these facilities become widespread, it is now believed that the investigations in new field of “picobiology” are now possible as a result of the significant advances in these time-resolved X-ray and infrared techniques.

## Acknowledgments

This work is supported by a Grant-in-Aid for the Global Center of Excellence Program, for the Targeted Protein Research Program, for Scientific Research (A) 2247012 and (B) 26234567, by the Japanese Ministry of Education, Culture, Sports, Science and Technology, and by JST, CREST. S. Yoshikawa is a Senior Visiting Scientist in the RIKEN Harima Institute.

## References

- Antonini E, Brunori M, Colosimo A, Greenwood C, Wilson MT (1977) Oxygen “pulsed” cytochrome *c* oxidase: functional properties and catalytic relevance. *Proc Natl Acad Sci U S A* 74:3128–3132
- Aoyama H, Muramoto K, Shinzawa-Itoh K, Hirata K, Yamashita E, Tsukihara T, Ogura T, Yoshikawa S (2009) A peroxide bridge between Fe and Cu ions in the O<sub>2</sub> reduction site of fully oxidized cytochrome *c* oxidase could suppress the proton pump. *Proc Natl Acad Sci U S A* 106:2165–2169
- Artzbatanov VY, Konstantinov AA, Skulachev VP (1978) Involvement of intramitochondrial protons in redox reactions of cytochrome alpha. *FEBS Lett* 87:180–185
- Baker GM, Noguchi M, Palmer G (1987) The reaction of cytochrome oxidase with cyanide. Preparation of the rapidly reacting form and its conversion to the slowly reacting form. *J Biol Chem* 262:595–604
- Bloch D, Belevich I, Jasaitis A, Ribacka C, Puustinen A, Verkhovsky MI, Wikström M (2004) The catalytic cycle of cytochrome *c* oxidase is not the sum of its two halves. *Proc Natl Acad Sci U S A* 101:529–533
- Brandt U, Schägger H, von Jagow G (1989) Purification of cytochrome-*c* oxidase retaining its pulsed form. *Eur J Biochem* 182:705–711
- Burke JM, Kincaid JR, Peters S, Gagne RR, Collman JP, Spiro TG (1978) Structure-sensitive resonance Raman bands of tetraphenyl and “picket fence” porphyrin-iron complexes, including an oxy-hemoglobin analog. *J Am Chem Soc* 100:6083–6088
- Chang H-Y, Hemp J, Chen Y, Fee JA, Gennis RB (2009) The cytochrome *ba*<sub>3</sub> oxygen reductase from *Thermus thermophilus* uses a single input channel for proton delivery to the active site and for proton pumping. *Proc Natl Acad Sci U S A* 106:16169–16173
- Cheesman MR, Oganessian VS, Watmough NJ, Butler CS, Thomson AJ (2004) The nature of the exchange coupling between high-spin Fe(III) heme *o*<sub>3</sub> and Cu<sub>B</sub>II in *Escherichia coli* quinol oxidase, cytochrome *bo*<sub>3</sub>: MCD and EPR studies. *J Am Chem Soc* 126:4157–4166
- Collman JP, Sunderland CJ, Berg KE, Vance MA, Solomon EI (2003) Spectroscopic evidence for a heme-superoxide/Cu(I) intermediate in a functional model of cytochrome *c* oxidase. *J Am Chem Soc* 125:6648–6649
- Cooper CE, Salerno JC (1992) Characterization of a novel g' = 2.95 EPR signal from the binuclear center of mitochondrial cytochrome *c* oxidase. *J Biol Chem* 267:280–285
- Day EP, Peterson J, Sendova MS, Schoonover J, Palmer G (1993) Magnetization of fast and slow oxidized cytochrome *c* oxidase. *Biochemistry* 32:7855–7860
- Dodson ED, Zhao XJ, Caughey WS, Elliott CM (1996) Redox dependent interactions of the metal sites in carbon monoxide-bound cytochrome *c* oxidase monitored by infrared and UV/visible spectroelectrochemical methods. *Biochemistry* 35:444–452
- Du W-GH, Noodleman L (2013) Density functional study for the bridged dinuclear center based on a high-resolution X-ray crystal structure of *ba*<sub>3</sub> cytochrome *c* oxidase from *Thermus thermophilus*. *Inorg Chem* 52:14072–14088
- Hirata K, Shinzawa-Itoh K, Yano N, Takemura S, Kato K, Hatanaka M, Muramoto K, . . . , Ago H (2014) Determination of damage-free crystal structure of an X-ray-sensitive protein using an XFEL. *Nat Methods* 11:734–736
- Isaacs NS (1995) *Physical Organic Chemistry*, 2nd edn. Longman Scientific & Technical, Harlow
- Kaila VRI, Verkhovsky MI, Wikström M (2010) Proton-coupled electron transfer in cytochrome oxidase. *Chem Rev* 110:7062–7081
- Kim E, Chufán EE, Kamaraj K, Karlin KD (2004) Synthetic models for heme-copper oxidases. *Chem Rev* 104:1077–1133
- Koepke J, Olkhova E, Angerer H, Müller H, Peng G, Michel H (2009) High resolution crystal structure of *Paracoccus denitrificans* cytochrome *c* oxidase: new insights into the active site and the proton transfer pathways. *Biochim Biophys Acta* 1787:635–645
- Konstantinov AA, Siletsky S, Mitchell D, Kaulen A, Gennis RB (1997) The roles of the two proton input channels in cytochrome *c* oxidase from *Rhodobacter sphaeroides* probed by the effects of site-directed mutations on time-resolved electrogenic intraprotein proton transfer. *Proc Natl Acad Sci U S A* 94:9085–9090
- Kubo M, Nakashima S, Yamaguchi S, Ogura T, Mochizuki M, Kang J, Tateno M, . . . , Yoshikawa S (2013) Effective pumping proton collection facilitated by a copper site (Cu<sub>B</sub>) of bovine heart cytochrome *c* oxidase, revealed by a newly developed time-resolved infrared system. *J Biol Chem* 288:30259–30269
- Mitchell R, Brown S, Mitchell P, Rich PR (1992) Rates of cyanide binding to the catalytic intermediates of mammalian cytochrome *c* oxidase, and the effects of cytochrome *c* and poly(L-lysine). *Biochim Biophys Acta* 1100:40–48
- Mochizuki M, Aoyama H, Shinzawa-Itoh K, Usui T, Tsukihara T, Yoshikawa S (1999) Quantitative reevaluation of the redox active sites of crystalline bovine heart cytochrome *c* oxidase. *J Biol Chem* 274:33403–33411

- Moody AJ (1996) 'As prepared' forms of fully oxidised haem/Cu terminal oxidases. *Biochim Biophys Acta* 1276:6–20
- Muramoto T, Ohta K, Shinzawa-Itoh K, Kanda K, Taniguchi M, Nabekura H, Yamashita E, . . . , Yoshikawa S (2010) Bovine cytochrome *c* oxidase structures enable O<sub>2</sub> reduction with minimization of reactive oxygens and provide a proton-pumping gate. *Proc Natl Acad Sci U S A* 107:7740–7745
- Nakamoto K (1997) Infrared and Raman spectra of inorganic and coordination compounds, Part B, 5th edn. Wiley, New York
- Naqui A, Kumar C, Ching YC, Powers L, Chance B (1984) Structure and reactivity of multiple forms of cytochrome oxidase as evaluated by X-ray absorption spectroscopy and kinetics of cyanide binding. *Biochemistry* 23:6222–6227
- Ogura T, Takahashi S, Hirota S, Shinzawa-Itoh K, Yoshikawa S, Appelman EH, Kitagawa T (1993) Time-resolved resonance Raman elucidation of the pathway for dioxygen reduction by cytochrome *c* oxidase. *J Am Chem Soc* 115:8527–8536
- Pereira MM, Sousa FL, Veríssimo AF, Teixeira M (2008) Looking for the minimum common denominator in haem-copper oxygen reductases: towards a unified catalytic mechanism. *Biochim Biophys Acta* 1777:929–934
- Proshlyakov DA, Ogura T, Shinzawa-Itoh K, Yoshikawa S, Appelman EH, Kitagawa T (1994) Selective resonance Raman observation of the "607 nm" form generated in the reaction of oxidized cytochrome *c* oxidase with hydrogen peroxide. *J Biol Chem* 269:29385–29388
- Proshlyakov DA, Ogura T, Shinzawa-Itoh K, Yoshikawa S, Kitagawa T (1996) Microcirculating system for simultaneous determination of Raman and absorption spectra of enzymatic reaction intermediates and its application to the reaction of cytochrome *c* oxidase with hydrogen peroxide. *Biochemistry* 35:76–82
- Qin L, Hiser C, Mulichak A, Garavito RM, Ferguson-Miller S (2006) Identification of conserved lipid/detergent-binding sites in a high-resolution structure of the membrane protein cytochrome *c* oxidase. *Proc Natl Acad Sci U S A* 103:16117–16122
- Sakaguchi M, Shinzawa-Itoh K, Yoshikawa S, Ogura T (2010) A resonance Raman band assignable to the O–O stretching mode in the resting oxidized state of bovine heart cytochrome *c* oxidase. *J Bioenerg Biomembr* 42:241–243
- Siletsky SA, Konstantinov AA (2012) Cytochrome *c* oxidase: charge translocation coupled to single-electron partial steps of the catalytic cycle. *Biochim Biophys Acta* 1817:476–488
- Tiefenbrunn T, Liu W, Chen Y, Katritch V, Stout CD, Fee JA, Cherezov V (2011) High resolution structure of the *ba*<sub>3</sub> cytochrome *c* oxidase from *Thermus thermophilus* in a lipidic environment. *PLoS One* 6:e22348
- Tsubaki M, Nagai K, Kitagawa T (1980) Resonance Raman spectra of myoglobins reconstituted with spiroporphyrin and isosprioporphyrin hemes and iron 2,4-diformylprotoporphyrin IX. Effect of formyl substitution at the heme periphery. *Biochemistry* 19:379–385
- Tsukihara T, Aoyama H, Yamashita E, Tomizaki T, Yamaguchi H, Shinzawa-Itoh K, Nakashima R, . . . , Yoshikawa S (1995) Structures of metal sites of oxidized bovine heart cytochrome *c* oxidase at 2.8 Å. *Science* 269:1069–1074
- Tsukihara T, Aoyama H, Yamashita E, Tomizaki T, Yamaguchi H, Shinzawa-Itoh K, Nakashima R, . . . , Yoshikawa S (1996) The whole structure of the 13-subunit oxidized cytochrome *c* oxidase at 2.8 Å. *Science* 272:1136–1144
- van Wart HE, Zimmer J (1985) Resonance Raman evidence for the activation of dioxygen in horseradish oxyperoxidase. *J Biol Chem* 260:8372–8377
- Verkhovskiy MI, Jasaitis A, Verkhovskaya ML, Morgan JE, Wikström M (1999) Proton translocation by cytochrome *c* oxidase. *Nature* 400:480–483
- Verkhovskiy MI, Tuukkanen A, Backgren C, Puustinen A, Wikström M (2001) Charge translocation coupled to electron injection into oxidized cytochrome *c* oxidase from *Paracoccus denitrificans*. *Biochemistry* 40:7077–7083
- Weng LC, Baker GM (1991) Reaction of hydrogen peroxide with the rapid form of resting cytochrome oxidase. *Biochemistry* 30:5727–5733
- Wikström M (2012) Active site intermediates in the reduction of O<sub>2</sub> by cytochrome oxidase, and their derivatives. *Biochim Biophys Acta* 1817:468–475
- Wigglesworth JM (1984) Formation and reduction of a 'peroxy' intermediate of cytochrome *c* oxidase by hydrogen peroxide. *Biochem J* 217:715–719
- Wigglesworth JM, Elsdon J, Chapman A, Van der Water N, Grahn MF (1988) Activation by reduction of the resting form of cytochrome *c* oxidase: tests of different models and evidence for the involvement of Cu<sub>B</sub>. *Biochim Biophys Acta* 936:452–464
- Yonetani T (1961) Studies on cytochrome oxidase III. Improved preparation and some properties. *J Biol Chem* 236:1680–1688
- Yoshikawa S, Shinzawa-Itoh K, Nakashima R, Yaono R, Yamashita E, Inoue N, Yao M, . . . , Tsukihara T (1998) Redox-coupled crystal structural changes in bovine heart cytochrome *c* oxidase. *Science* 280:1723–1729
- Yoshikawa S, Muramoto K, Shinzawa-Itoh K (2011) Proton-pumping mechanism of cytochrome *c* oxidase. *Ann Rev Biophys* 40:205–223

# Chapter 19

## Structure and Mechanism of Action of the Alternative Quinol Oxidases

Luke Young<sup>a</sup>, Benjamin May<sup>a</sup>, Tomoo Shiba<sup>b</sup>, Shigeharu Harada<sup>b</sup>, Daniel Ken Inaoka<sup>c</sup>, Kiyoshi Kita<sup>c</sup>,  
and Anthony L. Moore<sup>a,\*</sup>

<sup>a</sup>*Biochemistry and Molecular Sciences, School of Life Sciences,  
University of Sussex, Falmer, Brighton BN1 9QG, UK*

<sup>b</sup>*Department of Applied Biology, Graduate School of Science  
and Technology, Kyoto Institute of Technology, 606-8585 Kyoto,  
Japan*

<sup>c</sup>*Department of Biomedical Chemistry, Graduate School of  
Medicine, The University of Tokyo, 113-0033 Tokyo, Japan*

Summary.....	375
I. General Introduction.....	376
II. Overall Structure of the Alternative Oxidases.....	377
A. Role and Location of Universally Conserved Residues.....	377
B. The Hydrophobic Nature of the Protein.....	380
C. Structure of the Di-iron Core.....	381
III. Mechanism of Di-oxygen Reduction by the Alternative Oxidases.....	385
A. General Characteristics of Oxygen Reduction.....	385
B. Proposed Reaction Mechanism.....	385
1. Structure of the Fully Reduced Di-iron Core.....	385
2. Initial Reaction of the Di-iron Core with Oxygen.....	386
3. Rearrangement of the Core.....	388
C. Quinol Oxidation Mechanism.....	389
IV. Concluding Remarks.....	391
Acknowledgments.....	392
References.....	392

### Summary

In addition to heme-copper oxidases, all higher plants, some algae, yeasts, molds, metazoans, and pathogenic microorganisms such as *Trypanosoma brucei* contain an additional terminal oxidase, the cyanide- and antimycin-insensitive alternative oxidase (AOX). It is a di-iron carboxylate protein that catalyzes the four-electron reduction of dioxygen to water by ubiquinol, short-circuiting the mitochondrial electron-transport chain prior to proton

---

\*Author for correspondence, e-mail: [a.l.moore@sussex.ac.uk](mailto:a.l.moore@sussex.ac.uk)



translocation by complexes III and IV, thereby dramatically reducing ATP formation. In plants, it plays a key role in cellular metabolism, thermogenesis, and energy homeostasis and is generally considered to be a major stress-induced protein. In *T. brucei*, a parasite that causes human African sleeping sickness, AOX plays a critical role in the survival of the parasite in its bloodstream form. Because AOX is absent from mammals, this protein represents a unique and promising therapeutic target. Despite its bioenergetic and medical importance, however, until recently structural features of any AOX were unknown. In this review we describe recent advances in our understanding of this protein's structure following the recent successful crystallization of the alternative oxidase from *T. brucei*. We focus on the nature of the active site and ubiquinol-binding channels and describe a mechanism for the reduction of oxygen to water based on these structural insights.

## I. General Introduction

The alternative oxidase (AOX) is a monotopic protein with a diverse profile of postulated roles within cells, with each role being dependent upon the cell in which it is located. The protein is ubiquitous within the plant kingdom, in which it predominantly plays an energy homeostatic role. Readers are referred to recent reviews on this topic (Moore et al. 2013; Vanlerberghe 2013).

The most well documented role of AOX is in thermogenic plants, particularly those from the *Araceae* family. Thermogenic plants generate heat well above ambient temperatures through engagement of the alternative pathway (Meeuse 1975; Seymour et al. 2003). Energy released as a result of the direct reduction of oxygen through to water during the operation of this pathway results in heat generation since AOX is non-protonmotive (Moore et al. 1978). In thermogenic plants heat is used to either volatilize primary amines to attract insects for pollination purposes, as is the case in the voodoo lily (*Sauromatum guttatum*) and *Arum maculatum* (Lords & Ladies), or to melt the

surrounding ice, as occurs in skunk cabbage (*Symplocarpus foetidus*) (Seymour 2010).

In trypanosomes, the protozoa responsible for diseases such as Human African Trypanosomiasis (HAT) and nagana in livestock, AOX plays a more pivotal role within the electron transport chain. In its bloodstream form within the host, trypanosomes down regulate the expression of respiratory chain complexes III and IV (Grant et al. 1961), leaving the parasite dependent solely upon AOX as the terminal oxidase. Since oxidative phosphorylation can now no longer occur within the bloodstream form of the parasite, ATP is generated via glycolysis (Bienen et al. 1993) and the principal role of AOX is to regenerate cytosolic  $\text{NAD}^+$  via a glycerol-3-phosphate re-oxidation system. Such a critical metabolic role for AOX, coupled with the lack of the protein in mammalian systems, has led to AOX being considered as a potential chemotherapeutic target for the treatment of HAT (Nihei et al. 2002).

The recent success in crystallisation of the AOX (Shiba et al. 2013) from *Trypanosoma brucei brucei* (TAO) allows a much more detailed investigation of the active site and highly conserved residues than has hitherto been possible. Previous structural predictions that the protein contains a non-heme di-iron center surrounded by a four-helix bundle in which the metal core is ligated by four glutamic acids and two histidines (Moore et al. 1995; Siedow et al. 1995; Andersson and Nordlund 1999; Berthold et al. 2000) have proven essentially correct and, alongside the

---

*Abbreviations:* AOX – Alternative oxidase; Asco – Ascofuranone; CB – Colletochlorin B; HAT – Human African Trypanosomiasis; MMO – Methane monooxygenase; OG – Octyl gallate; PCET – Proton-coupled electron transport;  $\text{Q}(\text{H}_2)$  – (Reduced) ubiquinone; RBR – Rubrerythrin; RNR – Ribonucleotide reductase; rSgAOX' – Recombinant *Sauromatum guttatum* alternative oxidase; SHAM – Salicylic hydroxamic acid; TAO – Trypanosomal alternative oxidase

crystal structure, confirm that the AOX is indeed a legitimate member of the di-iron carboxylate superfamily, which includes other oxygen reductive species such as methane monooxygenase (MMO) and ribonucleotide reductase (RNR) (Lipscomb 1994; Kolberg et al. 2004).

While the active-sites of these proteins are similar, they undergo very different enzymatic reactions. MMO uses the oxygen to generate a high valent Fe(IV) (Shu et al. 1997) state for the conversion of methane to methanol, a reaction that has resulted in considerable scientific interest due to its catalytic conversion of a volatile gas into a transportable liquid at room temperature. RNR on the other hand uses the di-iron core to reduce ribonucleotides through to deoxyribonucleotides for use in DNA synthesis (Kolberg et al. 2004).

In this review we will consider in detail the crystallographic structure of the trypanosomal enzyme since it provides a useful framework in which to examine the mechanism of oxygen reduction by this family of proteins. Unlike the plant variant, the parasitic AOX, however, does not appear to be regulated either by a disulfide/sulfhydryl system (Umbach and Siedow 1993; Rhoads et al. 1998) nor activated by pyruvate (Millar et al. 1993; Umbach et al. 2002), effectively existing as a 'stripped-down' more simplistic version of the protein which is found in plant and fungi. We discuss salient structural features that are common to all AOX proteins and suggest a mechanism for the four-electron reduction of oxygen to water. For a discussion of terminal oxidases of cyanobacteria, including alternative respiratory terminal oxidases (ARTOs), see the Chap. 17 by Schmetterer in this volume.

## II. Overall Structure of the Alternative Oxidases

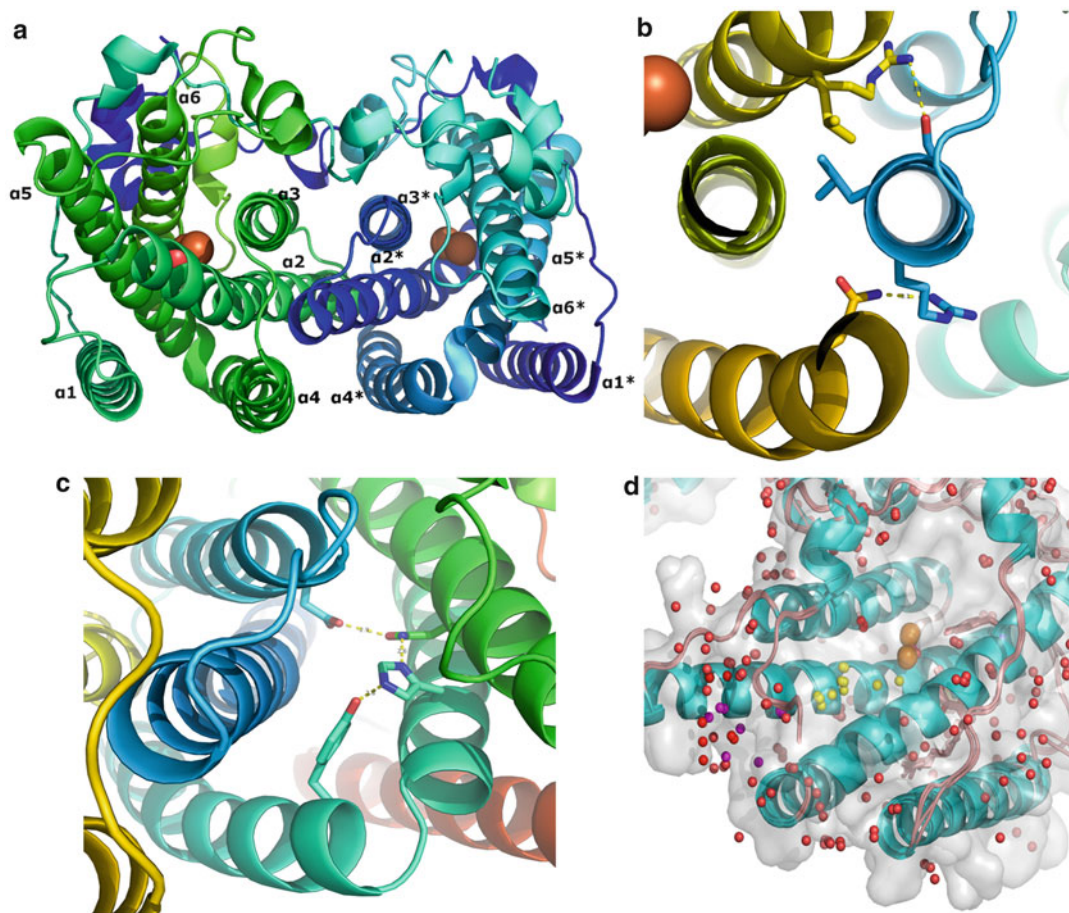
TAO was crystallised as a homodimer (Fig. 19.1a), with each monomer being comprised of six  $\alpha$ -helices arranged in an anti-parallel fashion, four of which form

a characteristic four helix bundle which acts as a scaffold to bind the di-ion core. The two remaining helices (helices 1 and 4) are membrane binding, anchoring the protein to the phospholipid bilayer. Since there are in excess of 850 AOX sequences deposited in the database it is possible to determine the identity and location of those residues that are either partially or fully conserved across the AOX protein family. Conservation of amino acids within a protein family suggests that specific amino acids are important to the overall function of the protein, and can usually be attributed to either fulfilling a structural or mechanistic role, with some undertaking both functions. Sequence alignment of a cross section of AOX sequences from fungal, pathogenic and plant species reveals that there are a total of 72 conserved residues, 46 of which appear to be fully conserved across the entire currently sequenced AOX family. In this section we attempt to ascribe a function to a number of what we consider to be the most important of these conserved residues.

### A. Role and Location of Universally Conserved Residues

In order to understand the possible role of conserved residues or regions it is important to consider their structural location. Table 19.1 summarizes the location of these residues in addition to suggesting a predicted function of the residue based on an analysis of the crystal structure. It is readily apparent from Table 19.1 that in addition to a number of single residues that are conserved throughout the structure, there are also regions of highly conserved amino-acids.

The larger conserved regions are predominantly residues surrounding the metal binding ligands, namely in the LETVA, NERMHL, GYLEEEA and RADEAxHR regions (where red letters are the metal ligands). A high level of conservation in this region is not surprising, given the crucial nature of the metallic core to the overall function of the protein, since perturbations caused by mutation would likely render the protein



*Fig. 19.1.* (a) Crystal structure of TAO dimer (PDB accession code 3VV9). Di-iron center shown as *brown spheres*, with helical numbering added for reference. (b) Cross section of the SLR region between dimers, showing hydrogen bonds between S141 and R163\*, and potentially between R143 and Q187\*. L142 and L166\* also shown, capping the interdimer gap with hydrophobic residues. (c) Hydrogen bond network linking four helices, consisting of Y198, H206, N273 and E158, non hydrogen bonding amino acids removed for clarity. (d) Water distribution throughout the crystal structure, shown with the four monomers of AOX inhibited with coltochlorin B overlaid (PDB: 3W54). *Yellow spheres* denote water within the structure, *red spheres* are water on the surface, and iron is shown as *orange spheres* in the centre. Helix 6 removed for clarity.

inactive. As expected, mutation of the iron binding residues in both the TAO (Ajayi et al. 2002; Nakamura et al. 2005) and plant AOX (Albury et al. 2002; Berthold et al. 2002) leads to a complete loss of enzymatic activity.

The SLR region (Fig. 19.1b) is located at the C-terminal end of helix 2 and is largely responsible for capping the dimer interface to either end of the protein. S141 forms a hydrogen bond with R163 (of NERMHL) to maintain the dimer formation between helices  $\alpha 2$  and the neighbouring monomer

$\alpha 3^*$ . A similar bond is also found at the opposite end of these two helices, with identical bond formation between helices  $\alpha 2^*$  and  $\alpha 3$  thereby effectively locking the helices together. The role of the R143 is less defined, given its location on the membrane face of helix  $\alpha 2$ . There is potential for hydrogen bond formation between R143 and Q187 on helix  $\alpha 4^*$ , but given the variability on the rotameric positions between monomers it is more likely that both amino acids play a role in anchoring the protein to the membrane. L142

Table 19.1. Highly conserved amino acids throughout the sequence alignment, and their predicted roles within the structure based upon crystal structure analysis.

AA sequence	TAO numbering	Region	Role
W	65	N-terminal	
H	77	N-terminal	
D	85	Helix 1	
R	96	Helix 1	Substrate binding
D	100	Helix 1	Substrate bind
R	118	Helix 2	Substrate binding
LETVA	122-126	Helix 2	Iron ligation
VPGMV	128-132	Helix 2	Varied
H	138	Helix 2	
SLR	141-143	Helix 2	Varied
GWI	150-152	Helix 3	Varied
L	155	Helix 3	
EA	158-159	Helix 3	
E	160	Helix 3	
NERMHL	161-166	Helix 3	iron ligation
F	169	Helix 3	
P	175	Between 3 + 4	Interhelix bend
R	180	Helix 4	
Q	187	Helix 4	
Y	198	Helix 4	Interhelical binding
L	199	Between 4 and 5	
SPR	201-203	Between 4 and 5	Interhelix bend
HR	206-207	Helix 5	
VGYLEEEA	209-216	Helix 5	Varied
YT	220-221	Helix 5	Redox active tyr
D	228	Helix 5	
G	230	Helix 5	
P	240	Between 5 and 6	
A	243	Between 5 and 6	
YW	246-247	Short helix	Structural/electron transport
D	257	Helix 6	Structural
RADEA	263-267	Helix 6	Iron ligation
HR	269-270	Helix 6	Iron ligation
VNH	272-274	Helix 6	Interhelical
P	290	C terminal	

Numbering taken from the *Sauromatum guttatum* sequence. Residues in red correspond to universally conserved amino acids

probably also plays a dual role, effectively capping the dimer interface with a hydrophobic residue and locking the helix into place through interaction with L166 located in the NERMHL region.

The membrane face of helix 4 is coated with hydrophobic residues which provide additional interaction with the phospholipid bilayer. While the conserved residues on helix

1 and 4 are mainly polar in nature and will bind directly to anchor points on the membrane surface, valine residues provide repulsion from the water layer on the membrane, thereby preventing the protein from embedding too far into the phospholipid bilayer.

The totally conserved tyrosine residue (Y198), which is located towards the C-terminal end of helix 4, is part of a hydrogen

bond network, which spans 4 helices. It appears that one of its main functions is to provide structural stability (Fig. 19.1c). It maintains the helical turn caused by P202 via formation of a hydrogen bond to H206 (Helix 5), which itself is further stabilised by N273 (helix 6) and E158 (Helix 3). While a majority of amino acids have a highly conserved rotameric position, the E158 appears to be fixed in one of two positions perpendicular from one-another dependent upon the location of the proximal crystallized water which co-crystallized with TAO (Shiba et al. 2013). CAVER (Chovancova et al. 2012) analysis reveals that a channel runs directly through these residues (E158, Y198, H206 and N273) from the protein exterior to the di-iron core. One of the features of the protein is the use of an aqueous channel, either for the transport of water away from the active site after the reaction is complete, or for the transport of protons into the active site. This notion is supported by the structures depicted in Fig. 19.1d which show an overlay of the four monomers from a single TAO crystal, revealing a pathway of internal water molecules (shown as yellow spheres) co-crystallised within the structure.

The hydrophobic channel itself is reasonably well conserved, consisting of a combination of hydrophobic and polar residues. Analysis of the pKa values of these polar residues, namely E158, Y198 and H206, using PropKa (Li et al. 2005), reveals a directional increase in pKa from the core to Y198 at the entrance of the tunnel, suggesting that if this channel is indeed used to transfer protons, the residues are aligned in such a manner that the route of proton transfer is towards the active site. While mutation of Y198 or H206 to alanine results in an inactive protein (Albury et al. 2010), this is most probably due to disruption of the tertiary structure rather than to a loss of the aqueous channel. Interestingly, a Y198F mutant retains approximately 50 % of its activity (Albury et al. 2002), suggesting that it is the presence of a hydrophobic residue in this pathway, rather than disruption of

the hydrogen bond network, that reduces the overall function of the protein.

H274 is the main focal point of interhelical interaction between helices 5 and 6, forming hydrogen bonds to both R207 and E214, effectively locking the helices together. While Y211 is found within this region, we suggest its role is to lock H274 in place, effectively preventing movement towards helix 1. At the C terminal end of helix 5, a highly conserved H-bond is formed between T221 and R263. The high conservation of these residues tends to suggest that their role is to stabilise the position of Y220, the redox-active tyrosine residue, in the region of the active site. The terminus of the interface is capped by a semi-conserved D228-R256 interaction, which also interacts with E71 in short helix  $\alpha 2$ . While the amino-acid sequence of TAO is the only one within the AOX family to contain a carboxylate at this position, alcohol containing amino acids are also found to occupy this location in all other AOX containing species and it is therefore likely that they undertake similar functions.

The YW pair (246 and 247) on short helix 3 is most likely used to stabilise the two histidines at the active site (Fig. 19.2). Hydrogen bonding between Y246 and N161 orientates helix 3 in such a way to facilitate a H-bond network between W247 and the iron-ligating residue H165 via D265. D265 is held in position by W65, a semi-conserved residue. It is important to note that this region is identical to that found in RNR, in which it has been suggested to be part of a proton-coupled electron transport (PCET) network (Stubbe et al. 2003). Mutation of Y246 to alanine results in 90 % inhibition of activity (Nakamura et al. 2005), demonstrating that this region is important to the overall function of the protein.

### *B. The Hydrophobic Nature of the Protein*

Helices 1 and 4 are predicted to be the membrane binding helices. As previously indicated the surface of the membrane side of the protein is largely hydrophobic, with the

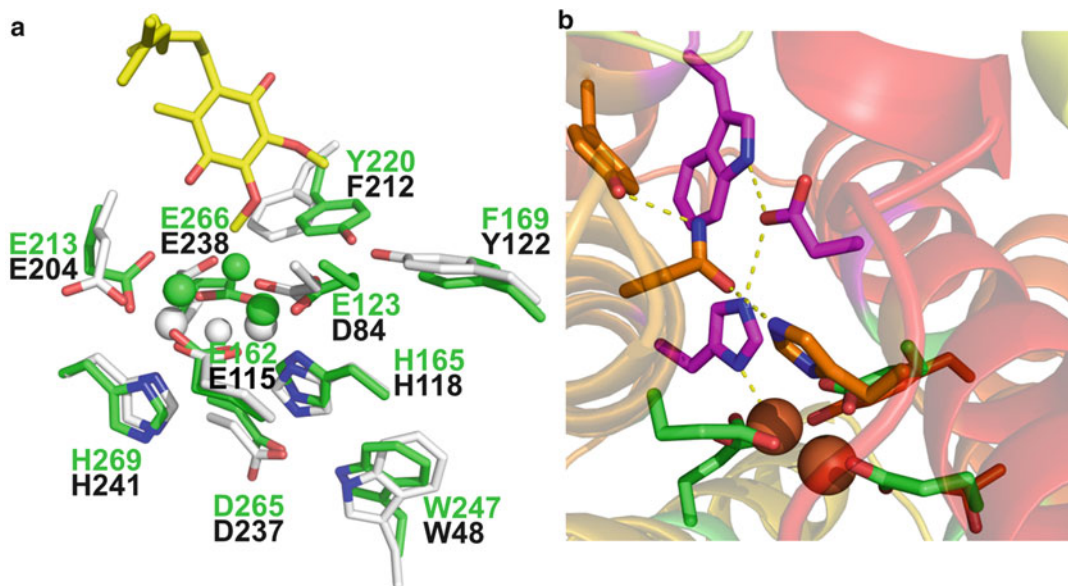


Fig. 19.2. The proton coupled electron transport (PCET) system within AOX. Figure (a) is an overlay of AOX (green – PDB:3VV9) and RNR (white – PDB:1RIB), showing good spatial alignment of the histidine, aspartic acid and tryptophan. (b) shows the PCET network in purple, with the proposed support network of tyrosine, asparagine and histidine shown in orange.

hydrophobicity extending to slightly above helices 1 & 4, indicating that this region resides below the polar head groups of the phospholipid bilayer and hence extends into the membrane (Fig. 19.3). Highly conserved arginine residues (R106, R143, R180 and R203) are present on the outside surface of the protein, probably acting as anchor points to the membrane itself.

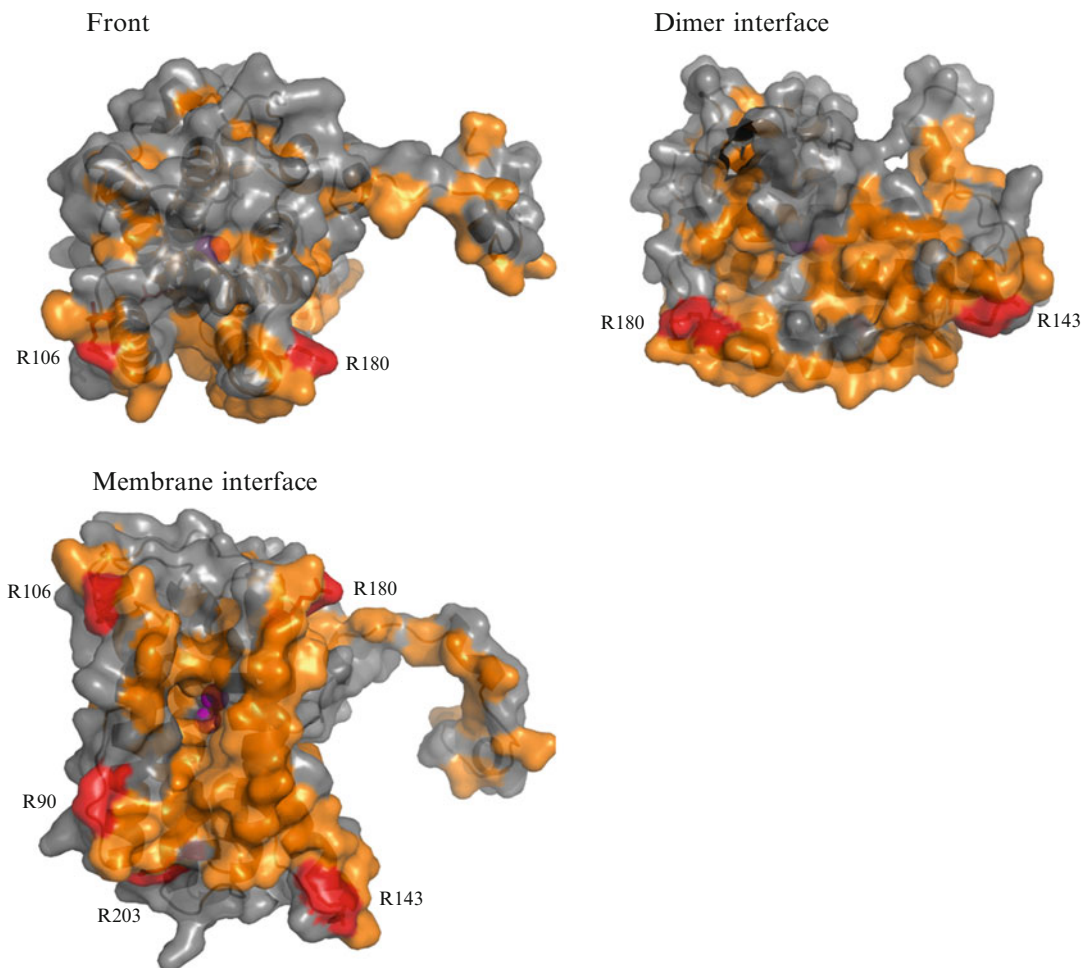
The opening that is visible in the membrane facing-side of the protein illustrated in Fig. 19.3 is the entrance to a larger hydrophobic cavity that leads directly to the di-iron core of the protein. CAVER (Chovancova et al. 2012) analysis of the crystal structure produced an outline of the cavity as indicated in Fig. 19.4. It is more than likely that the cavity leads to the quinol binding region. The hydrophobic nature of the cavity is an ideal binding environment for the isoprenoid tail of the quinol, and the cavity allows direct access from the quinone pool within the membrane into the di-iron core.

Of particular note is the location of highly conserved leucine residues flanking the cavity (L177 and L267). These residues form

a bottleneck for the cavity (approximately 6.3 Å wide), probably serving to correctly orientate the substrate as it enters the hydrophobic pocket in order to reach the active site. Recent site-directed mutagenesis studies on these residues indicate that mutation to alanine markedly decreases the sensitivity of the AOX protein to AOX inhibitors (Young et al. 2014). Inhibitory efficacy was considerably decreased in the mutants suggesting that these residues are crucial ligands for inhibitor binding, which in turn would also suggest that they play a critical role in quinol binding. Whether this is a direct effect of losing *Van der Waals* binding, or a consequential effect of incorrect orientation of the inhibitor into the binding pocket remains to be elucidated.

### C. Structure of the Di-iron Core

As with the other di-iron carboxylate proteins, the central core consists of two iron atoms ligated by four carboxylates. Figure 19.5 depicts the typical arrangement of ligands around the metal centres. Of



*Fig. 19.3.* Surface representation of a monomer from the TAO crystal structure, depicting the hydrophobic residues in orange. Membrane interface depicts the underside of the protein, and the di-iron core (magenta spheres) can be seen via the cavity. Residues coloured red are proposed to be responsible for membrane binding. N-terminal arm removed from dimer interface diagram for clarity.

particular note is the observation that the orientation of E123 appears to be dependent upon the location of the ligating oxygen species. While E123 is consistently observed to be in a bidentate binding mode, the closer the oxygen atom is located to E123 the more it induces rotational movement of E123, thereby resulting in hydrogen bond formation between the amino acid and the oxygen species.

A particular uniqueness about the ligation sphere of AOX is that although two histidines are universally conserved within the

primary ligation sphere of all AOXs, neither one appears to be within co-ordination distance when the protein is in its oxidized form (Table 19.2). Interestingly when overlaid on top of the oxidised forms of MMO and RNR, as depicted in Fig. 19.6, it is apparent that the lack of ligation is not due to movement of the histidine ligands, but rather due to migration of the iron atoms. Furthermore if the PCET network within AOX does indeed include these histidines, it would suggest that in its oxidized form there is a disconnection of the iron atoms from

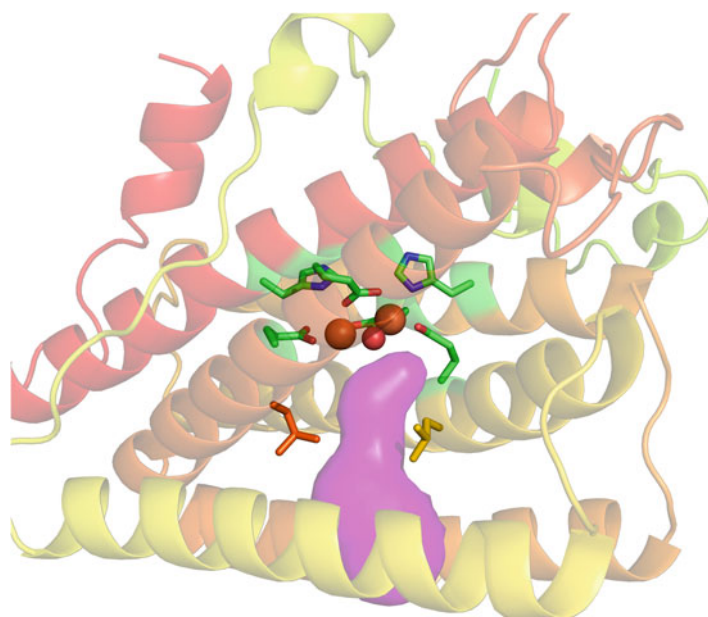


Fig. 19.4. Hydrophobic cavity (shown in magenta) leading towards the di-iron core between helices 1 and 4. Iron shown as orange spheres, oxygen as red, and the primary ligation sphere is shown as green sticks. Also shown are L177 and L267, the cause of the bottleneck in the cavity.

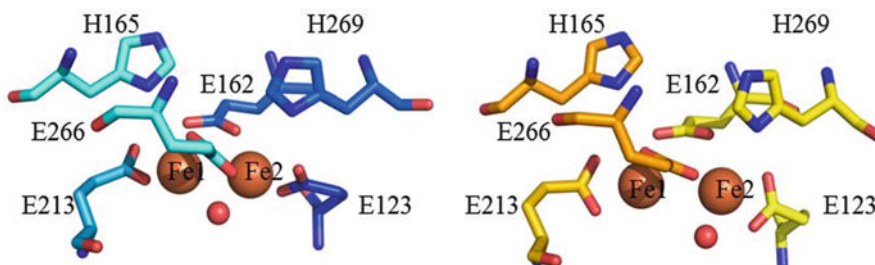


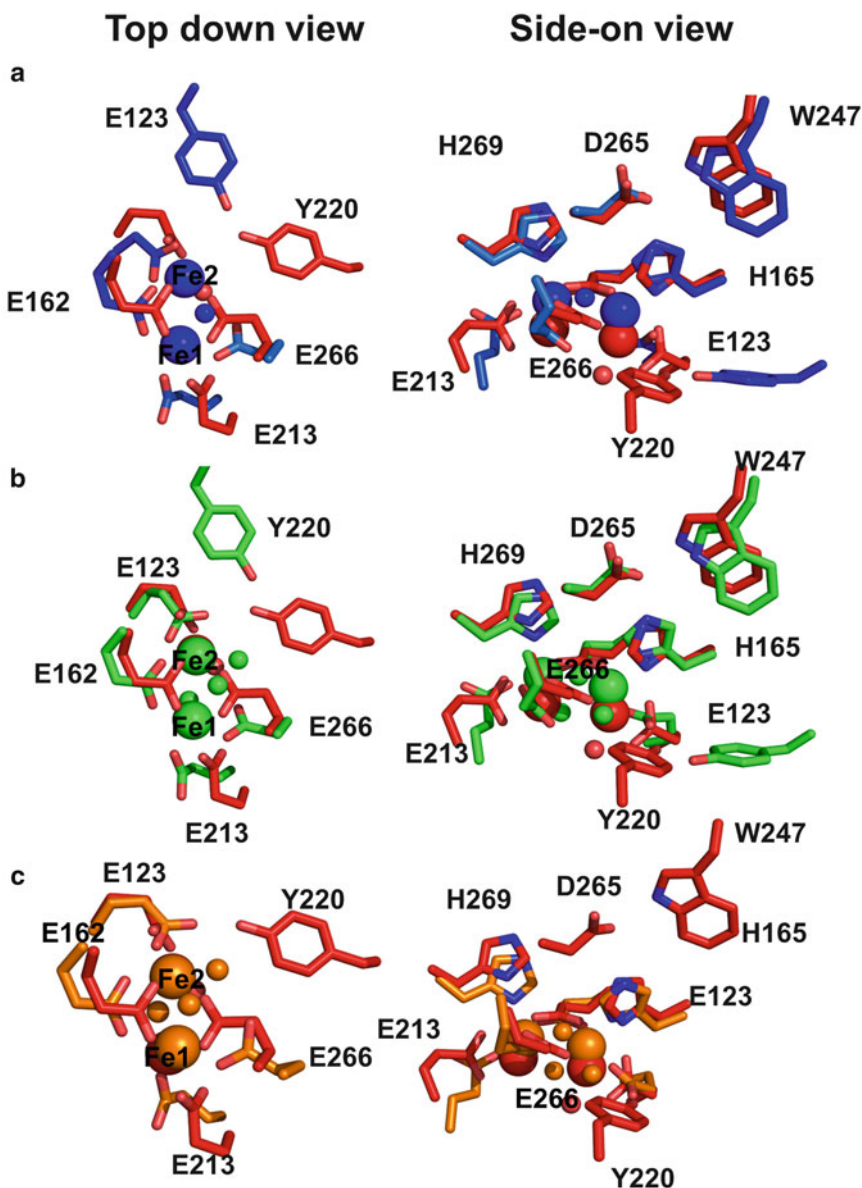
Fig. 19.5. Di-iron core of TAO (PDB:3VV9) from different monomers. Cyan figure on the left is monomer A, yellow on the right is monomer B. Large orange sphere corresponds to iron, with the small red sphere corresponding to oxygen.

Table 19.2. Bond distances in Angstroms for iron ligation sphere relative to the TAO numbering system.

Monomer	E123 (Fe2/Fe2)	E162 (Fe1/Fe2)	E213 (Fe1/Fe1)	E266 (Fe1/Fe2)	H165	H269
AOX	2.2/2.0	2.5/2.3	2.3/2.5	2.0/2.1	3.3	4.4
RNR	2.2/2.5	2.0/1.8	2.1/NB	2.1/NB	2.1	2.3
RNR D84E	2.2/2.9	2.2/2.1	2.1/NB	2.0/NB	2.4	2.1
MMO	2.0/NB	2.6/2.2	2.1/NB	2.0/NB	2.2	2.1
RBR	2.1/2.3	2.0/2.2	2.2/2.2	2.1/2.0	4.1	2.2

NB signifies no second bond towards to metal centre for that ligand





*Fig. 19.6.* Oxidized di-iron core of AOX aligned to; (a): RNR (PDB:1RIB), (b): RNR D84E (PDB:1PIU) and (c): MMO (PDB: 1MTY). AOX is shown in red, RNR wild type in blue, RNR D84E in green and MMO in orange. Alignment performed according to best fit with respect to the iron binding ligands. Atoms colored according to element, with oxygen shown in red and nitrogen in blue, with the exception of the di-iron core (*large spheres*) and ligating oxygens (*smaller spheres*), which were coloured according to crystal structure for visibility. Histidines removed from the top-down view for clarity. TAO numbering added for orientation purposes.

this network. It is conceivable that this may be necessary during the oxidative part of the catalytic cycle and not during the reaction with quinol.

The location of the proximal tyrosine (Y220) within the active site has also altered in comparison to RNR. Mutation of this tyrosine to phenylalanine results in 100 %

inhibition of activity (Nakamura et al. 2005; Albury et al. 2010), confirming the importance of the hydroxide moiety. The difference in location of Y220 in AOX in comparison to the position of Y122 in RNR is important since such a location, directly on top of the substrate binding cavity, in all probability allows the amino acid to interact directly with bound substrate.

### III. Mechanism of Di-oxygen Reduction by the Alternative Oxidases

#### A. General Characteristics of Oxygen Reduction

While the full reduction of oxygen through to water requires four electrons, several mechanistic possibilities exist with respect to how this may occur. For instance, when oxygen binds to the protein it becomes fully reduced, leaving the protein in an overall  $4^+$  oxidation state, or alternatively it could get reduced to a peroxo-type species, thereby leaving the protein in an overall  $2^+$  oxidation state. It is worth emphasising that the overall oxidation state refers to that of the protein and does not necessarily imply that it is the oxidation state of the di-iron center. Both tryptophan and tyrosine residues have been well documented for their ability to retain radical charges within RNR (Saleh and Bollinger 2006). A lower oxidation state around the metal center would reduce the reduction potential of the metal itself, allowing an effective tuning of the protein to specific substrates.

While there is no direct spectroscopic evidence with respect to the mechanism by which AOX reduces oxygen to water, inferences can be drawn from EPR (Berthold et al. 2002; Moore et al. 2008) and FTIR (Marechal et al. 2009) studies. Other di-iron proteins, such as MMO and RNR, have been studied in depth with respect to their catalytic cycles and are a reasonable starting point for examining the reactivity

of AOX with oxygen. While outside the scope of this review, readers are referred to some recent articles on the mechanistic nature of soluble methane monooxygenase (MMO (Tinberg and Lippard 2009, 2011; Lee et al. 2013)) ribonulceotide reductase (RNR (Tomter et al. 2013)) and cryo-crystallographic time course studies of RBR (Dillard et al. 2011).

#### B. Proposed Reaction Mechanism

The suggested reaction mechanism depicted in Fig. 19.7 is similar to those proposed for MMO and RNR with some subtle differences. One of the key differences between AOX and MMO is the lack of visible absorbance band at 720 nm. Such a band can be observed in MMO and has been attributed to a ligand to metal charge transfer event (Valentine et al. 1999). Given that this event is likely due to energy transfer from the superoxo species to a bridging peroxo species, we suggest that an alternative route probably exists in AOX involving the quenching of the radical superoxide species by the proximal tyrosine prior to rearrangement of the core. The ‘diamond core’ formed after the peroxodi-iron species is a common intermediate found in di-iron enzymes (Shu et al. 1997) and reduction of this highly reactive core either by the PCET network or via protons derived from the solvent would result in a di-iron center which, in redox potential terms, is closer to that of bound ubiquinol.

##### 1. Structure of the Fully Reduced Di-iron Core

EPR studies of the fully reduced protein resulted in a signal of  $g = 16.9$  in parallel mode (Moore et al. 2008), which is characteristic signature of di-iron proteins (Solomon et al. 2000). This suggests that the protein in its fully reduced form is an  $\text{Fe}^{2+}/\text{Fe}^{2+}$  state, and coupled with the lack of an EPR signal in the perpendicular mode (Moore et al. 2008), suggests the irons are paramagnetically linked,

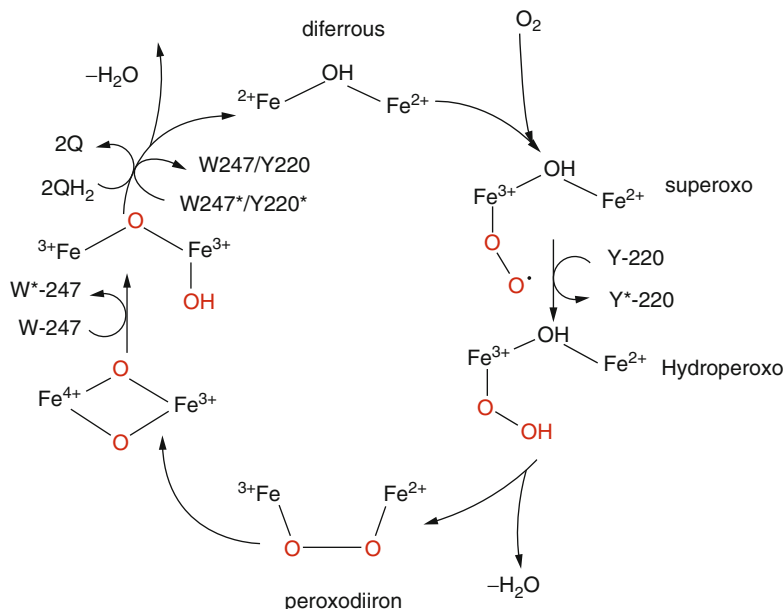


Fig. 19.7. Proposed mechanism for the oxygen reduction cycle within AOX.

either via a bridging hydroxide ion or one of the carboxylate ligands.

While a fully reduced species of AOX has yet to be crystallised, inferences as to the electronic state of the core can be made from an examination of the reduced structures of other di-iron proteins depicted in Fig. 19.8. Scrutiny of the wild type RNR and D84E mutant core (Nordlund and Eklund 1993; Voegtli et al. 2000; Voegtli et al. 2003) reveals that the effects of such a mutation are translated through the active site to the other terminal carboxylate, with movement of the carboxylate from a bidentate binding mode within the wild type to monodentate within the mutant. With the apparent lack of induction of movement caused by the proximal tyrosine in the RBR structure that occupies the same special region as Y220 in AOX, it would suggest that AOX would likely conform to an arrangement similar to that observed in the RNR-D84E mutant.

## 2. Initial Reaction of the Di-iron Core with Oxygen

EPR analysis with *Arabidopsis thaliana* AOX1a expressed in *E. coli* membranes provides some further insight into the possible

stepwise nature of the oxidation mechanism. Berthold and colleagues detected a stable  $\text{Fe}^{3+}/\text{Fe}^{2+}$  species (Berthold et al. 2002) under oxidizing conditions suggesting that the initial binding of oxygen occurs via an ‘end-on’ binding mode, generating a superoxo species. It is worth noting that this mixed valence species was stable enough to detect by EPR suggesting, given the high reactivity of the superoxo species, that the terminal oxygen was reduced in a manner that does not affect the oxidation state of the metal centres.

Of particular importance in a consideration of the initial steps in the oxidation mechanism is the role of the PCET network. It has previously been demonstrated in RNR that a tryptophan radical is generated prior to the generation of the tyrosine radical (Saleh and Bollinger 2006). It is likely that this would buffer the change in oxidation state that would accompany the reaction with oxygen, spreading the otherwise highly reactive radical between the iron and the tryptophan. If such a reaction occurred it could provide the di-iron core with some degree of stereochemical control thereby allowing oxygen to distinguish which of the two irons it will react with. Mutational studies of residues flanking

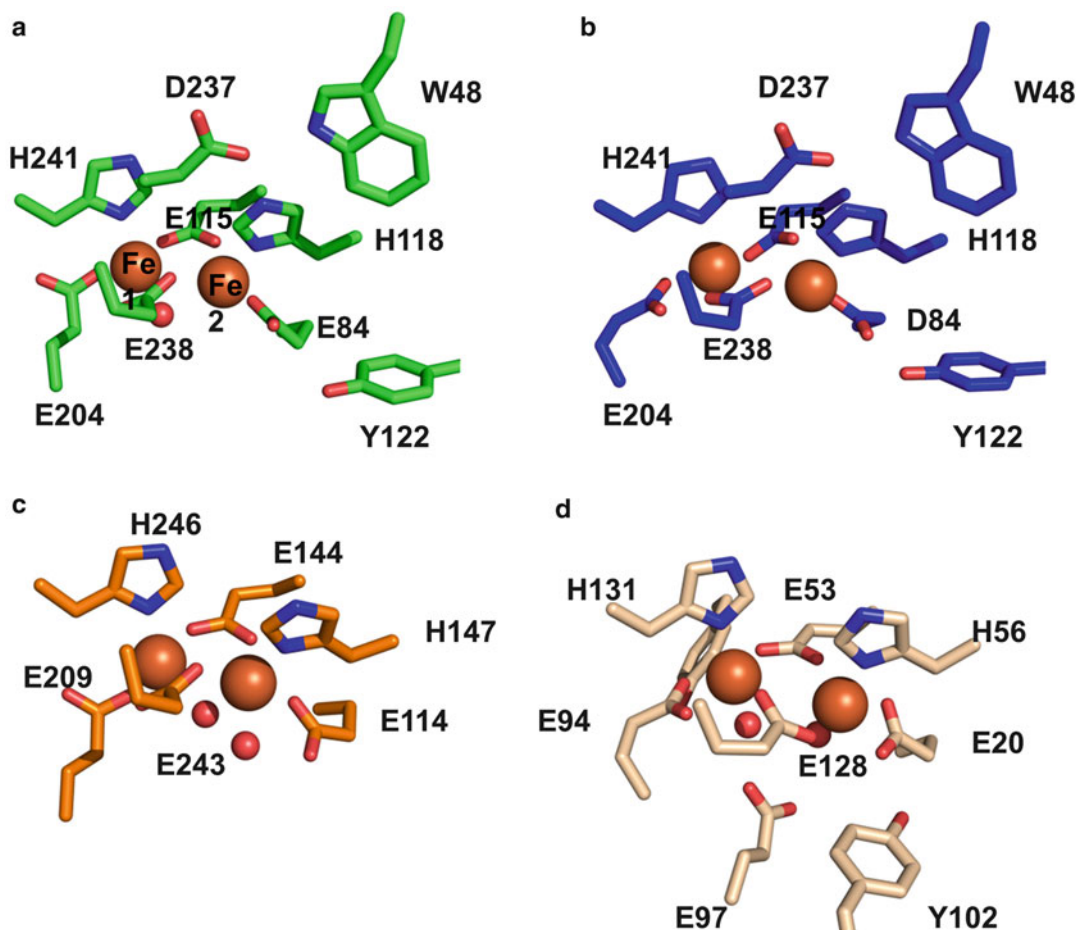
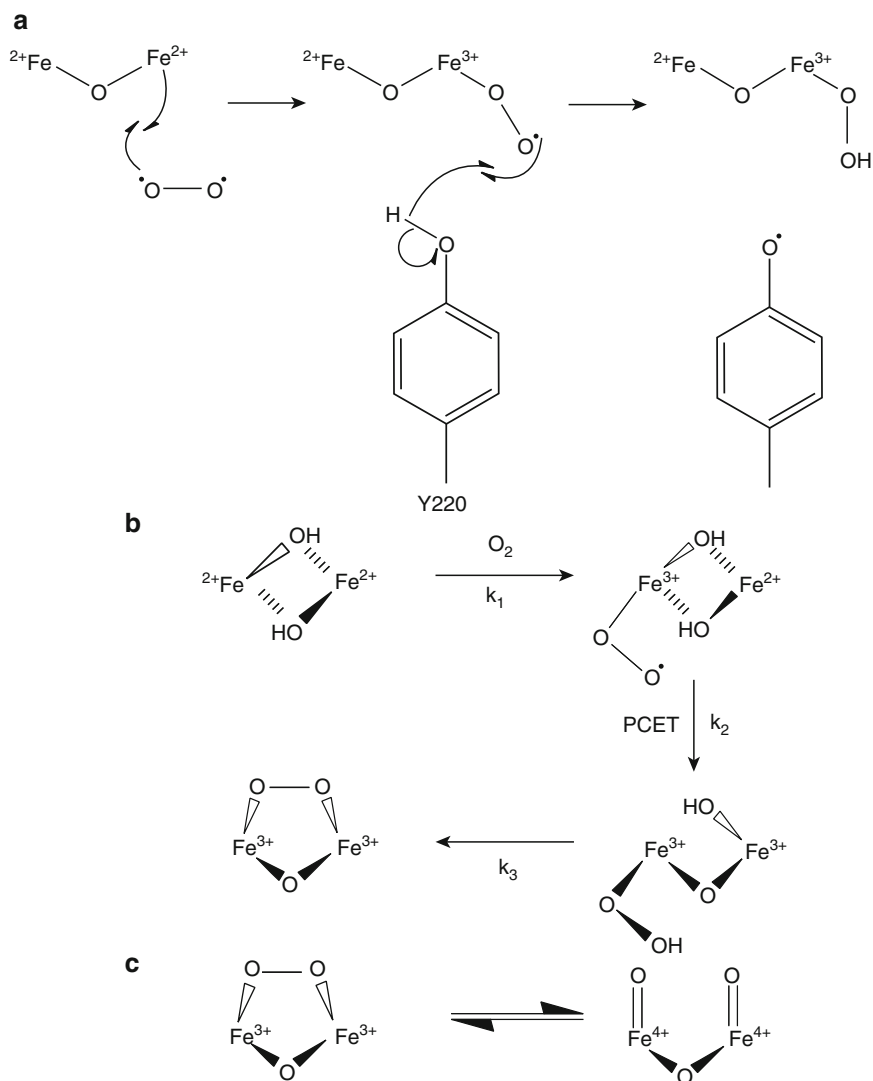


Fig. 19.8. Di-iron core of fully reduced species. (a): RNR-D84E mutant (PDB: 1PIM) in *green* (b): RNR wild type (1R56) in *blue*, (c): MMO (PDB:1FYZ) in *orange* and (d): RBR (PDB:1LKO) in *wheat*. Heteroatoms coloured with *blue* being nitrogen, oxygen being *red*, and iron as *orange spheres*. Numbering indicates amino acid position in respective protein.

the glutamate residue (L122A and T124A) on the PCET network side of the active site revealed that alterations within this region causes significant changes to the oxygen  $K_m$ , further implicating a selective initial binding of oxygen to one of the irons within the active site (Young et al. 2014).

It is noteworthy that an Fe(III)-O-O\* superoxo species has been crystallised in dioxygenase, with bond distances of 1.99 Å (Fe-O) and 1.47 Å (O-O\*) (Kovaleva and Lipscomb 2007). Given an Fe(1)-Tyr-O distance of 6 Å in AOX, (~5 Å to the proton), a reactive distance of 1.5 Å is sufficient for the required orbital overlap

necessary for hydrogen atom extraction. Fe(III)O<sub>2</sub>•<sup>-</sup> has also been demonstrated to be much more reactive than its Fe(IV)=O counterpart that is part of the ‘diamond core’ (Cho et al. 2012) existing in the singlet state thereby permitting for spin allowed hydrogen atom abstraction from the tyrosine, as depicted in Fig. 19.9a. In RNR (Atkin et al. 1973) repeated reduction by ferricyanide and reintroduction of oxygen into the sample gave rise to a characteristic signal for a tyrosine radical at 410 nm, and similar observations have been made with AOX (A. Maréchal, P. R. Rich, and A.L. Moore, unpublished observations). While



*Fig. 19.9. (a) Initial reaction of oxygen with the di-iron core, followed by hydrogen abstraction from the neighbouring tyrosine to generate a tyrosyl radical. (b) Proposed oxygen binding reaction in  $[\text{Fe}_2(\mu\text{-OH})_2(6\text{-Me}_3\text{-TPA})_2]$ , adapted from (Shan and Que 2005). (c) Scission of the  $[\text{Fe}_2(\mu\text{-O})(\mu\text{-O-O})]$  unit, adapted from (Kodera et al. 2012).*

such observations would suggest that the tyrosine radical is generated upon oxidation of the di-iron center, it does not necessarily imply that it occurs this early in the catalytic cycle and may indeed occur at a later point.

### 3. Rearrangement of the Core

Synthetic chemical systems that mimic the di-iron core present an alternative source of

information. One such system is the  $[\text{Fe}_2(\mu\text{-OH})_2(6\text{-Me}_3\text{-TPA})_2](\text{OTf})_2$  complex, which contains a comparable hydroperoxo species as a reaction mechanism intermediate shown in Fig. 19.9b (Shan and Que 2005). The interesting aspect about this system is that it facilitated an estimation of the maximal concentration of intermediates that could be formed. For instance it was calculated that if the core rearrangement was the rate-limiting

step, the maximal observed concentration of the mixed valent species would be approximately 7 %. Interestingly this is identical to that detected within AOX by EPR (Berthold et al. 2002). Given the highly clustered nature of the active site and the necessitation of carboxylate movement to open ligation sites, it is likely that the AOX di-iron core would indeed be the rate-limiting step in this part of the mechanism.

An  $[\text{Fe}_2(\mu\text{-O})(\mu\text{-O-O})]$  species has been shown (Kodera et al. 2012) to undergo spontaneous rearrangement between an Fe(III)/Fe(III) and Fe(IV)/Fe(IV) species via a reversible scission of the O-O bond (as shown in Fig. 19.9c). This reaction is dependent upon the surrounding acidity, with evidence that protonation of the bridging oxide increases scission rate (Kodera et al. 2012). We suggest that a potential source for protonation of the active site would be the water channels discussed earlier. The reaction could also be accelerated due to mechanical constraints on the active site; if the bridging species in the di-iron core is a carboxylate ligand, the increased energy provided by a ligand in a now unfavorable position may shift the equilibrium in favor of an Fe(IV)/Fe(IV) species. As with the previous step, the bridging oxygen is likely to be a carboxylate ligand which would affect the oxidation states of the metals, and a simple rearrangement would allow formation of the diamond core favored by other di-iron proteins (Shu et al. 1997).

Figure 19.10 depicts a potential proton-based mechanism for the rearrangement of the scissioned species to the oxo-species

using a proton-based system to liberate a molecule of water. One factor that is difficult to take into account at this time is the extent to which the primary ligation sphere affects the reaction mechanics, with respect to co-ordination saturation and electronic configuration of the metal centers. Computational examination of pKa values using PropKa (Li et al. 2005) reveals that if this rearrangement step is indeed coupled with a carboxylate shift, the acidity of the iron ligating histidine increases significantly, with a pKa decrease from 10.4 to 1.7.

It is also conceivable that this is not the route of electron transport since a shift in the ligation core may well force the reaction in a separate direction. We also have to consider that the picture given by the crystal structure does not truly represent an intermediate in the regular catalytic cycle but is rather a decomposition of the quinol reactive species, which is more stable.

### C. Quinol Oxidation Mechanism

TAO has been co-crystallised with col-letochlorin B and ascofuranone (Shiba et al. 2013), novel inhibitors of AOXs (Minagawa et al. 1996). The inhibitors are analogs of ubiquinone containing a fully functionalized phenol ring and an isoprene tail. Given the similarities between inhibitor and substrate, these structures add further validity to the idea of the hydrophobic cavity being the quinol-binding site. Both compounds ligate to the protein in an identical fashion, with 2-OH occupying the space between R96, R118 and T219, as depicted in Fig. 19.11.

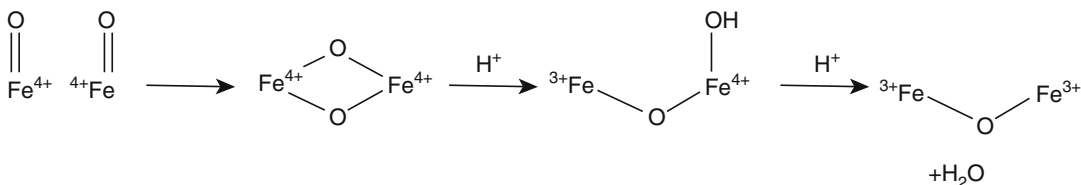


Fig. 19.10. Proposed mechanism for the formation of the quinol reactive species post scission. Formation of the diamond core that is a common intermediate within the di-iron reaction schemes, followed by successive protonation to liberate the first molecule of water. Bridging carboxylate removed for clarity.

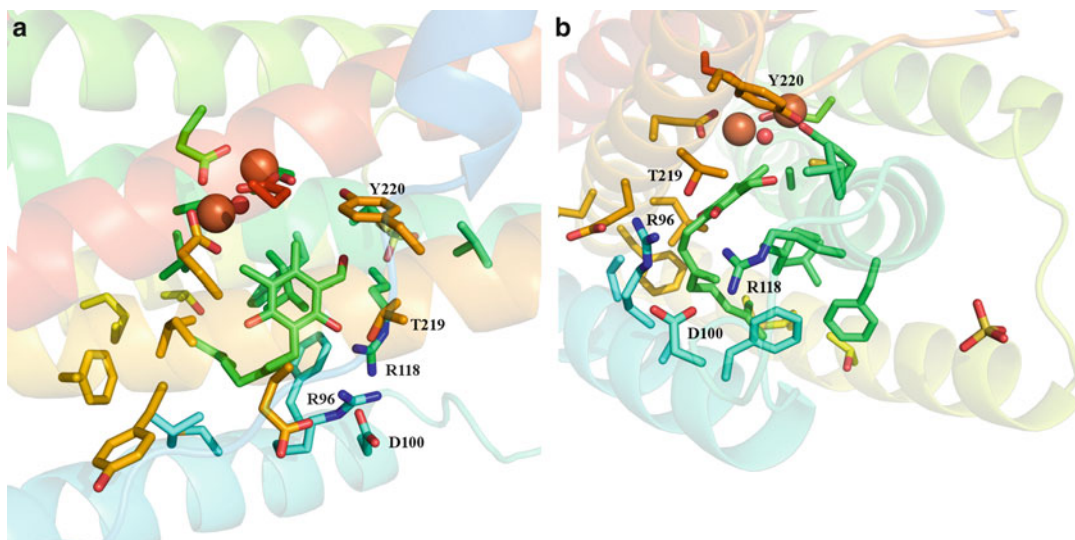


Fig. 19.11. Binding of Colletochlorin B (PDB:3w54), shown primarily in green. Amino acids shown are those within 6 Å of the inhibitor, with labelled amino acids indicating potential interaction with the inhibitor. Figure (a) depicts the head group interactions with the protein, with 2-OH within hydrogen bond distance to T219, R118 and R96. Figure (b) depicts the location of the isoprenoid tail.

Given the polar nature of these residues in an otherwise highly hydrophobic environment, it is highly likely they are involved in the overall reaction mechanism of the quinol-oxidation reaction. Docking studies (Seeliger and de Groot 2010) confirm the validity of the hydrophobic pocket as the substrate binding region since they suggest an identical binding pocket to that seen with the inhibitors in the crystal structure.

The important studies of Maréchal and colleagues (Marechal et al. 2009) demonstrated that the oxygen reactive species was the fully reduced form of the AOX and that reduction of the fully oxidized species occurs in a stepwise fashion of two 2 sequential electron reductions, as depicted in Fig. 19.12. From this, it can be inferred that each reduction step would correspond to a quinol:quinone oxidation step which enters the protein in a stepwise fashion as opposed to simultaneously. While it could theoretically be the case that both quinols bind at once and undergo a single electron reduction each between steps the relative instability of the semiquinone species, combined with the lack of a second substrate

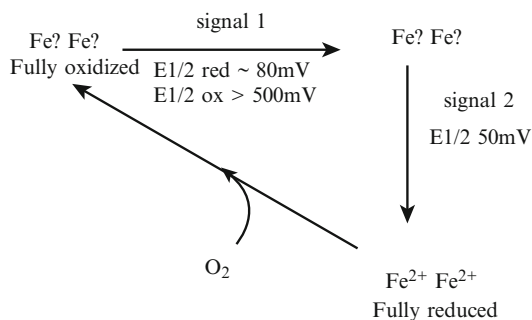


Fig. 19.12. Electrochemical studies adapted from (Marechal et al. 2009). Redox potentials in both oxidative and reductive direction quoted for signal 1, with signal 2 operating under standard reversible redox conditions.

binding site, would suggest that this is probably not the case.

Mutational studies performed on recombinant *Saurumattum guttatum* AOX within the quinol binding pocket revealed that while substitution of the arginine (R96) and aspartic acid (D100) with alanine reduces overall catalytic activity, such mutations do not completely inhibit activity suggesting that their role in the catalytic cycle is non-essential (Young et al. 2014).

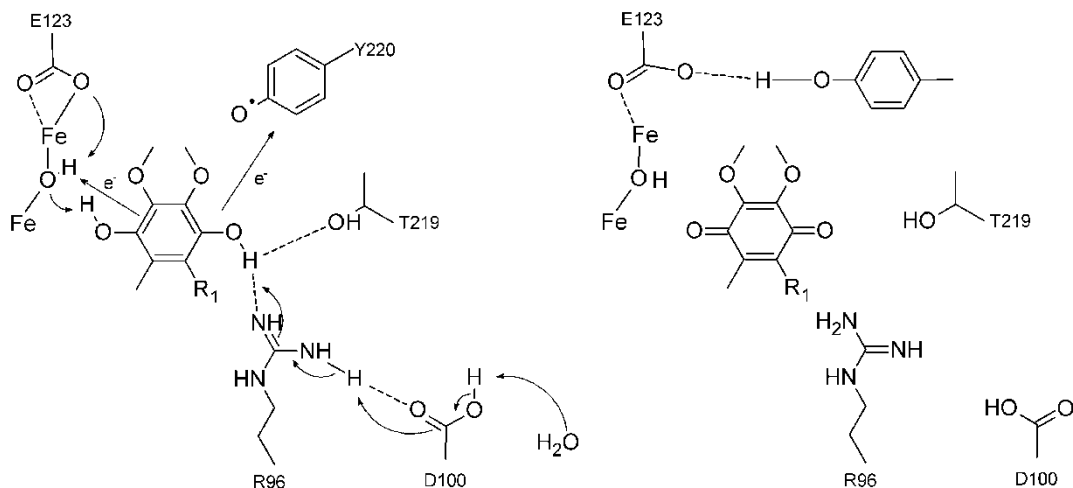


Fig. 19.13. Potential quinol oxidation mechanism based on the docked quinol species. Proton translocation towards the solvent facilitated via R96 and D100, with the second proton entering the di-iron active site, with a potential final resting place between E123 and Y220. Electrons transferred to the di-iron core and tyrosine respectively.

A possible initial reaction with quinol is depicted in Fig. 19.13. As indicated above, docking studies orientate the quinol in a similar manner to that observed for colletochlorin B and ascofuranone in the crystal structures, with one hydroxide between the tyrosine and di-iron core and the second hydroxide ligating to T219 and R96. Given the detection of the tyrosyl radical within the fully oxidized form (A. Maréchal, P.R. Rich and A.L. Moore, unpublished observations), it is likely that the radical reacts with the substrate abstracting a proton and electron from the quinol to form a neutral tyrosine and a semiquinone. While the second electron would transfer to the di-iron core, the fate of the second proton is questionable and probably dependent upon the nature of the water channels. If they do indeed transfer protons into the active site early within the reaction cycle it is feasible that the second proton is transferred out of the active site and into solvent via the arginine-aspartic acid pathway depicted in Fig. 19.13.

#### IV. Concluding Remarks

A full mechanism for the catalytic cycle of the alternative oxidases has been pro-

posed. While the initial stages for reactivity are fairly well characterized from a number of different sources, the intermediates after the mixed valent species are currently implied from synthetic chemical structures designed to mimic the active site which may not necessarily give a true representation of the catalytic cycle. One of the major problems with attempts to elucidate the mechanism for AOX is its lack of solubility, preventing probing the nature of intermediates to a suitable degree.

On the basis that a peroxo species has been predicted as an intermediate within the cycle, examination of whether the system is able to reduce hydrogen peroxide should confirm whether this is a likely intermediate. Given that rubrerythrin, the closest di-iron structure to AOX, demonstrates a preference for peroxide over oxygen as a substrate (Coulter et al. 2000), it should prove interesting to probe the reactivity of this oxidase towards peroxide.

A fully reduced crystal structure would also go a long way towards elucidation of the full mechanism. While prediction would suggest that the AOX active site adopts a conformation similar to that of the RNR-D84E mutant, there may be structural movements that



we are currently unable to accurately predict. Within the plant species, EPR work on the T179A mutation has revealed a semi-quinone species (P. Heathcote and A.L. Moore, unpublished observations). While this is not necessarily a trapping of an intermediate, a crystal structure of this mutant may well help to clarify what transitional states occur within the di-iron core itself during the oxygen reduction cycle.

## Acknowledgments

This work was supported in part by Creative Scientific Research Grant 18GS0314 (to K.K.), Grant-in-aid for Scientific Research on Priority Areas 18073004 (to K.K.) from the Japanese Society for the Promotion of Science (JSPS), and Targeted Proteins Research Program (to K.K. and S.H.) from the Japanese Ministry of Education, Science, Culture, Sports and Technology (MEXT), Grant-in-aid for research on emerging and re-emerging infectious diseases from the Japanese Ministry of Health and Welfare (to K.K.), and partly by the Programme for Promotion of Basic and Applied Researches for Innovations in Bio-oriented Industry (BRAINI) (to K.K. and S.H.). A.L.M. gratefully acknowledges BBSRC and the University of Sussex for financial support, with K.K. the Prime Ministers Initiative 2 (Connect – British Council) fund for collaborative twinning and JSPS for a Travel Fellowship. LY and BS gratefully acknowledge the University of Sussex for studentship support.

## References

- Ajayi WU, Chaudhuri M, Hill GC (2002) Site-directed mutagenesis reveals the essentiality of the conserved residues in the putative diiron active site of the trypanosome alternative oxidase. *J Biol Chem* 277:8187–8193
- Albury MS, Affourtit C, Crichton PG, Moore AL (2002) Structure of the plant alternative oxidase. Site-directed mutagenesis provides new information on the active site and membrane topology. *J Biol Chem* 277:1190–1194
- Albury MS, Elliott C, Moore AL (2010) Ubiquinol-binding site in the alternative oxidase mutagenesis reveals features important for substrate binding and inhibition. *Biochim Biophys Acta Bioenerg* 1797:1933–1939
- Andersson ME, Nordlund P (1999) A revised model of the active site of alternative oxidase. *FEBS Lett* 449:17–22
- Atkin CL, Thelander L, Reichard P, Lang G (1973) Iron and free-radical in ribonucleotide reductase – exchange of iron and Mossbauer-spectroscopy of protein-B2 subunit of *Escherichia coli* enzyme. *J Biol Chem* 248:7464–7472
- Berthold DA, Andersson ME, Nordlund P (2000) New insight into the structure and function of the alternative oxidase. *Biochim Biophys Acta Bioenerg* 1460:241–254
- Berthold DA, Voevodskaya N, Stenmark P, Graslund A, Nordlund P (2002) EPR studies of the mitochondrial alternative oxidase. Evidence for a diiron carboxylate center. *J Biol Chem* 277:43608–43614
- Bienen EJ, Maturi RK, Pollakis G, Clarkson AB Jr (1993) Non-cytochrome mediated mitochondrial ATP production in bloodstream form *Trypanosoma brucei brucei*. *Eur J Biochem* 216:75–80
- Cho KB, Chen H, Janardanan D, de Visser SP, Shaik S, Nam W (2012) Nonheme iron-oxo and -superoxo reactivities: O<sub>2</sub> binding and spin inversion probability matter. *Chem Commun (Camb)* 48:2189–2191
- Chovancova E, Pavelka A, Benes P, Strnad O, Brezovsky J, Kozlikova B, Gora A, . . . , Damborsky J (2012) CAVER 3.0: a tool for the analysis of transport pathways in dynamic protein structures. *PLoS Comput Biol* 8:e1002708
- Coulter ED, Shenvi NV, Beharry ZM, Smith JJ, Prickril BC, Kurtz DM (2000) Rubrerythrin-catalyzed substrate oxidation by dioxygen and hydrogen peroxide. *Inorg Chim Acta* 297:231–241
- Dillard BD, Demick JM, Adams MWW, Lanzilotta WN (2011) A cryo-crystallographic time course for peroxide reduction by rubrerythrin from *Pyrococcus furiosus*. *J Biol Inorg Chem* 16:949–959
- Grant PT, Sargent JR, Ryley JF (1961) Respiratory systems in the Trypanosomidae. *Biochem J* 81:200–206
- Kodera M, Kawahara Y, Hitomi Y, Nomura T, Ogura T, Kobayashi Y (2012) Reversible O-O bond scission of peroxodiiron(III) to high-spin oxodiiron(IV) in dioxygen activation of a diiron center with a bis-tpa dinucleating ligand as a soluble methane monooxygenase model. *J Am Chem Soc* 134:13236–13239

- Kolberg M, Strand KR, Graff P, Andersson KK (2004) Structure, function, and mechanism of ribonucleotide reductases. *Biochim Biophys Acta Protein Proteomics* 1699:1–34
- Kovaleva EG, Lipscomb JD (2007) Crystal structures of Fe<sup>2+</sup> dioxygenase superoxo, alkylperoxo, and bound product intermediates. *Science* 316:453–457
- Lee SJ, McCormick MS, Lippard SJ, Cho US (2013) Control of substrate access to the active site in methane monooxygenase. *Nature* 494:380–384
- Li H, Robertson AD, Jensen JH (2005) Very fast empirical prediction and rationalization of protein pKa values. *Proteins* 61:704–721
- Lipscomb JD (1994) Biochemistry of the soluble methane monooxygenase. *Annu Rev Microbiol* 48:371–399
- Marechal A, Kido Y, Kita K, Moore AL, Rich PR (2009) Three redox states of *Trypanosoma brucei* alternative oxidase identified by infrared spectroscopy and electrochemistry. *J Biol Chem* 284:31827–31833
- Meeuse BJD (1975) Thermogenic respiration in aroids. *Annu Rev Plant Physiol* 26:117–126
- Millar AH, Wiskich JT, Whelan J, Day DA (1993) Organic acid activation of the alternative oxidase of plant mitochondria. *FEBS Lett* 329:259–262
- Minagawa N, Yabu Y, Kita K, Nagai K, Ohta N, Meguro K, Sakajo S, Yoshimoto A (1996) An antibiotic, ascofuranone, specifically inhibits respiration and in vitro growth of long slender bloodstream forms of *Trypanosoma brucei brucei*. *Mol Biochem Parasitol* 81:127–136
- Moore AL, Bonner WD Jr, Rich PR (1978) The determination of the proton-motive force during cyanide-insensitive respiration in plant mitochondria. *Arch Biochem Biophys* 186:298–306
- Moore AL, Umbach AL, Siedow JN (1995) Structure-function-relationships of the alternative oxidase of plant-mitochondria – a model of the active-site. *J Bioenerg Biomembr* 27:367–377
- Moore AL, Carre JE, Affourtit C, Albury MS, Crichton PG, Kita K, Heathcote P (2008) Compelling EPR evidence that the alternative oxidase is a diiron carboxylate protein. *Biochim Biophys Acta Bioenerg* 1777:327–330
- Moore AL, Shiba T, Young L, Harada S, Kita K, Ito K (2013) Unraveling the heater: new insights into the structure of the alternative oxidase. *Annu Rev Plant Biol* 64:637–663
- Nakamura K, Sakamoto K, Kido Y, Fujimoto Y, Suzuki T, Suzuki M, Yabu Y, . . . , Kita K (2005) Mutational analysis of the *Trypanosoma vivax* alternative oxidase: the E(X)(6)Y motif is conserved in both mitochondrial alternative oxidase and plastid terminal oxidase and is indispensable for enzyme activity. *Biochem Biophys Res Commun* 334:593–600
- Nihei C, Fukai Y, Kita K (2002) Trypanosome alternative oxidase as a target of chemotherapy. *Biochim Biophys Acta Mol Basis Dis* 1587:234–239
- Nordlund P, Eklund H (1993) Structure and function of the *Escherichia coli* ribonucleotide reductase protein R2. *J Mol Biol* 232:123–164
- Rhoads DM, Umbach AL, Sweet CR, Lennon AM, Rauch GS, Siedow JN (1998) Regulation of the cyanide-resistant alternative oxidase of plant mitochondria. Identification of the cysteine residue involved in alpha-keto acid stimulation and intersubunit disulfide bond formation. *J Biol Chem* 273:30750–30756
- Saleh L, Bollinger JM Jr (2006) Cation mediation of radical transfer between Trp48 and Tyr356 during O<sub>2</sub> activation by protein R2 of *Escherichia coli* ribonucleotide reductase: relevance to R1-R2 radical transfer in nucleotide reduction? *Biochemistry* 45:8823–8830
- Seeliger D, de Groot BL (2010) Ligand docking and binding site analysis with PyMOL and Autodock/Vina. *J Comput Aided Mol Des* 24:417–422
- Seymour RS (2010) Scaling of heat production by thermogenic flowers: limits to floral size and maximum rate of respiration. *Plant Cell Environ* 33:1474–1485
- Seymour RS, Gibernau M, Ito K (2003) Thermogenesis and respiration of inflorescences of the dead horse arum *Heliconia muscivora*, a pseudo-thermoregulatory aroid associated with fly pollination. *Funct Ecol* 17:886–894
- Shan X, Que L Jr (2005) Intermediates in the oxygenation of a nonheme diiron(II) complex, including the first evidence for a bound superoxo species. *Proc Natl Acad Sci U S A* 102:5340–5345
- Shiba T, Kido Y, Sakamoto K, Inaoka DK, Tsuge C, Tatsumi R, Takahashi G, . . . , Kita K (2013) Structure of the trypanosome cyanide-insensitive alternative oxidase. *Proc Natl Acad Sci U S A* 110:4580–4585
- Shu L, Nesheim JC, Kauffmann K, Munck E, Lipscomb JD, Que L Jr (1997) An Fe<sub>2</sub>IIVO<sub>2</sub> diamond core structure for the key intermediate Q of methane monooxygenase. *Science* 275:515–518
- Siedow JN, Umbach AL, Moore AL (1995) The active-site of the cyanide-resistant oxidase from plant-mitochondria contains a binuclear iron center. *FEBS Lett* 362:10–14
- Solomon EI, Brunold TC, Davis MI, Kemsley JN, Lee SK, Lehnert N, Neese F, . . . , Zhou J (2000) Geometric and electronic structure/function correlations in non-heme iron enzymes. *Chem Rev* 100:235–349

- Stubbe J, Nocera DG, Yee CS, Chang MC (2003) Radical initiation in the class I ribonucleotide reductase: long-range proton-coupled electron transfer? *Chem Rev* 103:2167–2201
- Tinberg CE, Lippard SJ (2009) Revisiting the mechanism of dioxygen activation in soluble methane monooxygenase from *M. capsulatus* (Bath): evidence for a multi-step, proton-dependent reaction pathway. *Biochemistry* 48:12145–12158
- Tinberg CE, Lippard SJ (2011) Dioxygen activation in soluble methane monooxygenase. *Acc Chem Res* 44:280–288
- Tomter AB, Zoppellaro G, Andersen NH, Hersleth HP, Hammerstad M, Rohr AK, Sandvik GK, . . . , Andersson KK (2013) Ribonucleotide reductase class I with different radical generating clusters. *Coord Chem Rev* 257:3–26
- Umbach AL, Siedow JN (1993) Covalent and non-covalent dimers of the cyanide-resistant alternative oxidase protein in higher plant mitochondria and their relationship to enzyme activity. *Plant Physiol* 103:845–854
- Umbach AL, Gonzalez-Meler MA, Sweet CR, Siedow JN (2002) Activation of the plant mitochondrial alternative oxidase: insights from site-directed mutagenesis. *Biochim Biophys Acta* 1554:118–128
- Valentine AM, Stahl SS, Lippard SJ (1999) Mechanistic studies of the reaction of reduced methane monooxygenase hydroxylase with dioxygen and substrates. *J Am Chem Soc* 121:3876–3887
- Vanlerberghe GC (2013) Alternative oxidase: a mitochondrial respiratory pathway to maintain metabolic and signaling homeostasis during abiotic and biotic stress in plants. *Int J Mol Sci* 14:6805–6847
- Voegtli WC, Khidekel N, Baldwin J, Ley BA, Bollinger JM, Rosenzweig AC (2000) Crystal structure of the ribonucleotide reductase R2 mutant that accumulates a  $\mu$ -1,2-peroxodiiron(III) intermediate during oxygen activation. *J Am Chem Soc* 122:3255–3261
- Voegtli WC, Sommerhalter M, Saleh L, Baldwin J, Bollinger JM Jr, Rosenzweig AC (2003) Variable coordination geometries at the diiron(II) active site of ribonucleotide reductase R2. *J Am Chem Soc* 125:15822–15830
- Young L, May B, Pendlebury-Watt A, Shearman J, Elliott C, Albury MS, Shiba T, . . . , Moore AL (2014) Probing the ubiquinol-binding site of recombinant *Sauromatum guttatum* alternative oxidase expressed in *E. coli* membranes through site-directed mutagenesis. *Biochim Biophys Acta* 1837:1219–1225

# Part IV

## **Superoxide Generation in Cytochrome *bc* Complexes**

# Chapter 20

## Mechanisms of Superoxide Generation and Signaling in Cytochrome *bc* Complexes

Danas Baniulis<sup>a</sup>, S. Saif Hasan<sup>b</sup>, Inga Miliute<sup>a</sup>,  
and William A. Cramer<sup>b,\*</sup>

<sup>a</sup>*Institute of Horticulture, Lithuanian Research Centre for  
Agriculture and Forestry, Kaunas str. 30, Babtai, Kaunas 54333,  
Lithuania*

<sup>b</sup>*Department of Biological Sciences, Hockmeyer Building of  
Structural Biology, Purdue University, West Lafayette, IN 47907,  
USA*

Summary.....	397
I. Introduction.....	398
II. Mechanisms of Superoxide Generation in Cytochrome <i>bc</i> Complexes.....	400
A. Electron Transfer at the Q <sub>n</sub> Site.....	400
B. Electron Transfer at the Q <sub>p</sub> Site and Q-Cycle Bypass Reactions of Oxygen Reduction.....	400
C. Unique Superoxide Production Mechanism of <i>b<sub>6</sub>f</i> Complex.....	403
III. Signaling Function of ROS Produced by Cytochrome <i>bc</i> Complexes.....	405
A. Role of Superoxide Produced in the <i>bc</i> <sub>1</sub> Complex in Regulation of Mitochondrial Function.....	405
B. Signaling Role of O <sub>2</sub> <sup>•-</sup> in Chloroplasts.....	406
C. Interaction Between O <sub>2</sub> <sup>•-</sup> Producing Activities of the Photosynthetic ET Chain.....	407
D. Regulation of Photosynthetic State Transitions.....	408
E. ROS in Chloroplast Retrograde Signaling and Modulation of Abiotic Stress Response and Pathogen Defense.....	409
References.....	410

### Summary

The mechanisms of action of reactive oxygen species (ROS) in plant and animal cells, in chloroplasts, mitochondria, and other sub-cellular compartments such as the endoplasmic reticulum and nucleus, which result in deleterious effects as well as intra-organelle and metabolically significant signaling reactions, are discussed, as well as physiological effects

---

\*Author for correspondence, e-mail: [waclab@purdue.edu](mailto:waclab@purdue.edu)

induced by the signaling functions of ROS. The role of ROS in chloroplast retrograde signaling and modulation of abiotic stress response and pathogen defense is discussed. Attention is focused on mechanisms of ROS production, and particularly on the intra-organelle reactions mediated through reduction of oxygen to superoxide in the mitochondrial cytochrome  $bc_1$  and the chloroplast  $b_6f$  complexes, for which understanding of the mechanistic details is facilitated by the existence of high resolution crystal structures. Attention is directed to the structure-based details that underlie the more than tenfold larger specific rate of superoxide production in the  $b_6f$  complex compared to that of the mitochondrial  $bc_1$  complex. Because plastoquinol oxidation by the cytochrome  $b_6f$  complex is known to initiate chloroplast state transitions, the effect of superoxide on the intra-membrane chlorophyll protein kinase that is integral to the cytochrome  $b_6f$  complex, and which underlies the photosynthetic state transitions that regulate the distribution of light energy between the two photosystems, is considered.

## I. Introduction

Superoxide anion radical ( $O_2^{\bullet-}$ ) is a primary product of the univalent pathway of molecular oxygen ( $O_2$ ) reduction. The complete reduction of  $O_2$  to  $H_2O$  requires four electrons. Molecular oxygen, in the ground state, contains paired electron spins. Therefore, a two electron reduction reaction would involve a spin restriction. Instead, the oxygen reduction reaction is favored to proceed through a series of one-electron reduction steps leading to formation of the free radical (Cadenas 1995). The intermediates of the reaction,  $O_2^{\bullet-}$ , hydrogen peroxide ( $H_2O_2$ ), and hydroxyl radical ( $OH^{\bullet}$ ), are reactive oxygen

species (ROS) that are common by-products of the aerobic metabolism of living cells. Superoxide is a short-lived molecule and, in aqueous solutions, dismutates to  $O_2$  and  $H_2O_2$  spontaneously or via mediation by superoxide dismutase (Miwa et al. 2008).

Mitochondria are a major source of ROS in animal cells (Marchi et al. 2012). Respiratory chain complexes I (NADH:ubiquinone oxidoreductase) and III (ubiquinol:cytochrome c oxidoreductase; cytochrome  $bc_1$  complex) are considered to be the main producers of  $O_2^{\bullet-}$  and derived ROS (Boveris et al. 1976; Cadenas et al. 1977; Kushnareva et al. 2002; Turrens and Boveris 1980). Similar ROS production linked to the respiratory electron transfer chain proceeds in plant mitochondria (Suzuki et al. 2012). However, chloroplasts are one of the most significant sources of ROS in plant cells.  $O_2$  reduction is associated with photosynthesis and photorespiration in chloroplasts and peroxisomes, respectively (Foyer and Shigeoka 2011; Mittler et al. 2004). Production of  $H_2O_2$  associated with photosystem I (PSI) was first described (Mehler 1951). Subsequently, the primary reduced product was identified to be superoxide anion, and its disproportionation to  $H_2O_2$  and  $O_2$  was demonstrated (Asada et al. 1974). By analogy to the mitochondrial  $bc_1$  complex,  $O_2^{\bullet-}$  production by the  $b_6f$  complex (plastoquinol:plastocyanin oxidoreductase) in the oxygenic photosynthetic

---

*Abbreviations:*  $b_p, b_n$  –  $b$ -type hemes on electrochemically positive, negative sides of membrane; cyt – Cytochrome; DBMIB – 2,5-dibromo-3-methyl-6-isopropyl-*p*-benzoquinone;  $E_m$  – midpoint oxidation-reduction potential; ET – Electron transport; Fe-S – Iron-sulfur center;  $H_2O_2$  – Hydrogen peroxide; HPV – Hypoxic pulmonary vasoconstriction; ISP – Rieske iron-sulfur protein; LHC – Light harvesting complex; NQNO – 2-n-nonyl-4-hydroxyquinoline N-oxide; n-, p-side – Electrochemically negative-, positive side of membrane;  $^1O_2$  – Singlet oxygen;  $O_2^{\bullet-}$  – Superoxide; PC – Plastocyanin; PEWY – Proline-glutamate-tryptophan-tyrosine; PQ – Plastoquinone;  $PQH_2$  – Plastoquinol; PQH – Plastosemiquinone;  $PQ^{\bullet-}$  – Anionic plastosemiquinone; PSI, II – Photosystem I, II;  $Q_p, Q_n$  – Quinone binding site on p-, n-side of membrane; ROS – Reactive oxygen species; TDS – Tridecyl-stigmatellin; UQ – Ubiquinone;  $UQH_2$  – Ubiquinol;  $UQ_2^{\bullet-}$  – Anionic ubisemiquinone

electron transport chain was proposed (Cape et al. 2006; Cramer et al. 2008), and was subsequently demonstrated quantitatively (Baniulis et al. 2013; Sang et al. 2011).

In addition to respiratory and photosynthetic electron transport systems, ROS production in the endoplasmic reticulum and nucleus has been reported (Ashtamker et al. 2007). Animal and plant cells contain additional  $O_2^{\bullet-}$  producing enzymes, such as NADPH oxidase, which generates ROS mostly in the extracellular space outside the plasma membrane (Jiang et al. 2011; Marino et al. 2012).

Traditionally, ROS have been regarded as cytotoxic agents that cause oxidative stress and molecular damage. Biochemical pathways including ROS scavenging compounds, such as ascorbate and glutathione, and enzymes including superoxide dismutase, catalase, glutathione reductase that are important for ROS neutralization have been described (Apel and Hirt 2004; Foyer and Shigeoka 2011; Moller et al. 2007). More recently, however, it has been recognized that ROS act not only as toxic compounds but also as signaling molecules associated with responses to abiotic and biotic stress in animals, plants, and microbes (Apel and Hirt 2004; Foyer and Shigeoka 2011; Mittler et al. 2004, 2011; Suzuki et al. 2012). ROS also constitutes a central part of the oxygen sensing mechanism in mitochondria of animal cells, and might be important in a similar capacity in plant cells (Bell et al. 2007; Sasidharan and Mustroph 2011; Schumacker 2014).

A versatile role was disclosed for ROS produced in chloroplasts. Initially, it was regarded as a regulator of activity of the photosynthetic electron transport chain through the balance between different photosynthetic reactions, and a role in excess energy dissipation was investigated. A signaling role for ROS in retrograde signaling from chloroplasts to the nucleus was also demonstrated to be involved in regulation of plant responses to environmental stress, and transcriptional regulation

of photosynthesis (Galvez-Valdivieso and Mullineaux 2010; Nott et al. 2006). ROS produced in chloroplasts has been shown to play a role in triggering a plant response to pathogen infection (Kangasjarvi et al. 2014).

Evidence for  $O_2^{\bullet-}$  production and its physiological relevance has been presented for *bc* complexes of respiratory and photosynthetic electron transport chains. The two protein complexes catalyze analogous ubiquinol/plastoquinol oxidation reactions linked to electron transport and proton pumping pathways defined in the Q-cycle model proposed by Mitchell (Cramer et al. 2011; Mitchell 1975a, b, 1976; Trumppower 2002).

$O_2^{\bullet-}$  production is manifested in *bc* complexes as a bypass reaction of the bifurcated two electron oxidation reaction implicated in Q-cycle electron transfer. Much of the experimental evidence for  $O_2^{\bullet-}$  production has been presented for the mitochondrial *bc*<sub>1</sub> complex (Cape et al. 2007; Droese and Brandt 2008, 2012; Forquer et al. 2006; Muller et al. 2002, 2003; Sarewicz et al. 2010; Sun and Trumppower 2003). Similar Q-cycle bypass reactions occur in the *b*<sub>6</sub>*f* complex (Baniulis et al. 2013; Sang et al. 2011). Despite the fact that general principles of the Q-cycle reactions are considered to be well established [See additional perspective in this volume by Cramer and Hasan], the specific sequence of oxidation-reduction events leading to  $O_2^{\bullet-}$  production remains a subject of debate (Cape et al. 2006; Rutherford et al. 2012). In addition, many unsolved problems exist for the physiological role of  $O_2^{\bullet-}$  produced in *bc* complexes. Especially vague is the understanding of the function of  $O_2^{\bullet-}$  produced in the photosynthetic *b*<sub>6</sub>*f* complex. Although the general mechanism of Q-cycle bypass reactions may be similar in *bc*<sub>1</sub> and the *b*<sub>6</sub>*f* complexes, the surrounding environment and enzymatic reactions, such as oxygen concentration, compartmentalization of reactions, and functional significance of the complexes to other cellular sources of ROS, suggest the possibility of unique functions for the  $O_2^{\bullet-}$  generated by the *b*<sub>6</sub>*f* complex.

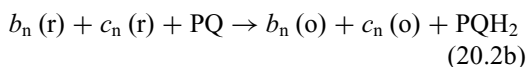
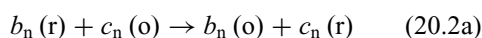
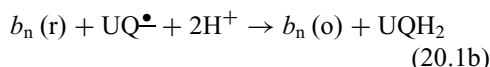
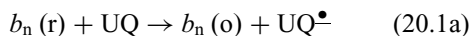
## II. Mechanisms of Superoxide Generation in Cytochrome *bc* Complexes

The mitochondrial Q-cycle involves ubiquinol oxidase activity at the  $Q_p$  site of the  $bc_1$  complex and ubiquinol reductase activity at the  $Q_n$  site (Crofts and Berry 1998). The analogous reaction of plastoquinol oxidation and reduction proceeds at *n*- and *p*-side sites of the  $b_6f$  complex (Cramer et al. 2011). It has been proposed that  $O_2^{\bullet-}$  is produced as a bypass reaction of the Q-cycle in the  $bc_1$  complex (Cape et al. 2006). While analogous oxido-reductase functions and structural similarity of the  $b_6f$  complex suggest a similar mechanism for  $O_2^{\bullet-}$  generation, the unique structural properties of the latter complex may have resulted in differences in the mechanism and control of the reaction (Baniulis et al. 2013).

### A. Electron Transfer at the $Q_n$ Site

Different electron transfer reactions might function for the mitochondrial and chloroplast *bc* complexes at the negative side of the complex where the ubiquinol/plastoquinol reduction reaction takes place. One electron reactions would involve formation of an intermediate, plasto-semiquinone, analogous to the reaction in the  $bc_1$  complex. Two step ubiquinone reduction reactions proposed for the  $bc_1$  complex are described in reactions 20.1a and 20.1b. Ubisemiquinone stabilization at the  $Q_n$  site of the  $bc_1$  complex has been demonstrated (Dikanov et al. 2004), and it is believed that this prevents Q-cycle bypass reactions and reduction of  $O_2$ . Structural differences at the  $Q_n$  site of the  $b_6f$  complex involves an additional prosthetic group, heme  $c_n$ , which overlaps  $Q_n$  in the  $bc_1$  complex (Kurusu et al. 2003). One side of the central heme Fe of heme  $c_n$ , 4 Å from the propionate of heme  $b_n$  (pdb 1VF5, updated to pdb 40GO), with which it shares electrons (Zatsman et al. 2006) and ligates the  $Q_n$  (Hasan et al. 2013). These properties provide a possibility for different mechanisms

of PQ reduction reaction including the possibility of a two electron exchange with quinone/quinol. Two-electron reduction of PQ could be mediated by the two hemes present at the negative side of the complex (reactions 20.2a and 20.2b). The latter mechanism would prevent  $O_2^{\bullet-}$  formation by the  $b_6f$  complex in spite of the hyperoxic conditions in oxygenic photosynthetic membranes.



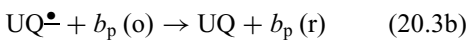
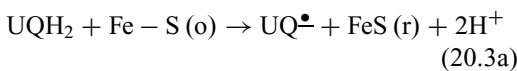
### B. Electron Transfer at the $Q_p$ Site and Q-Cycle Bypass Reactions of Oxygen Reduction

At the  $Q_p$  site of  $bc_1$  complex, ubiquinol is oxidized in a bifurcated reaction that leads to reduction of the [2Fe-2S] iron-sulfur cluster of the Rieske iron-sulfur protein (ISP) (high potential chain) and heme  $b_p$  of cyt *b* in the low potential chain. While the overall principles of the reaction at the  $Q_p$  site are well established, several theories on the mechanism of ubiquinol oxidation at the  $Q_p$  site of the mitochondrial  $bc_1$  complex have been proposed (Bleier and Droese 2013; Crofts et al. 2013; Xia et al. 2013). Single occupancy models propose simultaneous or sequential electron transfer to the [2Fe-2S] and heme  $b_p$ , electron acceptors, while the double-occupancy model involves a cooperation of ubiquinone molecules at the  $Q_p$  site during the ubiquinol oxidation reaction.

During the bifurcated sequential electron transfer reaction of ubiquinol oxidation at the  $Q_p$  site, a limiting first electron transfer to the FeS center of the Rieske

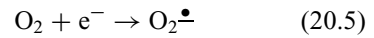
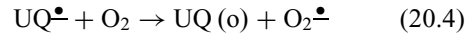


ISP (reaction 20.3a) generates a neutral ubisemiquinone intermediate that interacts with glutamate residue (Glu87 in cyanobacterial and Glu271 or Glu272 in the mitochondrial *bc*<sub>1</sub> complex) of the conserved Pro-Glu-Trp-Tyr (PEWY) sequence (Widger et al. 1984) of the cyt *b* subunit (Crofts 2004; Crofts et al. 2013). The interaction is essential for reduction of heme *b*<sub>p</sub> and electron transfer to the low potential chain (reaction 20.3b) as the glutamate residue is proposed to mediate proton delivery to the p-side exit channel by rotational displacement (Crofts et al. 1999b; Yu et al. 2009; Zhang et al. 2001, 2003; Zito et al. 1998) and opens up a niche for the closer access of anionic ubisemiquinone to heme *b*<sub>p</sub>. It has been suggested that the movement of semiquinone to the proximal domain facilitates rapid electron transfer and insulates it from further reaction with the reoxidized Rieske ISP, or with O<sub>2</sub> (Crofts et al. 1999a). Results of kinetic studies using yeast mutants were inconsistent with this sequential semiquinone mechanism and supported the model in which both electrons are transferred simultaneously from UQH<sub>2</sub> located at the same domain of the Q<sub>p</sub> site (Covian and Trumpower 2009). However, the formation of UQ<sup>•-</sup> has been demonstrated by Cape et al. (2007) and the role of the glutamate residue has been supported by later studies using *Rh. sphaeroides* Glu-295 mutants (Cape et al. 2007; Victoria et al. 2013; Zhang et al. 2007).



Because ubisemiquinone is a reductant of the low potential heme *b*<sub>p</sub> in the *bc*<sub>1</sub> complex, it has been inferred that the UQ<sup>•-</sup> formed at the Q<sub>p</sub> site during UQH<sub>2</sub> oxidase activity has a sufficiently reducing potential to form O<sub>2</sub><sup>•-</sup> in (reaction 20.4) (Trumpower and Gennis 1994). The midpoint redox potential for ubiquinone/quinol is E<sub>m7</sub> = + 60 mV, (Ohnishi and Trumpower 1980). O<sub>2</sub><sup>•-</sup> can be

formed through a one electron reduction of the oxygen molecule, with a midpoint redox potential = -0.14 V (reaction 20.5) (Wood 1988).



A model for formation of O<sub>2</sub><sup>•-</sup> at the Q<sub>p</sub> site involving the semiquinone intermediate was first proposed by (Turrens et al. 1985). Subsequently, O<sub>2</sub><sup>•-</sup> production by the *bc*<sub>1</sub> complex was characterized in vitro (Cape et al. 2007; Drose and Brandt 2008, 2012; Forquer et al. 2006; Muller et al. 2002, 2003; Sarewicz et al. 2010; Sun and Trumpower 2003). The latter studies revealed that O<sub>2</sub><sup>•-</sup> producing activity is effectively controlled under non-inhibited conditions for electron transport. The Q-cycle bypass reaction is activated by *n*-side inhibitors of the *bc*<sub>1</sub> complex, such as antimycin A, or by an over-reduced state of the electron transfer chain (Fig. 20.1a). When the low-potential electron transport chain is blocked, an unstable semiquinone species can escape from the reaction, or oxygen can diffuse into the reaction site, forming superoxide. It was demonstrated that destruction of protein structural integrity by heat inactivation or proteinase K digestion leads to increased production of O<sub>2</sub><sup>•-</sup>, suggesting that “loosening” of structural integrity may facilitate access of molecular oxygen to the Q<sub>p</sub> site or the release of produced O<sub>2</sub><sup>•-</sup> to the aqueous medium (Yin et al. 2010).

Based on the model of consecutive one electron oxidation of UQH<sub>2</sub>, it is inferred that UQ<sup>•-</sup> is formed as an intermediate of the reaction that follows reduction of Fe-S cluster of ISP. Under inhibited conditions, transfer of electrons to the low-potential chain would be hindered and oxidation of ubiquinone would result in accumulation of the UQ<sup>•-</sup> at the Q<sub>p</sub> site (Crofts et al. 2013). The formation of UQ<sup>•-</sup> is followed by O<sub>2</sub> reduction. However, recent studies have demonstrated that O<sub>2</sub><sup>•-</sup> production from the Q<sub>p</sub> site is stimulated by

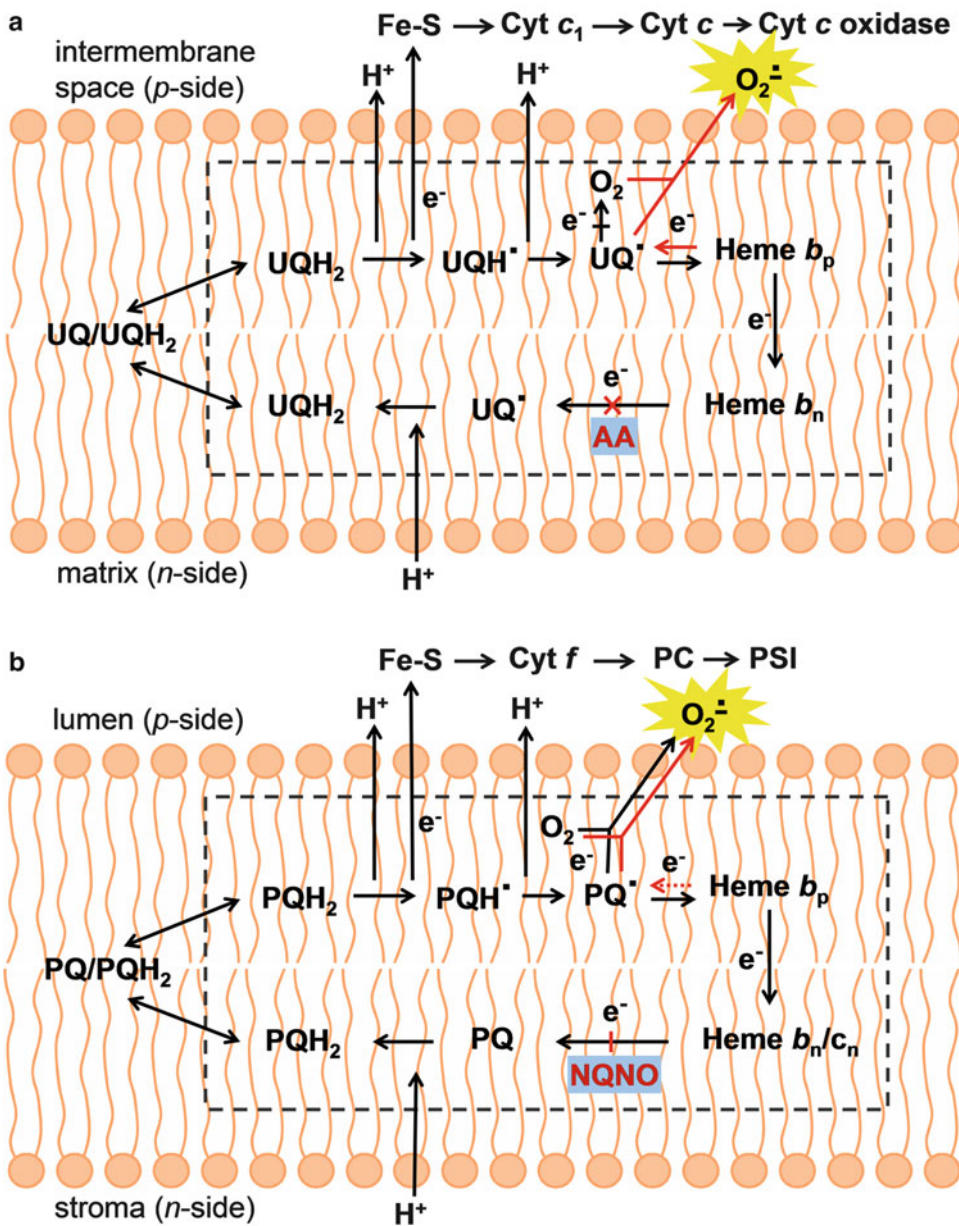
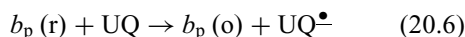


Fig. 20.1. Superoxide producing Q cycle bypass reactions in cytochromes  $bc$ . Black and red arrows indicate Q cycle reactions under uninhibited conditions (reactions 20.1a, 20.1b, 20.2a, 20.2b, 20.3a and 20.3b described in text) and in presence of  $n$ -side inhibitor, respectively, for cyt  $bc_1$  (a) and cyt  $b_6f$  (b) complexes. Reaction stoichiometry is not represented in the figure and could be obtained from the corresponding reactions presented in text. Oxygen reduction by  $UQ^{\bullet-}$  intermediate (reaction 20.4) is largely suppressed under uninhibited conditions for the cyt  $bc_1$  and Q-cycle bypass reaction is activated by  $n$ -side inhibitor antimycin A (a). Accumulation of  $UQ^{\bullet-}$  due to over-reduced state of the low potential electron transfer chain or through a backward Q-cycle reaction, that involves oxidation of the quinone by heme  $b_p$  (reaction 20.6), leads to formation of  $O_2^{\bullet-}$  (reaction 20.4). The  $O_2^{\bullet-}$  production equivalent to approx. 2% of overall ET is sustained in uninhibited cyt  $b_6f$  complex (b). It is proposed that due to structural differences at the  $Q_p$ -site, the life-time of the neutral semiquinone intermediate is expected to be larger and would be important for the enhanced superoxide production (reaction 20.4). Inhibition by  $n$ -side inhibitor NQNO has small effect on linear ET and has no significant effect on  $O_2^{\bullet-}$  production, therefore the role of the over-reduced state of the electron transfer chain and “semireverse” pathway (shown as dashed arrow) in the Q-cycle bypass reaction remains unconfirmed.

the presence of oxidized ubiquinone, suggesting that the dominant reaction for electron transfer to  $O_2$  via ubiquinone might be initiated by reduction of the UQ by heme  $b_p$  (reaction 20.6) (Borek et al. 2008; Drose and Brandt 2008; Rutherford et al. 2012; Sarewicz et al. 2010). The reverse Q-cycle reaction leads to formation of  $UQ^{\bullet-}$  that is followed by the  $O_2$  reduction reaction (reaction 20.4).



Different mechanisms were also proposed for the control of the Q-cycle bypass reaction leading to  $O_2$  reduction that is largely suppressed in the non-inhibited  $bc_1$  complex (Cape et al. 2006). In agreement with different models of  $UQH_2$  oxidation at  $Q_p$  site, the control mechanisms could involve (1) control of stability of the  $UQ^{\bullet-}$  anionic semiquinone (Junemann et al. 1998; Link 1997), (2) formation of the reaction intermediates that support the oxidation reaction of heme  $b_p$  (Cooley et al. 2004; Crofts et al. 1999a; Rich 2004), (3) a structural barrier that prevents diffusion of  $O_2$  into the reaction site or  $UQ^{\bullet-}$  into surrounding media (Yin et al. 2010), (4) a gating mechanism (Mulکیدjianian 2005; Osyczka et al. 2005), or (5) overall avoidance of formation of the semiquinone intermediate (Ding et al. 1995).

### C. Unique Superoxide Production Mechanism of $b_{6f}$ Complex

A high rate of  $O_2^{\bullet-}$  production by the cytochrome  $b_{6f}$  complex of oxygenic photosynthesis has been demonstrated experimentally under in vitro conditions using isolated  $b_{6f}$  complex (Baniulis et al. 2013; Sang et al. 2011). Based on structural analogy with the cytochrome  $bc_1$  complex, it is presumed that bifurcated Q-cycle reactions following oxidation of  $PQH_2$ , at the  $Q_p$  site of the  $b_{6f}$  complex, are analogous to the  $Q_p$  site reactions of the  $bc_1$  complex (reactions 20.1a, 20.1b, 20.2a, 20.2b, 20.3a and 20.3b) (Cramer et al. 2011). While this is supported by observations for Q-cycle

reactions involved in photosynthetic electron transfer, considerable differences may be present when Q-cycle bypass reactions that involve reduction of  $O_2$  are considered (Fig. 20.1b). Experiments with isolated yeast mitochondrial cytochrome  $bc_1$  complex and  $b_{6f}$  complex from cyanobacterial thylakoid membranes demonstrated a greater than one order of magnitude higher  $O_2^{\bullet-}$  production rate by the  $b_{6f}$  complex compared to the mitochondrial  $bc_1$  complex (Baniulis et al. 2013). Such a high rate of  $O_2^{\bullet-}$  production in the  $b_{6f}$  complex could, in principle, be a consequence of a more negative redox potential of heme  $b_p$  which, however, is not supported by existing redox titration data, or an increased residence time of the  $PQ^{\bullet-}$  in its binding niche near the 2Fe-2S cluster of the Rieske ISP.

Regarding redox potentials, there is appreciable variation in  $E_m$  values of the  $b$  hemes in cytochrome  $bc$  complexes (e. g., (Baymann et al. 1999)), which are pH-dependent, dependent on heme exposure to solvent (Kassner 1972), and on the presence of uncoupling agents (Böhme and Cramer 1973). For the isolated yeast  $bc_1$  complex, the  $E_m$  of heme  $b_p$  is  $-90$  mV (Brandt and Trumpower 1994). There is a large variation in the literature of midpoint redox potentials for heme  $b_p$  in the isolated  $b_{6f}$  complex, which may be partly attributed to a difference between titrations done in vitro with isolated  $b_{6f}$  complex compared to those done with thylakoid membranes. Reported  $E_m$  values are:  $-90$  mV, pH 7 (Böhme et al. 1971);  $-172$  mV, pH 6.5 (Gwak et al. 1987);  $-80$  mV, pH 6 (Rich and Bendall 1980);  $-158$  mV, pH 8.0 (Hurt and Hauska 1982). Thus, it seems unlikely that a difference in redox potentials is responsible for the difference in efficiency of superoxide formation.

According to the model of a sequential one-electron quinol oxidation reaction at the  $Q_p$  site of the  $bc_1$  complex (Crofts et al. 2013), the one-electron oxidation of  $PQH_2$  leads to formation of  $PQ^{\bullet-}$ , and this would be followed by generation of  $O_2^{\bullet-}$  in the Q-cycle bypass reaction (reaction 20.5). The high rate of  $O_2^{\bullet-}$  production implies that the

rate constant for the one-electron oxidation of PQH<sub>2</sub> leading to O<sub>2</sub> reduction by PQ<sup>•</sup> is increased relative to that for electron transfer from UQ<sup>•</sup> to heme b<sub>p</sub> in the bc<sub>1</sub> complex. The source of this difference can be PQ<sup>•</sup> generated in the b<sub>6f</sub> complex having a longer life-time in the Q<sub>p</sub> pocket relative to UQ<sup>•</sup> in the bc<sub>1</sub> complex. A suggested structure-based cause of this longer residence time may be the partial occlusion of the Q<sub>p</sub>-portal for quinone entry/exit by the phytyl chain of the unique chlorophyll *a* molecule embedded in each monomer of the complex (Hasan et al. 2013). However, this occlusion would not affect the overall rate of electron transfer through the b<sub>6f</sub> complex and the isolated b<sub>6f</sub> complex supports electron transfer rates (approx. 250–300 s<sup>-1</sup> for spinach and cyanobacterium *M. laminosus* b<sub>6f</sub> complexes) comparable to the activity of the bc<sub>1</sub> complex from yeast (approx. 150 s<sup>-1</sup>) (Baniulis et al. 2013).

As described earlier, the neutral semiquinone species bound within the Q<sub>p</sub> site of cytochrome bc<sub>1</sub> complex undergoes deprotonation via the Glu residue of the conserved PEWY motif (Widger et al. 1984) to form an anionic semiquinone, which can be an electron donor to the low potential chain containing the *b* hemes (Crofts et al. 2013). It has been suggested that Glu78 in subunit IV of the b<sub>6f</sub> complex is similarly involved the second electron transfer in the b<sub>6f</sub> complex. However motion of the Glu78 side chain is expected to be restricted due to the interaction with Arg87 (Hasan et al. 2013). It has previously been reported that the conserved Arg87 of transmembrane helix B in the cytochrome b<sub>6</sub> polypeptide (b<sub>6f</sub> complex) is replaced by a small uncharged residue, such as Ala84 (or Ala83), in the cytochrome *b* (bc<sub>1</sub> complex) (Widger et al. 1984). In the crystal structure of the b<sub>6f</sub> complex, the Glu78 side chain is found to be distant from the quinone analogue inhibitor TDS and it is found in a heme b<sub>p</sub>-proximal position, in which it interacts with the Arg87 over a short distance of 2.8 Å (Hasan et al. 2013). The TDS-distal orientation of the Glu78 side chain in the cytochrome b<sub>6f</sub> complex is in

contrast to the position of the homologous Glu271 in the cytochrome bc<sub>1</sub> complex, where the Glu271 side chain is oriented toward the quinol analog stigmatellin bound within the Q<sub>p</sub>-site (Esser et al. 2004). It is suggested that this interaction restricts motion of Glu78, thereby making proton translocation a less efficient process. As a consequence, the life-time of the neutral semiquinone would be larger within the Q<sub>p</sub>-site of the cytochrome b<sub>6f</sub> complex. This mechanism would be important for enhanced superoxide production assuming a one-electron oxidation of PQH<sub>2</sub> takes place at the Q<sub>p</sub> site of the b<sub>6f</sub> complex, and that it is involved in superoxide production (reaction 20.4) (Baniulis et al. 2013). Another mechanism for formation of semiquinone through a backward Q-cycle reaction would involve oxidation of the semiquinone by heme b<sub>p</sub> as proposed for bc<sub>1</sub> complex, and return of the electron to heme b<sub>p</sub>, a “semireverse” reaction (reaction 20.6). As shown for the Q<sub>n</sub> site of the bc complexes, it cannot be excluded that the Q<sub>p</sub> site of the b<sub>6f</sub> complex might have unique structural and functional aspects that lead to differences in electron transfer, as well as a Q-cycle bypass reaction mechanism. Therefore, in the absence of experimental evidence, it is suggested that either mechanism of formation of the PQ<sup>•</sup> intermediate could be involved in O<sub>2</sub> reduction that takes place at the Q<sub>p</sub> site of the b<sub>6f</sub> complex, and this might be associated with unique functions involved in cell signaling.

In the case of the bc<sub>1</sub> complex, only negligible quantities of O<sub>2</sub><sup>•</sup> are produced by the enzyme in the uninhibited state, meanwhile O<sub>2</sub><sup>•</sup> producing activity is a result of over-reduction of the low potential chain (that could also be invoked by application of *n*-side inhibitors of the bc<sub>1</sub> complex, such as antimycin A) and would signal the reduced state of the electron transfer chain. For the b<sub>6f</sub> complex, O<sub>2</sub><sup>•</sup> is produced at rates that constitute a significant part of uninhibited electron transfer rate and accumulation of substantial amounts of ROS in lumen of thylakoids would be associated with high photo-

synthetic electron transfer activity. An effect of over-reduced state of the photosynthetic electron transfer chain on  $O_2^{\bullet-}$  production could thus far not be confirmed explicitly (Baniulis et al. 2013).

The study of the Q-cycle bypass reactions in the *b<sub>6f</sub>* complex has been impeded due to absence of an *n*-side inhibitor comparable in efficacy to that of antimycin A used in studies with *bc<sub>1</sub>* complex. A quinone binding site homologous to that utilized by antimycin is altered by the presence of the heme *c<sub>n</sub>*, unique to the *b<sub>6f</sub>* complex, whose presence would hinder interactions with an *n*-side quinone analogue inhibitor such as antimycin (Hasan et al. 2013; Kurisu et al. 2003). Another quinone analogue inhibitor, NQNO, binds specifically to the *n*-side heme *c<sub>n</sub>* (Yamashita et al. 2007), and inhibits the oxidation of heme *b<sub>n</sub>* (Furbacher et al. 1989; Jones and Whitmarsh 1988; Rich et al. 1991). However, unlike the inhibition of the respiratory chain that results from the action of antimycin A, the inhibition of linear ET in the *b<sub>6f</sub>* complex is small (Jones and Whitmarsh 1988) and does not have a significant effect on  $O_2^{\bullet-}$  production under *in vitro* conditions (Baniulis et al. 2013). An increase in ROS production in the presence of NQNO was demonstrated for cyanobacteria *in vivo*, but the mechanism that leads to this effect and the implications for  $O_2^{\bullet-}$  producing activity at the *Q<sub>p</sub>* site are unknown (Brantmier 2013).

### III. Signaling Function of ROS Produced by Cytochrome *bc* Complexes

#### A. Role of Superoxide Produced in the *bc<sub>1</sub>* Complex in Regulation of Mitochondrial Function

Lipid membranes are highly impermeable to the charged superoxide anion (Takahashi and Asada 1983). Therefore  $O_2^{\bullet-}$  produced from sources including complex I, pyruvate dehydrogenase, 2-oxoglutarate dehydrogenase and electron transfer proteins may accumulate in the mitochondrial matrix

(Brand 2010). It is notable that alongside glycerol-3-phosphate dehydrogenase, the *Q<sub>p</sub>* site of the *bc<sub>1</sub>* complex is the major source for  $O_2^{\bullet-}$  accumulation in the intermembrane space of mitochondria (Brand 2010). It could also be expected that  $O_2^{\bullet-}$  produced in the intermembrane space could also be released to the cytoplasm through voltage-dependent anion channels (Han et al. 2003) or other outer membrane channels such as the translocase of the outer membrane (Perry et al. 2008) and the peptide-sensitive channel (Henry et al. 1996).  $O_2^{\bullet-}$  can also be scavenged by cytochrome *c* that is electrostatically bound at the surface of the inner mitochondrial membrane (Lenaz 1988). In addition, reaction with nitric oxide would yield peroxynitrite, another reactive species important in cell signaling (Liaudet et al. 2009). However, most of the  $O_2^{\bullet-}$  could be expected to dismutate to  $H_2O_2$  spontaneously or at rates higher by three orders of magnitude through the superoxide dismutase catalyzed reaction in the intermembrane space and cytoplasm (Miwa et al. 2008). Due to the short lifetime of the  $O_2^{\bullet-}$  the implications of the separation of  $O_2^{\bullet-}$  production and transfer between different mitochondrial compartments and the cytoplasm for cell signaling pathways are unclear. It is possible that superoxide signaling generated by the *bc<sub>1</sub>* complex is mostly mediated by  $H_2O_2$  or nitric oxide. Under hypoxia conditions,  $H_2O_2$  has been shown to mediate mitochondrial signaling that involves  $O_2^{\bullet-}$  production at the *Q<sub>p</sub>* site of the *bc<sub>1</sub>* complex (Chandel et al. 1998).

Generation of ROS from the *bc<sub>1</sub>* complex in mammals (including humans) is increased under hypoxia conditions (Chandel et al. 1998). The molecular reactions that follow the increase in ROS generation under low  $O_2$  conditions are not fully understood. However, it has been suggested that ROS produced by the *bc<sub>1</sub>* complex is involved in stabilization of Hypoxia-Inducible Factor-1 $\alpha$  (HIF-1) and the vasoconstriction response to alveolar hypoxia in the lungs (Waypa and Schumacker 2005). In addition, it has been demonstrated that low concentrations of ROS

are involved in protective mechanisms during the ischemic preconditioning that diminishes cardiac damage by ischemia reperfusion injury (Penna et al. 2009).

Production of ROS was shown to be important as an O<sub>2</sub> sensor to trigger a physiological response under hypoxic conditions (Schumacker 2014). Genetic studies using knockdown mutants and application of inhibitors of the Q<sub>p</sub> site of the bc<sub>1</sub> complex linked the response to O<sub>2</sub><sup>•</sup>-producing activity of the bc<sub>1</sub> complex (Bell et al. 2007; Brunelle et al. 2005; Chandel et al. 2000; Mansfield et al. 2005). The molecular basis through which lower O<sub>2</sub> concentrations increased the O<sub>2</sub><sup>•</sup> production at the Q<sub>p</sub> site is unknown. In addition, other mitochondrial sources of ROS could be involved in the response to hypoxic conditions (Chandel 2010; Paddenberget al. 2003). A model has been proposed in which hypoxia induces increased generation of ROS within mitochondria resulting in activation of signaling cascades leading to: (1) a decrease in Na<sup>+</sup>/K<sup>+</sup> ATPase activity that decreases cellular demand for O<sub>2</sub> and diminishes the risk of cells reaching anoxia; (2) accumulation of HIF-1 protein which leads to transcriptional up-regulation of vascular endothelial growth factor that stimulates angiogenesis and ensures a better supply of O<sub>2</sub>.

As part of the mechanism of control of O<sub>2</sub> concentration in body tissues, mitochondrial ROS might be implicated in hypoxic pulmonary vasoconstriction (HPV) (Sylvester et al. 2012). The process is mediated through an increase of intracellular calcium concentration in the pulmonary artery smooth muscle cells and evokes constriction of pulmonary arteries that is important for maintaining ventilation-perfusion ratio and blood oxygenation during hypoxia. Several mechanisms have been proposed for the O<sub>2</sub> sensing required to initiate HPV (Connolly and Aaronson 2010), including the suggestion that reduced O<sub>2</sub> levels cause a fall in ROS production and a shift of cells to a more reduced state that triggers calcium-mediated HVP response (Weir and Archer 1995). However, recent

evidence suggests that acute hypoxia leads to an increase in mitochondrial ROS production (Waypa et al. 2006, 2010). In this case, O<sub>2</sub><sup>•</sup> released from the bc<sub>1</sub> complex diffuses into the cytosol, triggering a calcium release from sarcoplasmic reticulum and secondary Ca<sup>2+</sup> entry through sarcolemmal store-operated Ca<sup>2+</sup> channels into the cytosol (Wang et al. 2012) and the HPV response of smooth muscle cells (Waypa et al. 2013).

O<sub>2</sub><sup>•</sup> and H<sub>2</sub>O<sub>2</sub> generated by electron transfer complexes of mitochondria might play a role in the triggering of cardioprotection by heart pre-conditioning (Baines et al. 1997; Tritto et al. 1997). Although the mechanism of redox signaling involved in preconditioning is still not completely understood, it was demonstrated that cardioprotection is mediated by mitochondrial ATP-sensitive potassium channels and mitochondrial ROS. Mitochondrial ROS signaling that occurs during the early phase of reperfusion was shown to be necessary for effective protection of the preconditioned heart (Hausenloy et al. 2007; Liu et al. 2008).

Concerning plant mitochondria, a similar signaling function might be expected to be involved in hypoxic stress of plant cells that is induced by water flooding or high metabolic activity. Although the mechanism of oxygen sensing involved in response to such hypoxic conditions is unknown, an increase in ROS accumulation is observed under hypoxic conditions (Ershova et al. 2011), and a role for ROS in oxygen sensing mechanisms has been proposed (Sasidharan and Mustroph 2011).

### B. Signaling Role of O<sub>2</sub><sup>•</sup> in Chloroplasts

Chloroplasts, on the other hand, are plant cell organelles specialized for light energy transduction. In addition, the components of the electron transport system can function as mediators of environmental signals (Pfannschmidt et al. 2001). High irradiance and photosynthetic activity create hyperoxic conditions in chloroplasts. Therefore, O<sub>2</sub> reduction in chloroplasts is inevitable and leads to the formation of ROS. In

chloroplasts, O<sub>2</sub> photoreduction is estimated to be about 5–27 % of the total electron flow (Cakmak and Marschner 1992) and the organelle is a major source of ROS in plant cells (Foyer and Shigeoka 2011).

The major sources of ROS generated in chloroplasts are PSII (<sup>1</sup>O<sub>2</sub>) and PSI (O<sub>2</sub><sup>•-</sup>) (Asada et al. 1974; Telfer et al. 1994; Hideg et al. 1998). In addition, O<sub>2</sub><sup>•-</sup> production *in vivo* by the *b<sub>6</sub>f* complex has been documented (Horn 2004), and the activity has been characterized *in vitro* (Baniulis et al. 2013; Sang et al. 2011). The accumulated O<sub>2</sub><sup>•-</sup> is metabolized to a more stable form of ROS H<sub>2</sub>O<sub>2</sub>, as well as other reactive species such as hydroxyl radical or peroxynitrite, the latter in the presence of iron ions or NO (Apel and Hirt 2004; Huie and Padmaja 1993).

The production of ROS during photosynthetic reactions in chloroplasts is a major cause of oxidative damage of membrane lipids, proteins and DNA (Moller et al. 2007). However, ROS that evolve during photosynthetic ET are important for dissipation of excess excitation energy (Mullineaux and Karpinski 2002), and as the ROS produced in mitochondria, the reactive oxygen species mediate signals from the organelle to the cytosol and nucleus in stress response and pathogen defense (Foyer and Noctor 2003; Galvez-Valdivieso and Mullineaux 2010; Trotta et al. 2014; Zurbriggen et al. 2010).

As discussed above, the signaling function of ROS produced in mitochondria is mostly linked to cell adaptation under hypoxic and anoxic conditions. However, O<sub>2</sub><sup>•-</sup> production during photosynthesis proceeds under different conditions compared to mitochondrial respiratory electron transfer. High irradiance and photosynthetic activity create hyperoxic conditions in chloroplasts. Therefore, functions other than oxygen sensing would be expected for O<sub>2</sub><sup>•-</sup> generated by the *b<sub>6</sub>f* complex during photosynthetic electron transfer. In addition, spatial localization of O<sub>2</sub><sup>•-</sup> production is different in mitochondria and chloroplasts. While O<sub>2</sub><sup>•-</sup> generated by *bc<sub>1</sub>* complex is directed to the intermembrane space of mitochondria, the Q<sub>p</sub> site of the *b<sub>6</sub>f* complex is oriented towards the luminal side

of the thylakoid membrane and, therefore, O<sub>2</sub><sup>•-</sup> produced by the *b<sub>6</sub>f* complex is released to the thylakoid lumen.

### C. Interaction Between O<sub>2</sub><sup>•-</sup> Producing Activities of the Photosynthetic ET Chain

In addition to the linear electron flow from water to NADP<sup>+</sup> used for CO<sub>2</sub> assimilation and photorespiration, photosynthetic ET includes a cyclic electron transfer pathway and ‘pseudocyclic electron pathway’ or a water–water cycle (Asada 1999). For the latter, electrons that are transferred by photosynthetic ET chain from the oxygen evolving complex of PSII are donated to O<sub>2</sub> through photoreduction, leading to formation of O<sub>2</sub><sup>•-</sup> by the PSI reaction center coupled to the PSI electron acceptors ferredoxin, thioredoxin and ferredoxin:NADP<sup>+</sup> oxidoreductase (Mehler reaction) (Foyer et al. 2012; Mehler 1951). The O<sub>2</sub><sup>•-</sup> subsequently disproportionates to H<sub>2</sub>O<sub>2</sub> and is detoxified to water by the ascorbate peroxidase pathway (Asada 1999). The Mehler reaction is important as a bypass or branch used to control over-reduction of the photosynthetic ET chain. In addition, the production of ROS mediates redox signaling that regulates activity of photosynthetic ET chain and gene expression, as discussed above and in Foyer et al. (2012).

While the Mehler reaction proceeds in the chloroplast stroma, O<sub>2</sub><sup>•-</sup> produced by *b<sub>6</sub>f* complex is released to the thylakoid lumen. The presence of Cu, Zn-superoxide dismutase in the lumen has been demonstrated (Hayakawa et al. 1984). This ensures fast dismutation of O<sub>2</sub><sup>•-</sup> to H<sub>2</sub>O<sub>2</sub> that can diffuse from the lumen through thylakoid and chloroplast membranes. Therefore, O<sub>2</sub><sup>•-</sup> production by the *b<sub>6</sub>f* complex inside the lumen contributes to signaling or excess energy dissipation mediated by the ROS produced during the Mehler reaction that proceeds in the stroma. It could be presumed that distribution of ROS between the two compartments, thylakoid lumen and stroma, might contribute to control of redox balance between the PQ pool in the thylakoid membrane and PSI acceptors in the stroma. Under favorable light conditions and the presence of a

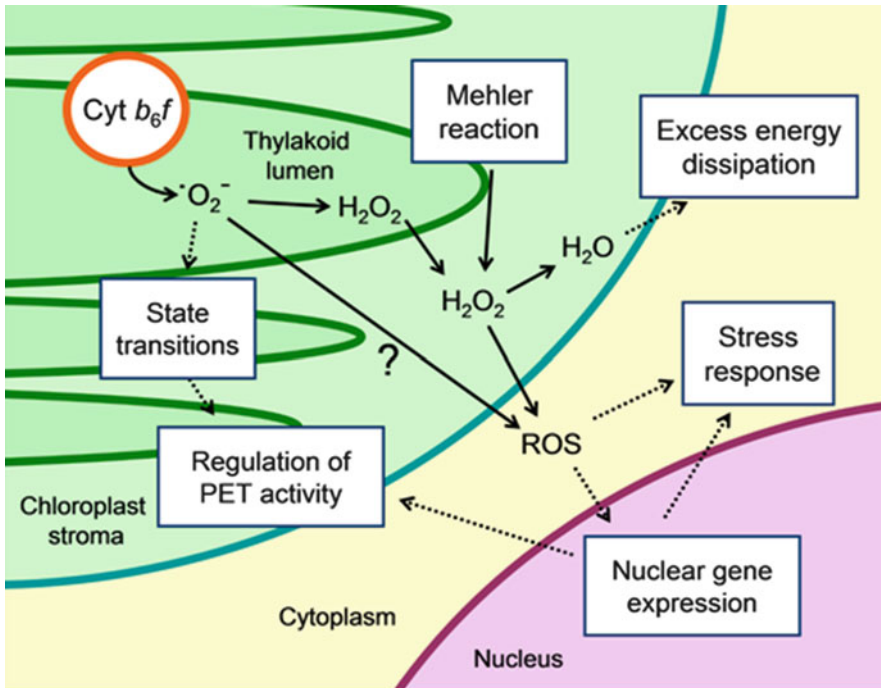


Fig. 20.2. Function of superoxide produced in chloroplasts. Schematic representation shows translocation within the cell of  $O_2^{\bullet-}$  produced by photosynthetic *cyt b<sub>6</sub>f* complex and its transformation reactions to other ROS (solid arrows). Cellular processes regulated by the ROS in different cellular compartments linked with dashed arrows. Mehler reaction is shown in the figure as another major contributor to  $H_2O_2$  production in chloroplast stroma that might have synergistic effect in regulation of photosynthetic and other cellular processes together with the *cyt b<sub>6</sub>f* complex producing  $O_2^{\bullet-}$  in chloroplast lumen.

reduced PQ pool and oxidized stroma, linear ET would cause ROS accumulation in the lumen, due to the  $O_2^{\bullet-}$  producing activity of the *b<sub>6</sub>f* complex and the Mehler reaction would proceed at a slow rate. Over-reduction of both ET chain components, PQ pool and PSI acceptors in the stroma, would cause an increase in the rate of the Mehler reaction, and ROS accumulation would become balanced between the lumenal and stromal sides of the thylakoid membrane. In addition, this balance would be modulated by the activity of PSI, as a low PSI activity would cause: (1) over-reduction of the plastocyanin pool which would slow down linear ET, and  $O_2^{\bullet-}$  producing activity of the *b<sub>6</sub>f* complex; (2) a decrease in the rate of the Mehler reaction which would lead to reduction of overall  $O_2^{\bullet-}$ -producing activity by the ET chain (Fig. 20.2).

#### D. Regulation of Photosynthetic State Transitions

Photosynthetic state transitions maintain the redox poise of the thylakoid membrane PQ pool (Allen 1992; Wollman 2001). Light harvesting complexes preferentially associate with PSII when the PQ pool and the *b<sub>6</sub>f* complex is oxidized, and with PS I when the PQ pool is reduced. The presence of reduced plastoquinone activates an Stt7/Stn7 protein kinase that phosphorylates light-harvesting complex LHCII and leads to the reversible displacement of the mobile LHCII between the photosystems (Rochaix 2007). The *b<sub>6</sub>f* complex plays a key role in the activation of the kinase (Wollman 2001). It has been demonstrated that the Stt7/Stn7 is bound to the *b<sub>6</sub>f* complex in thylakoid membranes, in a molar ratio of



approximately 1:20 kinase:*b<sub>6f</sub>* complex (Lemeille et al. 2009). In spite of the identification of the kinase and the PQH<sub>2</sub> binding to *b<sub>6f</sub>* as a key step in the activation of the kinase, the mechanism by which the PQH<sub>2</sub> is sensed in the Q<sub>p</sub>-portal and the nature of the transmembrane signal remain unknown.

It was proposed that redox signaling that involves *b<sub>6f</sub>* complex might be associated with regulation of state transitions (Kallas 2012), which could be linked to the O<sub>2</sub><sup>•-</sup>-producing activity of the *b<sub>6f</sub>* complex (Fig. 20.2). Although *in vivo* experiments with application of exogenous ROS did not confirm that ROS signaling is required for regulation of state transitions in cyanobacteria (Brantmier 2013), this does not exclude the possibility that regulation of the Stt7/Stn7 kinase activity could be directly linked to Q-cycle bypass reactions that proceed at the Q<sub>p</sub>-site.

Vener et al., proposed a model according to which the Stt7/Stn7 kinase activation is related to occupancy of the Q<sub>p</sub> site of the cytochrome *b<sub>6f</sub>* complex by plastoquinol (Vener et al. 1997). In addition, it has been suggested that upon binding of PQH<sub>2</sub> at the Q<sub>p</sub>-site, a signal is transduced from the ISP soluble domain through the ISP transmembrane helix to the N-terminus of the ISP on the *n*-side, which may provide the interaction site for the kinase (Hasan and Cramer 2012). As discussed in previous sections, the high rate of O<sub>2</sub><sup>•-</sup> production in the *b<sub>6f</sub>* complex could be associated with an increased residence time of the PQ<sup>•</sup> in its binding niche near the Fe-S cluster of the Rieske ISP. Therefore, it was proposed that the increased residence time of PQ<sup>•</sup> generated at the Q<sub>p</sub>-site in the *b<sub>6f</sub>* complex may be a consequence of the formation of a long-lived ISP- PQ<sup>•</sup> interaction that is required to provide enough time for the transmission of the signal through the ISP transmembrane helix to the *n*-side of the complex, where the Stt7/Stn7 kinase is recruited for interaction with the *b<sub>6f</sub>* complex.

### *E. ROS in Chloroplast Retrograde Signaling and Modulation of Abiotic Stress Response and Pathogen Defense*

Chloroplast proteins are encoded by genes located in genomes of both the nucleus and the plastid. Bidirectional signaling pathways ensures coordination of the protein synthesis and transport. Chloroplasts not only receive signals from the nucleus, but can also influence nuclear gene expression via chloroplast-to-nucleus retrograde signaling (Jung and Chory 2010; Nott et al. 2006). The redox state of photosynthetic electron transport components and ROS production comprise one of the retrograde signaling pathways that is crucial in regulation of plant responses to environmental stress (Barajas-Lopez et al. 2013; Fey et al. 2005; Nott et al. 2006). Increased levels of ROS serve as a signal of the functional and developmental state of the chloroplasts that is transferred to the nucleus and leads to change in nuclear gene expression. Chloroplast ROS-initiated signaling is implicated not only in the regulation of expression of nuclear genes associated with chloroplast development but has also been shown to be involved in plant acclimation to a variety of environmental stresses (Li et al. 2013; Pfalz et al. 2012; Suzuki et al. 2012) and pathogen defense signaling (Kangasjarvi et al. 2014; Karpinski et al. 2003, 2013; Trotta et al. 2014; Zurbriggen et al. 2010).

ROS accumulation in different plant cell compartments and routes by which such signal might reach the nucleus has been reviewed recently (Shapiguzov et al. 2012). Several major ROS signals that evolve from the activity of the photosynthetic ET chain, including <sup>1</sup>O<sub>2</sub>, O<sub>2</sub><sup>•-</sup> and H<sub>2</sub>O<sub>2</sub>, may act as signal mediators of the retrograde signaling network (Barajas-Lopez et al. 2013; Inaba et al. 2011; Yurina and Odintsova 2011). The function of different ROS molecules is defined by their chemical properties and sites of generation. Singlet oxygen (<sup>1</sup>O<sub>2</sub>) generated in PSII is most likely retained within chloroplasts considering its short lifetime (on the

order of 0.1  $\mu$ s (Baker and Kanofsky 1992)) and distance traveled. Despite this fact, it was demonstrated that  $^1\text{O}_2$  accumulates in chloroplasts and affects the expression of several nuclear genes (Kim et al. 2008).

As discussed in the previous section,  $\text{O}_2^{\bullet-}$  produced by components of the ET chain (such as PSI or  $b_6f$  complex) could be converted into  $\text{H}_2\text{O}_2$  that has a longer half life-time and diffuses across the chloroplast membrane into the cytoplasm (Pfannschmidt 2003). It has been demonstrated that  $\text{H}_2\text{O}_2$  can interact with downstream mediators of signaling networks, including MAP kinase cascades or *rimb* (redox imbalanced) components (Heiber et al. 2007; Kovtun et al. 2000), which lead to activation of Rcd1 and Rap2.4 transcription factors and expression of stress responsive genes (Shaikhali et al. 2008). The Gun1 (*genomes uncoupled 1*) protein was demonstrated to be a ROS signal mediator, although the mechanism underlying its function remains undefined (Cottage et al. 2008).

To identify ROS-responsive genes and to clarify the function of ROS as signaling molecules, transcript analyses have been performed using ROS-generating agents or mutants lacking antioxidative enzymes (Gadjev et al. 2006; Gechev et al. 2004; Vandenamee et al. 2004). Increases in  $\text{H}_2\text{O}_2$  concentrations have been shown to be important for the induction of the ascorbate peroxidase gene, APX2, and for the expression of a number of genes involved in plant development and stress responses (Vanderauwera et al. 2005). Recently, light was shed on  $\text{H}_2\text{O}_2$  signaling and expression of ROS-responsive genes through the use of plants expressing glycolate oxidase that generate endogenous  $\text{H}_2\text{O}_2$  in chloroplasts (Balazadeh et al. 2012). The study revealed a rapid and coordinated expression response of ROS-affected genes. These studies demonstrated the existence of multiple pathways implicated in ROS signaling. Interactions between signaling pathways are thought to modulate plant responses to abiotic and biotic stress.

ROS produced in chloroplasts interacts with signals from other intracellular and extracellular ROS sources in the modulation of local and systemic responses of plant immune defense (Kangasjarvi et al. 2014; Karpinski et al. 2013; Zurbriggen et al. 2010) (Fig. 20.2). Conditions that stimulate reduction of the photosynthetic electron transport chain and the overproduction of ROS induce gene expression of pathogen resistance and trigger a pathogen-induced hypersensitive response (Karpinski et al. 1999; Rossel et al. 2007). Studies with the *LSD1* gene mutant *Arabidopsis thaliana* plants demonstrated that induction of the “cell death response” is regulated by ET transfer chain activity and the redox status of the PQ pool (Muhlenbock et al. 2008). Treatment of plant leaves with the quinone analog inhibitor DBMIB decreases the rate of  $\text{PQH}_2$  pool oxidation and triggers production of  $\text{H}_2\text{O}_2$  required for induction of defense response. This observation suggests that the  $\text{O}_2^{\bullet-}$ -producing activity of the  $b_6f$  complex does not contribute to the ROS production required for the plant defense signaling process, as  $\text{O}_2^{\bullet-}$  production at the  $\text{Q}_p$  site is blocked by the presence of DBMIB (Baniulis et al. 2013).

The research during last decade revealed that the redox state of photosynthetic electron transport components acting through multiple ROS-mediated chloroplast retrograde signaling pathways is crucial in regulation of plant responses to environmental stress. Despite the fact that the role of plant ROS has been the subject of intensive research, the available data about the extent to which the ROS evolving from activity of different photosynthetic ET chain components, and specifically the  $b_6f$  complex, contribute to plant responses to environmental stress are still fragmented.

## References

- Allen JF (1992) Protein phosphorylation in regulation of photosynthesis. *Biochim Biophys Acta* 1098:275–335

- Apel K, Hirt H (2004) Reactive oxygen species: metabolism, oxidative stress, and signal transduction. *Annu Rev Plant Biol* 55:373–399
- Asada K (1999) The water-water cycle in chloroplasts: scavenging of active oxygens and dissipation of excess photons. *Annu Rev Plant Physiol Plant Mol Biol* 50:601–639
- Asada K, Kiso K, Yoshikawa K (1974) Univalent reduction of molecular oxygen by spinach chloroplasts on illumination. *J Biol Chem* 249:2175–2181
- Ashtamker C, Kiss V, Sagi M, Davydov O, Fluhr R (2007) Diverse subcellular locations of cryptogein-induced reactive oxygen species production in tobacco Bright Yellow-2 cells. *Plant Physiol* 143:1817–1826
- Baines CP, Goto M, Downey JM (1997) Oxygen radicals released during ischemic preconditioning contribute to cardioprotection in the rabbit myocardium. *J Mol Cell Cardiol* 29:207–216
- Baker A, Kanofsky JR (1992) Quenching of singlet oxygen by biomolecules from L1210 leukemia cells. *Photochem Photobiol* 55:523–528
- Balazadeh S, Jaspert N, Arif M, Mueller-Roeber B, Maurino VG (2012) Expression of ROS-responsive genes and transcription factors after metabolic formation of H<sub>2</sub>O<sub>2</sub> in chloroplasts. *Front Plant Sci* 3:234
- Baniulis D, Hasan SS, Stoffleth JT, Cramer WA (2013) Mechanism of enhanced superoxide production in the cytochrome b(6)f complex of oxygenic photosynthesis. *Biochemistry* 52:8975–8983
- Barajas-Lopez JD, Blanco NE, Strand A (2013) Plastid-to-nucleus communication, signals controlling the running of the plant cell. *Biochim Biophys Acta* 1833:425–437
- Baymann F, Robertson DE, Dutton PL, Mantele W (1999) Electrochemical and spectroscopic investigations of the cytochrome bc<sub>1</sub> complex from *Rhodobacter capsulatus*. *Biochemistry* 38:13188–13199
- Bell EL, Klimova TA, Eisenbart J, Moraes CT, Murphy MP, Budinger GR, Chandel NS (2007) The Q<sub>o</sub> site of the mitochondrial complex III is required for the transduction of hypoxic signaling via reactive oxygen species production. *J Cell Biol* 177:1029–1036
- Bleier L, Drose S (2013) Superoxide generation by complex III: from mechanistic rationales to functional consequences. *Biochim Biophys Acta* 1827:1320–1331
- Böhme H, Cramer WA (1973) Uncoupler-dependent decrease in midpoint potential of the chloroplast cytochrome b<sub>6</sub>. *Biochim Biophys Acta* 325:275–283
- Böhme H, Reimer S, Trebst A (1971) Role of plastoquinone in photosynthesis: effect of dibromothymoquinone, an antagonist of plastoquinone, on non cyclic and cyclic electron flow systems in isolated chloroplasts. *Z Naturforsch B* 26:341–352
- Borek A, Sarewicz M, Osyczka A (2008) Movement of the iron-sulfur head domain of cytochrome bc<sub>1</sub> transiently opens the catalytic Q<sub>o</sub> site for reaction with oxygen. *Biochemistry* 47:12365–12370
- Boveris A, Cadenas E, Stoppani AO (1976) Role of ubiquinone in the mitochondrial generation of hydrogen peroxide. *Biochem J* 156:435–444
- Brand MD (2010) The sites and topology of mitochondrial superoxide production. *Exp Gerontol* 45:466–472
- Brandt U, Trumpower B (1994) The protonmotive Q cycle in mitochondria and bacteria. *Crit Rev Biochem Mol Biol* 29:165–197
- Brantmier PJ (2013) Redox regulation of photosynthesis by the cytochrome bf complex: mechanisms and consequences. Thesis/Dissertation, University of Wisconsin Oshkosh. pp 1–151
- Brunelle JK, Bell EL, Quesada NM, Vercauteren K, Tiranti V, Zeviani M, Scarpulla RC, Chandel NS (2005) Oxygen sensing requires mitochondrial ROS but not oxidative phosphorylation. *Cell Metab* 1:409–414
- Cadenas E (1995) Mechanisms of oxygen activation and reactive oxygen species detoxification. In: Ahmad S (ed) *Oxidative Stress and Antioxidant Defenses in Biology*. Springer, New York, pp 1–16
- Cadenas E, Boveris A, Ragan CI, Stoppani AO (1977) Production of superoxide radicals and hydrogen peroxide by NADH-ubiquinone reductase and ubiquinol-cytochrome c reductase from beef-heart mitochondria. *Arch Biochem Biophys* 180:248–257
- Cakmak I, Marschner H (1992) Magnesium deficiency and high light intensity enhance activities of superoxide dismutase, ascorbate peroxidase, and glutathione reductase in bean leaves. *Plant Physiol* 98:1222–1227
- Cape JL, Bowman MK, Kramer DM (2006) Understanding the cytochrome bc complexes by what they don't do. The Q-cycle at 30. *Trends Plant Sci* 11:46–55
- Cape JL, Bowman MK, Kramer DM (2007) A semiquinone intermediate generated at the Q<sub>o</sub> site of the cytochrome bc<sub>1</sub> complex: importance for the Q-cycle and superoxide production. *Proc Natl Acad Sci USA* 104:7887–7892
- Chandel NS (2010) Mitochondrial regulation of oxygen sensing. *Adv Exp Med Biol* 661:339–354
- Chandel NS, Maltepe E, Goldwasser E, Mathieu CE, Simon MC, Schumacker PT (1998) Mitochondrial

- reactive oxygen species trigger hypoxia-induced transcription. *Proc Natl Acad Sci USA* 95:11715–11720
- Chandel NS, McClintock DS, Feliciano CE, Wood TM, Melendez JA, Rodriguez AM, Schumacker PT (2000) Reactive oxygen species generated at mitochondrial complex III stabilize hypoxia-inducible factor-1 $\alpha$  during hypoxia: a mechanism of O<sub>2</sub> sensing. *J Biol Chem* 275:25130–25138
- Connolly MJ, Aaronson PI (2010) Cell redox state and hypoxic pulmonary vasoconstriction: recent evidence and possible mechanisms. *Respir Physiol Neurobiol* 174:165–174
- Cooley JW, Roberts AG, Bowman MK, Kramer DM, Daldal F (2004) The raised midpoint potential of the [2Fe2S] cluster of cytochrome bc<sub>1</sub> is mediated by both the Qo site occupants and the head domain position of the Fe-S protein subunit. *Biochemistry* 43:2217–2227
- Cottage A, Mott E, Wang JH, Sullivan J, MacLean D, Tran L, Choy MK, . . . , Gray J (2008) GUN1 (GENOMES UNCOUPLED1) Encodes a pentatricopeptide repeat (PPR) protein involved in plastid protein synthesis-responsive retrograde signaling to the nucleus. In: Allen J, Gantt E, Golbeck J, Osmond B (eds) *Photosynthesis: Energy From The Sun*. Springer, Dordrecht, pp 1201–1205
- Covian R, Trumppower BL (2009) The rate-limiting step in the cytochrome bc<sub>1</sub> complex is not changed by inhibition of cytochrome b-dependent deprotonation: implications for the mechanism of ubiquinol oxidation at center P of the bc<sub>1</sub> complex. *J Biol Chem* 284:14359–14367
- Cramer WA, Baniulis D, Yamashita E, Zhang H, Zatsman AI, Hendrich MP (2008) Cytochrome b<sub>6</sub>f complex, structure, spectroscopy, and function of the heme cn and n-side electron and proton transfer reactions. In: Fromme P (ed) *Photosynthetic Protein Complexes: A Structural Approach*. Wiley-VCH Verlag GmbH & Co. KGaA, Weinheim, pp 155–179
- Cramer WA, Hasan SS, Yamashita E (2011) The Q cycle of cytochrome bc complexes: a structure perspective. *Biochim Biophys Acta* 1807:788–802
- Crofts AR (2004) Proton-coupled electron transfer at the Qo-site of the bc<sub>1</sub> complex controls the rate of ubihydroquinone oxidation. *Biochim Biophys Acta* 1655:77–92
- Crofts AR, Berry EA (1998) Structure and function of the cytochrome bc<sub>1</sub> complex of mitochondria and photosynthetic bacteria. *Curr Opin Struct Biol* 8:501–509
- Crofts AR, Barquera B, Gennis RB, Kuras R, Guergova-Kuras M, Berry EA (1999a) Mechanism of ubiquinol oxidation by the bc<sub>1</sub> complex: different domains of the quinol binding pocket and their role in the mechanism and binding of inhibitors. *Biochemistry* 38:15807–15826
- Crofts AR, Barquera B, Gennis RB, Kuras R, Guergova-Kuras M, Berry EA (1999b) Pathways for proton release during ubihydroquinone oxidation by the bc<sub>1</sub> complex. *Proc Natl Acad Sci USA* 96:10021–10026
- Crofts AR, Hong S, Wilson C, Burton R, Victoria D, Harrison C, Schulten K (2013) The mechanism of ubihydroquinone oxidation at the Qo-site of the cytochrome bc<sub>1</sub> complex. *Biochim Biophys Acta* 1827:1362–1377
- Dikanov SA, Samoilova RI, Kolling DR, Holland JT, Crofts AR (2004) Hydrogen bonds involved in binding the Qi-site semiquinone in the bc<sub>1</sub> complex, identified through deuterium exchange using pulsed EPR. *J Biol Chem* 279:15814–15823
- Ding H, Moser CC, Robertson DE, Tokito MK, Daldal F, Dutton PL (1995) Ubiquinone pair in the Qo site central to the primary energy conversion reactions of cytochrome bc<sub>1</sub> complex. *Biochemistry* 34:15979–15996
- Drose S, Brandt U (2008) The mechanism of mitochondrial superoxide production by the cytochrome bc<sub>1</sub> complex. *J Biol Chem* 283:21649–21654
- Drose S, Brandt U (2012) Molecular mechanisms of superoxide production by the mitochondrial respiratory chain. *Adv Exp Med Biol* 748:145–169
- Ershova AN, Popova NV, Berdnikova OS (2011) Production of reactive oxygen species and antioxidant enzymes of pea and soybean plants under hypoxia and high CO<sub>2</sub> concentration in medium. *Russ J Plant Physiol* 58:982–990
- Esser L, Quinn B, Li YF, Zhang M, Elberry M, Yu L, Yu CA, Xia D (2004) Crystallographic studies of quinol oxidation site inhibitors: a modified classification of inhibitors for the cytochrome bc<sub>1</sub> complex. *J Mol Biol* 341:281–302
- Fey V, Wagner R, Brautigam K, Wirtz M, Hell R, Dietzmann A, Leister D, . . . , Pfannschmidt T (2005) Retrograde plastid redox signals in the expression of nuclear genes for chloroplast proteins of *Arabidopsis thaliana*. *J Biol Chem* 280:5318–5328
- Forquer I, Covian R, Bowman MK, Trumppower BL, Kramer DM (2006) Similar transition states mediate the Q-cycle and superoxide production by the cytochrome bc<sub>1</sub> complex. *J Biol Chem* 281:38459–38465
- Foyer CH, Noctor G (2003) Redox sensing and signalling associated with reactive oxygen in chloroplasts, peroxisomes and mitochondria. *Physiol Plant* 119:355–364

- Foyer CH, Shigeoka S (2011) Understanding oxidative stress and antioxidant functions to enhance photosynthesis. *Plant Physiol* 155:93–100
- Foyer CH, Neukermans J, Queval G, Noctor G, Harbinson J (2012) Photosynthetic control of electron transport and the regulation of gene expression. *J Exp Bot* 63:1637–1661
- Furbacher PN, Girvin ME, Cramer WA (1989) On the question of interheme electron transfer in the chloroplast cytochrome *b6* in situ. *Biochemistry* 28:8990–8998
- Gadjev I, Vanderauwera S, Gechev TS, Laloi C, Minkov IN, Shulaev V, Apel K, ... , Van BF (2006) Transcriptomic footprints disclose specificity of reactive oxygen species signaling in Arabidopsis. *Plant Physiol* 141:436–445
- Galvez-Valdivieso G, Mullineaux PM (2010) The role of reactive oxygen species in signalling from chloroplasts to the nucleus. *Physiol Plant* 138:430–439
- Gechev TS, Gadjev IZ, Hille J (2004) An extensive microarray analysis of AAL-toxin-induced cell death in Arabidopsis thaliana brings new insights into the complexity of programmed cell death in plants. *Cell Mol Life Sci* 61:1185–1197
- Gwak SH, Yang FD, Yu L, Yu CA (1987) Phospholipid-dependent interaction between dibromothymoquinone and iron-sulfur protein in mitochondrial ubiquinol-cytochrome *c* reductase. *Biochim Biophys Acta* 890:319–325
- Han D, Antunes F, Canali R, Rettori D, Cadenas E (2003) Voltage-dependent anion channels control the release of the superoxide anion from mitochondria to cytosol. *J Biol Chem* 278:5557–5563
- Hasan SS, Cramer WA (2012) Lipid functions in cytochrome *bc* complexes: an odd evolutionary transition in a membrane protein structure. *Philos Trans R Soc B* 367:3406–3411
- Hasan SS, Yamashita E, Baniulis D, Cramer WA (2013) Quinone-dependent proton transfer pathways in the photosynthetic cytochrome *b6f* complex. *Proc Natl Acad Sci USA* 110:4297–4302
- Hausenloy DJ, Wynne AM, Yellon DM (2007) Ischemic preconditioning targets the reperfusion phase. *Basic Res Cardiol* 102:445–452
- Hayakawa T, Kanematsu S, Asada K (1984) Occurrence of Cu, Zn-superoxide dismutase in the intrathylakoid space of spinach chloroplasts. *Plant Cell Physiol* 25:883–889
- Heiber I, Stroher E, Raatz B, Busse I, Kahmann U, Bevan MW, Dietz KJ, Baier M (2007) The redox imbalanced mutants of Arabidopsis differentiate signaling pathways for redox regulation of chloroplast antioxidant enzymes. *Plant Physiol* 143:1774–1788
- Henry JP, Juin P, Vallette F, Thieffry M (1996) Characterization and function of the mitochondrial outer membrane peptide-sensitive channel. *J Bioenerg Biomembr* 28:101–108
- Hideg E, Kalai T, Hideg K, Vass I (1998) Photoinhibition of photosynthesis in vivo results in singlet oxygen production detection via nitroxide-induced fluorescence quenching in broad bean leaves. *Biochemistry* 37:11405–11411
- Horn DM (2004) Superoxide production in the cytochrome *bf* complex of photosynthesis. Thesis/Dissertation, University of Wisconsin-Oshkosh, pp 1–80
- Huie RE, Padmaja S (1993) The reaction of NO with superoxide. *Free Radic Res Commun* 18:195–199
- Hurt E, Hauska G (1982) Identification of the polypeptides in the cytochrome *b6/f* complex from spinach chloroplasts with redox-center-carrying subunits. *J Bioenerg Biomembr* 14:405–424
- Inaba T, Yazu F, Ito-Inaba Y, Kakizaki T, Nakayama K (2011) Retrograde signaling pathway from plastid to nucleus. *Int Rev Cell Mol Biol* 290:167–204
- Jiang F, Zhang Y, Dusting GJ (2011) NADPH oxidase-mediated redox signaling: roles in cellular stress response, stress tolerance, and tissue repair. *Pharmacol Rev* 63:218–242
- Jones RW, Whitmarsh J (1988) Inhibition of electron transfer and the electrogenic reaction in the cytochrome *bf* complex by 2-n-nonyl-4-hydroxyquinoline-N-oxide (NQNO) and 2,5-dibromo-3-methyl-6-isopropyl-p-benzoquinone (DBMIB). *Biochim Biophys Acta (BBA) Bioenergetics* 933:258–268
- Junemann S, Heathcote P, Rich PR (1998) On the mechanism of quinol oxidation in the *bc1* complex. *J Biol Chem* 273:21603–21607
- Jung HS, Chory J (2010) Signaling between chloroplasts and the nucleus: can a systems biology approach bring clarity to a complex and highly regulated pathway? *Plant Physiol* 152:453–459
- Kallas T (2012) Cytochrome *b6f* complex at the heart of energy transduction and redox signaling. In: Eaton-Rye JJ, Tripathy BC, Sharkey TD (eds) Photosynthesis. Springer, Dordrecht, pp 501–560
- Kangasjarvi S, Tikkanen M, Durian G, Aro EM (2014) Photosynthetic light reactions – an adjustable hub in basic production and plant immunity signaling. *Plant Physiol Biochem* 81:128–134
- Karpinski S, Reynolds H, Karpinska B, Wingsle G, Creissen G, Mullineaux P (1999) Systemic signaling and acclimation in response to excess excitation energy in Arabidopsis. *Science* 284:654–657
- Karpinski S, Gabrys H, Mateo A, Karpinska B, Mullineaux PM (2003) Light perception in plant

- disease defence signalling. *Curr Opin Plant Biol* 6:390–396
- Karpinski S, Szechynska-Hebda M, Wituszynska W, Burdiak P (2013) Light acclimation, retrograde signalling, cell death and immune defences in plants. *Plant Cell Environ* 36:736–744
- Kassner RJ (1972) Effects of nonpolar environments on the redox potentials of heme complexes. *Proc Natl Acad Sci U S A* 69:2263–2267
- Kim C, Meskauskiene R, Apel K, Laloi C (2008) No single way to understand singlet oxygen signalling in plants. *EMBO Rep* 9:435–439
- Kovtun Y, Chiu WL, Tena G, Sheen J (2000) Functional analysis of oxidative stress-activated mitogen-activated protein kinase cascade in plants. *Proc Natl Acad Sci USA* 97:2940–2945
- Kurisu G, Zhang H, Smith JL, Cramer WA (2003) Structure of the cytochrome b6f complex of oxygenic photosynthesis: tuning the cavity. *Science* 302:1009–1014
- Kushnareva Y, Murphy AN, Andreyev A (2002) Complex I-mediated reactive oxygen species generation: modulation by cytochrome c and NAD(P)<sup>+</sup> oxidation-reduction state. *Biochem J* 368:545–553
- Lemeille S, Willig A, Depege-Fargeix N, Delessert C, Bassi R, Rochaix JD (2009) Analysis of the chloroplast protein kinase Stt7 during state transitions. *PLoS Biol* 7, e45
- Lenaz G (1988) Role of mobility of redox components in the inner mitochondrial membrane. *J Membr Biol* 104:193–209
- Li B, Kronzucker HJ, Shi W (2013) Molecular components of stress-responsive plastid retrograde signalling networks and their involvement in ammonium stress. *Plant Signal Behav* 8, e23107
- Liaudet L, Vassalli G, Pacher P (2009) Role of peroxynitrite in the redox regulation of cell signal transduction pathways. *Front Biosci (Landmark Ed)* 14:4809–4814
- Link TA (1997) The role of the ‘Rieske’ iron sulfur protein in the hydroquinone oxidation (Q(P)) site of the cytochrome bc1 complex. The ‘proton-gated affinity change’ mechanism. *FEBS Lett* 412:257–264
- Liu Y, Yang XM, Iliodromitis EK, Kremastinos DT, Dost T, Cohen MV, Downey JM (2008) Redox signaling at reperfusion is required for protection from ischemic preconditioning but not from a direct PKC activator. *Basic Res Cardiol* 103:54–59
- Mansfield KD, Guzy RD, Pan Y, Young RM, Cash TP, Schumacker PT, Simon MC (2005) Mitochondrial dysfunction resulting from loss of cytochrome c impairs cellular oxygen sensing and hypoxic HIF- $\alpha$  activation. *Cell Metab* 1:393–399
- Marchi S, Giorgi C, Suski JM, Agnoletto C, Bononi A, Bonora M, De ME, . . . , Pinton P (2012) Mitochondria-ros crosstalk in the control of cell death and aging. *J Signal Transduct* 2012:329635
- Marino D, Dunand C, Puppo A, Pauly N (2012) A burst of plant NADPH oxidases. *Trends Plant Sci* 17:9–15
- Mehler AH (1951) Studies on reactions of illuminated chloroplasts. I. Mechanism of the reduction of oxygen and other Hill reagents. *Arch Biochem Biophys* 33:65–77
- Mitchell P (1975a) Protonmotive redox mechanism of the cytochrome b-c1 complex in the respiratory chain: protonmotive ubiquinone cycle. *FEBS Lett* 56:1–6
- Mitchell P (1975b) The protonmotive Q cycle: a general formulation. *FEBS Lett* 59:137–139
- Mitchell P (1976) Possible molecular mechanisms of the protonmotive function of cytochrome systems. *J Theor Biol* 62:327–367
- Mittler R, Vanderauwera S, Gollery M, Van BF (2004) Reactive oxygen gene network of plants. *Trends Plant Sci* 9:490–498
- Mittler R, Vanderauwera S, Suzuki N, Miller G, Tognetti VB, Vandepoele K, Gollery M, . . . , Van BF (2011) ROS signaling: the new wave? *Trends Plant Sci* 16:300–309
- Miwa S, Muller FL, Beckman KB (2008) The basics of oxidative biochemistry. In: Miwa S, Beckman KB, Muller FL (eds) *Oxidative Stress in Aging: From Model Systems to Human Diseases*. Humana Press, Totowa, pp 11–35
- Moller IM, Jensen PE, Hansson A (2007) Oxidative modifications to cellular components in plants. *Annu Rev Plant Biol* 58:459–481
- Muhlenbock P, Szechynska-Hebda M, Plaszczycza M, Baudo M, Mateo A, Mullineaux PM, Parker JE, . . . , Karpinski S (2008) Chloroplast signaling and LESSION SIMULATING DISEASE1 regulate crosstalk between light acclimation and immunity in Arabidopsis. *Plant Cell* 20:2339–2356
- Mulkidjanian AY (2005) Ubiquinol oxidation in the cytochrome bc1 complex: reaction mechanism and prevention of short-circuiting. *Biochim Biophys Acta* 1709:5–34
- Muller F, Crofts AR, Kramer DM (2002) Multiple Q-cycle bypass reactions at the Qo site of the cytochrome bc1 complex. *Biochemistry* 41:7866–7874
- Muller FL, Roberts AG, Bowman MK, Kramer DM (2003) Architecture of the Qo site of the cytochrome bc1 complex probed by superoxide production. *Biochemistry* 42:6493–6499
- Mullineaux P, Karpinski S (2002) Signal transduction in response to excess light: getting out of the chloroplast. *Curr Opin Plant Biol* 5:43–48

- Nott A, Jung HS, Koussevitzky S, Chory J (2006) Plastid-to-nucleus retrograde signaling. *Annu Rev Plant Biol* 57:739–759
- Ohnishi T, Trumpower BL (1980) Differential effects of antimycin on ubisemiquinone bound in different environments in isolated succinate-cytochrome *c* reductase complex. *J Biol Chem* 255:3278–3284
- Osyczka A, Moser CC, Dutton PL (2005) Fixing the Q cycle. *Trends Biochem Sci* 30:176–182
- Paddenberg R, Ishaq B, Goldenberg A, Faulhammer P, Rose F, Weissmann N, Braun-Dullaues RC, Kummer W (2003) Essential role of complex II of the respiratory chain in hypoxia-induced ROS generation in the pulmonary vasculature. *Am J Physiol Lung Cell Mol Physiol* 284:L710–L719
- Penna C, Mancardi D, Rastaldo R, Pagliaro P (2009) Cardioprotection: a radical view free radicals in pre and postconditioning. *Biochim Biophys Acta* 1787:781–793
- Perry AJ, Rimmer KA, Mertens HD, Waller RF, Mulhern TD, Lithgow T, Gooley PR (2008) Structure, topology and function of the translocase of the outer membrane of mitochondria. *Plant Physiol Biochem* 46:265–274
- Pfalz J, Liebers M, Hirth M, Grubler B, Holtzegel U, Schroter Y, Dietzel L, Pfannschmidt T (2012) Environmental control of plant nuclear gene expression by chloroplast redox signals. *Front Plant Sci* 3:257
- Pfannschmidt T (2003) Chloroplast redox signals: how photosynthesis controls its own genes. *Trends Plant Sci* 8:33–41
- Pfannschmidt T, Schutze K, Brost M, Oelmüller R (2001) A novel mechanism of nuclear photosynthesis gene regulation by redox signals from the chloroplast during photosystem stoichiometry adjustment. *J Biol Chem* 276:36125–36130
- Rich PR (2004) The quinone chemistry of *bc* complexes. *Biochim Biophys Acta* 1658:165–171
- Rich PR, Bendall DS (1980) The redox potentials of the *b*-type cytochromes of higher plant chloroplasts. *Biochim Biophys Acta* 591:153–161
- Rich PR, Madgwick SA, Moss DA (1991) The interactions of duroquinol, DBMIB and NQNO with the chloroplast cytochrome *bc* complex. *Biochim Biophys Acta (BBA) Bioenergetics* 1058:312–328
- Rochaix JD (2007) Role of thylakoid protein kinases in photosynthetic acclimation. *FEBS Lett* 581:2768–2775
- Rossel JB, Wilson PB, Hussain D, Woo NS, Gordon MJ, Mewett OP, Howell KA, . . . , Pogson BJ (2007) Systemic and intracellular responses to photooxidative stress in *Arabidopsis*. *Plant Cell* 19:4091–4110
- Rutherford AW, Osyczka A, Rappaport F (2012) Back-reactions, short-circuits, leaks and other energy wasteful reactions in biological electron transfer: redox tuning to survive life in O(2). *FEBS Lett* 586:603–616
- Sang M, Xie J, Qin XC, Wang WD, Chen XB, Wang KB, Zhang JP, . . . , Kuang TY (2011) High-light induced superoxide radical formation in cytochrome *b(6)f* complex from *Bryopsis corticulans* as detected by EPR spectroscopy. *J Photochem Photobiol B* 102:177–181
- Sarewicz M, Borek A, Cieluch E, Swierczek M, Osyczka A (2010) Discrimination between two possible reaction sequences that create potential risk of generation of deleterious radicals by cytochrome *bc(1)*. Implications for the mechanism of superoxide production. *Biochim Biophys Acta* 1797:1820–1827
- Sasidharan R, Mustruph A (2011) Plant oxygen sensing is mediated by the N-end rule pathway: a milestone in plant anaerobiosis. *Plant Cell* 23:4173–4183
- Schumacker P (2014) Cellular and molecular mechanisms of O<sub>2</sub> sensing. In: Swenson ER, Bärtsch P (eds) *High Altitude*. Springer, New York, pp 1–22
- Shaikhali J, Heiber I, Seidel T, Stroher E, Hiltscher H, Birkmann S, Dietz KJ, Baier M (2008) The redox-sensitive transcription factor Rap2.4a controls nuclear expression of 2-Cys peroxiredoxin A and other chloroplast antioxidant enzymes. *BMC Plant Biol* 8:48
- Shapiguzov A, Vainonen JP, Wrzaczek M, Kangasjarvi J (2012) ROS-talk – how the apoplast, the chloroplast, and the nucleus get the message through. *Front Plant Sci* 3:292
- Sun J, Trumpower BL (2003) Superoxide anion generation by the cytochrome *bcl* complex. *Arch Biochem Biophys* 419:198–206
- Suzuki N, Koussevitzky S, Mittler R, Miller G (2012) ROS and redox signalling in the response of plants to abiotic stress. *Plant Cell Environ* 35:259–270
- Sylvester JT, Shimoda LA, Aaronson PI, Ward JP (2012) Hypoxic pulmonary vasoconstriction. *Physiol Rev* 92:367–520
- Takahashi MA, Asada K (1983) Superoxide anion permeability of phospholipid membranes and chloroplast thylakoids. *Arch Biochem Biophys* 226:558–566
- Telfer A, Bishop SM, Phillips D, Barber J (1994) Isolated photosynthetic reaction center of photosystem II as a sensitizer for the formation of singlet oxygen. Detection and quantum yield determination using a chemical trapping technique. *J Biol Chem* 269:13244–13253
- Tritto I, D’Andrea D, Eramo N, Scognamiglio A, De SC, Violante A, Esposito A, . . . , Ambrosio G (1997) Oxygen radicals can induce preconditioning in rabbit hearts. *Circ Res* 80:743–748

- Trotta A, Rahikainen M, Konert G, Finazzi G, Kangasjarvi S (2014) Signalling crosstalk in light stress and immune reactions in plants. *Philos Trans R Soc Lond B Biol Sci* 369:20130235
- Trumpower BL (2002) A concerted, alternating sites mechanism of ubiquinol oxidation by the dimeric cytochrome bc(1) complex. *Biochim Biophys Acta* 1555:166–173
- Trumpower BL, Gennis RB (1994) Energy transduction by cytochrome complexes in mitochondrial and bacterial respiration: the enzymology of coupling electron transfer reactions to transmembrane proton translocation. *Annu Rev Biochem* 63:675–716
- Turrens JF, Boveris A (1980) Generation of superoxide anion by the NADH dehydrogenase of bovine heart mitochondria. *Biochem J* 191:421–427
- Turrens JF, Alexandre A, Lehninger AL (1985) Ubisemiquinone is the electron donor for superoxide formation by complex III of heart mitochondria. *Arch Biochem Biophys* 237:408–414
- Vandenabeele S, Vanderauwera S, Vuylsteke M, Rombauts S, Langebartels C, Seidlitz HK, Zabeau M, ..., Van BF (2004) Catalase deficiency drastically affects gene expression induced by high light in *Arabidopsis thaliana*. *Plant J* 39:45–58
- Vanderauwera S, Zimmermann P, Rombauts S, Vandenabeele S, Langebartels C, Gruijssem W, Inze D, Van BF (2005) Genome-wide analysis of hydrogen peroxide-regulated gene expression in *Arabidopsis* reveals a high light-induced transcriptional cluster involved in anthocyanin biosynthesis. *Plant Physiol* 139:806–821
- Vener VA, van Kan PJM, Rich PR, Ohad I, Andersson B (1997) Plastoquinol at the quinol oxidation site of reduced cytochrome bf mediates signal transduction between light and protein phosphorylation: thylakoid protein kinase deactivation by a single-turnover flash. *Proc Natl Acad Sci USA* 94:1585–1590
- Victoria D, Burton R, Crofts AR (2013) Role of the -PEWY-glutamate in catalysis at the Q(o)-site of the Cyt bc(1) complex. *Biochim Biophys Acta* 1827:365–386
- Wang J, Shimoda LA, Sylvester JT (2012) Ca<sup>2+</sup> responses of pulmonary arterial myocytes to acute hypoxia require release from ryanodine and inositol trisphosphate receptors in sarcoplasmic reticulum. *Am J Physiol Lung Cell Mol Physiol* 303:L161–L168
- Waypa GB, Schumacker PT (2005) Hypoxic pulmonary vasoconstriction: redox events in oxygen sensing. *J Appl Physiol* 98:404–414
- Waypa GB, Guzy R, Mungai PT, Mack MM, Marks JD, Roe MW, Schumacker PT (2006) Increases in mitochondrial reactive oxygen species trigger hypoxia-induced calcium responses in pulmonary artery smooth muscle cells. *Circ Res* 99:970–978
- Waypa GB, Marks JD, Guzy R, Mungai PT, Schriewer J, Dokic D, Schumacker PT (2010) Hypoxia triggers subcellular compartmental redox signaling in vascular smooth muscle cells. *Circ Res* 106:526–535
- Waypa GB, Marks JD, Guzy RD, Mungai PT, Schriewer JM, Dokic D, Ball MK, Schumacker PT (2013) Superoxide generated at mitochondrial complex III triggers acute responses to hypoxia in the pulmonary circulation. *Am J Respir Crit Care Med* 187:424–432
- Weir EK, Archer SL (1995) The mechanism of acute hypoxic pulmonary vasoconstriction: the tale of two channels. *FASEB J* 9:183–189
- Widger WR, Cramer WA, Herrmann RG, Trebst A (1984) Sequence homology and structural similarity between the b cytochrome of mitochondrial complex III and the chloroplast b6f complex: position of the cytochrome b hemes in the membrane. *Proc Natl Acad Sci USA* 81:674–678
- Wollman FA (2001) State transitions reveal the dynamics and flexibility of the photosynthetic apparatus. *EMBO J* 20:3623–3630
- Wood PM (1988) The potential diagram for oxygen at pH 7. *Biochem J* 253:287–289
- Xia D, Esser L, Tang WK, Zhou F, Zhou Y, Yu L, Yu CA (2013) Structural analysis of cytochrome bc1 complexes: implications to the mechanism of function. *Biochim Biophys Acta* 1827:1278–1294
- Yamashita E, Zhang H, Cramer WA (2007) Structure of the cytochrome b6f complex: quinone analogue inhibitors as ligands of heme cn. *J Mol Biol* 370:39–52
- Yin Y, Yang S, Yu L, Yu CA (2010) Reaction mechanism of superoxide generation during ubiquinol oxidation by the cytochrome bc1 complex. *J Biol Chem* 285:17038–17045
- Yu L, Yang S, Yin Y, Cen X, Zhou F, Xia D, Yu CA (2009) Chapter 25 Analysis of electron transfer and superoxide generation in the cytochrome bc1 complex. *Methods Enzymol* 456:459–473
- Yurina N, Odintsova M (2011) Plant organelles to nucleus retrograde signaling. In: Shanker A (ed) *Abiotic stress response in plants – physiological, biochemical and genetic Perspectives*. InTech, Rijeka, pp 55–74
- Zatsman AI, Zhang H, Gunderson WA, Cramer WA, Hendrich MP (2006) Heme-heme interactions in the cytochrome b6f complex EPR spectroscopy and correlation with structure. *J Am Chem Soc* 128:14246–14247



- Zhang H, Whitelegge JP, Cramer WA (2001) Ferredoxin:NADP<sup>+</sup> oxidoreductase is a subunit of the chloroplast cytochrome *b6f* complex. *J Biol Chem* 276:38159–38165
- Zhang H, Kurisu G, Smith JL, Cramer WA (2003) A defined protein-detergent-lipid complex for crystallization of integral membrane proteins: the cytochrome *b6f* complex of oxygenic photosynthesis. *Proc Natl Acad Sci U S A* 100: 5160–5163
- Zhang H, Osyczka A, Dutton PL, Moser CC (2007) Exposing the complex III Qo semiquinone radical. *Biochim Biophys Acta* 1767:883–887
- Zito F, Finazzi G, Joliot P, Wollman FA (1998) Glu78, from the conserved PEWY sequence of subunit IV, has a key function in cytochrome *b6f* turnover. *Biochemistry* 37:10395–10403
- Zurbriggen MD, Carrillo N, Hajirezaei MR (2010) ROS signaling in the hypersensitive response: when, where and what for? *Plant Signal Behav* 5:393–396

# Chapter 21

## Electron Transfer Reactions at the Q<sub>o</sub> Site of the Cytochrome *bc*<sub>1</sub> Complex: The Good, the Bad, and the Ugly

Nicholas Fisher<sup>a</sup>, Michael K. Bowman<sup>b</sup>,  
and David M. Kramer<sup>a,\*</sup>

<sup>a</sup>MSU-DOE Plant Research Laboratory, and Department of  
Biochemistry and Molecular Biology, Michigan State University,  
East Lansing, MI 48824, USA

<sup>b</sup>Department of Chemistry, The University of Alabama,  
Tuscaloosa, AL 35487-0336, USA

Summary.....	419
I. Introduction.....	420
II. Superoxide Production by the <i>bc</i> <sub>1</sub> Complex and the Question of SQ <sub>o</sub> Reactivity.....	421
A. Thermodynamic Control of SQ <sub>o</sub> Reactivity.....	422
B. Kinetic Control of SQ <sub>o</sub> Reactivity.....	422
III. Structure and Mechanism of the Q <sub>o</sub> Site: Keeping the Chemistry Under Control.....	422
A. Electron and Proton Transfers, and Associated Gating Mechanisms.....	423
1. The First Electron Transfer Reaction.....	423
2. The Second Electron Transfer Reaction.....	424
3. Double-Gated and 'Kinetic' Mechanisms for Controlling Electron Transfer and Chemistry at Q <sub>o</sub> .....	425
B. Spectroscopic Investigation of SQ <sub>o</sub> and Implications for Mechanism.....	427
Acknowledgments.....	430
References.....	431

### Summary

The cytochrome *bc*<sub>1</sub> complex of eukaryotic mitochondrial and prokaryotic energy transducing membranes functions as a protonmotive quinol:cytochrome *c* oxidoreductase. The enzyme utilizes a highly characteristic 'Q-cycle' reaction mechanism in which oxidation of substrate quinol leads to a bifurcated electron transfer pathway. This mechanism generates a highly-reducing, reactive radical semiquinone (SQ<sub>o</sub>) intermediate at the site of quinol oxidation (Q<sub>o</sub>) within cytochrome *b* which must be tightly managed to prevent energetically wasteful electron transfer side reactions or reduction of dioxygen to biologically harmful superoxide. In this chapter we discuss mechanistic strategies harnessed by the *bc*<sub>1</sub> complex

---

\*Author for correspondence, e-mail: [kramerd8@msu.edu](mailto:kramerd8@msu.edu)

to minimize unproductive electron transfer from SQ<sub>o</sub> with particular reference to superoxide generation. Recent work suggests that the *bc*<sub>1</sub> complex achieves this by kinetically trapping the SQ<sub>o</sub> anion within a hydrophobic region of the Q<sub>o</sub> pocket as a destabilized, low-occupancy intermediate, conserving redox energy to reduce the native electron acceptor (ferriheme *b*<sub>L</sub>) while minimizing the probability of unwanted (and potentially damaging) electron transfer bypass reactions.

## I. Introduction

The cytochrome *bc*<sub>1</sub> complex (cyt *bc*<sub>1</sub>, respiratory complex III) is a homodimeric, multimeric enzyme that functions as a protonmotive (ubi)quinol:cytochrome *c* oxidoreductase that is central to the respiratory biochemistry of eukaryotes and many prokaryotic organisms (Crofts 2004). The cytochrome *b*<sub>6f</sub> complex, a close cousin of *bc*<sub>1</sub>, is found in the thylakoid membrane of oxygenic photosynthesisers (Baniulis et al. 2008; Cramer et al. 2011). The monomeric unit of cyt *bc*<sub>1</sub> in eukaryotic organisms has a molecular mass of approximately 240 kDa and is formed from 10 to 11 discrete polypeptides. The hydrophobic cytochrome *b* subunit is encoded by mitochondrial DNA, with the remaining subunits encoded within the nucleus. During a complete catalytic cycle, cyt *bc*<sub>1</sub> oxidizes two molecules of ubiquinol, reducing two molecules of cytochrome *c* and one molecule of ubiquinone. Four protons are translocated into the intermembrane space (IMS) against the electrochemical gradient

---

*Abbreviations:* [2Fe-2S] – The iron-sulfur cluster of the ‘Rieske’ iron-sulfur protein; Cyt – Cytochrome; ENDOR – Electron nuclear double resonance spectroscopy; EPR – Electron paramagnetic resonance spectroscopy; ESEEM – Electron spin echo envelope modulation spectroscopy; HHDBT – 5-*n*-heptyl- 6-hydroxy-4,7-dioxobenzothiazole; ISP – The ‘Rieske’ iron-sulfur protein; PEWY – The Pro<sub>271</sub>-Glu-Trp-Tyr<sub>274</sub> sequence within the Q<sub>o</sub> site of cytochrome *b* (yeast numbering); QH<sub>2</sub> – Quinol or hydroquinone; Q<sub>i</sub> – Quinone reductase site of the cytochrome *bc*<sub>1</sub> complex; Q<sub>o</sub> – Quinol oxidase site of the cytochrome *bc*<sub>1</sub> complex; SQ – Semiquinone; SQ<sub>o</sub> – Semiquinone associated with the quinol oxidase site of the cytochrome *bc*<sub>1</sub> complex

per two electrons transferred to the soluble acceptor, cytochrome *c*, with the associated uptake of two protons from the matrix (Berry et al. 2000; Schultz and Chan 2001).

Three subunits form the highly conserved electron transferring catalytic core of the enzyme; cytochromes *b* (cyt *b*) and *c*<sub>1</sub> (cyt *c*<sub>1</sub>), and the ‘Rieske’ iron-sulfur protein (ISP) (Berry et al. 2000; Hunte et al. 2003). Cytochrome *b* is located within the inner mitochondrial membrane (IMM) and contains the substrate binding sites for quinol oxidation (Q<sub>o</sub>) and quinone reduction (Q<sub>i</sub>), located on opposite sides of the energy transducing membrane. Cyt *b* binds two heme *b* molecules, of differing potential (approximately –100 and +50 mV) forming a low potential electron transfer chain across the membrane. The prosthetic groups of cyt *c*<sub>1</sub> and the ISP, which are within protein domains located within the intermembrane space, form a high potential electron transfer chain within the cyt *bc*<sub>1</sub> complex.

Cyt *bc*<sub>1</sub> operates via the unique and energy-conserving ‘Q-cycle’ mechanism (Fig. 21.1), proposed by Peter Mitchell (1975) and since modified by others (see, for example Trumpower 1990; Crofts 2005; Zhang et al. 2008; Crofts et al. 2008). This mechanism requires the bifurcation of electron flow between the high- and low-potential electron transfer chains from the site of quinol oxidation at Q<sub>o</sub>, reducing a quinone molecule bound at Q<sub>i</sub>, recycling one electron back into the quinone pool per quinol molecule oxidized at Q<sub>o</sub>. This recycling mechanism doubles the number of protons translocated across the energy transducing membrane per quinol molecule oxidized at Q<sub>o</sub> compared to that achieved by

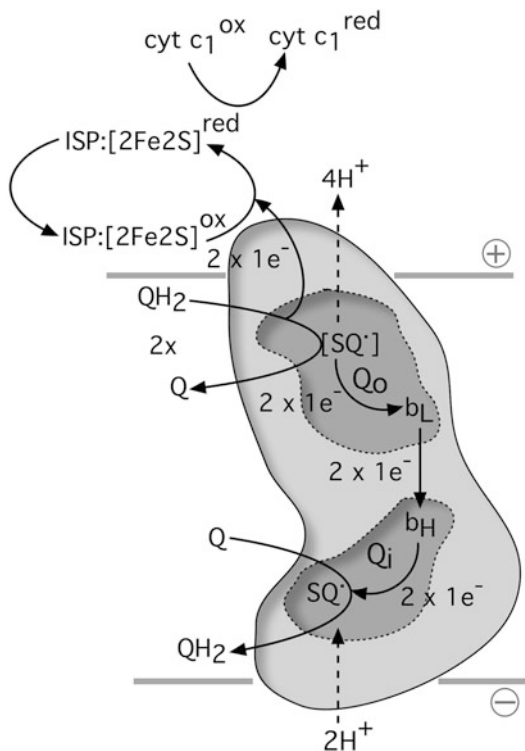


Fig. 21.1. The modified Q-cycle of the cytochrome  $bc_1$  complex. Cytochrome  $b$  is represented in cartoon form, with the  $Q_o$  and  $Q_i$  pockets indicated by dark shading. Oxidation of two molecules of (ubi)quinol at  $Q_o$  results in the transfer of two electrons through the 'high-potential' chain (the Rieske ISP/cytochrome  $c_1$ ) with the reduction of one molecule of (ubi)quinone at  $Q_i$  mediated by the transmembrane 'low-potential' chain of hemes  $b_L$  and  $b_H$ . In mitochondria, four protons are translocated into the intermembrane space against the electrochemical gradient with the associated uptake of two protons from the matrix during the complete catalytic cycle of the  $bc_1$  complex.

simple double reduction of the high potential chain. The first electron transfer reaction at  $Q_o$ , from quinol to the ISP, generates a highly reducing semiquinone ( $SQ_o$ ) intermediate, which serves as the reductant for heme  $b_L$ . Reduced  $b_L$  ( $-100$  mV) is oxidized by heme  $b_H$  ( $+50$  mV), which then reduces a quinone at the  $Q_i$ -site, generating a tightly bound and relatively unreactive semiquinone intermediate ( $SQ_i$ ). A second quinol molecule is then oxidized at  $Q_o$ , and the cycle repeats itself. In contrast to  $SQ_i$ , the  $SQ_o$  species is kinetically

unstable and capable of transferring its electron to oxygen, generating harmful superoxide (Rutherford et al. 2012; Bleier and Dröse 2013; Lanciano et al. 2013). The bifurcation mechanism at the  $Q_o$ -site must thus be controlled to avoid energetically wasteful (and biologically damaging) electron transfer reactions (Osyczka et al. 2005; Cape et al. 2006). Note that  $Q_p$  and  $Q_n$  are alternative designations for the  $Q_o$  and  $Q_i$  sites, respectively, referring to their locations near the electrochemically positive (p) and negative (n) sides of the membrane (see Chap. 9 by Cramer and Hasan in this volume for further discussion).

## II. Superoxide Production by the $bc_1$ Complex and the Question of $SQ_o$ Reactivity

Electron leakage to oxygen during normal catalytic turnover of the  $bc_1$  complex is often undetectably low (Muller et al. 2002). In general superoxide production is only observed in the presence of (i)  $Q_i$ -site antagonists (such as antimycin) which maintain a reduced low potential chain within the enzyme (Chance et al. 1979; Turrens et al. 1985; Zhang et al. 1998a; Sun and Trumpower 2003), (ii) mutant forms of the cyt  $bc_1$  complex, some of which have been implicated in human mitochondrial disorders (Sun and Trumpower 2003; Borek et al. 2008; Meunier et al. 2013), (iii) under conditions of high membrane potential and/or a highly-reduced UQ pool, impeding electron egress at  $Q_i$  (Dröse and Brandt 2008; Rottenberg et al. 2009) or (iv) certain types of  $Q_o$  inhibitors, such as myxothiazol and mucidin, which bind proximal to haem  $b_L$  (Muller et al. 2002, 2003; Sun and Trumpower 2003). It should be noted that semiquinone is essentially the only progenitor for superoxide at the  $Q_o$ -site; autooxidation of ferrocycytochrome  $b_L$  or the reduced  $[2Fe-2S]$  cluster are kinetically insignificant sources of superoxide production (Muller et al. 2002; Forquer et al. 2005; Cape et al. 2009).

Aside from oxygen reduction, there are a number of thermodynamically favorable SQ-mediated bypass reactions that can occur at  $Q_o$ . These include (i) double reduction of the high potential chain, lowering the proton-motive efficiency of the  $bc_1$  complex, similarly (ii) reduction of cytochrome  $c$  by SQ that has escaped the confines of the  $Q_o$  site, and (iii) futile reduction of  $SQ_o$  (or  $Q$ ) by ferroheme  $b_L$ . Typically, however, these reactions are not observed during uninhibited turnover of the native enzyme. The  $bc_1$  complex has evolved to minimize the probability of these energetically wasteful (and potentially biologically harmful) reactions from occurring.

*A priori*, bypass reactions at  $Q_o$ , with particular reference to electron transfer from  $SQ_o$  to oxygen, may be controlled by thermodynamic or kinetic mechanisms (or combination thereof), or may be avoided completely by the absence of a semiquinone intermediate during the reaction cycle (Cape et al. 2006; Rutherford et al. 2012). This latter phenomenon necessitates a concerted electron transfer mechanism requiring the simultaneous reduction of the ISP and ferricytochrome  $b_L$  with proton movements orchestrated accordingly (Snyder et al. 2000; Osyczka et al. 2004). A study of the activation energetics for superoxide production and quinol oxidation at  $Q_o$  in the presence and absence of antimycin using wild type and engineered forms of the yeast  $bc_1$  complex with altered ISP redox potentials revealed identical activation enthalpies for superoxide production and normal catalytic turnover of the  $Q_o$  site, strongly suggestive of common transition states (Forquer et al. 2006). As such, a truly concerted electron transfer mechanism at  $Q_o$  can be ruled out, and the quinol oxidation reaction can be considered to occur sequentially.

#### A. Thermodynamic Control of $SQ_o$ Reactivity

Protein-bound SQ species may be strongly stabilized (by five to ten orders of magnitude) by local environmental interactions (such as

hydrogen bonding), as is observed at the  $Q_i$  site of the  $bc_1$  complex and in other enzymes such as prokaryotic  $bo_3$  and  $aa_3$  quinol oxidases, and the  $Q_B$  site of photosystem II (Ingledeew et al. 1995; Hastings et al. 2000; Gunner et al. 2008; Yi et al. 2010). A stabilised SQ may be expected to be relatively unreactive with oxygen as additional energy must be supplied to the system for electron transfer to occur. Such a SQ species is expected to be relatively long-lived (with a lifetime of tens to hundreds of milliseconds) (Gunner et al. 2008), and thus be present at a relatively high concentration (occupancy) under equilibrium conditions. In contrast, the reactivity of a destabilized SQ intermediate with oxygen is expected to be moderated by the very short lifetime of the former species, with a correspondingly low equilibrium concentration.

#### B. Kinetic Control of $SQ_o$ Reactivity

Superoxide production during the catalytic cycle at  $Q_o$  may be moderated by ‘kinetic steering’ of semiquinone oxidation pathways towards productive Q-cycle chemistry (i.e. reduction of cytochrome  $b_L$ ) and away from deleterious side reactions. By controlling the orientation and distance between reacting centers, the  $Q_o$  site influences the activation entropies for the respective electron transfer pathways (with minimal effect on the overall driving force for the reaction) to lessen the probability of electron leak to oxygen. Such kinetic steering is implicit in many ‘gating’ mechanism models (discussed in Osyczka et al. 2005; Cape et al. 2006; Crofts et al. 2006 and references therein), which are described further in Sect. III.A.

### III. Structure and Mechanism of the $Q_o$ Site: Keeping the Chemistry Under Control

The  $Q_o$  site forms a large, bifurcated and predominantly hydrophobic volume within cyt  $b$ . It is composed from components encompassing the C-terminal region of trans-

membrane helix C, surface helix cd1 and the stretch encompassing the “PEWY” (Pro<sub>271</sub>-Glu-Trp-Tyr<sub>274</sub>, yeast notation) loop/ef helix to transmembrane helix F1 of cytochrome *b* (Zhang et al. 1998b; Berry et al. 1999; Hunte et al. 2000; Esser et al. 2004, 2008). Ligands binding within  $Q_o$  may be broadly classified as ‘ $b_L$  proximal’ or ‘ $b_L$  distal’ species depending on their positioning within the site. The  $b_L$ -proximal inhibitors, such as the natural antibiotics myxothiazol and strobilurin, characteristically have hydrogen bonding interactions with the backbone amide moiety of glutamate residue E272 in the  $Q_o$  ef helix, in close proximity to heme  $b_L$ . In contrast,  $b_L$  distal inhibitors, such as stigmatellin bind in a volume of the  $Q_o$  site in close proximity to the ISP, typically forming a strong hydrogen bond to a histidine ligand (H181) of the [2Fe-2S] cluster (Berry et al. 2000; Crofts et al. 1999; Gao et al. 2002).

The  $b_L$ -proximal inhibitors stimulate superoxide production at 50 % of the rate observed for the  $Q_i$  inhibitor antimycin as they permit the generation of  $SQ_o$  by the (forward) one-electron transfer reaction from distally-bound quinol to the oxidized ISP, but inhibit its oxidation by ferricytochrome  $b_L$ . Accordingly, superoxide production is not observed in the presence of the  $b_L$ -distal inhibitor stigmatellin, as this initial electron transfer reaction to form  $SQ_o$  cannot occur (Muller et al. 2002, 2003).

### A. Electron and Proton Transfers, and Associated Gating Mechanisms

#### 1. The First Electron Transfer Reaction

If we accept the assertion that substrate quinol is oxidized to quinone in a sequential manner at  $Q_o$ , which is the probable case (Forquer et al. 2006), then a generally accepted mechanism for the first electron transfer reaction (to the oxidized [2Fe-2S] cluster of the Rieske protein) is outlined below. For a more comprehensive treatment of electron and proton transfer chemistry within the  $Q_o$  site, the reader is referred to (Crofts et al. 2006, 2013, and references therein).

The atomic structure of stigmatellin-inhibited  $bc_1$  provides a useful model for the initial enzyme-substrate complex for  $Q_o$ -bound quinol (Zhang et al. 1998b; Crofts et al. 1999; Berry and Huang 2003). Accordingly, it is assumed that the enzyme-substrate complex for the initial electron transfer consists of quinol occupying the distal region of the  $Q_o$  site, with a hydrogen bond between the benzoquinone hydroxyl and the histidyl sidechain of the H181 ligand of the [2Fe2S] cluster. The donor-to-acceptor distance for electron transfer is approximately 7 Å. A weaker hydrogen bond may be present between the carboxylate group of E272 (yeast notation, equivalent to E271 in the bovine structure and located within the highly conserved ‘PEWY’  $Q_o$  motif of cyt *b*) and the benzoquinone hydroxyl *para* to that interacting with H181 (Berry and Huang 2011). It is through the hydrogen bond to H181 (which is considered to confer a bell-shaped pH dependency on the quinol oxidation reaction in the pH 6.0–8.0 range (Brandt and Okun 1997)) that the electron transfer proceeds in a strongly rate-limiting, energetically uphill, proton-coupled electron transfer reaction (Guergova-Kuras et al. 2000). This results in the formation of a semiquinone species within the  $Q_o$  distal region, and a reduced [2Fe-2S] cluster with H181 in the protonated form. The headgroup of the ISP then rotates away from the surface of cytochrome *b*, and reduces cytochrome  $c_1$ , releasing the proton carried by H181 to the bulk phase. The diffusion of the extrinsic domain of the ISP between cytochromes *b* and  $c_1$  is not rate-limiting for catalysis at the  $Q_o$  site in the native enzyme (Crofts et al. 2003). The initial (neutral) semiquinone generated at  $Q_o$  is likely to have a very transient existence and has not been detected spectroscopically (Cape et al. 2007). Its remaining proton is immediately stripped away to generate a quasi-stable semiquinone anion prior to the second electron transfer reaction (see Sect. III.A.2).

Subtle,  $Q_o$  inhibitor-dependent structural and hydrogen-bonding changes within the  $Q_o$  site that affect the positioning of the ISP

headgroup and cyt *b* cd1 helix and loop connecting transmembrane helices E and F, have been analysed by Berry and Huang (2011). These structural perturbations, many of which were recognized in early crystallographic studies (Crofts et al. 1999; Berry et al. 2000), have been interpreted in the context of ‘conformational’ gating mechanisms for the first electron transfer reaction. Allosteric control of the ISP movement and positioning by occupants at Q<sub>o</sub> forms a component of the ‘catalytic switch,’ electron bifurcation control mechanism proposed by Brandt and colleagues (Brandt and von Jagow 1991; Brandt 1999). Berry and Haung identified a potential hydrogen bonding interaction from the tyrosyl group of the Q<sub>o</sub>-site ef helix residue Y279 to the histidyl sidechain of ISP residue H181 in famaxodone-inhibited avian *bc*<sub>1</sub>, offering a possible explanation as to why the ISP headgroup exhibits high occupancy at the surface of cytochrome *b* in the associated atomic structure even though no hydrogen bonding interaction is predicted between this inhibitor and the ISP. Y279 is proposed to act as a ‘surrogate quinol’ in this instance (Berry and Huang 2011). A subtly different hydrogen-bonding interaction is observed between Y279 and H181 in the stigmatellin-inhibited complex, with the peptide carbonyl group of H181 acting as the hydrogen bond acceptor (Berry and Huang 2011). Y279 has been proposed as the gating ‘trapdoor tyrosine’ controlling access to the *b*<sub>L</sub> proximal region of Q<sub>o</sub> through simple steric hindrance, the positioning of which is governed by displacement of the PEWY loop (Crofts et al. 2013). Mutation of Y279 is frequently deleterious to the catalytic activity of the *bc*<sub>1</sub> complex (Fisher et al. 2004) with a concomitant increase in superoxide production, and has been implicated in human mitochondrial disorders (Meunier et al. 2013). Mutation of the equivalent residue (Y268) in the human malarial parasite (*Plasmodium falciparum*) confers resistance to the anti-malarial drug atovaquone, but at the cost of a fitness penalty to the organism (Fisher et al. 2012).

## 2. The Second Electron Transfer Reaction

The mechanism of the second electron transfer reaction at Q<sub>o</sub>, from the semiquinone to oxidized heme *b*<sub>L</sub>, is a matter of debate. A plausible scenario as proposed by Crofts et al. (2006, 2013, and references therein) is sketched here. The first electron transfer results in the semiquinone in the distal region of the Q<sub>o</sub> site, hydrogen bonded to the carboxylate sidechain of E272, which immediately deprotonates, generating the semiquinone anion. The sidechain of E272, considered a mobile actor within the Q<sub>o</sub> site (Crofts et al. 1999; Palsdottir et al. 2003), rotates by >130° about its C<sub>α</sub>-C<sub>β</sub> bond, transferring the proton to water molecules in an internal chain, that forms an effective proton channel to the bulk phase. Rotation of the E272 sidechain opens the *b*<sub>L</sub>-proximal volume of the Q<sub>o</sub> site to diffusion of the semiquinone anion into position to reduce heme *b*<sub>L</sub>. In contrast to the first electron transfer reaction, electron transfer from the semiquinone to heme *b*<sub>L</sub> is exergonic and rapid, minimizing the lifetime of the SQ<sub>o</sub> intermediate. Movement of SQ<sub>o</sub> from the distal to proximal domains of the Q<sub>o</sub> site decreases the distance for electron transfer to *b*<sub>L</sub>, exponentially increasing the rate constant for *b*<sub>L</sub> reduction. Oxidation of the semiquinone by *b*<sub>L</sub> generates quinone, which diffuses back to the distal pocket of Q<sub>o</sub>, and out of the enzyme.

Changes in the local electric field of the proximal domain by the redox state of heme *b*<sub>L</sub> are proposed as a key component of an elegant ‘Coulombic’ gating mechanism (Crofts et al. 2013; Victoria et al. 2013). The anionic semiquinone is suggested to be attracted to the partial positive charge of ferriheme *b*<sub>L</sub>, decreasing the rate constant for electron transfer to *b*<sub>L</sub>. Contrastingly, ferroheme *b*<sub>L</sub>, which will persist if the membrane potential is high or heme *b*<sub>H</sub> reduced (due to the absence of an electron acceptor at Q<sub>i</sub>), is predicted to present a repulsive field to the anionic semiquinone, lessening the probability of the re-reduction of SQ

by  $b_L$ . Additionally, the pK of the carboxylic sidechain of E272 is predicted to be lowered by the presence of ferriheme  $b_L$ , facilitating proton transfer through this residue from the semiquinone to the water channel (Crofts et al. 2013; Victoria et al. 2013).

E272 is completely conserved in mitochondrial cyt  $b$ , but is replaced by valine or proline in  $\beta$ - and  $\gamma$ -proteobacterial sequences (Kao and Hunte 2014). Whether this residue is essential for catalysis at  $Q_o$  has been examined by site-directed mutagenesis studies in yeast, *Paracoccus denitrificans* and *R. capsulatus bc\_1* (Osyczka et al. 2006; Wenz et al. 2006; Kleinschroth et al. 2008; Seddiki et al. 2008; Victoria et al. 2013). Typically, replacement of this residue has relatively minor effects on substrate binding at  $Q_o$ , although the kinetics of steady-state and single turnover ( $b_L/b_H$  reduction) are significantly affected. However, changes in the residue can result in large changes in superoxide production at the  $Q_o$  site. Of particular interest is the effect of E272 mutants. It has been suggested that there are considerable structural and mechanistic redundancies within the  $Q_o$  site to maintain activity, and that protonatable residues within the site (such as H253 in the yeast  $bc_1$  complex) may partly compensate for the missing E272 in site-directed mutants (Osyczka et al. 2006; Wenz et al. 2006). On the other hand, it is argued that because E272 is essential only for the semiquinone-oxidation step at  $Q_o$ , which is not rate limiting; the degree of inhibition due to mutagenesis of E272 may be underestimated in steady-state kinetic assays with the mitochondrial enzyme (Crofts et al. 2013).

### 3. Double-Gated and 'Kinetic' Mechanisms for Controlling Electron Transfer and Chemistry at $Q_o$

The important concept of the reversibility of electron- and proton-transfers associated with quinone chemistry in the Q-cycle (Mitchell 1975) has been emphasized by Osyczka et al. (2004), and used as a conceptual framework in the proposal of the 'double-gated' mechanism for control of

the electron transfer reactions at the  $Q_o$  site (Osyczka et al. 2005).

The 'double gated' models have one dominant feature: quinol oxidation is only permitted when *both* the ISP [2Fe-2S] and heme  $b_L$  are oxidized (or reduced, for the reverse electron transfer reaction to quinone). Quinol oxidation is forbidden if the [2Fe-2S] is reduced, or if heme  $b_L$  is reduced. This requires that SQ reactivity be gated in some fashion by the redox state of the complex.

A fully reversible, 'logic-gated' scheme was proposed by Rich (2004) for orchestrating electron transfer at  $Q_o$  that depends on the redox-linked protonation status of the hydrogen bond donors and acceptors (H161 and E272 in this instance). Partly in response to the controversy concerning the essential role of E272 for catalysis, Osyczka et al. (2005) independently proposed a 'double-gated' model wherein  $Q_o$  occupancy is gated by the hydrogen-bonding of a quinoid molecule to the water molecules in the  $Q_o$  site. The orientation of these water molecules was proposed to be influenced by the redox status of heme  $b_L$  and the [2Fe-2S] cluster, moderating quinoid reactivity accordingly. These double-gated models have been criticized for lacking experimental tractability (Crofts et al. 2006), although that proposed by Rich may be amenable to Fourier transform infra-red spectroscopic investigation.

Osyczka and colleagues developed a 'kinetic' model of control of  $Q_o$  site chemistry (Borek et al. 2008; Sarewicz et al. 2010) in which superoxide generation is a function of (i) the occupancy of the [2Fe-2S] cluster at  $Q_o$  and (ii) the midpoint potential of cytochrome  $c_1$ . Relative to wild type, superoxide production by *R. capsulatus bc\_1* in the presence of antimycin decreased when the mobility of the ISP was reduced by insertion of alanine residues in its flexible linker region, increasing the occupancy of the 2Fe-2S cluster at  $Q_o$ . Contrastingly, when the midpoint potential of heme  $c_1$  was markedly lowered by mutagenesis of the cyt  $c_1$  residue M183, impeding 2Fe-2S oxidation, superoxide production increased. These results were



interpreted as a simple kinetic competition for electrons between the semiquinone occupant, heme and [2Fe-2S] cofactors at  $Q_o$ , and oxygen (Borek et al. 2008; Sarewicz et al. 2010). Steric hindrance, which could limit access of oxygen to  $SQ_o$  when the ISP headgroup is docked at cytochrome *b*, was downplayed as a factor regulating superoxide production in the discussion of Osyczka's data, although it seems likely that this is a contributory factor.

A kinetic model for the control of  $Q_o$ -site chemistry was recently proposed by Quinlan and colleagues (Quinlan et al. 2011). The basic premise is that the reduction status of both hemes  $b_L$  and  $b_H$ , as influenced by the membrane potential or redox state of the Q pool, affects the kinetics of quinol oxidation and the occupancy of  $SQ$  at  $Q_o$ , which accordingly moderates superoxide generation. A similar model linking Q-pool redox status with  $bc_1$ -mediated ROS production has been described by Dröse and Brandt (Dröse and Brandt 2008). Using succinate (in the presence of malonate) as the electron donor in antimycin-inhibited rat mitochondrial preparations, Quinlan observed that maximal rates of hydrogen peroxide production showed a bell-shaped response, peaking when heme  $b_L$  was 70–80 % reduced. Imposition of a membrane potential by addition of ATP altered the redox equilibration between hemes  $b_L$  and  $b_H$ , disfavoring electron accumulation on  $b_H$ , and limiting peak hydrogen peroxide production. Mathematical modelling suggested that quinol oxidation (i.e.  $SQ_o$  generation) was slowed when  $b_H$  was reduced, and slowed further by reduction of  $b_L$ , perhaps by redox-induced conformational change within the enzyme (Quinlan et al. 2011). Coulombic effects on the redox potential of  $b_L$  due to reduction of  $b_H$  are also expected (Crofts et al. 2013).

It is notable that the transfer of the *first* pair of electrons from quinol at  $Q_o$  in the fully oxidized enzyme is unaffected by antimycin (Crofts et al. 1983), while some proteolytic and EPR spectroscopic data suggest that antimycin can act as an effector of the ISP and perturb its interaction with cytochrome *b*

(Valkova-Valchanova et al. 2000; Cooley et al. 2005; Cooley 2010). Intra- and intermonomeric allosteric regulation of  $Q_o$  chemistry was investigated by Trumpower and co-workers, and used to develop the 'half-of-sites' model for anti-cooperative regulation of  $bc_1$  activity (Covian and Trumpower 2008a, b). They concluded that only one  $Q_o$  site per  $bc_1$  dimer could be occupied by quinol during turnover, and that occupancy of the opposing  $Q_o$  site was excluded by conformational changes transmitted cross-dimer. Antimycin was also proposed to have a similar cross-dimer, anti-cooperative effect on  $Q_o$  turnover. Intermonomer electron transfer, mediated by the  $b_L$  hemes (which are separated by an edge-to-edge distance of 12 Å) was suggested to prevent accumulation of  $SQ_o$  (and subsequent electron leak to oxygen) in the half-of-sites model. The thermodynamic and kinetic basis of this model has been criticized by Crofts et al. (2008), although it has since been demonstrated that cross-dimer electron transfer can occur at physiologically relevant rates in  $Q_o/Q_i$  knockout mutants of *R. capsulatus*  $bc_1$  (Swierczek et al. 2010). This latter study, however, did not support the half-of-sites hypothesis for anti-cooperative control of  $bc_1$  activity, neither do quinone binding studies that indicate complete occupancy of both monomers (Bartoschek et al. 2001).

The data of Dröse and Brandt (2008) and Sarewicz et al. (2010) have been interpreted as supporting the 'semireverse' model for electron transfer at  $Q_o$  in which the predominant pathway for superoxide generation is by reverse electron transfer from ferrocycytochrome  $b_L$  to oxygen via a semiquinone intermediary (Fig. 21.2). In contrast, the observation by Forquer and colleagues (2006) that the rate-limiting step for quinol oxidation and superoxide generation at  $Q_o$  was essentially identical strongly supports the 'semiforward' model, with superoxide generation occurring prior to electron transfer to  $b_L$  (Fig. 21.2). The 'semiforward' mechanism is also favored by the kinetic models of  $Q_o$  chemistry by Quinlan (Quinlan et al. 2011). Strong support for the 'semiforward' model is also

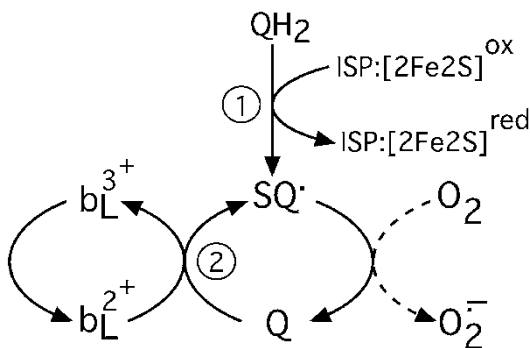


Fig. 21.2. Semiquinone (SQ) formation by the ‘semi-forward’ (1) and ‘semi-reverse’ (2) electron transfer pathways at  $Q_0$ . In the ‘semi-forward’ reaction the predominant pathway for SQ formation is oxidation of quinol by the ISP. Contrastingly, SQ is formed by reduction of  $Q_0$ -bound quinone by ferroheme  $b_L$  in the ‘semi-reverse’ reaction. Superoxide generation is mediated by SQ in both schemes.

provided by the observation of enhanced superoxide production in the presence of  $Q_0$ -proximal domain inhibitors (which prevent  $b_L$  reduction) and similarly in mutants of *Rhodobacter sphaeroides*  $bc_1$  lacking heme  $b_L/b_H$  (Muller et al. 2002; Yang et al. 2008).

### B. Spectroscopic Investigation of $SQ_0$ and Implications for Mechanism

The transient nature of  $SQ_0$  has made it a difficult species for spectroscopic investigation. Additionally, it has been questioned whether antiferromagnetic coupling between  $SQ_0$  and the reduced ISP would render it invisible to EPR investigation (Link 1997; Jünemann et al. 1998; Sarewicz et al. 2013). Initial EPR experiments detected a radical species in bovine submitochondrial particles under conditions of oxidant-induced reduction of  $bc_1$ , which was ascribed to  $SQ_0$  due to its abolition by treatment with British Anti-Lewisite (a covalent modifier of the ISP’s [2Fe-2S] center) and aerobic sensitivity (De Vries et al. 1981). However, this identification was questioned in later studies where the radical signal was shown to be stigmatellin-insensitive (Jünemann et al. 1998). It is likely that the species reported by de Vries was

located externally from  $Q_0$  (or indeed the  $bc_1$  complex in general).

Rapid freeze quench studies under anaerobic conditions have been used to trap  $SQ_0$  in *Rhodobacter* chromatophore and  $bc_1$  preparations, prior to EPR analysis (Cape et al. 2007; Zhang et al. 2007). Antimycin was present in these investigations to block semiquinone formation at  $Q_i$  and allow electron accumulation on the low potential chain in cytochrome  $b$ . Zhang observed a stigmatellin-sensitive  $SQ_0$  radical in chromatophores of *R. capsulatus* mutants (lacking heme  $b_H$ ) after flash excitation of the photosynthetic reaction centers to oxidize the  $bc_1$  complex followed by freezing. Cape et al rapidly mixed *Rhodobacter*  $bc_1$  with decylubiquinol prior to freezing in liquid propane after the reaction had been allowed to proceed for two to three enzymatic turnovers (approximately 10 ms), trapping  $SQ_0$  in a small population of centers.  $SQ_0$  occupancy was estimated to be approximately 0.01–0.1 SQ per  $bc_1$  monomer. EPR investigation of the frozen samples revealed that accumulation of the radical species (identified as an anionic semiquinone) was sensitive to stigmatellin, as expected, and furthermore was eliminated in a mutant  $bc_1$  complex lacking the ISP [2Fe-2S] cluster. Electron spin echo envelope modulation (ESEEM) analysis, a pulsed EPR technique, indicated an absence of hydrogen bonds between the trapped  $SQ_0$  and nitrogen atoms or backbone amide residues, suggesting that the anionic semiquinone was not interacting with H181 of the ISP, and was located in the vicinity of the  $b_L$ -proximal niche in the  $Q_0$ -site.

The existence of an SQ with occupancy greater than a few percent is not supported by ultra-fast freeze quench experiments on uninhibited  $bc_1$  (Zhu et al. 2007). Oxidation of quinol reduced the [2Fe-2S] center and  $b_L$  at the same rates. Even 100  $\mu$ s after mixing, equal amounts of these two reduced species were produced indicating that either the rate for movement of SQ to the proximal niche and reduction of  $b_L$  is much faster than the initial electron transfer to [2Fe-2S], resulting in very low  $SQ_0$  concentrations.

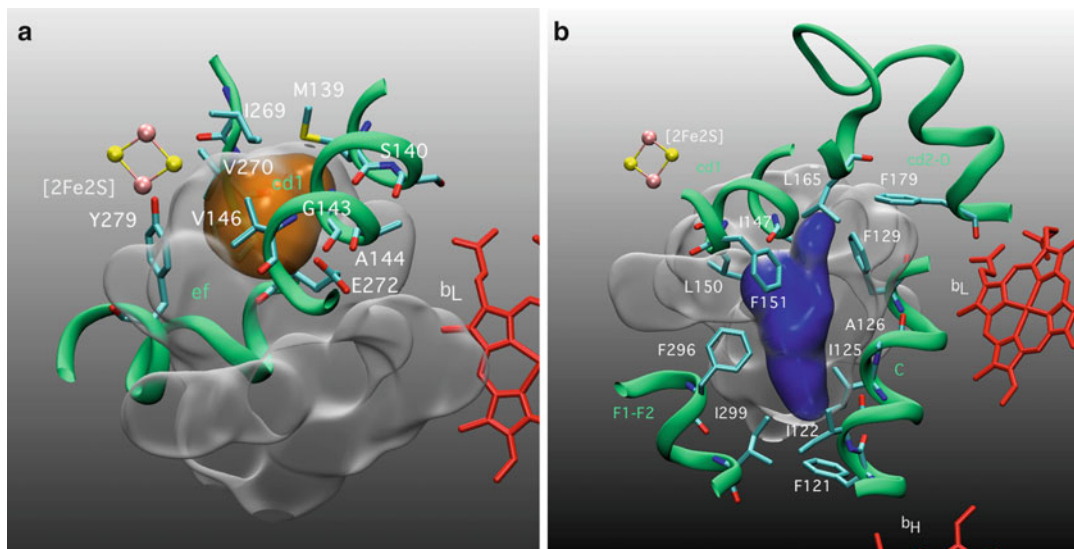
A more recent freeze-quench study by the Osyczka group (Sarewicz et al. 2013) examined a broader timescale of 0.012–300 s. SQ was not detected until after about 1 s, peaking near 10 s with antimycin bound. A new EPR line was detected at  $g = 1.94$  whose intensity paralleled that of the SQ. These observations were interpreted as indicating accumulation of large occupancy of SQ stabilized in the  $Q_o$ -site. The new EPR signal was considered to be from the triplet state of a spin-coupled pair of SQ and reduced [2Fe-2S] center in  $Q_o$ . The new signal, seen only when SQ and reduced [2Fe-2S] were both present, was taken to be a state of very-reduced  $bc_1$ . These measurements were made in air-equilibrated buffers with oxygen present, and it was argued that a hydrogen bond between SQ and the reduced [2Fe2S] would prevent the SQ from generating superoxide. However, a considerable fraction of the SQ was not in the form of this new EPR signal and is very efficient at generating superoxide (Muller et al. 2003). The measurements, per the Materials and Methods section (Sarewicz et al. 2013), were made with as many as 26 electrons from decylubiquinol per  $bc_1$ , of which only eight could be accepted by cyt  $c$ . Up to 18 superoxide molecules (some of which can be free radicals with lifetimes on the order of minutes) would be generated for each  $bc_1$  complex, leading to extensive oxidative damage of the enzyme. Unfortunately, it appears that SOD was never added to the reaction mixture as a control to prevent oxidative damage show that the SQ and triplet signals were not products of superoxide.

The new EPR signal at  $g = 1.94$  was assigned to a triplet state formed by an interacting SQ and [2Fe-2S] largely on the basis of simulating the new EPR spectrum. There are two major problems with this assignment. First, only one of the three potential EPR peaks from the triplet were clearly observed, the other two are either too broad to detect or obscured by overlap with the EPR spectra of the SQ and reduced [2Fe-2S]. A fit of one EPR line is not very conclusive given the number of parameters that potentially could be involved. Second, the spin coupling

model is not very appropriate for the supposed triplet. The [2Fe-2S] does not have a single unpaired spin as assumed in the spin Hamiltonian used by Sarewicz et al. in their supporting information to simulate the  $g = 1.94$  line. Rather, the [2Fe-2S] is itself a pair of interacting Fe(II) and Fe(III) ions and their  $S = 2$  and  $S = 5/2$  spin couple to produce the observed [2Fe-2S] EPR spectrum (Bertrand and Gayda 1979; Bertrand et al. 1985; Gurbiel et al. 1996; Shubin and Dikanov 2006). Rather, a simulation of the EPR spectrum for the triplet proposed by Sarewicz et al. needs to include spin couplings of the SQ, Fe(II) and Fe(III) to provide strong support for a triplet state. The proposal that a triplet composed of SQ and [2Fe-2S] has finally been found is intriguing, but would appear to contradict a large amount of past experimental evidence that  $SQ_o$  concentrations are low (see above). In our opinion, this proposal requires more substantial evidence that the signal does not arise from oxidative damage products from superoxide generation and that it is a triplet state composed of SQ and reduced [2Fe-2S] by simulation of its entire EPR spectrum by a realistic spin Hamiltonian.

Recently, the freeze quench studies of Cape et al. (2007) have been developed further using yeast  $bc_1$  preparations, which serves as a more appropriate model for the mammalian enzyme (Vennam et al. 2013). As in the *Rhodobacter*  $SQ_o$  study (Cape et al. 2007), ESEEM studies revealed no hydrogen bonding interactions between the yeast  $SQ_o$  and the surrounding protein structure. This result was confirmed by electron-nuclear double resonance (ENDOR) spectroscopy indicating that the SQ anion was located within at unusual trapping site within the  $Q_o$ -site when compared to other protein-bound SQ species (Vennam et al. 2013).

The temperature dependency of the paramagnetic relaxation enhancement (PRE) between paramagnetic centers in proteins provides useful information concerning the distance between these centers (Bertini and Turano 1995). As such, the PRE effect between the trapped SQ anion and hemes  $c_1$  and  $b_L/b_H$

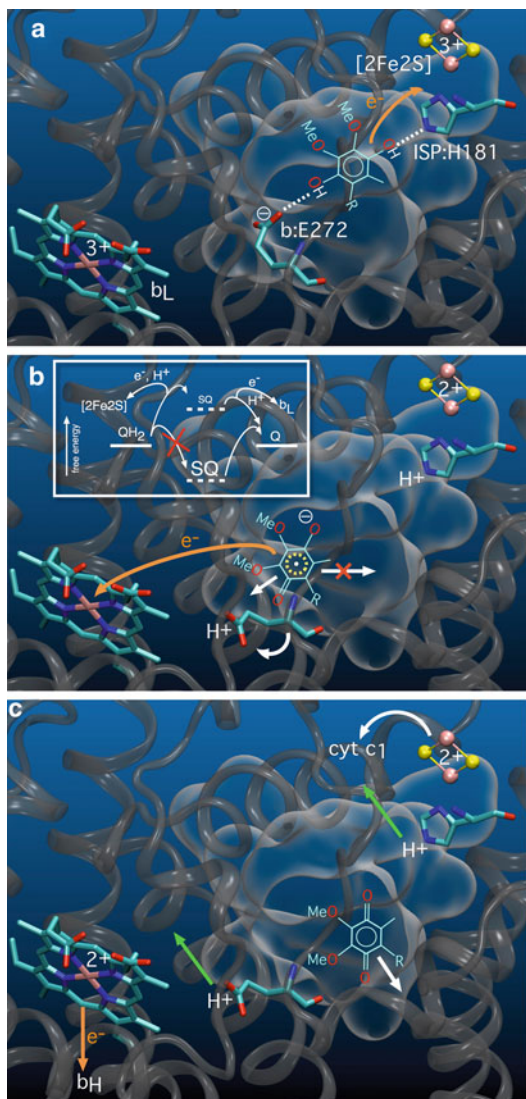


*Fig. 21.3.* Volumetric representation of the SQ binding sites within yeast *bc<sub>1</sub>* (constructed using the PDB coordinates 3CX5 (Solmaz and Hunte 2008)). The  $Q_o$  void volume is represented by a glass surface. The  $Q_o$  site void volume overlapping the intersection of the spherical regions defined by the  $b_L/c_1$  (intramonomer) paramagnetic relaxation enhancement distance constraints (site I) is represented in orange (panel **a**). Heme  $c_1$  itself is not shown in the figure. The  $b_L$  (intramonomer)/ $b_L$  (cross-dimer) distance constraints (site II) are shown in blue (panel **b**). Also shown are hemes  $b_L$  and  $b_H$  (red) of *cyt b* and the [2Fe-2S] cluster of the ISP (yellow/pink). *Cyt b* residues in close contact ( $<4 \text{ \AA}$ ) with site I and site II are labelled and shown in stick form. The *cyt b* polypeptide backbone is represented in green, with helices identified as shown.

of the freeze-quenched yeast *bc<sub>1</sub>* samples was used to calculate a set of distance constraints for identification of the location of the binding niche for SQ within  $Q_o$  (Vennam et al. 2013). It should be noted that the spin relaxation arising from the reduced [2Fe-2S] centre was too slow to contribute to the PRE effect in this study. As it was not possible to distinguish between the PRE effect of hemes  $c_1$  and  $b_L$  on the trapped SQ species, two possible localities for  $SQ_o$  that satisfied the PRE distance constraints (1.65–1.95 nm from the iron atom of one heme, and 2.55–3.00 nm from the iron of another) were identified within  $Q_o$  (Fig. 21.3a, b).

Site I is within the vicinity of the  $b_L$ -distal (stigmatellin-binding) niche, however no hydrogen-bonding interactions between  $SQ_o$  and the headgroup of the ISP or E272 of *cyt b* were observed. In comparison, Site II is localized in a hydrophobic niche deep within  $Q_o$ , located more proximally to heme  $b_L$ , in concordance with the mobile  $SQ_o$  models

of Crofts et al. (Crofts 2004; Crofts et al. 2013). The enthalpic cost of accommodating the anionic  $SQ_o$  species within the relatively aprotic environment of this hydrophobic region within  $Q_o$  is likely met by entropic terms; i.e. the trapped  $SQ_o$  can adopt multiple conformations within this volume. These data support the model of a destabilized, low occupancy and mobile SQ anion that is stripped of both hydroxyl protons during the first electron transfer reaction to the ISP (Fig. 21.4) (Kramer et al. 2005). The anionic SQ becomes kinetically (electrostatically) trapped within the hydrophobic confines of  $Q_o$ , conserving redox energy for reduction of heme  $b_L$  and minimizing the possibility of diffusion into the lipid bilayer. The lack of hydrogen bonding interactions to the surrounding protein structure will result in a highly destabilized, strongly reducing  $SQ_o$  (as evidenced by the observed low occupancy (Cape et al. 2007; Zhang et al. 2007)). Thus the redox properties of  $SQ_o$  resemble those



**Fig. 21.4.** The ‘proton-stripping’ model for catalysis at  $Q_0$ . Electron and proton movements are indicated by orange and green arrows, respectively. (a) A quinol molecule binds in the  $b_L$ -distal region at  $Q_0$ , forming hydrogen bonds between the benzoquinol hydroxyls, the imidazole ring of ISP residue H181 and an acceptor species within cytochrome *b*, here shown as the sidechain carboxylate of E272. The  $Q_0$  site is shown as a glass volume, as in Fig. 21.3. (b) Proton-coupled ET between the bound quinol and the ISP [2Fe-2S] cluster occurs through the QH2:H181 H-bond, reducing the [2Fe-2S] cluster and converting the sidechain of H181 to the imidazolium form. A second proton transfer occurs between the neutral semiquinone and an acceptor at  $Q_0$  (the carboxylate of E272 in this model), resulting in a semiquinone anion, which diffuses to the  $b_L$ -proximal niche within  $Q_0$  after this volume is opened up by the rotational flipping

of the photosystem I phylloquinone, which is considered to be destabilized with respect to the solution (Shinkarev et al. 2000). The destabilized  $SQ_0$  is consistent with the minimization of Q-cycle bypass reactions as its reduction by ferroheme  $b_L$  is thermodynamically unfavorable, and the probability of electron transfer to oxygen greatly reduced due to its very low occupancy. Contrastingly, a stabilized  $SQ_0$ , while present at high occupancy and likely to be a poor reductant for oxygen, would also be expected to lack sufficient free energy for the reduction of ferriheme  $b_L$ . Thus the  $Q_0$  site has evolved to strike a balance between maintaining the kinetic efficiency of the Q-cycle while minimizing the probability of bypass reactions through substrate destabilization (Fig. 21.4, panel B) – in contravention of the Pauling paradigm for enzymatic catalysis (Pauling 1948), using the simple device of hydrophobic containment. For further perspectives on reaction mechanisms and superoxide formation in  $bc_1$ - $b_6f$  complexes, see the Chaps. 14 and 20 by Sarewicz et al., and Baniulis et al., in this volume.

## Acknowledgments

Financial support from the National Institute of General Medical Sciences of the Na-

**Fig. 21.4.** (continued) of the protonated sidechain of E272. The semiquinone anion is enthalpically trapped within  $Q_0$  as it cannot be solvated by the hydrophobic residues surrounding the entrance to the site. It should be noted that oxidation of reduced  $b_L$  by anionic SQ is thermodynamically unfavorable, considerably lessening the probability of this unproductive bypass reaction. The inset represents the energetics for the overall reaction at  $Q_0$ ; a low occupancy, energetically destabilized  $SQ_0$  intermediate is the preferred model. (c) Oxidized  $b_L$  is reduced by the SQ anion, with the resulting neutral quinone molecule diffusing away into the membrane. The timing of proton transfer as represented in this panel is indicative only, although deprotonation is assumed to occur more quickly than the competing bypass reactions. Coordinates from yeast  $bc_1$  structure 3CX5.PDB (Solmaz and Hunte 2008) were used to generate this figure.

tional Institutes of Health (R01GM061904 to MKB) and the Division of Chemical Sciences, Geosciences, and Biosciences, Office of Basic Energy Sciences of the US Department of Energy (DE-FG02-11ER16220 to DMK) is gratefully acknowledged. Foundational support for the Plant Research Lab provided by Division of Chemical Sciences, Geosciences, and Biosciences, Office of Basic Energy Sciences of the US Department of Energy Grant DE-FG02-91ER20021.

## References

- Baniulis D, Yamashita E, Zhang H, Hasan SS, Cramer WA (2008) Structure-function of the cytochrome  $b_6f$  complex. *Photochem Photobiol* 84:1349–1358
- Bartoschek S, Johansson M, Geierstanger BH, Okun JG, Lancaster CRD, Humpfer E, Yu L, . . . , Brandt U (2001) Three molecules of ubiquinone bind specifically to mitochondrial cytochrome  $bc_1$  complex. *J Biol Chem* 276:35231–35234
- Berry EA, Huang L-S (2003) Observations concerning the quinol oxidation site of the cytochrome  $bc_1$  complex. *FEBS Lett* 555:13–20
- Berry EA, Huang L-S (2011) Conformationally linked interaction in the cytochrome  $bc_1$  complex between inhibitors of the  $Q_o$  site and the Rieske iron–sulfur protein. *Biochim Biophys Acta* 1807:1349–1363
- Berry EA, Huang LS, Zhang Z, Kim SH (1999) Structure of the avian mitochondrial cytochrome  $bc_1$  complex. *J Bioenerg Biomembr* 31:177–190
- Berry EA, Guergova-Kuras M, Huang LS, Crofts AR (2000) Structure and function of cytochrome  $bc$  complexes. *Annu Rev Biochem* 69:1005–1075
- Bertini I, Turano P (1995) Nuclear Magnetic Resonance of Paramagnetic Molecules. Kluwer, Dordrecht, pp 29–54
- Bertrand P, Gayda JP (1979) Theoretical interpretation of the variations of some physical parameters within the [2Fe-2S] ferredoxin group. *Biochim Biophys Acta* 579:107–121
- Bertrand P, Guigliarelli B, Gayda JP, Beardwood P, Gibson JF (1985) A ligand-field model to describe a new class of 2Fe-2S clusters in proteins and their synthetic analogues. *Biochim Biophys Acta* 831:261–266
- Bleier L, Dröse S (2013) Superoxide generation by complex III: from mechanistic rationales to functional consequences. *Biochim Biophys Acta* 1827:1320–1331
- Borek A, Sarewicz M, Osyczka A (2008) Movement of the iron-sulfur head domain of cytochrome  $bc_1$  transiently opens the catalytic  $Q_o$  site for reaction with oxygen. *Biochemistry* 47:12365–12370
- Brandt U (1999) Control of ubiquinol oxidation at center P ( $Q_o$ ) of the cytochrome  $bc_1$  complex. *J Bioenerg Biomembr* 31:243–250
- Brandt U, Okun JG (1997) Role of deprotonation events in ubihydroquinone: cytochrome  $c$  oxidoreductase from bovine heart and yeast mitochondria. *Biochemistry* 36:11234–11240
- Brandt U, von Jagow G (1991) Analysis of inhibitor binding to the mitochondrial cytochrome  $c$  reductase by fluorescence quench titration. Evidence for a ‘catalytic switch’ at the  $Q_o$  center. *Eur J Biochem* 195:163–170
- Cape JL, Bowman MK, Kramer DM (2006) Understanding the cytochrome  $bc$  complexes by what they don’t do. The Q-cycle at 30. *Trends Plant Sci* 11:46–55
- Cape JL, Bowman MK, Kramer DM (2007) A semiquinone intermediate generated at the  $Q_o$  site of the cytochrome  $bc_1$  complex: importance for the Q-cycle and superoxide production. *Proc Natl Acad Sci USA* 104:7887–7892
- Cape JL, Aidasani D, Kramer DM, Bowman MK (2009) Substrate redox potential controls superoxide production kinetics in the cytochrome  $bc_1$  complex. *Biochemistry* 48:10716–10723
- Chance B, Sies H, Boveris A (1979) Hydroperoxide metabolism in mammalian organs. *Physiol Rev* 59:527–605
- Cooley JW (2010) A structural model for across membrane coupling between the  $Q_o$  and  $Q_i$  active sites of cytochrome  $bc_1$ . *Biochim Biophys Acta* 1797:1842–1848
- Cooley JW, Ohnishi T, Daldal F (2005) Binding dynamics at the quinone reduction ( $Q_i$ ) site influence the equilibrium interactions of the iron sulfur protein and hydroquinone oxidation ( $Q_o$ ) site of the cytochrome  $bc_1$  complex. *Biochemistry* 44:10520–10532
- Covian R, Trumppower BL (2008a) The dimeric structure of the cytochrome  $bc_1$  complex prevents center P inhibition by reverse reactions at center N. *Biochim Biophys Acta* 1777:1044–1052
- Covian R, Trumppower BL (2008b) Regulatory interactions in the dimeric cytochrome  $bc_1$  complex: the advantages of being a twin. *Biochim Biophys Acta* 1777:1079–1091
- Cramer WA, Hasan SS, Yamashita E (2011) The Q cycle of cytochrome  $bc$  complexes: a structure perspective. *Biochim Biophys Acta* 1807:788–802

- Crofts AR (2004) The cytochrome  $bc_1$  complex: function in the context of structure. *Annu Rev Physiol* 66:689–733
- Crofts AR (2005) The Q-cycle – a personal perspective. *Photosynth Res* 80:223–243
- Crofts AR, Meinhardt SW, Jones KR (1983) The role of the quinone pool in the cyclic electron-transfer chain of *Rhodopseudomonas sphaeroides*. A modified Q-cycle mechanism. *Biochim Biophys Acta* 723:202–218
- Crofts AR, Barquera B, Gennis RB, Kuras R, Guergova-Kuras M, Berry EA (1999) Mechanism of ubiquinol oxidation by the  $bc_1$  complex: different domains of the quinol binding pocket and their role in the mechanism and binding of inhibitors. *Biochemistry* 38:15807–15826
- Crofts AR, Shinkarev VP, Kolling DRJ, Hong S (2003) The modified Q-cycle explains the apparent mismatch between the kinetics of reduction of cytochromes  $c_1$  and  $b_H$  in the  $bc_1$  complex. *J Biol Chem* 278:36191–36201
- Crofts AR, Lhee S, Crofts SB, Cheng J, Rose S (2006) Proton pumping in the  $bc_1$  complex: a new gating mechanism that prevents short circuits. *Biochim Biophys Acta* 1757:1019–1034
- Crofts AR, Holland JT, Victoria D, Kolling DRJ, Dikanov SA, Gilbreth R, Lhee S, . . . , Kuras MG (2008) The Q-cycle reviewed: how well does a monomeric mechanism of the  $bc_1$  complex account for the function of a dimeric complex? *Biochim Biophys Acta* 1777:1001–1019
- Crofts AR, Hong S, Wilson C, Burton R, Victoria D, Harrison C, Schulten K (2013) The mechanism of ubihydroquinone oxidation at the  $Q_0$ -site of the cytochrome  $bc_1$  complex. *Biochim Biophys Acta* 1827:1362–1377
- De Vries S, Albracht SP, Berden JA, Slater EC (1981) A new species of bound ubisemiquinone anion in  $QH_2$ : cytochrome  $c$  oxidoreductase. *J Biol Chem* 256:11996–11998
- Dröse S, Brandt U (2008) The mechanism of mitochondrial superoxide production by the cytochrome  $bc_1$  complex. *J Biol Chem* 283:21649–21654
- Esser L, Quinn B, Li Y-F, Zhang M, Elberry M, Yu L, Yu CA, Xia D (2004) Crystallographic studies of quinol oxidation site inhibitors: a modified classification of inhibitors for the cytochrome  $bc_1$  complex. *J Mol Biol* 341:281–302
- Esser L, Elberry M, Zhou F, Yu C-A, Yu L, Xia D (2008) Inhibitor-complexed structures of the cytochrome  $bc_1$  from the photosynthetic bacterium *Rhodobacter sphaeroides*. *J Biol Chem* 283:2846–2857
- Fisher N, Castleden CK, Bourges I, Brasseur G, Dujardin G, Meunier B (2004) Human disease-related mutations in cytochrome  $b$  studied in yeast. *J Biol Chem* 279:12951–12958
- Fisher N, Abd-Majid R, Antoine T, Al-Helal M, Warman AJ, Johnson DJ, Lawrenson AS, . . . , Biagini GA (2012) Cytochrome  $b$  mutation Y268S conferring atovaquone resistance phenotype in malaria parasite results in reduced parasite  $bc_1$  catalytic turnover and protein expression. *J Biol Chem* 287:9731–9741
- Forquer I, Cape JL, Bowman MK, Kramer DM (2005) Sequential two-electron oxidation of ubiquinol by the cytochrome  $bc_1$  complex. In: *Photosynthesis: Fundamental Aspects to Global Perspectives*. Pacific Northwest National Laboratory, Richland, pp 430–432
- Forquer I, Covian R, Bowman MK, Trumpower BL, Kramer DM (2006) Similar transition states mediate the Q-cycle and superoxide production by the cytochrome  $bc_1$  complex. *J Biol Chem* 281:38459–38465
- Gao X, Wen X, Yu C, Esser L, Tsao S, Quinn B, Zhang L, . . . , Xia D (2002) The crystal structure of mitochondrial cytochrome  $bc_1$  in complex with famoxadone: the role of aromatic-aromatic interaction in inhibition. *Biochemistry* 41:11692–11702
- Guergova-Kuras M, Kuras R, Ugulava N, Hadad I, Crofts AR (2000) Specific mutagenesis of the Rieske iron–sulfur protein in *Rhodobacter sphaeroides* shows that both the thermodynamic gradient and the pK of the oxidized form determine the rate of quinol oxidation by the  $bc_1$  complex. *Biochemistry* 39:7436–7444
- Gunner MR, Madeo J, Zhu Z (2008) Modification of quinone electrochemistry by the proteins in the biological electron transfer chains: examples from photosynthetic reaction centers. *J Bioenerg Biomembr* 40:509–519
- Gurbiel RJ, Doan PE, Gassner GT, Macke TJ, Case DA, Ohnishi T, Fee JA, . . . , Hoffman BM (1996) Active site structure of Rieske-type proteins: electron nuclear double resonance studies of isotopically labeled phthalate dioxygenase from *Pseudomonas cepacia* and Rieske protein from *Rhodobacter capsulatus* and molecular modeling studies of a Rieske center. *Biochemistry* 35:7834–7845
- Hastings SF, Heathcote P, Ingledew WJ, Rigby SE (2000) ENDOR spectroscopic studies of stable semiquinone radicals bound to the *Escherichia coli* cytochrome  $bo_3$  quinol oxidase. *Eur J Biochem* 267:5638–5645

- Hunte C, Koepke J, Lange C, Rossmann T, Michel H (2000) Structure at 2.3 Å resolution of the cytochrome  $bc_1$  complex from the yeast *Saccharomyces cerevisiae* co-crystallized with an antibody Fv fragment. *Structure* 8:669–684
- Hunte C, Palsdottir H, Trumpower BL (2003) Proton-motive pathways and mechanisms in the cytochrome  $bc_1$  complex. *FEBS Lett* 545:39–46
- Inglede WJ, Ohnishi T, Salerno JC (1995) Studies on a stabilisation of ubisemiquinone by *Escherichia coli* quinol oxidase, cytochrome  $bo$ . *Eur J Biochem* 227:903–908
- Jünemann S, Heathcote P, Rich PR (1998) On the mechanism of quinol oxidation in the  $bc_1$  complex. *J Biol Chem* 273:21603–21607
- Kao WC, Hunte C (2014) The molecular evolution of the  $Q_0$  motif. *Genome Biol Evol* 6:1894–1910
- Kleinschroth T, Anderka O, Ritter M, Stocker A, Link TA, Ludwig B, Hellwig P (2008) Characterization of mutations in crucial residues around the  $Q_0$  binding site of the cytochrome  $bc$  complex from *Paracoccus denitrificans*. *FEBS J* 275:4773–4785
- Kramer DM, Cape JL, Forquer IP, Bowman MK (2005) Kinetic steering of quinol oxidation by ‘proton stripping’ at the cytochrome  $bc_1$  complex  $Q_0$  site. In: *Photosynthesis: Fundamental Aspects to Global Perspectives*. Pacific Northwest National Laboratory, Richland, pp 424–427
- Lanciano P, Khalifaoui-Hassani B, Selamoglu N, Ghelli A, Rugolo M, Daldal F (2013) Molecular mechanisms of superoxide production by complex III: a bacterial versus human mitochondrial comparative case study. *Biochim Biophys Acta* 1827:1332–1339
- Link TA (1997) The role of the ‘Rieske’ iron sulfur protein in the hydroquinone oxidation ( $Q_p$ ) site of the cytochrome  $bc_1$  complex. The ‘proton-gated affinity change’ mechanism. *FEBS Lett* 412:257–264
- Meunier B, Fisher N, Ransac S, Mazat JP, Brasseur G (2013) Respiratory complex III dysfunction in humans and the use of yeast as a model organism to study mitochondrial myopathy and associated diseases. *Biochim Biophys Acta* 1827:1346–1361
- Mitchell P (1975) Protonmotive Q-cycle – general formulation. *FEBS Lett* 59:137–139
- Muller F, Crofts AR, Kramer DM (2002) Multiple Q-cycle bypass reactions at the  $Q_0$  site of the cytochrome  $bc_1$  complex. *Biochemistry* 41:7866–7874
- Muller FL, Roberts AG, Bowman MK, Kramer DM (2003) Architecture of the  $Q_0$  site of the cytochrome  $bc_1$  complex probed by superoxide production. *Biochemistry* 42:6493–6499
- Osyczka A, Moser CC, Daldal F, Dutton PL (2004) Reversible redox energy coupling in electron transfer chains. *Nature* 427:607–612
- Osyczka A, Moser CC, Dutton PL (2005) Fixing the Q cycle. *Trends Biochem Sci* 30:176–182
- Osyczka A, Zhang H, Mathé C, Rich PR, Moser CC, Dutton PL (2006) Role of the PEWY glutamate in hydroquinone-quinone oxidation-reduction catalysis in the  $Q_0$  site of cytochrome  $bc_1$ . *Biochemistry* 45:10492–10503
- Palsdottir H, Lojero CG, Trumpower BL, Hunte C (2003) Structure of the yeast cytochrome  $bc_1$  complex with a hydroxyquinone anion  $Q_0$  site inhibitor bound. *J Biol Chem* 278:31303–31311
- Pauling L (1948) Nature of forces between large molecules of biological interest. *Nature* 161:707–709
- Quinlan CL, Gerencser AA, Treberg JR, Brand MD (2011) The mechanism of superoxide production by the antimycin-inhibited mitochondrial Q-cycle. *J Biol Chem* 286:31361–31372
- Rich PR (2004) The quinone chemistry of  $bc$  complexes. *Biochim Biophys Acta* 1658:165–171
- Rottenberg H, Covian R, Trumpower BL (2009) Membrane potential greatly enhances superoxide generation by the cytochrome  $bc_1$  complex reconstituted into phospholipid vesicles. *J Biol Chem* 284:19203–19210
- Rutherford AW, Osyczka A, Rappaport F (2012) Back-reactions, short-circuits, leaks and other energy wasteful reactions in biological electron transfer: redox tuning to survive life in  $O_2$ . *FEBS Lett* 586:603–616
- Sarewicz M, Borek A, Cieluch E, Swierczek M, Osyczka A (2010) Discrimination between two possible reaction sequences that create potential risk of generation of deleterious radicals by cytochrome  $bc_1$ . *Biochim Biophys Acta* 1797:1820–1827
- Sarewicz M, Dutka M, Pintscher S, Osyczka A (2013) Triplet state of the semiquinone-Rieske cluster as an intermediate of electronic bifurcation catalysed by cytochrome  $bc_1$ . *Biochemistry* 52:6388–6395
- Schultz BE, Chan SI (2001) Structures and proton-pumping strategies of mitochondrial respiratory enzymes. *Annu Rev Biophys Biomol Struct* 30:23–65
- Seddiki N, Meunier B, Lemesle-Meunier D, Brasseur G (2008) Is cytochrome  $b$  glutamic acid 272 a quinol binding residue in the  $bc_1$  complex of *Saccharomyces cerevisiae*? *Biochemistry* 47:2357–2368
- Shinkarev VP, Vassiliev IR, Golbeck JH (2000) A kinetic assessment of the sequence of electron transfer from  $F_X$  to  $F_A$  and further to  $F_B$  in photosystem I: the value of the equilibrium constant between  $F_X$  and  $F_A$ . *Biophys J* 78:363–372
- Shubin AA, Dikanov SA (2006) Variations of g-tensor principal values in reduced [2Fe-2S] cluster of iron-sulfur proteins. *Appl Magn Reson* 30:399–416



- Snyder CH, Gutierrez-Cirlos EB, Trumpower BL (2000) Evidence for a concerted mechanism of ubiquinol oxidation by the cytochrome *bc*<sub>1</sub> complex. *J Biol Chem* 275:13535–13541
- Solmaz SRN, Hunte C (2008) Structure of complex III with bound cytochrome *c* in reduced state and definition of a minimal core interface for electron transfer. *J Biol Chem* 283:17542–17549
- Sun J, Trumpower BL (2003) Superoxide anion generation by the cytochrome *bc*<sub>1</sub> complex. *Arch Biochem Biophys* 419:198–206
- Swierczek M, Cieluch E, Sarewicz M, Borek A, Moser CC, Dutton PL, Osyczka A (2010) An electronic bus bar lies in the core of cytochrome *bc*<sub>1</sub>. *Science* 329:451–454
- Trumpower BL (1990) The protonmotive Q cycle. Energy transduction by coupling of proton translocation to electron transfer by the cytochrome *bc*<sub>1</sub> complex. *J Biol Chem* 265:11409–11412
- Turrens JF, Alexandre A, Lehninger AL (1985) Ubisemiquinone is the electron donor for superoxide formation by complex III of heart mitochondria. *Arch Biochem Biophys* 237:408–414
- Valkova-Valchanova M, Darrouzet E, Moomaw CR, Slaughter CA, Daldal F (2000) Proteolytic cleavage of the Fe-S subunit hinge region of *Rhodobacter capsulatus bc*<sub>1</sub> complex: effects of inhibitors and mutations. *Biochemistry* 39:15484–15492
- Vennam PR, Fisher N, Krzyaniak MD, Kramer DM, Bowman MK (2013) A caged, destabilized, free radical intermediate in the Q-Cycle. *Chembiochem* 14:1745–1753
- Victoria D, Burton R, Crofts AR (2013) Role of the -PEWY-glutamate in catalysis at the Q<sub>o</sub>-site of the Cyt *bc*<sub>1</sub> complex. *Biochim Biophys Acta* 1827:365–386
- Wenz T, Hellwig P, MacMillan F, Meunier B, Hunte C (2006) Probing the role of E272 in quinol oxidation of mitochondrial complex III. *Biochemistry* 45:9042–9052
- Yang S, Ma H-W, Yu L, Yu C-A (2008) On the mechanism of quinol oxidation at the Q<sub>P</sub> site in the cytochrome *bc*<sub>1</sub> complex: studied using mutants lacking cytochrome *b*<sub>L</sub> or *b*<sub>H</sub>. *J Biol Chem* 283:28767–28776
- Yi SM, Narasimhulu KV, Samoilova RI, Gennis RB, Dikanov SA (2010) characterization of the semiquinone radical stabilized by the cytochrome *aa*<sub>3</sub>-600 menaquinol oxidase of *Bacillus subtilis*. *J Biol Chem* 285:18241–18251
- Zhang L, Yu L, Yu CA (1998a) Generation of superoxide anion by succinate-cytochrome *c* reductase from bovine heart mitochondria. *J Biol Chem* 273:33972–33976
- Zhang Z, Huang L, Shulmeister VM, Chi YI, Kim KK, Hung LW, Crofts AR, . . . , Kim SH (1998b) Electron transfer by domain movement in cytochrome *bc*<sub>1</sub>. *Nature* 392:677–684
- Zhang H, Osyczka A, Dutton PL, Moser CC (2007) Exposing the complex III Q<sub>o</sub> semiquinone radical. *Biochim Biophys Acta* 1767:883–887
- Zhang H, Chobot SE, Osyczka A, Wraight CA, Dutton PL, Moser CC (2008) Quinone and non-quinone redox couples in Complex III. *J Bioenerg Biomembr* 40:493–499
- Zhu J, Egawa T, Yen SR, Yu L, Yu CA (2007) Simultaneous reduction of iron-sulfur protein and cytochrome *b*<sub>L</sub> during ubiquinol oxidation in cytochrome *bc*<sub>1</sub> complex. *Proc Natl Acad Sci USA* 104:4864–4869

# Part V

## **Cytochrome Complexes, Signaling, and Regulation**

# Chapter 22

## The Cytochrome $b_6f$ Complex: A Regulatory Hub Controlling Electron Flow and the Dynamics of Photosynthesis?

Giovanni Finazzi<sup>a</sup>, Jun Minagawa<sup>b</sup>, and Giles N. Johnson<sup>c,\*</sup>

<sup>a</sup>Centre National Recherche Scientifique, Unité Mixte Recherche  
5168, Laboratoire Physiologie Cellulaire et Végétale,  
F-38054 Grenoble, France

<sup>b</sup>National Institute for Basic Biology (NIBB), Nishigonaka 38,  
Myodaiji, Okazaki 444-8585, Japan

<sup>c</sup>Faculty of Life Sciences, University of Manchester, Michael  
Smith Building, Oxford Road, Manchester M13 9PT, UK

Summary.....	437
I. Introduction.....	438
II. $H^+/e^-$ Coupling in the Cytochrome $b_6f$ Complex and Its Role in Photosynthetic Control.....	440
III. A Redox Kinetic Control of Cytochrome $b_6f$ ?.....	443
IV. Linear Versus Cyclic Electron Flow.....	445
V. Role of Cytochrome $b_6f$ in State Transitions.....	446
VI. Conclusions.....	449
Acknowledgments.....	449
References.....	449

### Summary

Photosynthetic organisms must respond to several external stimuli to adjust their photosynthetic performances in order to keep a high capacity of carbon assimilation and avoid photodamage. They do so integrating processes occurring at different time scales starting from very fast light harvesting, down to slow changes of electron flow and protein composition of the photosynthetic apparatus. Central to these regulatory mechanisms is the cytochrome  $b_6f$  complex, which regulates intersystem electron flow via photosynthetic control and modulates light harvesting capacity by acting as a redox sensor to trigger an acclimation process named state transitions. In this chapter we describe how the

---

\*Author for correspondence, e-mail: [giles.johnson@manchester.ac.uk](mailto:giles.johnson@manchester.ac.uk)

cytochrome *b<sub>6</sub>f* complex performs to regulate these different functions in both plants and microalgae, proposing new mechanisms of regulation, and critically discussing how these processes are compatible with the existing literature on the structure and function of this complex.

## I. Introduction

Photosynthesis is an old invention of nature, which, since its onset, has drastically shaped life on earth (Gould et al. 2008). O<sub>2</sub> evolution by early oxygenic photosynthetic organisms opened up the possibility of land colonization, while imposing new constraints on photosynthesis, mostly related to the interactions between molecular oxygen produced by water splitting in photosystem (PS) II and excited states of the pigment. This interaction triggers the generation of reactive oxygen species (ROS), which are harmful for the photosynthetic apparatus and biological systems in general. ROS production becomes particularly high when photochemical light conversion (charge separation) is impaired by a decrease in electron flow capacity, leading to a reduction of the electron acceptors for the two photosystems. Thus, the photosynthetic electron transfer chain must be regulated to avoid ROS production. Key regulatory processes are linked to the generation

of a proton motive force (a pH gradient,  $\Delta\text{pH}$ ) across the thylakoid membrane. Acidification of the thylakoid lumen results in down regulation of light harvesting capacity of PSII via the onset of Non Photochemical Quenching (NPQ), a process which dissipates excess light energy as heat. This mainly occurs in the pigment-containing proteins of PSII, thanks to the  $\Delta\text{pH}$  induced synthesis of specific xanthophylls (e.g. zeaxanthin in plants and green algae, diatoxanthin in other microalgae) and the activation of protein sensors (PsbS in plants and LHCSR3 in eukaryotic algae) (Li et al. 2009).

Regulation of the pH gradient across the thylakoid membrane is central to the regulation of photosynthesis. To understand how the  $\Delta\text{pH}$  is controlled, however, we need to consider the (literally) central role of the cytochrome *b<sub>6</sub>f* complex (Cyt *b<sub>6</sub>f*). This complex is both crucial in generating  $\Delta\text{pH}$  but is also itself directly affected by that gradient. Lumen acidification modulates the rate of electron flow through the Cyt *b<sub>6</sub>f* complex (termed “*photosynthetic control*”, see Eberhard et al. 2008 and Fig. 22.1).

In what is usually seen as its primary role, in the linear electron flow (LEF) pathway, Cyt *b<sub>6</sub>f* catalyzes the transfer of electrons originating from PSII, and transferred through the membrane via the plastoquinone (PQ) pool, to a hydrophilic one-electron acceptor protein (plastocyanin (PC) or a *c*-type cytochrome (Cyt *c<sub>6</sub>*)). The electron transfer activity is coupled to proton translocation across the membrane. Reduced PC or Cyt *c<sub>6</sub>* (depending on species and growth conditions) is released from Cyt *b<sub>6</sub>f* and binds to PSI, where it reduces the primary electron

---

*Abbreviations:* CBB – Calvin Benson Bassham cycle; CEF – Cyclic electron flow; Cyt – *b<sub>6</sub>f* the cytochrome *b<sub>6</sub>f* complex; Cyt – Cytochrome; Fd – Ferredoxin; FNR – Ferredoxin-NADP<sup>+</sup> oxidoreductase; FQR – Ferredoxin quinone reductase; GAPDH – Glyceraldehyde-3-phosphate dehydrogenase; LEF – Linear electron flow; NDH – NAD(P)H dehydrogenase; NPQ – Non Photochemical Quenching; P<sub>700</sub> – Primary electron donor to PSI; PC – Plastocyanin; PQ – Plastoquinone; PQH<sub>2</sub> – Plastoquinol; PS – Photosystem; ROS – Reactive oxygen species

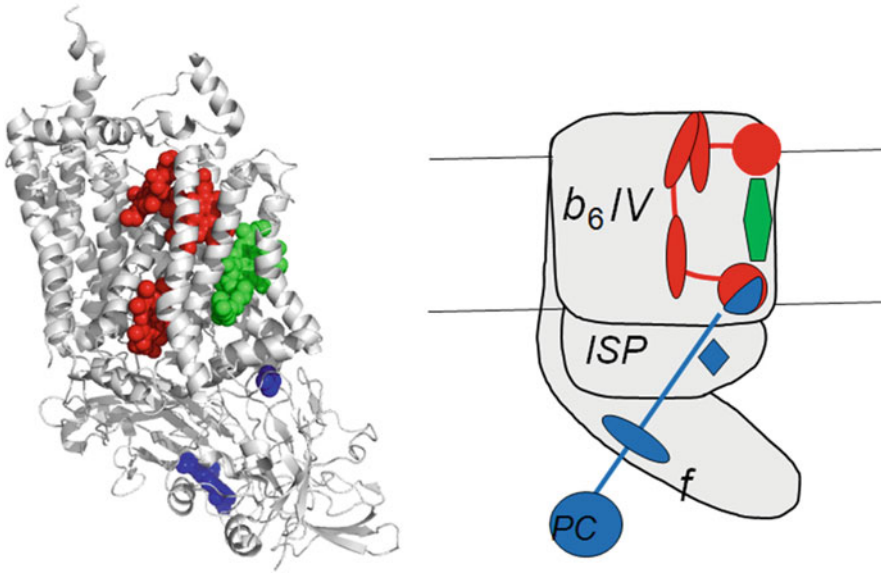


Fig. 22.1. Structure of the cytochrome  $b_6f$  complex (Stroebel et al. 2003). *Left*: atomic structure of the complex from *Chlamydomonas reinhardtii*. *Right*: Schematic representation of the complex. The low potential and high potential paths are represented in *red* and *blue*, respectively. The chlorophyll is shown in *green*. Catalytic activity of the high potential path is linked to  $H^+$  release in the lumen, and consequently regulated by the establishment of a  $\Delta pH$  across the membranes. The main subunits of the complex are represented: IV, subunit IV;  $b_6$  and  $f$ , cytochrome  $b_6$  and  $f$ , respectively; *ISP* Rieske protein containing and Fe-S cluster (*square*). *Closed circles, ellipses and polygons* indicate the quinone binding sites, hemes and chlorophyll, respectively. Note that only one monomer of the cytochrome  $b_6f$  dimer is shown.

donor of this complex,  $P_{700}$ . Electrons arriving at the donor side of PSI are transferred to its acceptor side via charge separation and there, either continue their journey towards the Calvin Benson Bassham cycle (CBB) via ferredoxin (Fd), ferredoxin NADP reductase (FNR) and then  $NADP^+$ , or are employed directly to provide reducing power for other cellular metabolic processes (such as nitrogen and sulfur metabolism, lipid, amino acid, pigment biosynthesis) via Fd oxidation (Eberhard et al. 2008). In addition to this linear pathway, the electrons from PSI can also be transferred back to Cyt  $b_6f$  via cyclic electron flow (CEF) around PSI (Shikanai 2007; Johnson 2011). This process, the significance of which was debated for many years, is now thought to occur in all oxygenic photosynthetic systems. Cyt  $b_6f$  is critical in

controlling the relative efficiency of linear and cyclic flow, either indirectly (by setting the rate of plastoquinol ( $PQH_2$ ) oxidation) or directly, e.g. via the formation of a biochemically stable PSI-Cyt  $b_6f$  complex (CEF supercomplex), which is seen in the green alga *Chlamydomonas reinhardtii* (see Chap. 23 by Minagawa). Finally, Cyt  $b_6f$  plays a specific role, which is not seen in its respiratory counterparts, the cytochrome  $bc_1$  complexes. Being the site of  $PQH_2$  oxidation, this complex senses the redox state of the photosynthetic electron transfer chain, and triggers the induction of state transitions, a process regulating the relative light absorption capacity of the two photosystems via the reversible migration of (a part of) the light harvesting complexes between the two photosystems (see Chap. 24 by Rochaix).

## II. $H^+/e^-$ Coupling in the Cytochrome $b_6f$ Complex and Its Role in Photosynthetic Control

Photosynthetic electron flow is kinetically controlled at the level of PQH<sub>2</sub> oxidation at the luminal side of the Cyt  $b_6f$  complex. Regulation can occur in response to acidification of the thylakoid lumen. This kinetic effect, known as “photosynthetic control,” is the consequence of the tight coupling between electron and proton transfer during oxidation of PQH<sub>2</sub> (West and Wiskich 1968). During this reaction, electrons originating from PQH<sub>2</sub> are divided between the Rieske Fe-S protein, the first step in the so-called high-potential chain (Fig. 22.1) and a cyclic route that comprises the  $b$  hemes (Q cycle; reviewed in Cramer et al. 2011), and possibly the  $c'$  (or  $c_n$ ) heme located on the stromal side of the complex (see Chap. 15 by Zito and Alric). In isolated Cyt  $b_6f$  isolated from *Chlamydomonas* (Nitschke et al. 1992; Pierre et al. 1995) the Rieske protein has an  $E_m$  of +290 mV. Cyt  $f$ , which oxidizes the Rieske Fe-S cluster, has an  $E_m$  of +330 mV, and the two Cyt  $b_6$  hemes have  $E_m$  values of –84 and –158 mV, respectively.

Due to the less positive  $E_m$  of the cytochrome comprising the  $b$ -heme pathway (as compared with Cyt  $f$  and the Rieske Fe-S protein), this route is referred to as the low-potential chain. According to the Q cycle mechanism proposed by Mitchell (1975) and modified by Crofts et al. (1983), quinones are oxidized and reduced at two distinct sites in the protein, the Q<sub>o</sub> and Q<sub>i</sub> (or Q<sub>p</sub> and Q<sub>n</sub>) sites, respectively, which are located on opposite sides of the membrane (Cramer et al. 2011). PQH<sub>2</sub> oxidation on the luminal side is associated with the reduction of both Cyt  $f$  and heme  $b_L$  (Crofts et al. 1983) and the release of protons into the lumen. Oxidation of the  $b_6$  hemes occurs through a two-step reduction of a PQ molecule at the Q<sub>i</sub> site, possibly involving the recently discovered  $c'$  heme (Cramer et al. 2011; and Chap. 15 by Zito and Alric). The electron transfer sequence is (1) the reduction of Cyt

$b_L$  by PQH<sub>2</sub>, a process that is coupled to proton release to the lumen, (2) electron transfer to  $b_H$ , and then (3) most likely a double electron transfer from these hemes to a PQ molecule bound at the Q<sub>i</sub> site, a process that is coupled to proton uptake from the stroma. Overall, the Q cycle results in additional proton pumping into the lumen, and therefore increases the  $H^+/e^-$  ratio of photosynthetic electron transfer.

Previous work has suggested that this cycle is constitutively active in physiological conditions (Sacksteder et al. 2000), and can be bypassed only upon drastic modifications of the redox features of the low potential chain (Malnoe et al. 2011). On average, each electron passes twice through the Cyt  $b_6f$  complex, once through the low- and once through the high-potential pathways and transports 2 protons from the stroma to the lumen. The reaction  $PQH_2 + PC^+ \leftrightarrow PQ + PC + 2H^+$  is expected to be sensitive to the luminal  $H^+$  concentration and this is simply as a result of a mass transfer effect. In particular, the pH effect would reflect the pH modulation of the formation of hydrogen bonds between the PQH<sub>2</sub> and protonatable residues in the Q<sub>o</sub> site. One of these protonatable residues is His126 of the Rieske protein of *C. reinhardtii*. The role of His126 in the modulation of the pH effect on the quinol oxidation rate has been first demonstrated in the case of cytochrome  $bc_1$  complexes (reviewed in Berry et al. 2000). Its involvement in the control of Cyt  $b_6f$  activity was confirmed by the pH profile of this complex in *Chlamydomonas*, where a pK of 6.25–6.5 has been detected (Finazzi 2002). This value is very close to the one previously attributed to His126 (Berry et al. 2000) of the Rieske protein in bacterial systems. The second residue involved in proton release in the lumen during PQH<sub>2</sub> oxidation is Glu78 of the PEWY sequence, which is extensively conserved in respiratory and photosynthetic cytochromes (Berry et al. 2000). This residue is located in a key position in the luminal binding pocket

(see e.g. Hasan et al. 2013) and its removal significantly altered the pH dependence of PQH<sub>2</sub> oxidation in *Chlamydomonas* cells (Zito et al. 1998).

Although plausible, a careful examination of the features of PQH<sub>2</sub> oxidation in the Cyt  $b_6f$  complex suggests that the simple mass effect explanation invoked previously to explain the photosynthetic control is probably a too simplistic view. Indeed the  $E_m$  differences between the initial electron donor (PQH<sub>2</sub>  $\sim$  0 mV) and the terminal acceptor (PC) is  $\sim$ 300 mV. This means that a very large pH gradient would be needed to counteract the driving force for electron transfer under steady state coupled conditions. However, it has been proposed that no such large proton gradient can be built in the thylakoid membranes under physiological conditions (Kramer et al. 2004). Measurements of the kinetics of P<sub>700</sub> reduction following a light-dark transition, an indicator of the flux through the Cyt  $b_6f$  complex, indicate that no inhibition of PQH<sub>2</sub> oxidation normally occurs in unstressed plants across the range of light intensities experienced in nature (Harbinson and Hedley 1989; Ott et al. 1999). This also implies that the in vivo lumen pH is not acidic enough to inhibit Cyt  $b_6f$  activity, consistent with previous in vivo measurements of the size of the H<sup>+</sup> gradient in microalgae (pH gradient of about 1.5 units; Finazzi and Rappaport 1998).

Interestingly, a mutant of *Arabidopsis*, *pgr1*, has been shown to have a mutation in the Rieske protein that results in an altered pH sensitivity, with a pK of 6.5–7 (Jahns et al. 2002). This shift results in plants that are deficient in qE (the  $\Delta$ pH-mediated ‘high-energy’ quenching of PSII), and the electron flux through Cyt  $b_6f$  is inhibited at a pH that is too high to induce significant quenching. This is in principle consistent with the notion that the luminal pH does not affect the turnover of the Cyt  $b_6f$  complex in vivo, unless its pH sensitivity is modified. On the other hand, Joliot and Johnson (2011) demonstrated that partial uncoupling of the thylakoid membrane, by infiltrating leaves with nigericin, resulted in an inhibition of

NPQ, as expected if the  $\Delta$ pH is inhibited, but also in a net reduction of the electron transport chain. Overall, these observations can be rationalized assuming that the lumen pH is involved in regulating the activity of the Cyt  $b_6f$  complex, although possibly via a different mechanism than a simple H<sup>+</sup>-mediated mass effect.

As an alternative explanation for the photosynthetic control, one can assume the existence of a pH dependent equilibrium between two kinetic states of the Cyt  $b_6f$  complex (characterized by a fast or a slow electron transfer rate). Under the hypothesis that the equilibration rate between the two states is faster than the electron transfer reaction, the pH dependence of Cyt  $b_6f$  activity can be mimicked in the frame of this very simple model, where only two kinetic states and a pK regulating their equilibration is conceived (Rappaport and Finazzi, unpublished data). The resolution of the structure of the Cyt  $b_6f$  and of its respiratory counterpart (cytochrome  $bc_1$ ) has provided a structural basis supporting this model. It has been shown that diversion of electrons into the high and low potential branches occurs via a conformational change at the level of the Rieske iron sulfur protein. In the related mitochondrial  $bc_1$  cytochrome complexes, the rotational swing of the Rieske protein extra-membrane domain leads to a cluster movement over 20 Å, which prevents a double electron injection into the high potential chain (for a review see Berry et al. 2000). Evidence for this movement was provided by three-dimensional Cyt  $bc_1$  structures (Xia et al. 1997; Iwata et al. 1998; Zhang et al. 1998), electron paramagnetic resonance spectroscopy (Brugna et al. 2000), and mutagenesis studies (for review, see Darrouzet et al. 2001). Several lines of evidence support the existence of a similar movement in the  $b_6f$  complex. These are two-dimensional crystals (Breyton 2000a), viscosity studies (Heimann et al. 2000), electron transfer from the Rieske ISP to Cyt  $f$  in vitro (Soriano et al. 2002), inhibitor binding (Schoepp et al. 1999), mutagenesis studies (de Vitry et al. 2004), and three-

dimensional Cyt *b<sub>6</sub>f* structures (Kurisu et al. 2003; Stroebel et al. 2003). Thus, one may speculate that the fast kinetics would be the one where the ISP and the PQH<sub>2</sub> lie close together in the luminal site, while the slow one would correspond to the ISP protein being close to the Cyt *f* moiety, thereby preventing proper interaction of PQH<sub>2</sub> with its binding site. The pK involved in this regulation would mainly be the one of His126, which is involved in making H-bonds with the quinone.

As mentioned above, the main consequence of the Q cycle is the increase in the H<sup>+</sup>/e<sup>-</sup> stoichiometry. A corollary of this model is that, although increased, the stoichiometry of protons pumped into the lumen per electron is fixed, being set by the conformational changes in the luminal site. This could be a limitation for photosynthesis where the H<sup>+</sup> gradient is required not only for photoprotection, but obviously also for ATP synthesis. In oxygenic photosynthesis, carbon assimilation is mainly driven by LEF, which produces NADPH as well as ATP, although probably in a ratio not sufficient to support the formation of glyceraldehyde-3-phosphate, the exported product of the CBB cycle (see Allen 2003 for a discussion). On the other hand, other electron fluxes, e.g. to reduce nitrogen, have different ATP:NADPH requirements. Thus every means available to modulate the H<sup>+</sup>/e<sup>-</sup> ratio in a flexible way, depending on demand, would allow plants to better regulate carbon assimilation, other metabolism and photoprotective responses. This possibility was investigated in *Chlamydomonas* using a genetic approach.

Mutants with an engineered Glu78 residue in subunit IV of Cyt *b<sub>6</sub>f* were generated and their responses to pH changes were tested (Zito et al. 1998; Finazzi 2002). Spectroscopic analysis revealed that this residue not only controls PQH<sub>2</sub> oxidation, as previously reported (Finazzi 2002), but also modulates the number of charges that are transferred through the Cyt *b<sub>6</sub>f* complex. This suggests that a transfer of protons from the stroma to the lumen during catalysis takes place in the complex itself, and that this is linked

to PQH<sub>2</sub> oxidation at the luminal pocket; suggesting the existence of a H<sup>+</sup> pumping activity in the complex (Finazzi 2002). This is in agreement with the finding of a relevant isotopic effect on the initial rate of charge transfer within the complex (Deniau and Rappaport 2000).

To account for this observation a model was proposed (Fig. 22.2), which reconciles the Q cycle with experimental observations showing that dicyclohexylcarbodiimide (DCCD), a chemical capable of modifying protonatable residues, induces a significant proton slip during catalysis (Brandt and Trumppower 1994). The model assumes that a channel exists between the luminal and stromal sites for PQ redox reactions, providing an internal shuttle for protons (Finazzi 2002). This channel would be operational either in the stroma to lumen direction (proton pumping) or in the opposite way (proton slip) depending on the pH of the two compartments and on the redox state of the electron flow cofactors within Cyt *b<sub>6</sub>f* (i.e. the high and low potential *b<sub>6</sub>* hemes). The transition from proton slip to proton pumping, observed in the pH 5–6 region, i.e. in the range compatible with the pK of this residue was compatible with the observation that the number of charges transferred through the cytochrome complex during turnover becomes constant in mutants where the Glu78 residue has been changed to a neutral residue, suggesting that this glutamic acid residue would act as a gate, modulating the opening and closing of this channel depending on luminal pH. Overall the activity of the redox-linked proton could represent a useful mean to help maintain pH homeostasis in the chloroplast lumen by modulating the H<sup>+</sup>/e<sup>-</sup> stoichiometry in vivo.

Although appealing, this hypothesis has not yet found a solid structural support. Indeed, no clear proton wire has been detected between the stromal and luminal sides in the structure of Cyt *b<sub>6</sub>f* complexes, at variance with the H<sup>+</sup> chain that is observed at the level of Cyt *f*, to channel proton release into the lumen (Cramer et al. 2011).



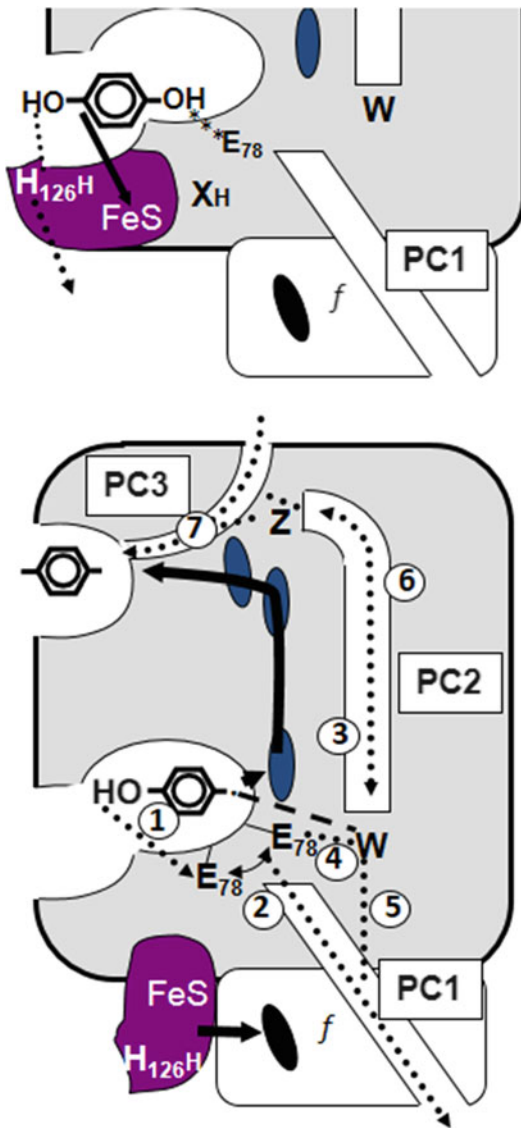


Fig. 22.2. Proposed mechanism for the redox controlled  $H^+$  pump in the Cyt  $b_6f$  complex. PQH<sub>2</sub> binding at the luminal sites occurs via  $H^+$  interaction with the H<sub>126</sub> and E<sub>78</sub> residues. This results in  $H^+$  and electron transfer to the Rieske protein (*top*). The Rieske protein is then oxidized by Cyt  $f$  (*thick arrow*) thanks to conformational changes of its head. In parallel, a movement of the protonated semiquinone allows the transfer of an electron to the  $b_L$  heme. Oxidation of neutral semiquinone is proposed to take place via the E<sub>78</sub> residue (1), which is connected to a proton channel PC1 (2). E<sub>78</sub> would modulate the activity of a transmembrane  $H^+$  channel (PC2, (2)) gated by two protonatable residues ( $W$  and  $Z$ ). Their protonation would be regulated by electrostatic interactions with the semiquinone (*dashed line*) and the  $b_6$  hemes.

### III. A Redox Kinetic Control of Cytochrome $b_6f$ ?

As discussed above (Sect. II), the effective rate limiting step in the electron transport chain is generally thought to be the oxidation of PQH<sub>2</sub> by Cyt  $b_6f$ . However, the factor that limits overall photosynthesis will often be downstream of this, either the supply of CO<sub>2</sub> for ribulose-5-phosphate reduction or the recycling of inorganic phosphate. For example, if a leaf is deprived of CO<sub>2</sub>, either naturally, due to drought induced stomatal closure, or artificially, by lowering the external CO<sub>2</sub> supply, demand for both NADPH and ATP declines. In simple terms this should result in a reduction of the whole electron transport chain, through a simple blockage of electron flow. This is not, however, what is seen. If CO<sub>2</sub> is abruptly removed, PSII acceptors, including the PQH<sub>2</sub> pool, become reduced, but Cyt  $f$  and the high potential chain become more oxidized, the opposite of what might be expected (Golding and Johnson 2003; Golding et al. 2005). This observation clearly shows that flux through the high potential chain is regulated at the level of the Cyt  $b_6f$  complex.

As already discussed, a simple effect of pH on the oxidation of PQH<sub>2</sub> might explain this observation; however various observations suggest that more is occurring. Importantly, another major pH-dependent process, high-energy state quenching, differs both in terms of kinetics of induction and steady state levels from the down-regulation of electron transport. For example, a wide range of NPQ values can be observed with no change in the flux through Cyt  $b_6f$  and, conversely, Cyt  $b_6f$  can be downregulated without a corresponding increase in NPQ (Ott et al. 1999).

Fig. 22.2. (continued) The activity of this channel would affect the  $H^+/e^-$  stoichiometries of PQH<sub>2</sub> oxidation, because of oscillation between proton pumping ((3) + (4) + (5)) and proton slip (6). (7) Protonation of the quinone at the stromal side. *Dotted lines*: proton transfer reactions. *Solid lines* electron transfer reactions (Modified from Finazzi 2002).

This led Johnson (2003) to put forward a model for feedback regulation by the redox poise of the PSI acceptor pool. Initially it was suggested that this may be via thioredoxin; however, later evidence pointed to NADPH redox poise being the crucial factor (Hald et al. 2008). Mutants in which photosynthesis was inhibited by antisense repression of glyceraldehyde-3-phosphate dehydrogenase, which consumes NADPH, showed a strong downregulation of Cyt  $b_6f$  activity and an oxidation of the high potential chain. Meanwhile, mutants repressed in FNR had a reduced electron transport chain. Both showed high levels of pH-dependent fluorescence quenching (a form of NPQ), indicating that the difference could not be explained by lumen pH alone.

Experiments such as these speak against a simple role for lumen pH controlling the flux of electrons through the Cyt  $b_6f$  complex. A notable example would be the *Arabidopsis pgr5* mutant, where the control of electron flux through Cyt  $b_6f$  fails to operate (Munekage et al. 2002b; Nandha et al. 2007; Joliot and Johnson 2011). This mutant was first

identified as a result of a screen for plants deficient in NPQ (Munekage et al. 2002a); however, in contrast to the *pgr1* mutant (Jahns et al. 2002), identified in the same screen, *pgr5* has a reduced electron transport chain across all conditions, implying that the PQH<sub>2</sub> oxidation is not being down regulated. At low CO<sub>2</sub> it does, however, generate NPQ, implying the formation of a large  $\Delta$ pH (Nandha et al. 2007). This alone is not sufficient to cause an inhibition of PQH<sub>2</sub> oxidation. In another study by Joliot and Johnson (2011) it was shown that infiltration of leaves with the ionophore nigericin, which dissipates  $\Delta$ pH without affecting the potential gradient, did not inhibit PSII electron transport but did prevent both NPQ formation and the down-regulation of Cyt  $b_6f$  activity. Results such as these speak in favor of a role of pH in regulating electron flow, but not through a simple photosynthetic control mechanism. Rather, the pH may modulate the redox sensitivity, shifting the  $E_m$  of redox sensitive components involved in regulation (Fig. 22.3). Johnson (2003) showed that inhibition of the Cyt  $b_6f$  complex by dithiothreitol is pH

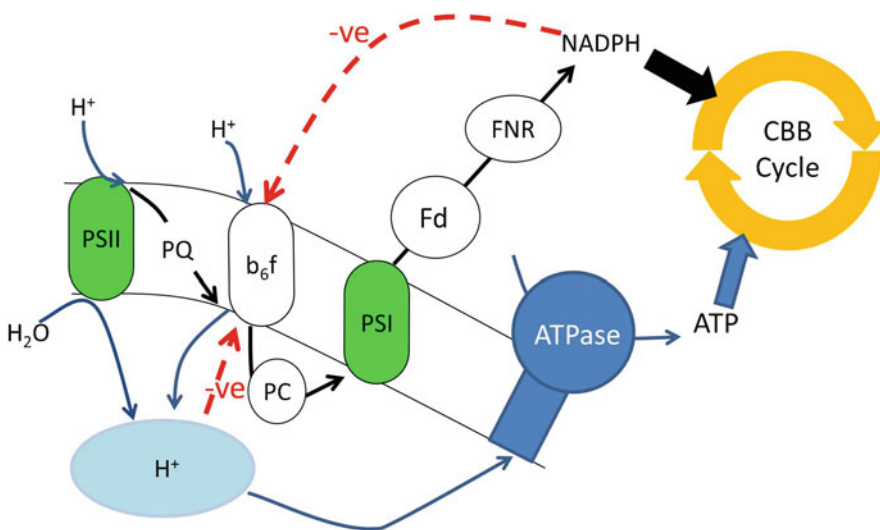


Fig. 22.3. Feedback control of Cyt  $b_6f$ . Linear electron transport generates NADPH (black arrows). At the same time, there is a net movement of protons into the thylakoid lumen, generating a  $\Delta$ pH, which is used to drive ATP synthesis (blue arrows). Under optimal conditions, NADPH and ATP are used in the Calvin-Benson-Basham (CBB) cycle. If the CBB cycle is inhibited, e.g. due to drought, NADPH feeds back to down-regulate the Cyt  $b_6f$  complex, while the  $\Delta$ pH, which is no longer being dissipated in ATP synthesis, inhibits electron flow either by directly inhibiting PQH<sub>2</sub> oxidation or indirectly by modulating the sensitivity to NADPH. See text for further explanation.

sensitive, with a shift in  $E_m$  of  $-90$  mV/pH. Hence, changes in the pH in the thylakoid lumen may increase the sensitivity of the Cyt  $b_6f$  complex to reducing agents, promoting at the same time redox regulation of electron flow, most likely exerted by NADPH.

#### IV. Linear Versus Cyclic Electron Flow

Among electron transport processes alternative to LEF, cyclic electron flow (CEF), which only involves PSI, has a major role in allowing plants and algae to control their ATP production via the regulation of the proton gradient,  $\Delta$ pH. CEF in flowering plants has been the subject of a number of reviews in recent years (e.g. Shikanai 2007; Johnson 2011) and we do not intend here to review in detail the evidence for its occurrence. Rather the focus will be on the regulation of this pathway and the involvement of the Cyt  $b_6f$  complex. The functioning of CEF in plants follows the same mechanism: electrons produced at the PSI acceptor side are oxidized in a way that results in the reduction of PQ, feeding electrons back into the electron transport chain between the two photosystems. That reaction may be catalyzed by either an NAD(P)H dehydrogenase (NDH) complex homologous to Complex I in mitochondrial electron transport (Rumeau et al. 2007; Shikanai 2007), or via an alternative reaction possibly involving Cyt  $b_6f$ . The relative contribution of the two paths is still under debate. Plants deficient in the NDH complex appear to perform well across a wide range of conditions, though there is evidence that they have increased sensitivity to drought stress (Rumeau et al. 2007; Lehtimäki et al. 2010). It seems, however, that NDH is not essential for plant growth. On the other hand, a recently identified mutant with enhanced CEF activity in *Arabidopsis* shows higher accumulation levels of this complex (Livingston et al. 2010), and it was recently proposed that this complex could mediate an  $H_2O_2$  driven activation of CEF (Strand et al. 2015).

In addition to the NDH pathway, electron transfer can take place via a pathway often referred to as the FQR (ferredoxin quinone reductase) pathway (Bendall and Manasse 1995). In early studies, the FQR pathway was proposed to involve the Cyt  $b_6f$  complex (Tagawa et al. 1963). However, later studies hypothesized a distinct enzyme for FQR that bypasses Cyt  $b_6f$  and directly interfaces with PQ pool reduction by Fd (Bendall and Manasse 1995). No one, however, was able to identify or purify the FQR specific enzyme until recently where evidence was presented for FQR being a complex of PGR5-PGRL1 (Hertle et al. 2013).

The physical association of the Cyt  $b_6f$  complex with PSI and FNR has also been suggested as a platform for the electron transfer in the FQR pathway (Carrillo and Vallejos 1983; Arnon 1995). Mathematical modeling of the electron transfer (Laisk 1993) and in vivo observation of its high efficiency (Joliot and Joliot 2002) suggest that FQR activity might operate in a complex involving Cyt  $b_6f$  and PSI. Indeed, Cramer and his co-workers reported that the Cyt  $b_6f$  complex co-purified with FNR and was reduced by Fd (Zhang et al. 2001). Physical interactions between PGRL1 and PsaD (subunit of PSI), PetB (Cyt  $b_6$ ), FNR, and PGR5 were shown by a yeast two-hybrid assay using the corresponding genes from *Arabidopsis* (DaCorso et al. 2008). This suggests that the formation of a CEF competent supercomplex is likely required to stabilize this pathway in a system where it could otherwise be outcompeted by linear flow.

While no such supercomplex was found in spinach leaves (Breyton et al. 2006) and indeed it has been argued that no such complexes are required (Johnson 2011; Joliot and Johnson 2011), biochemical analysis of thylakoid membranes from *Chlamydomonas* allowed Minagawa and colleagues (Iwai et al. 2010) to isolate such a complex from State 2-locked cells, where CEF is the prominent electron flow pathway. Using a sucrose density gradient, they purified a super-supercomplex composed of the PSI-LHCI supercomplex

with LHCIIs, Cyt  $b_6f$ , FNR, and PGRL1 in a fraction heavier than that of the PSI-LHCI supercomplex alone. Spectroscopic analyses of this super-supercomplex indicated that, upon illumination, reducing equivalents downstream of PSI were transferred to Cyt  $b_6f$ , while the oxidized PSI was re-reduced by reducing equivalents from Cyt  $b_6f$  (Iwai et al. 2010; see Chap. 23 by Minagawa for a further description of this CEF supercomplex).

What is the role of this supercomplex, and why is it observed only in *Chlamydomonas*? To answer these questions one has to consider that a key point in our understanding of CEF is the question of how the relative fluxes through LEF and CEF are regulated. It is acknowledged that photosynthetic complexes are not evenly distributed in the thylakoid membrane (Albertsson 2001). Functional PSII is localized in the membrane stacks. PSI is distributed between the grana margins (~70 %) and the stromal lamellae. Cyt  $b_6f$  is evenly distributed throughout the membrane. It has been shown that the diffusion of PQ/PQH<sub>2</sub> in the thylakoid membrane is highly restricted, probably due to the very high protein concentrations that characterize this membrane (Tremmel et al. 2003). This means that PQ localized in the granal stacks will primarily act in mediating electron transport between PSII and those Cyt  $b_6f$  complexes localized in the stacked regions. For reasons of access, it is unlikely that electrons will be transferred from Fd to Cyt  $b_6f$  complexes localized in the granal regions. Rather, a separate pool of Cyt  $b_6f$ , with associated PQ will be found in the stromal membranes. The physical distance between the different domains and the limitations on PQ diffusion mean that these different pools could be quite separate, thus promoting independent functioning of the photosynthetic complexes present in the grana and grana margins (LEF) and the stromal lamellae (CEF). On the other hand, thylakoid stacking is less defined in *Chlamydomonas* and algae in general, and therefore the functional segregation of LEF and CEF based on the physical segregation of the photosynthetic complexes in two distinct domains hardly applies to

these algae. It is therefore possible that the super-supercomplex, which localizes the mobile electron carriers (PQ, Fd, and PC) within a physically restricted space would ensure the compartmentation of the two pathways, thereby preventing CEF from being outcompeted by LEF activity. By doing this, super-supercomplex formation would play a similar role to that suggested for the segregation of PSI and PSII in the granal and stromal lamellae in plants.

## V. Role of Cytochrome $b_6f$ in State Transitions

In oxygenic photosynthesis, the two photosystems working in series have distinct pigment containing antenna complexes with distinct light absorbance properties. PS I has an enriched absorption capacity in the far-red region, whereas PS II lacks the far-red absorption capacity, but has a higher efficiency in the spectral regions where chlorophyll *b* absorbs (i.e. around 475 and 650 nm). Thus, in natural environments, where light quality and quantity fluctuate with time (Allen 1992; Bellafiore et al. 2005) unbalanced absorption can take place. This effect can be minimized by a phenomenon known as state transitions. Discovered independently by Murata and Sugahara (1969) and Bonaventura and Myers (1969), this process relies on a redox-triggered phosphorylation of the PSII antenna complexes (LHCII), which leads to a physiological displacement of LHCII from PSII to PSI under conditions where absorption of the former is enhanced (i.e. by enhanced light absorption by chlorophyll *b*). This state is called State 2. Conversely, over-excitation of PSI (e.g. by far red light) leads to the reassociation of LHCII with PSII (State 1; Allen 1992).

Pharmacological and genetic work has shown that state transitions are triggered by the PQ pool, which acts as a redox regulator of the phosphorylation of LHCII (Wollman 2001), via the activation of an LHCII kinase. However, reports exist claiming that LHCII

kinase(s) is/are not only activated by the reduced PQ pool, but also deactivated by the reduced thioredoxin pool that is downstream of PS I in the stroma of the chloroplasts in pumpkin (Rintamaki et al. 2000) and pea (Hou et al. 2002), and in *C. reinhardtii* (Vink et al. 2004). Why is the PQ pool responsible for such a redox signaling role? Being functionally located between PSII and PSI this redox active molecule can “sense” the relative light harvesting capacity of the two photosystems, being largely reduced when PSII activity overcomes that of PSI, and becoming oxidized when PSI prevails.

The nature of the kinase responsible for LHCII phosphorylation has been first identified in *Chlamydomonas* thanks to a genetic screening: it is a Ser/Thr kinase (Stt7) present in the chloroplast thylakoid membranes (Depege et al. 2003). Later, it was shown that an ortholog exist in plants (STN7; Bellafiore et al. 2005). The reversible phosphorylation of LHCII observed with thylakoids during state transitions implies that a phosphatase (TAP38/PPH1) is also active, being responsible for the dephosphorylation of LHCII (Pribil et al. 2010; Shapiguzov et al. 2010).

Signal transduction from PQH<sub>2</sub> to the Stt7/STN7 kinase is performed by the Cyt  $b_6f$  complex, as shown by several independent pieces of evidence. Wollman and Lemaire (1988) found that *C. reinhardtii* mutants lacking Cyt  $b_6f$  were unable to undergo a State 2 transition, indicating an essential role of this complex in the kinase activation. Later, spectroscopic (Vener et al. 1997) and genetic approaches (Zito et al. 1999) revealed that the committed step in kinase activation is the binding of PQH<sub>2</sub> to the luminal quinone-binding pocket (Q<sub>o</sub> site) of Cyt  $b_6f$ . While a consensus exists on the nature of the partners involved in the signaling from light to the kinase, the mechanism leading to the activation of Stt7/STN7 by reduced PQ is still under debate.

Based on a pharmacological analysis of kinase activation (Finazzi et al. 2001) a model has been built for this activation (Finazzi 2005), which involves several steps (Fig. 22.4). The signal from PQH<sub>2</sub> would be

transduced by an “active” Cyt  $b_6f$  complex, capable of switching between a docking conformation, which activates the kinase, and a releasing one, where the active kinase becomes capable of interacting with LHCII. Docking would involve conformational changes at the level of the Rieske protein and results in the phosphorylation of the Cyt  $b_6f$ -associated subunit PetO (Hamel et al. 2000; Finazzi et al. 2001; Wollman 2001). This step would precede phosphorylation of LHCII, which likely requires the release of the Stt7 kinase by a subsequent conformational change. This is suggested by the observation that while the PQ analog tridecylstigmatellin blocks Cyt  $b_6f$  catalysis and LHCII phosphorylation by preventing the movement of the Rieske protein head (Zhang et al. 1998; Breyton 2000b; Finazzi et al. 2001), this chemical does not affect the phosphorylation of PetO (Wollman 2001).

How are the conformational changes occurring in the luminal region of the complex transduced to the stromal site where the active moiety of the kinase is located? Analysis of the Stt7 kinase has suggested that this protein contains a putative transmembrane helix. This helix might, therefore, be directly involved in sensing PQH<sub>2</sub> binding to the Q<sub>o</sub> site, as already suggested (Vener et al. 1997). However, the existence of a direct signaling within the cytochrome complex is also possible, and supported by phenotypic analysis of Cyt  $b_6f$  mutants of *Chlamydomonas*. In particular, a mutant was generated (Zito et al. 2002) to fuse a small Cyt  $b_6f$  subunit (PetL) with subunit IV to “transform” the  $b_6f$  complex, which contains seven helices in its core subunits (Cyt  $b_6$  and subunit IV), into a  $bc_1$ -type complex (which contains eight helices in its unique core complex subunit, Cyt  $b$ ). At variance with expectations, this mutation did not lead to an altered electron flow, or PQH<sub>2</sub> binding to the luminal Q<sub>o</sub> site of the modified  $b_6f$  complex, but led to a complete abolition of state transitions.

Based on these results, it was proposed that docking of the kinase, which follows the structural changes induced by the PQH<sub>2</sub>-

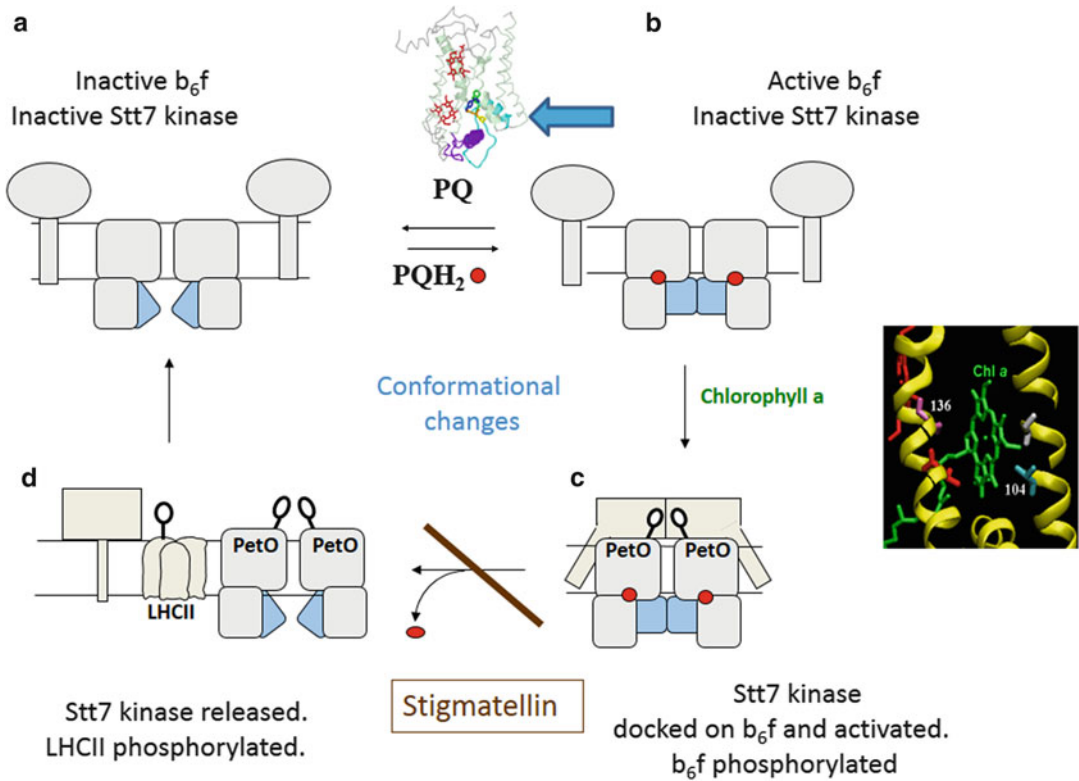


Fig. 22.4. Hypothetical mechanism of Stt7 activation by the cytochrome  $b_6f$  complex. The model conceives that upon binding of the PQH<sub>2</sub> molecule (red dot) to the lumenal Q<sub>o</sub> site of Cyt  $b_6f$ , conformational changes in the lumenal part of the Rieske protein (blue) would take place (transition from "a" to "b"). This would allow docking of the kinase (spheres and sticks) on the "lipid exposed" part of the complex, in close vicinity to the chlorophyll ring (c), leading to kinase activation (represented as boxes and sticks) and phosphorylation of the Cyt  $b_6f$  associated subunit PetO (black loops). Release of the active kinase after dissociation of the quinone from its binding pocket (d) would trigger LHCII trimer-kinase interactions, as required for antenna complex phosphorylation. The site of PQH<sub>2</sub> and kinase docking on Cyt  $b_6f$ , as well as the site of inhibition by stigmatellin are shown.

Cyt  $b_6f$  interaction, might take place on the cytochrome portion located in the proximity of the C terminus of subunit IV (where the PetL subunit was fused). This being the case, the mutant phenotype could be explained assuming that because of the presence of an additional helix close to its docking site, the formation of the kinase-Cyt  $b_6f$  complex was prevented, even if the cytochrome complex was in its "active" state. Interestingly, the 3D structure of Cyt  $b_6f$  from *Chlamydomonas*, (Stroebel et al. 2003), has revealed the presence of a chlorophyll molecule, which is exposed to the lipid phase through its tetrapyrrole ring, being sandwiched between helices F and G of subunit IV (see also Chap. 9

by Cramer and Hasan). Its phytol chain goes deeply into the complex structure ending up in the lumenal, PQH<sub>2</sub> binding pocket. Thus it is conceivable that the chlorophyll could "sense" the binding of PQH<sub>2</sub> to the Cyt  $b_6f$  complex via the phytol chain and transduce this information to the kinase docking site, via the chlorophyll ring (Finazzi 2005).

The possible involvement of the chlorophyll ring in kinase activation was later confirmed by the analysis of mutants affecting the environment of the chlorophyll ring in the complex, again in *Chlamydomonas* (de Lavalette et al. 2008). This study showed that in one mutant strain where the chlorine ring was likely displaced from its original site

because of steric hindrance, state transitions were largely compromised, although PQH<sub>2</sub> binding to the Q<sub>o</sub> site was not significantly affected. Based on these results, a scenario can be proposed to account for the mechanism of Stt7 activation by the Cyt  $b_6f$  complex (Fig. 22.4). However, further work will be needed to further confirm this model at the experimental level.

## VI. Conclusions

The role of the cytochrome  $b_6f$  complex in electron flow is a topic that has been investigated for many years combining functional and genetic approaches in both plants and microalgae. The resolution of the structure of this complex has led to major advances in this field, bridging the functional mechanism to the precise structural changes within the complex. Biochemical analyses have since then been instrumental in defining a further level of regulation, which involves a different interaction of the cytochrome with other photosynthetic complexes, as exemplified by the isolation of the PSI-Cyt  $b_6f$  supercomplex from *Chlamydomonas*. However, despite these major achievements, big questions are still open concerning both the intimate electron transfer mechanisms (the proton electron stoichiometry during catalysis, the obligatory occurrence of the Q cycle during turnover, proton versus redox regulation of the activity, and the possible existence of a signal transduction pathway within the complex allowing the activation of the kinase responsible for state transitions by reduced plastoquinone molecules). Major multidisciplinary efforts will be needed in the future to cast light on these fundamental aspects of bioenergetics.

## Acknowledgments

We would like to thank Dr. Cecile Breyton for her help in preparing Fig. 22.1. GF acknowledges the Marie Curie Initial Training Network Accliphot [FP7-PEOPLE-2012-

ITN, grant agreement number 316427], the French National Agency “DiaDomOil” [ANR-NT09\_567009], a grant from the region Rhone Alpes and the Centre National de la Recherche Scientifique program “Defi PF-ENRS13-1 Milli\_Oil”. JM was supported by JSPS and NEDO through KAKENHI (26251033) and a project for the strategic development of next-generation bioenergy utilization technology (P07015). GNJ acknowledges support from the UK Biotechnology and Biological Sciences Research Council (BB/C508877/1) and the Royal Society (ref: 24718)

## References

- Albertsson P-A (2001) A quantitative model of the domain structure of the photosynthetic membrane. *Trends Plant Sci* 6:349–354
- Allen JF (1992) Protein-phosphorylation in regulation of photosynthesis. *Biochim Biophys Acta* 1098:275–335
- Allen JF (2003) Cyclic, pseudocyclic and noncyclic photophosphorylation: new links in the chain. *Trends Plant Sci* 8:15–19
- Arnon DI (1995) Divergent pathways of photosynthetic electron transfer: the autonomous oxygenic and anoxygenic photosystems. *Photosynth Res* 46:47–71
- Bellafiore S, Barneche F, Peltier G, Rochaix JD (2005) State transitions and light adaptation require chloroplast thylakoid protein kinase STN7. *Nature* 433:892–895
- Bendall DS, Manasse RS (1995) Cyclic photophosphorylation and electron-transport. *Biochim Biophys Acta* 1229:23–38
- Berry EA, Guergova-Kuras M, Huang LS, Crofts AR (2000) Structure and function of cytochrome bc complexes. *Annu Rev Biochem* 69:1005–1075
- Bonaventura C, Myers J (1969) Fluorescence and oxygen evolution from *Chlorella pyrenoidosa*. *Biochim Biophys Acta* 189:366–383
- Brandt U, Trumppower B (1994) The protonmotive Q-cycle in mitochondria and bacteria. *Crit Rev Biochem Mol Biol* 29:165–197
- Breyton C (2000a) The cytochrome b(6)f complex: structural studies and comparison with the bc(1) complex. *Biochim Biophys Acta* 1459:467–474
- Breyton C (2000b) Conformational changes in the cytochrome  $b_6f$  complex induced by inhibitor binding. *J Biol Chem* 275:13195–13201

- Breyton C, Nandha B, Johnson GN, Joliot P, Finazzi G (2006) Redox modulation of cyclic electron flow around photosystem I in C3 plants. *Biochemistry* 45:13465–13475
- Brugna M, Rodgers S, Schrickler A, Montoya G, Kazmeier M, Nitschke W, Sinning I (2000) A spectroscopic method for observing the domain movement of the Rieske iron-sulfur protein. *Proc Natl Acad Sci USA* 97:2069–2074
- Carrillo N, Vallejos RH (1983) The light-dependent modulation of photosynthetic electron-transport. *Trends Biochem Sci* 8:52–56
- Cramer WA, Hasan SS, Yamashita E (2011) The Q cycle of cytochrome bc complexes: a structure perspective. *Biochim Biophys Acta* 1807:788–802
- Crofts AR, Meinhardt SW, Jones KR, Snozzi M (1983) The role of the quinone pool in the cyclic electron-transfer chain of *Rhodospseudomonas spaeroides*. A modified Q-cycle mechanism. *Biochim Biophys Acta* 723:202–218
- DalCorso G, Pesaresi P, Masiero S, Aseeva E, Nemann DS, Finazzi G, Joliot P, . . . , Leister D (2008) A complex containing PGRL1 and PGR5 is involved in the switch between linear and cyclic electron flow in *Arabidopsis*. *Cell* 132:273–285
- Darrouzet E, Moser CC, Dutton PL, Daldal F (2001) Large scale domain movement in cytochrome bc(1): a new device for electron transfer in proteins. *Trends Biochem Sci* 26:445–451
- de Lavalette AL, Finazzi G, Zito G (2008) b(6)f-Associated chlorophyll: structural and dynamic contribution to the different cytochrome functions. *Biochemistry* 47:5259–5265
- de Vitry C, Ouyang YX, Finazzi G, Wollman FA, Kallas T (2004) The chloroplast Rieske iron-sulfur protein – at the crossroad of electron transport and signal transduction. *J Biol Chem* 279:44621–44627
- Deniau C, Rappaport F (2000) New insights on the proton pump associated with cytochrome b(6)f turnovers from the study of H/D substitution effects on the electrogenicity and electron transfer reactions. *Biochemistry* 39:3304–3310
- Depege N, Bellafiore S, Rochaix JD (2003) Role of chloroplast protein kinase Stt7 in LHCII phosphorylation and state transition in *Chlamydomonas*. *Science* 299:1572–1575
- Eberhard S, Finazzi G, Wollman F-A (2008) The dynamics of photosynthesis. *Annu Rev Genet* 42:463–515
- Finazzi G (2002) Redox-coupled proton pumping activity in cytochrome b(6)f, as evidenced by the pH dependence of electron transfer in whole cells of *Chlamydomonas reinhardtii*. *Biochemistry* 41:7475–7482
- Finazzi G (2005) The central role of the green alga *Chlamydomonas reinhardtii* in revealing the mechanism of state transitions. *J Exp Bot* 56:383–388
- Finazzi G, Rappaport F (1998) In vivo characterization of the electrochemical proton gradient generated in darkness in green algae and its kinetic effects on cytochrome b(6)f turnover. *Biochemistry* 37:9999–10005
- Finazzi G, Zito F, Barbagallo RP, Wollman FA (2001) Contrasted effects of inhibitors of cytochrome b(6)f complex on state transitions in *Chlamydomonas reinhardtii* – the role of Q(o) site occupancy in LHCII kinase activation. *J Biol Chem* 276:9770–9774
- Golding AJ, Johnson GN (2003) Down-regulation of linear and activation of cyclic electron transport during drought. *Planta* 218:107–114
- Golding AJ, Joliot P, Johnson GN (2005) Equilibration between cytochrome f and P700 in intact leaves. *Biochim Biophys Acta Bioenerg* 1706:105–109
- Gould SB, Waller RR, McFadden GI (2008) Plastid evolution. *Annu Rev Plant Biol* 59:491–517
- Hald S, Nandha B, Gallois P, Johnson GN (2008) Feedback regulation of photosynthetic electron transport by NADP(H) redox poise. *Biochim Biophys Acta* 1777:433–440
- Hamel P, Olive J, Pierre Y, Wollman FA, de Vitry C (2000) A new subunit of cytochrome b(6)f complex undergoes reversible phosphorylation upon state transition. *J Biol Chem* 275:17072–17079
- Harbinson J, Hedley CL (1989) The kinetics of P-700<sup>+</sup> reduction in leaves – a novel in situ probe of thylakoid functioning. *Plant Cell Environ* 12:357–369
- Hasan SS, Yamashita E, Baniulis D, Cramer WA (2013) Quinone-dependent proton transfer pathways in the photosynthetic cytochrome b(6)f complex. *Proc Natl Acad Sci USA* 110:4297–4302
- Heimann S, Ponamarev MV, Cramer WA (2000) Movement of the Rieske iron-sulfur protein in the p-slide bulk aqueous phase: effect of luminal viscosity on redox reactions of the cytochrome b(6)f complex. *Biochemistry* 39:2692–2699
- Hertle AP, Blunder T, Wunder T, Pesaresi P, Pribil M, Armbruster U, Leister D (2013) PGRL1 is the elusive ferredoxin-plastoquinone reductase in photosynthetic cyclic electron flow. *Mol Cell* 49:511–523
- Hou CX, Pursiheimo S, Rintamaki E, Aro EM (2002) Environmental and metabolic control of LHCII protein phosphorylation: revealing the mechanisms for dual regulation of the LHCII kinase. *Plant Cell Environ* 25:1515–1525



- Iwai M, Takizawa K, Tokutsu R, Okamuro A, Takahashi Y, Minagawa J (2010) Isolation of the elusive supercomplex that drives cyclic electron flow in photosynthesis. *Nature* 464:1210–U1134
- Iwata S, Lee JW, Okada K, Lee JK, Iwata M, Rasmussen B, Link TA, . . . , Jap BK (1998) Complete structure of the 11-subunit bovine mitochondrial cytochrome  $bc_1$  complex. *Science* 281:64–71
- Jahns P, Graf M, Munekage Y, Shikanai T (2002) Single point mutation in the Rieske iron-sulfur subunit of cytochrome  $b_6/f$  leads to an altered pH dependence of plastoquinol oxidation in *Arabidopsis*. *FEBS Lett* 519:99–102
- Johnson GN (2003) Thiol regulation of the thylakoid electron transport chain – a missing link in the regulation of photosynthesis? *Biochemistry* 42:3040–3044
- Johnson GN (2011) Physiology of PSI cyclic electron transport in higher plants. *Biochim Biophys Acta* 1807:384–389
- Joliot P, Johnson GN (2011) Regulation of cyclic and linear electron flow in higher plants. *Proc Natl Acad Sci USA* 108:13317–13322
- Joliot P, Joliot A (2002) Cyclic electron transport in plant leaf. *Proc Natl Acad Sci USA* 99:10209–10214
- Kramer DM, Avenson TJ, Edwards G (2004) Dynamic flexibility in the light reactions of photosynthesis governed by both electron and proton transfer reactions. *Trends Plant Sci* 9:339–348
- Kurusu G, Zhang HM, Smith JL, Cramer WA (2003) Structure of the cytochrome  $b_6/f$  complex of oxygenic photosynthesis: tuning the cavity. *Science* 302:1009–1014
- Laisk A (1993) Mathematical modelling of free-pool and channelled electron transport in photosynthesis: evidence for a functional supercomplex around photosystem I. *Proc R Soc Lond Ser B Biol Sci* 251:243–251
- Lehtimäki N, Lintala M, Allahverdiyeva Y, Aro EM, Mulo P (2010) Drought stress-induced upregulation of components involved in ferredoxin-dependent cyclic electron transfer. *J Plant Physiol* 167:1018–1022
- Li Z, Wakao S, Fischer BB, Niyogi KK (2009) Sensing and responding to excess light. *Annu Rev Plant Biol* 60:239–260
- Livingston AK, Cruz JA, Kohzuma K, Dhingra A, Kramer DM (2010) An *Arabidopsis* mutant with high cyclic electron flow around photosystem I (hcef) involving the NADPH dehydrogenase complex. *Plant Cell* 22:221–233
- Malnoe A, Wollman F-A, de Vitry C, Rappaport F (2011) Photosynthetic growth despite a broken Q-cycle. *Nat Commun* 2:301
- Mitchell P (1975) The protonmotive Q cycle: a general formulation. *FEBS Lett* 59:137–199
- Munekage Y, Hojo M, Endo T, Shikanai T (2002a) *Arabidopsis pgr5* is defective in cyclic electron flow around photosystem I. *Plant Cell Physiol* 43:S23–S23
- Munekage Y, Hojo M, Meurer J, Endo T, Tasaka M, Shikanai T (2002b) PGR5 is involved in cyclic electron flow around photosystem I and is essential for photoprotection in *Arabidopsis*. *Cell* 110:361–371
- Murata N, Sugahara K (1969) Control of excitation transfer in photosynthesis. III. Light-induced decrease of chlorophyll a fluorescence related to photophosphorylation system in spinach chloroplasts. *Biochim Biophys Acta* 189:182–189
- Nandha B, Finazzi G, Joliot P, Hald S, Johnson GN (2007) The role of PGR5 in the redox poising of photosynthetic electron transport. *Biochim Biophys Acta* 1762:1252–1259
- Nitschke W, Joliot P, Liebl U, Rutherford AW, Hauska G, Muller A, Riedel A (1992) The pH-dependence of the redox midpoint potential of the 2Fe2S cluster from cytochrome-B $_6f$  complex (the Rieske center). *Biochim Biophys Acta* 1102:266–268
- Ott T, Clarke J, Birks K, Johnson G (1999) Regulation of the photosynthetic electron transport chain. *Planta* 209:250–258
- Pierre Y, Breyton C, Kramer D, Popot JL (1995) Purification and characterization of the cytochrome B(6)F complex from *Chlamydomonas reinhardtii*. *J Biol Chem* 270:29342–29349
- Pribil M, Pesaresi P, Hertle A, Barbato R, Leister D (2010) Role of plastid protein phosphatase TAP38 in LHCII dephosphorylation and thylakoid electron flow. *PLoS Biol* 8:e1000288
- Rintamäki E, Martinsuo P, Pursiheimo SAro EM (2000) Cooperative regulation of light-harvesting complex II phosphorylation via the plastoquinol and ferredoxin-thioredoxin system in chloroplasts. *Proc Natl Acad Sci USA* 97:11644–11649
- Rumeau D, Peltier G, Cournac L (2007) Chlororespiration and cyclic electron flow around PSI during photosynthesis and plant stress response. *Plant Cell Environ* 30:1041–1051
- Sacksteder CA, Kanazawa A, Jacoby ME, Kramer DM (2000) The proton to electron stoichiometry of steady-state photosynthesis in living plants: a proton-pumping Q cycle is continuously engaged. *Proc Natl Acad Sci USA* 97:14283–14288
- Schoepp B, Brugna M, Riedel A, Nitschke W, Kramer DM (1999) The Q(o)-site inhibitor DBMIB favours the proximal position of the chloroplast Rieske protein and induces a pK-shift of the redox-linked proton. *FEBS Lett* 450:245–250

- Shapiguzov A, Ingelsson B, Samol I, Andres C, Kessler F, Rochaix J-D, Vener AV, Goldschmidt-Clermont M (2010) The PPH1 phosphatase is specifically involved in LHCII dephosphorylation and state transitions in *Arabidopsis*. *Proc Natl Acad Sci USA* 107:4782–4787
- Shikanai T (2007) Cyclic electron transport around photosystem I: genetic approaches. *Annu Rev Plant Biol* 58:199
- Soriano GM, Guo L-W, de Vitry C, Kallas T, Cramer WA (2002) Electron transfer from the Rieske Iron-Sulfur Protein (ISP) to cytochrome f in vitro: is a guided trajectory of the ISP necessary for competent docking? *J Biol Chem* 277:41865–41871
- Strand DD, Livingston AK, Satoh-Cruz M, Froehlich JE, Maurino VG, Kramer DM (2015) Activation of cyclic electron flow by hydrogen peroxide in vivo. *Proc Natl Acad Sci* 112:5539–5544
- Stroebel D, Choquet Y, Popot JL, Picot D (2003) An atypical haem in the cytochrome b(6)f complex. *Nature* 426:413–418
- Tagawa K, Tsujimoto HY, Arnon DI (1963) Role of chloroplast ferredoxin in the energy conversion process of photosynthesis. *Proc Natl Acad Sci USA* 49:567–572
- Tremmel IG, Kirchhoff H, Weis E, Farquhar GD (2003) Dependence of plastoquinol diffusion on the shape, size, and density of integral thylakoid proteins. *Biochim Biophys Acta* 1607:97–109
- Vener AV, VanKan PJM, Rich PR, Ohad I, Andersson B (1997) Plastoquinol at the quinol oxidation site of reduced cytochrome bf mediates signal transduction between light and protein phosphorylation: thylakoid protein kinase deactivation by a single-turnover flash. *Proc Natl Acad Sci USA* 94:1585–1590
- Vink M, Zer H, Alumot N, Gaathon A, Niyogi K, Herrmann RG, Andersson B, Ohad I (2004) Light-modulated exposure of the light-harvesting complex II (LHCII) to protein kinase(s) and state transition in *Chlamydomonas reinhardtii* xanthophyll mutants. *Biochemistry* 43:7824–7833
- West KR, Wiskich JT (1968) Photosynthetic control by isolated pea chloroplasts. *Biochem J* 109:527–532
- Wollman FA (2001) State transitions reveal the dynamics and flexibility of the photosynthetic apparatus. *EMBO J* 20:3623–3630
- Wollman FA, Lemaire C (1988) Studies on kinase-controlled state transitions in photosystem II and b6f mutants from *Chlamydomonas reinhardtii* which lack quinone-binding proteins. *Biochim Biophys Acta* 933:85–94
- Xia D, Yu CA, Kim H, Xian JZ, Kachurin AM, Zhang L, Yu L, Deisenhofer J (1997) Crystal structure of the cytochrome bc(1) complex from bovine heart mitochondria (vol 277, pg 60, 1997). *Science* 278:2037–2037
- Zhang ZL, Huang LS, Shulmeister VM, Chi YI, Kim KK, Hung LW, Crofts AR, . . . , Kim SH (1998) Electron transfer by domain movement in stockbroker bc(1). *Nature* 392:677–684
- Zhang HM, Whitelegge JP, Cramer WA (2001) Ferredoxin: NADP(+) oxidoreductase is a subunit of the chloroplast cytochrome b(6)f complex. *J Biol Chem* 276:38159–38165
- Zito F, Finazzi G, Joliot P, Wollman FA (1998) Glu78, from the conserved PEWY sequence of subunit IV, has a key function in cytochrome b(6)f turnover. *Biochemistry* 37:10395–10403
- Zito F, Finazzi G, Delosme R, Nitschke W, Picot D, Wollman FA (1999) The Qo site of cytochrome b(6)f complexes controls the activation of the LHCII kinase. *EMBO J* 18:2961–2969
- Zito F, Vinh J, Popot JL, Finazzi G (2002) Chimeric fusions of subunit IV and PetL in the b6f complex of *Chlamydomonas reinhardtii* – structural implications and consequences on state transitions. *J Biol Chem* 277:12446–12455

## A Supercomplex of Cytochrome *b<sub>f</sub>* and Photosystem I for Cyclic Electron Flow

Jun Minagawa\*

*Division of Environmental Photobiology, National Institute for Basic Biology (NIBB), Okazaki 444–8585, Japan  
Core Research for Evolutional Science and Technology (CREST), Japan Science and Technology Agency (JST), Saitama 332–0012, Japan*

Summary.....	453
I. Introduction.....	454
II. Cyclic Electron Flow Is Essential.....	454
III. Cyclic Electron Flow and the Redox Status of the Chloroplast.....	456
IV. A Supercomplex in Charge of Cyclic Electron Flow in <i>Chlamydomonas</i> .....	456
V. Perspectives.....	460
Acknowledgments.....	461
References.....	461

### Summary

In oxygen-evolving photosynthesis, photochemical energy conversion occurs via electron transport in the thylakoid membranes, resulting in the reduction of NADP<sup>+</sup> in the stroma and the concomitant pumping of protons into the thylakoid lumen. Those electrons flow into two different pathways in the thylakoid membranes: the linear electron flow pathway from water to NADP<sup>+</sup> via photosystem II and photosystem I (PSI) in series and the cyclic electron flow pathway around PSI. While the operational site(s) for the cyclic electron flow has been elusive, recent studies are unraveling its molecular details. After providing an overview of the general understanding of the cyclic electron flow, this review focuses on a recent report on the super-supercomplex that is composed of the cytochrome *b<sub>6</sub>f* complex, photosystem I with its own light-harvesting complex, the light-harvesting complex for photosystem II, and the ferredoxin-NADPH oxidoreductase, which exhibits cyclic electron flow in the green unicellular alga *Chlamydomonas reinhardtii*.

---

\*Author for correspondence, e-mail: [minagawa@nibb.ac.jp](mailto:minagawa@nibb.ac.jp)

## I. Introduction

Because plants and algae typically do not have means to escape from adverse environments, their ability to acclimate to the environments is essential if they are to survive in their niche. In natural environments where the quality and quantity of light fluctuates, photoacclimation of the photosynthetic machinery is particularly important for photosynthetic organisms to optimize their photosynthetic efficiency and to protect their machineries from photooxidative damage. Photosynthesis is a process of photochemical energy conversion that occurs via electron transport in the thylakoid membranes of chloroplasts and results in the reduction of  $\text{NADP}^+$  in the stroma and the concomitant pumping of protons into the thylakoid lumen. The NADPH that is generated by electron flow and the ATP that is synthesized by using the proton motive force across the thylakoid membrane are required to assimilate  $\text{CO}_2$  in the Calvin-Benson cycle. Photosystem I (PSI) and II (PSII) are multi-subunit pigment-protein complexes where the charge separations elicited by light energy take place to drive electron flow. Electrons that are generated in the photosystems flow into two different pathways in the thylakoid membranes: the linear electron flow (LEF) pathway from water to  $\text{NADP}^+$  via PSII and PSI in series and the cyclic electron flow (CEF) pathway around PSI. While

the operational site(s) for CEF has been elusive, recent studies are unraveling its molecular details. In this chapter, I introduce a recent study on a super-supercomplexes that is composed of the cytochrome *b<sub>6</sub>f* complex (Cyt *bf*), PSI with its own light-harvesting complex (LHCI), the PSII light-harvesting complex (LHCII), the ferredoxin (Fd)-NADPH oxidoreductase (FNR), as well as several other membrane proteins showing CEF activity in the green unicellular alga *Chlamydomonas reinhardtii* (Iwai et al. 2010).

## II. Cyclic Electron Flow Is Essential

It is crucial to achieve an ATP:NADPH ratio of 3:2 in the stroma in order to assimilate  $\text{CO}_2$  in the Calvin-Benson cycle; however, this balance cannot be achieved by LEF alone (Allen 2003). As illustrated in Fig. 23.1, 4 protons are released into the lumen and 2 reduced plastoquinone (PQ) molecules are released into the intersystem pool after 4 turnovers of PSII upon capturing 5 photons assuming the quantum yield of the photochemistry is 0.8 (Björkman and Demmig 1987). At the  $\text{Q}_o$  (or  $\text{Q}_p$ ) site of Cyt *bf*, 2 molecules of  $\text{PQH}_2$  release 4 protons into the lumen and transfer 2 electrons to Pc. The yield of protons and electrons is doubled here (Sacksteder et al. 2000) by the so-called ‘Q cycle mechanism’ (Mitchell 1976). In total, 8 protons are released from Cyt *bf* into the lumen, and 4 Pc and then 2  $\text{NADP}^+$  are reduced. After all, 12 protons that are released into the lumen via LEF are used to rotate the  $\text{CF}_o$  subcomplex of ATP synthase, where 3 ADP molecules are phosphorylated per single rotation. Because the number of the proton-binding c-subunits in the  $\text{CF}_o$  subcomplex is 14 (Seelert et al. 2000), the 12 protons generated by LEF can only rotate the  $\text{CF}_o$  subcomplex 0.86 rounds, which is coupled to the synthesis of 2.6 molecules of ATP. To synthesize 3 molecules of ATP, plants and algae therefore need to re-route 1 electron from PSI to Cyt *bf* in order to

---

*Abbreviations:* AA – Antimycin A; CEF – Cyclic electron flow; Cyt *bf* – cytochrome *b<sub>6</sub>f* complex; DBMIB – 2,5-dibromo-3-methyl-6-isopropylbenzoquinone; DCMU – 3-(3,4-Dichlorophenyl)-1,1-dimethylurea; DMBQ – 2,6-dimethyl-p-benzoquinone; FCCP – Carbonyl cyanide 4-(trifluoromethoxy)phenylhydrazone; Fd – Ferredoxin; FNR – Ferredoxin-NADPH oxidoreductase; FQR – Ferredoxin-plastoquinone oxidoreductase; LEF – Linear electron flow; LHCI and LHCII – Light-harvesting complex protein I and II; NDH – NAD(P)H dehydrogenase; NPQ – Non-photochemical quenching; Pc – Plastocyanin; PQ – Plastoquinone; PSI and PSII – Photosystem I and II

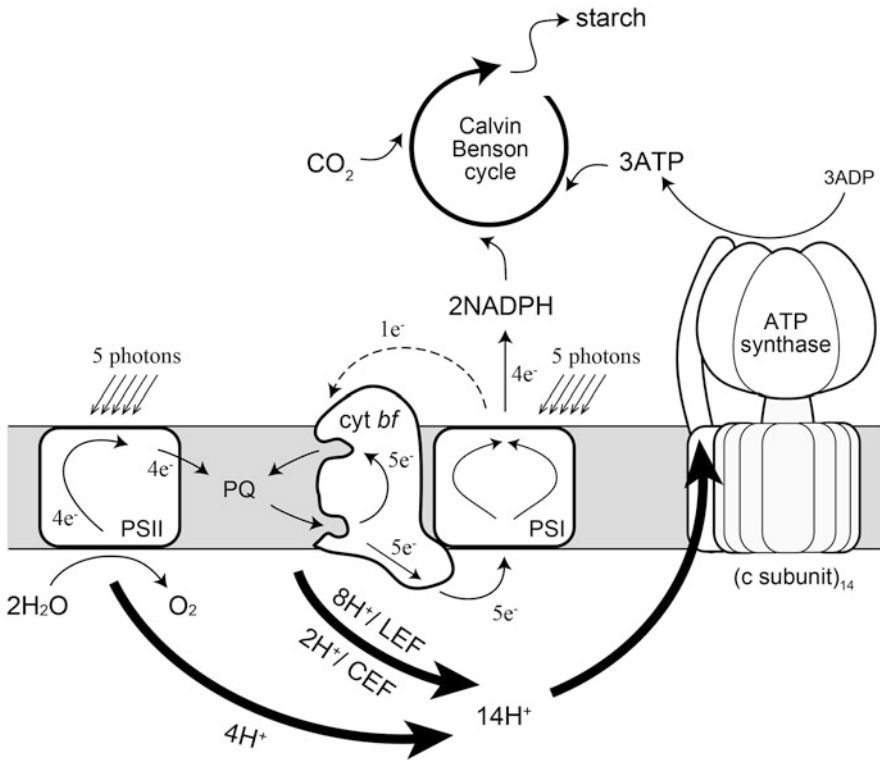


Fig. 23.1. Schematic representation of the movement of protons and electrons by the photosynthetic electron transport chain in chloroplasts. The pathways and stoichiometry of light-driven electron transport, proton translocation, and ATP synthesis in the thylakoid membranes are shown. *Thick arrows* represent the pathways of protons; *thin solid* and *thin dashed arrows* represent LEF and CEF, respectively.

pump 2 extra protons into the lumen. It is CEF that enables such electron re-routing from PSI to Cyt *bf*. CEF is thus essential for CO<sub>2</sub> assimilation (Munekage et al. 2004). The scheme described here indicates that the quantum yield of PSII, in which 5 photons are required for 4 turnovers, is lower than that of PSI, where 5 photons are required for 5 turnovers (Fig. 23.1). To put it another way, the quantum yield in PSII is 20 % lower than in PSI because 20 % of the electrons in PSI are re-circulated by the CEF pathway. In natural systems, ATP and NADPH could be consumed in various other cellular reactions and the demand for each fluctuates from time to time. Therefore, photosynthetic organisms need to constantly adjust the relative ratio of the two modes of electron flow. Another role of CEF in chloroplasts is to establish a high ΔpH across the thylakoid membrane to ac-

tivate non-photochemical quenching (NPQ). This is especially important under adverse environmental conditions where the capacity for CO<sub>2</sub> fixation cannot catch up with the amount of absorbed light. CEF is therefore crucial for achieving the correct balance of NADPH and ATP in the thylakoid stroma for CO<sub>2</sub> assimilation and for protecting its photosynthetic machineries from photodamage. Two possible electron transfer pathways have been proposed for CEF: an Fd-dependent pathway and an NAD(P)H dehydrogenase (NDH)-dependent pathway (Shikanai 2007). In the NDH-dependent pathway, NDH mediates NADPH oxidation and PQ pool reduction in much the same way as the complex I does in mitochondria (Ogawa 1991). However, how electrons on Fd are transferred to the PQ pool in Fd-dependent CEF (Fd-CEF) has, until recently, been unclear.

### III. Cyclic Electron Flow and the Redox Status of the Chloroplast

Each of the two charge separation devices in the thylakoid membranes, PSI and PSII, has a distinct pigment system with unique absorption characteristics. Thus, an imbalance in the distribution of energy between the two photosystems tends to occur in natural environments, where light quality and quantity fluctuate with time (Allen 1992; Bellafiore et al. 2005; Minagawa 2011). Because the two photosystems are connected in series under normal conditions, plants and algae need to constantly balance their excitation levels to ensure an optimal efficiency of electron flow. State transitions occur under such conditions to balance the light-harvesting capacities of the two photosystems and to minimize the unequal distribution of light energy. This short-term adaptation involves thylakoid-bound protein kinase(s) that are responsible for the phosphorylation of LHCII is a process called state transitions. When PSII is preferentially excited, LHCII are phosphorylated, and the light-harvesting capacity of PSII decreases (State 2). Conversely, when PSI is preferentially excited, LHCII are dephosphorylated, and the light-harvesting capacity for PSII increases (State 1). At room temperature, State 1 can be characterized by a high yield of chlorophyll fluorescence, arising primarily from PSII, and State 2 can be characterized by a low yield of chlorophyll fluorescence. In *C. reinhardtii*, it was suggested that the modulation of CEF occurs in parallel with state transitions (Finazzi et al. 2002). When the light-induced reduction of Cyt *bf* was probed in State 1- and State 2-adapted cells, a differential sensitivity to the addition of the Q<sub>B</sub> site inhibitor of PSII 3-(3,4-dichlorophenyl)-1,1-dimethylurea (DCMU) was observed. DCMU blocked the reduction of Cyt *bf* in State 1 but not in State 2. An identical sensitivity to an inhibitor of Cyt *bf*, 2,5-dibromo-3-methyl-6-isopropylbenzoquinone

(DBMIB), was observed in both State 1 and State 2, suggesting that PSII-independent CEF only occurs when the cells are in State 2 (Finazzi et al. 1999).

Other reports provided more information about CEF in *C. reinhardtii*. Under anaerobic conditions, the independent knock-down of three thylakoid membrane proteins, PGRL1, CAS, and ANR1, resulted in a decreased CEF activity (Terashima et al. 2012). The ability to undergo state transitions, however, was unaffected in these mutants, suggesting state transitions do not switch between LEF and CEF but rather that state transitions and LEF/CEF switching are coincidental. This was further supported by examining CEF activity in the State 2-locked mutant of *C. reinhardtii* (Takahashi et al. 2013). Although the lateral migration of mobile LHCII occurred in the *ptox2* mutant, which has a constantly reduced PQ pool due to the lack of plastid terminal oxidase 2 (Houille-Vernes et al. 2011), CEF was negligible much as in wild type cells in State 1. Thus, the CEF/LEF switching and state transitions can be hypothesized as follows: The chloroplast stroma and PQ pool are oxidized when PSI is preferentially excited. Under these conditions, LHCII are bound to PSII (State 1). Upon reduction of the stroma, Cyt *bf* and FNR are associated with PSI to form a super-supercomplex (CEF supercomplex) as described below; and on the other hand, the PQ pool, and the Q<sub>o</sub>-site of Cyt *bf*, gets reduced to bring the cells into State 2, where migration of the mobile LHCII occurs to the PsaH side of PSI, and a large scale reorganization of the thylakoids occurs to make the remained LHCII attached to PSII energy-dissipative (Nagy et al. 2014) (Fig. 23.2).

### IV. A Supercomplex in Charge of Cyclic Electron Flow in *Chlamydomonas*

The machinery for Fd-CEF was identified in *C. reinhardtii* cells treated with carbonyl cyanide 4-(trifluoromethoxy)phenylhydra-

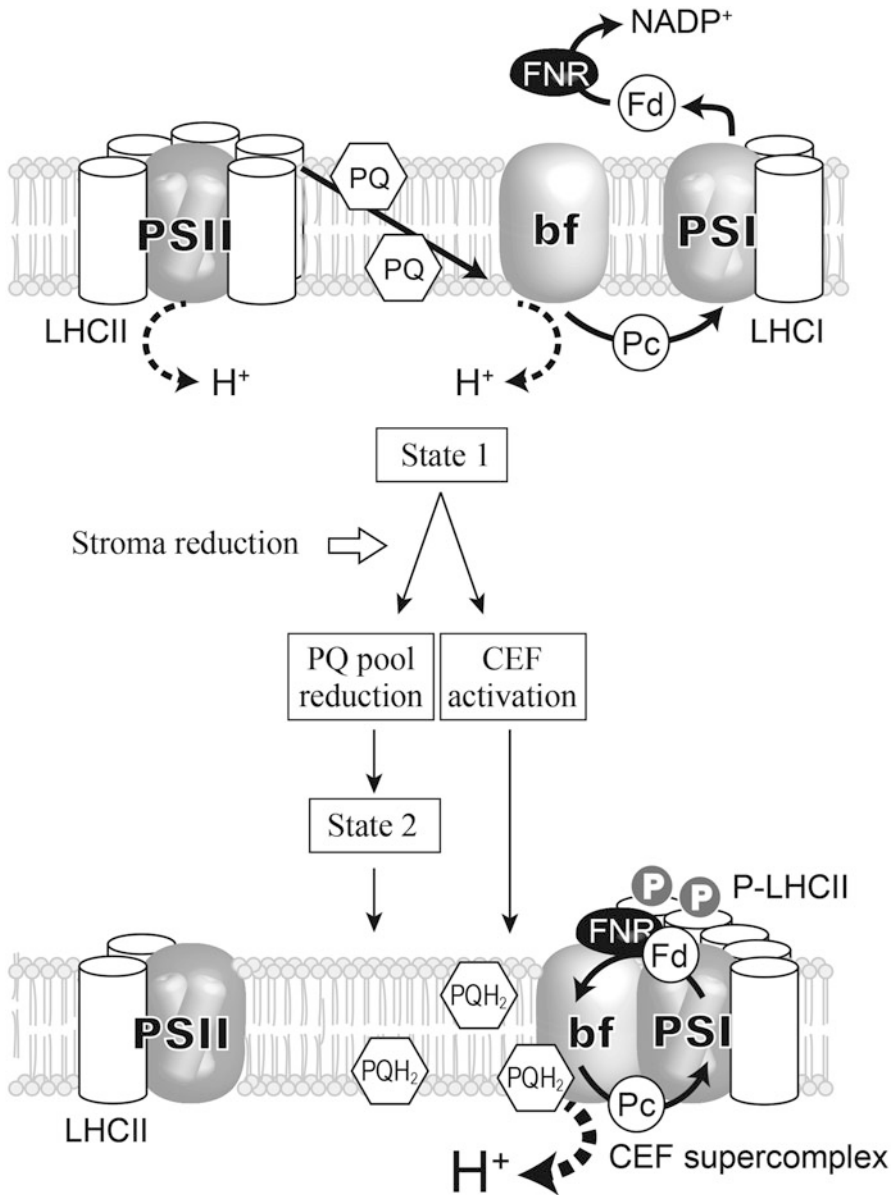


Fig. 23.2. Schematic representation of the regulation of state transitions and electron flow in *C. reinhardtii*. *Upper*, when PSI is preferentially excited, the chloroplast stroma and the PQ pool are oxidized. Under these conditions, LHCII is bound to PSII (State 1). The photosynthetic electron flow proceeds in LEF mode, generating NADPH as well as a proton gradient across the thylakoid membrane that is used for ATP production. *Middle*, when the stroma is reduced, on one hand, migration of the mobile LHCII from PSII to PSI occurs to establish State 2; on the other hand, CEF becomes activated by association of Cyt *bf* and FNR with PSI to form a super-supercomplex (CEF supercomplex). *Lower*, the cells are in State 2 and the photosynthetic electron flow proceeds in the CEF mode. PQ pool-reduced. Abbreviations: *bf* Cyt *bf*, *Fd* ferredoxin, *Pc* plastocyanin.

zone (FCCP) (Iwai et al. 2010). When FCCP depletes intracellular ATP pools by uncoupling the energized membranes

and stimulating glycolysis according to the Pasteur effect, the stroma of the chloroplast is reduced, and probably because of this,

CEF gets activated and the PQ pool in the thylakoid membrane becomes reduced to lead the cells to State 2 (Bulté et al. 1990). We solubilized these thylakoid membranes and loaded them onto a sucrose density gradient, which yielded four discrete green bands including the heaviest fraction (the A4 fraction). The A4 fraction contained PSI with its own antenna system (the PSI-LHCI supercomplex), major LHCII, minor LHCII, Cyt *bf* (Cyt *b<sub>6</sub>*, Cyt *f*, PetC, PetD, PetO, FNR, and PGRL1 with equimolar amount of Cyt *bf* and PSI. Four different methods were employed to confirm the proteins in the A4 fraction formed a single supercomplex: (1) A single peak with a molecular mass corresponding to 1400–1600 kDa was observed on a gel-filtration chromatogram. (2) The constituents of the A4 band were disassembled by salt treatment into smaller molecular mass complexes, indicating they originally formed a super-supercomplex. (3) The A4 fraction was not present either in the mutant of PSI or the Cyt *bf* complex. (4) The affinity-purified supercomplex by using a His-tagged PsaA subunit of PSI contained the same protein composition as the original A4 fraction.

To address the question as to whether the supercomplex in the A4 fraction is a functional unit for CEF, we examined the electron

transfer activities of the supercomplex on its stromal and luminal sides by a series of spectroscopic analyses. The stromal side electron transfer was first probed by measuring the reduction of Cyt *b* in the supercomplex. When Cyt *b* in the supercomplex was reduced after incubation with NADPH together with Fd, the resulting signal was approximately half as large as that produced upon the reduction of both *b*-type hemes with dithionite. This suggested that only one of the *b*-type hemes in Cyt *bf*, most likely the high-potential heme *b<sub>H</sub>*, was reduced (Fig. 23.3). When we illuminated the supercomplex in the presence of Fd, Cyt *b* was reduced, manifesting the photoreduction of heme *b<sub>H</sub>* by the electrons from P700. We then evaluated the luminal side electron transfer by studying the flash-induced kinetics of P700<sup>+</sup> re-reduction and Cyt *f* oxidation within the supercomplex. After oxidized by a single-turnover actinic flash, most of the P700 in the supercomplex accepted electrons from Pc. Cyt *f* in the supercomplex was rapidly oxidized upon illumination in the presence of Pc (Fig. 23.3).

The physical association of PSI, Cyt *bf*, and FNR has long been suggested as a platform for Fd-CEF (Joliot and Joliot 2002). Mathematical modelling of electron transfer (Laik 1993) and the observation of

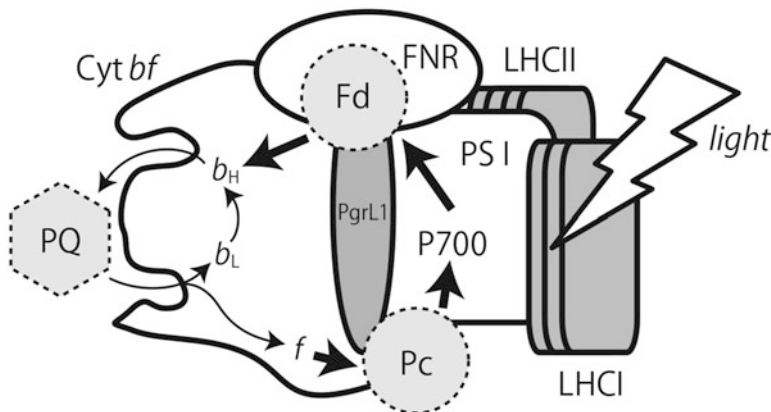


Fig. 23.3. Fd-CEF model in the CEF supercomplex. Major components of the CEF supercomplex (PSI, LHCI, LHCII, FNR, Cyt *bf*, and PGRL1) and possible electron transfer pathways are schematically drawn along with the mobile electron carriers (Fd, PQ, and Pc). Abbreviations: P700 primary electron donor in PSI, *b<sub>H</sub>* and *b<sub>L</sub>* high and low potential *b* hemes in Cyt *bf*, *f* heme *f* in Cyt *bf*.



its high efficiency *in vivo* (Joliot and Joliot 2002) suggested that Fd-CEF operates in a supercomplex. Cramer and co-workers reported that Cyt *bf* was co-purified with FNR and was reduced by Fd (Zhang et al. 2001). More recently, physical interactions between PGRL1, PsaD (a subunit of PSI), PetB (Cyt *b<sub>6</sub>*), FNR, and PGR5 were proposed based on a yeast two-hybrid assay using the corresponding genes from *A. thaliana* (DalCorso et al. 2008). However, the enigmatic all-star “super-supercomplex” comprising PSI, Cyt *bf*, and FNR has never been detected or isolated (Breyton et al. 2006; DalCorso et al. 2008). The study in *C. reinhardtii*, however, demonstrated that the CEF supercomplex indeed exists. Moreover, the isolated supercomplex contained PGRL1 as well as a loosely bound Cyt *bf* subunit, PetO (Hamel et al. 2000). Notably, electron transfer activity was detected on both stromal and luminal sides of the complex (Fig. 23.3). The exact electron transfer pathway within Cyt *bf* is still unclear, but we speculate that the reducing equivalent on heme *b<sub>H</sub>* is transported to *b<sub>L</sub>* via PQ molecules much as proposed for the Q-cycle (Mitchell 1976) (Fig. 23.3). Because CEF and LEF share many redox carriers including PQ, Cyt *bf*, Pc, PSI, Fd, and FNR, the two pathways are potentially in competition with one another. Furthermore, the redox poise of the CEF components could be disturbed if reduced LEF components coexist. However, the formation of a super-supercomplex specific for Fd-CEF (a PSI-LHCI-LHCII-FNR-Cyt *bf*-PGRL1 super-supercomplex or CEF supercomplex) seemingly compartmentalizes CEF by localizing the mobile electron carriers, forming a functional pool of CEF components to sustain the increased CEF activity.

As mentioned above, mutants carrying a mutation in one of the three thylakoid membrane proteins, PgrL1, CAS, and ANR1, have decreased CEF activities under anaerobic conditions (Terashima et al. 2012). Because these three proteins were included in the CEF supercomplex, they are likely additional components for the super-supercomplex (Terashima et al. 2012).

Furthermore, Rappaport and his colleagues showed that the CEF supercomplex is formed under anaerobic, but not aerobic conditions in wild type *Chlamydomonas*. It is also formed in *ptox2* (State 2-locked) and *stt7-9* (State 1-locked) mutant cells, leading them to propose that a reduced stromal environment (which was experimentally substantiated under anaerobic conditions) was responsible for the LEF/CEF switching. The mechanism of how such an increase in reducing power in the stroma promotes the formation of the CEF supercomplex still remains to be unraveled (Takahashi et al. 2013).

Last but not least, I will discuss the possible CEF inhibitor antimycin (AA) and the intriguing CEF components PGR5 and PGRL1. Among NPQ mutant lines, Shikanai and his colleagues isolated several *pgr* mutants that have restricted accumulation of proton motive force across the thylakoid membranes (Munekage et al. 2002). Because the reduction of the PQ pool by way of CEF was earlier described as AA-sensitive (Tagawa et al. 1963), an elusive AA-binding enzyme, Fd-PQ oxidoreductase (FQR), had been proposed to bypass Cyt *bf*, which is not sensitive to AA in contrast to the sister enzyme Cyt *bc<sub>1</sub>* complex in mitochondria (Huang et al. 2005), when it reduces the PQ pool (Moss and Bendall 1984). Because *pgr5* affected the AA-sensitive fluorescence rise, which is generally ascribed to Fd-mediated PQ pool reduction, PGR5 was postulated to be a component of the FQR enzyme (Shikanai 2007). PGR5 is only an 8 kDa polypeptide, therefore more likely forming a complex with other membrane spanning subunit(s) to constitute any FQR. A *pgrL1* mutant was subsequently reported to display the same phenotype as *pgr5* in *A. thaliana* (DalCorso et al. 2008). A recombinant PGRL1 was shown to be reduced by Fd when it formed a heterocomplex with PGR5, although such a heterocomplex was not detected *in vivo* (Hertle et al. 2013). The reduced and monomerized PGRL1 in turn reduced the PQ analog 2,6-dimethyl-p-benzoquinone (DMBQ) in an AA-dependent manner *in vitro* (Hertle et al. 2013).

While genes for both PGR5 and PGRL1 are present in the genome of *C. reinhardtii* (Merchant et al. 2007), and the transcription of both of these genes is at least elicited under specific conditions (e.g., iron deficient conditions) (Petroutsos et al. 2009), only PGRL1 was detected in the CEF supercomplex from *C. reinhardtii* (Iwai et al. 2010). A recent report indicated an impaired electrochromic shift upon switching from light to dark in the presence of DCMU in the *pgr5* mutant and an absence of PGR5 in the *pgrL1* mutant in *C. reinhardtii* (Johnson et al. 2014). These results suggest that Fd-CEF might also be dependent upon both PGRL1 and PGR5 in *C. reinhardtii* as in *A. thaliana*. PGR5 might have been present in the CEF supercomplex, but escaped our scrutiny since it is expressed at a level that is seven times lower than its binding partner PGRL1 (Hertle et al. 2013). Alternatively, it is probable that PGR5 is indeed absent in the isolated CEF supercomplex and so the complex did not exert its maximal CEF activity. The latter scenario is more likely because a significant amount of the reduced form of PGRL1 was present even in the *pgr5* background despite the amount of the reduced form and the reduction rate was somewhat lower than the control (Hertle et al. 2013). These scenarios, however, cannot account for the result in *C. reinhardtii* cells that the re-reduction of P700<sup>+</sup> was not sensitive to AA in the presence of DCMU, namely the condition where only CEF can reduce P700<sup>+</sup> (Iwai et al. 2010). A recent study on AA sensitivity and the sequence variations of PGR5 in two plant species might provide a possible clue for this problem (Sugimoto et al. 2013). They found CEF was sensitive to AA in *A. thaliana*, but not in pine. PGR5 in the former has Val and in the latter has Lys in the third residue. Because a common wild type strain of *C. reinhardtii* 137c, which was used in our isolation of the CEF supercomplex, harbors Lys at this position in its PGR5, any PGR5-dependent CEF would be AA resistant. We should, however, bear in mind that “AA has multiple effects on photosynthesis, and thus ascribing functional significance to

any one process may be misleading” (Fisher and Kramer 2014).

## V. Perspectives

In this chapter, I provided an overview of the PSI-Cyt<sub>b</sub>f-PgrL1 supercomplex that conducts Fd-CEF in *C. reinhardtii* (Iwai et al. 2010). Recently, an alternative PGR5-PGRL1 heterocomplex model, which was originally reported for *A. thaliana* (Hertle et al. 2013), was also proposed for *C. reinhardtii* (Johnson et al. 2014). The induction of *Pgr5* transcription was only reported under Fe-limiting conditions in *C. reinhardtii* (Petroutsos et al. 2009), another study reported the PGR5-dependent CEF pathway is constitutively active (Johnson et al. 2014). While PGR5 was not detected in the CEF supercomplex (Iwai et al. 2010), a *pgr5* mutant exhibits decreased CEF activity (Johnson et al. 2014). Although there are currently several differences and discrepancies among these studies and others, such recent studies set the framework toward unraveling the long lasting CEF story at the molecular level. One critical point to push these efforts even further would be sorting out the techniques for measuring CEF activity. These discrepancies may have in part arisen from differences in the methodologies employed for the measurements of CEF activity, such as a rise of PSII fluorescence as a marker of the PQ pool reduction in osmotically ruptured chloroplasts (Munekage et al. 2002; DalCorso et al. 2008; Hertle et al. 2013), the rapid re-reduction of P700<sup>+</sup> in the absence of PSII activity in the cells (Munekage et al. 2002; DalCorso et al. 2008; Petroutsos et al. 2009), the dark-interval relaxation of the electrochromic shift in the absence of PSII activity in the cells (Johnson et al. 2014), the reduction of a PQ analog DMBQ by a recombinant polypeptide (Hertle et al. 2013), the Cyt *b*<sub>H</sub> photoreduction in the isolated complex (Iwai et al. 2010), and so on. Future efforts are expected to sort

out these methodological differences. A recent attempt by Fisher and Kramer indeed provided an important step toward clarifying the problem (Fisher and Kramer 2014). They reevaluated the induction kinetics and inhibitor sensitivity of PSII fluorescence from ruptured spinach chloroplasts and pointed out that the fluorescence did not rapidly equilibrate with the redox state of the PQ pool. They concluded the fluorescence rise therefore may not reflect the CEF-dependent reduction of the PQ pool, but the reduction of the low potential variants of the primary acceptor ( $Q_A$ ) in PSII. Further efforts, especially those using key mutants of *A. thaliana* and *C. reinhardtii*, will be much awaited.

## Acknowledgments

The work done in my laboratory was supported in part by the New Energy and Industrial Technology Development Organization, the Japan Science and Technology Agency, the Japan Society for the Promotion of Science, and the Ministry of Education, Culture, Sports, Science and Technology.

## References

- Allen JF (1992) Protein phosphorylation in regulation of photosynthesis. *Biochim Biophys Acta* 1098:275–335
- Allen JF (2003) Cyclic, pseudocyclic and noncyclic photophosphorylation: new links in the chain. *Trends Plant Sci* 8:15–19
- Bellafiore S, Barneche F, Peltier G, Rochaix J-D (2005) State transitions and light adaptation require chloroplast thylakoid protein kinase STN7. *Nature* 433:892–895
- Björkman O, Demmig B (1987) Photon yield of  $O_2$  evolution and chlorophyll fluorescence characteristics at 77 K among vascular plants of diverse origins. *Planta* 170:489–504
- Breyton C, Nandha B, Johnson GN, Joliot P, Finazzi G (2006) Redox modulation of cyclic electron flow around photosystem I in C3 plants. *Biochemistry* 45:13465–13475
- Bulté L, Gans P, Rebéillé F, Wollman F-A (1990) ATP control on state transitions in vivo in *Chlamydomonas reinhardtii*. *Biochim Biophys Acta* 1020:72–80
- DalCorso G, Pesaresi P, Masiero S, Aseeva E, Schunemann D, Finazzi G, Joliot P, . . . , Leister D (2008) A complex containing PGRL1 and PGR5 is involved in the switch between linear and cyclic electron flow in *Arabidopsis*. *Cell* 132:273–285
- Finazzi G, Furia A, Barbagallo RP, Forti G (1999) State transitions, cyclic and linear electron transport and photophosphorylation in *Chlamydomonas reinhardtii*. *Biochim Biophys Acta* 1413:117–129
- Finazzi G, Rappaport F, Furia A, Fleischmann M, Rochaix J-D, Zito F, Forti G (2002) Involvement of state transitions in the switch between linear and cyclic electron flow in *Chlamydomonas reinhardtii*. *EMBO Rep* 3:280–285
- Fisher N, Kramer DM (2014) Non-photochemical reduction of thylakoid photosynthetic redox carriers in vitro: relevance to cyclic electron flow around photosystem I? *Biochim Biophys Acta* 1837:1944–1954
- Hamel P, Olive J, Pierre Y, Wollman F-A, de Vitry C (2000) A new subunit of cytochrome  $b_6f$  complex undergoes reversible phosphorylation upon state transition. *J Biol Chem* 275:17072–17079
- Hertle AP, Blunder T, Wunder T, Pesaresi P, Pribil M, Armbruster U, Leister D (2013) PGRL1 is the elusive ferredoxin-plastoquinone reductase in photosynthetic cyclic electron flow. *Mol Cell* 49:511–523
- Houille-Vernes L, Rappaport F, Wollman F-A, Alric J, Johnson X (2011) Plastid terminal oxidase 2 (PTOX2) is the major oxidase involved in chlororespiration in *Chlamydomonas*. *Proc Natl Acad Sci U S A* 108:20820–20825
- Huang L, Cobessi D, Tung EY, Berry EA (2005) Binding of the respiratory chain inhibitor antimycin to the mitochondrial  $bc_1$  complex: a new crystal structure reveals an altered intramolecular hydrogen-bonding pattern. *J Mol Biol* 351:573–597
- Iwai M, Takizawa K, Tokutsu R, Okamuro A, Takahashi Y, Minagawa J (2010) Isolation of the elusive supercomplex that drives cyclic electron flow in photosynthesis. *Nature* 464:1210–1213
- Johnson X, Steinbeck J, Dent RM, Takahashi H, Richaud P, Ozawa S, Houille-Vernes L, . . . , Alric J (2014) Proton gradient regulation 5-mediated cyclic electron flow under ATP- or redox-limited conditions: a study of  $\Delta ATPase pgr5$  and  $\Delta rbcL pgr5$  mutants in the green alga *Chlamydomonas reinhardtii*. *Plant Physiol* 165:438–452

- Joliot P, Joliot A (2002) Cyclic electron transfer in plant leaf. *Proc Natl Acad Sci U S A* 99:10209–10214
- Laisk A (1993) Mathematical modelling of free-pool and channelled electron transport in photosynthesis: evidence for a functional supercomplex around photosystem I. *Proc Biol Sci* 251:243–251
- Merchant SS, Prochnik SE, Vallon O, Harris EH, Karpowicz SJ, Witman GB, Terry A, . . . , Grossman AR (2007) The *Chlamydomonas reinhardtii* genome reveals the evolution of key animal and plant functions. *Science* 318:245–250
- Minagawa J (2011) State transitions – the molecular remodeling of photosynthetic supercomplexes that controls energy flow in the chloroplast. *Biochim Biophys Acta* 1807:897–905
- Mitchell P (1976) Possible molecular mechanisms of the protonmotive function of cytochrome systems. *J Theor Biol* 62:327–367
- Moss DA, Bendall DS (1984) Cyclic electron transport in chloroplasts. The Q-cycle and the site of action of antimycin. *Biochim Biophys Acta* 767:389–395
- Munekage Y, Hojo M, Meurer J, Endo T, Tasaka M, Shikanai T (2002) PGR5 is involved in cyclic electron flow around photosystem I and is essential for photoprotection in *Arabidopsis*. *Cell* 110:361–371
- Munekage Y, Hashimoto M, Miyake C, Tomizawa K, Endo T, Tasaka M, Shikanai T (2004) Cyclic electron flow around photosystem I is essential for photosynthesis. *Nature* 429:579–582
- Nagy G, Unnep R, Zsiros O, Tokutsu R, Takizawa K, Porcar L, Moyet L, . . . , Minagawa J (2014) Chloroplast remodeling during state transitions in *Chlamydomonas reinhardtii* as revealed by noninvasive techniques in vivo. *Proc Natl Acad Sci U S A* 111:5042–5047
- Ogawa T (1991) A gene homologous to the subunit-2 gene of NADH dehydrogenase is essential to inorganic carbon transport of *Synechocystis* PCC6803. *Proc Natl Acad Sci U S A* 88:4275–4279
- Petroutsos D, Terauchi AM, Busch A, Hirschmann I, Merchant SS, Finazzi G, Hippler M (2009) PGRL1 participates in iron-induced remodeling of the photosynthetic apparatus and in energy metabolism in *Chlamydomonas reinhardtii*. *J Biol Chem* 284:32770–32781
- Sacksteder CA, Kanazawa A, Jacoby ME, Kramer DM (2000) The proton to electron stoichiometry of steady-state photosynthesis in living plants: a proton-pumping Q cycle is continuously engaged. *Proc Natl Acad Sci U S A* 97:14283–14288
- Seelert H, Poetsch A, Dencher NA, Engel A, Stahlberg H, Muller DJ (2000) Structural biology. Proton-powered turbine of a plant motor. *Nature* 405:418–419
- Shikanai T (2007) Cyclic electron transport around photosystem I: genetic approaches. *Annu Rev Plant Biol* 58:199–217
- Sugimoto K, Okegawa Y, Tohri A, Long TA, Covert SF, Hisabori T, Shikanai T (2013) A single amino acid alteration in PGR5 confers resistance to antimycin A in cyclic electron transport around PSI. *Plant Cell Physiol* 54:1525–1534
- Tagawa K, Tsujimoto HY, Arnon DI (1963) Role of chloroplast ferredoxin in the energy conversion process of photosynthesis. *Proc Natl Acad Sci U S A* 49:567–572
- Takahashi H, Clowez S, Wollman FA, Vallon O, Rapaport F (2013) Cyclic electron flow is redox-controlled but independent of state transition. *Nat Commun* 4:1954
- Terashima M, Petroutsos D, Hudig M, Tolstygina I, Trompelt K, Gabelein P, Fufezan C, . . . , Hippler M (2012) Calcium-dependent regulation of cyclic photosynthetic electron transfer by a CAS, ANR1, and PGRL1 complex. *Proc Natl Acad Sci U S A* 109:17717–17722
- Zhang H, Whitelegge JP, Cramer WA (2001) Ferredoxin:NADP<sup>+</sup> oxidoreductase is a subunit of the chloroplast cytochrome *b<sub>6</sub>f* complex. *J Biol Chem* 276:38159–38165

# Chapter 24

## State Transition Kinases and Redox Signal Transduction in Chloroplasts

Jean-David Rochaix\*

*Departments of Molecular Biology and Plant Biology, University of Geneva, 30, Quai Ernest Ansermet, 1204 Geneva, Switzerland*

Summary.....	463
I. Introduction.....	464
II. The Role of the Stt7/STN7 Protein Kinase in State Transitions.....	466
III. Mobility and Location of LHCII.....	468
IV. How Is the Stt7/STN7 Kinase Activated?.....	469
V. Involvement of Stt7/STN7 in the Long Term Response.....	470
VI. Relationship Between Stt7/STN7 and Cyclic Electron Flow.....	471
VII. Conclusions and Perspectives.....	473
Acknowledgements.....	474
References.....	474

### Summary

Both linear (LEF) and cyclic electron flow (CEF) occur in the photosynthetic electron transfer chain and are essential to meet the cellular demands in energy and reducing power. Because photosynthetic organisms are constantly subjected to changes in light and nutrient availability, they need to continuously adapt the relative levels of LEF and CEF. A key parameter in this response is the redox state of the photosynthetic electron transport chain. While the molecular mechanisms underlying the regulation of the CEF/LEF ratio by the chloroplast redox state are still poorly understood, considerable progress has been achieved in elucidating how the redox state of the plastoquinone pool is sensed by the Stt7/STN7 protein kinase associated with the cytochrome *b<sub>6</sub>f* complex. This kinase induces both a short term and a long term response, both of which tend to restore the redox poise of the plastoquinone pool and thus to optimize the photosynthetic efficiency. The short term response, called “state transitions,” involves the phosphorylation of the light harvesting system of PSII and its reversible migration from photosystem II to photosystem I. The long term response involves a signaling information chain from the chloroplast to the nucleus which ultimately adjusts the stoichiometry between the two photosystems for re-equilibrating their redox state and that of the intervening cytochrome *b<sub>6</sub>f* complex. The Stt7/STN7 kinase together with the Stt1/STN8 kinase and their associated phosphatases form a central quartet which is part of an extended chloroplast signaling network that is important for the dynamic response of the photosynthetic apparatus, especially under adverse environmental conditions.

---

\*Author for correspondence, e-mail: [Jean-David.Rochaix@unige.ch](mailto:Jean-David.Rochaix@unige.ch)

## I. Introduction

The primary reactions of oxygenic photosynthesis occur on the thylakoid membranes within chloroplasts of land plants and algae. They are mediated by the three major protein-pigment complexes photosystem II (PSII), photosystem I (PSI) with their corresponding light-harvesting systems LHCII and LHCI, and the cytochrome *b<sub>6</sub>f* complex (*Cytb<sub>6</sub>f*). Light energy captured by the two antenna systems is transferred to the reaction centers of PSII and PSI where it induces a charge separation across the thylakoid membrane with ensuing electron flow along the photosynthetic electron transport chain from water to PSII, the plastoquinone pool (PQ pool), *Cytb<sub>6</sub>f*, PSI and NADP<sup>+</sup>, the final electron acceptor (Fig. 24.1). This electron flow is coupled to proton pumping into the thylakoid lumen and the resulting pH gradient across the membrane is utilized by a fourth major complex, the ATP synthase, to produce ATP from ADP and inorganic phosphate. Besides linear electron flow (LEF) there is a cyclic electron pathway (CEF) in which PSI transfers electrons back to the PQ pool and the *Cytb<sub>6</sub>f* complex through the Ndh (Burrows et al. 1998; Shikanai et al. 1998) and Pgr (Munekage et al. 2002) pathways, respectively (Fig. 24.1). This cyclic electron pathway generates a proton gradient and ultimately ATP, but does not produce reducing power. In addition, a third electron transfer route exists, called the chlororespiratory chain, which feeds reducing power from the stroma to the PQ pool through the Ndh complex with plastid terminal oxidase (Ptox) as final electron

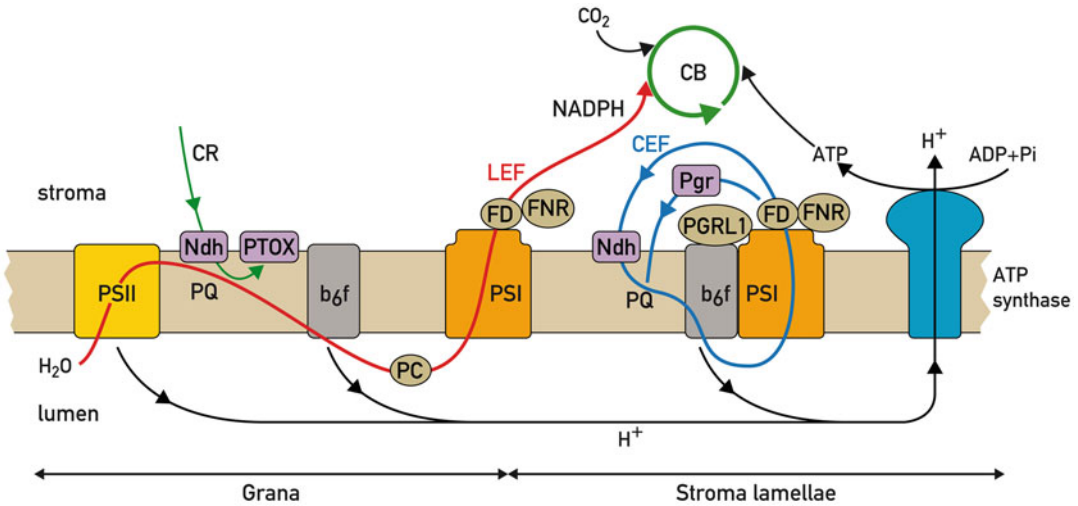
acceptor (Fig. 24.1). Ultimately, the products of the primary reactions of photosynthesis, NADPH and ATP are used to fuel the reactions of the Calvin-Benson cycle for carbon assimilation. To meet the demands of this metabolic cycle ATP and NADPH have to be delivered at a ratio of 3:2, a value that exceeds the maximum capacity of LEF which is 2.6:2 (Allen 2003). Moreover other specific cellular processes, e.g. translation and the carbon concentrating mechanism in algae require an even higher ratio of ATP/NADPH. Therefore fine-tuning of LEF and CEF is essential for maintaining cellular growth and metabolism.

The thylakoid membranes consist of two distinct domains, the grana regions and the stromal lamellae. Grana regions usually consist of cylindrical stacks of 5–20 layers of thylakoid membrane linked together by stroma lamellae. Each granum is surrounded by two stroma-exposed membranes and the highly curved margins that connect the adjacent grana membranes (Shimoni et al. 2005). Importantly, the photosynthetic complexes are not uniformly distributed between these two domains giving rise to lateral heterogeneity (Andersson and Andersson 1980). Because of their bulky extrusion into the stromal phase, PSI and the ATP synthase are confined to the stromal lamellae and the end membranes of the grana but excluded from the interior of the grana where most of PSII resides while *Cyt b<sub>6</sub>f* partitions equally between both domains.

Because PSII and PSI are connected in series through the electron transport chain, their activities need to be coordinated to maintain a proper redox poise of the PQ pool. Over-excitation of PSII relative to PSI would lead to an over-reduction of the PQ pool whereas the reverse case would result in its over-oxidation. In both of these extreme cases this would seriously compromise photosynthetic electron flow and lower the photosynthetic yield. Thus, different processes contribute to the maintenance of a balanced redox state of the electron transport chain. Some of these processes proceed through the transfer of reducing power to molecular

---

*Abbreviations:* CEF – Cyclic electron transfer; *Cytb<sub>6</sub>f* – Cytochrome *b<sub>6</sub>f* complex; DCMU – 3-(3,4-Dichlorophenyl)-1,1-dimethylurea; LEF – Linear electron flow; LHC – Light harvesting system; Ndh – NAD dehydrogenase; PQ – Plastoquinone; PQH<sub>2</sub> – Plastoquinol; PSI – Photosystem I; PSII – Photosystem II; Ptox – Plastid terminal oxidase; Q<sub>o</sub> Q<sub>p</sub> – The quinone binding site on the electrochemically positive side of the membrane



*Fig. 24.1.* Linear and cyclic electron transfer pathways. Linear electron flow (LEF) and cyclic electron flow (CEF) are shown in *red* and *blue*, respectively with *arrows* indicating the direction of electron flow. The LEF pathway is driven by the two photochemical reactions of PSII and PSI: electrons are extracted by PSII from water and transferred subsequently to the PQ pool, *Cytb<sub>6</sub>f*, plastocyanin (PC), PSI and ferredoxin (FD). Ferredoxin-NADPH reductase (FNR) catalyzes the formation of NADPH at the expense of reduced FD. The CEF pathway with the two Ndh and Pgr branches is driven by PSI in the stroma lamellae. In *C. reinhardtii* PSI forms a supercomplex with *Cytb<sub>6</sub>f*, FNR, PGRL1 and additional factors (Iwai et al. 2010a). Upon reduction of FD, electrons are returned to the PQ pool either through the NADH complex (Ndh) or via PGRL1 (Pgr) which acts as a FD-PQ oxidoreductase. Both LEF and CEF are associated with proton pumping into the lumen. The resulting proton gradient is used by ATP synthase to produce ATP, which together with NADPH drives CO<sub>2</sub> assimilation by the Calvin-Benson cycle (CB). CR, chlororespiratory chain (*green*) which feeds stromal reducing power into the PQ pool with plastid terminal oxidase (PTOX) as terminal electron acceptor. *G* grana, *SL* stroma lamellae (Adapted from Rochaix (2014)) with permission).

oxygen. This can occur on the acceptor side of PSI through the Mehler reaction in which electrons react with oxygen to form H<sub>2</sub>O<sub>2</sub>. Alternatively, Ptox, the plastid terminal oxidase is able to reoxidize the PQ pool on the stromal side of the thylakoid membrane. These reactions lead to the formation of a proton-motive force and hence to ATP synthesis. Excess reducing power can also be dissipated through the malate shuttle to the mitochondrial respiratory chain also resulting in oxygen consumption and ATP formation (Nunes-Nesi et al. 2008). Another process for avoiding over-reduction of the PQ pool involves state transitions, originally recognized as a mechanism that allows for the balancing in the short term of the light excitation energy of the LHCII and LHCI antenna systems of PSII and PSI, respectively. In the long term the maintenance of this balanced redox state is achieved through

compensatory changes in the expression of the LHC genes and involves a signaling chain from the chloroplast to the nucleus. While state transitions were discovered 45 years ago (Bonaventura and Myers 1969; Murata 1969), it is only recently that the underlying molecular mechanisms have been partially unraveled and they continue to be intensively investigated.

A key feature of state transitions is that the redox state of the PQ pool is perceived through a protein kinase which is associated with the thylakoid membranes. Because this kinase phosphorylates the LHCII proteins, it was named LHCII kinase. Although the activity of this kinase was noticed early (Bennett 1977), the kinase protein was identified only recently and named Stt7 in *Chlamydomonas* and STN7 in *Arabidopsis* (Depège et al. 2003; Bellafiore et al. 2005). Whenever PSII is overexcited relative to PSI, reduction

of the PQ pool promotes the occupancy of the Qo site of *Cytb<sub>6</sub>f* by plastoquinol (PQH<sub>2</sub>) and leads to the activation of the kinase and phosphorylation of LHCII (Vener et al. 1997; Zito et al. 1999). This causes the dissociation of LHCII from PSII and its association with PSI and hence an increase in size of the antenna of PSI at the expense of that of PSII and consequently restores the redox poise of the PQ pool. Dephosphorylation of the LHCII proteins is achieved by a phosphatase TAP38/PPH1 which counteracts the action of the Stt7/STN7 kinase (Pribil et al. 2010; Shapiguzov et al. 2010). Besides its involvement in state transitions, the Stt7/STN7 kinase is also implicated in a signaling chain which transmits signals from the chloroplast to the nucleus, a process also called retrograde signaling. This chapter reviews recent advances on the role of the Stt7/STN7 kinase and the TAP38/PPH1 phosphatase in state transitions and retrograde signaling. Earlier work on this topic has been covered in several recent reviews (Eberhard et al. 2008; Lemeille and Rochaix 2010; Rochaix 2013).

## II. The Role of the Stt7/STN7 Protein Kinase in State Transitions

The classic model of state transitions is shown in Fig. 24.2. Over-excitation of PSII relative to PSI leads to a reduced redox state of the PQ pool which in turn favors docking of PQH<sub>2</sub> to the Qo site of the *Cytb<sub>6</sub>f* complex. This process activates the Stt7/STN7 kinase (Vener et al. 1997; Zito et al. 1999) and leads to the phosphorylation of LHCII (Depège et al. 2003; Bellafiore et al. 2005). Subsequently, a portion of LHCII, called mobile LHCII, dissociates from PSII and associates with PSI thereby equilibrating the excitation energy between PSII and PSI. This state is called state 2. Conversely, over-excitation of PSI relative to PSII oxidizes the PQ pool which leads to the inactivation of the Stt7/STN7 kinase and to the dephosphorylation of LHCII mediated by the PPH1/TAP38 phosphatase (Pribil et al. 2010; Shapiguzov et al. 2010). The

dephosphorylated mobile LHCII dissociates from PSI and moves back to PSII. This state is called state 1. As seen below this view of state transitions may be too simplistic although its major features are still valid.

Although a direct phosphorylation of LHCII by the Stt7/STN7 kinase could not be demonstrated *in vivo*, it is very likely that this kinase qualifies as the LHCII kinase because it can be co-immunoprecipitated with LHCII and the phosphorylation of several LHCII proteins depends on Stt7/STN7 (Lemeille et al. 2010). Moreover, this kinase is always associated with large molecular weight complexes and in particular with the Cyt *b<sub>6</sub>f* complex in *Chlamydomonas* (Lemeille et al. 2009). The kinase is phosphorylated under state 2 conditions most likely through autophosphorylation (Lemeille and Rochaix 2010) because, *in vitro*, recombinant Stt7 kinase autophosphorylates readily (G. Fucile and J.D. Rochaix, unpublished results). In *Chlamydomonas* six phosphorylation sites within Stt7 sites have been identified (Lemeille et al. 2010; Wang et al. 2014) whereas four were found in STN7 of *Arabidopsis* (Reiland et al. 2009). The phosphorylation of the Stt7/STN7 kinase does not appear to play any major role in state transitions as changes of all four sites through site-directed mutagenesis in *Arabidopsis* did not impair LHCII phosphorylation and state transitions (Willig et al. 2011). However replacement of the four phosphorylated amino acids by phosphor-mimetic amino acids prevented the decline of STN7 which normally occurs upon prolonged state 1 conditions (Willig et al. 2011).

The Stt7/STN7 kinase is conserved in land plants and algae. It contains a single transmembrane region bounded by a conserved kinase domain on the stromal side and a short conserved N-terminal domain with two conserved Cys residues on the lumen side. These two residues play a crucial role because changes of either of these Cys abolishes the activity of the kinase and state transitions although they are outside of the catalytic domain (Lemeille et al. 2009).



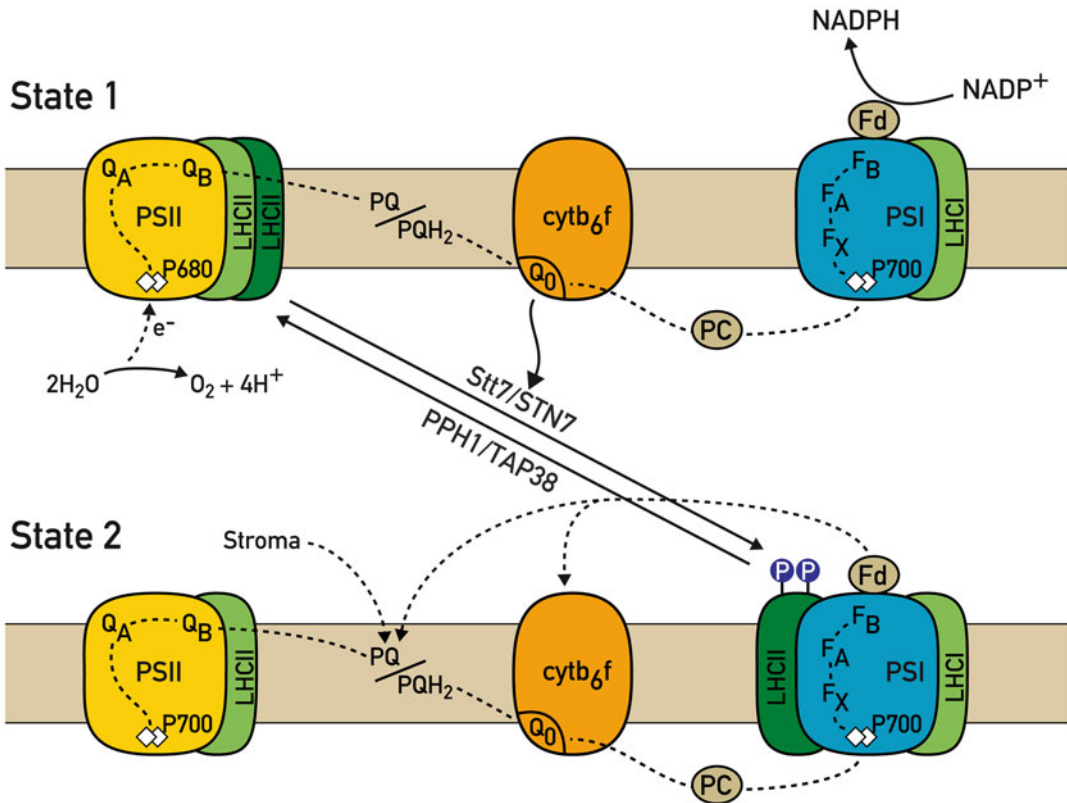


Fig. 24.2. State transitions. Transition from state 1 to state 2 occurs when the redox state of the plastoquinone pool (PQ) is reduced following preferential excitation of PSII relative to PSI. Docking of plastoquinol (PQH<sub>2</sub>) to the Q<sub>0</sub> site of Cytb<sub>6</sub>f leads to the activation of the protein kinase Stt7/STN7 which phosphorylates LHCII either directly or indirectly. Phosphorylated LHCII dissociates from PSII and binds to PSI (state 2). Upon preferential excitation of PSI relative to PSII, the kinase is inactivated and the PPH1/TAP38 phosphatase dephosphorylates LHCII which moves back to PSII (state 1). Under reducing conditions cyclic electron flow is induced independently of state transitions (Takahashi et al. 2013) (Adapted from Rochaix (2007)) with permission).

However during state transitions induced by changes in light quality or quantity, the redox state of these Cys does not change. It is only under prolonged anaerobic conditions that these Cys are fully reduced (A. Shapiguzov and J.D. Rochaix, unpublished results). Although state transitions can also be induced by anaerobiosis in *Chlamydomonas*, this process occurs significantly faster than the reduction of the Cys residues. One possibility is that these two Cys are involved in intersubunit disulfide bridges and thus responsible for the dimerization of the kinase. In this view only the kinase dimer would be active. The crystal structure of the dimeric Cytb<sub>6</sub>f complex of *Chlamydomonas* reveals

a cavity on the lumen side which could accommodate the interacting N-terminal domains of the kinase dimer (Stroebel et al. 2003). This cavity is presumably also conserved in the cyanobacterial Cytb<sub>6</sub>f complex (Hasan et al. 2013a).

There is significant sequence identity between the Stt7/STN7 and Stl1/STN8 kinases. The latter is also associated with the thylakoid membrane and appears to be mainly responsible for the phosphorylation of the PSII core proteins (Bonardi et al. 2005; Vainonen et al. 2005). There is some overlap between the substrates of these two kinases based first on the fact that in the absence of STN7 some residual LHCII phosphorylation

still occurs and reciprocally in the absence of STN8 residual phosphorylation of the PSII core proteins is detectable. Second, these protein phosphorylations are abolished in a double mutant lacking both kinases.

In land plants and *Chlamydomonas* the LHCII kinase is inactivated under high light (1000  $\mu\text{mol photons m}^{-2} \text{s}^{-1}$ ) (Schuster et al. 1986; Rintamaki et al. 2000). In plants, this process appears to be mediated by ferredoxin and thioredoxin. The question thus arises whether these two proteins localized in the stromal phase could modulate the redox state of the luminal Cys of Stt7/STN7. This is in principle possible because CCDA and HCF164, two thylakoid proteins required for heme attachment on the lumen side and for the biosynthesis of the *Cytb<sub>6</sub>f* complex, are able to transfer thiol-reducing equivalents across the thylakoid membrane and could therefore mediate the redox control of Stt7/STN7 (Lennartz et al. 2001; Page et al. 2004). However, high light treatment did not change the redox state of the conserved luminal Cys in *Chlamydomonas* indicating that the inactivation of the kinase occurs through a different mechanism (A. Shapiguzov and J.D. Rochaix, unpublished results). Besides the conserved luminal Cys, a TRX-like Cxxx motif within the kinase domain of STN7 exposed to the stroma exists in land plants. This motif has been proposed as a possible target for TRX (Puthiyaveetil 2011). However, site-directed mutagenesis of the Cys of this motif did not affect state transitions and LHCII phosphorylation in *Arabidopsis* (A. Shapiguzov and J.D. Rochaix, unpublished results). Furthermore, while this motif is conserved in land plants and several algae, it is absent from *Chlamydomonas*. Also, the decreased accumulation of Stt7/STN7 under extended state 1 conditions is unlikely to play a role in the control of the activity of the kinase because this decrease is significantly slower than that of its activity under high light (Schuster et al. 1986; Lemeille et al. 2009; Willig et al. 2011). It is therefore not yet clear how the LHCII kinase is inactivated under high light.

Besides its role in state transitions the Stt7/STN7 kinase is also required for optimal adaptation to fluctuations in light intensity. Reversible LHCII protein phosphorylation occurs when *Arabidopsis* plants are subjected to alternative periods of low light and high light with LHCII phosphorylation and dephosphorylation, respectively (Tikkanen et al. 2007). However surprisingly, the distribution of light excitation energy between the two photosystems does not change significantly during these changes in phosphorylation. The STN7 kinase appears to promote a balanced distribution of excitation to both photosystems under these conditions because in its absence the excitation of PSII rises during the low light phases and growth of the plants is strongly diminished (Tikkanen et al. 2007).

Although one cannot exclude that the activity of the PPH1/TAP38 phosphatase is also subjected to redox control, there is no evidence supporting this possibility. It is more likely that this phosphatase is constantly active and that the Stt7/STN7 is the major regulatory factor of the phosphorylation of the LHCII proteins.

### III. Mobility and Location of LHCII

Recent results have led to a reconsideration of the classical state transition model which raise new questions concerning the different locations of the mobile LHCII during state transitions. In land plants a PSII supercomplex with four LHCII trimers was identified (Wientjes et al. 2013). It contains up to two additional loosely associated trimers in state 1 which are displaced to PSI during a transition to state 2 so that in the end the PSII supercomplex remains intact (Wientjes et al. 2013). Earlier studies had indicated that stroma lamellae enriched in PSI contain more phosphorylated LHCII than the grana fraction which is enriched in PSII (Kyle et al. 1983; Bassi et al. 1988). The studies of Wientjes et al. however indicate that phosphorylation is not limited to the mobile LHCII but also includes LHCII

within the PSII supercomplex indicating that LHCII phosphorylation is not sufficient for the dissociation of certain LHCII trimers from PSII. In contrast to the earlier view which assumed that a small part of LHCII migrates to PSI in response to low light irradiance, the new results show that a large fraction of the PSI complexes binds one LHCII trimer. This system can transfer excitation energy efficiently to PSI after acclimation to different light conditions, indicating that LHCII is associated with the PSI antenna under many different growth conditions (Wientjes et al. 2013). Thus in land plants the mobile LHCII functions as a highly efficient antenna system for PSI under different light conditions. Mobile LHCII moves back to PSII only under specific conditions, e.g., upon a sudden increase in light intensity or when PSI is over-excited by far red light.

Whereas, evidence for the migration of LHCII between PSII and PSI comes mainly from in vitro studies with thylakoid membranes (Kargul et al. 2005; Takahashi et al. 2006), fluorescence lifetime imaging microscopy has provided new insights into this process in vivo. This technique allows one to differentiate chlorophyll auto-fluorescence based on its lifetime. It revealed a 250 ps lifetime fluorescence component during a state 1 to state 2 transition in live wild-type but not in *stt7* mutant cells of *Chlamydomonas* (Iwai et al. 2010b). This component diffused through the cell and formed large spotted areas. The fact that it could be detected in a mutant lacking PSII and PSI but containing LHCII and that its appearance correlated with LHCII phosphorylation suggest that it originates from phosphorylated LHCII dissociated from PSII in vivo. The existence of a free LHCII pool raises many questions. In particular, does it only form transiently and how and where does LHCII bind to PSI?

State transitions have been thought to represent a process which is mainly involved in acclimation under low light conditions. While this appears to be true for land plants, recent work with *Chlamydomonas* indicates

that besides qE defined as energy-dependent quenching through thermal dissipation of absorbed excess light, state transitions also have a photoprotective role during high light acclimation (Allorent et al. 2013). Comparative analysis of the *Chlamydomonas* mutants *stt7*, *npq4*, lacking the Lhcsr3 protein and the double mutant *stt7-npq4* showed that both qE and state transitions are induced during acclimation to high light and that the double mutant is significantly more affected than either of the single mutants. The *Chlamydomonas* PsbS protein, a major component of the qE response in land plants is not expressed under normal light and does not appear to play a significant role in this response (Bonente et al. 2008). Instead, induction of Lhcr3, an essential factor for qE, requires several hours upon exposure to high light stress (Peers et al. 2009). It was proposed that state transitions could play an important photoprotective role during this induction phase by decreasing the excitation photo-pressure on PSII through the displacement of a large part of the LHCII antenna to PSI, and thereby would diminish the production of reactive oxygen species before qE becomes operational (Allorent et al. 2013).

#### IV. How Is the Stt7/STN7 Kinase Activated?

While it is well established that the Stt7/STN7 kinase is activated as a result of a more reduced state of the PQ pool and more specifically through the docking of plastoquinol to the Qo site of the Cytb<sub>6</sub>f complex, the underlying molecular mechanisms are still unknown. As indicated above, the two conserved luminal Cys residues are essential for the activity of the kinase and need to be maintained in an oxidized state. They may be involved in two disulfide bridges responsible for dimer formation. Presumably the binding of PQH<sub>2</sub> induces a conformational change in the N-terminal luminal domain of the kinase which is transduced through the transmembrane

domain to the catalytic stromal domain of the kinase. Alternatively, PQH<sub>2</sub> binding could provoke a conformational change on the luminal side of Cyt *b*<sub>6</sub>*f* which is transmitted to its stromal side where it modulates the kinase activity. Finally, both the kinase and the Cyt*b*<sub>6</sub>*f* complex could be involved in this transmembrane signaling chain. New insights into this problem have come from the comparison of the chloroplast Cyt*b*<sub>6</sub>*f* and the yeast Cyt*b*<sub>c1</sub> complex crystal structures. It is well documented that cytochrome *b* with its eight transmembrane domains has been replaced by two polypeptides in the Cyt*b*<sub>6</sub>*f* complex, cytochrome *b*<sub>6</sub> with four and PetD with three trans-membrane helices (Widger et al. 1984). Thus, one transmembrane domain has been lost in the Cyt*b*<sub>6</sub>*f* complex. Interestingly, the crystal structure of this complex reveals the presence of a lipid and chlorophyll *a* chlorin ring in place of the lost eighth trans-membrane helix in the cytochrome *b* subunit (Hasan et al. 2011, 2013b). This replacement raises the question whether it occurred as a result of a selective advantage for signaling the redox state of the PQ pool or for coupling the oxidation of PQH<sub>2</sub> in the lumen to the reduction of a factor on the stromal side of the thylakoid membrane. It was proposed that this lipid may mediate this function or could substitute for the transmembrane domain of a signaling protein lost during crystallization of the complex (Hasan et al. 2013b). A prime candidate is the Stt7/STN7 kinase with its single trans-membrane domain.

Clearly, determination of the crystal structure of the Stt7/STN7 kinase is likely to provide key insights into the activation process of the kinase. An important step forward was achieved recently with the determination of the crystal structure of the kinase domain (KD) of the MsStt7d kinase from the marine microalga *Micromonas* sp. *RCC299*, which is related to that of Stt7/STN7 (Guo et al. 2013). Although MsStt7d does not contain a transmembrane domain and lacks the conserved Cys residues at its N-terminal end, the kinase domain is well conserved. MsStt7d-KD contains two

lobes, a small N-terminal lobe with a sheet of six antiparallel  $\beta$  strands and a single  $\alpha$  helix and a larger C-terminal lobe with nine  $\alpha$  helices and a pair of short  $\beta$  strands. The protein forms a dimer and is capable of autophosphorylation. A unique characteristic feature of this kinase and of the Stt7/STN7 family is a hairpin structure, essential for the stability of the enzyme, which interacts with the activation loop and thereby activates the kinase. Moreover, MsStt7d is a dual specificity kinase phosphorylating both Thr and Tyr residues that is able to phosphorylate a consensus pentapeptide of the antenna proteins from *Micromonas* (Guo et al. 2013). In this respect, it should be noted that an extensive phosphoproteomic analysis of plastid proteins of *Arabidopsis* did not reveal any Tyr phosphorylation site (Reiland et al. 2009). However this appears to be different in algae as Tyr phosphorylation could be detected in *Chlamydomonas* (Wang et al. 2014). The approach used with the *Micromonas* kinase opens a new framework for a better understanding of the activation process of Stt7/STN7 and raises the question whether the dual specificity of MsStt7d-KD may correspond to the dual role of Stt7/STN7 in both state transitions and in the long term response.

## V. Involvement of Stt7/STN7 in the Long Term Response

In addition to its role in short term response, the Stt7/STN7 kinase is also involved in a long term response with alterations in nuclear and chloroplast gene expression which lead to compensatory changes in thylakoid protein accumulation. In this way balancing of the excitation energy occurs between PSII and PSI and the redox poise of the PQ pool is maintained (Brautigam et al. 2009; Pesaresi et al. 2009). In the *stn7* *Arabidopsis* mutant the chloroplast *psaAB* operon is upregulated at the transcriptional level and the level of the nucleus-encoded PSI antenna protein Lhca1 is increased post-transcriptionally. This long term response

does not involve LHCII phosphorylation and state transitions and diverges from the short term response at, or immediately downstream, of STN7 (Pesaresi et al. 2009). As a consequence the Stt7/STN7 kinase must have other targets that act in the long term response pathway but that are still largely unknown. Comparison of the known LHCII phosphorylation sites of Stt7 in *Chlamydomonas* led to the identification of a consensus motif for these sites. A striking feature of this motif is that the phosphorylated Ser/Thr is flanked on each side by two basic residues (Lemeille et al. 2010) which is similar to that proposed for the specific signature of STN7 phosphorylation sites of *Arabidopsis* (Vainonen et al. 2005). Searching the predicted chloroplast proteins from *Chlamydomonas* for the presence of the Stt7 target phosphorylation motif led to the identification of additional putative substrates of Stt7. Interestingly they include several low-abundance chloroplast- and nucleus-encoded proteins involved in post-transcriptional steps of chloroplast gene expression, such as Tab2 required for translation of the *psaB* mRNA and the chloroplast  $\sigma$ -factor RpoD (Lemeille et al. 2010). These observations raise the possibility that Stt7 may also play a role in chloroplast gene expression. Additional putative target sites of Stt7 were identified amongst proteins required for chlorophyll synthesis (ChlH, Cpx1, PorB, Ppo) and subunits of ATP synthase (AtpA, AtpB).

Further indications that state transitions are not involved in the long term response have emerged from the analysis of several mutants of *Arabidopsis* affected in PSI. Thus *psaI-1* which lacks the PSI subunit PsaI and thereby the docking site of PSI for LHCII (Lunde et al. 2000) is deficient in state transitions but still displays a long term response (Pesaresi et al. 2009). The *psaD1* and *psaE1* mutants which lack one of the isoforms of the PsaD and PsaE proteins, respectively, still accumulate PSI but are impaired in electron flow and deficient in both state transitions and in the long term response. However, in these mutants LHCII is phosphorylated

under all light conditions because of the over-reduction of the PQ pool (Pesaresi et al. 2009). The growth defect in these mutants is exacerbated in the double mutants *stn7 psaD1* and *stn7 psaE1*. Taken together, these observations indicate that the STN7 kinase does not operate properly when it is permanently activated and that the long term response only occurs if the activity of STN7 can be modulated.

## VI. Relationship Between Stt7/STN7 and Cyclic Electron Flow

A salient feature of thylakoid membranes is their lateral heterogeneity with PSII and PSI localized mainly in the grana and stromal lamellae, respectively. In contrast, the Cyt *b*<sub>6</sub>*f* complex is equally distributed between these two regions but it is partially redistributed to the stroma lamellae during a transition from state 1 to state 2 (Vallon et al. 1991; Fleischmann et al. 1999). Enrichment of the Cyt *b*<sub>6</sub>*f* complex in the stroma lamellae did not lead to an increase in the maximal rate of CEF suggesting that the Cyt *b*<sub>6</sub>*f* complex is not the limiting step in CEF. Rather, it is likely that this limitation arises from the Ndh and Pgr pathways.

The picture that emerges from recent studies is that CEF is involved in the response to a wide range of environmental and metabolic changes to modulate the ATP/NADPH output ratio according to the cellular needs. Moreover, CEF induces a lumenal pH-dependent photoprotection through non-photochemical quenching (Lucker and Kramer 2013). The relationship between CEF and state transitions has been examined under a variety of experimental conditions including both continuous illumination, inhibition of photosynthesis with different inhibitors, darkness, anoxia and nutrient limitation. Studies aimed at determining whether there is a causal relationship between state transitions and CEF have given rise to conflicting results that can be at least partially attributed to the different experimental conditions used. It was initially

reported that CEF is induced in darkness in *Chlamydomonas* under anaerobic conditions that are also known to induce a transition to state 2 (Finazzi et al. 1999). Moreover, this activation of CEF did not occur in the *stt7* mutant which is blocked in state 1 (Finazzi et al. 2002). Reciprocally, CEF was shown to be inhibited by treatment with DCMU in the light which blocks electron transfer in PSII and leads to the oxidation of the PQ pool, a condition that promotes state 1. These results reveal a correlation between the induction of CEF and a transition from state 1 to state 2 and led to the suggestion that state transitions may act as a switch between LEF and CEF (Finazzi et al. 2002). Along the same line, a large PSI-Cyt<sub>b<sub>6</sub>f</sub> supercomplex including FNR and Pgr11 was identified in *Chlamydomonas* under state 2 but not under state 1 conditions (Iwai et al. 2010a). The fact that this complex could perform light-induced oxidation of cytochrome *f* and reduction of cytochrome *b* of the Cyt<sub>b<sub>6</sub>f</sub> complex suggested that it is involved in CEF.

However, other reports appear to contradict the idea that CEF is controlled by state transitions. In one study wild-type levels of CEF were obtained in the *Chlamydomonas stt7* mutant under limiting light conditions in the presence of DCMU (Cardol et al. 2009). Wild-type and *stt7* mutant cells were also examined for CEF under conditions in which inorganic and organic carbon availability changes (Lucker and Kramer 2013). These studies indicated that CEF is activated when the metabolic demand for ATP increases due to the induction of the carbon concentrating mechanism when CO<sub>2</sub> is limiting. However, CEF activation as measured by the decay of the electrochromic shift signal upon a light to dark transfer still occurred in the *stt7* mutant of *Chlamydomonas* as in the wild type, indicating that CEF is not dependent on state transitions in this case (Alric 2014). Moreover, time course experiments revealed that CEF occurred faster than state transitions revealing that there is no causal relationship between state transitions and CEF.

A similar conclusion was reached from a comparative study of wild type and two mutants *stt7* and *ptox2*, locked in state 1 and 2, respectively, independent of the redox conditions (Takahashi et al. 2013). The *ptox2* mutant is deficient in the plastid terminal oxidase which controls the redox state of the PQ pool in the dark (Houille-Vernes et al. 2011). While the accumulation of reducing power and transition to state 2 correlated well with the enhancement of CEF in the wild type, this was not the case for *ptox2*. In this mutant, CEF was not enhanced under aerobic conditions in the dark even though it is locked in state 2 with phosphorylated LHCII. Moreover, CEF enhancement and formation of the PSI-Cyt<sub>b<sub>6</sub>f</sub> supercomplex were still observed in the *stt7* mutant when the PQ pool was reduced. Thus both of these processes occurred under reducing conditions with no correlation with state transitions and their associated LHCII reorganization (Takahashi et al. 2013).

Further progress has been achieved in the identification of components involved in CEF. Pgr11 was shown to transfer electrons from ferredoxin to the plastoquinone pool in vitro and could thus qualify as the ferredoxin-plastoquinone reductase (Bendall and Manasse 1995), a hypothetical enzyme which had escaped biochemical detection (Hertle et al. 2013). The fact that the rate of electron transfer was rather low in these experiments suggests that other components are required for efficient CEF. A prime candidate remains the PSI-Cyt<sub>b<sub>6</sub>f</sub> supercomplex. The latter identified in *Chlamydomonas* under state 2 conditions and proposed to be involved in CEF is also formed in the absence of the Stt7 kinase further weakening the causal link between state transitions and CEF (Takahashi et al. 2013). Furthermore, a similar PSI-Cyt<sub>b<sub>6</sub>f</sub> supercomplex was also identified under anaerobic conditions (Terashima et al. 2012). It contains, in addition, the CAS (Ca<sup>++</sup>sensing protein) and ANR1 (anaerobic response), a protein that is required for acclimation to anoxia. A decrease of

CAS and ANR1 levels led to a strong inhibition of CEF which could be rescued by addition of external  $\text{Ca}^{++}$  in the case of CAS but not of ANR1 down regulation. These two proteins interact together, and with PGRL1 *in vivo*, suggesting that they may be involved in  $\text{Ca}^{++}$ -dependent regulation of CEF (Terashima et al. 2012). The fact that a decrease in the level of PGRL1, CAS or ANR1 leads to inhibition of CEF but that neither of these proteins is required for state transitions also agrees with the notion that these two processes are independent from each other. Taken together, these studies indicate that CEF is subjected to a rapid redox regulation through several components including metabolic pools (PQ, NADPH, ferredoxin) (Takahashi et al. 2013), reactive oxygen species (Livingston et al. 2010), and ions ( $\text{Ca}^{++}$ ) (Terashima et al. 2012), independent of state transitions.

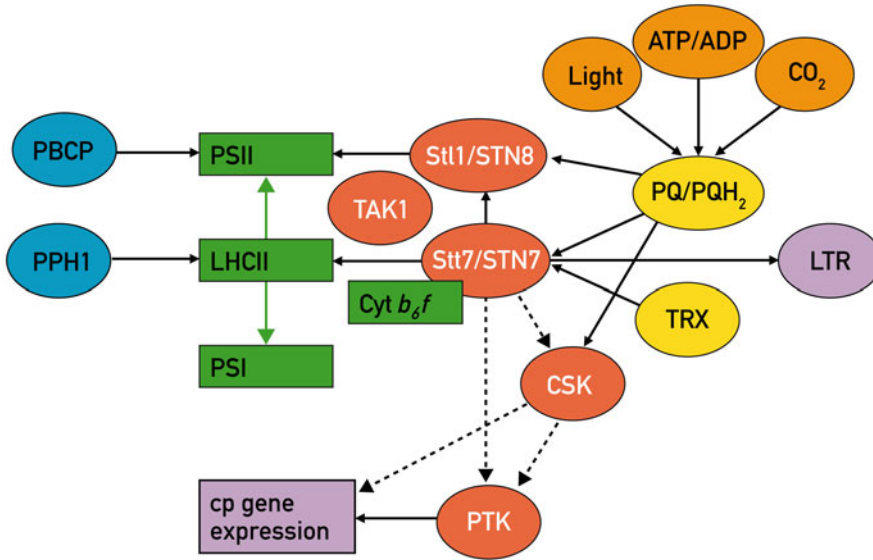
## VII. Conclusions and Perspectives

During the past years an increasing number of protein kinases and phosphatases have been identified that participate in a complex chloroplast signaling network involved in the acclimation response towards changes in environmental conditions (Fig. 24.3). A key parameter in this response is the redox state of the photosynthetic PQ pool which is influenced by intrinsic factors such as the cellular energy balance and by environmental factors including light quality and quantity,  $\text{CO}_2$  level, temperature and micronutrient availability. How the redox state is perceived by the chloroplast is still not fully elucidated although some potential candidates involved in this process have been identified. Amongst them a protein quartet consisting of the Stt7/STN7 (Depège et al. 2003; Bellafiore et al. 2005) and ST11/STN8 (Bonardi et al. 2005; Vainonen et al. 2005) kinases and their counterpart PPH1/TAP38 (Pribil et al. 2010; Shapiguzov et al. 2010) and PBCP (Samol et al. 2012) phosphatases plays an important role. The most promising candidate for sensing the redox state of the PQ pool is the Stt7/STN7 kinase. Through its close associa-

tion with the Cyt  $b_6f$  complex it is intimately connected to the PQ pool and activated upon binding of  $\text{PQH}_2$  to the  $\text{Q}_0$  site of the complex. Besides its role in state transitions, a short term response, the Stt7/STN7 kinase is also involved in the long term response which links the redox state of the PQ pool to nuclear gene expression (Pesaresi et al. 2009). However, little is known about the components of this signaling chain except that the two pathways branch off at the level of the kinase.

Another aspect of the chloroplast signaling network is the linkage of chloroplast kinases and phosphatases with each other and, in particular, how they relate to the Stt7/STN7 kinase (Fig. 24.3). The fact that Stl1 is a substrate of the Stt7 kinase suggests the existence of signaling cascade between these two kinases (Lemeille et al. 2010). Although another kinase, CSK, has been proposed to be a redox sensor in the chloroplast based mostly on its relation to bacterial two-component systems (Puthiyaveetil et al. 2008), it remains to be seen whether this kinase acts in an autonomous way or whether it is also linked to Stt7/STN7. CSK is conserved in land plants and some algae, but appears to be absent from *Chlamydomonas*. The casein kinase 2 (PTK) is implicated in the phosphorylation of proteins involved in chloroplast transcription and post-transcriptional regulation (Link 2003; Bollenbach et al. 2004). One phosphorylation site of STN7 was proposed to be a potential substrate for PTK, raising the possibility that this kinase could also be involved in LHCII phosphorylation through STN7 (Reiland et al. 2009). However, the connection of STN7 to the plastid-signaling network is still largely unknown.

Finally, the essential role of chloroplast reducing power for the enhancement of cyclic electron transfer raises the question of the underlying molecular mechanisms, which could involve any of the other kinases mentioned except Stt7/STN7. As pointed out by Takahashi et al. (2013), an interesting aspect of this new conceptual view is that it could apply to the entire green lineage, especially to those photosynthetic organisms in which



*Fig. 24.3.* Chloroplast signaling network. The redox state of the plastoquinone pool (PQ/PQH<sub>2</sub>) is dependent on irradiance, CO<sub>2</sub> level and cellular ATP/ADP ratio. PQH<sub>2</sub>, plastoquinol, activates the Stt7/STN7 kinase through the *Cyt b<sub>6</sub>f* complex. The major substrates of the Stt7/STN7 and Stt1/STN8 kinases are LHCII and the PSII core proteins. STN7 is also involved in retrograde signaling (LTR). The LHCII kinase has been proposed to be inactivated through reduced thioredoxin (TRX). The PPH1 and the PBCP phosphatases act as the counterparts of the Stt7/STN7 and Stt1/STN8 kinases, respectively. The kinases PTK and CSK act on the chloroplast gene expression system and may be redox-controlled through STN7. The TAK1 kinase has been proposed to be involved in LHCII phosphorylation (Snyders and Kohorn 1999) but its precise role remains to be determined (Adapted from Rochaix (2013)) with permission).

state transitions involve the mobility of only a limited portion of the antenna.

## Acknowledgements

I thank Nicolas Roggli for preparing the figures. The work in the author's laboratory was supported by grant 31003A\_133089/1 from the Swiss National Foundation.

## References

- Allen JF (2003) Cyclic, pseudocyclic and noncyclic photophosphorylation: new links in the chain. *Trends Plant Sci* 8:15–19
- Allorent G, Tokutsu R, Roach T, Peers G, Cardol P, Girard-Bascou J, Seigneurin-Berny D, . . . , Finazzi G (2013) A dual strategy to cope with high light in *Chlamydomonas reinhardtii*. *Plant Cell* 25:545–557

- Alric J (2014) Redox and ATP control of photosynthetic cyclic electron flow in *Chlamydomonas reinhardtii*: (II) involvement of the PGR5-PGRL1 pathway under anaerobic conditions. *Biochim Biophys Acta* 1837:825–834
- Andersson B, Andersson J (1980) Lateral heterogeneity in the distribution of chlorophyll-protein complexes of the thylakoid membranes of spinach chloroplasts. *Biochim Biophys Acta* 593:427–440
- Bassi R, Giacometti GM, Simpson DJ (1988) Changes in the organization of stroma membranes induced by in vivo state 1 – state 2 transition. *Biochim Biophys Acta* 935:152–165
- Bellaïfiore S, Barneche F, Peltier G, Rochaix JD (2005) State transitions and light adaptation require chloroplast thylakoid protein kinase STN7. *Nature* 433:892–895
- Bendall DS, Manasse RS (1995) Cyclic photophosphorylation and electron transport. *Biochim Biophys Acta* 1229:21–28
- Bennett J (1977) Phosphorylation of chloroplast membrane proteins. *Nature* 269:344–346



- Bollenbach TJ, Schuster G, Stern DB (2004) Cooperation of endo- and exoribonucleases in chloroplast mRNA turnover. *Prog Nucleic Acid Res Mol Biol* 78:305–337
- Bonardi V, Pesaresi P, Becker T, Schleiff E, Wagner R, Pfannschmidt T, Jahns P, Leister D (2005) Photosystem II core phosphorylation and photosynthetic acclimation require two different protein kinases. *Nature* 437:1179–1182
- Bonaventura C, Myers J (1969) Fluorescence and oxygen evolution from *Chlorella pyrenoidosa*. *Biochim Biophys Acta* 189:366–383
- Bonente G, Passarini F, Cazzaniga S, Mancone C, Buia MC, Tripodi M, Bassi R, Caffarri S (2008) The occurrence of the PsbS gene product in *Chlamydomonas reinhardtii* and in other photosynthetic organisms and its correlation with energy quenching. *Photochem Photobiol* 84:1359–1370
- Brautigam K, Dietzel L, Kleine T, Stroher E, Wormuth D, Dietz KJ, Radke D, . . . , Pfannschmidt T (2009) Dynamic plastid redox signals integrate gene expression and metabolism to induce distinct metabolic states in photosynthetic acclimation in *Arabidopsis*. *Plant Cell* 21:2715–2732
- Burrows PA, Sazanov LA, Svab Z, Maliga P, Nixon PJ (1998) Identification of a functional respiratory complex in chloroplasts through analysis of tobacco mutants containing disrupted plastid *ndh* genes. *EMBO J* 17:868–876
- Cardol P, Alrich J, Girard-Bascou J, Franck F, Wollman FA, Finazzi G (2009) Impaired respiration discloses the physiological significance of state transitions in *Chlamydomonas*. *Proc Natl Acad Sci USA* 106:15979–15984. Epub 12009 Sep 15971
- Depège N, Bellafiore S, Rochaix JD (2003) Role of chloroplast protein kinase Stt7 in LHCII phosphorylation and state transition in *Chlamydomonas*. *Science* 299:1572–1575
- Eberhard S, Finazzi G, Wollman FA (2008) The dynamics of photosynthesis. *Annu Rev Genet* 42:463–515
- Finazzi G, Furia A, Barbagallo RP, Forti G (1999) State transitions, cyclic and linear electron transport and photophosphorylation in *Chlamydomonas reinhardtii*. *Biochim Biophys Acta* 1413:117–129
- Finazzi G, Rappaport F, Furia A, Fleischmann M, Rochaix JD, Zito F, Forti G (2002) Involvement of state transitions in the switch between linear and cyclic electron flow in *Chlamydomonas reinhardtii*. *EMBO Rep* 3:280–285
- Fleischmann MM, Ravanel S, Delosme R, Olive J, Zito F, Wollman FA, Rochaix JD (1999) Isolation and characterization of photoautotrophic mutants of *Chlamydomonas reinhardtii* deficient in state transition. *J Biol Chem* 274:30987–30994
- Guo J, Wei X, Li M, Pan X, Chang W, Liu Z (2013) Structure of the catalytic domain of a state transition kinase homolog from *Micromonas* algae. *Protein Cell* 4:607–619
- Hasan SS, Yamashita E, Ryan CM, Whitelegge JP, Cramer WA (2011) Conservation of lipid functions in cytochrome bc complexes. *J Mol Biol* 414:145–162
- Hasan SS, Yamashita E, Baniulisc D, Cramer WA (2013a) Quinone-dependent proton transfer pathways in the photosynthetic cytochrome *b6f* complex. *Proc Natl Acad Sci USA* 110:4297–4303
- Hasan SS, Stofleth JT, Yamashita E, Cramer WA (2013b) Lipid-induced conformational changes within the cytochrome *b6f* complex of oxygenic photosynthesis. *Biochemistry* 52:2649–2654
- Hertle AP, Blunder T, Wunder T, Pesaresi P, Pribil M, Armbruster U, Leister D (2013) PGRL1 is the elusive ferredoxin-plastoquinone reductase in photosynthetic cyclic electron flow. *Mol Cell* 49:511–523
- Houille-Vernes L, Rappaport F, Wollman FA, Alric J, Johnson X (2011) Plastid terminal oxidase 2 (PTOX2) is the major oxidase involved in chlororespiration in *Chlamydomonas*. *Proc Natl Acad Sci USA* 108:20820–20825
- Iwai M, Takizawa K, Tokutsu R, Okamuro A, Takahashi Y, Minagawa J (2010a) Isolation of the elusive supercomplex that drives cyclic electron flow in photosynthesis. *Nature* 464:1210–1213
- Iwai M, Yokono M, Inada N, Minagawa J (2010b) Live-cell imaging of photosystem II antenna dissociation during state transitions. *Proc Natl Acad Sci USA* 107:2337–2342
- Kargul J, Turkina MV, Nield J, Benson S, Vener AV, Barber J (2005) Light-harvesting complex II protein CP29 binds to photosystem I of *Chlamydomonas reinhardtii* under state 2 conditions. *FEBS J* 272:4797–4806
- Kyle DJ, Staehelin LA, Arntzen CJ (1983) Lateral mobility of the light-harvesting complex in chloroplast membranes controls excitation energy distribution in higher plants. *Arch Biochem Biophys* 222:527–541
- Lemeille S, Rochaix JD (2010) State transitions at the crossroad of thylakoid signalling pathways. *Photosynth Res* 106:33–46
- Lemeille S, Willig A, Depège-Fargeix N, Delessert C, Bassi R, Rochaix JD (2009) Analysis of the chloroplast protein kinase Stt7 during state transitions. *PLoS Biol* 7:e45
- Lemeille S, Turkina MV, Vener AV, Rochaix JD (2010) Stt7-dependent phosphorylation during state transitions in the green alga *Chlamydomonas reinhardtii*. *Mol Cell Proteomics* 9:1281–1295

- Lennartz K, Plucken H, Seidler A, Westhoff P, Bechtold N, Meierhoff K (2001) HCF164 encodes a thioredoxin-like protein involved in the biogenesis of the cytochrome b(6)f complex in *Arabidopsis*. *Plant Cell* 13:2539–2551
- Link G (2003) Redox regulation of chloroplast transcription. *Antioxid Redox Signal* 5:79–87
- Livingston AK, Kanazawa A, Cruz JA, Kramer DM (2010) Regulation of cyclic electron flow in C(3) plants: differential effects of limiting photosynthesis at ribulose-1,5-bisphosphate carboxylase/oxygenase and glyceraldehyde-3-phosphate dehydrogenase. *Plant Cell Environ* 33:1779–1788
- Lucker B, Kramer DM (2013) Regulation of cyclic electron flow in *Chlamydomonas reinhardtii* under fluctuating carbon availability. *Photosynth Res* 117:449–459
- Lunde C, Jensen PE, Haldrup A, Knoetzel J, Scheller HV (2000) The PSI-H subunit of photosystem I is essential for state transitions in plant photosynthesis. *Nature* 408:613–615
- Munekage Y, Hoyo M, Meurer J, Endo T, Tasaka M, Shikanai T (2002) PGR5 is involved in cyclic electron flow around photosystem I and is essential for photoprotection in *Arabidopsis*. *Cell* 110:361–371
- Murata N (1969) Control of excitation transfer in photosynthesis. I. Light-induced change of chlorophyll a fluorescence in *Porphyridium cruentum*. *Biochim Biophys Acta* 172:242–251
- Nunes-Nesi A, Sulpice R, Gibon Y, Fernie AR (2008) The enigmatic contribution of mitochondrial function in photosynthesis. *J Exp Bot* 59:1675–1684
- Page ML, Hamel PP, Gabilly ST, Zegzouti H, Perea JV, Alonso JM, Ecker JR, . . . , Merchant S (2004) A homolog of prokaryotic thiol disulfide transporter CcdA is required for the assembly of the cytochrome b6f complex in *Arabidopsis* chloroplasts. *J Biol Chem* 279:32474–32482. Epub 32004 May 32424
- Peers G, Truong TB, Ostendorf E, Busch A, Elrad D, Grossman AR, Hippler M, Niyogi KK (2009) An ancient light-harvesting protein is critical for the regulation of algal photosynthesis. *Nature* 462:518–521
- Pesaresi P, Hertle A, Pribil M, Kleine T, Wagner R, Strissel H, Ihnatowicz A, . . . , Leister D (2009) *Arabidopsis* STN7 kinase provides a link between short- and long-term photosynthetic acclimation. *Plant Cell* 21:2402–2423
- Pribil M, Pesaresi P, Hertle A, Barbato R, Leister D (2010) Role of plastid protein phosphatase TAP38 in LHCII dephosphorylation and thylakoid electron flow. *PLoS Biol* 8:e1000288
- Puthiyaveetil S (2011) A mechanism for regulation of chloroplast LHC II kinase by plastoquinol and thioredoxin. *FEBS Lett* 585:1717–1721
- Puthiyaveetil S, Kavanagh TA, Cain P, Sullivan JA, Newell CA, Gray JC, Robinson C, . . . , Allen JF (2008) The ancestral symbiont sensor kinase CSK links photosynthesis with gene expression in chloroplasts. *Proc Natl Acad Sci U S A* 105:10061–10066
- Reiland S, Messerli G, Baerenfaller K, Gerrits B, Endler A, Grossmann J, Gruissem W, Baginsky S (2009) Large-scale *Arabidopsis* phosphoproteome profiling reveals novel chloroplast kinase substrates and phosphorylation networks. *Plant Physiol* 150:889–903. Epub 2009 Apr 2017
- Rintamaki E, Martinsuo P, Pursiheimo S, Aro EM (2000) Cooperative regulation of light-harvesting complex II phosphorylation via the plastoquinol and ferredoxin-thioredoxin system in chloroplasts. *Proc Natl Acad Sci USA* 97:11644–11649
- Rochaix JD (2007) Role of thylakoid protein kinases in photosynthetic acclimation. *FEBS Lett* 581:2768–2775. Epub 2007 Apr 2725
- Rochaix JD (2013) Redox regulation of thylakoid protein kinases and photosynthetic gene expression. *Antioxid Redox Signal* 18:2184–2201
- Rochaix JD (2014) Regulation and dynamics of the light-harvesting system. *Annu Rev Plant Biol* 65:287–309
- Samol I, Shapiguzov A, Ingelsson B, Fucile G, Crevecoeur M, Vener AV, Rochaix JD, Goldschmidt-Clermont M (2012) Identification of a photosystem II phosphatase involved in light acclimation in *Arabidopsis*. *Plant Cell* 24:2596–2609
- Schuster G, Dewit M, Staehelin LA, Ohad I (1986) Transient inactivation of the thylakoid photosystem II light-harvesting protein kinase system and concomitant changes in intramembrane particle size during photoinhibition of *Chlamydomonas reinhardtii*. *J Cell Biol* 103:71–80
- Shapiguzov A, Ingelsson B, Samol I, Andres C, Kessler F, Rochaix JD, Vener AV, Goldschmidt-Clermont M (2010) The PPH1 phosphatase is specifically involved in LHCII dephosphorylation and state transitions in *Arabidopsis*. *Proc Natl Acad Sci U S A* 107:4782–4787
- Shikanai T, Endo T, Hashimoto T, Yamada Y, Asada K, Yokota A (1998) Directed disruption of the tobacco *ndhB* gene impairs cyclic electron flow around photosystem I. *Proc Natl Acad Sci USA* 95:9705–9709
- Shimoni E, Rav-Hon O, Ohad I, Brumfeld V, Reich Z (2005) Three-dimensional organization of higher-plant chloroplast thylakoid membranes revealed by electron tomography. *Plant Cell* 17:2580–2586

- Snyders S, Kohorn BD (1999) TAKs, thylakoid membrane protein kinases associated with energy transduction. *J Biol Chem* 274:9137–9140
- Stroebel D, Choquet Y, Popot JL, Picot D (2003) An atypical haem in the cytochrome b(6)f complex. *Nature* 426:413–418
- Takahashi H, Iwai M, Takahashi Y, Minagawa J (2006) Identification of the mobile light-harvesting complex II polypeptides for state transitions in *Chlamydomonas reinhardtii*. *Proc Natl Acad Sci USA* 103:477–482
- Takahashi H, Clowez S, Wollman FA, Vallon O, Rapaport F (2013) Cyclic electron flow is redox-controlled but independent of state transition. *Nat Commun* 4:1954
- Terashima M, Petroustos D, Hudig M, Tolstygina I, Trompelt K, Gabelein P, Fufezan C, . . . , Hippler M (2012) Calcium-dependent regulation of cyclic photosynthetic electron transfer by a CAS, ANR1, and PGRL1 complex. *Proc Natl Acad Sci U S A* 109:17717–17722
- Tikkanen M, Grieco M, Kangasjärvi S, Aro EM (2007) Thylakoid protein phosphorylation in higher plant chloroplasts optimizes electron transfer under fluctuating light. *Biochim Biophys Acta* 152:723–735
- Vainonen JP, Hansson M, Vener AV (2005) STN8 protein kinase in *Arabidopsis thaliana* is specific in phosphorylation of photosystem II core proteins. *J Biol Chem* 280:33679–33686
- Vallon O, Bulte L, Dainese P, Olive J, Bassi R, Wollman FA (1991) Lateral redistribution of cytochrome b6/f complexes along thylakoid membranes upon state transitions. *Proc Natl Acad Sci USA* 88:8262–8266
- Vener AV, van Kan PJ, Rich PR, Ohad II, Andersson B (1997) Plastoquinol at the quinol oxidation site of reduced cytochrome b<sub>6</sub> mediates signal transduction between light and protein phosphorylation: thylakoid protein kinase deactivation by a single-turnover flash. *Proc Natl Acad Sci USA* 94:1585–1590
- Wang H, Gau H, Slade WO, Juergens M, Li P, Hicks LM (2014) The global phosphoproteome of *Chlamydomonas reinhardtii* reveals complex organellar phosphorylation in the flagella and thylakoid membrane. *Mol Cell Prot* 13: 2337–2357. In press, published on 10 June 2014
- Widger WR, Cramer WA, Herrmann RG, Trebst A (1984) Sequence homology and structural similarity between cytochrome b of mitochondrial complex III and the chloroplast b<sub>6</sub>-f complex: position of the cytochrome b hemes in the membrane. *Proc Natl Acad Sci USA* 81:674–678
- Wientjes E, Drop B, Kouril R, Boekema EJ, Croce R (2013) During state 1 to state 2 transition in *Arabidopsis thaliana*, the photosystem II supercomplex gets phosphorylated but does not disassemble. *J Biol Chem* 288:32821–32826
- Willig A, Shapiguzov A, Goldschmidt-Clermont M, Rochaix JD (2011) The phosphorylation status of the chloroplast protein kinase STN7 of *Arabidopsis* affects its turnover. *Plant Physiol* 157:2102–2107
- Zito F, Finazzi G, Delosme R, Nitschke W, Picot D, Wollman FA (1999) The Q<sub>o</sub> site of cytochrome b<sub>6</sub>f complexes controls the activation of the LHCII kinase. *EMBO J* 18:2961–2969

# Chapter 25

## Regulating Synthesis of Cytochromes

Sébastien Zappa and Carl E. Bauer\*

*Department of Molecular and Cellular Biochemistry, Indiana University, Simon Hall MSB, 212 S Hawthorne Dr, Bloomington, IN 47405, USA*

Summary.....	479
I. Introduction.....	480
II. The Bi- and Tri-furcated Tetrapyrrole Pathway.....	481
III. Regulating Heme Biosynthesis.....	482
A. Regulation by Heme or Other Tetrapyrrole Precursors.....	482
B. Redox Control of <i>hem</i> Gene Expression.....	484
1. CrtJ/PpsR.....	484
2. RegB-RegA.....	485
3. FnrL.....	487
IV. Regulating Cytochrome Apoprotein Synthesis.....	487
A. Transcription Control.....	487
1. Redox Regulation.....	487
2. Promoter Selectivity.....	489
B. Post-translational Regulation.....	489
V. Metal Homeostasis and Cytochrome Regulation.....	490
A. Iron Homeostasis.....	490
B. Copper Homeostasis.....	491
C. Iron and Copper Homeostasis Interplay with Cytochrome Regulation.....	492
VI. Concluding Remarks.....	493
References.....	493

### Summary

Detailed understanding of the regulation of cytochrome synthesis is an area that remains substantially undefined. Evidence to date suggests that the synthesis of cytochromes involves complex coordination of heme biosynthesis with expression of cytochrome apoproteins. Heme biosynthesis in turn is coordinated with the import of iron, as the presence of a coordinated iron in the heme tetrapyrrole is a key feature that allows heme to undertake redox reactions, redox sensing, and to carry diatomic gases such as O<sub>2</sub>, CO or NO. Some cytochrome oxidases also contain copper centers that are involved in shuttling electrons to and from heme groups. Since excess of iron and/or copper is toxic to cells, the proper import of these metals is also a significant consideration for the synthesis of some respiratory cytochromes. This review will cover both transcriptional and post-transcriptional control mechanisms that affect the synthesis of heme, the expression of cytochrome apoproteins and homeostasis of iron and copper in photosynthetic organisms.

---

\*Author for correspondence, e-mail: [bauer@indiana.edu](mailto:bauer@indiana.edu)

## I. Introduction

As discussed in other chapters of this volume, cytochromes are essential components in photosynthesis where they function to safely shuttle electrons to and from the photosystems (PS) as well as to a variety of other cellular components. Notable cytochromes include the *b<sub>6</sub>f* complex in cyanobacteria and plants that are essential for shuttling electrons between photosystem II (PSII) and photosystem I (PSI), and the homologous *bc<sub>1</sub>* complex in anoxygenic photosynthetic bacteria that is essential for photosynthetic cyclic electron transport in these bacteria. Not to be overlooked are various cytochrome oxidases and related reductases that generate membrane potential through the reduction of oxygen or other components such as dimethyl sulfoxide (DMSO).

By definition, all cytochromes contain one or more bound hemes that are either non-covalently or covalently attached to an apoprotein. Heme is composed of a heterocyclic tetrapyrrole ring, termed a porphyrin, that has iron bound to four pyrrolic groups. The synthesis of heme is highly regulated, as unbound free heme is a lipophilic toxic moiety that can catalyze damaging lipid peroxidation, oxidation of proteins and DNA damage (Kumar and Bandyopadhyay 2005; Graça-Souza et al. 2006; Anzaldi and Skaar 2010). All of these deleterious reactions are catalyzed by oxidative and reductive properties of an iron that bound to four pyrrole groups in a porphyrin ring. Free iron is also highly toxic as it can generate damaging oxygen radicals

through a process known as the Fenton reaction (Touati 2000; Chiancone et al. 2004; Cornelis et al. 2011). One can therefore think of cytochromes as a protein moiety that has evolved to safely and effectively control the redox properties of iron bound to heme that additionally is also capable of providing substrate and product specificity. It is because of the toxic nature of free iron and free heme that evolution has selected complex cellular mechanisms of coordinating the transport of iron with the synthesis of the tetrapyrrole ring that binds the iron, which is in turn coordinated with synthesis of cytochrome apoproteins. Coordination of these events ensures that there is minimal free iron or free heme present in most cells. Finally, some cytochrome oxidases also contain two copper centers as prosthetic groups that are also involved in electron transport (Wainio et al. 1959; Tsukihara et al. 1995). As is the case of iron, unbound copper is also highly toxic, necessitating tight control on its transport (Wainio et al. 1959; Tsukihara et al. 1995; Osman and Cavet 2008; Macomber and Imlay 2009; Dupont et al. 2011).

This review is centered on what is known about the control of cytochrome apoprotein synthesis, its relation to iron and copper transport, and the synthesis of the tetrapyrrole component of heme (Fig. 25.1). We will discuss evidence that heme is itself an important feedback regulator of its own synthesis at both the transcriptional and post-transcriptional levels. We also will cover evidence that there is coordination of heme synthesis gene expression with the expression of cytochrome apoproteins. Most of the studies on the control of cytochrome biosynthesis in photosynthetic organisms have been undertaken with purple photosynthetic bacteria, specifically *Rhodobacter capsulatus* and *Rhodobacter sphaeroides*. This review will therefore be focused on these studies, although we will touch on what is known in other classes of photosynthetic organisms.

---

*Abbreviations:* ALA –  $\delta$ -aminolevulinic acid; BChl – Bacteriochlorophyll; *cbb<sub>3</sub>*-Cox – *cbb<sub>3</sub>* cytochrome oxidase; Chl – Chlorophyll; Cys – Cysteine; DMSO – Dimethyl sulfoxide; GluTR – Glutamyl-tRNA reductase; PAS – Per-Arnt-Sim; PBG – Porphobilinogen; PPIX – Protoporphyrin IX; PS – Photosystem; *Rb.* – *Rhodobacter*

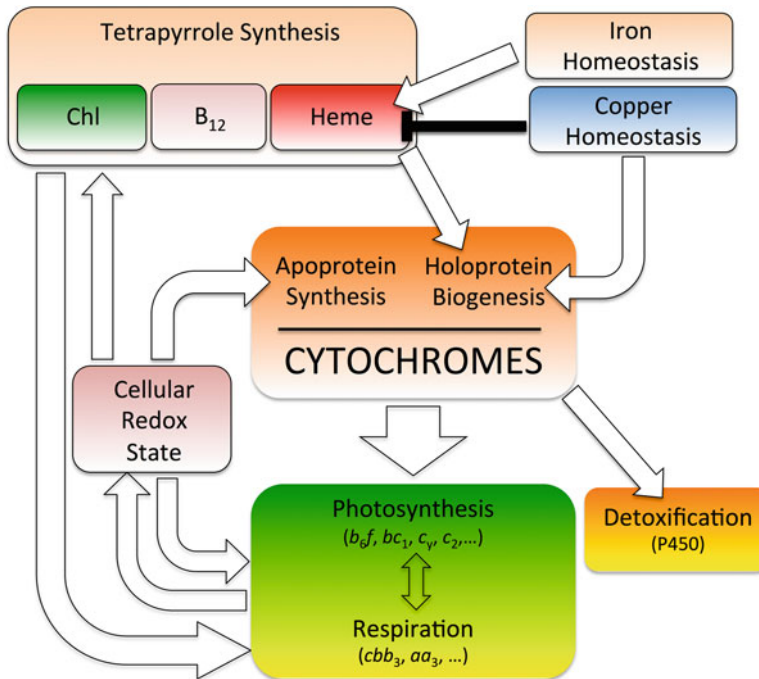


Fig. 25.1. Overview of major cellular signals controlling cytochrome biosynthesis and major cellular functions of cytochromes. Only prokaryotic photosynthetic organisms can synthesize vitamin B<sub>12</sub>. Only a subset of cytochromes, the terminal oxidases, uses copper as a cofactor. Copper was shown to inhibit heme synthesis (Azzouzi et al. 2013). B<sub>12</sub> cobalamin/vitamin B<sub>12</sub>, Chl chlorophyll, aa<sub>3</sub> and cbb<sub>3</sub>, aa<sub>3</sub> and cbb<sub>3</sub> cytochrome oxidases, P450 cytochrome P450.

## II. The Bi- and Tri-furcated Tetrapyrrole Pathway

As indicated in Fig. 25.2, the tetrapyrrole biosynthetic pathway is quite complex involving many enzymes and a branched pathway that leads to the synthesis of heme, chlorophyll (Chl) or bacteriochlorophyll (BChl in anoxygenic phototrophs) and cobalamin (vitamin B<sub>12</sub>). Heme is present in all branches of life (including all photosynthetic organisms) and is thus thought to be the most ancient of these three tetrapyrroles (Yin and Bauer 2013). In contrast, Chl is not present in Archaea. In eukaryotes, Chl is thought to be derived from endosymbiosis of a cyanobacterium that led to the formation of chloroplasts (Xiong et al. 2000; Xiong and Bauer 2002). As a result, in addition to complexities of regulating heme synthesis, photosynthetic cells are also faced with

the challenge of balancing heme synthesis with the synthesis of the second important tetrapyrrole, Chl/BChl, which has bound Mg instead of iron. Heme and Chl biosynthesis branch from each other at protoporphyrin IX (PPIX), which is the point where metal chelation into the tetrapyrrole PPIX occurs (Suzuki et al. 1997; Yin and Bauer 2013). As is the case with heme, free Chl/BChl is toxic, as light excited Chl/BChl is capable of forming a triplet state that can transfer energy to oxygen in the ground state to form highly reactive singlet oxygen. This necessitates that Chl/BChl synthesis also be highly regulated. To add further complexity, bacteria in general and photosynthetic bacteria in particular (anoxygenic and cyanobacteria) also synthesize a third tetrapyrrole cobalamin (vitamin B<sub>12</sub>) that contains cobalt bound to a tetrapyrrole ring (Yin and Bauer 2013). Cobalamin is not synthesized by algae and

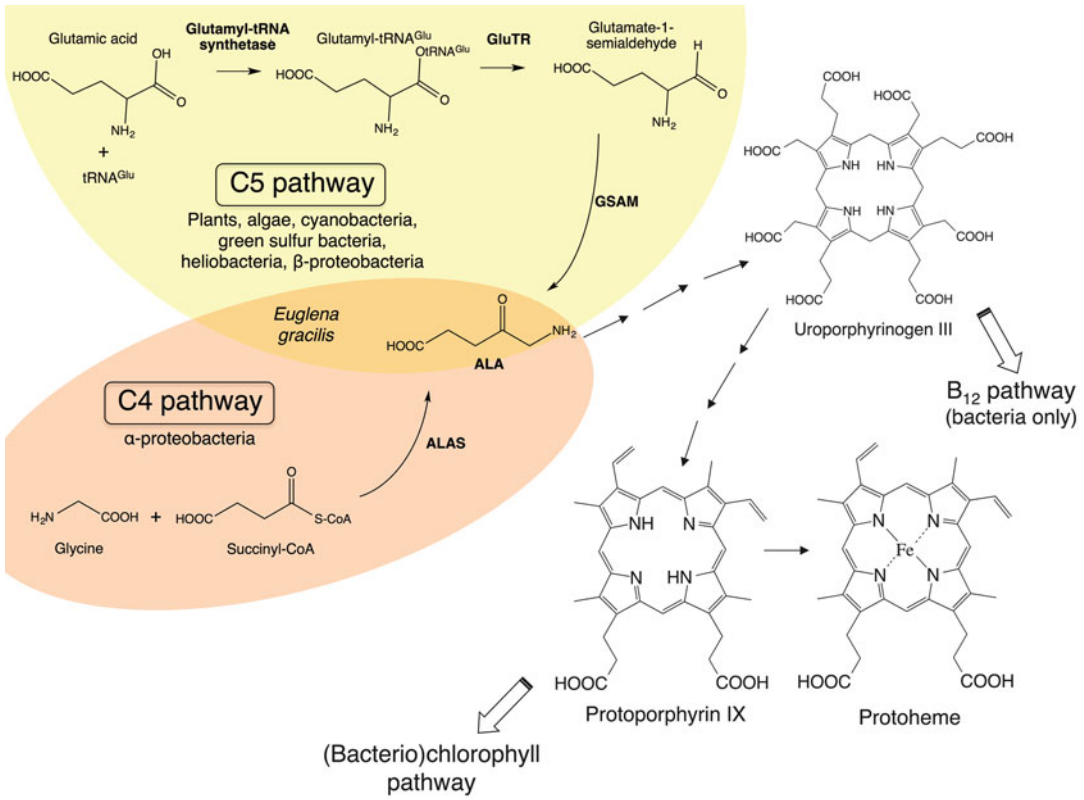


Fig. 25.2. Overview of heme synthesis pathways in photosynthetic organisms. Note that the C4 pathway is also known as the Shemin pathway. The only known organism to harbor both the C4 and C5 machinery is *Euglena gracilis* (Frankenberg et al. 2003). ALA  $\delta$ -aminolevulinic acid, ALAS  $\delta$ -aminolevulinic acid synthase, GluTR glutamyl-tRNA reductase, GSAM glutamate-1-semialdehyde-2,1-aminomutase.

plants, so these photosynthetic organisms only have to balance the synthesis of two tetrapyrroles instead of three.

Heme and Chl are both involved in redox chemistry as they accept and donate electrons. By definition, cytochromes are proteins containing a bound heme that is used to perform redox chemistry. Heme has the additional characteristic of functioning as a gas carrier as the heme iron bound to a protein such as hemoglobin is capable of forming an axial ligand to diatomic gasses such as O<sub>2</sub>, CO, and NO. Chlorophylls are not gas carriers but they do very effectively donate an electron when the tetrapyrrole ring is excited by light. Typically, an electron is donated to a neighboring Chl, pheophytin (a Chl derivative that lacks Mg), or to a ubiquinone. Cobalamin does not undergo re-

dox chemistry like that of heme and Chl, and is instead involved as a cofactor in enzymatic reactions such as the donation of a methyl group or the reduction of nucleotides (Banerjee and Ragsdale 2003).

### III. Regulating Heme Biosynthesis

#### A. Regulation by Heme or Other Tetrapyrrole Precursors

One mechanism of regulating heme synthesis is feedback inhibition in which free heme inhibits the activity of the first enzyme of the pathway,  $\delta$ -aminolevulinic acid synthase. This enzyme catalyzes the formation of  $\delta$ -aminolevulinic acid (ALA) from glycine and succinyl-CoA as first established by

Shemin and Russell (1953) and is known as the C-4 pathway (Fig. 25.2). In most characterized species, this enzyme is rate limiting and is feedback-inhibited by free heme (Burnham and Lascelles 1963). Such heme-based regulation was suggested in the purple bacterium *Rb. sphaeroides* as early as 1960, in which excess ALA was observed to decrease the activity of ALA synthase and the downstream enzyme porphobilinogen (PBG) synthase in vivo. Likewise, exogenous heme was shown to specifically decrease ALA synthase activity. On the contrary, PPIX and Mg-PPIX did not exert any influence on these enzymes (Lascelles 1960; Lascelles and Hatch 1969).

Plants, algae, and many bacterial species also synthesize ALA by an alternative route called the C-5 pathway (Beale and Castelfranco 1973; Beale 1978; von Wettstein et al. 1995; Kumar et al. 1996). This alternative route involves several enzymes such as glutamate tRNA synthase where glutamate is coupled to tRNA<sub>glu</sub> followed by glutamyl-tRNA<sub>Glu</sub> reductase (GluTR) that catalyzes the reduction of glutamyl-tRNA<sub>Glu</sub> to a glutamate 1-semialdehyde (Schön et al. 1986). A third enzyme then converts the glutamate 1-semialdehyde into ALA. Early studies in cyanobacteria, green algae (*Chlorella* and *Chlamydomonas*), and plant extracts indicated that the C-5 pathway for ALA production is also inhibited by free heme through a direct interaction with GluTR (Chereskin and Castelfranco 1982; Weinstein and Beale 1985; Huang and Wang 1986a, b; Rieble and Beale 1991; Pontoppidan and Kannangara 1994; Vothknecht et al. 1996).

In addition to feedback control of enzyme activity, the expression of many genes coding for enzymes in the common heme branch of the pathway (*hem* genes) is also regulated through heme availability. In the alga *Chlamydomonas*, Huang and Wang (1986a, b) initially reported that ALA synthesis was regulated in response to heme availability both at the gene expression and enzyme activity levels. Recombinant GluTRs from *Chlorobium vibrioforme* and *Chlamydomonas reinhardtii*

were purified and showed to bind heme. While heme displayed an inhibitory effect on the *Chlorobium* GluTR, this was not the case for the purified *Chlamydomonas* GluTR (Srivastava and Beale 2005; Srivastava et al. 2005). Interestingly, such inhibition was observed in the presence of a crude extract of *Chlamydomonas* in the enzyme reaction mixture (Srivastava et al. 2005). Beside heme, Mg-PPIX the first intermediate of the chlorophyll biosynthesis pathway, was found to activate the transcription of the GluTR-encoding gene, while inhibiting ALA synthesis at the enzyme level (Vasileuskaya et al. 2005; Meinecke et al. 2010; Voss et al. 2011). In purple photosynthetic bacteria, Smart and Bauer (2006) demonstrated that expression of many of the common trunk *hem* genes (*hemA*, *hemB*, *hemC*, *hemE* and *hemH*) was reduced when *Rb. capsulatus* cells were grown in the presence of exogenous heme. Smart and Bauer (2006) further reported the discovery of a heme-binding transcription factor termed HbrL that appears to have a central role in controlling *hem* gene expression in response to heme availability. Sequence analysis of HbrL indicates that it is a member of the LysR family of transcription factors (Smart and Bauer 2006). Spectral analysis of isolated HbrL indicates that it is capable of binding heme (Smart and Bauer 2006).

Studies of *hem* gene expression in *Rb. capsulatus* cells grown in the absence of excess heme, as well as in the presence of an iron chelator that decreases heme levels, show that HbrL functions as an activator of *hemA* (ALA-synthase), *hemB* (PBG synthase), *hemC* (PBG deaminase), *hemE* (uroporphyrinogen decarboxylase), *hemN2/hemZ* (coproporphyrinogen III oxidase), *hemJ* (protoporphyrinogen oxidase), and *hemH* (ferrochelatase) (Smart and Bauer 2006; Zappa and Bauer 2013). In contrast, when cells are grown in the presence of excess heme, HbrL appears to function as a repressor of *hemB* (Smart and Bauer 2006).

In addition to HbrL, there is a second heme-binding transcription factor called PpsR in *Rb. sphaeroides* and the related



CrtJ in *Rb. capsulatus* that is involved in controlling *hem* gene expression in these species (Smart et al. 2004; Yin et al. 2012). PpsR/CrtJ is a well characterized transcription factor that is also involved in redox control of the Mg-tetrapyrrole branch leading from PPIX to BChl (Penfold and Pemberton 1991, 1994; Gomelsky and Kaplan 1995; Ponnampalam and Bauer 1997; Elsen et al. 1998; Ponnampalam et al. 1998). Smart et al. (2004) demonstrated that CrtJ is capable of functioning as a repressor of *hemA*, *hemC* and *hemE* expression, as well as a significant activator of *hemZ* and *hemH* expression in *Rb. capsulatus*. Moskvina et al. (2005) also demonstrated the presence of three PpsR binding site in the divergent *hemC* and *hemE* promoter region of *Rb. sphaeroides*. Recently, it was demonstrated that PpsR from *Rb. sphaeroides* is itself a heme binding transcription factor and that the presence of excess heme in vivo results in decreased ability of PpsR to repress the expression of genes in the Mg-tetrapyrrole (BChl) branch (Yin et al. 2012). There is no effect of excess heme on the ability of PpsR to repress *hemC* or *hemE*, so it was reasoned that excess heme specifically disrupts the ability of PpsR to bind to a subset of genes leading to increased BChl biosynthesis. Presumably, this would allow the cell to “bleed off” excess PPIX into the Mg-tetrapyrrole (BChl) branch leading to a reduction in heme biosynthesis (Yin et al. 2012).

### B. Redox Control of hem Gene Expression

As discussed above, there are a common steps in the heme and BChl biosynthetic pathways, from the synthesis of ALA to PPIX. These two pathways separate at the point of metal insertion (Fe versus Mg) into PPIX (Fig. 25.3). In many species of purple photosynthetic bacteria, the synthesis of the BChl is quite variable as it is highly repressed (>100-fold) in response to the presence of molecular oxygen and to a lesser degree by high light intensity. Thus, there is a considerable flux of tetrapyrrole

intermediates that pass through the common heme/BChl trunk of the tetrapyrrole pathway depending on oxygen tension and light intensity. This has an impact on how the cell must control and coordinate the synthesis of heme with that of BChl and cobalamin as well as the cytochrome and photosystem apoproteins that bind heme and BChl, respectively.

Several studies on the control of heme synthesis in the purple bacteria *Rb. capsulatus* and *Rb. sphaeroides* have shown that expression of *hem* genes is altered in response to oxygen tension. In *Rb. sphaeroides*, aeration of the growth medium was observed to impact negatively the two first enzymes of the heme biosynthesis pathway, ALA synthase and PBG synthase (Lascelles 1960). Neidle and Kaplan (1993a, b) demonstrated that the expression of ALA synthase encoding genes *hemA* and *hemT* was oxygen repressed. In *Rb. capsulatus*, Smart et al. (2004) demonstrated that expression of *hemA* (ALA-synthase), *hemB* (PBG synthase), *hemC* (PBG deaminase), *hemE* (uroporphyrinogen decarboxylase), and *hemN2/hemZ* (coproporphyrinogen III oxidase) increased significantly when *Rb. capsulatus* cells are grown under anaerobic conditions where BChl biosynthesis occurs at a maximum rate. Presumably, this is in response to the shunting of tetrapyrrole intermediates from the common trunk into the Mg-tetrapyrrole branch necessitating that *hem* gene expression be increased to allow increased synthesis of these early intermediates. Interestingly, *hemH* (ferrochelatase) expression was not highly regulated by oxygen, indicating that the pool of PPIX must remain fairly static even under anaerobic conditions where much PPIX is shunted into the Mg-branch.

#### 1. CrtJ/PpsR

One of the regulators identified to be involved in redox control of heme gene expression is CrtJ/PpsR, which as discussed above is also capable of binding heme

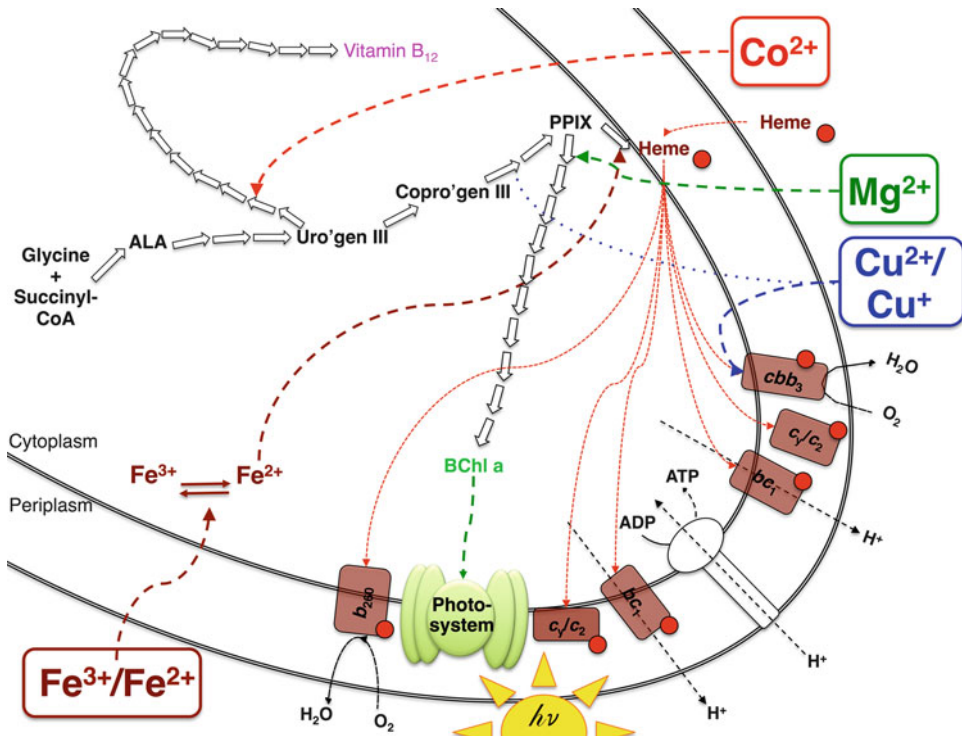


Fig. 25.3. Interdependence of metal import and tetrapyrrole and cytochrome biosynthesis. The trifurcated tetrapyrrole biosynthetic pathway leads to the formation of the Co-, Fe- and Mg-containing tetrapyrroles, namely cobalamin (vitamin B<sub>12</sub>), heme and BChl, respectively. Cytochromes are dependent on heme synthesis, which itself relies on iron availability, and those represented are involved in the photosynthetic and respiratory electron chains. Copper is a cofactor of respiratory terminal oxidase *cbb<sub>3</sub>-Cox* and was shown to inhibit coproporphyrinogen III oxidase in the tetrapyrrole pathway (dotted blue line). ALA  $\delta$ -aminolevulinic acid, *b<sub>260</sub>* ubiquinol oxidase, *bc<sub>1</sub>* cytochrome *c* oxidoreductase, BChl *a* bacteriochlorophyll *a*, *c<sub>2</sub>* cytochrome *c<sub>2</sub>*, *c<sub>y</sub>* cytochrome *c<sub>y</sub>*, *cbb<sub>3</sub>cbb<sub>3</sub>* cytochrome oxidase, Copro'gen III coproporphyrinogen III, PPIX protoporphyrin IX, Uro'gen III uroporphyrinogen III.

(Smart et al. 2004; Yin et al. 2012). The primary sequence of CrtJ consists of two Per-Arnt-Sim (PAS) domains at the N-terminal followed by a helix-turn-helix DNA binding domain at the C-terminal. In addition to heme binding, CrtJ contains a redox active cysteine (Cys) that is located in the helix-turn-helix DNA binding domain (Masuda and Bauer 2002; Masuda et al. 2002; Cheng et al. 2012). This Cys is capable of forming a disulfide bond with a second Cys in the PAS domain, as well as forming a stable sulfonic acid (Cys-OH) derivative (Masuda et al. 2002; Cheng et al. 2012). Genetic studies suggest that the oxidized Cys-OH form of CrtJ is an aerobic repressor of *hemA* (ALA synthase) *hemC* (PBG

deaminase), and *hemE* (uroporphyrinogen decarboxylase) (Smart et al. 2004). Interestingly, CrtJ appears to be both a strong aerobic and anaerobic activator of *hemH*, under both aerobic and anaerobic conditions (Smart et al. 2004).

## 2. RegB-RegA

In addition to CrtJ, the redox responding RegB-RegA two-component signal transduction cascade is known to anaerobically activate *hemA*, *hemC*, *hemE*, *hemZ* and *hemH* expression in *Rb. capsulatus* (Smart et al. 2004) and *hemA* in *Rb. sphaeroides* (Ranson-Olson et al. 2006; Ranson-Olson and Zeilstra-Ryalls 2008). RegA is known to

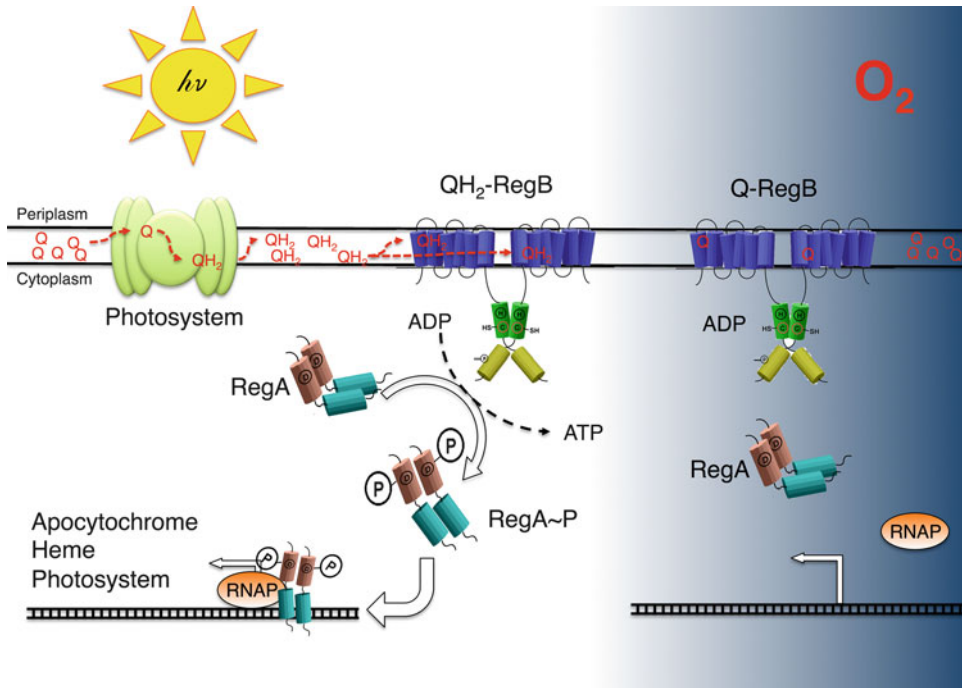


Fig. 25.4. Redox regulation of tetrapyrrole, photosystem and cytochrome biosynthesis by RegBA. The cellular redox state is monitored by the equilibrium between oxidized and reduced ubiquinones, Q and QH<sub>2</sub>, respectively. Light energy induces the formation of QH<sub>2</sub>. In turn, QH<sub>2</sub>-activated RegB triggers the ATP-dependent phosphorylation of RegA. Phosphorylated RegA activates the transcription of a plethora of genes, including ones involved in the synthesis of heme, apocytochrome and photosystem structural protein.

regulate nearly all of the *bch* genes coding for enzymes in the Mg-branch leading to the synthesis of BChl (Willett et al. 2007). RegA thus appears to be a major anaerobic activator of the pathway to ensure increased flux of tetrapyrroles through this pathway under anaerobic conditions where there is maximal synthesis of BChl. As shown in Fig. 25.4 this signal transduction cascade involves the membrane spanning histidine kinase RegB that phosphorylates the DNA binding response regulator RegA. Phosphorylation stimulates the DNA binding activity of RegA (Inoue et al. 1995; Bird et al. 1999). Under anaerobic conditions, RegB kinase activity is active leading to phosphorylation of RegA (Mosley et al. 1994).

RegB has multiple input signals that control its kinase activity in response to environmental redox conditions. One input is the redox state of the ubiquinone pool which is affected by both photosynthesis

and respiration (Fig. 25.4). Four membrane-spanning helices of RegB have been shown to interact with both oxidized and reduced forms of ubiquinone with nearly equal low affinities (Swem et al. 2006; Wu and Bauer 2010). It is proposed that a loosely bound ubiquinone to RegB is therefore in equilibrium with the ubiquinone pool. Thus, when the ubiquinone pool is oxidized, as in aerobic respiratory conditions, then the bound ubiquinone would be in an oxidized state. However when the ubiquinone pool is in a reduced state, as would occur under anaerobic photosynthetic growth conditions, then RegB contains bound reduced ubiquinone. Interestingly, the presence of oxidized ubiquinone effectively inhibits the kinase activity of RegB assuring that the kinase is inactive under respiratory growth conditions (Swem et al. 2006; Wu and Bauer 2010). A second level of control is offered by a redox active Cys in RegB that is

known to undergo oxidation in the presence of oxygen to form a stable Cys sulfonic acid derivative (Swem et al. 2003; Wu et al. 2013). Oxidation of this Cys also inhibits the kinase activity of RegB assuring that there is rapid shut off of kinase activity when the cells are exposed to molecular oxygen. Finally, it has also been proposed that a RegB homolog from *Rb. sphaeroides* called PrrB interacts directly with *cbb3* cytochrome oxidase (*cbb3*-Cox) and that this interaction affects PrrB activity (O’Gara et al. 1998; Oh and Kaplan 1999; Kim et al. 2007).

### 3. FnrL

In *Rb. capsulatus* and in *Rb. sphaeroides* the redox responding transcription factor FnrL is also thought to have a role in controlling *hem* gene expression. In *Rb. capsulatus*, Smart et al. (2004) identified putative FnrL binding sites in the *hemB* and *hemZ* promoter regions. In *Rb. sphaeroides* there are two promoters identified that control *hemA* expression with a putative FnrL binding site overlapping the start site of the upstream promoter (Zeilstra-Ryalls and Kaplan 1995; Ranson-Olson and Zeilstra-Ryalls 2008). A role of FnrL in controlling *hem* gene expression is intriguing given that the *E. coli* Fnr homolog has an oxygen labile 4Fe-4S cluster that is needed for DNA binding (Bauer et al. 1999). One would presume that, in times of Fe limitation, FnrL would be devoid of this Fe-S cluster leading to an alteration of *hem* gene expression. In *Rubrivivax gelatinosus*, FnrL was shown to control heme synthesis by regulating *hemN* expression (Ouchane et al. 2007) (Table 25.1).

## IV. Regulating Cytochrome Apoprotein Synthesis

### A. Transcription Control

#### 1. Redox Regulation

Evidence to date indicates that purple photosynthetic bacteria (and by conjecture other photosynthetic organisms) regulate apocytochrome synthesis by both transcriptional and post-transcriptional mechanisms. At the transcription level, several studies in *Rb. capsulatus* and in *Rb. sphaeroides* show that cytochrome encoding gene expression is redox-controlled by many of the same regulators that regulate heme synthesis. For example, as summarized in Fig. 25.3, the RegB-RegA signal transduction cascade, which is a major regulator of heme synthesis, also controls the expression of cytochrome encoding genes in both *Rb. capsulatus* and in *Rb. sphaeroides* (Eraso and Kaplan 1994; Karls et al. 1999; Swem et al. 2001). For example, reporter studies, coupled with DNA binding footprint assays, have demonstrated that phosphorylated RegA binds to the promoter regions of *cycA* (cytochrome *c*<sub>2</sub>), *cycY* (cytochrome *c*<sub>y</sub>), *ccoNOQP* (*cbb3*-Cox), *cydAB* (ubiquinol oxidase) and *petABC* (cytochrome *bc*<sub>1</sub>) in *Rb. capsulatus* (Swem et al. 2001). It has also been demonstrated that *cycA* is directly regulated by PrrA, the RegA homolog in *Rb. sphaeroides* (Eraso and Kaplan 1994; Karls et al. 1999). In *Rb. capsulatus*, each of these cytochromes are involved in either the photosynthetic or respiratory electron transport chain or both. Specifically, two electrons from the photosynthesis reaction center oxi-

Table 25.1. Known transcription factors that affect synthesis of heme and cytochromes.

Transcription factor	Cofactor	Function regulated
RegB-RegA	Ubiquinone, Cu <sup>+</sup>	Heme, BChl, PS, cytochrome apoprotein synthesis
CrtJ/PpsR	Heme	Heme, BChl, PS, cytochrome apoprotein synthesis
HbrL	Heme	Heme synthesis, iron transport
FnrL	4Fe-4S cluster	Heme synthesis
FixLJ-FiK	Heme	Heme, BChl, PS, cytochrome apoprotein synthesis
FurA	Heme	Heme synthesis, iron transport

dized by light, enter the ubiquinone pool by release of reduced ubiquinone from the reaction center. Electrons from the ubiquinone pool are shuttled back to the reaction center by first passing through the membrane bound cytochrome *bc*<sub>1</sub> complex and to either cytochrome *c*<sub>2</sub> or cytochrome *c*<sub>y</sub> that then reduces the oxidized reaction center (Fig. 25.3). When oxygen is present, the electrons preferentially pass from cytochrome *c*<sub>2</sub> or cytochrome *c*<sub>y</sub> to *cbb*<sub>3</sub>-Cox, essentially bypassing the reaction center and thereby ensuring that respiration occurs preferentially relative to photosynthesis. Ubiquinol oxidase can also reduce oxygen to water by obtaining electrons directly from the ubiquinone pool (Fig. 25.2). Given that photosynthesis adds electrons to the ubiquinone pool, and that respiration removes electrons from the ubiquinone pool, it is not surprising that the ubiquinone pool is significantly more reduced under photosynthetic growth conditions than under respiratory growth conditions (Grammel and Ghosh 2008; Klamt et al. 2008). Thus, controlling RegB kinase activity in response to alterations of the redox state of the ubiquinone pool provides a facile way of monitoring whether oxygen is present or absent as a substrate for respiration (Fig. 25.4).

One interesting aspect of respiratory cytochrome synthesis in *Rb. capsulatus* is that *cbb*<sub>3</sub>-Cox is maximally expressed under semi-aerobic and aerobic growth conditions, whereas ubiquinol oxidase is maximally expressed under anaerobic/semi-aerobic conditions (Swem and Bauer 2002; Swem et al. 2003). It is proposed that *cbb*<sub>3</sub>-Cox has a lower affinity but a higher turnover for substrate oxygen than does ubiquinol oxidase, which is proposed to have a higher affinity for oxygen with a lower substrate turnover (Swem and Bauer 2002). Thus, as cultures go from high to low oxygen tension *cbb*<sub>3</sub>-Cox will be used preferentially followed by ubiquinol oxidase. It is of interest that unphosphorylated RegA appears to function as an aerobic activator of *cbb*<sub>3</sub>-Cox while RegA~P appears to function as an anaerobic repressor (Swem and Bauer

2002; Swem et al. 2003). In contrast, both RegA and RegA~P function as aerobic and anaerobic activators of ubiquinol oxidase (Swem and Bauer 2002; Swem et al. 2003).

Additional studies on respiratory cytochrome gene expression in *Rb. capsulatus* indicate that ubiquinol oxidase expression is also aerobically repressed by CrtJ and by its coregulator AerR, while *cbb*<sub>3</sub>-Cox is anaerobically activated by FnrL (Swem and Bauer 2002; Swem et al. 2003). Such an FnrL-dependent activation of *ccoNOQP*, which encodes *cbb*<sub>3</sub>-Cox, was also observed in *Rb. sphaeroides* under microaerophilic conditions (Mouncey and Kaplan 1998). This latter result is supported by the presence of a putative FnrL binding site located between two RegA binding sites in the *Rb. capsulatus ccoNOQP* promoter region, indicating that FnrL has a direct role in controlling *cbb*<sub>3</sub>-Cox biosynthesis (Swem et al. 2003). In addition, FnrL is also absolutely required for anaerobic synthesis of dimethyl sulfoxide (DMSO) reductase that utilizes the alternative respiratory electron acceptors DMSO and trimethylamine oxide (Zeilstra-Ryalls et al. 1997). This requirement of FnrL is of interest given that it has an oxygen labile 4Fe-4S cluster that is needed for DNA binding (Bauer et al. 1999). Thus, the expression of *cbb*<sub>3</sub>-Cox, DMSO reductase and heme biosynthesis are all likely to be impaired under periods of iron stress.

In *Rubrivivax gelatinosus*, deletion of *fnrL* also resulted in the loss of *c*-type cytochromes and PpsR was found to be involved in the expression of the cytochrome *bd* quinol oxidase in aerobic conditions (Ouchane et al. 2007; Hassani et al. 2010b). In this organism, a model was established that described the equilibrium between the use of *bd* quinol oxidase and *cbb*<sub>3</sub>-Cox under aerobic and micro-aerobic conditions, respectively. Such equilibrium is dependent on both FnrL and PprsR (Ouchane et al. 2007; Hassani et al. 2010b).

Another redox control of *cbb*<sub>3</sub>-Cox occurs through the FixLJ-FixK system in *Rhodospseudomonas palustris*, where the oxygen sensor FixL phosphorylates FixJ

that, in turn, activates the transcription factor FixK. FixL uses a heme group to sense O<sub>2</sub> and to subsequently control the phosphorylation of FixJ in an oxygen dependent manner. Phosphorylated FixJ subsequently transcribes FixK which then activates transcription of heme synthesis genes as well as *ccoNOPQ* and *coxBAEFGC*, coding for *cbb*<sub>3</sub>-type and putative *aa*<sub>3</sub>-type cytochrome oxidases, respectively. Moreover, the FixK regulon also includes a putative homolog of the response regulator, Irr, that is known to control expression of iron transport genes in response to heme availability (Qi and O'Brian 2002). This complex regulatory cascade further illustrates the interconnection that exists between iron homeostasis, heme biosynthesis, and cytochrome regulation (Rey and Harwood 2010).

Beyond purple bacteria, the control of cytochrome gene expression is widely unstudied. In the cyanobacterium *Synechocystis* sp. PCC 6803, it has been shown that the addition of glucose to the culture results in increased expression of cytochrome *c* oxidase and ubiquinol oxidase (Lee et al. 2007). The mechanism of this regulation has not been studied.

## 2. Promoter Selectivity

Schilke and Donohue (1992) initially demonstrated that expression of the *cycA* gene coding for cytochrome *c*<sub>2</sub> was affected by heme availability. They reported that addition of ALA to cells resulted in a five to sevenfold increase in expression of *cycA*. A genetic selection for mutants that were altered in heme regulation of *cycA* expression was subsequently found to result in the isolation of a *Rb. sphaeroides* mutant, ChrR, that has increased *cycA* and *hemA* expression (Schilke and Donohue 1992).

Detailed analysis of the *Rb. sphaeroides cycA* gene has demonstrated that it contains three promoters driving its expression (Karls et al. 1998; MacGregor et al. 1998). The P1 promoter is recognized by the alternative heat shock sigma factor  $\sigma^{32}$  (Karls et al.

1998). The P2 promoter is recognized by the housekeeping sigma factor  $\sigma^{70}$  and is also regulated by PrrA (Karls et al. 1999), and the third promoter P3 is recognized by  $\sigma^E$  that is regulated by ChrR (Schilke and Donohue 1992; Newman et al. 1999). Detailed studies of  $\sigma^E$  and ChrR show that ChrR is a zinc binding anti-repressor of  $\sigma^E$  with the binding of ChrR to  $\sigma^E$  affected by singlet oxygen (<sup>1</sup>O<sub>2</sub>). Because ChrR was originally found to respond to a signal from the tetrapyrrole synthesis pathway, this latter involvement of <sup>1</sup>O<sub>2</sub> is intriguing given that <sup>1</sup>O<sub>2</sub> is generated as a byproduct of light excitation of Chl.

## B. Post-translational Regulation

In addition to transcriptional regulation of cytochrome synthesis, there is considerable evidence that the stability of cytochrome apoproteins is regulated in order to achieve proper assembly of cytochromes with their cofactors (heme and copper) and partner subunits as detailed below. An excellent review on this topic has recently been published by Ekici et al. (2012a) and only highlights of this process will be covered here. Briefly, the biogenesis of *cbb*<sub>3</sub>-Cox involves a plethora of actors (cofactors, chaperones, subunits, ...) and mechanisms. Maturation of the catalytic subunit CcoN requires integration of heme *b* and copper co-factors, while CcoO and CcoP are targets of the heme *c* maturation pathway Ccm. The biogenesis involves copper chaperones, disulphide oxidoreductases, and specific membrane lipids (Ekici et al. 2012a). In addition, Oh and Kaplan (2002) initially demonstrated that loss of CcoQ resulted in destabilization of *cbb*<sub>3</sub>-Cox in *Rb. sphaeroides*. They proposed that CcoQ was involved in protecting the *cbb*<sub>3</sub>-Cox core complex (CcoN, CcoO and CcoP) from oxidation and loss of heme. In *Rb. capsulatus*, Peters et al. (2008) also demonstrated that loss of CcoQ resulted in instability of *cbb*<sub>3</sub>-Cox and further showed that CcoQ specifically interacted with CcoP. A second assembly protein called CcoH has also been identified that affects stability

of the CcoP-CcoQ complex (Pawlik et al. 2010). As heme-copper cytochrome CcoN and *c*-type cytochromes CcoO and CcoP follow separate post-translational maturation process, fine-tuned regulation has to occur to obtain a functional *ccb*<sub>3</sub>-Cox complex. On the one hand, strains harboring mutations in CcoN have proven to display abnormal amounts of CcoO and CcoP (Koch et al. 1998). On the other hand, biogenesis of CcoN was shown to still occur in Ccm defective mutants (Ekici et al. 2013).

Finally, the coupling of heme and cytochrome synthesis was further illustrated by a *Rb. capsulatus* strain that lacks *c*-type cytochromes while having a normal content of *b*-type cytochromes. This strain was shown to excrete a massive amount of coproporphyrin and protoporphyrin (1.8 and 0.9 μM, respectively), while synthesizing less BChl. Although the mechanism is not clear, it involves a mutation in the cytochrome *c* maturation system (Biel and Biel 1990). Chlorophyll were also found in purified preparations of cytochrome *b*<sub>6f</sub> in *Chlamydomonas reinhardtii* (Pierre et al. 1997). Interestingly, synthesis of chlorophyll is also found to be necessary to accumulate cytochrome *b*<sub>6f</sub> in both *Chlamydomonas reinhardtii* and *Arabidopsis thaliana* (Pierre et al. 1997; Pontier et al. 2007; Meinecke et al. 2010). Heme and Mg-PPIX were also showed to exert influence on the expression of cytochrome *b*<sub>5</sub> and a putative cytochrome *c* oxidase assembly protein COX17 (Voss et al. 2011).

## V. Metal Homeostasis and Cytochrome Regulation

### A. Iron Homeostasis

Harnessed by four linked pyrroles, iron is the key component of heme that provides this tetrapyrrole a capability to accept and donate electrons and gases. As such, iron bound to heme is *the* critical element of cytochromes. Owing to the toxicity of free iron, its acquisition is highly regulated

and also has an impact on both heme and cytochrome synthesis. The coupling of iron homeostasis with heme biosynthesis was initially observed in the purple bacterium *Rb. sphaeroides* by Lascelles (1956). In conditions of iron deficiency, *Rb. sphaeroides* was observed to produce limited amounts of heme coupled to an increased accumulation of the heme precursor coproporphyrin (Lascelles 1956; Lascelles and Hatch 1969). More recent studies show that numerous genes coding for iron transporters and heme synthesizing enzymes were simultaneously upregulated in the purple bacterium *Rb. capsulatus* under conditions of iron scarcity (Zappa and Bauer 2013). As mentioned earlier, the LysR-type transcription factor appeared critical in this global activation that couples iron homeostasis and heme synthesis (Zappa and Bauer 2013). Likewise, in the cyanobacterium *Anabaena* sp. PCC 7120, iron deficiency induced the transcription of genes involved in iron homeostasis, heme synthesis and heme degradation. A homologue of the ferric uptake regulator, FurA, was found to be involved in coupling iron homeostasis and heme synthesis in these cyanobacteria (González et al. 2012). This coregulation is, however not universal in all species and nor even at the strain level in cyanobacteria. For example, the transcription of *hemA*, which encodes GluTR, was found to be down-regulated in a MED4 strain of *Prochlorococcus*, while it was stable in the MIT9313 strain under low iron conditions (Thompson et al. 2011).

Interdependence of iron homeostasis with the synthesis of cytochromes involved in photosynthesis has been extensively studied in cyanobacteria. Iron stress in cyanobacteria triggers a number of survival strategies such as the excretion of siderophores to take up iron from the environment, and the reduction of iron demand. The latter strategy consists of replacing an iron-utilizing enzyme by a non-iron utilizing enzyme, e.g. ferredoxin by flavodoxin. Overall, iron-containing enzymes in the photosynthetic electron chain, such as cytochromes, have their cellular level reduced during iron starvation (Ferreira and

Straus 1994). Under low iron conditions, the transcription of *petA* and *petC*, encoding cytochrome *b<sub>6f</sub>* subunits, is down-regulated in *Prochlorococcus* (Thompson et al. 2011). Similar observations were made regarding the PetB and PetC subunits of cytochrome *b<sub>6f</sub>* in *Trichodesmium erythraeum* (Shi et al. 2007). The content of cytochrome *b<sub>6f</sub>*, as observed from the assay of the PetC (Rieske) subunit, was found to be reduced in *Synechococcus elongatus* PCC 7942, and even more in *Synechocystis* sp. PCC 6803, where this results in a dramatic fourfold decrease of the *b<sub>6f</sub>*:PSII ratio (Fraser et al. 2013). Similarly, cytochrome *f* of *Synechococcus* sp. PCC 7942 was reduced to 40 % of its original content under iron limitation (Sandström et al. 2002).

### B. Copper Homeostasis

Several cytochrome *c* oxidases, such as *cbb<sub>3</sub>* and *aa<sub>3</sub>*, are both heme and copper containing enzymes. The biogenesis of *cbb<sub>3</sub>*-Cox in *Rb. capsulatus* and *Rb. sphaeroides* has been recently reviewed (Ekici et al. 2012a). Since proper enzyme activity is dependent on copper availability, this section first focuses on cellular processes that connect copper homeostasis to the regulation of *cbb<sub>3</sub>*-Cox. In both *Rhodobacter* species, *cbb<sub>3</sub>*-Cox apoprotein is the product of the *ccoNOQP* operon, where CcoN is a membrane-embedded catalytic subunit that harbors both heme *b* and a copper center. How the cell imports copper and integrates it into cytochromes is not fully understood, but in the case of *cbb<sub>3</sub>*-Cox, the copper acquisition protein CcoA was recently discovered (Ekici et al. 2012b, 2014). CcoA is a member of the “Major Facilitator Superfamily” of transporters, members of which have 12 transmembrane helices (Reddy et al. 2012). Deletion of *ccoA* induces lower cellular copper content and a failure to achieve normal assembly of an active *cbb<sub>3</sub>*-Cox, with such a phenotype being partially alleviated by exogenous copper supplementation (Ekici et al. 2012b). CcoA showed limited influence on both

transcription and translation of CcoN, which suggests post-translational regulation (Ekici et al. 2012b). Suppressors of a *ccoA* mutant displaying functional *cbb<sub>3</sub>*-Cox harbor mutations that impair the activity of CopA, a copper efflux transporter (Ekici et al. 2014). Thus, proper assembly of *cbb<sub>3</sub>*-Cox depends on a copper homeostasis system consisting (at least) of the importer CcoA and the exporter CopA. Moreover, screening for a subset of *ccoA* mutants that do not respond to copper supplementation led to strains harboring mutations in the Ccm cytochrome maturation system. Interestingly, porphyrin secretion that can be observed in Ccm deleted strains seems to be decreased by addition of exogenous copper (Ekici et al. 2013). Although no clear model exists at this time, these findings indicate an influence of copper on post-translational maturation of both *b*- and *c*-type subunits of *cbb<sub>3</sub>*-Cox. Other *cbb<sub>3</sub>*-Cox maturation components include CcoI and, possibly, CcoG. CcoI is critical for *cbb<sub>3</sub>*-Cox biogenesis and is a P-type ATPase that transports copper across the cytoplasmic membrane to the periplasm. It takes part in the insertion of the copper ion into CcoN, although the detailed mechanism remains to be elucidated (Ekici et al. 2012a). The role of CcoG is still unclear, partially due to lack of a defined phenotype of the CcoG mutant. However, involvement in redox balance of Cu<sup>+</sup>/Cu<sup>2+</sup> between copper import (CcoA) and export (CcoI) has been hypothesized (Ekici et al. 2012a).

In addition to the copper transport proteins described above, the putative copper chaperone SenC in *Rb. capsulatus*, is involved in maturation of *cbb<sub>3</sub>*-Cox (Lohmeyer et al. 2012). SenC is a membrane-anchored protein that was shown to bind copper. Moreover, mutants lacking SenC are defective in *cbb<sub>3</sub>*-Cox, with this phenotype capable of being rescued by copper supplementation. SenC interacts with the subunits CcoP and CcoH (Lohmeyer et al. 2012). Interestingly, the impact of a SenC deletion on *cbb<sub>3</sub>*-Cox maturation is pronounced at the usual and optimum growth temperature (35 °C), but not at 20 °C. Finally, whereas SenC seems



to affect the assembly of *cbb<sub>3</sub>*-Cox post-translationally, the transcription of *senC* itself depends on the presence of the copper efflux pump CcoI (Lohmeyer et al. 2012). Interestingly, PrrC, the SenC homologue in *Rb. sphaeroides*, does not appear to be involved in *cbb<sub>3</sub>*-Cox assembly (Eraso and Kaplan 2000). Finally, a periplasmic *Cu<sub>A</sub>*-chaperone (PCu<sub>A</sub>C) homologue was identified in *Rb. capsulatus*, despite this species not harboring a *aa<sub>3</sub>*-type *Cu<sub>A</sub>*-containing cytochrome oxidase (Ekici et al. 2012a; Lohmeyer et al. 2012). A potential role in trafficking copper between CcoI and CcoN has been suggested, although no evidence has been provided (Lohmeyer et al. 2012).

A model was recently proposed to describe how purple bacteria manage the toxicity of copper with its requirement for cytochrome *c* oxidases. In *Rubrivivax gelatinosus*, two *Cu<sup>2+</sup>*-P1-type ATPases were characterized: CtpA (a homologue to *Rb. capsulatus* CcoI and *Rb. sphaeroides* RdxI), and CopA. Interestingly, CtpA was shown necessary for assembly of both cytochrome oxidases *cbb<sub>3</sub>* and *caa<sub>3</sub>*, while CopA does not take part in cytochrome biogenesis but alleviates copper toxicity (Hassani et al. 2010a; Azzouzi et al. 2013). In copper replete conditions, a *copA* mutant was shown to excrete coproporphyrin III, and have less cytochrome *c* oxidase. In the absence of CopA, copper seems to deregulate the synthesis of heme at the HemN step, which results in a decrease in cytochrome oxidase. The mechanism of copper toxicity on the HemN enzyme may involve the destabilization of the 4Fe-4S cluster. Such a mechanism highlights the delicate equilibrium of copper necessity in cytochrome assembly versus its toxic impact on heme precursor synthesis (Hassani et al. 2010a; Azzouzi et al. 2013). Moreover, CopA homologues are present in *Rb. capsulatus* and *Rb. sphaeroides* so this model could be extended to other purple bacteria (Ekici et al. 2012b; Azzouzi et al. 2013; Ekici et al. 2014).

### C. Iron and Copper Homeostasis Interplay with Cytochrome Regulation

Cyanobacteria display a useful example of the influence of iron and copper homeostasis on the synthesis/stability of cytochromes in the photosynthetic electron transport chain. Indeed, cytochrome *b<sub>6</sub>f* transfers electrons to PSI through either cytochrome *c<sub>553</sub>* (cytochrome *c<sub>6</sub>*) or plastocyanin, which utilizes copper as a co-factor. Under iron stress, cyanobacterial siderophore production also lowers copper availability, since iron binding siderophores also display a high affinity for copper (Ferreira and Straus 1994). However, unlike ferrisiderophores, the *Cu<sup>2+</sup>*-siderophore complexes are not imported into the cell, hence generating copper limiting conditions. As a result, copper limitation is induced under iron stress, resulting in the preferential use of cytochrome *c<sub>6</sub>* over plastocyanin. This situation, starting with iron limitation and ending with the preferential use of an iron-using cytochrome over a copper-using protein, is counterintuitive. However, the rationale underlying these observations is that the pool of cytochrome *c<sub>6</sub>* is limited. Such an “imperfection” in the iron-sparing mechanism may be a small price to pay for an effective siderophore machinery that enables both iron scavenging and alleviation of copper toxicity. Interestingly, some cyanobacteria have lost the plastocyanin homologue in the process of natural selection and rely solely on cytochrome *c<sub>6</sub>*, even during iron starvation (Ferreira and Straus 1994). Moreover, the *Fe<sup>3+</sup>* transporter FutA<sub>2</sub> in *Synechocystis* sp. PCC 6803 was shown to be involved in this plastocyanin-cytochrome *c<sub>6</sub>* switch. Indeed, the *futA<sub>2</sub>* deleted mutant showed low cytochrome *c* activity and fails to produce cytochrome *c<sub>6</sub>* instead of plastocyanin (Waldron et al. 2007).

Copper interference with cytochrome regulation takes place also at the aforementioned switch between plastocyanin and cytochrome *c<sub>6</sub>* in cyanobacteria. Indeed, such

a switch depends not only on iron but also on copper availability, as extracellular copper levels were shown to regulate transcription of both electron transporters (Zhang et al. 1992). In *Synechocystis* sp. PCC 6803, two  $\text{Cu}^{2+}$  transporters of the P1-ATPase family were described, as required for an efficient switch: CtaA and PacS, involved in cellular import and compartmentalization into thylakoids, respectively (Tottey et al. 2001). A copper chaperone, Atx1, acting with PacS, is also involved (Tottey et al. 2002).

## VI. Concluding Remarks

Cytochromes are major electron carriers in photosynthetic organisms responsible for moving electrons among various components of the photosynthetic apparatus as well as to terminal electron acceptor complexes such as cytochrome oxidases. As such, they are, in large part, responsible for keeping a proper redox poise in cells that are continually challenged by a highly varying input of electrons from photosynthesis as well as from cellular metabolic pathways.

Cytochromes use iron bound to heme and, in some cases one or more bound coppers, as redox active centers to accept and donate electrons (Fig. 25.1). Both of these metals are toxic when not bound to cytochrome apoproteins. The same toxicity occurs when heme is not bound to cytochrome apoprotein. Not surprisingly, a high level of coordination occurs between the import of iron and copper for the synthesis of heme and cytochrome apoproteins. When iron, copper or heme synthesis is impaired, then the synthesis of cytochrome apoproteins is also inhibited.

Clearly the synthesis of cytochrome apoproteins depends on highly regulated events, and a molecular understanding of this regulation remains incomplete. Evidence is accumulating that there is a complex connection in the coregulation of cytochrome apoproteins with enzymes involved in iron transport and heme biosynthesis. It is intriguing that the redox state of the

ubiquinone pool, which is highly affected by the activity of cytochromes, is a major input to the control of the RegB-RegA signal transduction cascade. This signaling cascade is responsible for controlling expression of genes that code for enzymes in heme biosynthesis and cytochrome apoproteins in anoxygenic phototrophs. The interconnections of iron transport with heme and cytochrome synthesis is further highlighted in anoxygenic bacteria where the DNA-binding transcription factors FnrL, PpsR and HbrL, which control iron transport, heme synthesis and apocytochrome synthesis, themselves bind either iron or heme as a cofactor. A major challenge will be to extend similar studies on the regulation of cytochrome biosynthesis to eukaryotic algae and plants where additional cellular processes such as organelle compartmentalization add further layers of complexity.

## References

- Anzaldi LL, Skaar EP (2010) Overcoming the heme paradox: heme toxicity and tolerance in bacterial pathogens. *Infect Immun* 78:4977–4989
- Azzouzi A, Steunou A-S, Durand A, Khalfouli-Hassani B, Bourbon M-L, Astier C, Bollivar DW, Ouchane S (2013) Coproporphyrin III excretion identifies the anaerobic coproporphyrinogen III oxidase HemN as a copper target in the  $\text{Cu}^{+}$ -ATPase mutant copA<sup>-</sup> of *Rubrivivax gelatinosus*. *Mol Microbiol* 88:339–351
- Banerjee R, Ragsdale SW (2003) The many faces of vitamin B12: catalysis by cobalamin-dependent enzymes. *Annu Rev Biochem* 72:209–247
- Bauer CE, Elsen S, Bird TH (1999) Mechanisms for redox control of gene expression. *Annu Rev Microbiol* 53:495–523
- Beale SI (1978)  $\delta$ -Aminolevulinic acid in plants: its biosynthesis, regulation, and role in plastid development. *Annu Rev Plant Physiol* 29:95–120
- Beale SI, Castelfranco PA (1973)  $^{14}\text{C}$  incorporation from exogenous compounds into  $\delta$ -aminolevulinic acid by greening cucumber cotyledons. *Biochem Biophys Res Commun* 52:143–149
- Biel SW, Biel AJ (1990) Isolation of a *Rhodobacter capsulatus* mutant that lacks *c*-type cytochromes and excretes porphyrins. *J Bacteriol* 172:1321–1326

- Bird TH, Du S, Bauer CE (1999) Autophosphorylation, phosphotransfer, and DNA-binding properties of the RegB/RegA two-component regulatory system in *Rhodobacter capsulatus*. *J Biol Chem* 274:16343–16348
- Burnham BF, Lascelles J (1963) Control of porphyrin biosynthesis through a negative-feedback mechanism. Studies with preparations of  $\delta$ -aminolaevulate synthetase and  $\delta$ -aminolaevulate dehydratase from *Rhodopseudomonas spheroides*. *Biochem J* 87:462–472
- Cheng Z, Wu J, Setterdahl A, Reddie K, Carroll K, Hammad LA, Karty JA, Bauer CE (2012) Activity of the tetrapyrrole regulator CrtJ is controlled by oxidation of a redox active cysteine located in the DNA binding domain. *Mol Microbiol* 85:734–746
- Chereskin BM, Castelfranco PA (1982) Effects of iron and oxygen on chlorophyll biosynthesis: II. Observations on the biosynthetic pathway in isolated etiochloroplasts. *Plant Physiol* 69:112–116
- Chiancone E, Ceci P, Ilari A, Ribacchi F, Stefanini S (2004) Iron and proteins for iron storage and detoxification. *Biometals* 17:197–202
- Cornelis P, Wei Q, Andrews SC, Vinckx T (2011) Iron homeostasis and management of oxidative stress response in bacteria. *Metallomics* 3:540–549
- Dupont CL, Grass G, Rensing C (2011) Copper toxicity and the origin of bacterial resistance – new insights and applications. *Metallomics* 3:1109–1118
- Ekici S, Pawlik G, Lohmeyer E, Koch H-G, Daldal F (2012a) Biogenesis of cbb(3)-type cytochrome c oxidase in *Rhodobacter capsulatus*. *Biochim Biophys Acta* 1817:898–910
- Ekici S, Yang H, Koch H-G, Daldal F (2012b) Novel transporter required for biogenesis of cbb3-type cytochrome c oxidase in *Rhodobacter capsulatus*. *mBio* 3:e00293-11
- Ekici S, Jiang X, Koch H-G, Daldal F (2013) Missense mutations in cytochrome c maturation genes provide new insights into *Rhodobacter capsulatus* cbb3-type cytochrome c oxidase biogenesis. *J Bacteriol* 195:261–269
- Ekici S, Turkarlan S, Pawlik G, Dancis A, Baliga NS, Koch HG, Daldal F (2014) Intracytoplasmic copper homeostasis controls cytochrome c oxidase production. *mBio* 5:e01055-13
- Elsen S, Ponnampalam SN, Bauer CE (1998) CrtJ bound to distant binding sites interacts cooperatively to aerobically repress photopigment biosynthesis and light harvesting II gene expression in *Rhodobacter capsulatus*. *J Biol Chem* 273:30762–30769
- Eraso JM, Kaplan S (1994) *prpA*, a putative response regulator involved in oxygen regulation of photosynthesis gene expression in *Rhodobacter sphaeroides*. *J Bacteriol* 176:32–43
- Eraso JM, Kaplan S (2000) From redox flow to gene regulation: role of the PrrC protein of *Rhodobacter sphaeroides* 2.4.1. *Biochemistry* 39:2052–2062
- Ferreira F, Straus NA (1994) Iron deprivation in cyanobacteria. *J Appl Phycol* 6:199–210
- Frankenberg N, Moser J, Jahn D (2003) Bacterial heme biosynthesis and its biotechnological application. *Appl Microbiol Biotechnol* 63:115–127
- Fraser JM, Tulk SE, Jeans JA, Campbell DA, Bibby TS, Cockshutt AM (2013) Photophysiological and photosynthetic complex changes during iron starvation in *Synechocystis* sp. PCC 6803 and *Synechococcus elongatus* PCC 7942. *PLoS One* 3:e59861
- Gomelsky M, Kaplan S (1995) Genetic evidence that PpsR from *Rhodobacter sphaeroides* 2.4.1 functions as a repressor of *puc* and *bchF* expression. *J Bacteriol* 177:1634–1637
- González A, Bes MT, Valladares A, Peleato ML, Fillat MF (2012) FurA is the master regulator of iron homeostasis and modulates the expression of tetrapyrrole biosynthesis genes in *Anabaena* sp. PCC 7120. *Environ Microbiol* 14:3175–3187
- Graça-Souza AV, Maya-Monteiro C, Paiva-Silva GO, Braz GRC, Paes MC, Sorgine MHF, Oliveira MF, Oliveira PL (2006) Adaptations against heme toxicity in blood-feeding arthropods. *Insect Biochem Mol Biol* 36:322–335
- Grammel H, Ghosh R (2008) Redox-state dynamics of ubiquinone-10 imply cooperative regulation of photosynthetic membrane expression in *Rhodospirillum rubrum*. *J Bacteriol* 190:4912–4921
- Hassani BK, Astier C, Nitschke W, Ouchane S (2010a) CtpA, a copper-translocating P-type ATPase involved in the biogenesis of multiple copper-requiring enzymes. *J Biol Chem* 295:19330–19337
- Hassani BK, Steunou A-S, Liotenberg S, Reiss-Husson F, Astier C, Ouchane S (2010b) Adaptation to oxygen: role of terminal oxidases in photosynthesis initiation in the purple photosynthetic bacterium, *Rubrivivax gelatinosus*. *J Biol Chem* 285:19891–19899
- Huang D-D, Wang W-y (1986a) Genetic control of chlorophyll biosynthesis: regulation of delta-aminolevulinatase synthesis in *Chlamydomonas*. *Mol Gen Genet* 205:217–220
- Huang D-D, Wang W-y (1986b) Chlorophyll biosynthesis in *Chlamydomonas* starts with the formation of glutamyl-tRNA. *J Biol Chem* 261:13451–13455
- Inoue K, Kouadio JL, Mosley CS, Bauer CE (1995) Isolation and in vitro phosphorylation of sensory transduction components controlling anaerobic induction of light harvesting and reaction center gene expression in *Rhodobacter capsulatus*. *Biochemistry* 34:391–396

- Karls RK, Brooks J, Rossmeissl P, Luedke J, Donohue TJ (1998) Metabolic roles of a *Rhodobacter sphaeroides* member of the sigma32 family. *J Bacteriol* 180:10–19
- Karls RK, Wolf JR, Donohue TJ (1999) Activation of the *cycA* P2 promoter for the *Rhodobacter sphaeroides* cytochrome c2 gene by the photosynthesis response regulator. *Mol Microbiol* 34:822–835
- Kim Y-J, Ko I-J, Lee J-M, Kang H-Y, Kim YM, Kaplan S, Oh J-I (2007) Dominant role of the *cbb3* oxidase in regulation of photosynthesis gene expression through the PrrBA system in *Rhodobacter sphaeroides* 2.4.1. *J Bacteriol* 189:5617–5625
- Klamt S, Grammel H, Straube R, Ghosh R, Gilles ED (2008) Modeling the electron transport chain of purple non-sulfur bacteria. *Mol Syst Biol* 4:1–19
- Koch HG, Hwang O, Daldal F (1998) Isolation and characterization of *Rhodobacter capsulatus* mutants affected in cytochrome *cbb3* oxidase activity. *J Bacteriol* 180:969–978
- Kumar S, Bandyopadhyay U (2005) Free heme toxicity and its detoxification systems in human. *Toxicol Lett* 157:175–188
- Kumar AM, Schaub U, Söll D, Ujwal ML (1996) Glutamyl-transfer RNA: at the crossroad between chlorophyll and protein biosynthesis. *Trends Plant Sci* 1:371–376
- Lascelles J (1956) The synthesis of porphyrins and bacteriochlorophyll in cell suspensions of *Rhodospseudomonas sphaeroides*. *Biochem J* 62:78–93
- Lascelles J (1960) The synthesis of enzymes concerned in bacteriochlorophyll formation in growing cultures of *Rhodospseudomonas sphaeroides*. *J Gen Microbiol* 23:487–498
- Lascelles J, Hatch TP (1969) Bacteriochlorophyll and heme synthesis in *Rhodospseudomonas sphaeroides*: possible role of heme in regulation of the branched biosynthetic pathway. *J Bacteriol* 98:712–720
- Lee S, Ryu J-Y, Kim SY, Jeon J-H, Song JY, Cho H-T, Choi S-B, . . . , Park YI (2007) Transcriptional regulation of the respiratory genes in the cyanobacterium *Synechocystis* sp. PCC 6803 during the early response to glucose feeding. *Plant Physiol* 145:1018–1030
- Lohmeyer E, Schröder S, Pawlik G, Trasnea P-I, Peters A, Daldal F, Koch H-G (2012) The ScoI homologue SenC is a copper binding protein that interacts directly with the *cbb3*-type cytochrome oxidase in *Rhodobacter capsulatus*. *Biochim Biophys Acta* 1817:2005–2015
- MacGregor BJ, Karls RK, Donohue TJ (1998) Transcription of the *Rhodobacter sphaeroides cycA* P1 promoter by alternate RNA polymerase holoenzymes. *J Bacteriol* 180:1–9
- Macomber L, Imlay JA (2009) The iron-sulfur clusters of dehydratases are primary intracellular targets of copper toxicity. *Proc Natl Acad Sci U S A* 106:8344–8349
- Masuda S, Bauer CE (2002) AppA is a blue light photoreceptor that antirepresses photosynthesis gene expression in *Rhodobacter sphaeroides*. *Cell* 110:613–623
- Masuda S, Dong C, Swem D, Setterdahl AT, Knaff DB, Bauer CE (2002) Repression of photosynthesis gene expression by formation of a disulfide bond in CrtJ. *Proc Natl Acad Sci U S A* 99:7078–7083
- Meinecke L, Alawady A, Schroda M, Willows R, Kobayashi MC, Niyogi KK, Grimm B, Beck CF (2010) Chlorophyll-deficient mutants of *Chlamydomonas reinhardtii* that accumulate magnesium protoporphyrin IX. *Plant Mol Biol* 72:643–658
- Moskvin OV, Gomelsky L, Gomelsky M (2005) Transcriptome analysis of the *Rhodobacter sphaeroides* PpsR regulon: PpsR as a master regulator of photosystem development. *J Bacteriol* 187:2148–2215
- Mosley CS, Suzuki JY, Bauer CE (1994) Identification and molecular genetic characterization of a sensor kinase responsible for coordinately regulating light harvesting and reaction center gene expression in response to anaerobiosis. *J Bacteriol* 176:7566–7573
- Mouncey NJ, Kaplan S (1998) Oxygen regulation of the *ccoN* gene encoding a component of the *cbb3* oxidase in *Rhodobacter sphaeroides* 2.4.1 T: involvement of the FnrL protein. *J Bacteriol* 180:2228–2231
- Neidle EL, Kaplan S (1993a) Expression of the *Rhodobacter sphaeroides* hemA and hemT genes, encoding two 5-aminolevulinic acid synthase isozymes. *J Bacteriol* 175:2292–2303
- Neidle EL, Kaplan S (1993b) 5-Aminolevulinic acid availability and control of spectral complex formation in hemA and hemT mutants of *Rhodobacter sphaeroides*. *J Bacteriol* 175:2304–2313
- Newman JD, Falkowski MJ, Schilke BA, Anthony LC, Donohue TJ (1999) The *Rhodobacter sphaeroides* ECF sigma factor, sigma(E), and the target promoters *cycA* P3 and *rpoE* P1. *J Mol Biol* 294:307–320
- O’Gara JP, Eraso JM, Kaplan S (1998) A redox-responsive pathway for aerobic regulation of photosynthesis gene expression in *Rhodobacter sphaeroides* 2.4.1. *J Bacteriol* 180:4044–4050
- Oh JI, Kaplan S (1999) The *cbb3* terminal oxidase of *Rhodobacter sphaeroides* 2.4.1: structural and

- functional implications for the regulation of spectral complex formation. *Biochemistry* 38:2688–2696
- Oh JI, Kaplan S (2002) Oxygen adaptation. The role of the CcoQ subunit of the cbb3 cytochrome c oxidase of *Rhodobacter sphaeroides* 2.4.1. *J Biol Chem* 277:16220–16228
- Osman D, Cavet JS (2008) Copper homeostasis in bacteria. *Adv Appl Microbiol* 65:217–247
- Ouchane S, Picaud M, Therizols P, Reiss-Husson F, Astier C (2007) Global regulation of photosynthesis and respiration by FnrL: the first two targets in the tetrapyrrole pathway. *J Biol Chem* 282:7690–7699
- Pawlik G, Kulajta C, Sachelaru I, Schröder S, Waidner B, Hellwig P, Daldal F, Koch H-G (2010) The putative assembly factor CcoH is stably associated with the cbb3-type cytochrome oxidase. *J Bacteriol* 192:6378–6389
- Penfold RJ, Pemberton JM (1991) A gene from the photosynthetic gene cluster of *Rhodobacter sphaeroides* induces trans suppression of bacteriochlorophyll and carotenoid levels in *R. sphaeroides* and *R. capsulatus*. *Curr Microbiol* 23:259–263
- Penfold RJ, Pemberton JM (1994) Sequencing, chromosomal inactivation, and functional expression in *Escherichia coli* of *ppsR*, a gene which represses carotenoid and bacteriochlorophyll synthesis in *Rhodobacter sphaeroides*. *J Bacteriol* 176:2869–2876
- Peters A, Kulajta C, Pawlik G, Daldal F, Koch H-G (2008) Stability of the cbb3-type cytochrome oxidase requires specific CcoQ-CcoP interactions. *J Bacteriol* 190:5576–5586
- Pierre Y, Breyton C, Lemoine Y, Robert B, Vernotte C, Popot JL (1997) On the presence and role of a molecule of chlorophyll a in the cytochrome *b<sub>6</sub>f* complex. *J Biol Chem* 272:21901–21908
- Ponnampalam SN, Bauer CE (1997) DNA binding characteristics of CrtJ. A redox-responding repressor of bacteriochlorophyll, carotenoid, and light harvesting-II gene expression in *Rhodobacter capsulatus*. *J Biol Chem* 272:18391–18396
- Ponnampalam SN, Elsen S, Bauer CE (1998) Aerobic repression of the *Rhodobacter capsulatus* *bhcC* promoter involves cooperative interactions between CrtJ bound to neighboring palindromes. *J Biol Chem* 273:30757–30761
- Pontier D, Albrieux C, Joyard J, Lagrange T, Block MA (2007) Knock-out of the magnesium protoporphyrin IX methyltransferase gene in *Arabidopsis*. Effects on chloroplast development and on chloroplast-to-nucleus signaling. *J Biol Chem* 282:2297–2304
- Pontoppidan B, Kannangara CG (1994) Purification and partial characterisation of barley glutamyl-tRNA(Glu) reductase, the enzyme that directs glutamate to chlorophyll biosynthesis. *Eur J Biochem* 225:529–537
- Qi Z, O'Brian MR (2002) Interaction between the bacterial iron response regulator and ferredoxin-like protein mediates genetic control of heme biosynthesis. *Mol Cell* 9:155–162
- Ranson-Olson B, Zeilstra-Ryalls JH (2008) Regulation of the *Rhodobacter sphaeroides* 2.4.1 *hemA* gene by PrrA and FnrL. *J Bacteriol* 190:6769–6778
- Ranson-Olson B, Jones DF, Donohue TJ, Zeilstra-Ryalls JH (2006) In vitro and in vivo analysis of the role of PrrA in *Rhodobacter sphaeroides* 2.4.1 *hemA* gene expression. *J Bacteriol* 188:3208–3218
- Reddy VS, Shlykov MA, Castillo R, Sun EI, Saier MH (2012) The major facilitator superfamily (MFS) revisited. *FEBS J* 279:2022–2035
- Rey FE, Harwood CS (2010) FixK, a global regulator of microaerobic growth, controls photosynthesis in *Rhodospseudomonas palustris*. *Mol Microbiol* 75:1007–1020
- Rieble S, Beale SI (1991) Purification of glutamyl-tRNA reductase from *Synechocystis* sp. PCC 6803. *J Biol Chem* 266:9740–9745
- Sandström S, Ivanov AG, Park YI, Öquist G, Gustafsson P (2002) Iron stress responses in the cyanobacterium *Synechococcus* sp. PCC7942. *Physiol Plant* 116:255–263
- Schilke BA, Donohue TJ (1992) delta-Aminolevulinic acid couples *cycA* transcription to changes in heme availability in *Rhodobacter sphaeroides*. *J Mol Biol* 226:101–115
- Schön A, Krupp G, Gough SP, Berry-Lowe S, Kannangara CG, Söll D (1986) The RNA required in the first step of chlorophyll biosynthesis is a chloroplast glutamate tRNA. *Nature* 322:281–284
- Shemin D, Russell CS (1953)  $\delta$ -Aminolevulinic acid, its role in the biosynthesis of porphyrins and purines. *J Am Chem Soc* 75:4873–4874
- Shi T, Sun Y, Falkowski PG (2007) Effects of iron limitation on the expression of metabolic genes in the marine cyanobacterium *Trichodesmium erythraeum* IMS101. *Environ Microbiol* 9:2945–2956
- Smart JL, Bauer CE (2006) Tetrapyrrole biosynthesis in *Rhodobacter capsulatus* is transcriptionally regulated by the heme-binding regulatory protein, HbrL. *J Bacteriol* 188:1567–1576
- Smart JL, Willett JW, Bauer CE (2004) Regulation of *hem* gene expression in *Rhodobacter capsulatus* by redox and photosystem regulators RegA, CrtJ, FnrL, and AerR. *J Mol Biol* 342:1171–1186
- Srivastava A, Beale SI (2005) Glutamyl-tRNA reductase of *Chlorobium vibrioforme* is a dissociable homodimer that contains one tightly bound heme per subunit. *J Bacteriol* 187:4444–4450

- Srivastava A, Lake V, Nogaj LA, Mayer SM, Willows RD, Beale SI (2005) The *Chlamydomonas reinhardtii* *gtr* gene encoding the tetrapyrrole biosynthetic enzyme glutamyl-tRNA reductase: structure of the gene and properties of the expressed enzyme. *Plant Mol Biol* 58:643–658
- Suzuki JY, Bollivar DW, Bauer CE (1997) Genetic analysis of chlorophyll biosynthesis. *Annu Rev Genet* 31:61–89
- Swem DL, Bauer CE (2002) Coordination of ubiquinol oxidase and cytochrome *cbb(3)* oxidase expression by multiple regulators in *Rhodobacter capsulatus*. *J Bacteriol* 184:2815–2820
- Swem LR, Elsen S, Bird TH, Swem DL, Koch HG, Myllykallio H, Daldal F, Bauer CE (2001) The RegB/RegA two-component regulatory system controls synthesis of photosynthesis and respiratory electron transfer components in *Rhodobacter capsulatus*. *J Mol Biol* 309:121–138
- Swem LR, Kraft BJ, Swem DL, Setterdahl AT, Masuda S, Knaff DB, Zaleski JM, Bauer CE (2003) Signal transduction by the global regulator RegB is mediated by a redox-active cysteine. *EMBO J* 22:4699–4708
- Swem LR, Gong X, Yu C-A, Bauer CE (2006) Identification of a ubiquinone-binding site that affects autophosphorylation of the sensor kinase RegB. *J Biol Chem* 281:6768–6775
- Thompson AW, Huang K, Saito MA, Chisholm SW (2011) Transcriptome response of high- and low-light-adapted *Prochlorococcus* strains to changing iron availability. *ISME J* 5:1580–1594
- Tottey S, Rich PR, Rondet SA, Robinson NJ (2001) Two Menkes-type atpases supply copper for photosynthesis in *Synechocystis* PCC 6803. *J Biol Chem* 276:19999–20004
- Tottey S, Rondet SAM, Borrelly GPM, Robinson PJ, Rich PR, Robinson NJ (2002) A copper metallochaperone for photosynthesis and respiration reveals metal-specific targets, interaction with an importer, and alternative sites for copper acquisition. *J Biol Chem* 277:5490–5497
- Touati D (2000) Iron and oxidative stress in bacteria. *Arch Biochem Biophys* 373:1–6
- Tsukihara T, Aoyama H, Yamashita E, Tomizaki T, Yamaguchi H, Shinzawa-Itoh K, Nakashima R, . . . , Yoshikawa S (1995) Structures of metal sites of oxidized bovine heart cytochrome *c* oxidase at 2.8 Å. *Science* 269:1069–1074
- Vasileuskaya Z, Oster U, Beck CF (2005) Mg-protoporphyrin IX and heme control HEMA, the gene encoding the first specific step of tetrapyrrole biosynthesis, in *Chlamydomonas reinhardtii*. *Eukaryot Cell* 4:1620–1628
- von Wettstein D, Gough SP, Kannangara CG (1995) Chlorophyll biosynthesis. *Plant Cell* 7:1039–1057
- Voss B, Meinecke L, Kurz T, Al-Babili S, Beck CF, Hess WR (2011) Hemin and magnesium-protoporphyrin IX induce global changes in gene expression in *Chlamydomonas reinhardtii*. *Plant Physiol* 155:892–905
- Vothknecht UC, Kannangara CG, von Wettstein D (1996) Expression of catalytically active barley glutamyl tRNA<sub>Glu</sub> reductase in *Escherichia coli* as a fusion protein with glutathione S-transferase. *Proc Natl Acad Sci U S A* 93:9287–9291
- Wainio WW, Vander Wende C, Shimp NF (1959) Copper in cytochrome C oxidase. *J Biol Chem* 234:2433–2436
- Waldron KJ, Tottey S, Yanagisawa S, Dennison C, Robinson NJ (2007) A periplasmic iron-binding protein contributes toward inward copper supply. *J Biol Chem* 282:3837–3846
- Weinstein JD, Beale SI (1985) Enzymatic conversion of glutamate to delta-aminolevulinic acid in soluble extracts of the unicellular green alga, *Chlorella vulgaris*. *Arch Biochem Biophys* 237:454–464
- Willett JW, Smart JL, Bauer CE (2007) RegA control of bacteriochlorophyll and carotenoid synthesis in *Rhodobacter capsulatus*. *J Bacteriol* 189:7765–7773
- Wu J, Bauer CE (2010) RegB kinase activity is controlled in part by monitoring the ratio of oxidized to reduced ubiquinones in the ubiquinone pool. *mBio* 1:e00272-10
- Wu J, Cheng Z, Reddie K, Carroll K, Hammad LA, Karty JA, Bauer CE (2013) RegB kinase activity is repressed by oxidative formation of cysteine sulfenic acid. *J Biol Chem* 288:4755–4762
- Xiong J, Bauer CE (2002) Complex evolution of photosynthesis. *Annu Rev Plant Biol* 53:503–521
- Xiong J, Fischer WM, Inoue K, Nakahara M, Bauer CE (2000) Molecular evidence for the early evolution of photosynthesis. *Science* 289:1724–1730
- Yin L, Bauer CE (2013) Controlling the delicate balance of tetrapyrrole biosynthesis. *Philos Trans R Soc B* 368:20120262
- Yin L, Dragnea V, Bauer CE (2012) PpsR, a regulator of heme and bacteriochlorophyll biosynthesis, is a heme-sensing protein. *J Biol Chem* 287:13850–13858
- Zappa S, Bauer CE (2013) The LysR-type transcription factor HbrL is a global regulator of iron homeostasis and porphyrin synthesis in *Rhodobacter capsulatus*. *Mol Microbiol* 90:1277–1292

- Zeilstra-Ryalls JH, Kaplan S (1995) Aerobic and anaerobic regulation in *Rhodobacter sphaeroides* 2.4.1: the role of the *fnrL* gene. *J Bacteriol* 177:6422–6431
- Zeilstra-Ryalls JH, Gabbert KK, Mouncey NJ, Kaplan S, Kranz RG (1997) Analysis of the *fnrL* gene and its function in *Rhodobacter capsulatus*. *J Bacteriol* 179:7264–7273
- Zhang L, McSpadden B, Pakrasi HB, Whitmarsh J (1992) Copper-mediated regulation of cytochrome c553 and plastocyanin in the cyanobacterium *Synechocystis* 6803. *J Biol Chem* 267:19054–19059

# Part VI

## **Assembly of Cytochrome Complexes and Super-Complexes**



# Chapter 26

## Cofactor Assembly of Cytochrome $bc_1$ - $b_6f$ Complexes

Sara Guenther Cline<sup>a,\*</sup>, Stéphane Thierry Gabilly<sup>b</sup>,  
Nitya Subrahmanian<sup>c</sup>, and Patrice Paul Hamel<sup>c,\*</sup>

<sup>a</sup>Department of Mathematics, Computer and Natural Sciences,  
Athens State University, S303C Waters Hall, 300 N. Beaty Street,  
Athens, AL 35611, USA

<sup>b</sup>Department of Plant and Microbial Biology, University of  
California, Berkeley, 441 Koshland Hall, Berkeley,  
CA 94720-3120, USA

<sup>c</sup>Department of Molecular Genetics and Department of  
Biological Chemistry and Pharmacology, The Ohio State  
University, 500 Aronoff Laboratory, 318 W. 12th Avenue,  
Columbus, OH 43210, USA

Summary.....	502
I. Introduction.....	502
II. Prosthetic Groups in $bc_1$ and $b_6f$ .....	503
A. Common and Unique Prosthetic Groups in $bc$ Complexes.....	503
B. Incorporation of Prosthetic Groups in $bc_1$ and $b_6f$ Subunits.....	504
III. Pathways for the Covalent Attachment of Heme.....	505
A. Six Distinct Pathways for Heme Attachment in $bc_1/b_6f$ .....	505
B. Biochemical Requirements for Thioether Bond Formation.....	505
1. Transport of Pre-apocytochrome $c$ and Heme.....	506
2. Maintenance of Sulfhydryls and Heme Iron in the Reduced Form.....	506
3. Stereospecific Formation of Thioether Bond Formation.....	507
C. System I or CCM Pathway (Cytochrome $C$ Maturation).....	507
1. Overview of the CCM Pathway in Bacteria.....	507
2. A Variant of Bacterial System I in Land Plant Mitochondria.....	507
D. System II or CCS (Cytochrome $C$ Synthesis) Pathway.....	510
1. Discovery of System II in Plastids.....	510
2. A Transmembrane Heme Channel with Cytochrome $c$ Synthase Activity.....	511
3. Operation of a Transmembrane Disulfide Reducing Pathway.....	511
4. Additional System II Components in Plastids?.....	513
E. System III or HCCS (HoloCytochrome $C$ Synthase) Pathway.....	513
1. Discovery of HCCS, the Signature Component of System III.....	513
2. Missing Components in System III?.....	515

\*Author for correspondence, e-mail: [sara.cline@athens.edu](mailto:sara.cline@athens.edu); [hamel.16@osu.edu](mailto:hamel.16@osu.edu)

F. System IV or CCB (Cofactor Assembly on Complex C Subunit B).....	516
1. A Multi-step Pathway for Heme <i>c</i> <sub>i</sub> Formation in the <i>b</i> <sub>6</sub> <i>f</i> Complex.....	516
2. Identification of Novel Proteins Required for Heme <i>c</i> <sub>i</sub> Assembly.....	516
Acknowledgments.....	517
References.....	517

## Summary

Cytochromes *bc*<sub>1</sub> and *b*<sub>6</sub>*f* are enzyme complexes catalyzing essential electron transfer reactions in bacterial and organellar energy-transducing membranes. Electron transport relies on heme and Fe-S redox cofactors contained in the three catalytic subunits common to *bc*<sub>1</sub> and *b*<sub>6</sub>*f* complexes: a *b*-type cytochrome (cytochrome *b*), a *c*-type cytochrome (cytochrome *c*<sub>1</sub> or *f*) and a [2Fe-2S]-containing protein (Rieske). Maturation of the *b*-type and *c*-type cytochromes requires conversion of the subunit from the apoform to the holoform by the incorporation of two hemes (*b*<sub>L</sub> and *b*<sub>H</sub>) in cytochrome *b* of the *bc*<sub>1</sub> complex, three hemes (*b*<sub>L</sub>, *b*<sub>H</sub> and *c*<sub>i</sub>) in cytochrome *b*<sub>6</sub> of the *b*<sub>6</sub>*f* complex, and a single heme (*c*) in both cytochromes *c*<sub>1</sub> and *f*. Assembly of heme *c* requires the formation of two thioether bonds at a CXXCH motif in cytochrome *c*<sub>1</sub> and *f* on the *p*-side, and for *c*<sub>i</sub>, a single thioether bond in cytochrome *b*<sub>6</sub> on the *n*-side of the membrane, respectively. It is not known how non-covalently bound hemes (*b*<sub>L</sub> and *b*<sub>H</sub>) are inserted into cytochrome *b* and *b*<sub>6</sub>, but covalent linkage of heme is known to be a catalyzed process. The chemistry of thioether linkage formation appears, on the surface, to be simple (i.e. addition of a sulfhydryl to the α carbon of the vinyl group of heme). However, experimental investigations in bacteria, mitochondria and plastids have revealed an unsuspected biochemical complexity for this process. At least six different pathways for thioether bond formation have been described. Four of these, System I, II, III (on the *p*-side) and IV (on the *n*-side), are defined by prototypical components and have been extensively studied.

## I. Introduction

Cytochrome *bc*<sub>1</sub> and cytochrome *b*<sub>6</sub>*f* complexes (hereafter referred to as *bc*<sub>1</sub> and *b*<sub>6</sub>*f*) are multimeric enzymes responsible for electron transfer reactions in bacterial and eukaryotic energy-transducing membranes (Dibrova et al. 2013; Hasan et al. 2013). Cytochrome *bc*<sub>1</sub> complexes are quinol-cytochrome *c* oxido-reductases that function

in aerobic respiration in diverse bacterial phyla and all mitochondria, with the exception of some protozoan parasites and one photosynthetic alveolate (Nawathean and Maslov 2000; Stechmann et al. 2008; Flegontov et al. 2015). In photosynthetic bacteria, *bc*<sub>1</sub> are also key enzymes in anoxygenic photosynthesis (see Chap. 10). On the other hand, cytochrome *b*<sub>6</sub>*f* complexes are essential to oxygenic photosynthesis and operate as quinol-plastocyanin (or cytochrome *c*<sub>6</sub>) oxido-reductases in all cyanobacteria and plastids of both algae and land plants (see Chap. 9). In cyanobacteria, *b*<sub>6</sub>*f* is also required for the respiratory electron transfer chain (see Chap. 17). Variations of the typical *bc*<sub>1</sub>/*b*<sub>6</sub>*f* enzymes also exist in several eubacterial and archeal lineages. Such a variant is the *bc* complex, an enzyme related to the *b*<sub>6</sub>*f*, and

---

*Abbreviations:* BN-PAGE – Blue native polyacrylamide gel electrophoresis; Fe-S – Iron-sulfur; HHP – Heme handling protein; HO – Heme oxygenase; HRM – Heme regulatory motif; IMS – Intermembrane space; ISP – Iron-sulfur protein; OPR – Octotricopeptide repeat; PSI – Photosystem I; TDOR – Thiol-disulfide oxido-reductase; TMD – Transmembrane domain; Y2H – Yeast two-hybrid; WWD – tryptophan rich domain containing the tryptophan-tryptophan-aspartic acid signature

present in both anoxygenic phototrophic and non-phototrophic bacteria of the Firmicutes phylum (see Chap. 3).

Common to  $bc_1$  and  $b_6f$  are three catalytic subunits, a  $b$ -type cytochrome, a  $c$ -type cytochrome ( $c_1$  or  $f$ ), and a Rieske iron-sulfur protein (ISP), which harbor the prosthetic groups required for catalysis (Dibrova et al. 2013; Hasan et al. 2013). In addition to the catalytic subunits,  $bc_1$  and  $b_6f$  contain subunits which do not participate directly in electron transfer, but are required for assembly/activity of a functional complex. While mitochondrial  $bc_1$  contains additional seven or eight subunits that are absent in bacterial  $bc_1$  complexes (see Chap. 10), the four additional subunits found in the chloroplast  $b_6f$  have counterparts in the cyanobacterial complex (see Chap. 9). The biogenesis of  $bc_1$  and  $b_6f$  is an intricate process, requiring the synthesis of the structural subunits, the maturation of the redox subunits by attachment/incorporation of the prosthetic groups and the stepwise integration of the different subunits in the membrane. In this chapter, we will focus on the pathways controlling prosthetic group attachment to the catalytic subunits of  $bc_1$  and  $b_6f$ , with emphasis on the heme attachment reaction.

## II. Prosthetic Groups in $bc_1$ and $b_6f$

### A. Common and Unique Prosthetic Groups in $bc_1/b_6f$ Complexes

Iron-sulfur (Fe-S) cluster and heme (ferroprotoporphyrin IX) are the prosthetic groups common to both  $bc_1$  and  $b_6f$  complexes and are present in the three conserved catalytic subunits (Dibrova et al. 2013; Hasan et al. 2013). The membrane-anchored Rieske subunit, present in both  $bc_1$  and  $b_6f$ , contains a single [2Fe-2S] cluster in a domain facing the  $p$ -side<sup>1</sup> of the membrane

<sup>1</sup> $p$ - and  $n$ -sides refer to the positive and negative side of the energy-transducing membrane system, respectively. The  $p$ -side corresponds to the bacterial

(Dibrova et al. 2013; Hasan et al. 2013). Rieske ISPs are characterized by unique ligand coordination of their Fe-S cluster, with one of the two iron centers being coordinated by two cysteine residues and the other by two histidine residues (Schmidt and Shaw 2001). In  $bc_1/b_6f$ , cytochromes  $b$  and  $b_6$  are membrane-embedded proteins containing two  $b$ -hemes,  $b_L$  and  $b_H$ , on the  $p$ - and  $n$ -side of the membrane, respectively. Both hemes of cytochromes  $b$  and  $b_6$  are coordinated by two conserved histidines in a four-helix bundle. Cytochromes  $c_1$  and  $f$  are membrane-anchored,  $c$ -type cytochromes, also generically referred to as cytochromes  $c$ . Cytochromes of the  $c$ -type are a large family of hemoproteins with one or several heme moieties covalently attached to a  $CX_nC(H/K)^2$  motif, known as the heme-binding site (Thony-Meyer 1997). Axial ligands of covalently linked heme in  $c$ -type cytochromes are provided by the H/K residue in the heme-binding site and an amino acid in the protein, usually a methionine residue (Thony-Meyer 1997). Histidine in the heme-binding site is the most common axial ligand and lysine is only found in nitrate-reducing enzymes (Einsle et al. 1999). In cytochrome  $c_1$  and cytochrome  $f$ , a single heme  $c$  is attached on the  $p$ -side of the membrane. This attachment occurs via two thioether bonds between the vinyl-2 and -4 groups of heme and the sulfhydryl groups on the first and second cysteines occurring in a CXXCH motif of the protein. A notable exception occurs in the phylum Euglenozoa where the vinyl-4 of heme is linked to a single cysteine contained within a FXXCH motif in mitochondrial cytochrome  $c_1$  (Priest and Hajduk 1992).

periplasm, thylakoid lumen and mitochondria IMS while the  $n$ -side is the bacterial cytoplasm, plastid stroma and mitochondrial matrix.

<sup>2</sup>Where  $X$  can be any amino-acid except cysteine. The number of intervening residues ( $n$ ) is usually 2, with the rare exception of some bacterial cytochromes where  $n = 3, 4$  or 15 (Jungst et al. 1991; Jentzen et al. 1998; Aragão et al. 2003; Hartshorne et al. 2007).

Another type of covalent linkage of a single heme, referred to as heme  $c_1$  (or  $c_n$ ), has been found in cytochrome  $b_6$ . This heme is covalently linked via one thioether bond between the  $\alpha$  carbon of the vinyl-2 group of heme and a cysteine residue (Kurisu et al. 2003; Stroebel et al. 2003). Heme  $c_1$  was also detected as covalently linked to the cytochrome  $b$  subunit of the  $bc$  complexes in *Bacilli* and *Heliobacteria* representatives of the Firmicutes phylum (Kutoh and Sone 1988; Yu and Le Brun 1998; Ducluzeau et al. 2008). Unlike heme  $c$  in cytochromes  $c_1$  and  $f$ , heme  $c_1$  is not attached to a recognizable consensus motif and is localized on the  $n$ -side of the membrane (de Vitry 2011). Because  $b$ -type and  $c$ -type cytochromes refer to cytochromes with non-covalently and covalently bound heme(s), respectively, cytochrome  $b_6$ , which was initially defined as a  $b$ -type based on  $b_L$  and  $b_H$  hemes is now also referred to as a  $c$ -type cytochrome because of the presence of heme  $c_1$  (Thony-Meyer 1997; Kuras et al. 2007).

In addition to Fe-S and heme, subunit IV of the  $b_6f$  contains two non-covalently bound pigments, one molecule of chlorophyll  $a$  (Huang et al. 1994; Pierre et al. 1997) and one molecule of  $\beta$ -carotene (Zhang et al. 1999), which are absent in the  $bc_1$ . The typical carotenoid in  $b_6f$  is 9-*cis*- $\beta$ -carotene but other carotenoids, such as 9-*cis*- $\alpha$ -carotene and echinenone have been found in some algal and cyanobacterial enzymes (Boronowsky et al. 2001; Li et al. 2005). The function of chlorophyll  $a$  and  $\beta$ -carotene remains enigmatic as light is not required for electron transfer catalyzed by the  $b_6f$  complex.

### ***B. Incorporation of Prosthetic Groups in $bc_1$ and $b_6f$ Subunits***

Maturation of the redox subunits of the  $bc_1$  and  $b_6f$  requires apo- to holoform conversion of the subunit by the incorporation of one or several prosthetic groups. Failure to incorporate the prosthetic group yields a  $bc_1/b_6f$

assembly defect as the apoform of the subunit is usually unstable and degraded. One notable exception is the Rieske ISP in *Saccharomyces cerevisiae*, whose apoform was shown to assemble in the  $bc_1$  in the absence of Fe-S cluster incorporation (Graham and Trumppower 1991).

While the requirement for catalysis in the covalent attachment of heme has long been acknowledged, it is not known if incorporation of non-covalently bound cofactors, such as  $b$ -hemes into apocytochrome  $b/b_6$ , chlorophyll  $a$  and  $\beta$ -carotene into subunit IV and the Fe-S cluster in the Rieske ISP are also enzymatically assisted in vivo. The fact that these cofactors are retained by non-covalent interactions, and were shown, in some cases, to be correctly inserted into their corresponding apoprotein(s) in vitro, has led to the assumption that incorporation of non-covalently bound cofactors is not a catalyzed reaction in vivo (Robertson et al. 1994; Holton et al. 1996; Gubernator et al. 2006). The recent discovery that different assembly factors of mitochondrial  $bc_1$  associate with cytochrome  $b$  intermediates containing either  $b_L$  only or  $b_L$  and  $b_H$  suggests that incorporation of non-covalent heme might also be an assisted process (Hildenbeutel et al. 2014). Another example, highlighting the role of factors in assisting the delivery of non-covalently bound heme, is that of NO synthase. Its biogenesis requires thioredoxin, the Hsp90 chaperone, and glycerolphosphate-dehydrogenase for insertion of  $b$ -heme into the apoenzyme (Chakravarti et al. 2010; Ghosh et al. 2011; Hannibal et al. 2012). The concept of protein-assisted incorporation of non-covalently bound prosthetic group extends to molecules other than heme, as shown by the description of dedicated carriers facilitating Fe-S cluster insertion in a subset of apoprotein target(s) (Balk and Schaedler 2014). Hence, it is possible that incorporation of the Fe-S cluster in the apoform of  $bc_1/b_6f$  Rieske ISP also requires dedicated factor(s).

### III. Pathways for the Covalent Attachment of Heme

#### A. Six Distinct Pathways for Heme Attachment in $bc_1/b_6f$

Covalent heme attachment to apocytochromes  $c_1$  and  $f$  is a post-translational modification, occurring on the  $p$ -side of the energy-transducing membrane of bacteria, mitochondria and plastids (Kranz et al. 2009; Allen 2011; Mavridou et al. 2013; Verissimo and Daldal 2014). In cyanobacteria and plastids, heme  $c_1$  is formed by covalent linkage of heme to apocytochrome  $b_6$  on the  $n$ -side of the thylakoid membrane. By analogy, it is reasonable to assume that heme  $c_1$  in Firmicute  $bc$  is also attached on the cytoplasmic side of the membrane (de Vitry 2011). Heme attachment can take place independently of the presence of other  $bc_1/b_6f$  complex subunits but the steady-state level of the holoprotein is usually dependent upon association/assembly with other subunits (Kuras et al. 1997; Zara et al. 2007).

At least three distinct mechanisms for the covalent attachment of heme to the apofoms of cytochromes  $c_1$  and  $f$ , the so-called Systems I, II and III, have been described (Kranz et al. 2009; Allen 2011; Mavridou et al. 2013; Verissimo and Daldal 2014; Babbitt et al. 2015). All of these systems are not unique to the maturation of cytochrome  $c_1$  and  $f$ , but some also control the heme ligation reaction to multiple apocytochrome  $c$  substrates in the bacterial periplasm, soluble apocytochrome  $c$  in the mitochondrial IMS (intermembrane space) and soluble apocytochrome  $c_6$  in the thylakoid lumen of green algae. A fourth pathway for covalent heme attachment, System IV, is solely dedicated to the attachment of heme  $c_1$  to apocytochrome  $b_6$ , and hence is specific to the biogenesis of the  $b_6f$  (de Vitry 2011).

Because each system can be recognized on the basis of unique assembly factors, the distribution of the different maturation pathways was analyzed in the three domains of life. While the occurrence of a heme attachment pathway cannot be entirely predicted, a few

generalities about the distribution of the three systems in energy-transducing membranes have been noted (Bertini et al. 2007; Allen et al. 2008a; Giegé et al. 2008; Allen 2011; Babbitt et al. 2015). While all bacteria utilize System I or System II, archaea have so far been found to have only System I. All plastids appear to use System II and mitochondria possess System I or System III.

Mitochondrial cytochromes  $c$  and  $c_1$ , with a heme attached via a single thioether bond, were found to occur in all three major taxonomic groups of the Euglenozoa (diplonemids, kinetoplastids and euglenids), even in the absence of any component of the known  $c$ -type cytochrome maturation system. This was taken as an indication that a novel pathway for cytochrome  $c$  maturation (also referred to as System V) must operate in mitochondria of organisms belonging to this phylum (Allen et al. 2008a; Allen 2011). Similarly, as no prototypical component of System IV can be detected in the genomes of Firmicutes, a novel pathway for thioether bond formation in cytochrome  $b$ , System VI, was postulated (Allen 2011; Mavridou et al. 2013). Note that because Systems V and VI are yet to be experimentally investigated, their designations as novel systems still await confirmation.

#### B. Biochemical Requirements for Thioether Bond Formation

The biochemical requirements to complete the covalent attachment of heme on the  $p$ -side are presumed to be universal and common to all energy-transducing membranes (Hamel et al. 2009; Bonnard et al. 2010). Covalent heme attachment is dependent on several steps including: (1) transport of the apocytochrome  $c$  and heme substrates to the  $p$ -side of the energy-transducing membrane, (2) maintenance of both the sulfhydryls of the  $CX_nC(H/K)$  motif and the heme iron in a reduced form, and (3) formation of two thioether linkages between the vinyl-2 and -4 of heme, with the N- and C-terminal cysteines of the heme-binding motif, respectively.

### 1. Transport of Pre-apocytochrome *c* and Heme

The transport of bacterial and organellar apocytochromes *c* from the site of their synthesis (cytoplasm or plastid stroma) to their final sub-cellular location (periplasm, mitochondrial IMS or thylakoid lumen) has been examined in many experimental systems. In most cases, this requires transport of both the heme and the protein via independent pathways, and pre-apoprotein cleavage prior to heme attachment.

Most *c*-type cytochromes are synthesized in a precursor form with appropriate targeting sequences that direct them, as unfolded polypeptides across at least one biological membrane, via general translocation routes such as Sec in bacteria, Toc/Tic/Sec in the plastid and Tom/Tim in the mitochondria (Thöny-Meyer and Künzler 1997; Nakamoto et al. 2000; Hamel et al. 2009). The pre-sequences are cleaved during translocation to yield the apoform of the protein, which is typically the substrate for the heme attachment reaction. Although less common, heme attachment has been found to occur first as a prerequisite for processing of the pre-cytochrome *c*<sub>1</sub> in *S. cerevisiae* mitochondria (Zollner et al. 1992; Steiner et al. 1996).

The final two steps of heme synthesis, catalyzed by protoporphyrinogen oxidase and ferrochelatase, take place on the *n*-side of the membrane (Ajioka et al. 2006). Ferrochelatase is required for the incorporation of reduced iron in protoporphyrin IX and seems to be membrane-associated, facing the *n*-side (Ajioka et al. 2006). This orientation implies that a mechanism for transmembrane “delivery” of heme from the *n*-side to the *p*-side must operate, since mature heme is produced on the *n*-side. Exceptions occur in organisms where heme is not synthesized in the mitochondria. Such organisms are either parasites relying on dietary heme, like helminths and some trypanosomes, or eukaryotes producing heme within the plastid (Atteia et al. 2005; Hamza and Dailey 2012; Koreny et al. 2013). In both cases,

heme is assumed to be transported from the cytoplasm or the plastid to the mitochondrial IMS. With the exception of System II, where a transmembrane heme delivery route was shown to be required for cytochrome *c* assembly (see Sect. III.D.2), the pathways controlling heme distribution from its site of synthesis are unknown.

### 2. Maintenance of Sulfhydryls and Heme Iron in the Reduced Form

In vitro, uncatalyzed conversion of apocytochrome *c* to its holoform can be achieved in the presence of heme, provided that a reducing agent is added to the reaction (Daltrop et al. 2002; Daltrop and Ferguson 2003, 2004). In the absence of a reductant, the apocytochrome *c* heme-binding site is disulfide-bonded and heme attachment does not proceed. This indicates that reduced apocytochrome *c* is the only competent substrate for the heme ligation reaction. In the case of heme, the need of reduced iron for thioether bond formation is less intuitive and was deduced from reconstitution experiments (Barker et al. 1993; Daltrop et al. 2002). In these experiments, iron in the ferric form was postulated to initiate a radical-based chemistry, yielding side products with incorrectly attached heme. Hence, the initial oxidation state of the heme iron, when it is presented to the apoprotein, is critical to the formation of the thioether bond linkage. Mechanisms for heme reduction have been postulated for System I (see Chap. 27 by Khalfaoui-Hassani et al. in this volume), System II (see Sect. II.D.2), and System III (see Sect. III.E.2). There are known mechanisms for maintaining the heme-binding site sulfhydryls in a reduced form in Systems I and II (see Sects. III.C.2 and III.D.3), but not in System III. It is likely that System V does not require a mechanism to maintain sulfhydryls in a reduced form, considering that there is a single thioether bond forming cysteine in the A/FXXCH heme-binding motif (Allen et al. 2008b).

### 3. Stereospecific Formation of Thioether Bond Formation

Chemical reaction of the heme-binding site sulfhydryls with the vinyl side chains of heme can yield eight possible combinations. Yet only one combination is found in all cytochromes *c*, where the  $\alpha$  carbons of vinyl-2 and -4 of heme are linked to the amino (N)- and carboxyl (C)-terminal cysteines in the C(X)<sub>n</sub>CH/K motif (Barker and Ferguson 1999). This stereospecificity of heme attachment also extends to mitochondrial cytochrome *c* of Euglenozoa, where the cysteine in the A/FXXCH motif is forming a thioether bond with the  $\alpha$ -carbon of the vinyl-4 of heme (Vilmos et al. 2009). The mechanisms controlling this stereoselectivity in the heme ligation reaction still remain undeciphered.

#### C. System I or CCM Pathway (Cytochrome C Maturation)

##### 1. Overview of the CCM Pathway in Bacteria

The most complex “CCM” (for Cytochrome C Maturation) pathway, is currently the best characterized in terms of identity of the components, their biochemical activities and the sequence of events (Kranz et al. 2009; Sanders et al. 2010; Verissimo and Daldal 2014). The CCM was initially discovered in  $\alpha$ - and  $\gamma$ -proteobacteria. Additionally, it was also assumed to operate in the mitochondria of vascular plants and some protozoa (e.g. *Paramecium* spp.), based on the occurrence of mitochondria-encoded Ccm-like proteins (Allen et al. 2003). Extensive functional studies in various microbial models, including *Escherichia coli* and *Rhodobacter capsulatus*, led to the identification of multiple cytochrome *c* assembly factors that can be categorized in three functional modules (Fig. 26.1): (1) heme handling/delivery, (2) preparation of apocytochrome *c* substrate via maintenance of the heme-linking sulfhydryls in a reduced form, and (3) thioether bond formation. The

bacterial CCM pathway is detailed in the Chap. 27 by Khalfaoui-Hassani et al. in this volume. In the following section, we review the findings of the mitochondrial CCM pathway from experimental investigation in the *Arabidopsis* plant model (Fig. 26.1).

##### 2. A Variant of Bacterial System I in Land Plant Mitochondria

(1) *Heme Handling and Delivery*. In bacteria, the heme relay pathway includes several steps in the periplasm: (i) loading of heme onto CcmC and transfer onto heme chaperone CcmE, (ii) formation of holoCcmE by covalent attachment of heme to a conserved histidine, and (iii) release of holoCcmE from interaction with CcmC by the ABC-transporter CcmAB and CcmD (see the Chap. 27 by Khalfaoui-Hassani et al.). In land plant mitochondria, the components controlling the delivery and relay of heme can be recognized on the basis to their sequence similarity to bacterial CcmABCE, with the exception of CcmD (Giegé et al. 2008). CcmD, a small membrane-anchored protein, is part of the bacterial CcmABC-holoCcmE complex and is required for the release of holoCcmE (Feissner et al. 2006a; Richard-Fogal et al. 2008, 2009). It is likely that CcmD cannot be identified in plants because there is little conservation of its primary sequence in System I in bacteria and archaea.

Bacterial CcmC is a polytopic membrane HHP (Heme Handling Protein). HHPs are heme-interacting proteins containing heme-coordinating residues (such as histidine) and hydrophobic amino acids that can interact with the porphyrin ring (such as tryptophan) (Li et al. 2011). Bacterial CcmC displays a characteristic tryptophan-rich “WWD” heme-binding motif, flanked by two conserved histidines which are essential for heme loading onto CcmE (Schulz et al. 1999, 2000; Richard-Fogal and Kranz 2010). Compatible with a function in mitochondrial cytochrome *c* assembly, the tryptophan-rich “WWD” domain and flanking histidines of

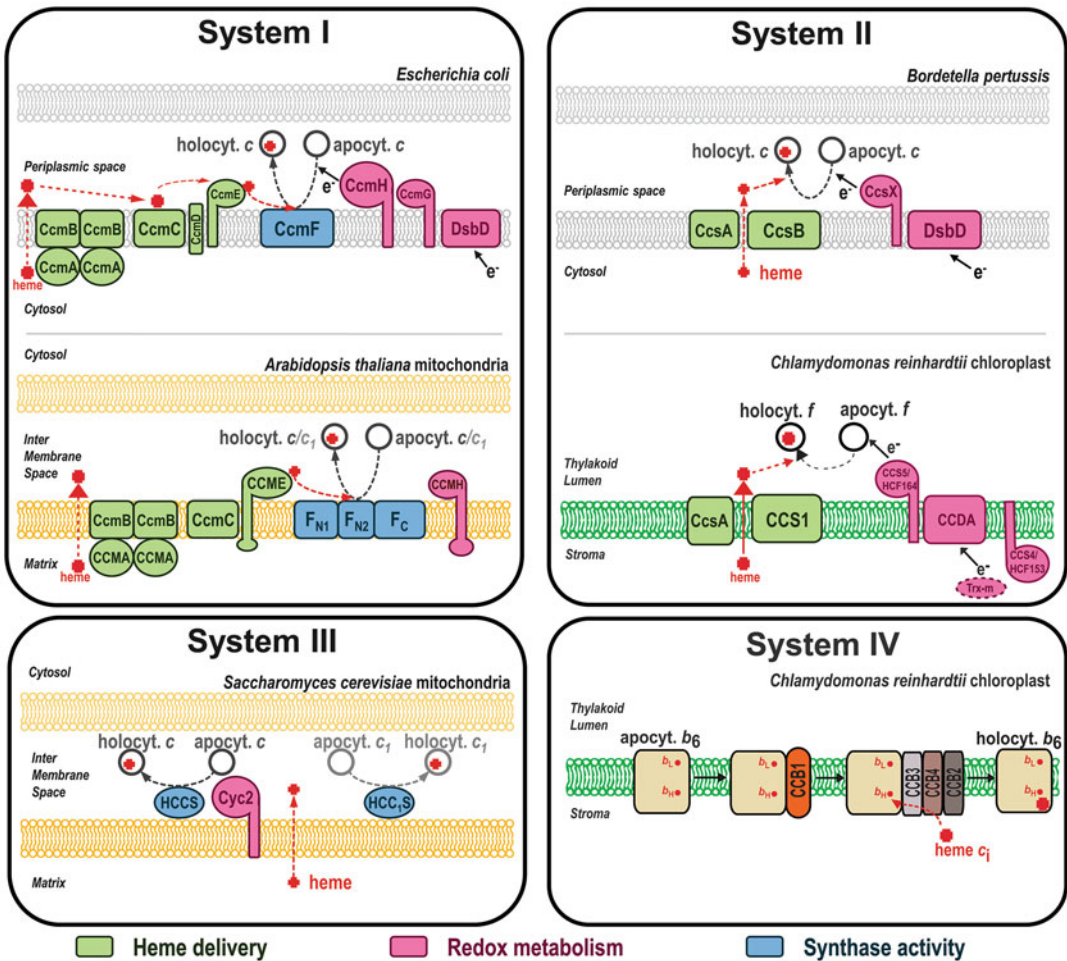


Fig. 26.1. Overview of pathways (Systems I, II, III and IV) for covalent heme attachment. The figure is adapted from Hamel et al. 2009. Bacterial membranes are shown in gray, thylakoid membranes are shown in green and mitochondrial membranes are shown in orange, the outer membrane (light orange) and the inner membrane (dark orange). For Systems I, II and III, the components shown in green are involved in heme handling/delivery, the ones in pink are involved in redox metabolism, and the blue components are postulated to have a holocytochrome *c* synthase activity. System I operates in mitochondria of land plants and some protists, and Gram<sup>-</sup> ( $\alpha$ ,  $\gamma$ ) bacteria. System II occurs in chloroplasts, Gram<sup>+</sup> and Gram<sup>-</sup> ( $\beta$ ,  $\delta$ ,  $\epsilon$ ) bacteria, aquificales and cyanobacteria. System III is restricted to mitochondria of fungi, animals, apicomplexan parasites, red and green algae and diatoms. CcdA or DsbD occur in bacterial System I and in System II and are Thiol-disulfide oxido-reductases (TDORs) of the DsbD family. Cyc2p is restricted to organisms where both HCCS and HCC<sub>1</sub>S are present. In animals, only one holocytochrome *c* synthase, HCCS is present. For System IV, a simplified pathway for the CCB-dependent heme attachment is shown (adapted from Saint-Marcoux et al. 2009).

plant CcmC are predicted to be exposed to the mitochondrial IMS (Giegé et al. 2008). Plant CcmC is mitochondria-encoded and detected in mitochondrial membrane fractions (Raczynska et al. 2006). A severe reduction of CcmC abundance, in a mutant

deficient for the processing of the *ccmC* transcript, has no impact on the activities of the *bc*<sub>1</sub> and cytochrome *c* oxidase complexes (Jonietz et al. 2011). However, the abundance of mitochondrial holocytochrome *c*<sub>1</sub> and *c* was not documented and the role of CcmC



in cytochrome *c* maturation remains to be demonstrated.

*Arabidopsis* CCME is a nuclear-encoded peripheral protein of the mitochondrial inner membrane with its heme-binding domain exposed to the mitochondrial IMS (Spielewoy et al. 2001). When expressed in the *E. coli* periplasm, mitochondrial CCME inserts correctly in the membrane but is unable to substitute for the function of bacterial CcmE in cytochrome *c* maturation (Spielewoy et al. 2001). However the fact that mitochondrial CCME binds heme covalently, via its conserved histidine when expressed in bacteria, was taken as an indication that its function as a heme chaperone is probably conserved (Spielewoy et al. 2001).

Nuclear-encoded CCMA, the ATP binding component of the ABC-transporter, localizes to the mitochondrial matrix, and was shown to be associated with the inner membrane (Rayapuram et al. 2007). In agreement with its sequence similarity to bacterial CcmA, a recombinant form of mitochondrial CCMA exhibits ATPase activity (Rayapuram et al. 2007). Interaction of CCMA at the inner membrane with CcmB, the mitochondria-encoded membrane component of the ABC transporter, is supported by yeast two-hybrid (Y2H) experiments (Rayapuram et al. 2007). ATP/Mg<sup>2+</sup> was shown to facilitate CCMA dissociation from the mitochondrial membrane, most likely because ATP hydrolysis induced conformational changes that modify the interaction with the transmembrane domains of CcmB (Rayapuram et al. 2007). Mitochondrial CCMA occurs in a 480 kDa complex that does not contain other Ccm proteins such as CcmF, CCME or CCMH (see below) (Rayapuram et al. 2007). It is likely that this complex contains CcmB but this could not be tested due to the lack of an antibody against this protein.

(2) *Preparation of the Apocytochrome c Substrate.* Maintenance of the heme-linking cysteines in a reduced form is essential for covalent attachment of heme to apocytochrome *c*. Bacterial CcmH is a membrane-anchored, periplasm-facing thiol-disulfide reductase proposed to be

involved in maintaining the heme-binding motif of apocytochromes *c* in a reduced form (Sanders et al. 2010; Verissimo and Daldal 2014). However, its mechanism of action still remains obscure (Verissimo and Daldal 2014) (see the Chap. 27 by Khalfaoui-Hassani et al.). In plants, the ortholog of CcmH is a nuclear-encoded, integral inner membrane protein with an IMS-facing domain containing a RCXXC redox motif (Meyer et al. 2005). Y2H experiments show an interaction between the IMS-facing domain of mitochondrial CCMH and apocytochrome *c*. Moreover, in vitro redox assays with a recombinant form of mitochondrial CCMH show that the RCXXC motif can reduce a disulfide in a model apocytochrome *c* peptide (Meyer et al. 2005). The thioredoxin-like CcmG and a TDOR (Thiol-disulfide oxido-reductase) of the DsbD family (see Fig. 26.1), which are proposed to maintain bacterial CcmH in a reduced form, cannot be identified in land plant genomes (Giegé et al. 2008; Sanders et al. 2010; Cho and Collet 2013). Hence, it is unclear how mitochondrial CCMH is maintained reduced in the IMS (Giegé et al. 2008; Bonnard et al. 2010).

(3) *Thioether Bond Formation.* CcmF was long considered to be the component catalyzing thioether bond formation but experimental evidence for this claim was only provided recently (Ren et al. 2002; Sanders et al. 2008; Richard-Fogal et al. 2009; San Francisco et al. 2014). Bacterial CcmF is a heme-handling protein (HHP) with a “WWD” domain and two flanking histidines on the *p*-side and two transmembrane histidines facing the *n*-side of the membrane (Richard-Fogal et al. 2009; San Francisco et al. 2011). The histidines on the *p*-side are proposed to bind the CcmE-attached heme while histidines on the *n*-side are ligands of a structural *b*-heme. The transmembrane *b*-heme was proposed to be involved in transferring electrons from the cytoplasm to the periplasmic side in order to maintain the heme substrate in a reduced form. *Arabidopsis* CcmF is encoded by the mitochondrial genome in the form of three

genes (*ccmF<sub>N1</sub>*, *ccmF<sub>N2</sub>*, *ccmF<sub>C</sub>*), each of which encodes an integral inner membrane protein with similarity to a corresponding domain of bacterial CcmF (Giegé et al. 2004; Rayapuram et al. 2008). Histidines on the *p*-side are in CcmF<sub>N1</sub> and CcmF<sub>N2</sub> while the *n*-side histidines are provided by CcmF<sub>N2</sub> and CcmF<sub>C</sub>. The occurrence of CcmF<sub>N1</sub>, -F<sub>N2</sub>, -F<sub>C</sub> in a mitochondrial membrane complex and Y2H-based interaction of CcmF<sub>N2</sub> with CcmF<sub>N1</sub> and CcmF<sub>C</sub> suggest that all three CcmF proteins constitute a functional unit in plant mitochondria (Giegé et al. 2004; Rayapuram et al. 2008). CcmF<sub>N2</sub> also contains the WWD domain that was shown to face the IMS and interact with apofoms of both cytochrome *c* and *c*<sub>1</sub> in an Y2H assay (Rayapuram et al. 2008). CcmF<sub>N2</sub> interacts with CCMH in Y2H assays and both proteins are also detected in a complex at the inner membrane (Rayapuram et al. 2008). It is likely that mitochondrial CcmF and CCMH form a complex controlling the heme ligation reaction, similar to the bacterial CcmFH, which was shown to carry the cytochrome *c* synthase activity (San Francisco et al. 2014). A role for *Arabidopsis* CcmF<sub>C</sub> in *c*-type cytochrome maturation was evidenced through the identification of a splicing defect of the *ccmF<sub>C</sub>* transcript that results in decreased accumulation of holoforms of cytochromes *c* and *c*<sub>1</sub> (Francs-Small et al. 2011). Similarly, an editing defect at a single position in the *ccmF<sub>N</sub>* transcript results in loss of CcmF<sub>N</sub> and severe reduction of mitochondrial *c*-type holoforms in maize (Sun et al. 2015).

#### D. System II or CCS (Cytochrome C Synthesis) Pathway

##### 1. Discovery of System II in Plastids

System II was originally discovered in the green alga *Chlamydomonas reinhardtii* through genetic studies of the *ccs* mutants (*ccs* for cytochrome *c* synthesis), a class of photosynthesis-minus mutants specifically deficient for the accumulation of the holoforms of plastid *c*-type cytochromes

(Howe and Merchant 1992; Howe et al. 1995; Xie et al. 1998). The *ccs* mutants are deficient for the thylakoid membrane-bound *c*-type cytochrome *f*, which is required for cytochrome *b<sub>6</sub>f* assembly, and also for soluble cytochrome *c*<sub>6</sub>, the functional replacement of plastocyanin in Cu-deficient conditions (see the Chaps. 30 and 31 by Bendall and Howe, and Diaz-Moreno et al. in this volume). All *ccs* mutants display a block in the conversion of apo- to holoform of plastid *c*-type cytochromes because the heme attachment to apocytochromes, a chemical reaction taking place in the thylakoid lumen, is compromised (Howe and Merchant 1993, 1994; Xie et al. 1998). It is also expected that lumen resident cytochrome *c*<sub>6A</sub>, the novel *c*-type cytochrome conserved in the green lineage (see the Chap. 33 by Howe et al.) is not assembled in the *ccs* mutants. However, this could not be determined because its holoform could not be detected in wild-type strains.

At least 7 loci, plastid *ccsA* and nuclear *CCS1* to *CCS6* were uncovered through genetic analysis of *ccs* mutants (Howe and Merchant 1992; Xie et al. 1998; Dreyfuss and Merchant 1999; Page et al. 2004). Sequence analysis of the cloned *ccsA* and *CCS1* genes (Xie and Merchant 1996; Inoue et al. 1997) revealed that the predicted protein products were novel integral membrane proteins co-occurring in cyanobacteria, the majority of the Gram-positive bacteria (e.g. *Bacillus subtilis*), proteobacteria of the β- (e.g. *Bordetella pertussis*), δ- (e.g. *Desulfovibrio desulfuricans*), and ε groups (e.g. *Helicobacter pylori*, *Wolinella succinogenes*), and aquificales (Simon and Hederstedt 2011). Forward and reverse genetics studies in several bacterial and cyanobacterial models have confirmed the roles of CcsA and CCS1-like proteins in the assembly of *c*-type cytochromes. This led to the definition of a distinct pathway for thioether bond formation in apocytochrome *c* (Tichy and Vermaas 1999; Beckett et al. 2000; Le Brun et al. 2000; Kern et al. 2010a, b). A representation of bacterial and plastid System II components is shown on Fig. 26.1.

## 2. A Transmembrane Heme Channel with Cytochrome *c* Synthase Activity

While CcsA was recognized as a member of the HHP family, based on the presence of the “WWD” domain and conserved histidines also found in System I CcmC and CcmF, there was no motif in CCS1 suggestive of a biochemical function in thioether bond formation (Inoue et al. 1997; Goldman et al. 1998; Hamel et al. 2003). Functional investigation of plastid CcsA and CCS1 proteins established that they are polytopic membrane proteins with functional domains exposed to the lumen and essential histidinyl residues on both the lumen and stromal side of the thylakoid membrane (Dreyfuss et al. 2003; Hamel et al. 2003). CcsA and CCS1 require each other for accumulation in vivo and were therefore proposed to function as a transmembrane heme delivery system from stroma to lumen in a complex, possibly with the products of some of the other CCS loci (Dreyfuss et al. 2003; Hamel et al. 2003). Experimental support for the biochemical activity of CcsA and CCS1 came with the discovery that naturally occurring Ccs1-CcsA fusion proteins called CcsBA, from several  $\epsilon$ -proteobacteria, could assemble reporter cytochrome(s) *c* in an *E. coli* strain lacking all of the Ccm components (Feissner et al. 2006b; Frawley and Kranz 2009; Goddard et al. 2010; Kern et al. 2010a; Richard-Fogal et al. 2012). The finding that CcsBA could substitute for all Ccm components indicated that the fusion protein was necessary and sufficient for thioether bond formation. The function of CcsBA as a transmembrane heme delivery system was confirmed from spectroscopic analysis of the purified CcsBA protein. This analysis revealed that heme can be trapped at an external binding domain where periplasmic localized histidines, provided by the CcsA moiety, act as axial ligands (Frawley and Kranz 2009). Histidines in transmembrane domains (TMD) of CcsB and CcsA, close to the cytoplasmic surface of the membrane, were postulated to act as an entry site for heme. This conclusion was based on the fact that heme was no longer detected at the

external binding domain when these residues are mutated. Imidazole-dependent rescue of the cytochrome *c* synthase activity of CcsBA carrying mutations in the TMD histidines also supported their implied involvement in providing a route for heme transport from the cytoplasm to the periplasm (Frawley and Kranz 2009). The mechanism by which heme is maintained reduced prior to the ligation reaction remains to be established. However, heme is bound to CcsBA in the oxidized form when either one of the heme-interacting histidines facing the periplasm is mutated (Frawley and Kranz 2009). This observation led to the proposal that histidine ligands act by protecting reduced heme from oxidation.

## 3. Operation of a Transmembrane Disulfide Reducing Pathway

(1) *A Two-Component Redox Pathway in Bacteria.* In System II, the involvement of thiol-based chemistry in the heme attachment reaction was first demonstrated in bacteria through the discovery of redox factors controlling cytochrome *c* assembly. Genetic screens in System II bacterial models led to the identification of a thiol-disulfide oxidoreductase (TDOR) from the DsbD family at the plasma membrane and a membrane-anchored, periplasm-facing thioredoxin-like ResA/CcsX, which are required for the covalent linkage of heme to apofoms of cytochromes *c* (Schiott et al. 1997a, b; Beckett et al. 2000; Erendsson et al. 2003). Loss of function of the redox cytochrome *c* assembly factors can be bypassed by provision of exogenous reduced thiols in the medium, a finding that led to the proposal that these components function in a disulfide reducing pathway (Beckett et al. 2000; Erendsson and Hederstedt 2002; Erendsson et al. 2003; Feissner et al. 2005; Small et al. 2013). One interpretation is that the thiols act as a substitute for the reducing activity of the assembly factors. A possible mechanism is that the thiols reduce a disulfide in the apocytochrome *c* heme-binding motif to free sulfhydryls. In

agreement with this view is the fact that the redox cytochrome *c* assembly factors are no longer required for heme attachment when the components of the disulfide forming pathway are inactivated (Erlendsson and Hederstedt 2002; Erlendsson et al. 2003; Small et al. 2013). One likely explanation is that disulfide bonds in apocytochromes *c* are formed by the disulfide forming pathway during their translocation to the periplasm. When the disulfide forming pathway no longer operates, sulfhydryls remain reduced and apocytochrome *c* is in the competent form to be acted upon by heme. So it appears that in bacteria the disulfide reducing pathway, in the context of thioether bond formation, is only needed to counter sulfhydryl oxidation of the heme-binding cysteines. In System I bacteria, a similar transmembrane disulfide reducing pathway (consisting of the thioredoxin-like CcmG and a TDOR) is also required for cytochrome *c* assembly (Fig. 26.1). As in System II, this pathway is only necessary for holocytochrome *c* maturation when the disulfide bond forming enzymes operate (Monika et al. 1997; Deshmukh et al. 2000, 2003; Bardischewsky and Friedrich 2001; Turkarslan et al. 2008).

In vivo, the disulfide bond in the heme-binding site of apocytochrome *c* is reduced to sulfhydryls by action of the thioredoxin-like ResA/CcsX. This is supported by extensive biochemical and structural studies of *B. subtilis* ResA, which reveal that the enzyme undergoes drastic conformational change and consequent increase in reactivity upon binding of oxidized apocytochrome *c* (Crow et al. 2004; Colbert et al. 2006; Lewin et al. 2006, 2008; Hodson et al. 2008). In the periplasm, ResA is maintained reduced by the activity of a TDOR of the DsbD family, which conveys the reducing power across the cytoplasmic membrane via thiol-disulfide exchange reactions. The primary source of electrons for this pathway is provided in the form of NADPH, via TrxA, the cytoplasmic thioredoxin (Möller and Hederstedt 2008).

(2) *A Bacterial-Like Redox Pathway in Plastids*. In plastids, the implication of

thiol-based chemistry in the assembly of plastid cytochrome *c* was inferred from (1) the observation that the *Chlamydomonas ccs4* and *ccs5* mutants could be phenotypically rescued by application of exogenous reductants, and (2) the occurrence in *Arabidopsis* of CCDA, another TDOR of the DsbD family at the thylakoid membrane, and HCF164, a membrane-anchored thioredoxin-like protein facing the lumen (Lennartz et al. 2001; Page et al. 2004; Motohashi and Hisabori 2010). Loss of function of CCDA and HCF164 yields a *b<sub>6</sub>f* assembly defect, an expected phenotype if heme attachment to apocytochrome *f* is compromised. However, this phenotype could not be attributed to a specific defect in cytochrome *c* assembly because the heme attachment reaction was not monitored in the *ccda* and *hcf164* mutants in *Arabidopsis* (Lennartz et al. 2001; Page et al. 2004). Molecular identification of the *Chlamydomonas CCS5* gene showed that the corresponding gene product is the ortholog of *Arabidopsis* HCF164. CCS5 was shown to interact with plastid apocytochromes *c* in a Y2H assay and a recombinant form of the molecule was active in reducing a disulfide-bonded CXXCH motif in a soluble form of apocytochrome *f* in vitro (Gabilly et al. 2010). Based on these findings, a role for CCS5/HCF164 as an apocytochrome *c* disulfide reductase in the heme attachment reaction was formulated. Oxidation of apocytochrome *c* CXXCH motif in the thylakoid lumen remains to be demonstrated, but the fact that the *ccs5*-null mutant is rescued in vivo by application of exogenous thiols is in agreement with the proposed disulfide reductase activity of CCS5/HCF164 (Gabilly et al. 2010). It is possible that, as in bacteria, apocytochrome *c* is a target of the disulfide bond forming pathway operating in the thylakoid lumen, but this remains to be experimentally tested (Karamoko et al. 2011; Lu et al. 2013).

The identification of CCS4 is intriguing, because this component does not display any motif suggesting a role in thiol-based redox chemistry (Gabilly et al. 2011). CCS4 displays limited similarity to *Arabidopsis*

HCF153, a thylakoid membrane-anchored protein required for the assembly of the cytochrome *b<sub>6</sub>f* complex (Lennartz et al. 2006). However, the activity and site of HCF153 action in the assembly process has so far remained undeciphered. The thiol-dependent photosynthetic rescue of the *ccs4* mutant, and the suppression of the *ccs4* phenotype by ectopic expression of CCDA, confirms the activity of CCS4 in a disulfide-reducing pathway for cytochrome *c* assembly (Gabilly et al. 2011). Moreover, the CCDA-dependent suppression of *ccs4* solidifies the placement of CCDA in plastid cytochrome *c* maturation, as earlier studies in *Arabidopsis* supported, but did not establish the requirement of plastid CCDA in the conversion of apo- to holocytochromes *c* (Page et al. 2004). By analogy to the bacterial disulfide reducing pathway, the proposed model is that CCDA and CCS5/HCF164 define a trans-thylakoid pathway for the delivery of reductants from stroma to lumen via thiol-disulfide exchanges (Page et al. 2004; Motohashi and Hisabori 2006, 2010; Gabilly et al. 2010, 2011). The involvement of CCS4 in the disulfide bond reducing pathway remains unclear, but a role in regulating the activity/stability of CCDA was postulated (Gabilly et al. 2011). The source of reductant is expected to originate from the stroma and *in organello* experiments support the role of the stromal thioredoxin Trx-*m* as a possible electron donor to both CCDA and HCF164 (Motohashi and Hisabori 2006, 2010).

#### 4. Additional System II Components in Plastids?

Saturating screens in System II bacteria have established the involvement of four assembly components CcsA, Ccs1/CcsB, a TDOR of the DsbD family and the thioredoxin-like ResA/CcsX (Beckett et al. 2000; Le Brun et al. 2000). In plastids, at least four additional CCS factors were revealed through genetic studies of *Chlamydomonas ccs* mutants, out of which, CCS3 and CCS6 still remain uncharacterized at the molecular level (Xie

et al. 1998; Page et al. 2004). The CCS2 locus was cloned and the corresponding gene shown to encode a plastid-resident OPR (ocotricopeptide repeat) protein (Cline et al., unpublished). Because all the OPR proteins characterized to date regulate translation, stability or maturation of chloroplast transcripts (Auchincloss et al. 2002; Balczun et al. 2005; Merendino et al. 2006; Eberhard et al. 2011; Rahire et al. 2012; Kleinknecht et al. 2014; Marx et al. 2015; Wang et al. 2015), the CCS2 protein is probably not directly involved in the heme attachment reaction. One possible function is that it controls the translation of the plastid-encoded *ccsA* transcript. It is plausible that cytochrome *c* maturation in the thylakoid lumen is more complicated than in bacteria and relies on additional components. The discovery that CCS4 functions in the disulfide reducing pathway and appears to be restricted to photosynthetic eukaryotes supports this view (Karamoko et al. 2013). The fact that the *Chlamydomonas* CCS3, CCS4, CCS5 and CCS6 loci are only defined by single alleles suggests that screens for plastid cytochrome *c* deficient mutants are not saturated and that additional CCS loci could be uncovered (Howe and Merchant 1992; Xie et al. 1998; Dreyfuss and Merchant 1999; Page et al. 2004).

#### E. System III or HCCS (HoloCytochrome C Synthase) Pathway

##### 1. Discovery of HCCS, the Signature Component of System III

System III, the first pathway for thioether bond formation to be described is defined by a single component, the prototypical HCCS or holocytochrome *c* synthase. This enzyme is responsible for the terminal step in the holocytochrome *c* synthesis pathway, that is, the formation of the thioether bonds in apocytochromes *c* and *c<sub>1</sub>* (Allen 2011; Babbitt et al. 2015). The HCCS pathway seems to be restricted to mitochondria of fungi, animals, apicomplexan parasites, red and green algae, and some protists (e.g. *Dictyostelium discoideum*), as gauged

from genome sequence analysis (Giegé et al. 2008; Allen 2011; Mavridou et al. 2013; Babbitt et al. 2015). Remarkably, the existence of two distinct mitochondrial enzymes, HCCS and HCC<sub>1</sub>S, catalyzing heme attachment onto apocytochrome *c* and *c*<sub>1</sub>, respectively, was first discovered more than 30 years ago from studies of holocytochrome *c* reconstitution using apoprotein, heme and mitochondrial extracts from fungi (Korb and Neupert 1978; Basile et al. 1980; Hennig and Neupert 1983; Visco et al. 1985). Identification of the HCCS and HCC<sub>1</sub>S-encoding genes came from later genetic studies of mutants deficient in mitochondrial cytochromes *c* and *c*<sub>1</sub> in fungi *S. cerevisiae*, *Neurospora crassa*, and *Candida albicans*, and these organisms have remained the focus of attention for the analysis of System III (Dumont et al. 1987; Nargang et al. 1988; Drygas et al. 1989; Zollner et al. 1992; Cervera et al. 1998). Genetic studies in *S. cerevisiae* established that apocytochrome *c* can only be assembled by HCCS, while apocytochrome *c*<sub>1</sub> is a substrate of both HCCS and HCC<sub>1</sub>S (Bernard et al. 2003). The holocytochrome *c*<sub>1</sub> synthase activity of HCCS is weak but can be enhanced if the substrate-enzyme interactions are modified via over-expression of the HCCS-encoding gene or point mutations in either HCCS or apocytochrome *c*<sub>1</sub> (Bernard et al. 2003). However, animals are the only System III organisms with a single HCCS, which was shown to act on both apocytochrome *c* and *c*<sub>1</sub> substrates (Schwarz and Cox 2002; Bernard et al. 2003).

Both HCCS and HCC<sub>1</sub>S are peripherally bound to the mitochondrial inner membrane and face the IMS, the compartment where the heme attachment reaction takes place (Dumont et al. 1991; Steiner et al. 1995; Bernard et al. 2005). All HCCSs are related in sequence (less than 20 % amino acid sequence identity in pairwise comparisons) and display zero to four typical HRMs (heme regulatory motif), also present in several other heme-binding proteins, such as the transcription factor Hap1p and HO (Heme oxygenase)

(Li et al. 2011). In intact or detergent-solubilized mitochondria, HCCSs were shown to interact with apocytochromes *c* (Nicholson et al. 1988; Nicholson and Neupert 1989; Mayer et al. 1995) and also with heme via the HRM (Steiner et al. 1996). Nevertheless, the HRMs are not strictly essential for formation of holocytochrome *c* and *c*<sub>1</sub>, suggesting that other domains of the HCCS must be important for their enzymatic activity (Steiner et al. 1996; Moore et al. 2011).

Because mitochondrial cytochrome *c* could be correctly matured in the bacterial periplasm or cytoplasm upon expression of HCCS alone, and did not require co-expression of any other assembly factors, HCCSs were proposed to participate in the biogenesis of *c*-type cytochromes by catalyzing thioether bond formation (Dumont et al. 1988; Pollock et al. 1998; Sanders and Lill 2000; Richard-Fogal et al. 2012).

However, despite the fact that HCCSs were the first *c*-type cytochrome assembly factors to be discovered, the specific enzymatic function of the proteins had remained elusive for a long time until recently. An important breakthrough in detailing the enzymology of HCCS came with the purification and spectroscopic analysis of the human enzyme co-expressed with its cognate apocytochrome *c* substrate in the bacterial cytoplasm (San Francisco et al. 2013; Babbitt et al. 2014a, b). Furthermore, the use of mutant forms of the enzyme and apocytochrome substrate enabled the trapping of intermediate complexes, which led to the delineation of possible steps in the heme attachment reaction. The first step in the HCCS-dependent heme attachment reaction is the binding of heme to the enzyme via two domains (I and II) containing conserved residues. One of these, a histidine in domain II, acts as an axial ligand of heme. Formation of the heme-HCCS complex triggers the recognition of the apocytochrome *c* substrate. The determinants for substrate recognition by HCCS were established using cytochrome *c* and found

to lie within a 9 residue sequence upstream the CXXCH motif (Stevens et al. 2011; Asher and Bren 2012; Verissimo et al. 2012; San Francisco et al. 2013). It is likely that the sequence requirements for recognition of cytochrome *c*<sub>1</sub> are similar but this awaits experimental testing.

The heme-HCCS-apocytochrome *c* together forms a ternary complex, where heme is coordinated by one histidine in domain II and another histidine in the CXXCH motif on apocytochrome *c* (San Francisco et al. 2013). The mechanism for thioether bond formation is still obscure, but bis-histidinylation of heme in the heme-HCCS-apocytochrome *c* complex is postulated to provide the ideal geometry for stereospecific thioether bond formation. In addition, the observation that some residues in HCCS control the retention of holocytochrome *c* in HCCS suggests that a mechanism for releasing the mature holoform from the enzyme is probably required for optimal cytochrome *c* synthesis (San Francisco et al. 2013; Babbitt et al. 2014a, b). Interestingly, none of the domains defined as important for the HCCS enzymatic activity include the HRMs initially postulated to be required for HCCS function (Allen 2011). In HO, another enzyme containing HRM motifs, the HRM cysteine sulfhydryls can switch between an oxidized or reduced form depending on the cellular redox state. Furthermore, thiol-disulfide interconversion at the HRMs was shown to regulate the heme-binding activity of HO and it is possible HRMs in HCCS perform the same function (Yi and Ragsdale 2007; Yi et al. 2009).

## 2. Missing Components in System III?

System III appears deceptively simple in terms of composition, in contrast to the complexity of Systems I and II, because extensive genetic screens in *S. cerevisiae* and *N. crassa* have so far revealed only HCCS and HCC<sub>1</sub>S as assembly factors for mitochondrial cytochromes *c* (Lang and Kaudewitz 1982; Dumont et al. 1987; Drygas et al. 1989; Sherman 1990; Zollner et al.

1992). Important future avenues for research include investigation into the mechanisms of heme delivery to the mitochondrial IMS. Furthermore, by analogy to System I and II, mechanisms for maintenance of the sulfhydryls and chemical reduction of heme prior to the ligation reaction must also operate. There is evidence that both of these are still biochemical requirements of the pathway from *in organello* reconstitution of holocytochromes *c* and *c*<sub>1</sub>. In the former instance, the CXXCH sulfhydryls were shown to be maintained reduced by an unknown mechanism until the heme ligation reaction (Nicholson et al. 1987). In the latter instance, both pyrimidine and flavin nucleotides were shown to be required for chemical reduction of heme iron (Basile et al. 1980; Nicholson and Neupert 1989; Nicholson et al. 1989; Tong and Margoliash 1998).

One candidate protein for the reduction of heme is Cyc2p, a mitochondrial protein first discovered in a screen for cytochrome *c* deficient mutants in yeast and initially assigned a function in the import of apocytochrome *c* (Dumont et al. 1993; Pearce et al. 1998; Sanchez et al. 2001). Cyc2p is an inner membrane anchored, IMS-facing, NAD(P)H-dependent flavoprotein and was re-isolated as a factor enhancing the holocytochrome *c*<sub>1</sub> synthase activity of HCCS through a multicopy suppressor screen (Bernard et al. 2003, 2005). An *in vivo* indication that Cyc2p controls a reductive step in the heme attachment reaction is the finding that the requirement for its function can be bypassed by exogenous reductants (Corvest et al. 2012), similar to what was observed for plastid and bacterial cytochrome *c* assembly mutants deficient in the disulfide reducing pathway (Deshmukh et al. 2000, 2003; Bardischewsky and Friedrich 2001; Turkarlan et al. 2008; Gabilly et al. 2010, 2011). However, although redox titrations of Cyc2p flavin indicate that reduction of a disulfide at the CXXCH site of apocytochrome *c* is a thermodynamically favorable reaction, Cyc2p does not act as an apocytochrome *c* CXXCH disulfide

reductase in vitro. Instead, Cyc2p is able to catalyze the NAD(P)H-dependent reduction of heme in vitro, indicating a possible role in reducing the heme iron prior to its attachment (Corvest et al. 2010, 2012). Y2H analysis showing that Cyc2p interacts with HCCS and also with apocytochromes *c* and *c*<sub>1</sub> led to the proposal that Cyc2p, possibly in a complex with HCCS, reduces the heme iron prior to co-factor attachment to the apoforms of cytochrome *c* and *c*<sub>1</sub>. Operation of a distinct heme reductase dedicated to the HCC<sub>1</sub>S enzyme was postulated based on the fact that Cyc2p is only required for the HCCS-dependent assembly of cytochrome *c* and *c*<sub>1</sub> and does not control the HCC<sub>1</sub>S-catalyzed heme attachment to apocytochrome *c*<sub>1</sub> (Corvest et al. 2010). Because Cyc2p appears to be restricted to fungi, additional mechanism(s) of heme reduction in System III mitochondria must exist in other organisms.

#### F. System IV or CCB (Cofactor Assembly on Complex C Subunit B)

##### 1. A Multi-step Pathway for Heme *c*<sub>i</sub> Formation in the *b*<sub>6</sub>*f* Complex

Covalently attached heme in cytochrome *b*<sub>6</sub> in the *b*<sub>6</sub>*f* and cytochrome *b* in the *bc* of Firmicutes was suspected from spectroscopic measurement and the observation that heme/cytochrome *b* association was unusually resistant to denaturing treatment (Lavergne 1983; Joliot and Joliot 1988; Kuras et al. 1997; Yu and Le Brun 1998). However, *b*<sub>L</sub> or *b*<sub>H</sub> heme was believed to be attached covalently at the time and the discovery of an additional heme (heme *c*<sub>i</sub>) bound via a single thioether bond in the X-ray structures of chloroplast and cyanobacterial *b*<sub>6</sub>*f* came as a surprise (Kurusu et al. 2003; Stroebel et al. 2003). Heme *c*<sub>i</sub> is located in close vicinity to heme *b*<sub>H</sub> and unlike heme *c* in canonical *c*-type cytochromes, does not appear to have any amino acid axial ligands (Kurusu et al. 2003; Stroebel et al. 2003; de Vitry et al. 2004). Heme *c*<sub>i</sub> has a unique axial ligand, a water molecule (or

possibly a hydroxide ion) also interacting with a propionate group of heme *b*<sub>H</sub>. A pathway for apo- to holocytochrome *b*<sub>6</sub> conversion was deduced from the analysis of *Chlamydomonas* strains depleted for heme or carrying mutations of the histidines coordinating *b*<sub>L</sub> and *b*<sub>H</sub> hemes (Kuras et al. 1997). While apocytochrome *b*<sub>6</sub> could be immunodetected in heme-deprived cells and mutants unable to ligate *b*<sub>L</sub>, a distinct immunoreactive species of cytochrome *b*<sub>6</sub> was present in mutants altered for *b*<sub>H</sub> ligation. The same species is also detected when the thioether bond forming cysteine in cytochrome *b*<sub>6</sub> is mutated (de Vitry et al. 2004). This indicates that loss of *b*<sub>H</sub> ligation prevents formation of heme *c*<sub>i</sub> and, reciprocally, that, in the absence of covalent attachment of heme, heme *b*<sub>H</sub> is presumably no longer retained. Spectroscopic analysis of the purified *b*<sub>6</sub>*f* complex altered for *b*<sub>H</sub> ligation showed that heme *b*<sub>L</sub> was present while hemes *b*<sub>H</sub> and *c*<sub>i</sub> were lost (Malnoë et al. 2011). Collectively, these results demonstrate that holocytochrome *b*<sub>6</sub> assembly proceeds through a *b*<sub>L</sub>-containing intermediate, followed by incorporation of *b*<sub>H</sub> and formation of heme *c*<sub>i</sub>.

##### 2. Identification of Novel Proteins Required for Heme *c*<sub>i</sub> Assembly

The accumulation of a *b*<sub>L</sub>-containing intermediate was exploited as a signature to identify assembly factors controlling heme *c*<sub>i</sub> formation, referred to as CCB (for Cofactor assembly of complex C subunit B<sup>3</sup>) (Kuras et al. 1997; de Vitry et al. 2004). In *Chlamydomonas*, four CCB loci were defined from the genetic analysis of *b*<sub>6</sub>*f*-deficient mutants that no longer assemble holocytochrome *b*<sub>6</sub> but still accumulate the *b*<sub>L</sub>-containing cytochrome *b*<sub>6</sub> intermediate (Gumpel et al. 1995; Kuras et al. 1997, 2007). The *ccb* mutants are unable to grow photosynthetically but still retain low levels of *b*<sub>6</sub>*f* (Lyska et al. 2007; Saint-Marcoux

<sup>3</sup>B is for petB (or cytochrome *b*<sub>6</sub>) of the cytochrome *b*<sub>6</sub>*f* complex (complex C).



et al. 2009). Wild-type levels of *b<sub>6</sub>f* lacking heme *c<sub>i</sub>* can be restored in *ccb* mutants with suppressor mutations attenuating the activity of the thylakoid FtsH protease (Malnoë et al. 2014). This result demonstrates that heme *c<sub>i</sub>* is not absolutely required for complex assembly/activity and that *b<sub>6</sub>f* lacking heme *c<sub>i</sub>* becomes prone to proteolytic degradation. The photosynthetic growth of the suppressed strains is light-sensitive, an indication that the presence of heme *c<sub>i</sub>* is required for optimal activity of the *b<sub>6</sub>f* complex (Malnoë et al. 2014).

The *CCB* genes were cloned and the corresponding gene products were shown to be novel thylakoid transmembrane proteins conserved in all organisms performing oxygenic photosynthesis (Kuras et al. 2007). In *Arabidopsis*, loss of function of CCB proteins yields a defect in heme *c<sub>i</sub>* formation (Lyska et al. 2007; Lezhneva et al. 2008). In cyanobacteria, *ccb* mutants are impaired for photosynthesis, but the function of CCB in heme *c<sub>i</sub>* biogenesis could not be ascertained because the impact on the *b<sub>6</sub>f* complex was not examined (Ishikawa et al. 2009).

The following pathway of action for the CCB machinery can be deduced from genetic and biochemical studies (Fig. 26.1). Interaction of CCB proteins with cytochrome *b<sub>6</sub>* is supported by BN-PAGE and co-immunoprecipitation experiments (Saint-Marcoux et al. 2009). Because subunit IV is not detected in association with the CCB factors, it was deduced that unassembled cytochrome *b<sub>6</sub>*, presumably a form containing both *b<sub>L</sub>* and *b<sub>H</sub>* hemes, is the substrate of the CCB machinery. The detection of a CCB1/cytochrome *b<sub>6</sub>* complex in *ccb2*, *ccb3* and *ccb4* mutants indicates that this complex is the first intermediate in the pathway and may chaperone the cytochrome *b<sub>6</sub>* substrate before the heme ligation step. This step is believed to be catalyzed by a CCB2/CCB4/CCB3 complex, also detected in association with cytochrome *b<sub>6</sub>* in a mutant altered for the thioether bond-forming cysteine. The presence of a stable CCB2/CCB4 heterodimer and a CCB3/cytochrome *b<sub>6</sub>* complex indicates

that these might also be intermediates in the assembly pathway. A model was postulated where CCB3/cytochrome *b<sub>6</sub>* is the second intermediate in the pathway and recruits the CCB2/CCB4 complex to form the CCB3/CCB2/CCB4 heme ligation complex (Fig. 26.1). Although the biochemical activity of the CCB factors remains to be elaborated, it is reasonable to postulate that some of the protein domains must interact with both heme and cytochrome *b<sub>6</sub>*. Moreover a mechanism for maintaining heme in a reduced form must exist, considering that the redox state of the heme iron is critical for the chemistry of thioether bond formation. Typical heme-binding motifs found in System I and II cytochrome *c* assembly factors, or conserved histidines, are not present in the CCB factors (Kuras et al. 2007). Occurrence of conserved, heme-interacting residues, such as tryptophan, tyrosine and/or phenylalanine, in regions exposed to the *n*-side of the membrane speaks to a possible heme handling/relay function, but this remains to be experimentally tested.

## Acknowledgments

This work is supported by a National Science Foundation grant (MCB-0920062), a U.S. Department of Energy (DOE), Office of Science, Basic Energy Sciences (BES) (DE-SC0014562) grant and a Muscular Dystrophy Association grant (MDA#4247) to P.H. We thank Dr. A. Simcox for critical reading of the manuscript and Dr. R. Kranz, Dr. A. Malnoë, Dr. J. Stevens, Dr. S. Ferguson and Dr. G. Bonnard for their valuable insights into cytochrome *c* maturation.

## References

- Ajioka RS, Phillips JD, Kushner JP (2006) Biosynthesis of heme in mammals. *Biochim Biophys Acta* 1763:723–736
- Allen JWA (2011) Cytochrome *c* biogenesis in mitochondria – Systems III and V. *FEBS J* 278: 4198–4216

- Allen JW, Daltrop O, Stevens JM, Ferguson SJ (2003) C-type cytochromes: diverse structures and biogenesis systems pose evolutionary problems. *Philos Trans R Soc Lond B Biol Sci* 358:255–266
- Allen JW, Jackson AP, Rigden DJ, Willis AC, Ferguson SJ, Ginger ML (2008a) Order within a mosaic distribution of mitochondrial *c*-type cytochrome biogenesis systems? *FEBS J* 275:2385–2402
- Allen JWA, Ferguson SJ, Ginger ML (2008b) Distinctive biochemistry in the trypanosome mitochondrial intermembrane space suggests a model for stepwise evolution of the MIA pathway for import of cysteine-rich proteins. *FEBS Lett* 582:2817–2825
- Aragão D, Frazão C, Sieker L, Sheldrick GM, LeGall J, Carrondo MA (2003) Structure of dimeric cytochrome *c*<sub>3</sub> from *Desulfovibrio gigas* at 1.2 Å resolution. *Acta Crystallogr D Biol Crystallogr* 59:644–653
- Asher WB, Bren KL (2012) Cytochrome *c* heme lyase can mature a fusion peptide composed of the amino-terminal residues of horse cytochrome *c*. *Chem Commun (Camb)* 48:8344–8346
- Attea A, van Lis R, Beale SI (2005) Enzymes of the heme biosynthetic pathway in the nonphotosynthetic alga *Polytomella* sp. *Eukaryot Cell* 4:2087–2097
- Auchincloss AH, Zerges W, Perron K, Girard-Bascou J, Rochaix JD (2002) Characterization of Tbc2, a nucleus-encoded factor specifically required for translation of the chloroplast *psbC* mRNA in *Chlamydomonas reinhardtii*. *J Cell Biol* 157:953–962
- Babbitt SE, San Francisco B, Bretsnyder EC, Kranz RG (2014a) Conserved residues of the human mitochondrial holocytochrome *c* synthase mediate interactions with heme. *Biochemistry* 53:5261–5271
- Babbitt SE, San Francisco B, Mendez DL, Lukat-Rodgers GS, Rodgers KR, Bretsnyder EC, Kranz RG (2014b) Mechanisms of mitochondrial holocytochrome *c* synthase and the key roles played by cysteines and histidine of the heme attachment site, Cys-XX-Cys-His. *J Biol Chem* 289:28795–28807
- Babbitt SE, Sutherland MC, Francisco BS, Mendez DL, Kranz RG (2015) Mitochondrial cytochrome *c* biogenesis: no longer an enigma. *Trends Biochem Sci* 40:446–455
- Balczun C, Bunse A, Hahn D, Bennoun P, Nickelsen J, Kuck U (2005) Two adjacent nuclear genes are required for functional complementation of a chloroplast trans-splicing mutant from *Chlamydomonas reinhardtii*. *Plant J* 43:636–648
- Balk J, Schaedler TA (2014) Iron cofactor assembly in plants. *Annu Rev Plant Biol* 65:125–153
- Bardischewsky F, Friedrich CG (2001) Identification of *ccdA* in *Paracoccus pantotrophus* GB17: disruption of *ccdA* causes complete deficiency in *c*-type cytochromes. *J Bacteriol* 183:257–263
- Barker PD, Ferguson SJ (1999) Still a puzzle: why is haem covalently attached in *c*-type cytochromes? *Struct Fold Des* 7:281–290
- Barker PD, Ferrer JC, Mylrajan M, Loehr TM, Feng R, Konishi Y, Funk, WD, . . . , Mauk AG (1993) Transmutation of a heme protein. *Proc Natl Acad Sci U S A* 90:6542–6546
- Basile G, Di Bello C, Taniuchi H (1980) Formation of an iso-1-cytochrome *c*-like species containing a covalently bonded heme group from the apoprotein by a yeast cell-free system in the presence of hemin. *J Biol Chem* 255:7181–7191
- Beckett CS, Loughman JA, Karberg KA, Donato GM, Goldman WE, Kranz RG (2000) Four genes are required for the system II cytochrome *c* biogenesis pathway in *Bordetella pertussis*, a unique bacterial model. *Mol Microbiol* 38:465–481
- Bernard DG, Gabilly ST, Dujardin G, Merchant S, Hamel PP (2003) Overlapping specificities of the mitochondrial cytochrome *c* and *c*<sub>1</sub> heme lyases. *J Biol Chem* 278:49732–49742
- Bernard DG, Quevillon-Cheruel S, Merchant S, Guiard B, Hamel PP (2005) Cyc2p, a membrane-bound flavoprotein involved in the maturation of mitochondrial *c*-type cytochromes. *J Biol Chem* 280:39852–39859
- Bertini I, Cavallaro G, Rosato A (2007) Evolution of mitochondrial-type cytochrome *c* domains and of the protein machinery for their assembly. *J Inorg Biochem* 101:1798–1811
- Bonnard G, Corvest V, Meyer EH, Hamel PP (2010) Redox processes controlling the biogenesis of *c*-type cytochromes. *Antioxid Redox Signal* 13:1385–1401
- Boronowsky U, Wenk S, Schneider D, Jager C, Rogner M (2001) Isolation of membrane protein subunits in their native state: evidence for selective binding of chlorophyll and carotenoid to the *b*<sub>6</sub> subunit of the cytochrome *b*<sub>6</sub>*f* complex. *Biochim Biophys Acta* 1506:55–66
- Cervera AM, Gozalbo D, McCreath KJ, Gow NA, Martinez JP, Casanova M (1998) Molecular cloning and characterization of a *Candida albicans* gene coding for cytochrome *c* haem lyase and a cell wall-related protein. *Mol Microbiol* 30:67–81
- Chakravarti R, Aulak KS, Fox PL, Stuehr DJ (2010) GAPDH regulates cellular heme insertion into inducible nitric oxide synthase. *Proc Natl Acad Sci U S A* 107:18004–18009
- Cho SH, Collet JF (2013) Many roles of the bacterial envelope reducing pathways. *Antioxid Redox Signal* 18:1690–1698

- Colbert CL, Wu Q, Erbel PJ, Gardner KH, Deisenhofer J (2006) Mechanism of substrate specificity in *Bacillus subtilis* ResA, a thioredoxin-like protein involved in cytochrome *c* maturation. *Proc Natl Acad Sci U S A* 103:4410–4415
- Corvest V, Murrey DA, Bernard DG, Knaff DB, Guiard B, Hamel PP (2010) *c*-type cytochrome assembly in *Saccharomyces cerevisiae*: a key residue for apocytochrome *c*<sub>1</sub>/lyase interaction. *Genetics* 186:561–571
- Corvest V, Murrey DA, Hirasawa M, Knaff DB, Guiard B, Hamel PP (2012) The flavoprotein Cyc2p, a mitochondrial cytochrome *c* assembly factor, is a NAD(P)H-dependent haem reductase. *Mol Microbiol* 83:968–980
- Crow A, Acheson RM, Le Brun NE, Oubrie A (2004) Structural basis of Redox-coupled protein substrate selection by the cytochrome *c* biosynthesis protein ResA. *J Biol Chem* 279:23654–23660
- Daltrop O, Ferguson SJ (2003) Cytochrome *c* maturation. The in vitro reactions of horse heart apocytochrome *c* and *Paracoccus denitrificans* apocytochrome *c*<sub>550</sub> with heme. *J Biol Chem* 278:4404–4409
- Daltrop O, Ferguson SJ (2004) In vitro studies on thioether bond formation between *Hydrogenobacter thermophilus* apocytochrome *c*<sub>552</sub> with metalloprotoporphyrin derivatives. *J Biol Chem* 279:45347–45353
- Daltrop O, Allen JW, Willis AC, Ferguson SJ (2002) In vitro formation of a *c*-type cytochrome. *Proc Natl Acad Sci U S A* 99:7872–7876
- de Vitry C (2011) Cytochrome *c* maturation system on the negative side of bioenergetic membranes: CCB or System IV. *FEBS J* 278:4189–4197
- de Vitry C, Desbois A, Redeker V, Zito F, Wollman FA (2004) Biochemical and spectroscopic characterization of the covalent binding of heme to cytochrome *b*<sub>6</sub>. *Biochemistry* 43:3956–3968
- Deshmukh M, Brasseur G, Daldal F (2000) Novel *Rhodobacter capsulatus* genes required for the biogenesis of various *c*-type cytochromes. *Mol Microbiol* 35:123–138
- Deshmukh M, Turkarslan S, Astor D, Valkova-Valchanova M, Daldal F (2003) The dithiol:disulfide oxidoreductases DsbA and DsbB of *Rhodobacter capsulatus* are not directly involved in cytochrome *c* biogenesis, but their inactivation restores the cytochrome *c* biogenesis defect of *CcdA*-null mutants. *J Bacteriol* 185:3361–3372
- Dibrova DV, Cherepanov DA, Galperin MY, Skulachev VP, Mulikidjanian AY (2013) Evolution of cytochrome *bc* complexes: from membrane-anchored dehydrogenases of ancient bacteria to triggers of apoptosis in vertebrates. *Biochim Biophys Acta* 1827:1407–1427
- Dreyfuss BW, Merchant S (1999) *CCS5*, a new locus required for chloroplast *c*-type synthesis. In: Pusztai J, Garab G (eds) *Proceedings of the XIth International Congress on Photosynthesis*. Kluwer, Dordrecht, pp 3139–3142
- Dreyfuss BW, Hamel PP, Nakamoto SS, Merchant S (2003) Functional analysis of a divergent system II protein, Ccs1, involved in *c*-type cytochrome biogenesis. *J Biol Chem* 278:2604–2613
- Drygas ME, Lambowitz AM, Nargang FE (1989) Cloning and analysis of the *Neurospora crassa* gene for cytochrome *c* heme lyase. *J Biol Chem* 264:17897–17906
- Ducluzeau AL, Chenu E, Capowiez L, Baymann F (2008) The Rieske/cytochrome *b* complex of *Helicobacter*. *Biochim Biophys Acta* 1777:1140–1146
- Dumont ME, Ernst JF, Hampsey DM, Sherman F (1987) Identification and sequence of the gene encoding cytochrome *c* heme lyase in the yeast *Saccharomyces cerevisiae*. *EMBO J* 6:235–241
- Dumont ME, Ernst JF, Sherman F (1988) Coupling of heme attachment to import of cytochrome *c* into yeast mitochondria. Studies with heme lyase-deficient mitochondria and altered apocytochromes *c*. *J Biol Chem* 263:15928–15937
- Dumont ME, Cardillo TS, Hayes MK, Sherman F (1991) Role of cytochrome *c* heme lyase in mitochondrial import and accumulation of cytochrome *c* in *Saccharomyces cerevisiae*. *Mol Cell Biol* 11:5487–5496
- Dumont ME, Schlichter JB, Cardillo TS, Hayes MK, Bethlendy G, Sherman F (1993) *CYC2* encodes a factor involved in mitochondrial import of yeast cytochrome *c*. *Mol Cell Biol* 13:6442–6451
- Eberhard S, Loiselay C, Drapier D, Bujaldon S, Girard-Bascou J, Kuras R, Choquet Y, Wollman FA (2011) Dual functions of the nucleus-encoded factor TDA1 in trapping and translation activation of *atpA* transcripts in *Chlamydomonas reinhardtii* chloroplasts. *Plant J* 67:1055–1066
- Einsle O, Messerschmidt A, Stach P, Bourenkov GP, Bartunik HD, Huber R, Kroneck PM (1999) Structure of cytochrome *c* nitrite reductase. *Nature* 400:476–480
- Erlendsson LS, Hederstedt L (2002) Mutations in the thiol-disulfide oxidoreductases BdbC and BdbD can suppress cytochrome *c* deficiency of *CcdA*-defective *Bacillus subtilis* cells. *J Bacteriol* 184:1423–1429
- Erlendsson LS, Acheson RM, Hederstedt L, Le Brun NE (2003) *Bacillus subtilis* ResA is a thiol-disulfide oxidoreductase involved in cytochrome *c* synthesis. *J Biol Chem* 278:17852–17858

- Feissner RE, Beckett CS, Loughman JA, Kranz RG (2005) Mutations in cytochrome assembly and periplasmic redox pathways in *Bordetella pertussis*. *J Bacteriol* 187:3941–3949
- Feissner RE, Richard-Fogal CL, Frawley ER, Kranz RG (2006a) ABC transporter-mediated release of a haem chaperone allows cytochrome *c* biogenesis. *Mol Microbiol* 61:219–231
- Feissner RE, Richard-Fogal CL, Frawley ER, Loughman JA, Earley KW, Kranz RG (2006b) Recombinant cytochromes *c* biogenesis systems I and II and analysis of haem delivery pathways in *Escherichia coli*. *Mol Microbiol* 60:563–577
- Flegontov P, Michalek J, Janouskovec J, Lai DH, Jirku M, Hajduskova E, Tomčala A, . . . , Lukes J (2015) Divergent mitochondrial respiratory chains in phototrophic relatives of apicomplexan parasites. *Mol Biol Evol* 32:1115–1131
- Francs-Small CC, Kroeger T, Zmudjak M, Ostersetzer-Biran O, Rahimi N, Small I, Barkan A (2011) A PORR domain protein required for *rpl2* and *ccmF<sub>C</sub>* intron splicing and for the biogenesis of *c*-type cytochromes in *Arabidopsis* mitochondria. *Plant J* 69:996–1005
- Frawley ER, Kranz RG (2009) CcsBA is a cytochrome *c* synthetase that also functions in heme transport. *Proc Natl Acad Sci U S A* 106:10201–10206
- Gabilly ST, Dreyfuss BW, Karamoko M, Corvest V, Kropat J, Page MD, Merchant SS, Hamel PP (2010) CCS5, a thioredoxin-like protein involved in the assembly of plastid *c*-type cytochromes. *J Biol Chem* 285:29738–29749
- Gabilly ST, Kropat J, Karamoko M, Page MD, Nakamoto SS, Merchant SS, Hamel PP (2011) A novel component of the disulfide-reducing pathway required for cytochrome *c* assembly in plastids. *Genetics* 187:793–802
- Ghosh A, Chawla-Sarkar M, Stuehr DJ (2011) Hsp90 interacts with inducible NO synthase client protein in its heme-free state and then drives heme insertion by an ATP-dependent process. *FASEB J* 25:2049–2060
- Giegé P, Rayapuram N, Meyer EH, Grienenberger JM, Bonnard G (2004) CcmF<sub>C</sub> involved in cytochrome *c* maturation is present in a large sized complex in wheat mitochondria. *FEBS Lett* 563:165–169
- Giegé P, Grienenberger JM, Bonnard G (2008) Cytochrome *c* biogenesis in mitochondria. *Mitochondrion* 8:61–73
- Goddard AD, Stevens JM, Rondelet A, Nomerotskaia E, Allen JW, Ferguson SJ (2010) Comparing the substrate specificities of cytochrome *c* biogenesis Systems I and II: bioenergetics. *FEBS J* 277:726–737
- Goldman BS, Beck DL, Monika EM, Kranz RG (1998) Transmembrane heme delivery systems. *Proc Natl Acad Sci U S A* 95:5003–5008
- Graham LA, Trumpower BL (1991) Mutational analysis of the mitochondrial Rieske iron-sulfur protein of *Saccharomyces cerevisiae*. III. Import, protease processing, and assembly into the cytochrome *bc<sub>1</sub>* complex of iron-sulfur protein lacking the iron-sulfur cluster. *J Biol Chem* 266:22485–22492
- Gubernator B, Kroliczewski J, Kallas T, Szczepaniak A (2006) Iron-sulfur cluster reconstitution of spinach chloroplast Rieske protein requires a partially prefolded apoprotein. *Biochim Biophys Acta* 1764:735–742
- Gumpel NJ, Ralley L, Girard-Bascou J, Wollman F-A, Nugent JHA, Purton S (1995) Nuclear mutants of *Chlamydomonas reinhardtii* defective in the biogenesis of the cytochrome *b<sub>6</sub>f* complex. *Plant Mol Biol* 29:921–932
- Hamel PP, Dreyfuss BW, Xie Z, Gabilly ST, Merchant S (2003) Essential histidine and tryptophan residues in CcsA, a system II polytopic cytochrome *c* biogenesis protein. *J Biol Chem* 278:2593–2603
- Hamel P, Corvest V, Giege P, Bonnard G (2009) Biochemical requirements for the maturation of mitochondrial *c*-type cytochromes. *Biochim Biophys Acta* 1793:125–138
- Hamza I, Dailey HA (2012) One ring to rule them all: trafficking of heme and heme synthesis intermediates in the metazoans. *Biochim Biophys Acta* 1823:1617–1632
- Hannibal L, Collins D, Brassard J, Chakravarti R, Vempati R, Dorlet P, Santolini J, . . . , Stuehr DJ (2012) Heme binding properties of glyceraldehyde-3-phosphate dehydrogenase. *Biochemistry* 51:8514–8529
- Hartshorne RS, Kern M, Meyer B, Clarke TA, Karas M, Richardson DJ, Simon J (2007) A dedicated haem lyase is required for the maturation of a novel bacterial cytochrome *c* with unconventional covalent haem binding. *Mol Microbiol* 64:1049–1060
- Hasan SS, Yamashita E, Cramer WA (2013) Transmembrane signaling and assembly of the cytochrome *b<sub>6</sub>f*-lipidic charge transfer complex. *Biochim Biophys Acta* 1827:1295–1308
- Hennig B, Neupert W (1983) Biogenesis of cytochrome *c* in *Neurospora crassa*. *Methods Enzymol* 97:261–274
- Hildenbeutel M, Hegg EL, Stephan K, Gruschke S, Meunier B, Ott M (2014) Assembly factors monitor sequential hemylation of cytochrome *b* to regulate mitochondrial translation. *J Cell Biol* 205:511–524
- Hodson CT, Lewin A, Hederstedt L, Le Brun NE (2008) The active-site cysteinyls and hydropho-

- bic cavity residues of ResA are important for cytochrome *c* maturation in *Bacillus subtilis*. J Bacteriol 190:4697–4705
- Holton B, Wu X, Tsapin AI, Kramer DM, Malkin R, Kallas T (1996) Reconstitution of the 2Fe-2S center and  $g = 1.89$  electron paramagnetic resonance signal into overproduced *Nostoc* sp. PCC 7906 Rieske protein. Biochemistry 35:15485–15493
- Howe G, Merchant S (1992) The biosynthesis of membrane and soluble plastidic *c*-type cytochromes of *Chlamydomonas reinhardtii* is dependent on multiple common gene products. EMBO J 11:2789–2801
- Howe G, Merchant S (1993) Maturation of thylakoid lumen proteins proceeds post-translationally through an intermediate in vivo. Proc Natl Acad Sci U S A 90:1862–1866
- Howe G, Merchant S (1994) Role of heme in the biosynthesis of cytochrome *c*<sub>6</sub>. J Biol Chem 269:5824–5832
- Howe G, Mets L, Merchant S (1995) Biosynthesis of cytochrome *f* in *Chlamydomonas reinhardtii*: analysis of the pathway in gabaculine-treated cells and in the heme attachment mutant B6. Mol Genet 246:156–165
- Huang D, Everly RM, Cheng RH, Heymann JB, Schagger H, Sled V, Ohnishi T, . . . , Cramer WA (1994) Characterization of the chloroplast cytochrome *b*<sub>6</sub>*f* complex as a structural and functional dimer. Biochemistry 33:4401–4409
- Inoue K, Dreyfuss BW, Kindle KL, Stern DB, Merchant S, Sodeinde OA (1997) *CCSI*, a nuclear gene required for the post-translational assembly of chloroplast *c*-type cytochromes. J Biol Chem 272:31747–31754
- Ishikawa M, Fujiwara M, Sonoike K, Sato N (2009) Orthogenomics of photosynthetic organisms: bioinformatic and experimental analysis of chloroplast proteins of endosymbiont origin in *Arabidopsis* and their counterparts in *Synechocystis*. Plant Cell Physiol 50:773–788
- Jentzen W, Ma JG, Shelnutt JA (1998) Conservation of the conformation of the porphyrin macrocycle in hemoproteins. Biophys J 74:753–763
- Joliot P, Joliot A (1988) The low-potential electron-transfer chain in the cytochrome *b*<sub>6</sub>*f* complex. Biochim Biophys Acta 933:319–333
- Jonietz C, Forner J, Hildebrandt T, Binder S (2011) RNA PROCESSING FACTOR3 is crucial for the accumulation of mature *ccmC* transcripts in mitochondria of *Arabidopsis* accession Columbia. Plant Physiol 157:1430–1439
- Jungst A, Wakabayashi S, Matsubara H, Zumft WG (1991) The *nirSTBM* region coding for cytochrome *cd*<sub>1</sub>-dependent nitrite respiration of *Pseudomonas stutzeri* consists of a cluster of mono-, di-, and tetraheme proteins. FEBS Lett 279:205–209
- Karamoko M, Cline S, Redding K, Ruiz N, Hamel PP (2011) Lumen Thiol Oxidoreductase1, a disulfide bond-forming catalyst, is required for the assembly of photosystem II in *Arabidopsis*. Plant Cell 23:4462–4475
- Karamoko M, Gabilly ST, Hamel PP (2013) Operation of trans-thylakoid thiol-metabolizing pathways in photosynthesis. Front Plant Sci 4:476
- Kern M, Eisel F, Scheithauer J, Kranz RG, Simon J (2010a) Substrate specificity of three cytochrome *c* haem lyase isoenzymes from *Wolinella succinogenes*: unconventional haem *c* binding motifs are not sufficient for haem *c* attachment by Nrfl and CcsA1. Mol Microbiol 75:122–137
- Kern M, Scheithauer J, Kranz RG, Simon J (2010b) Essential histidine pairs indicate conserved haem binding in epsilon proteobacterial cytochrome *c* haem lyases. Microbiology 156:3773–3781
- Kleinknecht L, Wang F, Stube R, Philippar K, Nickelsen J, Bohne AV (2014) RAP, the sole octotricopeptide repeat protein in *Arabidopsis*, is required for chloroplast 16S rRNA maturation. Plant Cell 26:777–787
- Korb H, Neupert W (1978) Biogenesis of cytochrome *c* in *Neurospora crassa*. Synthesis of apocytochrome *c*, transfer to mitochondria and conversion to holo-cytochrome *c*. Eur J Biochem 91:609–620
- Koreny L, Obornik M, Lukes J (2013) Make it, take it, or leave it: heme metabolism of parasites. PLoS Pathog 9, e1003088
- Kranz RG, Richard-Fogal C, Taylor J-S, Frawley ER (2009) Cytochrome *c* biogenesis: mechanisms for covalent modifications and trafficking of heme and for heme-iron redox control. Microbiol Mol Biol Rev 73:510–528
- Kuras R, de Vitry C, Choquet Y, Girard-Bascou J, Culler D, Buschlen S, Merchant S, Wollman FA (1997) Molecular genetic identification of a pathway for heme binding to cytochrome *b*<sub>6</sub>. J Biol Chem 272:32427–32435
- Kuras R, Saint-Marcoux D, Wollman FA, de Vitry C (2007) A specific *c*-type cytochrome maturation system is required for oxygenic photosynthesis. Proc Natl Acad Sci U S A 104:9906–9910
- Kurusu G, Zhang H, Smith JL, Cramer WA (2003) Structure of the cytochrome *b*<sub>6</sub>*f* complex of oxygenic photosynthesis: tuning the cavity. Science 302:1009–1014
- Kutoh E, Sone N (1988) Quinol-cytochrome *c* oxidoreductase from the thermophilic bacterium PS3. Purification and properties of a cytochrome *bc*<sub>1</sub>(*b*<sub>6</sub>*f*) complex. J Biol Chem 263:9020–9026

- Lang BF, Kaudewitz F (1982) Cytochrome *c*<sub>1</sub>-deficient mutants in *Saccharomyces cerevisiae*. *Curr Genet* 6:229–235
- Lavergne J (1983) Membrane potential-dependent reduction of cytochrome *b*-6 in an algal mutant lacking photosystem I centers. *Biochim Biophys Acta* 725:25–33
- Le Brun NE, Bengtsson J, Hederstedt L (2000) Genes required for cytochrome *c* synthesis in *Bacillus subtilis*. *Mol Microbiol* 36:638–650
- Lennartz K, Plücken H, Seidler A, Westhoff P, Bechtold N, Meierhoff K (2001) *HCF164* encodes a thioredoxin-like protein involved in the biogenesis of the cytochrome *b*<sub>6</sub>*f* complex in *Arabidopsis*. *Plant Cell* 13:2539–2551
- Lennartz K, Bossmann S, Westhoff P, Bechtold N, Meierhoff K (2006) HCF153, a novel nuclear-encoded factor necessary during a post-translational step in biogenesis of the cytochrome *b*<sub>6</sub>*f* complex. *Plant J* 45:101–112
- Lewin A, Crow A, Oubrie A, Le Brun NE (2006) Molecular basis for specificity of the extracytoplasmic thioredoxin ResA. *J Biol Chem* 281:35467–35477
- Lewin A, Crow A, Hodson CT, Hederstedt L, Le Brun NE (2008) Effects of substitutions in the CXXC active-site motif of the extracytoplasmic thioredoxin ResA. *Biochem J* 414:81–91
- Lezhneva L, Kuras R, Ephritikhine G, de Vitry C (2008) A novel pathway of cytochrome *c* biogenesis is involved in the assembly of the cytochrome *b*<sub>6</sub>*f* complex in *Arabidopsis* chloroplasts. *J Biol Chem* 283:24608–24616
- Li B, Mao D, Liu Y, Li L, Kuang T (2005) Characterization of the cytochrome *b*<sub>6</sub>*f* complex from marine green alga, *Bryopsis corticulans*. *Photosynth Res* 83:297–305
- Li T, Bonkovsky HL, Guo JT (2011) Structural analysis of heme proteins: implications for design and prediction. *BMC Struct Biol* 11:13
- Lu Y, Wang HR, Li H, Cui HR, Feng YG, Wang XY (2013) A chloroplast membrane protein LTO1/AtVKOR involving in redox regulation and ROS homeostasis. *Plant Cell Rep* 32:1427–1440
- Lyska D, Paradies S, Meierhoff K, Westhoff P (2007) HCF208, a homolog of *Chlamydomonas* CCB2, is required for accumulation of native cytochrome *b*<sub>6</sub> in *Arabidopsis thaliana*. *Plant Cell Physiol* 48:1737–1746
- Malnoë A, Wollman FA, de Vitry C, Rappaport F (2011) Photosynthetic growth despite a broken Q-cycle. *Nat Commun* 2:301
- Malnoë A, Wang F, Girard-Bascou J, Wollman FA, de Vitry C (2014) Thylakoid FtsH protease contributes to photosystem II and cytochrome *b*<sub>6</sub>*f* remodeling in *Chlamydomonas reinhardtii* under stress conditions. *Plant Cell* 26:373–390
- Marx C, Wunsch C, Kuck U (2015) The octatricopeptide repeat (OPR) protein Raa8 is required for chloroplast *trans*-splicing. *Eukaryot Cell* 14:998–1005
- Mavridou DAI, Ferguson SJ, Stevens JM (2013) Cytochrome *c* assembly. *IUBMB Life* 65:209–216
- Mayer A, Neupert W, Lill R (1995) Translocation of apocytochrome *c* across the outer membrane of mitochondria. *J Biol Chem* 270:12390–12397
- Merendino L, Perron K, Rahire M, Howald I, Rochaix JD, Goldschmidt-Clermont M (2006) A novel multifunctional factor involved in *trans*-splicing of chloroplast introns in *Chlamydomonas*. *Nucleic Acids Res* 34:262–274
- Meyer EH, Giege P, Gelhaye E, Rayapuram N, Ahuja U, Thony-Meyer L, Grienenberger JM, Bonnard G (2005) AtCCMH, an essential component of the *c*-type cytochrome maturation pathway in *Arabidopsis* mitochondria, interacts with apocytochrome *c*. *Proc Natl Acad Sci U S A* 102:16113–16118
- Möller MC, Hederstedt L (2008) Extracytoplasmic processes impaired by inactivation of *trxA* (thioredoxin gene) in *Bacillus subtilis*. *J Bacteriol* 190:4660–4665
- Monika EM, Goldman BS, Beckman DL, Kranz RG (1997) A thioreduction pathway tethered to the membrane for periplasmic cytochromes *c* biogenesis; in vitro and in vivo studies. *J Mol Biol* 271:679–692
- Moore RL, Stevens JM, Ferguson SJ (2011) Mitochondrial cytochrome *c* synthase: CP motifs are not necessary for heme attachment to apocytochrome *c*. *FEBS Lett* 585:3415–3419
- Motohashi K, Hisabori T (2006) HCF164 receives reducing equivalents from stromal thioredoxin across the thylakoid membrane and mediates reduction of target proteins in the thylakoid lumen. *J Biol Chem* 281:35039–35047
- Motohashi K, Hisabori T (2010) CcdA is a thylakoid membrane protein required for the transfer of reducing equivalents from stroma to thylakoid lumen in the higher plant chloroplast. *Antioxid Redox Signal* 13:1169–1176
- Nakamoto SS, Hamel P, Merchant S (2000) Assembly of chloroplast cytochromes *b* and *c*. *Biochimie* 82:603–614
- Nargang FE, Drygas ME, Kwong PL, Nicholson DW, Neupert W (1988) A mutant of *Neurospora crassa* deficient in cytochrome *c* heme lyase activity cannot import cytochrome *c* into mitochondria. *J Biol Chem* 263:9388–9394

- Nawathean P, Maslov DA (2000) The absence of genes for cytochrome *c* oxidase and reductase subunits in maxicircle kinetoplast DNA of the respiration-deficient plant trypanosomatid *Phytomonas serpens*. *Curr Genet* 38:95–103
- Nicholson DW, Neupert W (1989) Import of cytochrome *c* into mitochondria: reduction of heme, mediated by NADH and flavin nucleotides, is obligatory for its covalent linkage to apocytochrome *c*. *Proc Natl Acad Sci U S A* 86:4340–4344
- Nicholson DW, Kohler H, Neupert W (1987) Import of cytochrome *c* into mitochondria. Cytochrome *c* heme lyase. *Eur J Biochem* 164:147–157
- Nicholson DW, Hergersberg C, Neupert W (1988) Role of cytochrome *c* heme lyase in the import of cytochrome *c* into mitochondria. *J Biol Chem* 263:19034–19042
- Nicholson DW, Stuart RA, Neupert W (1989) Biogenesis of cytochrome *c*<sub>1</sub>. Role of cytochrome *c*<sub>1</sub> heme lyase and of the two proteolytic processing steps during import into mitochondria. *J Biol Chem* 264:10156–10168
- Page MLD, Hamel PP, Gabilly ST, Zegzouti H, Perea JV, Alonso JM, Ecker JR, . . . , Merchant S (2004) A homolog of prokaryotic thiol disulfide transporter CcdA is required for the assembly of the cytochrome *b*<sub>6</sub>*f* complex in *Arabidopsis* chloroplasts. *J Biol Chem* 279:32474–32482
- Pearce DA, Cardillo TS, Sherman F (1998) Cyc2p is required for maintaining ionic stability and efficient cytochrome *c* import and mitochondrial function in *Saccharomyces cerevisiae*. *FEBS Lett* 439:307–311
- Pierre Y, Breyton C, Lemoine Y, Robert B, Vernotte C, Popot JL (1997) On the presence and role of a molecule of chlorophyll *a* in the cytochrome *b*<sub>6</sub>*f* complex. *J Biol Chem* 272:21901–21908
- Pollock WB, Rosell FI, Twitchett MB, Dumont ME, Mauk AG (1998) Bacterial expression of a mitochondrial cytochrome *c*. Trimethylation of lys72 in yeast iso-1-cytochrome *c* and the alkaline conformational transition. *Biochemistry* 37:6124–6131
- Priest JW, Hajduk SL (1992) Cytochrome *c* reductase purified from *Crithidia fasciculata* contains an atypical cytochrome *c*<sub>1</sub>. *J Biol Chem* 267:20188–20195
- Raczynska KD, Le Ret M, Rurek M, Bonnard G, Augustyniak H, Gualberto JM (2006) Plant mitochondrial genes can be expressed from mRNAs lacking stop codons. *FEBS Lett* 580:5641–5646
- Rahire M, Laroche F, Cerutti L, Rochaix JD (2012) Identification of an OPR protein involved in the translation initiation of the PsaB subunit of photosystem I. *Plant J* 72:652–661
- Rayapuram N, Hagenmuller J, Grienberger JM, Giegé P, Bonnard G (2007) AtCCMA interacts with AtCcmB to form a novel mitochondrial ABC transporter involved in cytochrome *c* maturation in *Arabidopsis*. *J Biol Chem* 282:21015–21023
- Rayapuram N, Hagenmuller J, Grienberger JM, Bonnard G, Giegé P (2008) The three mitochondrial encoded CcmF proteins form a complex that interacts with CCMH and *c*-type apocytochromes in *Arabidopsis*. *J Biol Chem* 283:25200–25208
- Ren Q, Ahuja U, Thony-Meyer L (2002) A bacterial cytochrome *c* heme lyase. CcmF forms a complex with the heme chaperone CcmE and CcmH but not with apocytochrome *c*. *J Biol Chem* 277:7657–7663
- Richard-Fogal C, Kranz RG (2010) The CcmC:heme:CcmE complex in heme trafficking and cytochrome *c* biosynthesis. *J Mol Biol* 401:350–362
- Richard-Fogal CL, Frawley ER, Kranz RG (2008) Topology and function of CcmD in cytochrome *c* maturation. *J Bacteriol* 190:3489–3493
- Richard-Fogal CL, Frawley ER, Bonner ER, Zhu H, San Francisco B, Kranz RG (2009) A conserved haem redox and trafficking pathway for cofactor attachment. *EMBO J* 28:2349–2359
- Richard-Fogal CL, San Francisco B, Frawley ER, Kranz RG (2012) Thiol redox requirements and substrate specificities of recombinant cytochrome *c* assembly systems II and III. *Biochim Biophys Acta* 1817:911–919
- Robertson DE, Farid RS, Moser CC, Urbauer JL, Mulholland SE, Pidikiti R, Lear JD, . . . , Dutton PL (1994) Design and synthesis of multi-haem proteins. *Nature* 368:425–432
- Saint-Marcoux D, Wollman FA, de Vitry C (2009) Biogenesis of cytochrome *b*<sub>6</sub> in photosynthetic membranes. *J Cell Biol* 185:1195–1207
- San Francisco B, Bretsnyder EC, Rodgers KR, Kranz RG (2011) Heme ligand identification and redox properties of the cytochrome *c* synthetase, CcmF. *Biochemistry* 50:10974–10985
- San Francisco B, Bretsnyder EC, Kranz RG (2013) Human mitochondrial holocytochrome *c* synthase's heme binding, maturation determinants, and complex formation with cytochrome *c*. *Proc Natl Acad Sci U S A* 110:E788–E797
- San Francisco B, Sutherland MC, Kranz RG (2014) The CcmFH complex is the system I holocytochrome *c* synthetase: engineering cytochrome *c* maturation independent of CcmABCDE. *Mol Microbiol* 91:996–1008
- Sanchez NS, Pearce DA, Cardillo TS, Uribe S, Sherman F (2001) Requirements of Cyc2p and the porin, Por1p, for ionic stability and mitochondrial integrity in *Saccharomyces cerevisiae*. *Arch Biochem Biophys* 392:326–332
- Sanders C, Lill H (2000) Expression of prokaryotic and eukaryotic cytochromes *c* in *Escherichia coli*. *Biochim Biophys Acta* 1459:131–138

- Sanders C, Turkarslan S, Lee DW, Onder O, Kranz RG, Daldal F (2008) The cytochrome *c* maturation components CcmF, CcmH, and CcmI form a membrane-integral multisubunit heme ligation complex. *J Biol Chem* 283:29715–29722
- Sanders C, Turkarslan S, Lee D-W, Daldal F (2010) Cytochrome *c* biogenesis: the Ccm system. *Trends Microbiol* 18:266–274
- Schiott T, Throne-Holst M, Hederstedt L (1997a) *Bacillus subtilis* CcdA-defective mutants are blocked in a late step of cytochrome *c* biogenesis. *J Bacteriol* 179:4523–4529
- Schiott T, von Wachenfeldt C, Hederstedt L (1997b) Identification and characterization of the *ccdA* gene, required for cytochrome *c* synthesis in *Bacillus subtilis*. *J Bacteriol* 179:1962–1973
- Schmidt CL, Shaw L (2001) A comprehensive phylogenetic analysis of Rieske and Rieske-type iron-sulfur proteins. *J Bioenerg Biomembr* 33:9–26
- Schulz H, Fabianek RA, Pelliccioli EC, Hennecke H, Thöny-Meyer L (1999) Heme transfer to the heme chaperone CcmE during cytochrome *c* maturation requires the CcmC protein, which may function independently of the ABC-transporter CcmAB. *Proc Natl Acad Sci U S A* 96:6462–6467
- Schulz H, Pelliccioli EC, Thöny-Meyer L (2000) New insights into the role of CcmC, CcmD and CcmE in the haem delivery pathway during cytochrome *c* maturation by a complete mutational analysis of the conserved tryptophan-rich motif of CcmC. *Mol Microbiol* 37:1379–1388
- Schwarz QP, Cox TC (2002) Complementation of a yeast *CYC3* deficiency identifies an X-linked mammalian activator of apocytochrome *c*. *Genomics* 79:51–57
- Sherman F (1990) Studies of yeast cytochrome *c*: how and why they started and why they continued. *Genetics* 125:9–12
- Simon J, Hederstedt L (2011) Composition and function of cytochrome *c* biogenesis System II. *FEBS J* 278:4179–4188
- Small JL, Park SW, Kana BD, Ioerger TR, Sacchettini JC, Ehart S (2013) Perturbation of cytochrome *c* maturation reveals adaptability of the respiratory chain in *Mycobacterium tuberculosis*. *mBio* 4, e00475-13
- Spielewoy N, Schulz H, Grienenberger JM, Thony-Meyer L, Bonnard G (2001) CCME, a nuclear-encoded heme-binding protein involved in cytochrome *c* maturation in plant mitochondria. *J Biol Chem* 276:5491–5497
- Stechmann A, Hamblin K, Perez-Brocal V, Gaston D, Richmond GS, van der Giezen M, Clark CG, Roger AJ (2008) Organelles in *Blastocystis* that blur the distinction between mitochondria and hydrogenosomes. *Curr Biol* 18:580–585
- Steiner H, Zollner A, Haid A, Neupert W, Lill R (1995) Biogenesis of mitochondrial heme lyases in yeast. Import and folding in the intermembrane space. *J Biol Chem* 270:22842–22849
- Steiner H, Kispal G, Zollner A, Haid A, Neupert W, Lill R (1996) Heme binding to a conserved Cys-Pro-Val motif is crucial for the catalytic function of mitochondrial heme lyases. *J Biol Chem* 271:32605–32611
- Stevens JM, Zhang Y, Muthuvel G, Sam KA, Allen JW, Ferguson SJ (2011) The mitochondrial cytochrome *c* N-terminal region is critical for maturation by holocytochrome *c* synthase. *FEBS Lett* 585:1891–1896
- Stroebel D, Choquet Y, Popot JL, Picot D (2003) An atypical haem in the cytochrome *b<sub>6</sub>f* complex. *Nature* 426:413–418
- Sun F, Wang X, Bonnard G, Shen Y, Xiu Z, Li X, Gao D, . . . , Tan BC (2015) *Empty pericarp7* encodes a mitochondrial E-subgroup pentatricopeptide repeat protein that is required for *cmFN* editing, mitochondrial function and seed development in maize. *Plant J* 84:283–295
- Thony-Meyer L (1997) Biogenesis of respiratory cytochromes in bacteria. *Microbiol Mol Biol Rev* 61:337–376
- Thöny-Meyer L, Künzler P (1997) Translocation to the periplasm and signal sequence cleavage of preapocytochrome *c* depend on *Sec* and *Lep*, but not on the *ccm* gene products. *Eur J Biochem* 246:794–799
- Tichy M, Vermaas W (1999) Accumulation of pre-apocytochrome *f* in a *Synechocystis* sp. PCC 6803 mutant impaired in cytochrome *c* maturation. *J Biol Chem* 274:32396–32401
- Tong J, Margoliash E (1998) Cytochrome *c* heme lyase activity of yeast mitochondria. *J Biol Chem* 273:25695–25702
- Turkarslan S, Sanders C, Ekici S, Daldal F (2008) Compensatory thio-redox interactions between DsbA, CcdA and CcmG unveil the apocytochrome *c* holdase role of CcmG during cytochrome *c* maturation. *Mol Microbiol* 70:652–666
- Verissimo AF, Daldal F (2014) Cytochrome *c* biogenesis System I: an intricate process catalyzed by a maturase supercomplex? *Biochim Biophys Acta* 1837:989–998
- Verissimo AF, Sanders J, Daldal F, Sanders C (2012) Engineering a prokaryotic apocytochrome *c* as an efficient substrate for *Saccharomyces cerevisiae* cytochrome *c* heme lyase. *Biochem Biophys Res Commun* 424:130–135
- Vilmos F, Katharine AS, Stuart JF, Michael LG, James WAA (2009) Structure of a trypanosomatid mitochondrial cytochrome *c* with heme attached via only one thioether bond and implications for the substrate



- recognition requirements of heme lyase. FEBS J 276:2822–2832
- Visco C, Taniuchi H, Berlett BS (1985) On the specificity of cytochrome *c* synthetase in recognition of the amino acid sequence of apocytochrome *c*. J Biol Chem 260:6133–6138
- Wang F, Johnson X, Cavaiuolo M, Bohne A-V, Nickelsen J, Vallon O (2015) Two *Chlamydomonas* OPR proteins stabilize chloroplast mRNAs encoding small subunits of photosystem II and cytochrome *b*<sub>6</sub>*f*. Plant J 82:861–873
- Xie Z, Merchant S (1996) The plastid-encoded *ccsA* gene is required for heme attachment to chloroplast *c*-type cytochromes. J Biol Chem 271:4632–4639
- Xie Z, Culler D, Dreyfuss BW, Kuras R, Wollman FA, Girard-Bascou J, Merchant S (1998) Genetic analysis of chloroplast *c*-type cytochrome assembly in *Chlamydomonas reinhardtii*: one chloroplast locus and at least four nuclear loci are required for heme attachment. Genetics 148:681–692
- Yi L, Ragsdale SW (2007) Evidence that the heme regulatory motifs in heme oxygenase-2 serve as a thiol/disulfide redox switch regulating heme binding. J Biol Chem 282:21056–21067
- Yi L, Jenkins PM, Leichert LI, Jakob U, Martens JR, Ragsdale SW (2009) Heme regulatory motifs in heme oxygenase-2 form a thiol/disulfide redox switch that responds to the cellular redox state. J Biol Chem 284:20556–20561
- Yu J, Le Brun NE (1998) Studies of the cytochrome subunits of menaquinone:cytochrome *c* reductase (*bc* complex) of *Bacillus subtilis*. Evidence for the covalent attachment of heme to the cytochrome *b* subunit. J Biol Chem 273:8860–8866
- Zara V, Conte L, Trumpower BL (2007) Identification and characterization of cytochrome *bc*<sub>1</sub> subcomplexes in mitochondria from yeast with single and double deletions of genes encoding cytochrome *bc*<sub>1</sub> subunits. FEBS J 274:4526–4539
- Zhang H, Huang D, Cramer WA (1999) Stoichiometrically bound beta-carotene in the cytochrome *b*<sub>6</sub>*f* complex of oxygenic photosynthesis protects against oxygen damage. J Biol Chem 274:1581–1587
- Zollner A, Rodel G, Haid A (1992) Molecular cloning and characterization of the *Saccharomyces cerevisiae* *CYT2* gene encoding cytochrome-*c*<sub>1</sub>-heme lyase. Eur J Biochem 207:1093–1100

# Chapter 27

## Biogenesis of Cytochrome *c* Complexes: From Insertion of Redox Cofactors to Assembly of Different Subunits

Bahia Khalfaoui-Hassani<sup>a,1</sup>, Andreia F. Verissimo<sup>a,1</sup>,  
Namita P. Shroff<sup>a</sup>, Seda Ekici<sup>a</sup>, Petru-Iulian Trasnea<sup>b</sup>,  
Marcel Utz<sup>b</sup>, Hans-Georg Koch<sup>b</sup>, and Fevzi Daldal<sup>a,\*</sup>

<sup>a</sup>*Department of Biology, University of Pennsylvania,  
Philadelphia, PA 19104, USA*

<sup>b</sup>*Institut für Biochemie und Molekularbiologie, Albert-Ludwigs  
Universität Freiburg, 79104 Freiburg, Germany*

Summary.....	527
I. Introduction.....	528
II. The <i>cbb</i> <sub>3</sub> -Cox.....	530
A. Distribution and Role of <i>cbb</i> <sub>3</sub> -Cox.....	530
B. Subunit and Cofactor Composition of <i>cbb</i> <sub>3</sub> -Cox.....	531
C. Maturation of CcoN.....	533
1. Hemes <i>b</i> of <i>cbb</i> <sub>3</sub> -Cox.....	533
2. Cu <sub>B</sub> Biogenesis of <i>cbb</i> <sub>3</sub> -Cox.....	534
D. Maturation of CcoO and CcoP.....	538
1. Ccm-System I: Functional Organization.....	539
2. Do the Ccm Components form a Membrane-Integral Maturase Supercomplex?.....	543
E. Assembly of <i>cbb</i> <sub>3</sub> -Cox.....	545
Acknowledgments.....	546
References.....	546

### Summary

Cytochromes (cyts) are ubiquitous heme containing proteins that are key components of energy transduction pathways. They participate in a wide variety of electron transfer reactions, which are essential for cellular processes responsible for chemical energy (ATP) production. The *cbb*<sub>3</sub>-type cyt *c* oxidase (*cbb*<sub>3</sub>-Cox) provides an excellent model to study biogenesis of membrane-integral, oligomeric cyt *c* complexes. Its subunits contain three hemes *c*, two hemes *b* and a copper (Cu<sub>B</sub>) atom as cofactors that use distinct insertion processes. In cyts *c*, heme *b* is covalently ligated (referred to as heme *c*) via a complex maturation process that involves in some species up to nine components (Ccm-System I). In

---

<sup>1</sup>These authors contributed equally.

\*Author for correspondence, e-mail: [fdaldal@sas.upenn.edu](mailto:fdaldal@sas.upenn.edu)

addition to the cyts *c*, many cyt *c* containing complexes carry other cofactors, and insertion of these cofactors requires additional biogenesis components besides the Ccm-system I. In the case of *cbb*<sub>3</sub>-Cox, the mechanisms underlying incorporation of hemes *b* into the catalytic subunit are not well understood. However, remarkable progress was achieved recently on how the single Cu<sub>B</sub> atom at the catalytic heart of this heme-copper oxidase is acquired. Finally, insertion of the cofactors must be temporally and spatially coordinated with the assembly of the subunits in order to yield a functional *cbb*<sub>3</sub>-Cox enzyme. In this chapter, we discuss the biogenesis of *cbb*<sub>3</sub>-Cox from the insertion of its catalytic heme-copper (Cu<sub>B</sub>) center and maturation of its *c*-type cyts to the assembly of its mature subunits, mainly focusing on studies carried out with the anoxygenic phototrophic bacterium *Rhodobacter capsulatus*.

## I. Introduction

A vital characteristic of all living organisms is the ability to produce energy-rich molecules (ATP) required for central biological processes, such as biosynthesis and transport of molecules as well as cell motility and thermogenesis. Among the heme-containing proteins, cytochromes (cyts) are evolutionarily conserved components of biological energy transduction (Moore and Pettigrew 1990). They are ubiquitous to almost all forms of major electron transport pathways, including photosynthesis (Ps) and respiration (Res), and are crucial for energy production and cell viability (Pettigrew and Moore 1987). In the 1920s, Keilin classified cyts based on the spectroscopic properties of their different heme cofactors (Keilin 1925) [See Chap. 1 by Bendall]. Heme *b* (protoporphyrin IX-Fe) is an organic molecule composed of an iron (Fe) atom ligated to four nitrogen atoms of a porphyrin ring. Often, the side chains of specific amino acid residues (His or Met) from the polypeptide provide axial ligands to penta- or hexa-coordinate the Fe<sup>2+</sup> (reduced) or Fe<sup>3+</sup> (oxidized) ion. In cyts *b*, non-covalently bound hemes *b* are frequently coordinated by His, and rarely by other residues (Moore and Pettigrew 1990). Similarly, cyts *a*, *d* and *o* are also coordinated

to the corresponding polypeptides with one or two axial ligands. Their heme cofactors are derivatives of heme *b* that are chemically modified at different positions of the porphyrin ring. Both the hemes *a* and *o* contain a hydroxyl ethyl farnesyl group at position C3, and heme *a* contains an additional formyl group at position C18 of the porphyrin ring. Heme *d* has two hydroxyl groups at positions C12 and C13 (see e.g., Sanders et al. 2009 for detailed description). In contrast to the cyts *a*, *b*, *d* and *o*, all cyts *c* invariably contain a heme *b* cofactor that is stereo-specifically ligated to the polypeptide by two (rarely one) thioether bonds. These bonds are formed between the positions C3 (vinyl-2) and C8 (vinyl-4) of the porphyrin ring and the thiol groups of Cys<sub>1</sub> and Cys<sub>2</sub> located at a conserved heme-binding motif (C<sub>1</sub>XXC<sub>2</sub>H) within the apocytochromes (apocyts) *c* (Bowman and Bren 2008). The His residue of this motif axially coordinates the heme-iron together with another Met or His residue (Moore and Pettigrew 1990).

Over the last few decades, *Rhodobacter* (*R.*) species have emerged as model organisms for studying the structure, function and biogenesis of the cyts *c* and cyt *c* complexes (Sanders et al. 2009). For instance, the facultative anaerobic phototrophic  $\alpha$ -proteobacterium *R. capsulatus* produces a variety of soluble and membrane-bound cyts *c* (Fig. 27.1), including the cyts *c*<sub>1</sub>, *c*<sub>2</sub>, *c*'<sub>2</sub>, *c*<sub>Y</sub>, *c*<sub>0</sub> (CcoO), *c*<sub>p</sub> (CcoP) and DorC in order to sustain its versatile modes of growth (Daldal et al. 1987; Zannoni and Daldal 1993; Gray et al. 1994; Koch et al. 1998). Of these proteins, cyt *c*<sub>1</sub> is a carboxyl (C)-terminally membrane-anchored subunit of cyt *bc*<sub>1</sub>

---

*Abbreviations:* Ccm – Cytochrome *c* maturation system I; Cox – Cytochrome *c* oxidase; Cyt – Cytochrome; HCO – Heme-copper terminal oxidase; HHP – Heme handling protein; HMBD – Heavy metal binding domain; MFS – Major facilitator superfamily; Ps – Photosynthesis; Qox – Quinol (hydroquinone) oxidase; Res – Respiration

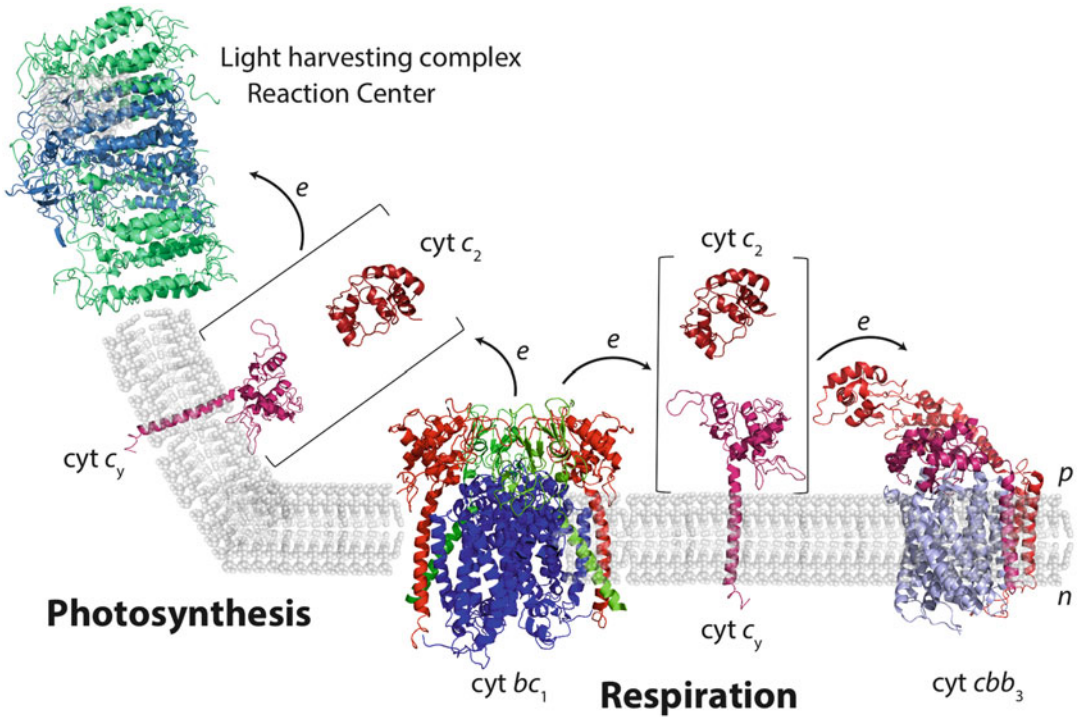


Fig. 27.1. 3D structures of *R. capsulatus* cyts *c* and *b* containing cyt complexes involved in photosynthesis and respiration. The structures shown are the *R. sphaeroides* light harvesting and reaction center (4JCB), *R. capsulatus* cyt *bc*<sub>1</sub> (1ZQT), *P. stutzeri* cyt *cbb*<sub>3</sub>-Cox (3MK7) and *R. capsulatus* cyt *c*<sub>2</sub> (1C2R), while that of cyt *c*<sub>γ</sub> is a hypothetical homology model. The membrane-anchored cyt *c*<sub>γ</sub> and the soluble cyt *c*<sub>2</sub> carry electrons between the cyt *bc*<sub>1</sub> and the reaction center during photosynthesis, and between the cyt *bc*<sub>1</sub> and the *cbb*<sub>3</sub>-Cox during respiration. Cyt *c* subunits are shown in different tones of red.

complex (cyt *bc*<sub>1</sub> or respiratory complex III) that is required for Ps growth (Daldal et al. 1987), whereas the cyts CcoO and CcoP are subunits of the *cbb*<sub>3</sub>-type cyt *c* oxidase (*cbb*<sub>3</sub>-Cox), which carries out aerobic and microaerophilic Res growth (Gray et al. 1994; Koch et al. 1998). The periplasmic small cyt *c*<sub>2</sub> together with the amino (N)-terminally membrane-anchored cyt *c*<sub>γ</sub> play critical roles as electron carriers during both Ps and Res (Fig. 27.1) (Jenney and Daldal 1993; Jenney et al. 1994; Hochkoepler et al. 1995). Under anaerobic conditions in the presence of dimethylsulfoxide (DMSO), or trimethylamine N-oxide (TMAO) (McEwan et al. 1985) *R. capsulatus* relies on the membrane-bound pentaheme cyt *c* DorC, which receives electrons from the membrane quinone/quinol (Q/QH<sub>2</sub>) pool and reduces DMSO to dimethyl sulfide (DMS), or TMAO to trimethylamine (TMA) (Shaw et al. 1999a, b).

The apocyts *c* are usually synthesized in the cytoplasm, translocated across the membrane, and matured to holocyts *c* in the periplasm. In Gram-negative bacteria, the periplasmic maturation process involves an elaborate pathway, referred to as cyt *c* maturation system I (Ccm-system I) (Sanders et al. 2010). It includes the translocation and delivery of heme *b*, chaperoning and thio-oxidoreduction of the apocyts *c* and heme ligation steps. Unlike the electron carrier cyts *c* (e.g., cyt *c*<sub>2</sub> and cyt *c*<sub>γ</sub>), some cyts *c* (e.g., cyt *c*<sub>1</sub>, CcoO and CcoP) associate together with other membrane bound proteins to form oligomeric enzyme complexes. Often, these enzymes also contain other cofactors whose biogenesis involves additional components along with the Ccm-system I. Thus, multifaceted interactions between multiple maturation components render biogenesis of cyt *c*

complexes highly complex. Coordinated incorporation of specific cofactors to specific subunits is needed to ensure the production of functional and stable multi-cofactor carrying complexes (Ekici et al. 2012a). As an example, the bacterial cyt *bc*<sub>1</sub> contains in addition to cyt *c*<sub>1</sub> two other catalytic subunits, which are the Rieske iron-sulfur (Fe-S) protein and cyt *b* (Iwata et al. 1995; Berry et al. 2004). The Fe-S protein is a membrane-anchored protein with a 2Fe-2S cluster as a redox cofactor, whereas cyt *b* is a multi-span integral membrane protein that carries two hemes *b* (*b*<sub>L</sub> and *b*<sub>H</sub>). Similarly, heme-copper oxidase (HCO) superfamily members, to which respiratory cyt *c* oxidase (Cox) belongs, are multi-cofactor containing complexes that have copper (Cu) atoms. The mitochondrial enzyme *aa*<sub>3</sub>-Cox (respiratory complex IV) has a bi-metallic center with two Cu atoms (Cu<sub>A</sub>) in its subunit II (Cox2), and two hemes *a* (*a* and *a*<sub>3</sub>) in its subunit I (Cox1). Heme *a*<sub>3</sub> forms with a third Cu atom (Cu<sub>B</sub>) the heme-Cu<sub>B</sub> catalytic center where O<sub>2</sub> is reduced to H<sub>2</sub>O (Iwata et al. 1995; Svensson-Ek et al. 2002). The bacterial *cbb*<sub>3</sub>-Cox has a similar heme-Cu<sub>B</sub> active site, but it contains two hemes *b* (*b* and *b*<sub>3</sub>) instead of the hemes *a* of *aa*<sub>3</sub>-Cox. In *cbb*<sub>3</sub>-Cox, the Cu<sub>A</sub> binuclear center is replaced by three hemes *c* of CcoO and CcoP (Buschmann et al. 2010). In addition, this enzyme is not essential for aerobic respiration of *R. capsulatus* as this species also contains a cyt *bc*<sub>1</sub>-independent and unrelated O<sub>2</sub> reductase (probably a *bb*- or *bd*-type quinol oxidase (Qox) devoid of heme *c*) (Marrs and Gest 1973; Daldal et al. 2001). This feature renders the cyts *c* non-essential in this species, thus permitting genetic analyses.

The *cbb*<sub>3</sub>-Cox provides a fascinating paradigm for investigating the biogenesis of cyt *c* complexes due to the presence of two axially coordinated hemes *b*, three covalently ligated hemes *c* and a single Cu atom (Cu<sub>B</sub>) as its cofactors (Sanders et al. 2009; Ekici et al. 2012a) (Fig. 27.1). Of the subunits of *cbb*<sub>3</sub>-Cox, CcoO and CcoP are *c*-type cyts that use Ccm-system I present in various

organisms. CcoN contains the heme-Cu<sub>B</sub> catalytic site and its maturation relies on homologues of the eukaryotic components dealing with Cu trafficking and assembly into the mitochondrial type *aa*<sub>3</sub>-Cox as well as on specific bacterial components. In this chapter, we focus on the structure and subunit composition of *cbb*<sub>3</sub>-Cox, and on the insertion of its Cu atom and maturation of its cyts *b* and *c*, using as an example *R. capsulatus* enzyme where most of the studies were conducted.

## II. The *cbb*<sub>3</sub>-Cox

### A. Distribution and Role of *cbb*<sub>3</sub>-Cox

The *cbb*<sub>3</sub>-Cox enzymes are widespread in the bacterial kingdom (Ducluzeau et al. 2008). They are commonly found in the  $\alpha$ -proteobacteria (e.g., *Rhodobacter* species) and the *cytophaga*, *flexibacter* and *bacteroides* (CFB) groups. The genes encoding *cbb*<sub>3</sub>-Cox are also found in the last mitochondrial ancestor *Midichloria mitochondrii* (Sassera et al. 2011), but so far, no *cbb*<sub>3</sub>-Cox related sequences have been identified in Archaea or Eukaryota (Hemp and Gennis 2008). Structural genes of *cbb*<sub>3</sub>-Cox were first identified in the facultative symbiotic N<sub>2</sub>-fixing *Rhizobiaceae* (Kahn et al. 1989; Preisig et al. 1993) and due to their importance for symbiotic N<sub>2</sub> fixation, they were initially termed *fixNOQP* (Preisig et al. 1993). For example, in *Bradyrhizobium japonicum* expression of *cbb*<sub>3</sub>-Cox is required for symbiotic N<sub>2</sub> fixation under very low O<sub>2</sub> conditions in soybean root nodules (Preisig et al. 1993). Subsequent studies identified the *cbb*<sub>3</sub>-Cox structural genes in non-symbiotic bacteria such as *R. capsulatus*, and referred to them as *ccoNOQP* (Garcia-Horsman et al. 1994; Gray et al. 1994; Thony-Meyer et al. 1994).

The *cbb*<sub>3</sub>-Cox enzymes are present in many microaerophilic pathogenic bacteria, and are implicated in host colonization. Moreover, in some species like *Campylobacter jejuni* (Parkhill et al. 2000), *Helicobacter*

*pylori* (Tomb et al. 1997; Alm et al. 1999), *Neisseria meningitidis* and *Neisseria gonorrhoea* (Li et al. 2010) *cbb*<sub>3</sub>-Cox is the only Cox enzyme. It is suggested that its higher O<sub>2</sub> affinity (compared to *aa*<sub>3</sub>-Cox) allows these pathogens to colonize low O<sub>2</sub> containing tissues (Pitcher and Watmough 2004). For example, *C. jejuni* mutants lacking *cbb*<sub>3</sub>-Cox are unable to colonize the chick caecum (Weingarten et al. 2008), which is primarily colonized by obligate anaerobic bacteria. Thus, *cbb*<sub>3</sub>-Cox was proposed to keep *C. jejuni* cytoplasmic O<sub>2</sub> tensions low enough to protect its O<sub>2</sub> sensitive metabolically important enzymes (Woodall et al. 2005; Weingarten et al. 2008). This so called “respiratory protection” phenomenon was first described in *Azotobacter vinelandii* as a way of using respiration to protect the O<sub>2</sub> sensitive nitrogenase from deleterious effects of O<sub>2</sub> (Jones et al. 1973). Similarly, facultative anaerobic phototrophs rely on *cbb*<sub>3</sub>-Cox to eliminate O<sub>2</sub> and reduce their environment in order to establish productive anaerobic Ps growth (Marrs and Gest 1973) (Fig. 27.1). For example, the terminal oxidases (including *cbb*<sub>3</sub>-Cox) of the purple non-sulfur phototrophic bacterium *Rubrivivax gelatinosus* are crucial for anoxygenic Ps gene expression (Hassani et al. 2010b).

### B. Subunit and Cofactor Composition of *cbb*<sub>3</sub>-Cox

The three dimensional (3D) structure of *cbb*<sub>3</sub>-Cox from *Pseudomonas stutzeri* was solved at a resolution of 3.2 Å (Fig. 27.2a) (Buschmann et al. 2010), revealing that even though the HCO enzymes are diverse in terms of their subunit and cofactor compositions, the overall architecture of the membrane-embedded part of *cbb*<sub>3</sub>-Cox is similar to that of *R. sphaeroides aa*<sub>3</sub>-Cox (Svensson-Ek et al. 2002) and *Thermus thermophilus ba*<sub>3</sub>-Cox, (Soulimane et al. 2000). The *cbb*<sub>3</sub>-Cox enzymes often have four structural subunits, CcoN (subunit I), CcoO (subunit II), CcoP (subunit III) and CcoQ (subunit IV) that are encoded by

the *ccoNOQP* operon (Ducluzeau et al. 2008). The catalytic subunit CcoN has 12 membrane-spanning helices. It forms a “clamshell”-like structure, with its N- and C-termini located close to each other on the cytoplasmic side of the membrane (Buschmann et al. 2010). CcoN contains a low-spin heme *b* (*b*) and a high-spin heme *b* (*b*<sub>3</sub>) associated with a single Cu atom (Cu<sub>B</sub>) to form the catalytic center that binds and reduces O<sub>2</sub> to H<sub>2</sub>O (Fig. 27.2b). The Cu<sub>B</sub> atom is coordinated with three His residues, and one of them is covalently ligated to a nearby, possibly redox-active, Tyr residue as in other Cox enzymes (Buse et al. 1999; Hosler et al. 2006). Two additional calcium atoms with a proposed stabilizing role are found in the structure of CcoN. One of these atoms interacts directly with the heme *b*<sub>3</sub>-Cu<sub>B</sub> catalytic center (Fig. 27.2b), while the second one is located between the loops of CcoN at the edge of the structure. CcoO and CcoP are mono- and di-heme containing *c*-type cyts, respectively, and have one or two N-terminally located transmembrane (TM) helices as membrane anchors (Buschmann et al. 2010).

The outer heme *c* of CcoP whose pyrrole rings C and D are solvent-exposed, is thought to accept electrons from a soluble or a membrane-bound electron donor (e.g., cyt *c*<sub>2</sub> or cyt *c*<sub>y</sub> in *R. capsulatus*), and transfers them to the inner heme *c* of CcoO, which convey them to heme *b* and subsequently to the heme *b*<sub>3</sub>-Cu<sub>B</sub> center of CcoN. CcoO makes strong contacts with CcoN  $\alpha$ -helices, specifically via a calcium atom that coordinates the heme *b* and heme *b*<sub>3</sub> at the binuclear catalytic center via its Ser residue (Ser102 for *P. stutzeri*) (Fig. 27.2b). O<sub>2</sub> binds to heme *b*<sub>3</sub> and is reduced via the electrons coming from heme *b*<sub>3</sub>, Cu<sub>B</sub>, and possibly the redox-active Tyr residue (Tyr251 for *P. stutzeri*) (Buschmann et al. 2010, 2014) (Fig. 27.2b).

CcoQ is a small, single TM helix containing protein that has no cofactor. Earlier, it was considered to play a regulatory role (Oh and Kaplan 2002), which remains to be proven. This subunit is absent in some *cbb*<sub>3</sub>-

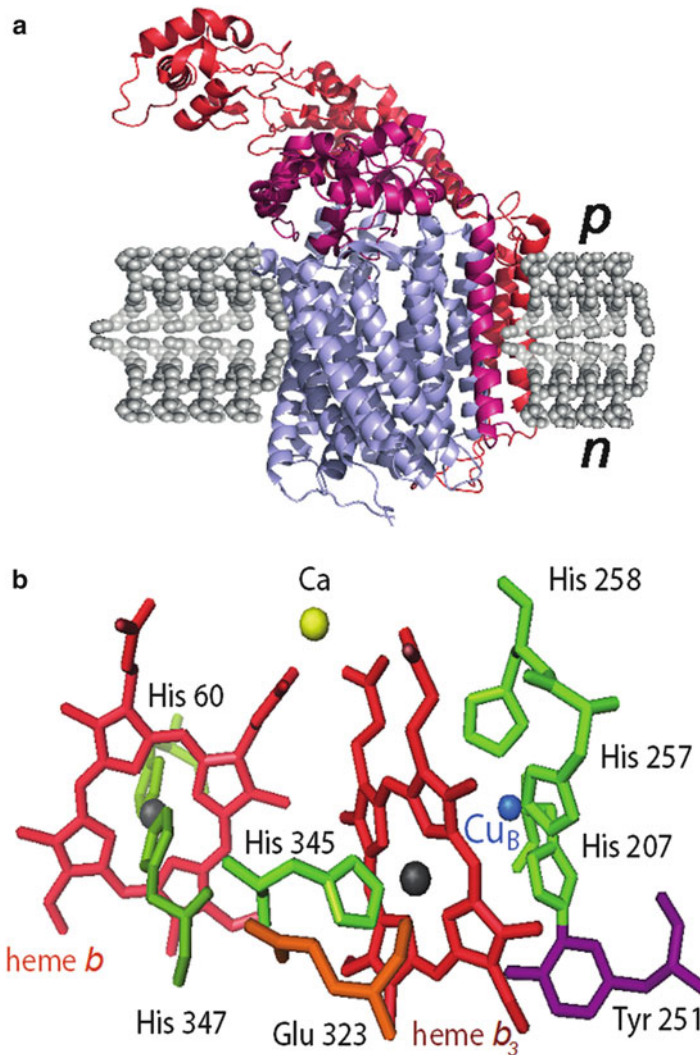


Fig. 27.2. Structure and subunit composition of *cbb*<sub>3</sub>-Cox. (a) 3D structure of *cbb*<sub>3</sub>-Cox of *P. stutzeri* (3MK7) as shown in Fig. 27.1. The 12 TM helix-containing CcoN subunit is shown in blue whereas the monoheme CcoO and the diheme CcoP are in magenta and red, respectively. The CcoQ subunit is not found in the structure of *cbb*<sub>3</sub>-Cox. (b) The heme *b* and heme *b*<sub>3</sub>-Cu<sub>B</sub> binuclear center of the catalytic subunit CcoN of *cbb*<sub>3</sub>-Cox. The color scheme is as follows: Heme *b*, light red and heme *b*<sub>3</sub>, dark red; His, green; Tyr, violet; Glu, orange; copper – blue; hexa-coordinate heme iron, light grey; penta-coordinate heme iron, dark grey; and calcium, yellow. Note the covalent bond between His 207 and Tyr 251.

Cox, and is not essential for the activity of *cbb*<sub>3</sub>-Cox in *R. sphaeroides* (Oh and Kaplan 1999), *R. capsulatus* (Peters et al. 2008) and *B. japonicum* (Zufferey et al. 1996), leaving its function undefined. Although a gene encoding *ccoQ* is present in the genome of *P. stutzeri*, curiously, CcoQ is not found in the 3D structure of *cbb*<sub>3</sub>-Cox (Buschmann

et al. 2010). Nevertheless, CcoQ appears to be a *bona fide* subunit of *cbb*<sub>3</sub>-Cox as it copurifies with the other subunits in *B. japonicum* (Zufferey et al. 1998). Moreover, it forms with CcoN, CcoO and CcoP an active complex of ~230-kDa in blue-native polyacrylamide gels (BN-PAGE) in *R. capsulatus* (Kulajta et al. 2006) and can be cross-linked

to CcoP, suggesting its close vicinity to this subunit in *cbb*<sub>3</sub>-Cox (Peters et al. 2008).

### C. Maturation of CcoN

CcoN is probably co-translationally inserted into the *R. capsulatus* cytoplasmic membrane (Koch et al. 2003; Koch 2007), and its hemes *b*, *b*<sub>3</sub> and Cu<sub>B</sub> cofactors are deeply buried within the protein. Incorporation of these cofactors into CcoN seems to be critical for proper folding and stabilization of *cbb*<sub>3</sub>-Cox. How, and in which order, these cofactors are inserted into CcoN is unknown, although a co-translational insertion process for hemes *a* and Cu cofactors for *aa*<sub>3</sub>-Cox has been proposed (Khalimonchuk et al. 2005).

#### 1. Hemes *b* of *cbb*<sub>3</sub>-Cox

Available structures of soluble and membrane-bound heme *b* containing proteins show that this cofactor is typically buried within the cognate protein without significant surface exposure (Smith et al. 2010). How the non-covalently attached heme groups are incorporated into their cognate proteins is still a largely unexplored process. Heme insertion into soluble cyts *b* was initially considered to occur spontaneously, but recent studies indicate that accessory proteins are required in vivo for efficient heme *b* incorporation into proteins. For example, insertion of the heme *b* cofactor into the NO synthase requires thioredoxin, Hsp90 chaperone, and glycerolphosphate-dehydrogenase (Chakravarti et al. 2010; Ghosh et al. 2011; Hannibal et al. 2012).

The process of non-covalently attached heme *b* (or *a*, or *o*) insertion into the HCO enzymes is mainly examined for the *aa*<sub>3</sub>-Cox of *P. denitrificans* and *R. sphaeroides*, and *bo*<sub>3</sub>-Qox of *E. coli*. In the case of *bo*<sub>3</sub>-Qox, use of <sup>55</sup>Fe-labeled heme showed that these cofactors were inserted at a late step during assembly (Palombo and Daley 2012). It is suggested that the heme-binding pocket within the catalytic subunit CyoB is only formed upon its interaction with a subcomplex containing the CyoD and CyoC

subunits, which do not contain any cofactor (Stenberg et al. 2007). However, it remains unknown whether any dedicated accessory protein(s) is involved in heme *b* or heme *o*<sub>3</sub> insertion into *bo*<sub>3</sub>-Qox. This process seems to be different in the case of the *aa*<sub>3</sub>-Cox, which requires Surf1 for the insertion of heme *a*<sub>3</sub> (Hannappel et al. 2012). Surf1 (called Shy1 in yeast) is a well-conserved membrane protein of about 30 kDa that binds heme via conserved His and Trp residues (Bundschuh et al. 2009). It consists of two TM domains, connected via a large loop facing the inter-membrane space in mitochondria or the periplasmic space in bacteria (Hannappel et al. 2012). In humans, Surf1 mutations are frequent causes of Leigh syndrome, a fatal neurological disorder associated with severe Cox deficiency (Tiranti et al. 1998; Zhu et al. 1998). Interestingly, insertion of the low-spin heme *a* into *R. sphaeroides aa*<sub>3</sub>-Cox does not seem to require Surf1 (Smith et al. 2005). As heme *a*<sub>3</sub> and Cu<sub>B</sub> insertion are suggested to occur simultaneously in the mitochondrial *aa*<sub>3</sub>-Cox (Cobine et al. 2006), Surf1 might be required for coordinating heme *a*<sub>3</sub> and Cu<sub>B</sub> insertions. In bacteria, heme *a* and Cu<sub>B</sub> insertions might be less tightly coupled, as heme *a*<sub>3</sub> insertion does not seem to require prior assembly of Cu<sub>B</sub> in *R. sphaeroides aa*<sub>3</sub>-Cox (Hiser et al. 2000). Likewise, Cu<sub>B</sub> insertion occurs even if heme *a*<sub>3</sub> insertion fails due to the absence of Surf1 (Smith et al. 2005), suggesting that alternative pathways might exist. In agreement with this possibility, *Bacillus subtilis*, which has no Surf1 homologue, contains two HCO enzymes that contain heme *a* (Hill and Andrews 2012). Interestingly, bacteria like *R. capsulatus* or *H. pylori* that have *cbb*<sub>3</sub>-Cox as their sole HCO do not have a Surf1 homologue. It remains unknown whether dedicated assembly proteins are absolutely required for heme *b* and/or *b*<sub>3</sub> insertion into *cbb*<sub>3</sub>-Cox.

A possible candidate for heme *b* insertion into *cbb*<sub>3</sub>-Cox might be CcoS, which is encoded by the *ccoGHIS* gene cluster located immediately downstream of the *ccoNOQP* operon (Koch et al. 1998;



Ducluzeau et al. 2008). CcoS is a small protein (56 amino acid residues) with a single TM helix. It has no recognizable secondary structure motif, and is resilient to mutations of its highly conserved amino acid residues (Pawlik et al. unpublished). Its exact function is unclear, and its overall biochemical properties (e.g., helical content or hydrophobicity) may be more important than its primary sequence. *R. capsulatus* mutants lacking CcoS assemble a completely inactive *cbb<sub>3</sub>-Cox* (i.e., the 230 kDa complex in BN-PAGE) due to the absence of heme *b* and a functional heme *b<sub>3</sub>-Cu<sub>B</sub>* binuclear center in CcoN (Koch et al. 2000; Kulajta et al. 2006). Absence of CcoS has no effect on CcoO and CcoP maturation via Ccm-System I. Whether *Cu<sub>B</sub>* is inserted into *cbb<sub>3</sub>-Cox* in the absence of CcoS is unknown, but available data suggest that Cu insertion is needed for CcoN stability (Kulajta et al. 2006; Ekici et al. 2013), suggesting that CcoS might be involved in heme *b* insertion into this subunit.

## 2. *Cu<sub>B</sub>* Biogenesis of *cbb<sub>3</sub>-Cox*

Cu is required as a cofactor for multiple cupro-enzymes, including various types of HCOs, Cu-Zn superoxide dismutases, multicopper oxidases and type II NADH dehydrogenases. However, free Cu is toxic for cells due to its chemical reactivity, thus cells control Cu homeostasis by monitoring its acquisition, trafficking, storage, and delivery to target proteins. *R. capsulatus* proteins that are known to be involved in this process so far are listed in Table 27.1.

### a. Cu Acquisition and Transport

During the last decade, Cu transport and delivery to HCOs was intensely studied, mainly motivated by Cu toxicity and Cu related diseases associated with Cox enzymes. In eukaryotic cells, Cu enters the cytoplasm via dedicated Cu importers called Ctr (Lutsenko and Petris 2003; Hardman et al. 2006; van den Berghe et al. 2007). However, bacteria have no homologues of Ctr proteins, leaving undefined how Cu enters the bacterial

cytoplasm (Rensing and Grass 2003). A major facilitator superfamily (MFS)-type Cu transporter, CcoA was recently identified in *R. capsulatus* by analyses of a mutant that exhibited Cu-dependent *cbb<sub>3</sub>-Cox* assembly and activity defects (Ekici et al. 2012b). CcoA is an integral membrane protein with 12 TM helices arranged into two subdomains that are separated by a large cytoplasmic loop, and contains the characteristic DRX-GRR motifs of the MFS-type transporters. CcoA also contains additional putative Cu binding Mets (MX<sub>x</sub>M) motifs (Khalifaoui-Hassani et al. 2016) as found in the Ctr-type eukaryotic Cu importers. The idea that CcoA is responsible for Cu transport was initially suggested by lower cellular Cu contents in *R. capsulatus* mutants lacking CcoA as compared with wild type strains (Ekici et al. 2012b). Additional studies, including decreased radioactive <sup>64</sup>Cu uptake ability (Ekici et al. 2014), and inter species heterologous complementation (Beaudoin et al. 2013), established that CcoA is a bacterial cytoplasmic Cu importer, which is required for *cbb<sub>3</sub>-Cox* production (Fig. 27.3). Interestingly, CcoA homologues are also present in eukaryotic organisms. For example, its *Schyzosaccharomyces pombe* homologue Mfc1 is located at the forespore membrane of this species, and is exclusively expressed during meiosis (Beaudoin et al. 2011). When Mfc1 is expressed in *S. pombe* mutants lacking the plasma membrane Cu importers Ctr4 and Ctr5, it complements the defective ability of these mutants to grow on respiratory carbon sources and to import <sup>64</sup>Cu (Beaudoin et al. 2011). Similarly, *R. capsulatus* CcoA also complements *S. pombe* mutants lacking Ctr4 and Ctr5, restoring their ability to grow on non-fermentable carbon sources and to import <sup>64</sup>Cu (Beaudoin et al. 2013). These findings established that the MFS-type transporter CcoA is a cytoplasmic Cu importer in *R. capsulatus*.

In bacteria, well-known cytoplasmic Cu exporters are members of the P1B-type ATPase superfamily that use ATP hydrolysis for Cu transport across the cytoplasmic membrane (Solioz and Vulpe 1996; Palmgren and

Table 27.1. Components involved in the biogenesis of the *R. capsulatus* CcoN subunit of *cbb*<sub>3</sub>-Cox.

Cu protein	Structural features	Proposed function
CcoI (FixI/CtpA/CopA2)	Eight TM helices with ATP-binding, phosphorylation and phosphatase domains. HMBD (CXXXC) and CPC are the Cu binding site	P1B-type ATPase that transports Cu to Cox and/or to other Cu containing proteins across the cytoplasmic membrane
CopA (CopA1)	Eight TM helices with ATP-binding, phosphorylation and phosphatase domains. HMBD (CXXXC) and CPC are the Cu binding site	P1B-type ATPase that exports Cu out of the cytoplasm to control Cu amounts in the cytoplasm
CcoA ( <i>S. pombe</i> Mfc1 homologue)	Twelve TM helices with conserved AVYGRR and AFRGRE motifs. Mets (MXXM) motifs are its putative Cu binding sites	MFS-type transporter that imports Cu into the cytoplasm, and is required for <i>cbb</i> <sub>3</sub> -Cox production
Sco (Sco1/Sco2/SenC/PrrC)	Single TM helix with a thioredoxin fold and a conserved Cu binding motif comprising the CXXXC sequence and a His ligand	Cu chaperone required for Cu <sub>A</sub> and/or Cu <sub>B</sub> insertion into various Cox enzymes. It might also affect oxidative stress and gene regulation
PCuAC (Pcc <sub>A</sub> )	Has a potential Cu binding motif MX <sub>10</sub> MX <sub>21</sub> HXM. Cu binds via one His and three Met residues	Periplasmic chaperone proposed to donate Cu to Sco protein (like eukaryotic Cox17)
CcoG (FixG)	Five TM helices with two putative ferredoxine-like 4Fe-4S cluster binding motifs	Proposed to affect intracellular Cu <sup>1+</sup> /Cu <sup>2+</sup> redox equilibrium
CcoS (FixS)	Small, single TM membrane protein (56 amino acids long) with no recognizable motif	Proposed to be involved in <i>b/b</i> <sub>3</sub> hemes and/or Cu <sub>B</sub> insertion in <i>cbb</i> <sub>3</sub> -Cox

Axelsen 1998; Rensing and Grass 2003). The recent 3D structure of *Legionella pneumophila* P1B-type transporter CopA revealed the direction of Cu transport, and locations of the characteristic motifs of this superfamily (Gourdon et al. 2011), including the ATP binding, phosphorylation and phosphatase domains. CopA also contains an N-terminal heavy metal binding domain (HMBD) with conserved metal binding motifs (CXXXC), and a membrane integral Cu binding site (CPX). The HMBD domain is thought to interact with specific cytoplasmic Cu chaperones via a docking platform as a Cu entry point (Gourdon et al. 2011). Cu transport by P1B-type transporters is from the cytoplasmic face of the membrane where ATP hydrolysis occurs to the other side of the lipid bilayer. Hence, in Gram-negative bacteria, CopA-like transporters seem mainly involved in Cu efflux from the cytoplasm. Earlier, the *Synechocystis* PCC

6803 P1B-type transporters CtaA and PacS were reported as Cu transporters to the cytoplasm and chloroplast stroma, respectively (Tottey et al. 2001, 2002). Whether they are indeed Cu importers deserves further studies.

Various Cu specific P1B-type transporters play distinct cellular functions depending on their efflux rates. For instance, *Pseudomonas aeruginosa* (Gonzalez-Guerrero et al. 2010), *R. capsulatus* (Koch et al. 2000; Ekici et al. 2014) and *Rubrivivax gelatinosus* (Hassani et al. 2010a; Azzouzi et al. 2013) express at least two homologous P1B-type ATPase involved in Cu export. The high flux *P. aeruginosa* CopA1 [homologue of *R. capsulatus* (Ekici et al. 2014) and *R. gelatinosus* CopA (Hassani et al. 2010a)] is involved in Cu detoxification, whereas the low flux CopA2 [homologue of *R. capsulatus* CcoI (Koch et al. 2000) and *R. gelatinosus* CtpA (Hassani et al. 2010a)] is dedicated to supply Cu to *cbb*<sub>3</sub>-Cox (Fig. 27.3).

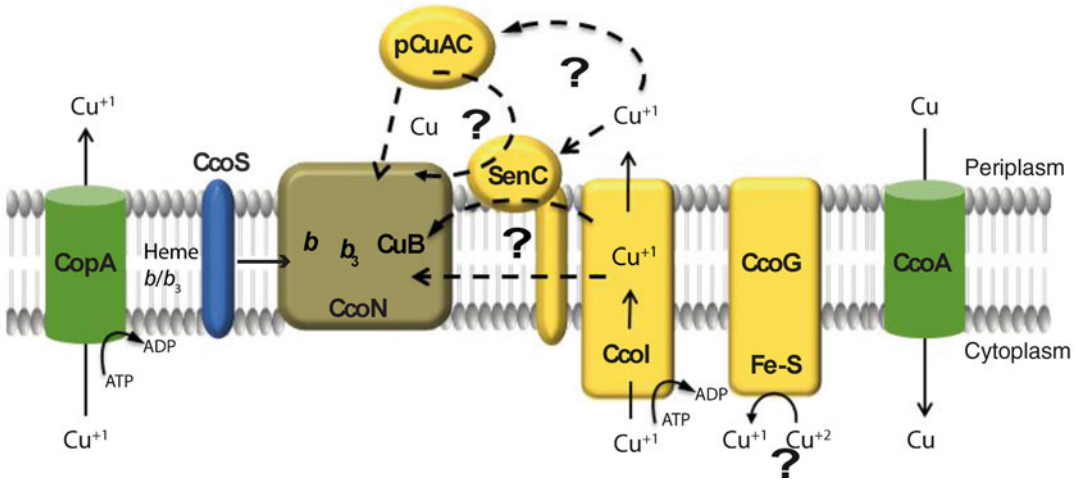


Fig. 27.3. A working model for maturation of the heme  $b_3$ -Cu<sub>B</sub> catalytic center of *R. capsulatus* CcoN subunit of *cbb*<sub>3</sub>-Cox. Cu (possibly Cu<sup>2+</sup>) is imported into the cytoplasm via a major facilitator superfamily (MFS)-type transporter CcoA. In the cytoplasm, Cu<sup>2+</sup> is thought to be reduced to Cu<sup>1+</sup> by the ferredoxin-like protein CcoG via its 4Fe-4S clusters, and exported across the cytoplasmic membrane via the PIB-type ATPase CcoI (shown on the right). CcoI delivers Cu to CcoN either during its co-translational insertion through the membrane (arrow in the membrane) or from the periplasm either directly, or via putative Cu chaperones like the membrane-anchored SenC and the periplasmic pCuAC. In all instances, the exact delivery route of Cu is not known, as indicated? with CcoS is proposed to be involved in incorporation of heme *b* and heme *b*<sub>3</sub> to CcoN. In order to maintain cytoplasmic Cu homeostasis and avoid toxicity while providing Cu to cuproproteins, the PIB-type transporter CopA (a high flux Cu exporter which is a homologue of the low flux CcoI) extrudes excess of Cu from the cytoplasm using ATP (shown on the left).

In the absence of these transporters (i.e., CopA2 or CcoI or CtpA) cells contain no *cbb*<sub>3</sub>-Cox, indicating a role of these transporters in Cu<sub>B</sub> incorporation into CcoN (Preisig et al. 1996; Koch et al. 1998, 2000). However, it is unknown whether Cu is inserted into CcoN without complete export across the membrane by a low flux Cu-transporter during its co-translational membrane insertion, or via specific periplasmic chaperone(s) that may differ among species (Fig. 27.3). Moreover, *R. gelatinosus* CtpA also supplies Cu to cupro-enzymes other than *cbb*<sub>3</sub>-Cox, like *caa*<sub>3</sub>-Cox and N<sub>2</sub>O reductase (Hassani et al. 2010a), suggesting a broader role for these transporters. The findings that the cytoplasmic Cu importer CcoA and the PIB-type Cu exporter CcoI are both required for *R. capsulatus* *cbb*<sub>3</sub>-Cox biogenesis indicate that Cu needs to be imported into, and then exported from, the cytoplasm in order to be incorporated into the CcoN subunit of *cbb*<sub>3</sub>-Cox. Currently,

*R. capsulatus* components involved in cytoplasmic Cu trafficking need further studies.

Two different ways of overcoming *cbb*<sub>3</sub>-Cox deficiency induced by the absence of CcoA have been observed. First, phenotypic suppression of mutants lacking CcoA can be achieved by supplementation of the growth medium with exogenous  $\mu$ M amounts of Cu<sup>2+</sup>. This finding suggests that a mechanism(s) independent of CcoA can also supply Cu to *cbb*<sub>3</sub>-Cox when Cu is not scarce (Ekici et al. 2012b). Second even when Cu is not abundant, bypass suppressors of *R. capsulatus* mutants lacking CcoA overcome *cbb*<sub>3</sub>-Cox deficiency by increasing cellular Cu content (Ekici et al. 2012b, 2014). These suppressor mutations occur at a unique ten consecutive cytosine base pair repeat in *copA* gene, inactivating the high flux PIB-type transporter CopA (Ekici et al. 2014). *R. capsulatus* mutants lacking CopA alone have no effect on *cbb*<sub>3</sub>-Cox biogenesis, but are hypersensitive to Cu. Indeed, a double mutant

lacking both CcoA and CopA restores *cbb*<sub>3</sub>-Cox production at the expense of cellular Cu hypersensitivity. Thus, homeostatic balance between the Cu importer CcoA and the Cu exporter CopA is crucial to ensure safe delivery of Cu to target cuproproteins like *cbb*<sub>3</sub>-Cox (Ekici et al. 2014).

#### b. Copper Insertion

Once imported into the cytoplasm, Cu is trafficked to various cuproproteins, including HCO enzymes. Although how Cu is specifically delivered to *cbb*<sub>3</sub>-Cox is not yet established, analyses of mutants lacking *cbb*<sub>3</sub>-Cox activity implicated into this process several gene products. The specificity of Cu delivery to the different Cu accepting proteins (e.g., Cu<sub>A</sub> and Cu<sub>B</sub> of *aa*<sub>3</sub>-Cox) is thought to be associated with specific putative Cu chaperones, as discussed below.

##### SCO (SenC/PrrC) Chaperones

SCO1 and SCO2 proteins are well studied in yeast and mammalian cells, and are mainly involved in Cu<sub>A</sub> insertion into the subunit II of *aa*<sub>3</sub>-Cox. Although both of these proteins were identified in yeast, only SCO1 participates in Cu<sub>A</sub> formation in this species (Schulze and Rodel 1988; Krummeck and Rodel 1990), whereas SCO1 and SCO2 are both required for Cox biogenesis in humans (Leary et al. 2004). Mutations in either of these proteins cause clinical disorders manifested as fatal encephalomyopathies (Shoubridge 2001; Stiburek et al. 2009). Homologues of the SCO proteins were also identified in a number of bacteria. The 3D structure of *B. subtilis* SCO1 depicts it as a membrane-anchored protein with a single TM helix (Balatri et al. 2003). Its periplasmic domain contains a thioredoxin fold, a Cys-rich Cu binding motif and a His ligand (Hill and Andrews 2012). Like their eukaryotic counterparts, bacterial SCO proteins seem to be specific to the insertion of Cu<sub>A</sub> of *aa*<sub>3</sub>-Cox. For example, a *B. japonicum* mutant lacking SCO1 has no *aa*<sub>3</sub>-Cox in its cytoplasmic membrane (Buhler et al. 2011), while in species like *R. sphaeroides*

(PrrC) (Eraso and Kaplan 2000), *Neisseria meningitidis*, or *Neisseria gonorrhoeae* (Eraso and Kaplan 2000; Seib et al. 2003), absence of SCO activity has no effect on *cbb*<sub>3</sub>-Cox (due the absence of Cu<sub>A</sub>). In addition, some SCO homologues were shown to have a thiol:disulfide oxidoreductase activity, possibly important for Cu insertion into the target proteins (McEwan et al. 2002; Hill and Andrews 2012).

Interestingly, genome surveys using bioinformatic approaches identified genes encoding for SCO proteins in a number of bacteria that also lack *aa*<sub>3</sub>-Cox, suggesting that in these cases, the role(s) of SCO proteins might extend beyond the Cu<sub>A</sub> insertion into this enzyme. Functions like Cu metallochaperoning for enzymes other than Cox (Banci et al. 2007), oxidative stress response (Seib et al. 2003) and photosynthetic gene regulation (Eraso and Kaplan 2000) were proposed for these proteins. Moreover, in some species like *R. capsulatus* (Swem et al. 2005) and *P. aeruginosa* (Frangipani and Haas 2009), absence of the SCO homologue SenC also impairs *cbb*<sub>3</sub>-Cox biogenesis in a manner commensurate with the availability of exogenous Cu (Fig. 27.3). Recent chemical cross-linking experiments in *R. capsulatus* indicated that SenC can be located near CcoP and CcoH proteins that are associated with *cbb*<sub>3</sub>-Cox (Lohmeyer et al. 2012). Finally, transcription of *senC* is enhanced by Cu addition in the absence of CcoI, linking it to Cu delivery to *cbb*<sub>3</sub>-Cox (Lohmeyer et al. 2012). Overall, the precise role(s) of SenC during *cbb*<sub>3</sub>-Cox biogenesis still remains unclear.

##### PCu<sub>A</sub>C (Pcc<sub>A</sub>) Chaperone

The gene for the periplasmic Cu<sub>A</sub> chaperone PCu<sub>A</sub>C, which has a potential metal binding motif, was first identified near that of SCO1 in *Deinococcus radiodurans* (Banci et al. 2005). In this species, PCu<sub>A</sub>C binds Cu<sup>1+</sup> through one His and three Met residues, donates Cu to SCO1, like the eukaryotic Cu chaperone Cox17. In *T. thermophiles*, PCu<sub>A</sub>C selectively inserts Cu<sup>1+</sup> into the subunit II of *ba*<sub>3</sub>-Cox to assemble a Cu<sub>A</sub> site with the

Cys ligands presumably reduced by Sco1 thiol:disulfide oxidoreductase activity prior to Cu insertion (Abriata et al. 2008). The role(s) of PCu<sub>A</sub>C together with and without PrrC (SenC) was also examined in *R. sphaeroides*, which produce both *aa*<sub>3</sub>-Cox and *cbb*<sub>3</sub>-Cox (Thompson et al. 2012). It was proposed that PrrC (SenC) might capture and deliver Cu to Cu<sub>A</sub> of the *aa*<sub>3</sub>-Cox and to Cu<sub>B</sub> of the *cbb*<sub>3</sub>-Cox (Fig. 27.3), while the predominant role of PCu<sub>A</sub>C may be to capture and deliver Cu to PrrC (SenC) and Cox11 involved in the maturation of *aa*<sub>3</sub>-Cox Cu<sub>B</sub> center, similar to Cox17 in mitochondria (Khalimonchuk et al. 2005). Homologues of PCu<sub>A</sub>C, called Pcc1, are also found in species that lack *aa*<sub>3</sub>-Cox like *R. capsulatus*. Unlike *D. radiodurans*, the structural gene of *R. capsulatus* Pcc1 is not located next to that of *senC*, but its product contains similar conserved metal-binding motifs. In the absence of Pcc<sub>A</sub>, *R. capsulatus cbb*<sub>3</sub>-Cox activity is reduced, but can be restored by addition of exogenous Cu (Trasnea et al. 2015).

#### CcoG Protein

CcoG is encoded by the *ccoGHIS* cluster located downstream of the *ccoNOQP* operon. It is an integral membrane protein with five predicted TM helices and has two putative 4Fe-4S cluster-binding motifs, but whether it contains any iron-sulfur cluster(s) is unknown. *R. capsulatus* mutants lacking CcoG exhibit a substantial amount of *cbb*<sub>3</sub>-Cox activity in a growth phase dependent manner (Koch et al. 2000) (Fig. 27.3), and its absence seems to affect *cbb*<sub>3</sub>-Cox activity mainly during the early phases of Res growth. It has been proposed that CcoG might affect the intracellular Cu<sup>1+</sup>/Cu<sup>2+</sup> redox equilibrium (Preisig et al. 1996), and its role might be partially redundant with some other component(s) especially in the absence of O<sub>2</sub>. In addition, a mutant lacking both CcoG and CcoA is phenotypically similar to a mutant lacking only CcoA (Ekici et al. 2012a, b), suggesting that CcoG acts downstream of CcoA.

#### D. Maturation of CcoO and CcoP

The CcoO and CcoP subunits of *cbb*<sub>3</sub>-Cox are matured through the Ccm-system I pathway that operates independently from CcoN maturation (Ekici et al. 2013). This process, which is present virtually in all organisms, occurs post-translationally, and is responsible for the covalent ligation of heme *b* to apocyts *c* to produce mature holocyts *c*. The Ccm pathway relies on major cellular functions like protein translocation, extra-cytoplasmic protein folding and degradation, redox homeostasis as well as heme synthesis, acquisition, and insertion into target proteins. Four variants of the cyt *c* biogenesis process (System I–IV) were identified in different organisms, and in spite of their different degrees of complexity, they all share common characteristics (Kranz et al. 2009; Sanders et al. 2010; Allen 2011; de Vitry 2011; Simon and Hederstedt 2011; Stevens et al. 2011). Both apocyts *c* and hemes are independently translocated across a membrane into a cellular compartment where dedicated chaperones and enzymes perform heme ligation. Apocyts *c* are translocated into the periplasm through the Sec pathway in Gram-negative bacteria (Natale et al. 2008; Facey and Kuhn 2010). These processes are coordinated spatially and temporally to minimize cytotoxic effects of free heme and proteolytic degradation of apocyts *c* (Goldman et al. 1996; Moore and Helmann 2005). Thioether bond formation requires reduced heme-Fe<sup>2+</sup> and thiol groups of the apocyt *c* heme-binding site Cys residues (Kranz et al. 1998; Sanders et al. 2010). Finally, mature cyts *c* are assembled into their respective cyt *c* complexes. Here, we focus on *R. capsulatus* cyt *c* biogenesis (Ccm-System I) pathway, which is similar to that found in  $\alpha$ - and  $\gamma$ -proteobacteria, archaea, and mitochondria of plants and red algae. Different components involved in this process are listed in Table 27.2.

The Ccm-System I displays broad substrate specificity and requires the presence of a C<sub>1</sub>XXC<sub>2</sub>H heme-binding site for efficient heme attachment (Allen et al. 2002, 2006,

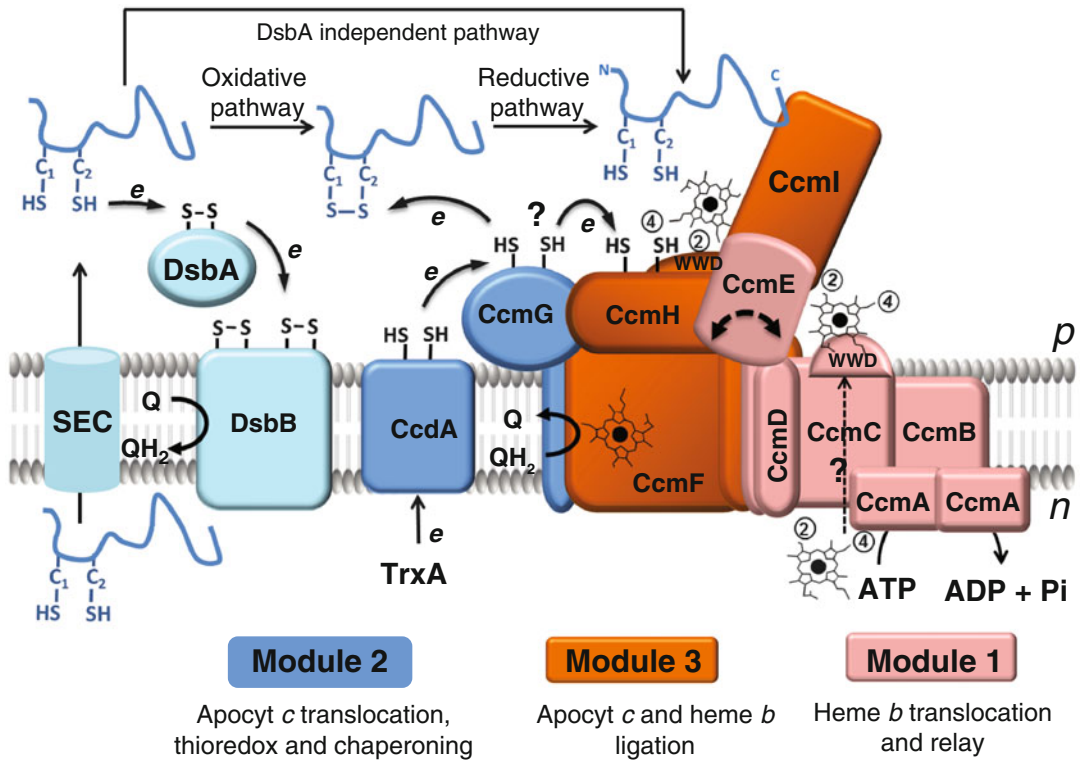
Table 27.2. Components involved in biogenesis of *R. capsulatus* CcoO and CcoP subunits of *cbb*<sub>3</sub>-Cox (Ccm-System I).

Ccm protein	Structural features	Proposed function
CcmA	Peripheral membrane protein with ATP binding domain Walker A (GX <sub>4</sub> GKS/T) and Walker B motifs (R/KX <sub>3</sub> GX <sub>3</sub> LX <sub>3</sub> D)	Part of CcmABCD, a putative ABC-type transporter; required for ATP-dependent “release” of holoCcmE from the CcmCDE complex
CcmB	Six TM helices and a conserved FXXDXXDGSL motif	Part of the CcmABCD, a putative ABC-type transporter; required for the “release” of holoCcmE from the CcmCDE complex
CcmC	Six TM helices with a tryptophan-rich (WGX <sub>F</sub> /Y/WXXWDXRLT) motif and two conserved His residues	Part of the CcmABCD, a putative ABC-type transporter; loads heme to apoCcmE and provides axial ligands to the heme-iron; acts as a CcmE-specific heme lyase
CcmD	Small single TM helix protein with no conserved domains	Part of the CcmABCD, a putative ABC-type transporter; improves CcmC activity; required for the release of holoCcmE from the CcmCDE complex
CcmE	Single TM helix with a periplasmic domain containing a conserved HXXX <sub>Y</sub> motif	Heme chaperone binding covalently vinyl-2 of heme via a conserved His residue; delivers heme to apocyts <i>c</i>
CcmF	Eleven TM helices with a tryptophan-rich (WGGXWFWDP-VEN) motif and four conserved His residues	Part of the CcmFHI heme ligation complex; interacts with apocyts <i>c</i> and holoCcmE; suggested to reduce heme of holoCcmE for its transfer to apocyts <i>c</i>
CcmG	Single TM helix with a periplasmic domain containing a thioredoxin motif (CXXC)	Binds poorly apocyts <i>c</i> ; involved in thiorreduction of apocyts <i>c</i> either directly, or indirectly via CcmH, or by resolving a CcmH-apocyt <i>c</i> mixed-disulfide bond
CcmH	Single TM helix with a periplasmic domain containing a thioredoxin-like motif (LRCXXC)	Part of the CcmFHI heme ligation complex; interacts with apocyts <i>c</i> and suggested to reduce its disulfide bond to enable stereo-specific heme ligation
CcmI	Two TM helices linked by a cytoplasmic loop with a leucine-zipper-like motif; has a large periplasmic domain containing three TPR repeats	Part of the CcmFHI heme ligation complex; is an apocyt <i>c</i> chaperone and binds the C-terminal portion of apocyt <i>c</i> via its periplasmic domain

2009). It ligates heme *b* to a variety of substrates, including natural and artificial cyts *c* (Sanders and Lill 2000) with single or multiple heme binding sites (Pitts et al. 2003), and even short peptides of a few residues (Braun and Thony-Meyer 2004; Lee et al. 2005). Below, we describe the Ccm proteins that are grouped into three functional modules with different roles. Then we discuss a working model for the mechanism of stereo-specific heme ligation, and the possible occurrence of a multi subunit Ccm supercomplex (dubbed a “Ccm machine”).

### 1. Ccm-System I: Functional Organization

*R. capsulatus* Ccm-System I has nine specific membrane-bound components (CcmABCDEFGHI) that can be grouped into three functional modules (Fig. 27.4). These three modules accomplish the (1) transport and relay of heme *b* (Module 1), (2) preparation and chaperoning of ligation-competent apocyts *c* (Module 2), and (3) ligation of heme-apocyt *c* (Module 3) to yield holocyts *c*.



*Fig. 27.4.* Modular organization of cyt *c* maturation (Ccm) system I in *R. capsulatus*. Three membrane-integral functional modules carry out Ccm in a coordinated manner: Module 1 (in pink) is responsible for heme *b* translocation across the membrane and holoCcmE production. The ATP-binding CcmA and its partners CcmB, CcmC, CcmD and the heme chaperone CcmE form an ABC-type transporter in a putative stoichiometry of CcmA<sub>2</sub>BCDE. Heme *b* is transported to the periplasm, and forms a non-covalent complex with CcmCD and CcmE. Oxidized heme-Fe<sup>3+</sup> binds covalently via its vinyl-2 to a conserved His residue at the CcmE heme-binding site. ATP hydrolysis by CcmA is postulated to induce a conformational change (indicated by the arrow in CcmE) that renders CcmE ready to deliver heme *b* to the apocyt *c* substrates. Module 2 (in dark blue) carries out the thio-reduction and chaperoning to the heme ligation site of the newly Sec-translocated apocyts. The periplasmic disulfide bond formation components DsbA and DsbB (light blue) form a disulfide bond at the heme-binding sites of the apocyts *c* to avoid their degradation, and the membrane-anchored thioredoxin-like CcmG reduces this intramolecular disulfide bond to allow heme ligation. CcdA receives electrons from the cytoplasmic thioredoxin TrxA and regenerates CcmG, completing the thioredox loop. DsbA, DsbB and CcdA are not exclusively involved in Ccm as they also play critical roles in other cellular processes. Module 3 (in orange) is composed by CcmFHI that forms the heme ligation complex. CcmI traps the C-termini of the apocyt *c* substrates while CcmF holds the heme delivered by holoCcmE, facilitating its covalent ligation to the apocyts *c* heme binding sites. The specific role of CcmH is still elusive, and suggested to ensure stereo-specificity of the thioether bonds during heme ligation.

a. Module 1. CcmABCD and CcmE:  
Heme *b* Translocation and Relay  
to Module 3

Module 1 has five (CcmABCD and CcmE) components of which CcmABCD are homologous to the ABC (ATP-binding cassette) transporters, and are involved in conveying heme *b* to the periplasm and

loading it on the heme-chaperone CcmE (Fig. 27.4). Of these proteins, CcmA is a peripheral membrane protein with a typical ATP-binding region containing Walker A and B domains (Walker et al. 1982). CcmB and CcmC are integral membrane proteins with six TM helices each, and together with CcmA form a putative ABC-type transporter complex with a stoichiometry of CcmA<sub>2</sub>BC

(Goldman et al. 1997; Page et al. 1997; Goldman and Kranz 2001; Feissner et al. 2006b; Rayapuram et al. 2007). CcmC has a hydrophobic tryptophan rich (WWD) motif and two conserved His residues exposed to the periplasm (Goldman et al. 1998; Richard-Fogal et al. 2009; Richard-Fogal and Kranz 2010). It belongs to the heme handling protein (HHP) family (Lee et al. 2007) and is the only protein necessary for loading heme *b* on apoCcmE to produce holoCcmE (Schulz et al. 1999). CcmD is a small polypeptide (about 60 residues) with a single TM helix and a hydrophilic C-terminal domain (Ahuja and Thony-Meyer 2005; Richard-Fogal et al. 2008) that enhances CcmC activity for holoCcmE synthesis (Feissner et al. 2006a; Richard-Fogal et al. 2008). CcmE is a member of the oligobinding family of proteins (Arcus 2002), has a single TM helix, and a large periplasmic  $\beta$  barrel core domain ending with a flexible C-terminus (Arnesano et al. 2002; Enggist et al. 2002; Aramini et al. 2012). It covalently and transiently binds vinyl-2 of heme *b* via its conserved His residue within the HXXXXY domain (Schulz et al. 1998; Lee et al. 2005; Harvat et al. 2009). Mutation of this His residue prevents holoCcmE formation, and blocks *cyts c* production (Schulz et al. 1999; Enggist et al. 2003). In spite of being the only protein necessary for holoCcmE formation, CcmC lacks any obvious heme delivery path, leaving the mechanism by which heme reaches the periplasm unknown. Once heme *b* is in the periplasm, it interacts with the WWD domain of CcmC (Ren and Thony-Meyer 2001) and the heme-binding region of apoCcmE (Enggist et al. 2003; Harvat et al. 2009). Heme is ligated covalently to the CcmE His residue, and CcmC provides the heme-Fe axial ligands (two His residues) in a CcmCD-heme-CcmE complex that contains oxidized heme (Fe<sup>3+</sup>) (Richard-Fogal et al. 2009; Richard-Fogal and Kranz 2010). The catalytic mechanism behind the formation of this His-heme unusual covalent bond between CcmE and heme is not yet established (Lee et al. 2005; Kranz et al. 2009). How heme *b* is delivered

from holoCcmE to apocyts *c* also remains unclear. Current models propose that ATP hydrolysis by CcmAB triggers the release of holoCcmE from the stable CcmCD-heme-CcmE complex (Feissner et al. 2006a). During this process, a Tyr residue at the heme-binding domain HXXXXY of CcmE replaces the heme-Fe axial ligands provided by CcmC (Uchida et al. 2004) to render holoCcmE proficient for Ccm.

#### b. Module 2. CcmG and CcmH: Apocyt *c* Thioredox and Relay to Module 3

The thiol:disulfide oxidoreductases CcmG and CcmH are specific components of module 2 that work together with the DsbA-DsbB oxidative protein-folding pathway. CcmG and CcmH are responsible for maintaining the apocyt heme-binding site Cys thiol groups in the reduced state. CcmH is also a component of Module 3, as part of the heme ligation complex together with CcmF and CcmI (see below) (Fig. 27.4). Apocyts *c* have processed signal sequences, and are translocated to the periplasm through the Sec pathway where the Cys residues of their heme-binding motifs undergo oxidation by the DsbA-DsbB (Hamel et al. 2009; Kranz et al. 2009; Bonnard et al. 2010; Sanders et al. 2010). DsbA has a highly reactive thioredoxin-like (CXXC) domain and acts upon a wide variety of substrates (Shouldice et al. 2011). DsbB is an integral membrane protein with two thioredoxin-like motifs that reoxidizes DsbA by shuttling the reducing power to the membrane Q/QH<sub>2</sub> pool, and eventually to the electron transport chain (Inaba and Ito 2008). This disulfide bond formation pathway is critical for folding of several proteins, providing resistance to proteolysis, and inducing conformational changes required for their functions and regulations (Depuydt et al. 2011). The Cys residues at the apocyts *c* heme-binding site need to be reduced for covalent heme ligation hence CcmG and probably CcmH are critical for keeping the apocyts ligation-competent. CcmG is a single TM helix protein with a *bona fide* thioredoxin fold with a CXXC



motif. Its active site is unusually acidic and has a groove that might be required for its interaction with CcdA or its substrate(s) (Edeling et al. 2002; Stirnimann et al. 2005). CcdA has six TM helices and two redox-active Cys residues, reduces CcmG (Deshmukh et al. 2000; Fabianek et al. 2000; Katzen et al. 2002; Stirnimann et al. 2006), and is regenerated by the cytoplasmic thioredoxin TrxA (Deshmukh et al. 2000; Katzen et al. 2002; Stirnimann et al. 2005). In *E. coli*, DsbD (the homologue of CcdA) is a larger membrane protein containing three distinct domains, each with a pair of Cys residues (Stewart et al. 1999; Stirnimann et al. 2006). Besides their involvement in cyt *c* biogenesis, CcdA and DsbD are thiol:disulfide oxidoreductases that act on numerous other substrates (Stirnimann et al. 2006), and involved in the expression of virulence genes or sporulation in some organisms (Han and Wilson 2013). The Cys residues from the CXXC motif in both CcdA and CcmG are essential for the Ccm pathway (Monika et al. 1997; Fabianek et al. 1998; Turkarslan et al. 2008). Addition of exogenous thiol compounds can compensate for the Ccm deficiency in CcmG and CcdA mutants (Deshmukh et al. 2000; Bardischewsky and Friedrich 2001; Erlendsson and Hederstedt 2002; Turkarslan et al. 2008). Similarly, addition of oxidants (e.g., Cu<sup>2+</sup> or diamide) was shown to improve production of cyts *c* in DsbA-DsbB mutants (Metheringham et al. 1995; Sambongi and Ferguson 1996; Erlendsson and Hederstedt 2002; Deshmukh et al. 2003; Turkarslan et al. 2008; Mavridou et al. 2012a). Interestingly, absence of DsbA or DsbB suppresses Ccm deficiency of CcdA-null (Erlendsson and Hederstedt 2002; Deshmukh et al. 2003) or CcmG-null mutants (Turkarslan et al. 2008), indicating that thio-reduction of the apocyts becomes unnecessary in the absence of their thio-oxidation (Turkarslan et al. 2008; Mavridou et al. 2012a). Besides being involved in thio-reduction, CcmG also participates in chaperoning the apocyts *c* (Turkarslan et al. 2008).

In *R. capsulatus*, CcmH has a single TM helix and a periplasmic domain with an unusual three helix-bundle fold with a conserved LRCXXCQ motif (Fig. 27.4) (Di Matteo et al. 2007; Ahuja et al. 2008; Zheng et al. 2012). *E. coli* CcmH is a fusion protein between this redox-active domain and a C-terminal extension homologous to CcmI (see below) as found in *R. capsulatus* and *P. aeruginosa* (Fabianek et al. 1999; Zheng et al. 2012). Both Cys residues of CcmH are important for Ccm but not essential under all conditions (Fabianek et al. 1999; Robertson et al. 2008). Remarkably, no thioredox compensation occurs in mutants lacking both DsbA and CcmH, suggesting an additional role for CcmH during Ccm (Turkarslan et al. 2008). Currently, the exact sequence of events during thio-reduction of apocyts *c* is not clear. Initially, a linear dithiol-disulfide cascade with CcmG reducing CcmH, followed by CcmH reducing the oxidized apocyts *c* substrates was proposed (Monika et al. 1997; Fabianek et al. 1999; Setterdahl et al. 2000; Reid et al. 2001; Schoepp-Cothenet et al. 2001; Meyer et al. 2005; Zheng et al. 2012). However, the unusual thioredoxin-fold and the redox properties of CcmH together with the fact that *P. aeruginosa* CcmG does not reduce in vitro the disulfide bond of CcmH but can reduce a 5-thio-2-nitrobenzoic acid (TNB)-CcmH mixed disulfide (Di Matteo et al. 2010), lead to alternative proposals (Verissimo and Daldal 2014). CcmH forms first an inter-molecular mixed-disulfide bond with apocyts *c* that is subsequently resolved by CcmG (Fabianek et al. 1999; Reid et al. 2001; Di Matteo et al. 2007, 2010). Establishing the exact sequence of thioredox reactions between CcmG, CcmH and the apocyts *c* is required for understanding the mechanism of heme ligation.

### c. Module 3. CcmFHI: Apocyt *c* and Heme Ligation

Heme-apocyt *c* ligation *per se* is attributed to Module 3, which in *R. capsulatus* contains at least the CcmF, CcmH and CcmI forming a

membrane-integral complex (Sanders et al. 2008). In *E. coli* the CcmFH complex is a functional homologue of *R. capsulatus* CcmFHI (Ren et al. 2002). CcmI has two distinct domains with different functions (Ritz et al. 1993; Delgado et al. 1995; Lang et al. 1996; Cinege et al. 2004). The membrane embedded N-terminal CcmI-1 domain has two TM helices and a cytoplasmic loop with a leucine zipper-like motif. The CcmI-2 domain is a large periplasmic C-terminal extension decorated with three tetratricopeptide repeats (TPR) (Lang et al. 1996; Sanders et al. 2007; Verissimo et al. 2011), which are ubiquitous protein-protein interaction domains (D'Andrea and Regan 2003). In *R. capsulatus*, the CcmI-1 domain is required for the production of all cyts *c* whereas CcmI-2 is unnecessary for the C-terminally membrane-anchored cyt *c*<sub>1</sub> (Lang et al. 1996). It is now established that CcmI is an apocyt *c* chaperone that binds the C-terminal helix of apocyt *c*<sub>2</sub> mainly via its periplasmic CcmI-2 domain (Han et al. 2008; Verissimo et al. 2011; Di Silvio et al. 2013). In addition, genetic data indicate that the CcmI-2 domain and CcmG can functionally substitute for each other during Ccm (Deshmukh et al. 2002; Sanders et al. 2005, 2007). CcmF is a large integral membrane protein that contains heme *b* (Richard-Fogal et al. 2009). It belongs to the HHP family and has a periplasmic WWD motif like CcmC (Lee et al. 2007). There are four conserved His residues in CcmF: two of them ligate its heme *b* cofactor (San Francisco et al. 2011), and the remaining two coordinate heme *b* of holoCcmE to form a stable CcmF-heme-CcmE complex (Richard-Fogal et al. 2009; San Francisco and Kranz 2014) at least in the absence of CcmGH. CcmF can be reduced by QH<sub>2</sub> in vitro and is proposed to reduce the oxidized heme-iron (Fe<sup>3+</sup>) in holoCcmE. However, mutations at the proposed QH<sub>2</sub> binding site in CcmF do not abolish cyt *c* production (Mavridou et al. 2013), leaving unknown how holoCcmE heme is reduced. Recent reports indicate that under optimized conditions CcmFH together with CcmG are sufficient for cyts

*c* production in *E. coli* (San Francisco et al. 2014). Although this is surprising because CcmABCDE are normally required for Ccm, it strengthens the proposal that *E. coli* CcmFH (or CcmFHI in other species) are responsible for heme ligation *per se* (San Francisco et al. 2014).

## 2. Do the Ccm Components form a Membrane-Integral Maturase Supercomplex?

The *E. coli* Ccm-System I components form a single operon, whose products were initially thought to co-localize in the inner membrane, forming a large “maturase” complex (Thony-Meyer 1997). However, in other organisms, these components are dispersed among multiple genomic loci (Beckman et al. 1992; Lang et al. 1996; Deshmukh et al. 2000). Regardless of the genomic distributions, the use of genetic strategies allowed accumulation and isolation of different intermediate complexes from dodecylmaltoside (DDM) solubilized membrane fractions. A CcmE-heme-apocyt *c* intermediate, with heme being covalently bound to both CcmE (via His) and apocyt *c* (via Cys), was isolated in the absence of CcmFHG (Mavridou et al. 2012b). In addition, apoCcmE devoid of heme was shown to interact with apocyt *c* in vitro, recognizing its heme-binding site (Verissimo et al. 2013). Similarly, CcmE is known to form a complex with CcmCD (Richard-Fogal et al. 2009; Richard-Fogal and Kranz 2010) and with CcmF in the presence of heme (San Francisco and Kranz 2014). *R. capsulatus* apoCcmE forms a ternary complex with apocyt *c*<sub>2</sub> and CcmI in vitro (Verissimo et al. 2013). Furthermore, using DDM-dispersed membrane fractions, apoCcmE was shown to interact directly with CcmI and CcmH (Verissimo et al. 2013). Additionally, CcmI, CcmH and CcmF co-purify with apocyt *c*<sub>2</sub>, and CcmG with CcmI (Verissimo and Daldal unpublished), in agreement with the observation that CcmFHG are sufficient for cyts *c* production (San Francisco et al. 2014). Altogether, these findings suggest

that the heme ligation complex CcmFHI also contains CcmE and CcmG, and raise the possibility of the occurrence of a CcmABCD-CcmE-CcmFHI-CcmG supercomplex (Ccm machine) that may catalyze the entire Ccm process in *R. capsulatus* (Verissimo and Daldal 2014) (Fig. 27.4). If so, then the single TM domain subunits like CcmD might be involved in the assembly, stabilization and regulation of this large supercomplex (Zickermann et al. 2010), by mediating tight associations between CcmABCDE and CcmFHIG complexes. In support of this proposal, co-localization of *R. capsulatus* heme ligation components CcmFHI was reported in high molecular weight (~800 kDa) chromatography column fractions (Sanders et al. 2008). Similar large entities containing different Ccm-System I components were also observed in *A. thaliana* (~500 kDa) (Meyer et al. 2005), and wheat (~700 kDa) mitochondria (Giege et al. 2004).

Large supercomplexes composed of several proteins interacting weakly with each other are difficult to isolate, and often require specific lipid dispersion conditions using mild detergents (e.g., digitonine or amphipoles) to maintain them together (Krause 2006). The intermediate complexes cited above were isolated in the presence of the non-ionic detergent DDM, known to disrupt membrane supercomplexes (e.g., mitochondrial case) (Krause 2006). Thus, whether the Ccm components form altogether a highly stable membrane supercomplex needs further studies. If a Ccm machine exists, then CcmE might act as a heme-shuttle interacting simultaneously with the heme handling (CcmABCD) and the heme ligation (CcmFHI) complexes (Fig. 27.4). The occurrence of such an apparatus may facilitate concerted availability of heme and apocyt *c* substrates, enhancing efficiency of the maturation process. This macromolecular organization is attractive for the maturation of multiheme cyts *c*, where several hemes have to be ligated successively. In this case, CcmI may keep the apocyt *c* trapped in the Ccm machine while the other Ccm

components ensure stereo-specific ligation and axial coordination of heme cofactors.

In the light of the new findings and the possible occurrence of a Ccm machine, we refined our heme ligation model (Sanders et al. 2010; Verissimo and Daldal 2014). In the absence of heme, apoCcmE may be associated more closely with CcmI-CcmH than CcmCD. Once an apocyt *c* is available, CcmI (which is together with CcmFH) traps its C-terminus while apoCcmE recognizes its heme-binding site. To ensure stereo-specific heme ligation, a mixed disulfide bond between the apocyt *c* Cys<sub>1</sub> and oxidized CcmH is formed, leaving Cys<sub>2</sub> available. When heme *b* reaches the periplasm it is oxidized (Fe<sup>3+</sup>), and binds covalently (through its vinyl-2) to the His residue of CcmE to form a CcmE-heme-CcmCD complex. CcmC then provides a heme platform via its WWD domain and its His residues axially ligate heme-iron. Following ATP hydrolysis by CcmAB, the occurrence of a conformational change in CcmC was suggested to render holoCcmE competent for interaction with other heme ligation components. CcmE then forms a CcmE-heme-CcmF complex, with CcmF providing the heme scaffold and the His axial ligands. Upon reduction of the heme-iron (Fe<sup>2+</sup>) (possibly via the heme cofactor of CcmF) the heme *b* vinyl-4 forms the first thioether bond with the reduced Cys<sub>2</sub> thiol of apocyt *c*. Next, CcmG (or possibly the free Cys of CcmH) resolves the mixed disulfide between CcmH and apocyt *c* Cys<sub>1</sub>, rendering it able to interact with heme *b*. This leads to the formation of the second thioether bond between vinyl-2 and apocyt Cys<sub>1</sub> and release of heme from holoCcmE. We note that at present many of the steps of this model, and their chronological orders are hypothetical, and multiple alternative possibilities are plausible. Yet, the in vivo trapped CcmCD-heme-CcmE (Richard-Fogal et al. 2009), CcmE-heme-apocyt *c* (Mavridou et al. 2012b) and CcmF-heme-CcmE (San Francisco and Kranz 2014) intermediates, as well as the in vitro observed CcmI-apocyt *c*<sub>2</sub>-apoCcmE (Verissimo et al. 2013), CcmHI-apoCcmE (Verissimo et al. 2013)

complexes are consistent with this working model which undoubtedly will be elucidated by future studies.

### E. Assembly of *cbb*<sub>3</sub>-Cox

In *R. capsulatus* membranes separated by BN-PAGE, *cbb*<sub>3</sub>-Cox is visualized as an active complex of ~230 kDa, which contains all four structural subunits (CcoNOQP) (Kulajta et al. 2006) (Fig. 27.5). The putative assembly factor CcoH, encoded by the *ccoGHIS* cluster, is also associated with this complex, suggesting that it may be a more permanent component of *cbb*<sub>3</sub>-Cox (Pawlik et al. 2010). Using similar BN-PAGE analyses, two inactive assembly intermediates of ~210 kDa and <70 kDa were also detected in *R. capsulatus* membranes. The ~210 kDa complex contains CcoN, CcoO and CcoH, but lacks CcoP, whereas the <70 kDa complex contains CcoP, CcoQ and CcoH (Kulajta et al. 2006; Pawlik et al. 2010). Although not essential for activity, CcoQ is required for full activity of *cbb*<sub>3</sub>-Cox enzyme, and chemical cross-linking

data show that CcoQ and CcoP interact with each other (Peters et al. 2008). Available data suggest that assembling together the CcoNOH and CcoQPH subcomplexes, possibly via CcoH dimerization, might yield the active *cbb*<sub>3</sub>-Cox (Fig. 27.5) (Pawlik et al. 2010).

CcoO found in the 210 kDa, and CcoP in the <70 kDa complexes contain their covalently attached heme groups as indicated by their peroxidase activity (Kulajta et al. 2006), suggesting that *cyt c* maturation occurs prior to their assembly into *cbb*<sub>3</sub>-Cox. Recent findings indicate that a defective Ccm-System I does not abolish membrane insertion and stability of CcoN (Ekici et al. 2013), although whether this subunit contains its cofactors is not known. Thus, maturation of CcoO and CcoP through the Ccm machinery and that of CcoN via its dedicated components (e.g., CcoA, CcoI, SenC, Pcc<sub>A</sub> and CcoS) are two independent events that are coordinated temporally and spatially for successful production of an active *cbb*<sub>3</sub>-Cox.

The unexpected finding that CcoH is associated with the assembly intermediates of

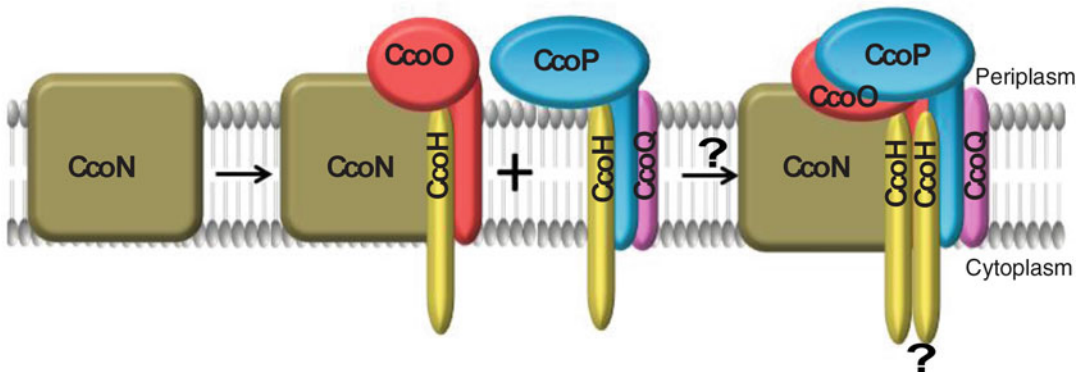


Fig. 27.5. Assembly model of *cbb*<sub>3</sub>-Cox in *R. capsulatus*. Insertion of CcoN into the membrane is independent of the maturation of the other *cbb*<sub>3</sub>-Cox subunits, but when heme *b*, heme *b*<sub>3</sub> and Cu<sub>B</sub> are incorporated is unknown. The assembly of an active *cbb*<sub>3</sub>-Cox enzyme (the 230 kDa active complex revealed by BN-PAGE) proceeds via two inactive subcomplex intermediates. The first subcomplex contains CcoN, CcoO and CcoH (the 210 kDa inactive complex revealed by BN-PAGE) while the second subcomplex contains CcoP, CcoQ and CcoH (the 70 kDa inactive complex revealed by BN-PAGE). Considering that CcoH is associated with both subcomplex intermediates the assembly of *cbb*<sub>3</sub>-Cox is thought to occur via a fusion between CcoNOH and CcoQPH possibly facilitated by CcoH. Whether CcoH is associated to *cbb*<sub>3</sub>-Cox as a dimer is not known. The *cyt c* CcoO and CcoP subunits present in the subcomplex intermediates contain their hemes *c*, further indicating that their maturation occurs prior to their assembly to *cbb*<sub>3</sub>-Cox.

*cbb<sub>3</sub>*-Cox suggests that this protein behaves like a *bona fide* subunit rather than an assembly factor of *R. capsulatus* enzyme. This notion is also supported by the observation that CcoH stability depends on the presence of *cbb<sub>3</sub>*-Cox. Interestingly, CcoH of *R. capsulatus* is a homologue of yeast (Rcf1 and Rcf2) and mammalian (HIG2A) putative supercomplex assembly factors (Strogolova et al. 2012). Yeast Rcf1 binds to the Cox13 subunit of mitochondrial *aa<sub>3</sub>*-Cox as a late assembly factor and affects its dimerization. Yeast cells lacking Rcf1 have reduced amounts of supercomplexes formed by the associations of cyt *bc<sub>1</sub>* and *aa<sub>3</sub>*-Cox and produce ROS (Vukotic et al. 2012). Similarly, depletion of HIG2A (a mammalian homologue of CcoH) alters supercomplex organization in mouse myoblast cells (Chen et al. 2012). The 3D reconstitutions of bovine supercomplexes suggest that these CcoH homologues might fill up a gap between cyt *bc<sub>1</sub>* and *aa<sub>3</sub>*-Cox, as seen by cryo-electron microscopy and electron tomography techniques (Dudkina et al. 2011). Whether CcoH affects supramolecular organizations of cyt *bc<sub>1</sub>* and *cbb<sub>3</sub>*-Cox in *R. capsulatus* membranes is an attractive possibility that deserves future studies. Identification of putative respiratory supercomplexes and their regulation in response to changing physiological conditions is clearly important for our complete understanding of energy transduction pathways.

## Acknowledgments

This work is supported by grants from the NIH GM 38237 and DOE, Division of Chemical Sciences, Geosciences, and Biosciences, Office of Basic Energy Sciences DE-FG02-91ER20052 to FD, and by grants from the Deutsche Forschungsgemeinschaft (GRK1487) and the German-French PhD College (Membrane Proteins and Biological Membranes) to HGK.

## References

- Abriata LA, Banci L, Bertini I, Ciofi-Baffoni S, Gkazonis P, Spyroulias GA, Vila AJ, . . . , Wang S (2008) Mechanism of Cu<sub>A</sub> assembly. *Nat Chem Biol* 4:599–601
- Ahuja U, Thony-Meyer L (2005) CcmD is involved in complex formation between CcmC and the heme chaperone CcmE during cytochrome *c* maturation. *J Biol Chem* 280:236–243
- Ahuja U, Rozhkova A, Glockshuber R, Thony-Meyer L, Einsle O (2008) Helix swapping leads to dimerization of the N-terminal domain of the *c*-type cytochrome maturation protein CcmH from *Escherichia coli*. *FEBS Lett* 582:2779–2786
- Allen JW (2011) Cytochrome *c* biogenesis in mitochondria – systems III and V. *FEBS J* 278:4198–4216
- Allen JW, Tomlinson EJ, Hong L, Ferguson SJ (2002) The *Escherichia coli* cytochrome *c* maturation (Ccm) system does not detectably attach heme to single cysteine variants of an apocytochrome *c*. *J Biol Chem* 277:33559–33563
- Allen JW, Harvat EM, Stevens JM, Ferguson SJ (2006) A variant system I for cytochrome *c* biogenesis in archaea and some bacteria has a novel CcmE and no CcmH. *FEBS Lett* 580:4827–4834
- Allen JW, Sawyer EB, Ginger ML, Barker PD, Ferguson SJ (2009) Variant *c*-type cytochromes as probes of the substrate specificity of the *E. coli* cytochrome *c* maturation (Ccm) apparatus. *Biochem J* 419:177–184
- Alm RA, Ling LS, Moir DT, King BL, Brown ED, Doig PC, Smith DR, . . . , Trust TJ (1999) Genomic-sequence comparison of two unrelated isolates of the human gastric pathogen *Helicobacter pylori*. *Nature* 397:176–180
- Aramini JM, Hamilton K, Rossi P, Ertekin A, Lee HW, Lemak A, Wang H, . . . , Montelione GT (2012) Solution NMR structure, backbone dynamics, and heme-binding properties of a novel cytochrome *c* maturation protein CcmE from *Desulfovibrio vulgaris*. *Biochemistry* 51:3705–3707
- Arcus V (2002) OB-fold domains: a snapshot of the evolution of sequence, structure and function. *Curr Opin Struct Biol* 12:794–801
- Arnesano F, Banci L, Barker PD, Bertini I, Rosato A, Su XC, Viezzoli MS (2002) Solution structure and characterization of the heme chaperone CcmE. *Biochemistry* 41:13587–13594

- Azzouzi A, Steunou AS, Durand A, Khalfaoui-Hassani B, Bourbon ML, Astier C, Bollivar DW, . . . , Ouchane S (2013) Coproporphyrin III excretion identifies the anaerobic coproporphyrinogen III oxidase HemN as a copper target in the Cu<sup>+</sup>-ATPase mutant CopA<sup>-</sup> of *Rubrivivax gelatinosus*. *Mol Microbiol* 88:339–351
- Balatri E, Banci L, Bertini I, Cantini F, Ciofi-Baffoni S (2003) Solution structure of Sco1: a thioredoxin-like protein involved in cytochrome *c* oxidase assembly. *Structure* 11:1431–1443
- Banci L, Bertini I, Ciofi-Baffoni S, Katsari E, Katsaros N, Kubicek K, Mangani S (2005) A copper(I) protein possibly involved in the assembly of Cu<sub>A</sub> center of bacterial cytochrome *c* oxidase. *Proc Natl Acad Sci USA* 102:3994–3999
- Banci L, Bertini I, Cavallaro G, Rosato A (2007) The functions of Sco proteins from genome-based analysis. *J Proteome Res* 6:1568–1579
- Bardischewsky F, Friedrich CG (2001) Identification of *ccdA* in *Paracoccus pantotrophus* GB17: disruption of *ccdA* causes complete deficiency in *c*-type cytochromes. *J Bacteriol* 183:257–263
- Beaudoin J, Ioannoni R, Lopez-Maury L, Bahler J, Ait-Mohand S, Guerin B, Dodani SC, . . . , Labbe S (2011) Mfc1 is a novel forespore membrane copper transporter in meiotic and sporulating cells. *J Biol Chem* 286:34356–34372
- Beaudoin J, Ekici S, Daldal F, Ait-Mohand S, Guerin B, Labbe S (2013) Copper transport and regulation in *Schizosaccharomyces pombe*. *Biochem Soc Trans* 41:1679–1686
- Beckman DL, Trawick DR, Kranz RG (1992) Bacterial cytochromes *c* biogenesis. *Genes Dev* 6: 268–283
- Berry EA, Huang LS, Saechao LK, Pon NG, Valkova-Valchanova M, Daldal F (2004) X-ray structure of *Rhodobacter capsulatus* cytochrome *bc*<sub>1</sub>: comparison with its mitochondrial and chloroplast counterparts. *Photosynth Res* 81:251–275
- Bonnard G, Corvest V, Meyer EH, Hamel PP (2010) Redox processes controlling the biogenesis of *c*-type cytochromes. *Antioxid Redox Signal* 13:1385–1401
- Bowman SE, Bren KL (2008) The chemistry and biochemistry of heme *c*: functional bases for covalent attachment. *Nat Prod Rep* 25:1118–1130
- Braun M, Thony-Meyer L (2004) Biosynthesis of artificial microperoxidases by exploiting the secretion and cytochrome *c* maturation apparatuses of *Escherichia coli*. *Proc Natl Acad Sci USA* 101:12830–12835
- Buhler D, Rossmann R, Landolt S, Balsiger S, Fischer HM, Hennecke H (2011) Disparate pathways for the biogenesis of cytochrome oxidases in *Bradyrhizobium japonicum*. *J Biol Chem* 285: 15704–15713
- Bundschuh FA, Hannappel A, Anderka O, Ludwig B (2009) Surf1, associated with Leigh syndrome in humans, is a heme-binding protein in bacterial oxidase biogenesis. *J Biol Chem* 284:25735–25741
- Buschmann S, Warkentin E, Xie H, Langer JD, Ermler U, Michel H (2010) The structure of *cbb*<sub>3</sub> cytochrome oxidase provides insights into proton pumping. *Science* 329:327–330
- Buschmann S, Richers S, Ermler U, Michel H (2014) A decade of crystallization drops: crystallization of the *cbb*<sub>3</sub> cytochrome *c* oxidase from *Pseudomonas stutzeri*. *Protein Sci* 23:411–422
- Buse G, Soulimane T, Dewor M, Meyer HE, Bluggel M (1999) Evidence for a copper-coordinated histidine-tyrosine cross-link in the active site of cytochrome oxidase. *Protein Sci* 8:985–990
- Chakravarti R, Aulak KS, Fox PL, Stuehr DJ (2010) GAPDH regulates cellular heme insertion into inducible nitric oxide synthase. *Proc Natl Acad Sci USA* 107:18004–18009
- Chen YC, Taylor EB, Dephoure N, Heo JM, Tonhato A, Papandreou I, Nath N, . . . , Rutter J (2012) Identification of a protein mediating respiratory supercomplex stability. *Cell Metab* 15: 348–360
- Cinege G, Kereszt A, Kertesz S, Balogh G, Dusha I (2004) The roles of different regions of the CycH protein in *c*-type cytochrome biogenesis in *Sinorhizobium meliloti*. *Mol Genet Genomics* 271:171–179
- Cobine PA, Pierrel F, Winge DR (2006) Copper trafficking to the mitochondrion and assembly of copper metalloenzymes. *Biochim Biophys Acta* 1763:759–772
- D'Andrea LD, Regan L (2003) TPR proteins: the versatile helix. *Trends Biochem Sci* 28:655–662
- Daldal F, Davidson E, Cheng S (1987) Isolation of the structural genes for the Rieske Fe-S protein, cytochrome *b* and cytochrome *c*<sub>1</sub> all components of the ubiquinol: cytochrome *c*<sub>2</sub> oxidoreductase complex of *Rhodospseudomonas capsulata*. *J Mol Biol* 195:1–12
- Daldal F, Mandaci S, Winterstein C, Myllykallio H, Duyck K, Zannoni D (2001) Mobile cytochrome *c*<sub>2</sub> and membrane-anchored cytochrome *c*<sub>y</sub> are both efficient electron donors to the *cbb*<sub>3</sub>- and *aa*<sub>3</sub>-type cytochrome *c* oxidases during respiratory growth of *Rhodobacter sphaeroides*. *J Bacteriol* 183:2013–2024
- de Vitry C (2011) Cytochrome *c* maturation system on the negative side of bioenergetic membranes: CCB or system IV. *FEBS J* 278:4189–4197
- Delgado MJ, Yeoman KH, Wu G, Vargas C, Davies AE, Poole RK, Johnston AW, Downie JA (1995) Characterization of the *cycHJKL* genes involved in cytochrome *c* biogenesis and symbiotic nitrogen fixation in *Rhizobium leguminosarum*. *J Bacteriol* 177:4927–4934

- Depuydt M, Messens J, Collet JF (2011) How proteins form disulfide bonds. *Antioxid Redox Signal* 15:49–66
- Deshmukh M, Brasseur G, Daldal F (2000) Novel *Rhodobacter capsulatus* genes required for the biogenesis of various *c*-type cytochromes. *Mol Microbiol* 35:123–138
- Deshmukh M, May M, Zhang Y, Gabbert KK, Karberg KA, Kranz RG, Daldal F (2002) Overexpression of *cell-2* can bypass the need for the putative apocytochrome chaperone CycH during the biogenesis of *c*-type cytochromes. *Mol Microbiol* 46:1069–1080
- Deshmukh M, Turkarslan S, Astor D, Valkova-Valchanova M, Daldal F (2003) The dithiol: disulfide oxidoreductases DsbA and DsbB of *Rhodobacter capsulatus* are not directly involved in cytochrome *c* biogenesis, but their inactivation restores the cytochrome *c* biogenesis defect of CcdA-null mutants. *J Bacteriol* 185:3361–3372
- Di Matteo A, Gianni S, Schinina ME, Giorgi A, Altieri F, Calosci N, Brunori M, Travaglini-Allocatelli C (2007) A strategic protein in cytochrome *c* maturation: three-dimensional structure of CcmH and binding to apocytochrome *c*. *J Biol Chem* 282:27012–27019
- Di Matteo A, Calosci N, Gianni S, Jemth P, Brunori M, Travaglini-Allocatelli C (2010) Structural and functional characterization of CcmG from *Pseudomonas aeruginosa*, a key component of the bacterial cytochrome *c* maturation apparatus. *Proteins* 78:2213–2221
- Di Silvio E, Di Matteo A, Malatesta F, Travaglini-Allocatelli C (2013) Recognition and binding of apocytochrome *c* to *P. aeruginosa* CcmI, a component of cytochrome *c* maturation machinery. *Biochim Biophys Acta* 1834:1554–1561
- Ducluzeau AL, Ouchane S, Nitschke W (2008) The *cbb<sub>3</sub>* oxidases are an ancient innovation of the domain bacteria. *Mol Biol Evol* 25:1158–1166
- Dudkina NV, Kudryashev M, Stahlberg H, Boekema EJ (2011) Interaction of complexes I, III, and IV within the bovine respirasome by single particle cryoelectron tomography. *Proc Natl Acad Sci USA* 108:15196–15200
- Edeling MA, Guddat LW, Fabianek RA, Thony-Meyer L, Martin JL (2002) Structure of CcmG/DsbE at 1.14 Å resolution: high-fidelity reducing activity in an indiscriminately oxidizing environment. *Structure* 10:973–979
- Ekici S, Pawlik G, Lohmeyer E, Koch HG, Daldal F (2012a) Biogenesis of *cbb<sub>3</sub>*-type cytochrome *c* oxidase in *Rhodobacter capsulatus*. *Biochim Biophys Acta* 1817:898–910
- Ekici S, Yang H, Koch HG, Daldal F (2012b) Novel transporter required for biogenesis of *cbb<sub>3</sub>*-type cytochrome *c* oxidase in *Rhodobacter capsulatus*. *MBio* 3:293–322
- Ekici S, Jiang X, Koch HG, Daldal F (2013) Missense mutations in cytochrome *c* maturation genes provide new insights into *Rhodobacter capsulatus cbb<sub>3</sub>*-type cytochrome *c* oxidase biogenesis. *J Bacteriol* 195:261–269
- Ekici S, Turkarslan S, Pawlik G, Dancis A, Baliga NS, Koch HG, Daldal F (2014) Intracytoplasmic copper homeostasis controls cytochrome *c* oxidase production. *MBio* 5:e01055–01013
- Enggist E, Thony-Meyer L, Guntert P, Pervushin K (2002) NMR structure of the heme chaperone CcmE reveals a novel functional motif. *Structure* 10:1551–1557
- Enggist E, Schneider MJ, Schulz H, Thony-Meyer L (2003) Biochemical and mutational characterization of the heme chaperone CcmE reveals a heme binding site. *J Bacteriol* 185:175–183
- Eraso JM, Kaplan S (2000) From redox flow to gene regulation: role of the PrrC protein of *Rhodobacter sphaeroides* 2.4.1. *Biochemistry* 39:2052–2062
- Erlendsson LS, Hederstedt L (2002) Mutations in the thiol-disulfide oxidoreductases BdbC and BdbD can suppress cytochrome *c* deficiency of CcdA-defective *Bacillus subtilis* cells. *J Bacteriol* 184:1423–1429
- Fabianek RA, Hennecke H, Thony-Meyer L (1998) The active-site cysteines of the periplasmic thioredoxin-like protein CcmG of *Escherichia coli* are important but not essential for cytochrome *c* maturation in vivo. *J Bacteriol* 180:1947–1950
- Fabianek RA, Hofer T, Thony-Meyer L (1999) Characterization of the *Escherichia coli* CcmH protein reveals new insights into the redox pathway required for cytochrome *c* maturation. *Arch Microbiol* 171:92–100
- Fabianek RA, Hennecke H, Thony-Meyer L (2000) Periplasmic protein thiol: disulfide oxidoreductases of *Escherichia coli*. *FEMS Microbiol Rev* 24:303–316
- Facey SJ, Kuhn A (2010) Biogenesis of bacterial inner-membrane proteins. *Cell Mol Life Sci* 67:2343–2362
- Feissner RE, Richard-Fogal CL, Frawley ER, Kranz RG (2006a) ABC transporter-mediated release of a haem chaperone allows cytochrome *c* biogenesis. *Mol Microbiol* 61:219–231
- Feissner RE, Richard-Fogal CL, Frawley ER, Loughman JA, Earley KW, Kranz RG (2006b) Recombinant cytochromes *c* biogenesis systems I and II and analysis of haem delivery pathways in *Escherichia coli*. *Mol Microbiol* 60:563–577

- Frangipani E, Haas D (2009) Copper acquisition by the SenC protein regulates aerobic respiration in *Pseudomonas aeruginosa* PAO1. *FEMS Microbiol Lett* 298:234–240
- Garcia-Horsman JA, Berry E, Shapleigh JP, Alben JO, Gennis RB (1994) A novel cytochrome *c* oxidase from *Rhodobacter sphaeroides* that lacks Cu<sub>A</sub>. *Biochemistry* 33:3113–3119
- Ghosh A, Chawla-Sarkar M, Stuehr DJ (2011) Hsp90 interacts with inducible NO synthase client protein in its heme-free state and then drives heme insertion by an ATP-dependent process. *FASEB J* 25:2049–2060
- Giege P, Rayapuram N, Meyer EH, Grienerberger JM, Bonnard G (2004) CcmF(C) involved in cytochrome *c* maturation is present in a large sized complex in wheat mitochondria. *FEBS Lett* 563:165–169
- Goldman BS, Kranz RG (2001) ABC transporters associated with cytochrome *c* biogenesis. *Res Microbiol* 152:323–329
- Goldman BS, Gabbert KK, Kranz RG (1996) Use of heme reporters for studies of cytochrome biosynthesis and heme transport. *J Bacteriol* 178:6338–6347
- Goldman BS, Beckman DL, Bali A, Monika EM, Gabbert KK, Kranz RG (1997) Molecular and immunological analysis of an ABC transporter complex required for cytochrome *c* biogenesis. *J Mol Biol* 268:724–738
- Goldman BS, Beck DL, Monika EM, Kranz RG (1998) Transmembrane heme delivery systems. *Proc Natl Acad Sci USA* 95:5003–5008
- Gonzalez-Guerrero M, Raimunda D, Cheng X, Arguello JM (2010) Distinct functional roles of homologous Cu<sup>+</sup> efflux ATPases in *Pseudomonas aeruginosa*. *Mol Microbiol* 78:1246–1258
- Gourdon P, Liu XY, Skjorringe T, Morth JP, Moller LB, Pedersen BP, Nissen P (2011) Crystal structure of a copper-transporting PIB-type ATPase. *Nature* 475:59–64
- Gray KA, Grooms M, Myllykallio H, Moomaw C, Slaughter C, Daldal F (1994) *Rhodobacter capsulatus* contains a novel *cb*-type cytochrome *c* oxidase without a Cu<sub>A</sub> center. *Biochemistry* 33:3120–3127
- Hamel P, Corvest V, Giege P, Bonnard G (2009) Biochemical requirements for the maturation of mitochondrial *c*-type cytochromes. *Biochim Biophys Acta* 1793:125–138
- Han H, Wilson AC (2013) The two CcdA proteins of *Bacillus anthracis* differentially affect virulence gene expression and sporulation. *J Bacteriol* 195:5242–5249
- Han D, Kim K, Oh J, Park J, Kim Y (2008) TPR domain of NrfG mediates complex formation between heme lyase and formate-dependent nitrite reductase in *Escherichia coli* O157:H7. *Proteins* 70:900–914
- Hannappel A, Bundschuh FA, Ludwig B (2012) Role of Surf1 in heme recruitment for bacterial COX biogenesis. *Biochim Biophys Acta* 1817:928–937
- Hannibal L, Collins D, Brassard J, Chakravarti R, Vempati R, Dorlet P, Santolini J, Stuehr DJ (2012) Heme binding properties of glyceraldehyde-3-phosphate dehydrogenase. *Biochemistry* 51:8514–8529
- Hardman B, Manuelpillai U, Wallace EM, Monty JF, Kramer DR, Kuo YM, Mercer JF, Ackland ML (2006) Expression, localisation and hormone regulation of the human copper transporter hCTR1 in placenta and choriocarcinoma Jeg-3 cells. *Placenta* 27:968–977
- Harvat EM, Redfield C, Stevens JM, Ferguson SJ (2009) Probing the heme-binding site of the cytochrome *c* maturation protein CcmE. *Biochemistry* 48:1820–1828
- Hassani BK, Astier C, Nitschke W, Ouchane S (2010a) CtpA, a copper-translocating P-type ATPase involved in the biogenesis of multiple copper-requiring enzymes. *J Biol Chem* 285:19330–19337
- Hassani BK, Steunou AS, Liotenberg S, Reiss-Husson F, Astier C, Ouchane S (2010b) Adaptation to oxygen: role of terminal oxidases in photosynthesis initiation in the purple photosynthetic bacterium, *Rubrivivax gelatinosus*. *J Biol Chem* 285:19891–19899
- Hemp J, Gennis RB (2008) Diversity of the heme-copper superfamily in archaea: insights from genomics and structural modeling. *Results Probl Cell Differ* 45:1–31
- Hill BC, Andrews D (2012) Differential affinity of BsSCO for Cu(II) and Cu(I) suggests a redox role in copper transfer to the Cu(A) center of cytochrome *c* oxidase. *Biochim Biophys Acta* 1817:948–954
- Hiser L, Di Valentin M, Hamer AG, Hosler JP (2000) Cox11p is required for stable formation of the Cu<sub>B</sub> and magnesium centers of cytochrome *c* oxidase. *J Biol Chem* 275:619–623
- Hochkoeppler A, Jenney FE Jr, Lang SE, Zannoni D, Daldal F (1995) Membrane-associated cytochrome *c<sub>y</sub>* of *Rhodobacter capsulatus* is an electron carrier from the cytochrome *bc*<sub>1</sub> complex to the cytochrome *c* oxidase during respiration. *J Bacteriol* 177:608–613
- Hosler JP, Ferguson-Miller S, Mills DA (2006) Energy transduction: proton transfer through the respiratory complexes. *Annu Rev Biochem* 75:165–187
- Inaba K, Ito K (2008) Structure and mechanisms of the DsbB-DsbA disulfide bond generation machine. *Biochim Biophys Acta* 1783:520–529
- Iwata S, Ostermeier C, Ludwig B, Michel H (1995) Structure at 2.8 Å resolution of cytochrome *c* oxidase from *Paracoccus denitrificans*. *Nature* 376:660–669



- Jenney FE Jr, Daldal F (1993) A novel membrane-associated *c*-type cytochrome, *cyt c<sub>y</sub>*, can mediate the photosynthetic growth of *Rhodobacter capsulatus* and *Rhodobacter sphaeroides*. *EMBO J* 12:1283–1292
- Jenney FE Jr, Prince RC, Daldal F (1994) Roles of the soluble cytochrome *c<sub>2</sub>* and membrane-associated cytochrome *c<sub>y</sub>* of *Rhodobacter capsulatus* in photosynthetic electron transfer. *Biochemistry* 33:2496–2502
- Jones CW, Brice JM, Wright V, Ackrell BA (1973) Respiratory protection of nitrogenase in *Azotobacter vinelandii*. *FEBS Lett* 29:77–81
- Kahn D, David M, Domergue O, Daveran ML, Ghai J, Hirsch PR, Batut J (1989) *Rhizobium meliloti fixGHI* sequence predicts involvement of a specific cation pump in symbiotic nitrogen fixation. *J Bacteriol* 171:929–939
- Katzen F, Deshmukh M, Daldal F, Beckwith J (2002) Evolutionary domain fusion expanded the substrate specificity of the transmembrane electron transporter DsbD. *EMBO J* 21:3960–3969
- Keilin D (1925) On cytochrome, a respiratory pigment, common to animals, yeast and higher plants. *Proc R Soc Lond B Biol Sci* 98:312–339
- Khalifaoui-Hassani B, Verissimo AF, Koch HG, Daldal F (2016) Uncovering the transmembrane metal binding site of the novel bacterial major facilitator superfamily-type copper importer CcoA. *MBio* 7(1), pii: e01981–15. doi:10.1128/mBio.01981-15
- Khalimonchuk O, Ostermann K, Rodel G (2005) Evidence for the association of yeast mitochondrial ribosomes with Cox1p, a protein required for the Cu<sub>B</sub> site formation of cytochrome *c* oxidase. *Curr Genet* 47:223–233
- Koch HG (2007) Folding, assembly, and stability of transmembrane cytochromes. *Curr Chem Biol* 1:59–74
- Koch HG, Hwang O, Daldal F (1998) Isolation and characterization of *Rhodobacter capsulatus* mutants affected in cytochrome *cbb<sub>3</sub>* oxidase activity. *J Bacteriol* 180:969–978
- Koch HG, Winterstein C, Saribas AS, Alben JO, Daldal F (2000) Roles of the *ccoGHIS* gene products in the biogenesis of the *cbb<sub>3</sub>*-type cytochrome *c* oxidase. *J Mol Biol* 297:49–65
- Koch HG, Moser M, Muller M (2003) Signal recognition particle-dependent protein targeting, universal to all kingdoms of life. *Rev Physiol Biochem Pharmacol* 146:55–94
- Kranz R, Lill R, Goldman B, Bonnard G, Merchant S (1998) Molecular mechanisms of cytochrome *c* biogenesis: three distinct systems. *Mol Microbiol* 29:383–396
- Kranz RG, Richard-Fogal C, Taylor JS, Frawley ER (2009) Cytochrome *c* biogenesis: mechanisms for covalent modifications and trafficking of heme and for heme-iron redox control. *Microbiol Mol Biol Rev* 73:510–528
- Krause F (2006) Detection and analysis of protein-protein interactions in organellar and prokaryotic proteomes by native gel electrophoresis: (Membrane) protein complexes and supercomplexes. *Electrophoresis* 27:2759–2781
- Krummeck G, Rodel G (1990) Yeast SCO1 protein is required for a post-translational step in the accumulation of mitochondrial cytochrome *c* oxidase subunits I and II. *Curr Genet* 18:13–15
- Kulajta C, Thumfart JO, Haid S, Daldal F, Koch HG (2006) Multi-step assembly pathway of the *cbb<sub>3</sub>*-type cytochrome *c* oxidase complex. *J Mol Biol* 355:989–1004
- Lang SE, Jenney FE Jr, Daldal F (1996) *Rhodobacter capsulatus* CycH: a bipartite gene product with pleiotropic effects on the biogenesis of structurally different *c*-type cytochromes. *J Bacteriol* 178:5279–5290
- Leary SC, Kaufman BA, Pellicchia G, Guercin GH, Mattman A, Jaksch M, Shoubridge EA (2004) Human SCO1 and SCO2 have independent, cooperative functions in copper delivery to cytochrome *c* oxidase. *Hum Mol Genet* 13:1839–1848
- Lee D, Pervushin K, Bischof D, Braun M, Thony-Meyer L (2005) Unusual heme-histidine bond in the active site of a chaperone. *J Am Chem Soc* 127:3716–3717
- Lee JH, Harvat EM, Stevens JM, Ferguson SJ, Saier MH Jr (2007) Evolutionary origins of members of a superfamily of integral membrane cytochrome *c* biogenesis proteins. *Biochim Biophys Acta* 1768:2164–2181
- Li Y, Hopper A, Overton T, Squire DJ, Cole J, Tovell N (2010) Organization of the electron transfer chain to oxygen in the obligate human pathogen *Neisseria gonorrhoeae*: roles for cytochromes *c<sub>4</sub>* and *c<sub>5</sub>*, but not cytochrome *c<sub>2</sub>*, in oxygen reduction. *J Bacteriol* 192:2395–2406
- Lohmeyer E, Schroder S, Pawlik G, Trasnea PI, Peters A, Daldal F, Koch HG (2012) The ScoI homologue SenC is a copper binding protein that interacts directly with the *cbb<sub>3</sub>*-type cytochrome oxidase in *Rhodobacter capsulatus*. *Biochim Biophys Acta* 1817:2005–2015
- Lutsenko S, Petris MJ (2003) Function and regulation of the mammalian copper-transporting ATPases:

- insights from biochemical and cell biological approaches. *J Membr Biol* 191:1–12
- Marrs B, Gest H (1973) Genetic mutations affecting the respiratory electron-transport system of the photosynthetic bacterium *Rhodospseudomonas capsulata*. *J Bacteriol* 114:1045–1051
- Mavridou DA, Ferguson SJ, Stevens JM (2012a) The interplay between the disulfide bond formation pathway and cytochrome *c* maturation in *Escherichia coli*. *FEBS Lett* 586:1702–1707
- Mavridou DA, Stevens JM, Monkemeyer L, Daltrop O, di Gleria K, Kessler BM, . . . , Allen JW (2012b) A pivotal heme-transfer reaction intermediate in cytochrome *c* biogenesis. *J Biol Chem* 287:2342–2352
- Mavridou DA, Clark MN, Choulat C, Ferguson SJ, Stevens JM (2013) Probing heme delivery processes in cytochrome *c* biogenesis system I. *Biochemistry* 52:7262–7270
- McEwan AG, Greenfield AJ, Wetzstein HG, Jackson JB, Ferguson SJ (1985) Nitrous oxide reduction by members of the family *Rhodospirillaceae* and the nitrous oxide reductase of *Rhodospseudomonas capsulata*. *J Bacteriol* 164:823–830
- McEwan AG, Lewin A, Davy SL, Boetzel R, Leech A, Walker D, Wood T, Moore GR (2002) PrrC from *Rhodobacter sphaeroides*, a homologue of eukaryotic Sco proteins, is a copper-binding protein and may have a thiol-disulfide oxidoreductase activity. *FEBS Lett* 518:10–16
- Metheringham R, Griffiths L, Crooke H, Forsythe S, Cole J (1995) An essential role for DsbA in cytochrome *c* synthesis and formate-dependent nitrite reduction by *Escherichia coli* K-12. *Arch Microbiol* 164:301–307
- Meyer EH, Giege P, Gelhaye E, Rayapuram N, Ahuja U, Thony-Meyer L, Grienenberger JM, Bonnard G (2005) AtCCMH, an essential component of the *c*-type cytochrome maturation pathway in *Arabidopsis* mitochondria, interacts with apocytochrome *c*. *Proc Natl Acad Sci USA* 102:16113–16118
- Monika EM, Goldman BS, Beckman DL, Kranz RG (1997) A thio-reduction pathway tethered to the membrane for periplasmic cytochromes *c* biogenesis; in vitro and in vivo studies. *J Mol Biol* 271:679–692
- Moore CM, Helmann JD (2005) Metal ion homeostasis in *Bacillus subtilis*. *Curr Opin Microbiol* 8:188–195
- Moore GR, Pettigrew GW (1990) Cytochromes *c* Evolutionary, Structural and Physicochemical Aspects. Springer, New York
- Natale P, Bruser T, Driessen AJ (2008) Sec- and Tat-mediated protein secretion across the bacterial cytoplasmic membrane—distinct translocases and mechanisms. *Biochim Biophys Acta* 1778:1735–1756
- Oh JI, Kaplan S (1999) The *cbb*<sub>3</sub> terminal oxidase of *Rhodobacter sphaeroides* 2.4.1: structural and functional implications for the regulation of spectral complex formation. *Biochemistry* 38:2688–2696
- Oh JI, Kaplan S (2002) Oxygen adaptation. The role of the CcoQ subunit of the *cbb*<sub>3</sub> cytochrome *c* oxidase of *Rhodobacter sphaeroides* 2.4.1. *J Biol Chem* 277:16220–16228
- Page MD, Pearce DA, Norris HA, Ferguson SJ (1997) The *Paracoccus denitrificans* ccmA, B and C genes: cloning and sequencing, and analysis of the potential of their products to form a haem or apo-*c*-type cytochrome transporter. *Microbiology* 143: 563–576
- Palmgren MG, Axelsen KB (1998) Evolution of P-type ATPases. *Biochim Biophys Acta* 1365:37–45
- Palombo I, Daley DO (2012) Heme incorporation into the cytochrome *bo*<sub>3</sub> occurs at a late stage of assembly. *FEBS Lett* 586:4197–4202
- Parkhill J, Wren BW, Mungall K, Ketley JM, Churcher C, Basham D, Chillingworth T, . . . , Barrell BG (2000) The genome sequence of the food-borne pathogen *Campylobacter jejuni* reveals hypervariable sequences. *Nature* 403:665–668
- Pawlik G, Kulajta C, Sachelaru I, Schroder S, Waidner B, Hellwig P, Daldal F, Koch HG (2010) The putative assembly factor CcoH is stably associated with the *cbb*<sub>3</sub>-type cytochrome oxidase. *J Bacteriol* 192:6378–6389
- Peters A, Kulajta C, Pawlik G, Daldal F, Koch HG (2008) Stability of the *cbb*<sub>3</sub>-type cytochrome oxidase requires specific CcoQ-CcoP interactions. *J Bacteriol* 190:5576–5586
- Pettigrew GW, Moore GR (1987) Cytochromes C - Biological Aspects. Springer, Berlin/Heidelberg/New York/Paris/Tokyo
- Pitcher RS, Watmough NJ (2004) The bacterial cytochrome *cbb*<sub>3</sub> oxidases. *Biochim Biophys Acta* 1655:388–399
- Pitts KE, Dobbin PS, Reyes-Ramirez F, Thomson AJ, Richardson DJ, Seward HE (2003) Characterization of the *Shewanella oneidensis* MR-1 decaheme cytochrome MtrA: expression in *Escherichia coli* confers the ability to reduce soluble Fe(III) chelates. *J Biol Chem* 278:27758–27765
- Preisig O, Anthamatten D, Hennecke H (1993) Genes for a microaerobically induced oxidase complex in *Bradyrhizobium japonicum* are essential for a nitrogen-fixing endosymbiosis. *Proc Natl Acad Sci USA* 90:3309–3313
- Preisig O, Zufferey R, Hennecke H (1996) The *Bradyrhizobium japonicum* *fixGHIS* genes are re-

- quired for the formation of the high-affinity *cbb<sub>3</sub>*-type cytochrome oxidase. *Arch Microbiol* 165:297–305
- Rayapuram N, Hagenmuller J, Grienenberger JM, Giege P, Bonnard G (2007) AtCCMA interacts with AtCcmB to form a novel mitochondrial ABC transporter involved in cytochrome *c* maturation in *Arabidopsis*. *J Biol Chem* 282:21015–21023
- Reid E, Cole J, Eaves DJ (2001) The *Escherichia coli* CcmG protein fulfils a specific role in cytochrome *c* assembly. *Biochem J* 355:51–58
- Ren Q, Thony-Meyer L (2001) Physical interaction of CcmC with heme and the heme chaperone CcmE during cytochrome *c* maturation. *J Biol Chem* 276:32591–32596
- Ren Q, Ahuja U, Thony-Meyer L (2002) A bacterial cytochrome *c* heme lyase. CcmF forms a complex with the heme chaperone CcmE and CcmH but not with apocytochrome *c*. *J Biol Chem* 277:7657–7663
- Rensing C, Grass G (2003) *Escherichia coli* mechanisms of copper homeostasis in a changing environment. *FEMS Microbiol Rev* 27:197–213
- Richard-Fogal C, Kranz RG (2010) The CcmC: heme: CcmE complex in heme trafficking and cytochrome *c* biosynthesis. *J Mol Biol* 401:350–362
- Richard-Fogal CL, Frawley ER, Kranz RG (2008) Topology and function of CcmD in cytochrome *c* maturation. *J Bacteriol* 190:3489–3493
- Richard-Fogal CL, Frawley ER, Bonner ER, Zhu H, San Francisco B, Kranz RG (2009) A conserved haem redox and trafficking pathway for cofactor attachment. *EMBO J* 28:2349–2359
- Ritz D, Bott M, Hennecke H (1993) Formation of several bacterial *c*-type cytochromes requires a novel membrane-anchored protein that faces the periplasm. *Mol Microbiol* 9:729–740
- Robertson IB, Stevens JM, Ferguson SJ (2008) Dispensable residues in the active site of the cytochrome *c* biogenesis protein CcmH. *FEBS Lett* 582:3067–3072
- Sambongi Y, Ferguson SJ (1996) Mutants of *Escherichia coli* lacking disulphide oxidoreductases DsbA and DsbB cannot synthesise an exogenous monohaem *c*-type cytochrome except in the presence of disulphide compounds. *FEBS Lett* 398:265–268
- San Francisco B, Kranz RG (2014) Interaction of holoccmE with CcmF in heme trafficking and cytochrome *c* biosynthesis. *J Mol Biol* 426:570–585
- San Francisco B, Bretsnyder EC, Rodgers KR, Kranz RG (2011) Heme ligand identification and redox properties of the cytochrome *c* synthetase, CcmF. *Biochemistry* 50:10974–10985
- San Francisco B, Sutherland MC, Kranz RG (2014) The CcmFH complex is the system I holo-cytochrome *c* synthetase: engineering cytochrome *c* maturation independent of CcmABCDE. *Mol Microbiol* 91:996–1008
- Sanders C, Lill H (2000) Expression of prokaryotic and eukaryotic cytochromes *c* in *Escherichia coli*. *Biochim Biophys Acta* 1459:131–138
- Sanders C, Deshmukh M, Astor D, Kranz RG, Daldal F (2005) Overproduction of CcmG and CcmFH(Re) fully suppresses the *c*-type cytochrome biogenesis defect of *Rhodobacter capsulatus* CcmI-null mutants. *J Bacteriol* 187:4245–4256
- Sanders C, Boulay C, Daldal F (2007) Membrane-spanning and periplasmic segments of CcmI have distinct functions during cytochrome *c* biogenesis in *Rhodobacter capsulatus*. *J Bacteriol* 189:789–800
- Sanders C, Turkarlan S, Lee DW, Onder O, Kranz RG, Daldal F (2008) The cytochrome *c* maturation components CcmF, CcmH, and CcmI form a membrane-integral multisubunit heme ligation complex. *J Biol Chem* 283:29715–29722
- Sanders C, Turkarlan S, Onder O, Frawley ER, Kranz RG, Koch H-G, Daldal F (2009) Biogenesis of *c*-type cytochromes and cytochrome complexes. In: Hunter CN, Daldal F, Beatty JT (eds) *The Purple Phototrophic Bacteria*. Springer Science, Netherlands
- Sanders C, Turkarlan S, Lee DW, Daldal F (2010) Cytochrome *c* biogenesis: the Ccm system. *Trends Microbiol* 18:266–274
- Sassera D, Lo N, Epis S, D’Auria G, Montagna M, Comandatore F, Horner D, . . . , Bandi C (2011) Phylogenomic evidence for the presence of a flagellum and *cbb<sub>3</sub>* oxidase in the free-living mitochondrial ancestor. *Mol Biol Evol* 28:3285–3296
- Schoepp-Cothenet B, Schutz M, Baymann F, Brugna M, Nitschke W, Myllykallio H, Schmidt C (2001) The membrane-extrinsic domain of cytochrome *b*(558/566) from the archaeon *Sulfolobus acidocaldarius* performs pivoting movements with respect to the membrane surface. *FEBS Lett* 487:372–376
- Schulz H, Hennecke H, Thony-Meyer L (1998) Prototype of a heme chaperone essential for cytochrome *c* maturation. *Science* 281:1197–1200
- Schulz H, Fabianek RA, Pelliccioli EC, Hennecke H, Thony-Meyer L (1999) Heme transfer to the heme chaperone CcmE during cytochrome *c* maturation requires the CcmC protein, which may function independently of the ABC-transporter CcmAB. *Proc Natl Acad Sci USA* 96:6462–6467
- Schulze M, Rodel G (1988) SCO1, a yeast nuclear gene essential for accumulation of mitochondrial cytochrome *c* oxidase subunit II. *Mol Gen Genet* 211:492–498

- Seib KL, Jennings MP, McEwan AG (2003) A Sco homologue plays a role in defence against oxidative stress in pathogenic *Neisseria*. FEBS Lett 546:411–415
- Setterdahl AT, Goldman BS, Hirasawa M, Jacquot P, Smith AJ, Kranz RG, Knaff DB (2000) Oxidation-reduction properties of disulfide-containing proteins of the *Rhodobacter capsulatus* cytochrome *c* biogenesis system. Biochemistry 39:10172–10176
- Shaw AL, Hochkoeppler A, Bonora P, Zannoni D, Hanson GR, McEwan AG (1999a) Characterization of DorC from *Rhodobacter capsulatus*, a *c*-type cytochrome involved in electron transfer to dimethyl sulfoxide reductase. J Biol Chem 274:9911–9914
- Shaw AL, Leimkuhler S, Klipp W, Hanson GR, McEwan AG (1999b) Mutational analysis of the dimethylsulfoxide respiratory (*dor*) operon of *Rhodobacter capsulatus*. Microbiology 145:1409–1420
- Shoubridge EA (2001) Cytochrome *c* oxidase deficiency. Am J Med Genet 106:46–52
- Shouldice SR, Heras B, Walden PM, Totsika M, Schembri MA, Martin JL (2011) Structure and function of DsbA, a key bacterial oxidative folding catalyst. Antioxid Redox Signal 14:1729–1760
- Simon J, Hederstedt L (2011) Composition and function of cytochrome *c* biogenesis system II. FEBS J 278:4179–4188
- Smith D, Gray J, Mitchell L, Antholine WE, Hosler JP (2005) Assembly of cytochrome *c* oxidase in the absence of assembly protein SurfI<sub>p</sub> leads to loss of the active site heme. J Biol Chem 280:17652–17656
- Smith LJ, Kahraman A, Thornton JM (2010) Heme proteins—diversity in structural characteristics, function, and folding. Proteins 78:2349–2368
- Soligo M, Vulpe C (1996) CPx-type ATPases: a class of P-type ATPases that pump heavy metals. Trends Biochem Sci 21:237–241
- Soulimane T, Buse G, Bourenkov GP, Bartunik HD, Huber R, Than ME (2000) Structure and mechanism of the aberrant *ba*<sub>3</sub>-cytochrome *c* oxidase from *Thermus thermophilus*. EMBO J 19:1766–1776
- Stenberg F, von Heijne G, Daley DO (2007) Assembly of the cytochrome *bo*<sub>3</sub> complex. J Mol Biol 371:765–773
- Stevens JM, Mavridou DA, Hamer R, Kritsiligkou P, Goddard AD, Ferguson SJ (2011) Cytochrome *c* biogenesis system I. FEBS J 278:4170–4178
- Stewart EJ, Katzen F, Beckwith J (1999) Six conserved cysteines of the membrane protein DsbD are required for the transfer of electrons from the cytoplasm to the periplasm of *Escherichia coli*. EMBO J 18:5963–5971
- Stiburek L, Vesela K, Hansikova H, Hulkova H, Zeman J (2009) Loss of function of Sco1 and its interaction with cytochrome *c* oxidase. Am J Physiol Cell Physiol 296:C1218–C1226
- Stirnemann CU, Rozhkova A, Grauschopf U, Grutter MG, Glockshuber R, Capitani G (2005) Structural basis and kinetics of DsbD-dependent cytochrome *c* maturation. Structure 13:985–993
- Stirnemann CU, Grutter MG, Glockshuber R, Capitani G (2006) nDsbD: a redox interaction hub in the *Escherichia coli* periplasm. Cell Mol Life Sci 63:1642–1648
- Strogolova V, Furness A, Robb-McGrath M, Garlich J, Stuart RA (2012) Rcf1 and Rcf2, members of the hypoxia-induced gene 1 protein family, are critical components of the mitochondrial cytochrome *bc*<sub>1</sub>-cytochrome *c* oxidase supercomplex. Mol Cell Biol 32:1363–1373
- Svensson-Ek M, Abramson J, Larsson G, Tornroth S, Brzezinski P, Iwata S (2002) The X-ray crystal structures of wild-type and EQ(I-286) mutant cytochrome *c* oxidases from *Rhodobacter sphaeroides*. J Mol Biol 321:329–339
- Swem DL, Swem LR, Setterdahl A, Bauer CE (2005) Involvement of SenC in assembly of cytochrome *c* oxidase in *Rhodobacter capsulatus*. J Bacteriol 187:8081–8087
- Thompson AK, Gray J, Liu A, Hosler JP (2012) The roles of *Rhodobacter sphaeroides* copper chaperones PCu(A)C and Sco (PrrC) in the assembly of the copper centers of the *aa*<sub>3</sub>-type and the *cbb*<sub>3</sub>-type cytochrome *c* oxidases. Biochim Biophys Acta 1817:955–964
- Thony-Meyer L (1997) Biogenesis of respiratory cytochromes in bacteria. Microbiol Mol Biol Rev 61:337–376
- Thony-Meyer L, Beck C, Preisig O, Hennecke H (1994) The *ccoNOQP* gene cluster codes for a *cb*-type cytochrome oxidase that functions in aerobic respiration of *Rhodobacter capsulatus*. Mol Microbiol 14:705–716
- Tiranti V, Hoertnagel K, Carrozzo R, Galimberti C, Munaro M, Granatiero M, Zelante L, . . . , Zeviani M (1998) Mutations of SURF-1 in Leigh disease associated with cytochrome *c* oxidase deficiency. Am J Hum Genet 63:1609–1621
- Tomb JF, White O, Kerlavage AR, Clayton RA, Sutton GG, Fleischmann RD, Ketchum KA, . . . , Venter JC (1997) The complete genome sequence of the gastric pathogen *Helicobacter pylori*. Nature 388:539–547
- Tottey S, Rich PR, Rondet SA, Robinson NJ (2001) Two Menkes-type ATPases supply copper for photosynthesis in *Synechocystis* PCC 6803. J Biol Chem 276:19999–20004

- Tottey S, Rondet SA, Borrelly GP, Robinson PJ, Rich PR, Robinson NJ (2002) A copper metallochaperone for photosynthesis and respiration reveals metal-specific targets, interaction with an importer, and alternative sites for copper acquisition. *J Biol Chem* 277:5490–5497
- Trasnea PI, Utz M, Khalfaoui-Hassani B, Lagies S, Daldal F, Koch HG (2015) Cooperation between two periplasmic copper chaperones is required for full activity of the *cbb3*-type cytochrome *c* oxidase and copper homeostasis in *Rhodobacter capsulatus*. *Mol Microbiol*. doi:10.1111/mmi.13321. [Epub ahead of print]
- Turkarlan S, Sanders C, Ekici S, Daldal F (2008) Compensatory thio-redox interactions between DsbA, CcdA and CcmG unveil the apocytochrome *c* holdase role of CcmG during cytochrome *c* maturation. *Mol Microbiol* 70:652–666
- Uchida T, Stevens JM, Daltrop O, Harvat EM, Hong L, Ferguson SJ, Kitagawa T (2004) The interaction of covalently bound heme with the cytochrome *c* maturation protein CcmE. *J Biol Chem* 279:51981–51988
- van den Berghe PV, Folmer DE, Malingre HE, van Beurden E, Klomp AE, van de Sluis B, Merckx M, . . . , Klomp LW (2007) Human copper transporter 2 is localized in late endosomes and lysosomes and facilitates cellular copper uptake. *Biochem J* 407:49–59
- Verissimo AF, Daldal F (2014) Cytochrome *c* biogenesis system I: an intricate process catalyzed by a maturase supercomplex? *Biochim Biophys Acta* 1837: 989–998
- Verissimo AF, Yang H, Wu X, Sanders C, Daldal F (2011) CcmI subunit of CcmFHI heme ligation complex functions as an apocytochrome *c* chaperone during *c*-type cytochrome maturation. *J Biol Chem* 286:40452–40463
- Verissimo AF, Mohtar MA, Daldal F (2013) The heme chaperone ApoCcmE forms a ternary complex with CcmI and apocytochrome *c*. *J Biol Chem* 288:6272–6283
- Vukotic M, Oeljeklaus S, Wiese S, Vogtle FN, Meisinger C, Meyer HE, Zieseniss A, . . . , Deckers M (2012) Rcf1 mediates cytochrome oxidase assembly and respirasome formation, revealing heterogeneity of the enzyme complex. *Cell Metab* 15:336–347
- Walker JE, Saraste M, Runswick MJ, Gay NJ (1982) Distantly related sequences in the alpha- and beta-subunits of ATP synthase, myosin, kinases and other ATP-requiring enzymes and a common nucleotide binding fold. *EMBO J* 1:945–951
- Weingarten RA, Grimes JL, Olson JW (2008) Role of *Campylobacter jejuni* respiratory oxidases and reductases in host colonization. *Appl Environ Microbiol* 74:1367–1375
- Woodall CA, Jones MA, Barrow PA, Hinds J, Marsden GL, Kelly DJ, Dorrell N, . . . , Maskell DJ (2005) *Campylobacter jejuni* gene expression in the chick cecum: evidence for adaptation to a low-oxygen environment. *Infect Immun* 73:5278–5285
- Zannoni D, Daldal F (1993) The role of *c*-type cytochromes in catalyzing oxidative and photosynthetic electron transport in the dual functional plasmamembrane of facultative phototrophs. *Arch Microbiol* 160:413–423
- Zheng XM, Hong J, Li HY, Lin DH, Hu HY (2012) Biochemical properties and catalytic domain structure of the CcmH protein from *Escherichia coli*. *Biochim Biophys Acta* 1824:1394–1400
- Zhu Z, Yao J, Johns T, Fu K, De Bie I, Macmillan C, Cuthbert AP, . . . , Shoubridge EA (1998) SURF1, encoding a factor involved in the biogenesis of cytochrome *c* oxidase, is mutated in Leigh syndrome. *Nat Genet* 20:337–343
- Zickermann V, Angerer H, Ding MG, Nubel E, Brandt U (2010) Small single transmembrane domain (STMD) proteins organize the hydrophobic subunits of large membrane protein complexes. *FEBS Lett* 584:2516–2525
- Zufferey R, Preisig O, Hennecke H, Thony-Meyer L (1996) Assembly and function of the cytochrome *cbb3* oxidase subunits in *Bradyrhizobium japonicum*. *J Biol Chem* 271:9114–9119
- Zufferey R, Arslan E, Thony-Meyer L, Hennecke H (1998) How replacements of the 12 conserved histidines of subunit I affect assembly, cofactor binding, and enzymatic activity of the *Bradyrhizobium japonicum cbb3*-type oxidase. *J Biol Chem* 273:6452–6459

## Assembly of Transmembrane *b*-Type Cytochromes and Cytochrome Complexes

Hans-Georg Koch<sup>a,\*</sup> and Dirk Schneider<sup>b,\*</sup>

<sup>a</sup>*Institut für Biochemie und Molekularbiologie, ZBMZ, Albert-Ludwigs-Universität Freiburg, 79104 Freiburg, Germany*

<sup>b</sup>*Institut für Pharmazie und Biochemie, Johannes Gutenberg-Universität Mainz, 55128 Mainz, Germany*

Summary.....	555
I. Introduction.....	556
II. Transmembrane <i>b</i> -Type Cytochromes in Respiratory and Photosynthetic $e^-$ -Transfer Chains.....	559
III. Targeting and Membrane Insertion of <i>b</i> -Type Apo-Cytochromes.....	559
A. Co-Translational Membrane Targeting by the Signal Recognition Particle (SRP) Pathway.....	559
B. The Integration Channels: The SecYEG Translocon and the YidC Integrase.....	562
C. The Insertion Mode of Membrane-Bound <i>b</i> -Type Cytochromes.....	564
D. Post-Translational Transport across the Sec Translocon.....	565
E. Alternative Protein Targeting and Transport Pathways.....	565
1. The Twin-Arginine Translocation Pathway.....	565
2. The Insertion of Tail-Anchored Membrane Proteins: The GET Pathway.....	566
3. The Insertion of Small Membrane Proteins.....	567
4. Translation-Independent Targeting Pathways.....	567
IV. Structural Features Determining Heme Binding to Membrane-Bound Apo-Cytochromes.....	567
V. Assembly of Individual Transmembrane Holo-Cytochromes.....	569
A. Cytochrome <i>b</i> <sub>559</sub> : A Mono-Heme TM <i>b</i> -Type Cytochrome.....	570
B. Cytochrome <i>b</i> <sub>6</sub> : A Di-Heme Transmembrane Four-Helix Bundle.....	572
VI. Naturally Occurring and Designed Transmembrane Four-Helix Bundle <i>b</i> -Type Cytochromes.....	574
VII. Assembly of Cytochrome <i>b</i> -Containing Membrane Protein Complexes.....	576
A. Cytochrome <i>b</i> <sub>03</sub> Oxidase Assembly.....	576
B. Cytochrome <i>b</i> <sub>c1</sub> and Cytochrome <i>b</i> <sub>6f</sub> Complex Assembly.....	577
Acknowledgements.....	578
References.....	578

### Summary

Cytochromes are involved in charge-transfer reactions, and many cytochromes contain a transmembrane domain and are part of membrane-localized electron transfer chains. Protoporphyrin IX (heme *b*) is the first heme product in the tetrapyrrole/heme biosynthesis

\*Author for correspondence, e-mail: [Hans-Georg.Koch@uni-freiburg.de](mailto:Hans-Georg.Koch@uni-freiburg.de); [Dirk.Schneider@uni-mainz.de](mailto:Dirk.Schneider@uni-mainz.de)

pathway. In contrast to *c*-type cytochromes, there is no need for a specialized machinery catalyzing covalent attachment of the heme molecule to a *b*-type apo-cytochrome, nor is the cofactor further modified, as in *a*-, *d*- and *o*-type cytochromes. Thus, formation of a holo-cytochrome is relatively simple for *b*-type cytochromes, and this class of proteins probably represents the most ancient members of transmembrane cytochromes. However, assembly of individual transmembrane *b*-type cytochromes as well as of larger cytochrome complexes involves multiple steps, which have to be tightly controlled and aligned: the apo-protein as well as the heme cofactor needs to be synthesized, targeted to, and integrated into a membrane prior to holo-cytochrome formation. Spontaneous folding and assembly of individual transmembrane *b*-type cytochromes involves folding of the polypeptide chain and formation of a heme-binding cavity, which allows specific and tight binding of the cofactor. Additional biogenesis steps are eventually required for maturation of transmembrane *b*-type cytochrome complexes.

## I. Introduction

Heme proteins are a class of soluble or membrane-bound proteins that carry one or multiple heme cofactors (Reedy and Gibney 2004). They are involved in binding and transport of small molecules, such as oxygen or nitric oxide, as well as in catalytic reactions, such as in case of oxygenases, catalases or peroxidases. When heme proteins are involved in charge-transfer reactions, the proteins are called cytochromes, a term introduced almost 100 years ago by Keilin (1925). However, it is noteworthy that some proteins, such as cytochrome monooxygenases of the cytochrome P-450 type, have obtained their name by accident, and these proteins are not involved in electron transfer reactions (Abramson et al. 2000; (NC-IUB) (1992)). Many cytochromes contain a transmembrane (TM) domain and are part of membrane-localized electron transfer chains (Koch and Schneider 2007; Thöny-Meyer 1997). Here, the individual cytochromes are typically

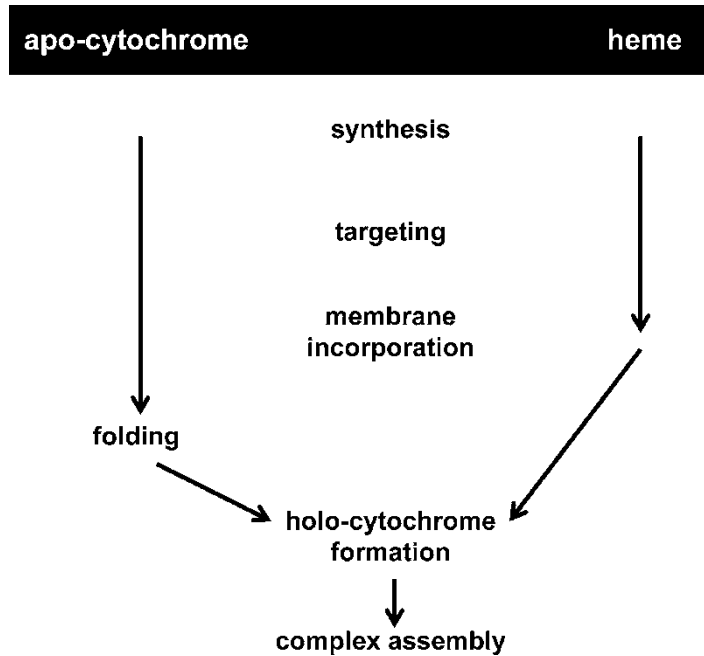
subunits of larger multi-subunit TM protein complexes.

Assembly of TM cytochromes involves multiple steps, which have to be tightly controlled and aligned (Fig. 28.1). The apo-protein as well as the heme cofactors need to be synthesized, targeted to, and integrated into a membrane prior to holo-cytochrome formation. Furthermore, as holo-cytochromes are typically part of larger cytochrome complexes, additional biogenesis steps are eventually required for their maturation.

Tetrapyrroles, such as hemes and chlorophylls, are synthesized by two common pathways. The initial precursor 5-aminolevulinic acid (ALA) is built from glycine and succinyl-CoA in animals, fungi, yeast and some bacteria, whereas plants, algae and most bacteria synthesize ALA from glutamate (Mochizuki et al. 2010). Eight ALA molecules assemble to the tetrapyrrole uroporphyrinogen III, which is subsequently converted to protoporphyrin IX. Incorporation of iron, catalyzed by the ferrochelatase, results in formation of Fe-protoporphyrin IX (heme *b*), whereas incorporation of magnesium by the magnesium-chelatase results in formation of Mg-protoporphyrin IX, which in plants is subsequently converted in multiple steps into chlorophyll (Mochizuki et al. 2010). In animals and fungi, the steps of heme biosynthesis, starting from ALA,

---

*Abbreviations:* b<sub>559</sub> – *b*-type heme with a reduced  $\alpha$ -band peak at 559 nm; GET – Guided entry of tail-anchored proteins; RNC – Ribosome-nascent-chain complex; SRP – Signal recognition particle; SR – SRP-receptor; TM – Transmembrane; TIM – Translocase of the inner mitochondrial membrane; TOM – Translocase of the outer mitochondrial membrane



*Fig. 28.1.* Multiple-step assembly of TM cytochromes and cytochrome complexes. Prior to the formation of a TM holo-cytochrome, the apo-protein as well as the heme cofactors need to be synthesized, targeted to, and integrated into a membrane. When holo-cytochromes are part of larger cytochrome complexes, additional biogenesis steps are required for their maturation. All steps need to be tightly controlled and aligned.

are localized within the cytoplasm, whereas the later steps of the heme biosynthesis are localized within mitochondria. In plants, heme biosynthesis takes place almost exclusively in plastids and only the final steps are possibly localized to both mitochondria and plastids (Mochizuki et al. 2010; Tanaka and Tanaka 2007).

Due to its hydrophobicity, free heme will intercalate into biological membranes, potentially leading to membrane rupture. Heme iron might also generate reactive oxygen species and free heme exhibits peroxidase activity. Thus, the cellular accumulation of free heme is highly unfavorable for cells and newly synthesized heme is immediately complexed by heme-binding proteins. However, the contribution of these proteins to heme transport and assembly of TM *b*-type cytochromes, is presently elusive (Hamza and Dailey 2012).

In all heme species, the central heme iron ion is ligated by four N-atoms of the heme tetrapyrrole ring system. In most cases the

iron center is additionally ligated via two histidine side-chains of a polypeptide chain, which serve as fifth and sixth ligands. However, the side-chains of Met, Cys and Tyr can also act as sixth ligand (Smith et al. 2010). When involved in  $e^-$ -transfer reactions, the redox state of the central heme iron switches between  $Fe^{3+}$  (ferri-heme) and  $Fe^{2+}$  (ferro-heme), allowing reversible reduction and oxidation.

Five major cytochrome classes can be differentiated (cytochrome *a*, *b*, *c*, *d*, *o*), and these differ in the nature of the bound heme (derivative) and/or in the mode of heme binding (Koch and Schneider 2007; Thöny-Meyer 1997). The structures of the heme cofactors bound in the respective cytochrome groups are shown in Fig. 28.2. Protoporphyrin IX (heme *b*) is the first heme product in the tetrapyrrole/heme biosynthesis pathway, and protoporphyrin IX derivatives are subsequently generated by heme *b* ring modifications. While in both *b*- and *c*-type cytochromes, protoporphyrin IX is bound



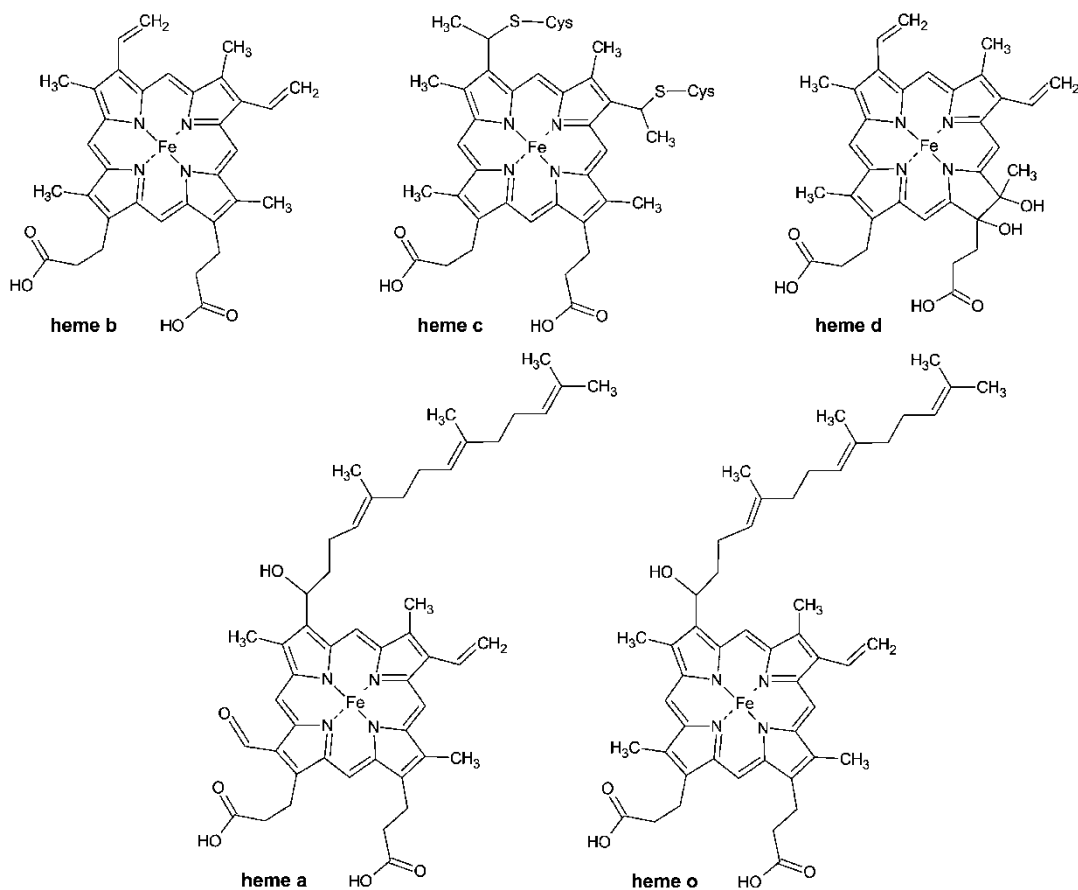


Fig. 28.2. Chemical Structures of naturally occurring hemes *b*, *c*, *d*, *a*, *o*. All hemes are derived from protoporphyrin IX (heme *b*) and thus have the same basic structure. The central iron is  $\text{Fe}^{2+}$  in the reduced and  $\text{Fe}^{3+}$  in the oxidized state. While most hemes are non-covalently bound by proteins, in *c*-type cytochromes heme *c* is bound covalently to a protein, typically via two thioether binds to cysteine (Cys) residues.

to the protein, *c*-type cytochromes have the heme covalently attached (typically via two thioether-linkages), whereas in *b*-type cytochromes the heme is non-covalently bound and bound only by two axial histidine residues. Similarly, in *a*-, *d*- and *o*-type cytochromes the heme molecules are non-covalently attached to proteins. In contrast to *c*-type cytochromes, there is no need for a specialized machinery catalyzing covalent attachment of the heme molecule to a *b*-type apo-cytochrome, nor is the cofactor further modified, as in *a*-, *d*- and *o*-type cytochromes. Thus, formation of a holo-cytochrome is relatively simple for *b*-type cytochromes, and they probably represent the

most ancient members of TM cytochromes. However, during evolution, some proteins have changed their heme cofactors. This is illustrated by the terminal cytochrome *c*-oxidases, which contain a variety of different heme species associated with subunit I. So far, *aa*<sub>3</sub>-, *ba*<sub>3</sub>-, *cb*<sub>3</sub>- or *bb*<sub>3</sub>-type cytochrome oxidases have been characterized (Garcia-Horsman et al. 1994; Thöny-Meyer 1997). The *cb*<sub>3</sub>-type cytochrome *c* oxidase contains two heme *b* cofactors and closely resembles the NO-reductases (Ekici et al. 2012). This led to the hypothesis that subunit I of cytochrome oxidases evolved from subunit I of the NO-reductase and that the *b*-type heme-containing oxidases appear to

be the primordial enzyme (Pereira et al. 2001; Saraste and Castresana 1994).

## II. Transmembrane *b*-Type Cytochromes in Respiratory and Photosynthetic $e^-$ -Transfer Chains

Several cofactor-containing TM protein complexes are involved in respiratory and photosynthetic electron transfer reactions. Cofactors involved in  $e^-$ -transfer include not only hemes but also iron-sulfur clusters and other metal centers, such as Fe, Mo, Cu or Ni. However, utilizing membrane-integrated cytochromes, and in particular *b*-type cytochromes, has evolved as an efficient principle to catalyze charge transfer across membranes. This is reflected by the fact that despite the great diversity of  $e^-$ -transfer chains, TM *b*-type cytochromes are key subunits of most multi-subunit TM complexes involved in aerobic and anaerobic respiratory electron transfer chains in eu- and prokaryotes. They are present in dehydrogenases, such as succinate or formate dehydrogenases, as well as in cytochrome *bc<sub>1</sub>* and *b<sub>6f</sub>* complexes, which transfer electrons from a quinol to the soluble  $e^-$ -carrier cytochrome *c<sub>6</sub>* or to plastocyanin. Furthermore, the bacterial quinol as well as cytochrome *c* oxidases mostly contain TM *b*-type cytochrome subunits. In addition, also photosystem II of cyanobacteria and higher plants contains a conserved TM *b*-type cytochrome subunit (cytochrome *b<sub>559</sub>*).

Despite the wealth of structural, biophysical and biochemical data on TM cytochromes, surprisingly little is known about their biogenesis. In case of *c*-type cytochromes, four defined systems have been identified and described, which are involved in covalent attachment of the heme cofactor to the protein moiety, and thus in the conversion of an apo- to a holo-cytochrome (Ferguson et al. 2008). In contrast, no specialized biogenesis system and/or heme chaperone system for delivery of heme to

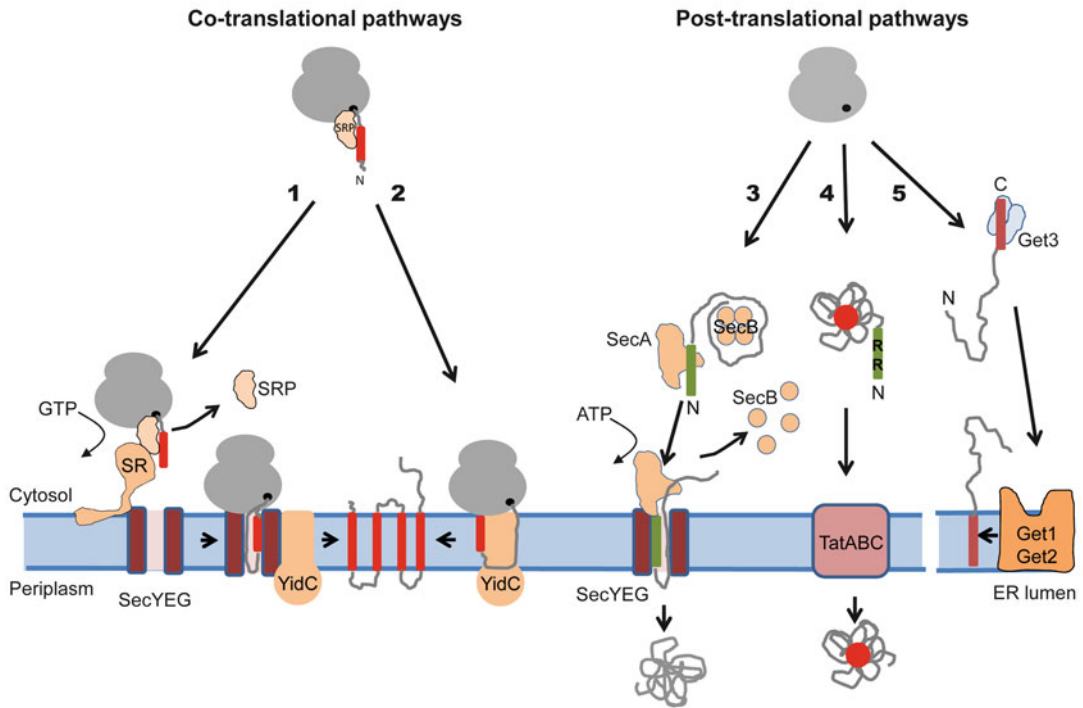
*b*-type cytochromes and/or for biogenesis of TM *b*-type cytochromes has been identified so far. Instead, it appears to be likely that *b*-type cytochromes assemble spontaneously from the apo-protein and free heme, as further discussed below.

## III. Targeting and Membrane Insertion of *b*-Type Apo-Cytochromes

*b*-type cytochromes execute their functions in different membrane environments, and correct targeting and membrane insertion is crucial for their function in electron transport processes. Prokaryotic and eukaryotic cells engage multiple targeting and insertion pathways to ensure the correct cellular localization of membrane-bound *b*-type cytochromes (Kudva et al. 2013). In this chapter we will mainly focus on their insertion into the bacterial cytoplasmic membrane and only briefly outline other membrane systems (Fig. 28.3).

### A. Co-Translational Membrane Targeting by the Signal Recognition Particle (SRP) Pathway

Lipid-anchoring of membrane proteins, such as *b*-type cytochromes, is usually achieved via a single or via multiple hydrophobic TM  $\alpha$ -helices. These  $\alpha$ -helices are not only involved in membrane insertion, but the N-terminal helix usually also serves as a recognition signal during the targeting process and is hence referred to as signal anchor sequence (SA) (Kudva et al. 2013). Upon synthesis on cytosolic ribosomes, hydrophobic  $\alpha$ -helices tend to aggregate in the aqueous cytosolic environment and this would impair subsequent targeting and insertion. Co-translational protein targeting overcomes this problem by coupling protein synthesis with protein targeting. Co-translational membrane targeting is facilitated by the signal recognition particle (SRP) and its membrane-bound receptor (SRP-receptor,



**Fig. 28.3.** Co- and post-translational protein-targeting pathways. Co-translational protein transport is initiated by binding of the signal recognition particle (SRP) to a signal anchor sequence (red) emerging from the ribosomal tunnel: (1) SRP then delivers the SRP-ribosome nascent chain complex (SRP-RNC) to the membrane-bound SRP receptor (SR) and the RNC is transferred to the SecYEG translocon. GTP hydrolysis by SRP and SR induce their dissociation allowing another round of targeting. The SecYEG translocon cooperates with YidC during membrane protein insertion and YidC is thought to facilitate folding and assembly processes. (2) YidC can also function independently of the SecYEG translocon and insert membrane proteins on its own. Targeting of most proteins to YidC also appears to be SRP-dependent. (3) The best studied example of a post-translational protein-targeting pathway is the bacterial SecA-dependent transport. Secretory proteins, i.e. periplasmic and outer membrane proteins, are recognized by the tetrameric chaperone SecB after their release from the ribosome. SecA binds to the signal sequence (green) and targets the protein to the SecYEG translocon. SecB is released and SecA translocates the protein in ATP-dependent steps across the SecYEG channel. The signal sequence is cleaved off by a signal peptidase and further degraded. Sec-independent post-translational protein transport pathways also exist in prokaryotes and eukaryotes. (4) The twin-arginine translocation (Tat) is able to transport cofactor-containing folded proteins across the bacterial cytoplasmic membrane or the chloroplast thylakoid membrane. The TatBC proteins serve as a signal sequence receptor, recognizing the canonical RR-motif. TatA oligomers are probably required for TM translocation, but the exact mechanism of transport is still unknown. (5) Proteins containing a C-terminal TM domain (tail-anchored (TA) proteins) are inserted into the endoplasmic reticulum (ER) membrane by the GET pathway. The homo-dimeric ATPase GET3 functions as an ER targeting factor. The minimal membrane insertion machinery for TA proteins in yeast appears to be provided by the ER-integral GET1 and GET2 proteins. The insertion mode of bacterial TA proteins is largely unknown, but might involve YidC (Aschtgen et al. 2012).

SR) (Koch et al. 1999). The SRP pathway is the only protein-targeting pathway that is universally conserved and essential in almost all domains of life. Notable known exceptions are *Saccharomyces cerevisiae* and the Gram-positive bacterium *Streptococcus*

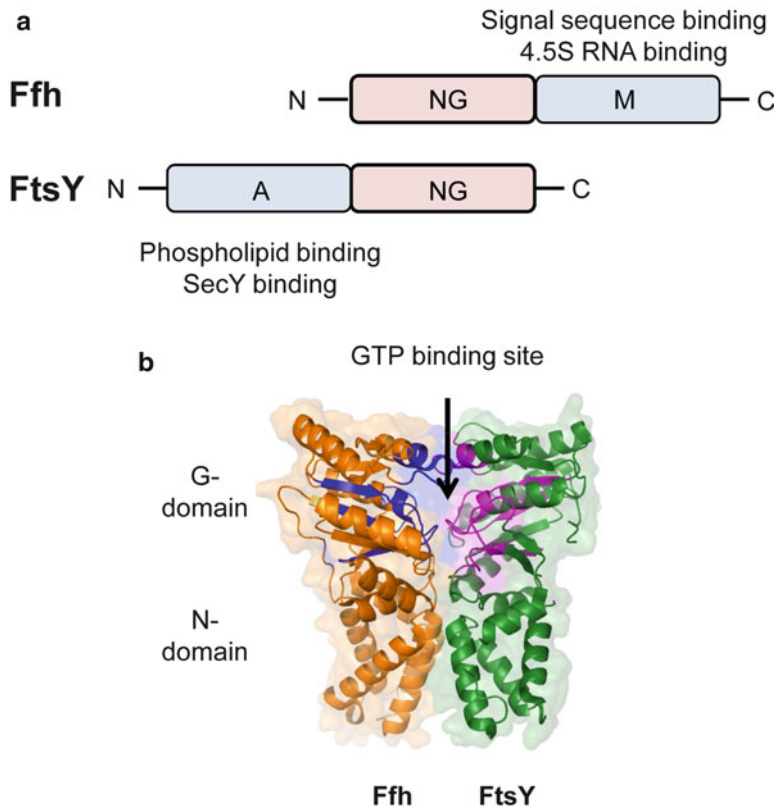
*mutans*, which tolerate SRP inactivation (Koch et al. 2003a, 2013).

SRP is a ribonucleoprotein complex that consists of 6 protein subunits in mammals, which are bound to the 300-nucleotide-long 7S RNA. The bacterial SRP is reduced

to a functional core comprising the signal sequence binding subunit Ffh (homologous to the eukaryotic SRP54 subunit) and the 4.5S SRP-RNA, which in *E. coli* is 114 nucleotides long. This minimal core is present in all organisms, with the intriguing exception of higher plant chloroplasts, where the SRP lacks the RNA subunit (Trager et al. 2012).

Ffh/SRP54 and the bacterial SRP receptor FtsY belong to the SIMIBI family (Signal recognition particle – MinD – BioD) of nucleotide-hydrolyzing enzymes (Grudnik et al. 2009) and display a modular organization (Fig. 28.4). Both, Ffh/SRP54

and FtsY, contain a highly similar four-helix bundle domain (N-Domain) that is connected to a Ras-like GTPase domain (G-domain). In contrast to classical GTP-hydrolyzing enzymes, such as Ras, EF-Tu or Ran, neither Ffh nor FtsY require external guanine nucleotide exchange factors (GEFs) or GTPase-activating enzymes (GAPs). Instead, the GTPase activities of Ffh and FtsY are stimulated upon Ffh-FtsY heterodimer formation, which occurs via their respective NG-domains (Bange and Sinning 2013). Both, Ffh and FtsY, contain an additional functional domain that is fused to their respective NG domains;



*Fig. 28.4.* Domain structure of the bacterial Signal Recognition Particle pathway (SRP) components. **(a)** Ffh is the protein component of the bacterial SRP and forms together with the 4.5S RNA the bacterial SRP. The conserved NG-domain is required for GTP hydrolysis and regulation, while the C-terminal M-domain harbors the signal sequence-binding site and the contact site for the 4.5S RNA. The NG-domain of FtsY is very similar to the NG domain of Ffh. The N-terminal A-domain contains in *E. coli* binding sites for SecY and for negatively charged phospholipids. The A-domain exhibits only low sequence conservation and has a variable size in different bacterial species (Kudva et al. 2013; Weiche et al. 2008). **(b)** The heterodimer of the NG-domains of Ffh and FtsY from *T. aquaticus* (PDB: 1OKK). The structure shows a large common surface area, which also includes a composite GTPase site.

the M-domain in Ffh and the A-domain in FtsY (Kuhn et al. 2014). The C-terminal M-domain in Ffh is the signal sequence binding region, which is characterized by an over-representation of methionine residues in mesophilic organisms. This flexible methionine-rich domain probably allows the accommodation of a large variety of signal anchor sequences. The N-terminal A-domain of FtsY is involved in membrane binding and contains two amphipathic lipid-binding helices with high affinity to anionic phospholipids, such as phosphatidylglycerol and cardiolipin (Braig et al. 2009; Weiche et al. 2008). The A-domain varies significantly in length and amino acid composition between different bacterial species (Weiche et al. 2008), and only the second lipid-binding helix, located close to the NG-domain, appears to be essential for function (Braig et al. 2011; Eitan and Bibi 2004; Parlitz et al. 2007). Lipid binding of FtsY triggers a conformational switch that strongly enhances its subsequent interaction with SRP (Braig et al. 2009, 2011; Klostermann et al. 2002; Lam et al. 2010; Stjepanovic et al. 2011).

SRP binds to ribosomes with high affinity ( $K_d \cong 50\text{--}70$  nM) (Bornemann et al. 2008). Its binding site is located close to the ribosomal tunnel exit, which allows SRP to scan emerging polypeptides for signal anchor sequences and to initiate membrane targeting of the translating ribosome (ribosome-nascent-chain complex (RNC)) (Gu et al. 2003). If the emerging protein does not contain a suitable signal sequence, the affinity of SRP for ribosomes drops significantly ( $>200$  nM). This probably explains why a rather small number of SRP molecules (approx. 200–300 in *E. coli*) can scan a vast number of ribosomes (approx. 20,000–30,000 in *E. coli*). Although SRP binding to emerging polypeptides is mainly determined by their hydrophobicity, other factors, such as the presence of helix-breaking amino acids (Beha et al. 2003) or the translation speed, also influence SRP binding (Zhang and Shan 2012).

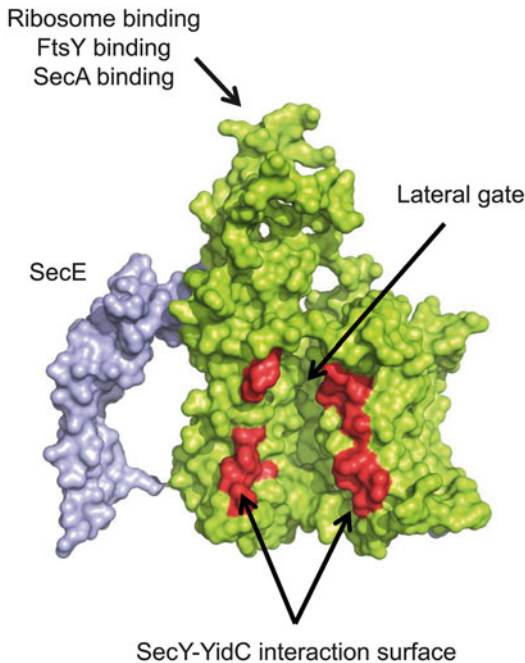
After binding to the polypeptide, SRP targets RNCs to the membrane-bound FtsY.

FtsY not only binds to phospholipids, but also directly to the surface-exposed loops of the membrane-bound SecYEG translocon (Angelini et al. 2006, 2005; Kuhn et al. 2011), the main protein transport channel in bacterial membranes (Kudva et al. 2013). Thus, FtsY recruits the SRP-RNC complex directly to the protein transport channel and is probably displaced by the SRP-RNC, because FtsY and ribosomes use partially overlapping binding sites on SecY (Kuhn et al. 2011). GTP hydrolysis by FtsY and SRP then induces their complete dissociation and allows for the next round of targeting. FtsY was also found to contact YidC, which can constitute a SecYEG-independent insertion site for some membrane proteins (Welte et al. 2012).

### *B. The Integration Channels: The SecYEG Translocon and the YidC Integrase*

In *E. coli* and probably most bacteria, SRP-dependent membrane proteins are preferentially targeted to the SecYEG translocon, which is homologous to the eukaryotic Sec61 complex in the endoplasmic reticulum (ER) membrane (Kudva et al. 2013; Zimmermann et al. 2011). The SecYEG translocon is a trimeric membrane protein complex that consists of the three integral membrane proteins SecY, SecE and SecG (du Plessis et al. 2011). Additional subunits associate at least transiently with the SecYEG/Sec61 core complexes and are required for substrate folding and processing (Fig. 28.5).

The protein conducting channel of the SecYEG translocon is formed by the SecY subunit, an hour-glass-like structure with a hydrophobic constriction in the center that is thought to seal the channel during protein transport (Van den Berg et al. 2004). In its inactive state, the channel is further blocked by a short helix on the periplasmic side of the constriction, which is believed to serve as a plug (Li et al. 2007). The SecYEG translocon is activated when RNCs bind to surface-exposed SecY loops (Park et al. 2013). The signal anchor sequence is threaded into the



*Fig. 28.5.* The SecYE translocon in *E. coli*. SecY and SecE form the core components of the bacterial Sec translocon and are essential for function. The structure is adapted from Frauenfeld et al. (2011, pdb:3J01). SecE is shown in blue and SecY in green. The cytosolically exposed loops of SecY provide overlapping binding sites for the ribosome, the SRP receptor FtsY and the ATPase SecA. Transmembrane domains are thought to exit the SecYE translocon via the lateral gate. Residues of the lateral gate helices that were shown to be in contact with YidC are shown in red.

channel, where it contacts TM helices 2 and 7 of SecY, relocating the plug slightly to the periphery of the channel. This probably results in the opening of a lateral gate within SecY that is formed by TM helices 2 and 3 on one side and TM helices 7 and 8 on the other side (Fig. 28.5) (Park et al. 2013). Opening of the SecY channel laterally towards the membrane probably allows membrane proteins to exit the channel and to partition into the lipid phase (du Plessis et al. 2009; Hizlan et al. 2012). The essential SecE subunit of the SecYEG translocon is located opposite to the lateral gate at the back of the SecY channel (Van den Berg et al. 2004). SecE probably stabilizes SecY, because in its absence, SecY is rapidly degraded by the protease FtsH

(Kihara et al. 1995). SecG, the third subunit of the eubacterial SecYEG translocon is not essential for protein transport. It also shows no sequence homology to Sec61 $\beta$ , the third subunit of the archaeal and eukaryotic Sec translocon (Park and Rapoport 2012). Available data indicate that SecG is required for SecA-dependent post-translational transport across the SecYEG channel (see below). This is consistent with the observation that both, SecA and SecG, are exclusively found in bacteria (Kudva et al. 2013).

TM helices exiting the SecY channel via the lateral gate have been shown to contact YidC before they encounter lipids. YidC and its homologues in mitochondria (Oxa1 & Oxa2) and chloroplasts (Alb3 & Alb4) are multi-spanning membrane proteins, containing a conserved core of five TM helices (Funes et al. 2011). In most Gram-negative bacteria, the N-terminus of the conserved core is connected via a large periplasmic loop to an additional TM helix (Saaf et al. 1998). It is believed that YidC assists in the transfer of TM helices from the SecY channel to lipids (Beck et al. 2001). In addition, YidC also facilitates the folding and assembly of membrane proteins (Chen et al. 2002). As YidC is located in immediate proximity to the lateral gate of SecY, it is perfectly positioned to interact with TM helices emerging from the SecY translocon (Sachelaru et al. 2013). Eukaryotic YidC homologues are absent in the ER, but instead located in the chloroplast thylakoid and inner mitochondrial membrane. A SecY-Alb3 interaction was shown in chloroplasts (Klostermann et al. 2002), but does not occur in mitochondria, since the inner mitochondrial membrane usually lacks a Sec machinery (Becker et al. 2012).

YidC not only functions in concert with SecYEG but it can also insert membrane proteins independently of SecYEG (Fig. 28.3). The SecYEG-independent insertion function of YidC was initially observed for small phage proteins (Samuelson et al. 2000), but later it was demonstrated that YidC can also insert small native membrane proteins, such as the c-subunit of the F<sub>1</sub>F<sub>0</sub> ATPase (Yi et al. 2003) and the mechano-sensitive

channel of large conductance MscL in *E. coli* (Facey et al. 2007). Further in vitro studies revealed that YidC is also able to insert multi-spanning membrane proteins that were previously considered to be exclusively SecYEG-dependent (Welte et al. 2012). It remains to be determined how YidC inserts single- and multi-spanning membrane proteins. Electrophysiological measurements indicate the presence of a cation-selective channel in the mitochondrial Oxa1, but whether YidC also forms a protein conducting channel is currently unknown. Targeting of most substrates to YidC is co-translational and mediated by the SRP pathway. Some Gram-positive bacteria, such as *Streptococcus mutans*, express YidC derivatives with an extended C-terminus, which serves as a ribosome-binding site (Palmer et al. 2012). In these bacteria sufficient membrane protein targeting occurs even when the SRP pathway is inactivated. This probably explains why *S. mutans* SRP mutants are viable.

It is currently unknown why bacteria contain two integration sites for membrane proteins and to which extent they are engaged in vivo. In *E. coli*, YidC is present in approx. 5-fold excess over SecYEG (Kudva et al. 2013). In addition, the limited number of SecYEG translocons is also required for the post-translational translocation of periplasmic and outer membrane proteins (see below; Fig. 28.3). This could suggest that YidC is the preferred integration site. However, YidC is unable to insert membrane proteins with large periplasmic loops (Welte et al. 2012). Membrane proteins, which harbor periplasmic loops of more than approx. 30 amino acids, are still targeted to the membrane by the SRP pathway, but the translocation of the periplasmic loop requires the SecA motor protein ATPase (Deitermann et al. 2005). SecA can interact with SecYEG but probably not with YidC (Kuhn et al. 2011; Welte et al. 2012). Thus, membrane proteins which harbor large periplasmic domains are probably strictly dependent on SecYEG for insertion, while closely spaced

membrane proteins can probably be inserted by either SecYEG or YidC.

### C. The Insertion Mode of Membrane-Bound b-Type Cytochromes

The exact insertion mode has been experimentally verified only for a few membrane-bound b-type cytochromes and in most cases it can only be predicted based on the topological features of b-type cytochromes. In *E. coli*, the heme b-containing subunits CyoB of the cytochrome *bo*<sub>3</sub> oxidase and HybB of the Ni/Fe hydrogenase 2 both contain only small periplasmic loops and can probably be inserted into the *E. coli* membrane by either, SecYEG or YidC. On the other hand, larger periplasmic loops are present in the CydA and CydB subunits of cytochrome *bd* oxidase (146 amino acids between TM helices 6 and 7; 51 amino acids between TM helices 1 and 2, respectively) (Borisov et al. 2011) or in cytochrome *b*<sub>561</sub> (36 amino acids between TM3 and TM4), which would probably render both proteins SecYEG-dependent. In addition to the size of periplasmic loops, the charge composition of a membrane protein also influences whether a protein is able to insert via SecYEG or YidC (Price and Driessen 2010; Zhu et al. 2013). A situation, thus far unique, is observed for the CyoA subunit of cytochrome *bo*<sub>3</sub> oxidase. The N-terminus of CyoA is inserted via YidC, while the large periplasmic loop is translocated via SecYEG (du Plessis et al. 2006). This could indicate that when YidC encounters large periplasmic domains during insertion, SecYEG is recruited for further translocation. However, this needs to be experimentally verified for additional substrates.

The mitochondrial YidC homologue Oxa1 is believed to provide the main integration site for the strongly hydrophobic subunits of the cytochrome *bc*<sub>1</sub> complex, cytochrome *c* oxidase, and F<sub>1</sub>F<sub>0</sub> ATP synthase into the mitochondrial membrane (Hell et al. 2001). These proteins are encoded by the mitochondrial genome and assemble with

less hydrophobic nuclear encoded subunits, which are post-translationally imported into mitochondria via the TOM-TIM machinery (Becker et al. 2012). Oxa1 consists of an extended C-terminus that serves as a high affinity binding site for ribosomes. This extended C-terminus causes targeting to Oxa1 SRP-independent, in line with the lack of an SRP-dependent targeting system in mitochondria (Funes et al. 2013; Ott and Herrmann 2010). Importantly, bacterial Ffh can partially rescue the co-translational insertion defect in Oxa1 mutants lacking the ribosome-binding site (Funes et al. 2013). Ribosome binding to the mitochondrial membrane involves at least two additional proteins, Mba1 and Mdm38 (Bauerschmitt et al. 2010; Ott et al. 2006). Both bind to the large ribosomal subunit and *mba1-mdm38* double mutants lack a functional respiratory chain (Bauerschmitt et al. 2010).

#### *D. Post-Translational Transport across the Sec Translocon*

The co-translational SRP pathway is highly advantageous because it minimizes the risk of misfolding/aggregation of nascent membrane proteins before they encounter their target membrane. Still, several post-translational protein-targeting pathways are also utilized and both the bacterial and the eukaryotic Sec channels can operate in a post-translational mode (Rapoport et al. 1996). In eukaryotes, this mode depends on the Sec62/63 complex, which associates with the Sec61 complex. Substrate recognition requires the Hsp70 and Hsp90 chaperone systems. So far, mainly short proteins/peptides and GPI-anchored proteins appear to be transported post-translationally in eukaryotes (Zimmermann et al. 2011).

The post-translational mode of the bacterial SecYEG translocon depends on the interaction with the cytosolic ATPase SecA and is required for the ATP-dependent translocation of secretory, *i.e.* periplasmic and outer membrane proteins across the SecYEG translocon (du Plessis et al. 2011). After the release of a fully synthesized

protein from the ribosome, the homotetrameric chaperone SecB binds to the protein and keeps it in a transport-competent conformation. The substrate-SecB complex is then recognized by the ATPase SecA that binds with high affinity to the N-terminal signal sequences of secretory proteins. In comparison to the signal anchor sequences mentioned above, these signal sequences display lower hydrophobicity and contain a signal peptidase cleavage site that is characterized by an Ala-x-Ala motif (Kudva et al. 2013). SecA binds, like FtsY, directly to the cytosolic loops of the SecYEG translocon and to anionic phospholipids, with recent data suggesting that FtsY and SecA compete for binding to the limited number of SecYEG translocons (Kuhn et al. 2011). SecA-dependent translocation of secretory proteins across the SecYEG translocon is a stepwise process that is coupled with multiple rounds of ATP hydrolysis. During translocation, the signal sequence is cleaved off and further degraded by peptidases; the mature protein is then released into the periplasmic space. The SecA/SecY pathway also operates at the thylakoid membrane in plants, but SecB homologues have so far not been identified (Koch et al. 2003b; Muller et al. 2001).

Cytochrome *b*<sub>562</sub> (CybC) is the only periplasmic *b*-type cytochrome in *E. coli* and it contains a typical signal sequence (Nikkila et al. 1991) that routes it very likely into the post-translational SecB/SecA targeting pathway. The periplasmic protein NikA also contains a cleavable Sec signal sequence and was shown to bind heme (Shepherd et al. 2007). However, whether heme binding is required for the function of NikA in Ni uptake remains to be determined.

#### *E. Alternative Protein Targeting and Transport Pathways*

##### *1. The Twin-Arginine Translocation Pathway*

The twin-arginine translocation (Tat) pathway is a protein transport system that exists in bacteria, archaea and chloroplasts (Palmer



and Berks 2012). Its ability to export proteins in a fully folded conformation makes it distinct from most other protein transport systems. The Tat system in *E. coli* consists of three membrane proteins TatA, TatB and TatC. TatC and TatB form a receptor complex that is required for the initial recognition of the N-terminal S-R-R-x-F-L-K consensus sequence of Tat substrates (Alami et al. 2003). The name-giving arginine pair within the signal sequence is almost invariant and required for transport. However, a few naturally occurring exceptions have been described, in which one Arg is replaced by Lys, Asn or Gln (Kudva et al. 2013). Translocation of Tat substrates across the membrane is mediated by TatA oligomers (Kudva et al. 2013). It is however being debated whether TatA oligomers form a membrane pore, like the SecYEG translocon, or whether they destabilize the membrane, thereby weakening the permeability barrier (Kudva et al. 2013). The number of Tat substrates in different bacterial species varies significantly. 27 substrates have been identified so far in *E. coli*, while almost 190 predicted Tat substrates exist in *Streptomyces coelicolor* (Palmer and Berks 2012). Several reasons have been established for explaining why proteins engage the Tat pathway instead of the Sec pathway: (1) The dependence on cytosolic cofactor insertion machineries that induces a partial or complete folding of the protein. This applies to *E. coli* proteins containing [Fe-S] clusters (e.g. HyaA, HybO, NapG or NrfC), Cu-cofactors (CueO or PcoA), or molybdenum cofactors (TorA, DmsA); (2) Avoidance of uncontrolled cofactor insertion in the periplasm. This has been established for the Mn<sup>2+</sup> binding protein MncA of *Synechocystis* sp. PCC 6803 (Tottey et al. 2008), which would incorporate Cu or Zn if exported into the periplasm in an unfolded conformation; (3) the association with partner proteins in the cytosol before transport. This was shown for Hydrogenase-1 and -2 in *E. coli*, where only the small subunits (HyaA, HybO) contain a Tat signal sequence. By association with the small subunits, the large subunits (HyaB, HybC) can be translocated across

the membrane by a hitchhiker mechanism (Palmer and Berks 2012); (4) the requirement for cytosolic folding catalysts or unfavorable extracellular conditions for protein folding. The latter argument might explain why many halophilic archaea employ the Tat pathway (Pohlschroder et al. 2005).

So far, the DyP-like periplasmic peroxidase EfeB (YcdB) is the only Tat-dependent heme-containing protein identified in *E. coli* (Sturm et al. 2006). The Tat pathway is nevertheless important for the assembly of several cytochrome *b*-containing membrane protein complexes, as they contain Tat-dependent subunits. HybB is a membrane integral cytochrome *b* subunit of the *E. coli* hydrogenase. It contains 10 TM domains and is likely a substrate for the SRP pathway, while HybO and HybC are translocated together via the Tat pathway. A similar situation is encountered for formate dehydrogenases in *E. coli*, which contain a membrane integral *b*-type cytochrome subunit ( $\gamma$ -subunit) that assembles with the G- and H-subunits. The G- and H-subunits are translocated together as a heterodimer via the Tat pathway due to a Tat signal sequence present in the G-subunit.

## 2. The Insertion of Tail-Anchored Membrane Proteins: The GET Pathway

Several membrane proteins are membrane-anchored via a C-terminal TM domain (Tail-anchored (TA) proteins), which escape co-translational SRP binding and targeting. Bioinformatics screens have identified 411 TA proteins in humans (Kalbfleisch et al. 2007), 55 TA proteins in *S. cerevisiae* (Beilharz et al. 2003) and 11–14 TA proteins in *E. coli* (Borgese and Righi 2010; Renthal 2010). Examples are cytochrome *b*<sub>5</sub> of mammalian and plant cells or the  $\beta$ -subunit of *E. coli* formate dehydrogenase-N (Borgese and Righi 2010). In eukaryotic cells, TA proteins of the ER employ a post-translational insertion pathway, the **Guided Entry of Tail-anchored proteins (GET)** system (Sinning et al. 2011). The central component of the GET pathway is the homodimeric ATPase GET3, which functions as an

ER targeting factor. GET3 shows homology to the bacterial ATP-dependent arsenite transporter ArsA, and belongs, together with Ffh/FtsY, to the SIMIBI family of NTPases. The minimal membrane insertion machinery for TA proteins in yeast appears to be provided by the GET1 and GET2 proteins, which are integral ER membrane proteins that interact with GET3. For a subset of eukaryotic TA proteins an involvement of the SRP-Sec pathway has also been suggested (Rabu et al. 2009).

How TA proteins are inserted into bacterial membranes is largely unknown. YidC has been implicated in the insertion of the *E. coli* TA protein TssL (Aschtgen et al. 2012) and some *Streptomyces coelicolor* TA proteins (Craney et al. 2011). The osmosensor ProW contains a 100-amino-acid-long periplasmic N-tail followed by seven closely spaced TM helices. Biochemical studies indicate that ProW follows an SRP-dependent but SecYEG-independent insertion pathway (Cristobal et al. 1999), which could involve YidC. The involvement of chaperones of the Hsp70/Hsp40 families in recognition and targeting of TA proteins has also been suggested (Borgese and Righi 2010).

### 3. The Insertion of Small Membrane Proteins

Small, single-spanning membrane proteins are frequently found as accessory subunits of respiratory complexes, and it has been suggested that they are involved in organizing the large hydrophobic subunits within the membrane (Pawlik et al. 2010; Zickermann et al. 2010). *E. coli* synthesizes more than 60 proteins less than 50 amino acids long that are predicted to be membrane-inserted (Fontaine et al. 2011). Co-translational recognition and insertion of these proteins by the SRP-Sec or SRP-YidC pathway is conceptually difficult because approximately 30–40 amino acids are shielded by the ribosomal peptide tunnel during synthesis. However, data from conditional depletion strains suggest that the insertion of some of these proteins appears to be impaired upon

SecYEG or YidC depletion (Fontaine et al. 2011).

### 4. Translation-Independent Targeting Pathways

The general concept of protein targeting and transport relies on the presence of a transport signal within the protein itself. However, recent data have indicated that mRNAs encoding membrane proteins localize to the inner membrane in *E. coli* by a translation-independent mechanism (Nevo-Dinur et al. 2011). Although details on the recognition and membrane targeting of these mRNAs are still missing, it has been shown that mRNAs coding for membrane proteins have a significantly higher uracil content than mRNAs encoding cytoplasmic proteins (Bibi 2011).

## IV. Structural Features Determining Heme Binding to Membrane-Bound Apo-Cytochromes

It still is not entirely clear why the heme cofactors are covalently attached in *c*-type cytochromes (Barker and Ferguson 1999). Covalent attachment reduces the need for stabilizing heme-protein interactions via additional forces, such as Van der Waals or hydrophobic interactions, which are involved in stabilizing heme-protein contacts in *a*-, *b*-, *d*- or *o*-type cytochromes. At least four different systems exist, which are involved in covalent attachment of hemes to the protein moiety of *c*-type cytochromes. Thus, in case of soluble *c*-type cytochromes, the three-dimensional protein structure might fold after covalent heme attachment to small polypeptide stretches, and the heme might be involved in formation of a folding core. However, in case of TM *c*-type cytochromes, where the heme is bound in the TM region, it appears to be rather unlikely that major parts of a polypeptide chain fold after heme attachment, as unfolded polypeptide

chains are energetically unfavorable in the hydrophobic membrane environment (Popot and Engelman 1990). As all TM cytochromes belong to the class of  $\alpha$ -helical TM proteins, which span the lipid bilayer in an  $\alpha$ -helical conformation and form TM helix bundles (in contrast to  $\beta$ -barrel TM proteins), it appears to be likely that at least the membrane-integrated TM  $\alpha$ -helices are pre-structured. In case of TM *c*-type cytochromes, it still is possible that individual TM helices assemble around the cofactor after covalent attachment of the heme to a single TM helix and thereafter form the final three-dimensional structure. However, as in case of all other cytochrome types, the heme cofactors are non-covalently bound, such folding pathways appear to be rather unlikely. More likely, heme molecules will bind to predefined, small hydrophobic pockets, which have a shape complementary to the shape of the heme cofactor. Such steric complementation results in a close fit between the heme cofactor and the protein moiety. Existence of a predefined heme-binding pocket and specific packing interactions maximizes non-polar contacts of the heme cofactor with the protein, resulting in tight heme binding. Initially, it was suggested that ligation of the heme central iron via the two ligating amino acid side chains (mostly His residues) is the major force driving formation of *b*-type cytochromes and mainly stabilizes the final cytochrome structures (Schneider et al. 2007). In line with this suggestion, in synthetic heme proteins, resembling TM cytochrome structures, essentially only the crucial His residues were incorporated and the resulting *b*-type cytochrome structures were competent to bind heme (Robertson et al. 1994). However, after mutating the His ligands in soluble *b*-type cytochromes, binding of the heme cofactor was still observed, indicating that additional forces guide specific heme recruitment (Barrick 1994; McRae et al. 1994). Also, after mutation of a conserved heme ligand in the TM protein cytochrome *b*<sub>6</sub> of spinach, which binds two heme cofactors, binding of the hemes was still observed (Dreher

et al. 2008), and a naturally occurring cytochrome *b*<sub>6</sub> variant, in which a (otherwise conserved) His ligand is replaced by an Ala, has been described in the cyanobacterium *Gloeobacter violaceus* (Dreher et al. 2010). Thus, while binding of heme via the fifth and sixth His ligand is important, it appears to be dispensable in some cases, and other forces must be involved in binding of heme cofactors to proteins.

Structural analyses of multiple (soluble as well as membrane-integrated) cytochromes has indicated that the heme cofactor is typically deeply buried within a protein structure without significant surface exposure (Smith et al. 2010). However, it must be noted that solvent accessibility might be especially problematic for soluble cytochromes, where the hydrophobic heme group is exposed to an aqueous environment, whereas in TM cytochromes the solvent is mainly represented by the hydrophobic acyl side chains of the membrane lipids. Thus, in a membranous environment an increased solvent exposure might be less problematic than in aqueous environments. In line with this, in the simple TM *b*-type cytochrome *b*<sub>559</sub>, which is formed by only two TM  $\alpha$ -helices that sandwich a single heme (Herrmann et al. 1984), the heme cofactor is rather exposed to the lipid environment (Prodöhl et al. 2005). However, in naturally occurring TM di-heme proteins the heme molecules are almost completely buried within the protein (Smith et al. 2010). Maximizing heme-protein contacts will stabilize the holo-cytochrome structure, and additionally, due to an involvement in charge transfer reactions the heme cofactors need to be bound in a hydrophobic pocket with little solvent exposure. Within the rather non-polar heme-binding pockets the character of individual amino acids, rather than the exact identity, appears to be conserved (Smith et al. 2010). The binding pocket typically contains a large number of amino acids with non-polar side chains, and especially aromatic residues are over-represented (Smith et al. 2010). The three aromatic amino acids Phe, Tyr and Trp are involved in contacts with the

heme face, and they predominantly stabilize the heme-protein contact via aromatic-aromatic  $\pi$ -stacking interactions (Schneider et al. 2007). Furthermore, aromatic residues are frequently involved in Van der Waals contacts with the non-polar “edges” of the heme molecules. Similarly, also Leu, Ala and Val residues have been observed to frequently pack at the “edges” of heme molecules (Schneider et al. 2007). These residues are additionally involved in building a fairly rigid heme-binding surface, which keeps the heme cofactor in a rather fixed position (Schneider et al. 2007).

It was previously recognized that in many cytochrome structures the heme propionyl side chains interact with the positively charged amino acids Arg and Lys via the formation of salt bridges. Such interaction anchor and orient a heme molecule within a protein structure (Schneider et al. 2007; Smith et al. 2010). A structural survey has further revealed that also His side chains (other than the Fe-ligands), as well as tyrosine residues, might be involved in specific interactions with a heme propionyl chain, and thus in orienting and anchoring of the cofactor (Schneider et al. 2007; Smith et al. 2010).

Besides those defined interactions with the heme cofactors, other residues are indirectly involved in heme binding, but still crucial for its correct positioning. Some amino acids interact with His side chains and thereby orient the His imidazole ring to a position, which allows optimal interactions with heme (Schneider et al. 2007). Contacts between the heme and the protein moiety strikingly depend on the His rotamer (i.e. low energy side chain conformations), which has a severe impact on the energetics of heme binding and on positioning of the heme cofactor (Huang et al. 2004; Negron et al. 2009). Thus, a defined heme-binding cavity enables selective and high-affinity binding of heme, and such a cavity would have coevolved with the integration of heme *b* derivatives, such as heme *a*, *d* or *o*. Binding of different heme species to a TM *b*-type cytochrome might be possible, although with rather low

affinities, to circumvent nonspecific binding of undesired heme species in vivo. For example, in plant chloroplasts, the concentration of chlorophyll, which is formed from protoporphyrin IX in various steps, is up to 100 times higher than the concentration of heme *b* (Moulin and Smith 2005), and thus, binding of chlorophyll or chlorophyll precursors needs to be excluded. While the mechanisms leading to specific binding are not yet completely resolved, the geometry of the heme-binding pocket, as well as the tetrapyrrole ring substituents and the central metal ion ( $\text{Fe}^{2+/3+}$  in heme;  $\text{Mg}^{2+}$  in chlorophyll) might control selective binding of heme *b* (Tome et al. 2013).

## V. Assembly of Individual Transmembrane Holo-Cytochromes

Following membrane integration of the apo-cytochrome, individual apo-proteins interact with heme, resulting in formation of the holo-cytochrome. However, in contrast to *c*-type cytochromes, the assembly of *b*-type cytochromes is largely unclear. Originally, based on studies with designed four-helix-bundle heme proteins it has been concluded that heme integrates spontaneously into a protein moiety, resulting in formation of *b*-type cytochrome structures (Robertson et al. 1994). However, these studies were conducted using water-soluble proteins. Thus, the hydrophobic effect might promote intercalation of the hydrophobic heme cofactor into the hydrophobic protein interior of the designed proteins in an aqueous environment. Therefore, only minimal additional forces are needed to generate some specificity in heme-binding, e.g., provided by the rational placement of heme-ligating His residues. In recent years, such designed heme-binding proteins have been characterized in the more hydrophobic environment of detergent micelles or membranes, and hydrophobic heme-binding proteins have been designed, which mimic TM *b*-type cytochromes more closely

(Discher et al. 2003, 2005; Korendovych et al. 2010). Nevertheless, in these cases the heme-binding affinities were quite low, indicating weak interactions and low binding energies.

Folding and assembly of naturally occurring TM *b*-type cytochromes, which bind heme with high affinities, has been studied in only a few cases. In the following, we discuss recent results obtained by analyzing assembly of the simple mono-heme TM *b*-type cytochrome *b*<sub>559'</sub> as well as of the more complex di-heme TM cytochrome *b*<sub>6</sub>.

#### A. Cytochrome *b*<sub>559'</sub>: A Mono-Heme TM *b*-Type Cytochrome

Cytochrome *b*<sub>559</sub> is part of the large TM protein complex photosystem II, where it is the only TM cytochrome subunit. The physiological function of cytochrome *b*<sub>559</sub> is still under discussion but its involvement in secondary electron transfer processes and protection of photosystem II have been discussed (Shinopoulos and Brudvig 2012). In vivo, this protein is composed of two subunits, PsbE and PsbF (Babcock et al. 1985; Herrmann et al. 1984; Widger et al. 1985), which both span the membrane with a single TM  $\alpha$ -helix (Shinopoulos and Brudvig 2012). As PsbF is only around 40–50 amino acids long, a large portion of this protein is membrane-embedded. In contrast, the PsbE subunit is >100 amino acids long, and thus this protein contains more extended extra-membrane domains. The two TM helices of PsbE and PsbF form a TM helix dimer, and a single heme molecule is sandwiched and non-covalently bound in between the two TM helices. Interestingly, the amino acid sequence of the TM regions of both proteins is highly similar, and amino acids, which are involved in heme binding, are strictly conserved in both sequences (Prodöhl et al. 2005). Consequently, it has been shown some time ago that synthetic PsbF peptides spontaneously form a dimeric, heme-binding TM protein structure (Francke et al. 1999). In the following years this cytochrome *b*<sub>559</sub>-like protein (cytochrome *b*<sub>559'</sub>) has been used as a

simple cytochrome *b*<sub>559</sub> model to rationalize individual steps of cytochrome *b*<sub>559</sub> assembly (Prodöhl et al. 2005, 2007; Volkmer et al. 2006; Weber et al. 2011).

Understanding assembly of this simple TM *b*-type cytochrome can be helpful for understanding folding pathways of more complex TM cytochromes and may provide hints for an improved rational design of TM *b*-type cytochromes. Based on mutational analyses it has been concluded that the apo-cytochrome *b*<sub>559'</sub> assembles without heme, and thus TM helix dimerization is not heme-dependent (Prodöhl et al. 2005). In fact, presence or absence of heme has no impact on the interaction propensity of the TM helices (Prodöhl et al. 2005; Volkmer et al. 2006). Addition of heme after TM helix dimerization resulted in the formation of the holo-cytochrome, and thus the heme cofactor integrates into the dimeric apo-cytochrome. Consequently, when dimerization of the PsbF TM helix was disturbed, heme could not bind and formation of the holo-cytochrome was abolished (Prodöhl et al. 2005). This indicates that the heme cofactor inserts into a predefined heme-binding niche. In the apo-cytochrome, the heme-binding domain is still flexible and only after heme binding, the cytochrome structure tightens up like a clam-shell, resulting in formation of the final holo-cytochrome structure (Akdogan et al. 2012) (Fig. 28.6). The PsbF TM region can be divided into a dimerization domain and a heme-binding domain, which are separated by a conserved kink-inducing Pro-residue (Weber et al. 2012). While the TM helices in the dimerization domain have a crossing angle of about 20°, the Pro residue induces a kink, which results in an almost parallel orientation of the two TM helices in the heme-binding domain. Thus, the heme-binding niche is predefined and heme binds to an open state resulting in structural alterations and clam-shell-like closing of the structure (Fig. 28.6). Inspection of the PsbF heme-binding region nicely illustrates that a heme-binding niche is predefined on each monomeric TM helix and many of the aspects derived from in silico

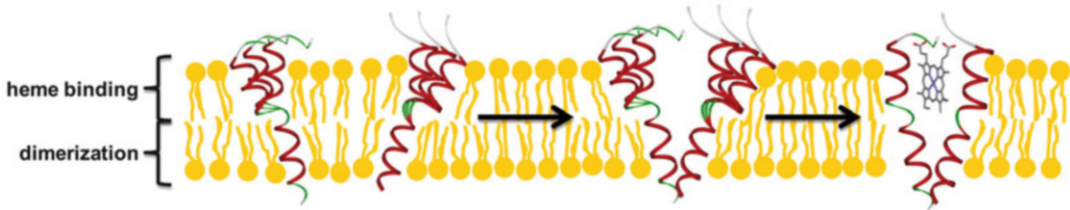


Fig. 28.6. The cytochrome  $b_{559}'$  folding pathway. For assembly of a heme-binding TM helix dimer, two monomeric PsbF TM peptides first interact via their dimerization domain and thereby form a homodimer with a flexible heme-binding domain. Heme binding constricts the flexibility of the heme-binding domain, resulting in formation of the final holo-cytochrome structure.

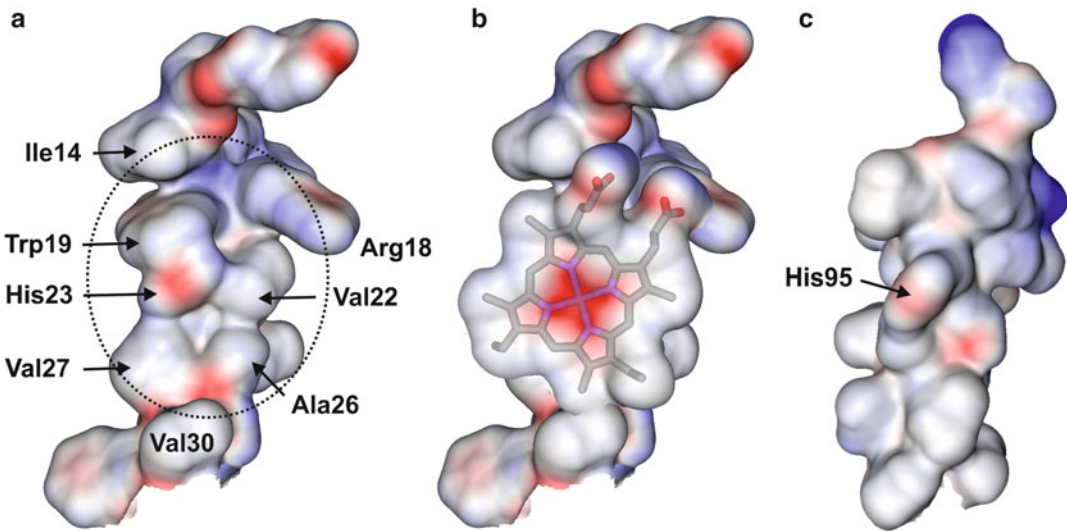


Fig. 28.7. Structure of PsbF in the apo- and holo-cytochrome  $b_{559}'$  protein. (a) Residues involved in heme binding at the heme-binding cavity formed by a single PsbF protein are shown. The protein surface is visualized with red and blue colors, indicating positive and negatively charged regions, respectively. Hydrophobic surfaces are colored in gray. The circle marks the heme-binding cavity. (b) The structure shown in (a) with heme bound. The structures shown in (a) and (b) are derived from the pdb-file 1S5L. (c) Modeled surface structure of the designed, heme-binding GpA peptide. The His residue introduced for heme binding (His95) is indicated. The structural model was generated using pdb-file 1AFO as a template.

analyses described above are confirmed (Fig. 28.7a).

On a single PsbF TM helix a cavity is formed, which is confined by Ile14 and Arg18 on one side and Val30 on the other side of the helix. This cavity has a rather flat and hydrophobic surface, composed of Val22, Ala26 and Val27, and the heme-ligating His23 is part of the surface without protruding out of the heme-binding plane. Additionally, Trp19 is in an almost parallel orientation to His23 and positions the His

imidazole ring, which most likely improves the stability of the His-iron bond. As can be seen in Fig. 28.7b, the heme molecule nicely fits into the predefined heme-binding cavity, and hydrophobic contacts are maximized. Furthermore, the heme propionyl side chains are positioned in a way that one side chain interacts with Arg18 of one TM helix (shown) and the other will interact with the corresponding Arg residue on the adjacent TM helix (removed in Fig. 28.6a, b). Such a perfect fit results in tight heme binding.

Nevertheless, deletion of the heme-ligating His residue completely abolished heme binding (Prodöhl et al. 2005). In contrast, when a heme-ligating His residue together with an Arg residue, which potentially salt-bridges the propionyl side-chain, are placed into the sequence context of the simple TM helix dimer glycophorin A (GpA), the protein was shown to bind heme (Cordova et al. 2007; Shinde et al. 2012). While this illustrates the predominant role of the His and Arg/Lys residues in heme binding, the heme-binding affinity of the designed protein was low. Inspection of the modeled surface structure of the designed TM *b*-type cytochrome nicely illustrates likely reasons for the low heme-binding affinity: In contrast to PsbF, in the designed protein no heme-binding cavity is preformed, the heme-ligating His side-chain protrudes out of the heme-binding surface, and besides interactions with the heme-ligating His and the Arg residues, the heme cofactor will not establish additional stabilizing Van der Waals interactions, as observed for cytochrome *b*<sub>559'</sub> (Fig. 28.7c). Furthermore, the kink introduced in the cytochrome *b*<sub>559'</sub> structure by Pro28 establishes formation of a parallel helix dimer in the heme-binding region, and thus the distance of the two adjacent TM helices to the heme cofactor is almost identical throughout the length of the heme molecules. In contrast, in the case of the designed heme-binding TM helix dimer, the heme-binding cavity narrows down, and thus the distance of the individual TM helices to the heme molecules differs throughout the length of the heme-protein contacts. Therefore, it appears to be rather difficult to establish stabilizing Van der Waals interactions at major heme parts. Consequently, future design of dimeric mono-heme TM cytochromes may include optimization of hydrophobic contacts in the heme-binding region. Furthermore, in case of cytochrome *b*<sub>559'</sub>, an induced fit has been observed upon heme binding (Akdogan et al. 2012), and thus the apo-cytochrome structure was flexible to some extent in the heme-binding region. Such flexibility appears to

be a prerequisite if the heme-binding cavity will enclose the heme molecules perfectly to establish maximal Van der Waals contacts. The designed TM helix cytochrome dimer is based on the rather rigid structure of the TM helix dimer GpA, and thus engineering some flexibility might further improve heme-binding affinities.

### *B. Cytochrome b<sub>6</sub>: A Di-Heme Transmembrane Four-Helix Bundle*

The role of individual amino acids in formation of the TM cytochrome *b* subunit of cytochrome *bc*<sub>1</sub> complexes has been analyzed by site-directed mutagenesis years ago [summarized in (Brasseur and Brivet-Chevillotte 1995)]. In earlier studies it has been observed that mutation of the heme-ligating His residues results in loss of heme binding and thus in disturbed assembly of the cytochrome *b* subunit (Gennis et al. 1993). Furthermore, a crucial importance of positively charged Lys or Arg residues, which interact with the heme propionyl side chains, has also been described early on. In addition, small residues located in the TM helices, which are not directly involved in heme binding but are part of the four-helix bundle, sandwiching the two *b*-type hemes, have been identified to be crucial for assembly of the proteins (Esposti et al. 1993; Gennis et al. 1993; Rau and Haehnel 1998). Thus, in case of the four-helix bundle proteins of the cytochrome *b*-type class of proteins, heme-ligating His residues are conserved as well as positively charged residues, which salt-bridge the heme propionyl side chains. Furthermore, the heme-binding niches are pre-defined and involve conserved Gly residues, since residues with small side chains are crucial to exclude steric clashes in the structure caused by heme incorporation. Thus, cytochrome *b* proteins contain symmetric motifs of conserved Gly and His residues in their TM regions and positively charged amino acids in the juxtamembrane regions of the TM helices (Esposti et al. 1993). This has been recognized and used in the improved design of (soluble) four-helix bundle proteins,

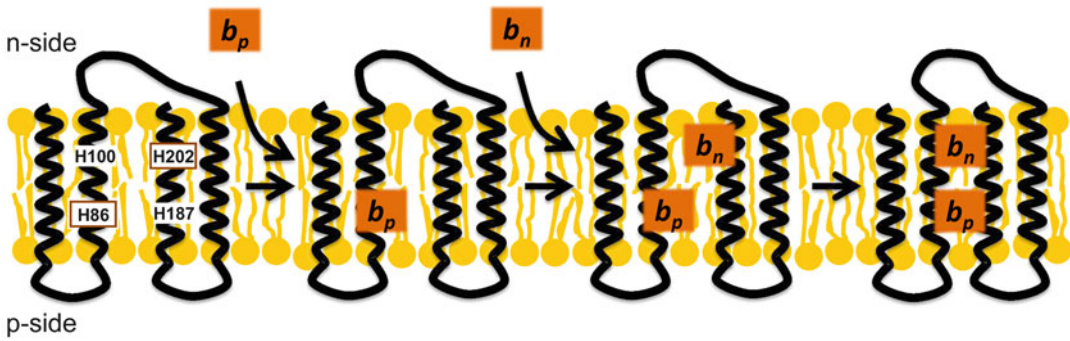


Fig. 28.8. The cytochrome  $b_6$  assembly pathway. Conversion of the apo- to the holo-cytochrome  $b_6$  involves multiple steps. Following membrane integration of the apo-cytochrome, the heme cofactor on the electrochemically negative side (n-side), heme  $b_p$ , binds predominantly via His86 to the protein moiety. Subsequently, the heme on the electrochemically positive side of the membrane (p-side), heme  $b_n$ , binds primarily via His202 to an assembly intermediate, finally resulting in a structural rearrangement and formation of the holo-cytochrome. The two residues His187 and His100 are involved in stabilization of bound heme  $b_p$  and heme  $b_n$ , respectively. In the case of chloroplast thylakoid membranes, the n- and p-side of the membrane correspond to stroma and lumen, respectively.

which bind two heme molecules, as further discussed below. The first four TM helices of cytochrome  $b$ , found in some prokaryotes and in eukaryotic mitochondria, are homologous to the four-TM protein cytochrome  $b_6$  (Widger et al. 1984), which also binds two heme cofactors non-covalently. The two hemes located on the n- and p-sides of the membrane, are designated hemes  $b_n$  and  $b_p$ , respectively (Fig. 28.8).

As individual assembly steps are analyzed in greater detail in case of the cytochrome  $b_6$  protein, in the following we use the amino acid numbering of the spinach cytochrome  $b_6$  protein (See Chap. 9 by Cramer and Hasan).

Deletion of the His residues, ligating the high-potential heme  $b_n$  in the cytochrome  $b$  protein of *Rhodobacter* species, has resulted in loss of heme  $b_n$  as expected (Gennis et al. 1993). However, mutation of the His residue, ligating the low-potential heme  $b_p$  to large polar or charged residues has resulted in completely abolished heme binding (Gennis et al. 1993). Similarly, when both His residues of the spinach cytochrome  $b_6$  protein, which are involved in heme  $b_n$  binding, are mutated to Ala, binding of heme  $b_p$  was abolished, and when the two heme  $b_n$  ligating His residues were mutated to Ala, both, heme  $b_p$  and heme  $b_n$ , were absent

(Dreher et al. 2008). These observations indicate that binding of heme  $b_p$  is a prerequisite for binding of heme  $b_n$  and thus, heme  $b_n$  binds after heme  $b_p$ . However, while in the originally described mutational study replacement of individual His residues by large polar or even charged residues resulted in complete loss of heme binding, the effects observed after replacement of the individual His residues by the small Ala residues were slightly different. In case of the spinach cytochrome  $b_6$  protein, replacement of His100 still resulted in binding of heme  $b_p$ , indicating that a single heme-ligating His residue is sufficient for heme binding (Dreher et al. 2008). This observation is not completely unexpected as such heme coordination mimics binding of heme in catalytically active heme proteins or e.g. in oxygen-transporting myoglobins and hemoglobins, where the sixth ligand position is free. However, mutation of solely the second heme  $b_n$  ligating His residue (His 202) resulted in complete loss of heme  $b_n$  binding, indicating that the importance of the two heme-binding half-niches located on the helix hairpins differs (Dreher et al. 2008). Most likely, dominant interactions between the heme molecule and defined amino acids within the heme  $b_p$  binding niche of TM helices C and D promote



heme binding even in the absence of His100. In fact, a cytochrome  $b_6$  protein has been identified in the cyanobacterium *Gloeobacter violaceus*, which has a naturally occurring mutation at the His100 equivalent position but binds two heme molecules with high affinity (Dreher et al. 2010). In contrast to the heme  $b_n$  ligating residues, replacement of the heme  $b_p$  ligating residues His 86 and His187 in combination resulted in absence of both, heme  $b_p$  and heme  $b_n$ . However, mutation of solely His187 did not impair binding of the two heme molecules, whereas mutation of solely His86 completely abolished binding of any  $b$ -type heme (Dreher et al. 2008). Based on these observations a likely folding pathway involves initial formation of two helical-hairpins (helix pairs AB and CD) after integration of the TM helices into the membrane. Subsequently, heme  $b_p$  binds, and His86 appears to have a predominate function in retaining this heme cofactor bound. Most likely, the structure of the four-helix bundle has not closed, as the second heme has to bind and the heme  $b_n$  binding niche has to be accessible. Thus, it appears to be likely that molecular interactions stabilize binding of heme  $b_n$  primarily at the helical hairpin formed by the TM helices A and B. After initial binding of heme  $b_p$ , heme  $b_n$  binds and here interactions mediated by His202 and the heme-binding half-cavity formed by the helical hairpin CD predominantly stabilize the bound heme cofactor. Binding of heme  $b_p$  obviously triggers formation of the final two-heme-binding four TM helix bundle structure, which appears to be a prerequisite for subsequent assembly of the entire cytochrome  $b_{6f}$  complex (Hasan et al. 2013; Saint-Marcoux et al. 2009).

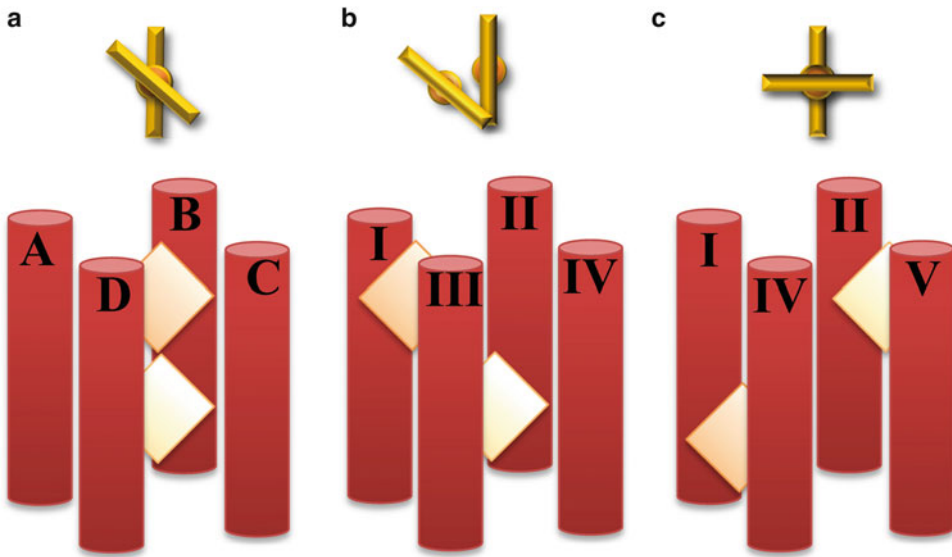
Thus, on each helical hairpin of the heme-binding four helix bundle, two His residues are conserved in one helix, and one of these His residues has a predominant function. Furthermore, Gly residues are conserved in the other TM helix of the helical TM hairpin, as discussed above. The two helical hairpins (AB and CD) have an inverse TM topology, and thus the di-heme cytochrome  $b_6$  protein has an internal quasi-two-fold symmetry

with the two helical hairpins oriented at  $180^\circ$  to each other. Such organization has been mimicked in some approaches aiming to design a four-helix bundle  $b$ -type cytochrome, as further discussed below.

## VI. Naturally Occurring and Designed Transmembrane Four-Helix Bundle $b$ -Type Cytochromes

Noteworthy, TM four-helix bundle structures, which bind two  $b$ -type heme molecules, are also found in other TM proteins, the structure of which has been solved, such as the  $\gamma$  subunit of the formate dehydrogenase, and subunit C of the fumarate reductase (Jormakka et al. 2003; Lancaster 2002). In all three cases, two heme molecules are non-covalently bound by a TM four-helix bundle and the heme residues are always ligated via two His residues. Nevertheless, the occurrence of two related helical-hairpin structures in cytochrome  $b$  and  $b_6$  proteins and the symmetric motifs of conserved His and Gly residues found in these two helical-hairpin structures is not seen in the other di-heme TM proteins. In fact, the three structures have very diverse heme coordination patterns (Fig. 28.9). In the formate dehydrogenase  $\gamma$ -subunit, the heme-ligating His residues are provided by three TM helices, and in case of the fumarate reductase C subunit all four heme-ligating His residues belong to different TM helices. Consequently, the three TM four-helix bundle proteins have no sequence homology, and thus may have evolved independently (Jormakka et al. 2003; Lancaster 2002).

As the structural organization of the first four TM helices of cytochrome  $b$  proteins, which correspond to the cytochrome  $b_6$  protein, is the least complex organization, these structures have served in the past as models for the design of water-soluble, di-heme-binding TM cytochrome models. In the initial design, a potential role of conserved cytochrome  $b$  amino acids has



*Fig. 28.9.* Structures of transmembrane four-helix bundle *b*-type cytochromes. Three types of TM four-helix bundles, which bind two *b*-type hemes non-covalently, have been identified in TM protein structures, represented by the cytochrome *b/b<sub>6</sub>* subunit of cytochrome *bc<sub>1</sub>/b<sub>6</sub>f* complexes (illustrated in **a**), the  $\gamma$  subunit of the formate dehydrogenase (**b**), and the subunit *c* of the fumarate reductase (**c**) (Jormakka et al. 2003; Lancaster 2002). Two heme molecules are always non-covalently bound by a TM four-helix bundle and the heme residues are always ligated via two His residues. However, different TM helices are involved in heme binding, as discussed in detail in the text. The orientation of the two heme molecules with respect to each other is indicated above each four-helix bundle.

been recognized, though the identified residues were not completely included in the sequence of a synthetic peptide, which assembled to a water-soluble, heme-binding four-helix bundle (Robertson et al. 1994). Here, only the heme-ligating His residues, together with Arg residues involved in interaction with the heme propionyl groups, have been retained in the synthetic peptide. This initial design of a so-called molecular “Maquette” structure was a key step, as it was shown for the first time that heme-binding four helix bundles spontaneously assemble in aqueous solutions. However, in this design more specific heme-binding cavities or caves, as seen in naturally occurring *b*-type cytochromes, were not considered, and four identical helices assembled to form the four-helix bundle structure. Two identical helices were dimerized by disulfide linkage and these helix dimers finally assembled into a four-helix bundle with parallel topology. All four helices of the four-helix bundle

protein contained His residue potentially involved in heme binding. For enhancing Van der Waals packing of the heme to the protein moiety, topologically defined four-helix bundles were subsequently designed and synthesized, which mimic the heme-binding core of cytochrome *b* proteins more closely (Rau and Haehnel 1998). Two different helices were synthesized: a heme-binding helix, which contains the conserved His and Arg residues involved in heme binding, as well as a heme-shielding helix, which contains the conserved Gly residues crucial for heme packing as they provide space for tight packing and an optimal fit for the heme. Later on it has been shown that all residues needed for heme binding (His & Arg) and for heme space organization (Gly) might be included in a single helix (Ghirlanda et al. 2004). Furthermore, in the latter study a Thr residue was included, which was involved in correctly positioning the His residues, as the His residue position has been

shown to be crucial for high-affinity binding of heme molecules (Huang et al. 2004; Negron et al. 2009). In subsequent studies, heme-binding four-helix bundles have been designed, which reside in the hydrophobic environment of micelles or lipid bilayers (Discher et al. 2005; Korendovych et al. 2010; Ye et al. 2005). In these cases, heme binding occurred with rather low affinity, indicating that the forces driving assembly of *b*-type cytochromes severely differ in a polar aqueous vs. non-polar membranous environment. In contrast to a membrane environment, formation of a water-soluble four-helix bundle is mainly driven by formation of the hydrophobic bundle core. Consequently, further optimization of heme-binding properties within the hydrophobic membrane environment is needed.

## VII. Assembly of Cytochrome *b*-Containing Membrane Protein Complexes

The vast majority of the membrane-bound *b*-type cytochromes function as part of larger protein assemblies, but there is surprisingly little information available on how these complexes assemble within the membrane. The best studied example in the *E. coli* inner membrane is cytochrome *bo*<sub>3</sub> oxidase, the major terminal oxidase under high oxygen conditions. Another well studied example is the assembly of cytochrome *cbb*<sub>3</sub> oxidase of *Rhodobacter capsulatus*, which is described in more detail in the chapter in this volume by Daldal and Koch. Finally, recent data have also shed light on the assembly of the cytochrome *bc*<sub>1</sub> complex in the bacterial and mitochondrial membrane (Gruschke et al. 2011, 2012) and the cytochrome *b*<sub>6f</sub> complex in the thylakoid membrane (Hasan et al. 2013).

### A. Cytochrome *bo*<sub>3</sub> Oxidase Assembly

Cytochrome *bo*<sub>3</sub> oxidase is a four-subunit membrane complex containing heme *b*, heme

*o* and a Cu<sub>B</sub> center within the large subunit I (CyoB), which spans the membrane 15 times (Pereira et al. 2001; Stenberg et al. 2007). Subunit II (CyoA) contains two TM helices and a large periplasmic loop, while subunits III (CyoC) and IV (CyoD) are closely spaced membrane proteins, containing five and three TM helices, respectively. An elegant study by the Daley group (Stenberg et al. 2007) has revealed a sequential assembly process in which subunits III and IV assemble first within the membrane, forming an intermediate migrating at approx. 63 kDa during Blue-native polyacrylamide gel electrophoresis (BN-PAGE). CyoB is then recruited to this intermediate, resulting in a 123 kDa complex when visualized on BN-PAGE. Finally, CyoA binds to the CyoB-CyoC-CyoD sub-complex to form the holo-complex. The process and timing of cofactor insertion into respiratory complexes, such as the cytochrome *bo*<sub>3</sub> oxidase, is still unresolved. The cofactors are deeply buried within CyoB and their insertion is probably important for its folding and stability. It was therefore generally assumed that cofactor insertion occurs early during assembly, and probably even co-translationally (Ekici et al. 2012; Koch and Schneider 2007; Stenberg et al. 2007). However, the only indication for co-translational cofactor insertion so far is the observed interaction between ribosomal proteins and Cox11, a protein required for Cu<sub>B</sub> center formation in the cytochrome *aa*<sub>3</sub> oxidase (Khalimonchuk et al. 2005). Strikingly, a recent study using <sup>55</sup>Fe-labeled heme indicates that at least the heme groups are inserted at a late step in cytochrome *bo*<sub>3</sub> oxidase assembly pathway (Palombo and Daley 2012). It has been suggested that the heme-binding pocket is only formed upon the interaction of CyoB with the CyoDC subcomplex. This would also explain why monomeric CyoB binds heme only with low efficiency (Nakamura et al. 1990). Whether Cu<sub>B</sub> insertion also occurs at a late step during assembly, is currently unknown. Multiple accessory proteins assist in the stepwise assembly process of cytochrome *aa*<sub>3</sub> oxidases (Kim

et al. 2012; Mick et al. 2011) or cytochrome *ccb<sub>3</sub>* oxidases (Ekici et al. 2012), but similar proteins have not yet been described for cytochrome *bo<sub>3</sub>* oxidase.

### *B. Cytochrome bc<sub>1</sub> and Cytochrome b<sub>6</sub>f Complex Assembly*

The cytochrome *bc<sub>1</sub>* complex (or its thylakoidal equivalent, the cytochrome *b<sub>6</sub>f* complex) is a central component of respiratory and photosynthetic electron transport chains in bacteria and eukaryotes, although it is absent in some bacteria, such as *E. coli* (Cramer et al. 2005). All *bc<sub>1</sub>* complexes contain three core subunits with redox prosthetic groups (Daldal et al. 1987). Cytochrome *b* is an integral membrane protein with 8 TM helices that ligates two heme groups of different redox potentials and absorbance maxima, *b<sub>p</sub>* (*b<sub>562</sub>*) and *b<sub>n</sub>* (*b<sub>565</sub>*), located near the electrochemically positive (p) and negative (n) side of the membrane (compare above). Cytochrome *c<sub>1</sub>* and the Rieske Fe/S protein both consist of a single TM helix and a larger periplasmic/soluble domain harboring a covalently attached heme group and a 2Fe-2S cluster, respectively. As for the cytochrome *bo<sub>3</sub>* oxidase, so far no accessory proteins have been identified that are required for the attachment of heme *b* to apo-cytochrome *b*, and it is therefore assumed that heme is spontaneously inserted into the apo-protein, as discussed above. Heme *b* insertion is considered to occur early during assembly and probably concomitantly with folding. Mutating the heme-ligating residues in apo-cytochrome *b* impairs *bc<sub>1</sub>* complex assembly (Brasseur et al. 1996). Cytochrome *b* and cytochrome *c<sub>1</sub>* probably assemble first and form a protease-resistant intermediate to which the Rieske Fe/S protein is later recruited (Valkova-Valchanova et al. 1998). Mutations that interfere with cofactor insertion into the Rieske Fe/S protein have no impact on cytochrome *b* or cytochrome *c<sub>1</sub>* maturation, suggesting that these processes occur independently (Davidson et al. 1992).

The eukaryotic *bc<sub>1</sub>* complex contains additional subunits and its assembly pathway is far more complex compared to its prokaryotic homologue. The *S. cerevisiae* cytochrome *bc<sub>1</sub>* complex consists of 10 subunits and forms a dimer in the mitochondrial membrane. Translation of the cytochrome *b*-encoding mRNA requires processing by the matrix protein Cbp2 and the translational activators Cbs1 and Cbs2. In addition, Cbp3-Cbp6 has to bind to the ribosomal tunnel exit to allow efficient cytochrome *b* synthesis (Gruschke et al. 2011). After synthesis is completed, the Cbp3-Cbp6 complex is released from the ribosome but maintains contact to cytochrome *b*. Sequential recruitment of the assembly factor Cbp4 and the Qcr7 and Qcr8 subunits induces the release of Cbp3-Cbp6 and allows subsequent binding of the two additional subunits Cor1 and Cor2, which do not contain cofactors. During this step Cbp4 is also released. Stepwise binding of Qcr6, cytochrome *c<sub>1</sub>* and of Qcr9, Qcr10 and the Rieske Fe/S protein then completes the assembly process (Gruschke et al. 2012). Blocking later stages of assembly sequesters Cbp3-Cbp6 in the early intermediates and prevents further translational activation of the cytochrome *b* synthesis. This feed-back loop regulates cytochrome *b* synthesis in response to the efficiency of cytochrome *bc<sub>1</sub>* complex assembly.

The cytochrome *b<sub>6</sub>f* complex is a symmetric dimer of eight TM subunits. The *b<sub>6</sub>f* monomer contains two multi-spanning membrane subunits (Cramer et al. 2005). Cytochrome *b<sub>6</sub>* has four TM helices and a short N-terminal helix, which is surface-exposed. Subunit IV contains three TM helices, which surround the four-helix bundle of cytochrome *b<sub>6</sub>*. This core assembles with additional six TM helices, which are provided by the additional single-spanning subunits cytochrome *f*, the Rieske protein and the four small single TM proteins, PetG, PetL, PetM and PetN at the periphery of each monomer of the complex (Hasan et al. 2013).

Seven prosthetic groups are present in the cytochrome *b<sub>6f</sub>* complex monomer (Kurisu et al. 2003; Stroebel et al. 2003). The cytochrome *b<sub>6</sub>* subunit harbors two bis-His ligated *b*-hemes (*b<sub>p</sub>* and *b<sub>n</sub>*) and a covalently linked heme *c<sub>n</sub>*, which is unique in not having any amino acid as an axial ligand (Kurisu et al. 2003; Stroebel et al. 2003). In addition, a chlorophyll-*a* (chl-*a*) and a  $\beta$ -carotene ( $\beta$ -car) molecule are intercalated within the four TM domains of cytochrome *b*. An additional heme molecule is covalently attached to the cytochrome *f* subunit and one [2Fe–2S] cluster is bound to the Rieske subunit.

The current model suggests that the cytochrome *b<sub>6</sub>* and subunit IV assemble first to form the core of the monomeric cytochrome *b<sub>6f</sub>* complex, which subsequently undergoes dimerization (Hasan et al. 2013). At this stage, lipids are thought to stabilize the monomer–monomer interactions (Breyton et al. 1997) (See Chap. 20 by Baniulis et al.). The Rieske FeS protein and the cytochrome *f* subunit also form a subcomplex that is stabilized by a native acidic sulfolipid interacting with basic residues of both TM helices. This sub-complex then interacts with the cytochrome *b<sub>6</sub>*-SU IV polytopic core nucleus to form a cytochrome *b<sub>6</sub>*-SU IV-ISP-cytochrome *f* sub-complex. The four small subunits are thought to insert spontaneously into the membrane and to assemble as a four-helix bundle around the  $\beta$ -carotene molecule at the periphery of the cytochrome *b<sub>6f</sub>* complex core. Mutagenesis studies suggest that the presence of the PetG, L, M, N subunits is required for a stable cytochrome *b<sub>6f</sub>* complex dimer (Hasan et al. 2013).

Heme binding is probably an important step in the stabilization of the assembly intermediates. In the absence of heme, the cytochrome *b<sub>6</sub>* and cytochrome *f* apo-proteins are highly susceptible to protease cleavage (Kuras et al. 1995). Heterologous expression and stable membrane insertion of cytochrome *b<sub>6f</sub>* subunits in *E. coli* is possible, when heme is added to the medium, suggesting that no dedicated assembly factors/chaperones are required for heme insertion (Dreher et al. 2007). However, the exact

timing of subunit assembly and cofactor insertion still needs to be determined.

## Acknowledgements

The authors thank all previous and current lab members. This work was funded by grants from the Deutsche Forschungsgemeinschaft.

## References

- Abramson J, Riistama S, Larsson G, Jasaitis A, Svensson-Ek M, Laakkonen L, Puustinen A, ... Wikstrom M (2000) The structure of the ubiquinol oxidase from *Escherichia coli* and its ubiquinone binding site. 7:910–917
- Akdogan Y, Anbazhagan V, Hinderberger D, Schneider D (2012) Heme binding constricts the conformational dynamics of the cytochrome b(559)' heme binding cavity. *Biochemistry* 51:7149–7156
- Alami M, Luke I, Deitermann S, Eisner G, Koch HG, Brunner J, Muller M (2003) Differential interactions between a twin-arginine signal peptide and its translocase in *Escherichia coli*. *Mol Cell* 12:937–946
- Angelini S, Deitermann S, Koch HG (2005) FtsY, the bacterial signal-recognition particle receptor, interacts functionally and physically with the SecYEG translocon. *EMBO Rep* 6:476–481
- Angelini S, Boy D, Schiltz E, Koch HG (2006) Membrane binding of the bacterial signal recognition particle receptor involves two distinct binding sites. *J Cell Biol* 174:715–724
- Aschtgen M-S, Zoued A, Lloubes R, Journet L, Cascales E (2012) The C-tail anchored TssL subunit, an essential protein of the enteroaggregative *Escherichia coli* Sci-1 Type VI secretion system, is inserted by YidC. *MicrobiologyOpen* 1:71–82
- Babcock GT, Widger WR, Cramer WA, Oertling WA, Metz JG (1985) Axial ligands of chloroplast cytochrome b-559: identification and requirement for a heme-crosslinked polypeptide structure. *Biochemistry* 24:3638–3645
- Bange G, Sinning I (2013) SIMIBI twins in protein targeting and localization. *Nat Struct Mol Biol* 20:776–780
- Barker PD, Ferguson SJ (1999) Still a puzzle: why is haem covalently attached in c-type cytochromes? *Structure* 7:R281–R290

- Barrick D (1994) Replacement of the proximal ligand of sperm whale myoglobin with free imidazole in the mutant His-93 → Gly. *Biochemistry* 33: 6546–6554
- Bauerschmitt H, Mick DU, Deckers M, Vollmer C, Funes S, Kehrein K, Ott M, ... Herrmann JM (2010) Ribosome-binding proteins Mdm38 and Mba1 display overlapping functions for regulation of mitochondrial translation. *Mol Biol Cell* 21:1937–1944
- Beck K, Eisner G, Trescher D, Dalbey RE, Brunner J, Muller M (2001) YidC, an assembly site for polytopic *Escherichia coli* membrane proteins located in immediate proximity to the SecYE translocon and lipids. *EMBO Rep* 2:709–714
- Becker T, Bottinger L, Pfanner N (2012) Mitochondrial protein import: from transport pathways to an integrated network. *Trends Biochem Sci* 37:85–91
- Beha D, Deitermann S, Muller M, Koch HG (2003) Export of beta-lactamase is independent of the signal recognition particle. *J Biol Chem* 278: 22161–22167
- Beilharz T, Egan B, Silver PA, Hofmann K, Lithgow T (2003) Bipartite signals mediate subcellular targeting of tail-anchored membrane proteins in *Saccharomyces cerevisiae*. *J Biol Chem* 278:8219–8223
- Bibi E (2011) Early targeting events during membrane protein biogenesis in *Escherichia coli*. *Biochim Biophys Acta* 1808:841–850
- Borgese N, Righi M (2010) Remote origins of tail-anchored proteins. *Traffic* 11:877–885
- Borisov VB, Gennis RB, Hemp J, Verkhovsky MI (2011) The cytochrome bd respiratory oxygen reductases. *Biochim Biophys Acta* 1807:1398–1413
- Bornemann T, Jockel J, Rodnina MV, Wintermeyer W (2008) Signal sequence-independent membrane targeting of ribosomes containing short nascent peptides within the exit tunnel. *Nat Struct Mol Biol* 15:494–499
- Braig D, Bar C, Thumfart JO, Koch HG (2009) Two cooperating helices constitute the lipid-binding domain of the bacterial SRP receptor. *J Mol Biol* 390:401–413
- Braig D, Mircheva M, Sachelaru I, van der Sluis EO, Sturm L, Beckmann R, Koch HG (2011) Signal sequence-independent SRP-SR complex formation at the membrane suggests an alternative targeting pathway within the SRP cycle. *Mol Biol Cell* 22:2309–2323
- Brasseur G, Brivet-Chevillotte P (1995) Characterization of mutations in the mitochondrial cytochrome b gene of *Saccharomyces cerevisiae* affecting the quinone reductase site (QN). *Eur J Biochem* 230:1118–1124
- Brasseur G, Saribas AS, Daldal F (1996) A compilation of mutations located in the cytochrome b subunit of the bacterial and mitochondrial bc1 complex. *Biochim Biophys Acta* 1275:61–69
- Breyton C, Tribet C, Olive J, Dubacq JP, Popot JL (1997) Dimer to monomer conversion of the cytochrome b6 f complex. Causes and consequences. *J Biol Chem* 272:21892–21900
- Chen M, Xie K, Jiang F, Yi L, Dalbey RE (2002) YidC, a newly defined evolutionarily conserved protein, mediates membrane protein assembly in bacteria. *Biol Chem* 383:1565–1572
- Cordova JM, Noack PL, Hilcove SA, Lear JD, Ghirlanda G (2007) Design of a functional membrane protein by engineering a heme-binding site in glycophorin A. *J Am Chem Soc* 129:512–518
- Cramer WA, Yan J, Zhang H, Kurisu G, Smith JL (2005) Structure of the cytochrome b6f complex: new prosthetic groups, Q-space, and the ‘hors d’oeuvres hypothesis’ for assembly of the complex. *Photosynth Res* 85:133–143
- Craney A, Tahlan K, Andrews D, Nodwell J (2011) Bacterial transmembrane proteins that lack N-terminal signal sequences. *PLoS ONE* 6:e19421
- Cristobal S, Scotti P, Luirink J, von Heijne G, de Gier JW (1999) The signal recognition particle-targeting pathway does not necessarily deliver proteins to the sec-translocase in *Escherichia coli*. *J Biol Chem* 274:20068–20070
- Daldal F, Davidson E, Cheng S (1987) Isolation of the structural genes for the Rieske Fe-S protein, cytochrome b and cytochrome c1 all components of the ubiquinol: cytochrome c2 oxidoreductase complex of *Rhodospseudomonas capsulata*. *J Mol Biol* 195:1–12
- Davidson E, Ohnishi T, Tokito M, Daldal F (1992) *Rhodobacter capsulatus* mutants lacking the Rieske FeS protein form a stable cytochrome bc1 subcomplex with an intact quinone reduction site. *Biochemistry* 31:3351–3358
- Deitermann S, Sprie GS, Koch HG (2005) A dual function for SecA in the assembly of single spanning membrane proteins in *Escherichia coli*. *J Biol Chem* 280:39077–39085
- Discher BM, Koder RL, Moser CC, Dutton PL (2003) Hydrophilic to amphiphilic design in redox protein maquettes. *Curr Opin Chem Biol* 7:741–748
- Discher BM, Noy D, Strzalka J, Ye S, Moser CC, Lear JD, Blasie JK, Dutton PL (2005) Design of amphiphilic protein maquettes: controlling assembly, membrane insertion, and cofactor interactions. *Biochemistry* 44:12329–12343
- Dreher C, Prodöhl A, Weber M, Schneider D (2007) Heme binding properties of heterologously expressed spinach cytochrome b(6): implications for transmembrane b-type cytochrome formation. *FEBS Lett* 581:2647–2651

- Dreher C, Prodöhl A, Hielscher R, Hellwig P, Schneider D (2008) Multiple step assembly of the transmembrane cytochrome b<sub>6</sub>. *J Mol Biol* 382:1057–1065
- Dreher C, Hielscher R, Prodöhl A, Hellwig P, Schneider D (2010) Characterization of two cytochrome b<sub>6</sub> proteins from the cyanobacterium *Gloeobacter violaceus* PCC 7421. *J Bioenerg Biomembr* 42:517–526
- du Plessis DJF, Nouwen N, Driessen AJM (2006) Subunit a of cytochrome o oxidase requires both YidC and SecYEG for membrane insertion. *J Biol Chem* 281:12248–12252
- du Plessis DJ, Berrelkamp G, Nouwen N, Driessen AJ (2009) The lateral gate of SecYEG opens during protein translocation. *J Biol Chem* 284:15805–15814
- du Plessis DJF, Nouwen N, Driessen AJM (2011) The sec translocase. *Biochim Biophys Acta* 1808:851–865
- Eitan A, Bibi E (2004) The core *Escherichia coli* signal recognition particle receptor contains only the N and G domains of FtsY. *J Bacteriol* 186:2492–2494
- Ekici S, Pawlik G, Lohmeyer E, Koch HG, Daldal F (2012) Biogenesis of cbb(3)-type cytochrome c oxidase in *Rhodobacter capsulatus*. *Biochim Biophys Acta* 1817:898–910
- Esposti MD, De Vries S, Crimi M, Ghelli A, Patarinello T, Meyer A (1993) Mitochondrial cytochrome b: evolution and structure of the protein. *Biochim Biophys Acta* 1143:243–271
- Facey SJ, Neugebauer SA, Krauss S, Kuhn A (2007) The mechanosensitive channel protein MscL is targeted by the SRP to the novel YidC membrane insertion pathway of *Escherichia coli*. *J Mol Biol* 365:995–1004
- Ferguson SJ, Stevens JM, Allen JWA, Robertson IB (2008) Cytochrome c assembly: a tale of ever increasing variation and mystery? *Biochim Biophys Acta - Bioenergetics* 1777:980–984
- Fontaine F, Fuchs RT, Storz G (2011) Membrane localization of small proteins in *Escherichia coli*. *J Biol Chem* 286:32464–32474
- Francke C, Loyal R, Ohad I, Haehnel W (1999) In vitro assembly of a beta<sub>2</sub> cytochrome b<sub>559</sub>-like complex from the chemically synthesised beta-subunit encoded by the *Synechocystis* sp. 6803 psbF gene. *FEBS Lett* 442:75–78
- Frauenfeld J, Gumbart J, van der Sluis EO, Funes S, Gartmann M, Beatrix B, Mielke T, Berninghaus O, Becker T, Schulten K, Beckmann R (2011) Cryo EM structure of the ribosome-SecYE complex in the membrane environment. *Nat Struct Mol Biol* 18:614–621
- Funes S, Kauff F, van der Sluis EO, Ott M, Herrmann JM (2011) Evolution of YidC/Oxa1/Alb3 insertases: three independent gene duplications followed by functional specialization in bacteria, mitochondria and chloroplasts. *Biol Chem* 392:13–19
- Funes S, Westerburg H, Jaimes-Miranda F, Woellhaf MW, Aguilar-Lopez JL, Janssen L, Bonnefoy N, ... Herrmann JM (2013) Partial suppression of Oxa1 mutants by mitochondria-targeted signal recognition particle provides insights into the evolution of the cotranslational insertion systems. *Febs J* 280:904–915
- Garcia-Horsman JA, Barquera B, Rumbley J, Ma J, Gennis RB (1994) The superfamily of heme-copper respiratory oxidases. *J Bacteriol* 176:5587–5600
- Gennis RB, Barquera B, Hacker B, Van Doren SR, Arnaud S, Crofts AR, Davidson E, ... Daldal F (1993) The bc<sub>1</sub> complexes of *Rhodobacter sphaeroides* and *Rhodobacter capsulatus*. *J Bioenerg Biomembr* 25:195–209
- Ghirlanda G, Osyczka A, Liu W, Antolovich M, Smith KM, Dutton PL, Wand AJ, DeGrado WF (2004) De novo design of a D<sub>2</sub>-symmetrical protein that reproduces the diheme four-helix bundle in cytochrome bc<sub>1</sub>. *J Am Chem Soc* 126:8141–8147
- Grudnik P, Bange G, Sinning I (2009) Protein targeting by the signal recognition particle. *Biol Chem* 390:775–782
- Gruschke S, Kehrein K, Rompler K, Grone K, Israel L, Imhof A, Herrmann JM, Ott M (2011) Cbp3-Cbp6 interacts with the yeast mitochondrial ribosomal tunnel exit and promotes cytochrome b synthesis and assembly. *J Cell Biol* 193:1101–1114
- Gruschke S, Rompler K, Hildenbeutel M, Kehrein K, Kuhl I, Bonnefoy N, Ott M (2012) The Cbp3-Cbp6 complex coordinates cytochrome b synthesis with bc<sub>1</sub> complex assembly in yeast mitochondria. *J Cell Biol* 199:137–150
- Gu SQ, Peske F, Wieden HJ, Rodnina MV, Wintermeyer W (2003) The signal recognition particle binds to protein L23 at the peptide exit of the *Escherichia coli* ribosome. *RNA* 9:566–573
- Hamza I, Dailey HA (2012) One ring to rule them all: trafficking of heme and heme synthesis intermediates in the metazoans. *Biochim Biophys Acta* 1823:1617–1632
- Hasan SS, Yamashita E, Cramer WA (2013) Transmembrane signaling and assembly of the cytochrome b<sub>6</sub>f-lipidic charge transfer complex. *Biochim Biophys Acta - Bioenergetics* 1827:1295–1308
- Hell K, Neupert W, Stuart RA (2001) Oxa1p acts as a general membrane insertion machinery for proteins encoded by mitochondrial DNA. *Embo J* 20:1281–1288

- Herrmann RG, Alt J, Schiller B, Widger WR, Cramer WA (1984) Nucleotide sequence of the gene for apocytochrome *b*-559 on the spinach plastid chromosome: implications for the structure of the membrane protein. *FEBS Lett* 176:239–244
- Hizlan D, Robson A, Whitehouse S, Gold VA, Vonck J, Mills D, Kuhlbrandt W, Collinson I (2012) Structure of the SecY complex unlocked by a preprotein mimic. *Cell Rep* 1:21–28
- Huang SS, Koder RL, Lewis M, Wand AJ, Dutton PL (2004) The HP-1 maquette: from an apoprotein structure to a structured hemoprotein designed to promote redox-coupled proton exchange. *Proc Natl Acad Sci USA* 101:5536–5541
- Jormakka M, Byrne B, Iwata S (2003) Formate dehydrogenase—a versatile enzyme in changing environments. *Curr Opin Struct Biol* 13:418–423
- Kalbfleisch T, Cambon A, Wattenberg BW (2007) A bioinformatics approach to identifying tail-anchored proteins in the human genome. *Traffic* 8:1687–1694
- Keilin DD (1925) On cytochrome, a respiratory pigment, common to animals, yeast, and higher plants. In: *Proceedings of the royal society of London Series B, containing papers of a biological character* 98:312–339 (CR - Copyright &#169; 1925 The Royal Society)
- Khalimonchuk O, Ostermann K, Rodel G (2005) Evidence for the association of yeast mitochondrial ribosomes with Cox11p, a protein required for the Cu(B) site formation of cytochrome *c* oxidase. *Curr Genet* 47:223–233
- Kihara A, Akiyama Y, Ito K (1995) FtsH is required for proteolytic elimination of uncomplexed forms of SecY, an essential protein translocase subunit. *Proc Natl Acad Sci USA* 92:4532–4536
- Kim HJ, Khalimonchuk O, Smith PM, Winge DR (2012) Structure, function, and assembly of heme centers in mitochondrial respiratory complexes. *Biochim Biophys Acta* 1823:1604–1616
- Klostermann E, Droste Gen Helling I, Carde JP, Schunemann D (2002) The thylakoid membrane protein ALB3 associates with the cpSecY-translocase in *Arabidopsis thaliana*. *Biochem J* 368:777–781
- Koch HG, Schneider D (2007) Assembly and stability of transmembrane cytochromes. *Curr Chem Biol* 1:59–74
- Koch HG, Hengelage T, Neumann-Haefelin C, MacFarlane J, Hoffschulte HK, Schimz KL, Mechler B, Muller M (1999) In vitro studies with purified components reveal signal recognition particle (SRP) and SecA/SecB as constituents of two independent protein-targeting pathways of *Escherichia coli*. *Mol Biol Cell* 10:2163–2173
- Koch HG, Moser M, Muller M (2003) Signal recognition particle-dependent protein targeting, universal to all kingdoms of life. *Rev Physiol Biochem Pharmacol* 146:55–94
- Korendovych IV, Senes A, Kim YH, Lear JD, Fry HC, Therien MJ, Blasie JK, . . . Degrado WF (2010) De novo design and molecular assembly of a transmembrane diporphyrin-binding protein complex. *J Am Chem Soc* 132:15516–15518
- Kudva R, Denks K, Kuhn P, Vogt A, Muller M, Koch HG (2013) Protein translocation across the inner membrane of Gram-negative bacteria: the Sec and Tat dependent protein transport pathways. *Res Microbiol* 164:505–534
- Kuhn P, Weiche B, Sturm L, Sommer E, Drepper F, Warscheid B, Sourjik V, Koch HG (2011) The bacterial SRP receptor, SecA and the ribosome use overlapping binding sites on the SecY translocon. *Traffic* 12:563–578
- Kuhn P, Kudva R, Welte T, Sturm L, Koch H-G (2014) Targeting and integration of bacterial membrane proteins. In: Remaut H, Fronzes R (eds) *Bacterial Membranes: Structural and Molecular Biology*. Caister Academic Press, Norfolk
- Kuras R, Buschlen S, Wollman FA (1995) Maturation of pre-apocytochrome *f* in vivo. A site-directed mutagenesis study in *Chlamydomonas reinhardtii*. *J Biol Chem* 270:27797–27803
- Kurisu G, Zhang H, Smith JL, Cramer WA (2003) Structure of the cytochrome *b6f* complex of oxygenic photosynthesis: tuning the cavity. *Science* 302:1009–1014
- Lam VQ, Akopian D, Rome M, Henningsen D, Shan SO (2010) Lipid activation of the signal recognition particle receptor provides spatial coordination of protein targeting. *J Cell Biol* 190:623–635
- Lancaster CR (2002) *Wolinella succinogenes* quinol: fumarate reductase-2.2-A resolution crystal structure and the E-pathway hypothesis of coupled transmembrane proton and electron transfer. *Biochim Biophys Acta* 1565:215–231
- Li W, Schulman S, Boyd D, Erlandson K, Beckwith J, Rapoport TA (2007) The plug domain of the SecY protein stabilizes the closed state of the translocation channel and maintains a membrane seal. *Mol Cell* 26:511–521
- McRee DE, Jensen GM, Fitzgerald MM, Siegel HA, Goodin DB (1994) Construction of a bisquo heme enzyme and binding by exogenous ligands. *Proc Natl Acad Sci USA* 91:12847–12851
- Mick DU, Fox TD, Rehling P (2011) Inventory control: cytochrome *c* oxidase assembly regulates mitochondrial translation. *Nat Rev Mol Cell Biol* 12:14–20



- Mochizuki N, Tanaka R, Grimm B, Masuda T, Moulin M, Smith AG, Tanaka A, Terry MJ (2010) The cell biology of tetrapyrroles: a life and death struggle. *Trends Plant Sci* 15:488–498
- Moulin M, Smith AG (2005) Regulation of tetrapyrrole biosynthesis in higher plants. *Biochem Soc Trans* 33:737–742
- Muller M, Koch HG, Beck K, Schafer U (2001) Protein traffic in bacteria: multiple routes from the ribosome to and across the membrane. *Prog Nucleic Acid Res Mol Biol* 66:107–157
- Nakamura H, Yamato I, Anraku Y, Lemieux L, Gennis RB (1990) Expression of *cyoA* and *cyoB* demonstrates that the CO-binding heme component of the *Escherichia coli* cytochrome *o* complex is in subunit I. *J Biol Chem* 265:11193–11197
- NCotIUoB (NC-IUB) (1992) Nomenclature of electron-transfer proteins. Recommendations 1989. *J Biol Chem* 267:665–677
- Negron C, Fufezan C, Koder RL (2009) Geometric constraints for porphyrin binding in helical protein binding sites. *Proteins* 74:400–416
- Nevo-Dinur K, Nussbaum-Shochat A, Ben-Yehuda S, Amster-Choder O (2011) Translation-independent localization of mRNA in *E. coli*. *Science* 331:1081–1084
- Nikkila H, Gennis RB, Sligar SG (1991) Cloning and expression of the gene encoding the soluble cytochrome *b*562 of *Escherichia coli*. *Eur J Biochem* 202:309–313
- Ott M, Herrmann JM (2010) Co-translational membrane insertion of mitochondrially encoded proteins. *Biochim Biophys Acta* 1803:767–775
- Ott M, Prestele M, Bauerschmitt H, Funes S, Bonnefoy N, Herrmann JM (2006) Mba1, a membrane-associated ribosome receptor in mitochondria. *Embo J* 25:1603–1610
- Palmer T, Berks BC (2012) The twin-arginine translocation (Tat) protein export pathway. *Nat Rev Microbiol* 10:483–496
- Palmer SR, Crowley PJ, Oli MW, Ruelf MA, Michalek SM, Brady LJ (2012) YidC1 and YidC2 are functionally distinct proteins involved in protein secretion, biofilm formation and cariogenicity of *Streptococcus mutans*. *Microbiology* 158:1702–1712
- Palombo I, Daley DO (2012) Heme incorporation into the cytochrome *bo*3 occurs at a late stage of assembly. *FEBS Lett* 586:4197–4202
- Park E, Rapoport TA (2012) Mechanisms of Sec61/SecY-mediated protein translocation across membranes. *Annu Rev Biophys* 41:21–40
- Park E, Menetret JF, Gumbart JC, Ludtke SJ, Li W, Whynot A, Rapoport TA, Akey CW (2013) Structure of the SecY channel during initiation of protein translocation. *Nature* 506:102–106
- Parlitz R, Eitan A, Stjepanovic G, Bahari L, Bange G, Bibi E, Sinning I (2007) *Escherichia coli* signal recognition particle receptor FtsY contains an essential and autonomous membrane-binding amphipathic helix. *J Biol Chem* 282:32176–32184
- Pawlik G, Kulajta C, Sachelaru I, Schroder S, Waidner B, Hellwig P, Daldal F, Koch HG (2010) The putative assembly factor CcoH is stably associated with the *cbb*3-type cytochrome oxidase. *J Bacteriol* 192:6378–6389
- Pereira MM, Santana M, Teixeira M (2001) A novel scenario for the evolution of haem-copper oxygen reductases. *Biochim Biophys Acta* 1505:185–208
- Pohlschroder M, Hartmann E, Hand NJ, Dilks K, Haddad A (2005) Diversity and evolution of protein translocation. *Annu Rev Microbiol* 59:91–111
- Popot JL, Engelman DM (1990) Membrane protein folding and oligomerization: the two-stage model. *Biochemistry* 29:4031–4037
- Price CE, Driessen AJ (2010) Conserved negative charges in the transmembrane segments of subunit K of the NADH: ubiquinone oxidoreductase determine its dependence on YidC for membrane insertion. *J Biol Chem* 285:3575–3581
- Prodöhl A, Volkmer T, Finger C, Schneider D (2005) Defining the structural basis for assembly of a transmembrane cytochrome. *J Mol Biol* 350:744–756
- Prodöhl A, Weber M, Dreher C, Schneider D (2007) A mutational study of transmembrane helix-helix interactions. *Biochimie* 89:1433–1437
- Rabu C, Schmid V, Schwappach B, High S (2009) Biogenesis of tail-anchored proteins: the beginning for the end? *J Cell Sci* 122:3605–3612
- Rapoport TA, Jungnickel B, Kutay U (1996) Protein transport across the eukaryotic endoplasmic reticulum and bacterial inner membranes. *Annu Rev Biochem* 65:271–303
- Rau HK, Haehnel W (1998) Design, synthesis, and properties of a novel cytochrome *b* model. *J Am Chem Soc* 120:468–476
- Reedy CJ, Gibney BR (2004) Heme protein assemblies. *Chem Rev* 104:617–649
- Renthal R (2010) Helix insertion into bilayers and the evolution of membrane proteins. *Cell Mol Life Sci* 67:1077–1088
- Robertson DE, Farid RS, Moser CC, Urbauer JL, Mulholland SE, Pidikiti R, Lear JD, ... Dutton PL (1994) Design and synthesis of multi-haem proteins. *Nature* 368:425–432
- Saaf A, Monne M, de Gier JW, von Heijne G (1998) Membrane topology of the 60-kDa Oxa1p homologue from *Escherichia coli*. *J Biol Chem* 273:30415–30418
- Sachelaru I, Petriman NA, Kudva R, Kuhn P, Welte T, Knapp B, Drepper F, ... Koch HG (2013) YidC

- occupies the lateral gate of the SecYEG translocon and is sequentially displaced by a nascent membrane protein. *J Biol Chem* 288:16295–16307
- Saint-Marcoux D, Wollman F-A, de Vitry C (2009) Biogenesis of cytochrome b6 in photosynthetic membranes. *J Cell Biol* 185:1195–1207
- Samuelson JC, Chen M, Jiang F, Moller I, Wiedmann M, Kuhn A, Phillips GJ, Dalbey RE (2000) YidC mediates membrane protein insertion in bacteria. *Nature* 406:637–641
- Saraste M, Castresana J (1994) Cytochrome oxidase evolved by tinkering with denitrification enzymes. *FEBS Lett* 341:1–4
- Schneider S, Marles-Wright J, Sharp KH, Paoli M (2007) Diversity and conservation of interactions for binding heme in *b*-type heme proteins. *Nat Prod Rep* 24:621–630
- Shepherd M, Heath MD, Poole RK (2007) NikA binds heme: a new role for an *Escherichia coli* periplasmic nickel-binding protein. *Biochemistry* 46:5030–5037
- Shinde S, Cordova JM, Woodrum BW, Ghirlanda G (2012) Modulation of function in a minimalist heme-binding membrane protein. *J Biol Inorg Chem* 17:557–564
- Shinopoulos KE, Brudvig GW (2012) Cytochrome b559 and cyclic electron transfer within photosystem II. *Biochim Biophys Acta* 1817:66–75
- Sinning I, Bange G, Wild K (2011) It takes two to Get3. *Structure* 19:1353–1355
- Smith LJ, Kahraman A, Thornton JM (2010) Heme proteins—diversity in structural characteristics, function, and folding. *Proteins* 78:2349–2368
- Stenberg F, von Heijne G, Daley DO (2007) Assembly of the cytochrome bo3 complex. *J Mol Biol* 371:765–773
- Stjepanovic G, Kapp K, Bange G, Graf C, Parltz R, Wild K, Mayer MP, Sinning I (2011) Lipids trigger a conformational switch that regulates signal recognition particle (SRP)-mediated protein targeting. *J Biol Chem* 286:23489–23497
- Stroebel D, Choquet Y, Popot JL, Picot D (2003) An atypical haem in the cytochrome b(6)f complex. *Nature* 426:413–418
- Sturm A, Schierhorn A, Lindenstrauss U, Lilie H, Bruser T (2006) YcdB from *Escherichia coli* reveals a novel class of Tat-dependently translocated hemo-proteins. *J Biol Chem* 281:13972–13978
- Tanaka R, Tanaka A (2007) Tetrapyrrole biosynthesis in higher plants. *Annu Rev Plant Biol* 58:321–346
- Thöny-Meyer L (1997) Biogenesis of respiratory cytochromes in bacteria. *Microbiol Mol Biol Rev* 61:337–376
- Tome L, Schaetzel C, Dreher C, Schneider D (2013) Fe- but not Mg-protoporphyrin IX binds to a transmembrane *b*-type cytochrome. *Mol Membr Biol* 31:37–45
- Totley S, Waldron KJ, Firbank SJ, Reale B, Bessant C, Sato K, Cheek TR, ... Robinson NJ (2008) Protein-folding location can regulate manganese-binding versus copper- or zinc-binding. *Nature* 455:1138–1142
- Trager C, Rosenblad MA, Ziehe D, Garcia-Petit C, Schrader L, Kock K, Richter CV, ... Schunemann D (2012) Evolution from the prokaryotic to the higher plant chloroplast signal recognition particle: the signal recognition particle RNA is conserved in plastids of a wide range of photosynthetic organisms. *Plant Cell* 24:4819–4836
- Valkova-Valchanova MB, Saribas AS, Gibney BR, Dutton PL, Daldal F (1998) Isolation and characterization of a rho-subunit cytochrome *b*-c1 sub-complex from *Rhodobacter capsulatus* and reconstitution of its ubihydroquinone oxidation (Qo) site with purified Fe-S protein subunit. *Biochemistry* 37:16242–16251
- Van den Berg B, Clemons WM Jr, Collinson I, Modis Y, Hartmann E, Harrison SC, Rapoport TA (2004) X-ray structure of a protein-conducting channel. *Nature* 427:36–44
- Volkmer T, Becker C, Prodöhl A, Finger C, Schneider D (2006) Assembly of a transmembrane *b*-type cytochrome is mainly driven by transmembrane helix interactions. *Biochim Biophys Acta* 1758:1815–1822
- Weber M, Prodöhl A, Dreher C, Becker C, Underhaug J, Svane AS, Malmendal A, ... Schneider D (2011) SDS-facilitated in vitro formation of a transmembrane *b*-type cytochrome is mediated by changes in local pH. *J Mol Biol* 407:594–606
- Weber M, Tome L, Otzen D, Schneider D (2012) A Ser residue influences the structure and stability of a Pro-kinked transmembrane helix dimer. *Biochim Biophys Acta - Biomembr* 1818:2103–2107
- Weiche B, Bürk J, Angelini S, Schiltz E, Thumfart JO, Koch H-G (2008) A cleavable N-terminal membrane anchor is involved in membrane binding of the *Escherichia coli* SRP receptor. *J Mol Biol* 377:761–773
- Welte T, Kudva R, Kuhn P, Sturm L, Braig D, Müller M, Warscheid B, ... Koch H-G (2012) Promiscuous targeting of polytopic membrane proteins to SecYEG or YidC by the *Escherichia coli* signal recognition particle. *Mol Biol Cell* 23:464–479
- Widger WR, Cramer WA, Herrmann RG, Trebst A (1984) Sequence homology and structural similarity between cytochrome *b* of mitochondrial complex III

- and the chloroplast b6-f complex: position of the cytochrome b hemes in the membrane. *Proc Natl Acad Sci USA* 81:674–678
- Widger WR, Cramer WA, Hermodson M, Herrmann RG (1985) Evidence for a hetero-oligomeric structure of the chloroplast cytochrome b-559. *FEBS Lett* 191:186–190
- Ye S, Discher BM, Strzalka J, Xu T, Wu SP, Noy D, Kuzmenko I, ... Blasie JK (2005) Amphiphilic four-helix bundle peptides designed for light-induced electron transfer across a soft interface. *Nano Lett* 5:1658–1667
- Yi L, Jiang F, Chen M, Cain B, Bolhuis A, Dalbey RE (2003) YidC is strictly required for membrane insertion of subunits a and c of the F1F0 ATP synthase and SecE of the SecYEG translocase. *Biochemistry* 42:10537–10544
- Zhang D, Shan SO (2012) Translation elongation regulates substrate selection by the signal recognition particle. *J Biol Chem* 287:7652–7660
- Zhu L, Wasey A, White SH, Dalbey RE (2013) Charge composition features of model single-span membrane proteins that determine selection of YidC and SecYEG translocase pathways in *Escherichia coli*. *J Biol Chem* 288:7704–7716
- Zickermann V, Angerer H, Ding MG, Nubel E, Brandt U (2010) Small single transmembrane domain (STMD) proteins organize the hydrophobic subunits of large membrane protein complexes. *FEBS Lett* 584:2516–2525
- Zimmermann R, Eyrisch S, Ahmad M, Helms V (2011) Protein translocation across the ER membrane. *Biochim Biophys Acta* 1808:912–924

# Chapter 29

## Respiratory Cytochrome Supercomplexes

Giorgio Lenaz\* and Maria Luisa Genova

Section of Biochemistry, Department of Biomedical and  
Neuromotor Sciences (DIBINEM), University of Bologna,  
Via Imerio 48, 40126 Bologna, Italy

Summary.....	585
I. Introduction.....	586
A. The Respiratory Chain of Mitochondria.....	586
B. Organization of the Respiratory Chain: Historical Outline.....	588
II. Distribution and Composition of Respiratory Supercomplexes.....	589
A. Distribution in Different Organisms.....	589
B. Composition of Respiratory Supercomplexes.....	589
C. Megacomplexes or Respiratory Strings.....	591
III. Structure of Supercomplexes.....	592
A. Molecular Structure by Electron Microscopy and Modeling.....	592
B. Lipid Content and Composition.....	595
1. Lipid Composition of Mitochondria.....	595
2. Roles of Mitochondrial Lipids.....	595
3. Lipids and Supercomplex Stabilization.....	596
C. Biogenesis of Respiratory Supercomplexes.....	598
IV. Functions of Respiratory Supercomplexes.....	600
A. Respiratory Supercomplexes are Functional.....	600
B. Kinetic Advantage.....	600
1. From Complex I to Complex III.....	602
2. From Complex III to Complex IV.....	606
3. Respiratory Enzymes Not Associated in Supercomplexes.....	607
C. Supercomplexes and Energy Conservation.....	609
D. Modulation of Generation of Reactive Oxygen Species.....	610
E. Effect of Supercomplex Association on Stability of Individual Complexes.....	612
F. Dynamic Nature of Supercomplexes: The Plasticity Model.....	613
1. Role of Membrane Electrochemical Potential.....	615
2. Role of Post-translational Changes.....	616
V. A Role of Supercomplexes in Cell Physiology.....	616
References.....	617

### Summary

Evidence from several investigations demonstrates the existence of supramolecular units of Complex I, Complex III, and multiple copies of Complex IV in mitochondria and indicates that specific respiratory complexes may preferentially associate to form cytochrome-containing supercomplexes in the native membrane. There are now indications that

---

\*Author for correspondence, e-mail: [giorgio.lenaz@unibo.it](mailto:giorgio.lenaz@unibo.it)

cardiolipin, a distinctive mitochondrial lipid, stabilizes the respiratory assemblies. The isolated supercomplexes are active with respect to both their component individual complexes and the entire respiratory function that relies on Coenzyme Q and cytochrome c as intermediate substrates. The latter finding argues against previous models of a random distribution of the respiratory complexes in mitochondria. The supercomplex organization is compatible with electron transfer, but experimental evidence is scant for an effective mechanism via substrate channeling compared to free diffusion of substrates in accordance with the random collision model. The finding that Complex I is almost totally associated in a supercomplex with Complex III seems to exclude a role for the ubiquinone pool in physiological electron transfer between these two complexes, whereas it is certainly required for electron transfer from Complex II or from other dehydrogenases to Complex III; likely, only a small fraction of Complex IV forms a functional supercomplex with channeling of cytochrome c. Nevertheless, the supercomplexes may physiologically exist in equilibrium with free complexes (plasticity model). The supercomplex organization appears to prevent excessive generation of reactive oxygen species from the respiratory chain; accordingly, many pathological conditions and the mitochondrial aging phenotype characterized by a loss of supercomplex assembly correlate with mitochondrial dysfunction and increased oxidative stress. Specific metabolic signals may also arise in the cell in response to a tuned production of reactive oxygen species as a consequence of the controlled dynamics of supercomplex assembling/disassembling at different physio-pathological conditions. The present review paper provides an updated and extensive discussion on the subject.

## I. Introduction

### A. The Respiratory Chain of Mitochondria

The *electron transfer chain* or *respiratory chain* is a multi-enzyme system that collects reducing equivalents (hydrogen atoms)

released from oxidations of intermediary metabolism and conveys them to molecular oxygen, reducing it to water (four electron reduction). In eukaryotes the respiratory chain is associated to the inner membrane of mitochondria and collects reducing equivalents mostly from oxidations occurring in the mitochondrial matrix. Most oxidizable substrates have redox potentials close to the midpoint potential of the  $\text{NAD}^+/\text{NADH}$  couple ( $E_{m7} = -320$  mV). Therefore, NADH is used to shuttle electrons from these substrates to the respiratory chain; a few oxidizable substrates, however, have midpoint potentials close to zero on the biochemists' scale, and their reducing equivalents must reach the respiratory chain at a site downstream energetically relative to the entry of electrons from NADH.

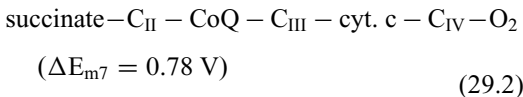
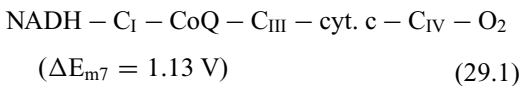
The free energy decrease accompanying electron transfer is exploited to create an electrochemical proton gradient ( $\Delta\tilde{\mu}_{\text{H}}^+$ ) by proton translocation from the mitochondrial inner space, the matrix, to the space existing between the inner and outer mitochondrial membranes (Nicholls and Ferguson 2013). The proton gradient is then used as a

---

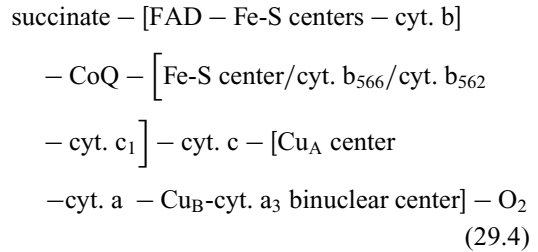
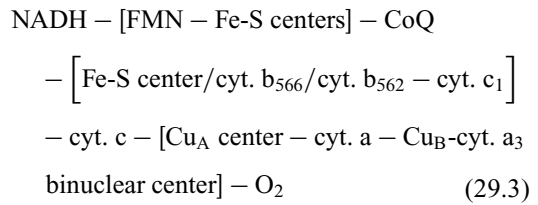
*Abbreviations:* AOX – Alternative oxidase; BHM – Bovine heart mitochondria; BN-PAGE – Blue-native polyacrylamide gel electrophoresis;  $\text{C}_I$  – Complex I, NADH-coenzyme Q reductase;  $\text{C}_{II}$  – Complex II, succinate-CoQ reductase;  $\text{C}_{III}$  – Complex III, ubiquinol-cytochrome c reductase;  $\text{C}_{IV}$ , COX – Complex IV, cytochrome c oxidase; CJ – Cristae junction; CL – Cardiolipin; CN-PAGE – Colorless-native polyacrylamide gel electrophoresis; Complex V – ATP synthase; CoQ – Coenzyme Q, ubiquinone; cyt. c – Cytochrome c;  $\Delta\tilde{\mu}_{\text{H}}^+$  – Electrochemical proton gradient; ETF – Electron transfer flavoprotein; FAO – Fatty acid  $\beta$ -oxidation; IM – Inner mitochondrial membrane; OM – Outer mitochondrial membrane; OXPHOS – Oxidative phosphorylation; PC – Phosphatidyl choline; PE – Phosphatidyl ethanolamine; R4B – Crude mitochondrial preparation enriched in complexes I and III; ROS – Reactive oxygen species

source of energy mainly to synthesize ATP from ADP and Pi by the ATP synthase complex: the overall process is called oxidative phosphorylation (OXPHOS). The ATP synthesized is moved to the cytoplasm in exchange with ADP by the ATP/ADP translocase at the expense of the proton gradient. Alternatively, the proton gradient is used to drive other energy-linked reactions such as NADH/NADP<sup>+</sup> transhydrogenation and up-hill ion movements across the inner membrane.

The classic electron transfer chain was first described by Hatefi et al. (1962a) in David Green's laboratory (cf. Green and Tzagoloff 1966, for a comprehensive review) as the functional sequence of four major multi-subunit complexes, randomly dispersed in the inner mitochondrial membrane, and designated as NADH-Coenzyme Q reductase (Complex I, C<sub>I</sub>), succinate-CoQ reductase (Complex II, C<sub>II</sub>), ubiquinol-cytochrome c reductase (Complex III, C<sub>III</sub>) and cytochrome c oxidase (Complex IV, C<sub>IV</sub>); the enzyme complexes are connected by two mobile redox-active molecules, i.e. a lipophilic quinone, designated Coenzyme Q (CoQ) or ubiquinone, embedded in the membrane lipid bilayer, and a hydrophilic heme protein, cytochrome c (cyt. c), localized on the external surface of the inner membrane (see Sect. 1.B for details). The chain functions in the following sequences, where  $\Delta E_{m7}$  is the change in redox potential between the initial electron donor and the final acceptor,



and in which several redox centers (Schemes 29.3 and 29.4) that are associated with the enzyme complexes allow electron transfer down the midpoint potential gradient:



The best fit unit stoichiometry between complexes in beef heart mitochondria is: 1 Complex I : 1.3 Complex II : 3 Complex III : 6.7 Complex IV (Schägger and Pfeiffer 2001). In addition, there are 0.5 ATP synthase (also called Complex V) and 3–5 units of the ADP/ATP translocase (catalyzing the equimolar exchange of ADP and ATP across the inner membrane) for each cytochrome oxidase, and there is one NADH/NADP<sup>+</sup> transhydrogenase per Complex I (Capaldi 1982). Nevertheless, wide differences in cytochrome, Coenzyme Q, and pyridine nucleotide contents of mitochondria from different species, as well as from different organs and tissues of the same species, have been reported (Lenaz and Genova 2010); data in the literature indicate that the molar ratios of the respiratory components vary significantly.

The inner membrane contains other proteins having electron transfer activity in smaller amounts (Lenaz and Genova 2010); among these there are electron transfer flavoproteins capable of feeding electrons to the respiratory chain by pathways not involving Complex I and/or NADH, i.e. glycerol-3-phosphate dehydrogenase, electron transfer flavoprotein (ETF)-ubiquinone oxidoreductase, dihydro-orotate dehydrogenase, choline dehydrogenase, in addition to alternative NADH dehydrogenases in mitochondria from several organisms, especially plants

and fungi. Moreover, alternative or branched pathways of electron transfer also occur, departing from CoQ: these are the alternative ubiquinol oxidases from bacteria and plant and fungi mitochondria.

### *B. Organization of the Respiratory Chain: Historical Outline*

The systematic resolution and reconstitution of four respiratory complexes from mitochondria was accomplished by Hatefi et al. (1962a), leading Green (Green and Tzagoloff 1966) to postulate that the overall respiratory activity is the result of both intra-complex electron transfer in the ‘solid’ state between redox components having fixed steric relation and, in addition, of inter-complex electron transfer ensured by rapid diffusion of the mobile components acting as co-substrates, i.e. CoQ and cyt. c. This proposal was substantially confirmed over the following years, leading to the postulation by Hackenbrock et al. (1986) of the *Random Collision Model of Electron Transfer*. The organization of the respiratory chain has represented a major research subject in the 1970–1980s, culminating with acceptance of the random collision model by the majority of investigators in the field.

The accumulation of recent experimental evidence obtained with newly developed techniques has replaced the random collision model of electron transfer, based on random interactions between randomly dispersed components, with a model of supramolecular organization based upon specific, though dynamic, interactions between individual components, and leading to the acquisition of new properties (substrate channeling, assembly, morphological organization) that were unpredictable in the previous reductionist approach.

A retrospective analysis of the literature reveals that the idea of supramolecular associations between respiratory enzymes has been present since the early times, dating from the original view derived from the pioneering studies of Chance and Williams (1955), who depicted the respiratory chain

as a solid-state assembly of flavins and cytochromes in a protein matrix.

Evidence against a random distribution of respiratory complexes was also derived from early investigations reporting isolation of Complex I–Complex III (Hatefi et al. 1962b) and Complex II–Complex III units (Yu et al. 1974), indicating that such units may be preferentially associated in the native membrane. The authors of the original studies were well aware that these preferential associations were physiological and indicated the existence of supramolecular units of electron transfer. Hatefi et al. (1962a) in their paper on the reconstitution of the electron transfer system stated that the four primary enzyme systems may be suitably combined to form secondary units capable of catalyzing the sums of the reactions catalyzed by the respective subunits. A careful examination of these pioneering papers allows one to conclude that respiratory supercomplexes, as well as the entire DPNH oxidase (the *respirasome*, see later) had been isolated and reconstituted. The appearance of the fluid mosaic model of membranes (Singer and Nicolson 1972) strongly influenced the researchers involved in the study of mitochondrial membranes, and this is probably the reason that the random collision model of Hackenbrock was so well and uncritically accepted.

There were, however, a few reports before the year 2000 on the possible presence of specific associations between respiratory complexes, either fixed (Ozawa et al. 1987) or dynamic (Hochman et al. 1985).

A breakthrough occurred in 2000 when Schagger applied the previously introduced technique of Blue-Native Polyacrylamide Gel Electrophoresis (BN-PAGE) to digitonin-solubilized yeast and mammalian mitochondria (Schagger and Pfeiffer 2000). The newly discovered associations were considered to represent the physiological state of the respiratory complexes and were called *respirasomes* (see Sect. II). In the same paper the authors also described a dimeric state for the ATP-synthase complex.

Today the evidence of supercomplex association of the respiratory chain is well

consolidated (Wittig and Schagger 2009; Lenaz and Genova 2010), although its possible relation with a random distribution of the individual complexes is not completely clarified (Genova and Lenaz 2013, 2014). This aspect will be widely discussed subsequently in this chapter.

## II. Distribution and Composition of Respiratory Supercomplexes

### A. Distribution in Different Organisms

BN-PAGE and the closely related though milder colorless native PAGE (CN-PAGE) are the preferred experimental strategy for the detection of the respiratory supercomplexes from various biological samples and for the analysis of their protein composition (Wittig et al. 2006; Krause and Seelert 2008) (Fig. 29.1).

Respiratory supercomplexes have been found in a wide range of living organisms; they were first discovered in yeast and mammalian mitochondria (Schagger and Pfeiffer 2000, 2001). They were subsequently revealed and characterized in several mammalian tissues, such as rat brain (Reifschneider et al. 2006; Dencher et al. 2007; Wernicke et al. 2010), liver (Lenaz et al. 2010; Dani et al. 2009; Reifschneider et al. 2006), kidney (Reifschneider et al. 2006), skeletal muscle (Reifschneider et al. 2006; Lombardi et al. 2009), and heart (Reifschneider et al. 2006; G3mez et al. 2009), in bovine heart (Schagger and Pfeiffer 2001; Schagger 2002; Krause 2006), in human skin fibroblasts (Kovarova et al. 2012; Miyake et al. 2013), human syncytiotrophoblast (De Los Rio Castillo et al. 2011) and human tumor cells (Genova et al. 2008) and in many other organisms, e.g., fish (Schafer et al. 2007a), fungi (Krause et al. 2004b; Marques et al. 2007; Maas et al. 2009; Nubel et al. 2009; Davies et al. 2011; Cabrera-Orefice et al. 2014), *Caenorhabditis elegans* (Brys et al. 2010), *Drosophila* (Le Pecheur et al. 2009), and also in plants (Eubel et al. 2004; Krause et al. 2004a; Genova

et al. 2008; Peters et al. 2008; Kakizaki et al. 2012), and many bacteria (Schagger 2002; Stroh et al. 2004; Krause 2006; Sousa et al. 2012, 2013).

### B. Composition of Respiratory Supercomplexes

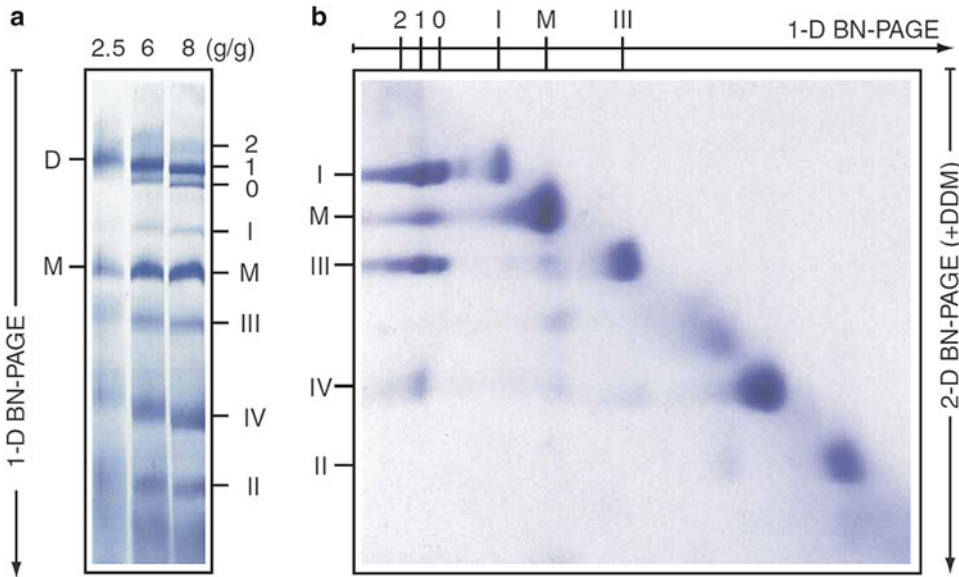
All the supercomplexes investigated exhibit highly ordered architectures, thus discarding most doubts on artificial protein-protein interactions, and supporting the idea that such interactions may also be species- or kingdom- specific (Vonck and Schafer 2009).

Most evidence presently favors the view that supercomplexes are formed by the three “core” complexes of the respiratory chain, i.e. Complexes I, III, and IV, whereas the other respiratory enzymes should be free in the lipid bilayer (Lenaz and Genova 2010). These “core” complexes have the common feature of carrying out proton translocation and of having subunits encoded by mitochondrial DNA.

In bovine heart mitochondria (BHM), only 14–16 % of total Complex I was found in free form in the presence of digitonin (Schagger and Pfeiffer 2001); thus, it seems likely that all Complex I is bound to Complex III in the absence of detergents. According to the stoichiometry of BHM OXPHOS complexes reported by Schagger and Pfeiffer (2001), it is plausible that approximately one-third of total Complex III and >85 % of total Complex IV are not bound in supercomplexes.

The fundamental features of the supra-molecular organization of the standard respiratory complexes I, III, and IV as a respirasome are conserved in all higher eukaryotes. The supercomplex I-III<sub>2</sub>-IV<sub>1.4</sub> is one of the most intriguing supercomplexes because it contains all the redox enzymes required for the complete pathway of electron transfer from NADH to molecular oxygen, and for this reason was called “*respirasome*”. However, supercomplexes containing only two partners are also present in detectable quantities, as the supercomplex I-III<sub>2</sub> in which Complex IV is not present, as well as respiratory assemblies comprising only Complex





**Fig. 29.1.** Separation of supramolecular assemblies of oxidative phosphorylation complexes by 1D BN-PAGE and identification of their constituent individual complexes by 2D BN/BN-PAGE. **(a)** Bovine sonic particles were solubilized by digonin using the indicated digonin/protein ratios (g/g). The solubilized complexes were separated by 1D BN-PAGE. I, II, III and IV indicate mitochondrial complexes I-IV. Bands 0, 1 and 2 indicate respiratory supercomplexes containing monomeric Complex I, dimeric Complex III and zero (0), one (1) or two (2) copies of Complex IV, respectively. M and D indicate monomeric (M) and dimeric (D) ATP synthase. **(b)** The lane for the digonin/protein ratio of 8 (g/g) excised from **(a)** was processed by 2D BN/BN-PAGE using 0.02 % dodecylmaltoside added to the cathode buffer. Respiratory supercomplexes were thereby disassembled into the individual constituent complexes I, III and IV (Reprinted from Wittig et al. (2006), with permission).

III and Complex IV. In particular, BN-PAGE in digonin-solubilized mitochondria of *S. cerevisiae*, which possesses no Complex I, revealed two bands with apparent masses of ~750 and 1000 kDa containing the subunits of complexes III and IV, as assigned after two dimensional SDS-PAGE followed by N-terminal protein sequencing (Schägger and Pfeiffer 2000). The smaller super complex ( $\text{III}_2\text{IV}_1$ ) consists of a Complex III dimer and a Complex IV monomer while the larger super complex ( $\text{III}_2\text{IV}_2$ ) is comprised of a Complex III dimer associated with two Complex IV monomers (Stuart 2008; Mileykovskaya et al. 2012).

Although Complex I is usually a monomer, a putative dimeric Complex I has also been described in mitochondria from *Neurospora crassa*, *Yarrowia lipolytica*, *Podospora anserina* and *Solanum tuberosum* where it may be involved in forming string-like and patch-like megacomplexes

composed of repeated units of respiratory supercomplexes (Krause 2006; Krause et al. 2004b; Bultema et al. 2009; Marques et al. 2007; Nübel et al. 2009) (see Sect. II.C).

A higher level of complexity in the organisation state of supercomplexes is due to the presence of further interaction partners such as the ADP/ATP carrier, some chaperones for cytochrome c oxidase (COX) assembly and the carbonic anhydrase subunits, which co-assemble with the OXPHOS supercomplexes (Stuart 2009; Mick et al. 2007; Sunderhaus et al. 2006). Several additional proteins are probably able to interact with cytochrome c oxidase, and some examples such as monocarboxylate transporters, mitochondrial nitric oxide synthase, and the large-conductance  $\text{Ca}^{2+}$ -activated  $\text{K}^+$  channel have already been identified by immunoprecipitation (Hashimoto et al. 2008; Persichini et al. 2005; Ohya et al. 2005). Recently it was

reported that mitochondrial superoxide dismutases associate with a documented respirasome (Suthammarak et al. 2013).

Wang et al. (2010) provided evidence for a multifunctional fatty acid  $\beta$ -oxidation (FAO) complex within mitochondria that is physically associated with supercomplexes. However, Schönfeld et al. (2010) could not find such an association (see Sect. IV.B.3.b).

It has been observed that several mitochondrial soluble  $\text{NAD}^+$ -dependent dehydrogenases such as malate dehydrogenase,  $\beta$ -hydroxyacyl-CoA dehydrogenase,  $\alpha$ -ketoglutarate dehydrogenase complex, and the pyruvate dehydrogenase complex specifically associate with Complex I (Sumegi and Srere 1984; Ovádi et al. 1994; Fukushima et al. 1989). However, their functional role remains controversial (Kotlyar et al. 2004).

The other respiratory enzymes not comprising the “core” of the proton translocation machinery appear not to be associated in supercomplexes (Lenaz and Genova 2010), although only Complex II has been investigated in some detail.

Association of Complex II with other complexes of the respiratory chain has not been identified thus far by BN-PAGE, except in a few cases (Acín-Pérez et al. 2008; Schönfeld et al. 2010). It was recently found that digitonin-solubilised Complex II quantitatively forms high molecular weight structures that can be resolved by CN-PAGE (Kovářová et al. 2013). These structures are enzymatically active and differ in electrophoretic mobility between tissues (500–over 1000 kDa) and cultured cells (400–670 kDa). Complex II has been proposed to be a candidate for physiological association with Complex III (Yu et al. 1974; Gwak et al. 1986).

Mitochondrial glycerol phosphate dehydrogenase has been suggested not to be associated in a supercomplex on the basis of functional studies (Rauchová et al. 1992). This absence has been confirmed in the respirasome, although the enzyme was found to associate in the form of homo-oligomers (Mráček et al. 2014). According to Hildebrandt (2011), sulfide-quinone oxidoreduc-

tase and sulfite oxidase, the two membrane bound enzymes of the pathway catalyzing sulfide oxidation, which transfer electrons into the respiratory chain, might also be associated with a supercomplex in vivo.

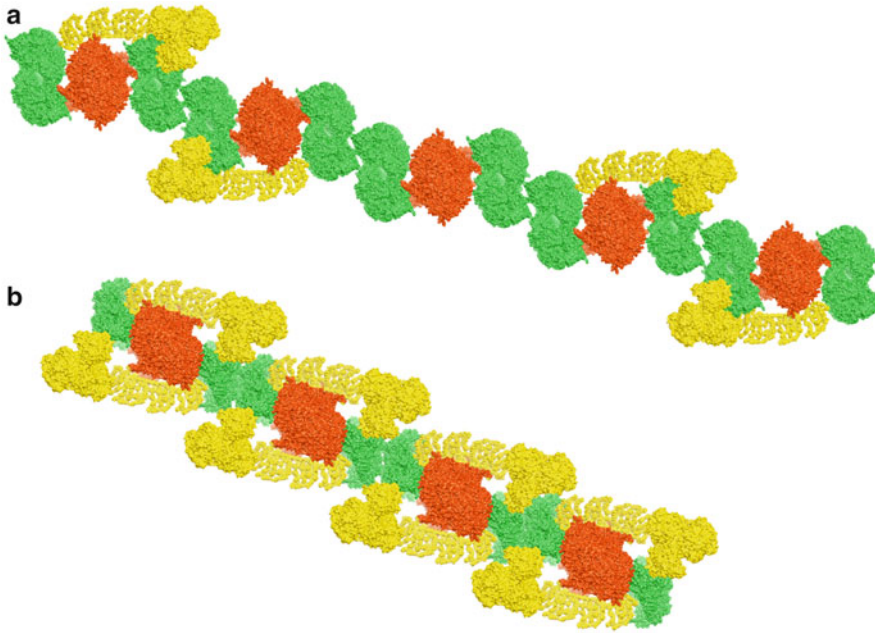
### C. Megacomplexes or Respiratory Strings

It has been postulated that the assembly of respiratory complexes into supercomplexes is just the first step in the formation of much larger supramolecular structures called *respiratory strings* or *megacomplexes*.

The model of respiratory strings proposed by Wittig et al. (2006) envisions a linear aggregate of alternating Complex III homodimers and Complex IV tetramers, with Complex I bound to some of these units. The existence of these assemblies was demonstrated as the isolation by large pore BN-PAGE of very high mass (35–45 MDa) assemblies of Complex I, III, and IV in bovine heart mitochondria (Strecker et al. 2010). These higher assemblies can be split into individual Complex I, III, and IV complexes under 2D BN/BN-PAGE with dodecylmaltoside, allowing the identification of tetrameric Complex IV and showing the lack of oligomeric Complex I and Complex III. According to Wittig et al. (2006), this evidence suggests a specific and ordered association of these complexes as core pieces of respiratory strings and not random aggregates of respiratory supercomplexes (Fig. 29.2a).

Bultema et al. (2009) postulated a model based on a single-particle electron microscopy of potato mitochondria supercomplex  $\text{I}_2\text{III}_2$  consisting of two copies of Complex I bound to both sides of a Complex III homodimer (Fig. 29.2b). The model string has a basic unit of Complex III dimer with a Complex I and Complex IV bound to either side, and the contacts are formed by Complex IV dimers.

It is noteworthy that ATP synthase and Complex I occupy different regions of the mitochondrial cristae (Davies et al. 2011). In particular, ATP synthase forms



*Fig. 29.2.* Hypothetical models for a higher organization of respiratory chain complexes (respiratory strings). The model for bovine heart mitochondria in (a) is built from a linear combination of  $I_1III_2IV_4$  and  $III_2IV_4$  supercomplexes, connected via complex IV tetramers, as described by Wittig and Schägger (2009). The model for potato mitochondria in (b) is based on the discussion in Bultema et al. (2009) and consists of  $I_2III_2IV_2$  supercomplexes, connected via Complex IV dimers. Complex I is shown in *yellow*, III in *orange*, IV in *green* (Reprinted from Vonck (2012), with permission).

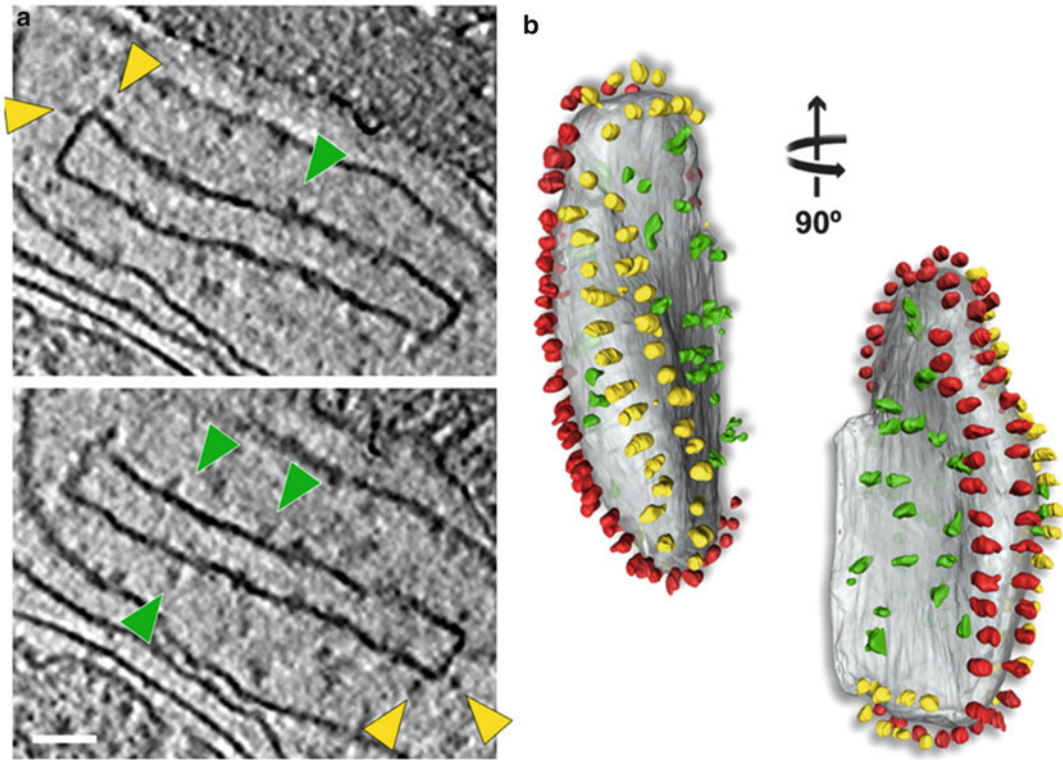
rows of dimers at the cristae tips, whereas the proton pumps of the electron transfer chain reside predominantly on the flat surface of the adjacent membrane regions (Fig. 29.3). The possible correlation between oligomeric rows of ATP synthase and the morphology of the mitochondrial cristae is debated (Habersetzer et al. 2013); electron microscopic studies have shown that the membrane domains of the two partners in the ATP synthase dimer are at an angle to each other, indicating that *in vivo* the dimers would cause the membrane to bend (Vonck and Schäfer 2009; Chaban et al. 2014). Interestingly, in tomographic reconstructions of mitochondria from some organisms as bovine, yeast and *Arabidopsis*, it is difficult to observe oligomeric chains of dimeric ATP synthases, but the green alga *Polytomella* is an exception to the rule. The tubular cristae of *Polytomella* appear fully covered by oligomeric rows of ATP synthases, suggesting that the other OXPHOS enzymes might be arranged in between, but these

can not be easily visualized due to the tight packing of ATP synthases (Dudkina et al. 2010). Few attempts have been made to correlate physiological processes to a potential regulation of the ATP synthase oligomerization. Profound age-dependent changes can be observed in membrane architecture; with increasing age, the typical cristae disappear and the inner membrane vesiculates, the ATP synthase dimers that form rows at the cristae tips dissociate into monomers in inner-membrane vesicles, and the membrane curvature at the ATP synthase inverts (Daum et al. 2013).

### III. Structure of Supercomplexes

#### A. Molecular Structure by Electron Microscopy and Modeling

Supercomplexes can be isolated in their active form after mild detergent solubilization (Stroh et al. 2004; Braun et al. 2009). Partial



**Fig. 29.3.** Isolated vesicle from *P. anserina* cristae. **(a)** Two tomographic slices of the same *box-shaped* cristae vesicle showing ATP synthase dimers at approximately  $90^\circ$  bends in the membrane (*yellow arrowheads*) and Complex I densities (*green arrowheads*) in flat membrane regions of the vesicle. **(b)** Segmented surface representation. Two rows of ATP synthase dimers (*yellow and red*) in the membrane (*gray*) run along the  $90^\circ$  membrane ridges. Irregularly distributed particles of Complex I or other respiratory chain complexes (*green*) are confined to flat membrane regions. Scale bar, 50 nm (Reprinted from Davies et al. (2011), with permission).

elucidation of the interaction of the individual respiratory complexes within the supercomplex was achieved by single-particle electron microscopy.

Shortly after the first 2D electron projection maps of a supercomplex  $I_1III_2$  from *Arabidopsis* (Dudkina et al. 2005), Schäfer et al. (2006, 2007b) provided initial insights into the shape and size of two respiratory chain supercomplexes isolated from bovine heart mitochondria ( $I_1III_2$  and  $I_1III_2IV_1$ ), whose composition was confirmed by peptide mass fingerprinting.

More recently, new 3D maps at nanoscale resolution allowed interpretation of the architecture of plant and mammalian supercomplexes at the level of secondary structure, confirming the lateral association of dimeric Complex III with the membrane

arm of Complex I, while Complex IV, when present, interacts with the distal portion of the same arm. In the new model by Dudkina et al. (2011), the single complexes I,  $III_2$  and IV appear to be at some distance in the bovine respirasome, suggesting that there is little close contact. In particular, the section through the model on the level of the membrane demonstrates gaps between complexes  $III_2$  and IV within the membrane, whereas the same two complexes appear to contact each other in their matrix portions close to the membrane.

Althoff et al. (2011) also proposed that only few points of direct contact are allowed between the three complexes in the mammalian supercomplex  $I_1III_2IV_1$  because average distances between the individual complexes exceed 2 nm. Moreover, at 19

Å resolution the membrane-embedded part of the supercomplex shows intermediate values of density between that of the soluble protein and the hydrophobic membrane interior, suggesting that the supercomplex is held together at least partly by lipid-protein interaction. A gap filled with membrane lipid might also facilitate the diffusion of CoQ between Complex I and Complex III. It is interesting to note that the CoQ-binding sites in Althoff's model are conveniently placed for the efficient electron transfer between Complex I and the proximal Complex III monomer over a short distance of about 13 nm to be covered by CoQ. It is proposed that the proximal monomer may be more effective in ubiquinol oxidation, while the distal one may be needed to transfer the electron to cytochrome *c* via its flexible Rieske domain, in accordance with the half-of-the-sites reactivity model of Complex III (Castellani et al. 2010). Furthermore, a trajectory of 10 nm is envisaged in the respirasome along which cytochrome *c* may travel to shuttle electrons towards Complex IV (Fig. 29.4).

In agreement with the results of Althoff et al. (2011), three-dimensional density maps of yeast supercomplexes by electron cryo-microscopy show gaps between the transmembrane-localized interfaces of individual complexes consistent with the large excess of cardiolipin in supercomplexes compared to that integrated into the structure of individual respiratory complexes (Mileykovskaya et al. 2012; Mileykovskaya and Dowhan 2014) (cf. Sect. III.B.3).

It has to be borne in mind that, beside the lack of a high resolution crystal structure of the mammalian Complex I, several uncertainties are still present in the interpretation of the 3D maps: for example, there are additional density areas that cannot be filled by the current structural models of complexes III and IV, suggesting that additional proteins may participate in the supercomplexes. This is the case of SCAFI, a recently reported protein required for the super-assembly of complexes III and IV that is not present in the free complexes (Lapuente-Brun et al. 2013), or of the reassignment of NDUF4A as a structural subunit of Complex IV not present in the x-ray structure (Balsa et al. 2012).

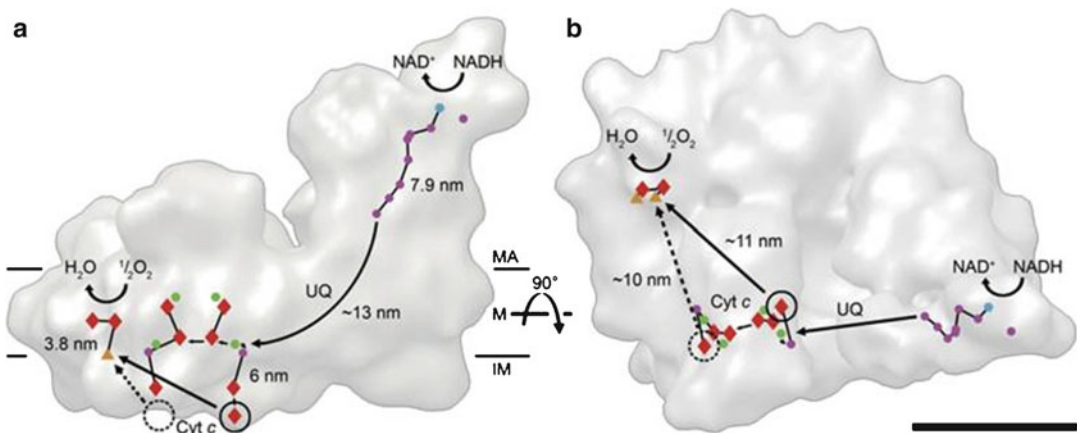


Fig. 29.4. Electron transfer pathways in the supercomplex. Outline of the supercomplex with cofactors active in electron transport marked in *blue* (FMN), *purple* (iron–sulfur-clusters), *green* (quinols/stigmatellins), *red* (hemes) and *orange* (copper atoms), seen from the membrane (a) and from the matrix (b). Electron trajectories are marked in *black*. The *dashed circle* marks the distal cytochrome *c* binding site, which is unoccupied in the supercomplex. *Straight arrows* in (a) indicate the shortest distances from the cytochrome *c* binding sites on complex III to the site of cytochrome *c* oxidation in complex IV. The shorter, proximal branch may be preferred for electron transport. MA matrix, M membrane, IM intermembrane space, UQ ubiquinol, Cyt *c* cytochrome *c*. Scale bar, 10 nm (Image taken from Althoff et al. (2011) and reprinted by permission from Macmillan Publishers Ltd, copyright 2011).

### B. Lipid Content and Composition

Lipids are essential determinants of supercomplex association (Lenaz and Genova 2007). However, they can modify the nature and extent of the associations only in long time-scales, since their metabolism is affected by the organism species, by the tissue and, within a given tissue and species, by diet and life style.

#### 1. Lipid Composition of Mitochondria

Mitochondria from different cell types have high protein to lipid ratios, as a consequence of the high protein density of the inner membrane (Horvath and Daum 2013), that had been recognized since the early studies (Fleischer et al. 1967). The major phospholipids, accounting for about 80 % of total phospholipids, are phosphatidyl choline (PC) and phosphatidyl ethanolamine (PE). A distinctive feature of mitochondria is the high diphosphatidyl glycerol or cardiolipin (CL) content, in the range of 15–20 %. Phospholipids are not evenly distributed in the inner (IM) and in the outer (OM) mitochondrial membrane nor across their lipid bilayers but rather arranged asymmetrically (Horvath and Daum 2013). Sterols and sphingolipids are only found at low amounts. In different mammalian cells and tissues, the mitochondrial lipid composition is more or less identical. Mitochondria from heart, brain, kidney, adrenal cortex and spleen contain PC and PE plasmalogens in the range of 5–30 % of total phospholipids. Plasmalogens are a class of phospholipids carrying a vinyl ether bond in the *sn-1* and an ester bond in the *sn-2* position of the glycerol backbone. This structure leads to strong lipophilic properties and allows plasmalogens to form inverse hexagonal phase structures. Marine bivalves have considerable amounts of plasmalogens (Kraffe et al. 2004).

Ectotherms tend to have more monounsaturated membranes (lipids with fatty acids with only one C=C) than endotherms of the same size and body temperature (Else et al. 2004).

Decreasing the environment temperature induces fatty acid changes in membrane lipids that have been proposed to help maintaining the fluidity of cellular membranes (*homeoviscous adaptation* (Sinensky 1974)), including mitochondria (Cossins et al. 1980), by producing a generally higher degree of unsaturation (Nozawa 2011).

A unique modification is the presence of non-methylene-interrupted unsaturated fatty acids and branched fatty acids in marine bivalves (Kraffe et al. 2004).

#### 2. Roles of Mitochondrial Lipids

Lipids, and specifically phospholipids, are required for the activity of membrane-bound enzymes (Green and Fleischer 1963; Lenaz 1979). This is achieved in part by a mere dispersive solubilization effect that can be duplicated by appropriate detergents; moreover, lipids are believed to confer on membrane proteins the correct conformation for optimal activity (Lenaz 1979, 1987; Hunte and Richers 2008) and a correct template for membrane protein topogenesis (Dowhan and Bogdanov 2009). In addition, lipids have a specific catalytic effect that is mostly fulfilled by cardiolipin (Vik and Capaldi 1977; Fry and Green 1980, 1981; Robinson et al. 1980; Lee 2004; Wenz et al. 2009). Furthermore, in mitochondria, phospholipids provide a sufficiently lipophilic environment for the interaction of the lipophilic electron carrier, ubiquinone (Lenaz 1988). A further role of lipids is to participate in linking together the protein components of the membrane.

CL differs from all other phospholipids by its dimeric structure, with two headgroups carrying two negative charges and four fatty acyl chains. The fatty acid composition of CL is peculiar (Mileykovskaya et al. 2005; Paradies et al. 2014b): in animals and higher plants, CL almost exclusively contains polyunsaturated linoleic acid (C18:2), while in yeast *S. cerevisiae* there are 16 and 18 monounsaturated chains. CLs in bacteria contain monounsaturated and saturated fatty acids with 14–18 carbons.

It is worth noting that newly synthesized CL contains primarily saturated fatty acids, but CL fatty acyl chains are remodeled in mature CL by phospholipid transacylation in mammalian and yeast cells by a transacylase denominated *tafazzin* (Bogdanov et al. 2008; Baile et al. 2014a, b; Mejia et al. 2014; Horvath and Daum 2013). Although *tafazzin per se* promotes random fatty acyl replacements, it is the physical state of the lipid substrates that provides specificity to the transacylation process (Schlame et al. 2012). Both the precursor phosphatidic acid and mature CL are distributed between the different mitochondrial compartments by the action of protein factors, among which apoprotein O-like (APOOL) (Koob and Reichert 2014) demonstrates a role of CL in determining cristae morphology.

Although CL has two phosphate groups, it is not fully ionized at physiological pH due to intra-molecular hydrogen bonding between the free hydroxyl of the central glycerol and a protonated phosphate (Kates et al. 1993). Due to the four acyl chains and a small headgroup, CL can organize into domains, which have the potential to serve as a proton sink in membranes particularly when in close proximity to OXPHOS complexes that generate and consume  $\Delta\tilde{\mu}_{\text{H}}^+$  (Haines and Dencher 2002). Being a dimeric lipid, CL can serve as a “flexible linker”, which fills cavities at protein interfaces and thus stabilizes interactions between individual subunits of oligomeric proteins as well as between multi-subunit individual complexes organized into supercomplexes (Hunte 2005; Bogdanov et al. 2008; Mileyskoykaya and Dowhan 2009; Schlame et al. 2000; Houtkooper and Vaz 2008) (Sect. III.B.3). The ubiquitous and intimate association between CL and energy-transducing membranes suggests an important role for CL in mitochondrial bioenergetic processes (Mileyskoykaya et al. 2005; Paradies et al. 2009, 2014a).

Indeed, CL is required for optimal activity of complexes I, III, IV, and V. Crystallographic studies have shown the presence of a few tightly bound CL molecules in each of the crystal structures of Complex III (Lange et al. 2001; Hunte 2005), Com-

plex IV (Ozawa et al. 1982; Shinzawa-Itoh et al. 2007), and ADP/ATP carrier (Pebay-Peyroula et al. 2003). These results suggest that CL is an integral component of these proteins, the presence of which is critical to protein folding and function. In Complex III, one CL molecule resides at the Qi site (the inner site where CoQ is reduced in the Q-cycle mechanism) suggesting direct involvement of CL in proton uptake at the ubiquinone reduction site. A second CL was found in the hydrophobic cleft close to the homodimer interface of Complex III (Hunte 2005). Two CLs were resolved in Complex IV (Shinzawa-Itoh et al. 2007). A third CL, found by photolabeling with arylazido-containing CL analogues (Sedlák et al. 2006), is located near the entrance to the putative proton pumping channel of Complex IV and thus might facilitate proton entry into the channel.

CL is also observed in the crystal structure of *R. sphaeroides* reaction center, where one CL molecule stabilizes two membrane-spanning  $\alpha$ -helices of the M polypeptide (Fyfe and Jones 2005), in *E. coli* succinate dehydrogenase (Yankovskaya et al. 2003), formate dehydrogenase-N (Jormakka et al. 2002) and cytochrome c (Musatov et al. 2013; Muenzner and Pletneva 2014).

### 3. Lipids and Supercomplex Stabilization

The forces responsible for supercomplex association strongly depend on the lipid content and composition and likely on the shape of the inner mitochondrial membrane (Lenaz and Genova 2007).

At low protein concentrations in lipid bilayers, proteins are usually randomly dispersed (Lee 2004), whereas at high concentrations they tend to aggregate. The forces involved in protein aggregation are both of entropic and enthalpic origin.

Lipid-mediated protein-protein interactions originate by hydrophobic mismatch: the same reasons inducing the formation of a lipid annulus to compensate for the mismatch by attracting the lipids having the best fit would be operative by attracting

together proteins having mismatch of the same sense (Bloom et al. 1991). For the same reason, however, proteins having hydrophobic mismatch of opposite sense should repel each other (Gil et al. 1998).

In the mitochondrial inner membrane, integral proteins of the OXPHOS system are densely packed so that the average distance between complexes may be calculated to be few nanometers (Lenaz 1988). Thus, the presence of protein aggregates of the transmembrane respiratory complexes would not be unexpected on theoretical grounds. Changing the nature of the lipids would dramatically change their matching conditions to the proteins. This could be due to presence and number of electrostatic charges, different lengths of the fatty acyl chains, and of physical state and phases existing at the body temperature. Lipid peroxidation removes *cis* double bonds from the fatty acyl chains, inducing profound biophysical changes in the lipid bilayer (Stark 2005), such as increased disorder and possible breakdown of membrane structure and of lipid-protein interactions (Megli and Sabatini 2003), and presumably affecting the membrane thickness. Therefore, a change in membrane protein aggregation induced by lipid peroxidation can be expected on theoretical grounds.

Since the integral membrane proteins are not fully deformable entities, their insertion in a lipid bilayer can distort the shape of the membrane locally; the lowest energy would be achieved in a system able to induce the least possible mismatch of the protein with the acyl chains in the surrounding lipid domain of *boundary lipids* or *annular lipids* (Jost et al. 1973; Hesketh et al. 1976). The lipid annulus is not a static entity, but rather a dynamic one, where the exchange of lipid molecules with the surrounding bulk phase is very fast (Marsh and Horvath 1998). The annular lipids must not be confused with those lipids that are usually detected in high-resolution crystal structures of membrane proteins and defined *non-annular* or *cofactor lipids* (Lee 2004) (see Sect. III.B.2). In particular, the studies by Ragan (Ragan and

Heron 1978; Heron et al. 1978) and Genova et al. (2008) have shown that reconstitution of a binary I/III mitochondrial protein fraction (R4B) at a high lipid to protein ratio (>10:1) prevents formation of the I-III supercomplex. Thus, it appears that dilution of the proteins with an excess of phospholipids may weaken the forces holding together the respiratory complexes.

Among the lipids, CL and PE are both non-bilayer-forming phospholipids, due to their small polar heads compared with the bulky nonpolar tails (Van den Brink-van der Laan et al. 2004; Osman et al. 2011). The phospholipids in closest vicinity to the protein surface, as well as those in the free bilayer, are highly mobile and free to exchange, but CL is tightly bound being more likely buried within the protein complexes, as in Complex IV and Complex III (Kang et al. 1979; Lange et al. 2001).

The structural studies of the purified mammalian and yeast respiratory supercomplexes by single particle cryoelectron microscopy (Althoff et al. 2011; Mileykovskaya et al. 2012) and cryoelectron tomography (Dudkina et al. 2011) (see Sect. III.A), resulting in three-dimensional density maps of atomic models for these structures, showed the presence of spaces between transmembrane domains of individual complexes which may be filled with phospholipids and suggested that CL may be an essential component for the assembly of supercomplexes.

Further evidence concerning this subject has been collected for the III<sub>2</sub>-IV<sub>2</sub> supercomplex in yeast mutants lacking CL (Pfeiffer et al. 2003; Zhang et al. 2002; Mileykovskaya et al. 2005). The putative direct protein-protein interaction of cytochrome oxidase and Complex III in yeast is proposed to involve also one molecule of CL and one of PE, tightly bound in a cavity of the membrane imbedded domain of Complex III (Lange et al. 2001). It has been suggested that these two phospholipids can provide a flexible linkage between the interacting subunits of Complexes III and IV as well as with the ADP/ATP carrier that is also known to exist in physical association with the III-IV



supercomplex (Claypool et al. 2008). Site-directed mutagenesis investigations (Wenz et al. 2009) indicated that CL stabilizes supercomplex formation by neutralizing the charges of lysine residues in the interaction domain of Complex III with cytochrome c oxidase.

In addition, the stability and assembly of Complex IV was found to be reduced in yeast cells lacking Taz1 (Brandner et al. 2005; Li et al. 2007), the orthologue of human Tafazzin, the acyl transferase involved in the maturation of CL (see previous section).

Mutations of Tafazzin in humans result in Barth syndrome, a cardio-skeletal myopathy with neutropenia, characterized by respiratory chain dysfunction. Patient mitochondria display lower CL content and a polydispersity in acyl chain composition of CL (Schlame and Ren 2006). BN-PAGE reveals an increase in free CIV monomer and a decrease in the supercomplex I<sub>1</sub>III<sub>2</sub>IV<sub>1</sub> in patient lymphocytes (McKenzie et al. 2006). In a pluripotent stem cell model system of this disorder Dudek et al. (2013) found an impaired remodeling of CL, a dramatic decrease in basal oxygen consumption rate, and in the maximal respiratory capacity; BN-PAGE analyses revealed that decreased respiration coincided with dramatic structural changes in respiratory chain supercomplexes leading to a massive increase in generation of reactive oxygen species.

Significantly, the CL defect in Barth syndrome results in destabilization of the supercomplexes by weakening the interactions between respiratory complexes (McKenzie et al. 2006). Gonzalez et al. (2013) confirmed that in immortalized lymphoblasts from Barth's syndrome patients the amount of supercomplexes is decreased, as well as the amount of individual complexes I and IV; these changes were compensated by increasing mitochondrial mass.

A recent study from Claypool's group (Baile et al. 2014b) confirmed the absolute requirement for CL, although changes in fatty acid composition did not affect mitochondrial morphology and oxidative phosphorylation, concluding that the mi-

tochondrial changes in Barth's syndrome are not due to changes of fatty acid composition, but are probably the result of accumulation of lysoCL and/or the concomitant decrease of fully acylated CL.

The dependence on CL for supercomplex formation was clearly demonstrated in a study by Bazán et al. (2013). By employing a system composed of purified CIII and CIV from *S. cerevisiae* and liposomes of different phospholipid composition, these authors demonstrated, for the first time, the reconstitution of the supercomplexes III<sub>2</sub>IV<sub>1</sub> and III<sub>2</sub>IV<sub>2</sub> from individual CIII and CIV in proteoliposomes and specific dependence of III<sub>2</sub>IV<sub>2</sub> formation on liposomes containing CL in strong preference over other phospholipids.

It is well documented that exposure of mitochondria to reactive oxygen species (ROS) can affect the respiratory activity via oxidative damage of CL, which is required for the optimal functioning of the enzyme complexes (Paradies et al. 2000, 2002; Petrosillo et al. 2003), reviewed by Paradies et al. (2010, 2014a). Genova et al. (2008) demonstrated by flux control analysis that the maintenance of a I-III supercomplex in proteoliposomes is abolished if lipid peroxidation is induced by 2,2'-azobis-(2-amidinopropane) dihydrochloride before reconstitution. Evidently, the distortion of the lipid bilayer induced by peroxidation and the alteration of the tightly bound phospholipids determine dissociation of the supercomplex originally present in the preparation.

### C. Biogenesis of Respiratory Supercomplexes

Acín-Pérez et al. (2008) performed pulse-chase experiments, labeling the 13 mtDNA-encoded proteins from cultured mouse cells, and analyzing the time course of their incorporation into respiratory complexes and supercomplexes by 2D electrophoresis.

The labeling of large supercomplexes showed a different pattern depending on whether or not they contained Complex IV. Thus, supercomplexes I/III appear labeled

as soon as after a 0.5 h chase. On the contrary, no labeling of supercomplexes I/III/IV was observed after a 0.5 and 2 h chase despite the fact that fully assembled Complex IV already could be observed. The labeling of the supercomplexes did not reach the characteristic pattern until after a 12 h chase. These results support the idea that supercomplexes are structures formed by the specific and ordered association of previously assembled individual complexes (Acín-Pérez et al. 2008).

The existence of protein factors that regulate the assembly of the different respiratory complexes into respirasomes is fully compatible with this model. A number of independent reports recently described two related *S. cerevisiae* proteins (renamed as Rcf1 and Rcf2) that might be important for the assembly between complexes III and IV (Chen et al. 2012; Strogolova et al. 2012; Vukotic et al. 2012; Shoubridge 2012). Rcf1 is a member of the hypoxia inducible gene 1 (HIG1) family, and it has at least two mammalian orthologs, HIG1A and HIG2A. Human HIG2A partially suppressed the phenotype caused by deletion of the yeast Rcf1 (Vukotic et al. 2012), and siRNA-mediated knockdown of the murine homolog of HIG2A resulted in a decrease in supercomplexes containing CIV (Chen et al. 2012), suggesting that the mammalian protein is also important in stabilizing CIV-containing supercomplexes. According to Acín-Peréz and Enriquez (2014), however, the role of HIG2A in supercomplex assembly seems to be marginal, and these factors can therefore be understood as being required for Complex IV function rather than specific supercomplex assembly factors.

In contrast, SCAFI, a recently described protein factor that is required to allow the integration of Complex IV into supercomplexes (Lapiente-Brun et al. 2013), modulates the interaction between Complex III and IV without affecting their assembly or stability, and is thus a true supercomplex assembly factor (Lapiente-Brun et al. 2013).

Moreno Lastres et al. (2012) proposed a different path for supercomplex formation.

After depleting cells of OXPHOS complexes by treatment with doxycycline, an inhibitor of mitochondrial translation, they followed complex and supercomplex assembly by BN-PAGE and immunodetection of individual proteins as markers of the overall complexes or subcomplexes. This analysis led them to propose that biogenesis of the respirasome involves the coordinated and sequential association of specific combinations of partially assembled respiratory complexes and free subunits. This model has major implications because it concludes that Complex I cannot be fully assembled nor catalytically active in the absence of Complex III and/or IV. In other words, the respirasome assembly is intimately linked to Complex I assembly and function.

The latter model cannot explain the normal assembly, stability and functionality of Complex I in cells lacking Complex IV (Balsa et al. 2012) and Complex III (Diaz et al. 2012a) in different culture conditions (Enríquez and Lenaz 2014). Nor can it explain either the stability or function of Complex I in fungi that lack Complex III and IV but naturally respire by an alternative oxidase (AOX) (Maas et al. 2009).

Recently, Davoudi et al. (2014) used a transgenic mouse model with decreased expression of BCS1L leading to loss of the Rieske protein of Complex III. In young healthy homozygous mutant mice, liver mitochondria had normal supercomplexes as in wild type; in the same aged mice that had developed hepatopathy, the main supercomplex contained Complex III in a pre-complex form lacking the Rieske protein. No disassembly of Complex I was evident in this model in which ROS generation was not enhanced, supporting the conclusions of Diaz et al. (2012b) that Complex I disassembly in the absence of active Complex III is the result of ROS damage (see Sect. IV.E).

Besides the above mentioned assembly factors required for the biogenesis and assembly of the supercomplexes, to our knowledge one more protein has been recently described that may be involved in the reversible regulation of supercomplex

association and activity: Hatle et al. (2013) identified MCJ/DnaJC15 as a distinct co-chaperone that localizes at the mitochondrial inner membrane, where it interacts preferentially with Complex I and functions as a negative regulator of the respiratory chain by impairing the formation of supercomplexes.

It is also worth mentioning that genetic ablation or overexpression of OPA1 with consequent disorganization of the cristae structure of the inner mitochondrial membrane can affect assembly and activity of supercomplexes (Cogliati et al. 2013).

#### IV. Functions of Respiratory Supercomplexes

There is now extensive evidence that supercomplexes are not artifacts due to detergent-induced associations, but are present physiologically and have a definite function, providing several physiological advantages.

##### A. Respiratory Supercomplexes are Functional

The supercomplexes were found to possess the in-gel activities of the individual complexes (Schägger and Pfeiffer 2000, 2001). However, the first demonstration that they are indeed functional and capable of full activity came from the chromatographic isolation of a functional respirasome from *P. denitrificans* (Stroh et al. 2004). The respirasome contained complexes I, III, and IV in a fixed stoichiometry, was enriched in CoQ with respect to the original membrane, but was considerably deficient in cytochrome  $c_{552}$ ; for this reason, although the activity of NADH cytochrome c reductase was close to that expected from the rate-limiting activity of Complex I, the whole NADH oxidase was strongly impaired with respect to the expected rate.

The respiratory activity of a respirasome isolated from mammalian mitochondria was reported by Acín-Pérez et al. (2008) who performed an extensive study on isolated mouse liver mitochondria and mitochondria

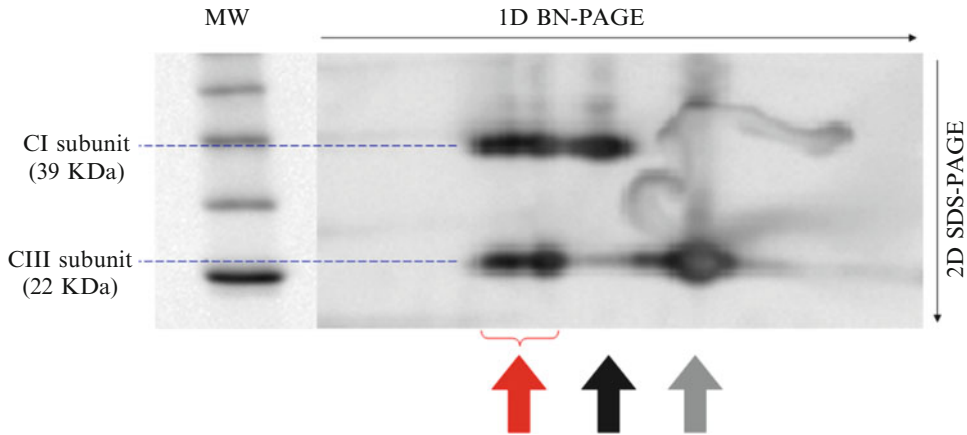
from mouse fibroblast cell lines. They demonstrated that BN-PAGE bands containing both CoQ<sub>9</sub> (the major CoQ homologue in rodents) and cytochrome c showed complete NADH oxidase activity, as measured using a Clark electrode, whereas a mixture of the bands of the individual complexes I, III, and IV, was inactive. In contrast to previous studies, some bands of supercomplexes also contained Complex II and ATP synthase and showed full respiratory activity from succinate that was sensitive to the specific respiratory inhibitors of all involved complexes. It is, however, possible that co-migrations of complexes II and V are due to overlapping and not to real associations.

A crude mitochondrial preparation (R4B) containing complexes I and III (Hatefi and Rieske 1967) is largely in the form of supercomplex I-III, as shown by BN-PAGE (Fig. 29.5), and exhibits high NADH-cytochrome c reductase activity, demonstrating that the isolated supercomplex is fully functional (Maranzana et al. 2013).

These findings directly confirm that supercomplex organization is compatible with electron transfer; however, it does not exclude the idea that electron transfer is still possible in the membrane in the absence of supercomplex organization, in accordance with the random collision model (see Sect. IV.B.1.a).

##### B. Kinetic Advantage

Immediately after the discovery of supercomplexes it was proposed that the natural consequence of such assemblies is substrate channeling or enhanced catalysis in inter-complex electron transfer. Substrate channeling is the direct transfer of an intermediate between the active sites of two enzymes catalyzing consecutive reactions (Ovádi 1991); in the case of electron transfer, this means direct transfer of electrons between two consecutive enzymes by successive reduction and reoxidation of the intermediate without its diffusion in the bulk medium. In such a case, inter-complex electron transfer becomes indistinguishable



*Fig. 29.5.* Respiratory supercomplexes and complexes from a crude mitochondrial fraction (R4B) enriched in Complex I and Complex III. The digitonin-solubilized R4B sample (detergent to protein ratio 8:1 w:w) was separated by 2D-BN/SDS-PAGE and resolved by Western blotting followed by immunodetection using monoclonal antibodies (MitoSciences, Inc., Eugene, OR; available for sale through Abcam) specific for single respiratory subunits as follows: NDUFA9 (39 kDa) of Complex I and Rieske protein (22 kDa) of Complex III. Arrows point to monomeric Complex I (*black*), dimeric Complex III (*gray*), and high molecular weight supercomplexes (*red*) containing both Complex I and Complex III.

from intra-complex electron transfer, so that the so-called mobile intermediates, predicted to exhibit substrate-like behavior in the classic view of the random collision model, function more efficiently when buried in the interface between the two consecutive complexes (Lenaz and Genova 2007).

The mechanism of electron transfer in supercomplexes is still uncertain. Ideally, we should have a detailed knowledge of the molecular structure and/or distances of the interacting sites, and this knowledge is still lacking. The extreme models are i) close docking of the active sites with real inter-protein tunneling, up to relatively long distances that may be covered either by important conformation changes, or ii) restricted diffusion (microdiffusion) of the “mobile” components within the space between the two active sites. All of these alternatives have in common obligate channeling between two fixed sites, so that even the last mechanism, microdiffusion, would be quite distinguishable from pool behavior of CoQ or cyt. c. In the latter case, the interaction of the mobile component may stochastically occur with a great number of possible sites located on several different protein targets

which can be reached by random diffusion (Genova and Lenaz 2011). In the interaction between Complex I and Complex III within a supercomplex, if the sites are connected by CoQ microdiffusion, it is possible that it takes place within a lipid milieu, although we cannot exclude that the sites are put together by movement of CoQ on the protein or by movement of the protein itself.

Some evidence for possible channeling comes from the 3D structure of the mitochondrial supercomplex  $I_1III_2IV_1$  described by Althoff et al. (2011); a unique arrangement of the three component complexes indicates the pathways along which ubiquinone and cytochrome c can travel to shuttle electrons between their respective protein partners (cf. Sect. III.A). In the model of Althoff et al (2011), one of the Complex III monomers faces the lipid bilayer while the other is surrounded by Complex I. Therefore, Coenzyme Q is likely to run a trajectory through a 13 nm gap within the membrane core of the supercomplex which is presumably filled with membrane lipids. It was estimated that approximately 300 lipid molecules would fit the gap that extends between complexes I, III, and IV on the level

of the membrane-embedded portion of the supercomplex (Althoff et al 2011; Dudkina et al. 2011; Chaban et al. 2014).

### 1. From Complex I to Complex III

The rate of electron transfer between membrane-bound electron carriers depends on their structural organization in the membrane. If two redox enzymes are connected by a mobile redox carrier undergoing long-range random diffusion in the medium, the overall reaction rate would be governed by the frequency of useful collisions between the mobile carrier and its two redox partners. On the other hand, if the system is fixed in a solid state assembly, the frequency of encounters will be dictated by the constraints that determine the interaction between the redox partners (*channeling*).

#### a. Evidence of Channeling

The random collision model of electron transfer (Hackenbrock et al. 1986) had been anticipated by an extensive kinetic evidence in the previous decade, that led investigators in the field to advance the notion of a homogeneous and freely diffusible Coenzyme Q pool in the lipid milieu of the inner mitochondrial membrane, whose redox state determines the overall electron flux observed during steady-state respiration. Evidence was provided by the effect of changing the rate of ubiquinol oxidation by means of inhibitor titration of Complex III (Kröger and Klingenberg 1973b), which shows a characteristic convex hyperbolic relationship between the overall rate of electron transfer and the fraction of Complex III inhibited by antimycin. On the contrary, a linear relationship is expected in the case of a stoichiometric association between Complex III and the CoQ-reducing enzymes. However, most available data on CoQ pool concern succinate oxidation (i.e. Complex II and Complex III integrated activity) in submitochondrial particles, whereas fewer data are available for Complex I-dependent activity (reviewed

in Lenaz and Genova 2007, 2009; Genova and Lenaz 2011).

Interestingly, Kröger and Klingenberg (1973a, b) already noticed that 10–20 % of CoQ in submitochondrial particles is not reduced by any substrate. More recently Benard et al. (2008) described the existence of three different pools of CoQ in rat liver and muscle mitochondria: one pool is utilized during succinate-dependent steady-state respiration, another (approx. 8 % in muscle and 23 % in liver) is mobilized as a reserve in case of a perturbation to maintain the energy fluxes at normal values (e.g. due to inhibition of the respiratory complexes or in case of mitochondrial diseases), and a third one (approx. 79 % in muscle and 21 % in liver) cannot be mobilized at all. These results are compatible with CoQ compartmentalization, although similar results with NADH oxidation were not provided in order to functionally prove that the fraction of CoQ that is not utilizable for succinate oxidation is channeled within supercomplex I-III.

This compartmentalization prevents significant cross talk between NADH oxidation (Complex I-dependent) (Fig. 29.6a, b) and succinate oxidation (dependent on Complex II) or other flavoenzyme-dependent oxidations (Fig. 29.6c).

Those Complex III molecules that physically interact with Complex I in the formation of supercomplexes are exclusively dedicated to NADH oxidation by a dedicated subset of CoQ molecules ( $C_{III_{NADH}}$ ), while those that are not bound to Complex I are mainly responsible for oxidation of succinate and other substrates using the free CoQ pool (Lapuente-Brun et al. 2013). Complex I has a very high affinity for Complex III, so that this association is preferred to the free state of either Complex I or Complex III. When a partial loss of Complex III occurs, NADH oxidation by the  $C_{III_{NADH}}$  enzyme is preferentially maintained despite the risk of compromising the oxidation of FAD-linked substrates that, on the contrary, rely on the diminished availability of CIII enzyme in free form.

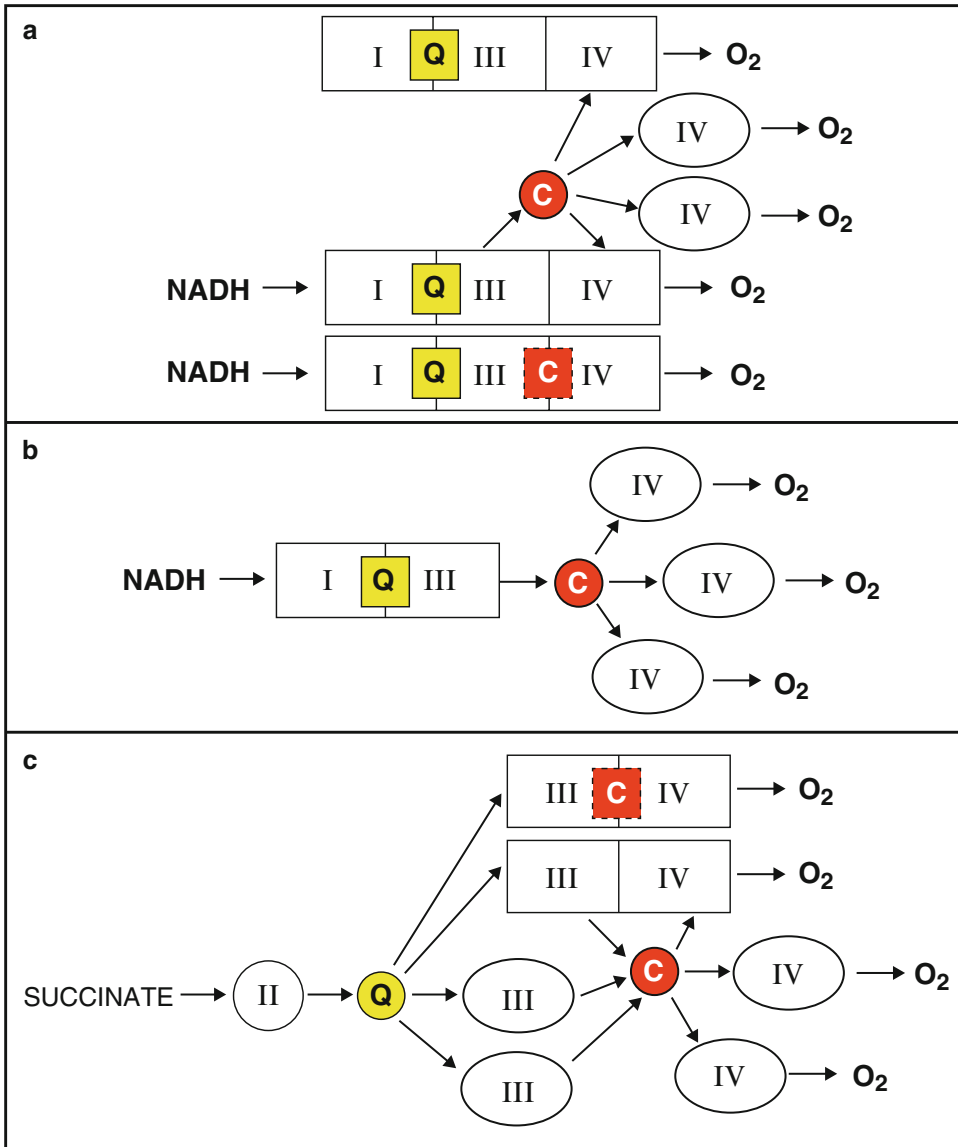


Fig. 29.6. Proposed organization of the respiratory chains in mammalian mitochondria. (a) Representation of respirasomes (I-III-IV) and free cytochrome oxidase (IV) molecules; in this model, electron transfer between CI and CIII always occurs by CoQ (Q) channeling, whereas fast dissociation of cytochrome c (C) from CIII may also allow electron transfer by random collisions of free cytochrome c with CIV, either free or bound in other respirasomes. (b) scheme of the possible function of the supercomplex formed by CI and CIII; it is postulated that free cytochrome c collides with uncomplexed CIV units. (c) Depiction of the mechanism of electron transfer from succinate via free CII and the CoQ pool. This model may also apply to other enzymes feeding electrons to the CoQ pool (see text for details). In this case, the CoQ pool interacts with either free CIII or associated CIII/CIV. The CIII units are shown as monomers for the sake of simplicity (Reprinted from Genova and Lenaz (2013), with permission from De Gruyter Publisher (<http://www.degruyter.com/>)).

The first studies on the mechanism of electron transfer between Complexes I and III were performed by Ragan (Ragan and

Heron 1978; Heron et al 1978). They showed that these Complexes can be mixed in stoichiometric ratios to give rise to a functional

unit having NADH cytochrome c reductase activity; the formation of a stable unit depended on a specific lipid environment.

A more direct comparison of the effect of channeling with respect to CoQ-pool behavior was performed in a simpler experiment. A system obtained by fusing R4B with different amounts of phospholipids and CoQ<sub>10</sub> (Lenaz et al. 1999) was used to discriminate whether the reconstituted protein fraction behaves as individual enzymes (CoQ-pool behavior), or as assembled supercomplexes depending on the experimental distances between the intramembrane particles. The comparison of the experimentally determined NADH-cytochrome c reductase activity with the values expected by theoretical calculation applying the pool equation (Eq. (29.5), Kröger and Klingenberg 1973a), where  $V_{\text{obs}}$  is the overall flux observed,  $V_{\text{red}}$  is the rate of CoQ reduction and  $V_{\text{ox}}$  is the rate of ubiquinol oxidation,

$$V_{\text{obs}} = (V_{\text{red}} \cdot V_{\text{ox}}) / (V_{\text{red}} + V_{\text{ox}}) \quad (29.5)$$

showed overlapping results at phospholipid dilutions (w:w) greater than 1:10, i.e. for theoretical distances >50 nm. On the contrary, pool behavior was not effective and the observed rates of NADH-cytochrome c reductase activity were higher than the theoretical values (Lenaz et al. 1999; Bianchi et al. 2003; Genova et al. 2008) at low protein:lipid dilution (1:1 w:w). This ratio corresponds to the mean nearest neighbor distance between respiratory complexes in mitochondria (Lenaz 1988). Moreover, when the same proteoliposomes at 1:1 lipid:protein ratios were treated with dodecyl maltoside to dissolve the supercomplex organization, the NADH cytochrome c reductase activity fell dramatically, whereas both Complex I and Complex III individual activities were unchanged (Maranzana et al. 2013); an analogous behavior was detected by treating bovine heart mitochondria with the same detergent.

Additional evidence for channeling between complexes I and III derives from

the demonstration that selective decrease of Complex III content under a given threshold induces a preferential decrease of electron transfer rate between complexes II and III, while the transfer of electrons between Complex I and III remains unaltered (Lapuente-Brun et al. 2013).

The assumption that supercomplex association has the major function of conferring a rate advantage by substrate channeling arose together with the discovery of supercomplexes (Schägger and Pfeiffer 2000). Although the theoretical basis of channeling by metabolic control analysis was already established (Kholodenko and Westerhoff 1993), the first demonstration of respiratory supercomplex association on a functional basis was achieved some years later (Bianchi et al. 2003, 2004). The study by Bianchi et al. (2004) exploited flux control analysis (Kholodenko and Westerhoff 1993) and the principle that the sum of the flux control coefficients of the individual enzymes in an integrated pathway must equal 1 unless these enzymes form supramolecular units and establish substrate channeling. In the latter case, these enzymes would all be equally rate-limiting and the sum of the control coefficients would be greater than 1 (Kholodenko and Westerhoff 1993). Using specific inhibitor titrations, the flux control coefficients were investigated of the complexes involved in aerobic NADH oxidation (I, III, IV) and succinate oxidation (II, III, IV) in bovine heart mitochondria and submitochondrial particles (Bianchi et al. 2004). Both Complex I and Complex III were found to be rate-limiting for NADH oxidation, kinetics that suggest the existence of functionally relevant association between the two complexes, whereas Complex IV appears randomly distributed. That is, a large excess of active Complex IV exists in free form in the pathway from NADH to oxygen (see Sect. IV.B.2). Moreover, Complex II is rate-limiting for succinate oxidation, clearly indicating the absence of substrate channeling toward Complexes III and IV. This approach

is similar to that of Boumans et al. (1998), who had found that CoQ does not follow pool behavior in yeast mitochondria unless they are treated with chaotropic agents.

Other studies addressed to the functional aspects of supercomplexes using metabolic control analysis (Quarato et al. 2011; Kaambre et al. 2012, 2013) confirmed that the respiratory chain, at least under certain conditions, is organized in functionally relevant supramolecular structures. In digitonin-permeabilized HepG2 cells, it was observed that under conditions of high membrane potential the sum of the flux control coefficients calculated for the activities of Complexes I, III and IV exceeded 1, supporting the proposition that they are complexed in a supramolecular unit Quarato et al. (2011) (see Sect. IV.F.1 for further discussion of the role of membrane potential). In saponin-permeabilized breast and colorectal tumor samples Kaambre et al. (2012, 2013) observed flux control coefficients for mitochondrial oxidative phosphorylation activities whose sum approached 4, in contrast with lower values for normal tissues; they also interpret the data as due to the presence of supercomplex association.

#### b. Saturation Kinetics

The finding that Complex I is almost totally associated in a supercomplex with Complex III seems to exclude a role for the CoQ pool in physiological electron transfer between these two complexes. Surprisingly, strong evidence exists that NADH cytochrome c reductase activity follows saturation kinetics with respect to CoQ.

The relation between electron transfer rate and CoQ concentration was seen for NADH and succinate oxidation in reconstituted systems (Norling et al. 1974; Estornell et al. 1992) and in phospholipid-enriched mitochondria (Schneider et al. 1982). Direct titrations of CoQ-depleted mitochondria reconstituted with different CoQ supplements yielded a “ $K_m$ ” for

NADH oxidation by CoQ in the range of 2–5 nmol CoQ  $\text{mg}^{-1}$  mitochondrial protein (Estornell et al. 1992), corresponding to a CoQ concentration of 4–10 mM in the lipid bilayer.

The presence of saturation kinetics demonstrates that free CoQ in the pool is also necessary for proper channeling between Complex I and Complex III. In fact, the bound inter-complex quinone that allows electron flow directly from Complex I to Complex III must be in dissociation equilibrium with the CoQ pool, so that its amount, at steady state, would be dictated by the size of the pool: this equilibrium explains the saturation kinetics for total ubiquinone exhibited by the integrated activity of Complex I and Complex III and the decrease of respiratory activities in mitochondria fused with phospholipids with subsequent dilution of the CoQ pool. To be in agreement with the experimental observation obtained by metabolic flux analysis, this proposition requires that the dissociation rate constants of bound CoQ be considerably slower than the rates of inter-complex electron transfer via the same bound quinone molecules (Lenaz and Genova 2007). Earlier studies by Heron et al. (1978) also reported that endogenous ubiquinone-10 leaks out of the Complex I-III unit when extra phospholipid is present, causing a decrease in activity that could be alleviated by adding more ubiquinone. It is likely that the function of the large amount of ubiquinone in the natural membrane may be, therefore, to maintain the ubiquinone-10 content in the supercomplex unit when it is formed.

The notion that inter-complex bound CoQ is in chemical equilibrium with CoQ in the pool is sufficient to explain the improved cell bioenergetics upon addition of exogenous CoQ. It is expected that even a slight decrease of CoQ content in the membrane is sufficient to dissociate part of the quinone from the supercomplex, thus decreasing the rate of electron channeling.

This observation may be particularly important in view of the assumption that the



supercomplex association is physiologically dynamic according to the plasticity model of supercomplex association (Acín-Pérez et al. 2008). It also means that, if supercomplexes are dissociated in physiological or pathological conditions, the CoQ content of the membrane becomes less saturating for electron transfer; the obvious consequence is that in this condition an exogenous CoQ supplementation may be extremely useful to sustain a high respiratory rate. The efficacy of exogenous CoQ<sub>10</sub> supplementation in several disease states has been shown in many studies (cf. Genova and Lenaz 2011).

## 2. From Complex III to Complex IV

### a. Early Kinetic and Biophysical Studies

Although the pool equation has been developed for CoQ between dehydrogenases and bc<sub>1</sub> complexes, the same reasoning is valid for cytochrome c that shares with ubiquinone the postulated role of a mobile substrate-like component of the respiratory chain (Froud and Ragan 1984a, b).

Nevertheless, the role of cytochrome c mobility between Complex III and Complex IV is even more intriguing than that of ubiquinone (Fig. 29.6) (Lenaz 1988). Hackenbrock and coworkers (Gupte and Hackenbrock 1988a, b) observed that under physiological conditions of 150 mM ionic strength, cytochrome c is readily dissociated from the membrane and undergoes three-dimensional diffusion in the inter-membrane space. In reconstituted enzyme systems in the presence of excess cytochrome c, “pool behavior” is followed (Froud and Ragan 1984a); in liposomes consisting of cardiolipin and dimyristoyl lecithin, however, when the latter lipid is in the gel phase, the rotational diffusion of spin-labelled cytochrome c is slowed, suggesting that the cytochrome c pool is bound to cardiolipin molecules, whose lateral and rotational diffusion in the bilayer is adequate to account for electron-transport rates (Froud and Ragan 1984a). Likewise, the rotation rates of

cytochrome oxidase reconstituted in lipid vesicles are not influenced by simultaneous incorporation of Complex III (Kawato et al. 1981), suggesting that Complex III and Complex IV act as independent entities.

However, a similar study in mammalian mitochondrial membranes allowed the conclusion that only about one-half of cytochrome oxidase contributed to the observed rotational relaxation rate, the remainder being relatively immobile, and that the fraction of aggregated protein progressively decreases with decreasing concentration of proteins in the membrane following the fusion of soybean phospholipid vesicles with mitoplasts (Kawato et al. 1980, 1982).

### b. Flux Control Analysis

Flux control studies clearly established that CI and CIII behave as a functional supercomplex in bovine heart and rat liver mitochondria, whereas Complex IV does not since it has a low flux control coefficient, despite the BN-PAGE showing that a fraction of Complex IV is physically associated in the respirasome in the same mitochondrial samples (Bianchi et al. 2004; Genova et al. 2008; Lenaz et al. 2010).

The reason for this discrepancy is not clear. The flux control studies allow to conclude that the free molecules of CIV are involved in electron transfer from NADH, and imply that the CIV molecules in the supercomplex do not receive electrons from CIII by channeling of cytochrome c (Fig. 29.6) (Genova and Lenaz 2013, 2014). Of course, branched pathways are difficult to approach by metabolic control analysis and measurements in isolated mitochondria by inhibitor titration of the relevant enzymes inevitably involves using assay conditions (i.e. substrate concentrations) that are not necessarily intended to reproduce *in vivo* conditions.

Moreover, the non-artifactual nature of the lack of functional channeling shown by the flux control coefficients in mammalian mitochondria is supported by the fact that in

potato tuber mitochondria the respirasome seems to be completely functional in channeling (Genova et al. 2008). The reason for the difference may be in a tighter binding of cytochrome *c* in the respirasome. Likewise, Boumans et al. (1998) found evidence for cytochrome *c* channeling in *S. cerevisiae* mitochondria; accordingly, single particle cryo-electron microscopy revealed that the supercomplex consisting of a III<sub>2</sub>IV<sub>2</sub> unit (there is no Complex I in this yeast species) is arranged in such way that the distance between the binding sites of cytochrome *c*, i.e. cytochrome *c*<sub>1</sub> in CIII and subunit II of CIV (containing the Cu<sub>A</sub>), is considerably shorter than in bovine mitochondria (Mileykovskaya et al. 2012). To further confuse the issue, it is also worth noting that Trouillard et al. (2011) recently demonstrated in yeast mitochondria that the time-resolved oxidation of cytochrome *c* by CIV is a random process not involving substrate compartmentalization.

The purified supercomplex I<sub>1</sub>III<sub>2</sub>IV<sub>1</sub> obtained from bovine heart (Althoff et al. 2011) and some putative respirasomes isolated from rat liver mitochondria (Acín-Pérez et al. 2008) also contained traces of cytochrome *c*; therefore, it cannot be excluded that substrate channeling on this level occurs also in mammalian mitochondria. It was also found that, after incubating samples of isolated mammalian mitochondria with an excess of cytochrome *c*, the I<sub>1</sub>III<sub>2</sub>IV<sub>1</sub> supercomplex contains cytochrome *c* (Lenaz et al. 2010). It is likely that the native supercomplex contains loosely bound cytochrome *c* that is easily dissociated. The question is, therefore, to understand if such an easy dissociation occurs in the living cell: in other words, this means that if the dissociation rate is of the same order of the respiratory turnover, cytochrome *c* would exhibit pool behavior even if present in a supercomplex.

Using a different approach, Enriquez' group recently demonstrated that at least part of Complex IV forms a functional supercomplex with channeling of cytochrome *c* (Lapuenta-Brun et al. 2013). In particular,

they demonstrated in isolated liver mitochondria that the assembling of Complex IV in supercomplexes defines three types of Complex IV, one dedicated exclusively to receive electrons from NADH oxidation (forming supercomplex I-III-IV), another dedicated to receive electrons from FAD-dependent enzymes (forming supercomplex III-IV) and a third major one that is in free form and that is able to receive electrons from both NADH and FADH<sub>2</sub> oxidation.

On the contrary, if Complex IV is maintained permanently detached from supercomplexes by elimination of SCAF1 (Sect. III.C), the maximum respiratory activity of intact cells under glucose-rich medium parallels the maximum respiratory activity obtained in the same cells by feeding directly electrons to Complex IV. In this case, since all Complex IV is in free form and electron transfer takes place via diffusion of the cytochrome *c* pool, this experiment demonstrates that the cytochrome *c* pool function is also very efficient.

### 3. Respiratory Enzymes Not Associated in Supercomplexes

#### a. Electron Transfer Between Complex II and Complex III

The CoQ pool is certainly required for electron transfer from Complex II to Complex III (Fig. 29.6): in bovine heart mitochondria and submitochondrial particles, Complex II kinetically follows pool behavior in reconstitution experiments (Estornell et al. 1992) and also in intact mitochondria (Stoner 1984); this is in complete accordance with the lack of Complex II-containing supercomplexes as found by BN-PAGE (Schägger and Pfeiffer 2001). Flux control analysis (Bianchi et al. 2004) confirmed that Complex II is the only rate-limiting step in succinate oxidation, and both Complex III and Complex IV have low flux control coefficients in contrast with NADH oxidation (Sect. IV.B.1.a). The existence of small amounts of supercomplexes including Complex II molecules, described by Acín-Pérez et al. (2008) in mouse cell

lines and in mouse liver mitochondria, does not contradict the fact that most of succinate oxidation takes place via the CoQ pool between Complexes II and III.

In contrast with the BN-PAGE and kinetic data outlined above, earlier studies had provided some evidence for a specific association of Complex II with Complex III. Ziegler and Doeg (1959) in Green's laboratory had isolated a succinic dehydrogenase:cytochrome b complex from beef heart mitochondria, that can be dissociated into its components (Complex II and Complex III) and reconstituted therefrom (Hatefi et al. 1962a). At the same time Tsou King's laboratory isolated a succinate cytochrome c reductase from beef heart Keilin-Hartree particles, that could be dissociated into a soluble succinate dehydrogenase and a particulate bc<sub>1</sub> complex (Takemori and King 1964) and reconstituted from the isolated components (King and Takemori 1964). Subsequently, the reconstitution could also be achieved using a detergent-solubilized bc<sub>1</sub> complex (Yu et al. 1974).

Further studies (Yu and Yu 1980) yielded similar results using highly purified succinate dehydrogenase and ubiquinol cytochrome c reductase preparations. The effective interaction between the two components of the succinate cytochrome c reductase preparation was demonstrated by Gwak et al. (1986) in the same laboratory. These results indicate that succinate-ubiquinone reductase and ubiquinol-cytochrome c reductase are indeed present in the membrane as a super-macromolecular complex. Strangely enough, no such super-macromolecular complex could be detected between NADH-ubiquinone and ubiquinol-cytochrome c reductases (Gwak et al. 1986).

Another study whose conclusions contradicted the notion of a free Complex II was the kinetic study of Boumans et al. (1998) in yeast, showing that succinate oxidation did not obey pool behavior unless the mitochondria were treated with chaotropic agents.

A likely explanation of these contrasting findings is the existence of very loose but specific contacts between Complex II and

Complex III, not giving rise to any kind of channeling even in phosphorylating mitochondria (Stoner 1984). As appears by BN-PAGE, these contacts are lost in frozen mitochondria and in submitochondrial particles, or by digitonin treatment, but may be strongly non-physiologically enhanced by some treatments used for mitochondrial respiratory chain fractionation.

#### b. Electron Transfer to Complex III from Other Enzymes Using Coenzyme Q

The CoQ pool behavior must fully apply to other enzymes that deliver electrons to CoQ in the respiratory chain (glycerol-3-phosphate dehydrogenase, electron transfer flavoprotein (ETF)-ubiquinone oxidoreductase, dihydroorotate dehydrogenase, choline dehydrogenase, sulfide CoQ reductase and proline dehydrogenase). These enzymes are likely to be in minor amounts and strongly rate-limiting in integrated electron transfer (Lenaz et al. 2010). Few direct studies are, however, available on possible associations of these enzymes. The only study directly addressed to this problem (Rauchová et al. 1997) demonstrated that in brown fat mitochondria the inhibition curve of glycerol phosphate-cytochrome c reductase is sigmoidal in the presence of myxothiazol and antimycin, suggesting the presence of a homogeneous CoQ pool between glycerol phosphate dehydrogenase and Complex III.

Wang et al. (2010) provided evidence of a multifunctional fatty acid  $\beta$ -oxidation (FAO) complex within mitochondria that is physically associated with OXPHOS supercomplexes. They also showed that metabolic channeling of electrons occurs from FAO directly to the respiratory chain since the reduction of cytochrome c is efficiently promoted by the addition of palmitoyl-CoA in a reaction mixture containing excess cytochrome c, CoQ and a sucrose gradient fraction of rat liver mitochondrial proteins enriched in respiratory supercomplexes, thus indicating that the necessary FAO components are also present in the fraction to mediate oxidation of

acyl-CoAs with no accumulation of pathway intermediates. However, Schönfeld et al. (2010) could not find such an association between Complex I and ETF that participates in fatty acid oxidation in rat heart and liver mitochondria, nor could they find any evidence of channeling between fatty acid oxidation and respiratory supercomplexes.

### c. Is There a Direct Connection Between Complex I and Complex II?

The hyperbolic relation experimentally found by Gutman (1985) between succinate oxidase and the rate of reverse electron transfer from succinate to  $\text{NAD}^+$ , involving sequential interaction of complexes II and I by means of CoQ, is in complete accordance with the pool equation. This observation poses a particularly puzzling question (Lenaz and Genova 2007) about how ubiquinol reduced by Complex II interacts from the pool with the CoQ site in Complex I, since Complex I is totally engaged in the supercomplex. The same dilemma applies to the NADH fumarate reductase activity that also involves interaction of Complex I and Complex II (Gutman 1985).

It must be noted that the ATP-driven reverse electron transfer from succinate to  $\text{NAD}^+$  occurs in the presence of a high mitochondrial transmembrane protonmotive force that, according to Piccoli et al. (2006), might be the physiological signal causing the structural reorganization of the respiratory complexes. The model hypothesis suggests that the I-III supercomplex would dissociate its constituting complexes under conditions of high  $\Delta\tilde{\mu}_{\text{H}^+}$ , and this would no longer limit the access from the CoQ pool to the binding site in Complex I. This model is however incompatible with the observation reported by Gutman (1985) that NADH-fumarate reductase, assayed at low membrane potential, shares the same pathway of the reverse reduction of  $\text{NAD}^+$  by succinate. According to this consideration, the pathways linking Complex II and Complex I during either direct or reverse electron transfer most probably

require the interaction between the CoQ pool and Complex I within the supercomplex. If this is true, it must be concluded that Complex I in the supercomplex is somewhat accessible to the CoQ pool (Genova and Lenaz 2014).

### C. Supercomplexes and Energy Conservation

There are several reasons why supercomplex assembly might enhance the efficiency of oxidative phosphorylation, although there has been no direct study to address this question.

First, the presence of channeling *per se*, by enhancing electron flow in the respiratory chain, allows a higher rate of proton translocation and hence indirectly of ATP synthesis.

There are additional indications that supercomplex association may provide further kinetic advantages besides substrate channeling. The study of Schäfer et al. (2007b) showed that a supercomplex comprising cytochrome c oxidase ( $\text{I}_1\text{III}_2\text{IV}_1$ ) had higher Complex I and Complex III activities than the supercomplex devoid of the terminal oxidase ( $\text{I}_1\text{III}_2$ ); evidently, the presence of Complex IV modifies the conformation of the partner complexes in such a way to enhance their catalytic activity. Likewise, Hildebrandt (2011) showed that supercomplex dissociation abolishes the protective effect of dehydro-ascorbic acid on sulfide toxicity to cytochrome c oxidase, suggesting a conformational effect of supramolecular association on the allosteric properties of cytochrome c oxidase. Such a kinetic advantage would be competent by itself to enhance the creation of the membrane potential; however, it is not known whether such conformational changes also improve the efficiency of proton translocation.

Too little is known presently about the possibility that protein-protein interactions within the supercomplex I-III-IV might affect the subunits that appear to be important in the proton-pumping mechanism of Complex I, Complex III and Complex IV (Genova and Lenaz 2014). The redox

potential span that provides the driving force for proton translocation across the inner mitochondrial membrane depends on the reduction level of the electron donors/acceptors at steady state, as catalyzed by the respiratory supercomplex. It would be of interest to know whether the supercomplex association improves the proton pumping efficiency of the respiratory chain by increasing the redox potential span of the substrates that are channeled within the protein assembly itself, in comparison to the homogenous donor/acceptor pool. However, to our knowledge, a thermodynamic analysis that specifically addresses this problem in the respiratory supercomplex is still lacking, possibly because it is challenging to measure the redox potentials of the ubiquinol/ubiquinone and ferro/ferricytochrome c couples directly in the supercomplex.

There is yet another reason why supercomplexes may enhance the efficiency of energy conservation. As extensively described in Sect. III.B, CL is required for the stabilization of supercomplexes and participates in their structural integrity. In addition, CL is only found at high levels in membranes that pump protons. The high pK(2) (above 8.0) of CL provides a role for its head-group as a proton trap for oxidative phosphorylation. The high pK(2) also indicates that the head-group has but one negative charge in the neutral pH range. Data on the binding of CL to all of the oxidative phosphorylation proteins suggest that the CL may aggregate the oxidative phosphorylation proteins into a patch while it restricts pumped protons within its headgroup domain, supplying protons to the ATP synthase with minimal changes in the bulk phase pH (Haines and Dencher 2002). Adjacent to the respiratory proton pumps, the buffering by CL would increase the voltage component,  $\Delta\Psi$ , of the electrochemical gradient within the supercomplex. Therefore, in addition to connecting proteins and enhancing efficiency of electron flow, CL could locally contribute to creating a high local  $\Delta\Psi$  that is needed to drive the directional ATP export vs. ADP import through the

adenylate carrier across the mitochondrial membrane. Through facilitating respiratory supercomplex assembly and recruiting the adenylate carrier, it has been suggested that, under optimal conditions, CL increases the efficiency of OXPHOS by at least 35 % (Claypool 2009).

#### *D. Modulation of Generation of Reactive Oxygen Species*

The possibility that supercomplex assembly prevents excessive ROS generation from the respiratory chain has been suggested in the past, without, however, direct experimental evidence (Panov et al. 2007; Lenaz and Genova 2012; Seelert et al. 2009). In a recent study, Maranzana et al. (2013) induced a primary condition in mitochondrial samples enhancing free Complex I with respect to Complex I bound to the supercomplex; using this approach, the first direct demonstration was obtained that loss of supercomplex organization causes an enhancement of ROS generation by Complex I. The above study showed an enhanced ROS generation by Complex I in two experimental systems in which the supramolecular organization of the respiratory assemblies was destroyed by: (i) treatment either of bovine heart mitochondria or liposome-reconstituted supercomplex I-III with dodecyl maltoside; (ii) reconstitution of Complexes I and III at high phospholipid to protein ratio.

The ROS increase does not appear to be the mere result of Complex I damage as a consequence of the treatment in the presence of detergents, since the NADH-ubiquinone redox activity is only slightly depressed, although Complex I is mostly in its free form. Moreover, the hypothesis that facilitation of electron flow by substrate channeling within the respirasome helps to maintain the redox components of the complexes in the oxidized state, thus limiting ROS formation, cannot be the only explanation. In fact, in the study of Maranzana et al. (2013), ROS production is investigated in the presence of inhibitors (mucidin and rotenone) that prevent electron transfer to any possible accep-

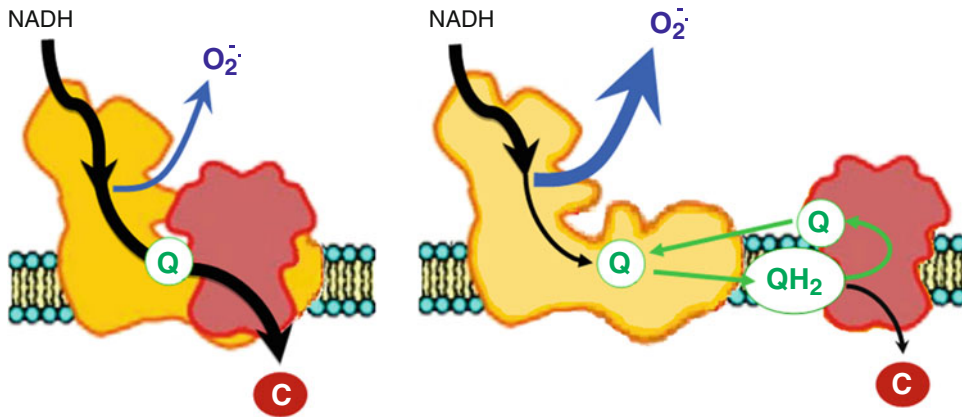


Fig. 29.7. Scheme of electron flux in two models of integrated NADH-cytochrome *c* reductase activity in the respiratory chain. (Left) In a supercomplex I<sub>1</sub>III<sub>2</sub>, any step in the obligatory pathway is regarded as a component of a single enzyme unit where the overall transfer of electrons to the final acceptor is optimized by channeling of the intermediate substrates. Protein-protein interactions modulate the reactivity of the intra-complex redox centers with dioxygen and prevent excessive ROS generation from Complex I (yellow). (Right) In a linear pathway composed of individual Complex I (yellow) and Complex III (red), as a consequence of supercomplex disaggregation, the overall electron transfer to cytochrome *c* is mediated by pool behavior of CoQ. The efficiency of electron flux is modified by the absence of protein-protein interactions and superoxide O<sub>2</sub><sup>-</sup> production by Complex I is strongly enhanced.

tor, so that the redox centers in Complex I are maximally reduced both in the situations where supercomplexes are maintained and in the situation where Complex I is free (Fig. 29.7).

The two potential sites for oxygen reduction that exist in Complex I (i.e. FMN and iron-sulfur cluster N2) might distinctly prevail in generating ROS under different conditions (Fato et al. 2009; Hirst et al. 2008; Lenaz and Genova 2010). Possibly, the dissociation of Complex I from Complex III may render the 51 kDa subunit containing the FMN more “loose” allowing it to interact with oxygen (Radermacher et al. 2006). Indeed, the actual shape of the I<sub>1</sub>III<sub>2</sub>IV<sub>1</sub> supercomplex from bovine heart (Schäfer et al. 2007b) suggests a slightly different conformation of Complex I in the supercomplex, showing a higher bending of the matrix arm toward the membrane (and presumably Complex III) which may limit exposure of the redox centers of Complex I to oxygen.

Several observations in cellular and animal models link together supercomplex dissociation and enhanced ROS production.

In mouse fibroblasts expressing the activated form of the k-ras oncogene, a strong decrease of high molecular weight supercomplexes correlating with higher ROS generation was observed in comparison with wild type fibroblasts (Baracca et al. 2010; Lenaz et al. 2010). Moreover, enhanced ROS generation and oxidative stress were found in yeast mutants lacking the supercomplex assembly factor Rcf1 and thus devoid of supercomplexes III-IV (Chen et al. 2012; Strogolova et al. 2012; Vukotic et al. 2012) since the yeast *S. cerevisiae* lacks Complex I; in this case the origin of the extra ROS is presumably Complex III.

Numerous pathological states are accompanied by enhanced generation of ROS (Lenaz 2012, 2014). In an experimental model of heart failure, the decrease of oxidative phosphorylation has been associated with a decrease of respiratory supercomplexes (Rosca and Hoppel 2008, 2009; Rosca et al. 2008).

Lymphoblasts from patients affected by Barth Syndrome, due to genetic loss of tafazzin, an enzyme involved in cardiolipin remodeling, have altered mitochondrial

supercomplexes (McKenzie et al. 2006); likewise, in a yeast experimental model of tafazzin mutation, Chen et al. (2008) observed an increased oxidative stress in response to ethanol.

Aging is also accompanied by a decline of supercomplex association (Gómez et al. 2009; Frenzel et al. 2010); despite some uncertainties and challenges, aging is generally associated with increased ROS and oxidative damage (for recent reviews cf. Cui et al. 2012; Barja 2013). Gómez and Hagen (2012) reason that age-associated destabilization of respiratory supercomplexes may be important for the development of the mitochondrial aging phenotype by means of impaired bioenergetics and enhanced ROS production; in addition Frenzel et al. (2010) on the basis of the 3D-structures of supercomplexes and the close spatial arrangement of the respective electron carrier binding sites (Schäfer et al. 2007b) conclude that less superoxide radical formation is expected to occur in supercomplexes than in randomly distributed individual complexes. These latter studies, however, fail to show which is the causative event (i.e. supercomplex dissociation causing ROS increase or, alternatively, ROS increase causing supercomplex dissociation) or even if they are independent phenomena. [See Chaps. 20 and 21 (Baniulis et al. 2015; Fisher et al. 2015) in this volume on mechanism and consequences of superoxide production in photosynthetic and mitochondrial electron transport chains].

#### *E. Effect of Supercomplex Association on Stability of Individual Complexes*

Since the discovery of supercomplexes it was noticed that the stability of Complex I is altered when it is not assembled in the respirasome.

The attempts to isolate Complex I from mutant strains of *Paracoccus denitrificans* lacking complexes III or IV led to the complete dissociation of Complex I under the conditions of BN-PAGE. Reduced stability of free Complex I in those mutant strains was also apparent from an almost complete loss

of NADH CoQ reductase activity (Stroh et al. 2004).

Analysis of the state of supercomplexes in human patients with an isolated deficiency of Complex III (Acín-Peréz et al. 2004; Schägger et al. 2004) and in cultured cell models harboring Complex III (Acín-Peréz et al. 2004), Complex IV (Diaz et al. 2006) or cytochrome c (Vempati et al. 2009) depletion, led to the proposal that the formation of respirasomes may be essential for the assembly/stability of Complex I. Genetic alterations leading to a loss of Complex III led to secondary loss of Complex I, therefore primary Complex III assembly deficiencies presented as Complex III/I defects (Laman-tea et al. 2002; Acín-Peréz et al. 2004).

D'Aurelio et al. (2006) studied the complementation of mitochondrial DNA (mtDNA) upon fusion of human cell lines, one containing a homoplasmic mutation in a subunit of respiratory chain Complex IV, COX-I, and the other with a distinct homoplasmic mutation in the cytochrome b subunit of Complex III: respiration was recovered in correlation with the presence of supercomplexes containing complexes I, III and IV. From these findings, supercomplex assembly was proposed as a necessary step for respiration.

In a different study, deletion of the *ndufs4* gene, encoding an accessory subunit of Complex I, in mouse tissues results in decreased stability and activity of Complex I: however, the portion of Complex I that is still active is bound in the supercomplexes, indicating that the supramolecular association improves the stability of Complex I (Calvaruso et al. 2011).

Conversely, mutations of Complex I had controversial effects, since in some studies they did not affect the amount of other complexes (Schägger et al. 2004; Pineau et al. 2005), while in others they significantly reduced the amounts of Complexes III and IV (Acín-Peréz et al. 2009a; Ugalde et al. 2004; Grad and Lemire 2004, 2006). The reason for this discrepancy is not known, but might be related to the specificity of the mutation affecting subunits of Complex I, which may

be involved in the contacts with the other complexes.

Animal models of the effects of Complex III and Complex IV mutations on Complex I should prove useful for a better understanding of the role of supercomplexes. In one study, ‘knock down’ of predicted homologues of COX-IV and COX-Va in the nematode *Caenorhabditis elegans* showed that intrinsic Complex I enzymatic activity is dependent on the presence of Complex IV, despite no overall decrease in the amount of Complex I (Suthammarak et al. 2009). In a further study in *C. elegans* the same group showed that Complex III defects inhibit Complex I by several different mechanisms involving supercomplex destabilization (Suthammarak et al. 2010). Mutant analysis revealed that Complex III affects supercomplex I-III-IV formation by acting as an assembly/stabilizing factor.

Is the stabilization of Complex I by its association in a supercomplex a primary effect on assembly during biogenesis or is it a secondary effect on the stability of the Complex after its assembly? It is possible that both explanations are valid.

Moreno Lastres et al. (2012) report that at early supercomplex assembly stages Complex I is neither fully assembled nor active when it binds to other respiratory chain complexes (cf. Sect. III.C), thus suggesting that the supercomplex constitutes the structural unit in which Complex I arrives at complete assembly.

On the other hand, Enriquez’ group (Acín-Peréz et al. 2004; Lapuente-Brun et al. 2013) reported that the assembly of supercomplexes temporally follows the full assembly of the individual complexes and that association of Complex I and Complex III is devoted to the storage and preservation of Complex I since the enzyme stability and not its normal assembly is compromised in the absence of Complex III.

Ghelli et al. (2013) characterized the biochemical properties of cybrids carrying a human cytochrome *b* missense mutation (m.15579A>G) identified in a patient with severe exercise intolerance and multisystem

pathological alterations. This mutation does not induce disassembly of the supercomplex containing Complex I. Evidently, there must be specific structural consequences of Complex III mutations in order to disassemble the I<sub>1</sub>III<sub>2</sub>IV supercomplex with consequent destabilization of Complex I.

Recently Cui et al. (2014) demonstrated that the N-terminal portion of the Rieske protein of Complex III in *S. cerevisiae* is required for stable association with Complex IV in a supercomplex.

From all of these results the evidence would favor the following course of events: misassembled CIII prevents formation of supercomplex; the lack of the supercomplex association induces an enhanced ROS generation from Complex I (see Sect. IV.D), with consequent damage to neighbor molecules and to Complex I itself which is vulnerable to oxidative stress (Choksi et al. 2004), both directly and through the lipid peroxidation, particularly of cardiolipin (Paradies et al. 2004). This series of events can create a vicious circle of oxidative stress and supercomplex disorganization (Fig. 29.8) (Lenz and Genova 2010).

Indeed, the fragility of free Complex I is not the result of inherent instability of the enzyme, since the isolated Complex I is stable and active for a long time, as evidenced by the early studies of Hatefi and coworkers (Hatefi et al. 1962b), and also by the analysis of Complex I activity in proteoliposomes by Maranzana et al. (2013). However, Complex I shows some fragility due to its sensitivity to the increased production of ROS during the activity of the respiratory chain.

A study on fibroblasts lacking the Rieske iron sulfur protein (Diaz et al. 2012b) also supports the hypothesis that Complex I destabilization in the absence of the Complexes III or IV depends on its particular sensitivity to oxidative damage.

#### F. Dynamic Nature of Supercomplexes: The Plasticity Model

All the BN-PAGE studies reported in Sect. II.B showed that different types of



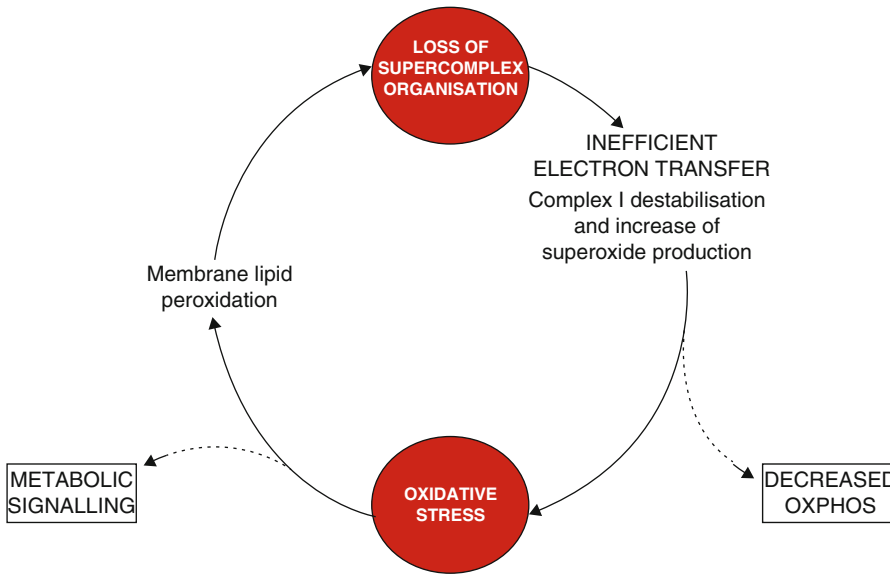


Fig. 29.8. Scheme showing how the loss of supercomplex organization may be involved in a ‘vicious cycle’ of oxidative stress and energy failure. ROS production by Complex I is enhanced as a consequence of supercomplex disassembly. Membrane phospholipid peroxidation and consequent further loss of supercomplex organization may occur due to mitochondrial oxidative stress, thus perpetuating a ‘vicious cycle.’ Depending on the amount produced, ROS can also operate as signaling molecules from mitochondria to the cell. See text for explanations.

associations exist between the three core respiratory complexes besides the I+III+IV units or respirasomes, such as I+III or III+IV, which were formed regardless the presence of the third partner of the respirasome, strongly suggesting that they can also be present *in vivo*. For this reason Acín-Pérez et al. (2008) also concluded that the free complexes likely co-exist with supercomplexes. In this context they proposed an integrated model, *the plasticity model*, for the organization of the mitochondrial electron transport chain. The previous opposed models, solid vs. fluid, would be two extreme functional situations of a dynamic range of different molecular associations between respiratory complexes. The plasticity model and the dynamics of mitochondrial supercomplexes are extensively discussed by Acín-Pérez and Enriquez (2014) in a recent review.

A fundamental prediction of the plasticity model is that, *in vivo*, the mitochondrial respiratory chain should be able to work both when supercomplexes are present and when the formation of supercomplexes is

prevented. Indeed, several studies *in vitro* support the view that electron transfer in the respiratory chain can occur in absence of supercomplexes, as described in Sect. IV.B.1.a.

Maas et al. (2009) have been able to express functional AOX in a mutant of *Podospora anserina* cells lacking complexes III and IV. Under these conditions, Complex I is stable and works perfectly in combination with AOX, which is able to oxidize ubiquinol supplanting the combined role of Complex III, cytochrome *c* and Complex IV. This demonstrates *in vivo* that Complex I-dependent respiration does not strictly require supercomplex I-III formation.

The early studies of Hackenbrock in the ‘80s showed that the intramembrane particles are randomly distributed in the plane of the inner membrane where they diffuse with relatively high diffusion coefficients in the range of  $10^{-10} \text{ cm}^2\text{s}^{-1}$  (Gupte et al. 1984; Hackenbrock et al. 1986). Those accurate studies cannot be dismissed as artefacts, therefore they must be explained within the frame of a dynamic equilibrium between su-

percomplexes and randomly diffusing individual complexes. To this respect, the time window of the experimental approaches is of paramount importance and must be taken in account.

The first attempt to follow the temporal dynamics of the respiratory complexes *in situ* was made by Muster et al. (2010) who suggested that supercomplex dissociation into a fully random distribution may not be a fast event. By fusing cells containing mitochondria with respiratory complexes labeled with different fluorescent proteins and resolving their time dependent re-localization in living cells, the authors found that a complete reshuffling of respiratory complexes throughout the entire chondriome in single HeLa cells occurs within 2–3 h by organelle fusion and fission. Moreover, polykaryons of fused cells completely re-mixed their complexes in 10–24 h in a progressive way.

In a recent study, Wilkens et al. (2013) investigated the impact of mitochondrial fusion/fission on the reorganization of OXPHOS complexes in the inner mitochondrial membrane of different HeLa cells tagged with fluorescent proteins (GFP and DsRed-HA). After cell fusion by polyethylene glycol treatment, the outer membrane and matrix proteins mix quickly and homogeneously upon mitochondrial fusion, whereas the mixing and redistribution of the tagged OXPHOS complexes of inner membrane is decelerated. In particular, the comparison of the localization profiles of OXPHOS complexes I, III and IV in the inner membrane compartments clearly showed an overlap: 80 % of CI coincided with 80 % of CIII and CIV, thus supporting the idea of a physical assembly constituted by the three enzymes. Interestingly the diffusion coefficients reported by Wilkens et al. (2013) are of the order of those reported by Hackenbrock et al. (1986).

### 1. Role of Membrane Electrochemical Potential

A study of the influence of the mitochondrial trans-membrane potential on the flux control exerted by cytochrome *c* oxidase on the respi-

ratory indicated that, under conditions mimicking state 4 respiration in intact cells and isolated mitochondria, the control exerted by the oxidase over respiration is decreased relative to endogenous state 3 respiration (Piccoli et al. 2006). The control of Cytochrome *c* oxidase seems to be exerted by the electrical component of  $\Delta\tilde{\mu}_H^+$  (Dalmonte et al 2009). More recently, Quarato et al. (2011) extended these studies to the other proton-translocating respiratory complexes (I and III) analyzing the sum of the flux control coefficients, which describe the control that each individual step in a pathway exerts over the global flux of the pathway (Kacser and Burns 1995): under conditions of low potential, the sum exceeded 1, whereas at high potential, the coefficients were much lower.

Although the interpretation of the results in such a complex system is very difficult, the authors suggest that such a change in control strength might be expressed in terms of supercomplex plasticity. In particular, the results showing that the sum of the flux control coefficients of Complexes I, III, and IV exceeds 1, in state 3, were compatible with respirasome organization at lower membrane potential and with a random organization of cytochrome oxidase with respect to other complexes at high membrane potential (state 4); since the respiratory rate is high in state 3 conditions, the supercomplex organization would produce an extra advantage by raising the rate through electron channeling.

The molecular mechanisms leading to the assembly/disassembly of the supercomplexes have been not yet defined, but it is conceivable that, given the membrane-integrated nature of the single complexes, electrostatic/hydrophobic interactions may enter into play in response to  $\Delta\tilde{\mu}_H^+$ . In this respect, recent investigations have revealed a surprising interplay between pH gradients, lipid composition and packing and membrane cristae shape (Khalifat et al. 2008, 2011).

In potato tuber mitochondria, it was found that hypoxia dissociates the supercomplex I-III<sub>2</sub>-IV into individual Complex I plus Complex III-IV units (Ramirez-Aguilar

et al. 2011). It was shown that the change was due to the acidification of the medium caused by hypoxia and that acidification could reproduce the same effect of hypoxia; moreover, the effect was not due to changes in membrane potential.

## 2. Role of Post-translational Changes

Mitochondria contain protein kinases and phosphatases and both serine/threonine phosphorylation (Deng et al. 2011; Grimsrud et al. 2012) and tyrosine phosphorylation (Hébert-Chatelain et al. 2012; Hébert-Chatelain 2013; Bellomo et al. 2006) of mitochondrial proteins are important in the regulation of the activity of these organelles (Acín-Peréz et al. 2011a, b).

Phosphorylation of Complex I has been shown to modify the activity of the enzyme and its ROS generating capacity (Bellomo et al. 2006; Iuso et al. 2006; Maj et al. 2004; Papa et al. 2008; Raha et al. 2002). Cyclic AMP-dependent phosphorylation of the 18 kDa subunit of Complex I, encoded by the nuclear *NDUFS4* gene, is required for import of the subunit; modulation of subunit phosphorylation by intramitochondrial protein kinase A and phosphoprotein phosphatase contributes to the stability of Complex I and stimulation of its activity (De Rasmio et al. 2008). It is tempting to speculate that the increase of activity of Complex I and the decrease of ROS generation by phosphorylation may be, in part, the result of enhanced stability of the I-III supercomplex. However, to our knowledge, no studies to date have established any correlation between them. Phosphorylation of Complex III subunits has also been reported although its functional role remains undetermined (Zhao et al. 2011).

Complex IV is a target of the intramitochondrial cAMP-PKA signaling pathway (Acín-Peréz et al. 2009a, b; Ramzan et al. 2012). It is tempting to speculate that endocrine alterations may affect the assembly state of Complex IV, by hyper- or hypo-phosphorylation of some subunits in the complex. Indeed, cAMP- and PKA-

dependent phosphorylation of Complex IV in heart mitochondria (Rosca et al. 2011) was found to be higher in free Complex IV not associated in supercomplex than in the bound enzyme, suggesting that phosphorylation prevents supercomplex association. Nevertheless, caution must be exerted in the interpretation of the role of post-translational changes in supercomplex formation, since no causal correlation has yet been established.

Recent evidence indicates that thiol-based redox regulation of the respiratory chain activity and especially S-nitrosylation of Complex I could be a strategy to prevent elevated ROS production, oxidative damage and tissue necrosis during ischemia-reperfusion injury (Dröse et al. 2014). It is possible that these redox modifications can also affect the supramolecular structure of the respiratory chain complexes, since they are able to induce important conformational changes; this possibility has not been however as yet explored.

## V. A Role of Supercomplexes in Cell Physiology

The supercomplex organization of the mitochondrial electron transport chain imposes functional features to mitochondrial physiology that are a consequence of the different properties that supercomplexes assume with respect to individual cytochrome complexes (Genova and Lenaz 2014).

The dynamic character of the supercomplexes provides a mechanism to optimize the use of available substrates. In fact, glucose utilization as a fuel contributes largely to feed electrons to the respiratory chain through NADH and Complex I, whereas fatty acid oxidation feeds more electrons through a FAD-linked pathway (ETF dehydrogenase). Furthermore, in CD1 mouse mitochondria, fasting reduces maximal Complex I and Complex I+III activities (NADH route) without influencing Complex II or Complex II+III (Lapuente-Brun et al. 2013), and the proportion of Complex III assembled with

Complex I is reduced accordingly. How this change is produced and what would happen if this adaptation was impeded remain to be investigated. At present, no known molecular mechanism can be invoked to explain the exquisite regulation of the balance between Complex III<sub>NADH</sub> (i.e. Complex III dedicated to Complex I) and Complex III<sub>FAD</sub>. Further understanding of this behavior is of paramount importance.

The modulation of supercomplex assembly may have further consequences ensuring the possibility to modulate ATP levels and ROS production by changing the rate of electron flow in the respiratory chain. Dissociation of supercomplexes would contribute to a low level of NADH oxidation, and hence a high NADH/NAD<sup>+</sup> ratio within mitochondria, which could contribute a metabolic switch to the control of the cellular activity. In addition, the plasticity of the respiratory chain supercomplexes can be envisaged as a possible mechanism of intracellular signaling achieved by ROS molecular recognition (“mitochondrial retrograde signaling”, Whelan and Zuckerbraun 2013). One notable example is Nrf2 that, in the presence of ROS, is translocated from the cytoplasm to the nucleus, where it stimulates the antioxidant response element (ARE) of cytoprotective genes (Itoh et al. 1999).

Deficiency of respiratory supercomplexes and mitochondrial dysfunction is also correlated with mitochondrial morphology/quality maintenance in the development of the mitochondrial aging phenotype (Gómez et al. 2009; Frenzel et al. 2010; Gómez and Hagen 2012) and in the etiopathology of several diseases (cf. Lenaz and Genova 2012 for a review).

## References

- Acín-Peréz R, Enriquez JA (2014) The function of respiratory supercomplexes: the plasticity model. *Biochim Biophys Acta* 1837:444–450
- Acín-Peréz R, Bayona-Bafaluy MP, Fernández-Silva P, Moreno-Loshuertos R, Pérez-Martos A, Bruno C, Moraes CT, Enriquez JA (2004) Respiratory complex III is required to maintain complex I in mammalian mitochondria. *Mol Cell* 13:805–815
- Acín-Peréz R, Fernández-Silva P, Peleato ML, Pérez-Martos A, Enriquez JA (2008) Respiratory active mitochondrial supercomplexes. *Mol Cell* 32:529–539
- Acín-Peréz R, Salazar E, Brosel S, Yang H, Schon EA, Manfredi G (2009a) Modulation of mitochondrial protein phosphorylation by soluble adenylyl cyclase ameliorates cytochrome oxidase defects. *EMBO Mol Med* 1:392–406
- Acín-Peréz R, Salazar E, Kamenetsky M, Buck J, Levin LR, Manfredi G (2009b) Cyclic AMP produced inside mitochondria regulates oxidative phosphorylation. *Cell Metab* 9:265–276
- Acín-Peréz R, Gatti DL, Bai Y, Manfredi G (2011a) Protein phosphorylation and prevention of cytochrome oxidase inhibition by ATP: coupled mechanisms of energy metabolism regulation. *Cell Metab* 13:712–719
- Acín-Peréz R, Russwurm M, Gunnewig K, Gertz M, Zoidl G, Ramos L, Buck J, . . . , Steegborn C (2011b) A phosphodiesterase 2A isoform localized to mitochondria regulates respiration. *J Biol Chem* 286:30423–30432
- Althoff T, Mills DJ, Popot JL, Kühlbrandt W (2011) Arrangement of electron transport chain components in bovine mitochondrial supercomplex I(1)III(2)IV(1). *EMBO J* 30:4652–4664
- Baile MG, Lu YW, Claypool SM (2014a) The topology and regulation of cardiolipin biosynthesis and remodeling in yeast. *Chem Phys Lipids* 179:25–31
- Baile MG, Sathappa M, Lu YW, Pryce E, Whited K, McCaffery JM, Han X, . . . , Claypool SM (2014b) Unremodeled and remodeled cardiolipin are functionally indistinguishable in yeast. *J Biol Chem* 289:1768–1778
- Balsa E, Marco R, Perales-Clemente E, Szklarczyk R, Calvo E, Landázuri MO, Enriquez JA (2012) ND-UFA4 is a subunit of complex IV of the mammalian electron transport chain. *Cell Metab* 16:378–386
- Baniulis D, Saif Hasan S, Miliute I, Cramer WA (2015) Mechanisms of superoxide generation and signaling in cytochrome bc complexes. In: Cramer WA, Kallas T (eds) *Cytochrome Complexes: Evolution, Structures, Energy Transduction, and Signaling*. Springer, Dordrecht
- Baracca A, Chiaradonna F, Sgarbi G, Solaini G, Alberghina L, Lenaz G (2010) Mitochondrial complex I decrease is responsible for bioenergetic dysfunction in K-ras transformed cells. *Biochim Biophys Acta* 1797:314–323
- Barja G (2013) Updating the mitochondrial free radical theory of aging: an integrated view, key aspects,

- and confounding concepts. *Antioxid Redox Signal* 19:1420–1445
- Bazán S, Mileyskoykaya E, Mallampalli VK, Heacock P, Sparagna GC, Dowhan W (2013) Cardiolipin-dependent reconstitution of respiratory supercomplexes from purified *Saccharomyces cerevisiae* complexes III and IV. *J Biol Chem* 288:401–411
- Bellomo F, Piccoli C, Cocco T, Scacco S, Papa F, Gaballo A, Boffoli D, . . . , Papa S (2006) Regulation by the cAMP cascade of oxygen free radical balance in mammalian cells. *Antioxid Redox Signal* 8:495–502
- Benard G, Faustin B, Galinier A, Rocher C, Bellance N, Smolkova K, Casteilla L, . . . , Letellier T (2008) Functional dynamic compartmentalization of chain intermediate substrates: implications for the control of energy production and mitochondrial diseases. *Int J Biochem Cell Biol* 40:1543–1554
- Bianchi C, Fato R, Genova ML, Parenti Castelli G, Lenaz G (2003) Structural and functional organization of complex I in the mitochondrial respiratory chain. *Biofactors* 18:3–9
- Bianchi C, Genova ML, Parenti Castelli G, Lenaz G (2004) The mitochondrial respiratory chain is partially organized in a supercomplex assembly: kinetic evidence using flux control analysis. *J Biol Chem* 279:36562–36569
- Bloom M, Evans E, Mouritsen OG (1991) Physical properties of the fluid lipid-bilayer component of cell membranes: a perspective. *Q Rev Biophys* 24:293–397
- Bogdanov M, Mileyskoykaya E, Dowhan W (2008) Lipids in the assembly of membrane proteins and organization of protein supercomplexes: implications for lipid-linked disorders. *Subcell Biochem* 49:197–239
- Boumans H, Grivell LA, Berden JA (1998) The respiratory chain in yeast behaves as a single functional unit. *J Biol Chem* 273:4872–4877
- Brandner K, Mick DU, Frazier AE, Taylor RD, Meisinger C, Rehling P (2005) Taz1, an outer mitochondrial membrane protein, affects stability and assembly of inner membrane protein complexes: implications for Barth syndrome. *Mol Biol Cell* 16:5202–5214
- Braun HP, Sunderhaus S, Boekema EJ, Kouril R (2009) Purification of the cytochrome c reductase/cytochrome c oxidase super complex of yeast mitochondria. *Methods Enzymol* 456:183–190
- Brys K, Castelein N, Matthijssens F, Vanfleteren JR, Braeckman BP (2010) Disruption of insulin signalling preserves bioenergetic competence of mitochondria in ageing *Caenorhabditis elegans*. *BMC Biol* 8:91
- Bultema JB, Braun HP, Boekema EJ, Kouril R (2009) Megacomplex organization of the oxidative phosphorylation system by structural analysis of respiratory supercomplexes from potato. *Biochim Biophys Acta* 1787:60–67
- Cabrera-Orefice A, Chiquete-Félix N, Espinasa-Jaramillo J, Rosas-Lemus M, Guerrero-Castillo S, Peña A, Uribe-Carvajal S (2014) The branched mitochondrial respiratory chain from *Debaryomyces hansenii*: components and supramolecular organization. *Biochim Biophys Acta* 1837:73–84
- Calvaruso MA, Willems P, van den Brand M, Valsecchi F, Kruse S, Palminter R, Smeitink J, Nijtmans L (2011) Mitochondrial complex III stabilizes complex I in the absence of NDUFS4 to provide partial activity. *Hum Mol Genet* 21:115–120
- Capaldi RA (1982) Arrangement of proteins in the mitochondrial inner membrane. *Biochim Biophys Acta* 694:292–306
- Castellani M, Covian R, Kleinschroth T, Anderka O, Ludwig B, Trumpower BL (2010) Direct demonstration of half-of-the-sites reactivity in the dimeric cytochrome bc1 complex: enzyme with one inactive monomer is fully active but unable to activate the second ubiquinol oxidation site in response to ligand binding at the ubiquinone reduction site. *J Biol Chem* 285:502–510
- Chaban Y, Boekema EJ, Dudkina NV (2014) Structures of mitochondrial oxidative phosphorylation supercomplexes and mechanisms for their stabilization. *Biochim Biophys Acta* 1837:418–426
- Chance B, Williams GR (1955) A method for the localization of sites for oxidative phosphorylation. *Nature* 176:250–254
- Chen S, He Q, Greenberg ML (2008) Loss of tafazzin in yeast leads to increased oxidative stress during respiratory growth. *Mol Microbiol* 68:1061–1072
- Chen Y-C, Taylor EB, Dephore N, Heo J-M, Tonhato A, Papandreou I, Nath N, . . . , Rutter J (2012) Identification of a protein mediating respiratory supercomplex stability. *Cell Metab* 15:348–360
- Choksi KB, Boylston WH, Rabek JP, Widger WR, Papaconstantinou J (2004) Oxidatively damaged proteins of heart mitochondrial electron transport complexes. *Biochim Biophys Acta* 1688:95–101
- Claypool SM (2009) Cardiolipin, a critical determinant of mitochondrial carrier protein assembly and function. *Biochim Biophys Acta* 1788:2059–2068
- Claypool SM, Oktay Y, Boontheung P, Loo JA, Koehler CM (2008) Cardiolipin defines the interactome of the major ADP/ATP carrier protein of the mitochondrial inner membrane. *J Cell Biol* 182:937–950
- Cogliati S, Frezza C, Soriano ME, Varanita T, Quintana-Cabrera R, Corrado M, Cipolat S, . . . ,

- Scorrano L (2013) Mitochondrial cristae shape determines respiratory chain supercomplexes assembly and respiratory efficiency. *Cell* 155:160–171
- Cossins AR, Kent J, Prosser CL (1980) A steady state and differential polarised phase fluorimetric study of the liver microsomal and mitochondrial membranes of thermally acclimated green sunfish (*Lepomis cyanellus*). *Biochim Biophys Acta* 599:341–358
- Cui H, Kong Y, Zhang H (2012) Oxidative stress, mitochondrial dysfunction, and aging. *J Signal Transduct* 2012:646354
- Cui TZ, Conte A, Fox JL, Zara V, Winge DR (2014) Modulation of the respiratory supercomplexes in yeast: enhanced formation of cytochrome oxidase increases the stability and abundance of respiratory supercomplexes. *J Biol Chem* 289:6133–6141
- D'Aurelio M, Gajewski CD, Lenaz G, Manfredi G (2006) Respiratory chain supercomplexes set the threshold for respiration defects in human mtDNA mutant cybrids. *Hum Mol Genet* 15:2157–2269
- Dalmonte ME, Forte E, Genova ML, Giuffrè A, Sarti P, Lenaz G (2009) Control of respiration by cytochrome c oxidase in intact cells: role of the membrane potential. *J Biol Chem* 284:32331–32335
- Dani D, Shimokawa I, Komatsu T, Higami Y, Warnken U, Schokraie E, Schnölzer M, ..., Dencher NA (2009) Modulation of oxidative phosphorylation machinery signifies a prime mode of anti-ageing mechanism of calorie restriction in male rat liver mitochondria. *Biogerontology* 11:321–334
- Daum B, Walter A, Horst A, Osiewacz HD, Kühlbrandt W (2013) Age-dependent dissociation of ATP synthase dimers and loss of inner-membrane cristae in mitochondria. *Proc Natl Acad Sci USA* 110:15301–15306
- Davies KM, Strauss M, Daum B, Kief JH, Osiewacz HD, Rycovska A, Zickermann V, Kühlbrandt W (2011) Macromolecular organization of ATP synthase and complex I in whole mitochondria. *Proc Natl Acad Sci USA* 108:14121–14126
- Davoudi M, Kotarsky H, Hansson E, Fellman V (2014) Complex I function and supercomplex formation are preserved in liver mitochondria despite progressive complex III deficiency. *PLoS ONE* 9:e86767
- De los Rios Castillo D, Zarco-Zavala M, Olvera-Sanchez S, Pardo JP, Juarez O, Martinez F, Mendoza-Hernandez G, ..., Flores-Herrera O (2011) Atypical cristae morphology of human syncytiotrophoblast mitochondria: role for complex V. *J Biol Chem* 286:23911–23919
- de Rasmio D, Panelli D, Sardanelli AM, Papa S (2008) cAMP-dependent protein kinase regulates the mitochondrial import of the nuclear encoded NDUFS4 subunit of complex I. *Cell Signal* 20:989–997
- Dencher NA, Frenzel M, Reifschneider NH, Sugawa M, Krause F (2007) Proteome alterations in rat mitochondria caused by aging. *Ann NY Acad Sci* 1100:291–298
- Deng N, Zhang J, Zong C, Wang Y, Lu H, Yang P, Wang W, ..., Ping P (2011) Phosphoproteome analysis reveals regulatory sites in major pathways of cardiac mitochondria. *Mol Cell Proteomics* 10:M110.000117
- Diaz F, Fukui H, Garcia S, Moraes CT (2006) Cytochrome c oxidase is required for the assembly/stability of respiratory complex I in mouse fibroblasts. *Mol Cell Biol* 26:4872–4881
- Diaz F, Garcia S, Padgett KR, Moraes CT (2012a) A defect in the mitochondrial complex III, but not complex IV, triggers early ROS-dependent damage in defined brain regions. *Hum Mol Genet* 21:5066–5077
- Diaz F, Enriquez JA, Moraes CT (2012b) Cells lacking Rieske iron-sulfur protein have a reactive oxygen species-associated decrease in respiratory complexes I and IV. *Mol Cell Biol* 32:415–429
- Dowhan W, Bogdanov M (2009) Lipid-dependent membrane protein topogenesis. *Annu Rev Biochem* 78:515–540
- Dröse S, Brandt U, Wittig I (2014) Mitochondrial respiratory chain complexes as sources and targets of thiol-based redox-regulation. *Biochim Biophys Acta* 1844:1344–1354
- Dudek J, Cheng IF, Balleininger M, Vaz FM, Streckfuss-Bömeke K, Hübscher D, Vukotic M, ..., Guan K (2013) Cardiolipin deficiency affects respiratory chain function and organization in an induced pluripotent stem cell model of Barth syndrome. *Stem Cell Res* 11:806–819
- Dudkina NV, Eubel H, Keegstra W, Boekema EJ, Braun HP (2005) Structure of a mitochondrial supercomplex formed by respiratory-chain complexes I and III. *Proc Natl Acad Sci USA* 102:3225–3229
- Dudkina NV, Oostergetel GT, Lewejohann D, Braun HP, Boekema EJ (2010) Row-like organization of ATP synthase in intact mitochondria determined by cryo-electron tomography. *Biochim Biophys Acta* 1797:272–277
- Dudkina NV, Kudryashev M, Stahlberg H, Boekema EJ (2011) Interaction of complexes I, III, and IV within the bovine respirasome by single particle cryoelectron tomography. *Proc Natl Acad Sci USA* 108:15196–15200
- Else PL, Turner N, Hulbert AJ (2004) The evolution of endothermy: role for membranes and molecular activity. *Physiol Biochem Zool* 77:950–958
- Enriquez JA, Lenaz G (2014) Coenzyme Q and the respiratory chain: coenzyme Q pool and mitochondrial supercomplexes. *Mol Syndromol* 5:119–140

- Estornell E, Fato R, Castelluccio C, Cavazzoni M, Parenti Castelli G, Lenaz G (1992) Saturation kinetics of coenzyme Q in NADH and succinate oxidation in beef heart mitochondria. *FEBS Lett* 311:107–109
- Eubel H, Heinemeyer J, Sunderhaus S, Braun HP (2004) Respiratory chain supercomplexes in plant mitochondria. *Plant Physiol Biochem* 42:937–942
- Fato R, Bergamini C, Bortolus M, Maniero AL, Leoni S, Ohnishi T, Lenaz G (2009) Differential effects of complex I inhibitors on production of reactive oxygen species. *Biochim Biophys Acta* 1787:384–392
- Fisher N, Bowman MK, Kramer D (2015) Electron transfer reactions at the Q<sub>o</sub> site of the cytochrome *bc*<sub>1</sub> complex: the good, the bad, and the ugly. In: Cramer WA, Kallas T (eds) *Cytochrome Complexes: Evolution, Structures, Energy Transduction, and Signaling*. Springer, Dordrecht
- Fleischer S, Fleischer B, Stoeckenius W (1967) Fine structure of lipid-depleted mitochondria. *J Cell Biol* 32:193–208
- Frenzel M, Rommelspacher H, Sugawa MD, Dencher NA (2010) Ageing alters the supramolecular architecture of OxPhos complexes in rat brain cortex. *Exp Gerontol* 45:563–572
- Froud RJ, Ragan CI (1984a) Cytochrome c-mediated electron transfer between ubiquinol-cytochrome c reductase and cytochrome c oxidase. Kinetic evidence for a mobile cytochrome c pool. *Biochem J* 217:551–560
- Froud RJ, Ragan CI (1984b) Cytochrome c mediates electron transfer between ubiquinol-cytochrome c reductase and cytochrome c oxidase by free diffusion along the surface of the membrane. *Biochem J* 217:561–571
- Fry M, Green DE (1980) Cardiolipin requirement by cytochrome oxidase and the catalytic role of phospholipid. *Biochem Biophys Res Commun* 93:1238–1246
- Fry M, Green DE (1981) Cardiolipin requirement for electron transfer in complex I and III of the mitochondrial respiratory chain. *J Biol Chem* 256:1874–1880
- Fukushima T, Decker RV, Anderson WM, Spivey HO (1989) Substrate channeling of NADH and binding of dehydrogenases to complex I. *J Biol Chem* 264:16483–16488
- Fyfe PK, Jones MR (2005) Lipids in and around photosynthetic reaction centres. *Biochem Soc Trans* 33:924–930
- Genova ML, Lenaz G (2011) New developments on the functions of coenzyme Q in mitochondria. *Biofactors* 37:330–354
- Genova ML, Lenaz G (2013) A critical appraisal of the role of respiratory supercomplexes in mitochondria. *Biol Chem* 394:631–639
- Genova ML, Lenaz G (2014) Functional role of mitochondrial respiratory supercomplexes. *Biochim Biophys Acta* 1837:427–443
- Genova ML, Baracca A, Biondi A, Casalena G, Facioli M, Falasca AI, Formiggini G, . . . , Lenaz G (2008) Is supercomplex organization of the respiratory chain required for optimal electron transfer activity? *Biochim Biophys Acta* 1777:740–746
- Ghelli A, Tropeano CV, Calvaruso MA, Marchesini A, Iommarini L, Porcelli AM, Zanna C, . . . , Rugolo M (2013) The cytochrome b p.278Y>C mutation causative of a multisystem disorder enhances superoxide production and alters supramolecular interactions of respiratory chain complexes. *Hum Mol Genet* 22:2141–2151
- Gil T, Ipsen JH, Mouritsen OG, Sabra MC, Sperotto MM, Zuckermann MJ (1998) Theoretical analysis of protein organization in lipid membranes. *Biochim Biophys Acta* 1376:245–266
- Gómez LA, Hagen TM (2012) Age-related decline in mitochondrial bioenergetics: does supercomplex destabilization determine lower oxidative capacity and higher superoxide production? *Semin Cell Dev Biol* 23:758–767
- Gómez LA, Monette JS, Chavez JD, Maier CS, Hagen TM (2009) Supercomplexes of the mitochondrial electron transport chain decline in the aging rat heart. *Arch Biochem Biophys* 490:30–35
- Gonzalvez F, D'Aurelio M, Boutant M, Moustapha A, Puech JP, Landes T, Arnauné-Pelloquin L, . . . , Petit PX (2013) Barth syndrome: cellular compensation of mitochondrial dysfunction and apoptosis inhibition due to changes in cardiolipin remodeling linked to tafazzin (TAZ) gene mutation. *Biochim Biophys Acta* 1832:1194–1206
- Grad LI, Lamire D (2006) Riboflavin enhances the assembly of mitochondrial cytochrome c oxidase in *C. elegans* NADH ubiquinone reductase mutants. *Biochim Biophys Acta* 1757:115–122
- Grad LI, Lemire D (2004) Mitochondrial complex I mutations in *Caenorhabditis elegans* produce cytochrome c oxidase deficiency, oxidative stress and vitamin-response lactic acidosis. *Hum Mol Genet* 13:303–314
- Green DE, Fleischer S (1963) The role of lipids in mitochondrial electron transfer and oxidative phosphorylation. *Biochim Biophys Acta* 70:554–582
- Green DE, Tzagoloff A (1966) The mitochondrial electron transfer chain. *Arch Biochem Biophys* 116:293–304

- Grimsrud PA, Carson JJ, Hebert AS, Hubler SL, Niemi NM, Bailey DJ, Jochem A, . . . , Pagliarini DJ (2012) A quantitative map of the liver mitochondrial phosphoproteome reveals posttranslational control of ketogenesis. *Cell Metab* 16:672–683
- Gupte SS, Hackenbrock CR (1988a) Multidimensional diffusion modes and collision frequencies of cytochrome c with its redox partners. *J Biol Chem* 263:5241–5247
- Gupte SS, Hackenbrock CR (1988b) The role of cytochrome c diffusion in mitochondrial electron transport. *J Biol Chem* 263:5248–5253
- Gupte SS, Wu ES, Hoechli L, Hoechli M, Jacobson K, Sowers AE, Hackenbrock CR (1984) Relationship between lateral diffusion, collision frequency, and electron transfer of mitochondrial inner membrane oxidation-reduction components. *Proc Natl Acad Sci USA* 81:2606–2610
- Gutman M (1985) Kinetic analysis of electron flux through the quinones in the mitochondrial system. In: Lenaz G (ed) *Coenzyme Q*. Wiley, Chichester, pp 215–234
- Gwak SH, Yu L, Yu CA (1986) Spin-label electron paramagnetic resonance and differential scanning calorimetry studies of the interaction between mitochondrial succinate-ubiquinone and ubiquinol-cytochrome c reductases. *Biochemistry* 25:7675–7682
- Habersetzer J, Ziani W, Larrieu I, Stines-Chaumeil C, Giraud MF, Brèthes D, Dautant A, Paumard P (2013) ATP synthase oligomerization: from the enzyme models to the mitochondrial morphology. *Int J Biochem Cell Biol* 45:99–105
- Hackenbrock CR, Chazotte B, Gupte SS (1986) The random collision model and a critical assessment of diffusion and collision in mitochondrial electron transport. *J Bioenerg Biomembr* 18:331–368
- Haines TH, Dencher NA (2002) Cardiolipin: a proton trap for oxidative phosphorylation. *FEBS Lett* 528:35–39
- Hashimoto T, Hussien R, Cho H-S, Kaufer D, Brooks GA (2008) Evidence for the mitochondrial lactate oxidation complex in rat neurons: demonstration of an essential component of brain lactate shuttles. *PLoS ONE* 3, e2915
- Hatefi Y, Rieske JS (1967) Preparation and properties of DPNH-coenzyme Q reductase (Complex I of the respiratory chain). *Methods Enzymol* 10:235–239
- Hatefi Y, Haavik AG, Fowler LR, Griffiths DE (1962a) Studies on the electron transfer system. XLII. Reconstitution of the electron transfer system. *J Biol Chem* 237:2661–2669
- Hatefi Y, Haavik AG, Griffiths DE (1962b) Studies on the electron transfer system. XL. Preparation and properties of mitochondrial DPNH-Coenzyme Q reductase. *J Biol Chem* 237:1676–1680
- Hatle KM, Gummadidala P, Navasa N, Bernardo E, Dodge J, Silverstrim B, Fortner K, . . . , Rincon M (2013) MCJ/DnaJC15, an endogenous mitochondrial repressor of the respiratory chain that controls metabolic alterations. *Mol Cell Biol* 33:2302–2314
- Hébert-Chatelain E (2013) Src kinases are important regulators of mitochondrial functions. *Int J Biochem Cell Biol* 45:90–98
- Hébert-Chatelain E, Jose C, Gutierrez Cortes N, Dupuy JW, Rocher C, Dachary-Prigent J, Letellier T (2012) Preservation of NADH ubiquinone-oxidoreductase activity by Src kinase-mediated phosphorylation of NDUFB10. *Biochim Biophys Acta* 1817:718–725
- Heron C, Ragan CI, Trumpower BL (1978) The interaction between mitochondrial NADH-ubiquinone oxidoreductase and ubiquinol-cytochrome c oxidoreductase - restoration of ubiquinone-pool behaviour. *Biochem J* 174:791–800
- Hesketh TR, Smith GA, Houslay MD, McGill KA, Birdsall NJ, Metcalfe JC, Warren GB (1976) Annular lipids determine ATPase activity of a calcium transport protein complexes with dipalmitoyllecithin. *Biochemistry* 15:4145–4151
- Hildebrandt TM (2011) Modulation of sulfide oxidation and toxicity in rat mitochondria by dehydroascorbic acid. *Biochim Biophys Acta* 1807:1206–1213
- Hirst J, King MS, Pryde KR (2008) The production of reactive oxygen species by complex I. *Biochem Soc Trans* 36:976–980
- Hochman J, Ferguson-Miller S, Schindler M (1985) Mobility in the mitochondrial electron transport chain. *Biochemistry* 24:2509–2516
- Horvath SE, Daum G (2013) Lipids of mitochondria. *Prog Lipid Res* 52:590–614
- Houtkooper RH, Vaz FM (2008) Cardiolipin, the heart of mitochondrial metabolism. *Cell Mol Life Sci* 65:2493–2506
- Hunte C (2005) Specific protein-lipid interactions in membrane proteins. *Biochem Soc Trans* 33:938–942
- Hunte C, Richers S (2008) Lipids and membrane protein structures. *Curr Opin Struct Biol* 18:406–411
- Itoh K, Wakabayashi N, Katoh Y, Ishii T, Igarashi K, Engel JD, Yamamoto M (1999) Keap1 represses nuclear activation of antioxidant responsive elements by Nrf2 through binding to the amino-terminal Neh2 domain. *Genes Dev* 13:76–86
- Iuso A, Scacco S, Piccoli C, Bellomo F, Petruzzella V, Trentadue R, Minuto M, . . . , Papa S (2006) Dysfunctions of cellular oxidative metabolism in



- patients with mutations in the NDUFS1 and NDUFS4 genes of complex I. *J Biol Chem* 281: 10374–10380
- Jormakka M, Törnroth S, Byrne B, Iwata S (2002) Molecular basis of proton motive force generation: structure of formate dehydrogenase-N. *Science* 295:1863–1868
- Jost P, Griffith OH, Capaldi RA, Vanderkooi G (1973) Evidence for boundary lipids in membranes. *Proc Natl Acad Sci USA* 70:480–484
- Kaambre T, Chekulayev V, Shevchuk I, Karu-Varikmaa M, Timohhina N, Tepp K, Bogovskaja J, . . . , Saks V (2012) Metabolic control analysis of cellular respiration in situ in intraoperational samples of human breast cancer. *J Bioenerg Biomembr* 44:539–558
- Kaambre T, Chekulayev V, Shevchuk I, Tepp K, Timohhina N, Varikmaa M, Bagur R, . . . , Saks V (2013) Metabolic control analysis of respiration in human cancer tissue. *Front Physiol* 4:151
- Kacsner H, Burns JA (1995) The control of flux. *Biochem Soc Trans* 23:341–366
- Kakizaki Y, Moore AL, Kikukatsu I (2012) Different molecular bases underlie the mitochondrial respiratory activity in the homoeothermic spadices of *Symplocarpus renifolius* and the transiently thermogenic appendices of *Arum maculatum*. *Biochem J* 445:237–246
- Kang SY, Gutowsky HS, Hsung JC, Jacobs R, King TE, Rice D, Oldfield E (1979) Nuclear magnetic resonance investigation of the cytochrome oxidase-phospholipid interaction: a new model for boundary lipid. *Biochemistry* 18:3257–3267
- Kates M, Syz JY, Gosser D, Haines TH (1993) pH-dissociation characteristics of cardiolipin and its 2'-deoxy analogue. *Lipids* 28:877–882
- Kawato S, Sigel E, Carafoli E, Cherry RJ (1980) Cytochrome oxidase rotates in the inner membrane of intact mitochondria and submitochondrial particles. *J Biol Chem* 255:5508–5510
- Kawato S, Sigel E, Carafoli E, Cherry RJ (1981) Rotation of cytochrome oxidase in phospholipid vesicles. Investigations of interactions between cytochrome oxidases and between cytochrome oxidase and cytochrome bc1 complex. *J Biol Chem* 256:7518–7527
- Kawato S, Lehner C, Müller M, Cherry RJ (1982) Protein-protein interactions of cytochrome oxidase in inner mitochondrial membranes. The effect of liposome fusion on protein rotational mobility. *J Biol Chem* 257:6470–6476
- Khalifat N, Puff N, Bonneau S, Fournier JB, Angelova MI (2008) Membrane deformation under local pH gradient: mimicking mitochondrial cristae dynamics. *Biophys J* 95:4924–4933
- Khalifat N, Fournier JB, Angelova MI, Puff N (2011) Lipid packing variations induced by pH in cardiolipin-containing bilayers: the driving force for the cristae-like shape instability. *Biochim Biophys Acta* 1808:2724–2733
- Kholodenko NB, Westerhoff HV (1993) Metabolic channelling and control of the flux. *FEBS Lett* 320:71–74
- King TE, Takemori S (1964) Reconstitution of respiratory chain enzyme systems. XIV. Reconstitution of succinate cytochrome c reductase from soluble succinate dehydrogenase and the cytochrome bc1 particle. *J Biol Chem* 239:3559–3569
- Koob S, Reichert AS (2014) Novel intracellular functions of apolipoproteins: the ApoO protein family as constituents of the Mitofilin/MINOS complex determines cristae morphology in mitochondria. *Biol Chem* 395:285–296
- Kotlyar AB, Maklashina E, Cecchini G (2004) Absence of NADH channeling in coupled reaction of mitochondrial malate dehydrogenase and complex I in alamethicin-permeabilized rat liver mitochondria. *Biochem Biophys Res Commun* 318:987–991
- Kovářová N, Cížková Vrbacká A, Pecina P, Stránecký V, Pronicka E, Kmoch S, Houštěk J (2012) Adaptation of respiratory chain biogenesis to cytochrome c oxidase deficiency caused by SURF1 gene mutations. *Biochim Biophys Acta* 1822:1114–1124
- Kovářová N, Mráček T, Nůsková H, Holzerová E, Vrbacký M, Pecina P, Hejzlarová K, . . . , Houštěk J (2013) High molecular weight forms of mammalian respiratory chain complex II. *PLoS ONE* 8:e71869
- Kraffe E, Soudant P, Marty Y (2004) Fatty acids of serine, ethanolamine, and choline plasmalogens in some marine bivalves. *Lipids* 39:59–66
- Krause F (2006) Detection and analysis of protein-protein interactions in organellar and prokaryotic proteomes by native gel electrophoresis: (membrane) protein complexes and supercomplexes. *Electrophoresis* 27:2759–2781
- Krause F, Seelert H (2008) Detection and analysis of protein-protein interactions of organellar and prokaryotic proteomes by blue native and colorless native gel electrophoresis. *Curr Protoc Protein Sci* 19:Unit 19.18
- Krause F, Reifschneider NH, Vocke D, Seelert H, Rexroth S, Dencher NA (2004a) Respirasome-like supercomplexes in green leaf mitochondria of spinach. *J Biol Chem* 279:48369–48375
- Krause F, Scheckhuber CQ, Werner A, Rexroth S, Reifschneider NH, Dencher NA, Osiewacz HD (2004b) Supramolecular organization of cytochrome c oxidase- and alternative oxidase-

- dependent respiratory chains in the filamentous fungus *Podospora anserina*. *J Biol Chem* 279:26453–26461
- Kröger A, Klingenberg M (1973a) The kinetics of the redox reactions of ubiquinone related to the electron-transport activity in the respiratory chain. *Eur J Biochem* 34:358–368
- Kröger A, Klingenberg M (1973b) Further evidence of the pool function of ubiquinone as derived from the inhibition of the electron transport by antimycin. *Eur J Biochem* 39:313–323
- Lamantea E, Carrara F, Mariotti C, Morandi L, Tiranti V, Zeviani M (2002) A novel nonsense mutation (Q352X) in the mitochondrial cytochrome b gene associated with a combined deficiency of complexes I and III. *Neuromuscul Disord* 12:49–52
- Lange C, Nett JH, Trumpower BL, Hunte C (2001) Specific roles of protein-phospholipid interactions in the yeast cytochrome bc1 complex structure. *EMBO J* 20:6591–6600
- Lapuente-Brun E, Moreno-Loshuertos R, Acín-Peréz R, Latorre-Pellicer A, Colás C, Balsa E, Perales-Clemente E, . . . , Enríquez JA (2013) Supercomplex assembly determines electron flux in the mitochondrial electron transport chain. *Science* 340:1567–1570
- Le Pécheur M, Morrow G, Kim H-J, Schäfer E, Dencher N, Tanguay RM (2009) Characterization of OXPHOS complexes in long-lived flies overexpressing Hsp22. Mitochondria in ageing and age-related disease, MiMage final meeting (and LINK-AGE Topic Research) group meeting, abstract 16:35
- Lee AG (2004) How lipids affect the activities of integral membrane proteins. *Biochim Biophys Acta* 1666:62–87
- Lenaz G (1979) The role of lipids in the structure and function of membranes. *Subcell Biochem* 6:233–343
- Lenaz G (1987) Lipid fluidity and membrane protein dynamics. *Biosci Rep* 7:823–837
- Lenaz G (1988) Role of mobility of redox components in the inner mitochondrial membrane. *J Membr Biol* 104:193–209
- Lenaz G (2012) Mitochondrial and reactive oxygen species. Which role in physiology and pathology? *Adv Exp Med Biol* 942:93–136
- Lenaz G (2014) Role of mitochondria in the generation of reactive oxygen species. In: Suzuki M, Yamamoto S (eds) *Handbook of Reactive Oxygen Species (ROS)*. Nova Biomedical, New York, pp 1–108
- Lenaz G, Genova ML (2007) Kinetics of integrated electron transfer in the mitochondrial respiratory chain: random collisions vs. solid state electron channeling. *Am J Physiol Cell Physiol* 292:C1221–C1239
- Lenaz G, Genova ML (2009) Mobility and function of coenzyme Q (ubiquinone) in the mitochondrial respiratory chain. *Biochim Biophys Acta* 1787:563–573
- Lenaz G, Genova ML (2010) Structure and organization of mitochondrial respiratory complexes: a new understanding of an old subject. *Antioxid Redox Signal* 12:961–1008
- Lenaz G, Genova ML (2012) Supramolecular organization of the mitochondrial respiratory chain: a new challenge for the mechanism and control of oxidative phosphorylation. *Adv Exp Med Biol* 748:107–144
- Lenaz G, Fato R, Di Bernardo S, Jarreta D, Costa A, Genova ML, Parenti Castelli G (1999) Localization and mobility of coenzyme Q in lipid bilayers and membranes. *Biofactors* 9:87–93
- Lenaz G, Baracca A, Barbero G, Bergamini C, DalmonTE ME, del Sole M, Faccioli M, . . . , Solaini G (2010) Mitochondrial respiratory chain supercomplex I-III in physiology and pathology. *Biochim Biophys Acta* 1797:633–640
- Li G, Chen S, Thompson MN, Greenberg ML (2007) New insights into the regulation of cardiolipin biosynthesis in yeast: implications for Barth syndrome. *Biochim Biophys Acta* 1771:432–441
- Lombardi A, Silvestri E, Cioffi F, Senese R, Lanni A, Goglia F, de Lange P, Moreno M (2009) Defining the transcriptomic and proteomic profiles of rat ageing skeletal muscle by the use of a cDNA array, 2D- and Blue native-PAGE approach. *J Proteomics* 72:708–721
- Maas MF, Krause F, Dencher NA, Sainsard-Chanet A (2009) Respiratory complexes III and IV are not essential for the assembly/stability of complex I in fungi. *J Mol Biol* 387:259–269
- Maj MC, Raha S, Myint T, Robinson BH (2004) Regulation of NADH/CoQ oxidoreductase: do phosphorylation events affect activity? *Protein J* 23:25–32
- Maranzana E, Barbero G, Falasca AI, Lenaz G, Genova ML (2013) Mitochondrial respiratory supercomplex association limits production of reactive oxygen species from complex I. *Antioxid Redox Signal* 19:1469–1480
- Marques I, Dencher NA, Videira A, Krause F (2007) Supramolecular organization of the respiratory chain in *Neurospora crassa* mitochondria. *Eukaryot Cell* 6:2391–2405

- Marsh D, Horvath LI (1998) Structure, dynamics and composition of the lipid-protein interface. Perspectives from spin-labelling. *Biochim Biophys Acta* 1376:267–296
- McKenzie M, Lazarou M, Thorburn DR, Ryan MT (2006) Mitochondrial respiratory chain supercomplexes are destabilized in Barth syndrome patients. *J Mol Biol* 361:462–469
- Megli FM, Sabatini K (2003) EPR studies of phospholipid bilayers after lipoperoxidation. I. Inner molecular order and fluidity gradient. *Chem Phys Lipids* 125:161–172
- Mejia EM, Nguyen H, Hatch GM (2014) Mammalian cardiolipin biosynthesis. *Chem Phys Lipids* 179:11–16
- Mick DU, Wagner K, van der Laan M, Frazier AE, Perschil I, Pawlas M, Meyer HE, . . . , Rehling P (2007) Shy1 couples Cox1 translational regulation to cytochrome c oxidase assembly. *EMBO J* 26:4347–4358
- Mileykovskaya E, Dowhan W (2009) Cardiolipin membrane domains in prokaryotes and eukaryotes. *Biochim Biophys Acta* 1788:2084–2091
- Mileykovskaya E, Dowhan W (2014) Cardiolipin-dependent formation of mitochondrial respiratory supercomplexes. *Chem Phys Lipids* 179:42–48
- Mileykovskaya E, Zhang M, Dowhan W (2005) Cardiolipin in energy transducing membranes. *Biochemistry (Mosc)* 70:154–158
- Mileykovskaya E, Penczek PA, Fang J, Mallampalli VK, Sparagna GC, Dowhan W (2012) Arrangement of the respiratory chain complexes in *Saccharomyces cerevisiae* supercomplex III<sub>2</sub>IV<sub>2</sub> revealed by single particle cryo-electron microscopy. *J Biol Chem* 287:23095–23103
- Miyake N, Yano S, Sakai C, Hatakeyama H, Matsushima Y, Shiina M, Watanabe Y, . . . , Matsumoto N (2013) Mitochondrial complex III deficiency caused by a homozygous UQCRC2 mutation presenting with neonatal-onset recurrent metabolic decompensation. *Hum Mutat* 34:446–452
- Moreno Lastres D, Fontanesi F, García-Consuegra I, Martín MA, Arenas J, Barrientos A, Ugalde C (2012) Mitochondrial complex I plays an essential role in human respirasome assembly. *Cell Metab* 15:324–335
- Mráček T, Holzerová E, Drahotka Z, Kovářová N, Vrbacký M, Ješina P, Houštěk J (2014) ROS generation and multiple forms of mammalian mitochondrial glycerol-3-phosphate dehydrogenase. *Biochim Biophys Acta* 1837:98–111
- Muenzner J, Pletneva EV (2014) Structural transformations of cytochrome c upon interaction with cardiolipin. *Chem Phys Lipids* 179:57–63
- Musatov A, Fabian M, Varhač R (2013) Elucidating the mechanism of ferrocytochrome c heme disruption by peroxidized cardiolipin. *J Biol Inorg Chem* 18:137–144
- Muster B, Kohl W, Wittig I, Strecker V, Joos F, Haase W, Bereiter-Hahn J, Busch K (2010) Respiratory chain complexes in dynamic mitochondria display a patchy distribution in life cells. *PLoS ONE* 5, e11910
- Nicholls DG, Feguson SJ (2013) *Bioenergetics*, 4th edn. Academic, New York
- Norling B, Glazek E, Nelson BD, Ernster L (1974) Studies with ubiquinone-depleted submitochondrial particles. Quantitative incorporation of small amounts of ubiquinone and its effects on the NADH and succinate oxidase activities. *Eur J Biochem* 47:475–482
- Nozawa Y (2011) Adaptive regulation of membrane lipids and fluidity during thermal acclimation in *Tetrahymena*. *Proc Jpn Acad Ser B Phys Biol Sci* 87:450–462
- Nübel E, Wittig I, Kerscher S, Brandt U, Schägger H (2009) Two-dimensional native electrophoretic analysis of respiratory supercomplexes from *Yarrowia lipolytica*. *Proteomics* 9:2408–2418
- Ohya S, Kuwata Y, Sakamoto K, Muraki K, Imaizumi Y (2005) Cardioprotective effects of estradiol include the activation of large-conductance Ca<sup>2+</sup>-activated K<sup>+</sup> channels in cardiac mitochondria. *Am J Physiol Heart Circ Physiol* 289:H1635–H1642
- Osman C, Voelker DR, Langer T (2011) Making heads or tails of phospholipids in mitochondria. *J Cell Biol* 192:7–16
- Ovådi J (1991) Physiological significance of metabolic channelling. *J Theor Biol* 152:135–141
- Ovådi J, Huang Y, Spivey HO (1994) Binding of malate dehydrogenase and NADH channeling to complex I. *J Mol Recognit* 7:265–272
- Ozawa T, Tanaka M, Wakabayashi T (1982) Crystallization of mitochondrial cytochrome oxidase. *Proc Natl Acad Sci USA* 179:7175–7179
- Ozawa T, Nishikimi M, Suzuki H, Tanaka M, Shimomura Y (1987) Structure and assembly of mitochondrial electron-transfer complexes. In: Ozawa T, Papa S (eds) *Bioenergetics: Structure and Function of Energy-Transducing Systems*. The Japan Science Society Press, Tokyo, pp 101–119
- Panov A, Dikalov S, Shalbuyeva N, Hemendinger R, Greenamyre JT, Rosenfeld J (2007) Species- and tissue-specific relationships between mitochondrial permeability transition and generation of ROS in brain and liver mitochondria of rats and mice. *Am J Physiol Cell Physiol* 292:C708–C718

- Papa S, De Rasmio D, Scacco S, Signorile A, Technikova-Dobrova Z, Palmisano G, Sardanelli AM, . . . , Santeramo A (2008) Mammalian complex I: a regulable and vulnerable pacemaker in mitochondrial respiratory function. *Biochim Biophys Acta* 1777:719–728
- Paradies G, Petrosillo G, Pistolese M, Ruggiero FM (2000) The effect of reactive oxygen species generated from the mitochondrial electron transport chain on the cytochrome c oxidase activity and on the cardiolipin content in bovine heart submitochondrial particles. *FEBS Lett* 466:323–326
- Paradies G, Petrosillo G, Pistolese M, Ruggiero FM (2002) Reactive oxygen species affect mitochondrial electron transport complex I activity through oxidative cardiolipin damage. *Gene* 286:135–141
- Paradies G, Petrosillo G, Pistolese M, Di Venosa N, Federici A, Ruggiero FM (2004) Decrease in mitochondrial complex I activity in ischemic/reperfused rat heart: involvement of reactive oxygen species and cardiolipin. *Circ Res* 94:53–59
- Paradies G, Petrosillo G, Paradies V, Ruggiero FM (2009) Role of cardiolipin peroxidation and Ca<sup>2+</sup> in mitochondrial dysfunction and disease. *Cell Calcium* 45:643–650
- Paradies G, Petrosillo G, Paradies V, Ruggiero FM (2010) Oxidative stress, mitochondrial bioenergetics, and cardiolipin in aging. *Free Radic Biol Med* 48:1286–1295
- Paradies G, Paradies V, De Benedictis V, Ruggiero FM, Petrosillo G (2014a) Functional role of cardiolipin in mitochondrial bioenergetics. *Biochim Biophys Acta* 1837:408–417
- Paradies G, Paradies V, Ruggiero FM, Petrosillo G (2014b) Cardiolipin and mitochondrial function in health and disease. *Antioxid Redox Signal* 20:1925–1953
- Pebay-Peyroula E, Dahout-Gonzalez C, Kahn R, Trézéguet V, Lauquin GJ, Brandolin G (2003) Structure of mitochondrial ADP/ATP carrier in complex with carboxyatractyloside. *Nature* 426:39–44
- Persichini T, Mazzone V, Polticelli F, Moreno S, Venturini G, Clementi E, Colasanti M (2005) Mitochondrial type I nitric oxide synthase physically interacts with cytochrome c oxidase. *Neurosci Lett* 384:254–259
- Peters K, Dudkina NV, Jansch L, Braun HP, Boekema EJ (2008) A structural investigation of complex I and I+III<sub>2</sub> supercomplex from *Zea mays* at 11–13 Å resolution: assignment of the carbonic anhydrase domain and evidence for structural heterogeneity within complex I. *Biochim Biophys Acta* 1777:84–93
- Petrosillo G, Ruggiero FM, Di Venosa N, Paradies G (2003) Decreased complex III activity in mitochondria isolated from rat heart subjected to ischemia and reperfusion: role of reactive oxygen species and cardiolipin. *FASEB J* 17:714–716
- Pfeiffer K, Gohil V, Stuart RA, Hunte C, Brandt U, Greenberg ML, Schägger H (2003) Cardiolipin stabilizes respiratory chain supercomplexes. *J Biol Chem* 278:52873–52880
- Piccoli C, Scrima R, Boffoli D, Capitanio N (2006) Control by cytochrome c oxidase of the cellular oxidative phosphorylation system depends on the mitochondrial energy state. *Biochem J* 396:573–583
- Pineau B, Mathieu C, Gérard-Hirne C, De Paepe R, Chétrit P (2005) Targeting the NAD7 subunit in mitochondria restores a functional complex I and a wild type phenotype in the *Nicotiana sylvestris* CMS II mutant lacking nad7. *J Biol Chem* 280:25994–26001
- Quarato G, Piccoli C, Scrima R, Capitanio N (2011) Variation of flux control coefficient of cytochrome c oxidase and of the other respiratory chain complexes at different values of protonmotive force occurs by a threshold mechanism. *Biochim Biophys Acta* 1807:1114–1124
- Radermacher M, Ruiz T, Clason T, Benjamin S, Brandt U, Zickermann V (2006) The three-dimensional structure of complex I from *Yarrowia lipolytica*: a highly dynamic enzyme. *J Struct Biol* 154:269–279
- Ragan CI, Heron C (1978) The interaction between mitochondrial NADH-ubiquinone oxidoreductase and ubiquinol-cytochrome c oxidoreductase - evidence for stoichiometric association. *Biochem J* 174:783–790
- Raha S, Myint AT, Johnstone L, Robinson BH (2002) Control of oxygen free radical formation from mitochondrial complex I: roles for protein kinase A and pyruvate dehydrogenase kinase. *Free Radic Biol Med* 32:421–430
- Ramirez-Aguilar SJ, Keuthe M, Rocha M, Fedyaev VV, Kramp K, Gupta KJ, Rasmusson AG, . . . , van Dongen JT (2011) The composition of plant mitochondrial supercomplexes changes with oxygen availability. *J Biol Chem* 286:43045–43053
- Ramzan R, Weber P, Kadenbach B, Vogt S (2012) Individual biochemical behaviour versus biological robustness: spotlight on the regulation of cytochrome c oxidase. *Adv Exp Med Biol* 748:265–281
- Rauchová H, Battino M, Fato R, Lenaz G, Drahotová Z (1992) Coenzyme Q pool function in glycerol-3-phosphate oxidation in hamster brown adipose tissue mitochondria. *J Bioenerg Biomembr* 24:235–241

- Rauchová H, Fato R, Drahotka Z, Lenaz G (1997) Steady-state kinetics of reduction of coenzyme Q analogs by glycerol-3-phosphate dehydrogenase in brown adipose tissue mitochondria. *Arch Biochem Biophys* 344:235–241
- Reifschneider NH, Goto S, Nakamoto H, Takahashi R, Sugawa M, Dencher NA, Krause F (2006) Defining the mitochondrial proteomes from five rat organs in a physiologically significant context using 2D blue-native/SDS-PAGE. *J Proteome Res* 5:1117–1132
- Robinson NC, Strey F, Talbert L (1980) Investigation of the essential boundary layer phospholipids of cytochrome c oxidase using Triton X-100 delipidation. *Biochemistry* 19:3656–3661
- Rosca MG, Hoppel CL (2008) Mitochondria in heart failure. *Cardiovasc Res* 88:40–50
- Rosca MG, Hoppel CL (2009) New aspects of impaired mitochondrial function in heart failure. *J Bioenerg Biomembr* 41:107–112
- Rosca M, Vazquez E, Kerner J, Parland W, Chandler M, Stanley W, Sabbah H, Hoppel C (2008) Cardiac mitochondria in heart failure: decrease in respirasomes and oxidative phosphorylation. *Cardiovasc Res* 80:30–39
- Rosca M, Minkler P, Hoppel CL (2011) Cardiac mitochondria in heart failure: normal cardiolipin profile and increased threonine phosphorylation of complex IV. *Biochim Biophys Acta* 1807:1373–1382
- Schäfer E, Seelert H, Reifschneider NH, Krause F, Dencher NA, Vonck J (2006) Architecture of active mammalian respiratory chain supercomplexes. *J Biol Chem* 281:15370–15375
- Schäfer E, Cellerino A, Englert C, Frenzel M, Terzibasi E, Dencher NA (2007a) Partial mitochondrial proteome and supramolecular organisation of OXPHOS complexes in the short-lived fish *Nothobranchius furzeri*. *Ann Conf German Genetic Soc Abstract* 43:38
- Schäfer E, Dencher NA, Vonck J, Parcej DN (2007b) Three-dimensional structure of the respiratory chain supercomplex I<sub>1</sub>III<sub>2</sub>IV<sub>1</sub> from bovine heart mitochondria. *Biochemistry* 46:12579–12585
- Schägger H (2002) Respiratory chain supercomplexes of mitochondria and bacteria. *Biochim Biophys Acta* 1555:154–159
- Schägger H, Pfeiffer K (2000) Supercomplexes in the respiratory chains of yeast and mammalian mitochondria. *EMBO J* 19:1777–1783
- Schägger H, Pfeiffer K (2001) The ratio of oxidative phosphorylation complexes I–V in bovine heart mitochondria and the composition of respiratory chain supercomplexes. *J Biol Chem* 276:37861–37867
- Schägger H, de Coo R, Bauer MF, Hofmann S, Godinot C, Brandt U (2004) Significance of respirasomes for the assembly/stability of human respiratory chain complex I. *J Biol Chem* 279:36349–36353
- Schlame M, Ren M (2006) Barth syndrome, a human disorder of cardiolipin metabolism. *FEBS Lett* 580:5450–5455
- Schlame M, Rua D, Greenberg ML (2000) The biosynthesis and functional role of cardiolipin. *Prog Lipid Res* 39:257–288
- Schlame M, Acehan D, Berno B, Xu Y, Valvo S, Ren M, Stokes DL, Epan RM (2012) The physical state of lipid substrates provides transacylation specificity for tafazzin. *Nat Chem Biol* 8:862–869
- Schneider H, Lemasters JJ, Hackenbrock CR (1982) Lateral diffusion of ubiquinone during electron transfer in phospholipid- and ubiquinone-enriched mitochondrial membranes. *J Biol Chem* 257:10789–10793
- Schönfeld P, Wiecekowiński MR, Lebidzińska M, Wojtczak L (2010) Mitochondrial fatty acid oxidation and oxidative stress: lack of reverse electron transfer-associated production of reactive oxygen species. *Biochim Biophys Acta* 1797:929–938
- Sedláček E, Panda M, Dale MP, Weintraub ST, Robinson NC (2006) Photolabeling of cardiolipin binding subunits within bovine heart cytochrome c oxidase. *Biochemistry* 45:746–754
- Seelert H, Dani DN, Dante S, Hauß T, Krause F, Schäfer E, Frenzel M, ..., Dencher NA (2009) From protons to OXPHOS supercomplexes and Alzheimer's disease: structure-dynamics-function relationships of energy-transducing membranes. *Biochim Biophys Acta* 1787:657–671
- Shinzawa-Itoh K, Aoyama H, Muramoto K, Terada H, Kurauchi T, Tadehara Y, Yamasaki A, ..., Yoshikawa S (2007) Structures and physiological roles of 13 integral lipids of bovine heart cytochrome c oxidase. *EMBO J* 26:1713–1725
- Shoubridge EA (2012) Supersizing the mitochondrial respiratory chain. *Cell Metab* 15:271–272
- Sinensky M (1974) Homeoviscous adaptation—a homeostatic process that regulates the viscosity of membrane lipids in *Escherichia coli*. *Proc Natl Acad Sci USA* 71:522–525
- Singer SJ, Nicolson GL (1972) The fluid mosaic model of the structure of cell membranes. *Science* 175:720–731
- Sousa PM, Videira MA, Bohn A, Hood BL, Conrads TP, Goulao LF, Melo AM (2012) The aerobic respiratory chain of *Escherichia coli*: from genes to supercomplexes. *Microbiology* 158:2408–2418
- Sousa PM, Videira MA, Santos FA, Hood BL, Conrads TP, Melo AM (2013) The bc<sub>1</sub>caa3 supercomplexes

- from the gram positive bacterium *Bacillus subtilis* respiratory chain: a megacomplex organization? Arch Biochem Biophys 537:153–160
- Stark G (2005) Functional consequences of oxidative membrane damage. J Membrane Biol 205:1–16
- Stoner C (1984) Steady-state kinetics of the overall oxidative phosphorylation reaction in heart mitochondria. Determination of the coupling relationships between the respiratory reactions and miscellaneous observations concerning rate-limiting steps. J Bioenerg Biomembr 16:115–141
- Strecker V, Wumaier Z, Wittig I, Schägger H (2010) Large pore gels to separate mega protein complexes larger than 10 MDa by blue native electrophoresis: isolation of putative respiratory strings or patches. Proteomics 10:3379–3387
- Strogolova V, Furness A, Robb-McGrath M, Garlich J, Stuart RA (2012) Rcf1 and Rcf2, members of the hypoxia induced gene 1 protein family, are critical components of the mitochondrial cytochrome bc1-cytochrome c oxidase supercomplex. Mol Cell Biol 32:1363–1373
- Stroh A, Anderka O, Pfeiffer K, Yagi T, Finel M, Ludwig B, Schägger H (2004) Assembly of respiratory complexes I, III, and IV into NADH oxidase supercomplex stabilizes complex I in *Paracoccus denitrificans*. J Biol Chem 279:5000–5007
- Stuart RA (2008) Supercomplex organization of the oxidative phosphorylation enzymes in yeast mitochondria. J Bioenerg Biomembr 40:411–417
- Stuart RA (2009) Supercomplex organization of the yeast respiratory chain complexes and the ADP/ATP carrier proteins. Methods Enzymol 456:191–208
- Sumegi B, Srere PA (1984) Complex I binds several mitochondrial NAD-coupled dehydrogenases. J Biol Chem 259:15040–15045
- Sunderhaus S, Dudkina NV, Jansch L, Klodmann J, Heinemeyer J, Perales M, Zabaleta E, . . . , Braun HP (2006) Carbonic anhydrase subunits form a matrix-exposed domain attached to the membrane arm of mitochondrial complex I in plants. J Biol Chem 281:6482–6488
- Suthammarak W, Yang Y-Y, Morgan PG, Sedensky MM (2009) Complex I function is defective in complex IV-deficient *Caenorhabditis elegans*. J Biol Chem 284:6425–6435
- Suthammarak W, Morgan PG, Sedensky MM (2010) Mutations in mitochondrial complex III uniquely affect complex I in *Caenorhabditis elegans*. J Biol Chem 285:40724–40731
- Suthammarak W, Somerlot BH, Opheim E, Sedensky M, Morgan PG (2013) Novel interactions between mitochondrial superoxide dismutases and the electron transport chain. Aging Cell 12:1132–1140
- Takemori S, King TE (1964) Reconstitution of respiratory chain enzyme systems. 13. Sequential fragmentation of succinate oxidase: preparation and properties of succinate cytochrome c reductase and the cytochrome bc1 particle. J Biol Chem 239:3546–3558
- Trouillard M, Meunier B, Rappaport F (2011) Questioning the functional relevance of mitochondrial supercomplexes by time-resolved analysis of the respiratory chain. Proc Natl Acad Sci USA 108:1027–1034
- Ugalde C, Janssen RJ, Van den Heuvel LP, Smeitink JA, Nijtmans LG (2004) Differences in the assembly and stability of complex I and other OXPHOS complexes in inherited complex I deficiency. Hum Mol Genet 13:659–667
- Van den Brink-van der Laan E, Killian JA, de Kruijff B (2004) Nonbilayer lipids affect peripheral and integral membrane proteins via changes in the lateral pressure profile. Biochim Biophys Acta 1666:275–288
- Vempati U, Han X, Moraes CT (2009) Lack of cytochrome c in mouse fibroblasts disrupts assembly/stability of respiratory complexes I and IV. J Biol Chem 284:4383–4391
- Vik SB, Capaldi RA (1977) Lipid requirements for cytochrome c oxidase activity. Biochemistry 16:5755–5759
- Vonck J (2012) Supramolecular organization of the respiratory chain. In: Sazanov L (ed) A Structural Perspective on Complex I: Structure and Function of NADH: Ubiquinone Oxidoreductase. Springer, Dordrecht, pp 247–277
- Vonck J, Schäfer E (2009) Supramolecular organization of protein complexes in the mitochondrial inner membrane. Biochim Biophys Acta 1793:117–124
- Vukotic M, Oeljeklaus S, Wiese S, Vögtle F-N, Meisinger C, Meyer HE, Zieseniss A, . . . , Deckers M (2012) Rcf1 mediates cytochrome oxidase assembly and respirasome formation, revealing heterogeneity of the enzyme complex. Cell Metab 15:336–347
- Wang Y, Mohsen A-W, Mihalik SJ, Goetzman ES, Vockley J (2010) Evidence for physical association of mitochondrial fatty acid oxidation and oxidative phosphorylation complexes. J Biol Chem 285:29834–29841
- Wenz T, Hielscher R, Hellwig P, Schägger H, Richers S, Hunte C (2009) Role of phospholipids in respiratory cytochrome bc(1) complex catalysis and supercomplex formation. Biochim Biophys Acta 1787:609–616

- Wernicke C, Hellmann J, Zięba B, Kuter K, Ossowska K, Frenzel M, Dencher NA, Rommelspacher H (2010) 9-Methyl- $\beta$ -carboline has restorative effects in an animal model of Parkinson's disease. *Pharmacol Rep* 62:35–53
- Whelan SP, Zuckerbraun BS (2013) Mitochondrial signaling: forwards, backwards, and in between. *Oxid Med Cell Longev* 2013:351613
- Wilkens V, Kohl W, Busch K (2013) Restricted diffusion of OXPHOS complexes in dynamic mitochondria delays their exchange between cristae and engenders a transitory mosaic distribution. *J Cell Sci* 126:103–116
- Wittig I, Schägger H (2009) Supramolecular organization of ATP synthase and respiratory chain in mitochondrial membranes. *Biochim Biophys Acta* 1787:672–680
- Wittig I, Braun HP, Schägger H (2006) Blue native PAGE. *Nat Protoc* 1:418–428
- Yankovskaya V, Horsefield R, Törnroth S, Luna-Chavez C, Miyoshi H, Léger C, Byrne B, . . . , Iwata S (2003) Architecture of succinate dehydrogenase and reactive oxygen species generation. *Science* 299:700–704
- Yu A, Yu L (1980) Resolution and reconstitution of succinate-cytochrome c reductase: preparations and properties of high purity succinate dehydrogenase and ubiquinol-cytochrome c reductase. *Biochim Biophys Acta* 591:409–420
- Yu A, Yu L, King TE (1974) Soluble cytochrome b-c1 complex and the reconstitution of succinate-cytochrome c reductase. *J Biol Chem* 249:4905–4910
- Zhang M, Mileykovskaya E, Dowhan W (2002) Gluing the respiratory chain together. Cardiolipin is required for supercomplex formation in the inner mitochondrial membrane. *J Biol Chem* 277:43553–43556
- Zhao X, Leon IR, Bak S, Mogensen M, Wrzesinski K, Hojlund K, Jensen ON (2011) Phosphoproteome analysis of functional mitochondria isolated from resting human muscle reveals extensive phosphorylation of inner membrane protein complexes and enzymes. *Mol Cell Proteomics* 10:M110.000299
- Ziegler DM, Doeg KA (1959) The isolation of a functionally intact succinic dehydrogenase-cytochrome b complex from beef heart mitochondria. *Arch Biochem Biophys* 85:282–284

# Part VII

## **Branched Pathways and Cryptic Cytochromes**



# Chapter 30

## The Interaction Between Cytochrome *f* and Plastocyanin or Cytochrome *c*<sub>6</sub>

Derek S. Bendall<sup>a</sup> (deceased) and Christopher J. Howe<sup>b,\*</sup>

<sup>a</sup>*Department of Biochemistry, University of Cambridge, Cambridge, UK*

<sup>b</sup>*Department of Biochemistry, University of Cambridge, Downing Site, Cambridge CB2 1QW, UK*

Summary.....	631
I. Introduction.....	632
II. Evolution of Plastocyanin and Cytochrome <i>c</i> <sub>6</sub> .....	633
III. Structure of Cytochrome <i>f</i> .....	635
IV. Structure of Plastocyanin and Cytochrome <i>c</i> <sub>6</sub> .....	636
V. Structure of Specific Complexes.....	637
VI. Dynamics of Interaction.....	639
VIII. The Reaction In Vivo.....	646
Acknowledgements.....	649
References.....	649

### Summary

Cytochrome *f* is bound to the cytochrome *b*<sub>6</sub>*f* complex embedded in the thylakoid membrane, but plastocyanin is a small protein that diffuses between cytochrome *f* and photosystem I in the thylakoid lumen. The essential feature of electron transfer from cytochrome *f* to plastocyanin is that a weak, transient complex is formed so as to allow both rapid formation of the reaction complex, and rapid dissociation of products. The reaction has been studied with the proteins in solution, using preparations of the large, heme-containing luminal domain of cytochrome *f*, by kinetic methods, NMR and computer simulation. The reaction sites have been identified as small areas of hydrophobic residues on the surface immediately above the heme or Cu atom and including ligand residues (Tyr1 for cytochrome *f* and His87 for plant plastocyanin). A model of the reaction has been developed in which an intermediate encounter complex is formed covering a relatively large area of the surface and serving the purpose of steering the proteins towards a reactive configuration. With plant and algal proteins the main attractive force forming the encounter complex is electrostatic, but the reactive complex depends on desolvation energy to which electrostatics can make little contribution. With cyanobacterial proteins there is considerable species variation. Hydrophobic attraction plays a significant role in formation of the encounter complex as well as the reaction complex and sometimes may dominate. NMR relaxation studies and Brownian dynamics simulations suggest that rather than a single reaction complex, several (encounter)

---

\*Author for correspondence, e-mail: [c.j.howe@bioc.cam.ac.uk](mailto:c.j.howe@bioc.cam.ac.uk)

configurations contribute to  $k_{\text{et}}$ . There are additional features governing the reaction in vivo. Plastocyanin diffuses within the tight luminal space which forms a sheet no more than about 10 nm thick, obstructed by the large luminal domains of photosystem II and other complexes. Solution studies with added viscosogens suggest that other soluble luminal proteins would cause little inhibition. The lumen is now thought to expand in the light, contrary to previous evidence, raising the intriguing possibility that expansion and contraction of the thylakoid lumen is a significant method of regulation of electron transport. The role of electrostatic attraction in vivo has been tested with *Chlamydomonas* mutants. The surprising result was that charge neutralisation had very little effect on either cell growth or the rate of oxidation of cytochrome *f*, suggesting that the dominant attraction forming the encounter complex in vivo is probably hydrophobic in all oxygenic organisms.

## I. Introduction

Electron transfer between cytochrome *f* and plastocyanin or cytochrome  $c_6$  is an essential part of the electron transport system of all oxygenic organisms even though it does not contribute directly to energy conservation. A diffusive process is necessary to connect the cytochrome  $b_6f$  complex to the reaction centre of photosystem I, and for this part of the chain the high redox potential ( $\sim +400$  mV) that might be provided either by a cupredoxin or a cytochrome is required. These are soluble proteins, so that diffusion occurs within the lumen of the thylakoid rather than in the lipid phase of the membrane, as for plastoquinone as the intermediate in the reduction of the cytochrome complex by photosystem II. In addition to the high redox potential the other essential feature of the reaction is that it must be very rapid, without formation of a tight complex between cytochrome *f* and plastocyanin. In other words the interaction must be transient so that plastocyanin can rapidly shuttle electrons between cytochrome *f* and the P700 reaction center of photosystem I. In this context ‘transient’ implies that the complex formed between the two proteins has a lifetime of no more than about 1 ms, and that the binding constant as a rule lies in the range  $10^2$ – $10^6$   $\text{M}^{-1}$ . Understanding this reaction thus depends on detailed knowledge of both electron transfer theory and

the factors governing the diffusive interaction between two protein molecules in solution.

Electron transfer is essentially a promiscuous reaction. It depends on quantum mechanical tunnelling between reactant and product wavefunctions, rather than specific activation in a well defined complex, and as such is the simplest kind of chemical reaction and potentially very fast. The theory, which is discussed in more detail in Chaps. 5 and 6 of this volume, leads to a simple statement that the rate constant for electron transfer depends on the product of an electronic factor and a nuclear factor. The electronic factor represents the electronic coupling between the two wavefunctions. For our present purposes the important feature of the electronic coupling,  $H^2$ , is that it decays exponentially with distance  $r$  between the two redox centers according to Gamow’s tunnelling equation

$$H_r^2 = H_0^2 e^{-\beta r}$$

where  $\beta = h(2mV)^{1/2}$ ,  $h$  being Planck’s constant,  $m$  the mass of the electron and  $V$  the height of the potential energy barrier through which the electron has to tunnel. For tunnelling through protein  $\beta$  is often taken to be  $1.4 \text{ \AA}^{-1}$  (Moser et al. 1995) which leads to the conclusion that to achieve  $k_{\text{et}} \geq 10^3 \text{ s}^{-1}$   $r$  should be not more than  $14 \text{ \AA}$ . The structures of the two proteins should thus allow this degree of proximity to be achieved by diffusion. The figure of  $14 \text{ \AA}^{-1}$  is only a rough guide, partly because of uncertainty regarding the precise points that  $r$  refers to—in the case

---

Abbreviations: NMR – Nuclear magnetic resonance; P700 – The P700 reaction center of photosystem I

of heme proteins Moser et al. prefer to measure the distance from the edge of the heme macrocycle rather than from the iron atom.

The nuclear factor, on the other hand, can be described by the activation free energy term of classical transition state theory.  $\Delta G^\ddagger$  is given by the ‘Energy Gap’ law derived by Marcus (Marcus and Sutin 1985)

$$\Delta G^\ddagger = \frac{(\lambda + \Delta G^0)^2}{4\lambda}$$

so that it depends on the reorganization energy,  $\lambda$ , and the driving force, that is the standard free energy change for the reaction,  $\Delta G^0$ . For the reaction between cytochrome *f* and plastocyanin or cytochrome *c*<sub>6</sub> the driving force is normally small, 10–15 mV for plastocyanin, and even smaller for cytochrome *c*<sub>6</sub>. Both proteins are small, rigid molecules so that  $\lambda$  is mainly the result of the relatively large solvent contribution.

A protein molecule diffuses in solution by a Brownian process. It is continually being buffeted by a myriad of relatively tiny water molecules pushing it this way and that, which results overall in a series of small movements of the protein in a random walk. The rate at which two molecules collide can be calculated with the diffusion equation:

$$k_a = 4\pi N_A r (D_A + D_B) \cdot 10^3$$

where  $N_A$  is Avogadro’s constant,  $r$  the sum of their radii and  $D_A$ ,  $D_B$ , are the diffusion constants in  $\text{m}^2\text{s}^{-1}$ . For two molecules the size of plastocyanin the collision rate is found to be in the range  $10^9$ – $10^{10}$   $\text{M}^{-1}\text{s}^{-1}$  if charges on the proteins are ignored. However, we are interested in contacts with a specific orientation so that the reactive sites become close to each other, and then the great majority of initial contacts are non-productive and  $k_a$  for productive contacts becomes orders of magnitude smaller than the above figure. In practice the rate is not as small as one would predict by calculation from the sizes of the reactive sites because when two protein molecules collide in solution they are trapped by surrounding

solvent (the solvent cage effect) to form an ‘encounter complex’ in which they can explore numerous relative conformations by surface diffusion (Northrup and Erickson 1992), as expected from the principle of reduction of dimensionality (Adam and Delbrück 1968). The rate can be enhanced if the two proteins carry complementary charges. The process has been modelled for the interaction of cytochrome *f* and plastocyanin of higher plants, *Chlamydomonas reinhardtii* and the cyanobacterium *Phormidium laminosum* by the Brownian dynamics algorithm with a fair degree of success (Pearson and Gross 1998; Gross and Pearson 2003; Gross 2004; Haddadian and Gross 2005; Gross and Rosenberg 2006). The simulations confirm the very similar performance of plastocyanin and cytochrome *c*<sub>6</sub> with the *Chlamydomonas* proteins.

The Brownian dynamics algorithm of UHBD (Madura et al. 1995), SDA (Gabdouline and Wade 1998) or MacroDox (Northrup et al. 1987), mimics the Brownian random walk together with the long-range effect of the interaction of the electrostatic fields of the two proteins, calculated with a finite difference Poisson-Boltzmann equation, and the short-range entropic contribution to binding by hydrophobic desolvation as the two proteins come into contact. The electrostatic calculations emphasize the fact that whereas complementary charges on the two proteins provide a long range attractive force and can exert a steering effect to encourage contact between the two reactive sites, at short range a large desolvation penalty is involved which severely weakens the attraction between a positive and a negative charge and can even result in repulsion.

## II. Evolution of Plastocyanin and Cytochrome *c*<sub>6</sub>

Plastocyanin and cytochrome *c*<sub>6</sub> are functionally interchangeable (Bohner and Böger 1978; Wood 1978). There are only minor differences between the two proteins

in the kinetics of reduction of P700 (Medina et al. 1993; Hervás et al. 1994, 1995; Navarro et al. 1997), and Wood (1978) demonstrated that in vitro cytochrome *f* from *Chlamydomonas reinhardtii* reduces both plastocyanin and cytochrome *c*<sub>6</sub> with a rate constant  $>1 \times 10^7 \text{ M}^{-1}\text{s}^{-1}$ , whereas cytochrome *c*<sub>6</sub> reduces plastocyanin two orders of magnitude more slowly. Why then is there a need for the two proteins? The answer seems to lie in the availability of iron and copper in the environment, which are required for formation of the respective cofactors. Both metals have highly insoluble redox states, oxidized in the case of iron, Fe(III) and reduced in the case of copper, Cu(I), with alternative states soluble and therefore available. The proteins do not normally occur together in any one organism, although many are capable of synthesizing both, under appropriate conditions.

The primitive earth on which life evolved was anoxic. Under these conditions iron, in the form of the highly soluble Fe<sup>2+</sup>, was freely available. Protoporphyrin IX is a common intermediate in the biosynthesis of both chlorophyll and heme (Hohmann-Marriott and Blankenship 2011) and all known anaerobic photosynthetic organisms depend on a form of chlorophyll in their reaction centers. Thus heme proteins could be expected to be extremely ancient, preceding the origins of oxygenic photosynthesis and cyanobacteria, and cytochromes occur in every photosynthetic anaerobe today. By contrast, copper would not have been so readily available, because Cu(I), which would predominate under reducing conditions, forms an extremely insoluble sulphide. The earliest oxygenic organisms are therefore more likely to have contained cytochrome *c*<sub>6</sub> than plastocyanin. Nevertheless, the anaerobic phototroph *Chloroflexus aurantiacus* employs a cupredoxin, auracyanin, in its electron transport system. This organism belongs to the filamentous anoxygenic phototrophs, which show an early branching from all the other groups of photosynthetic eubacteria (Van Driessche et al. 1999). Given that the latter also exhibit the cupredoxin

protein fold, as in the plastocyanin of cyanobacteria (see below for structure), the most parsimonious explanation is that the cupredoxin fold is also ancient.

The relative availabilities of iron and copper on the primitive earth probably persisted until the Great Oxidation Event, about 2.4 billion years ago, brought about a conversion of the reducing atmosphere of the primitive earth to an oxidizing atmosphere as a result of the development by cyanobacteria of water as the electron donor for photosynthetic metabolism, leaving molecular oxygen as the byproduct. This was the first great biological modification of the earth environment. The availabilities of iron and copper would then have been reversed as Fe(III) is highly insoluble in water whereas Cu(II) is readily soluble. By this time iron compounds had been employed in a wide variety of metabolic processes so that cells had to find ways of making iron available, but replacing cytochrome *c*<sub>6</sub> by plastocyanin would have represented a significant saving. Even so, the aqueous environment was not homogeneous and anaerobic environments would have persisted. To this day aquatic organisms, that is most cyanobacteria and green algae, have in many cases found it an advantage to retain the genes for both cytochrome *c*<sub>6</sub> and plastocyanin, and use plastocyanin in preference unless copper becomes unavailable in the environment although other algal lineages use only cytochrome *c*<sub>6</sub>.

The controlling factor is the availability of copper rather than iron. By omitting copper from the growth medium of *Chlamydomonas reinhardtii* Wood (1978) was able to change the ratio of plastocyanin to cytochrome *c*<sub>6</sub> in cultured cells by a factor of at least 5000. On the other hand, *C. mundana*, a species isolated from an anaerobic sewage pool containing free H<sub>2</sub>S, contained cytochrome *c*<sub>6</sub> but no plastocyanin. Sandmann et al. (1983) found a number of species of green algae that were unable to synthesize cytochrome *c*<sub>6</sub> under copper deficiency, and correspondingly organisms in other groups of algae that were unable to synthesize plastocyanin even when copper was freely available. Merchant

and Bogorad (1986) demonstrated directly with *C. reinhardtii* that copper in the medium stimulated production of plastocyanin and inhibited production of cytochrome *c*<sub>6</sub>. Plants, like some green algae, have lost the ability to synthesize cytochrome *c*<sub>6</sub>, but it is not clear exactly why this should be so. Although a form of cytochrome *c*<sub>6</sub>, referred to as *c*<sub>6A</sub>, has been reported in green algae and plants, with related molecules in cyanobacteria, they have a different function. Cytochrome *c*<sub>6A</sub>, as well as the cyanobacterial *c*<sub>6</sub>-like cytochromes, is discussed elsewhere in this volume.

### III. Structure of Cytochrome *f*

Cytochrome *f* is a unique protein with no known evolutionary forebears and, having a largely  $\beta$ -sheet structure, is unrelated to other *c*-type cytochromes. Two unusual features should be noted. The first is that it uses the N-terminal residue, almost invariably tyrosine, as a heme ligand, and as the residue is surface exposed it forms a favourable site for electron transfer to acceptors. The second is that cytochrome *f* contains a conserved chain of five internal water molecules (Martinez et al. 1996) which have been suggested to provide a proton channel for operation of the Q cycle in the cytochrome *b*<sub>6</sub>*f* complex (Ponamarev and Cramer 1998; Sainz et al. 2000). Another suggestion is that the buried waters have a structural function (Chi et al. 2000; Griffin et al. 2002). A study of mutants in which one or more of the waters have been eliminated by mutation of conserved binding residues within the protein shows that any effects on electron transfer are on cytochrome *f* reduction rather than its oxidation (Ponamarev and Cramer 1998), so the function of the water chain will not be discussed further in this chapter.

Cytochrome *f* is a membrane-bound protein which requires detergent to solubilize it, as well as being an integral component of the cytochrome *b*<sub>6</sub>*f* complex. The major part of the molecule (the first 250 residues) is exposed to the aqueous phase of the thylakoid lumen and is anchored

to the membrane by a single  $\alpha$ -helix and a short section of polypeptide chain (14 residues) on the stromal or cytoplasmic side (Gray 1992). This large luminal domain contains the heme prosthetic group, the plane of which lies at about 30° to the membrane plane, as shown originally by EPR (Crowder et al. 1982) and confirmed by the more recent X-ray structures of the whole complex. These structures have been obtained at 3.0 Å resolution for the cyanobacterium *Mastigocladus laminosum* (Kurusu et al. 2003) and 3.1 Å for the green alga *Chlamydomonas reinhardtii* (Stroebele et al. 2003) which is sufficient to resolve  $\alpha$ -helices but not to resolve accurately the sidechains of individual amino acids. The most accurate structures have been obtained with the isolated luminal domain which is liberated spontaneously by proteolysis at the membrane surface when leaves of certain crucifers (e.g. turnip, charlock or rape) are homogenized in butanone, or by heterologous expression of the appropriately truncated gene in *Escherichia coli*. Structures for the protein from a higher plant (turnip, *Brassica rapa*), a green alga (*Chlamydomonas reinhardtii*) and the cyanobacterium *Phormidium laminosum* have been reported at a resolution of 1.9–2.0 Å (Martinez et al. 1996; Carrell et al. 1999; Chi et al. 2000). These structures effectively encompass the whole spectrum of oxygenic organisms, but are remarkably similar. The tertiary structures show virtually identical elongated molecules. The heme group is buried but close to the lumen-exposed surface. The molecule as a whole is acidic in all cases but the major difference is that the plant and algal proteins possess a cluster of basic residues close to the heme (58, 65, 66, 187, 209) which complement an acidic patch in plastocyanin, whereas in the cyanobacterial case several of these basic residues are either acidic or neutral. This truncated, soluble preparation of cytochrome *f* is the form which has been used for nearly all the studies of the interaction with plastocyanin or cytochrome *c*<sub>6</sub>.

#### IV. Structure of Plastocyanin and Cytochrome $c_6$

Plastocyanin is a blue copper protein or cupredoxin with a type 1 copper center (Malmström 1970). It has a Greek-key  $\beta$ -barrel structure which is highly conserved throughout all oxygenic organisms, as determined for several species of higher plant, a fern, green algae and several cyanobacteria (Colman et al. 1978; Guss and Freeman 1983; Collyer et al. 1990; Moore et al. 1991; Guss et al. 1992; Redinbo et al. 1993; Bagby et al. 1994; Badsberg et al. 1996; Romero et al. 1998; Xue et al. 1998; Babu et al. 1999; Bond et al. 1999; Inoue et al. 1999a, b; Kohzuma et al. 1999; Shibata et al. 1999; Sugawara et al. 1999; Bertini et al. 2001; Schmidt et al. 2006) either by X-ray crystallography or by NMR to give the solution structure. The structure of the copper center, in which the single copper atom is coordinated in a distorted tetrahedral structure, is also conserved. The three equatorial ligands, the  $N^\delta$  atoms of His37 and His87 and the  $S^\gamma$  atom of Cys84 lie in a plane slightly below the copper atom, and the axial ligand is the  $S^\delta$  of Met92 (higher plant numbering system) with an unusually long bond length. His87 is exposed to the surface at one end of the molecule within a patch of hydrophobic residues, and has been favoured as the site for electron transfer to or from its natural redox partners. A second, 'remote' site centered on Tyr83, adjacent to the Cys84 ligand, has been identified by kinetic and NMR experiments observing paramagnetic line broadening with inorganic reactants (Sykes 1985). Tyr83 is located between two groups of acidic residues, 42–45 and 59–61 in higher plants. Positively charged complexes such as  $[\text{Co}(\text{phen})_3]^{3+}$  react at this site, whereas negatively charged complexes such as ferricyanide react at the 'northern' site involving His87 (Sinclair-Day and Sykes 1986). NMR experiments with proteins from several different sources have shown conclusively that the electron transfer site with cytochrome  $f$  involves His87 (or its cyanobacterial homologue)

(Ubbink et al. 1998; Crowley et al. 2001; Díaz-Moreno et al. 2005a; Lange et al. 2005; Hulsker et al. 2008). The charge properties of plastocyanin from plants and algae are highly conserved. They are all acidic proteins, with a pair of conserved acidic patches which complement the basic ridge of cytochrome  $f$ . The larger of these includes residues at positions 42, 43, 44 and 45 whereas the smaller one, which is closer to His87, often includes residues 59, 60 and 61, but is more variable than the large patch. In cyanobacterial plastocyanins, on the other hand, some of the equivalent positions are occupied by basic or neutral residues. A particularly significant residue is Arg93, corresponding to Gln88 in plant plastocyanins, which lies immediately below the hydrophobic patch (Schlarb-Ridley et al. 2002a). The pI varies from acidic to basic, according to species. In particular, plastocyanins from *Synechococcus* sp. PCC 6301 and *Prochlorococcus marinus* have pIs almost as low as those of the plant proteins, but the characteristic plant pattern of acidic patches in plastocyanin and a basic cluster in cytochrome  $f$  is lacking.

Cytochrome  $c_6$  is a type 1 cytochrome  $c$  which occurs in many cyanobacteria and green algae but not in higher plants. Its structure bears no relation to that of plastocyanin. Nevertheless, one edge of the heme prosthetic group is exposed to the medium and is surrounded by hydrophobic residues, providing a potential reaction site similar to that of H92 in plastocyanin (numbering system of *P. laminosum*). Furthermore, there is a conserved arginine residue, R66, on the edge of this site which has been shown to be essential for reaction of cytochrome  $c_6$  with photosystem I of cyanobacteria (De la Cerda et al. 1999; Molina-Heredia et al. 2001). This residue is in a similar position relative to the reaction site as the conserved R93 in plastocyanin. The reaction of cytochrome  $f$  with cytochrome  $c_6$  has not been as thoroughly investigated as with plastocyanin in the mistaken belief that the two  $c$ -type cytochromes are not easily distinguished spectroscopically.

## V. Structure of Specific Complexes

Electron transfer complexes are inherently unstable; crystallisation has often proved difficult and so far impossible for a complex between cytochrome *f* and plastocyanin, even though the separate proteins have been crystallized. X-ray crystal structures have, however, been obtained for several electron transfer complexes, the first of these being the 1:1 complex between cytochrome *c* and cytochrome *c* peroxidase from yeast by Pelletier and Kraut (1992). This system has become a paradigm for the development of our understanding of electron transfer reactions between proteins in solution. The structure observed in the crystals is very similar both to that of a covalently cross-linked complex which has been shown to be active in electron transfer (Guo et al. 2004), and to the solution structure obtained by NMR (Volkov et al. 2006).

When two proteins interact in solution residues involved in specific binding sites can be identified by observing NMR chemical shift changes due to the change in chemical environment. If one of the proteins contains a paramagnetic nucleus in its active site, such as the ferric atom of oxidized cytochromes, an actual structure can be obtained by observing pseudocontact shifts in the other protein, because these depend upon relative orientation and the distance between the two nuclei. The fact that electron transfer proteins are usually in fast exchange on the NMR time scale, and by assuming that they behave as rigid bodies, the crystal structures of the individual proteins, together with restrained rigid-body molecular dynamics, can be used to calculate the most probable structure for a specific complex. This was first reported for the complex between turnip cytochrome *f* and spinach plastocyanin by Ubbink et al. (1998) and the method has since been extended to several other complexes. More recently the technique has been extended and made more general by measuring paramagnetic relaxation enhancement ( $T_2$ ) in nuclei of one protein in response to paramagnetic

centers containing unpaired electrons introduced at specific sites in the other. Clore et al. have developed the method with several protein complexes (Iwahara and Clore 2006; Tang et al. 2006; Clore and Iwahara 2009) and Ubbink et al. with electron-transfer complexes (Volkov et al. 2006, 2010a, b; Bashir et al. 2010). The effect is highly localized because of the  $r^{-6}$  distance dependence and also very sensitive. As a result the technique provides additional, precise information about the structure of the specific complex, and can also identify minor, transiently occupied complexes of the encounter ensemble. The latter aspect will be discussed below in relation to the dynamics of interaction, but for the moment we will concentrate on the structure of the single, specific complex.

The most striking feature of all the complexes is that they include binding of the hydrophobic patch of plastocyanin which contains the copper ligand His87, to a hydrophobic patch on cytochrome *f* which is immediately above the heme group and contains Tyr1 and Phe3. This provides a good coupling pathway for electron transfer between the iron atom of cytochrome *f* and the copper atom of plastocyanin via the copper ligand His87 and the heme ligand Tyr1. The relative orientation of the proteins can differ, however, and in the case of *Phormidium laminosum* it appears to shift the closest contact of His87 from Tyr1 to Phe3 (Crowley et al. 2001). At one orientational extreme there is the complex from the cyanobacterium *P. laminosum*, in which plastocyanin binds ‘head-on’ to cytochrome *f*, and at the other the higher-plant complex which has a ‘side-on’ orientation (Ubbink et al. 1998) (Fig. 30.1). The latter corresponds closely to the structure DC2 previously identified by calculation of electrostatic energies by Soriano et al. (1997) and is determined in plants by electrostatic interaction between the basic ridge of cytochrome *f* lying to one side of the heme site, and the acidic patches of plastocyanin. In the cyanobacterium *Nostoc* PCC 7119 (subsequently referred to as *Nostoc*) the binding is also side-on,

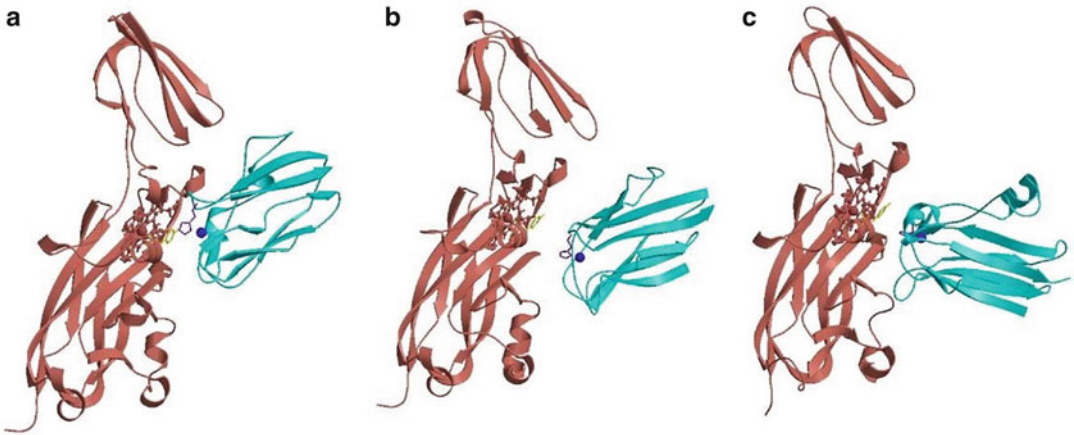


Fig. 30.1. NMR structures of the solution complex between cytochrome *f* and plastocyanin. Higher plant proteins (a) *Brassica rapa*, turnip, cytochrome *f*; *Spinacea oleracea*, spinach, plastocyanin, 2pcf.pdb model 6; cyanobacterial proteins (b) *Nostoc* sp. PCC 7119, 1tu2.pdb model 1; (c) *Phormidium laminosum*, Crowley et al. 2001). Cytochrome *f*, backbone salmon, heme indianred, heme ligand Tyr1 yellow; plastocyanin, backbone cyan, copper blue, copper ligand (a, His87, b and c, His92) purple. Figure drawn with MolScript (Kraulis 1991) and Raster3D (Merritt and Bacon 1997).

but the charges on the two proteins are reversed (Díaz-Moreno et al. 2005a). The same is true for the complex from another cyanobacterium, *Prochlorothrix hollandica*, in which an involvement of electrostatics in complex formation can be demonstrated by the effects of ionic strength (Crowley et al. 2002; Hulsker et al. 2008). In this case, however, there is no evidence for specific interactions at the interface between acidic residues in cytochrome *f* and basic residues in plastocyanin, as is the case with the *Nostoc* complex. The balance between electrostatics and the relatively short-range hydrophobic interactions can vary, particularly amongst cyanobacteria. In *P. laminosum* electrostatics are much less important and hydrophobic interactions are significant (Crowley et al. 2001; Schlarb-Ridley et al. 2002a). In higher plants and green algae the nature of the hydrophobic patch and the pattern of charged residues is remarkably constant, but in at least three species of fern (*Dryopteris crassirhizoma*, *Nephrolepis exaltata*, and *Polystichum longifrons*) the distribution of acidic residues in plastocyanin is significantly different (Navarro et al. 2004). Thus, only one of the

four acidic residues in the lower acidic patch of spinach (residues 42–45) remains in ferns which also have several glutamate residues on the edge of the smaller hydrophobic patch. A further difference, which may be significant, is that the highly conserved glutamine residue at position 88 in spinach, adjacent to the copper ligand His87, has become a positively charged lysine residue, where cyanobacteria have a conserved arginine (except in *Gloeobacter* which has lysine).

A significant feature of the hydrophobic interface is that it has a relatively open, loosely packed structure porous to water molecules (Crowley and Carrondo 2004; Bendall et al. 2011). This ensures weak binding and a short lifetime (large  $k_{\text{off}}$ ), in other words the transient nature of the interaction. The idea of ‘hot spots’ providing most of the binding energy is generally inappropriate for transient complexes. They often involve tryptophan, tyrosine or arginine residues surrounded by a more hydrophobic ‘O ring’ to exclude water, and tend to be characteristic of tight, static complexes (Clackson and Wells 1995; Bogan and Thorn 1998). Even so, a hot spot involving



Arg13 of cytochrome *c* bound to Tyr39 of cytochrome *c* peroxidase has been identified in the interface between these two proteins in the electron transfer complex (Volkov et al. 2009). This complex has a relatively high binding constant, but in general the magnitude of the binding constant is not a good guide to the kinetic significance of the encounter complex (Worrall et al. 2002).

## VI. Dynamics of Interaction

The dynamics of interaction between plastocyanin and the soluble luminal domain of cytochrome *f* have been extensively studied in vitro in the expectation that the properties of the two proteins so revealed would be directly relevant for understanding the reaction in vivo. We will see later that the relevance is, in fact, not straightforward, but for the moment we will concentrate on the solution reaction because there is no doubt that there are important principles that must apply to both sets of conditions.

There are two questions that we need to answer. The first is how the rate of reaction is enhanced from the low value that could be expected for simple diffusional collision when only small patches on the proteins are reactive ( $k_2 \sim 10^5\text{--}10^6 \text{ M}^{-1}\text{s}^{-1}$ ) to the experimentally observed rate ( $k_2 \sim 10^8 \text{ M}^{-1}\text{s}^{-1}$ ). The second is how restrictive the distance dependence of electron transfer is on the size of the reactive patches and the nature of the reactive complex between the two proteins.

The first question, appropriately rephrased, is relevant to all cases of specific protein-protein interactions. The most directly relevant to electron transfer systems are those reactions involving enzymes and their specific inhibitor proteins in which the inhibitor must bind extremely rapidly to a specific site in the enzyme to form a very stable complex. This might be either because of the lethality of the enzyme to its parent cell or for physiological reasons. A well studied example of the former is the bacterial ribonuclease known as barnase, which is lethal until excreted,

so that the small inhibitor protein barstar binds rapidly to the intracellular enzyme as soon as it is synthesized. A physiological example is the inhibition by fasciculin of acetylcholine esterase, the terminator of nerve impulses involving acetylcholine. The rate of formation of these enzyme-inhibitor complexes,  $k_{\text{on}}$ , is often diffusion limited, but dissociation of the complex,  $k_{\text{off}}$ , is very slow, giving a large binding constant,  $K_A = k_{\text{on}}/k_{\text{off}}$ . In electron transfer reactions  $k_{\text{on}}$  is also usually very fast, although not necessarily diffusion-limited, but  $k_{\text{off}}$  must also be fast to provide a transient complex with a small  $K_A$ .

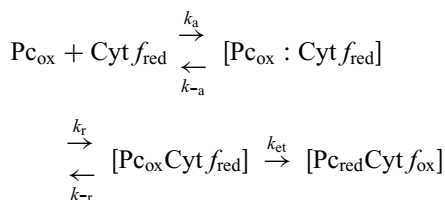
The model which has been used successfully to explain rapid binding kinetics postulates that the final complex is reached via a transient intermediate complex, the structure of which effectively broadens out the size of the restricted patches through which the two proteins bind to each other in the final complex (Berg and von Hippel 1985; Schreiber and Fersht 1996; Gabdouliline and Wade 1999). This encounter complex is the endpoint of the diffusional interaction which is reached by liquid phase diffusion and may be followed by a rapid two-dimensional surface diffusion. The kinetic advantage provided by the encounter complex depends on relatively long-range inter-protein forces guiding the two proteins towards a productive configuration. In many cases this steering effect is the result of complementary charges on the proteins situated in the region of the target site, but these cannot bring the proteins into close contact because of the strong desolvation penalty that would be incurred in so doing. Movement into the final, specific complex involves short-range hydrophobic and van der Waals forces.

Electron transfer from soluble cytochrome *f* to plastocyanin or cytochrome *c*<sub>6</sub> is also strongly dependent on electrostatic attraction between the two proteins (Takenaka and Takabe 1984; Anderson et al. 1987; Modi et al. 1992; Meyer et al. 1993; Lee et al. 1995; Kannt et al. 1996; Gong et al. 2000; De Rienzo et al. 2001; Schlarb-Ridley et al. 2002a; Hart et al. 2003; Albarrán et al. 2007).

The steering effect can increase the rate by orders of magnitude by preorienting the two proteins to bring their active sites close enough for electron transfer. The strength of the attraction is strongly dependent on ionic strength, and a pictorial impression of the effectiveness of a charge is given by the concept of the Debye length or screening distance which gives a measure of the way in which the field around an ion is compressed by other ions in the solution. The Debye length is the distance at which the field is reduced by  $1/e$  and is defined by the reciprocal of the Debye-Hückel factor,  $\kappa$ , which in SI units is given by

$$\kappa^2 = \frac{2000N_A e^2}{\epsilon_0 \epsilon k_B T} I$$

where  $I$  is ionic strength,  $k_B$  is Boltzmann's constant,  $e$  the charge on an electron and  $\epsilon_0$  and  $\epsilon$  the permittivity of vacuum and dielectric constant respectively. At high ionic strength  $1/\kappa$  is vanishingly small and the field effectively disappears, but at  $I = 100$  mM it is about  $10 \text{ \AA}$  which is large enough for the field around a group of charges on a protein surface to be smeared out into a single surface. Simple electrostatics might suggest that the field (and its effect on the rate of electron transfer) would continue to increase exponentially as  $I$  is decreased further, but in fact an optimum value of  $I$  is normally observed, with decreasing rates as  $I$  is lowered still further. Meyer et al. (1993) found the optimum to be at about 40 mM where  $1/\kappa$  has a value of about  $15 \text{ \AA}$ . In terms of the encounter complex model this can be explained with the following scheme



if it is supposed that at low ionic strength the rate constant for rearrangement,  $k_r$ , becomes progressively smaller so that the sys-

tem tends to get stuck in the essentially electrostatic encounter complex, represented as  $[\text{Pc}_{\text{ox}} : \text{Cyt } f_{\text{red}}]$ . The kinetic behaviour of this scheme depends on which of the three steps is rate limiting (Schlarb-Ridley et al. 2005). When  $k_{\text{et}}$  is fast and initial binding is limiting, the reaction is diffusion controlled, and when, on the other hand  $k_{\text{et}}$  is limiting the reaction may be described as activation controlled. Taking rearrangement into account, Davidson described the latter type of reaction as 'coupled', that is to say the overall rate is determined not only by  $k_{\text{et}}$  but also by rearrangement, so that  $k_r/k_{-r} < 1$  (Harris et al. 1994; Davidson 1996, 2000). The intermediate case of slow rearrangement but rapid  $k_{\text{et}}$  is commonly referred to as 'conformationally gated' in the terminology introduced by Hoffman and Ratner (1987).

The existence of the rearrangement step has been reinforced by studies of the effects of viscosity and temperature on several reactions in which electron transfer has been initiated by laser flash photolysis. Millett and coworkers have developed the use of ruthenium complexes as photosensitizers (Mei et al. 1999; Millett and Durham 2002). An early study by Qin and Kostić (1994) involved the accelerated decay of the flash-induced triplet state of zinc-substituted cytochrome *c* (zinc replacing the iron) in the presence of cytochrome *b*<sub>5</sub>. Quenching is due to electron transfer from the excited triplet state of Zn cytochrome *c* to ferric cytochrome *b*<sub>5</sub>. Although the reaction is unphysiological it can reveal the dynamics within the protein complex. Electron transfer within the preformed complex was found to be biphasic and sensitive to viscosity, which was interpreted to indicate more than one reactive configuration interconverting by orientational fluctuations. This conclusion agrees with more recent NMR studies of the system by Volkov et al. (2005) who found evidence for a dynamic complex from the small size of chemical shift perturbations on binding. The flash photolysis technique has been used by Hoffman and colleagues in studies, discussed below, of the interaction between cytochrome *b*<sub>5</sub> and myoglobin.

Hydrophobic forces arise from the entropy increase as two non-polar surfaces approach one another and become dehydrated, and are effective over a shorter distance. This effect normally extends about two water diameters from the surface of a protein, which is sufficient to provide a weak steering effect and a significant rate enhancement by providing pathways into an encounter ensemble. Camacho et al. (2000) have studied this theoretically in relation to the binding of ovomucoid to  $\alpha$ -chymotrypsin and elastase. Hydrophobic effects have been shown to be a significant factor in the kinetics of electron transfer from cytochrome *f* to plastocyanin, the best known example being the proteins from *P. laminosum* with which electrostatics have only a minor role to play (Schlarb-Ridley et al. 2002a) and, indeed, ionic strength changes have no detectable effect on the magnitude of chemical shift changes resulting from binding (Crowley et al. 2001). The rate enhancement is not as great as it is for plant proteins when measured under standard conditions at 300 K, but this is compensated by the fact that *P. laminosum* is thermophilic, with a natural growth temperature of 45 °C. Moreover, when electrostatic forces are virtually eliminated at high ionic strength, the *P. laminosum* proteins react an order of magnitude faster than the higher plant proteins (Schlarb-Ridley et al. 2003), which presumably reflects a more effective hydrophobic channelling into the reactive configuration.

It may be worth mentioning that it is not impossible for hydrophobic attraction to extend very much further from a hydrophobic surface (Tsao et al. 1993). This is thought to be an electrostatic effect resulting from the polarization field of water molecules oriented at the surface (Despa and Berry 2007), but is unlikely to be significant for protein interactions.

Electrostatics are not entirely irrelevant in the *Phormidium* system, however. The effects of ionic strength on  $k_2$  reveal a weak electrostatic attraction, but this is the result of a balance between basic and acidic residues

on the surface of plastocyanin. The most important basic residue is Arg93, the conserved residue adjacent to the copper ligand, His 92, with minor contributions from Lys46 and Lys53. These residues would provide an attractive force to the acidic surface of cytochrome *f*, but this is offset by a repulsion originating with Asp44 and Asp45 (Schlarb-Ridley et al. 2002a), so that *Phormidium* plastocyanin has not evolved to give the highest possible rate of reaction with cytochrome *f*. Nor can one say that these charge residues are present to satisfy the requirements for rapid reaction with Photosystem I, as the mutants have similar effects on both reactions (Schlarb-Ridley et al. 2002b). The pseudo-neutrality which results for the reaction with cytochrome *f* is important in determining the 'head-on' collision. Thus there is a balance between the steering effects of electrostatic and hydrophobic forces which can vary from one organism to another, at least amongst cyanobacteria.

The failure to detect an effect of ionic strength on the binding constant ( $K_A$ ) for *P. laminosum* proteins, despite an effect on  $k_2$ , was previously explained by the reaction being diffusion controlled, when  $k_2 = k_a$  and  $K_A = \frac{k_a k_r}{k_{-a} k_{-r}}$  (Hart et al. 2003). One would then expect that an electrostatic attraction influencing the encounter complex would increase  $k_a$  and decrease  $k_{-a}$  but have opposite effects on  $k_r$  and  $k_{-r}$  so that  $k_2$  would be stimulated without any significant effect on  $K_A$ . Even if the reaction is not fully diffusion controlled and thermal activation makes some contribution to  $k_2$  (Gabdoulline and Wade 2009) this argument is likely to remain the basis of the explanation of the apparent anomaly. A small effect of ionic strength on  $k_{et}$  is a possibility in view of the uncertainty surrounding the structure of the single reaction complex (see above).

The second question posed at the beginning of this section, the effective size of the reactive patches, is partially answered by emphasizing the fact that a contribution to electron transfer is significant in any orientation provided the heme-Cu distance

remains below roughly 14 Å. The reaction scheme above assumes that there is a single, specific active complex, represented by  $[\text{Pc}_{\text{ox}}\text{Cyt } f_{\text{red}}]$ . The encounter complex, by contrast, does not have a single configuration but consists of an ensemble of different complexes close to the position of the final complex or, more likely, allows rapid movement between these positions until rearrangement into the reaction position occurs. The loose distance requirement of electron transfer suggests that this concept of the encounter complex is too restrictive and that some encounter configurations might make a significant direct contribution. In an extreme case one might say that there is no single specific configuration responsible for most of the electron transfer. An analysis along these lines has been carried out for the reaction between *P. laminosum* cytochrome *f* and plastocyanin by Gabdoulline and Wade (2009). They modelled the reaction by Brownian dynamics simulation in which they took account of both electrostatic forces and a non-polar desolvation term to allow for close contact orientations. For each configuration the probability of electron transfer was calculated using the semi-classical formulation of Marcus (Marcus and Sutin 1985) with the PATHWAY method of Beratan et al. (1991) to calculate electronic coupling, and the results were summed to give the overall value of  $k_{\text{et}}$ .

The value of  $k_{\text{et}}$  has been measured directly by laser flash photolysis in the presence of deazariboflavin to generate a free radical which rapidly reduces cytochrome *f*. The subsequent reoxidation by plastocyanin can then be recorded. Turnip cytochrome *f* reducing French bean plastocyanin gave  $k_{\text{et}} = 2800 \text{ s}^{-1}$  (Qin and Kostić 1992), but the homologous *Nostoc* proteins gave  $13,400 \text{ s}^{-1}$  (Albarrán et al. 2005). These figures are surprising. The dominant factor determining  $k_{\text{et}}$  is the distance between the Fe and Cu atoms, so this should be shorter for *Nostoc* than for the higher plant proteins, remembering that according to Gamow's tunnelling equation with a value of  $\beta = 1.4 \text{ Å}^{-1}$  the rate declines by a factor of 10 for every

1.6 Å. In fact, the opposite seems to be the case. The NMR structures give average values of  $\sim 16 \text{ Å}$  for *Nostoc* (Díaz-Moreno et al. 2005a) and  $10.9 \text{ Å}$  for turnip/spinach (Ubbink et al. 1998). Although in the latter case plastocyanin was from spinach rather than French bean, the difference in structure would be expected to be small. The relatively large distance for *Nostoc* is probably partially offset by the dynamic nature of the complex, that is to say electron transfer from configurations of the encounter complex is significant, as demonstrated by Scanu et al. (2013) but it is difficult to judge just how important this is. However, a further factor favouring a relatively high value of  $k_{\text{et}}$  in the higher plant combination of turnip cytochrome *f* and spinach plastocyanin (which favours a single reactive configuration) is the value expected for  $k_{\text{et}}$  from stopped-flow measurement of  $k_2$ , the second-order rate constant, and NMR measurement of the binding constant for which values of  $1.8 \times 10^8 \text{ M}^{-1}\text{s}^{-1}$  and  $7 \times 10^3 \text{ M}^{-1}$  respectively have been obtained (Kannt et al. 1996). According to a simple kinetic analysis (Bendall 1996; Kannt et al. 1996)  $k_{\text{et}}$  has a minimum value of  $k_2/K_{\text{A}}$  or  $2.6 \times 10^4 \text{ s}^{-1}$ . For the *Phormidium* system of homologous proteins the measured values are  $k_2 = 4.7 \times 10^7 \text{ s}^{-1}$  (Schlarb-Ridley et al. 2002a) and  $K_{\text{A}} \sim 10^3 \text{ M}^{-1}$  (Crowley et al. 2001), giving  $k_{\text{et}} \geq 4.7 \times 10^4 \text{ s}^{-1}$ .

The *Phormidium* system presents further unsolved kinetic problems. In the first place analysis of chemical shift and pseudocontact shift changes described above did not converge on a single structure for the complex and yielded a much larger variation of configurations than did the higher plant proteins (Crowley et al. 2001). The correct interpretation of this situation is uncertain, and one possibility is that there is no single reactive structure but an ensemble of closely related configurations in fast exchange (an encounter complex), each of which has a somewhat lower probability of electron transfer than a single optimum configuration. Each of the calculated structures showed the head-on orientation of plastocyanin relative to cytochrome *f* but the point of closest

approach of the copper ligand, His92, was always to Phe3 rather than Tyr1 (the heme ligand) and gave an average Fe to Cu distance of 15 Å. An interesting comparison can be made with the proteins from *Prochlorothrix hollandica*. The wild type proteins form a defined complex with an orientation similar to that of *Nostoc*, but the plastocyanin has an unusual structure of its hydrophobic interaction site in which G12 has become Y and L14 has become P, compared with plastocyanins from most other sources. Hulsker et al. (2008) characterized the dynamics of both the wild type plastocyanin and the Y12G/P14L mutant with cytochrome *f* by NMR spectroscopy. Chemical shift perturbations and pseudocontact shifts showed that the transient complex formed by the mutant was much more dynamic than that of the wild type, so that the encounter state had become more highly populated. Despite this increase in dynamics the binding constant and overall rate of electron transfer showed little change.

A second problem concerning *P. laminosum* arose from a study of the effects of viscosity on  $k_2$  (Schlarb-Ridley et al. 2005). This rate was previously thought to be diffusion controlled and would therefore be expected to be inversely proportional to the viscosity of the solvent. In practice a series of different viscogens, glycerol, ethane diol and sucrose, gave almost identical rates which depended not on  $\eta^{-1}$  but on  $\eta^{-1.8}$ . This result was inconsistent with a reaction which was purely diffusion controlled, as was the high temperature coefficient, but is supported by the most recent Brownian dynamics simulations (Gabdouline and Wade 2009). Several possible, but conflicting, explanations for the power function viscosity dependence remain possible. One would be that each of the viscogens had similar specific effects on the proteins that would inhibit the rate, although plotting against molality rather than viscosity gave markedly different responses. Schlarb-Ridley et al. (2005) attempted to explain the result in terms of a multistep reaction, assuming a single active configuration, which might involve Tyr1 rather than Phe3, and so could be described as a conformationally

gated reaction. It is not clear, however, what effect of viscosity might be expected if no such single configuration exists, as discussed above.

Hoffman and colleagues have made extensive studies of the more extreme case of the reaction between cytochrome  $b_5$  and myoglobin. The native reaction is the reduction of metmyoglobin to its functional form, but the reaction studied has been the triplet quenching of zinc-heme myoglobin by reduction of ferric cytochrome  $b_5$  (Nocek et al. 1997). The interaction is clearly strongly dependent on electrostatic attraction. The problem is that the reaction center of both proteins is the exposed heme edge, so that the two sets of heme propionate groups would be expected to repel each other. If electron transfer were dependent on a single configuration of low energy (simple docking) one would expect neutralisation of the propionate charges on Zn-myoglobin to increase  $k_2$ , the second-order process, by increasing the binding constant  $K_A$ , but although  $k_2$  was observed to increase 100-fold, there was very little effect on binding (Liang et al. 2002). This could not be explained by the simple docking model but was consistent with a dynamic docking model in which numerous configurations of the complex exist with similar but not identical energies, but only a few, not those with the lowest energy, are effective in electron transfer. The effect of heme neutralisation was to increase the probability of the complex finding the most reactive configurations involving close contact between the two hemes.

The question arising, then, is how to identify the configurations that contribute to the encounter ensemble. Camacho et al. (1999) have calculated three dimensional maps of free energy landscapes for formation of encounter complexes of several protein-inhibitor complexes. Harel et al. (2007) have used double mutant cycle analysis to identify pairs of surface residues of the two proteins that are involved in the transition state for rearrangement of the encounter complex for two enzyme-inhibitor complexes, and in a third case a Type I interferon binding to the extracellular domain of its receptor.

Mutagenesis studies can reveal kinetically significant residues that either enhance or inhibit the rate of reaction. The most powerful technique currently for providing steady-state information about the structure and surface distribution of the encounter complex involves paramagnetic NMR, and has been developed by Ubbink and colleagues for study of electron transfer complexes. As described above, the first method made use of pseudocontact shifts of  $^{15}\text{N}$ -labelled nuclei of one protein induced by a paramagnetic cofactor of the other. This provided distance and orientational information for individual nuclei which made it possible to calculate the structure of the single, specific complex. It gave no information about the structure of the encounter complex, but hinted strongly (without being quantitative) at the balance between the encounter complex and the specific complex, that is the size of  $K_r$  in Scheme 1, by considering the amplitude of the pseudocontact shifts. In the case of the complex between turnip cytochrome *f* and spinach plastocyanin it was suggested that the equilibrium lay well over towards the specific complex, with a large  $K_r$ , except at low ionic strength when the situation becomes reversed (Ubbink et al. 1998). On the other hand, in the unphysiological reaction between plastocyanin and cytochrome *c* small diamagnetic chemical shift changes could be observed when cytochrome *c* was in the reduced state and these were sufficient to identify relatively large binding areas on the surface of each protein, but no additional pseudocontact shifts were observed when the iron atom of cytochrome *c* was in the oxidized, paramagnetic state (Ubbink and Bendall 1997). This suggested that no single, specific complex was formed, but that the complex consisted of a dynamic ensemble of structures forming an encounter complex, which still yielded a rate constant for electron transfer of  $3.5 \times 10^6 \text{ M}^{-1}\text{s}^{-1}$  (Modi et al. 1992). Similarly dynamic complexes, with small chemical shift perturbations, have been found for cytochrome *b*<sub>5</sub> and myoglobin (Worrall et al. 2002), cytochrome *b*<sub>5</sub> and cytochrome *c* (Volkov et al. 2005), and

adrenodoxin and cytochrome *c* (Worrall et al. 2003).

As described above, measurements of paramagnetic relaxation can be used to calculate the regions of each protein surface that contribute to the encounter ensemble. To achieve this it is necessary to introduce cysteine residues, one at a time, at several different sites distributed over the surface of the protein, and then to label them covalently with a nitroxide spin label. The method has been developed in relation to the reaction between yeast cytochrome *c* and cytochrome *c* peroxidase (Volkov et al. 2006, 2010a, b; Bashir et al. 2010). With the wild type proteins 70 % of the lifetime of the complex as a whole is spent in the single, specific configuration and 30 % in the encounter ensemble, but single site mutations of residues shown to be important in the specific form can shift the equilibrium in either direction. Thus the mutation T12A of cytochrome *c* reduces the encounter form to only 10 % of the total, while R13A increases it to 80 %. A similar qualitative increase in dynamics by mutation was earlier described for *Prochlorothrix hollandica*, as mentioned above (Hulsker et al. 2008). *Nostoc* provides an interesting intermediate case, the only one reported so far for the reaction between cytochrome *f* and plastocyanin. Pseudocontact shifts were sufficiently large to enable the calculation of a definite orientation (side-on) for the single specific complex, but provided no information about the encounter state (Díaz-Moreno et al. 2005a). More recently paramagnetic relaxation has been used to demonstrate that the complex is, in fact, highly dynamic and that the encounter ensemble must be significantly populated (Scanu et al. 2012). The relative population of the encounter ensemble for an interaction giving rapid electron transfer is likely to depend on whether the distance between redox centers is adequate in the configurations that contribute.

The above considerations lead to some general conclusions about the essential features of the reaction. Above all there is the need for a high  $k_{\text{off}}$  to allow plastocyanin and cytochrome *c*<sub>6</sub> to perform their function

of rapid shuttling of electrons between cytochrome *f* and photosystem I. This can be achieved with a suitable structure of the interface in a specific complex. It is composed of a small group of hydrophobic residues in a loose structure which is not sealed off completely from the surrounding solvent (Crowley and Carrondo 2004; Bendall et al. 2011). There are few, if any, hydrogen bonds or ‘hot spots’ of binding energy.

A high  $k_{\text{off}}$  implies a much larger  $k_{\text{on}}$  which is greater by more than one order of magnitude than the simple collisional rate makes possible. This enhancement is achieved by a steering effect which is the result of either long range electrostatic forces or shorter range hydrophobic interactions that bring the two proteins into a relatively loose configuration that forms the encounter complex. Electrostatic steering is the more common, and is probably never completely absent, but hydrophobic steering can be important and may even dominate (especially, perhaps, in thermophilic organisms) although it gives a smaller rate enhancement. The ensemble of configurations of the encounter complex can make a significant contribution to electron transfer if they bring the redox centers sufficiently close together. In extreme cases the specific complex may be dispensed with altogether (that is become just one component of the reactive encounter complex), but such a case has not been described for the reaction between cytochrome *f* and plastocyanin. A more extensive analysis of the *Nostoc* system by Scanu et al. (2013), using the paramagnetic relaxation technique described above, has provided new insight into the nature of the encounter complex in transient interactions. In this organism electrostatic attraction plays a significant part in binding and a specific complex with the side-on orientation has been identified. Nevertheless, electrostatics play no part in the definition of the specific complex because negative charges of cytochrome *f* are distributed over the whole surface of the protein, rather than localised (Albarrán et al. 2007). The similarity of the relaxation data for paramagnetic probes

placed in a variety of positions around the specific site shows that plastocyanin always approaches cytochrome *f* in the same orientation, with the hydrophobic northern site pointed towards the hydrophobic patch near the heme of the cytochrome. The model that results from these observations is that the role of electrostatics is limited to a favourable preorientation of plastocyanin as a result of the strongly localised charges on plastocyanin and delocalised charges on cytochrome *f*. Hence both the encounter complex and the specific complex are stabilized predominantly by hydrophobic interactions. This situation allows rapid electron transfer without strong, specific electrostatic attraction because the activation energy that is required for desolvation of charged residues in passing from the encounter to the specific complex is no longer necessary.

Only a limited comparison can be made between the reactions with plastocyanin and cytochrome  $c_6$  as acceptors because there have been few studies with the latter. Grove and Kostić (2003), however, have used the triplet decay technique to investigate the reaction between cytochrome *f* and Zn-heme cytochrome  $c_6$  from *Chlamydomonas reinhardtii*, and their results show a surprising difference in the behaviour of cytochrome  $c_6$  and plastocyanin as acceptor proteins. With plastocyanin the *Chlamydomonas* proteins behave much like those from higher plants, which is to say that both  $k_2$  and  $K_A$  are strongly dependent on ionic strength, indicating electrostatic steering (Soriano et al. 1998). With cytochrome  $c_6$ , on the other hand, Grove and Kostić found very little effect of ionic strength on either parameter. It would seem, therefore, that the reaction is predominantly hydrophobic, despite the fact that both proteins have well-defined acidic patches. This conclusion is at odds with that reached on the basis of Brownian dynamics simulations of each protein interacting with cytochrome *f* (Gross and Pearson 2003; Haddadian and Gross 2005) from which models of the structure of the complex were obtained. In the case of the cyanobacterial

proteins from *Nostoc* sp. PCC 7119 an NMR study of the chemical shift perturbations in the complex between cytochrome *f* and cytochrome *c*<sub>6</sub> tends to confirm the similarity between the behaviour of cytochrome *c*<sub>6</sub> and plastocyanin, both of which show an interaction between basic groups in the acceptor with acidic groups in cytochrome *f* (Díaz-Moreno et al. 2005b).

Mutagenesis of the reactants in individual species has demonstrated that evolution has not produced sequences that optimise the rate of electron transfer as it occurs in solution *in vitro*. This suggests that the wild type proteins have already achieved rates considerably in excess of the maximum that may be required *in vivo*, when other limiting factors presumably come into play, and when other constraints may also be significant. The factors discussed above nevertheless provide the basis of what is possible under *in vivo* conditions. So we must now turn to the question of what is known about the physiological reaction *in vivo*.

### VIII. The Reaction *In Vivo*

The detailed studies of the interaction between plastocyanin and the soluble fragment of cytochrome *f* in solution, as described above, provide only a crude model of the physiological process, but it has led to a basic understanding of the physical constraints on the reaction. In the living plant the reaction occurs under conditions far from those of free solution. The *in vitro* studies pretend that both cytochrome *f* and plastocyanin are free to diffuse in an aqueous medium of infinite extent. *In vivo* the reaction occurs in the severely confined space of the thylakoid lumen which is a sheet of aqueous solution no more than about 10 nm thick. Moreover, this thin space is crowded with protein complexes anchored to the membrane, especially photosystem II and, to a lesser extent, the cytochrome *b*<sub>6</sub>*f* complex. The luminal domains of these complexes can occupy much of the trans-luminal dimension. The diffusion space is further complicated in higher plants

by the structure of thylakoids, with differentiation into the appressed membranes of granal stacks and unappressed stroma lamellae. This differentiation is associated with a functional differentiation involving segregation of the major membrane complexes. Most of photosystem II, and all the active form, occurs in the appressed granal membranes, whereas photosystem I is confined to the stroma lamellae and the end membranes and possibly the disc margins of the grana. Fractionation of disrupted thylakoid membranes by phase partitioning has shown that each of the three fractions containing photosystem I has about one-third of the total (Albertsson 2001), but the origin of the fraction corresponding to disc margins according to Albertsson has been questioned (Anderson et al. 2012). The cytochrome *b*<sub>6</sub>*f* complex, on the other hand, is evenly distributed between appressed and unappressed membranes (Cox and Andersson 1981; Anderson 1982). Connexion between the two photosystems is mostly dependent on diffusion by plastocyanin, as plastoquinone is largely confined to small domains (Joliot et al. 1992; Kirchoff et al. 2000) and the thylakoid lumen is thought to be one continuous space.

The complexity of the thylakoid membrane suggests diffusion paths for plastocyanin of very different lengths. The longest is that between the cytochrome *b*<sub>6</sub>*f* complex in the grana and photosystem I in the stroma lamellae, and there is evidence for an increase in granal plastocyanin at the expense of that in stroma lamellae in the light (Haehnel et al. 1989). Linear electron flow, however, is more likely to depend predominantly on diffusion only as far as the disc margins and the end membrane of granal stacks. Diffusion within a granum would be facilitated in the model of thylakoid structure of Shimoni et al. (2005) according to which there are direct connections between the individual sacs of a granum. Photosystem I in the stroma lamellae is primarily concerned with cyclic electron flow and can occur as a supercomplex with the cytochrome *b*<sub>6</sub>*f* complex (Joliot and Joliot 2002; Iwai et al. 2010). This



provides the shortest possible diffusion path. Diffusion paths also vary with the type of organism. Chloroplasts from higher plants have been the most intensively studied, but green algae, such as *Chlamydomonas reinhardtii*, lack the highly organized separation of thylakoid membranes into grana and stroma lamellae, although some appression of membranes does occur. Thylakoid membranes of cyanobacteria are completely unappressed, as might be expected from the need to accommodate phycobilisomes. Corresponding to the uniformity of the thylakoid membranes, no lateral segregation between the photosystems has been detected (Mullineaux 1999), so that diffusion paths are likely to be short.

The various factors that may affect the rate of diffusion are difficult to evaluate. The confined space represents a reduction in dimensionality which would enhance the rate, but this would be offset by the greater length of the tortuous path available. An attempt was made to gain information about the effect of macromolecular crowding in the lumen by examining the effect of the artificial polymers, Ficoll and Dextran, on the reaction in solution between cytochrome *f* and plastocyanin of the cyanobacterium *Phormidium laminosum* (Schlarb-Ridley et al. 2005). The surprising result was that there was no detectable effect up to a concentration that increased the viscosity threefold. Phillip et al. (2012) have explained a similar lack of effect with the reaction between  $\beta$ -lactamase and its inhibitor protein as the combination of two opposing effects, an enhancement of binding because of the excluded volume, and an inhibition by decreased diffusion rate.

Plastocyanin diffusion may also be influenced by physiological conditions, as well as by thylakoid structure. The total concentration of plastocyanin in the thylakoid is of the order of 1 mM and one could expect a substantial proportion of this to be bound to the cytochrome *b<sub>6</sub>f* complex and photosystem I. Isolated cytochrome *b<sub>6</sub>f* complex has indeed been found to contain plastocyanin (Romanowska and Albertsson 1994). Early experiments with 'broken' chloroplasts from

higher plants (i.e. those that have lost their outer membrane and stroma but possess intact thylakoids) showed that photooxidation of cytochrome *f* and photosystem I activity were inhibited at low osmotic pressure (Avron and Chance 1967; Bendall and Wood 1978; Lockau 1979). Lockau showed that this is probably due to a decrease in internal ionic strength, rather than an effect on luminal volume, which would be consistent with the inhibition observed in vitro (but see below). By contrast Cruz et al. (2001) showed that hyperosmotic shock of whole cells of *Chlamydomonas reinhardtii* caused inhibition of light-induced electron transfer through plastocyanin, and electron micrographs suggested that inhibition was associated with a contraction of the thylakoid space. The idea that electron transfer through plastocyanin is influenced by the dimensions of the thylakoid lumen has been followed up by Kirchoff et al. (2011)). They found that the thylakoid lumen of grana in the chloroplasts of *Arabidopsis* leaves expands from about 5 nm in the dark to 9 nm when illuminated. Modelling demonstrated how the known density of photosystem II complexes in the membrane provided extremely limited space for plastocyanin diffusion, which would be significantly alleviated by expansion of the lumen in the light. Measurements of the redox state of cytochrome *f* and P700 confirmed the limited effectiveness of plastocyanin diffusion and its improvement in the light. These results seem to contradict the long-standing view that the lumen contracts on illumination, which originated with the experiments of Murakami and Packer (1970), but Kirchoff et al. argue that their own use of cryo-electron microscopy gives more realistic results than the slow chemical fixation used by Murakami and Packer. Simulation of the diffusion of plastocyanin within a narrowly confined space such as the thylakoid lumen by Kovalenko et al. (2008) showed a remarkably sharp optimum in the rate of complexing to cytochrome *f* at a lumen thickness of 8 nm. This conclusion is consistent with the experimental result of Kirchoff et al.

Whether or not variations in luminal thickness provide an effective system for regulation of photosynthetic electron transport is not known. Observations need to be extended to other organisms in order to establish the generality of such an effect. In higher plants it seems that plastocyanin diffusion is not normally a limiting factor for linear electron flow but may become so under some circumstances, with variation in lumen thickness an unexpected controlling factor. It is also unlikely to be limiting for cyclic electron flow.

The question now arises as to whether diffusion of plastocyanin in the lumen is influenced by electrostatics as it is *in vitro*. Experimental work attempting to answer this question is limited. The first point is that as far as plastocyanin is concerned there is little difference in solution between the behaviour of cytochrome *f* either in its truncated, soluble form, or as a component of the cytochrome *b<sub>6</sub>f* complex, as shown by Illerhaus et al. (2000) for plant preparations. This is consistent with the X-ray structures of the cytochrome *b<sub>6</sub>f* complex that show that in the complex the reaction site of cytochrome *f* for plastocyanin around Tyr1 is exposed to the lumen (Kurisu et al. 2003; Stroebel et al. 2003).

The question has been most thoroughly investigated with mutants of *Chlamydomonas reinhardtii* by Soriano et al. (1996, 1998), but their results do not provide a clear-cut answer. Cytochrome *f* of *Chlamydomonas* is overall an acidic protein, but it contains a group of five basic residues thought to be important for binding to plastocyanin, Lys58, Lys65 and Lys66 in the large domain which contains the heme, and Lys188 and Lys189 in the small domain. The approach used was to prepare mutant cultures in which all these residues were neutralized or only those of either the small or large domain. Small increases in doubling time of phototrophically grown cultures could be demonstrated, but there was no consistent effect on the half-time for flash-induced oxidation of cytochrome *f*. These observations suggest that the oxidation of cytochrome *f* is not rate limiting under

these growth conditions although it might become so at an earlier stage of development or under stress (Soriano et al. 1998). There is experimental evidence that the release of oxidized plastocyanin from photosystem I is rate limiting in *Chlamydomonas* (Finazzi et al. 2005), and the complexity of diffusion paths in the lumen suggests that diffusion of plastocyanin might become limiting under some circumstances. It has also been shown that a small domain deletion mutant is viable, although there is a small increase in doubling time, but no significant effect on flash-induced oxidation of cytochrome *f* was detected (Gong et al. 2001). The lack of importance of electrostatic attraction *in vivo* as compared with the *in vitro* reaction in solution is also consistent with the fact that hydrophobic channelling is also effective. We have already commented above that the charge pattern on the two proteins has not been optimised to give the maximum rate, again suggesting that the reaction is not limiting for overall photosynthesis. Nevertheless, we have to account for the fact that the charge pattern on the two proteins is highly conserved among plants and green algae, but at the present time there is no satisfactory explanation.

The above discussion provides a rough sketch of the interaction between plastocyanin and cytochrome *f* *in vivo*, particularly for higher plants and green algae, in so far as *Chlamydomonas* can be taken as being representative of the latter, but clearly there are many details to be filled in and much that is still probably controversial. Moreover there is very little information concerning cyanobacteria which after all are a major group of oxygenic organisms. Nevertheless a strong impression is beginning to emerge that electrostatics are much less important for the reaction between cytochrome *f* and plastocyanin than studies in solution indicated (Scanu et al. 2013). The intracellular reaction in *Chlamydomonas*, at least, can manage quite well without help from electrostatic steering, and there are other indications that the electrostatic properties of the two proteins have not been

optimised to achieve the maximum rate of reaction. This implies that hydrophobic channelling is more generally important than has hitherto been recognized. It also indicates that the ridge of basic residues in cytochrome *f*, which is such a consistent feature of most, possibly all, higher plants and green algae, has another function which has not been clearly identified.

Studies of the behaviour of the purified proteins in solution have emphasized the need for a fast  $k_{\text{off}}$  to maintain the shuttle property of plastocyanin, which is of the essence of the reaction in vivo, and this property of the proteins does not depend on salt bridges in the reaction site. Although much of the luminal plastocyanin is likely to be bound to the cytochrome  $b_6f$  complex this must be in fast exchange with free plastocyanin. From the evolutionary point of view a fast  $k_{\text{off}}$  would not have been difficult to achieve. Whereas for many protein-protein interactions of physiological importance the key factor would have been the slowing down of  $k_{\text{off}}$ , for transient electron transfer reactions it would have been the development of hydrophobic channelling to establish a sufficiently rapid binding to a more or less specific reaction site to provide a modest increase in  $K_A$ . Short-range hydrophobic interactions seem to be adequate for this purpose, and would have been achieved at an early stage in the evolution of oxygenic photosynthetic organisms. The establishment of a rapid reaction between the cytochrome  $b_6f$  complex and plastocyanin is part of the essential background for efficient photosynthesis, but does not seem to present a limitation to the flexibility of thylakoid organisation in response to fluctuating illumination (Anderson et al. 2012).

### Acknowledgements

We thank Dr Marcellus Ubbink for helpful comments and Dr P.B. Crowley for the coordinates of the *P. laminosum* complex. Work in the authors' laboratory was supported by the Biotechnology and Biological Sciences

Research Council and the European Commission.

### References

- Adam G, Delbrück M (1968) Reduction of dimensionality in biological diffusion processes. In: Rich A, Davidson N (eds) *Structural Chemistry and Molecular Biology*. Freeman, San Francisco, pp 198–215
- Albarrán C, Navarro JA, Molina-Heredia FP, Murdoch PS, De la Rosa MA, Hervás M (2005) Laser flash-induced kinetic analysis of cytochrome *f* oxidation by wild-type and mutant plastocyanin from the cyanobacterium *Nostoc* sp. PCC 7119. *Biochemistry* 44:11601–11607
- Albarrán C, Navarro JA, De la Rosa MA, Hervás M (2007) The specificity in the interaction between cytochrome *f* and plastocyanin from the cyanobacterium *Nostoc* sp. PCC 7119 is mainly determined by the copper protein. *Biochemistry* 46:997–1003
- Albertsson P-Å (2001) A quantitative model of the domain structure of the photosynthetic membrane. *Trends Plant Sci* 6:349–354
- Anderson JM (1982) Distribution of the cytochromes of spinach chloroplasts between the appressed membranes of grana stacks and stroma-exposed thylakoid regions. *FEBS Lett* 138:62–66
- Anderson GP, Sanderson DG, Lee CH, Durell S, Anderson LB, Gross EL (1987) The effect of ethylenediamine chemical modification of plastocyanin on the rate of cytochrome *f* oxidation and P-700 reduction. *Biochim Biophys Acta* 894:386–398
- Anderson JM, Horton P, Kim E-H, Chow WS (2012) Towards elucidation of dynamic structural changes of plant thylakoid architecture. *Philos Trans R Soc Lond B* 367:3515–3524
- Avron M, Chance B (1967) Relation of phosphorylation to electron transport in isolated chloroplasts. In: Olson JM (ed) *Brookhaven Symposia in Biology Number 19 Energy Conversion by the Photosynthetic Apparatus*. Brookhaven National Laboratory, Upton, pp 149–160
- Babu CR, Volkman BF, Bullerjahn GS (1999) NMR solution structure of plastocyanin from the photosynthetic prokaryote, *Prochlorothrix hollandica*. *Biochemistry* 38:4988–4995
- Badsberg U, Jorgensen AMM, Gesmar H, Led JJ, Hammerstad JM, Jespersen L-L, Ulstrup J (1996) Solution structure of reduced plastocyanin from the blue-green alga *Anabaena variabilis*. *Biochemistry* 35:7021–7031
- Bagby S, Driscoll PC, Harvey TS, Hill HAO (1994) High-resolution solution structure of reduced parsley plastocyanin. *Biochemistry* 33:6611–6622

- Bashir Q, Volkov AN, Ullmann GM, Ubbink M (2010) Visualization of the encounter ensemble of the transient electron transfer complex of cytochrome *c* and cytochrome *c* peroxidase. *J Am Chem Soc* 132:241–247
- Bendall DS (1996) Interprotein electron transfer. In: Bendall DS (ed) *Protein Electron Transfer*. Bios Scientific, Oxford, pp 43–68
- Bendall DS, Wood PM (1978) Kinetics of electron transfer through higher-plant plastocyanin. In: Hall DO, Coombs J, Goodwin TW (eds) *Photosynthesis '77 Proceedings of the Fourth International Congress on Photosynthesis*. The Biochemical Society, London/Colchester, pp 771–775
- Bendall DS, Schlarb-Ridley BG, Howe CJ (2011) Transient interactions between soluble electron transfer proteins. The case of plastocyanin and cytochrome *f*. In: Peschek GA, Obinger C, Renger G (eds) *Bioenergetic Process of Cyanobacteria*. Springer, Dordrecht, pp 541–571
- Beratan DN, Betts JN, Onuchic JN (1991) Protein electron transfer rates set by the bridging secondary and tertiary structure. *Science* 252:1285–1288
- Berg OG, von Hippel PH (1985) Diffusion-controlled macromolecular interactions. *Annu Rev Biophys Chem* 14:131–160
- Bertini I, Ciurli S, Dikly A, Fernández CO, Luchinat C, Safarov N, Shumilin S, Vila AJ (2001) The first solution structure of a paramagnetic copper(II) protein: the case of oxidized plastocyanin from the cyanobacterium *Synechocystis* PCC6803. *J Am Chem Soc* 123:2405–2413
- Bogan AA, Thorn KS (1998) Anatomy of hot spots in protein interfaces. *J Mol Biol* 280:1–9
- Bohner H, Böger P (1978) Reciprocal formation of cytochrome *c*-553 and plastocyanin in *Scenedesmus*. *FEBS Lett* 85:337–339
- Bond CS, Bendall DS, Freeman HC, Guss JM, Howe CJ, Wagner MJ, Wilce MCJ (1999) The structure of plastocyanin from the cyanobacterium *Phormidium laminosum*. *Acta Crystallogr D* 55:414–421
- Camacho CJ, Weng ZP, Vajda S, Delisi C (1999) Free energy landscapes of encounter complexes in protein-protein association. *Biophys J* 76:1166–1178
- Camacho CJ, Kimura SR, Delisi C, Vajda S (2000) Kinetics of desolvation-mediated protein-protein binding. *Biophys J* 78:1094–1105
- Carrell CJ, Schlarb BG, Bendall DS, Howe CJ, Cramer WA, Smith JL (1999) Structure of the soluble domain of cytochrome *f* from the cyanobacterium, *Phormidium laminosum*: convergent evolution of the membrane-bound *c*-type cytochromes from photosynthetic and respiratory cytochrome *bc* complexes. *Biochemistry* 38:9590–9599
- Chi Y-I, Huang L-S, Zhang Z, Fernández-Velasco JG, Berry EA (2000) X-ray structure of a truncated form of cytochrome *f* from *Chlamydomonas reinhardtii*. *Biochemistry* 39:7689–7701
- Clackson T, Wells JA (1995) A hot spot of binding energy in a hormone-receptor interface. *Science* 267:383–386
- Clore GM, Iwahara J (2009) Theory, practice, and applications of paramagnetic relaxation enhancement for the characterization of transient low-population states of biological macromolecules and their complexes. *Chem Rev* 109:4108–4139
- Collyer CA, Guss JM, Sugimura Y, Yoshizaki F, Freeman HC (1990) Crystal structure of plastocyanin from a green alga, *Enteromorpha prolifera*. *J Mol Biol* 211:617–632
- Colman PM, Freeman HC, Guss JM, Murata M, Norris VA, Ramshaw JAM, Venkatappa MP (1978) X-ray crystal structure analysis of plastocyanin at 2.7 Å resolution. *Nature* 272:319–324
- Cox RP, Andersson B (1981) Lateral and transverse organisation of cytochromes in the chloroplast thylakoid membrane. *Biochem Biophys Res Commun* 103:1336–1342
- Crowder MS, Prince RC, Bearden A (1982) Orientation of membrane-bound cytochromes in chloroplasts, detected by low-temperature EPR spectroscopy. *FEBS Lett* 144:204–208
- Crowley PB, Carrondo MA (2004) The architecture of the binding site in redox protein complexes: implications for fast dissociation. *Proteins* 55:603–612
- Crowley PB, Otting G, Schlarb-Ridley BG, Canters GW, Ubbink M (2001) Hydrophobic interactions in a cyanobacterial plastocyanin-cytochrome *f* complex. *J Am Chem Soc* 123:10444–10453
- Crowley PB, Vintonenko N, Bullerjahn GS, Ubbink M (2002) Plastocyanin-cytochrome *f* interactions: the influence of hydrophobic patch mutations studied by NMR spectroscopy. *Biochemistry* 41:15698–15705
- Cruz JA, Salbilla BA, Kanazawa A, Kramer DM (2001) Inhibition of plastocyanin to P<sub>700</sub><sup>+</sup> electron transfer in *Chlamydomonas reinhardtii* by hyperosmotic shock. *Plant Physiol* 127:1167–1179
- Davidson VL (1996) Unraveling the kinetic complexity of interprotein electron transfer reactions. *Biochemistry* 35:14035–14039
- Davidson VL (2000) What controls the rates of interprotein electron-transfer reactions. *Acc Chem Res* 33:87–93
- De la Cerda B, Díaz-Quintana A, Navarro JA, Hervás M, De la Rosa MA (1999) Site-directed mutagenesis of cytochrome *c*<sub>6</sub> from *Synechocystis* sp. PCC6803 – the heme protein possesses a negatively charged area that may be isofunctional with the acidic patch of plastocyanin. *J Biol Chem* 274:13292–13297

- De Rienzo F, Gabdoulline RR, Menziani MC, De Benedetti PG, Wade RC (2001) Electrostatic analysis and Brownian dynamics simulation of the association of plastocyanin and cytochrome *f*. *Biophys J* 81:3090–3104
- Despa F, Berry RS (2007) The origin of long-range attraction between hydrophobes in water. *Biophys J* 92:373–378
- Díaz-Moreno I, Díaz-Quintana A, De la Rosa MA, Ubbink M (2005a) Structure of the complex between plastocyanin and cytochrome *f* from the cyanobacterium *Nostoc* sp. PCC 7119 as determined by paramagnetic NMR. *J Biol Chem* 280:18908–18915
- Díaz-Moreno I, Díaz-Quintana A, Ubbink M, De la Rosa MA (2005b) An NMR-based docking model for the physiological transient complex between cytochrome *f* and cytochrome *c<sub>6</sub>*. *FEBS Lett* 579:2891–2896
- Finazzi G, Sommer F, Hippler M (2005) Release of oxidized plastocyanin from photosystem I limits electron transfer between photosystem I and cytochrome *b<sub>6</sub>f* complex in vivo. *Proc Natl Acad Sci USA* 102:7031–7036
- Gabdoulline RR, Wade RC (1998) Brownian dynamics simulation of protein-protein diffusional encounter. *Methods* 14:329–341
- Gabdoulline RR, Wade RC (1999) On the protein-protein diffusional encounter complex. *J Mol Recognit* 12:226–234
- Gabdoulline RR, Wade RC (2009) On the contributions of diffusion and thermal activation to electron transfer between *Phormidium laminosum* plastocyanin and cytochrome *f*: Brownian dynamics simulations with explicit modeling of nonpolar desolvation interactions and electron transfer events. *J Am Chem Soc* 131:9230–9238
- Gong X-S, Wen JQ, Fisher NE, Young S, Howe CJ, Bendall DS, Gray JC (2000) The role of individual lysine residues in the basic patch on turnip cytochrome *f* for electrostatic interactions with plastocyanin in vitro. *Eur J Biochem* 267:3461–3468
- Gong X-S, Chung S, Fernández-Velasco JG (2001) Electron transfer and stability of the cytochrome *b<sub>6</sub>f* complex in a small domain deletion mutant of cytochrome *f*. *J Biol Chem* 276:24365–24371
- Gray JC (1992) Cytochrome *f*: structure, function and biosynthesis. *Photosynth Res* 34:359–374
- Griffin S, Vitello A, Wittung-Stafshede P (2002) Buried water molecules contribute to cytochrome *f* stability. *Arch Biochem Biophys* 404:335–337
- Gross EL (2004) A Brownian dynamics study of the interaction of *Phormidium laminosum* plastocyanin with *Phormidium laminosum* cytochrome *f*. *Biophys J* 87:2043–2059
- Gross EL, Pearson DC (2003) Brownian dynamics simulations of the interaction of *Chlamydomonas* cytochrome *f* with plastocyanin and cytochrome *c<sub>6</sub>*. *Biophys J* 85:2055–2068
- Gross EL, Rosenberg I (2006) A Brownian dynamics study of the interaction of *Phormidium* cytochrome *f* with various cyanobacterial plastocyanins. *Biophys J* 90:366–380
- Grove TZ, Kostić NM (2003) Metalloprotein association, self-association, and dynamics governed by hydrophobic interactions: simultaneous occurrence of gated and true electron-transfer reactions between cytochrome *f* and cytochrome *c<sub>6</sub>* from *Chlamydomonas reinhardtii*. *J Am Chem Soc* 125:10598–10607
- Guo M, Bhasker B, Li H, Barrows TP, Poulos TL (2004) Crystal structure and characterization of a cytochrome *c* peroxidase-cytochrome *c* site-specific cross-link. *Proc Natl Acad Sci USA* 101:5940–5945
- Guss JM, Freeman HC (1983) Structure of oxidized poplar plastocyanin at 1.6 Å resolution. *J Mol Biol* 169:521–563
- Guss JM, Bartunik HD, Freeman HC (1992) Accuracy and precision in protein structure analysis: restrained least-squares refinement of the structure of poplar plastocyanin at 1.33 Å resolution. *Acta Cryst B* 48:790–811
- Haddadian EJ, Gross EL (2005) Brownian dynamics study of cytochrome *f* interactions with cytochrome *c<sub>6</sub>* and plastocyanin in *Chlamydomonas reinhardtii* plastocyanin, and cytochrome *c<sub>6</sub>* mutants. *Biophys J* 88:2323–2339
- Haehnel W, Ratajczak R, Robenek H (1989) Lateral distribution and diffusion of plastocyanin in chloroplast thylakoids. *J Cell Biol* 108:1397–1405
- Harel M, Cohen M, Schreiber G (2007) On the dynamic nature of the transition state for protein-protein association as determined by double-mutant cycle analysis and simulation. *J Mol Biol* 371:180–196
- Harris TK, Davidson VL, Chen L, Mathews FS, Xia Z-X (1994) Ionic strength dependence of the reaction between methanol dehydrogenase and cytochrome *c-551i*: Evidence of conformationally coupled electron transfer. *Biochemistry* 33:12600–12608
- Hart SE, Schlarb-Ridley BG, Delon C, Bendall DS, Howe CJ (2003) Role of charges on cytochrome *f* from the cyanobacterium *Phormidium laminosum* in its interaction with plastocyanin. *Biochemistry* 42:4829–4836
- Hervás M, Ortega JM, Navarro JA, De la Rosa MA, Bottin H (1994) Laser flash kinetic analysis of *Synechocystis* PCC 6803 cytochrome *c<sub>6</sub>* and plastocyanin oxidation by photosystem I. *Biochim Biophys Acta* 1184:235–241

- Hervás M, Navarro JA, Díaz A, Bottin H, De la Rosa MA (1995) Laser-flash kinetic analysis of the fast electron transfer from plastocyanin and cytochrome *c*<sub>6</sub> to photosystem I. Experimental evidence on the evolution of the reaction mechanism. *Biochemistry* 34:11321–11326
- Hoffman BM, Ratner MA (1987) Gated electron transfer: when are observed rates controlled by conformational interconversion? *J Am Chem Soc* 109:6237–6243
- Hohmann-Marriott MF, Blankenship RE (2011) Evolution of photosynthesis. *Annu Rev Plant Biol* 62:515–548
- Hulsker R, Baranova MV, Bullerjahn GS, Ubbink M (2008) Dynamics in the transient complex of plastocyanin-cytochrome *f* from *Prochlorothrix hollandica*. *J Am Chem Soc* 130:1985–1991
- Illerhaus J, Altschmied L, Reichert J, Zak J, Zak E, Herrmann RG, Haehnel W (2000) Dynamic interaction of plastocyanin with the cytochrome *bf* complex. *J Biol Chem* 275:17590–17595
- Inoue T, Gotowda M, Sugawara H, Kohzuma T, Yoshizaki F, Sugimura Y, Kai Y (1999a) Structure comparison between oxidized and reduced plastocyanin from a fern, *Dryopteris crassirhizoma*. *Biochemistry* 38:13853–13861
- Inoue T, Sugawara H, Hamanaka S, Tsukui H, Suzuki E, Kohzuma T, Kai Y (1999b) Crystal structure determinations of oxidized and reduced plastocyanin from the cyanobacterium *Synechococcus* sp PCC 7942. *Biochemistry* 38:6063–6069
- Iwahara J, Clore GM (2006) Detecting transient intermediates in macromolecular binding by paramagnetic NMR. *Nature* 440:1227–1230
- Iwai M, Takizawa K, Tokutsu R, Okamuro A, Takahashi Y, Minagawa J (2010) Isolation of the elusive supercomplex that drives cyclic electron flow in photosynthesis. *Nature* 464:1210–1214
- Joliot P, Joliot A (2002) Cyclic electron transfer in plant leaf. *Proc Natl Acad Sci USA* 99:10209–10214
- Joliot P, Lavergne J, Béal D (1992) Plastoquinone compartmentation in chloroplasts. I. Evidence for domains with different rates of photo-reduction. *Biochim Biophys Acta* 1101:1–12
- Kannt A, Young S, Bendall DS (1996) The role of acidic residues of plastocyanin in its interaction with cytochrome *f*. *Biochim Biophys Acta* 1277:115–126
- Kirchhoff H, Horstmann S, Weis E (2000) Control of the photosynthetic electron transport by PQ diffusion microdomains in thylakoids of higher plants. *Biochim Biophys Acta* 1459:148–168
- Kirchhoff H, Hall C, Wood M, Herbstová M, Tsaabari O, Nevo R, Charuvi D, ... Reich Z (2011) Dynamic control of protein diffusion within the granal thylakoid lumen. *Proc Nat Acad Sci USA* 108:20248–20253
- Kohzuma T, Inoue T, Yoshizaki F, Sasakawa Y, Onodera K, Nagatomo S, Kitagawa T, ... Kai Y (1999) The structure and unusual pH dependence of plastocyanin from the fern *Dryopteris crassirhizoma*. *J Biol Chem* 274:11817–11823
- Kovalenko IB, Abaturova AM, Gromov PA, Ustinin DM, Riznichenko GY, Grachev EA, Rubin AB (2008) Computer simulation of plastocyanin-cytochrome *f* complex formation in the thylakoid lumen. *Biophysics* 53:140–146
- Kraulis PJ (1991) MOLSCRIPT: a program to produce both detailed and schematic plots of protein structures. *J Appl Cryst* 24:946–950
- Kurisu G, Zhang H, Smith JL, Cramer WA (2003) Structure of the cytochrome *b<sub>6</sub>f* complex of oxygenic photosynthesis: tuning the cavity. *Science* 302:1009–1014
- Lange C, Cornvik T, Diaz-Moreno I, Ubbink M (2005) The transient complex of poplar plastocyanin with cytochrome *f*: effects of ionic strength and pH. *Biochim Biophys Acta* 1707:179–188
- Lee BH, Hibino T, Takabe T, Weisbeek PJ (1995) Site-directed mutagenetic study on the role of negative patches on *Silene* plastocyanin in the interactions with cytochrome *f* and photosystem I. *J Biochem (Tokyo)* 117:1209–1217
- Liang Z-X, Nocek JM, Huang K, Hayes RT, Kuminov IV, Beratan DN, Hoffman BM (2002) Dynamic docking and electron transfer between Zn-myoglobin and cytochrome *b<sub>5</sub>*. *J Am Chem Soc* 124:6849–6859
- Lockau W (1979) The inhibition of photosynthetic electron transport in spinach chloroplasts by low osmolarity. *Eur J Biochem* 94:365–373
- Madura JD, Briggs JM, Wade RC, Davis ME, Luty BA, Illin A, Antosiewicz J, ... McCammon JA (1995) Electrostatics and diffusion of molecules in solution: simulations with the University of Houston Brownian Dynamics program. *Comp Phys Commun* 91:57–95
- Malmström BG (1970) The ‘unique’ metal-binding properties of metalloenzymes. *Pure Appl Chem* 24:393–406
- Marcus RA, Sutin N (1985) Electron transfers in chemistry and biology. *Biochim Biophys Acta* 811:265–322
- Martinez SE, Huang D, Ponomarev M, Cramer WA, Smith JL (1996) The heme redox center of chloroplast cytochrome *f* is linked to a buried five-water chain. *Protein Sci* 5:1081–1092
- Medina M, Díaz A, Hervás M, Navarro JA, Gómez-Moreno C, De la Rosa MA, Tollin G (1993) A com-

- parative laser-flash absorption spectroscopy study of *Anabaena* PCC 7119 plastocyanin and cytochrome *c*<sub>6</sub> photooxidation by photosystem I particles. *Eur J Biochem* 213:1133–1138
- Mei HK, Wang KF, Peffer N, Weatherly G, Cohen DS, Miller M, Pielak G, ... Millett F (1999) Role of configurational gating in intracomplex electron transfer from cytochrome *c* to the radical cation in cytochrome *c* peroxidase. *Biochemistry* 38:6846–6854
- Merchant S, Bogorad L (1986) Regulation by copper of the expression of plastocyanin and cytochrome *c*-552 in *Chlamydomonas reinhardtii*. *Mol Cell Biol* 6:462–469
- Merritt EA, Bacon DJ (1997) Raster3D photorealistic molecular graphics. *Methods Enzymol* 277:505–524
- Meyer TE, Zhao ZG, Cusanovich MA, Tollin G (1993) Transient kinetics of electron transfer from a variety of *c*-type cytochromes to plastocyanin. *Biochemistry* 32:4552–4559
- Millett F, Durham B (2002) Design of photoactive ruthenium complexes to study interprotein electron transfer. *Biochemistry* 41:11315–11324
- Modi S, Nordling M, Lundberg LG, Hansson Ö, Bendall DS (1992) Reactivity of cytochromes *c* and *f* with mutant forms of spinach plastocyanin. *Biochim Biophys Acta* 1102:85–90
- Molina-Heredia FP, Hervás M, Navarro JA, De la Rosa MA (2001) A single arginyl residue in plastocyanin and cytochrome *c*<sub>6</sub> from the cyanobacterium *Anabaena* sp. PCC 7119 is required for efficient reduction of photosystem I. *J Biol Chem* 276:601–605
- Moore JM, Lepre CA, Gippert GP, Chazin WJ, Case DA, Wright PE (1991) High-resolution solution structure of reduced French bean plastocyanin and comparison with the crystal structure of poplar plastocyanin. *J Mol Biol* 221:533–555
- Moser CC, Page CC, Farid RS, Dutton PL (1995) Biological electron transfer. *J Bioenerg Biomembr* 27:263–274
- Mullineaux CW (1999) The thylakoid membranes of cyanobacteria: structure, dynamics and function. *Aus J Plant Physiol* 26:671–677
- Murakami S, Packer L (1970) Protonation and chloroplast membrane structure. *J Cell Biol* 47:332–351
- Navarro JA, Hervás M, De la Rosa MA (1997) Co-evolution of cytochrome *c*<sub>6</sub> and plastocyanin, mobile proteins transferring electrons from cytochrome *b*<sub>6</sub>*f* to photosystem I. *J Biol Inorg Chem* 2:11–22
- Navarro JA, Lowe CE, Amons R, Kohzuma T, Canters GW, De la Rosa MA, Ubbink M, Hervás M (2004) Functional characterization of the evolutionarily divergent fern plastocyanin. *Eur J Biochem* 271:3449–3456
- Nocek JM, Sishta BP, Cameron JC, Mauk AG, Hoffman BM (1997) Cyclic electron transfer within the [Zn-myoglobin, cytochrome *b*<sub>5</sub>] complex. *J Am Chem Soc* 119:2146–2155
- Northrup SH, Erickson HP (1992) Kinetics of protein-protein association explained by Brownian dynamics computer simulation. *Proc Natl Acad Sci USA* 89:3338–3342
- Northrup SH, Boles JO, Reynolds JCL (1987) Electrostatic effects in the Brownian dynamics of association and orientation of heme proteins. *J Phys Chem* 91:5991–5998
- Pearson DC, Gross EL (1998) Brownian dynamics study of the interaction between plastocyanin and cytochrome *f*. *Biophys J* 75:2698–2711
- Pelletier H, Kraut J (1992) Crystal structure of a complex between electron transfer partners, cytochrome *c* peroxidase and cytochrome *c*. *Science* 258:1748–1755
- Phillip Y, Harel M, Khait R, Qin S, Zhou H-X, Schreiber G (2012) Contrasting factors on the kinetic path to protein complex formation diminish the effects of crowding agents. *Biophys J* 103:1011–1019
- Ponamarev MV, Cramer WA (1998) Perturbation of the internal water chain in cytochrome *f* of oxygenic photosynthesis: loss of the concerted reduction of cytochromes *f* and *b*<sub>6</sub>. *Biochemistry* 37:17199–17208
- Qin L, Kostić NM (1992) Electron-transfer reactions of cytochrome *f* with flavin semiquinones and with plastocyanin. Importance of protein-protein electrostatic interactions and of donor-acceptor coupling. *Biochemistry* 31:5145–5150
- Qin L, Kostić NM (1994) Photoinduced electron transfer from the triplet state of zinc cytochrome *c* to ferricytochrome *b*<sub>5</sub> is gated by configurational fluctuations of the diprotein complex. *Biochemistry* 33:12592–12599
- Redinbo MR, Cascio D, Choukair MK, Rice D, Merchant S, Yeates TO (1993) The 1.5-Å crystal structure of plastocyanin from the green alga *Chlamydomonas reinhardtii*. *Biochemistry* 32:10560–10567
- Romanowska E, Albertsson P-Å (1994) Isolation and characterization of the cytochrome *bf* complex from whole thylakoids, grana, and stroma lamellae vesicles from spinach chloroplasts. *Plant Cell Physiol* 35:557–568
- Romero A, De la Cerda B, Varela PF, Navarro JA, Hervás M, De la Rosa MA (1998) The 2.15 Å crystal structure of a triple mutant plastocyanin from the cyanobacterium *Synechocystis* sp. PCC 6803. *J Mol Biol* 275:327–336

- Sainz G, Carrell CJ, Ponamarev MV, Soriano GM, Cramer WA, Smith JL (2000) Interruption of the internal water chain of cytochrome *f* impairs photosynthetic function. *Biochemistry* 39:9164–9173
- Sandmann G, Reck H, Kessler E, Böger P (1983) Distribution of plastocyanin and soluble plastidic cytochrome *c* in various classes of algae. *Arch Microbiol* 134:23–27
- Scanu S, Förster J, Finiguerra MG, Shabestari MH, Huber M, Ubbink M (2012) The complex of cytochrome *f* and plastocyanin in *Nostoc* sp. PCC 7119 is highly dynamic. *Chembiochem* 13:1312–1318
- Scanu S, Foerster JM, Ullmann GM, Ubbink M (2013) Role of hydrophobic interactions in the encounter complex formation of the plastocyanin and cytochrome *f* complex revealed by paramagnetic NMR spectroscopy. *J Am Chem Soc* 135:7681–7692
- Schlarb-Ridley BG, Bendall DS, Howe CJ (2002a) Role of electrostatics in the interaction between cytochrome *f* and plastocyanin of the cyanobacterium *Phormidium laminosum*. *Biochemistry* 41:3279–3285
- Schlarb-Ridley BG, Navarro JA, Spencer M, Bendall DS, Hervás M, Howe CJ, De la Rosa MA (2002b) Role of electrostatics in the interaction between plastocyanin and photosystem I of the cyanobacterium *Phormidium laminosum*. *Eur J Biochem* 269:5893–5902
- Schlarb-Ridley BG, Bendall DS, Howe CJ (2003) Relation between interface properties and kinetics of electron transfer in the interaction of cytochrome *f* and plastocyanin from plants and the cyanobacterium *Phormidium laminosum*. *Biochemistry* 42:4057–4063
- Schlarb-Ridley BG, Mi H, Teale WD, Meyer VS, Howe CJ, Bendall DS (2005) Implications of the effects of viscosity, macromolecular crowding, and temperature for the transient interaction between cytochrome *f* and plastocyanin from the cyanobacterium *Phormidium laminosum*. *Biochemistry* 44:6232–6238
- Schmidt L, Christensen HEM, Harris P (2006) Structure of plastocyanin from the cyanobacterium *Anabaena variabilis*. *Acta Crystallogr D* 62:1022–1029
- Schreiber G, Fersht AR (1996) Rapid, electrostatically assisted association of proteins. *Nat Struct Biol* 3:427–431
- Shibata N, Inoue T, Nagano C, Nishio N, Kohzuma T, Onodera K, Yoshizaki F, . . . Kai Y (1999) The crystal structure of *Ulva pertusa* plastocyanin at 1.6 Å resolution, structural basis for regulation of the copper site by residue 88. *J Biol Chem* 274:4225–4230
- Shimoni E, Rav-Hon O, Ohad I, Brumfeld V, Reich Z (2005) Three-dimensional organization of higher-plant chloroplast thylakoid membranes revealed by electron tomography. *Plant Cell* 17:2580–2586
- Sinclair-Day JD, Sykes AG (1986) Kinetic studies on 1:1 electron-transfer reactions involving blue copper proteins. Part 12. Reactions of spinach plastocyanin with inorganic redox partners. *J Chem Soc Dalton Trans* 10:2069–2073
- Soriano GM, Ponamarev MV, Tae GS, Cramer WA (1996) Effect of the interdomain basic region of cytochrome *f* on its redox reactions *in vivo*. *Biochemistry* 35:14590–14598
- Soriano GM, Cramer WA, Krishtalik LI (1997) Electrostatic effects on electron-transfer kinetics in the cytochrome *f* plastocyanin complex. *Biophys J* 73:3265–3276
- Soriano GM, Ponamarev MV, Piskowski RA, Cramer WA (1998) Identification of the basic residues of cytochrome *f* responsible for electrostatic docking interactions with plastocyanin *in vitro*: relevance to the electron transfer reaction *in vivo*. *Biochemistry* 37:15120–15128
- Stroebel D, Choquet Y, Picot D (2003) An atypical heme in the cytochrome *b<sub>6</sub>f* complex. *Nature* 426:413–418
- Sugawara H, Inoue T, Li C, Gotawda M, Hibino T, Takabe T, Kai Y (1999) Crystal structures of wild-type and mutant plastocyanins from a higher plant, *Silene*. *J Biochem* 125:899–903
- Sykes AG (1985) Structure and electron-transfer reactivity of the blue copper protein plastocyanin. *Chem Soc Rev* 14:283–314
- Takenaka K, Takabe T (1984) Importance of local positive charges on cytochrome *f* for electron transfer to plastocyanin and potassium ferricyanide. *J Biochem* 96:1813–1821
- Tang C, Iwahara J, Clore GM (2006) Visualization of transient encounter complexes in protein-protein association. *Nature* 444:383–386
- Tsao Y-H, Evans DF, Wennerström H (1993) Long-range attractive force between hydrophobic surfaces observed by atomic force microscope. *Science* 262:547–550
- Ubbink M, Bendall DS (1997) Complex of plastocyanin and cytochrome *c* characterized by NMR chemical shift analysis. *Biochemistry* 36:6326–6335
- Ubbink M, Ejdebäck M, Karlsson BG, Bendall DS (1998) The structure of the complex of plastocyanin and cytochrome *f*, determined by paramagnetic NMR and restrained rigid-body molecular dynamics. *Structure* 6:323–335
- Van Driessche G, Hu W, Van de Werken G, Selvaraj F, McManus JD, Blankenship RE, Van Beeumen JJ



- (1999) Auracyanin A from the thermophilic green gliding photosynthetic bacterium *Chloroflexus aurantiacus* represents an unusual class of small blue copper proteins. *Protein Sci* 8:947–957
- Volkov AN, Ferrari D, Worrall JAR, Bonvin AMJJ, Ubbink M (2005) The orientations of cytochrome *c* in the highly dynamic complex with cytochrome *b*<sub>5</sub> visualized by NMR and docking using HADDOCK. *Protein Sci* 14:799–811
- Volkov AN, Worrall JAR, Holtzmann E, Ubbink M (2006) Solution structure and dynamics of the complex between cytochrome *c* and cytochrome *c* peroxidase determined by paramagnetic NMR. *Proc Natl Acad Sci USA* 103:18945–18950
- Volkov AN, Bashir Q, Worrall JAR, Ubbink M (2009) Binding hot spot in the weak protein complex of physiological redox partners yeast cytochrome *c* and cytochrome *c* peroxidase. *J Mol Biol* 385:1003–1013
- Volkov AN, Bashir Q, Worrall JAR, Ullmann GM, Ubbink M (2010a) Shifting the equilibrium between the encounter state and the specific form of a protein complex by interfacial point mutations. *J Am Chem Soc* 132:11487–11495
- Volkov AN, Ubbink M, Van Nuland NAJ (2010b) Mapping the encounter state of a transient protein complex by PRE NMR spectroscopy. *J Biomol NMR* 48:225–236
- Wood PM (1978) Interchangeable copper and iron proteins in algal photosynthesis. Studies on plastocyanin and cytochrome *c*-552 in *Chlamydomonas*. *Eur J Biochem* 87:9–19
- Worrall JAR, Liu Y, Crowley PB, Nocek JM, Hoffman BM, Ubbink M (2002) Myoglobin and cytochrome *b*<sub>5</sub>: a nuclear magnetic resonance study of a highly dynamic protein complex. *Biochemistry* 41:11721–11730
- Worrall JAR, Reinle W, Bernhardt R, Ubbink M (2003) Transient protein interactions studied by NMR spectroscopy: the case of cytochrome *c* and adrenodoxin. *Biochemistry* 42:7068–7076
- Xue YF, Ökvist M, Hansson Ö, Young S (1998) Crystal structure of spinach plastocyanin at 1.7 Å resolution. *Protein Sci* 7:2099–2105

# Chapter 31

## Cytochrome $c_6$ of Cyanobacteria and Algae: From the Structure to the Interaction

Irene Díaz-Moreno\*, Antonio Díaz-Quintana,  
and Miguel A. De la Rosa

*Instituto de Bioquímica Vegetal y Fotosíntesis, Centro de  
Investigaciones Científicas Isla de la Cartuja, Universidad de  
Sevilla-CSIC, Sevilla, Spain*

Summary.....	657
I. Introduction.....	658
II. Cytochrome $c_6$ Structure and Properties.....	658
III. $Cc_6$ -Involving Photosynthetic Complexes.....	662
A. $Cc_6$ as the Electron Donor to PSI.....	662
B. $Cc_6$ as the Electron Acceptor from the $Cb_6f$ Complex.....	665
1. The Structure of Algal and Cyanobacterial $Cb_6f$ .....	665
2. Kinetics of Electron Transfer Between Cf and $Cc_6$ .....	665
3. Structural Model of the Cf and $Cc_6$ Complex.....	665
IV. $Cc_6$ -Involving Respiratory Complexes.....	667
A. The Structure of Cyanobacterial CcO.....	668
B. Kinetics of Electron Transfer Between $Cc_6$ and CcO.....	668
C. Structural Model of the $Cc_6$ and CcO Complex.....	669
V. Conclusions and Perspectives.....	671
Acknowledgements.....	671
References.....	671

### Summary

Cytochrome  $c_6$  is a small, globular and soluble heme protein—found in algae and cyanobacteria, but not in higher plants—that usually serves as a redox carrier between the cytochrome  $b_6f$  complex and photosystem I in the photosynthetic electron transport chain. In cyanobacteria, in particular, it can also donate electrons to cytochrome  $c$  oxidase and can thus serve as a switch between photosynthesis and respiration as these two processes share the same cellular location.

Cytochrome  $c_6$  can be replaced by the blue copper protein plastocyanin in many cyanobacteria and eukaryotic algae, which are all able to synthesize one or the other protein depending on the relative availability of iron and copper. Such a metabolic versatility lets these organisms rapidly adapt to environmental changes. Although the three-dimensional structures of cytochrome  $c_6$  and plastocyanin are evolutionary unrelated, their similar physicochemical properties and surface features make them easily exchangeable within each organism. Plants,

---

\*Author for correspondence, e-mail: [idiuzmoreno@us.es](mailto:idiuzmoreno@us.es)

however, only synthesize plastocyanin but not cytochrome  $c_6$  as the increase in atmospheric molecular oxygen throughout the Earth's life made copper more readily available than iron.

This chapter also focuses on cytochrome  $c_6$  and its physiological transient interactions with photosynthetic or respiratory membrane-complexes, namely cytochrome  $b_6f$ , photosystem I and cytochrome  $c$  oxidase. In all three cases, an optimal coupling between redox centers within the adducts is essential for electron transfer although the interactions of cytochrome  $c_6$  with its partners must be weak enough to guarantee a rapid turnover. So rather than forming a well-defined system, the two partners adopt multiple conformations within encounter complexes that exchange among them with low activation barriers to eventually yield a final productive orientation. Accordingly, cyanobacterial and algal cytochrome  $c_6$ -involving dynamic ensembles result from a balance between hydrophobic contacts and electrostatic interactions, thus allowing cytochrome  $c_6$  to scan the surface of its partner.

## I. Introduction

In oxygenic photosynthesis, either cytochrome  $c_6$  ( $Cc_6$ ) or plastocyanin (Pc) carries out the electron transport from the cytochrome  $b_6f$  complex ( $Cb_6f$ ) to photosystem I (PSI). The structures of these two small metalloproteins are unrelated, but the analogies between their surface properties make them exchangeable in organisms that are able to synthesize both. Indeed, the two proteins show similar dissociation constants towards their physiological partners (De la Rosa et al. 2002, 2011; Díaz et al. 1994a; Díaz-Quintana et al. 2003, 2008).

A few years ago, we proposed that  $Cc_6$  is the most ancient of the two soluble carriers. The reducing nature of the primitive Earth's atmosphere favored the availability of iron rather than copper (De la Rosa et al. 2002, 2011). This context eventually reversed as the concentration of molecular oxygen heightened due to photosynthetic activity, and Pc started to replace  $Cc_6$ . In soils, copper was not a limiting element

for plants and Pc became a constitutively synthesized protein. Many cyanobacteria and eukaryotic algae still maintain their ability to adapt to changing aqueous environments by synthesizing either of the two metalloproteins. Recently,  $Cc_6$ -like proteins have been reported, and they are described in the final chapters in this book.

In this chapter, we summarize the major features that enable  $Cc_6$  as a functional and efficient electron carrier in algae and cyanobacteria. In addition, we sum up our current knowledge on the interactions of  $Cc_6$  with its physiological partners.

## II. Cytochrome $c_6$ Structure and Properties

$Cc_6$  is a typical type-I  $c$ -cytochrome (Moore and Pettigrew 1990) with a folding different from other cyanobacterial cytochromes (Navarro et al. 1995; Frazao et al. 2001).  $Cc_6$  shows a characteristic globular fold comprising four  $\alpha$ -helical regions separated by loops with different sequence lengths. The first of these regions is split into two helices (Ia and Ib) because of covalent binding to heme. Figure 31.1a shows an overlay of the structures of  $Cc_6$  from several cyanobacteria and algae. Figure 31.1b shows a ribbon diagram of  $Cc_6$  from *Monoraphidium braunii* (pdb 1ctj; Frazao et al. 1995) colored according to residue conservation. A structure-based sequence

---

*Abbreviations:*  $Cb_6f$  – Cytochrome  $b_6f$ ;  $Cc$  – Cytochrome  $c$ ;  $Cc_6$  – Cytochrome  $c_6$ ;  $CcO$  – Cytochrome  $c$  oxidase;  $Cf$  – Cytochrome  $f$ ; NDH – NADPH Dehydrogenase; NMR – Nuclear magnetic resonance; Pc – Plastocyanin; PQ – Plastoquinone; PRE – Paramagnetic relaxation enhancement; PSI – Photosystem I; PSII – Photosystem II; SDH – Succinate Dehydrogenase; TROSY – Transverse relaxation-optimized spectroscopy

alignment is shown in Fig. 31.1c. Most of the identities between  $Cc_6$  sequences in the UNIREF database (Suzek et al. 2007) fall in the range between 0.2 and 0.8 per amino acid residue. Besides those involved in binding the heme cofactor covalently, the most conserved residues (>85 % of sequences) are the hydrophobic ones that surround the heme group or help helices pack. In particular, three conserved aromatic amino acids form a core that stabilizes the interaction between helices Ia and IV. These residues are a Phe at helix I, a Tyr from helix IV and a Trp at the C-terminus. At the protein surface, only the patch surrounding the heme-lodging cleft is highly conserved. Notably, a Lys is the only invariable charged residue in the alignments. This residue makes a salt bridge with the solvent accessible carboxyl of propionate 6 and is located in the  $\Omega$  loop joining helices III and IV.

In all  $Cc_6$  species, helix IV packs with helices Ia and III, whereas helices Ib and 2 do not interact with another regular structure. The analysis of the 12 aligned structures in Fig. 31.1c indicates that helices III and IV pack according to the canonical side chain “ridges and grooves” model (Chotia et al. 1985). The average angles between these two elements are  $52.4 \pm 1.1^\circ$ , and the distance between their main axes is  $8.4 \pm 0.1 \text{ \AA}$ . Helix IV also packs with helix Ia but, in this case, they are almost perpendicular. Average angle and distance between the main axes of these two elements are  $82.5 \pm 1.4^\circ$  and  $7.3 \pm 0.3 \text{ \AA}$ , respectively. These values correspond to an “extended” or non-canonical “ridges and grooves” packing model, which is made possible by the presence of an invariable Gly residue in helix Ia that faces another low-volume residue in helix IV. This slot-to-slot helix packing is conserved in all of the  $Cc$  family. In the PDB structures of  $Cc_6$  from green algae, the nearby residue in helix IV is either Ala or Gly, while the cyanobacterial, brown, and red algal structures show either Asn or Asp instead. A still larger variability is found among the sequences deposited at UNIREF: In addition to the residues above, Glu, Gln, Ser and Thr are also found. No-

tably, when the residue at that position is Asp, it makes a salt bridge with a positively charged residue in helix Ia. The D70R mutation in  $Cc_6$  from *Nostoc* destabilizes the protein as it turns the salt bridge into a repulsive interaction (Lange et al. 2003). The Hammond behavior (Matouschek and Fersht 1993) associated with this mutant indicates that it needs to set more native interactions to arrange the two helices properly along the folding pathway.

The heme cofactor is located in a cleft of the protein. The peptide binds the cofactor by two thioether bridges involving the two Cys residues from a CXXCH motif. This motif is conserved in all type-I  $c$ -cytochromes. The proximity of the two Cys strains the macrocycle, bringing on a major  $B_{1u}$ -symmetry distortion of the equatorial plane to yield a ruffled structure (García-Heredia et al. 2011). The geometry of the iron first coordination sphere fits a distorted octahedron. Nitrogen atoms from the tetrapyrrole are the equatorial ligands while the imidazole  $N\epsilon 2$  nitrogen from the CXXCH motif and a thioether sulfur (S8) from a conserved Met act as axial ligands. The last residue is located in the conserved  $\Omega$  loop joining helical regions III and IV. An octahedral distortion comes from the distance between S8 and Fe ( $2.15 \pm 0.003 \text{ \AA}$ ), which is slightly longer than those between the nitrogen atoms and the metal (ranging from 1.96 to 2.00  $\text{ \AA}$ ) (Díaz-Moreno et al. 2006a).

Physical-chemical properties affecting the functionality of the protein depend on the amino acid composition, the tertiary structure of the protein and the nature of the cofactor. The  $pK_a$  value for the alkaline transition is 9.3 (Dikiy et al. 2002), identical to that of mitochondrial  $Cc$  (García-Heredia et al. 2010), which can be drastically modified upon nitration (Díaz-Moreno et al. 2011; García-Heredia et al. 2012; Ly et al. 2012).

As  $Cc_6$  is a photosynthetic electron carrier, its surface and redox properties are of major importance to assure efficient binding to physiological partners and electron transfer between cofactors, respectively. The redox potential of  $Cc_6$  is ca. 330 mV at pH 7.



It is similar to that of Pc, the alternative soluble electron carrier. In part, this value is determined by the His-Met axial coordination. As expected, replacement of the thioether ligand by a more basic group, such as imidazole or thiolate, drops the midpoint potential drastically. The observed values for M58H and M58C  $Cc_6$  mutants are  $-140$  and  $-235$  mV, respectively (Kranich et al. 2009; Díaz-Moreno et al. 2014). Still, the value for wild-type  $Cc_6$  differs from those reported for other  $c$ -type cytochromes showing a His-Met axial coordination of the metal cofactor.

A more polar heme environment stabilizes the oxidized form, thereby lowering the redox potential of the protein. This depends on structural features such as solvent accessibility of the porphyrin ring or the polarity of side chains and hydrogen bonding close to the cofactor moiety (Dikiy et al. 2002). Notably, the heme moiety is mostly buried inside the protein: it only exposes methyl 3 and vinyl 4 residues at ring C, and the carboxyl group of propionate 6 at ring D. Further, no water molecule dwells near the porphyrin inside the protein. In its turn, side chain polarity modulates the midpoint potential depending on the neighboring region of the macrocycle. Thus, removing the internal aromatic ring from the  $\Omega$  loop, as in the F67A mutant by De la Cerda et al. (1999) decreases the redox potential by 37 mV. In addition, the conserved glutamine at helix III is responsible for the large differences in the redox potential between  $Cc_6$  and the cryptic cytochrome  $c_6$ -like homologues (Marcaida et al. 2006; Worrall et al. 2007) that show a hydrophobic residue in its place. The side chain amide of this Gln stacks on top of ring A of the heme.

It is worth mentioning that the NMR structures of the two redox forms of *Monoraphidium*  $Cc_6$  (PDB: 1ced, Banci et al. 1996; PDB: 1a2s, Banci et al. 1998) barely show differences in the backbone (RMSD 0.89 Å). Still, the two structures differ in the orientation of several side chains. These belong to His30 and Gln53, along with several hydrophobic residues located near the porphyrin ring. In fact, the Gln53 side chain is the one lying on top of the heme ring A. However, X-ray Diffraction (XRD) structures of the two forms of  $Cc_6$  from *Scenedesmus* (PDB: 1c6o, 1c6r; Schnackenberg et al. 1999) show no change as regards the side chains in these structures. Indeed, the RMSD for all the heavy atoms is 0.8 Å and that of the backbone is 0.39 Å.

Surface properties are essential for the functionality of  $Cc_6$ . The surface is mostly hydrophilic, showing a small hydrophobic patch near the heme cleft (Fig. 31.2). As its analog Pc, the heme protein displays an asymmetric charge distribution leading to a well-defined dipole moment (Frazao et al. 1995). This is common to all the  $Cc_6$  family, though its magnitude changes from one organism to another as does the isoelectric point. The torque induced by the opposite electrostatic interactions with the surface of the physiological partners may be responsible for the dynamics of the encounter complex. Indeed NMR data shows that even when the complex is highly dynamic,  $Cc_6$  always shows the rim of the heme cleft to the surface of its partner (Díaz-Moreno et al. 2005a, b, 2014).

---

←

Fig. 31.1. (continued) (Landau et al. 2005) on the full UNIREF dataset. The orientation is similar to that of the left image in panel (a). Conserved residues are in blue, variable in red, and those not evaluable in green. The side chains of the most conserved residues are represented by cyan sticks. (c) Sequence alignment based on the above structural overlay. Consensus sequence is colored in blue for fully conserved residues, cyan for partially conserved residues and black for those showing variability. Individual sequences are colored according to their hydrophobicity index (Kyte and Doolittle 1982). Residues in bold are in close vicinity to the heme porphyrin (Graphics created with UCSF Chimera (Pettersen et al. 2004)).

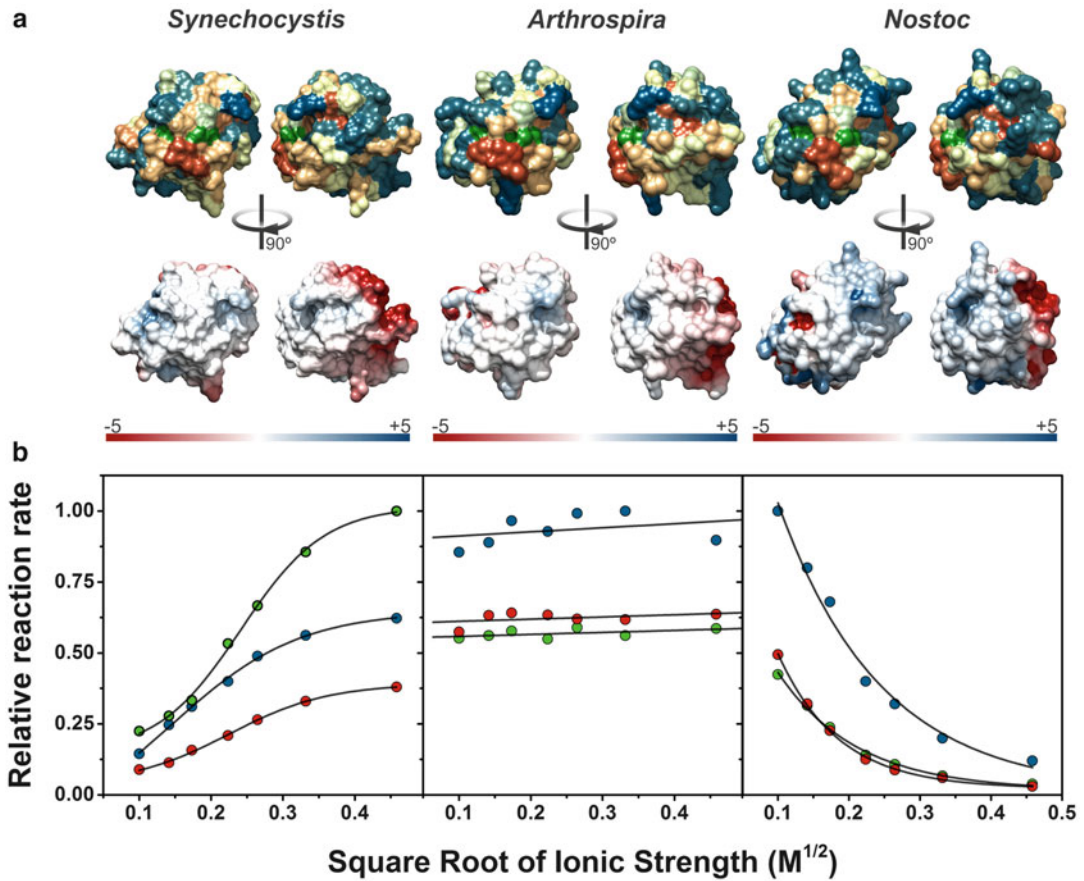


Fig. 31.2. Surface properties and functionality of  $Cc_6$ . (a) Surface solvation properties and electrostatic potential maps of  $Cc_6$  from *Synechocystis* sp. PCC 6803, *Arthrospira maxima* CS-328 and *Nostoc* sp. PCC 7119. The top row shows hydrophathy maps according to their Kyte and Doolittle (1982) score. Hydrophobic residues are shown in brown, hydrophilic are blue and the heme group is green. Below the hydrophathy profiles, the surface electrostatic potential maps are shown with similar orientations. The scales are in  $k_B T/e$  units. Computations were performed with DelPhi (Nicholls and Honig 1991) at 150 mM ionic strength. (b) Ionic strength dependencies of the electron transfer rates from the three cytochromes to PSI from *Synechocystis* (green circles), *Arthrospira* (red circles) and *Nostoc* (blue circles), as reported by Hervás et al. (2005).

### III. $Cc_6$ -Involving Photosynthetic Complexes

The electron transfer from the  $Cb_6f$  complex to PSI is carried out by Pc and  $Cc_6$  (Díaz et al. 1994b; Díaz-Quintana et al. 2003). Most cyanobacteria and green algae synthesize either Pc or  $Cc_6$  depending on the availability of copper and iron, their respective cofactor metals (De la Rosa et al. 2002; Durán et al. 2004). Higher plants only contain Pc, although a  $Cc_6$ -like protein has been identified in *Arabidopsis* (Gupta et al. 2002),

but it is unable to transfer electrons to PSI (Molina-Heredia et al. 2003).

#### A. $Cc_6$ as the Electron Donor to PSI

PSI is the electron acceptor for  $Cc_6$  (Hope 2000). Solar energy absorbed by PSI sparks the translocation of an electron from either  $Cc_6$  or Pc at the luminal face of the membrane to flavodoxin and ferredoxin at the stroma (Medina et al. 1992; Casaus et al. 2002). The membrane-embedded assembly comprises a heterodimeric core bearing the

intrinsic pigments and cofactors for excitation energy and electron transfer. A peripheral antenna system provides additional pigments for effective light-harvesting. The X-ray coordinates of PSI from cyanobacteria (PDB code: 1jb0; Jordan et al. 2001; PDB code: 4kt0; Mazor et al. 2013) and plants (PDB code: 3lw5; Amunts et al. 2010) are available. The structural features of PSI have been described by Nelson and Mazor in another chapter in this volume.

An indentation of the luminal surface of the PsaA-PsaB heterodimer provides the binding site for Pc and  $Cc_6$ . It is located around the pseudo- $C_2$  axis of the reaction center, close to the P700 cofactor. There, two solvent-exposed helices form a hydrophobic patch to interact with the electron donors. Each one contains a highly-conserved Trp residue, essential for the binding and the subsequent electron transfer process (Sun et al. 1999; Sommer et al. 2004). Two acidic residues in these helices seem to destabilize the complex in algae, to warrant an efficient turnover of Pc (Kuhlgert et al. 2012). In addition, the cyanobacterial and eukaryotic complexes differ in the donor binding site. Compared to the prokaryotic N-terminal domain of PsaF, the eukaryotic domain has an 18-residue insertion. This spans the first helical region of the subunit and provides four additional Lys residues to the donor binding site. In eukaryotes, this basic patch of PsaF and the acidic regions of the soluble carriers undergo long-range electrostatic attractions. This favors the subsequent hydrophobic interaction with the reaction center core. However, the N-terminus of the luminal domain of the prokaryotic PsaF subunit lies more distant from the  $C_2$  axis. These changes account for the different abilities of the distinct PsaF subunits to bind the donor. Indeed, inserting a Lys-rich helix into *Synechococcus elongatus* PsaF makes the cyanobacterial PSI behave as the plant complex when reacting with algal Pc.

The mechanism for the electron transfer from  $Cc_6$  to PSI has been widely analyzed using fast-kinetics approaches. Light oxidizes the special chlorophyll pair P700 in

PSI to trigger charge separation within the reaction complex. Then, the electron transfer reaction from any donor to the oxidized P700<sup>+</sup> species is recorded by UV-Visible spectroscopy (Díaz-Quintana et al. 2003). The changes in the redox state of the P700 cofactor are measurable at either 698 nm (Hiyama and Ke 1972) or 820 nm (Mathis and Sétif 1981). Pulsed laser devices provide a fast excitation of the pigment, keeping the monitor dead times to within the sub-microsecond time scale.

Early kinetic analyses of P700 reduction used Pc as the electron donor. Notably, collision-limited models mismatched the reaction mechanism. Indeed, the reaction showed a two-exponential trace with half-times of 12 and 160  $\mu$ s (Bottin and Mathis 1985). The fast and slow phases fitted to first-order and second-order reactions, respectively. Hence, the initial phase was attributed to direct electron transfer in a preformed Pc/PSI complex and the second one to a binding-limited, two-step reaction model reported by Tollin et al. (1986). The first analyses using  $Cc_6$  (Hervás et al. 1992, 1994; Medina et al. 1993) displayed a similar behavior.

Further insight into the reaction with proteins from different sources demonstrated the variability of its performance under different conditions. To integrate this information, we first proposed a single three-step kinetic model that accounted for three observable kinetic behaviors (Hervás et al. 1995). Thus, the properties of the reaction partners and the experimental conditions determine the limiting step in each case.

The initial, second-order binding step limits the rate of the slow exponential decay at low protein concentrations. Viscosity affects the kinetics of this phase. According to the observed *in vitro* ionic strength profiles of kinetic rates, this event is influenced by long-range electrostatics. In some cyanobacteria such as *Synechocystis* sp. PCC 6803, this is the limiting step (Hervás et al. 1994, 1995, 1996). This is due to the subsequent phenomena lasting much less than the lifetime of the complex.



The encounter complex is highly dynamic, and suffers conformational re-arrangements that determine the probability for the intramolecular electron transfer. This heterogeneity of the encounter is responsible for the biphasic ionic strength dependencies of kinetic data (Watkins et al. 1994). In fact, the PSI reduction rate in eukaryotic organisms shows a bell-shaped ionic strength profile (Hervás et al. 1995). The drift across the encounter conformation landscape affects the relative amplitudes of the distinct exponential phases within the reaction trace. This step may limit the rate of the slow phase at saturating donor concentrations. In most green algae and plants, a rearrangement step is needed to fit all the kinetic data (Hervás et al. 1995; Sigfridsson et al. 1995). However, in other cases as in the green alga *Monoraphidium*, this event cannot be easily discriminated (Hervás et al. 1995), and the data are fit by the classical two-step mechanism (Yoneda and Holwerda 1978; Tollin et al. 1986).

Finally, donor dissociation is another important event in the reaction, but little is known about the dissociation of  $Cc_6$  from PSI. Still, double-flash excitation experiments and site-directed mutagenesis have shown that oxidized Pc dissociation may limit the donor turnover demanded in photosynthesis (Drepper et al. 1996; Kuhlert et al. 2012). An efficient turnover demands differences in the affinity of the partner towards the two redox forms of  $Cc_6$ . This may be due to some structural change in the partners during the reaction, or just to a change in electrostatics. Dissociation may be favored by the charge transfer during the reaction, as it affects the electrostatic interactions between the two partners. The donor gains a positive charge upon the electron transfer, and we may speculate that the two conserved acidic residues of helices at the binding site of PSI cause mismatching in the complex once P700 has been reduced.

The above schema helps to understand the reaction kinetics under different conditions. For instance, the effects of electrostatics on a reaction can be inferred from its ionic

strength profiles. Usually, depending on the organism,  $Cc_6$  holds either attractive or repulsive long-range electrostatic interactions with its partners under *in vitro* conditions (Fig. 31.2b). Sometimes, as in *Arthrospira*,  $Cc_6$  reduces PSI in an ionic strength independent way (Hervás et al. 2005; Fig. 31.2b). Moreover, the sign of the interaction and the reaction mechanism in cyanobacteria rely on the surface properties of  $Cc_6$  and they are independent of those of PSI (Hervás et al. 2005; Fig. 31.2b).

Thus, changes in the ionic strength or pH may decrease the encounter affinity while easing the re-arrangement (Hervás et al. 1998; Molina-Heredia et al. 1998, 1999). A single mutation may affect one or more events along the reaction pathway, thereby modifying the kinetic behavior (Molina-Heredia et al. 1999; Olesen et al. 1999). Notably, protein charge modifications showed that the collision-limited kinetics depend on the charge configuration of the protein (De la Cerda et al. 1999). The kinetics of  $Cc_6$  oxidation by PSI in *Synechocystis* correlate with the size of the positive region surrounding the heme cleft. Single mutations also serve to determine that a conserved Arg residue (Arg67) plays an essential role in the binding event (De la Cerda et al. 1999; Molina-Heredia et al. 1999) and that this feature is common to Pc (Molina-Heredia et al. 2001).

As opposed to the interaction between  $Cf$  and  $Cc_6$  (see below), little is known about the conformation of the electron-transfer complex between  $Cc_6$  and PSI. To the best of our knowledge, co-crystallization trials have failed, and the complex is too large to be characterized by NMR. Still, Transverse Relaxation-Optimized Spectroscopy (TROSY) NMR has provided a clue that  $Cc_6$  interacts with PSI using the same surface patch as with  $Cf$  (Díaz-Moreno et al. 2005b). Notably, most of the NMR signals from  $^{15}\text{N}$ -labeled  $Cc_6$  from cyanobacteria are still monitored in the presence of an excess of PSI trimers. This clearly indicates that the complex is highly dynamic. All the  $Cc_6$  signals should broaden

beyond the detection limits if the binding to PSI is tight, given the long diffusional correlation time of the reaction center. In addition, X-ray absorption spectroscopy (XAS) experiments have shown that binding to PSI induces subtle changes in the heme iron. Indeed, the absorption edge of  $\text{Fe}^{2+}$   $Cc_6$  shifts slightly towards lower energies (Díaz-Moreno et al. 2006a).

### B. $Cc_6$ as the Electron Acceptor from the $Cb_6f$ Complex

#### 1. The Structure of Algal and Cyanobacterial $Cb_6f$

The hetero-oligomeric  $Cb_6f$  complex contains eight tightly-bound polypeptide subunits that couple the electron transfer to proton translocation, generating the proton electrochemical potential gradient necessary for ATP synthesis. The three-dimensional crystal structure has been determined for the  $Cb_6f$  complex from the green alga *Chlamydomonas reinhardtii* (Stroebel et al. 2003), and the cyanobacteria *Mastigocladus laminosus* (Kurusu et al. 2003) and *Nostoc* sp. PCC 7120 (Baniulis et al. 2009). On the one hand, the first two  $Cb_6f$  crystallographic structures are essentially identical despite the great evolutionary distance between the prokaryote (*Mastigocladus*) and the eukaryotic organelle (*Chlamydomonas*). Both structures reveal the presence of a chlorophyll molecule and a  $\beta$ -carotene in unusual surroundings, whose functions are still unclear. On the other hand, the main difference between the cyanobacterial  $Cb_6f$  crystallographic structures is the acetylation of the *Nostoc* Rieske Fe-S protein at the N terminus, a post-translational modification uncommon in cyanobacterial membranes and electron transfer proteins (Baniulis et al. 2009).

Cytochrome *f* (*Cf*) is a subunit of the  $Cb_6f$  complex, anchored to the thylakoid membrane by a C-terminal transmembrane helix leaving a 28-kDa soluble portion exposed to the lumen with a clear two-domain structure. The large domain harbors the heme, and the

small domain possesses a patch of charged residues. *Cf* is considered an unusual *c*-type cytochrome because of its  $\beta$ -sheet structure, elongated form and particular, heme axial coordination with the amino group of the N-terminus residue, Tyr1 (Martínez et al. 1994; Stroebel et al. 2003; Kurisu et al. 2003; Díaz-Moreno et al. 2006b; Baniulis et al. 2009).

#### 2. Kinetics of Electron Transfer Between *Cf* and $Cc_6$

Fast-kinetics studies combined with Brownian dynamics using a *Chlamydomonas* Zn- $Cc_6$  derivative and *Cf* have been reported (Grove and Kostic 2003; Grove et al. 2012), concluding that the hydrophobic forces are crucial not only for protein docking but also for reactivity. The association of both redox metalloproteins is only weakly enhanced by electrostatic interactions. The kinetic rate constants are invariant with ionic strength over a wide range.

Such studies reveal that both cytochromes associate in broad, dynamic ensembles of configurations whose exchange is possible because they are close in energy. As the ensemble is driven by non-directional hydrophobic interactions that allow easy rearrangement, the oxidoreduction mechanism between *Cf* and  $Cc_6$  can be true, coupled, gated, or a combination of the three. In the first case, the electron transfer is the limiting step. In the gated mechanism, rearrangement is the reaction bottleneck. Finally, in the coupled electron transfer, rearrangement is thermodynamically unfavorable, but faster than the electron transfer event (Grove et al. 2012).

#### 3. Structural Model of the *Cf* and $Cc_6$ Complex

NMR-based structural approaches using heme proteins from several cyanobacterial sources unveil differences in the specificity, not only for *Cf*-Pc complexes (Díaz-Moreno et al. 2005c, d), but also for the *Cf*- $Cc_6$  complexes. The acidic  $Cc_6$  from *Synechococcus elongatus* forms a non-

specific and highly dynamic adduct with *Phormidium Cf*, which has a negative net charge (Crowley et al. 2002). On the contrary, the interaction site of the basic  $Cc_6$  from *Nostoc sp.* PCC 7119 when binding to *Cf* from *Phormidium* or *Nostoc sp.*, which is also negatively charged, consists of a predominantly hydrophobic patch surrounding the heme (Crowley et al. 2002; Díaz-Moreno et al. 2005a), as previously described in the reactive *Nostoc Cc<sub>6</sub>*-PSI complex (Díaz-Moreno et al. 2005b). The presence of positive residues near the heme cleft of *Nostoc Cc<sub>6</sub>* also favors the attractive electrostatic interactions with either *Phormidium Cf* or *Nostoc Cf*.

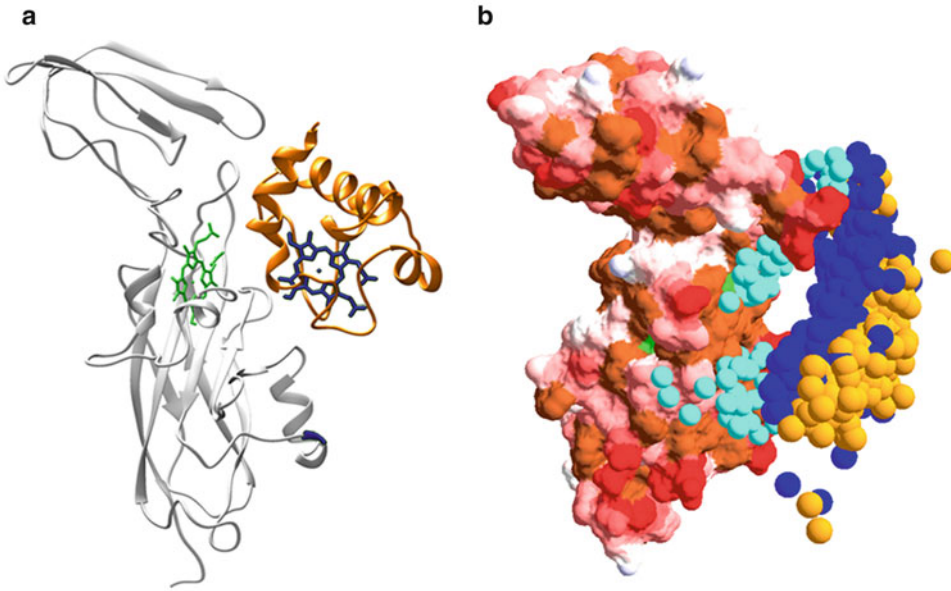
The binding constant of the physiological  $Cc_6$ -*Cf* interaction from *Nostoc* is identical to that of the  $Cc_6$ -*Cf* cross-complex, suggesting that *Nostoc Cc<sub>6</sub>* binds to *Nostoc* and *Phormidium Cf* in a similar way. However, significant differences are found between the homologous (*Nostoc Cc<sub>6</sub>* and *Nostoc Cf*) and the heterologous (*Nostoc Cc<sub>6</sub>* and *Phormidium Cf*) complexes. For instance, Arg64 of  $Cc_6$ , whose functional and structural relevance has been emphasized with PSI, its other redox partner (Molina-Heredia et al. 2001; Díaz-Moreno et al. 2005b), shows chemical-shift perturbations within the native complex but not within the non-physiological one.

The NMR-restraint docking simulations of *Nostoc Cc<sub>6</sub>*-containing adducts are similar (Crowley et al. 2002; Díaz-Moreno et al. 2005a) and resemble the models of the  $Cf$ - $Cc_6$  complex from the green alga *Chlamydomonas* (Gross and Pearson 2003) and of the cross-complex between turnip *Cf* and *Monoraphidium Cc<sub>6</sub>* (1jx8 PDB code). In all these complexes,  $Cc_6$  interacts with charged amino acids at the small domain of *Cf* (Fig. 31.3a). A positively charged ridge of positive charges on the small domain of *Cf* interacts with a cluster of negative charges on  $Cc_6$  in green algae while the opposite is true for cyanobacteria, despite the fact that the cyanobacterial  $Cc_6$  does not possess such well-defined, complementary charged patches.

*In silico* data on the *Chlamydomonas Cc<sub>6</sub>*-*Cf* complex shows not only the relevance of hydrophobic and electrostatic interactions in bringing the two heme proteins sufficiently close as to allow efficient electron transfer (Gross and Pearson 2003; Haddadian and Gross 2005) but also the key role of the *Cf* small domain in guiding  $Cc_6$  to dock with *Cf*, which suggests that  $Cc_6$  explores different positions on *Cf* (Haddadian and Gross 2006).

This finding, along with the kinetic study demonstrating that multiple conformations of  $Cc_6$  contribute to electron transfer within the  $Cf$ - $Cc_6$  complex (Grove et al. 2012), is in agreement with recent paramagnetic relaxation enhancement (PRE) NMR data (Díaz-Moreno et al. 2014), which are not compatible with a well-defined *Nostoc Cf*- $Cc_6$  complex (Díaz-Moreno et al. 2005a). In fact, the interaction can be described as a highly dynamic ensemble comprising multiple orientations without any one orientation being predominant (Fig. 31.3b). Then, after an electrostatic pre-orientation to bring both cytochromes closer, an ensemble of orientations are formed with extensive hydrophobic contacts between the heme groups, which must be sufficiently close to allow rapid electron transfer. The importance of hydrophobic contacts in the interactions of  $Cc_6$  with photosynthetic *Cf* (Crowley et al. 2002; Díaz-Moreno et al. 2005a; Grove et al. 2012) and PSI (Molina-Heredia et al. 1999, 2001; Díaz-Moreno et al. 2005b), as well as with its respiratory partners (Hart et al. 2008), have been corroborated using NMR, kinetic measurements and docking calculations.

An efficient electron transfer within the  $Cf$ - $Cc_6$  ensemble is as important as a high off-rate to avoid reduction of the electron flow rate. To make the turnover high enough,  $Cc_6$  binds to *Cf* with relatively low affinity and with no dominant stereospecific orientation; multiple contacts make the encounter complex avoid dissociation before electron transfer takes place. Then, an ensemble of conformations, governed by a gradual increase and decrease of the hydrophobic interactions between both cytochromes during association and dissociation, ensures a low

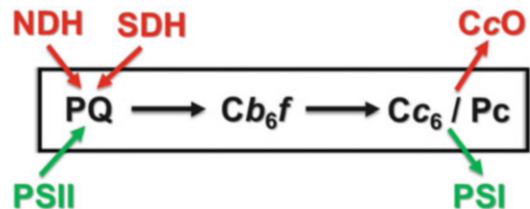


*Fig. 31.3.* Structural models of the complex between  $C_f$  and  $Cc_6$ . **(a)** The well-defined  $C_f$ - $Cc_6$  structure as calculated by NMR-restraint docking.  $C_f$  and  $Cc_6$  are represented by *light grey* and *orange ribbons*, respectively. Heme groups are shown as *green sticks* for  $C_f$  and *blue sticks* for  $Cc_6$ . **(b)** The ensemble of  $Cc_6$  around  $C_f$  as determined by PRE NMR restraints.  $C_f$  is shown in surface representation according to its electrostatic potential. Negative potential is displayed in *red*. Non-polar and Tyr residues are shown in *brown* and the heme, in *green*. The cyan spheres indicate the positions of the spin label oxygen atoms in the ensemble structures. The *yellow-orange* and *blue spheres* represent the centers-of-mass and iron atoms of  $Cc_6$  in the ensemble, respectively. Images have been adapted from Díaz-Moreno et al. 2005a (panel a) and Díaz-Moreno et al. 2014 (panel b) (Figure was created with Chimera software (Pettersen et al. 2004)).

transition state barrier that accelerates the disruption of the  $C_f$ - $Cc_6$  complex (Díaz-Moreno et al. 2014).

#### IV. $Cc_6$ -Involving Respiratory Complexes

In cyanobacteria, oxygenic photosynthesis and aerobic respiration occur within a single prokaryotic cell. The cyanobacterial thylakoid membrane contains not only photosynthetic but also respiratory electron transport complexes forming transport chains that intersect with each other and share the plastoquinone pool, the  $Cb_6f$  complex and the soluble electron carriers Pc and  $Cc_6$  (Fig. 31.4). It has been firmly established that  $Cc_6$  or Pc, at the thylakoid lumen, are able to reduce both PSI and Cytochrome  $c$  Oxidase ( $CcO$ ). However, the



*Fig. 31.4.* Schematic representation of the intersecting photosynthetic and respiratory electron reactions in thylakoid membranes of cyanobacteria. Electron transfer complexes specifically involved in photosynthesis are Photosystem II (PSII) and PSI, which are shown in *green*, whereas those specific for respiratory electron flow include NADPH DeHydrogenase (NDH), Succinate DeHydrogenase (SDH) and  $CcO$ , which are represented in *red*. Plastoquinone (PQ),  $Cb_6f$ , Pc and  $Cc_6$  are shared by both metabolic pathways. The *arrows* represent electron transfer reactions.

nature of the periplasmic carrier transferring electrons to  $CcO$  at the plasma membrane, which separates the cytosol from the

periplasm and contains only respiratory components, is still under discussion. So far, only  $Cc_6$  has been identified at the periplasmic space of cyanobacteria (Obinger et al. 1990).

#### A. The Structure of Cyanobacterial CcO

No structural information is yet available for any cyanobacterial CcO complexes, but they can be modeled by using the high-resolution structures of the PDB as templates. Such three-dimensional structures are from *Paracoccus denitrificans* (Koepke et al. 2009; Harrenga and Michel 1999; Ostermeier et al. 1997), *Rhodobacter sphaeroides* (Svensson-Ek et al. 2002; Qin et al. 2006, 2009), *Rhodothermus marinus* (Srinivasan et al. 2005), *Thermus thermophilus* (Williams et al. 1999; Soulimane et al. 2000; Liu et al. 2009; Lyons et al. 2012; Tiefenbrunn et al. 2011; Luna et al. 2012) and *Bos taurus* (Tsukihara et al. 1996, 2003; Yoshikawa et al. 1998; Muramoto et al. 2007; Suga et al. 2011).

Cyanobacterial CcO belongs to the superfamily of heme-copper oxidases and transfers electrons from  $Cc_6$  to oxygen. CcO is usually an  $aa_3$ -type protein complex, whereas those described for *T. thermophilus* are  $aa_3$ - or  $ba_3$ -type. It is composed of three core subunits (Fig. 31.5). Subunit I (also called CtaD) ligates heme *a* and the binuclear center formed by heme  $a_3$  and  $Cu_B$ . Subunit II (CtaC) ligates the  $Cu_A$  center. Subunit III (CtaE) does not ligate any redox centers, but could play a role in complex stability and assembly.

The assembly of the  $Cu_A$  cofactor in the CtaC of eukaryotic CcO is performed by Sco proteins, which work as copper transporters (Herrmann and Funes 2005; Cobine et al. 2006; Banci et al. 2011). The Sco proteins are also found in prokaryotic organisms where their function goes beyond the assembly of the  $Cu_A$  center. Sequenced prokaryotic genomes reveal that ca. 12 % of them code for Sco proteins but not for  $Cu_A$ -containing proteins (Banci et al. 2007). It has been proposed that such Sco proteins in bacteria, namely *Neisseria gonorrhoeae* and

*Rhodobacter capsulatus*, protect periplasmic proteins from oxidative damage (Seib et al. 2003; Borsetti et al. 2005). Unlike eukaryotes and most bacteria, archaea and cyanobacteria do not contain either the Sco proteins or their metallochaperones, although the CcO complexes harbor  $Cu_A$  cofactors. Therefore, the mechanism by which the copper delivery to CtaC occurs in cyanobacteria, if one exists, is still unknown.

#### B. Kinetics of Electron Transfer Between $Cc_6$ and CcO

In the thylakoid lumen,  $Cc_6$  can deliver electrons to two distinct acceptors, namely PSI and CcO, with similar  $Cc_6$ -mediated reduction rates within the same organism. However, there are some discrepancies in the oxidation rate of  $Cc_6$  by CcO among different organisms. The  $Cc_6$ -CcO electron transfer kinetics in the cyanobacterium *Nostoc sp.* PCC 7119 (Navarro et al. 2005) is one order of magnitude higher than that reported for the interaction of *Paracoccus* bacterial cytochrome  $c_{552}$  with the extrinsic  $Cu_A$ -binding domain of the CcO subunit II (Lappalainen et al. 1993). The electron flow in the *Nostoc*  $Cc_6$ -CcO system is two to three orders of magnitude higher than that observed for the interaction of *Synechocystis sp.* PCC 6803  $Cc_6$  with the  $Cu_A$ -binding domain of the CcO subunit II (Paumann et al. 2004). Of particular interest is the fact that the electron transfer constant of the *Nostoc*  $Cc_6$ -CcO system resembles the constant recently estimated in human mitochondrial complexes between Cc and CcO (Rodríguez-Roldán et al. 2008).

The ionic strength dependence shown by the  $Cc_6$ -CcO system relates to the cyanobacterial organism. The oxidation of  $Cc_6$  by CcO in *Synechocystis* occurs without the formation of any electrostatically governed and kinetically detectable complex between these proteins (Paumann et al. 2004). On the contrary, the *Nostoc*  $Cc_6$ -CcO adduct is impaired by added salt, which reveals the existence of strong electrostatic attractive interactions, as previously reported for other respiratory Cc and CcO systems (Hazzard et al. 1991;

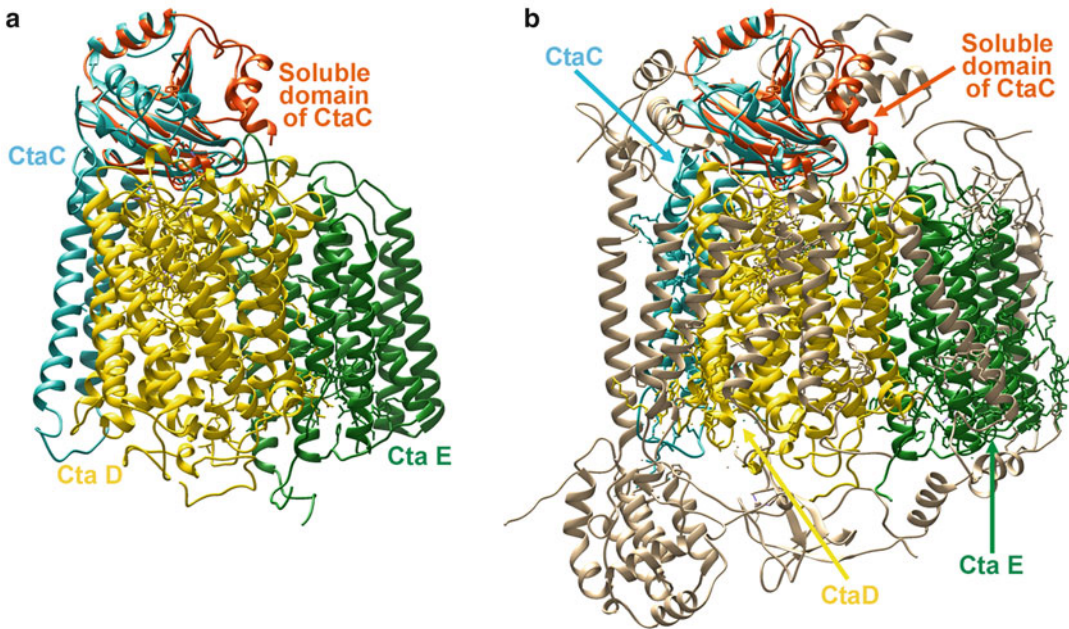


Fig. 31.5. Comparison between Bacterial and Eukaryotic CcO Structures. (a) *Rhodobacter sphaeroides* CcO (PDB: 1 m56; Svensson-Ek et al. 2002). (b) Bovine heart CcO in the fully reduced state (PDB: 2ejj; Muramoto et al. 2007). The CtaC subunit is colored in light blue, CtaD in yellow and CtaE in green. The remaining subunits, only present in eukaryotic CcO complexes, are shown in grey. The soluble domain of the CtaC subunit from *Phormidium laminosum*, in orange, has been aligned with respect to that from *Rhodobacter* and from *Bos taurus* in panels a and b, respectively (Figure was created with Chimera software (Pettersen et al. 2004)).

Lappalainen et al. 1993; Wang et al. 1999; Maneg et al. 2003, 2004; Navarro et al. 2005; Rodríguez-Roldán et al. 2008).

Such differences between *Nostoc* and *Synechocystis*  $Cc_6$ -CcO could be due to the use of the entire membrane-bound CcO complex in the case of *Nostoc*, yielding an affinity binding constant similar to that of the human mitochondrial Cc-CcO complex. However, these differences could be inherent to these cyanobacteria. Kinetic discrepancies are also observed in the interaction of  $Cc_6$  with PSI, with the *Nostoc* system exhibiting high electron transfer rates and strong ionic strength effects as compared with *Synechocystis* (Díaz-Quintana et al. 2003).

### C. Structural Model of the $Cc_6$ and CcO Complex

In cyanobacteria, there is only one docking simulation analysis of  $Cc_6$  and its physiological electron acceptor, the  $Cu_A$ -binding

domain of CcO subunit II, from *Phormidium laminosum* (Hart et al. 2008). The resulting models show seven different docking orientations, with the heme to copper distances being close enough to guarantee an efficient electron transfer. The lowest-energy docking solution is similar to that observed for the docking between Pc and CcO (Hart et al. 2008). Both complexes are mainly mediated by hydrophobic and non-ionic contacts, thus resembling the NMR restraint-based model proposed for the interaction between cytochrome  $c_{552}$  and the  $ba_3$ -type CcO subunit II from *Thermus thermophilus* (Muresanu et al. 2006). This is in agreement with previous studies on the photosynthetic electron transfer complexes formed by  $Cc_6$  or Pc with PSI in *Phormidium*, which are independent of ionic strength (Schlarb-Ridley et al. 2002a; Hervás et al. 2003). However, the available structural and functional data on the *Phormidium* Pc-Cf adduct shows an apparent contradiction on the role of elec-

trostatics in the interaction between the two metalloproteins. Whereas the ionic strength does not have any effect on the binding equilibrium according to NMR analysis (Crowley et al. 2001), the electron transfer between Pc and Cf is slightly affected by the addition of salt (Schlarb-Ridley et al. 2002b; Hart et al. 2003). Molecular Dynamics (MD) simulations harmonize such discrepancies showing changes in dynamics of Cf caused by repulsive electrostatic interactions with Pc. Unlike the complexes in *Phormidium* and *Thermus*, the complex between the soluble cytochrome *c*<sub>552</sub> domain and CcO from *Paracoccus denitrificans* (Flöck and Helms 2002), as well as the mitochondrial Cc-CcO complex (Roberts and Pique 1999) are exclusively driven by electrostatic steering.

A plausible explanation in *Phormidium* CcO is the lack of acidic residues close to the ligands of the copper center and to the electron accepting Tyr. These acidic residues should guide the proteins to the correct docking site via long-range electrostatic interactions in bacterial and mitochondrial CcO complexes but not in the cyanobacterial complexes. Therefore, the cyanobacterial

surface-exposed ligands of the copper center and the Tyr residue are on a relatively non-polar surface, leading to a docking mainly dominated by hydrophobic contacts (Hart et al. 2008).

The orientations of the mitochondrial Cc-CcO and bacterial cytochrome *c*<sub>552</sub>-CcO complexes are quite different with respect to the cyanobacterial Cc<sub>6</sub>-CcO complex (Fig. 31.6). In *Phormidium*, Cc<sub>6</sub> samples a region on the CcO subunit II surface that would be occupied by a loop surrounding the copper center in other organisms. This loop becomes more prominent in *Paracoccus* and mitochondria, shifting to Cc or to cytochrome *c*<sub>552</sub> towards a different spatial location to decrease the steric hindrance. Actually, the C-terminal  $\alpha$ -helix extension at the cyanobacterial CcO subunit II prevents the docking of Cc<sub>6</sub> in a similar relative position as Cc or cytochrome *c*<sub>552</sub>. The relative orientation of *c*<sub>552</sub> when interacting with CcO in *Thermus thermophilus* clashes with that of CcO in *Phormidium*, although the cytochromes are roughly located in the same space region but with different orientations (Fig. 31.6).

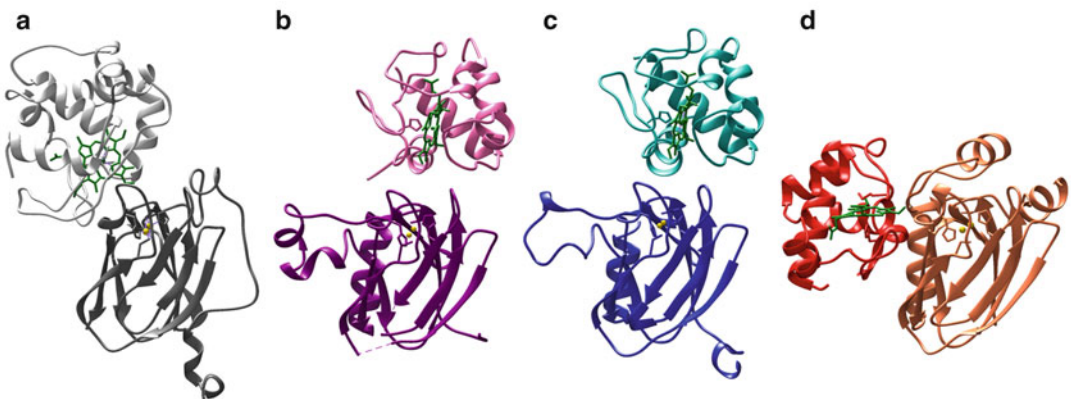


Fig. 31.6. The lowest energy docking solutions of CcO CtaC and *c*-type Cytochromes. (a) Cytochrome *c*<sub>552</sub> (light grey) and the soluble domain of *ba*<sub>3</sub>-type CcO subunit II (dark grey) from *Thermus thermophilus*. (b) The soluble cytochrome *c*<sub>552</sub> domain (pink) with the soluble domain of CcO subunit II (purple) from *Paracoccus denitrificans*. (c) Mitochondrial Cc (cyan) bound to the soluble domain of CcO subunit II (blue). (d) Cc<sub>6</sub> (red) and the soluble domain of *aa*<sub>3</sub>-type CcO subunit II (orange) from *Phormidium laminosum*. All the CcO soluble domains are equally oriented with respect to their copper centers. Heme groups are represented by green sticks, and copper centers by yellow spheres. Proteins are represented by ribbons (Figure was created with Chimera software (Pettersen et al. 2004)).

The finding of alternative conformations in *Phormidium*  $Cc_6$ -CcO docking calculations suggests that the proteins form an ensemble of interactions rather than a well-defined and fixed complex governed by multiple contacts, as previously reported for the mitochondrial  $Cc$ -CcO (Roberts and Pique 1999) and the cytochrome  $c_{552}$  domain with CcO from *Paracoccus denitrificans* (Flöck and Helms 2002). These electron transfer complexes require an optimal coupling between redox centers by weak and unstable associations to guarantee a rapid dissociation and an efficient turnover. As already described for other cyanobacterial photosynthetic  $Cc_6$ -involving interactions (see Sect. III), the ensemble of orientations between  $Cc_6$  and CcO in *Phormidium* might also be dominated by hydrophobic contacts, rather than by electrostatic interactions.

## V. Conclusions and Perspectives

Photosynthesis and respiration in cyanobacteria are two redox processes sharing the same cellular location and several redox components, but occurring at different time and under distinct conditions. Cyanobacteria require aerobic respiration for the generation of energy in darkness and under certain stress conditions, which impair photosynthesis. A concerted regulation of the whole electron transfer process is crucial, with  $Cc_6$  facilitating a rapid switching between photosynthesis and respiration.

To bring the redox centers within the  $Cf$ - $Cc_6$ ,  $Cc_6$ -CcO and  $Cc_6$ -PSI adducts sufficiently close is thus essential, but the formation of a well-defined complex is not required if multiple orientations exist in which electron transfer can occur. Such a specific complex is not desirable from the point of view of fast dissociation, because a well-defined state has a lower free energy than all similar states and thus a higher transition state energy to dissociate. Further discussion of  $Cf$  interactions with  $Cc_6$  or Pc and of cyanobacterial terminal oxidases may be found in subsequent chapters in this volume.

## Acknowledgements

We would like to thank all former and present members of the Biointeractomics group at the Institute for Plant Biochemistry and Photosynthesis (icCartuja, University of Seville—CSIC). We also thank to Prof. Helms, Prof. Roberts and Prof. Fernández-Recio for providing us the coordinates of *Paracoccus c<sub>552</sub>*-CcO,  $Cc$ -CcO and  $Cc_6$ -CcO complexes, respectively. Financial support was provided by the Spanish Ministry of Economy and Competitiveness for several years (Grant No. BFU2003-00458/BMC, BFU2006-01361/BMC, BFU2009-07190/BMC and BFU2012-31670/BMC), by Ramon Areces Foundation and by the Andalusian Government (Grant PAI, BIO198, P07-CVI-02896 and P11-CVI-7216).

## References

- Akazaki H, Kawai F, Chida H, Matsumoto Y, Hirayama M, Hoshikawa K, Unzai S, Hakamata W, Nishio T, Park SY, Oku T (2008) Cloning, expression and purification of cytochrome  $c(6)$  from the brown alga *Hizikia fusiformis* and complete X-ray diffraction analysis of the structure. *Acta Crystallogr Sect F Struct Biol Cryst Commun* 64:674–680
- Amunts A, Toporik H, Borovikova A, Nelson N (2010) Structure determination and improved model of plant photosystem I. *J Biol Chem* 285:3478–3486
- Banci L, Bertini B, Quacquareni G, Walter O, Díaz A, Hervás M, De la Rosa MA (1996) The solution structure of cytochrome  $c_6$  from the green alga *Monoraphidium braunii*. *J Biol Inorg Chem* 1:330–340
- Banci L, Bertini I, De la Rosa MA, Koulougliotis D, Navarro JA, Walter O (1998) The solution structure of oxidized cytochrome  $c_6$  from the green alga *Monoraphidium braunii*. *Biochemistry* 37:4831–4843
- Banci L, Bertini I, Cavallaro G, Rosato A (2007) The functions of Sco proteins from genome-based analysis. *J Proteome Res* 6:1568–1579
- Banci L, Bertini I, Cavallaro G, Ciafi-Baffoni S (2011) Seeking the determinants of the elusive functions of Sco proteins. *FEBS J* 278:2244–2262
- Baniulis D, Yamashita E, Whitelegge JP, Zatsman AI, Hendrich MP, Hasan SS, Ryan CM, Cramer WA



- (2009) Structure-function, stability, and chemical modification of the cyanobacterial cytochrome *b<sub>6</sub>f* complex from *Nostoc sp* PCC 7120. *J Biol Chem* 284:9861–9869
- Beissinger M, Sticht H, Sutter M, Ejchart A, Haehnel W, Rösch P (1998) Solution structure of cytochrome *c<sub>6</sub>* from the thermophilic cyanobacterium *Synechococcus elongatus*. *EMBO J* 17:27–36
- Bialek W, Krzywda S, Jaskolski M, Szczepaniak A (2009) Atomic-resolution structure of reduced cyanobacterial cytochrome *c<sub>6</sub>* with an unusual sequence insertion. *FEBS J* 276:4426–4436
- Borsetti F, Tremaroli V, Michelacci F, Borghese R, Winterstein C, Daldal F, Zannoni D (2005) Tellurite effects on *Rhodobacter capsulatus* cell viability and superoxide dismutase activity under oxidative stress conditions. *Res Microbiol* 156:807–813
- Bottin H, Mathis P (1985) Interaction of plastocyanin with the Photosystem I reaction center: a kinetic study by flash absorption spectroscopy. *Biochemistry* 24:6453–6460
- Casaus JL, Navarro JA, Hervás M, Lostao A, De la Rosa MA, Gómez-Moreno C, Sancho J, Medina M (2002) *Anabaena sp.* PCC 7119 flavodoxin as electron carrier from photosystem I to Ferredoxin-NADP(+) reductase - Role of Trp57 and Tyr94. *J Biol Chem* 277:22338–22344
- Chotia C, Levitt M, Robertson D (1985) Helix to helix packing in proteins. *J Mol Biol* 145:215–250
- Cobine PA, Pierrel F, Wing DR (2006) Copper trafficking to the mitochondrion and assembly of copper metalloenzymes. *Biochim Biophys Acta* 1763:759–772
- Crowley PB, Otting G, Schlarb-Ridley BG, Canters GW, Ubbink M (2001) Hydrophobic interactions in a cyanobacterial plastocyanin–cytochrome *f* complex. *J Am Chem Soc* 123:10444–10453
- Crowley PB, Díaz-Quintana A, Molina-Heredia FP, Nieto P, Sutter M, Haehnel W, De la Rosa MA, Ubbink M (2002) The interactions of cyanobacterial cytochrome *c<sub>6</sub>* and cytochrome *f*, characterized by NMR. *J Biol Chem* 277:48685–48689
- De la Cerda B, Díaz-Quintana A, Navarro JA, Hervás M, De la Rosa MA (1999) Site-directed mutagenesis of cytochrome *c<sub>6</sub>* from *Synechocystis sp.* PCC 6803. The heme-protein possesses a negatively charged area that may be isofunctional with the acidic patch of plastocyanin. *J Biol Chem* 274:13292–13297
- De la Rosa MA, Navarro JA, Díaz-Quintana A, De la Cerda B, Molina-Heredia FP, Balme A, Murdoch Pdel S, Díaz-Moreno I, Durán RV, Hervás M (2002) An evolutionary analysis of the reaction mechanisms of photosystem I reduction by cytochrome *c<sub>6</sub>* and plastocyanin. *Bioelectrochemistry* 55:41–45
- De la Rosa MA, Navarro JA, Hervás M (2011) The convergent evolution of cytochrome *c<sub>6</sub>* and plastocyanin has been driven by geochemical changes. In: Peschek GA, Obinger C, Renger G (eds) *Bioenergetic Processes of Cyanobacteria*. Springer, Dordrecht
- Díaz A, Navarro F, Hervás M, Navarro JA, Chávez S, Florencio FJ, De la Rosa MA (1994a) Cloning and correct expression in *Escherichia coli* of the *petJ* gene encoding cytochrome *c<sub>6</sub>* from *Synechocystis* 6803. *FEBS Lett* 347:173–177
- Díaz A, Hervás M, Navarro JA, De la Rosa MA, Tollin G (1994b) A thermodynamic study by laser-flash photolysis of plastocyanin and cytochrome *c<sub>6</sub>* oxidation by photosystem I from the green alga *Monoraphidium braunii*. *Eur J Biochem* 222:1001–1007
- Díaz-Moreno I, Díaz-Quintana A, Ubbink M, De la Rosa MA (2005a) An NMR-based docking model for the physiological transient complex between cytochrome *f* and cytochrome *c<sub>6</sub>*. *FEBS Lett* 579:2891–2896
- Díaz-Moreno I, Díaz-Quintana A, Molina-Heredia FP, Nieto PM, Hansson O, De la Rosa MA, Karlsson BG (2005b) NMR analysis of the transient complex between membrane photosystem I and soluble cytochrome *c<sub>6</sub>*. *J Biol Chem* 280:7925–7931
- Díaz-Moreno I, Díaz-Quintana A, De la Rosa MA, Crowley PB, Ubbink M (2005c) Different modes of interaction in cyanobacterial complexes of plastocyanin and cytochrome *f*. *Biochemistry* 44:3176–3183
- Díaz-Moreno I, Díaz-Quintana A, De la Rosa MA, Ubbink M (2005d) Structure of the complex between plastocyanin and cytochrome *f* from the cyanobacterium *Nostoc sp.* PCC 7119 as determined by paramagnetic NMR: the balance between electrostatic and hydrophobic interactions within the transient complex determines the relative orientation of the two proteins. *J Biol Chem* 280:18908–18915
- Díaz-Moreno I, Díaz-Quintana A, Subías G, Mairs T, De la Rosa MA, Díaz-Moreno S (2006a) Detecting transient protein–protein interactions by X-ray absorption spectroscopy: the cytochrome *c<sub>6</sub>*-photosystem I complex. *FEBS Lett* 580:3023–3028
- Díaz-Moreno I, Díaz-Moreno S, Subías G, De la Rosa MA, Díaz-Quintana A (2006b) The atypical iron-coordination geometry of cytochrome *f* remains unchanged upon binding to plastocyanin, as inferred by XAS. *Photosynth Res* 90:23–28
- Díaz-Moreno I, García-Heredia JM, Díaz-Quintana A, Teixeira M, De la Rosa MA (2011) Nitration of

- tyrosines 46 and 48 induces the specific degradation of cytochrome  $c$  upon change of the heme iron state to high-spin. *Biochim Biophys Acta – Bioenerg* 1807:1616–1623
- Díaz-Moreno I, Hulsker R, Skubak P, Foerster JM, Cavazzini D, Finiguerra MG, Díaz-Quintana A, Moreno-Beltrán B, Rossi GL, Ullmann GM, Pannu NS, De la Rosa MA, Ubbink M (2014) The dynamic complex of cytochrome  $c_6$  and cytochrome  $f$  studied with paramagnetic NMR spectroscopy. *Biochim Biophys Acta* 1837:1305–1315
- Díaz-Quintana A, Navarro JA, Hervás M, Molina-Heredia FP, De la Cerda B, De la Rosa MA (2003) A comparative structural and functional analysis of cyanobacterial plastocyanin and cytochrome  $c_6$  as alternative electron donors to photosystem I. *Photosynth Res* 75:97–110
- Díaz-Quintana A, Hervás M, Navarro JA, De la Rosa MA (2008) Plastocyanin and cytochrome  $c_6$ : the soluble electron carriers between the cytochrome  $b_6f$  complex and photosystem I. In: Fromme P (ed) *Photosynthetic Protein Complexes: A Structural Approach*. Wiley-Blackwell, Weinheim, pp 181–200
- Dikiy A, Carpentier W, Vandenberghe I, Borsari M, Safarov N, Dikaya E, Van Beeumen J, Ciurli S (2002) Structural basis for the molecular properties of cytochrome  $c_6$ . *Biochemistry* 17:14689–14699
- Drepper F, Hippler M, Nitschke W, Haehnel W (1996) Binding dynamics and electron transfer between plastocyanin and Photosystem I. *Biochemistry* 35:1282–1295
- Durán RV, Hervás M, De la Rosa MA, Navarro JA (2004) The efficient functioning of photosynthesis and respiration in *Synechocystis* sp. PCC 6803 strictly requires the presence of either cytochrome  $c_6$  or plastocyanin. *J Biol Chem* 279:7229–7233
- Flöck D, Helms V (2002) Protein-protein docking of electron transfer complexes: cytochrome  $c$  oxidase and cytochrome  $c$ . *Proteins* 47:75–85
- Frazaõ C, Soares CM, Carrondo MA, Pohl E, Dauter Z, Wilson KS, Hervás M, Navarro JA, De la Rosa MA, Sheldrick GM (1995) Ab initio determination of the crystal structure of cytochrome  $c_6$  and comparison with plastocyanin. *Structure* 3:1159–1169
- Frazaõ C, Enguita FJ, Coelho R, Sheldrick GM, Navarro JA, Hervás M, De la Rosa MA, Carrondo MA (2001) Crystal structure of low-potential cytochrome  $c_{549}$  from *Synechocystis* sp. PCC 6803 at 1.21 angstrom resolution. *J Biol Inorg Chem* 6:324–332
- García-Heredia JM, Díaz-Moreno I, Nieto PM, Orzáez M, Kocanis S, Teixeira M, Pérez-Payá E, Díaz-Quintana A, De la Rosa MA (2010) Nitration of tyrosine 74 prevents human cytochrome  $c$  to play a key role in apoptosis signaling by blocking caspase-9 activation. *Biochim Biophys Acta* 1797:981–993
- García-Heredia JM, Díaz-Quintana A, Salzano M, Orzáez M, Pérez-Payá E, Teixeira M, De la Rosa MA, Díaz-Moreno I (2011) Tyrosine phosphorylation turns alkaline transition into a biologically relevant process and makes human cytochrome  $c$  behave as an anti-apoptotic switch. *J Biol Inorg Chem* 16:1155–1168
- García-Heredia JM, Díaz-Moreno I, Díaz-Quintana A, Orzáez M, Navarro JA, Hervás M, De la Rosa MA (2012) Specific nitration of tyrosines 46 and 48 makes cytochrome  $c$  assemble a non-functional apoptosome. *FEBS Lett* 586:154–158
- Gross EL, Pearson DC (2003) Brownian dynamics simulations of the interaction of *Chlamydomonas* cytochrome  $f$  with plastocyanin and cytochrome  $c_6$ . *Biophys J* 85:2055–2068
- Grove TZ, Kostic NM (2003) Metalloprotein association, self-association, and dynamics governed by hydrophobic interactions: simultaneous occurrence of gated and true electron-transfer reactions between cytochrome  $f$  and cytochrome  $c_6$  from *Chlamydomonas reinhardtii*. *J Am Chem Soc* 125:10598–10607
- Grove TZ, Ullmann GM, Kostic NM (2012) Simultaneous true, gated, and coupled electron-transfer reactions and energetics of protein rearrangement. *J Inorg Biochem* 106:143–150
- Gupta R, He ZY, Luan S (2002) Functional relationship of cytochrome  $c_6$  and plastocyanin in *Arabidopsis*. *Nature* 417:567–571
- Haddadian EJ, Gross EL (2005) Brownian dynamics study of cytochrome  $f$  interactions with cytochrome  $c_6$  and plastocyanin in *Chlamydomonas reinhardtii* plastocyanin, and cytochrome  $c_6$  mutants. *Biophys J* 88:2323–2339
- Haddadian EJ, Gross EL (2006) A Brownian dynamics study of the effects of cytochrome  $f$  structure and deletion of its small domain in interactions with cytochrome  $c_6$  and plastocyanin in *Chlamydomonas reinhardtii*. *Biophys J* 90:566–577
- Harrenga A, Michel H (1999) The cytochrome  $c$  oxidase from *Paracoccus denitrificans* does not change the metal center ligation upon reduction. *J Biol Chem* 274:33296–33299
- Hart SE, Schlarb-Ridley BG, Delon C, Bendall DS, Howe CJ (2003) Role of charges on cytochrome  $f$  from the cyanobacterium *Phormidium laminosum* in its interaction with plastocyanin. *Biochemistry* 42:4829–4836
- Hart SE, Howe CJ, Mizuguchi K, Fernandez-Recio J (2008) Docking of cytochrome  $c_6$  and plasto-

- cyanin to the aa<sub>3</sub>-type cytochrome *c* oxidase in the cyanobacterium *Phormidium laminosum*. Protein Eng Des Sel 21:689–698
- Hazzard JT, Rong SY, Tollin G (1991) Ionic strength dependence of the kinetics of electron transfer from bovine mitochondrial cytochrome *c* to bovine cytochrome *c* oxidase. Biochemistry 30:213–222
- Herrmann JM, Funes S (2005) Biogenesis of cytochrome oxidase-sophisticated assembly lines in the mitochondrial inner membrane. Gene 354:43–52
- Hervás M, De la Rosa MA, Tollin G (1992) A comparative laser flash photolysis study of algal plastocyanin and cytochrome *c*<sub>552</sub> photooxidation by Photosystem I particles. Eur J Biochem 203:115–120
- Hervás M, Ortega JM, Navarro JA, De la Rosa MA, Bottin H (1994) Laser flash kinetic analysis of *Synechocystis* PCC 6803 cytochrome *c*<sub>6</sub> and plastocyanin oxidation by PSI. Biochim Biophys Acta 1184:235–241
- Hervás M, Navarro JA, Díaz A, Bottin H, De la Rosa MA (1995) Laser-flash kinetic analysis of the fast electron transfer from plastocyanin and cytochrome *c*<sub>6</sub> to PSI. Experimental evidence on the evolution of the reaction mechanism. Biochemistry 34:11321–11326
- Hervás M, Navarro JA, Díaz A, De la Rosa MA (1996) A comparative thermodynamic analysis by laser-flash absorption spectroscopy of plastocyanin and cytochrome *c*<sub>6</sub> oxidation by Photosystem I in *Anabaena* PCC 7119, *Synechocystis* PCC 6803 and spinach. Biochemistry 35:2693–2698
- Hervás M, Navarro JA, Molina-Heredia FP, De la Rosa MA (1998) The reaction mechanism of Photosystem I reduction by plastocyanin and cytochrome *c*<sub>6</sub> follows two different kinetic models in the cyanobacterium *Pseudanabaena* sp. PCC 6903. Photosynth Res 57:93–100
- Hervás M, Navarro JA, De la Rosa MA (2003) Electron transfer between membrane complexes and soluble proteins in photosynthesis. Acc Chem Res 36:798–805
- Hervás M, Díaz-Quintana A, Kerfeld CA, Krogmann DW, De la Rosa MA, Navarro JA (2005) Cyanobacterial Photosystem I lacks specificity in its interaction with cytochrome *c*<sub>6</sub> electron donors. Photosynth Res 83:329–333
- Hiyama T, Ke B (1972) Difference spectra and extinction coefficient of P700. Biochim Biophys Acta 267:160–171
- Hope AB (2000) Electron transfer amongst cytochrome *f*, plastocyanin and Photosystem I: kinetics and mechanisms. Biochim Biophys Acta 1456:5–26
- Jordan P, Fromme P, Witt HT, Klukas O, Saenger W, Krauss N (2001) Three-dimensional structure of cyanobacterial photosystem I at 2.5 Å resolution. Nature 411:909–917
- Kerfeld CA, Sawaya MR, Krogmann DW, Yeates TO (2002) Structure of cytochrome *c*<sub>6</sub> from *Arthrospira maxima*: an assembly of 24 subunits in a nearly symmetric shell. Acta Crystallogr Sect D 58:1104–1110
- Kerfeld CA, Anwar HP, Interrante R, Merchant S, Yeates TO (1995) The structure of chloroplast cytochrome *c*<sub>6</sub> at 1.9 Å resolution: evidence for functional oligomerization. J Mol Biol 250:627–647
- Koepke J, Angerer H, Peng G (2009) High resolution crystal structure of *Paracoccus denitrificans* cytochrome *c* oxidase: new insights into the active site and the proton transfer pathways. Biochim Biophys Acta 1787:635–645
- Kranich A, Naumann H, Molina-Heredia FP, Moore HJ, Lee TR, Lecomte S, de la Rosa MA, Hildebrandt P, Murgida DH (2009) Gated electron transfer of cytochrome *c*<sub>6</sub> at biomimetic interfaces: a time-resolved SERR study. Phys Chem Chem Phys 11:7390–7397
- Kuhlgert S, Drepper F, Fufezan C, Sommer F, Hippler M (2012) Residues PsaB Asp612 and PsaB Glu613 of photosystem I confer pH dependent binding of plastocyanin and cytochrome *c*<sub>6</sub>. Biochemistry 51:7297–7303
- Kurusu G, Zhang HM, Smith JL, Cramer WA (2003) Structure of the cytochrome *b*<sub>6</sub>*f* complex of oxygenic photosynthesis: tuning the cavity. Science 302:1009–1014
- Kyte J, Doolittle RF (1982) A simple method for displaying the hydrophobic character of a protein. J Mol Biol 157:105–132
- Landau M, Mayrose I, Rosenberg Y, Glaser F, Martz E, Pupko T, Ben-Tal N (2005) ConSurf 2005: the projection of evolutionary conservation scores of residues on protein structures. Nucleic Acids Res 33:W299–W302
- Lange C, Hervás M, De la Rosa MA (2003) Analysis of the stability of cytochrome *c*<sub>6</sub> with an improved stopped-flow protocol. Biochem Biophys Res Commun 310:215–221
- Lappalainen P, Aasa R, Malmström BG, Saraste M (1993) Soluble Cu<sub>A</sub>-binding domain from the *Paracoccus* cytochrome *c* oxidase. J Biol Chem 268:26416–26421
- Liu B, Chen Y, Doukov T, Soltis SM, Stout CD, Fee JA (2009) Combined microspectrophotometric and crystallographic examination of chemically reduced and X-ray radiation-reduced forms of cytochrome *b*<sub>a3</sub> oxidase from *Thermus thermophilus*: structure of the reduced form of the enzyme. Biochemistry 48:820–826

- Luna VM, Fee JA, Deniz AA, Stout CD (2012) Mobility of Xe atoms within the oxygen diffusion channel of cytochrome  $ba_3$  oxidase. *Biochemistry* 51:4669–4676
- Ly HK, Utesch T, Díaz-Moreno I, García-Heredia JM, De La Rosa MA, Hildebrandt P (2012) Perturbation of the redox site structure of cytochrome  $c$  variants upon tyrosine nitration. *J Phys Chem B* 116:5694–5702
- Lyons JA, Aragao D, Slattery O, Pislakov AV, Soulimane T, Caffrey M (2012) Structural insights into electron transfer in  $caa_3$ -Type cytochrome oxidases. *Nature* 487:514–518
- Maneg O, Ludwig B, Malatesta F (2003) Different interaction modes of two cytochrome- $c$  oxidase soluble  $Cu_A$  fragments with their substrates. *J Biol Chem* 278:46734–46740
- Maneg O, Malatesta F, Ludwig B, Drosou V (2004) Interaction of cytochrome  $c$  with cytochrome oxidase: two different docking scenarios. *Biochim Biophys Acta* 1655:274–281
- Marcaida MJ, Schlarb-Ridley BG, Worrall JA, Wastl J, Evans TJ, Bendall DS, Luisi BF, Howe CJ (2006) Structure of cytochrome  $c_{6A}$ , a novel dithio-cytochrome of *Arabidopsis thaliana*, and its reactivity with plastocyanin: implications for function. *J Mol Biol* 360:968–977
- Martínez SE, Huang D, Szczepaniak A, Cramer WA, Smith JL (1994) Crystal-structure of chloroplast cytochrome  $f$  reveals a novel cytochrome fold and unexpected heme ligation. *Structure* 2:95–105
- Mathis P, Sétif P (1981) Near infra-red absorption spectra of the chlorophyll cations and triplet state in vitro and in vivo. *Isr J Chem* 21:316–320
- Matuschek A, Fersht AR (1993) Application of physical organic-chemistry to engineered mutants of proteins — Hammond postulate behavior in the transition state of protein folding. *Proc Natl Acad Sci USA* 90:7814–7818
- Mazor Y, Nataf D, Toporik H, Nelson N (2013) Crystal structures of virus-like photosystem I complexes from the mesophilic cyanobacterium *Synechocystis* PCC 6803. *eLIFE* 3, e01496
- Medina M, Hervás M, Navarro JA, De la Rosa MA, Gómez-Moreno C, Tollin G (1992) A laser flash absorption spectroscopy study of *Anabaena* sp. PCC 7119 flavodoxin photoreduction by photosystem I particles from spinach. *FEBS Lett* 313:239–242
- Medina M, Díaz A, Hervás M, Navarro JA, Gómez-Moreno C, De la Rosa MA, Tollin G (1993) A comparative laser-flash absorption-spectroscopy study of *Anabaena* PCC-7119 plastocyanin and cytochrome  $c_6$  photooxidation by Photosystem-I particles. *Eur J Biochem* 213:1133–1138
- Molina-Heredia FP, Hervás M, Navarro JA, De la Rosa MA (1998) Cloning and correct expression in *Escherichia coli* of the *petE* and *petJ* genes respectively encoding plastocyanin and cytochrome  $c_6$  from the cyanobacterium *Anabaena* sp. PCC 7119. *Biochem Biophys Res* 243:302–306
- Molina-Heredia FP, Díaz-Quintana A, Hervás M, Navarro JA, De la Rosa MA (1999) Site-directed mutagenesis of cytochrome  $c_6$  from *Anabaena* species PCC 7119 - Identification of surface residues of the hemeprotein involved in photosystem I reduction. *J Biol Chem* 274:33565–33570
- Molina-Heredia FP, Hervás M, Navarro JA, De la Rosa MA (2001) A single arginyl residue in plastocyanin and in cytochrome  $c_6$  from the cyanobacterium *Anabaena* sp. PCC 7119 is required for efficient reduction of photosystem I. *J Biol Chem* 276:601–605
- Molina-Heredia FP, Wastl J, Navarro JA, Bendall DS, Hervás M, Howe CJ, De la Rosa MA (2003) A new function for an old cytochrome? *Nature* 424:33–34
- Moore GR, Pettigrew GW (1990) Cytochromes  $c$  — Evolutionary, Structural and Physicochemical Aspects. Springer, Heidelberg
- Muramoto K, Hirata K, Shinzawa-Itoh K, Yoko-o S, Yamashita E, Aoyama H, Tsukihara T, Yoshikawa S (2007) A histidine residue acting as a controlling site for dioxygen reduction and proton pumping by cytochrome  $c$  oxidase. *Proc Natl Acad Sci USA* 104:7881–7886
- Muresanu L, Pristovsek P, Löhr F, Maneg O, Mukrasch MD, Rüterjans H, Ludwig B, Lücke C (2006) The electron transfer complex between cytochrome  $c_{552}$  and the  $Cu_A$  domain of the *Thermus thermophilus*  $ba_3$  oxidase. A combined NMR and computational approach. *J Biol Chem* 281:14503–14513
- Navarro JA, Hervás M, De la Cerda B, De la Rosa MA (1995) Purification and physicochemical properties of the low-potential cytochrome  $c_{549}$  from the cyanobacterium *Synechocystis* sp. PCC 6803. *Arch Biochem Biophys* 318:46–52
- Navarro JA, Durán RV, De la Rosa MA, Hervás M (2005) Respiratory cytochrome  $c$  oxidase can be efficiently reduced by the photosynthetic redox proteins cytochrome  $c_6$  and plastocyanin in cyanobacteria. *FEBS Lett* 579:3565–3568
- Nicholls A, Honig B (1991) A rapid finite difference algorithm, utilizing successive over-relaxation to solve the Poisson–Boltzmann equation. *J Comput Chem* 12:435–445
- Obinger C, Knepper JC, Zimmermann U, Peschek GA (1990) Identification of a periplasmic C-type cytochrome as electron donor to the plasma membrane-bound cytochrome oxidase of the cyanobacterium *Nostoc*. *Biochem Biophys Res Commun* 169:492–501
- Olesen K, Ejdebäck M, Crnogorac MM, Kostic NM, Hansson Ö (1999) Electron transfer to photosystem

- 1 from spinach plastocyanin mutated in the small acidic patch: ionic strength dependence of kinetics and comparison of mechanistic models. *Biochemistry* 38:16695–16705
- Ostermeier C, Harrenga A, Ermler U, Michel H (1997) Structure at 2.7 Å resolution of the *Paracoccus denitrificans* two-subunit cytochrome *c* oxidase complexed with an antibody FV fragment. *Proc Natl Acad Sci USA* 94:10547–10553
- Paumann M, Feichtinger M, Bernroither M, Goldfuhs J, Jakopitsch C, Furtmüller PG, Regelsberger G, Peschek GA, Obinger C (2004) Kinetics of interprotein electron transfer between cytochrome *c*<sub>6</sub> and the soluble CuA domain of cyanobacterial cytochrome *c* oxidase. *FEBS Lett* 576:101–106
- Pettersen EF, Goddard TD, Huang CC, Couch GS, Greenblatt DM, Meng EC, Ferrin TE (2004) UCSF Chimera—a visualization system for exploratory research and analysis. *J Comput Chem* 25:1605–1612
- Qin L, Hiser C, Mulichak A, Garavito RM, Ferguson-Miller S (2006) Identification of conserved lipid/detergent-binding sites in a high-resolution structure of the membrane protein cytochrome *c* oxidase. *Proc Natl Acad Sci USA* 103:16117–16122
- Qin L, Mills DA, Proshlyakov DA, Hiser C, Ferguson-Miller S (2009) Redox dependent conformational changes in cytochrome *c* oxidase suggest a gating mechanism for proton uptake. *Biochemistry* 48:5121–5130
- Roberts VA, Pique ME (1999) Definition of the interaction domain for cytochrome *c* on cytochrome *c* oxidase. III. Prediction of the docked complex by a complete, systematic search. *J Biol Chem* 274:38051–38060
- Rodríguez-Roldán V, García-Heredia JM, Navarro JA, De la Rosa MA, Hervás M (2008) A comparative kinetic analysis of the reactivity of plant, horse, and human respiratory cytochrome *c* towards cytochrome *c* oxidase. *Biochemistry* 47:12371–12379
- Schlarb-Ridley BG, Navarro JA, Spencer M, Bendall DS, Hervás M, Howe CJ, De la Rosa MA (2002a) Role of electrostatics in the interaction between plastocyanin and photosystem I of the cyanobacterium *Phormidium laminosum*. *Eur J Biochem* 269:5893–5902
- Schlarb-Ridley BG, Bendall DS, Howe CJ (2002b) Role of electrostatics in the interaction between cytochrome *f* and plastocyanin of the cyanobacterium *Phormidium laminosum*. *Biochemistry* 41:3279–3285
- Seib KL, Jennings MP, McEwan AG (2003) A Sco homologue plays a role in defence against oxidative stress in pathogenic *Neisseria*. *FEBS Lett* 546:411–415
- Sigfridsson K, Hansson Ö, Karlsson BG, Baltzer L, Nordling M, Lundberg LG (1995) Spectroscopic and kinetic characterization of the spinach plastocyanin mutant Tyr83-His: a histidine residue with a high pK<sub>a</sub> value. *Biochim Biophys Acta* 1228:28–36
- Schnackenberg J, Than ME, Mann K, Wiegand G, Huber R, Reuter W (1999) Amino acid sequence, crystallization and structure determination of reduced and oxidized cytochrome *c*<sub>6</sub> from the green alga *Scenedesmus obliquus*. *J Mol Biol* 290:1019–1030
- Sommer F, Drepper F, Haehnel W, Hippler M (2004) The hydrophobic recognition site formed by residues PsaA-Trp651 and PsaB-Trp627 of photosystem I in *Chlamydomonas reinhardtii* confers distinct selectivity for binding of plastocyanin and cytochrome *c*<sub>6</sub>. *J Biol Chem* 279:20009–20017
- Soulimane T, Buse G, Bourenkov GP, Bartunik HD, Huber R, Than ME (2000) Structure and mechanism of the aberrant ba<sub>3</sub>-cytochrome *c* oxidase from *Thermus thermophilus*. *EMBO J* 19:1766–1776
- Srinivasan V, Rajendran C, Sousa FL, Melo AM, Saraiva LM, Pereira MM, Santana M, Teixeira M, Michel H (2005) Structure at 1.3 Å resolution of *Rhodothermus marinus* caa(3) cytochrome *c* domain. *J Mol Biol* 345:1047–1057
- Stroebel D, Choquet Y, Popot JL, Picot D (2003) An atypical haem in the cytochrome *b<sub>6</sub>f* complex. *Nature* 426:413–418
- Suga M, Yano N, Muramoto K, Shinzawa-Itoh K, Maeda T, Yamashita E, Tsukihara T, Yoshikawa S (2011) Distinguishing between Cl<sup>-</sup> and O<sub>2</sub><sup>2-</sup> as the bridging element between Fe<sup>3+</sup> and Cu<sup>2+</sup> in resting-oxidized cytochrome *c* oxidase. *Acta Crystallogr* 67:742–744
- Sun J, Xu W, Hervás M, Navarro JA, De la Rosa MA, Chitnis PR (1999) Oxidising side of the cyanobacterial Photosystem I. Evidence for interaction between the electron donor proteins and a luminal surface helix of the PsaB subunit. *J Biol Chem* 274:19048–19054
- Suzek BBE, Huang H, McGarvey P, Mazumder R, Wu CH (2007) UniRef: comprehensive and non-redundant UniProt reference clusters. *Bioinformatics* 23:1282–1288
- Svensson-Ek M, Abramson J, Larsson G, Tornroth S, Brezezinski P, Iwata S (2002) The X-ray crystal structures of wild-type and EQ(I-286) mutant cytochrome *c* oxidases from *Rhodobacter sphaeroides*. *J Mol Biol* 321:329–339
- Tiefenbrunn T, Liu W, Chen Y, Katritch V, Stout CD, Fee JA, Cherezov V (2011) High resolution structure of the ba<sub>3</sub> cytochrome *c* oxidase from *Thermus thermophilus* in a lipidic environment. *Plos One* 6:e22348–e22348

- Tollin G, Meyer T, Cusanovich MA (1986) Elucidation of the factors which determine reaction-rate constants and biological specificity for electron transfer proteins. *Biochim Biophys Acta* 853:29–41
- Tsukihara T, Aoyama H, Yamashita E, Tomizaki T, Yamaguchi H, Shinzawa-Itoh K, Nakashima R, Yaono R, Yoshikawa S (1996) The whole structure of the 13-subunit oxidized cytochrome *c* oxidase at 2.8 Å. *Science* 272:1136–1144
- Tsukihara T, Shimokata K, Katayama Y, Shimada H, Muramoto K, Aoyama H, Mochizuki M, Shinzawa-Itoh K, Yamashita E, Yao M, Ishimura Y, Yoshikawa S (2003) The low-spin heme of cytochrome *c* oxidase as the driving element of the proton-pumping process. *Proc Natl Acad Sci U S A* 100:15304–15309
- Wang K, Zhen Y, Sadoski R, Grinnell S, Geren L, Ferguson-Miller S, Durham W, Millett F (1999) Definition of the interaction domain for cytochrome *c* on cytochrome *c* oxidase. II Rapid kinetic analysis of electron transfer from cytochrome *c* to *Rhodobacter sphaeroides* cytochrome oxidase surface mutants. *J Biol Chem* 274:38042–38050
- Watkins JA, Cusanovich MA, Meyer TE, Tollin G (1994) A ‘parallel plate’ electrostatic model of bimolecular rate constants applied to electron transfer proteins. *Protein Sci* 3:2104–2114
- Williams PA, Blackburn NJ, Sanders D, Bellamy H, Stura EA, Fee JA, McRee DE (1999) The  $Cu_A$  domain of *Thermus thermophilus*  $ba_3$ -type cytochrome *c* oxidase at 1.6 Å resolution. *Nat Struct Biol* 6:509–516
- Worrall JA, Schlarb-Ridley BG, Reda T, Marcaida MJ, Moorlen RJ, Wastl J, Hirst J, Bendall DS, Luisi BF, Howe CJ (2007) Modulation of heme redox potential in the cytochrome  $c_6$  family. *J Am Chem Soc* 129:9468–9475
- Yamada S, Park SY, Shimizu H, Koshizuka Y, Kadokura K, Satoh T, Suruga K, Ogawa M, Isogai Y, Nishio T, Shiro Y, Oku T (2000) Structure of cytochrome  $c_6$  from the red alga *Porphyra yezoensis* at 1.57 Å resolution. *Acta Crystallogr D Biol Crystallogr* 56:1577–1582
- Yoneda GS, Holwerda RA (1978) Kinetics of the oxidation of *Rhus vernicifera* stellacyanin by the  $Co(EDTA)^-$  ion. *Bioinorg Chem* 8:139–159
- Yoshikawa S, Shinzawa-Itoh K, Nakashima R, Yaono R, Yamashita E, Inoue N, Yao M, Fei MJ, Libeu CP, Mizushima T, Yamaguchi H, Tomizaki T, Tsukihara T (1998) Redox-coupled crystal structural changes in bovine heart cytochrome *c* oxidase. *Science* 280:1723–1729

# Chapter 32

## Electron Partitioning in Anoxic Phototrophic Bacteria

Melanie A. Spero<sup>a</sup>, Saheed Imam<sup>b</sup>, Daniel R. Noguera<sup>c</sup>,  
and Timothy J. Donohue<sup>a,\*</sup>

<sup>a</sup>*Department of Bacteriology, University of Wisconsin-Madison,  
1552 University Avenue, Madison, WI 53726, USA*

<sup>b</sup>*Program in Cellular and Molecular Biology, University of  
Wisconsin-Madison, 1552 University Avenue, Madison,  
WI 53726, USA*

<sup>c</sup>*Department of Civil and Environmental Engineering, University  
of Wisconsin-Madison, 1552 University Avenue, Madison,  
WI 53726, USA*

Summary.....	680
I. Introduction.....	680
II. Competition for Electrons of the Quinone Pool.....	681
A. Quinol Producing Reactions.....	683
B. Quinol Consuming Reactions.....	683
III. The Role of Cytoplasmic “Electron Sinks” During Photoheterotrophic Growth.....	685
A. The Calvin-Benson-Bassham Cycle.....	685
B. Nitrogenase Activity.....	686
C. Other Cytoplasmic Electron Sinks.....	687
IV. Recycling Reducing Power Captured in Pyridine Nucleotides.....	688
A. Role of Transhydrogenases in Maintaining Redox Balance of the Pyridine Nucleotide and Glutathione Pools.....	688
B. PntAB Is Required for Normal Photosynthetic Growth in <i>Rhodobacter sphaeroides</i> ..	689
C. Zwf Is an Alternative Route for NADPH Synthesis in <i>Rhodobacter sphaeroides</i> .....	690
V. Modeling the Metabolism of Photosynthetic Organisms.....	692
A. Constraint-Based Modeling.....	692
B. Constraint-Based Models for Photosynthetic Organisms.....	692
C. Challenges for Metabolic Modeling of Photosynthetic Cells.....	693
D. Metabolic Modeling as a Tool for Rational Design of Photosynthetic Organisms.....	693
VI. Concluding Remarks and Future Directions.....	694
Acknowledgements.....	694
References.....	695

---

\*Author for correspondence, e-mail: [tdonohue@bact.wisc.edu](mailto:tdonohue@bact.wisc.edu)

## Summary

Photosynthetic cells make major contributions to many important processes on this planet, including solar energy capture, nitrogen or carbon dioxide sequestration and production of useful biocommodities. The sheer number of photosynthetic cells also makes them significant contributors to global nutrient cycling, especially in aquatic ecosystems. For each of these activities, photosynthetic cells need efficient systems for production and distribution of reducing power among the myriad of cellular pathways that depend on reductant. This chapter focuses on the partitioning of reductant in purple nonsulfur photosynthetic bacteria. It summarizes known membrane and cytoplasmic enzymes and pathways that need the reductant produced via photochemical activity (quinol in these organisms). These observations illustrate that quinol is used to provide reducing power to a variety of crucial processes (cellular biosynthesis, maintenance of a proton motive force) and key assimilatory pathways (carbon dioxide and nitrogen fixation), depending on the availability of nutrients. We also summarize data illustrating that cells use a variety of pathways to recycle excess reductant. Finally, we illustrate how the recent use of genomic and computational approaches to the analysis of these and other photosynthetic organisms has provided testable predictions and considerable new insight into the partitioning of reductant that is produced from solar energy capture.

## I. Introduction

Photosynthetic organisms are among the most abundant organisms on earth. Their unique ability to harvest solar energy and use it to fix atmospheric carbon dioxide is at the foundation of the global food chain. Consequently, photosynthetic organisms have been the attention of intense study from chemical, energetic and biological perspectives. Other chapters in this volume illustrate that photosynthesis depends on the interplay of many components. This chapter focuses on the cellular distribution of electrons that are required to support energetic and biosynthetic processes in photosynthetic organisms. Specifically, we describe recent work analyzing this process in anoxic phototrophic bacteria, particularly the purple nonsulfur bacteria (PNSB).

PNSB contain some of the most thoroughly characterized bioenergetic pathways (Blankenship et al. 1995; Blankenship and Hartman 1998). The photosynthetic apparatus of Gram-negative bacteria is typically housed in the intracytoplasmic membrane, a specialized bioenergetic membrane that is the functional equivalent of the plant chloroplast thylakoid (Tavano and Donohue 2006). These bacteria convert light energy into chemical energy by using specialized light-harvesting complexes to capture photons. Once light is captured they couple light-driven oxidation of pigments in a reaction center complex to electron transfer through membrane-bound enzymes (Meyer and Donohue 1995). The ultimate product of photochemistry in the PNSB reaction center—quinol (QH<sub>2</sub>)—diffuses from the reaction center through the membrane where it binds to and is oxidized by the cytochrome *bc*<sub>1</sub> complex to form a trans-membrane H<sup>+</sup> gradient that supports ATP synthesis (Fig. 32.1) (Meyer and Donohue 1995). The reaction center of these bacteria lacks an O<sub>2</sub>-evolving complex to reduce the photochemically-oxidized reaction center complex. Instead, periplasmic proteins

---

*Abbreviations:* CBM – Constraint-based model; DMSO – Dimethylsulfoxide; FBA – Flux balance analysis; PHB – Poly- $\beta$ -hydroxybutyrate; PNSB – Purple nonsulfur bacteria; SMP – Soluble microbial products; TMAO – Trimethylamine *N*-oxide



(cytochrome  $c_2$ , iron-sulfur- or non-heme iron proteins) or another integral membrane protein complex acts in a cyclic electron transport chain to reduce the light-oxidized reaction center complex to its ground state (Fig. 32.1) (Meyer and Donohue 1995). PNSB lack photosystem I, so NADH is not formed directly from light energy conversion (Meyer and Donohue 1995). Instead, a proton-translocating NADH:quinone oxidoreductase (complex I) uses the proton gradient to pass electrons from quinol to  $\text{NAD}^+$ , producing the NADH needed for anabolic reactions (Fig. 32.1) (Herter et al. 1998; Tichi et al. 2001). The photosynthetic apparatus of PNSB is the ancestor of the photosystem II complex in modern plants and oxygenic phototrophs (Blankenship et al. 1995; Blankenship and Hartman 1998). The photocycle of PNSB is arguably the best understood bioenergetic membrane process in terms of structural, functional and genetic information (Blankenship et al. 1995; Blankenship and Hartman 1998).

PNSB are typically facultative anaerobes capable of several well-studied energetic and metabolic lifestyles (McEwan 1994). Individual species of PNSB are able to metabolize a wide variety of electron-rich carbon sources under anaerobic conditions in the presence of light (Imam et al. 2013). To maintain redox balance, cells grown under these photoheterotrophic conditions require a means to recycle excess reducing power (Richardson et al. 1988; McEwan 1994; Dubbs and Tabita 2004; McKinlay and Harwood 2010b). In many species of photosynthetic bacteria excess reducing power can be dissipated or recycled through poly- $\beta$ -hydroxybutyrate (PHB) synthesis (McKinlay and Harwood 2010a; Yilmaz et al. 2010; Kontur et al. 2011), the Calvin-Benson cycle (assimilating  $\text{CO}_2$  even in the presence of organic carbon) (Dubbs and Tabita 2004),  $\text{H}_2$  synthesis (Gest and Kamen 1949; Gest and Blankenship 2004), and respiration of alternative electron acceptors (Richardson et al. 1988). Products of uncharacterized genes also appear to recycle excess reducing

power under photoheterotrophic conditions in some species, suggesting there are yet to be identified additional uses for excess reducing power in these cells (Tavano et al. 2005).

Below, we summarize new information on the pathways used to partition or recycle reducing power in PNSB, focusing on studies or models that have been developed to analyze this in *Rhodobacter sphaeroides* and other photoheterotrophic species (Mackenzie et al. 2007; McKinlay and Harwood 2010a; Imam et al. 2011, 2013). The analysis of electron partitioning has been facilitated by prior knowledge of cytochromes and other electron carriers (Meyer and Cusanovich 1985; Bartsch et al. 1989; Meyer and Donohue 1995), the availability of complete genome sequences (Larimer et al. 2004; Mackenzie et al. 2007; Kontur et al. 2012b), the ability to generate mutants by a variety of techniques (Donohue and Kaplan 1991) and the incorporation of synthetic (Jaschke et al. 2011; Work et al. 2012; Tikh et al. 2014) or systems biology (Callister et al. 2006; McKinlay and Harwood 2010a; Imam et al. 2011, 2013, 2014, 2015a, b, c; Berghoff et al. 2013) techniques to analyze or model the metabolic or regulatory activities of these bacteria.

## II. Competition for Electrons of the Quinone Pool

During anoxic phototrophy, reduced quinones (quinol) are responsible for shuttling electrons from the reaction center to the cytochrome  $bc_1$  complex (Fig. 32.1). However, they also interact with a number of other integral membrane complexes that can alter the quinone:quinol ratio. Because the quinone pool is connected to many metabolic processes, it serves as a dynamic measure of cellular redox state. A number of energy-conserving (e.g. photosynthesis,  $\text{H}_2$  oxidation) or energy-consuming (e.g.  $\text{CO}_2$  fixation,  $\text{N}_2$  fixation) pathways are regulated by the RegB/RegA (PrrB/PrrA)

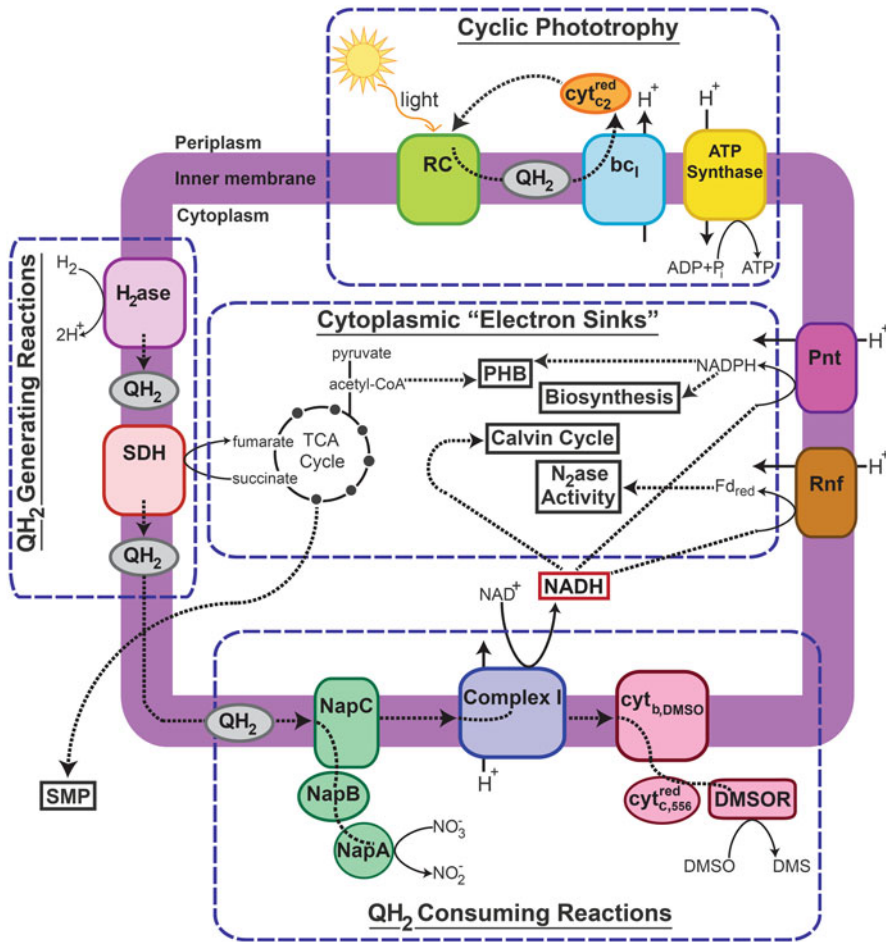


Fig. 32.1. Phototrophic electron transfer pathways in PNSB. During cyclic electron transfer, the reaction center (RC) reduces quinone to produce quinol (QH<sub>2</sub>), which donates electrons to the cytochrome *bc*<sub>1</sub> complex (*bc*<sub>1</sub>). Electrons are transferred to cytochrome *c*<sub>2</sub> (*cyt*<sub>*c*2</sub><sup>red</sup>) and are then carried back to the reaction center. This process generates a proton motive force (H<sup>+</sup>) that can be used by ATP synthase for ATP formation. Quinol generating reactions include uptake [NiFe] hydrogenase (H<sub>2</sub>ase) and succinate dehydrogenase (SDH). Quinol consuming reactions include nitrate reductase (NapABC) and DMSO reductase (DMSOR), which requires a *b*-type cytochrome (*cyt*<sub>*b*</sub>,DMSO) and a *c*-type cytochrome (*cyt*<sub>*c*</sub>,556<sup>red</sup>). Complex I also performs a quinol consuming reaction that uses the generated proton motive force to synthesize NADH. NADH is used in a variety of electron sinks to balance cellular redox components. It can be shuttled directly into the Calvin-Benson-Bassham cycle for CO<sub>2</sub> fixation, or electrons can be transferred from NADH to ferredoxin via the Rnf complex (Rnf), and the reduced ferredoxin (Fd<sub>red</sub>) can transfer electrons to nitrogenase (N<sub>2</sub>ase). Electrons can also be transferred from NADH to NADP<sup>+</sup> via pyridine nucleotide transhydrogenase (Pnt), and the resulting NADPH can be used for biosynthetic reactions or combined with acetate to synthesize poly-β-hydroxybutyrate (PHB). The cell can also excrete compounds, called soluble microbial products (SMP), to balance redox.

two-component regulatory system, which alters gene expression potentially in response to changes in the redox state of the quinone pool or electron transport chain (Elsen et al. 2004; Oh et al. 2004; Swem et al. 2006; Wu and Bauer 2010). Furthermore, many studies of PNSB show that mutations that alter

redox balance result in photoheterotrophic growth defects, which can be corrected by addition of the terminal electron acceptor dimethylsulfoxide (DMSO), which accepts reducing equivalents from quinol (Shaw et al. 1999). Thus, the redox state of the quinone pool is linked to a variety of critical

processes. Here, we discuss the enzymes that contribute to or utilize electrons from the quinone pool during phototrophic growth.

### A. Quinol Producing Reactions

In addition to the photochemical reaction center, other conserved respiratory enzymes can contribute electrons to the quinone pool. The first is the tricarboxylic acid (TCA) cycle enzyme succinate dehydrogenase, which transfers electrons from succinate to quinone (Fig. 32.1). While little work has investigated the role of succinate dehydrogenase in maintaining the quinone pool during phototrophy, its expression and synthesis has been observed during photoheterotrophic growth in *R. sphaeroides* (Callister et al. 2006; Arai et al. 2008). Metabolic modeling of *R. sphaeroides* predicts succinate dehydrogenase is essential for photoheterotrophic growth on succinate, but not for growth on many other substrates, including pyruvate or glucose (Imam, unpublished).

In addition to succinate dehydrogenase, many PNSB use [Ni-Fe] hydrogenases to oxidize H<sub>2</sub> and produce quinol (Vignais and Billoud 2007). Uptake [Ni-Fe] hydrogenases are often distinguished from other hydrogenases by their bimetallic [Ni-Fe] active site, and because they are membrane-bound respiratory enzymes (Vignais and Colbeau 2004). Uptake hydrogenases can transfer electrons to the quinone pool (via a *b*-type cytochrome), conserving the energy of this reaction by generating a proton motive force (Fig. 32.1) (Porte and Vignais 1980). Many environmental signals regulate the expression of uptake hydrogenases in PNSB. Uptake hydrogenase expression is activated in the presence of H<sub>2</sub> by a cytoplasmic, H<sub>2</sub>-sensing regulatory hydrogenase (HupUV/HoxBC) and a two-component signal transduction system (HupT/HoxJ and HupR/HoxA) (Dischert et al. 1999; Vignais et al. 2005; Rey et al. 2006). Uptake hydrogenase expression is negatively regulated by the presence of O<sub>2</sub>, and by the global anaerobic regulator RegB/RegA

(PrrB/PrrA) during conditions where the cell has other (non-H<sub>2</sub>) sources of electrons, such as photoheterotrophic growth (Elsen et al. 2000; Vignais 2009; Donohue and Kiley 2010; Wu and Bauer 2010). In diazotrophs, uptake hydrogenase gene expression is often co-regulated with nitrogen fixation genes, since nitrogenase produces H<sub>2</sub> as a byproduct of the nitrogen fixation reaction (Elsen et al. 2000; Hallenbeck and Benemann 2002). Related to this, work in *Rhodospirillum rubrum* and specific strains of *R. sphaeroides* have used hydrogenase-deletion strains to increase yields of nitrogenase-mediated H<sub>2</sub> production during photoheterotrophic growth (Kern et al. 1994; Kim et al. 2006; Kars et al. 2008; Kontur et al. 2011). While a hydrogenase-deletion mutant is able to grow photoheterotrophically, the enzyme is required for photoautotrophic growth with H<sub>2</sub> as the electron source (Xu et al. 1989; Rey et al. 2006; Kontur et al. 2011).

In addition, the *R. sphaeroides* genome is predicted to encode three other quinol-producing enzymes. The first (RSP\_1777) is annotated as an FAD-binding flavoprotein-quinone oxidoreductase. Homologs of this protein can be found in many PNSB genomes. The second (RSP\_3381) is a predicted NADPH-quinone oxidoreductase, homologous to the cytoplasmic *Escherichia coli* QOR enzyme, for which protein crystal structures have been described (Thorn et al. 1995; Shimomura et al. 2003). Lastly, RSP\_2673 is predicted to encode a quinoprotein glucose dehydrogenase (glucose:quinone oxidoreductase). The *E. coli* homolog of this enzyme is membrane-bound and contains a pyrroloquinoline quinone cofactor (Cozier et al. 1999; Anthony 2004). The physiological roles of each of these proteins in PNSB remain to be experimentally tested.

### B. Quinol Consuming Reactions

During phototrophic growth, quinol generated from the reaction center carries electrons to the cytochrome *bc*<sub>1</sub> complex. However, quinones can also be reduced

during central carbon metabolism (succinate dehydrogenase) or from alternative electron donors such as  $H_2$  (via uptake hydrogenase) during phototrophic growth (Fig. 32.1). As a result, the quinone pool can become over-reduced, halting cyclic electron transfer and slowing or even preventing growth (McEwan 1994). Consequently, under phototrophic growth conditions, electron transfer reactions that maintain the redox state of the quinone pool are essential.

One way that quinol can be oxidized is by transferring electrons to a terminal electron acceptor. DMSO and trimethylamine *N*-oxide (TMAO) are organic intermediates of the sulfur and nitrogen cycles, respectively, that are commonly found in surface waters (Andreae 1980; Gibb and Hatton 2004). Both compounds can act as terminal electron acceptors under photoheterotrophic conditions, where electrons are transferred from quinol through a membrane-bound cytochrome *b*, to a periplasmic cytochrome *c*, and finally to DMSO or TMAO via the periplasmic molybdoenzyme DMSO reductase (DMSOR) (Fig. 32.1) (McEwan et al. 1983, 1985, 1989; McEwan 1994; Shaw et al. 1999). DMSOR expression in *R. sphaeroides* and *Rhodobacter capsulatus* is controlled by the FNR (fumarate and nitrate reduction) homolog, FnrL, in response to  $O_2$  tension and by the two component regulatory system DorSR in response to the presence of DMSO (ZeilstraRyalls et al. 1997; Mouncey and Kaplan 1998; Tavano et al. 2004). Thus, DMSOR is only synthesized under anaerobic conditions in the presence of DMSO (Mouncey et al. 1997). DMSOR activity is required for anaerobic respiration with DMSO/TMAO in the dark. However, while the enzyme is active during phototrophic conditions in the presence of DMSO and provides an alternative quinol consuming reaction, it is not essential for growth under these conditions (Mouncey et al. 1997). Finally, the addition of DMSO to cultures can act as an electron sink to balance redox components and rescue growth phenotypes predicted to result from an altered redox state of the quinone pool (see below).

Many PNSB also contain complete or partial denitrification pathways. Denitrification is a dissimilatory process, whereby nitrate ( $NO_3$ ) is reduced to nitrogen gas ( $N_2$ ) (Zumft 1997). Denitrification can be used to generate a proton motive force for ATP synthesis in the absence of  $O_2$ ; however, that is not considered its only function in PNSB. Four enzymes are required for the conversion of nitrate to  $N_2$ , but many species of PNSB encode only partial denitrification pathways (Michalski and Nicholas 1988; Shapleigh 2009). Moreover, there is no apparent phylogenetic trend among the distribution of denitrification enzymes in these bacteria (Shapleigh 2009). The current hypothesis is that many PNSB encode partial denitrification pathways that serve to dissipate excess reducing power during phototrophic conditions, rather than to conserve energy for ATP synthesis. For example, *R. capsulatus* strains that encode nitrate reductase or nitrous oxide ( $N_2O$ ) reductase can grow photoheterotrophically on reduced substrates that typically do not support growth (such a butyrate) with the addition of nitrate or nitrous oxide (Richardson et al. 1988). Furthermore, work in *R. sphaeroides* strain DSM158 demonstrates that nitrate reductase activity increases during photoheterotrophic growth on highly reduced substrates, suggesting it plays a role in redox balance (Gavira et al. 2002). There are three types of nitrate reductases (Nas, Nar, Nap), none, some, or all of which can be found in any given purple nonsulfur bacterium (Richardson et al. 2001). Two of these enzymes, Nar and Nap (Nap, Fig. 32.1), accept electrons from the quinone pool (Richardson et al. 2001; Shapleigh 2006). However, the other enzymes involved in denitrification (nitrite reductase, nitric oxide reductase, and nitrous oxide reductase) accept electrons from reduced cytochromes generated by the cytochrome *bc*<sub>1</sub> complex (Shapleigh 2006). This allows denitrification enzymes to act as sinks for over-reduced components of cyclic phototrophic electron transfer reactions (quinol, reduced cytochromes). While the

transcriptional control of denitrification genes is complex, they are, in part, positively regulated by RegB/RegA (PrrB/PrrA), again suggesting a role for this pathway in balancing cellular redox state (Laratta et al. 2002; Imam et al. 2014, 2015b).

PNSB can also alter the redox state of the quinone pool by moving reductant from the membrane to the cytoplasm. This is typically accomplished by complex I, which utilizes the proton motive force to drive electron transfer from quinol to  $\text{NAD}^+$ , synthesizing NADH (Fig. 32.1) (McEwan 1994; Herter et al. 1998). Once generated, cytoplasmic NADH can be used by a variety of pathways to support biosynthesis, or this excess reductant can be dissipated via a variety of “electron sinks” (discussed below). In *R. capsulatus* and *R. sphaeroides*, complex I is required for photoautotrophic and photoheterotrophic growth, where it synthesizes NADH to oxidize the quinol pool. The phenotypes of complex I mutants can be rescued by the addition of the terminal electron acceptor DMSO (Dupuis et al. 1997; Tichi et al. 2001; Spero et al. 2015), suggesting that the growth defect of these strains is also associated with an alteration in the redox state (over-reduction) of the quinone pool. Thus, the requirement for complex I during phototrophy is predicted to be conserved across PNSB. Indeed, genomic analyses indicate that all bacteria that use solely a quinol-generating type-2 reaction center (purple bacteria, filamentous green nonsulfur bacteria) are predicted to encode complex I. However, bacteria that have a reduced ferredoxin-generating type-1 reaction center (cyanobacteria, green sulfur bacteria) do not encode complex I, but rather complex I-like enzymes predicted to use electron donors other than NADH (Bryant and Frigaard 2006; Battchikova et al. 2011; Spero et al. 2015; see also the chapter by Shikanai and Aro in this volume). These correlations support the hypothesis that complex I of PNSB serves to recycle quinol that is produced from photochemical activity in the reaction center. Interestingly, genomic analyses also find that a small number

(<4 %) of sequenced bacteria are predicted to encode two complex I isozymes, including all sequenced strains of *R. sphaeroides* and *Rhodopseudomonas palustris* (Spero et al. 2015). While the roles of these isozymes are currently unknown, gene expression studies in *R. sphaeroides* show the two complex I operons are differentially expressed in the presence or absence of  $\text{O}_2$  (Arai et al. 2008). However, both of the complex I operons are expressed (at different levels) during photoheterotrophic growth. Thus, additional experiments are needed to determine the roles of these complex I isozyme in maintaining the cellular redox balance.

### III. The Role of Cytoplasmic “Electron Sinks” During Photoheterotrophic Growth

When complex I transfers excess reducing power from membrane-bound quinol to  $\text{NAD}^+$ , the resulting NADH can be shuttled into a variety of cytoplasmic “electron sinks” to maintain the  $\text{NAD}^+:\text{NADH}$  ratio. Alternatively, the reducing power in NADH can be transferred to another electron carrier (ferredoxin,  $\text{NADP}^+$ ) and used to support other cellular processes (Fig. 32.1). Because complex I is required for phototrophic growth (Dupuis et al. 1997; Tichi et al. 2001), it is predicted to supply a large fraction of reducing power for biosynthesis or for passage to electron sinks. However, it is not known the extent to which electrons directed into electron sinks originate from complex I-mediated NADH synthesis, as opposed to other NADH-generating catabolic processes. Below we describe known electron sinks that are important for photoheterotrophic growth in PNSB.

#### A. The Calvin-Benson-Bassham Cycle

Excess NADH can be directed into the Calvin-Benson-Bassham (Calvin) cycle, which utilizes this reducing power and ATP to fix  $\text{CO}_2$  into organic carbon

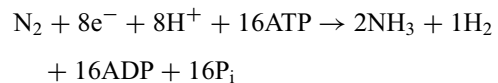
(Hallenbeck et al. 1990; Dubbs and Tabita 2004; McKinlay and Harwood 2010b, 2011). Though the role of the Calvin cycle during autotrophic growth has been known for a long time, its importance for photoheterotrophic growth is a more recent finding. The Calvin cycle is required for many photoheterotrophic growth conditions in *R. sphaeroides*, *R. capsulatus*, and *R. palustris* (Hallenbeck et al. 1990; Paoli et al. 1998; McKinlay and Harwood 2010b). Here, it is proposed that the Calvin cycle acts as an electron sink, oxidizing NADH so it can be used in catabolism (Fig. 32.1). Calvin cycle mutants can be rescued by the addition of exogenous DMSO, or in some organisms (*R. palustris*, *R. capsulatus*) by increasing the expression of another enzyme, such as nitrogenase, that can act as an electron sink (Hallenbeck et al. 1990; Tichi and Tabita 2000; McKinlay and Harwood 2010a). Additionally, an *R. sphaeroides* Calvin cycle mutant is able to grow on acetate, where the ethylmalonyl-CoA pathway that is used to assimilate acetate also balances the redox state of the pyridine nucleotide pool by oxidizing NADPH (Laguna et al. 2011). However, *R. palustris* uses the glyoxylate cycle to assimilate acetate, which produces NADH, leading to a requirement for the Calvin cycle during photoheterotrophic growth on acetate (Laguna et al. 2011).

In *R. palustris*, <sup>13</sup>C-metabolic flux analysis has demonstrated the extent to which the organism depends on the Calvin cycle for redox balance (McKinlay and Harwood 2010b). During growth on acetate, 22 % of the consumed acetate is released as CO<sub>2</sub>, most of which (67 %) is re-assimilated via the Calvin cycle. While most of the acetate carbon is used in biosynthetic pathways, only half of the reduced electron carriers generated during acetate catabolism are re-oxidized via biosynthetic pathways. Under these conditions, the Calvin cycle re-oxidizes almost all of the remaining reduced electron carriers (McKinlay and Harwood 2010b). Thus, most of the CO<sub>2</sub> produced during acetate metabolism is subsequently assimilated in order to maintain cellular

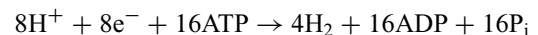
redox state. A similar study found that the *R. palustris* Calvin cycle oxidizes a large fraction of reduced electron carriers (38–55 %) during photoheterotrophic growth, regardless of the oxidation state of the provided carbon substrate (McKinlay and Harwood 2011). These observations demonstrate the important role of the Calvin cycle as an electron sink during photoheterotrophic growth.

### B. Nitrogenase Activity

In the absence of a preferred nitrogen source such as ammonium, photoheterotrophically growing PNSB activate expression of their N<sub>2</sub> fixation system, which can be used to convert N<sub>2</sub> to ammonia and thus dissipate excess reductant. N<sub>2</sub> fixation, which is performed by the nitrogenase enzyme, requires large amounts of ATP and reductant, according to the following reaction (McKinlay and Harwood 2010a):



However, nitrogenase can also function in the absence of N<sub>2</sub>. For example, when cells are grown in the presence of a fixed nitrogen source (such as glutamate), the reducing power consumed by nitrogenase activity is used to synthesize H<sub>2</sub>, according to (McKinlay and Harwood 2010a):



The electron donor to nitrogenase is not known in many PNSB, but because N<sub>2</sub> fixation requires low potential electrons, it is proposed that reduced ferredoxin is used for this purpose (Yoch and Arnon 1975; Jouanneau et al. 1995; Biegel et al. 2011; Kontur et al. 2011). Electrons are predicted to be transferred from NADH to ferredoxin by the *Rhodobacter* nitrogen fixation (Rnf) complex, which uses the proton motive force to drive the reaction (Fig. 32.1) (Schmehl et al. 1993; Biegel et al. 2011).

The role of nitrogenase-mediated H<sub>2</sub> production as an electron sink varies depending on the carbon substrate provided to the cells. When *R. sphaeroides* was grown in the presence of glutamate as a nitrogen source, nitrogenase activity (measured as H<sub>2</sub> production) was highest when cells were grown photoheterotrophically on lactate, and lowest when grown on glycerol (Kontur et al. 2011). In addition, an *R. sphaeroides* nitrogenase mutant grows very poorly on a reduced carbon source such as lactate, where nitrogenase activity is presumably important for redox balancing. Meanwhile, the nitrogenase mutant has the same growth rate as the wild type on glycerol, although no H<sub>2</sub> is produced by the mutant (Kontur et al. 2011).

In *R. palustris*, Calvin cycle mutants grow when nitrogenase is active, suggesting that this enzyme plays a substantial role in maintaining cellular redox state in this organism. When wild type *R. palustris* is grown photoheterotrophically on acetate in the absence of nitrogenase activity (i.e., on a preferred nitrogen source), half of reduced electron carriers generated during catabolism are re-oxidized by biosynthetic pathways, and the Calvin cycle re-oxidizes most of the remaining reduced electron carriers (McKinlay and Harwood 2010b). In contrast, when nitrogenase is active, electrons are diverted from the Calvin cycle into H<sub>2</sub> production. Under these conditions, half of the reduced electron carriers are still re-oxidized by biosynthetic pathways, but the Calvin cycle re-oxidizes a smaller fraction of reduced electron carriers (14 %) while nitrogenase activity re-oxidizes the remaining (34 %) reduced electron carriers (McKinlay and Harwood 2010b). The fraction of electrons that are diverted to nitrogenase or the Calvin cycle is regulated at the transcriptional level and depends on the carbon substrate, since transcription of the *R. palustris* Calvin cycle genes depends on the supplied carbon source (McKinlay and Harwood 2010b, 2011). Furthermore, the partitioning of electron flow to nitrogenase in *R. palustris* was influenced by how the carbon substrate was metabolized. Thus, the role of nitrogenase activity in cellular redox

balancing depends on the fraction of electrons diverted away from the Calvin cycle, and how the reductant is produced by carbon metabolism (McKinlay and Harwood 2011).

### C. Other Cytoplasmic Electron Sinks

While the Calvin cycle and nitrogenase are well-documented major electron sinks in PNSB, several others exist. Polyhydroxyalkanoic acids (PHA) are carbon storage polymers, the most common of which is poly- $\beta$ -hydroxybutyrate (PHB). PHB is synthesized in bacteria when carbon and energy, specifically acetyl-CoA and NAD(P)H, are in excess but nitrogen, sulfur, or phosphorous are limiting (Fig. 32.1) (Hustede et al. 1993; Steinbuchel and Fuchtenbusch 1998; Madison and Huisman 1999). *R. sphaeroides* and *R. rubrum* produce the highest levels of PHB when growing photoheterotrophically on acetate (which feeds directly into the PHB pathway), where it can account for 40–70 % of dry cell weight (Hustede et al. 1993; Khatipov et al. 1998). Despite the large contribution of PHB to cell mass, mutant strains defective in PHB synthesis still grow photoheterotrophically on acetate. To compensate for the loss of PHB as an electron sink, these mutants produce significantly more H<sub>2</sub> than wild type cells when grown on acetate under conditions where nitrogenase is active (Hustede et al. 1993). While PHB mutants have been made in a variety of PNSB with the goal of diverting excess reductant towards nitrogenase-mediated H<sub>2</sub> production, these strains show little or no increases in H<sub>2</sub> production as a function of growth conditions (Lee et al. 2002; Franchi et al. 2004; Kim et al. 2006; Yilmaz et al. 2010). The largest differences in H<sub>2</sub> production between wild type and PHB mutants were seen when strains were grown on substrates such as acetate or glucose, which typically result in the highest amount of PHB production in wild-type cells (Hustede et al. 1993; Yilmaz et al. 2010). These results indicate that there are still many unknown aspects of electron partitioning among different pathways in PNSB.

Additionally, photoheterotrophically grown cells will often excrete metabolic intermediates referred to as soluble microbial products (SMP) (Fig. 32.1) (Yilmaz et al. 2010). For example, *R. sphaeroides* grown photoheterotrophically on lactate excreted almost 20 % of the provided carbon in the form of SMP by late stationary phase (Yilmaz et al. 2010). A large fraction of the SMPs are central metabolic intermediates, such as pyruvate, succinate or fumarate (Yilmaz et al. 2010; McKinlay and Harwood 2011). These SMP can be thought of as a way to dissipate excess reducing power, or incompletely oxidized carbon skeletons that are not used to support biosynthetic activity and thereby “lost” to the cells. However, in some cases, a fraction of the SMP are eventually consumed by cells when other nutrients become limiting (McKinlay and Harwood 2011).

#### IV. Recycling Reducing Power Captured in Pyridine Nucleotides

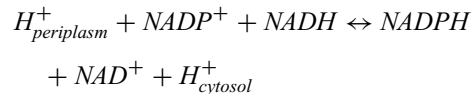
In phototrophic and other cells, biosynthetic reactions oxidize a large fraction of reduced electron carriers. For many anabolic processes, NADPH serves as the electron donor. Below, we discuss the major enzymatic routes of NADPH synthesis in *R. sphaeroides*, and the growth conditions that require these enzymes.

##### A. Role of Transhydrogenases in Maintaining Redox Balance of the Pyridine Nucleotide and Glutathione Pools

NADPH is an important cofactor used as a source of reducing power in a wide array of crucial anabolic processes including the Calvin cycle, fatty acid biosynthesis, and photosynthetic pigment biosynthesis, amongst others (Nelson and Cox 2005). NADPH also plays an important role in cellular resistance to oxidative and other stresses, where it provides reducing equivalents to maintain reduced pools of glutathione,

thioredoxin and other antioxidants (Hickman et al. 2002; Brumaghim et al. 2003). Thus, the NADP<sup>+</sup>:NADPH ratio needs to be tightly controlled for normal cellular function.

Pyridine nucleotide transhydrogenase plays an important role in maintenance of the cellular NAD(P)<sup>+</sup>:NAD(P)H ratios, catalyzing the reversible exchange of reducing equivalents between pyridine nucleotides, NADPH and NADH (Bragg et al. 1972; Rydström et al. 1976; Bragg 1998; Sauer et al. 2004):



Two forms of transhydrogenases have been identified: (i) the energy-dependent membrane-bound pyridine nucleotide (NADH/NADPH) transhydrogenase (PntAB); and (ii) the energy-independent soluble pyridine nucleotide (NADH/NADPH) transhydrogenase (STH or UdhA) (Voor-douw et al. 1983; Sauer et al. 2004). PntAB is a widely-distributed heterotetrameric  $\alpha_2\beta_2$  enzyme complex, which catalyzes a reversible reaction based on the direction or magnitude of the proton gradient across the cytoplasmic membrane (Bragg et al. 1972; Bragg 1998; Cao et al. 2011). On the other hand, STH is a less commonly found flavoprotein (Boonstra et al. 1999; Sauer et al. 2004; Cao et al. 2011). Only a few  $\gamma$ -Proteobacteria, such as *E. coli*, possess both forms of this enzyme (Boonstra et al. 1999; Sauer et al. 2004).

Both PntAB and STH have been extensively studied in *E. coli* by metabolic flux analysis and by analyzing the phenotypes of mutants under different growth conditions (Sauer et al. 2004). PntAB has been shown to typically function in the forward direction (i.e., synthesis of NADPH) and thus its expression is induced when there is a demand for NADPH (Sauer et al. 2004). In *E. coli*, PntAB is required for optimal growth on carbon sources whose metabolism does not directly result in the net production of NADPH, such as glycerol, where PntAB functions to provide the necessary NADPH for biosynthe-



Table 32.1. Growth phenotypes of transhydrogenase deletion strains in *E. coli* and *R. sphaeroides*<sup>a</sup>.

Growth substrate	<i>E. coli</i>		<i>R. sphaeroides</i>	
	$\Delta pntAB$	$\Delta udhA$	$\Delta pntAB$ (photo)	$\Delta pntAB$ (aero)
High NADPH producing (e.g., acetate in <i>E. coli</i> )	++	--	?	?
Moderate NADPH producing (e.g., glucose)	+–	++	++	++
NADPH-neutral (e.g., glycerol or succinate)	+– <sup>b</sup>	++	+– <sup>b</sup>	++
NADPH consuming (e.g., acetate in <i>R. sphaeroides</i> )	?	?	--	+–

<sup>a</sup>Observed growth phenotypes on different categories of carbon sources displayed by  $\Delta pntAB$  deletion strains in *E. coli* and *R. sphaeroides* and a  $\Delta udhA$  deletion strain in *E. coli*. (++) Normal growth rate relative to wild type cells; (+–), reduced growth rate relative to wild type cells; (–), No growth

<sup>b</sup>During growth on NADPH-neutral carbon sources such as glycerol or succinate, a long lag is observed in both *E. coli* and *R. sphaeroides* before growth commences

sis (Table 32.1). Conversely, during growth on substrates whose metabolism results in the production of excess NADPH (such as acetate, which is metabolized via the TCA cycle and glyoxylate shunt), PntAB is not required. Under these conditions, STH expression is induced, and the enzyme catalyzes the conversion of NADPH to NADP<sup>+</sup> with the concomitant production of NADH (Sauer et al. 2004; Lee et al. 2010). STH activity is essential under these conditions, since a *sth* deletion strain is incapable of growth on acetate. Thus, through the use of these two enzymes, *E. coli* is able to maintain NAD(P)<sup>+</sup>:NAD(P)H homeostasis. In addition to PntAB and STH, other enzymes such as glucose-6-phosphate dehydrogenase (Zwf), 6-phosphogluconate dehydrogenase (Gnd) and isocitrate dehydrogenase (Icd) are also known to make significant contributions to the cellular NADPH pool under specific conditions (Sauer et al. 2004; Lee et al. 2010).

### B. PntAB Is Required for Normal Photosynthetic Growth in *Rhodobacter sphaeroides*

In photosynthetic organisms, NADPH has additional roles. In oxygenic phototrophs it provides reducing equivalents required for CO<sub>2</sub> fixation via the Calvin cycle (Allen 2003), and in all phototrophs, including PNSB, NADPH is required for the biosynthesis of tetrapyrroles, photopigments and lipids

of the photosynthetic apparatus. The role of PntAB during anoxygenic phototrophy has been studied in *R. sphaeroides* by assessing the growth phenotypes of deletion mutants and by flux balance analysis (Imam et al. 2013). Unlike *E. coli*, *R. sphaeroides* does not possess a known homolog of STH, so PntAB is likely central to the maintenance of the cellular NAD(P)<sup>+</sup>:NAD(P)H ratios. During photosynthetic growth on substrates whose metabolism results in the net production of NADPH (such as glucose), PntAB is not required for growth (Imam et al. 2013), as NADPH produced through the Zwf reaction is sufficient to support normal photosynthetic growth (Table 32.1). Conversely, during growth on substrates that require a net consumption of NADPH (e.g. acetate metabolized via the ethylmalonyl-CoA pathway) (Alber 2011), PntAB is essential for photosynthetic growth (Imam et al. 2013). During growth with NADPH-neutral carbon sources (i.e. substrates whose metabolism does not result in the net production or consumption of NADPH) such as succinate and most of the carbon sources known to support *R. sphaeroides* growth, the loss of PntAB activity results in a significantly reduced photosynthetic growth rate, indicating that PntAB is needed to produce NADPH under most conditions (Imam et al. 2013).

Under aerobic respiratory conditions, the loss of PntAB activity has much less impact on *R. sphaeroides* (Table 32.1),

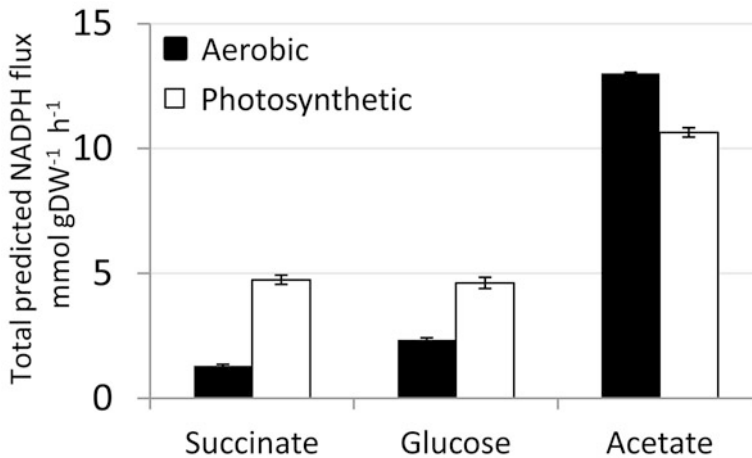


Fig. 32.2. Comparison of the predicted NADPH flux during photosynthetic or aerobic respiratory growth. Predictions were made for the total NADPH flux during growth of *R. sphaeroides* with succinate, glucose or acetate under photosynthetic and aerobic respiratory conditions. The larger predicted NADPH demand under aerobic conditions compared to photosynthetic conditions during growth with acetate is due to a larger predicted uptake rate of acetate under aerobic conditions (Figure adapted from Imam et al. (2013)).

suggesting there is a diminished need for either NADPH or activity of this enzyme under these conditions (Imam et al. 2013). However, it is also possible that other NADPH producing pathways are active aerobically but not photosynthetically. To assess the amount of NADPH required under individual conditions, a genome-scale metabolic model of *R. sphaeroides*, iRsp1095 (Imam et al. 2011), was used to predict the flux through the PntAB reaction in aerobic and photosynthetic cells that use different growth substrates (Fig. 32.2). This analysis indicated that, in general, more NADPH was required for growth under photosynthetic than aerobic conditions, consistent with the observation that the PntAB mutant had more severe growth defects during photosynthetic conditions (Imam et al. 2013).

Interestingly, more NADPH was predicted to be required for aerobic growth on acetate than photosynthetic growth on any other substrate (Fig. 32.2). This prediction was unexpected, as a strain lacking PntAB activity was able to grow aerobically on acetate (Imam et al. 2013). This suggested that alternative routes existed for aerobic NADPH synthesis, which were either not functional or insuffi-

cient to support photosynthetic growth. Indeed, the iRsp1095 model indicated that at least 6 other reactions could potentially contribute to the NADPH pool in *R. sphaeroides* under any growth condition (Table 32.2). Subsequent RNA abundance analysis showed that the genes encoding the enzymes that catalyze some of these reactions were differentially expressed in response to the loss of PntAB activity under aerobic conditions, depending on growth substrate (Table 32.2), suggesting they might function to provide NADPH to compensate for the loss of PntAB (Imam et al. 2013).

### C. *Zwf* Is an Alternative Route for NADPH Synthesis in *Rhodobacter sphaeroides*

The central carbon catabolism enzyme glucose-6-phosphate dehydrogenase (*Zwf*) is one of the alternative routes for NADPH synthesis predicted by the iRsp1095 model to be used by *R. sphaeroides* in the absence of PntAB activity (Table 32.2). iRsp1095 predicts that succinate is converted to glucose-6-phosphate via gluconeogenesis, which could then be metabolized via the Entner-Doudoroff glycolytic pathway,

Table 32.2. Reactions predicted by iRsp1095 to be involved in generation of NADPH in *Rhodobacter sphaeroides*.

Enzyme name	Gene identifier	Reaction catalyzed	EC number	Glucose <sup>a</sup>	Acetate <sup>a</sup>
PntAB	RSP_0239 & RSP_0240	$\text{NADP}^+ + \text{NADH} + 2 \text{H}^+ [\text{p}] \Rightarrow \text{NADPH} + \text{NAD}^+ + 2\text{H}^+$	1.6.1.2		
NADPH-ferredoxin reductase	RSP_1939	Reduced ferredoxin + $\text{NADP}^+ + \text{H}^+ \rightleftharpoons$ Oxidized ferredoxin + NADPH	1.18.1.2		↑
Zwf	RSP_2734	D-Glucose 6-phosphate + $\text{NADP}^+ \rightleftharpoons$ 6PGL + NADPH	1.1.1.49		
Malic enzyme	RSP_1217   RSP_1593	(S)-Malate + $\text{NADP}^+ \Rightarrow$ Pyruvate + $\text{CO}_2$ + NADPH	1.1.1.40	↑	
THF dehydrogenase	RSP_0661	$\text{mlthf} + \text{NADP}^+ \rightleftharpoons$ methf + NADPH	1.5.1.5	↑	
Icd	RSP_0446   RSP_1559	Isocitrate + $\text{NADP}^+ \rightleftharpoons$ 2-Oxoglutarate + $\text{CO}_2$ + NADPH	1.1.1.42	↑	
Glutamate synthase	RSP_1146 & RSP_1149	2L-Glutamate + $\text{NADP}^+ \rightleftharpoons$ L-Glutamine + 2-Oxoglutarate + NADPH + $\text{H}^+$	1.4.1.13		

6PGLD-Glucono-1,5-lactone 6-phosphate

*mlthf* 5,10-Methylenetetrahydrofolate

*THF dehydrogenase* 5,10-methylene-tetrahydrofolate dehydrogenase

<sup>a</sup>Genes differentially expressed in response to the loss of PntAB under aerobic conditions during growth on either glucose or acetate. Upward arrows indicate upregulation

generating NADPH via Zwf. Mutational analysis showed that this route is indeed employed by *R. sphaeroides* under both aerobic and photosynthetic conditions. While loss of either only PntAB or Zwf had little impact on aerobic growth, loss of both PntAB and Zwf resulted in significantly impaired aerobic growth on succinate (Imam et al. 2013). The residual growth of the PntAB and Zwf double deletion strain under aerobic conditions, likely indicates that other alternative NADPH generating reactions might exist under these conditions. Further analysis showed that Zwf also makes a significant contribution to the NADPH pool during photosynthetic growth on succinate. While loss of PntAB resulted

in significantly impaired photosynthetic growth on succinate, loss of both PntAB and Zwf resulted in a complete loss of growth on succinate (Imam et al. 2013).

In sum, these data indicate that PntAB and Zwf are the two major sources of NADPH during photosynthetic growth in *R. sphaeroides*. In addition, it appears that PntAB plays a crucial role in maintenance of NADPH:NADH homeostasis in *R. sphaeroides* and possibly other phototrophic bacteria, with added importance under photosynthetic conditions. As is the case in other well-studied bacteria, PntAB appears to generally function in the direction of NADPH production in *R. sphaeroides*.

Conditions of excess NADPH production have yet to be assessed in *R. sphaeroides*, but given its lack of a STH homolog, such conditions could be detrimental as the NADPH pool would become over-reduced. However, experiments to search for alternative reactions or pathways that could recycle excess NADPH have yet to be performed.

## V. Modeling the Metabolism of Photosynthetic Organisms

As highlighted in the previous sections, computational models of metabolism can play an important role in guiding the analysis of metabolism and electron flow through one or more pathways. By considering the genes, proteins, reactions and metabolites involved in individual pathways or the entire metabolic network of an organism, models have been used to make accurate qualitative and quantitative predictions about outcomes of growth conditions and genetic perturbations, which have led to novel discoveries and strategies for strain improvements (Oberhardt et al. 2009; McCloskey et al. 2013). Many approaches are utilized for modeling of cellular metabolism, including kinetic (Schallau and Junker 2010), ensemble (Tran et al. 2008; Tan and Liao 2012) and constraint-based (Varma and Palsson 1994; Palsson 2000) models. In recent years, constraint-based models (CBMs) have found widespread use.

### A. Constraint-Based Modeling

Constraint-based modeling assumes that the flux of metabolites through a network at steady state is dependent on enzyme capacity, the stoichiometry of the reactions that make up the network, and their inherent thermodynamic constraints (Varma and Palsson 1994; Palsson 2000). As a consequence, constraint-based modeling bypasses the need for kinetic parameters, which are often difficult to obtain. Simulations can be carried out with CBMs using flux balance analysis (FBA)

(Varma and Palsson 1994) and related approaches, which can be used to make experimentally testable qualitative or quantitative predictions about growth rates, phenotypes, electron flow, flux distributions and production rates of specific metabolites.

### B. Constraint-Based Models for Photosynthetic Organisms

Manually curated genome-scale CBMs have recently been constructed and applied for analysis of several photosynthetic bacteria, including *R. sphaeroides*. An initial genome-scale CBM for *R. sphaeroides* (iRsp1095) was later refined using high-throughput phenotypic data to generate a larger, more comprehensive model called iRsp1140, which accounts for 1140 genes (~26 % of the *R. sphaeroides* genome) and includes 1416 reactions and 878 metabolites (Imam et al. 2013). iRsp1095 and iRsp1140 have been used to study the various *R. sphaeroides* lifestyles, analyze its metabolic capabilities, predict the fate of gene deletions, study H<sub>2</sub> production and electron transport, identify alternative electron sinks, as well as general analysis of the metabolic network structure (Imam et al. 2011, 2013). Recently, the impact of light intensity on steady state photosynthetic growth has been used to extend and improve the modeling of photosynthetic growth in *R. sphaeroides* (Imam et al. 2015a).

Other photosynthetic organisms for which manually curated genome-scale CBMs have been reconstructed include: *Synechocystis* sp. PCC 6803 (Fu 2008; Montagud et al. 2010), *Cyanothece* sp. ATCC 51142 (Vu et al. 2012), *Dinoroseobacter shibae* DFL12T (Rex et al. 2013), *Chlamydomonas reinhardtii* (Chang et al. 2011), *Arabidopsis thaliana* (Poolman et al. 2009; de Oliveira Dal'Molin et al. 2010; Saha et al. 2011), *Zea mays* (Dal'Molin et al. 2010; Saha et al. 2011), and *Oryza sativa* (Poolman et al. 2013). These models have guided research in a variety of ways, including predicting the effects of gene deletions during photosynthetic growth and predicting

the flux of carbon and electrons during photosynthetic growth.

### C. Challenges for Metabolic Modeling of Photosynthetic Cells

CBMs for photosynthetic organisms appeared initially in ~2009, and have not yet undergone the sort of extensive refinements seen for models of non-phototrophic bacteria (e.g. *E. coli*). However, improving computational tools for genome annotation and automated network reconstruction are speeding up the process of CBM reconstruction and refinement (Overbeek et al. 2005; Aziz et al. 2008; Henry et al. 2010).

A unique challenge of constraint-based modeling in photosynthetic organisms is the measurement of the amount of light used by the cell. Given that a significant amount of exogenous light can be reflected or dissipated as heat, measurement of this parameter can prove difficult. In addition, the light source used can also impact cell growth and modeling predictions. To accurately measure light uptake in *Cyanothece*, custom photobioreactors were built that allowed quantitative measurements of incident and transmitted light, and provided light sources of the specific wavelengths used by the *Cyanothece* photosystems (Vu et al. 2012). Using these bioreactors, they were able to accurately measure light uptake for *Cyanothece* sp. ATCC 51142 and used it as a modeling constraint to study how incident light affects growth rate. In another attempt to quantitatively use supplied light in modeling, one study (Chang et al. 2011) developed a novel approach for modeling light emitted by different sources. These so called “prism reactions” enable decomposition of different light sources into wavelength ranges that correspond to the optimal absorption wavelength ranges of the various light utilizing reactions in *C. reinhardtii*. Thereby photons of different wavelength ranges supplied by a given light source can be apportioned to the different light utilizing components (e.g. photosystems) that can absorb them. Using

this approach, researchers were able to model *C. reinhardtii* growth on 11 different light sources, including light emitting diodes, solar, incandescent and fluorescent light sources (Chang et al. 2011). Future experimental and computational developments should further improve our ability to model light uptake in photosynthetic organisms.

### D. Metabolic Modeling as a Tool for Rational Design of Photosynthetic Organisms

Many photosynthetic microbes are metabolically versatile and naturally capable of producing compounds of socio-economic value. For instance, *R. sphaeroides* is capable of producing large amounts of H<sub>2</sub> gas (Mackenzie et al. 2007; Yilmaz et al. 2010; Imam et al. 2011). Further, given its ability to increase membrane synthesis, *R. sphaeroides* also produces more ubiquinone (Lu et al. 2015), fatty acids or membrane lipids per cell than many other bacteria (Kien et al. 2010; Lemmer-Christensen et al. 2015), which can serve as a biocommodity (Khan et al. 2015), pharmaceutical (Lemke et al. 2014), or food supplement (Kien et al. 2010). *R. sphaeroides* and several other species of PNSB also have the native ability to accumulate PHB, which can be used in the manufacture of biodegradable plastics (Khatipov et al. 1999). However, significant genetic, genomic or synthetic biology improvements in the capabilities of these organisms to produce these value-added commodities will be required before they can have an economic impact (Jaschke et al. 2011; Desai and Atsumi 2013; Tikh et al. 2014).

In this regard, another important application of CBMs is in the development of strategies for improving the performance of photosynthetic systems. These strategies could involve genetic changes to remove or add genes or reactions to the metabolic network. Approaches such as FBA, minimization of metabolic adjustment (MOMA) (Segre et al. 2002) and regulatory on/off minimization of metabolic flux changes (ROOM) (Shlomi et al. 2005) have been used to make

predictions of the effects of genetic perturbations to metabolic flux distributions in non-phototrophs (Alper et al. 2005; Park et al. 2007). In addition, several other approaches have been developed specifically geared towards strain optimization for improving metabolite production such as optknock (Burgard et al. 2003), optGene (Patil et al. 2005), optORF (Kim and Reed 2010), and optStrain (Pharkya et al. 2004), which have been used with varying levels of success. Recent efforts have been able to produce transcriptional regulatory network models that can predict previously unidentified genes that are involved in the low oxygen, photosynthetic, central carbon and other major pathways of PNSB (Imam et al. 2014, 2015b, c). In addition to providing new insight into these important transcriptional regulatory networks, they illustrate the need to integrate these predictions into CBMs. Despite their potential to improve performance of photosynthetic systems, to date, these modeling strategies have yet to be successfully applied or combined in any phototroph. As CBMs and transcriptional network models for phototrophs become more detailed and improve in their predictive accuracy, one would expect that these approaches and others developed in the future will prove to be successful for improving desired traits and production capabilities in PNSB.

## VI. Concluding Remarks and Future Directions

The analysis of PNSB and other photosynthetic bacteria has provided unique insights into photochemistry, bioenergetics, the assimilation of atmospheric nutrients ( $N_2$  and  $CO_2$ ) and the production of compounds of industrial value (Blankenship et al. 1995; Meyer and Donohue 1995; Blankenship and Hartman 1998; Steinbuchel and Fuchtenbusch 1998; Dubbs and Tabita 2004; Gest and Blankenship 2004; Kien et al. 2010; McKinlay and Harwood 2010a; Kontur et al. 2012a). Each of the above areas has in common the production or use of electrons. Despite the wealth of

biochemical and mechanistic information on individual pathways or processes that are summarized in studies cited in this and other chapters in this volume, there are still many unanswered questions about the coordination of electron partitioning within and between different pathways in photosynthetic and other organisms. Future analyses of PNSB and other photosynthetic bacteria have the ability to provide such knowledge about the pathways used for electron partitioning under different conditions.

Our ability to globally understand how cells divert electrons among different pathways is challenged by the number of membrane bound or soluble enzymes or electron carriers that can be present under given metabolic conditions (e.g. photosynthetic, respiratory, aerobic, or anaerobic). Despite this complexity, the integration of genomic and modeling approaches with traditional biochemical, genetic and physiological tools has the ability to predict, test and provide new and important insights into electron partitioning by photosynthetic organisms. Obtaining such a systems-level understanding can allow us to increase the utility of photosynthetic organisms for the production of food, fuel and other products of societal importance in the twenty-first Century.

## Acknowledgements

The analysis of electron partitioning in the author's lab has recently been funded by grants from the Department of Energy, Office of Science, Great Lakes Bioenergy Research Center (DE-FC02-07ER64494), the Genomics:GTL and SciDAC Programs (DE-FG02-04ER25627) and the National Institutes of General Medical Sciences (GM075273). SI was supported during part of this work by a William H. Peterson Predoctoral Fellowship from the University of Wisconsin-Madison Bacteriology Department. MAS was supported during part of this work by a traineeship from the NIH Biotechnology Training Program grant 5T32 GM08349.

## References

- Alber BE (2011) Biotechnological potential of the ethylmalonyl-CoA pathway. *Appl Microbiol Biotechnol* 89:17–25
- Allen JF (2003) Cyclic, pseudocyclic and noncyclic photophosphorylation: new links in the chain. *Trends Plant Sci* 8:15–19
- Alper H, Jin YS, Moxley JF, Stephanopoulos G (2005) Identifying gene targets for the metabolic engineering of lycopene biosynthesis in *Escherichia coli*. *Metab Eng* 7:155–164
- Andreae MO (1980) Dimethylsulfoxide in marine and fresh waters. *Limnol Oceanogr* 25:1054–1063
- Anthony C (2004) The quinoprotein dehydrogenases for methanol and glucose. *Arch Biochem Biophys* 428:2–9
- Arai H, Roh JH, Kaplan S (2008) Transcriptome dynamics during the transition from anaerobic photosynthesis to aerobic respiration in *Rhodobacter sphaeroides* 2.4.1. *J Bacteriol* 190:286–299
- Aziz RK, Bartels D, Best AA, DeJongh M, Disz T, Edwards RA, Formisano K, ... Zagnitko O (2008) The RAST server: rapid annotations using subsystems technology. *BMC Genomics* 9:75
- Bartsch RG, Ambler RP, Meyer TE, Cusanovich MA (1989) Effect of aerobic growth conditions on the soluble cytochrome content of the purple phototrophic bacterium *Rhodobacter sphaeroides*: induction of cytochrome *c*<sub>554</sub>. *Arch Biochem Biophys* 271:433–440
- Battchikova N, Eisenhut M, Aro EM (2011) Cyanobacterial NDH-1 complexes: novel insights and remaining puzzles. *BBA-Bioenergetics* 1807: 935–944
- Berghoff BA, Konzer A, Mank NN, Looso M, Rische T, Förstner KU, Krüger M, ... Klug G (2013) Integrative “Omics”-approach discovers dynamic and regulatory features of bacterial stress responses. *PLoS Genet* 9: e1003576
- Biegel E, Schmidt S, Gonzalez JM, Muller V (2011) Biochemistry, evolution and physiological function of the Rnf complex, a novel ion-motive electron transport complex in prokaryotes. *Cell Mol Life Sci* 68:613–634
- Blankenship RE, Hartman H (1998) The origin and evolution of oxygenic photosynthesis. *Trends Biochem Sci* 23:94–97
- Blankenship RE, Madigan MT, Bauer CE (1995) *Anoxygenic Photosynthetic Bacteria*. Kluwer Academic, Boston
- Boonstra B, French CE, Wainwright I, Bruce NC (1999) The *udhA* gene of *Escherichia coli* encodes a soluble pyridine nucleotide transhydrogenase. *J Bacteriol* 181:1030–1034
- Bragg PD (1998) Site-directed mutagenesis of the proton-pumping pyridine nucleotide transhydrogenase of *Escherichia coli*. *Biochim Biophys Acta* 1365:98–104
- Bragg PD, Davies PL, Hou C (1972) Function of energy-dependent transhydrogenase in *Escherichia coli*. *Biochem Biophys Res Commun* 47: 1248–1255
- Brumaghim JL, Li Y, Henle E, Linn S (2003) Effects of hydrogen peroxide upon nicotinamide nucleotide metabolism in *Escherichia coli*: changes in enzyme levels and nicotinamide nucleotide pools and studies of the oxidation of NAD(P)H by Fe(III). *J Biol Chem* 278:42495–42504
- Bryant DA, Frigaard NU (2006) Prokaryotic photosynthesis and phototrophy illuminated. *Trends Microbiol* 14:488–496
- Burgard AP, Parkya P, Maranas CD (2003) OptKnock: a bilevel programming framework for identifying gene knockout strategies for microbial strain optimization. *Biotechnol Bioeng* 84:647–657
- Callister SJ, Nicora CD, Zeng XH, Roh JH, Dominguez MA, Tavano CL, Monroe ME, ... Lipton MS (2006) Comparison of aerobic and photosynthetic *Rhodobacter sphaeroides* 2.4.1 proteomes. *J Microbiol Meth* 67:424–436
- Cao Z, Song P, Xu Q, Su R, Zhu G (2011) Overexpression and biochemical characterization of soluble pyridine nucleotide transhydrogenase from *Escherichia coli*. *Fems Microbiol Lett* 320:9–14
- Chang RL, Ghamsari L, Manichaikul A, Hom EF, Balaji S, Fu W, Shen Y, ... Papin JA (2011) Metabolic network reconstruction of *Chlamydomonas* offers insight into light-driven algal metabolism. *Mol Syst Biol* 7:518
- Cozier GE, Salleh RA, Anthony C (1999) Characterization of the membrane quinoprotein glucose dehydrogenase from *Escherichia coli* and characterization of a site-directed mutant in which histidine-262 has been changed to tyrosine. *Biochem J* 340:639–647
- Dal’Molin CG, Quek LE, Palfreyman RW, Brumbley SM, Nielsen LK (2010) C4GEM, a genome-scale metabolic model to study C4 plant metabolism. *Plant Physiol* 154:1871–1885
- de Oliveira Dal’Molin CG, Quek LE, Palfreyman RW, Brumbley SM, Nielsen LK (2010) AraGEM, a genome-scale reconstruction of the primary metabolic network in *Arabidopsis*. *Plant Physiol* 152:579–589
- Desai SH, Atsumi S (2013) Photosynthetic approaches to chemical biotechnology. *Curr Opin Biotech* 24:1031–1036
- Dischert V, Vignais PM, Colbeau A (1999) The synthesis of *Rhodobacter capsulatus* HupSL hydrogenase

- is regulated by the two-component HupT/HupR system. *Mol Microbiol* 34:995–1006
- Donohue TJ, Kaplan S (1991) Genetic techniques in *Rhodospirillaceae*. *Methods Enzymol* 204: 459–485
- Donohue TJ, Kiley PJ (2010) Bacterial responses to O<sub>2</sub> limitation. In: Storz G, Hengge R (eds) *Bacterial Stress Responses*. American Society for Microbiology, Washington, DC, pp 175–189
- Dubbs JM, Tabita RF (2004) Regulators of nonsulfur purple phototrophic bacteria and the interactive control of CO<sub>2</sub> assimilation, nitrogen fixation, hydrogen metabolism and energy generation. *FEMS Microbiol Rev* 28:353–376
- Dupuis A, Peinnequin A, Darrouzet E, Lunardi J (1997) Genetic disruption of the respiratory NADH-ubiquinone reductase of *Rhodobacter capsulatus* leads to an unexpected photosynthesis-negative phenotype. *Fems Microbiol Lett* 148:107–114
- Elsen S, Dischert W, Colbeau A, Bauer CE (2000) Expression of uptake hydrogenase and molybdenum nitrogenase in *Rhodobacter capsulatus* is coregulated by the RegB-RegA two-component regulatory system. *J Bacteriol* 182:2831–2837
- Elsen S, Swem LR, Swem DL, Bauer CE (2004) RegB/RegA, a highly conserved redox-responding global two-component regulatory system. *Microbiol Mol Biol Rev* 68:263–279
- Franchi E, Tosi C, Scolla G, Della Penna G, Rodriguez F, Pedroni PM (2004) Metabolically engineered *Rhodobacter sphaeroides* RV strains for improved biohydrogen photoproduction combined with disposal of food wastes. *Mar Biotechnol* 6:552–565
- Fu P (2008) Genome-scale modeling of *Synechocystis* sp. PCC 6803 and prediction of pathway insertion. *J Chem Technol Biotechnol* 84:473–483
- Gavira M, Roldan MD, Castillo F, Moreno-Vivian C (2002) Regulation of *nap* gene expression and periplasmic nitrate reductase activity in the phototrophic bacterium *Rhodobacter sphaeroides* DSM158. *J Bacteriol* 184:1693–1702
- Gest H, Blankenship R (2004) Time line of discoveries: anoxygenic bacterial photosynthesis. *Photosynth Res* 80:59–70
- Gest H, Kamen H (1949) Photoproduction of molecular hydrogen by *Rhodospirillum rubrum*. *Science* 109:558–559
- Gibb SW, Hatton AD (2004) The occurrence and distribution of trimethylamine-N-oxide in Antarctic coastal waters. *Mar Chem* 91:65–75
- Hallenbeck PC, Benemann JR (2002) Biological hydrogen production; fundamentals and limiting processes. *Int J Hydrog Energy* 27:1185–1193
- Hallenbeck PL, Lerchen R, Hessler P, Kaplan S (1990) Roles of CfxA, CfxB, and external electron acceptors in regulation of Ribulose 1,5-Bisphosphate Carboxylase Oxygenase expression in *Rhodobacter sphaeroides*. *J Bacteriol* 172:1736–1748
- Henry CS, DeJongh M, Best AA, Frybarger PM, Linsay B, Stevens RL (2010) High-throughput generation, optimization and analysis of genome-scale metabolic models. *Nat Biotechnol* 28: 977–982
- Herter SM, Kortluke CM, Drews G (1998) Complex I of *Rhodobacter capsulatus* and its role in reverted electron transport. *Arch Microbiol* 169:98–105
- Hickman JW, Barber RD, Skaar EP, Donohue TJ (2002) Link between the membrane-bound pyridine nucleotide transhydrogenase and glutathione-dependent processes in *Rhodobacter sphaeroides*. *J Bacteriol* 184:400–409
- Husted E, Steinbuchel A, Schlegel HG (1993) Relationship between the photoproduction of hydrogen and the accumulation of PHB in nonsulfur purple bacteria. *Appl Microbiol Biotechnol* 39: 87–93
- Imam S, Yilmaz S, Sohmen U, Gorzalski AS, Reed JL, Noguera DR, Donohue TJ (2011) iRsp1095: a genome-scale reconstruction of the *Rhodobacter sphaeroides* metabolic network. *BMC Syst Biol* 5:116
- Imam S, Noguera DR, Donohue TJ (2013) Global insights into energetic and metabolic networks in *Rhodobacter sphaeroides*. *BMC Syst Biol* 7:89
- Imam S, Noguera DR, Donohue TJ (2014) Global analysis of photosynthesis transcriptional regulatory networks. *PLoS Genet* 10:e1004837
- Imam S, Fitzgerald CM, Cook EM, Donohue TJ, Noguera DR (2015a) Quantifying the effects of light intensity on bioproduction and maintenance energy during photosynthesis. *Photosynth Res* 123:167–182
- Imam S, Noguera DR, Donohue TJ (2015b) An integrated approach to reconstructing genome-scale transcriptional regulatory networks. *PLoS Comput Biol* 11:e1004103
- Imam S, Noguera DR, Donohue TJ (2015c) CceR and AkgR regulate central carbon and energy metabolism in alphaproteobacteria. *Mbio* 6:02461–02464
- Jaschke PR, Saer RG, Noll S, Beatty JT (2011) Modification of the genome of *Rhodobacter sphaeroides* and construction of synthetic operons. *Methods in Enzymology*. In: *Synthetic Biology, Methods for Part/Device Characterization and Chassis Engineering, Part A*, vol 497. Elsevier, San Diego, pp 519–538
- Jouanneau Y, Meyer C, Naud I, Klipp W (1995) Characterization of an Fdxn mutant of *Rhodobacter capsulatus* indicates that Ferredoxin I serves as electron donor to nitrogenase. *BBA-Bioenergetics* 1232:33–42



- Kars G, Gunduz U, Rakhely G, Yucel M, Eroglu I, Kovacs KL (2008) Improved hydrogen production by uptake hydrogenase deficient mutant strain of *Rhodobacter sphaeroides* OU001. *Int J Hydrog Energy* 33:3056–3060
- Kern M, Klipp W, Klemme JH (1994) Increased nitrogenase-dependent H<sub>2</sub> photoproduction by Hup mutants of *Rhodospirillum rubrum*. *Appl Environ Microbiol* 60:1768–1774
- Khan N, Nybo SE, Chappell J, Curtis WR (2015) Triterpene hydrocarbon production engineered into a metabolically versatile host – rhodobacter capsulatus. *Biotechnol Bioeng*. doi:10.1002/bit.25573
- Khatipov E, Miyake M, Miyake J, Asada Y (1998) Accumulation of poly-beta-hydroxybutyrate by *Rhodobacter sphaeroides* on various carbon and nitrogen substrates. *Fems Microbiol Lett* 162: 39–45
- Khatipov E, Miyake M, Miyake J, Asada Y (1999) Polyhydroxybutyrate accumulation and hydrogen evolution by *Rhodobacter sphaeroides* as a function of nitrogen availability. *Biohydrogen III*: 157–161
- Kien NB, Kong IS, Lee MG, Kim JK (2010) Coenzyme Q<sub>10</sub> production in a 150-l reactor by a mutant strain of *Rhodobacter sphaeroides*. *J Ind Microbiol Biotechnol* 37:521–529
- Kim J, Reed JL (2010) OptORF: optimal metabolic and regulatory perturbations for metabolic engineering of microbial strains. *BMC Syst Biol* 4:53
- Kim MS, Baek JS, Lee JK (2006) Comparison of H<sub>2</sub> accumulation by *Rhodobacter sphaeroides* KD131 and its uptake hydrogenase and PHB synthase deficient mutant. *Int J Hydrog Energy* 31: 121–127
- Kontur WS, Ziegelhoffer EC, Spero MA, Imam S, Noguera DR, Donohue TJ (2011) Pathways involved in reductant distribution during photobiological H<sub>2</sub> production by *Rhodobacter sphaeroides*. *Appl Environ Microbiol* 77:7425–7429
- Kontur WS, Noguera DR, Donohue TJ (2012a) Maximizing reductant flow into microbial H<sub>2</sub> production. *Curr Opin Biotechnol* 23:1–8
- Kontur WS, Shackwitz W, Ivanova N, Martin J, LaButti K, Deshpande S, Tice HN, ... Donohue TJ (2012b) Revised sequence and annotation of the *Rhodobacter sphaeroides* 2.4.1 genome. *J Bacteriol* 194:7016–7017
- Laguna R, Tabita FR, Alber BE (2011) Acetate-dependent photoheterotrophic growth and the differential requirement for the Calvin-Benson-Bassham reductive pentose phosphate cycle in *Rhodobacter sphaeroides* and *Rhodopseudomonas palustris*. *Arch Microbiol* 193:151–154
- Laratta WP, Choi PS, Tosques IE, Shapleigh JP (2002) Involvement of the PrrB/PrrA two-component system in nitrite respiration in *Rhodobacter sphaeroides* 2.4.3: evidence for transcriptional regulation. *J Bacteriol* 184:3521–3529
- Larimer FW, Chain P, Hauser L, Lamerdin J, Malfatti S, Do L, Land ML, ... Harwood CS (2004) Complete genome sequence of the metabolically versatile photosynthetic bacterium *Rhodopseudomonas palustris*. *Nat Biotechnol* 22:55–61
- Lee IH, Park JY, Kho DH, Kim MS, Lee JK (2002) Reductive effect of H<sub>2</sub> uptake and poly-beta-hydroxybutyrate formation on nitrogenase-mediated H<sub>2</sub> accumulation of *Rhodobacter sphaeroides* according to light intensity. *Appl Microbiol Biotechnol* 60:147–153
- Lee HC, Kim JS, Jang W, Kim SY (2010) High NADPH/NADP<sup>+</sup> ratio improves thymidine production by a metabolically engineered *Escherichia coli* strain. *J Biotechnol* 149:24–32
- Lemke RAS, Peterson AC, Ziegelhoffer EC, Westphall MS, Tjellström H, Coon JJ, Donohue TJ (2014) Synthesis and scavenging role of furan fatty acids. *Proc Natl Acad Sci USA* 111:E3450–E3457
- Lemmer-Christensen KC, Dohnalkova A, Noguera DR, Donohue TJ (2015) Oxygen-dependent regulation of bacterial lipid production. *J Bacteriol* 197:1649–1658
- Lu W, Ye L, Lv X, Xie W, Gu J, Chen Z, Zhu Y, ... Yu H (2015) Identification and elimination of metabolic bottlenecks in the quinone modification pathway for enhanced coenzyme Q<sub>10</sub> production in *Rhodobacter sphaeroides*. *Metab Eng* 29:208–216
- Mackenzie C, Eraso JM, Choudhary M, Roh JH, Zeng X, Bruscella P, Puskás A, ... Kaplan S (2007) Postgenomic adventures with *Rhodobacter sphaeroides*. *Annu Rev Microbiol* 61: 283–307
- Madison LL, Huisman GW (1999) Metabolic engineering of poly(3-hydroxyalkanoates): from DNA to plastic. *Microbiol Mol Biol R* 63:21–53
- McCloskey D, Palsson BO, Feist AM (2013) Basic and applied uses of genome-scale metabolic network reconstructions of *Escherichia coli*. *Mol Syst Biol* 9:661
- McEwan AG (1994) Photosynthetic electron transport and anaerobic metabolism in purple nonsulfur phototrophic bacteria. *Anton Leeuw Int J G* 66:151–164
- McEwan AG, Ferguson SJ, Jackson JB (1983) Electron flow to dimethylsulfoxide or trimethylamine-N-oxide generates a membrane potential in *Rhodopseudomonas capsulata*. *Arch Microbiol* 136:300–305

- McEwan AG, Wetzstein HG, Ferguson SJ, Jackson JB (1985) Periplasmic location of the terminal reductase in trimethylamine N oxide and dimethylsulfoxide respiration in the photosynthetic bacterium *Rhodospseudomonas capsulata*. *Biochim Biophys Acta* 806:410–417
- McEwan AG, Richardson DJ, Hudig H, Ferguson SJ, Jackson JB (1989) Identification of cytochromes involved in electron transport to trimethylamine N oxide dimethylsulfoxide reductase in *Rhodobacter capsulatus*. *Biochim Biophys Acta* 973:308–314
- McKinlay JB, Harwood CS (2010a) Photobiological production of hydrogen gas as a biofuel. *Curr Opin Biotechnol* 21:244–251
- McKinlay JB, Harwood CS (2010b) Carbon dioxide fixation as a central redox cofactor recycling mechanism in bacteria. *Proc Natl Acad Sci USA* 107:11669–11675
- McKinlay JB, Harwood CS (2011) Calvin cycle flux, pathway constraints, and substrate oxidation state together determine the H<sub>2</sub> biofuel yield in photoheterotrophic bacteria. *Mbio* 2:e00323–00310
- Meyer TE, Cusanovich MA (1985) Soluble cytochrome composition of the purple phototrophic bacterium, *Rhodospseudomonas sphaeroides* ATCC 17023. *Biochim Biophys Acta* 807:308–319
- Meyer TE, Donohue TJ (1995) Cytochromes, iron-sulfur and copper proteins mediating electron transfer from the cytochrome *bc*<sub>1</sub> complex to photosynthetic reaction center complexes. In: Blankenship RE, Madigan MT, Madigan EBC (eds) *Anoxygenic Photosynthetic Bacteria: Advances in Photosynthesis*. Kluwer Academic, Dordrecht, pp 725–745
- Michalski WP, Nicholas DJD (1988) Identification of 2 new denitrifying strains of *Rhodobacter sphaeroides*. *Fems Microbiol Lett* 52:239–244
- Montagud A, Navarro E, Fernandez de Cordoba P, Urchueguia JF, Patil KR (2010) Reconstruction and analysis of genome-scale metabolic model of a photosynthetic bacterium. *BMC Syst Biol* 4: 156
- Mouncey NJ, Kaplan S (1998) Cascade regulation of dimethyl sulfoxide reductase (*dor*) gene expression in the facultative phototroph *Rhodobacter sphaeroides* 2.4.1(T). *J Bacteriol* 180:2924–2930
- Mouncey NJ, Choudhary M, Kaplan S (1997) Characterization of genes encoding dimethyl sulfoxide reductase of *Rhodobacter sphaeroides* 2.4.1(T): an essential metabolic gene function encoded on chromosome II. *J Bacteriol* 179:7617–7624
- Nelson DL, Cox MM (2005) *Lehninger: Principles of Biochemistry*. W. H. Freeman and Company, New York
- Oberhardt MA, Palsson BO, Papin JA (2009) Applications of genome-scale metabolic reconstructions. *Mol Syst Biol* 5:320
- Oh JI, Ko IJ, Kaplan S (2004) Reconstitution of the *Rhodobacter sphaeroides* *ccb*<sub>3</sub>-PrrBA signal transduction pathway *in vitro*. *Biochemistry* 43:7915–7923
- Overbeek R, Begley T, Butler RM, Choudhuri JV, Chuang HY, Cohoon M, de Crécy-Lagard V, . . . Vonstein V (2005) The subsystems approach to genome annotation and its use in the project to annotate 1000 genomes. *Nucleic Acids Res* 33:5691–5702
- Palsson B (2000) The challenges of *in silico* biology. *Nat Biotechnol* 18:1147–1150
- Paoli GC, Vichivanives P, Tabita FR (1998) Physiological control and regulation of the *Rhodobacter capsulatus* *ccb* operons. *J Bacteriol* 180: 4258–4269
- Park JH, Lee KH, Kim TY, Lee SY (2007) Metabolic engineering of *Escherichia coli* for the production of L-valine based on transcriptome analysis and *in silico* gene knockout simulation. *Proc Natl Acad Sci USA* 104:7797–7802
- Patil KR, Rocha I, Forster J, Nielsen J (2005) Evolutionary programming as a platform for *in silico* metabolic engineering. *BMC Bioinforma* 6:308
- Pharkya P, Burgard AP, Maranas CD (2004) Opt-Strain: a computational framework for redesign of microbial production systems. *Genome Res* 14:2367–2376
- Poolman MG, Miguet L, Sweetlove LJ, Fell DA (2009) A genome-scale metabolic model of *Arabidopsis* and some of its properties. *Plant Physiol* 151:1570–1581
- Poolman MG, Kundu S, Shaw R, Fell DA (2013) Responses to light intensity in a genome-scale model of rice metabolism. *Plant Physiol* 162:1060–1072
- Porte F, Vignais PM (1980) Electron transport chain and energy transduction in *Paracoccus denitrificans* under autotrophic growth conditions. *Arch Microbiol* 127:1–10
- Rex R, Bill N, Schmidt-Hohagen K, Schomburg D (2013) Swimming in light: a large-scale computational analysis of the metabolism of *Dinoroseobacter shibae*. *PLoS Comput Biol* 9:e1003224
- Rey FE, Oda Y, Harwood CS (2006) Regulation of uptake hydrogenase and effects of hydrogen utilization on gene expression in *Rhodospseudomonas palustris*. *J Bacteriol* 188:6143–6152
- Richardson DJ, King GF, Kelly DJ, McEwan AG, Ferguson SJ, Jackson JB (1988) The role of auxiliary oxidants in maintaining redox balance during phototrophic growth of *Rhodobacter capsulatus* on propionate or butyrate. *Arch Microbiol* 150:131–137
- Richardson DJ, Berks BC, Russell DA, Spiro S, Taylor CJ (2001) Functional, biochemical and genetic diversity of prokaryotic nitrate reductases. *Cell Mol Life Sci* 58:165–178

- Rydström J, Hoek JB, Ernster L (1976) Nicotinamide Nucleotide Transhydrogenases. Academic, New York
- Saha R, Suthers PF, Maranas CD (2011) *Zea mays* iRS1563: a comprehensive genome-scale metabolic reconstruction of maize metabolism. *PLoS ONE* 6:e21784
- Sauer U, Canonaco F, Heri S, Perrenoud A, Fischer E (2004) The soluble and membrane-bound transhydrogenases UdhA and PntAB have divergent functions in NADPH metabolism of *Escherichia coli*. *J Biol Chem* 279:6613–6619
- Schallau K, Junker BH (2010) Simulating plant metabolic pathways with enzyme-kinetic models. *Plant Physiol* 152:1763–1771
- Schmehl M, Jahn A, Vilsendorf AMZ, Hennecke S, Masepohl B, Schuppler M, Marxer M, . . . Klipp W (1993) Identification of a new class of nitrogen fixation genes in *Rhodobacter capsulatus* – a putative membrane complex involved in electron transport to nitrogenase. *Mol Gen Genet* 241:602–615
- Segre D, Vitkup D, Church GM (2002) Analysis of optimality in natural and perturbed metabolic networks. *Proc Natl Acad Sci USA* 99: 15112–15117
- Shapleigh JP (2006) The denitrifying prokaryotes. In: *Prokaryotes: A Handbook on the Biology of Bacteria*, vol 2, 3rd edn. Springer-Verlag, New York, pp 769–792
- Shapleigh JP (2009) Dissimilatory and assimilatory nitrate reduction in the purple photosynthetic bacteria. In: Neil Hunter C, Daldal F, Thurnauer MC, Thomas Beatty J (eds) *The Purple Phototrophic Bacteria*. Springer, Dordrecht
- Shaw AL, Hochkoeppler A, Bonora P, Zannoni D, Hanson GR, McEwan AG (1999) Characterization of DorC from *Rhodobacter capsulatus*, a c-type cytochrome involved in electron transfer to dimethyl sulfoxide reductase. *J Biol Chem* 274:9911–9914
- Shimomura Y, Kakuta Y, Fukuyama K (2003) Crystal structures of the quinone oxidoreductase from *Thermus thermophilus* HB8 and its complex with NADPH: implication for NADPH and substrate recognition. *J Bacteriol* 185:4211–4218
- Shlomi T, Berkman O, Ruppin E (2005) Regulatory on/off minimization of metabolic flux changes after genetic perturbations. *Proc Natl Acad Sci USA* 102:7695–7700
- Spero MA, Aylward FO, Currie CR, Donohue TJ (2015) Phylogenomic analysis and predicted physiological role of the proton-translocating NADH: quinone oxidoreductase (complex I) across bacteria. *Mbio* 6:e00389–00315
- Steinbuchel A, Fuchtenbusch B (1998) Bacterial and other biological systems for polyester production. *Trends Biotechnol* 16:419–427
- Swem LR, Gong X, Yu CA, Bauer CE (2006) Identification of a ubiquinone-binding site that affects autophosphorylation of the sensor kinase RegB. *J Biol Chem* 281:6768–6775
- Tan Y, Liao JC (2012) Metabolic ensemble modeling for strain engineers. *Biotechnol J* 7:343–353
- Tavano CL, Donohue TJ (2006) Development of the bacterial photosynthetic apparatus. *Curr Opin Microbiol* 9:625–631
- Tavano CL, Comolli JC, Donohue TJ (2004) The role of *dor* gene products in controlling the P2 promoter of the cytochrome  $c_2$  gene, *cycA*, in *Rhodobacter sphaeroides*. *Microbiology* 150:1893–1899
- Tavano CL, Podevels AM, Donohue TJ (2005) Identification of genes required for recycling reducing power during photosynthetic growth. *J Bacteriol* 187:5249–5258
- Thorn JM, Barton JD, Dixon NE, Ollis DL, Edwards KJ (1995) Crystal structure of *Escherichia coli* Qor quinone oxidoreductase complexed with NADPH. *J Mol Biol* 249:785–799
- Tichi MA, Tabita FR (2000) Maintenance and control of redox poise in *Rhodobacter capsulatus* strains deficient in the Calvin-Benson-Bassham pathway. *Arch Microbiol* 174:322–333
- Tichi MA, Meijer WG, Tabita FR (2001) Complex I and its involvement in redox homeostasis and carbon and nitrogen metabolism in *Rhodobacter capsulatus*. *J Bacteriol* 183:7285–7294
- Tikh I, Held M, Schmidt-Dannert C (2014) Bio-Brick™ compatible vector system for protein expression in *Rhodobacter sphaeroides*. *Appl Microbiol Biotechnol* 98:1–9
- Tran LM, Rizk ML, Liao JC (2008) Ensemble modeling of metabolic networks. *Biophys J* 95:5606–5617
- Varma A, Palsson BO (1994) Metabolic flux balancing: basic concepts, scientific and practical use. *Nat Biotechnol* 12:994–998
- Vignais PM (2009) Regulation of hydrogenase gene expression. In: Neil Hunter C, FD M, Thurnauer C, Thomas Beatty J (eds) *The Purple Phototrophic Bacteria*. Springer, The Netherlands, pp 743–757
- Vignais PM, Billoud B (2007) Occurrence, classification, and biological function of hydrogenases: an overview. *Chem Rev* 107:4206–4272
- Vignais PM, Colbeau A (2004) Molecular biology of microbial hydrogenases. *Curr Issues Mol Biol* 6:159–188
- Vignais PM, Elsen S, Colbeau A (2005) Transcriptional regulation of the uptake [NiFe]hydrogenase genes in *Rhodobacter capsulatus*. *Biochem Soc Trans* 33:28–32
- Voordouw G, van der Vies SM, Themmen AP (1983) Why are two different types of pyridine nucleotide transhydrogenase found in living organisms? *Eur J Biochem* 131:527–533

- Vu TT, Stolyar SM, Pinchuk GE, Hill EA, Kucek LA, Brown RN, Lipton MS, . . . Reed JL (2012) Genome-scale modeling of light-driven reductant partitioning and carbon fluxes in diazotrophic unicellular cyanobacterium *Cyanothece* sp. ATCC 51142. PLoS Comput Biol 8:e1002460
- Work VH, D'Adamo S, Radakovits R, Jinkerson RE, Posewitz MC (2012) Improving photosynthesis and metabolic networks for the competitive production of phototroph-derived biofuels. Curr Opin Biotechnol 23:290–297
- Wu JA, Bauer CE (2010) RegB kinase activity is controlled in part by monitoring the ratio of oxidized to reduced ubiquinones in the ubiquinone pool. Mbio 1:e00272-10
- Xu HW, Love J, Borghese R, Wall JD (1989) Identification and isolation of genes essential for H<sub>2</sub> oxidation in *Rhodobacter capsulatus*. J Bacteriol 171:714–721
- Yilmaz LS, Kontur WS, Sanders AP, Sohmen U, Donohue TJ, Noguera DR (2010) Electron partitioning during light- and nutrient-powered hydrogen production by *Rhodobacter sphaeroides*. Bioenergy Res 3:55–66
- Yoch DC, Arnon DI (1975) Comparison of 2 ferredoxins from *Rhodospirillum rubrum* as electron carriers for native nitrogenase. J Bacteriol 121:743–745
- ZeilstraRyalls JH, Gabbert K, Mouncey NJ, Kaplan S, Kranz RG (1997) Analysis of the *firL* gene and its function in *Rhodobacter capsulatus*. J Bacteriol 179:7264–7273
- Zumft WG (1997) Cell biology and molecular basis of denitrification. Microbiol Mol Biol R 61:533–616

# Chapter 33

## Cytochrome $c_{6A}$ of Chloroplasts

Christopher J. Howe<sup>a,\*</sup>, Robert H. Nimmo,<sup>a</sup>  
Adrian C. Barbrook,<sup>a</sup> and Derek S. Bendall<sup>b</sup> (deceased)

<sup>a</sup>*Department of Biochemistry, University of Cambridge, Downing  
Site, Cambridge CB2 1QW, UK*

<sup>b</sup>*Department of Biochemistry, University of Cambridge,  
Cambridge, UK*

Summary.....	701
I. Introduction.....	702
A. Cytochrome $c_6$ Family.....	702
B. Discovery of Cytochrome $c_{6A}$ .....	702
II. The Protein.....	703
A. Evidence Against Cytochrome $c_{6A}$ as a Substitute for Plastocyanin.....	703
B. Structure.....	704
C. Loop Insertion Peptide.....	704
D. Redox Midpoint Potential.....	705
E. Interaction Partners.....	706
III. 'Omics Studies.....	706
IV. Distribution Outside the Green Plant Lineage.....	707
V. Possible Functions.....	708
VI. Evolution of Cytochrome $c_{6A}$ .....	709
VII. General Conclusions.....	710
Acknowledgements.....	711
References.....	711

### Summary

Cytochrome  $c_{6A}$  must be an important protein, as it is conserved across plant and green algal lineages, yet its function remains as mysterious as when it was discovered over 10 years ago. The protein is similar in sequence to conventional cytochrome  $c_6$  proteins, which are well known as alternatives to plastocyanin in transferring electrons from the cytochrome  $b_6f$  complex to Photosystem I in the light reactions of photosynthesis. Yet cytochrome  $c_{6A}$  has a dramatically lower redox midpoint potential than conventional cytochrome  $c_6$ , meaning that it is an unsuitable electron acceptor from cytochrome  $f$ . The structure of cytochrome  $c_{6A}$  has been determined, and mutagenesis studies have pinpointed a single substitution compared to cytochrome  $c_6$  that is responsible for at least 100 mV of the lowering of the midpoint potential—a remarkable effect for a single residue. Another striking feature of cytochrome  $c_{6A}$ , absent from cytochrome  $c_6$ , is a 12-residue insertion in a loop region of the protein. This insertion has two conserved cysteine residues. The function of these is unknown, but

---

\*Author for correspondence, e-mail: [c.j.howe@bioc.cam.ac.uk](mailto:c.j.howe@bioc.cam.ac.uk)

may be structural rather than catalytic. Cytochrome  $c_{6A}$  is able to transfer electrons to plastocyanin. Transcriptomic and proteomic studies have provided remarkably little insight into the protein's function. Ironically, the recognition of cytochrome  $c_{6A}$  in plants—from which cytochrome  $c_6$  was long thought to be absent—has now led to the recognition of a previously unsuspected class of cytochrome  $c_6$ -like proteins in cyanobacteria, designated cytochrome  $c_{6B}$  and cytochrome  $c_{6C}$ .

## I. Introduction

### A. Cytochrome $c_6$ Family

Cytochrome  $c_{6A}$  is a low molecular weight protein that is clearly homologous, based on primary sequence, to the cytochrome  $c_6$  family of proteins. However, cytochrome  $c_{6A}$  differs from the conventional cytochrome  $c_6$  proteins in aspects of its primary structure, in redox and other biochemical properties, and in function. The conventional cytochrome  $c_6$  proteins have been known for many years to function in photosynthetic electron transfer between the cytochrome  $b_6f$  complex and Photosystem I (PSI). The established view was that some cyanobacterial and algal lineages rely on cytochrome  $c_6$  for this stage in the electron transfer chain, while others use either cytochrome  $c_6$  or, especially under copper-replete conditions, the copper-containing protein plastocyanin. In addition it was accepted that land plants no longer have a cytochrome  $c_6$ , having completely replaced it with plastocyanin (Sandmann et al. 1983; Ho and Krogmann 1984; Kerfeld and Krogmann 1988). Cytochrome  $c_6$  and plastocyanin were believed also to function in electron transfer to cytochrome oxidase in organisms with a cytochrome oxidase in the same compartment as the photosynthetic electron transfer chain, i.e. in photosynthetic bacteria (Peschek et al. 2004; Hart et al. 2005).

### B. Discovery of Cytochrome $c_{6A}$

It was therefore very surprising when the existence of a modified form of cytochrome  $c_6$  in plants was reported in 2002 independently by two groups (Gupta et al. 2002a; Wastl et al. 2002). Wastl et al. reported genomic and expressed sequence tag (EST) database searches that showed the existence in land plants of sequences encoding a protein with clear homology to cytochrome  $c_6$ , including the heme-binding motif —CXXCH— and a potential iron-ligating methionine, both of which were found in algal cytochrome  $c_6$  proteins. They also noted the existence of an insertion of 12 amino acids, including two cysteines, in all the novel cytochrome  $c_6$  proteins that was not found in the conventional ones, and suggested this was indicative of a recently acquired function, perhaps in redox regulation or signalling. They predicted, based on homology models, that the newly recognised protein would have significantly different surface charge distributions from conventional cytochrome  $c_6$ , again suggesting a different function. In addition, they noted that sequences encoding the novel protein were found in EST collections from non-photosynthetic, as well as from photosynthetic, tissue and suggested that this might indicate a function for the protein alternative or additional to any role in photosynthesis (Wastl et al. 2002).

Gupta et al. (2002a), by contrast, argued on the basis of a more detailed functional study that the novel protein serves as a substitute for plastocyanin, especially under copper-deficient conditions, in much the same way as conventional cytochrome  $c_6$ . They recognized the existence of sequences encoding the novel cytochrome in yeast two-hybrid screens of an *Arabidopsis* cDNA

---

*Abbreviations:* LIP – Loop insertion peptide; *pI* – Isoelectric point; PPI – Peptidyl-prolyl *cis-trans* isomerase; PS I – Photosystem I; PS II – Photosystem II

library for sequences encoding proteins interacting with a chloroplast immunophilin which was subsequently identified as the thylakoid-located immunophilin FKBP13 (Buchanan and Luan 2005). Based on RNA blot hybridizations and immunoblots, they reported that transcripts for the protein and the protein itself were found in leaves, but not in roots, and that when the gene was expressed under a powerful promoter, although transcripts were seen in both tissues, the protein accumulated only in leaves. Immunoblot analysis of chloroplast fractions from over-expressing lines indicated that the protein could be found in the thylakoid lumen, consistent with a putative targeting sequence at the N-terminus of the protein. A chloroplast location was subsequently supported by Nimmo (2011). Gupta et al. also reported that recombinant protein could restore oxygen evolution in inside-out thylakoid preparations in vitro, and that T-DNA insertion mutants of *Arabidopsis* lacking the cytochrome  $c_6$  were phenotypically normal. In addition, they reported that RNAi lines designed to down-regulate expression of both plastocyanin genes of *Arabidopsis* were viable, although impaired in growth, but that the combination of cytochrome  $c_6$  knockout and plastocyanin RNAi was lethal. On the basis of these experiments they concluded that the new cytochrome  $c_6$  was a functional substitute for plastocyanin, although they noted that less severe reduction of plastocyanin levels achieved by copper deprivation ultimately led to death of wild type plants, and did not cause elevation of transcript levels for cytochrome  $c_6$ .

Subsequently, Wastl et al. (2004a) reported that the genome of the eukaryotic green alga *Chlamydomonas* contained a sequence encoding the novel cytochrome  $c_6$ , as well as a sequence encoding the conventional form of the protein. Phylogenetic analysis showed that the novel *Chlamydomonas* protein formed a monophyletic group with those identified from land plants, consistent with the fact that they all contained the 12 amino-acid insertion. Reflecting their monophyletic nature, Wastl et al. proposed

the name cytochrome  $c_{6A}$  for this family of proteins in preference to a previous proposal of the name cytochrome  $c_x$ , arguing that the latter name was potentially confusing (the term had already been used for a different cytochrome), and did not reflect the relationship with other cytochromes  $c_6$ . The term cytochrome  $c_{6A}$  is now widely accepted, and, as discussed below and elsewhere in this volume, has been used as the basis for designating additional families as cytochrome  $c_{6B}$  and cytochrome  $c_{6C}$ .

## II. The Protein

### A. Evidence Against Cytochrome $c_{6A}$ as a Substitute for Plastocyanin

Notwithstanding the evidence provided by Gupta et al. (2002a) that cytochrome  $c_{6A}$  is a functional substitute for plastocyanin, a number of lines of evidence accumulated to the contrary. Molina-Heredia et al. (2003) showed that the redox midpoint potential of *Arabidopsis* cytochrome  $c_{6A}$  was over 200 mV lower than that of *Arabidopsis* plastocyanin or a conventional cytochrome  $c_6$ , meaning that it would be very unlikely to be able to oxidize cytochrome  $f$ , whose redox midpoint potential is similar to plastocyanin. Molina-Heredia et al. also showed that *Arabidopsis* cytochrome  $c_{6A}$  reduced *Arabidopsis* PSI preparations in vitro much more slowly than *Arabidopsis* plastocyanin or cytochrome  $c_6$  from the eukaryotic alga *Monoraphidium*. Modelling of *Arabidopsis* cytochrome  $c_{6A}$  indicated an overall predominantly positively charged surface, whereas both *Arabidopsis* plastocyanin and *Monoraphidium* cytochrome  $c_6$  would have a predominantly negatively charged surface, again suggesting that cytochrome  $c_{6A}$  and plastocyanin had different targets. Increasing ionic concentration (and thus screening charge repulsion) did not lead to increased rate of reaction between cytochrome  $c_{6A}$  and PS I, indicating that the failure of the two to react was not simply due to electrostatic effects.

Weigel et al. (2003a) provided compelling genetic evidence that cytochrome  $c_{6A}$  is not a direct substitute for plastocyanin. They generated stable null alleles of both plastocyanin genes in *Arabidopsis*, and showed that, although the double mutant was viable when propagated on medium containing sucrose, it was unable to grow photosynthetically, with fluorescence data indicating a block in photosynthetic electron transfer somewhere between Photosystem II (PSII) and PSI. Furthermore, overexpression of cytochrome  $c_{6A}$  from the powerful 35S promoter failed to alleviate the mutant phenotype, indicating that cytochrome  $c_{6A}$  was unable to compensate for the lack of plastocyanin. This study raises the question of why the plastocyanin knockdown lines of *Arabidopsis* studied by Gupta et al. (2002a) remained viable, even though plastocyanin was not detectable by immunoblot analysis. Given that these were knockdown lines, it seems likely that some plastocyanin expression remained, even though this was below the level of detection in immunoblots. The major reduction in plastocyanin levels was presumably responsible for the impaired growth of the plants. Why the loss of cytochrome  $c_{6A}$  was lethal in a background with low levels of plastocyanin is discussed below.

Weigel et al. (2003b) also argued for a different function for cytochrome  $c_6$  from plastocyanin on the basis of RNA profiles. They showed that in *Arabidopsis* lines mutant for cytochrome  $c_{6A}$  transcript profiles for more than 3000 genes in microarrays, most of which encoded chloroplast proteins, were significantly different from profiles for single or double plastocyanin mutants.

### B. Structure

Structures of cytochrome  $c_{6A}$  were reported independently by two groups in 2006. Marcaida et al. (2006) reported structures at 1.2 Å and 1.4 Å resolution for protein with the heme in the ferric and ferrous states respectively (Fig. 33.1), and Chida et al. (2006) reported the structure of the ferric form at 1.5 Å resolution. The structure was

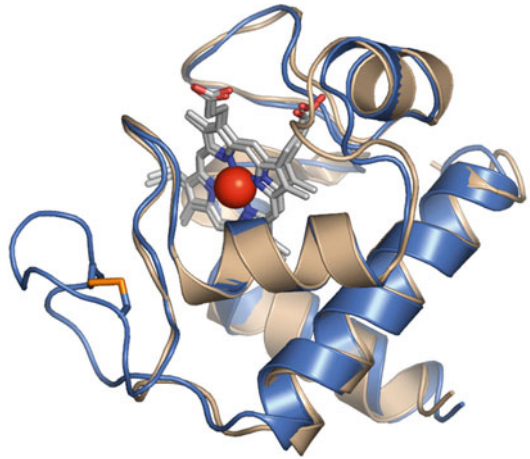


Fig. 33.1. Superposition of the structure of *Arabidopsis* ferri-cytochrome  $c_{6A}$  on that of ferro-cytochrome  $c_6$  from the green alga *Monoraphidium braunii* (pdb code 1ctj). Blue, cytochrome  $c_{6A}$ ; pink, cytochrome  $c_6$ . Reprinted from Journal of Molecular Biology, Vol 360, Marcaida MJ et al. 'Structure of cytochrome  $c_{6A}$ , a novel dithio-cytochrome of *Arabidopsis thaliana*, and its reactivity with plastocyanin: implications for function.' pp 968–977, Copyright (2006), with permission from Elsevier.

dominated by four alpha-helices, and was similar to predictions from modelling based on homology with cytochrome  $c_6$  (Molina-Heredia et al. 2003), with heme iron coordinated by the sulfur of a methionine residue and the nitrogen of a histidine. There was little difference between the structures of ferrous and ferric forms, a point discussed below. The 12 amino-acid insertion diagnostic of cytochrome  $c_{6A}$  was located on the outside of the molecule and was well-structured, with the two cysteines forming a disulfide bridge. The structures formed the basis for hypotheses to explain the big change in redox midpoint potential of cytochrome  $c_{6A}$  compared to cytochrome  $c_6$ , and this is discussed in more detail below.

### C. Loop Insertion Peptide

As previously described, the cytochrome  $c_{6A}$  proteins all showed an insertion of 12 amino acids in a loop connecting two alpha helices (Fig. 33.1), and this has been designated the



Loop Insertion Peptide, abbreviated to LIP (Howe et al. 2006). Wastl et al. (2004b) compared the biochemical properties of the wild type *Arabidopsis* protein and forms carrying site-directed mutations in the LIP that resulted in deletion of the LIP or replacement of the cysteine residues with serines. Deletion of the LIP led to a slight drop in the  $pI$  from 5.1 to 4.6, but not enough to bring it to the  $pI$  of *Arabidopsis* plastocyanin (4.1). The redox midpoint potentials were unchanged in the mutants, and the second order rate constants for reaction with PS I were essentially unchanged (or slightly reduced) and some 70-fold lower than the rate constants for reaction of plastocyanin with PS I. The authors concluded that the LIP was not responsible for the low redox midpoint potential, or the low rate of reaction with PS I, including the  $pI$  unsuitable for the reaction (Wastl et al. 2004b).

Chida et al. (2006) analysed the denaturation of wild type cytochrome  $c_{6A}$  and mutants with the cysteines in the LIP mutated to serine, or with the LIP deleted, and concluded that the disulfide bridge contributed to the stability of the protein. Worrall et al. (2008) analysed the disulfide bond angles, with reference to the work of Schmidt et al. (2006) on relating disulfide bond angles to their function. Worrall et al. concluded that the LIP disulfide bond was structural, rather than regulatory or catalytic, and that the LIP might be involved in interaction with other proteins. Mason et al. (2012) analysed the folding of wild type cytochrome  $c_{6A}$ , the mutant with the LIP cysteines replaced by serines, and a cytochrome  $c_6$  from a cyanobacterium, and also concluded that the disulfide makes a significant contribution to stability, with the formation of the structure of the region containing it occurring late in the folding pathway.

Overall, therefore, it seems that the LIP is not directly responsible for the failure to react with PS I. However, it may be involved in interaction with other substrates, and the disulfide bridge contained within it probably has a structural rather than a regulatory or catalytic role.

#### D. Redox Midpoint Potential

The low redox midpoint potential is one of the most striking differences between cytochrome  $c_{6A}$  and cytochrome  $c_6$  or plastocyanin. As summarized above, Wastl et al. (2004b) showed that this was not due to the LIP of cytochrome  $c_{6A}$ . Consideration of the three-dimensional structures of cytochrome  $c_{6A}$ , together with sequence comparisons with cytochrome  $c_6$ , led to the identification of a number of residues in the vicinity of the heme that might affect the redox midpoint potential (Marcaida et al. 2006; Chida et al. 2006). Worrall et al. (2007) tested the contribution of position 52 (*Arabidopsis* cytochrome  $c_{6A}$  numbering), which is consistently a glutamine in conventional cytochrome  $c_6$ , but a hydrophobic residue in cytochrome  $c_{6A}$  (valine in the *Arabidopsis* protein). The glutamine is within hydrogen-bonding distance of a water molecule that, in turn, is putatively able to interact with the propionate sidechains of the heme. Worrall et al. (2007) also tested the contribution of an alanine (A31 in *Arabidopsis* cytochrome  $c_{6A}$ ) whose corresponding position in cytochrome  $c_6$  is taken by a residue with an electropositive side chain that is again likely to interact with a heme propionate side chain. Substitution of V52 with glutamine in the *Arabidopsis* protein resulted in an increase in the redox midpoint potential of +109 mV, a remarkable change for a single residue. Consistent with this, replacement of the equivalent glutamine in cytochrome  $c_6$  from the cyanobacterium *Phormidium laminosum* with valine lowered the midpoint potential by 100 mV. Substitution of A31 with lysine in the *Arabidopsis* cytochrome  $c_{6A}$  protein raised the midpoint potential by +31 mV. Thus, the V52Q change alone is sufficient to account for a large part of the difference in midpoint potential between cytochrome  $c_{6A}$  and cytochrome  $c_6$ , which Worrall et al. estimated as approximately 250 mV, larger than previously indicated (Molina-Heredia et al. 2003). However, the detailed basis for the effect of the residue at position 52 on the midpoint potential is not fully clear

(Rajagopal et al. 2011). The low midpoint potential of cytochrome  $c_{6A}$  contrasts with the general situation with cytochrome  $c$  proteins, where evolution has acted to stabilize the reduced state (Worrall et al. 2008).

### E. Interaction Partners

A limited number of studies have considered possible interaction partners of cytochrome  $c_{6A}$ . The first of these was the study by Gupta et al. (2002a) that was one of the first to report the existence of cytochrome  $c_{6A}$ . In this study, a cDNA encoding the *Arabidopsis* cytochrome  $c_{6A}$  was identified through the ability of its product to interact with the immunophilin FKBP13 in a yeast two-hybrid assay. FKBP13 is one of a family of proteins predicted to be located in the thylakoid lumen with peptidyl-prolyl *cis-trans* isomerase (PPI) activity. The precursor of the FKBP13 protein had also been shown on the basis of a two-hybrid screen and assays in vitro to interact with the Rieske Fe-S protein component of the cytochrome  $b_6f$  complex (Gupta et al. 2002b). Surprisingly, although the precursor form of FKBP13 (including the chloroplast transit sequence) and the intermediate form (lacking the transit sequence but retaining the thylakoid targeting sequence) interacted with the Rieske protein, the mature form of FKBP13 did not (Gupta et al. 2002b). This was interpreted as indicating that interaction occurs at some stage during the import pathway. Downregulation of expression of FKBP13 by RNAi led to an increase in the level of Rieske protein. Structural analysis of FKBP13 (Gopalan et al. 2004) showed the presence of two disulfide bridges in the protein. The cysteines were shown to be redox-active with thioredoxin, with reduction leading to a loss of PPI activity. Similarly, loss of one or other disulfide bridge was also shown to lead to reduction in PPI activity, and it was proposed that reduction of the disulfides was a basis for redox regulation. Whether cytochrome  $c_{6A}$ , with its pair of cysteines in the LIP, was involved in this system was not known.

Marcaida et al. (2006) examined the possibility that cytochrome  $c_{6A}$  reacts with plastocyanin (see below), which would be thermodynamically feasible in terms of the midpoint potentials of the two proteins. They found that *Arabidopsis* cytochrome  $c_{6A}$  (with the heme reduced) could reduce pea plastocyanin in vitro, and obtained a value for the second order rate constant for the reaction of  $1.2 \times 10^7 \text{ M}^{-1}\text{s}^{-1}$  for the reaction at 300 K and pH 6.0. Although this was significantly lower than the value of  $8.7 \times 10^7 \text{ M}^{-1}\text{s}^{-1}$  for the reaction of plastocyanin with PS I in *Arabidopsis* (Wastl et al. 2004b), they argued that the value for the reaction between cytochrome  $c_{6A}$  and plastocyanin was potentially physiologically significant, especially if the reaction were involved in regulation or biogenesis.

Pesaresi et al. (2009) examined further the possible interaction between cytochrome  $c_{6A}$  and plastocyanin in yeast two-hybrid screens. Using this assay they were unable to detect interaction between *Arabidopsis* cytochrome  $c_{6A}$  and either of the plastocyanin isoforms. It should be noted, though, that interactions between redox proteins are typically very weak. For example, the  $K_D$  for the interaction between turnip cytochrome  $f$  and spinach plastocyanin is approximately 0.14 mM (Kannt et al. 1996). It is therefore possible that an interaction between cytochrome  $c_{6A}$  and plastocyanin would not have been detected in this assay. Unexpectedly, Pesaresi et al. (2009) found that cytochrome  $c_{6A}$  appeared to form a homodimer, based on the two hybrid screen, and this interaction was seen both with the wild type protein and with the mutant form with the LIP cysteines mutated to serine, indicating that the dimerization did not depend on the formation of disulfide bridges involving the LIP.

### III. 'Omics Studies

Apart from providing the genetic evidence for the existence of the protein, 'omics studies have provided few additional insights.

The protein is encoded on chromosome 5 of *Arabidopsis* (gene model AT5G45040.1) and contains 5 introns in the coding region. Curiously, the coding region overlaps with, but is on the opposite strand, to a region corresponding to the 3' untranslated region for a gene AT5G45030.1, encoding a trypsin-like protein (<http://www.arabidopsis.org/servlets/TairObject?name=AT5G45040&type=locus>, accessed 2 Feb 2014). The significance, if any, of this is unclear, as the arrangement is not conserved. The transcript has been recorded from a wide range of tissue types, from sperm cells to embryos and leaves. There is little evidence of strong regulation of transcript levels in response to environmental changes. Interestingly, though, transcript levels were markedly lower in *Arabidopsis* lines with the *vtc1* (vitamin C defective) mutation which results in loss of GDP-mannose pyrophosphorylase activity, and lowered ascorbate levels (Kerchev et al. 2011). However, the significance of the low transcript level is again difficult to assess, as a similar effect was not seen in the *vtc2* mutant, which lacks the GDP-L-galactose phosphorylase, also leading to lowered ascorbate levels. The apparent contradiction between *vtc1* and *vtc2* mutants may reflect the fact that the GDP-mannose pyrophosphorylase mutation (*vtc1*) is pleiotropic, influencing, for example, protein glycosylation and ammonium sensitivity, as well as ascorbate biosynthesis (Qin et al. 2008). Other genes showing a similar pattern to that for cytochrome *c*<sub>6A</sub> in *vtc1* mutants included *psbA*, *petG* and genes for a small number of components of the NADH dehydrogenase complex of the thylakoid membrane (Queval and Foyer 2012).

Gupta et al. (2002a) reported that immunoblot analysis indicated the presence of the protein in wild type *Arabidopsis* leaves, with much lower levels in roots. They also reported studies using isolated chloroplasts indicating a thylakoid lumen location in over-expression lines. However, proteomic studies have, to our knowledge, failed to detect cytochrome *c*<sub>6A</sub> directly in spite of the fact that transcripts for the protein have been detected in a wide range of tissues. It should be noted

that some studies have included the protein in chloroplast thylakoid luminal proteome databases on the basis of the literature or studies in silico (e.g. Zybailov et al. 2008; Karpowicz et al. 2011; Huang et al. 2012). The use of the literature appears to lead ultimately to the initial report of Gupta et al. and it is therefore important for this to be independently confirmed. Howe et al. (2006) discussed the reasons for the failure to detect the protein in proteomic studies, and concluded it was unlikely to be due to extremes of size or isoelectric points, as plastocyanin is smaller than cytochrome *c*<sub>6A</sub> (10.5 kDa compared to 11.8 kDa) and has a more extreme isoelectric point (4.1 for *Arabidopsis* plastocyanin as opposed to 5.1), yet is readily detected. This suggests that cytochrome *c*<sub>6A</sub> is at very low abundance under all the conditions used so far in proteomic studies.

#### IV. Distribution Outside the Green Plant Lineage

We consider here the distribution of cytochrome *c*<sub>6A</sub> proteins, as this may shed some light on their function. The evolutionary interpretation of their distribution is discussed in more detail below. Database searches indicate the widespread distribution of sequences encoding cytochrome *c*<sub>6A</sub> among green plants and algae (e.g. Howe et al. 2006). However, if the presence of the LIP with its two cysteines and a hydrophobic residue rather than a glutamine at the equivalent of position 52 (see above) are taken as diagnostic features in addition to sequence similarity, searches (as at March 2014) failed to identify any sequences encoding cytochrome *c*<sub>6A</sub> (as opposed to cytochrome *c*<sub>6</sub>) in organisms with secondary green chloroplasts, such as *Euglena* or *Chlorarachnion*. [See Walker et al. (2011) and Dorrell and Howe (2012) for detailed descriptions of the evolutionary positions of these organisms and a summary of the secondary and tertiary plastid endosymbioses that have taken place in eukaryote evolution].

On the criteria of LIP and a hydrophobic residue at position 52, cytochrome  $c_{6A}$  also appears to be absent from other photosynthetic eukaryotes, including those with primary chloroplasts but outside the green lineage (i.e. red algae and glaucophytes). However, there are a limited number of examples outside the green lineage of sequences encoding apparently similar polypeptides that lack the LIP, but which may have a hydrophobic residue at the equivalent of position 52, as in cytochrome  $c_{6A}$  (although this may depend on the details of the alignment). These include sequences from the red alga *Galdieria sulphuraria* (e.g. XM\_005704567.1), the haptophyte alga *Emiliania huxleyii* (e.g. XM\_005765899.1), the cryptophyte *Guillardia theta* (e.g. XM\_005827306.1), and the dinoflagellate *Amphidinium carterae* (e.g. CF065358.1). Whether these genuinely are homologues of cytochrome  $c_{6A}$ , including having a low redox midpoint potential, remains to be seen, but would repay further study.

Understanding the distribution of cytochrome  $c_{6A}$  became more complex with the recognition that proteins of the low potential cytochrome  $c_6$  family do in fact occur in cyanobacteria, typified by the PetJ2 protein of *Synechococcus* sp. PCC 7002 (Bialek et al. 2008). Although this protein also lacks the LIP with two cysteines, it has a hydrophobic residue (leucine) at the equivalent of position 52 for cytochrome  $c_{6A}$ , and a redox midpoint potential of  $148 \pm 1.7$  mV. This is much lower than for the conventional cytochrome  $c_6$  found in the same organism and, as for cytochrome  $c_{6A}$ , would make it unsuitable to act as an electron acceptor from cytochrome  $f$  (Bialek et al. 2008). On the basis of a phylogenetic analysis, Bialek et al. proposed the existence of two groups of these proteins in cyanobacteria, and designated them cytochrome  $c_{6B}$  and cytochrome  $c_{6C}$ . There is something of an irony here. Cytochrome  $c_{6A}$  was first described as a homologue of the cyanobacterial cytochrome  $c_6$  found, contrary to the understanding at the time, in plants. Cytochromes  $c_{6B}$  and  $c_{6C}$  were then described as cyanobacterial homologues

of the plant protein. The cyanobacterial cytochromes  $c_{6B}$  and  $c_{6C}$  are described in more detail elsewhere in this volume. Bialek et al. commented that the cyanobacteria containing the cytochrome  $c_{6C}$  family are largely nitrogen-fixing species and that ‘the *Nostoc punctiforme* NpF1886 gene for a  $c_6$ -like cytochrome is expressed at low but significant levels in ammonia-grown and nitrogen-starved cells and in hormogonia and akinetes’. Reyes-Sosa et al. (2011) reported that the *Nostoc* sp. PCC 7119 cytochrome  $c_{6C}$  protein was able to reduce PSI at a rate that could be physiologically significant, and proposed a function for the cytochrome in a different but unidentified electron transfer pathway from the conventional one between the cytochrome  $b_6f$  complex and PSI.

## V. Possible Functions

We now speculate on possible functions for cytochrome  $c_{6A}$ . Evidence presented above implies that it does not function as a simple substitute for plastocyanin in transfer of electrons from cytochrome  $f$  to PSI. A role in apoptosis has been suggested (Weigel et al. 2003b), although Howe et al. (2006) argued against this on the grounds that proteomic analysis of programmed cell death in plants had not indicated that cytochrome  $c_{6A}$  was upregulated under those conditions (Swidzinski et al. 2004). Howe et al. (2006) suggested the possibility of a regulatory role involving structural effects on some or all of the LIP, the heme, and interaction with FKBP13. They suggested that, given its midpoint potential, the protein might be involved in sensing the redox state of the plastoquinone pool. However, the fact that no significant difference in structure was later seen between the forms of the protein with the heme oxidized or reduced (Marcaida et al. 2006) makes the proposal of a regulatory role associated with conformational change less attractive.

In the light of the ability of cytochrome  $c_{6A}$  to react with plastocyanin (Marcaida et al. 2006), Schlarb-Ridley et al. (2006)

suggested the former protein might assist the formation of disulfide bridges in proteins of the thylakoid lumen, with electrons being transferred from two cysteines of the target protein to the disulfide in the bond in the LIP. This would generate a disulfide bond in the target protein, reducing the disulfide bond in the LIP. This might be re-formed by electrons being transferred from the cysteines of the LIP to plastocyanin directly, and also to the heme group of the protein and then to plastocyanin. Schlarb-Ridley et al. suggested that plastocyanin might also be able to form disulfides in target proteins directly, but that cytochrome  $c_{6A}$  took over this role under low plastocyanin concentrations. This would explain why the combination of knocked down levels of plastocyanin and knockout of cytochrome  $c_{6A}$  was lethal in the experiments of Gupta et al. (2002a). However, there is as yet no direct evidence in support of a role in disulfide bond formation, and the analysis suggesting a structural rather than a catalytic role for the disulfide (Worrall et al. 2008) argues against this.

It may be that we should look for an explanation involving an electron transfer process that is important under stress conditions that have not yet been properly identified. It is increasingly recognized that alternative electron transfer pathways exist in addition to the ‘standard’ ones, often to allow protection against light stress. For example, the cyanobacterial Flv1 and Flv3 flavodiiron proteins allow direct transfer of electrons generated by PSII activity to oxygen, to protect PSI against photodamage under conditions of rapidly pulsing light (Tikkanen et al. 2012; Allahverdiyeva et al. 2013). Similarly, the respiratory terminal oxidases located in the cyanobacterial thylakoid membrane are necessary for survival under rapidly changing light intensities, protecting against formation of reactive oxygen species and the occurrence of photoinhibition, probably by allowing electrons to be diverted from the plastoquinone pool or the cytochrome  $b_{6f}$  complex to oxygen (Lea-Smith et al. 2013). Given that its redox midpoint potential would be suitable for it to accept electrons

from PQH<sub>2</sub> it is tempting to suggest that cytochrome  $c_{6A}$  functions as a ‘safety valve’ to bypass the cytochrome  $b_{6f}$  complex and transfer electrons directly from PQH<sub>2</sub> to PSI (presumably via plastocyanin) when the plastoquinone pool is highly reduced. Although this would require the lipid soluble plastoquinone to interact directly with the soluble cytochrome, there is precedent for interaction between plastoquinone and extrinsic proteins, such as the chloroplast sensor kinase CSK (Puthiyaveetil et al. 2013), and respiratory complex I, where the quinol headgroup appears to protrude some distance from the membrane to participate in the redox reaction (Baradaran et al. 2013).

## VI. Evolution of Cytochrome $c_{6A}$

Before the existence of the cytochrome  $c_{6B}$  and cytochrome  $c_{6C}$  proteins was recognized in cyanobacteria, it was possible to propose a relatively simple model for the evolution of cytochrome  $c_{6A}$  (Howe et al. 2006). According to this, the cyanobacterium that entered endosymbiosis to give primary chloroplasts would have contained cytochrome  $c_6$  and plastocyanin. Duplication and divergence of the cytochrome  $c_6$  gene in the green chloroplast lineage led to the situation in algae such as *Chlamydomonas*, which contain both cytochrome  $c_6$  and cytochrome  $c_{6A}$  (Wastl et al. 2004a) as well as plastocyanin. In the land plant lineage, the cytochrome  $c_6$  gene was lost, and in the ancestor to the red algae and glaucophyte algae the plastocyanin gene was lost. In organisms with serial endosymbiosis involving a red algal symbiont, such as diatoms, there was no plastocyanin. (Limited instances of the existence of plastocyanin in such organisms, for example *Thalassiosira oceanica* (Peers and Price 2006) probably reflect horizontal gene transfer).

However, with the identification of the cytochrome  $c_{6B}$  and cytochrome  $c_{6C}$  proteins in cyanobacteria (Bialek et al. 2008) the situation became more complex. Only a limited number of phylogenetic analyses have been performed, and the shortness of

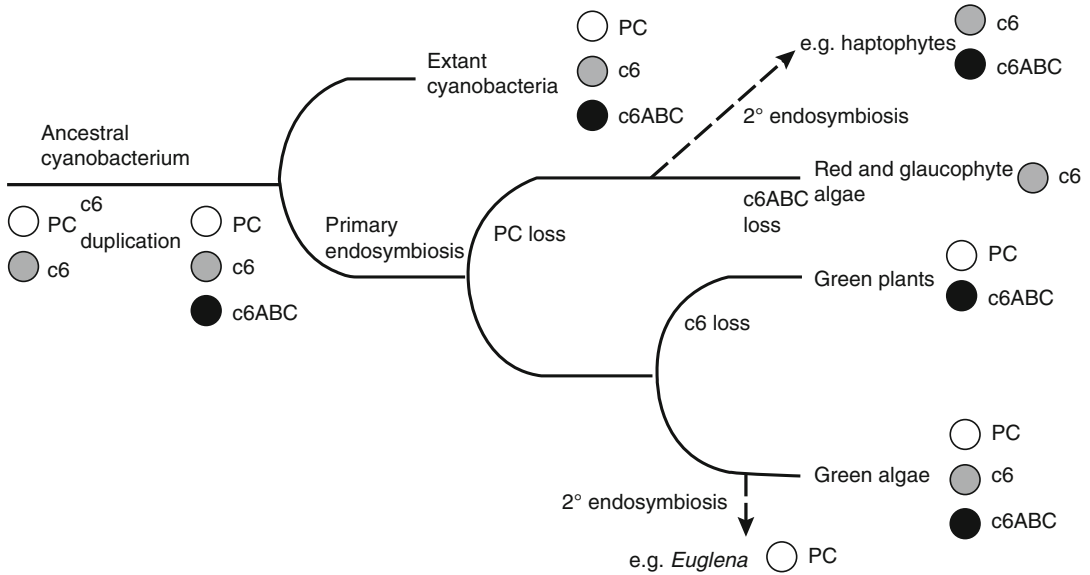


Fig. 33.2. Evolutionary history of cytochrome  $c_6$ , cytochromes  $c_{6A,B,C}$ , and plastocyanin. Secondary endosymbioses are shown by *dashed lines*. The figure assumes that cytochromes  $c_{6A,B,C}$  share a common ancestry to the exclusion of cytochrome  $c_6$ . It does not show horizontal gene transfer events.

the cytochrome  $c$  protein sequences makes phylogenetic analysis difficult. However, if we assume the low redox midpoint potential (demonstrated or inferred) to be indicative of common ancestry, this implies that the cytochrome  $c_{6A}$  found in green chloroplasts originated in the cyanobacterial ancestor of primary chloroplasts. Thus the ancestral chloroplast would have had the full complement of cytochrome  $c_6$ , low potential cytochrome  $c_6$ , and plastocyanin (as in *Chlamydomonas*). All three were retained in the green algal lineage, with the acquisition of the LIP by the low potential cytochrome  $c_6$ . Cytochrome  $c_6$  was lost in the land plant lineage. Plastocyanin was lost in the ancestor of red algae and glaucophytes (as there is no evidence for it in those organisms), and the low potential cytochrome  $c_6$  was also lost in a number of these algae. Secondary endosymbiosis involving the green lineage (as in e.g. *Euglena*) seems to have failed to transfer the low potential cytochrome  $c_6$ . Secondary endosymbiosis of the red lineage is likely to have involved a line that retained the low potential cytochrome  $c_6$ , as it is present

(assuming the features referred to in Sect. IV are diagnostic) in a number of the groups with secondary chloroplasts of red algal origin. This complex evolutionary history is summarized in Fig. 33.2. It will be instructive to test in more detail the phylogenetic relationships among the cyanobacterial cytochrome  $c_{6B}$  and cytochrome  $c_{6C}$ , cytochrome  $c_{6A}$  of the green lineage, and the putatively low potential cytochrome  $c_6$  proteins of lineages with secondary plastids. Might cytochrome  $c_{6A}$  instead represent an independent evolution of a low potential form of cytochrome  $c_6$ ?

## VII. General Conclusions

We now have a good knowledge of the structure of cytochrome  $c_{6A}$ , and the features responsible for its low redox midpoint potential compared to conventional cytochrome  $c_6$ . We recognize that it is not a simple substitute for plastocyanin, and it seems likely that the LIP, with its conserved pair of cysteine residues, is structural rather than catalytic. Beyond that, we have little more concrete information

about the function of this mysterious, but well conserved, protein than when it was first discovered over 10 years ago.

## Acknowledgements

We are grateful to the Biotechnology and Biological Sciences Research Council, the Leverhulme Trust, and the European Commission for their support of our work on this protein.

## References

- Allahverdiyeva Y, Mustila H, Ermakova M, Bersanini L, Richaud P, Ajlani G, Battchikova N, ... Aro E-M (2013) Flavodiiron proteins Flv1 and Flv3 enable cyanobacterial growth and photosynthesis under fluctuating light. *Proc Natl Acad Sci USA* 110:4111–4116
- Baradaran R, Berrisford JM, Minhas GS, Sazanov LA (2013) Crystal structure of the entire respiratory complex I. *Nature* 494:443–448
- Bialek W, Nelson M, Tamiola K, Kallas T, Szczepaniak A (2008) Deeply branching *c*<sub>6</sub>-like cytochromes of cyanobacteria. *Biochemistry* 47:5515–5522
- Buchanan BB, Luan S (2005) Redox regulation in the chloroplast thylakoid lumen: a new frontier in photosynthesis research. *J Exp Bot* 56:1439–1447
- Chida H, Yokoyama T, Kawai F, Nakazawa A, Akazaki H, Takayama Y, Hirano T, ... Oku T (2006) Crystal structure of oxidized cytochrome *c*<sub>6A</sub> from *Arabidopsis thaliana*. *FEBS Letts* 580:3763–3768
- Dorrell RG, Howe CJ (2012) What makes a chloroplast? Reconstructing the establishment of photosynthetic symbioses. *J Cell Sci* 125:1865–1875
- Gopalan G, He Z, Balmer Y, Romano P, Gupta R, Héroux A, Buchanan BB, ... Luan S (2004) Structural analysis uncovers a role for redox in regulating FKBP13, an immunophilin of the chloroplast thylakoid lumen. *Proc Natl Acad Sci USA* 101:13945–13950
- Gupta R, He Z, Luan S (2002a) Functional relationship of cytochrome *c*<sub>6</sub> and plastocyanin in *Arabidopsis*. *Nature* 417:567–571
- Gupta R, Mould RM, He Z, Luan S (2002b) A chloroplast FKBP interacts with and affects the accumulation of Rieske subunit of cytochrome *bf* complex. *Proc Natl Acad Sci USA* 99:15806–15811
- Hart SE, Schlarb-Ridley BG, Bendall DS, Howe CJ (2005) Terminal oxidases of cyanobacteria. *Biochem Soc Trans* 33:832–835
- Ho KK, Krogmann DW (1984) Electron donors to P700 in cyanobacteria and algae. An instance of unusual genetic variability. *Biochim Biophys Acta* 766:310–316
- Howe CJ, Schlarb-Ridley BG, Wastl J, Purton S, Bendall DS (2006) The novel cytochrome *c*<sub>6</sub> of chloroplasts: a case of evolutionary bricolage? *J Exp Bot* 57:13–22
- Huang M, Friso G, Nishimura K, Qu X, Olinares PDB, Majeran W, Sun Q, van Wijk KJ (2012) Construction of plastid reference proteomes for maize and *Arabidopsis* and evaluation of their orthologous relationships; the concept of orthoproteomics. *J Proteome Res* 12:491–504
- Kannt A, Young S, Bendall DS (1996) The role of acidic residues of plastocyanin in its interaction with cytochrome *f*. *Biochim Biophys Acta* 1277:115–126
- Karpowicz SJ, Prochnik SE, Grossman AR, Merchant SS (2011) The GreenCut2 resource, a phylogenomically derived inventory of proteins specific to the plant lineage. *J Biol Chem* 286:21427–21439
- Kerchev PI, Pellny TK, Vivancos PD, Kiddle G, Hedden P, Driscoll S, Vanacker H, ... Foyer CH (2011) The transcription factor ABI4 is required for the ascorbic acid-dependent regulation of growth and regulation of jasmonate-dependent defense signaling pathways in *Arabidopsis*. *Plant Cell* 23:3319–3334
- Kerfeld CA, Krogmann DW (1988) Photosynthetic cytochromes *c* in cyanobacteria, algae and plants. *Annu Rev Plant Physiol Plant Mol Biol* 49:397–425
- Lea-Smith DJ, Ross N, Zori M, Bendall DS, Dennis JS, Scott SA, Smith AG, Howe CJ (2013) Thylakoid terminal oxidases are essential for the cyanobacterium *Synechocystis* sp. PCC 6803 to survive rapidly changing light intensities. *Plant Physiol* 162:484–495
- Marcaida MJ, Schlarb-Ridley BG, Worrall JAR, Wastl J, Evans TJ, Bendall DS, Luisi BF, Howe CJ (2006) Structure of cytochrome *c*<sub>6A</sub>, a novel dithio-cytochrome of *Arabidopsis thaliana*, and its reactivity with plastocyanin: implications for function. *J Mol Biol* 360:968–977
- Mason JM, Bendall DS, Howe CJ, Worrall JAR (2012) The role of a disulfide bridge in the stability and folding kinetics of *Arabidopsis thaliana* cytochrome *c*<sub>6A</sub>. *Biochim Biophys Acta* 1824:311–318
- Molina-Heredia FP, Wastl J, Navarro JA, Bendall DS, Hervás M, Howe CJ, de la Rosa MA (2003) A new function for an old cytochrome. *Nature* 424:33–34

- Nimmo RH (2011) Location and function of cytochrome  $c_{6A}$ . PhD thesis, University of Cambridge
- Peers G, Price NM (2006) Copper-containing plastocyanin used for electron transport by an oceanic diatom. *Nature* 441:341–344
- Pesaresi P, Scharfenberg M, Weigel M, Granlund I, Schröder WP, Finazzi G, Rappaport F, ... Leister D (2009) Mutants, overexpressors, and interactors of *Arabidopsis* plastocyanin isoforms: revised roles of plastocyanin in photosynthetic electron flow and thylakoid redox state. *Mol Plant* 2:236–248
- Peschek GA, Obinger C, Paumann M (2004) The respiratory chain of blue-green algae (cyanobacteria). *Physiol Plant* 120:358–369
- Puthiyaveetil S, Ibrahim I, Allen JF (2013) Evolutionary rewiring: a modified prokaryotic gene-regulatory pathway in chloroplasts. *Philos Trans R Soc B* 368:20120260
- Qin C, Qian W, Wang W, Wu Y, Yu C, Jiang X, Wang D, Wu P (2008) GDP-mannose pyrophosphorylase is a genetic determinant of ammonium sensitivity in *Arabidopsis thaliana*. *Proc Natl Acad Sci USA* 105:18308–18313
- Queval G, Foyer CH (2012) Redox regulation of photosynthetic gene expression. *Philos Trans R Soc B* 367:3475–3485
- Rajagopal BS, Wilson MT, Bendall DS, Howe CJ, Worrall JAR (2011) Structural and kinetic studies of imidazole binding to two members of the cytochrome  $c_6$  family reveal an important role for a conserved heme pocket residue. *J Biol Inorg Chem* 16:577–588
- Reyes-Sosa FM, Gil-Martínez J, Molina-Heredia FP (2011) Cytochrome  $c_6$ -like protein as a putative donor of electrons to photosystem I in the cyanobacterium *Nostoc* sp. PCC 7119. *Photosynth Res* 110:61–72
- Sandmann G, Reck H, Kessler E, Boeger P (1983) Distribution of plastocyanin and soluble plastidic cytochrome  $c$  in various classes of algae. *Arch Microbiol* 134:23–27
- Schlarb-Ridley BG, Nimmo RH, Purton S, Howe CJ, Bendall DS (2006) Cytochrome  $c_6A$  is a funnel for thiol oxidation in the thylakoid lumen. *FEBS Lett* 580:2166–2169
- Schmidt B, Ho L, Hogg PJ (2006) Allosteric disulfide bonds. *Biochemistry* 45:7429–7433
- Swidzinski JA, Leaver CJ, Sweetlove LJ (2004) A proteomic analysis of plant programmed cell death. *Phytochemistry* 65:1829–1838
- Tikkanen M, Grieco M, Nurmi M, Rantala M, Suorsa M, Aro E-M (2012) Regulation of the photosynthetic apparatus under fluctuating growth light. *Philos Trans R Soc B* 367:3486–3493
- Walker G, Dorrell RG, Schlacht A, Dacks JB (2011) Eukaryotic systematics: a user's guide for cell biologists and parasitologists. *Parasitology* 138:1638–1663
- Wastl J, Bendall DS, Howe CJ (2002) Higher plants contain a modified cytochrome  $c_6$ . *Trends Plant Sci* 7:244–245
- Wastl J, Purton S, Bendall DS, Howe CJ (2004a) Two forms of cytochrome  $c_6$  in a single eukaryote. *Trends Plant Sci* 9:474–476
- Wastl J, Molina-Heredia FP, Hervàs M, Navarro JA, de la Rosa MA, Bendall DS, Howe CJ (2004b) Redox properties of *Arabidopsis* cytochrome  $c_6$  are independent of the loop extension specific to higher plants. *Biochim Biophys Acta* 1657:115–120
- Weigel M, Varotto C, Pesaresi P, Finazzi G, Rappaport F, Salamini F, Leister D (2003a) Plastocyanin is indispensable for photosynthetic electron flow in *Arabidopsis thaliana*. *J Biol Chem* 278:31286–31289
- Weigel M, Pesaresi P, Leister (2003b) Tracking the function of the cytochrome  $c_6$ -like protein in higher plants. *Trends Plant Sci* 8:513–517
- Worrall JAR, Schlarb-Ridley BG, Reda T, Marcaida MJ, Moorlen RJ, Wastl J, Hirst J, ... Howe CJ (2007) Modulation of heme redox potential in the cytochrome  $c_6$  family. *J Am Chem Soc* 129:9468–9475
- Worrall JAR, Luisi BF, Schlarb-Ridley BG, Bendall DS, Howe CJ (2008) Cytochrome  $c_{6A}$ : discovery, structure and properties responsible for its low haem redox potential. *Biochem Soc Trans* 36:1175–1179
- Zybailov B, Rutschow H, Friso G, Rudella A, Emanuelsson O, Sun Q, van Wijk KJ (2008) Sorting signals, N-terminal modifications and abundance of the chloroplast proteome. *PLoS ONE* 3:e1994



# Chapter 34

## Cryptic $c_6$ -Like and $c_M$ Cytochromes of Cyanobacteria

Wojciech Bialek<sup>a</sup>, Andrzej Szczepaniak<sup>a</sup>, Piotr Kolesinski<sup>a</sup>,  
and Toivo Kallas<sup>b,\*</sup>

<sup>a</sup>Faculty of Biotechnology, University of Wrocław, F. Joliot-Curie  
14a, Wrocław 50-383, Poland

<sup>b</sup>Department of Biology, University of Wisconsin-Oshkosh,  
Oshkosh, WI 54901, USA

Summary.....	713
I. Introduction.....	714
II. Discovery of the $c_6$ -Like and $c_M$ Cytochromes.....	714
III. Cytochromes $c_{6C}$ and $c_{6B}$ .....	715
A. Genome Analyses.....	715
B. Biophysical Features.....	717
C. Structures and Heme Environment.....	719
IV. Cytochrome $c_M$ .....	722
A. Genome Analyses.....	722
B. Biophysical Features.....	724
V. Possible Functions of $c_6$ -Like and $c_M$ Cytochromes.....	725
VI. Concluding Remarks.....	729
Acknowledgements.....	730
References.....	730

### Summary

Cytochromes  $c_6$  are widely-distributed monoheme proteins that transfer electrons from the cytochrome  $b_6f$  complex to photosystem I in cyanobacteria and certain eukaryotic algae. Cytochrome  $c_6$  has been replaced by plastocyanin in all known plant chloroplasts and in many cyanobacteria and algae, and was thought to be absent from plants until the discovery of chloroplast cytochrome  $c_6$ -like proteins, now named cytochromes  $c_{6A}$ . These have midpoint potentials substantially lower than those of typical cytochrome  $c_6$  or plastocyanin indicating that they could not effectively transfer electrons from the cytochrome  $b_6f$  complex to photosystem I. Additional  $c_6$ -like cytochromes have been discovered in cyanobacteria. The first of these was cytochrome  $c_M$ , discovered in *Synechocystis* sp. PCC 6803 followed by discovery of a  $c_6$ -like cytochrome encoded by the *petJ2* gene in *Synechococcus* sp. PCC 7002. Subsequent phylogenetic analysis revealed that most, but not all, cyanobacteria carry several genes for putative  $c_6$ -like cytochromes. Two deeply-branching clusters, designated

---

\*Author for correspondence, e-mail: [kallas@uwosh.edu](mailto:kallas@uwosh.edu)

cytochromes  $c_{6B}$  and  $c_{6C}$ , are distinct from either the classical  $c_6$  cytochromes, chloroplast cytochromes  $c_{6A}$ , cyanobacterial cytochromes  $c_M$  or  $c_{550}$ , or bacterial cytochromes  $c_{555}$ . Like cytochrome  $c_{6A}$ , representative cytochromes  $c_{6C}$ ,  $c_{6B}$ , and  $c_M$  have been analyzed and found to have low midpoint potentials unfavorable for electron transfer from the cytochrome  $b_6f$  complex. High-resolution structures have been solved for  $c_{6C}$  and  $c_{6B}$  cytochromes and key residues identified that govern their low midpoint potentials. However, despite these advances and the widespread distribution of these cryptic cytochromes among cyanobacteria, their functions have remained largely mysterious. Here we review the discovery of cyanobacterial  $c_6$ -like cytochromes and current understanding of their properties and possible functions.

## I. Introduction

In oxygenic photosynthesis, sunlight catalyzes electron flow from water through localized, membrane-bound protein complexes. Mobile carriers transfer electrons between these complexes. One of these is cytochrome (Cyt)  $c_6$ , a water-soluble, high-potential, monoheme protein found in the thylakoid lumen of cyanobacteria and some algal chloroplasts. Cyt  $c_6$  transfers electrons from the Cyt  $b_6f$  complex to photosystem I (PSI) and, in cyanobacteria, to a respiratory cytochrome oxidase (Schmetterer 1994; Kerfeld and Krogmann 1998). Crystal structures of Cyt  $c_6$  are available from several sources (Frazao et al. 1995; Kerfeld et al. 1995; Yamada et al. 2000; Sawaya et al. 2001; Bialek et al. 2009), and many additional sequences have been deposited in databases. These proteins are characterized by their low molecular masses (~80–90 amino acids in the mature protein), covalently bound,  $c$ -type heme, and high midpoint potentials of approximately +310 to +390 mV. Apart from these well characterized cytochromes, the genomes of many cyanobacteria carry sequences for cytochromes similar to cytochrome  $c_6$ . These are the so-called,  $c_6$ -like cytochromes that are widely distributed among cyanobacteria and include cytochromes  $c_M$  (Malakhov et al. 1994),  $c_{6B}$ , and  $c_{6C}$  (Bialek et al.

2008). They are characterized by midpoint potentials substantially lower than those of typical  $c_6$  cytochromes and surface charge properties that make them poorly suited for electron transfer from the Cyt  $b_6f$  complex to PSI. These proteins have been difficult to detect, their transcript levels are typically low although elevated under certain stresses, and despite detailed structural and biophysical analysis of some of these proteins expressed in bacteria, their functions have remained largely obscure. In this chapter we review current understanding of these cryptic  $c_6$ -like cytochromes of cyanobacteria, their distinguishing properties, structures, and possible functions.

## II. Discovery of the $c_6$ -Like and $c_M$ Cytochromes

Cytochrome  $c_M$  was initially described as Cyt  $c_{552}$  (Holton and Myers 1967). The  $c_M$  designation originates from Malakhov et al. (1994) who described a water-soluble, moderately basic protein with a redox potential of about +150 mV isolated from *Synechocystis* sp. PCC 6803 (hereafter *Synechocystis* 6803). To test the function of Cyt  $c_M$ , its gene was deleted but this mutation had no perceptible impact on photosynthetic growth, respiration, or oxygen evolution. However, Cyt  $c_M$  could not be inactivated in a PSI deletion strain of *Synechocystis* (Manna and Vermaas 1997), implying that at least under some conditions, Cyt  $c_M$  is indispensable. However, the same authors could not obtain a double deletion mutant of plastocyanin and cytochrome  $c_6$  in the same PSI-

---

*Abbreviations:* COX – Cytochrome oxidase; Cyt – Cytochrome; Cyt  $b_6f$  – Cytochrome  $b_6f$  complex; Cyt  $c_{6A}$  – Cytochrome  $c_{6A}$ ; Cyt  $c_{6B}$  – Cytochrome  $c_{6B}$ ; Cyt  $c_{6C}$  – Cytochrome  $c_{6C}$ ; Cyt  $c_M$  – Cytochrome  $c_M$ ; PC – Plastocyanin; PQ – Plastoquinone; PSI – Photosystem I; PSII – Photosystem II

minus background indicating that Cyt  $c_M$  could not substitute as an electron carrier for these proteins. Manna and Vermaas (1997) observed a sequence similarity between Cyt  $c_M$  and the Cyt  $c$ -binding region of the  $aa_3$  cytochrome oxidase (COX) from *Bacillus* sp. and *Thermus thermophilus*. They suggested that Cyt  $c_M$  may serve as a soluble or membrane-bound component of cytochrome oxidase. In that case the Cyt  $c_M$  N-terminal domain might function as a membrane anchor. Manna and Vermaas (1997) further proposed that plastocyanin or Cyt  $c_6$  may transfer electrons from the Cyt  $b_6f$  complex to COX through Cyt  $c_M$ . Indeed, Bernroitter et al. (2009) showed that Cyt  $c_M$  can donate electrons to cytochrome oxidase as efficiently as Cyt  $c_6$  and more efficiently than PC. However, it has also been shown that no additional component is needed for electron transfer from Cyt  $c_6$  or PC to COX (Paumann et al. 2004a, b) (see also Chap. 31 by Diaz-Moreno et al.). Thus a role for Cyt  $c_M$  in electron transfer to PSI or COX remains uncertain, at least under typical laboratory growth conditions.

A  $c_6$ -like cytochrome was subsequently discovered in plant chloroplasts (Gupta et al. 2002; Wastl et al. 2002). Because land plants, and some algae, exclusively use the blue-copper plastocyanin protein as an electron carrier between the Cyt  $b_6f$  complex and PSI, Cyt  $c_6$  was thought to be absent from chloroplasts prior to this discovery. However, genome and expressed sequence tag (EST) analyses of higher plants (Gupta et al. 2002; Wastl et al. 2002), as well as the green alga *Chlamydomonas reinhardtii* (Wastl et al. 2004), revealed sequences that encode the characteristic, CXXCH  $c$ -heme-binding motif (where XX represents any of a number of amino acids but is often AA or AG), and are strikingly similar to Cyt  $c_6$  sequences. Indeed the initial report by Gupta et al. (2002) presented evidence suggesting that these  $c_6$ -like cytochromes (then designated Cyt  $c_x$ ) could, at least to an extent, replace plastocyanin as an electron carrier. However, subsequent studies concluded that these novel cytochromes are unlikely substitutes for plas-

tocyanin because they have midpoint potentials 200 mV lower than those of typical chloroplast PC or cyanobacterial and algal Cyt  $c_6$ , and positive surface charges in contrast to the negative chloroplast PC (Molina-Heredia et al. 2003; Howe et al. 2006). In addition, Weigel et al. (2003) showed convincingly that an *Arabidopsis* double mutant, with both of its plastocyanin genes inactivated, could not grow photosynthetically. Wastl et al. (2004) showed by phylogenetic analysis that the novel  $c_6$  cytochromes are monophyletic, and although similar to Cyt  $c_6$ , are distinct from them, and thus named these ‘cytochrome  $c_{6A}$ .’ These are discussed in detail in Chap. 33 by Howe et al.

Nomura (2001) first discovered a gene for a second, putative  $c_6$  cytochrome in the cyanobacterium *Synechococcus* sp. PCC 7002 (hereafter *Synechococcus* 7002). The *petJ* gene encodes Cyt  $c_6$  and accordingly, the second gene for a  $c_6$ -like cytochrome was named *petJ2*. In a subsequent phylogenetic analysis of 40 some cyanobacterial genome sequences, Bialek et al. (2008) discovered that most of these carry genes for  $c_6$ -like cytochromes that are similar to the *PetJ2*,  $c_6$ -like cytochrome of *Synechococcus* 7002. Their analysis revealed two deeply-branching clusters, designated cytochromes  $c_{6B}$  and  $c_{6C}$ , that have features distinct from cytochrome  $c_6$ ,  $c_M$ , or other  $c$ -type cytochrome proteins. Bialek et al. (2008) found that the *PetJ2*,  $c_{6C}$  cytochrome of *Synechococcus* 7002 has a midpoint potential ( $E_{m,7}$ ) of +148 mV and a positive, overall surface charge, indicating that it, like cytochromes  $c_M$  and  $c_{6A}$ , would be poorly suited for electron transfer from the Cyt  $b_6f$  complex to PSI.

### III. Cytochromes $c_{6C}$ and $c_{6B}$

#### A. Genome Analyses

Figure 34.1 illustrates the phylogenetic relationships of cyanobacterial cytochrome  $c_M$ ,  $c_{6C}$ , and  $c_{6B}$  proteins relative to cyanobacterial  $c_{550}$ , bacterial  $c_{555}$ , and chloroplast

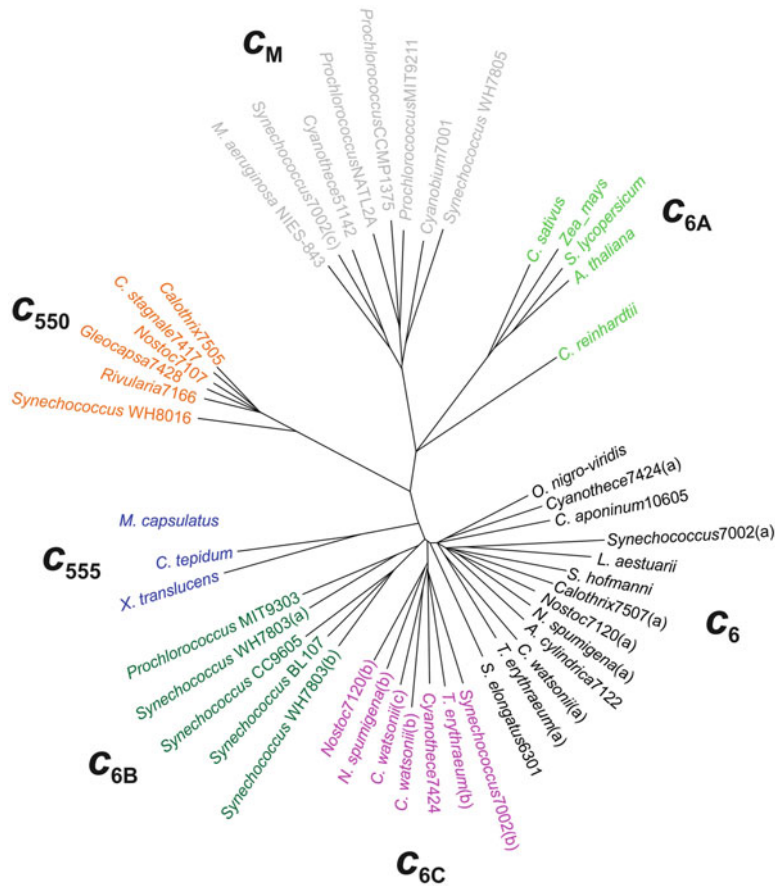


Fig. 34.1. Unrooted tree of *c*-type cytochrome proteins from cyanobacteria, algae, and plants. Cytochrome *c*<sub>6</sub> sequences are: *Oscillatoria nigro-viridis* (gi504991236), *Cyanothece* sp. PCC 7424 (gi506436589), *Cyanobacterium aponinum* PCC 10605 (gi428685443), *Synechococcus* sp. PCC 7002 (gi2522460), *Lyngbya aestuarii* BL J (gi550814042), *Scytonema hofmanni* (gi516352295), *Calothrix* sp. PCC 7507 (gi427350415), *Nostoc* sp. PCC 7120 (gi17133386), *Nodularia spumigena* (gi493209471), *Anabaena cylindrica* PCC 7122 (gi428677279), *Crocospaera watsonii* (gi494517037), *Trichodesmium erythraeum* (gi499931389), *Synechococcus elongatus* PCC 6301 (gi56751283). Cytochrome *c*<sub>6A</sub> sequences are: *Cucumis sativus* (gi449433475), *Zea mays* (gi293334331), *Solanum lycopersicum* (gi460374873), *Arabidopsis thaliana* (gi332007810), *Chlamydomonas reinhardtii* (gi158273740). Cytochrome *c*<sub>6B</sub> sequences are: *Prochlorococcus marinus* str. MIT 9303 (gi124023458), *Synechococcus* sp. WH 7803 (gi148239320), *Synechococcus* sp. CC9605 (gi499683262), *Synechococcus* sp. BL107 (gi497475850), *Synechococcus* sp. WH 7803 (gi148239088). Cytochrome *c*<sub>6C</sub> sequences are: *Synechococcus* sp. PCC 7002 (gi22652035), *Trichodesmium erythraeum* (gi499933174), *Cyanothece* sp. PCC 7424 (gi501597452), *Crocospaera watsonii* (gi494515064 and gi494518195), *Nodularia spumigena* (gi493209475), *Nostoc* sp. PCC 7120 (gi17135139). Cytochrome *c*<sub>550</sub> sequences are: *Calothrix* sp. PCC 7507 (gi427353344), *Cylindrospermum stagnale* PCC 7417 (gi428259159), *Nostoc* sp. PCC 7107 (gi427710663), *Gloeocapsa* sp. PCC 7428 (gi428265205), *Rivularia* sp. PCC 7116 (gi427374782), *Synechococcus* sp. WH 8016 (gi351677206). Cytochrome *c*<sub>555</sub> sequences are: *Methylococcus capsulatus* str. Bath (gi53756998), *Chlorobium tepidum* TLS (gi21672916), *Xanthomonas translucens* (gi497260364). Cytochrome *c*<sub>M</sub> sequences are: *Microcystis aeruginosa* NIES-843 (gi166363520), *Synechococcus* sp. PCC 7002 (gi169884672), *Cyanothece* sp. ATCC 51142 (gi171699631), *Prochlorococcus marinus* str. NATL2A (gi72382534), *Prochlorococcus marinus* subsp. *marinus* str. CCMP1375 (gi33240028), *Prochlorococcus marinus* str. MIT 9211 (gi159888850), *Cyanobium* sp. PCC 7001 (gi197624664), *Synechococcus* sp. WH 7805 (gi88786922). Sequence similarities were calculated with Neighbor Joining using BLOSUM62.

$c_{6A}$ . The diversity of cyanobacteria in which  $c_6$ -like cytochrome genes are found (single-celled, filamentous, and nitrogen-fixing) suggests that these cytochromes appeared early in cyanobacterial evolution. Distinguishing features of the  $c_{6B}$  and  $c_{6C}$  cytochromes include (i) absence of the 12-residue, cysteine-containing, ‘Loop Insertion Sequence’ that characterizes the  $c_{6A}$  family (see Wastl et al. (2004) and Bialek et al. (2008) for alignments), (ii) a hydrophobic residue (leucine, isoleucine, valine) adjacent to the heme edge (position 50 in the *Synechococcus* 7002 PetJ2,  $c_{6C}$  protein) relative to a conserved glutamine in the corresponding location in  $c_6$  cytochromes, and (iii) a conserved tyrosine (position 61 in the *Synechococcus* 7002 protein) relative to a phenylalanine or tryptophan at this location in cytochromes  $c_6$  and  $c_{6A}$ . The hydrophobic residue at position 50 in the  $c_{6A,B,C}$  cytochromes and the resulting more limited hydrogen-bonding network around the heme appear to play major roles in lowering the redox midpoint potential of these  $c_6$ -like cytochromes relative the classical,  $c_6$  cytochromes (Worrall et al. 2007; Rajagopal et al. 2011; Bialek et al. 2014; Zatwarnicki et al. 2014). Genes for the  $c_{6B}$  cytochromes are found mostly among the non-nitrogen-fixing, *Prochlorococcus* and *Synechococcus* strains, which are widely distributed in diverse marine environments (Ting et al. 2002). The *petJ2*, cytochrome  $c_{6C}$  gene in the marine, coastal cyanobacterium *Synechococcus* 7002 seems to be rather exceptional because these genes are found mainly in heterocyst-forming or unicellular, nitrogen-fixing strains (Bialek et al. 2008).

Among related cytochromes,  $c_{550}$  is named after its  $\alpha$ -band absorbance maximum at 550 nm and is an extrinsic component of PSII in cyanobacteria and some eukaryotic algae such as red algae, dinoflagellates, and stramenopiles such as diatoms and brown algae (reviewed in Roncel et al. (2012)). Cytochromes  $c_{550}$  help stabilize the Mn cluster and oxygen-evolving complex of PSII, but are not essential for PSII activity, at least under standard growth conditions

(Shen et al. 1995; Li et al. 2004). The  $c_{550}$  heme has a unique, bis-histidine axial ligation, and a role in dissipating over-reduction of PSII has been proposed, but its function remains unresolved. Cytochrome  $c_{550}$  is also found in non-photosynthetic organisms, such as *Bacillus subtilis* where it fulfills a regulatory role in initiation of sporulation (Shin et al. 2005). Cytochrome  $c_{555}$ -encoding genes were initially found in *Chlorobium* genomes but further sequencing projects have identified increasing numbers of their homologs. Members of this family, for example from the hyperthermophilic bacterium, *Aquifex aeolicus*, have representatives that include soluble as well as membrane-anchored variants (Baymann et al. 2001b). Cytochrome  $c_M$  proteins are discussed in detail in Sect. IV.

### B. Biophysical Features

All  $c$ -type cytochromes, including  $c_6$ ,  $c_6$ -like and Cyt  $f$  proteins exhibit characteristic absorbance features in the visible wavelength range (see Holton and Myers (1967); Ho and Krogmann (1980); Bialek et al. (2008); Zatwarnicki et al. (2014) for representative spectra). Spectra of the oxidized forms have two absorbance peaks—an intense, narrow peak with a maximum at 410 nm (the Soret or  $\gamma$  band) and a broad flattened peak with a maximum at 530 nm. Upon heme reduction, the Soret band shifts slightly to higher wavelengths and two new peaks appear—the  $\beta$  peak at 520 nm and the  $\alpha$  peak at 550 nm—with simultaneous disappearance of the 530 nm peak. Table 34.1 shows the spectral properties, midpoint potentials ( $E_{m,7}$ ), and isoelectric points of three, representative  $c_6$ -like cytochromes purified from *Synechococcus* sp. WH 8102 (Cyt  $c_{6B}$  Zatwarnicki et al. (2014)), *Synechococcus* 7002 (Cyt  $c_{6C}$ , Bialek et al. (2008, 2014)), and *Nostoc* sp. PCC 7119 (a Cyt  $c_6$ -like protein that falls within the  $c_{6C}$  group, Reyes-Sosa et al. (2011)). For example, the *Nostoc* sp. PCC 7119 (hereafter *Nostoc* 7119)  $c_{6C}$  cytochrome, when reduced, shows absorbance maxima at 417 (Soret band),

Table 34.1. Biophysical properties of cyanobacterial  $c_6$ -like cytochromes<sup>a</sup>.

Protein	Isoelectric point	$E_{m7}$ (mV)	Absorbance maxima (nm)		
			Band $\gamma$	Band $\beta$	Band $\alpha$
Cyt $c_{6B}$	8.4	113	418.3	523.5	557.0
Cyt $c_{6C}$	9.7	155	416.5	523.6	556.1
$c_6$ -like Cyt	8.0	199	417	523	553

<sup>a</sup>Data for cytochrome  $c_{6B}$  are from *Synechococcus* sp. WH 8102 (Zatwarnicki et al. 2014), for  $c_{6C}$  from *Synechococcus* sp. PCC 7002 (Bialek et al. 2008, 2014), and for a  $c_6$ -like ( $c_{6C}$ ) cytochrome from *Nostoc* sp. PCC 7119 (Reyes-Sosa et al. 2011). The peak absorbance bands are from the reduced cytochromes

523 ( $\beta$ -band) and 553 nm ( $\alpha$ -band), whereas the oxidized protein has peaks at 409 and 528 nm. The spectral features of the reduced forms of cytochrome  $c_{6B}$  from *Synechococcus* sp. WH 8102 and  $c_{6C}$  from *Synechococcus* 7002 are very similar to those of the *Nostoc* 7119 protein, with the exception of their  $\alpha$ -bands, which are red-shifted (to 556 and 557 nm, respectively) relative to the *Nostoc* Cyt  $c_{6C}$  and the  $\alpha$ -bands of typical  $c_6$  cytochromes.

In contrast to their similar spectral properties, the  $c_6$ -like cytochromes have significantly lower midpoint potentials than their cytochrome  $c_6$  counterparts (Table 34.1). Cytochromes  $c_6$  from *Nostoc* 7119 and *Synechococcus* 7002 have midpoint potentials ( $E_{m,7}$ ) of +337 mV (Molina-Heredia et al. 1998) and +319 mV (Bialek et al. 2008), respectively. Potentials in this range enable these proteins to efficiently transfer electrons from Cyt  $f$  in the  $b_6f$  complex (which has midpoint potentials in the +270 to +340 mV range in cyanobacteria (Ho and Krogmann 1980; Ponamarev et al. 2000; Baymann et al. 2001a) to PSI (with most estimates of cyanobacterial P700+/P700 midpoint potentials in the +420 to +450 mV range, Nakamura et al. (2005); Bailleul et al. (2008)). For detailed discussion of the protein-protein interactions and mechanism of Cyt  $c_6$ -mediated electron transfer from Cyt  $f$  to PSI, see Chap. 31 by Diaz-Moreno et al.

The low midpoint potentials of +113 to +199 mV for representative  $c_6$ -like cytochromes (Table 34.1) exclude the possibility that these proteins could readily oxidize cytochrome  $f$ . The same argument

applies to chloroplast  $c_{6A}$  cytochromes that have midpoint potentials in the +100 to +140 mV range (Molina-Heredia et al. 2003; Marcaida et al. 2006). Nonetheless, it remains possible that under some conditions the  $c$ -like cytochromes may conduct electrons from Cyt  $f$  to PSI. Despite the unfavorable equilibrium for Cyt  $f$  oxidation by Cyt  $c_{6A}$  or Cyt  $c_{6B,C}$ , the overall transfer to PSI would be favorable. There are several examples of ‘roller coaster’ electron transfer pathways with unfavorable, ‘uphill’ intermediate steps. These include transfer from soluble Cyt  $c_2$  ( $E_m$  +300 mV) to Cyt  $c_{554}$  ( $E_m$  -50 mV), the first heme in the tetraheme donor chain in reaction centers of purple photosynthetic bacteria such as *Rhodobacter viridis* and *Blastochloris viridis*. A second uphill transfer in the overall, downhill pathway from Cyt  $c_2$  to the reaction center is at the step from Cyt  $c_{556}$  ( $E_m$  +320 mV) to Cyt  $c_{552}$  ( $E_m$  +30 mV) (see Baymann and Rappaport (1998) and Alric et al. (2006) for further discussion). Although electron flow from the Cyt  $b_6f$  complex to PSI via a ‘roller coaster’ pathway involving a  $c_{6B,C,A}$  or  $c_M$  cytochrome remains theoretically possible, no evidence has been found to support this. In *Synechocystis* 6803 (Manna and Vermaas 1997) and *Arabidopsis* (Weigel et al. 2003) Cyt  $c_6$  and PC double mutants, and in a *Synechococcus* 7002 PetJ1 Cyt  $c_6$  mutant (Nomura and Bryant 1999), the respective  $c_M$ ,  $c_{6A}$ , or  $c_{6C}$  cytochromes were unable to support phototrophic growth under the conditions tested.

Electron transfer from the *Arabidopsis* Cyt  $c_{6A}$  to PSI as well as cytochrome oxidase has

been demonstrated *in vitro*, although at significantly lower rates than from *Arabidopsis* PC or algal Cyt  $c_6$  (Molina-Heredia et al. 2003). Moreover, a significant electron transfer rate has been shown *in vitro* from the *Nostoc* 7119 Cyt  $c_{6C}$  to PSI at rates only 3.8 and 2.4-fold lower, respectively, than for the native Cyt  $c_6$  and PC carriers (Reyes-Sosa et al. 2011). In *Nostoc* 7119, Cyt  $c_{6C}$  has a basic isoelectric point of 8.0, which is close to those of the Cyt  $c_6$  and PC proteins from this cyanobacterium. Reyes-Sosa et al. (2011) proposed that the  $c_{6C}$  cytochrome could serve as an alternative electron donor to PSI, perhaps under nitrogen-fixing conditions from a pathway that does not include the Cyt  $b_6f$  complex. Electron transfer to a cytochrome oxidase remains possible as well, and has been shown *in vitro* for Cyt  $c_M$  (Bernroitner et al. 2009). To our knowledge this has not been tested for the  $c_{6B}$  or  $c_{6C}$  cytochromes.

### C. Structures and Heme Environment

Numerous Cyt  $c_6$  structures have been deposited into databases (e.g. Frazao et al.

1995; Kerfeld et al. 1995; Yamada et al. 2000; Sawaya et al. 2001; Bialek et al. 2009). High-resolution structures of *Arabidopsis*  $c_{6A}$  have been solved by Marcaida et al. (2006) both with the heme oxidized (ferric state, at 1.2 Å) and reduced (ferrous state, 1.4 Å) and by Chida et al. (2006) with the heme oxidized. Oxidation or reduction of the heme had little impact on the protein structure. See Chap. 33 by Howe et al. for further discussion and comparison of the Cyt  $c_{6A}$  structure relative to Cyt  $c_6$  from *Monoraphidium braunii*. Among related cytochromes of cyanobacteria, structures have been solved for Cyt  $c_{550}$  both in isolated form and in association with PSII (reviewed by Roncel et al. (2012)). The structure of a cyanobacterial Cyt  $c_{6B}$  from *Synechococcus* sp. WH 8102 has been determined at 1.4 Å (Zatwarnicki et al. (2014), PDB accession number 4KMG) and that of Cyt  $c_{6C}$  from *Synechococcus* 7002 at 1.03 Å (Bialek et al. (2014), 4EIE). Despite efforts toward this, no structures are yet available for Cyt  $c_M$ . Figure 34.2a, b show the overall structures of the cyanobacterial  $c_{6C}$  and  $c_{6B}$  cytochromes.

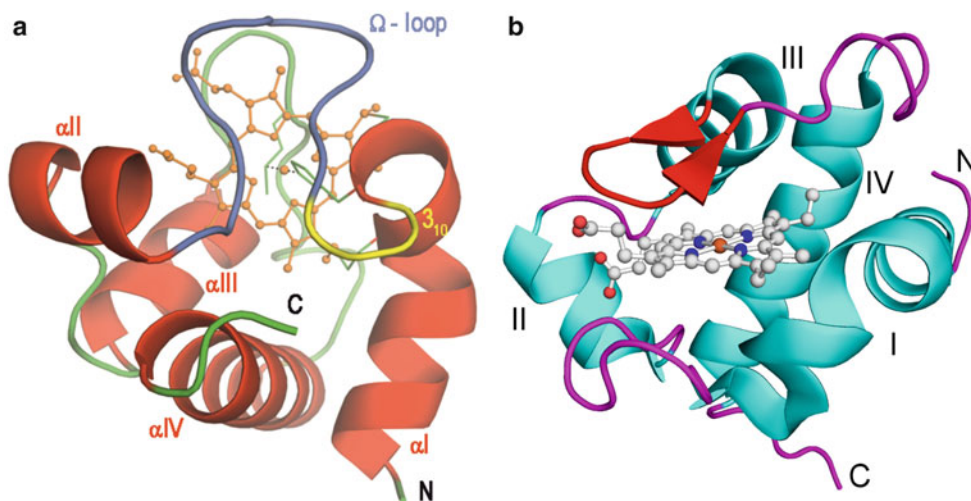


Fig. 34.2. Overall architecture of Cyt  $c_{6C}$  from *Synechococcus* sp PCC 7002 and Cyt  $c_{6B}$  from *Synechococcus* WH 8102. (a) Cyt  $c_{6C}$ . Secondary structures include  $\alpha$ -helices (red),  $3_{10}$ -helix (yellow) and several loops (green). The  $\Omega$ -loop characteristic of cytochromes  $c_{6C}$  is indicated in cyan. The heme group is shown as orange balls-and-sticks. (b) Cyt  $c_{6B}$ . The heme group is represented by balls and sticks. Secondary structures include  $\alpha$ -helices (cyan), loops (magenta), and a  $\beta$ -hairpin (red) (Figures a and b are reproduced from Bialek et al. (2014) and Zatwarnicki et al. (2014), respectively, with permission from the publishers).

The structures of classical  $c_6$  cytochromes as well as the  $c_6$ -like cytochromes share an overall architecture typical of class I cytochromes (Bialek et al. 2014). Their tertiary structure is determined by a four  $\alpha$ -helix bundle (with an additional  $3_{10}$  helix following the first  $\alpha$ -helix) wrapped around a single heme moiety. The first of these helices contains a characteristic kink at Cys14 belonging to the CXXCH heme-binding motif, which is involved in covalent attachment of the heme through a double, thioether linkage. The helices are separated by loops of varying lengths, with the characteristic, so-called  $\Omega$ -loop located between helices I and II. The central heme iron is axially coordinated by the imidazole ring of a conserved histidine (His18, in Cyt  $c_{6C}$  of *Synechococcus* 7002) and the sulfur atom of a specific methionine side chain (Met58 in Cyt  $c_{6C}$  of *Synechococcus* 7002). Whereas the overall fold of Cyt  $c_{6C}$  is not different from Cyt  $c_6$  proteins, the  $c_{6A}$  and  $c_{6B}$  proteins exhibit unique structural features. The  $c_{6A}$  proteins contain an additional, 12-residue, surface-exposed loop, designated the ‘Loop Insertion Sequence’ or ‘LIP’ (Howe et al. 2006). Because this loop contains two cysteines it was thought to have a role in redox-dependent regulation by oxidation of dithiol/disulfide groups via reduction of the LIP disulfide and electron transfer to the  $c_{6A}$  heme (Marcaida et al. 2006). However, a more recent study, in which the two cysteines were converted to serines, shows that the LIP disulfide has an important role in on-pathway folding and stability of the  $c_{6A}$  protein (Mason et al. 2012). Thus the postulated catalytic role of the LIP disulfide has fallen out of favor. In contrast to other known  $c_6$  and  $c_6$ -like protein structures, Cyt  $c_{6B}$  from *Synechococcus* sp. WH 8102 contains a  $\beta$ -hairpin located in the loop between helices III and IV (Fig. 34.2b). The significance of this feature is unclear at this time.

Key biophysical differences in the  $c_6$ -like cytochromes relative to  $c_6$  arise from the amino acids that surround the heme pocket and in surface charge distributions. In Cyt  $c_6$ , two separate surface domains have been

distinguished. The so called ‘north face’ consists of primarily hydrophobic residues surrounding the heme crevice, whereas the ‘east face’ has charged amino acids (Molina-Heredia et al. 1999). Both are considered important for rapid electron transfer from Cyt  $f$  to Cyt  $c_6$  and Cyt  $c_6$  to PSI. According to current models, efficient electron transfer and turnover first requires long-range electrostatic attractions via the Cyt  $c_6$  east face to establish initial, weak contacts. This is followed by hydrophobic interactions with the north face to bring donor-acceptor centers into proximity, followed by electron transfer and then rapid dissociation of the weakly bound encounter complex (Diaz-Moreno et al. 2014; Diaz-Moreno et al., Chap. 31). In cyanobacteria, cytochrome  $c_6$  may be acidic (as in *Synechococcus* 7002) or basic (as in *Nostoc* 7119) and the interacting Cyt  $f$  and PSI surfaces typically carry complementary charges (Hervas et al. 2005). Notably, in contrast to the acidic  $pI$  and surface charge of Cyt  $c_6$  from *Synechococcus* 7002, its Cyt  $c_{6C}$  has a basic  $pI$  and positively charged east face (Bialek et al. 2008, 2014). This further suggests that Cyt  $c_{6C}$  would not be an effective electron carrier from the Cyt  $b_6f$  complex to PSI or cytochrome oxidase and rather implies that it may interact with different partners or by a different mechanism. However, it has also been shown that PSI, at least from *Nostoc* 7119, can be relatively indiscriminate with respect to the surface charge of the Cyt  $c_6$  donor (Hervas et al. 2005). Table 34.2 shows the calculated molecular weights and  $pI$  values of  $c_{6A}$ ,  $c_{6B}$ , and  $c_{6C}$  cytochromes from a number of sources. As in *Synechococcus* 7002, the predicted  $pI$  values of  $c_{6C}$  cytochromes are basic, whereas those for the chloroplast  $c_{6A}$  cytochromes are slightly acidic. The cyanobacterial  $c_{6B}$  cytochromes cover a wide range of  $pI$  values from acidic to basic.

All cytochrome  $c_6$  and  $c_6$ -like proteins carry a covalently bound heme. Thioether bonds between the heme and polypeptide chain are established between the vinyl groups of the porphyrin ring and sulfhydryl groups of conserved cysteines (Cys14 and



Table 34.2. Calculated pI values and molecular weights of cytochrome  $c_6$ -like proteins<sup>a</sup>.

Cyt $c_{6A}$			Cyt $c_{6B}$			Cyt $c_{6C}$		
Species	pI	MW (Da)	Species	pI	MW (Da)	Species	pI	MW (Da)
<i>Glycine max</i>	5.3	10,986.4	<i>S. RCC307</i>	4.9	8884.0	<i>S. 7002</i>	8.7	9400.5
<i>Medicago</i>	5.1	11,948.4	<i>S. WH7803</i>	5.5	9045.1	<i>A. marina</i>	8.0	9448.7
<i>Solano</i>	5.1	11,387.7	<i>S. WH7805</i>	5.5	9235.3	<i>A. maxima</i>	8.0	9718.9
<i>Chlamydomonas</i>	5.8	10,585.0	<i>P. NAT1</i>	5.6	9662.7	<i>Cr. watsonii</i>	9.6	9709.2
<i>Arabidopsis</i>	5.1	11,703.1	<i>S. CC9311</i>	5.7	9325.4	<i>Cr. watsonii</i>	9.7	9779.2
<i>Triticum</i>	5.2	11,452.8	<i>S. RS9916</i>	6.0	9004.1	<i>S. 7942</i>	8.7	9134.4
<i>Aegilops</i>	6.5	10,883.3	<i>S. BL107</i>	6.0	9129.3	<i>S. 6301</i>	8.7	9134.4
<i>Hordeum</i>	6.5	12,412.0	<i>S. CC9902</i>	6.1	9290.5	<i>C. 51142</i>	9.0	10,006.4
<i>Oriza</i>	5.7	11,173.7	<i>S. CC9605</i>	6.1	9608.8	<i>C. CCY0110</i>	9.2	10,065.5
			<i>P. NAT2A</i>	6.1	9691.8	<i>C. 7424</i>	8.0	10,123.4
			<i>P. 9313</i>	6.9	9491.6	<i>C. 7425</i>	8.1	9251.4
			<i>P. 9303</i>	6.9	9519.6	<i>C. 7822</i>	9.6	9631.0
			<i>P. 9211</i>	7.0	9889.3	<i>C. 8801</i>	8.0	9618.9
			<i>S. WH8102</i>	8.0	9223.4	<i>C. 8802</i>	8.0	9618.9
			<i>P. 1375</i>	8.0	9733.9	<i>A. variabilis</i>	9.0	9494.8
			<i>Cy. 7001</i>	8.1	9494.7	<i>Nostoc 7120</i>	8.1	9668.9
			<i>S. RS9917</i>	8.1	9400.5	<i>N. punctiforme</i>	8.7	9597.9
			<i>S. WH5701</i>	8.1	9323.6	<i>N. spumigena</i>	8.7	9515.7
			<i>P. 9301</i>	9.0	9505.9	<i>T. erythraeum</i>	9.6	9848.3
			<i>P. 9312</i>	9.0	9550.0	<i>Lyngbya 8106</i>	9.5	9647.9

<sup>a</sup>Isoelectric points and predicted molecular weights were calculated with ProtParam software (Gasteiger et al. 2005)

Cys17) in the canonical CXXCH heme-binding motif located within a hydrophobic pocket of the protein (Fig. 34.3a). The residue numbers are those of the *Synechococcus* 7002 proteins. A typical feature of these proteins as well as other  $c$ -type cytochromes is a slight, saddle-shape bend of this ligand and coordination of its central iron ion by a nitrogen from a histidine (His18) imidazole ring and a sulfur atom from a conserved methionine (Met58). Despite the differences in redox properties between the Cyt  $c_6$  and  $c_6$ -like families, the distances from their central heme irons to their His-Met, axial coordination partners as well as their N-Fe-S angles remain virtually the same among the characterized  $c_6$  and  $c_6$ -like proteins (Marcaida et al. 2006; Bialek et al. 2014; Zatwarnicki et al. 2014).

Key structural features that govern the midpoint potential and presumably the

function of  $c_6$ -like cytochromes include the amino acids that occupy positions adjacent to the heme. The most important of these is a glutamine at position 50 (numbered according to the *Synechococcus* 7002 Cyt  $c_{6C}$ ) that is conserved among  $c_6$  cytochromes (Bialek et al. 2008). Its replacement by a hydrophobic residue such as valine, leucine or isoleucine in  $c_6$ -like cytochromes results in a significant decrease in the midpoint potential. The role of the amino acid at position 50 has been confirmed by directed mutagenesis. Re-introduction of glutamine at this site in cytochromes  $c_{6A}$  (Worrall et al. 2007) and  $c_{6C}$  (Bialek et al. 2014) led to a 50–100 mV increase in midpoint potential. Conversely, substitution of valine for Gln50 in the Cyt  $c_6$  heme crevice decreased the  $E_m$  by 100 mV in these proteins from *Synechococcus* 7002 (Bialek et al. 2014) and *Phormidium laminosum*

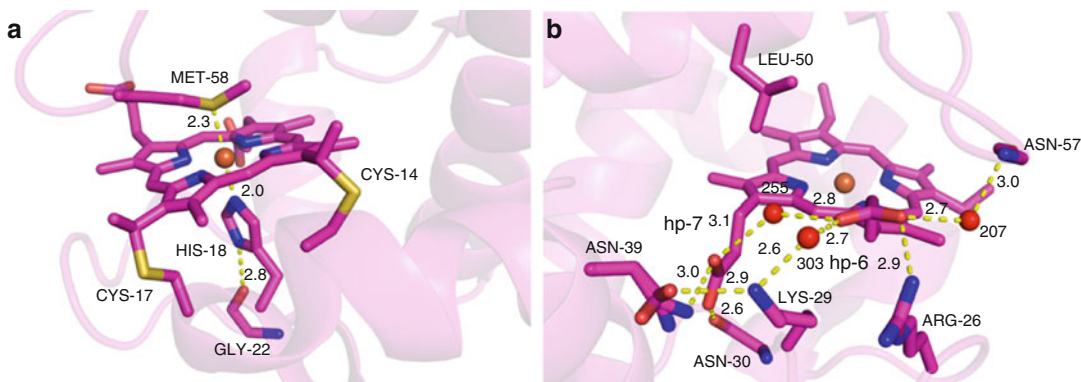


Fig. 34.3. Heme-binding pocket of Cyt  $c_{6C}$  from *Synechococcus* sp. PCC 7002. (a) Cyt  $c_{6C}$  heme pocket showing thioether linkages to Cys-14 and -17, and the His-18 and Met-58 axial ligands. The heme iron is depicted as an orange sphere. (b) Cyt  $c_{6C}$  heme environment showing three bound water molecules (large red spheres) and polar residues that participate in a hydrogen bonding network surrounding the heme. The heme iron is shown as an orange sphere. The H-bonding network does not extend above the heme plane as it does in Cyt  $c_6$ . The hydrophobic Leu-50 lies in proximity to the heme edge in a position occupied by the polar Gln-50 residue in Cyt  $c_6$  proteins. Dashed lines in both panels represent hydrogen bonds and distances are given in Å.

(Rajagopal et al. 2011). The structures of the  $c_6$  and  $c_6$ -like cytochromes indicate that in addition to the amino acid at position 50, an equally important determinant of redox properties may be the extent and distribution of structural water molecules and the hydrogen-bonding network around the heme group (Fig. 34.3b). Whereas all of these water molecules are located above the heme propionate-7 plane in cytochromes  $c_6$ , replacement of the conserved Gln50 in the heme cavity by a hydrophobic residue completely alters the pattern of the hydrogen bonding among amino acid side chains and structural water molecules around the heme (Bialek et al. 2014; Zatwarnicki et al. 2014). Thus the polar Gln residue in the heme pocket of Cyt  $c_6$ , as well as the H-bonding network around the heme, stabilize the reduced form of the heme resulting in the characteristically high midpoint potentials of  $c_6$  cytochromes. In contrast, a more hydrophobic environment and diminished H-bonding network around the  $c_{6A,B,C}$  hemes decreases the stability of an electron on the reduced heme resulting in a lower midpoint potential (Worrall et al. 2007; Rajagopal et al. 2011; Bialek et al. 2014; Zatwarnicki et al. 2014).

## IV. Cytochrome $c_M$

### A. Genome Analyses

The sequence alignments in Fig. 34.4 show the conserved heme-binding motif CXYCH (residues 16–20) near the predicted N-terminus of the mature Cyt  $c_M$  protein, where X is predominantly alanine and Y almost exclusively a glycine residue. Note, however, that it remains unclear whether the mature Cyt  $c_M$  protein is as shown in Fig. 34.4 or whether the N-terminal domain (not shown in this figure) is retained and functions as a membrane anchor. At least two studies (Cho et al. 2000; Bernroitner et al. 2009) support the latter hypothesis as discussed further below. The heme-binding motif is directly preceded by an asparagine in all of the aligned sequences (Fig. 34.4). His20 in the heme-binding motif provides the fifth ligand (an axial ligand) for the heme, but because of limited data, the sixth ligand (second axial ligand) of Cyt  $c_M$  remains unresolved. Based on sequence alignments, two methionine residues, Met56 and Met66 (as numbered in Fig. 34.4) are likely candidates. The former is a part of an absolutely conserved GXTTPMPXF motif,

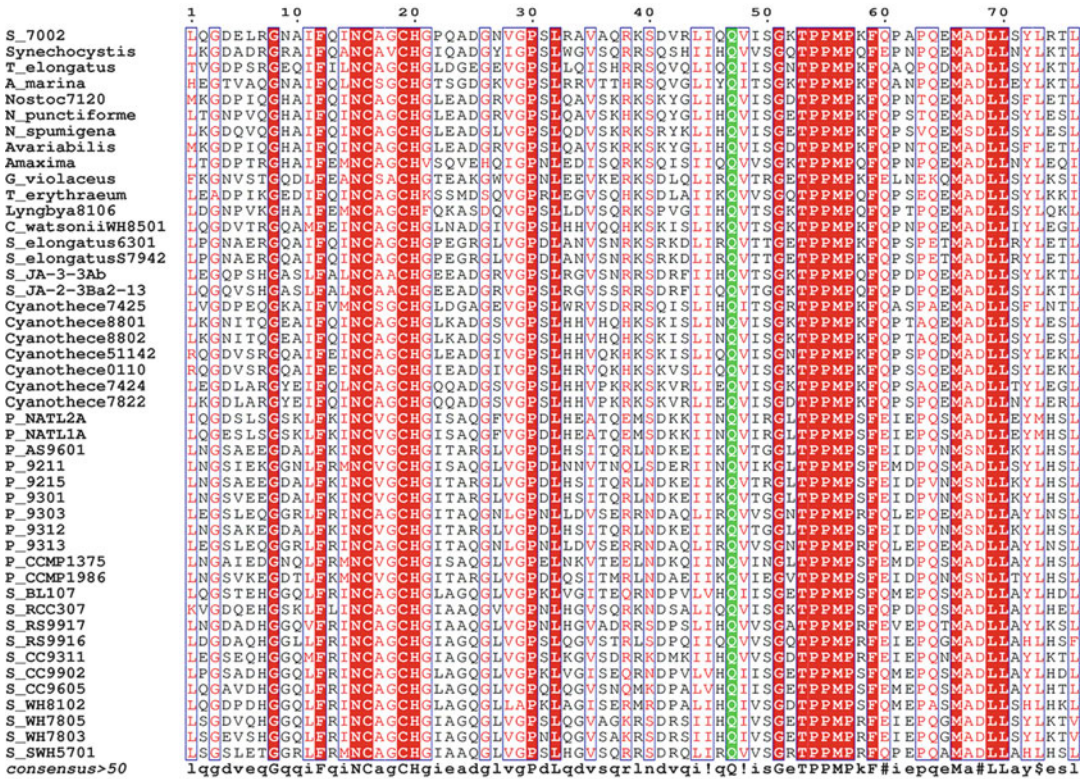


Fig. 34.4. Sequence alignments of the putative ‘mature,’ processed region of Cyt  $c_M$  proteins where the N-terminal targeting domain has been removed. It remains controversial whether this N-terminal domain is a targeting sequence or a membrane anchor. The glutamine (Q-47) residue in Cyt  $c_M$  that corresponds to an absolutely conserved glutamine in Cyt  $c_6$  and a small hydrophobic residue (I, L or V) in Cyt  $c_{6B}$  and Cyt  $c_{6C}$  is highlighted in green. In the strain designations, *P* represents *Prochlorococcus* and *S* represents *Synechococcus* strains (Figure prepared using ESPrnt (Gouet et al. 1999)).

and in our opinion is most likely to act as a heme ligand as Met66 may be too close to the C-terminus. Homology modeling of Cyt  $c_M$  from *A. maxima* using horse-heart Cyt  $c$  as a template did not clarify which methionine acts as the sixth ligand (Ho et al. 2011). In contrast to cytochromes  $c_6$ ,  $c_{6A,B,C}$  and  $c_{550}$ , Cyt  $c_M$  has yet to be crystallized. Surprisingly, all attempts at crystallization from *Synechocystis* 6803 (Ho et al. 2011) and *Synechococcus* 7002 (Bialek, unpublished results) have failed.

Analysis of currently available cyanobacterial genomes reveals a single copy gene, *cytM*, encoding the Cyt  $c_M$  protein, which occurs in almost all cyanobacterial species, with the exception of one known strain (*Prochlorococcus marinus* MIT9515). The

*cytM* gene is more common than either the Cyt  $c_{6B}$  or  $c_{6C}$  genes. Cyt  $c_M$  seems to be evenly distributed among species harboring Cyt  $c_{6B}$  or  $c_{6C}$  sequences (Fig. 34.5). As in Cyt  $c_6$ , but in contrast to Cyt  $c_{6A}$ ,  $c_{6B}$  and  $c_{6C}$ , all predicted Cyt  $c_M$  proteins harbor an absolutely conserved glutamine residue, Q47 (residue numbering as in Fig. 34.4). The amino acid at this position modulates redox potential, as shown for Cyt  $c_6$ ,  $c_{6A}$  and  $c_{6C}$  (Worrall et al. 2007; Bialek et al. 2014). On the one hand, Cyt  $c_M$  seems more similar to Cyt  $c_6$  because of the key, conserved glutamine residue at a homologous position. On the other hand, the measured redox midpoint potential ( $E_{m,7}$ ) of Cyt  $c_M$  is only +151 mV (Cho et al. 2000), which is less than half the typical value for Cyt  $c_6$ ,

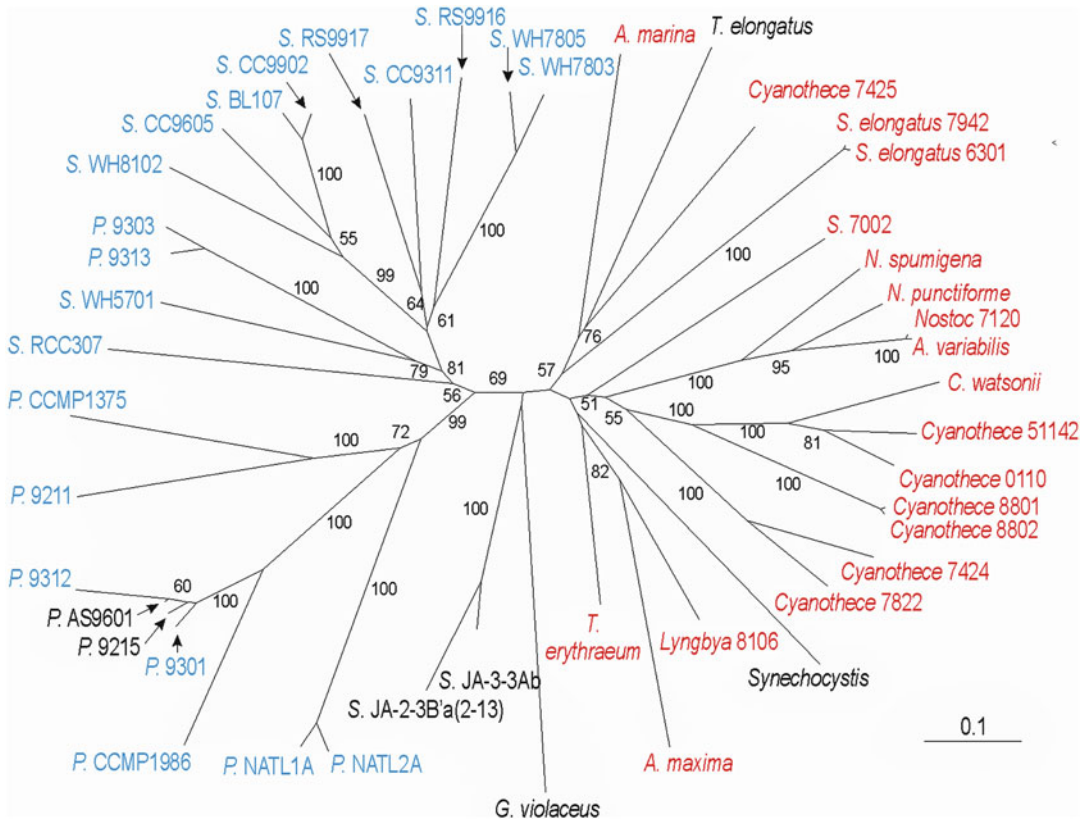


Fig. 34.5. Unrooted phylogenetic tree of Cyt  $c_M$  proteins. Cyanobacterial species harboring genes for Cyt  $c_{6B}$  or  $c_{6C}$  are shown in blue and red, respectively. Species harboring the Cyt  $c_M$  gene but lacking genes for  $c_{6B}$  or  $c_{6C}$  are shown in black. The bar represents evolutionary distance in substitutions per residue.

virtually the same as that of Cyt  $c_{6C}$  from *Synechococcus* 7002 (+148 mV, Bialek et al. (2008)), and similar to that of Cyt  $c_{6B}$  from *Synechococcus* sp. WH 8102 (+113 mV, Zatwarnicki et al. (2014)). In that regard, Cyt  $c_M$  appears to be more similar to the other Cyt  $c_6$ -like cytochromes in terms of its likely functional properties.

### B. Biophysical Features

The nucleotide sequence of Cyt  $c_M$  from *Synechocystis* 6803 contains two putative transcription start sites. Given the location of a probable ribosome binding site (RBS), Malakhov et al. (1994) proposed that transcription results in a pre-protein of 11.4 kDa. Analysis of the Cyt  $c_M$  N-terminal region suggested that it could be either a

transit peptide for targeting to the thylakoid lumen, the periplasm, or else a membrane anchor. Because this region resembles transit peptides of cytochromes  $c_6$ , Molina-Heredia et al. (2002) concluded that it most likely functions as a genuine transit peptide, which, after cleavage, results in a mature protein of 8.3 kDa. The presence of the VLA motif, as in the 18 kDa protein of the PSII oxygen-evolving complex (OEC) from spinach (Malakhov et al. 1994; Seidler 1996; Molina-Heredia et al. 2002), supported the view that the Cyt  $c_M$  N-terminus functions in targeting to the lumen. However, it was not clear whether the hydrophobic N-terminal domain is processed *in vivo*. Immunoblotting with antibodies against recombinant Cyt  $c_M$  revealed a protein from *Synechocystis* 6803 that is larger than the presumptive, ‘mature’

Cyt  $c_M$  expressed in *E. coli* (Cho et al. 2000). This suggested that the N-terminal domain functions as a membrane anchor. A subsequent immunoblot study supported this hypothesis. Bernroitner et al. (2009) detected Cyt  $c_M$  in both cytoplasmic and thylakoid membrane fractions but not cytosolic extracts, strongly suggesting that Cyt  $c_M$  is an integral membrane protein. Further confirmation is lacking but the apparent localization of Cyt  $c_M$  in cytoplasmic as well as thylakoid membranes raises intriguing questions about possible roles in specific electron transport chains.

Bernroitner et al. (2009) further showed that the Cyt  $c_M$  protein content increases under high salt stress, corroborating earlier findings showing that stresses such as low temperature and high light elevate Cyt  $c_M$  (*cytM*) transcripts (Malakhov et al. 1999; Shuvalov et al. 2001). Increased *cytM* transcript levels were subsequently also detected in *Synechocystis* 6803 grown under sulfur deprivation (Zhang et al. 2008). In depth 'RNA Seq,' transcriptomic studies of *Synechococcus* 7002 further revealed that low temperature, heat shock, oxidative stress, mixotrophic growth, high salt, and high light intensity increased, whereas low salt and phosphorus deprivation modestly decreased *cytM* (SynPCC7002\_A0375) transcripts (Ludwig and Bryant 2011, 2012a, b). The same authors showed that CO<sub>2</sub>, nitrogen, sulfur, and iron limitations also increased *cytM* transcripts. However, it should be noted that under standard growth conditions for *Synechococcus* 7002 (250  $\mu\text{mol photons m}^{-2} \text{s}^{-1}$ , 5 % CO<sub>2</sub>), the *petJ1* (SynPCC7002\_A0167) transcript for Cyt  $c_6$  represents 1 % of the total mRNA whereas the *cytM* transcript is less than 0.002 %, or >500-fold lower than that for *petJ1*. Under high salt, low nitrogen, and low sulfur, *cytM* transcripts increase by 12, 14, and 24-fold, respectively; whereas *petJ1* transcripts decline by 2–3-fold. Under these conditions, *cytM* transcripts comprise 0.025–0.05 % of the total mRNA, relative to *petJ1* at 0.35–0.6 %, but are still 10–20-fold lower than the *petJ1* mRNA. We are unaware

of any quantitative study of Cyt  $c_M$  specific protein content and turnover relative to Cyt  $c_6$ . Assuming that the mRNA transcript levels reflect protein abundance, these data suggest that even under stress conditions, Cyt  $c_M$  may not be present in quantities sufficient to play a large role in a major, photosynthetic electron transport pathway. However, these gene expression profiles may be compatible with a regulatory role for Cyt  $c_M$  or one that alleviates over reduction of electron carriers under certain stress conditions and the damaging consequences of this.

## V. Possible Functions of $c_6$ -Like and $c_M$ Cytochromes

The functions of  $c_6$ -like cytochromes remain obscure but interesting clues have begun to emerge. The most likely roles for Cyt  $c_{6C}$ ,  $c_{6B}$ , and  $c_M$  cytochromes are: (1) in alternative electron transfer pathways to alleviate sudden over-reduction of electron carriers and generation of damaging oxygen radicals, (2) in the cytoplasmic membrane in electron transfer pathways that energize that membrane for transport processes, or (3) in regulation, for example of electron transfer, metabolic pathways, or gene expression.

With respect to stress responses and redox homeostasis, it is well established that photosynthetic and respiratory electron transfer chains in cyanobacteria intersect through the plastoquinone pool, Cyt  $b_{6f}$  complex, and soluble carriers (Cyt  $c_6$  or PC) that conduct electrons to PSI or a terminal oxidase (see Kallas (2012); Mullineaux (2014) for reviews). The respiratory electron transfer pathways are much less active than photosynthetic pathways but may operate concurrently to maintain redox balance, mitigate photoinhibition, and minimize the formation of reactive oxygen species (ROS) (Helman et al. 2003, 2005). In addition, cyanobacteria have evolved a further suite of mechanisms to alleviate the sudden and dangerous over-reduction of electron carriers. These include photoprotective, non-photochemical quenching (qE) mediated by

the orange carotenoid protein (OCP), that when activated by blue-green light dissipates excitation energy as heat and thereby effectively decreases the phycobilisome antenna (reviewed by Kirilovsky and Kerfeld (2012)).

At the level of electron transfer, cyanobacteria have evolved a number of branched pathways to maintain redox balance and this is where the  $c_6$ -like cytochromes may have roles. Almost all cyanobacteria encode the Flv1/Flv3 flavodiiron proteins and a more limited number among the  $\beta$ -cyanobacteria have Flv2/Flv4 (reviewed by Allahverdiyeva et al. (2015)). Flv1/3 catalyze electron transfer from PSI to molecular oxygen in a harmless ‘Mehler-like’ reaction that does not generate the superoxide as in the classical Mehler reaction in chloroplasts (Mehler 1951). Interestingly,  $\Delta flv1/3$  knockout mutants have no noticeable impact on growth under either continuous light or light–dark cycles with steady illumination phases. However, the  $\Delta flv1/3$  mutation severely limits growth or even result in cell death in cultures grown under fluctuating light regimes such as those encountered in natural environments (Helman et al. 2003; Allahverdiyeva et al. 2011, 2013). Indeed it has now become evident that such fluctuating conditions with rapid shifts from very low to high light intensities are extremely stressful because they result in rapid over-reduction of electron carriers and production of damaging ROS (Lea-Smith et al. 2013). Thus the Flv1/3 flavodiiron proteins have been shown to provide crucial protection for PSI against acceptor side over-reduction and ROS production. In the cyanobacteria that have them, the Flv2/4 proteins protect PSII against damage from over excitation at high light intensities and low (ambient) CO<sub>2</sub> (Zhang et al. 2009, 2012; Bersanini et al. 2014). Part of this mechanism involves a not yet characterized electron transfer route that funnels electrons from the vicinity of the Q<sub>B</sub>, acceptor site of PSII into an unknown electron transfer pathway. Might this pathway involve the  $c_{6B}$ ,  $c_{6C}$ , or  $c_M$  cytochromes?

In *Synechocystis* 6803, *flv2/4* genes are upregulated in response to high light, oxidative stress, and particularly under CO<sub>2</sub> limitation (Allahverdiyeva et al. 2015). *Cyt c<sub>M</sub>* transcripts are upregulated, at least in *Synechococcus* 7002, under the same conditions. Note, however, that *Synechococcus* 7002 does not have *flv2/4* genes and *Synechocystis* 6803 is one of the few cyanobacteria that does not carry genes for *Cyt c<sub>6B</sub>* or  $c_{6C}$ . Thus a Q<sub>B</sub>>Flv2/4 route involving *Cyt c<sub>M</sub>* to mitigate acceptor side (PQ pool) over-reduction in cyanobacteria such as *Synechococcus* 7002 remains possible, but at present no evidence exists to support this. Given the emergent appreciation of mechanisms that have evolved to alleviate the hazards of fluctuating light exposures, it may be interesting to test knockout mutant of the  $c_{6B}$ ,  $c_{6C}$ , and  $c_M$  cytochromes under such conditions. To our knowledge, such experiments have not been conducted.

Other branched pathways and mechanisms that cyanobacteria may use to alleviate over-reduction and ROS production include photorespiration (Eisenhut et al. 2008; Allahverdiyeva et al. 2011), terminal oxidases (Lea-Smith et al. 2013), quinol (*Cyd*) oxidases (Berry et al. (2002); see also Chap. 19, Young et al.), alternative respiratory terminal (ARTO or Cta-II) oxidases (Howitt and Vermaas 1998; Nomura et al. 2006b), ‘plastid’ terminal oxidases (PTOX) (Bailey et al. 2008), and nitrate reductases (Flores et al. 2005). All cyanobacteria appear to have at least one terminal oxidase and may have different combinations or none of the *bd*-type quinol, ARTO, and PTOX oxidases that either take electrons from the PQ pool or from water soluble carriers (see Chap. 17 by Schmetterer). The  $c_6$ -like cytochromes may function in some of these pathways, perhaps again as safety-valves at specific electron transfer steps to help relieve over-reduction induced by sudden upswings in light intensity. PSI or terminal oxidases could be available as electron acceptors under some of these conditions. Electron transfer has been demonstrated at reasonable rates from *Cyt c<sub>6C</sub>* to PSI (Reyes-Sosa et al.

2011) and from Cyt  $c_M$  to the CtaI, *aa3* cytochrome oxidase (Bernroitner et al. 2009) and might be performed as well, at least in principle, by any of the  $c_6$ -like cytochromes. An intriguing, possible, ‘overflow’ pathway may be one from PQH<sub>2</sub> in the PQ pool to PSI or a terminal oxidase via the Rieske iron-sulfur protein (ISP) and one of the  $c_6$ -like cytochromes. This may confer an important selective advantage because PQH<sub>2</sub> oxidation by the Cyt *b<sub>6</sub>f* complex via the Rieske ISP and Cyt *f* is the usual rate-limiting step in electron transport (Kallas (2012) and references therein). The high-resolution, 2.0 Å structure of the PetC Rieske ISP of *Thermosynechococcus elongatus* reveals a deep hydrophobic pocket facing the membrane in the soluble 2Fe-2S cluster-bearing domain of the protein (Veit et al. 2012). This pocket appears to be conserved in PetC1 Rieske ISPs. As suggested by Veit et al. (2012) and Bernat et al. (Chap. 13), this pocket might serve as the binding site for a lipid, plastoquinone, chlorophyll, or carotenoid molecule, or perhaps the hydrophobic domain of a protein such as plastocyanin. A cytochrome  $c_{6B}$ ,  $c_{6C}$ , or  $c_M$  might similarly either bind here or accept electrons from plastoquinol bound to this site to provide an electron pathway that circumvents Cyt *f* en route to PSI or a terminal oxidase. This could provide an alternative, ‘safety-valve’ route to alleviate PQ pool over-reduction. Hydrophobic contacts are important in forming encounter complexes between both PC and Cyt  $c_6$  with Cyt *f* (see Chap. 30, Bendall and Howe, and Chap. 31, Diaz-Moreno et al.) and would likely be important as well in interactions involving the  $c_6$ -like cytochromes. Some experimental data suggest an electron pathway through the Cyt *b<sub>6</sub>f* complex that circumvents Cyt *f* (Fernandez-Velasco et al. 2001), but to our knowledge this has not been corroborated by further studies.

A possible problem with roles for the  $c_{6B}$ ,  $c_{6C}$ , or  $c_M$  cytochromes in ‘safety-valve’ electron flow pathways is that available transcription data, as discussed above, suggests a relatively low abundance of these proteins. For example, in *Synechococcus* 7002 grown

under standard photoautotrophic conditions, the *petJ1* transcript for Cyt  $c_6$  represents 1 % of total transcript counts (normalized per kb); whereas the Cyt  $c_{6C}$  and  $c_M$  counts under these conditions are 0.01 % and 0.002 % of the total, respectively (Ludwig and Bryant 2011, 2012a, b). Cyt  $c_{6C}$  transcripts increase up to 3–4-fold under stresses such as high salt or sulfur deprivation. Cyt  $c_M$  transcripts increase more dramatically up to 12–24-fold under stresses such as high salt or nitrogen and sulfur deprivation, where they may represent up to 0.05 % of total mRNA counts (Ludwig and Bryant 2011, 2012a, b). By comparison, the *flv1* (\_A1321) transcript for Flv1, with an established role in alleviating PSI acceptor-side over-reduction (Allahverdiyeva et al. 2013), represents 0.015 % of total transcripts under standard conditions in *Synechococcus* 7002. *Flv1* transcripts increase 19-fold up to 0.3 % of the total under limiting CO<sub>2</sub> but only 2–3-fold up to 0.02 % to 0.04 % of the total under high salt or limiting nitrogen or sulfur. The *flv1* transcript level is similar to that of *petJ2* for Cyt  $c_{6C}$  under standard conditions but 30-times higher under low CO<sub>2</sub>. However, under high salt or limiting N or S, the *flv1* transcript is similar within a factor or twofold or even lower than the transcript levels for *petJ2* or *cytM* (for Cyt  $c_M$ ) (Ludwig and Bryant 2011, 2012a, b). This does not answer the question of whether the Cyt  $c_{6C}$ ,  $c_{6B}$ , or  $c_M$  proteins may be present in sufficient quantity for roles in ‘overflow’ electron pathways, but does suggest that they could be significant under certain stress conditions.

Immunological data show that Cyt  $c_M$  is localized to both thylakoid and cytoplasmic membranes of *Synechocystis* sp. PCC 6803 (Bernroitner et al. 2009). The same authors showed that Cyt  $c_M$  transfers electrons to the Cu<sub>A</sub> center of cytochrome oxidase in vitro as efficiently as Cyt  $c_6$ . These findings raise interesting possibilities for participation of Cyt  $c_M$  (and possibly  $c_{6B}$  or  $c_{6C}$ ) in a cytoplasmic membrane electron pathway, possibly leading to a terminal oxidase. However, at this stage, it is not known what that pathway might be. Indeed the composition of cyanobacterial

cytoplasmic membranes remains unresolved but important differences exist among ecotypes. According to the model of Schultze et al. (2009), the cytoplasmic membrane of *Synechocystis* 6803 carries an electron transfer chain comprised of succinate (SDH) and NDH-2 NADH dehydrogenases, quinol oxidase (Cyd), a CtaII (or ARTO) terminal oxidase, and an ATP synthase. The dehydrogenases and oxidases are linked via a plastoquinone pool and a pH gradient across the membrane is established either by the quinone reduction-oxidation reactions or the ATP synthase operating in reverse. A similar model is presented by Lea-Smith et al. (2013) and supported by proteomics data (Huang et al. 2002; Agarwal et al. 2010). The thylakoid membrane of PCC 6803 also contains the Cyd quinol oxidase in addition to the CtaI cytochrome oxidase, succinate dehydrogenase, and NDH-I, NDH-2 NAD(P)H dehydrogenases. The importance of the CtaI (Howitt and Vermaas 1998) and Cyd (Berry et al. 2002) oxidases for redox balance is well established, and essential under some conditions as illustrated by the lethality of a CtaI mutant of *Synechocystis* sp. PCC 6803 grown at low light intensity (Kufryk and Vermaas 2006). Lea-Smith et al. (2013) have now demonstrated convincingly that one or the other of these oxidases is essential for survival under fluctuating light conditions. *Synechococcus* 7002 possesses only the CtaI and CtaII (ARTO) terminal oxidases and CtaII has been shown to have an important role in regulation of oxidative stress responses (Nomura et al. 2006a, b). See also Chap. 17 by Schmetterer for further discussion.

With respect to cytoplasmic membranes and  $c_6$ -like cytochromes, the immunological analysis of *Synechocystis* 6803 by Schultze et al. (2009) shows that these membranes exclusively contain the PetC3 Rieske iron-sulfur protein but not the PetC1 or PetC2 ISPs or other subunits of the Cyt  $b_6f$  complex. The role of the PetC3 ISP in the cytoplasmic membrane is not resolved but its midpoint potential of +135 mV

(Schneider et al. 2002) may be compatible with electron transfer to a Cyt  $c_{6C}$  or  $c_M$  with midpoint potentials of +150 to 200 mV or perhaps with reverse flow from some of these cytochromes or  $c_{6B}$  which has a lower potential (Table 34.1). In Chap. 13, Bernat et al. show that the PetC3 ISP shares similarity with Rieske-type subunits of periplasmic, membrane-bound arsenite oxidases (Lebrun et al. 2003) and propose that PetC3 may be a component of such an enzyme. Co-transcribed genes for sulfide:quinone oxidoreductase (*suoS*) and a putative arsenite importer (*suoT*) or arsenite:quinone oxidoreductase are extensively upregulated in the presence of sulfide or arsenite (Nagy et al. 2014). The involvement, if any, of  $c_{6C}$ ,  $c_{6B}$ , or  $c_M$  cytochromes in such pathways is not clear although their midpoint potentials would make them suitable as electron acceptors for arsenite ( $E_{m,7} + 60$  mV, van Lis et al. (2013)) or plastoquinol ( $E_{m,7} + 80$  mV, Schuurmans et al. (2014)). The terminal electron acceptor for a cytoplasmic membrane,  $c_6$ -like cytochrome is also unclear because these membranes may be limited to CtaII (ARTO) oxidases that accept electrons from quinol, thus apparently excluding electron transfer from Cyt  $c_{6C}$ ,  $c_{6B}$ , or  $c_M$ .

With respect to possible roles in regulation, Hiraide et al. (2015) uncovered an interesting phenotype for Cyt  $c_M$  relative to dark, heterotrophic growth. They show that Cyt  $c_M$  mutants exhibit faster dark, heterotrophic growth on glucose than the wild type *Leptolyngbya boryana* and enable genuine, dark heterotrophic growth (in contrast to 'light activated heterotrophic growth'—LAHG, Anderson and McIntosh (1991)) in *Synechocystis* 6803. They suggest that this curious phenotype may reflect an adaptation that spares respiratory, carbohydrate reserves under extended stress conditions that induce Cyt  $c_M$  expression. The basis for this may be related to the finding of Manna and Vermaas (1997) of sequence similarity between Cyt  $c_M$  and Cyt  $c$ -binding domains of CtaI,  $aa_3$ -type cytochrome oxidases and their proposal that Cyt  $c_M$  is subunit of this oxidase in cyanobacteria. Cyt  $c_M$  associated with the



CtaI oxidase may exert a suppressive effect as suggested by Hiraide et al. (2015). Because the CtaI oxidase is apparently not located in cytoplasmic membranes of typical cyanobacteria and because only a small fraction of known cyanobacteria can grow heterotrophically in darkness, Cyt  $c_M$  must have functions that extend beyond the modulation of heterotrophic growth.

Several heme-binding proteins, including  $c$ -type cytochromes, have known or postulated regulatory roles. The heme iron interacts with molecules such as  $O_2$ , CO, and nitric oxide (NO) and is thus well adapted as a sensor of such molecules as well as redox changes. For recent reviews of heme proteins in regulation, see Green et al. (2014) for a review of transcriptional regulation of bacterial virulence in response to  $O_2$  and NO, and Arora et al. (2015) for NO regulation of bacterial biofilms. Several regulators of tetrapyrrole synthesis such as HbrL and PpsR/CrtJ are heme-binding proteins. See Yin and Bauer (2013) and Chap. 25 by Zappa and Bauer for reviews.  $C$ -type cytochrome regulators include Cyt  $c_{550}$  of *Bacillus subtilis*, which has a midpoint potential of +190 mV (David et al. 1999) and a role in initiation of sporulation based on knockout and overexpression studies (Shin et al. 2005). Oxygen binding to the heme of the FixL sensor-kinase modulates nitrogen-fixation gene expression (Bauer et al. 1999). Other bacterial cytochrome sensors include the *Clostridium botulinum*  $b$ -heme SONO (Nioche et al. 2004) and the *Rhodobacter capsulatus* (Cross et al. 2001) and *Alcaligenes xylosoxidans* (Kruglik et al. 2007) periplasmic, pentacoordinate  $c'$  cytochromes for sensing and/or reductive detoxification of nitric oxide. NO production also occurs in nondenitrifying bacteria and some cyanobacteria possess quinol-nitric oxide reductases as a line of defense (Busch et al. 2002). Based on such precedents, roles for cyanobacterial  $c_6$ -like cytochromes in sensing-signaling pathways are conceivable but entirely speculative at this time.

## VI. Concluding Remarks

Cytochromes  $c_{6C}$ ,  $c_{6B}$ , or  $c_M$  are small,  $c_6$ -like cytochrome proteins of cyanobacteria. Despite the widespread distribution of genes for these cytochromes among cyanobacterial lineages, their functions remain largely unknown. Cytochrome  $c_M$  was the first of these to be discovered (Malakhov et al. 1994). Genes for cytochromes  $c_{6C}$  and  $c_{6B}$  were discovered from phylogenetic analysis (Bialek et al. 2008) and so named in relation to the previous, unexpected finding of genes for a  $c_6$ -like cytochrome, designated  $c_{6A}$ , in plants and some eukaryotic algae. Cytochrome  $c_M$  is found in almost all known cyanobacteria and cytochromes  $c_{6C}$  or  $c_{6B}$  are found in most cyanobacteria. One exception is the widely studied *Synechocystis* 6803, which carries a gene for cytochrome  $c_M$  but not for  $c_{6C}$  and  $c_{6B}$ . Representative  $c_M$ ,  $c_{6C}$ , and  $c_{6B}$  cytochromes have midpoint potentials in the +110 to +190 mV range, too low to effectively substitute for cytochromes  $c_6$  or plastocyanin in electron transfer from the cytochrome  $b_6f$  complex to photosystem I (Cho et al. 2000; Bialek et al. 2008; Zatwarnicki et al. 2014). Immunological data show that cytochrome  $c_M$  is located in both thylakoid and cytoplasmic membranes of *Synechocystis* 6803 (Bernroither et al. 2009). The localization of cytochromes  $c_{6C}$  and  $c_{6B}$  is unknown. The *petJ2* gene for cytochrome  $c_{6C}$  is transcribed at consistently low levels under most conditions tested in *Synechococcus* 7002 but increases up to 4-fold under certain stresses. Transcripts for cytochrome  $c_M$  in the same strain are still lower under standard conditions but increase as much as 24-fold, up to 0.05 % of total mRNA counts, under stresses such as high salt or nitrogen or sulfur limitation (Ludwig and Bryant 2012a, b). These findings suggest possible roles for these  $c_6$ -like cytochromes in overflow electron transfer pathways to alleviate over-reduction of electron carriers and the production of reactive oxygen species. Heme groups are well adapted for interactions with ligands such as molecular oxy-

gen, nitric oxide, or with electrons, and thus the  $c_6$ -like cytochromes may well serve in yet to be defined regulatory or signal transduction roles. A recently discovered regulatory role for cytochrome  $c_M$  in *Synechocystis* 6803 is in suppression of dark heterotrophic growth, possibly through interaction with the CtaI,  $aa_3$  cytochrome oxidase (Hiraide et al. 2015). Most likely, these widespread  $c_6$ -like cytochromes of cyanobacteria are not simply evolutionary relics and further research will reveal additional functions.

## Acknowledgements

TK gratefully acknowledges grants MCB 0450875 and MRI 0321545 from the U.S. National Science Foundation, which supported some of this work.

## References

- Agarwal R, Matros A, Melzer M, Mock HP, Sainis JK (2010) Heterogeneity in thylakoid membrane proteome of *Synechocystis* 6803. *J Proteomics* 73:976–991
- Allahverdiyeva Y, Ermakova M, Eisenhut M, Zhang P, Richaud P, Hagemann M, Laurent C, Aro EM (2011) Interplay between flavodiiron proteins and photorespiration in *Synechocystis* sp. PCC 6803. *J Biol Chem* 286:24007–24014
- Allahverdiyeva Y, Mustila H, Ermakova M, Bersanini L, Richaud P, Ajlani G, Battchikova N, ... Aro EM (2013) Flavodiiron proteins Flv1 and Flv3 enable cyanobacterial growth and photosynthesis under fluctuating light. *Proc Natl Acad Sci U S A* 110:4111–4116
- Allahverdiyeva Y, Isojarvi J, Zhang P, Aro EM (2015) Cyanobacterial oxygenic photosynthesis is protected by flavodiiron proteins. *Life* 5:716–743
- Alric J, Lavergne J, Rappaport F, Vermeglio A, Matsuura K, Shimada K, Nagashima KV (2006) Kinetic performance and energy profile in a roller coaster electron transfer chain: a study of modified tetraheme-reaction center constructs. *J Am Chem Soc* 128:4136–4145
- Anderson SL, McIntosh L (1991) Light-activated heterotrophic growth of the cyanobacterium *Synechocystis* sp. strain PCC 6803: a blue-light-requiring process. *J Bacteriol* 173:2761–2767
- Arora DP, Hossain S, Xu Y, Boon EM (2015) Nitric oxide regulation of bacterial biofilms. *Biochemistry* 54:3717–3728
- Bailey S, Melis A, Mackey KR, Cardol P, Finazzi G, van Dijken G, Berg G, ... Grossman A (2008) Alternative photosynthetic electron flow to oxygen in marine *Synechococcus*. *Biochim Biophys Acta* 1777:269–276
- Bailleul B, Johnson X, Finazzi G, Barber J, Rappaport F, Telfer A (2008) The thermodynamics and kinetics of electron transfer between cytochrome  $b_6f$  and photosystem I in the chlorophyll d-dominated cyanobacterium, *Acaryochloris marina*. *J Biol Chem* 283:25218–25226
- Bauer CE, Elsen S, Bird TH (1999) Mechanisms for redox control of gene expression. *Annu Rev Microbiol* 53:495–523
- Baymann F, Rappaport F (1998) Electrostatic interactions at the donor side of the photosynthetic reaction center of *Rhodospseudomonas viridis*. *Biochemistry* 37:15320–15326
- Baymann F, Rappaport F, Joliet P, Kallas T (2001a) Rapid electron transfer to photosystem I and unusual spectral features of cytochrome  $c(6)$  in *Synechococcus* sp. PCC 7002 in vivo. *Biochemistry* 40:10570–10577
- Baymann F, Tron P, Schoepp-Cothenet B, Aubert C, Bianco P, Stetter KO, Nitschke W, Schutz M (2001b) Cytochromes  $c555$  from the hyperthermophilic bacterium *Aquifex aeolicus* (VF5). 1. Characterization of two highly homologous, soluble and membranous, cytochromes  $c555$ . *Biochemistry* 40:13681–13689
- Bernroither M, Tangl D, Lucini C, Furtmuller PG, Peschek GA, Obinger C (2009) Cyanobacterial cytochrome  $c(M)$ : probing its role as electron donor for Cu(A) of cytochrome  $c$  oxidase. *Biochim Biophys Acta* 1787:135–143
- Berry S, Schneider D, Vermaas WF, Rogner M (2002) Electron transport routes in whole cells of *Synechocystis* sp. strain PCC 6803: the role of the cytochrome  $bd$ -type oxidase. *Biochemistry* 41:3422–3429
- Bersanini L, Battchikova N, Jokel M, Rehman A, Vass I, Allahverdiyeva Y, Aro EM (2014) Flavodiiron protein Flv2/Flv4-related photoprotective mechanism dissipates excitation pressure of PSII in cooperation with phycobilisomes in Cyanobacteria. *Plant Physiol* 164:805–818
- Bialek W, Nelson M, Tamiola K, Kallas T, Szczepaniak A (2008) Deeply branching  $c_6$ -like cytochromes of cyanobacteria. *Biochemistry* 47:5515–5522
- Bialek W, Krzywda S, Jaskolski M, Szczepaniak A (2009) Atomic-resolution structure of reduced

- cyanobacterial cytochrome *c6* with an unusual sequence insertion. *FEBS J* 276:4426–4436
- Bialek W, Krzywdka S, Zatwarnicki P, Jaskolski M, Kolesinski P, Szczepaniak A (2014) Insights into the relationship between the haem-binding pocket and the redox potential of *c6* cytochromes: four atomic resolution structures of *c6* and *c6*-like proteins from *Synechococcus* sp. PCC 7002. *Acta Crystallogr D Biol Crystallogr* 70:2823–2832
- Busch A, Friedrich B, Cramm R (2002) Characterization of the *norB* gene, encoding nitric oxide reductase, in the nondenitrifying cyanobacterium *Synechocystis* sp. strain PCC6803. *Appl Environ Microbiol* 68:668–672
- Chida H, Yokoyama T, Kawai F, Nakazawa A, Akazaki H, Takayama Y, Hirano T, . . . Oku T (2006) Crystal structure of oxidized cytochrome *c(6A)* from *Arabidopsis thaliana*. *FEBS Lett* 580:3763–3768
- Cho YS, Pakrasi HB, Whitmarsh J (2000) Cytochrome *cM* from *synechocystis* 6803. Detection in cells, expression in *Escherichia coli*, purification and physical characterization. *Eur J Biochem* 267:1068–1074
- Cross R, Lloyd D, Poole RK, Moir JW (2001) Enzymatic removal of nitric oxide catalyzed by cytochrome *c'* in *Rhodobacter capsulatus*. *J Bacteriol* 183:3050–3054
- David PS, Morrison MR, Wong SL, Hill BC (1999) Expression, purification, and characterization of recombinant forms of membrane-bound cytochrome *c*-550 nm from *Bacillus subtilis*. *Protein Expr Purif* 15:69–76
- Diaz-Moreno I, Hulsker R, Skubak P, Foerster JM, Cavazzini D, Finiguerra MG, Díaz-Quintana A, . . . Ubbink M (2014) The dynamic complex of cytochrome *c6* and cytochrome *f* studied with paramagnetic NMR spectroscopy. *Biochim Biophys Acta* 1837:1305–1315
- Eisenhut M, Ruth W, Haimovich M, Bauwe H, Kaplan A, Hagemann M (2008) The photorespiratory glycolate metabolism is essential for cyanobacteria and might have been conveyed endosymbiotically to plants. *Proc Natl Acad Sci U S A* 105:17199–17204
- Fernandez-Velasco JG, Jamshidi A, Gong XS, Zhou J, Ueng RY (2001) Photosynthetic electron transfer through the cytochrome *b<sub>6</sub>f* complex can bypass cytochrome *f*. *J Biol Chem* 276:30598–30607
- Flores E, Frias JE, Rubio LM, Herrero A (2005) Photosynthetic nitrate assimilation in cyanobacteria. *Photosynth Res* 83:117–133
- Frazao C, Dias JM, Matias PM, Romao MJ, Carrondo MA, Hervas M, Navarro JA, . . . Sheldrick GM (1995) Cytochrome *c6* from the green alga *Monoraphidium braunii*. Crystallization and preliminary diffraction studies. *Acta Crystallogr D Biol Crystallogr* 51:232–234
- Gasteiger E, Hoogland C, Gattiker A, Duvaud S, Wilkins MR, Appel RD, Bairoch A (2005) Protein identification and analysis tools on the ExPASy server. In: Walker JM (ed) *The proteomics protocols handbook*. Humana Press, New York, pp 571–607
- Gouet P, Courcelle E, Stuart DI (1999) ESPript: analysis of multiple sequence alignments in PostScript. *Bioinformatics* 15:305–308
- Green J, Rolfe MD, Smith LJ (2014) Transcriptional regulation of bacterial virulence gene expression by molecular oxygen and nitric oxide. *Virulence* 5:794–809
- Gupta R, He Z, Luan S (2002) Functional relationship of cytochrome *c(6)* and plastocyanin in *Arabidopsis*. *Nature* 417:567–571
- Helman Y, Tchernov D, Reinhold L, Shibata M, Ogawa T, Schwarz R, Ohad I, Kaplan A (2003) Genes encoding A-type flavoproteins are essential for photoreduction of O<sub>2</sub> in cyanobacteria. *Curr Biol* 13:230–235
- Helman Y, Barkan E, Eisenstadt D, Luz B, Kaplan A (2005) Fractionation of the three stable oxygen isotopes by oxygen-producing and oxygen-consuming reactions in photosynthetic organisms. *Plant Physiol* 138:2292–2298
- Hervas M, Diaz-Quintana A, Kerfeld CA, Krogmann DW, De la Rosa MA, Navarro JA (2005) Cyanobacterial Photosystem I lacks specificity in its interaction with cytochrome *c(6)* electron donors. *Photosynth Res* 83:329–333
- Hiraide Y, Oshima K, Fujisawa T, Uesaka K, Hirose Y, Tsujimoto R, Yamamoto H, . . . Fujita Y (2015) Loss of cytochrome *cM* stimulates cyanobacterial heterotrophic growth in the dark. *Plant Cell Physiol* 56:334–345
- Ho KK, Krogmann DW (1980) Cytochrome *f* from spinach and cyanobacteria. Purification and characterization. *J Biol Chem* 255:3855–3861
- Ho KK, Kerfeld CA, Krogmann DW (2011) The water-soluble cytochromes of cyanobacteria. In: Peschek GA, Obinger C, Renger G (eds) *Bioenergetic Processes of Cyanobacteria: From Evolutionary Singularity to Ecological Diversity*. Springer, Dordrecht, pp 515–540
- Holton RW, Myers J (1967) Water-soluble cytochromes from a blue-green alga. I. Extraction, purification, and spectral properties of cytochromes C (549, 552, and 554, *Anacystis nidulans*). *Biochim Biophys Acta* 131:362–374
- Howe CJ, Schlarb-Ridley BG, Wastl J, Purton S, Bendall DS (2006) The novel cytochrome *c6* of chloro-

- plasts: a case of evolutionary bricolage? *J Exp Bot* 57:13–22
- Howitt CA, Vermaas WF (1998) Quinol and cytochrome oxidases in the cyanobacterium *Synechocystis* sp. PCC 6803. *Biochemistry* 37:17944–17951
- Huang F, Parmryd I, Nilsson F, Persson AL, Pakrasi HB, Andersson B, Norling B (2002) Proteomics of *Synechocystis* sp. strain PCC 6803: identification of plasma membrane proteins. *Mol Cell Proteomics* 1:956–966
- Kallas T (2012) Cytochrome *b<sub>6</sub>f* complex at the heart of energy transduction and redox signaling. In: Eaton-Rye JJ, Tripathy BC, Sharkey TD (eds) *Photosynthesis: Plastid Biology, Energy Conversion and Carbon Assimilation*. Springer, Dordrecht, pp 501–560
- Kerfeld CA, Krogmann DW (1998) Photosynthetic cytochromes *c* in cyanobacteria, algae, and plants. *Annu Rev Plant Physiol Plant Mol Biol* 49:397–425
- Kerfeld CA, Anwar HP, Interrante R, Merchant S, Yeates TO (1995) The structure of chloroplast cytochrome *c<sub>6</sub>* at 1.9 Å resolution: evidence for functional oligomerization. *J Mol Biol* 250:627–647
- Kirilovsky D, Kerfeld CA (2012) The orange carotenoid protein in photoprotection of photosystem II in cyanobacteria. *Biochim Biophys Acta* 1817:158–166
- Kruglik SG, Lambry JC, Cianetti S, Martin JL, Eady RR, Andrew CR, Negrerie M (2007) Molecular basis for nitric oxide dynamics and affinity with *Alcaligenes xylosoxidans* cytochrome *c*. *J Biol Chem* 282:5053–5062
- Kufryk GI, Vermaas WF (2006) Sll 1717 affects the redox state of the plastoquinone pool by modulating quinol oxidase activity in thylakoids. *J Bacteriol* 188:1286–1294
- Lea-Smith DJ, Ross N, Zori M, Bendall DS, Dennis JS, Scott SA, Smith AG, Howe CJ (2013) Thylakoid terminal oxidases are essential for the cyanobacterium *Synechocystis* sp. PCC 6803 to survive rapidly changing light intensities. *Plant Physiol* 162:484–495
- Lebrun E, Brugna M, Baymann F, Muller D, Lievre-mont D, Lett MC, Nitschke W (2003) Arsenite oxidase, an ancient bioenergetic enzyme. *Mol Biol Evol* 20:686–693
- Li Z, Andrews H, Eaton-Rye JJ, Burnap RL (2004) In situ effects of mutations of the extrinsic cytochrome *c<sub>550</sub>* of photosystem II in *Synechocystis* sp. PCC6803. *Biochemistry* 43:14161–14170
- Ludwig M, Bryant DA (2011) Transcription profiling of the model Cyanobacterium *Synechococcus* sp. strain PCC 7002 by next-gen (SOLiD) SEQUENCING of cDNA. *Front Microbiol* 2:41
- Ludwig M, Bryant DA (2012a) Acclimation of the global transcriptome of the cyanobacterium *Synechococcus* sp. strain PCC 7002 to nutrient limitations and different nitrogen sources. *Front Microbiol* 3:145
- Ludwig M, Bryant DA (2012b) *Synechococcus* sp. strain PCC 7002 transcriptome: acclimation to temperature, salinity, oxidative stress, and mixotrophic growth conditions. *Front Microbiol* 3:354
- Malakhov MP, Wada H, Los DA, Semenenko VE, Murata N (1994) A new type of cytochrome *c* from *synechocystis* PCC6803. *J Plant Physiol* 144:259–264
- Malakhov MP, Malakhova OA, Murata N (1999) Balanced regulation of expression of the gene for cytochrome *c<sub>M</sub>* and that of genes for plastocyanin and cytochrome *c<sub>6</sub>* in *Synechocystis*. *FEBS Lett* 444:281–284
- Manna P, Vermaas W (1997) Lumenal proteins involved in respiratory electron transport in the cyanobacterium *Synechocystis* sp. PCC6803. *Plant Mol Biol* 35:407–416
- Marcaida MJ, Schlarb-Ridley BG, Worrall JA, Wastl J, Evans TJ, Bendall DS, Luisi BF, Howe CJ (2006) Structure of cytochrome *c<sub>6A</sub>*, a novel dithio-cytochrome of *Arabidopsis thaliana*, and its reactivity with plastocyanin: implications for function. *J Mol Biol* 360:968–977
- Mason JM, Bendall DS, Howe CJ, Worrall JA (2012) The role of a disulfide bridge in the stability and folding kinetics of *Arabidopsis thaliana* cytochrome *c(6A)*. *Biochim Biophys Acta* 1824:311–318
- Mehler AH (1951) Studies on reactions of illuminated chloroplasts. I. Mechanism of the reduction of oxygen and other Hill reagents. *Arch Biochem Biophys* 33:65–77
- Molina-Heredia FP, Hervas M, Navarro JA, De la Rosa MA (1998) Cloning and correct expression in *Escherichia coli* of the *petE* and *petJ* genes respectively encoding plastocyanin and cytochrome *c<sub>6</sub>* from the cyanobacterium *Anabaena* sp. PCC 7119. *Biochem Biophys Res Commun* 243:302–306
- Molina-Heredia FP, Diaz-Quintana A, Hervas M, Navarro JA, De La Rosa MA (1999) Site-directed mutagenesis of cytochrome *c(6)* from *Anabaena* species PCC 7119. Identification of surface residues of the hemeprotein involved in photosystem I reduction. *J Biol Chem* 274:33565–33570
- Molina-Heredia FP, Balme A, Hervas M, Navarro JA, De la Rosa MA (2002) A comparative structural and functional analysis of cytochrome *c<sub>M</sub>* cytochrome *c<sub>6</sub>* and plastocyanin from the cyanobacterium *Synechocystis* sp. PCC 6803. *FEBS Lett* 517:50–54
- Molina-Heredia FP, Wastl J, Navarro JA, Bendall DS, Hervas M, Howe CJ, De La Rosa MA (2003) Pho-

- tosynthesis: a new function for an old cytochrome? *Nature* 424:33–34
- Mullineaux CW (2014) Co-existence of photosynthetic and respiratory activities in cyanobacterial thylakoid membranes. *Biochim Biophys Acta* 1837: 503–511
- Nagy CI, Vass I, Rakhely G, Vass IZ, Toth A, Duza A, Peca L, ... Kos PB (2014) Coregulated genes link sulfide:quinone oxidoreductase and arsenic metabolism in *Synechocystis* sp. strain PCC6803. *J Bacteriol* 196:3430–3440
- Nakamura A, Suzawa T, Kato Y, Watanabe T (2005) Significant species-dependence of P700 redox potential as verified by spectroelectrochemistry: comparison of spinach and *Thermosynechococcus elongatus*. *FEBS Lett* 579: 2273–2276
- Nioche P, Berka V, Vipond J, Minton N, Tsai AL, Raman CS (2004) Femtomolar sensitivity of a NO sensor from *Clostridium botulinum*. *Science* 306: 1550–1553
- Nomura C (2001) Electron transport proteins of *Synechococcus* sp. PCC 7002. PhD thesis, Pennsylvania State University, University Park
- Nomura C, Bryant DA (1999) Cytochrome *c6* from *Synechococcus* sp. PCC 7002. In: Peschek G, Löffelhardt W, Schmetterer G (eds) *The Phototrophic Prokaryotes*. Kluwer Academic/Plenum Publishers, New York, pp 269–274
- Nomura CT, Persson S, Shen G, Inoue-Sakamoto K, Bryant DA (2006a) Characterization of two cytochrome oxidase operons in the marine cyanobacterium *Synechococcus* sp. PCC 7002: inactivation of *ctaDI* affects the PS I:PS II ratio. *Photosynth Res* 87:215–228
- Nomura CT, Sakamoto T, Bryant DA (2006b) Roles for heme-copper oxidases in extreme high-light and oxidative stress response in the cyanobacterium *Synechococcus* sp. PCC 7002. *Arch Microbiol* 185: 471–479
- Paumann M, Bernroither M, Lubura B, Peer M, Jakopitsch C, Furtmuller PG, Peschek GA, Obinger C (2004a) Kinetics of electron transfer between plastocyanin and the soluble CuA domain of cyanobacterial cytochrome *c* oxidase. *FEMS Microbiol Lett* 239:301–307
- Paumann M, Feichtinger M, Bernroither M, Goldfuhs J, Jakopitsch C, Furtmuller PG, Regelsberger G, ... Obinger C (2004b) Kinetics of interprotein electron transfer between cytochrome *c6* and the soluble CuA domain of cyanobacterial cytochrome *c* oxidase. *FEBS Lett* 576:101–106
- Ponamarev MV, Schlarb BG, Howe CJ, Carrell CJ, Smith JL, Bendall DS, Cramer WA (2000) Tryptophan-heme pi-electrostatic interactions in cytochrome *f* of oxygenic photosynthesis. *Biochemistry* 39:5971–5976
- Rajagopal BS, Wilson MT, Bendall DS, Howe CJ, Worrall JA (2011) Structural and kinetic studies of imidazole binding to two members of the cytochrome *c* (6) family reveal an important role for a conserved heme pocket residue. *J Biol Chem* 16:577–588
- Reyes-Sosa FM, Gil-Martinez J, Molina-Heredia FP (2011) Cytochrome *c6*-like protein as a putative donor of electrons to photosystem I in the cyanobacterium *Nostoc* sp. PCC 7119. *Photosynth Res* 110:61–72
- Roncel M, Kirilovsky D, Guerrero F, Serrano A, Ortega JM (2012) Photosynthetic cytochrome *c550*. *Biochim Biophys Acta* 1817:1152–1163
- Sawaya MR, Krogmann DW, Serag A, Ho KK, Yeates TO, Kerfeld CA (2001) Structures of cytochrome *c-549* and cytochrome *c6* from the cyanobacterium *Arthrospira maxima*. *Biochemistry* 40:9215–9225
- Schmetterer G (1994) Cyanobacterial respiration. In: Bryant DA (ed) *The Molecular Biology of Cyanobacteria*. Kluwer Academic, Dordrecht, pp 409–435
- Schneider D, Skrzypczak S, Anemuller S, Schmidt CL, Seidler A, Rogner M (2002) Heterogeneous rieske proteins in the cytochrome *b6f* complex of *synechocystis* PCC6803? *J Biol Chem* 277:10949–10954
- Schultze M, Forberich B, Rexroth S, Dyczmons NG, Roegner M, Appel J (2009) Localization of cytochrome *b6f* complexes implies an incomplete respiratory chain in cytoplasmic membranes of the cyanobacterium *Synechocystis* sp. PCC 6803. *Biochim Biophys Acta* 1787:1479–1485
- Schuermans RM, Schuurmans JM, Bekker M, Kromkamp JC, Matthijs HC, Hellingwerf KJ (2014) The redox potential of the plastoquinone pool of the cyanobacterium *Synechocystis* species strain PCC 6803 is under strict homeostatic control. *Plant Physiol* 165:463–475
- Seidler A (1996) The extrinsic polypeptides of photosystem II. *Biochim Biophys Acta* 1277:35–60
- Shen JR, Vermaas W, Inoue Y (1995) The role of cytochrome *c-550* as studied through reverse genetics and mutant characterization in *Synechocystis* sp. PCC 6803. *J Biol Chem* 270:6901–6907
- Shin I, Ryu HB, Yim HS, Kang SO (2005) Cytochrome *c550* is related to initiation of sporulation in *Bacillus subtilis*. *J Microbiol* 43:244–250
- Shuvalov VA, Allakhverdiev SI, Sakamoto A, Malakhov M, Murata N (2001) Optical study of cytochrome *cM* formation in *Synechocystis*. *IUBMB Life* 51:93–97
- Ting CS, Rocap G, King J, Chisholm SW (2002) Cyanobacterial photosynthesis in the oceans: the ori-

- gins and significance of divergent light-harvesting strategies. *Trends Microbiol* 10:134–142
- van Lis R, Nitschke W, Duval S, Schoepp-Cothenet B (2013) Arsenics as bioenergetic substrates. *Biochim Biophys Acta* 1827:176–188
- Veit S, Takeda K, Tsunoyama Y, Rexroth D, Rogner M, Miki K (2012) Structure of a thermophilic cyanobacterial *b<sub>6</sub>f*-type Rieske protein. *Acta Crystallogr D Biol Crystallogr* 68:1400–1408
- Wastl J, Bendall DS, Howe CJ (2002) Higher plants contain a modified cytochrome c(6). *Trends Plant Sci* 7:244–245
- Wastl J, Purton S, Bendall DS, Howe CJ (2004) Two forms of cytochrome c6 in a single eukaryote. *Trends Plant Sci* 9:474–476
- Weigel M, Varotto C, Pesaresi P, Finazzi G, Rappaport F, Salamini F, Leister D (2003) Plastocyanin is indispensable for photosynthetic electron flow in *Arabidopsis thaliana*. *J Biol Chem* 278:31286–31289
- Worrall JA, Schlarb-Ridley BG, Reda T, Marcaida MJ, Moorlen RJ, Wastl J, Hirst J, ... Howe CJ (2007) Modulation of heme redox potential in the cytochrome c6 family. *J Am Chem Soc* 129:9468–9475
- Yamada S, Park SY, Shimizu H, Koshizuka Y, Kadokura K, Satoh T, Suruga K, ... Oku T (2000) Structure of cytochrome c6 from the red alga *Porphyra yezoensis* at 1.57 Å resolution. *Acta Crystallogr D Biol Crystallogr* 56:1577–1582
- Yin L, Bauer CE (2013) Controlling the delicate balance of tetrapyrrole biosynthesis. *Philos Trans R Soc London B Biol Sci* 368:20120262
- Zatwarnicki P, Barciszewski J, Krzywda S, Jaskolski M, Kolesinski P, Szczepaniak A (2014) Cytochrome c(6B) of *Synechococcus* sp. WH 8102—crystal structure and basic properties of novel c(6)-like family representative. *Biochem Biophys Res Commun* 443:1131–1135
- Zhang Z, Pendse ND, Phillips KN, Cotner JB, Khodursky A (2008) Gene expression patterns of sulfur starvation in *Synechocystis* sp. PCC 6803. *BMC Genomics* 9:344
- Zhang P, Allahverdiyeva Y, Eisenhut M, Aro EM (2009) Flavodiiron proteins in oxygenic photosynthetic organisms: photoprotection of photosystem II by Flv2 and Flv4 in *Synechocystis* sp. PCC 6803. *PLoS ONE* 4:e5331
- Zhang P, Eisenhut M, Brandt AM, Carmel D, Silen HM, Vass I, Allahverdiyeva Y, ... Aro EM (2012) Operon *flv4-flv2* provides cyanobacterial photosystem II with flexibility of electron transfer. *Plant Cell* 24:1952–1971

# Index

## A

- Alternate respiratory terminal oxidases (ARTOs), 331, 340, 341, 343–345, 347, 377
- Alternative oxidases (AOXs), 52, 112, 117, 340, 347–348, 375–392, 599, 614
- Anoxygenic bacteria, 40, 493
- Anoxygenic chain, 40
- Anoxygenic phototrophic bacteria, 35, 38, 502–503, 679–694
- AOXs. *See* Alternative oxidases (AOXs)
- ARTOs. *See* Alternate respiratory terminal oxidases (ARTOs)
- Ascofuranone, 389, 391
- Assembly of Cox, 490–492, 545–546
- Assembly, prosthetic groups, 504

## B

- Bacterial cytochrome (bc) complex, 283, 300, 307–324, 503, 515, 668, 670, 713–714
- $b_H$  and  $b_L$ , high and low potential  $b$  hemes, 458
- Biogenesis, 150, 324, 489–491, 503–505, 514, 517, 527–546, 556, 557, 559, 599–600, 613, 706
- Butler, W. L., 3, 4

## C

- cbb*<sub>3</sub> type cytochrome *c* oxidase, 331, 345–346
- CBM. *See* Constraint-based model (CBM)
- CCB. *See* Complex C subunit B (CCB) pathway
- CCM. *See* Cytochrome *c* maturation (CCM) pathways
- Cc*<sub>6</sub> photosynthetic complexes, 662–667
- Cc*<sub>6</sub> respiratory complexes, 667–671
- CEF. *See* Cyclic electron flow (CEF)
- CET. *See* Cyclic electron transport (CET)
- CFX. *See* *Chloroflexus aurantiacus* (CFX)
- Channeling, 586, 588, 600–611, 615
- Chlamydomonas reinhardtii*, 38, 52–53, 136, 137, 146, 216, 242, 259–260, 266, 273–274, 297, 298, 301, 439–442, 445–449, 453, 454, 456–460, 465–473, 483, 490, 510, 512, 513, 516, 632–635, 645, 647, 648, 660, 665, 666, 692, 703, 709, 710, 715, 716, 721
- Chloroflexus aurantiacus* (CFX), 34, 38, 262, 634
- c*<sub>6</sub>-like cytochromes, 635, 704, 713–715, 717, 718, 720–722, 724–730
- Competition for electrons, 425–426, 681–685
- Complex C subunit B (CCB) pathway, 508, 516–517
- Complex III, 9, 212, 223, 266, 309, 585–591, 593, 594, 596–599, 601, 602, 604–617

- Constraint-based model (CBM), 692–693
- Continuum electrostatics, 87, 88, 100, 120–122
- Copper acquisition, transport, 491
- Copper chaperone, 489, 491, 493
- COX. *See* Cytochrome *c* oxidase (COX) assembly
- Cramer, W. A., 9, 22, 26, 34, 42, 43, 118, 132, 144, 147, 158, 169, 179–186, 190, 191, 193, 195, 200, 242, 260, 262, 266–268, 270, 273, 274, 282, 296, 399, 400, 403, 409, 420, 421, 440, 442, 445, 448, 459, 573, 577, 635
- Crystal structure,  $b_6f$  complex, 42
- CuA, CuB, unique copper binding sites on oxidase, 357, 535
- Cyanobacteria, 26, 41–44, 51–53, 56–62, 64, 65, 100, 131–140, 146, 147, 149–151, 163, 164, 179–182, 193, 194, 198, 211, 216, 242, 253–256, 259, 261, 262, 265–275, 296, 301, 308, 331–351, 377, 401, 403, 405, 409, 467, 480, 481, 483, 490, 492, 502–505, 508, 510, 516, 517, 559, 631, 634–636, 638, 641, 645, 647, 648, 657–671, 685, 702, 708–710, 713–730
- Cyclic electron flow (CEF), 42, 44, 146, 439, 445, 446, 454–461, 463–465, 471–473
- Cyclic electron transport (CET), 31, 34, 39–44, 52, 53, 57–58, 63, 180, 191–194, 196, 197, 253, 254, 256, 257, 262, 273, 274, 480, 681
- Cyt *bf*. *See* Cytochrome  $b_6f$  complex (Cyt *bf*)
- Cyt *c*<sub>6</sub>. *See* Cytochrome *c*<sub>6</sub> (Cyt *c*<sub>6</sub>)
- Cytochrome
  - a*, *b*, *bo*, *bo*<sub>3</sub>, *c*, *e*, *f*, *h*, *o*, 557
  - apoprotein synthesis, 480, 487–490
  - $b_6$ , 9, 259, 261, 301, 470, 502, 504, 516, 517, 568, 570, 572–574, 577, 578
  - $b_{559}$ , 9, 41, 143–169, 559, 568, 570–572
  - bc*, *bc*<sub>1</sub>,  $b_6f$  complexes, 179
  - bc*,  $b_6f$  complexes, 179, 188
  - bc* complex, 9, 10, 34–38, 42, 120, 132–133, 179, 188, 195, 200, 281–291, 397–410
  - bc*<sub>1</sub> complex, 9, 35, 36, 107, 132, 178, 179, 183, 209–230, 237, 260, 282, 296, 300, 304, 309, 398, 403, 404, 419–431, 440, 488, 502, 564, 572, 576, 577, 680, 682–684
  - $b_6f$  complex, cyanobacterial, 265–275
  - bo*<sub>3</sub>, 8, 564, 576–577
  - c*<sub>6</sub>A, 510, 701–711, 714–716
  - c*<sub>6</sub>A, evidence against substitute for plastocyanin, 703–704
  - c*<sub>6</sub>B and *c*<sub>6</sub>C, 702, 703, 708–710
  - c*<sub>6</sub> (Cyt *c*<sub>6</sub>) family, 702, 708
  - c*M, 343, 713–717, 722–725, 729, 730

Cytochrome *b<sub>6</sub>f* complex (Cyt *b<sub>f</sub>*), 9, 37, 41, 42, 57, 62, 65, 132, 178, 179, 182, 184, 185, 189, 191, 193, 196, 199, 200, 253–262, 295–304, 347, 398, 404, 409, 420, 437–449, 453–459, 463, 464, 502, 574, 576–578, 631, 632, 635, 646–649, 657, 702, 706, 708, 709, 713, 714, 729

Cytochrome *c*, 5–10, 32, 34, 36, 37, 39, 40, 43, 44, 90–92, 95, 101–103, 121, 132, 241, 283, 307–324, 331, 332, 341–343, 345–346, 348–350, 357–371, 398, 405, 419, 420, 422, 485, 489–492, 505–517, 527–546, 558, 559, 564, 586, 587, 590, 594, 596, 598, 600, 601, 603–609, 611, 612, 614, 615, 637, 639, 640, 644, 657, 658, 684, 705, 709

Cytochrome *c*6 (Cyt *c*6), 38, 41–44, 132, 134–139, 267, 296, 343, 438, 492, 502, 510, 559, 631–649, 657–671, 701–705, 707–710, 713–724, 727

Cytochrome *c* maturation (CCM) pathways, 490, 505, 507–510, 512, 513

Cytochrome *c* oxidase (COX) assembly, 333–350, 487, 488, 530–538, 545, 558, 590, 715

Cytochrome *f* (C*f*), 4, 6–10, 26, 37, 43, 44, 180, 186, 187, 242, 259–261, 296, 472, 491, 503, 510, 577, 578, 631–649, 664–667, 669–671, 701, 703, 706, 708, 718

Cytochrome maturation, 491, 505, 510

Cytoplasmic electron sinks, 687–688

**D**

Debye, 84, 109, 640

Dielectric constants, 73, 74, 77, 78, 86–88, 92, 109–111, 165, 183, 185, 186, 640

D-, K+, pathways for proton transfer, 309–311, 315–318

Domain movement, 187, 224, 230

**E**

ECS. *See* Electrochromic shift (ECS)

Electrochromic shift (ECS), 298, 299, 460, 472

Electron donor to PSI, 43, 458, 662–665, 719

Electron paramagnetic resonance (EPR), 146, 149, 150, 152, 183, 185, 189, 194, 197–198, 247, 284, 322, 323, 385–386, 389, 392, 426–428, 441

Electron-proton transfer pathways, 196

Electron transfer (ET), 8, 14, 26, 52, 73, 99, 132, 144, 178, 210, 238, 254, 270, 281, 295, 308, 341, 357, 398, 419, 438, 455, 463, 502, 527, 555, 586, 631, 658, 680, 702, 714

inter-monomer, 226–227, 281–291

pathways, 41, 104, 212, 225, 254, 262, 288, 319, 320, 407, 419, 422, 427, 455, 458, 459, 465, 594, 682, 718, 725, 726, 729

proton transfer pathways, 196, 423–427

at Q<sub>n</sub>, Q<sub>p</sub> site, 223

Electrostatic potential (ESP), 86, 105, 108, 109, 112, 118, 165, 260, 662, 667

EPR. *See* Electron paramagnetic resonance (EPR)

ESP. *See* Electrostatic potential (ESP)

ET. *See* Electron transfer (ET)

Evolution, 10, 14–16, 18–22, 26, 28, 30, 37, 38, 40–44, 51–65, 93, 132–133, 136, 138, 147, 180, 183, 186–188, 190, 192, 195, 211, 217, 262, 290, 368, 438, 480, 528, 558, 633–635, 646, 649, 657, 665, 703, 706, 707, 709–710, 714, 717, 724, 730

**F**

Femtoseconds (fs), 84, 357–359, 366, 368, 369, 371

Ferredoxin, 28, 41, 43, 51, 55–56, 87, 89–90, 134, 181, 191–194, 196, 197, 266, 271, 273, 407, 439, 445, 465, 468, 472, 473, 490, 535, 536, 662, 682, 685, 686, 691

Ferredoxin-NADP<sup>+</sup> reductase (FNR), 64, 181, 182, 188, 193–194, 196, 253–262, 273, 296, 439, 444–446, 453, 454, 456–459, 465, 472, 685

Ferredoxin-plastoquinone oxidoreductase (FQR), 193–194, 445, 459

Flavodiiron proteins, 62, 726

FNR. *See* Ferredoxin-NADP<sup>+</sup> reductase (FNR)

Fourier transform infra-red spectroscopy (FTIR), 166, 323, 385, 425

FQR. *See* Ferredoxin-plastoquinone oxidoreductase (FQR)

FTIR. *See* Fourier transform infra-red spectroscopy (FTIR)

**G**

GOE. *See* Great oxidation event (GOE)

Great oxidation event (GOE), 15, 19–21, 634

**H**

Haemochromogen, 5, 7, 8

Hartree, E. F., 5, 6, 9

HAT. *See* Human African Trypanosomiasis (HAT)

HCCS. *See* Holocytochrome *c* synthase (HCCS) pathway

HCO. *See* Heme copper oxidase (HCO)

Helical propensity, 247, 248

Heme

biosynthesis, 13–21, 479, 482–490, 493, 555–557

channel, 511

c<sub>i</sub>/c<sub>n</sub>, 295–304

cofactors, 13–22, 33, 35, 528, 544, 556–559, 567–570, 572–574, 659

Heme copper oxidase (HCO), 309–324, 340–341, 348, 530, 531, 533, 534, 537, 668

Heme handling protein (HHP), 507, 509, 511, 541, 543

Heterogeneity of *b<sub>6</sub>f* complex, 268–272

HGT. *See* Horizontal gene transfer (HGT)

HHP. *See* Heme handling protein (HHP)

High spin heme, 309, 311, 314, 531

Hill, R., 6, 7, 9, 43

Holocytochrome *c* synthase (HCCS) pathway, 508, 513–516

Horizontal gene transfer (HGT), 15, 18, 709, 710

Human African trypanosomiasis (HAT), 376

Hydrogen bond, 106, 108, 119, 152–156, 164, 166, 199, 222, 241, 246, 248, 270, 284, 316, 319, 320, 363, 366, 367, 370–371, 378, 380, 382, 390, 422–425, 427–430, 440, 596, 645, 661, 722, 771



**I**

- Insertion, small membrane proteins, 567
- Insertion, tail-anchored membrane proteins, 566–567
- Interaction, dynamics, 588
- Interaction partners, 274, 590, 706
- Inter heme electron transfer, 92, 320
- Iron, copper homeostasis, 492–493
- Iron sulfur protein (ISP), 89, 180, 182, 184–188, 190, 195, 196, 198, 199, 213, 215–220, 222–228, 230, 238–249, 259–261, 270, 296, 400–401, 403, 409, 420–427, 429, 430, 439, 441–442, 503, 504, 613, 727, 728
- ISP. *See* Iron sulfur protein (ISP)

**K**

- Keilin, D., 3–10, 528, 556, 608
- Kinases, 260, 272–273, 398, 408–410, 446–449, 456, 463–474, 486–488, 616, 709, 729
- Kinetics, 28, 29, 34, 39, 43, 73, 81, 91, 100, 120–124, 134–135, 139, 186, 194, 225, 226, 228, 238, 239, 247, 262, 270, 274, 282, 286, 287, 290, 302, 401, 420–422, 425–427, 429, 430, 440–445, 458, 461, 600–609, 631–634, 636, 639–644, 663–666, 668–669, 692

**L**

- Last universal common ancestor (LUCA), 13–22
- Light harvesting complex (LHC), 34, 136, 211, 212, 408, 439, 453, 680
- Linear and cyclic electron flow, 439
- Linear electron flow (LEF), 41, 42, 44, 273, 274, 407, 438, 442, 445, 446, 453–457, 459, 463–465, 472
- Linear electron transport (LET), 41, 58, 186, 189, 192–197, 254, 256, 258, 271, 274, 444
- Lipid content, 190–191, 595–598
- Lipoprotein, lipid content, 190–191
- LIPs. *See* Loop insertion peptides (LIPs)
- Loop insertion peptides (LIPs), 704–710, 720
- Loosely bound subunits, 273–275
- LUCA. *See* Last universal common ancestor (LUCA)

**M**

- Major facilitator superfamily (MFS), 491, 534–536
- Marcus theory, 100, 102–104, 114, 122
- MD. *See* Molecular dynamics (MD)
- Metabolic modeling, 683, 690, 693–694
- MFS. *See* Major facilitator superfamily (MFS)
- Microstate model, 100, 106, 117, 120, 121, 123, 125
- Mitochondrial alternate oxidase, 212
- Mitochondrial *bc<sub>1</sub>* complex (*Mtbc<sub>1</sub>*), 132, 186, 187, 190–191, 193, 198, 213, 215–218, 220, 222–224, 226, 228, 238, 242, 245, 248, 398–401, 403, 441, 503, 504
- Mitochondrial cytochrome *c* oxidase, 341, 342, 345
- MM. *See* Molecular mechanics (MM)
- Mobility of LHCII, 466

- Molecular dynamics (MD), 84–85, 87, 90, 91, 239, 241, 317, 320, 321, 637, 670
- Molecular mechanics (MM), 84, 107
- Molecular orbitals, 93–94
- Mtbc<sub>1</sub>*. *See* Mitochondrial *bc<sub>1</sub>* complex (*Mtbc<sub>1</sub>*)

**N**

- NADH: ubiquinone reductase, 308
- n* and *p*, electrochemically negative and positive side of the membrane, 180, 398
- Nitrate reductase, 682, 684, 726
- 2-*n*-nonyl-4-hydroxyquinoline-N-oxide (NQNO), 189, 227, 228, 303, 304, 347, 402, 405
- Non-photochemical quenching (NPQ), 57, 62, 63, 65, 438, 441, 443, 444, 455, 459, 471, 725
- NO-reductase, 16, 19, 21, 314, 323, 558
- Nuclear magnetic resonance (NMR), 249, 320, 631, 636–638, 640, 642–644, 646, 661, 664–667, 669, 670

**O**

- Oceanic complex, 133
- “Omics” studies, 706–707

**P**

- P700, 57, 134, 139, 181, 187, 194, 197, 274, 441, 458, 460, 632, 634, 647, 663, 664, 718
- Paramagnetic relaxation enhancement (PRE), 428, 429, 666, 667
- Pathways for heme attachment, 505
- PCET. *See* Proton-coupled electron transport (PCET)
- PEWY sequence, 198, 267, 401, 440
- Phage-encoded complex, 139–140
- Photosystem I
- Photosystem II, core complex (PSIIcc), 144–152, 154, 156, 157, 159, 162, 163, 167–169
- Photosystem I, II
- Photosystem I, Structure
- Phycobilisome, 133, 274, 647, 726
- Phylogeny, 14–16, 19–21
- Picobiology, 358, 368–371
- Plastidic type terminal oxidase (Pt<sub>ox</sub>), 331, 347–348, 350, 464, 465
- Plastid terminal oxidase, 52, 464, 465, 472, 726
- Plastocyanin, 39, 41, 43, 44, 132, 134, 179, 181, 187, 242, 253, 254, 267, 270, 296, 343, 398, 408, 438, 454, 457, 465, 492, 510, 559, 631–649, 657, 658, 701–711, 713–715, 727, 729
- Plastoquinone (PQ), 52, 53, 57, 58, 63, 64, 101, 132, 134, 139, 144–151, 154, 156, 167–169, 179, 181, 183, 193–197, 266–268, 270–272, 274, 296, 301, 304, 345, 346, 398–400, 403, 404, 407–410, 438–440, 442, 445–447, 449, 454–461, 463–467, 469, 470–474, 646, 658, 667, 708, 709, 714, 725–728
- PMF. *See* Proton motive force (PMF)
- Possible functions, 144, 156, 243, 513, 603, 708–709, 714, 725–729

Post-translational changes, 616  
 PQ. *See* Plastoquinone (PQ)  
 Pre-apocytochrome *c*, 506  
 Promoter selectivity, 489–490  
 Proton-coupled electron transport (PCET), 376, 380–382, 385–387  
 Proton/electron coupling, 107  
 Proton motive force (PMF), 34, 52, 57, 58, 63–65, 210–212, 225, 307, 308, 438, 454, 459, 465, 680, 682–686  
 Proton trans-membrane electrochemical potential gradient, 180, 665

## Q

Q cycle, 29, 30, 34–36, 39, 42, 101, 103, 107, 192, 194–197, 214–216, 267, 282, 288, 289, 296, 309, 399–405, 409, 419–422, 425, 430, 440, 442, 449, 454, 459, 596, 635  
 QM. *See* Quantum mechanics (QM)  
 QOX. *See* Quinol oxidases (QOX)  
 Quantum mechanics (QM), 73, 74, 80–85, 91, 283, 632  
 Quinol consuming reactions, 682, 683–685  
 Quinol oxidases (QOX), 7, 212, 331, 340, 341, 345–347, 375–392, 422, 533  
 Quinol oxidase site, 422  
 Quinol producing reactions, 683  
 Quinol/quinone oxidation, reduction sites, 181  
 Quinone pool, 42, 52, 147, 150, 156, 167, 168, 194, 289, 347, 348, 381, 420, 681–685  
 Quinone reductase site, 420  
 Quinones, 16, 20–22, 26, 27, 32, 34, 35, 42, 52, 100–103, 107, 117, 121, 132, 144, 145, 147, 148, 150, 151, 154, 156, 157, 167, 179, 181, 189, 194–200, 210, 212, 215, 222, 224, 225, 227, 247, 260, 262, 267, 268, 282, 285, 288–291, 296, 300–303, 347, 390, 392, 398, 400, 402, 404, 405, 410, 420, 421, 423–427, 430, 439, 440, 442, 443, 445, 448, 529, 587, 605, 632, 681–684, 728

## R

Reaction center (RC), 26–34, 37, 41, 102, 116, 120–124, 132, 144, 178, 181, 183, 187–190, 193–195, 197, 210–212, 262, 296, 407, 427, 464, 487, 488, 529, 596, 632, 634, 643, 663, 665, 680–685, 718  
 Reactive oxygen species (ROS), 41, 42, 100, 169, 229, 289, 290, 308, 309, 321, 348, 397–399, 404–410, 426, 438, 469, 473, 546, 557, 586, 598, 599, 610–614, 616, 617, 709, 725, 726, 729  
 Reactive oxygen species signaling function, 398, 405–410  
 Redox  
   buffers, 100, 101  
   regulation, 101, 271, 445, 449, 473, 486–489, 616, 706  
   signal transduction, 463–474  
   status, 410, 425, 426, 456  
 Regulation, apoprotein synthesis, 480, 487–490  
 Regulatory hub, 437–449  
 Resonance Raman (RR), 146, 357, 359, 361, 362, 364, 366, 367, 560

Resonance Raman spectroscopy, 323  
 Respiratory chain, 6, 8–10, 133, 178, 183, 187, 195, 197, 211, 230, 307–309, 376, 398, 405, 465, 565, 586–589, 591–593, 598, 600, 603, 605, 606, 608–614, 616–617  
 Respiratory terminal oxidases (RTOs), 331–351, 485, 709  
*Rhodobacter capsulatus* bc<sub>1</sub>, 425, 426  
*Rhodobacter Sphaeroides* bc<sub>1</sub> (*Rsb*c<sub>1</sub>), 211, 213, 216, 218–223, 226, 227, 229, 230, 427  
 Ribonucleotide reductase (RNR), 377, 380–387, 391  
 Rich, P., 9, 185, 189, 190, 195, 216, 228, 303, 317, 387, 391, 403, 405, 425  
 Rieske iron-sulfur protein; different positions, 237–249  
 Rieske iron-sulfur subunits, 265–275  
 Rieske Protein, 35, 180, 186, 237–249, 266, 268–272, 274, 423, 439–441, 443, 447, 448, 577, 599, 601, 613, 706  
 RNR. *See* Ribonucleotide reductase (RNR)  
 ROS. *See* Reactive oxygen species (ROS)  
 RR. *See* Resonance Raman (RR)  
 RTOs. *See* Respiratory terminal oxidases (RTOs)

## S

*Sauromatum Guttatum* alternative oxidase, 376  
 Scarisbrick, R., 6–9  
 Secondary structure, 26, 83, 165, 187, 220, 243, 245, 261, 534, 593, 719  
 Semiquinone (SQ), 35, 197, 199, 239, 289, 290, 304, 390, 391, 401–404, 419, 421–429, 443  
 Signaling, 213, 274, 397–410, 447, 463–474, 493, 614, 616, 617, 729  
 Siroheme, 14, 18–20  
 Six pathways for covalent heme attachment, 505, 508  
 Small electron donors, 134–139  
 Small polypeptides, 265–275, 541, 567  
 SQ. *See* Semiquinone (SQ)  
 State transitions, 260, 270, 271, 273, 274, 322, 398, 408–409, 438, 439, 446–449, 456, 457, 463–474  
 Structural model, 165, 367, 571, 594, 665–667, 669–671  
 Structure, 7, 16, 26, 53, 74, 100, 135, 144, 178, 210, 237, 253, 266, 281, 295, 308, 346, 357, 376, 398, 422, 438, 467, 486, 503, 528, 557, 591, 634, 657, 681, 705, 714  
 Stt7/STN7 kinase, 273, 408, 409, 447, 466–474  
 Super-complex, 183, 190, 193, 194, 253, 254, 590  
 Superoxide, 166, 169, 196, 213, 229–230, 289, 290, 385, 397–410, 419–428, 430, 534, 591, 611, 612, 614, 726

## T

TAO. *See* Trypanosomal alternative oxidase (TAO)  
 Tat. *See* Twin arginine translocation pathway (Tat)  
 Tetrapyrrole pathway, 481–482, 484, 485  
 Thylakoid and cytoplasmic membranes, 727, 729  
 Tridimensional structure, 300–301  
 Trypanosomal alternative oxidase (TAO), 376–380, 382–384, 389  
 Twin arginine translocation pathway (Tat), 560, 565–566

**U**

Ubiquinone (ol) (UQ), 7, 8, 10, 100, 103, 107, 132, 211–213, 216, 218, 219, 224, 226–228, 239, 289, 290, 308, 309, 346, 375, 376, 385, 389, 398–401, 403, 420, 482, 485–489, 493, 586–588, 594–596, 601, 602, 604–606, 608–610, 614, 693

**V**

Very low potential (VLP) heme, 158, 159, 163

**W**

Warburg, O., 3, 5  
Water-oxidizing complex (WOC), 144, 145, 148, 151, 156, 163, 167  
WOC. *See* Water-oxidizing complex (WOC)

**X**

XFEL. *See* X-ray free electron laser (XFEL)  
X-ray free electron laser (XFEL), 357–371